Synthesis of Astrochemically Relevant Small Molecules for Rotational Spectroscopy

By

Samuel M. Kougias

A dissertation submitted in partial fulfilment of the requirements for the degree of

Doctor of Philosophy

(Chemistry)

At the

UNIVERSITY OF WISCONSIN-MADISON

2022

Date of final oral examination: August 18, 2022

The dissertation is approved by the following members of the Final Oral Committee:

Robert J. McMahon, Professor, Materials, Organic and Physical Chemistry
R. Claude Woods, Professor, Physical Chemistry
Tehshik P. Yoon, Professor, Organic and Inorganic Chemistry
Shannon S. Stahl, Professor, Organic and Inorganic Chemistry

© Copyright by Samuel M. Kougias 2022
All Rights Reserved

Acknowledgements

Above all, I would like to thank my research advisors, Professors Bob McMahon and Claude Woods for their unwavering support and patience throughout my career as a graduate student. Bob and Claude have been amazing mentors, and have generously provided me with whatever I needed to succeed and grow as a scientist. I have truly enjoyed working in their lab, and I feel honored having been a member of their research group.

The Department of Chemistry at UW Madison has been a fantastic place to work. I would like to thank all the faculty, staff, and research scientists who have made my graduate career a positive experience. Even though the past two years have felt chaotic, the folks in the chemistry department have always contributed to provide a supportive community and to keep everything running. I would like to thank Jeff Nielsen, Tracy Drier, Blaise Thompson, Bill Goebel, Ariel Andrea, Kendall Schneider, Steve Myers, Charlie Fry, Heike Hofstetter, Cathy Clewett, Martha Vestling, Arrietta Clauss and Desiree Bates for their dedication to the department, the facilities, and the wellbeing of the folks that work there.

I would like to thank the members of the McMahon | Woods group, both past and current, for making the office such a welcoming place to work. Vanessa, Matisha, Andrew, Maria, Madison, Houston, Brian and Sam have all contributed massively to my development as a scientist. I am thankful for having worked alongside all of you over the past years, and I am excited to see what the future has in store for us!

I am grateful for the friendships I have formed throughout my time in Madison - both in and outside of lab. The adventures shared with Manar Alherech, Mike Croissant, Austin Kruger and Lu Liu made my time in Madison enjoyable (and memorable). Even events such as a car overheating in the Sonic parking lot became a hilarious ordeal. I'd like to thank Sam Wood for

being one of the most genuine people I've ever met - you are truly the proverbial diamond among silicates. Don't ever change! I want to thank Ryan Reeves – your technical expertise undoubtedly helped me become a more skilled chemist. I appreciate all the random projects involving fly fishing or flying drones or flying D-batteries. I want to thank Dan Glazier and Naomi Biok for all those rad camping trips. Thank you both for all the help over the past year. Every time I read an article from *Tetrahedron Lett.* it reminds me of Blue Mound State Park. Thanks to the friends I met at UW-Madison, I have a wealth of memories that I will appreciate for the rest of my life. They're also responsible for a bowling ball named "Larry" that's at the bottom of Lake Mendota. I'll *spare* you the details on how it got there.

I want to thank my undergraduate advisors and instructors from UW-Oshkosh. Professors Bill Wacholtz, Kevin Crawford, Jennifer Schuttlefield, Dennis Rioux, Linfeng Xie, Brant Kedrowski, Jonathan Gutow, Mark Lattery, Nenad Stojilovic, Barton Pritzl (and many others) not only taught me the skills and patience required to be a proficient scientist, but they also encouraged my decision to attend graduate school. I feel honored to have represented UW-Oshkosh throughout my experience in graduate school at UW-Madison.

Lastly, I would like to thank my family. Throughout my life, my folks have always cultivated an interest and appreciation for science and technology. They always encouraged me to learn about the world and investigate how things work. I have seriously lost count on how many times we visited the Museum of Science and Industry or the Adler Planetarium. My family has been incredibly supportive throughout my journey as a graduate student and throughout my life in general. This thesis is an accomplishment that would not have been possible without their encouragement, reassurance, and love.

SYNTHESIS OF ASTROCHEMICALLY RELEVANT SMALL MOLECULES FOR ROTATIONAL SPECTROSCOPY

Samuel Matthew Kougias

Under the supervision of Professor Robert J. McMahon and Professor R. Claude Woods

at the University of Wisconsin – Madison

Rotational spectroscopy is an essential technique used for the detection and characterization of molecules in the gas phase. While many techniques exist for the structural determination of molecules, rotational spectroscopy is an extremely precise tool for the structural characterization of gas-phase species. A key application of rotational spectroscopy is in the field of radioastronomy, where gaseous matter present in the cosmos is studied *via* the observation and assignment of rotational transitions emitted by celestial species. Rotational spectroscopy plays a pivotal role by providing the spectroscopic characterization data needed to search for novel species in the cosmos. The disciplines of radioastronomy, astrochemistry, molecular structure, and quantum theory are bound by the field of rotational spectroscopy.

The McMahon | Woods group seeks to further develop the library of known celestial molecules through the analysis of species theorized to be part of astrochemical systems. Our research involves rotational spectroscopy of target species to determine the spectroscopic constants and characterization data needed for radioastronomical searches, matrix isolation spectroscopy to investigate and describe the reactivity/stability of species in stellar environments, and detailed structural determinations to report highly-precise structure of our target molecules. The individual roles of the members in our group varies considerably with individual researchers contributing distinct specialties largely related to the field of physical organic chemistry. Our group is composed of specialists in theoretical chemistry, molecular spectroscopy, data analysis, analytical

chemistry, physical organic chemistry, and synthetic organic chemistry. The combined specialties of the members in the McMahon | Woods group is unique amongst molecular spectroscopy groups, and allows for the pursuit of highly detailed research projects.

During my time in the McMahon | Woods group, my research has centered around the synthesis, purification and isolation of target molecules for rotational spectroscopy studies within our group, and in collaboration with other groups. Many (but not all) of the molecules studied by the McMahon | Woods group have been synthetically produced in our laboratory. The synthesis of pure samples of target species enables the measurement and assignment of species not typically available to groups researching rotational spectroscopy. Our ability to synthetically produce target species (and isotopologues) yields data allowing our group to publish high-impact studies in the field of molecular spectroscopy and molecular structure.

The first three chapters of this thesis describe the synthesis and spectroscopic characterization of organic nitriles hypothesized to be present in the interstellar medium (ISM) and other carbon/nitrogen rich environments such as the atmosphere of Saturn's largest moon, Titan. Organic nitriles are a particularly interesting class of molecules that are highly desirable candidates for our group to investigate due to their pronounced dipole moments and ubiquity throughout the cosmos. The nitriles described in chapters 1-3 are isomeric to the nitrogenous heterocycle, pyridine, which has yet to be identified in the ISM. While the detection of aromatic/heteroaromatic species in the cosmos has been an area of interest in the field of astrochemistry, the presence of pyridine in celestial realms has important implications regarding prebiotic organic chemistry. The radioastronomical search or detection of these nitriles provides clues regarding the potential formation or presence of pyridine in the cosmos.

Chapter 1 describes the research of four cyanobutadiene (C_5H_5N) isomers that are of considerable interest to the organic chemistry, molecular spectroscopy, and astrochemistry communities. Upon joining the McMahon | Woods group in 2016, my initial project involved the synthesis and isolation of (*E*)-1-cyano-1,3-butadiene. The project was previously researched by Stephanie N. Knezz (Ph.D., 2016) who had graduated only a week before I had joined the group. While Stephanie succeeded in producing small quantities of (*E*)-1-cyano-1,3-butadiene, and was able to characterize the compound *via* NMR spectroscopy, she had encountered difficulty obtaining samples of pure material due to the tendency of (*E*)-1-cyano-1,3-butadiene to undergo polymerization. Since 2016, our group continued in the development of methodology permitting the isolation of four cyanobutadiene isomers as pure compounds: (*E*)-1-cyano-1,3-butadiene, (*Z*)-1-cyano-1,3-butadiene, 4-cyano-1,2-butadiene, and 2-cyano-1,3-butadiene. A diastereoselective synthesis was developed to generate (*E*)-1-cyano-1,3-butadiene (10:1 *E*:*Z*) *via* tandem S_N2 and E2′ reactions. The potential energy surfaces of the E2′ reactions leading to (*E*)- and (*Z*)-1-cyano-1,3-butadiene were analyzed by density functional theory calculations and the observed diastereoselectivity was rationalized in the context of the Curtin-Hammett principle. The preparation of pure samples of these reactive compounds enables measurement of their laboratory rotational spectra. Using samples prepared using the methodology described herein, our group assigned minimally perturbed, single-state least-squares fits of over 1000 transitions for each species, yielding sets of spectroscopic constants that are expected to enable accurate prediction of high-intensity transitions at frequencies up to 370 GHz for both 1-cyano-1,3-butadiene isomers. The assigned transitions and spectroscopic constants for these cyanobutadienes have already enabled the identification of two isomers in harsh reaction environments and should be sufficient to enable their identification in astronomical environments by radioastronomy.

Chapter 2 describes our research of a series of C_5H_5N nitrile isomers that contain a carbocyclic backbone. Upon the isolation of the cyanobutadiene isomers, it became clear to our research team that the C_5H_5N nitriles were intrinsically linked to each other through isomerization reactions, and to other smaller nitrile-containing molecules already detected in interstellar environments *via* photolysis reactions. The synthesis and spectroscopic characterization of additional nitrile isomers would not only be valuable for enabling radioastronomical searches, but also in gaining insight regarding the reactivity of such compounds in astrochemical environments *via* laboratory matrix isolation/photolysis and electrical discharge experiments. In chapter 2, we report the synthesis, purification and characterization of three carbocycle-containing C_5H_5N nitrile isomers: 3-cyano-3-methylcyclopropene, (cyanomethylene)cyclopropane, and 1-cyanocyclobutene. Characterization of (cyanomethylene)cyclopropane, and 1-cyanocyclobutene *via* rotational spectroscopy is discussed along with the study of a related small nitrile, methacrylonitrile. Additional carbocycle-containing C_5H_5N nitrile isomers are discussed to provide context and to build a foundation for future synthetic and spectroscopic endeavors within the McMahon/Woods group.

Chapter 3 presents our research regarding a series of four isomeric (C_5H_5N) open-chain nitriles that contain a concurrent alkynyl moiety: 4-cyano-1-butyne, 2-methyl-3-butynenitrile, 2-pentynenitrile (1-cyano-1-butyne, ethyl cyanoacetylene), and 3-pentynenitrile (methylpropargyl cyanide). Methods and techniques used for the synthesis, purification and characterization of each isomer are provided to serve as a guide for producing samples that are critical for the detailed spectroscopic characterization of these astrochemically relevant species, and to build the foundation for future synthetic and spectroscopic investigations within our group.

Chapter 4 covers methods and research regarding the deuterium-tagging of five heterocyclic organic compounds: thiophene, 1,2,4-triazole, 1,2,3-triazole, isoxazole, and pyridine. Aromatic and heterocyclic compounds has been an interest of our group for several years. Although many of the molecular species studied in these investigations are commercially available, the inclusion of rotational spectroscopy data collected from isotopically-tagged samples produced in our lab has enabled the high-precision semi-experimental equilibrium (r_e^{SE}) structural determination of each species. Details concerning the production of deuterium-tagged species and their analysis *via* rotational spectroscopy are discussed in detail.

Chapter 5 describes some of the research I pursued while working in the Stahl group from 2014 to 2015. This research focused on the development of a technique for the mediated electrochemical oxidation of methyl arenes to the corresponding benzonitriles *via* activation of relatively weak benzylic C-H bonds. Overall, the process was divided into two distinct electrochemically-driven steps: mediated anodic benzylic C-H activation/iodination of methyl arenes, and subsequent amination/anodic oxidation of the benzyl iodide to yield the respective benzonitrile. Project goals, method development, technical considerations regarding mediated electrochemical oxidations are discussed in detail.

Table of Contents

Acknowledgements i

Abstract iii

Table of Contents viii

List of Figures xiii

List of Schemes xvi

List of Tables xix

Chapter 1: Synthesis of Cyanobutadiene (C_5H_5N) Isomers – Molecules of Astrochemical Relevance. 1

Introduction 2

Background 9

Results and Discussion 16

1-Cyano-1,3-butadiene 16

(E)-1-Cyano-1,3-butadiene 20

(Z)-1-Cyano-1,3-butadiene 22

4-Cyano-1,2-butadiene 28

2-Cyano-1,3-butadiene 30

Conclusions 30

Experimental Section 31

References 43

Supporting Information 54

Chapter 2: Synthesis and Characterization of C_5H_5N Carbocycle-Containing Carbonitriles 148

Introduction 149

Background 154

3-Cyano-3-methylcyclopropene 154

(Cyanomethylene)cyclopropane 155

1-Cyanomethylcyclopropene and 3-Cyanomethylcyclopropene 157

2-Methylenecyclopropanecarbonitrile 158

3-Cyano-1-methylcyclopropene and 1-Cyano-3-methylcyclopropene 160

1-Cyano-2-methylcyclopropene 161

1-Cyanocyclobutene 161

1-Cyanobicyclo[1.1.0]butane 164

Results and Discussion 164

Methacrylonitrile 164

3-Cyano-3-Methylcyclobutene 167

(Cyanomethylene)Cyclopropane 167

1-Cyanocyclobutene 169

Conclusions 171

Experimental Section 172

Notes and References 183

Supporting Information 189

Chapter 3: C_5H_5N Alkynyl Nitrile Isomers. 208

Introduction 209

Background 212

Results and Discussion 217

Conclusions 221

Notes and References 223

Supporting Information 229

Chapter 4: Synthesis of Isotopically – Labeled Heterocyclic Molecules for Detailed Equilibrium Structure Determinations "Heavy Heterocycles" 245

Introduction 246

Background. 248

Thiophene 248

1,2,4-Triazole. 251

1*H*-1,2,3-Triazole 253

Isoxazole 255

Pyridine 256

Results and Discussion 258

Thiophene 258

1*H*-1,2,4-Triazole 261

1*H*-1,2,3-Triazole 262

Isoxazole 266

Pyridine 269

Conclusions 269

Experimental Section 270

Notes and References 281

Supporting Information 297

Chapter 5: Mediated Electrocatalytic Ammoxidation of Methyl Arenes 320

Introduction 321

Part 1: Electrocatalytic Benzylic Iodination of Methyl Arenes Using *N*-Hydroxypthalimide (NHPI). 326

Background 326

Results and Discussion 335

Part 2: Iodine-Mediated Electrochemical Oxidation of Benzyl Iodides to Benzonitriles 343

Background 343

Results and Discussion 345

Apparatus Design 352

Conclusions 355

Experimental Section 355

References 359

Supporting Information 362

Appendix A: Synthesis and Characterization of Cyanobutadiene Isomers – Molecules of Astrochemical Significance. *J. Org. Chem.* **2020**, *85* (9), 5787-5798. 366

Appendix B: Synthesis, Purification and Rotational Spectroscopy of (Cyanomethylene)Cyclopropane–An Isomer of Pyridine. *J. Phys. Chem. A* **2021,** *125* (25), 5601-5614. 379

Appendix C: Rotational Spectra of Three Cyanobutadiene Isomers (C_5H_5N) of Relevance to Astrochemistry and Other Harsh Reaction Environments. *J. Am. Chem. Soc.* **2021,** *143* (25), 9551-9564. 394

Appendix D: Precise Equilibrium Structure Determination of Thiophene (*c*-C_4H_4S) by Rotational Spectroscopy–Structure of a Five-Membered Heterocycle Containing a Third-Row Atom. *J. Chem. Phys.* **2021,** *154* (24), 244310. 409

Appendix E: The 130–360 GHz Rotational Spectrum of *syn*-2-Cyano-1,3-Butadiene (C_5H_5N) – A Molecule of Astrochemical Relevance. *Mol. Phys.* **2021,** *119* (21-22), e1964629. 427

Appendix F: Synthesis, Purification, and Rotational Spectroscopy of 1-Cyanocyclobutene (C_5H_5N). *J. Phys. Chem. A* **2022,** *126* (12), 1980-1993. 442

Appendix G: Rotational Spectrum of *anti*- and *gauche*-4-Cyano-1-Butyne (C_5H_5N) – An Open-Chain Isomer of Pyridine. *J. Mol. Spectrosc.* **2022,** *385*, 111604. 457

Appendix H: The 130–360 GHz Rotational Spectrum of Isocyanocyclobutane (C_4H_7NC) and Cyanocyclobutane (C_4H_7CN). *J. Mol. Spectrosc.* **2022**, *388*, 111684 467

Appendix I: Precise Equilibrium Structures of 1*H*- and 2*H*-1,2,3-Triazoles ($C_2H_3N_3$) by Millimeter-Wave Spectroscopy. *J. Chem. Phys.* **2022,** *157*, 084305 478

List of Figures

Chapter 1

Figure 1.1. Cyanobutadiene isomers: (*E*)-1-Cyano-1,3-butadiene (***E*-1**), (*Z*)-1-cyano-1,3-butadiene (***Z*-1**), 2-cyano-1,3-butadiene (**2**), 4-cyano-1,2-butadiene (**3**), 2-methylcyanoallene (**4**), and 4-methylcyanoallene (**5**).

Figure 1.2. (a) Discharge of benzene and nitrogen produces *E*-1-cyano-1,3-butadiene (***E*-1**) and *Z*-1-cyano-1,3-butadiene (***Z*-1**). (b) Pyrolysis of 1-cyano-2-butene produces *Z*-1-cyano-1,3-butadiene (***Z*-1**).

Figure 1.3. Electrical discharge experiment reported by Sagan *et al.* yielding 1-cyano-1,3-butadiene (**1**) and 2-cyano-1,3-butadiene (**2**). Reaction conditions and reagent gases designed to simulate conditions observed in Titan's atmosphere.

Figure 1.4. Gas-phase photolysis experiments yielding 2-cyano-1,3-butadiene (**2**) or 1-cyanocyclobutene from cyanoacetylene and ethylene.

Figure 1.5. Rearrangement regiochemistry of 1,2-butadienyl compounds.

Figure 1.6. Computed reaction coordinate diagram for E2′ reaction of (*Z*)-1-bromo-4-cyano-2-butene (***Z*-11**) with cyanide in water. Gibbs free energies at B3LYP/cc-pVTZ with polarized-continuum model for solvent (H_2O) at 273 K (0 °C). Solid line: lower energy transition state. Dashed line: higher energy transition state.

Figure 1.7. Computed reaction coordinate diagram for E2′ reaction of (*E*)-1-bromo-4-cyano-2-butene (***E*-11**) with cyanide in water. Gibbs free energies at B3LYP/cc-pVTZ with polarized-continuum model for solvent (H_2O) at 323 K (50 °C). Solid line: lower energy transition state. Dashed line: higher energy transition state.

Figure S1.1. GC-MS analysis of *E* and *Z* 1-cyano-1,3-butadiene (***E*-1** and ***Z*-1**) crude reaction mixture in acetonitrile. Top: GC trace with *Z* (red arrow) and *E* (blue arrow) cyanobutadiene. Middle: Mass spectra of the indicated GC peaks with solvent subtraction. Bottom: NIST library spectrum for cyanobutadiene ***E*-1**.

Figure S1.2. HRMS (ASAP-Q-IT) spectrum of 1-cyano-1,3-butadiene **1** (above). MS/MS below.

Figure S1.3. Vinyl region of 1-cyano-1,3-butadiene (**1**) ^{1}H NMR spectrum (400 MHz) in C_6D_6 (top), CD_3CN (middle), and $CDCl_3$ (bottom).

Figure S1.4. Assignment of protons in the ^{1}H-NMR spectrum (400 MHz) of 1-cyano-1,3-butadiene (***E*-1**) and (***Z*-1**) in C_6D_6.

Figure S1.5. Relaxed 2-D conformational scan of (*E*)-1-bromo-4-cyano-2-butene (***E*-11**) using B3LYP/cc-pVTZ electronic energies with PCM solvent correction for water. Relative energies in kcal/mol.

Figure S1.6. Relaxed 2-D conformational scan of (*Z*)-1-bromo-4-cyano-2-butene (***Z*-11**) using B3LYP/cc-pVTZ electronic energies with PCM solvent correction for water. Relative energies in kcal/mol.

Figure S1.7. Free energies (kcal/mol) for the isomerization of 4-cyano-1,2-butadiene (**2**) to 1-cyano-1,3-butadiene (**1**) at B3LYP/cc-pVTZ with PCM (H_2O) at 298 K.

Chapter 2

Figure 2.1. C_5H_5N Nitrile Isomers Containing a Three-Membered Carbocycle: 3-Cyano-3-methylcyclopropene (**1**), (Cyanomethylene)cyclopropane (**2**), 1-Cyanomethylcyclopropene (**3**), 3-Cyanomethylcyclopropene (**4**), 2-Methylenecyclopropanecarbonitrile (**5**), 3-Cyano-1-methylcyclopropene (**6**), 1-Cyano-3-methylcyclopropene (**7**) and 1-Cyano-2-methylcyclopropene (**8**).

Figure 2.2. C_5H_5N Nitrile Isomers Containing a Four-Membered Ring: 1-Cyanocyclobutene (**9**), 1-Cyanobicyclo[1.1.0]butane (**10**), 3-Cyanocyclobutene (**11**), and 2-Cyanobicyclo[1.1.0]butane (**12**)

Figure 2.3. Gas-phase Synthesis of 1-Cyanocyclobutene (**9**) *via* Photochemical [2+2] Cycloaddition of Cyanoacetylene and Ethylene.

Figure 2.4. Structurally Similar Four-membered Ring Species: Cyanocyclobutane (**14**), 1-Cyanocyclobutene (**9**), Cyano-1,3-cyclobutadiene (**15**), β–Propiolactone (**16**), and Diketene (**17**).

Chapter 3

Figure 3.1. C_5H_5N Nitrile Isomers Containing an Alkynyl Moiety: 4-Cyano-1-butyne (**1**), 2-Methyl-3-butynenitrile (**2**), 2-Pentynenitrile (**3**), and 3-Pentynenitrile (**4**).

Figure 3.2. Rotational spectrum of 4-cyano-1-butyne (**1**) from 188.0 GHz to 192.5 GHz (bottom) and stick spectrum of the ground vibrational states (top). Dashed green lines mark transitions of *gauche*-4-cyano-1-butyne, and solid-colored lines mark transitions of anti-4-cyano-1-butyne. Solid lines highlighted in magenta belong to the $J'' + 1 = 66$ series of *anti*-4-cyano-1-butyne, and the corresponding $K_a'' + 1$ values are marked above. Many transitions belonging to other vibrational satellites are also visible in the experimental spectrum.

Chapter 4

Figure 4.1. Aromatic heterocycles described in this chapter for isotopologue synthesis and detailed structural determination: thiophene, 1,2,4-triazole, 1,2,3-triazole, isoxazole, and pyridine.

Figure 4.2. Tautomers of 1,2,3- and 1,2,4-Triazole with Conventional Numbering of Ring Atoms and Relative Energies Calculated at B3LYP/6311G**.

Figure 4.3. Deuteration of Thiophene *via* Deuteration/Deprotonation at the C2 Site.

Figure 4.4. 3*H*-thiolium (a) and 2*H*-Thiolium (b) with their relative energies (B3LYP/6-311G+(2d,p)+ZPVE), the Natural Population Analysis (NPA) charges as spheres whose size correspond to the magnitude of the local charge (blue for positive and red for negative), and relevant resonance structures from the Natural Resonance Theory analysis.

Chapter 5

Figure 5.1. Nitrile-Containing Compounds Produced in the Materials (a) and Agrochemical (b) Industries.

Figure 5.2. Modern Pharmaceuticals Containing the Nitrile Pharmacophore

Figure 5.3. Structures of *N*-Hydroxypthalimide (NHPI) (a) and Phthalimido-*N*-Oxyl (PINO) (b).

Figure 5.4. Polar Effect Observed in the Stabilized Transition State of C-H Abstraction Events Involving PINO

Figure 5.5. Cyclic voltammograms of 0.01 M NHPI in acetonitrile (with 0.1 M $LiClO_4$ supporting electrolyte) at different concentrations of an added organic base, 2,6-lutidine (50 mV/s scan rate).

Figure 5.6. Potential Reduction of Bicarbonate (a) or Iodine (b) Occurring at the Cathodic Surface During Bulk Electrolyses

Figure 5.7. Trace of the currents observed in the electrolysis presented in Table 5.6. Points where additions were made are numbered in the order shown in Table 5.6.

Figure 5.8. Cyclic Voltammograms Collected of the Benzyl Iodide/Ammonia Reaction Mixture after every Five Degassing Cycles for Ammonia Removal (scan rate: 50 mV/s).

Figure 5.9. Divided and Undivided Electrochemical Cells Designed for Electroorganic Reactions. Sealable Design allows for Frequently used Practices in Organic Synthesis (Application of Vacuum, Controlled Atmospheres, etc.).

Figure 5.10. Low-Profile Short-Resistant Platinum Counter Electrode Design.

List of Schemes

Chapter 1

Scheme 1.1. Previous Syntheses of 1-Cyano-1,3-butadiene (**1**).

Scheme 1.2. Previous Syntheses of 2-Cyano-1,3-butadiene (**2**).

Scheme 1.3. Previous Syntheses of 2-Methylcyanoallene (**4**).

Scheme 1.4. Propargylic Substitution and Rearrangement Mechanisms.

Scheme 1.5. Published Synthetic Methods for 4-Methylcyanoallene and Related Congeners.

Scheme 1.6. Initial Synthetic Route to 1-Cyano-1,3-butadiene (**1**) from 2-Butyne-1,4-diol (**6**).

Scheme 1.7. Improved Synthetic Route to 1-Cyano-1,3-butadiene (mixture ***E*-1** and ***Z*-1**) from Propargyl Alcohol (**13**).

Scheme 1.8. Strategy for Diastereoselective Synthesis of (*E*)-1-Cyano-1,3-butadiene (***E*-1**).

Scheme 1.9. Diastereoselective Synthesis of (*E*)-1-Cyano-1,3-butadiene (***E*-1**) from (*Z*)-1,2-Dibromo-2-butene (***Z*-10**).

Scheme 1.10. Modified Reaction Conditions for Efficient Synthesis and Purification of (*E*)-1-Cyano-1,3-butadiene (***E*-1**).

Scheme 1.11. Modified Reaction Conditions for Semi-Selective Preparation of 1-Cyano-1,3-butadiene (***Z*-1**) from (*E*)-1,4-Dibromo-2-Butene (***E*-10**).

Scheme 1.12. Reaction Conditions for the Preparation of 4-Cyano-1,2-Butadiene (**3**).

Scheme 1.13. Preparation of 2-Cyano-1,3-butadiene (**2**).

Chapter 2

Scheme 2.1. Previous Syntheses of 3-Cyano-3-methylcyclopropene (**1**).

Scheme 2.2. Previous Syntheses of (Cyanomethylene)cyclopropane (**2**)

Scheme 2.3. Proposed Synthesis of 1-Cyanomethylcyclopropene (**3**) and 3-Cyanomethylcyclopropene (**4**).

Scheme 2.4. Proposed Synthesis of 2-Methylenecyclopropanecarbonitrile (**5**).

Scheme 2.5. Previous Synthesis of 3-Cyano-1-methylcyclopropene (**6**) by Tsuchiya *et. al.*

Scheme 2.6. Proposed Synthesis of 3-Cyano-1-methylcyclopropene (**6**) and 1-Cyano-3-methylcyclopropene (**7**) from (*E*)-Crotonitrile (**30**).

Scheme 2.7. Previous Syntheses of 1-Cyanocyclobutene (**9**)

Scheme 2.8. Previous Synthesis of 1-Cyanobicyclo[1.1.0]butane (**10**)

Scheme 2.9. Methods for Producing Methacrylonitrile (**35**) (a), and Deuterium-enriched Methacrylonitrile (**35-*d***) (b).

Scheme 2.10. Preparation of 3-Cyano-3-methylcyclopropene (**1**).

Scheme 2.11. Modified Synthesis of (Cyanomethylene)cyclopropane (**2**).

Scheme 2.12. Synthesis of 1,2-Dicyanocyclobutane (**34**) and 1-Cyanocyclobutene (**9**).

Chapter 3

Scheme 3.1. Previous Syntheses of 4-Cyano-1-butyne (**1**)

Scheme 3.2. Previous Syntheses of 2-Methyl-3-butynenitrile (**2**)

Scheme 3.3. Previous Syntheses of 2-Pentynenitrile (**3**)

Scheme 3.4. Previous Syntheses of 3-Pentynenitrile (**4**)

Scheme 3.5. Propargylic Substitution and Rearrangement Mechanisms

Scheme S3.1. Reaction Pathway for the Direct Cyanation of α-Aryl, and 2º-Propargyl Alcohols proposed by Rajagopal *et al.*

Chapter 4

Scheme 4.1. Synthesis of Deuterium-Containing Isotopologues of Thiophene.

Scheme 4.2. Recrystallizations of 1,2,4-Triazole in D_2O/H_2O for Accessing all Deuterated Isotopologue Combinations.

Scheme 4.3. Deuterium incorporation in 1*H*- and 2*H*-1,2,3-triazoles: (a) *N*-deuteriation by strong base, (b) C-deuteriation by weak base, (c) three-step sequence to achieve a high level of deuterium content at C-4 and C-5.

Scheme 4.4. Synthesis of Isoxazole from 1,1,3,3-Tetraethoxypropane and Hydroxylamine Reported by Wakefield *et. al.*

Scheme 4.5. Proposed Methods for Accessing Each Deuterated Isotopologue of Isoxazole via Modification of 1,1,3,3-Tetraethoxypropane.

Scheme 4.6. Preparation of 2- and 3-deuteropyridine *via* lithiation/D_2O quench of 2- and 3-bromopyridines.

Chapter 5

Scheme 5.1. Direct (a) and Indirect (b) Anodic Oxidation Configurations.

Scheme 5.2. Proposed Two-Step Indirect Electrochemical Ammoxidation Process for the Conversion of Methyl Arenes to the Corresponding Aryl Nitriles.

Scheme 5.3. NHPI/NOx Catalyzed Aerobic Benzylic Halogenation/Acetoxylation Methodology Described by Minisci *et al.*

Scheme 5.4. Proposed Method of Accessing Benzyl Iodides *via* NHPI/PINO Mediated Electrocatalytic Benzylic C-H Activation.

Scheme 5.5. Preliminary Bulk Electrolysis for Benzylic Iodination Conditions Derived from Minisci's Acetoxylation Methodology.

Scheme 5.6. Degradation Routes of 2,6-Lutidine (1) in the Presence of I_2 or PINO Through the Formation of Benzylic Radicals (2) or Unstable Complexes (3).

Scheme 5.7. Unimolecular and Bimolecular Degradation Routes of PINO

Scheme 5.8. Methodologies Reported by Togo *et al.* for Conversion of Multiple Benzylic Groups to Benzonitriles Using the NH_3/I_2 Oxidation System.

Scheme 5.9. Electrochemical Method Reported by Qu *et al.* for the Anodic Oxidation of Aldehydes *via in situ* Generation of I_2 from the Supporting Electrolyte.

Scheme 5.10. Formation of tris(4-Methylbenzyl)amine as the Only Product of Reacting 4-Methylbenzyliodide with Aqueous Ammonia.

Scheme 5.11. Formation and Cleavage of Aldehyde/Bisulfite Adducts.

List of Tables

Chapter 1

Table S1.1. ^{1}H NMR signal assignments of *E*-1 and *Z*-1 in $CDCl_3$ previously reported and found in this work. Estimated coupling constants affected by second order effects. For more accurate coupling constants, see data from spectrum in C_6D_6 (Figure S1.4).

Table S1.2. Summary of Absolute Electronic and Free Energies Determined by B3LYP/cc-pVTZ with PCM(H_2O).

Table S1.3. Summary of Relative Electronic and Free Energies Determined by B3LYP/cc-pVTZ with PCM(H_2O).

Chapter 5

Table 5.1. Evaluation of Bulk Electrolysis Solvent/Base Systems for Benzylic Iodinations.

Table 5.2. Optimization of the supporting electrolyte

Table 5.3. Evaluating Effect of Toluene : Iodine Ratio on Charge Efficiency and Yield.

Table 5.4. Substrate Scope and Yields of Electrochemical Iodination Using a Fourfold Excess of Methyl Arene Substrates.

Table 5.5. Optimization of Catholytic Sacrificial Oxidants for Benzylic Iodination Bulk Electrolyses

Table 5.6. Charge Course Evaluation of the Anodic Iodination on 4-*tert*-Butyltoluene with Incremental Additions of I_2, NHPI, and $KHCO_3$.

Table 5.7. Evaluation of the Voltage Applied During Bulk Electrolysis of 4-Methylbenzyl Iodide to *p*-tolunitrile

Table 5.8. Substrate Scope of the Electrochemical Conversion of Benzyl Iodides to Benzonitriles.

Chapter 1: Synthesis of Cyanobutadiene (C_5H_5N) Isomers – Molecules of Astrochemical Relevance.

Some content contained in this section has been submitted and accepted for publication. Contributions to the content in this section have been made by Stephanie N. Knezz, Andrew N. Owen, Rodrigo A. Sanchez, Grace E Hyland, Daniel J. Lee, Aatmik R. Patel and Brian J. Esselman.

Introduction

Over 250 different molecules have been detected in the interstellar medium (ISM) or circumstellar shells[1-2] and are theorized to be involved in complex reaction networks.[3-7] The vast majority of these detections have been made *via* radioastronomy, through observation and assignment of rotational spectra. Due to their large dipole moments,[8-10] which confer intense rotational transitions, and composition of relatively abundant elements, nitriles (R–CN) represent realistic targets for detection by radioastronomy. Approximately 10% of the known interstellar molecules are nitriles, including recently detected benzonitrile,[11] hydroxyacetonitrile,[12] and silyl cyanide.[13] The list of astronomically detected nitriles comprise a variety of chain lengths[14-18] from hydrogen cyanide (HCN)[17] to cyanodecapentayne ($HC_{11}N$)[19]. Additionally, interstellar nitriles are observed in various degrees of hydrogenation, from highly unsaturated cyanopolyynes, $RC_{2n+1}N$ (R = H, n = 1-4; R = CH_3, n = 1,2),[14-18, 20-21] to vinyl and phenyl derivatives (vinyl cyanide (acrylonitrile),[22] cyanoallene,[23] benzonitrile[11]), to compounds with fully saturated backbones (acetonitrile,[24] hydroxyacetonitrile,[12] propyl cyanide,[25] and isopropyl cyanide[26]). Recent detections of benzonitrile, the cyano-1,3-cyclopentadienes, and the cyanonaphthalenes represent a dramatic breakthrough in the field,[11, 27-28] revealing a glimpse of simple aromatic compounds in astronomical environments.[29] The McMahon/Woods group has been keenly interested in both structural and chemical relationships between open-chain organic nitriles and their cyclic counterparts for some time.[30] In this thesis chapter, we report the development of methods and techniques used for the synthesis, purification and characterization of four cyanobutadiene isomers: (*E*)-1-cyano-1,3-butadiene (***E*-1**), (*Z*)-1-cyano-1,3-butadiene (***Z*-1**), 2-cyano-1,3-butadiene (**2**), and 4-cyano-1,2-butadiene (**3**) (Figure 1.1). Additional cyanobutadiene isomers are

discussed to provide context and to build the foundation for future synthetic and spectroscopic investigations within our group.

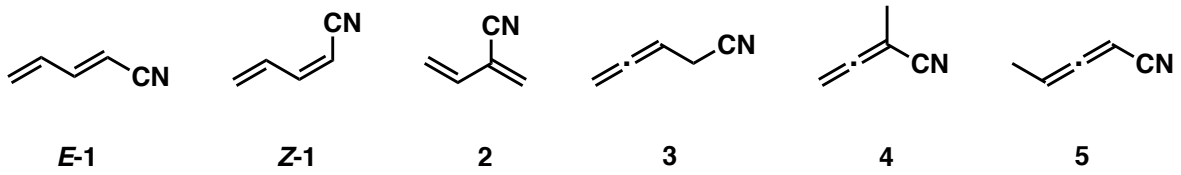


Figure 1.1. Cyanobutadiene isomers: (*E*)-1-Cyano-1,3-butadiene (***E*-1**), (*Z*)-1-cyano-1,3-butadiene (***Z*-1**), 2-cyano-1,3-butadiene (**2**), 4-cyano-1,2-butadiene (**3**), 2-methylcyanoallene (**4**), and 4-methylcyanoallene (**5**).

The nitrile-containing species detected in the cosmos exhibit a diverse array of structural arrangements and features. Of particular interest to the species investigated in this thesis chapter are vinyl cyanide (C_3H_3N; acrylonitrile),[22] cyanoallene (C_4H_3N),[23] cyanodiacetylene (HC_5N),[14] and propadienylidene (*l*-H_2C_3) due to the shared structural motifs with the cyanobutadiene (C_5H_5N) isomers (Figure 1.1). The cyanobutadienes are an important family of six isomeric (C_5H_5N), open-chain nitrile species that are especially interesting as candidate astromolecules. The cyanobutadiene isomers are further classified into two groups based on the structure of the carbon chain π bonds: 1,3- butadienes and 1,2-butadienes (allenes). Three species possess a 1,3-butadiene backbone ((*E*)-1-cyano-1,3-butadiene (***E*-1**), (*Z*)-1-cyano-1,3-butadiene (***Z*-1**), 2-cyano-1,3-butadiene (**2**)) and three species possess a 1,2-butadiene (allene) backbone (4-cyano-1,2-butadiene (**3**), 2-methylcyanoallene (**4**), and 4-methylcyanoallene (**5**)). The structural similarity, and the fact that both smaller and larger carbon-chain nitriles are known in extraterrestrial environments, suggest that the cyanobutadiene isomers represent highly plausible targets for detection in the ISM. Additionally, these nitriles are acyclic isomers of the aromatic heterocycle, pyridine, which has yet to be identified in the ISM.[31] Detection of any of these nitriles would provide additional motivation to detect pyridine and other aromatic heterocycles. The existence of organic nitriles in the interstellar medium is relevant not only to our understanding of the chemical processes in the

ISM, but also to our understanding of the origin of amino acids, nucleotides, and other pre-biotic compounds that are critical for life on Earth.

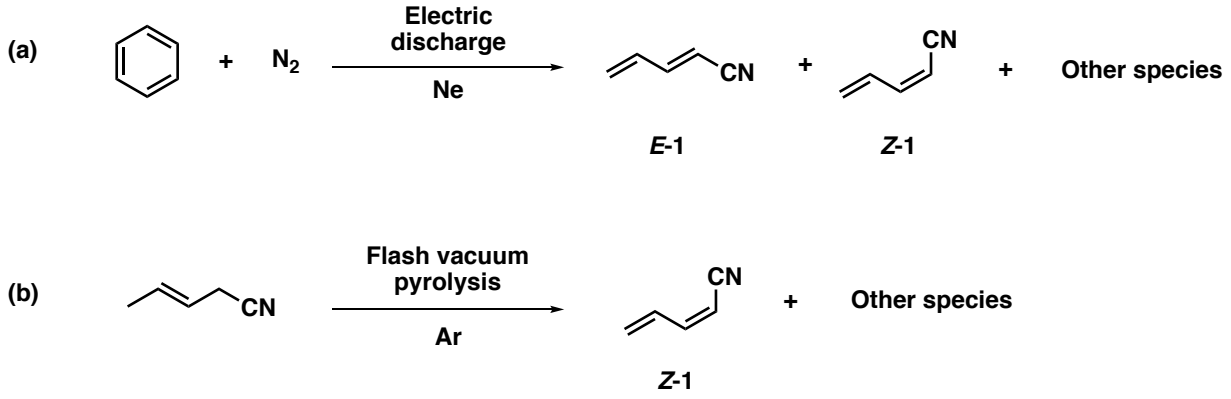


Figure 1.2. (a) Discharge of benzene and nitrogen produces *E*-1-cyano-1,3-butadiene (***E*-1**) and *Z*-1-cyano-1,3-butadiene (***Z*-1**).[32] (b) Pyrolysis of 1-cyano-2-butene produces *Z*-1-cyano-1,3-butadiene (***Z*-1**).[33]

Recent studies examined potential routes leading to the formation of the cyanobutadiene isomers under harsh reaction conditions or conditions modeled after cosmic environments. McCarthy *et al.* analyzed the products generated by electrical discharge of benzene and molecular nitrogen and identified both *E*- and *Z*-1-cyano-1,3-butadiene isomers (**1**) in the product spectra (Figure 1.2a).[32] Zwier and coworkers investigated the gas-phase pyrolysis of *trans*-3-pentenenitrile, which results in dehydrogenation to afford *Z*-1-cyano-1,3-butadiene (***Z*-1**), among many products (Figure 1.2b). Notably, pyridine was not detected, despite being lower in energy than the detected cyanobutadiene isomer.[33] The spectroscopic assignments used for the identification of the cyanobutadiene species in both of these experiments were made on the basis of data reported by our group using samples prepared using the methodology described herein.

Much earlier, Tsukamoto and Lichtin observed *E*- and *Z*-1-cyano-1,3-butadiene (**1**) as products in a reaction between 1,3-butadiene and nitrogen activated *via* microwave discharge.[34] They noted the possibility that this reaction involves the cyano radical as the primary intermediate.

More recent theoretical and experimental studies indicate the reaction between the cyano radical and 1,3-butadiene produces *E*-1-cyano-1,3-butadiene (***E*-1**), despite the open-chain molecule being less thermodynamically favorable than pyridine.[35-36] Although the cyano radical has been known in the ISM for decades,[37] 1,3-butadiene has not been detected. The predominant *s-trans* conformer of 1,3-butadiene does not possess a dipole moment, while the small dipole moment in the higher energy *syn* conformation makes it a difficult astronomical target.[38] Balucani *et al.* suggested that the reaction of the cyano radical with an unsaturated hydrocarbon species is a highly plausible route to formation of the nitriles in the ISM, as well as that the detection of a particular unsaturated hydrocarbon can be used to predict the presence of the corresponding nitrile.[39] Given the small dipole moment of 1,3-butadiene, however, it seems that the detection of the 1-cyano-1,3-butadiene isomers (**1**) could better serve as potential tracers for 1,3-butadiene. A theoretical study by Jamal and Mebel[40] suggested that reaction of the cyano radical with 1,2-butadiene would preferentially form 2-cyano-1,3-butadiene (**2**),[41] 1-cyano-3-propyne (C_4H_3N), or cyanoallene (C_4H_3N), and not 4-cyano-1,2-butadiene (**3**). This does not preclude, however, generation of 4-cyano-1,2-butadiene (**3**) *via* alternative reaction pathways.

The ISM is not the only location where detection of the cyanobutadiene isomers could be informative. Saturn's largest moon, Titan, possesses a nitrogenous atmosphere with complex atmospheric chemistry and photochemistry. The atmospheric chemistry of Titan has been suggested to be relevant to prebiotic Earth.[42] Small neutral nitriles, as well as their anions, have been detected in Titan's atmosphere and are implicated in the formation of tholins,[43-45] the organic polymers responsible for the reddish haze of various bodies in our solar system and suggested as potential prebiotic precursors in the presence of water. Pyrolysis of synthetic tholin analogues produces 1-cyano-1,3-butadiene (**1**).[46-47] Data from the Cassini-Huygens probe also suggests the

presence of benzene,[43-44] and data from the Atacama Large Millimeter Array (ALMA) recently revealed the presence of cyclopropenylidene (C_3H_2).[48] It is likely that other aromatics like pyridine or its isomers could be detected in this environment.

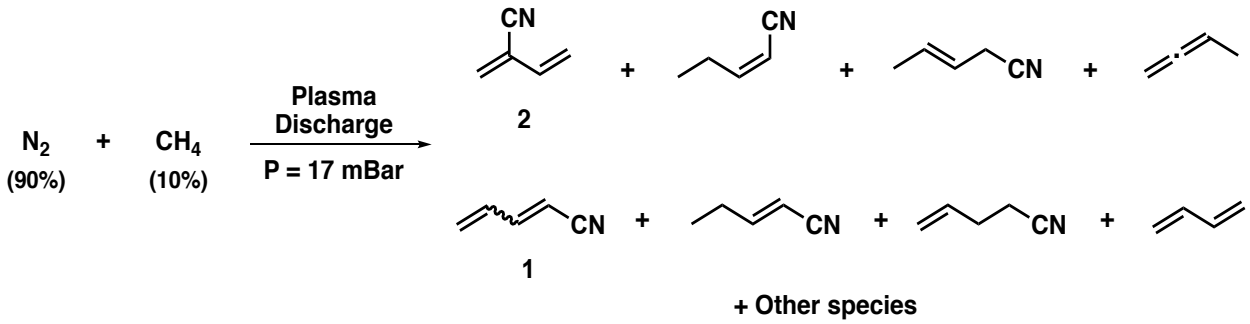


Figure 1.3. Electrical discharge experiment reported by Sagan *et al.* yielding 1-cyano-1,3-butadiene (**1**) and 2-cyano-1,3-butadiene (**2**). Reaction conditions and reagent gases designed to simulate conditions observed in Titan's atmosphere.[49]

Experimental studies aimed at understanding the origin and reactivity of organic species detected in the Titanian atmosphere show the cyanobutadienes are likely products in gaseous photochemical processes and atmospheric plasma reactions. Sagan *et al.* modeled electrical discharge experiments performed on gaseous mixtures of N_2 and CH_4 to simulate the composition and conditions of Titan's atmosphere.[49] Analysis of the resulting product mixture showed the formation of 1-cyano-1,3-butadiene (**1**), 2-cyano-1,3-butadiene (**2**), several 1-cyanobutene isomers, 1,3-butadiene and 1,2-butadiene amongst a myriad of other nitrile-containing small molecules (Figure 1.3). Ferris *et al.* demonstrated the photochemical formation of 2-cyano-1,3-butadiene (**2**) from species already detected (or highly likely present) in the Titanian atmosphere.[50-51] Irradiation of gaseous mixtures consisting of cyanoacetylene and ethylene with 254 nm UV radiation generates 2-cyano-1,3-butadiene (**2**) (Figure 1.4a). 2-Cyano-1,3-butadiene (**2**) is closely related to its cyclic isomer, 1-cyanocyclobutene. In comparison to the reaction in Figure 1.4a, the irradiation of gaseous cyanoacetylene and ethylene with higher energy 185 nm UV radiation yields 1-cyanocyclobutene as the primary product instead of **2** (Figure 1.4b).[50-51] Direct irradiation of **2**

with 254 nm UV radiation yields 1-cyanocyclobutene,[52] which readily undergoes thermolysis to form **2**[53-54] (Figure 1.4b). The relationship between cyanobutadiene species and their cyclic isomers and may indicate the possible presence of multiple C_5H_5N nitrile isomers in an environment when one is detected. The work pertaining to the synthesis and characterization of carbocycle-containing C_5H_5N carbonitriles will be discussed in further detail in the subsequent chapter.

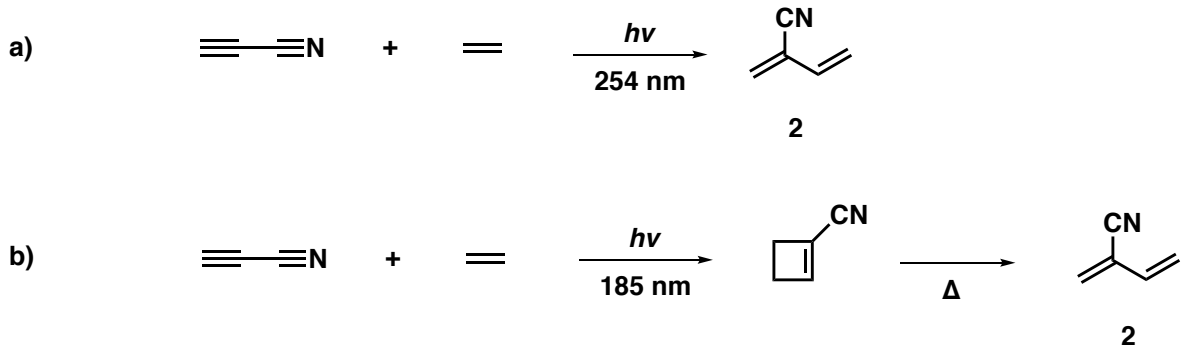


Figure 1.4. Gas-phase photolysis experiments yielding 2-cyano-1,3-butadiene (**2**) or 1-cyanocyclobutene from cyanoacetylene and ethylene. [50-51]

With respect to astrochemistry, electrical discharge, or other harsh reaction environments, the cyanobutadiene isomers (Figure 1.1) are important in that they may be considered proxies for pyridine in such environments. Pyridine is an aromatic molecule of substantial astrochemical interest that has thus far eluded detection in the ISM.[31] The cyanobutadiene isomers are more polar (μ = 3.7-4.7 D), and therefore more readily detectable, than pyridine (μ = 2.2 D). Mechanistically, it is not known whether the cyanobutadiene isomers might represent precursors to pyridine or decomposition products of pyridine, but the detection of any isomer of pyridine (C_5H_5N) would represent a significant observation in astrochemistry.[55-57] Pyridine is nearly 23.2 kcal/mol lower in energy than *E*-1-cyano-1,3-butadiene (***E*-1**), which itself is 0.3 kcal/mol and 16.3 kcal/mol lower in energy than *Z*-1-cyano-1,3-butadiene (***Z*-1**) and 4-cyano-1,2-butadiene (**3**) (B3LYP/ 6-311+G(2d,p)), respectively. Pyridine is a building block of nicotinic acid (Vitamin

B3) and nicotinamide, which are precursors to a key coenzyme used in metabolism, nicotinamide adenine dinucleotide (NAD).[58] A possible route to interstellar formation of nicotinic acid from pyridine has been suggested,[59] and nicotinic acid of interstellar origin has been detected on the Murchison meteorite.[60-61] Identification of extraterrestrial pyridine could assist our understanding of prebiotic chemistry occurring in extreme environments, as well as our understanding of formation of nitrogen-containing polycyclic aromatic hydrocarbons (NPAHs), in which pyridine has been suggested as a precursor.[62]

Despite the sophistication of modern synthetic chemistry, the synthesis, purification, and isolation of the simple organic nitriles shown in Figure 1.1 remains a challenge at the current time. The new procedures reported in this chapter enabled detailed studies of the high-resolution rotational spectroscopy of four cyanobutadiene isomers: (*E*)-1-cyano-1,3-butadiene (***E*-1**), (*Z*)-1-cyano-1,3-butadiene (***Z*-1**), 2-cyano-1,3-butadiene (**2**), and 4-cyano-1,2-butadiene (**3**) (Figure 1.1).[41, 63-64] The rotational spectrum of each compound is very complex; having a pure sample, for which spectral features are not obscured by impurities, is critical to achieve a sophisticated analysis of the complex spectrum. In measuring gas-phase spectra, volatile impurities are especially problematic. The synthetic and purification procedures described herein have been designed to minimize, or eliminate, these troubling contaminants. This work provides the foundation for the ultimate detection of nitriles ***E*-1**, ***Z*-1**, **2**, and **3** in extraterrestrial environments. With their relevance in the atmospheric chemistry of Titan and interstellar chemistry, the improved isolation of these nitriles allows new spectroscopic measurements of broad interest to the chemistry community.

Background

The earliest research pertaining to the synthesis of the cyanobutadiene isomers was accomplished during the heyday of early polymer chemistry. During the groundbreaking work of finding viable methods for producing synthetic rubber-like materials, several isoprene (2-methyl-1,3-butadiene, C_5H_8) derivatives were investigated as monomer units.[65-66] 2-Cyano-1,3-butadiene (**2**, cyanoprene) was originally sought by Wallace H. Carothers and co-workers at DuPont as a component in new synthetic nitrile rubbers. The reactivity of 2-cyano-1,3-butadiene (**2**) as a monomer was anticipated to polymerize several orders of magnitude faster than the structurally similar isoprene monomers and was considered a highly desirable target.

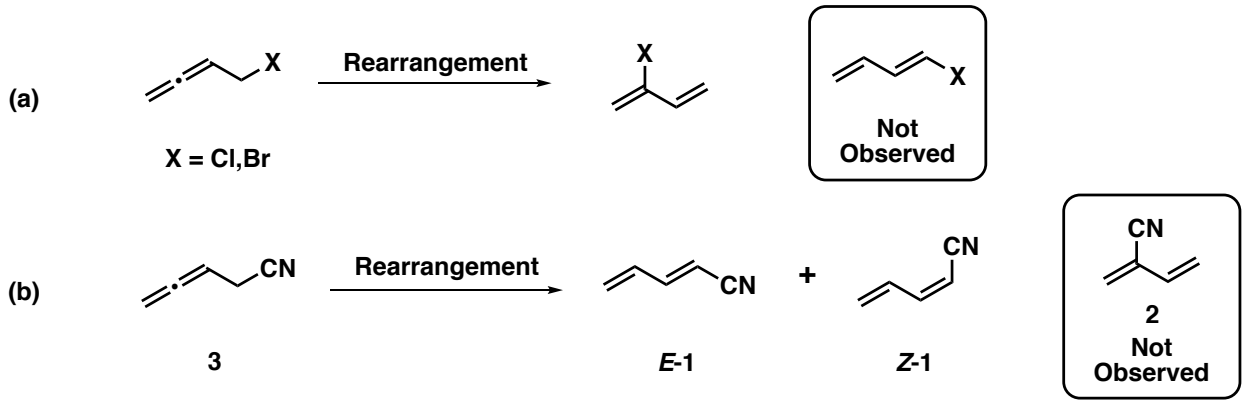


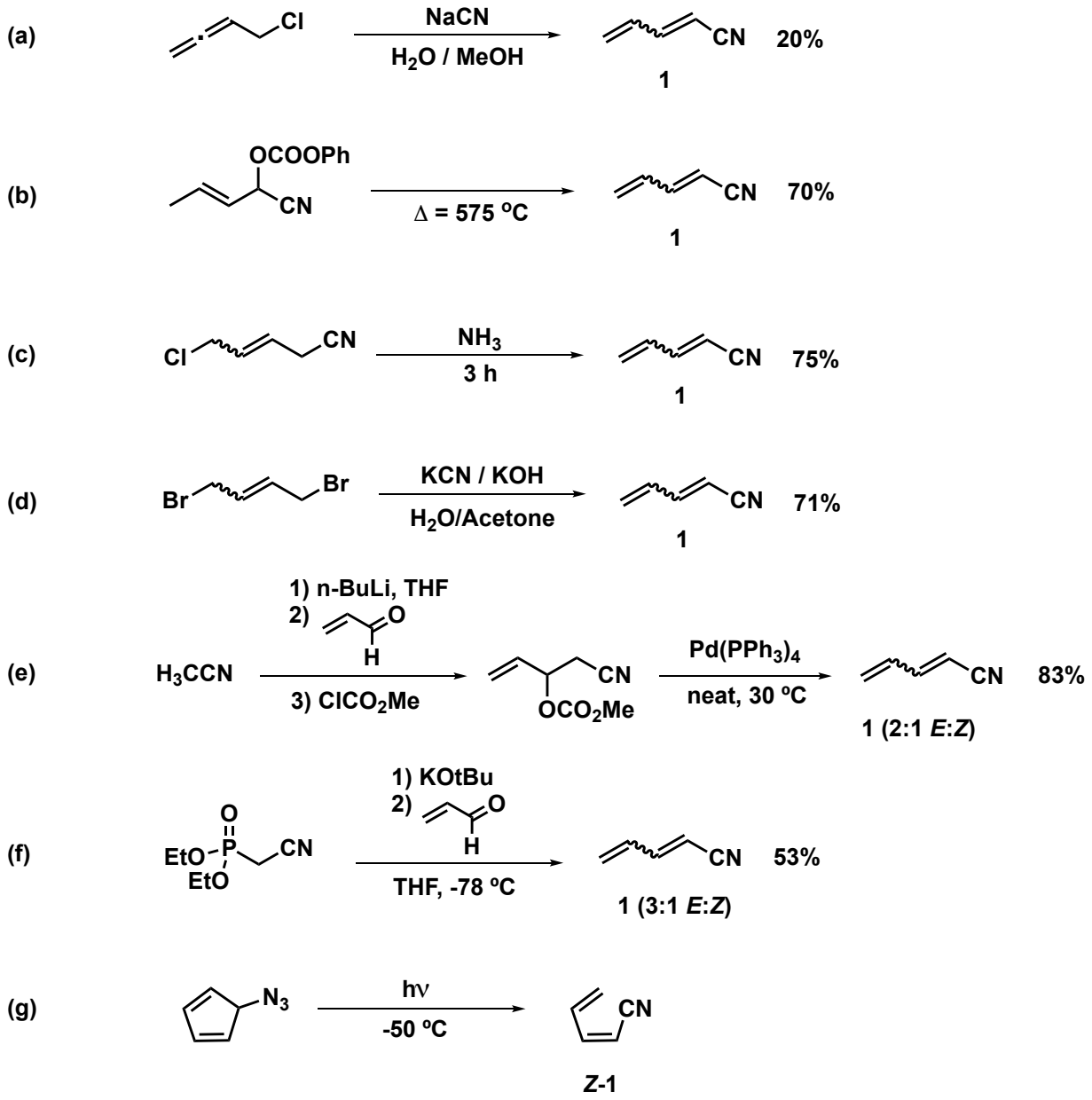
Figure 1.5. Rearrangement regiochemistry of 1,2-butadienyl compounds.

When designing a synthetic approach for producing 2-cyano-1,3-butadiene (**2**), Carothers observed that several 1,2-butadienyl (allenyl) derivatives underwent rearrangement to yield the 1,3-butadienyl structural isomer.[67] This reactivity was well documented for the 4-halo-1,2-butadiene compounds, and served as the earliest routes accessing haloprene monomers (Figure 1.5a). Carothers initially hypothesized that 2-cyano-1,3-butadiene (**2**) could be formed through a similar rearrangement from transient 4-cyano-1,3-butadiene (**3**) generated from 4-chloro-2-butyn-1-ol (**9**) *via* S_N2 metathesis (Scheme 1.1a). However, it was discovered that unlike the 4-halo-1,2-

butadienyl compounds, the rearrangement of 4-cyano-1,2-butadiene (**3**) exclusively yielded the 1-cyano-1,3-butadiene (**1**; mixture of *E* and *Z* isomers) instead of the anticipated 2-cyano-1,3-butadiene (**2**) (Figure 1.5b). Although obtaining a different cyanobutadiene isomer than initially planned, Carothers and co-workers succeeded in isolating 1-cyano-1,3-butadiene (**1**) (2,4-pentadienenitrile) as the first synthetic cyanobutadiene isomers (Scheme 1.1a).[67-70] Later, Snyder *et al.* prepared **1** by flash vacuum pyrolysis (Scheme 1.1b), separated the *E* and *Z* isomers by careful fractional distillation,[71] and investigated the reactivity of **1** in trapping, dimerization, and polymerization reactions.[72-74] Snyder's early investigations contain a wealth of useful data describing the synthesis and physical properties of ***E*-1** and ***Z*-1**, but the experimental procedures for synthesis, purification, and isolation were designed for a relatively large scale, and those reports predate modern methods for spectroscopic characterization.[75-84]

An efficient, selective synthesis of (*E*)-1-cyano-1,3-butadiene (***E*-1**) has not been described, although modern synthetic procedures for producing a mixture of diastereomers (***E*-1** and ***Z*-1**) have been reported (Scheme 1.1e/f/g). The preparation reported by Braun *et al.*[85] (Scheme 1.1e) involves the reaction of acetonitrile anion with acrolein and subsequent protection/elimination steps to yield diastereomers ***E*-1** and ***Z*-1** in a 2:1 ratio. The procedure described by Clary and Back [86] (Scheme 1.1f) combines a diethylcyanomethyl-phosphonate ylide with acrolein in a Horner-Wadsworth-Emmons olefination to afford diastereomers ***E*-1** and ***Z*-1** in a 3:1 ratio. Banert [87] reported the selective preparation of ***Z*-1** by thermolysis or photolysis of 1-azido-cyclopentadiene (Scheme 1.1g). These various procedures notwithstanding, details concerning both purification and characterization of ***E*-1** and ***Z*-1** remain incomplete because of the sensitivity and high reactivity of these compounds under a variety of conditions.

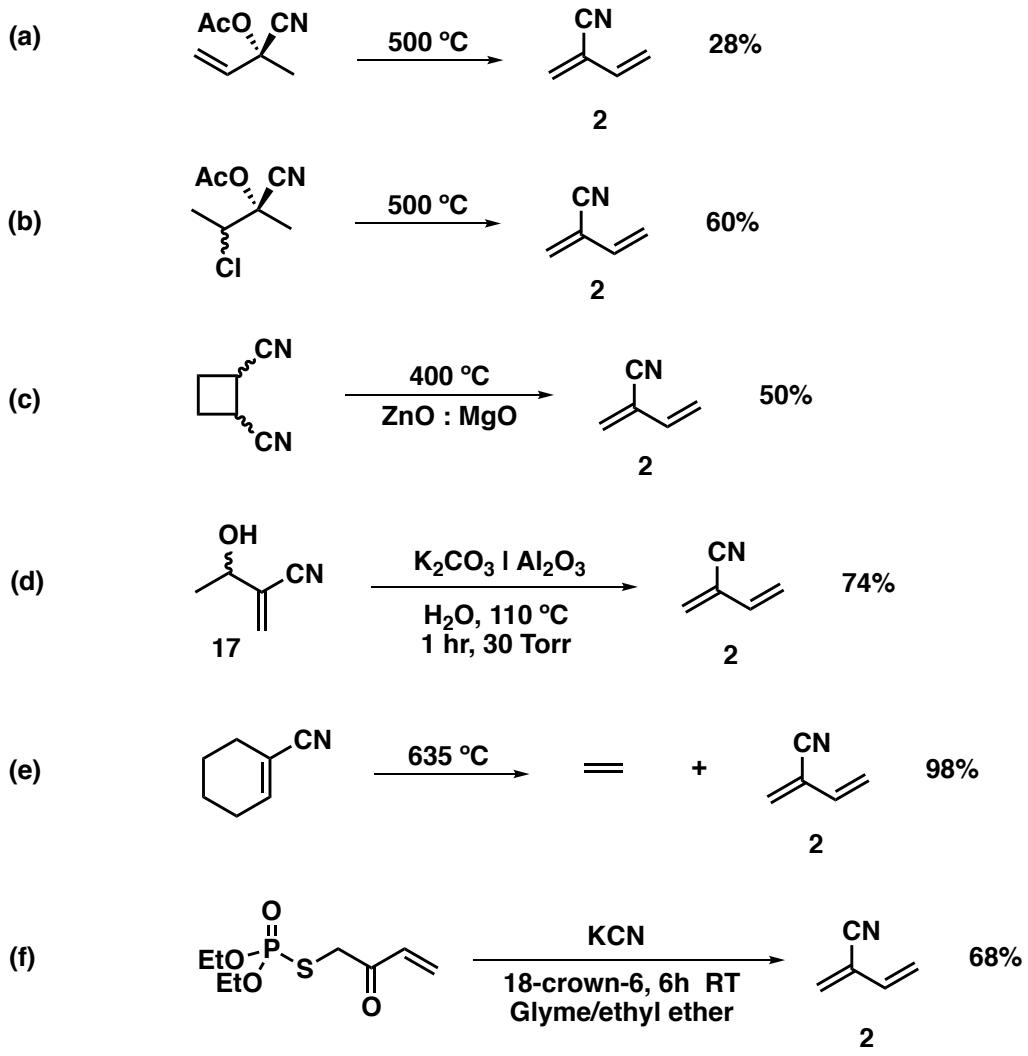
Scheme 1.1. Previous Syntheses of 1-Cyano-1,3-butadiene (1).



(a) Carothers and Berchet;[68] Coffman.[69] (b) Snyder *et al.*[71] (c) Daessle *et al.*[78] (d) Katagiri *et al.*[83] (e) Braun *et al.*[85] (f) Clary and Back.[86] (g) Banert.[87]

2-Cyano-1,3-butadiene attracted significant interest from rubber manufactures as the polymer technology advanced between the 1930's and 1950's.[88] Several methods are reported for the synthesis of 2-cyano-1,3-butadiene (**2**) and are presented chronologically in Scheme 1.2.

Scheme 1.2. Previous Syntheses of 2-Cyano-1,3-butadiene (2).



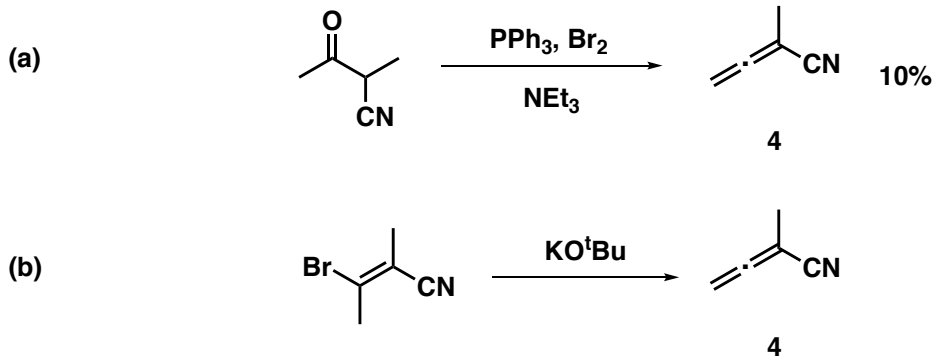
(a) Carter *et al.*[89-90] (b) Marvel *et al.*[89-90] (c) Grasselli *et al.*[91] (d) Nonaka *et al.*[92-95] (e) Rickborn[96] (f) Maciagiewicz *et al.*[97-98]

Carter *et al.* (DuPont) reported the production of 2-cyano-1,3- butadiene (**2**) *via* pyrolysis of aceylated methyl vinyl ketone cyanohydrin (Scheme 1.2a).[89-90] Carl "Speed" Marvel *et al.* reported improved pyrolysis methods involving simultaneous double bond formation using a 3-chloro-2-acetoxy-2-cyanobutane, 2,4-diacetoxy-2-cyanobutane or 2,3-diacetoxy-2-cyanobutane (Scheme 1.2b). [99-105] Grasselli *et al.* (Standard Oil Co.) reported the generation of 2-cyano-1,3-butadiene *via* pyrolysis of 1,2-dicyanocyclobutane on a metal oxide reactor bed (Scheme 1.2c).[91]

Nonaka *et al.* (Toyo Soda Manufacturing Co.) reported the facile production of **2** *via* dehydration of 3-hydroxy-2-methylenebutanenitrile (**17**) using various heterogeneous supported bases (Scheme 1.2d).[92-95] Rickborn demonstrated the efficient formation of **2** *via* retro-Diels-Alder reaction of cyanocyclohexene under pyrolysis conditions (Scheme 1.2e).[96] More recently Maciagiewicz *et al.* reported a one-pot method for producing **2** from a vinyl-thiirane (Scheme 1.2f). [97-98] Although multiple methods exist for producing **2**, details regarding the spectroscopic characterization remain incomplete.

Prior to the works published by our group, the literature does not include any reports describing the synthesis of 4-cyano-1,2-butadiene (**3**) or the determination of its physical properties.[97-98] 2-Methylcyanoallene (**4**) is the only remaining cyanobutadiene isomer without an experimentally determined rotational spectrum. While the synthesis and isolation of a pure sample of 2-methylcyanoallene (**4**) was not performed as part of the work listed in this thesis, the background information pertaining to the synthesis of 2-methylcyanoallene (**4**) is listed herein to provide a foundation for future synthetic and spectroscopic endeavors in our group. Prior literature reports describing the production of 2-methylcyanoallene (**4**) has been published (Scheme 1.3).

Scheme 1.3. Previous Syntheses of 2-Methylcyanoallene (4).

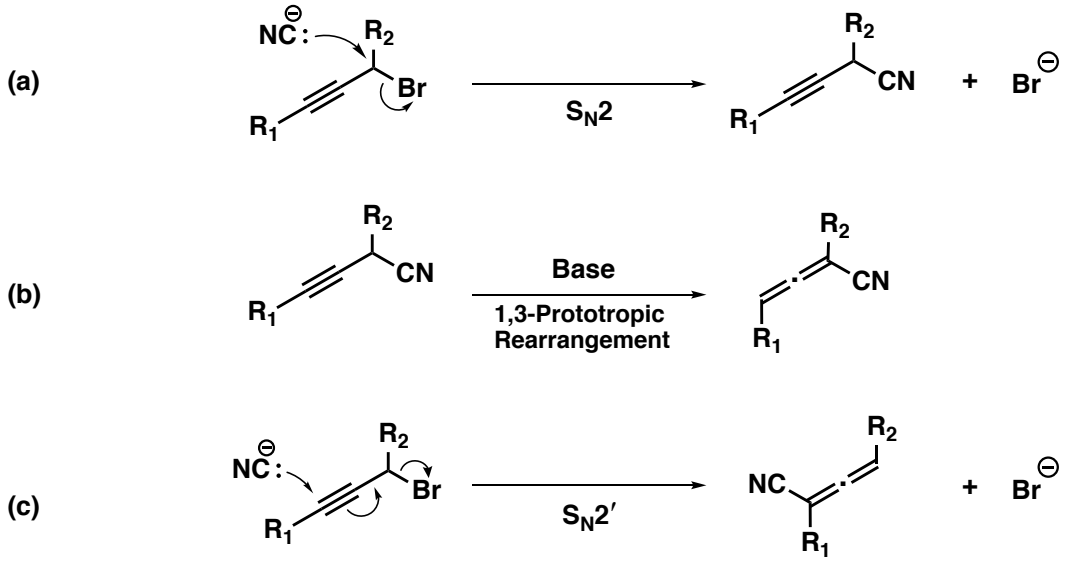


(a) Buono.[106] (b) Chalchat *et al.*[107]

Buono prepared 2-methylcyanoallene (**4**) *via* treatment of 2-cyano-3-butanone with Appel conditions in the presence of trimethylamine (Scheme 1.3a).[106] This procedure reports the boiling point, index of refraction and yield (defined as R_{dt} in French publications) for 2-methylcyanoallene (**4**), but the detailed experimental methodology, reaction conditions, and spectroscopic characterization are not discussed. Chalchat *et al.* reported the generation of 2-methylcyanoallene (**4**) *via* base-induced elimination of 3-bromo-2-methyl-2-butenenitrile (Scheme 1.3b).[107] In the report by Chalchat *et al.*, **4** was only detected in the reaction mixture and was not isolated. Although the ^{1}H-NMR chemical shifts and IR stretching frequencies were documented by Chalchat *et al.*, detailed methodology pertaining to the synthesis, purification and characterization of 2-methylcyanoallene (**4**) remain incomplete at the current time.

The synthetic methodology used to prepare and isolate related cyanoallene congeners could likely be applied in developing a procedure for isolating 2-methylcyanoallene (**4**). Typically, cyanoallene compounds are generated through the treatment of a propargyl bromide with a cyanide source. Two substitution mechanisms lead to the formation of the cyanoallene structure (Scheme 1.4) and are thought to be influenced by the substituents present on the propargyl bromide and the identity of the cationic metal present in the cyanide.[108] Cyanoallenes can be formed through an initial 1,1-substitution (S_N2) to yield a propargyl nitrile (Scheme 1.4a), and undergo a subsequent base-catalyzed 1,3-prototropic rearrangement to yield the allenic nitrile (Scheme 1.4b). Alternatively, nucleophilic attack can occur at the distal sp-hybridized carbon in the alkyne to form the allene structure through a 1,3-substitution (S_N2') (Scheme 1.4c). Sterically large substituents at the propargylic site, and the presence of catalytic or stoichiometric transition metal salts (such as copper) tends to favor the 1,3-substitution mechanism, while the absence of both factors the 1,1-substitution pathway prevails.

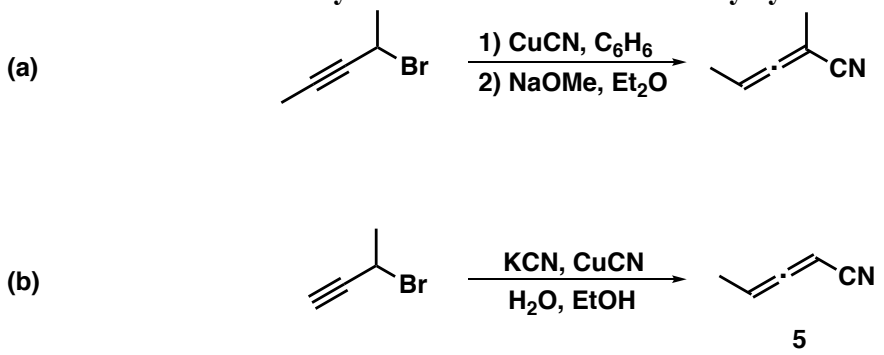
Scheme 1.4. Propargylic Substitution and Rearrangement Mechanisms.



A key step for isolating cyanoallene derivatives is to facilitate the complete prototropic rearrangement of the intermediate propargyl nitrile to the isomeric allenic nitrile.[109] The separation of cyanoallene derivatives from un-isomerized propargyl nitriles usually cannot be accomplished *via* fractional distillation or chromatography due to the thermal sensitivity of the allenic nitrile. To make matters worse, methods utilizing cuprous cyanide for synthesizing propargylic nitriles or cyanoallenes can form highly explosive copper acetylide salts. The distillation of crude propargyl nitriles often reaches an endpoint when the explosive conversion of the distillation rig to glass shrapnel (this result is apparently very reproducible).[110] Alkali cyanides are sufficiently basic to facilitate the complete base-catalyzed prototropic rearrangement of propargyl nitriles, and are typically used in combination with cuprous cyanide for cyanoallene syntheses. The base-catalyzed rearrangement of propargyl nitriles can also be accomplished as a separate step. During the synthesis and purification of 2,4-dimethylcyanoallene, Smith *et al.* assured the complete isomerization of intermediate 2-cyano-3-pentyne through treatment of the crude isolate with ethereal sodium methoxide (Scheme 1.5a).[109] The synthetic procedure for producing 4-

methylcyanoallene (**5**) described by Brandsma *et al.* was used by Carles *et al.* to prepare a pure sample for rotational spectroscopy *via* reaction of 3-bromo-1-butyne, cuprous cyanide, and potassium cyanide (Scheme 1.5b).[108, 111]

Scheme 1.5. Published Synthetic Methods for 4-Methylcyanoallene and Related Congeners.



(a) Smith *et al.*[109] (b) Brandsma *et al.*;[108] Carles *et al.*[111]

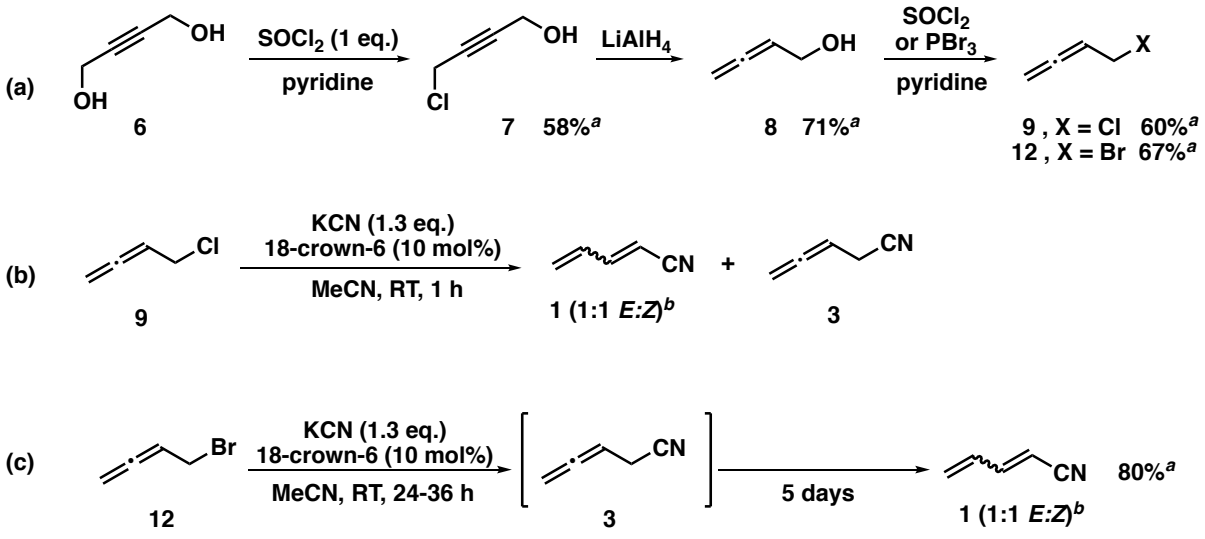
Results and Discussion

1-Cyano-1,3-butadiene (1)

From the time of the earliest interest in 1-cyano-1,3-butadiene (**1**) (Figure 1.1),[67-74] it has been evident that *generating* this compound has not been the obstacle to further study. Rather, the sensitivity of **1** to undergo reaction (dimerization, polymerization) or degradation (heat, light, strong bases, and silica/alumina gels) greatly complicates the task of purifying and characterizing **1**. Our attempts to replicate the procedure reported by Braun *et al.*[85] (Scheme 1.1e) failed to produce an isolable amount of the expected mixture of diastereomers. In our hands, the procedure described by Clary and Back[86] (Scheme 1.1f) afforded ***E*-1** and ***Z*-1** as components in a rather complex mixture of products. Analysis of the crude ^{1}H-NMR spectrum revealed the presence of suspected polymeric by-products generated through addition reactions between ***E*-1**/***Z*-1** and the strong base used to generate the phosphonate ylide. Thus, we sought alternate synthetic strategies to facilitate isolation, purification, and characterization of compound **1**.

We replicated the conditions for the synthesis of 1-cyano-1,3-butadiene (**1**) reported by the DuPont group (Scheme 1.1a).[68-69] To prepare the requisite starting material, 4-chloro-1,2-butadiene (**9**), we employed the sequence depicted in Scheme 1.6a. 2-Butyne-1,4-diol (**6**) was mono-chlorinated with $SOCl_2$ to produce 4-chloro-2-butyn-1-ol (**7**), and subsequent reduction of **7** with $LiAlH_4$ produced 1,2-butadien-4-ol (**8**).[112] Chlorination of **8** with $SOCl_2$ produced 4-chloro-1,2-butadiene (**9**),[113] which was isolated and subjected to the reaction conditions described by Coffman (Scheme 1.1a).[69] Analysis of the resulting product mixture *via* ^{1}H-NMR spectroscopy revealed the presence of both ***E*-1** and ***Z*-1** along with several methoxy-substituted species resulting from the addition of methanol across one (or both) of the double bonds present in **1**, as noted previously.[69] We suspected that the mixed solvent system (H_2O/MeOH) in Scheme 1.1a was used in an attempt to optimize the solubility of the ionic and the organic reactants (sodium cyanide and 4-chloro-1,2-butadiene (**9**), respectively), but the formation of methanol adducts is clearly problematic.

Scheme 1.6. Initial Synthetic Route to 1-Cyano-1,3-butadiene (1) from 2-Butyne-1,4-diol (6).

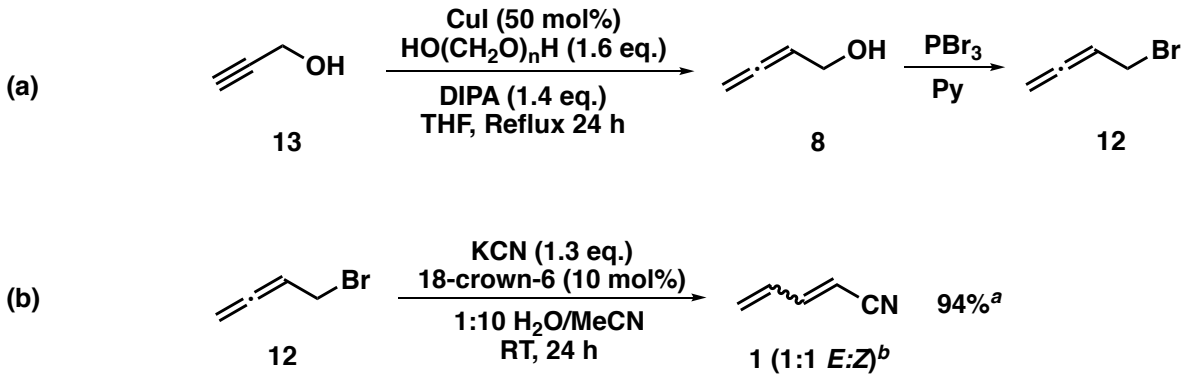


[a] Isolated (gravimetric) yield. [b] Yield and diastereomeric ratio determined *via* ^{1}H-NMR.

We changed the reaction solvent to acetonitrile, which seemed to be a more appropriate solvent for an S_N2 reaction. The solubility of alkali-metal cyanides in most polar-aprotic organic solvents is low, so a crown ether (18-crown-6)[114] was used as a phase-transfer catalyst. Although a solution of KCN and 18-crown-6 in acetonitrile was not completely homogenous, the increased solubility of cyanide was apparently sufficient that the reaction mixture rapidly turned a turbid, dark brown color as the reaction progressed (Scheme 1.6b). The $^{13}C\{^1H\}$NMR spectrum of the crude reaction mixture contained three signals characteristic of an allenic *sp*-hybridized ^{13}C atom, indicating the presence of alcohol **8**, chloride **9**, and a previously unreported allene derivative. Further analysis *via* two-dimensional NMR spectroscopy (HMBC/HSQC) showed correlation of the new allenic ^{13}C signal to three ^1H signals sharing a very similar coupling pattern as observed in alcohol **8** and chloride **9**, but with different *J*-coupling frequencies and chemical shifts. We suspected that the unassigned ^{13}C signal was due to 4-cyano-1,2-butadiene (**3**), the presumed product of initial S_N2 substitution in chloro-compound **9**, prior to rearrangement to 1-cyano-1,3-butadiene (**1**). This suspicion was later confirmed to be true. Details concerning the optimization of reaction conditions, isolation, and spectroscopic characterization of 4-cyano-1,2-butadiene (**3**) are discussed below.

Along with 4-cyano-1,2-butadiene (**3**), smaller amounts of 1-cyano-1,3-butadiene (***E*-1** and ***Z*-1**) were formed in this reaction, the product mixture also included a large amount of unreacted starting material **9**. Extending the reaction time to four hours resulted in the formation of a polymeric material and complete loss of both ***E*-1** and ***Z*-1** – yet there was still unreacted **9** present (evident *via* NMR). The same reaction sequence, employing the corresponding 4-bromo-1,2-butadiene (**12**) afforded a better result. 4-Bromo-1,2-butadiene (**12**) was prepared in two steps from propargyl alcohol (**13**) (Scheme 1.7a).[112, 115]

Scheme 1.7. Improved Synthetic Route to 1-Cyano-1,3-butadiene (mixture *E*-1 and *Z*-1) from Propargyl Alcohol (13).



[a] Reaction yield determined *via* ^{1}H-NMR using phenyltrimethylsilane (Ph-TMS) as an internal standard. [b] Diastereomeric ratio determined *via* ^{1}H-NMR.

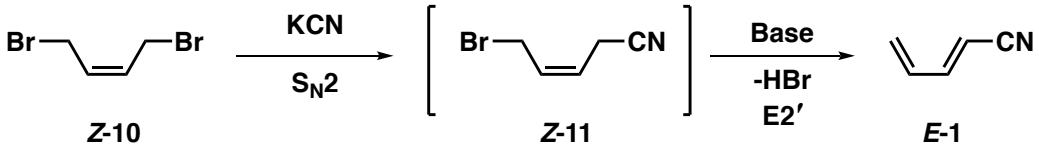
When treated with the same reaction conditions as allenic chloride **9**, allenic bromide **12** reacted in a more controlled, clean manner, yielding significantly less of the brown polymeric material. The reaction of allenic bromide (**12**) to form **3**, as well as the subsequent isomerization of **3** to **1** was unexpectedly slow; at room temperature and under anhydrous conditions, isomerization of 4-cyano-1,2-butadiene (**3**) to 1-cyano-1,3-butadiene (**1**) took five days (80% yield; approximately 1:1 mixture of ***E*-1** and ***Z*-1**) (Scheme 1.6c). Despite the use of a phase-transfer catalyst, the reaction in acetonitrile was not homogenous. Addition of water (~10% v/v) to the reaction mixture increased the solubility of KCN and decreased the reaction time to approximately twenty-four hours (Scheme 1.7b). The optimal conditions for producing a 1:1 mixture of ***E*-1** and ***Z*-1** with minimal byproducts are reported in Scheme 1.7b. Even though the reaction efficiently produced ***E*-1** and ***Z*-1**, we were confounded in our efforts to separate, purify, and isolate these isomers, as prepared in this procedure. Difficulties included the inability to remove small amounts of acetonitrile and propensity for dimerization and/or polymerization.

Requiring pure, neat materials in order to obtain their rotational spectra, we turned to other synthetic strategies that might afford a measure of selectivity in the preparation of ***E*-1** and ***Z*-1**.

(E)-1-Cyano-1,3-butadiene (*E*-1)

Daessle *et al*. demonstrated that 1-cyano-1,3-butadiene (**1**) can be accessed *via* an E2′ (1,4-elimination) reaction of a mixture of 1-chloro-4-cyano-2-butenes with anhydrous ammonia (Scheme 1.1c).[78] Katagiri *et al*. demonstrated that **1** can be produced in a one-pot synthesis involving the treatment of a mixture of 1,4-dibromo-2-butenes (**10**) with alkali-metal cyanides under basic conditions (Scheme 1.1d).[83] While the diastereoselectivity of these reactions was not previously investigated, we saw an opportunity to influence the diastereoselectivity of the reaction to favor the formation of ***E*-1** over ***Z*-1** *via* the stereochemistry of the 1,4-dibromo-2-butene precursor ***Z*-10** or ***E*-10** (Scheme 1.8). Consistent with similar precedents,[116-118] we hypothesized that E2′ reaction of (*Z*)-1-bromo-4-cyano-2-butene (***Z*-11**) would favor the formation of ***E*-1** over ***Z*-1** because of a steric preference for the cyano group to be rotated away from the *cis* $-CH_2Br$ group in the transition state for the elimination reaction. In fact, selectivity in favor of ***E*-1** was observed, and a computational analysis of the basis for the selectivity is described later in this chapter.

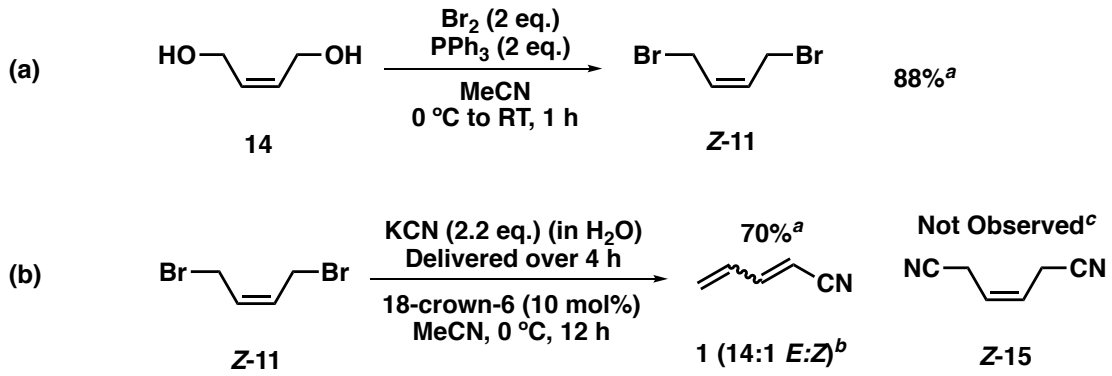
Scheme 1.8. Strategy for Diastereoselective Synthesis of (*E*)-1-Cyano-1,3-butadiene (*E*-1).



(*Z*)-1,4-Dibromo-2-butene (***Z*-10**), prepared from (*Z*)-2-buten-1,4-diol (**14**) *via* Appel conditions,[119] readily reacts with two equivalents of KCN through tandem S_N2/E2′ reactions to

form 1-cyano-1,3-butadiene (**1**; *E:Z* ratio 14:1) without the addition of an exogenous base (Scheme 1.9). The best results were observed using binary acetonitrile/water solvent systems. Reactions performed in pure acetonitrile (*via* addition of solid KCN to the stirring reaction) proceeded slowly and never to full conversion – likely due to the low solubility of KCN in acetonitrile. Several other polar-aprotic solvents were investigated for use in these reactions (DMF, THF, glyme, diethyl ether, PEG, and DMSO), though the cleanest reactions were observed with the acetonitrile/water solvent system. DMF and DMSO accelerated the reaction to the point of a rapid exotherm, which resulted in degradation of the product, likely due to the high concentration of cyanide in these solvents. We found that the best diastereoselectivity was observed (with near-complete conversion) in experiments where aqueous KCN was added slowly to a solution of ***Z*-10** and 18-crown-6 in acetonitrile at 0 ºC.

Scheme 1.9. Diastereoselective Synthesis of (*E*)-1-Cyano-1,3-butadiene (*E*-1) from (*Z*)-1,2-Dibromo-2-butene (*Z*-10).



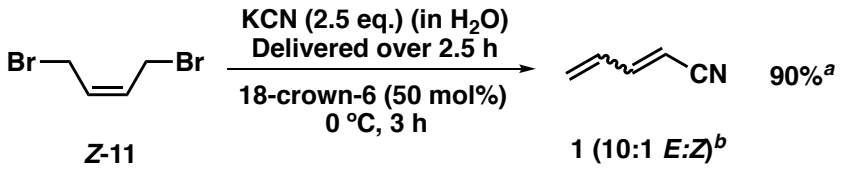
[a] Isolated (gravimetric) yield. [b] Diastereomeric ratio determined *via* ^{1}H-NMR. [c] 1,4-Dicyano-2-butene (***Z*-15**) not observed *via* ^{1}H-NMR.

Evaluation of the reaction progress *via* ^{1}H-NMR spectroscopy showed the rapid formation of ***E*-1**/***Z*-1** upon addition of KCN to ***Z*-10**. Signals corresponding to (*Z*)-1-bromo-4-cyano-2-butene (***Z*-11**) or (*Z*)-1,4-dicyano-2-butene (***Z*-15**), a potential by-product resulting from a second S_N2 displacement in ***Z*-11**, were not observed in the ^{1}H-NMR spectrum as the reaction progressed.

The rapid formation of ***E*-1**/***Z*-1** and absence of observable ***Z*-11** and ***Z*-15** signals in the ^{1}H-NMR evaluation suggests that the product-forming E2′ reaction occurs more rapidly than either of these competing reactions. The drawback of this procedure was the difficulty of removing residual acetonitrile solvent from the product ***E*-1**.

The following procedure was developed, with the goal of optimizing the ability to isolate and purify the target compound (*E*)-1-cyano-1,3-butadiene (***E*-1**). Addition of ***Z*-10** to 50 mol% 18-crown-6 resulted in a eutectic mixture, which remained a liquid when cooled to 0 ºC. Slow addition of aqueous KCN to a rapidly stirring eutectic mixture of ***Z*-10**/18-crown-6 at 0 ºC proceeded to full conversion while retaining good diastereoselectivity to produce ***E*-1**. Subsequent extraction with diethyl ether and fractional distillation of the product mixture yielded 1-cyano-1,3-butadiene (**1**) in 90% isolated yield (*E:Z* ratio 10:1) (Scheme 1.10).

Scheme 1.10. Modified Reaction Conditions for Efficient Synthesis and Purification of (*E*)-1-Cyano-1,3-butadiene (*E*-1).



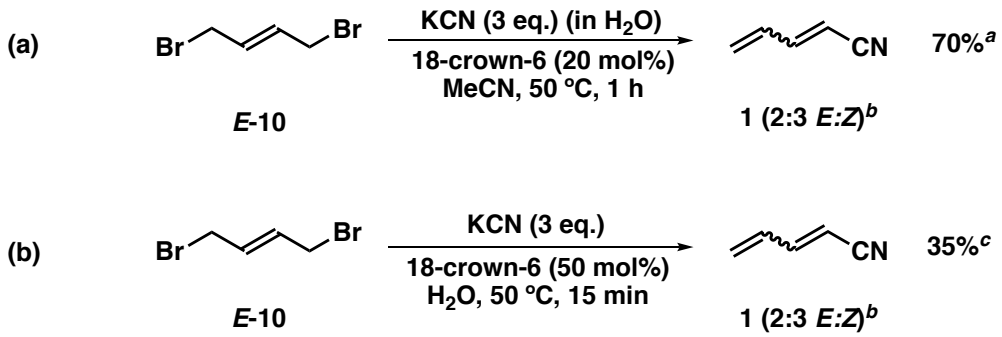
[a] Isolated (gravimetric) yield. [b] Diastereomeric ratio determined *via* ^{1}H-NMR.

(Z)-1-Cyano-1,3-butadiene (*Z*-1)

A selective route to produce (*Z*)-1-cyano-1,3-butadiene (***Z*-1**) has been reported,[87] although details of the experimental procedure and spectroscopic properties are not readily available. Multiple studies describe the separation, isolation, and physical properties of ***Z*-1**.[71, 120] As a counterpart to our development of a selective process for the preparation of ***E*-1** from *Z*-1,4-dibromo-2-butene (***Z*-10**), we observed that subjecting ***E*-10** to the reaction conditions shown in

Scheme 1.11 resulted in a mildly selective formation of ***Z*-1**. Although this procedure utilizes acetonitrile as the solvent, which was problematic in the isolation and purification of ***E*-1**, the slightly higher volatility of ***Z*-1** enables its separation from ***E*-1** and acetonitrile in a straightforward fashion. Iterative fractional distillation of the product mixture increased the relative concentration of ***Z*-1** in the distillate, resulting in a reasonably pure sample of ***Z*-1** after three distillations. Purity was sufficient that the ratio of *E* to *Z* by rotational spectroscopy was observed at approximately 1:8 (***E*-1**:***Z*-1**).

Scheme 1.11. Modified Reaction Conditions for Semi-Selective Preparation of 1-Cyano-1,3-butadiene (*Z*-1) from (*E*)-1,4-Dibromo-2-Butene (*E*-10).



[a] Reaction yield determined *via* ^{1}H-NMR. [b] Diastereomeric ratio determined *via* ^{1}H-NMR.
[c] Isolated (gravimetric) yield.

Computational Analysis of Diastereoselectivity in the Formation of 1-Cyano-1,3-butadiene (*E*-1 / *Z*-1)

The reaction to form (*E*)-1-cyano-1,3-butadiene (***E*-1)** from (*Z*)-1,4-dibromo-2-butene (***Z*-10**) is hypothesized to proceed through (*Z*)-1-bromo-4-cyano-2-butene (***Z*-11**), which, once formed, reacts with another equivalent of cyanide to eliminate HBr in a concerted 1,4-elimination mechanism (E2′ mechanism). Given that the *E* and *Z* diastereomers of 1-cyano-1,3-butadiene (**1**) are predicted to be very similar in energy (within 1 kcal/mol) and the reactions of different precursor stereoisomers lead to different product ratios, it is clear that a kinetically controlled

reaction is responsible for the observed diastereoselectivity. Thus, the E2′ transition state barriers leading to each diastereomer of **10** must be responsible for the selectivity, or lack thereof, in the formation of ***E*-1** and ***Z*-1**.

The proposed E2′ substrates, (*Z*)- and (*E*)-1-bromo-4-cyano-2-butene (**11**), exhibit multiple conformational isomers, which are analyzed in detail (see Supporting Information). The isomerization barriers for all conformations of both diastereomers are less than 6 kcal/mol. Contour plots and the detailed analysis of the complete conformational potential energy surfaces of ***Z*-11** and ***E*-11** are provided in the Supporting Information. Two pairs of E2′ transition states were found for each diastereomer ***Z*-11** and ***E*-11** reacting with cyanide ion leading to ***E*-1** and ***Z*-1** (Figures 1.6 and 1.7). In each of the transition state geometries, an acidic hydrogen atom at C-4 is perpendicular to the plane of the adjacent alkene unit. The bromide leaving group at C-1 can be in an *anti* or *syn* orientation with respect to the acidic hydrogen atom at C-4. The cyano substituent at C-4 may occupy a *syn*-periplanar conformation relative to the alkene moiety, which leads to formation of (*Z*)-1-cyano-1,3-butadiene (***Z*-1**), or an *anti*-periplanar conformation, which leads to formation of (*E*)-1-cyano-1,3-butadiene (***E*-1**). Each transition state was verified to connect one diastereomer of the starting material (**11**) to one diastereomer of the product (**1**) using an intrinsic reaction coordinate (IRC) calculation. Attempts to explore a step-wise pathway beginning with deprotonation of ***Z*-11** or ***E*-11** failed to obtain an anionic intermediate as a stationary point. Therefore, a stepwise mechanism was not considered further.

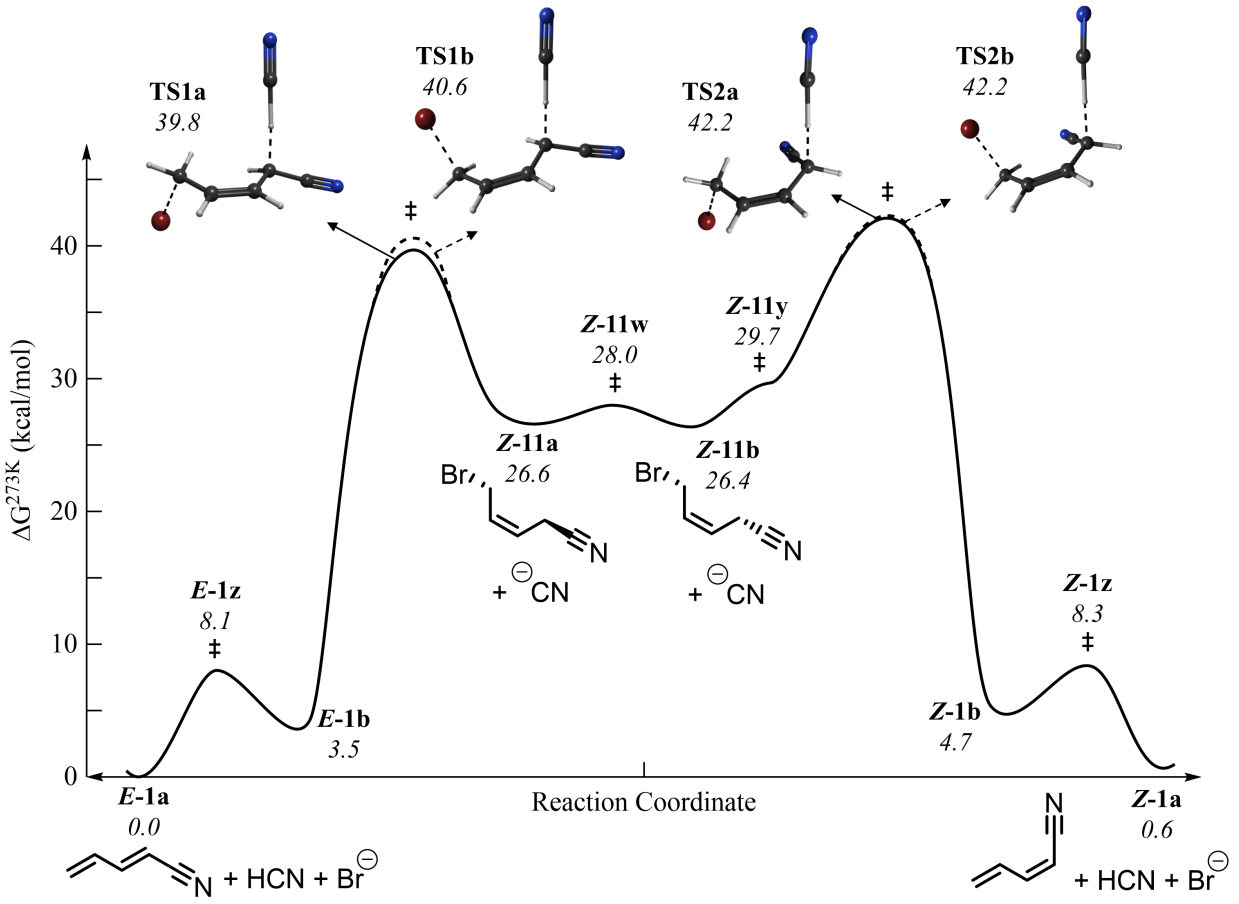


Figure 1.6. Computed reaction coordinate diagram for E2′ reaction of (*Z*)-1-bromo-4-cyano-2-butene (***Z*-11**) with cyanide in water. Gibbs free energies at B3LYP/cc-pVTZ with polarized-continuum model for solvent (H_2O) at 273 K (0 °C). Solid line: lower energy transition state. Dashed line: higher energy transition state.

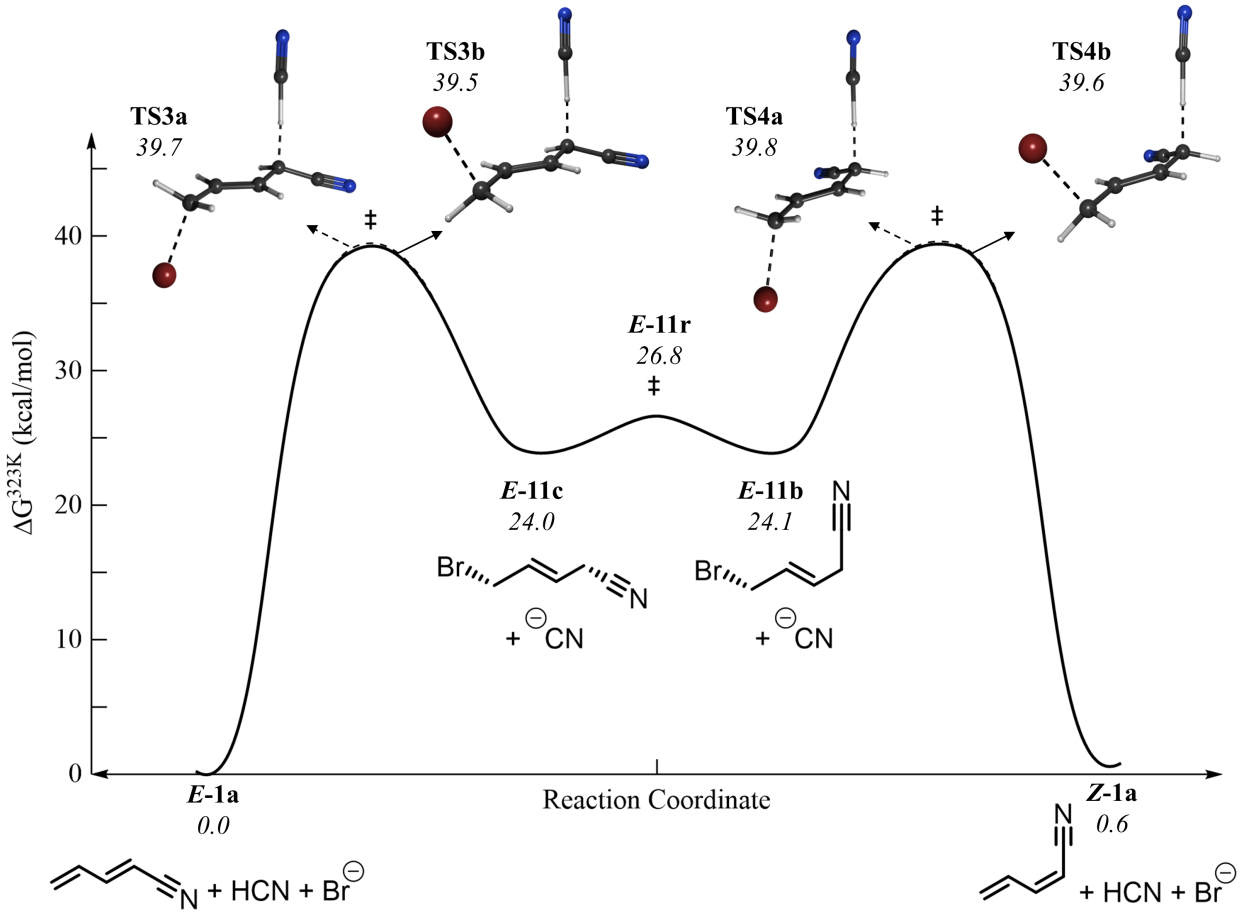


Figure 1.7. Computed reaction coordinate diagram for E2′ reaction of (*E*)-1-bromo-4-cyano-2-butene (***E*-11**) with cyanide in water. Gibbs free energies at B3LYP/cc-pVTZ with polarized-continuum model for solvent (H_2O) at 323 K (50 °C). Solid line: lower energy transition state. Dashed line: higher energy transition state.

For either diastereomer of 1-bromo-4-cyano-2-butene (***E*-11** or ***Z*-11**), the computed activation barriers of the E2′ transition states are significantly higher (by 7 to 14 kcal/mol) than the activation barriers for conformational interconversion. Thus, the diasteroselectivity in the elimination reaction is interpreted in terms of the Curtin-Hammett principle.[121] Product selectivity is governed by the difference in energy between the competing product-forming transition states ($\Delta\Delta G^{\ddagger}$); conformational equilibrium in the starting materials is rapid and does not govern the composition of products. As such, the potential energy surfaces for the E2′ reactions shown in

Figure 1.6 and Figure 1.7 contain a simplified surface for the conformational isomerization of each 1-bromo-4-cyano-2-butene (***E*-11** or ***Z*-11**).

In the E2′ reaction of (*Z)*-1-bromo-4-cyano-2-butene (***Z*-11**) with cyanide in water at 273 K (0 °C) (Figure 1.6), the transition states **TS2a** and **TS2b** that lead to (*Z*)-1-cyano-1,3-butadiene (***Z*-1**) are higher in energy than the transition states **TS1a** and **TS1b** that lead to (*E*)-1-cyano-1,3-butadiene (***E*-1**). Thus, the computational analysis is in qualitative accord with the experimental observation of diastereoselectivity favoring the formation of (*E*)-1-cyano-1,3-butadiene (***E*-1**). The difference in transition state energies ($\Delta\Delta G^{\ddagger}$) appears to arise from a steric interaction in the transition states involving the $-CH_2CN$ group. Both transition states leading to ***Z*-1** (**TS2a** and **TS2b**) have a larger interaction between –CN and $-CH_2Br$, relative to the transition states leading to ***E*-1** (**TS1a** and **TS1b**). The small energy difference between the ***E*-1**-forming transition states **TS1a** and **TS1b** (0.8 kcal/mol) is likely due to a subtle difference in electrostatic interactions (repulsion) between the bromo and cyano substituents in the *anti* vs. *syn* E2′ elimination pathways. Natural Bond Orbital (NBO) analysis of each transition state did not reveal any obvious hyperconjugation contribution to the energy differences among **TS1a**, **TS1b**, **TS2a**, and **TS2b**. Assuming that this potential energy surface reasonably models this reaction, the ***E*-1**/***Z*-1** ratio derived from the $\Delta\Delta G^{\ddagger}$ between **TS1a** and **TS2a** (2.4 kcal/mol) is expected to be ca. 60:1. This result is in qualitative agreement with the experimental observation of an ***E*-1**/***Z*-1** ratio of 10:1. This does indicate, however, that the computational prediction of $\Delta\Delta G^{\ddagger}$ is larger than its true value by about 1 kcal/mol.

In a similar fashion, the potential energy surface of the E2′ reaction of (*E)*-1-bromo-4-cyano-2-butene (***E*-11**) with cyanide in water at 323 K (50 °C) is presented in Figure 1.7. Unlike the reaction of the isomeric system (***Z*-11**), the transition states for the E2′ reaction of ***E*-11** leading

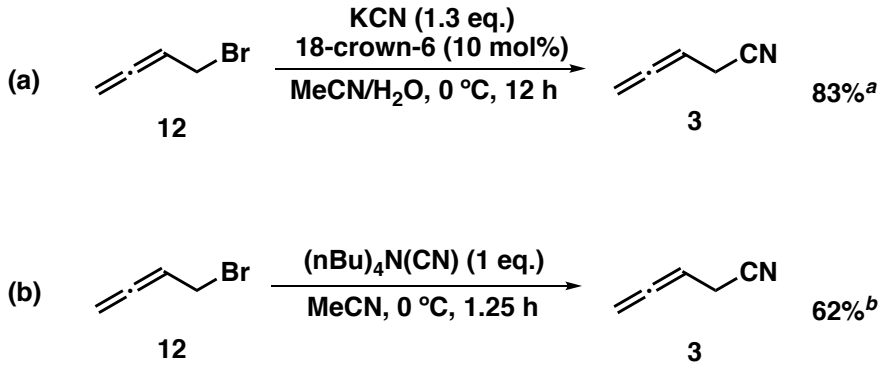
to (*E*)- and (*Z*)-1-cyano-1,3-butadiene (**1**) are computed to be virtually isoergic ($\Delta\Delta G^{\ddagger}$ = 0.1 kcal/mol favoring the formation of ***E*-1**). With the $-CH_2CN$ and $-CH_2Br$ groups in a *trans* orientation in the ground state of ***E*-11**, there is not a significant preference for the –CN substituent to adopt one conformation over the other. This situation is also manifest in the transition states (**TS3a**, **TS3b**, **TS4a**, **TS4b**); the relative energies of the transition states reveal no preference for the stereochemical course of the reaction. Thus, the rates of product formation would be expected to afford a diastereomeric ratio of nearly 1:1. This prediction is consistent with the experimentally observed product ratio of ***E*-1** : ***Z*-1** (*E*:*Z* ratio 2:3). The deviation of the experimental ratio from 1:1 reveals that there is a slight energetic preference (< 1 kcal/mol) for the transition states leading to the *Z* diastereomer. Our computational model is not expected to be of sufficient accuracy to account for such a small energetic difference.

4-Cyano-1,2-butadiene (3)

As described earlier, we observed 4-cyano-1,2-butadiene (**3**) as an intermediate during the preparation of 1-cyano-1,3-butadiene (**1**) from 4-halo-1,2-butadienes (**9** or **12**) (Scheme 1.6). In order to optimize conditions for the preparation and isolation of **3**, it was necessary to avoid the isomerization of **3** to **1** – a process that is typically observed under conditions that utilize both water and cyanide (a weak base) at ambient temperature. When the reaction of 4-bromo-1,2-butadiene (**12**) is performed under anhydrous conditions (dry solvent, vacuum-dried crown ether, vacuum-dried KCN), bromide **12** undergoes slow S_N2 reaction; minimal isomerization of **3** is observed. The rate of substitution, however, is too slow to be useful. Addition of water to the reaction mixture increases the solubility of cyanide, increases the rate of substitution, and increases the rate of isomerization of **3** to **1**. (Ultimately, the rate becomes very rapid and results in a

noticeable exotherm.) At a reaction temperature of 0 ºC, the isomerization is slow enough such that 4-cyano-1,2-butadiene (**3**) can be isolated (Scheme 1.12a). Absent aqueous acidic or basic conditions, **3** is stable when isolated. The slow addition of an organic-soluble cyanide source (tetrabutylammonium cyanide), under anhydrous conditions, allows for an efficient S_N2 reaction and isolation of pure **3** without significant isomerization (Scheme 1.12b).

Scheme 1.12. Reaction Conditions for the Preparation of 4-Cyano-1,2-Butadiene (3).



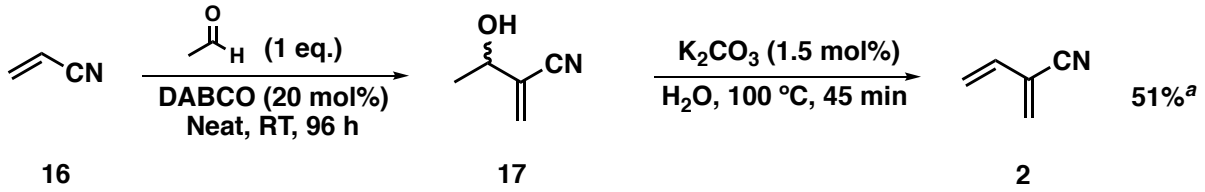
[a] Reaction yield determined *via* ^{1}H-NMR. [b] Isolated (gravimetric) yield.

Once the cyanide is consumed, exposure to water in the subsequent extraction (to remove the polar-aprotic solvent) does not promote significant isomerization of **3**. In fact, neat **3** can be left at ambient conditions for weeks without observable isomerization. Nitrile **3** is sufficiently stable that it can be distilled under a relatively low vacuum (100 Torr) without noticeable degradation. In contrast to the regioselectivity exhibited in the rearrangement of the corresponding allenic halides,[122] the isomerization of allenic nitrile **3** yields exclusively 1-cyano-1,3-butadiene (**1**). 2-Cyano-1,3-butadiene (**2**) is not observed, which is attributable to the absence of cyanide dissociation / recombination previously observed for the corresponding allenic halides.

2-Cyano-1,3-butadiene (2)

Although 2-cyano-1,3-butadiene (**2**) has been prepared previously, synthetic routes often involve a pyrolysis reaction as the last step. Preferring to avoid a pyrolysis reaction, we prepared 2-cyano-1,3-butadiene (**2**) using a combination of literature procedures from Strub *et al.* and Nonaka *et al.* (Scheme 1.13).[92-95, 123]

Scheme 1.13. Preparation of 2-Cyano-1,3-butadiene (2).



[a]Isolated (gravimetric) yield

Morita-Baylis-Hillman addition of acrylonitrile (**16**) and acetaldehyde using catalytic 1,4-diazabicyclo[2.2.2]octane (DABCO) afforded 3-hydroxy-2-methylenebutanenitrile (**17**) in quantitative yield. Subsequent dehydration of **17** was performed using catalytic K_2CO_3. The resulting 2-cyano-1,3-butadiene (**2**) was distilled from the reaction mixture under vacuum and collected as an aqueous emulsion that separated upon cooling. Compound **2** is prone to undergo polymerization, even at –20 ºC.

Conclusions

We describe the synthesis, isolation, purification, and spectroscopic characterization of four cyano-butadiene isomers: (*E*)-1-cyano-1,3-butadiene (***E*-1**), (*Z*)-1-cyano-1,3-butadiene (***Z*-1**), 4-cyano-1,2-butadiene (**3**), and 2-cyano-1,3-butadiene (**2**). These molecules are of considerable significance to the field of astrochemistry, as possible constituents of both planetary atmospheres and interstellar space. Because of the general experimental difficulties in handling these reactive

compounds, the literature data concerning the spectroscopic characterization (NMR, IR, MS) of these simple organic molecules is remarkably sparse. Our new procedures enable isolation and purification of these compounds, affording high quality NMR, IR, and MS data, for the first time. The preparation of pure samples of these molecules enabled the measurement of their laboratory rotational spectra – the critical data needed to search for these species in space by radioastronomy. Synthetic methodology and analysis/assignment of rotational spectrum were published as separate manuscripts,[41, 63-64] and continues to be used for the facile isolation of cyanobutadiene samples intended for matrix-isolation IR and UV-Vis spectroscopy.

Experimental Section

General Experimental Methods. All commercial reagents were purchased from Sigma-Aldrich, Acros, and Oakwood and used as received without further purification, unless otherwise noted. ^{1}H-NMR spectra (400 or 500 MHz) and ^{13}C{^{1}H}-NMR spectra (100 or 125 MHz) were obtained in $CDCl_3$, CD_3CN, or C_6D_6 on a Bruker 400 MHz Avance III or Bruker 500 MHz DCH Avance III spectrometer; chemical shifts (δ) are reported as ppm downfield from internal standard $SiMe_4$. Mass spectra were acquired using electrospray ionization (ESI) or Atmospheric Solids Analysis Probe (ASAP)[124] on a Thermo Scientific Q-Exactive Plus™ mass spectrometer. GC/MS analysis was performed on a Shimadzu GCMS-2010S. IR spectra were obtained on a Bruker Tensor FTIR instrument as neat samples using an attenuated total reflectance accessory (Bruker Platinum ATR).

Synthetic Procedures & Information

1-Cyano-1,3-butadiene (1). Our preliminary studies concerning the preparation, isolation, and identification of 1-cyano-1,3-butadiene (**1**) provide some context for the experimental difficulties encountered and detail concerning the spectroscopic assignments.[125] Following the procedure of Clary and Back:[86] to a suspension of sodium hydride (2.88 g, 120 mmol) in freshly distilled THF (500 mL) was added diethyl cyanomethylphosphonate (8.1 mL, 50.1 mmol) dropwise *via* syringe at 0 °C. After stirring for 1 h, freshly distilled acrolein (3.6 mL, 53.9 mmol) was added dropwise. The reaction was stirred for 5 h at 0 °C, warmed to room temperature, and quenched with saturated aqueous NH_4Cl solution. The solution was extracted with diethyl ether, washed with saturated aqueous NaCl, and dried over $MgSO_4$. After removal of the drying agent by filtration, ether was removed under reduced pressure at room temperature, and the resulting mixture was fractionally distilled (collection flask cooled to −78 °C, and distillation flask cooled to 0 °C). The distillate consisted of a mixture *E* and *Z* isomers of 1-cyano-1,3-butadiene (**1**) in a ratio of 2:1 in addition to residual THF.

^{1}H-NMR (400 MHz, $CDCl_3$): ***E***-isomer δ 6.31 (ddt, 1H, J = 16, 11, <1 Hz), 5.74 (tt, 1H, J = 10, <1 Hz), 4.94 (dm, 1H, J = 17, <1, <1 Hz), 4.93 (dm, 1H, J = 10, <1, <1 Hz), 4.65 (dd, 1H, J = 16, <1 Hz) ppm; ***Z***-isomer δ 6.59 (dtd, 1H, J = 17, 10, <1 Hz), 6.03 (tt, 1H, J = 10, <1 Hz), 5.03 (dm, 1H, J = 17, <1, <1 Hz), 5.02 (dm, 1H, J = 10, <1, <1 Hz), 4.55 (dd, 1H, J = 10, <1 Hz). HRMS (ASAP-Q-IT)[124] *m/z*: $[M+H]^+$ Calcd for C_5H_6N 80.0495; Found 80.0493.

The procedure involves the formation of a phosphonate ylide followed by reaction with acrolein in a Horner-Wadsworth-Emmons type olefination.[86] Although this reaction appears to be straightforward, the resulting ^{1}H-NMR spectrum does not agree with that described in the literature.[86] Upon closer investigation, the previously reported ^{1}H-NMR data do not account for

all hydrogen atoms in the molecule. Although each isomer (***E*-1** and ***Z*-1**) should have five signals in the spectrum, the *E*-isomer (***E*-1**) has four reported signals and the *Z*- (***Z*-1**) has only three.[86] Additionally, the reaction inherently undergoes a side reaction, and not all signals in the crude spectrum are attributable to **1**. The combination of the two issues combined with challenges encountered in purification created confusion in characterization and complicated the optimization and troubleshooting process. These issues are discussed in greater detail in the Supporting Information section.

Isolation of *E*- and *Z*-Isomers of 1-Cyano-1,3-butadiene (1). One of the challenges encountered during the isolation of neat ***E*-1**/***Z*-1** originates from their volatility and their tendency to form azeotropes with acetonitrile. The complete removal of acetonitrile was necessary for obtaining accurate spectra and isolated yields of the product. Solvent removal *via* rotary evaporation drastically reduced product yields due to the azeotropic losses. We found that most acetonitrile could be removed through aqueous washes of the crude ethereal extract during reaction workup. Remaining traces of acetonitrile could be fully removed from the products by low-temperature vacuum distillation (~100-500 mTorr, 0 ºC). Attempts to remove acetonitrile *via* careful vacuum fractional distillation were marginally effective, as a small amount of acetonitrile always co-distilled with the product diastereomers. We found that highly volatile solvents (such as the diethyl ether used during the biphasic extraction of the reaction mixture) were more easily removed *via* fractional distillation through a packed column under atmospheric pressure without co-distilling any ***E*-1** and ***Z*-1**. Additionally, product losses resulting from polymerization of ***E*-1** and ***Z*-1** during the distillation process were minimized *via* addition of a phenolic polymerization inhibitor. We found that hydroquinone was ideal for our purposes because its high boiling point

and extremely low volatility prevented its co-distillation with ***E*-1** and ***Z*-1** during the final purification.

(*Z*)-1,4-Dibromo-2-butene (*Z*-10). In a modification of literature procedures,[126-128] 52.55 g (200 mmol) of PPh_3 was added to 300 mL of acetonitrile in a 500 mL round-bottom flask equipped with a 100 mL dropping funnel. The reaction vessel was sealed with a septum and cooled to 0 ºC on ice. The reaction vessel and contents were subjected to three vacuum pump/N_2 purge cycles. Br_2 (10.2 mL, 197.8 mmol) was added dropwise to the stirring PPh_3 suspension *via* dropping funnel. (*Z*)-2-Buten-1,4-diol (**14**) (9.035 g, 103 mmol) was rapidly added to the stirring suspension *via* syringe. The cooling bath was removed, and the reaction stirred for 1 h. After the elapsed reaction time, approximately half of the acetonitrile solvent was removed by rotary evaporation. The resulting triphenylphosphine oxide precipitate was removed *via* vacuum filtration. The filtrate was then evaporated to dryness. The resulting orange solids were dissolved in 50 mL 1:4 EtOAc/*n*-hexane and filtered through a silica plug (5 cm) to remove any remaining triphenylphosphine oxide. Solvent was removed *in vacuo* to yield 18.07 g (88%) of (*Z*)-1,4-dibromo-2-butene (***Z*-10**) as a pale-yellow oil. **CAUTION: (*Z*)-1,4-Dibromo-2-butene is a potent lachrymator and vesicant and must be handled with caution. Samples of (*Z*)-1,4-dibromo-2-butene will isomerize upon heating and should be stored in a freezer (-20 ºC).** ^{1}H-NMR ($CDCl_3$, 500 MHz): δ (ppm) complex spin system, 5.89 (m, 2H), 4.02 (m, 4H). $^{13}C\{^1H\}$-NMR ($CDCl_3$, 125 MHz): δ (ppm) 129.9, 24.7.

(*E*)-1-Cyano-1,3-butadiene (*E*-1) ((*E*)-2,4-Pentadienenitrile). 5.38 g (25.2 mmol) (*Z*)-1,4-Dibromo-2-butene (***Z*-10**), 3.36 g (12.7 mmol) 18-crown-6, and 57 mg (0.52 mmol) hydroquinone were added to a 50 mL single-neck round-bottom flask. The reaction vessel was sealed with a septum and purged with N_2 *via* syringe needle inlet. The vessel was then cooled to 0

ºC on ice. Potassium cyanide (4.09 g, 62.8 mmol) was dissolved in 10 mL of deionized H_2O and delivered to the cooled reaction dropwise *via* syringe pump over the course of 2 h with vigorous stirring. As the addition completed, the reaction became biphasic with an orange top organic layer and a tan bottom aqueous layer. The reaction was stirred for an additional 15 min at 0 ºC after the addition was complete and then allowed to warm to room temperature. The reaction mixture was rinsed into a separatory funnel with 10 mL diethyl ether and 10 mL deionized H_2O, the organic layer was separated, and the aqueous layer was extracted with diethyl ether (4 × 10 mL). The combined organic layers were washed with 10 mL saturated aqueous NaCl and dried over anhydrous $CaCl_2$. After removal of the drying agent by gravity filtration, hydroquinone (97 mg) was added to the filtrate and the ethereal solvent was removed by fractional distillation at atmospheric pressure (45 cm Vigreux column). The crude product was cooled to room temperature, and a vacuum of ~400 Torr was applied to remove residual ether. The remaining yellow concentrate was purified *via* bulb-to-bulb (Kugelrohr) distillation to yield 1.8047 g of 1-cyano-1,3-butadiene (**1**) (90 %, 10:1 *E*:*Z*) as a colorless oil. Compound ***E*-1** is indefinitely stable as a neat substance at −80 ºC or in dilute solution of diethyl ether with hydroquinone inhibitor to prevent polymerization. ^{1}H-NMR (C_6D_6, 500 MHz): δ (ppm) ***E*-1**: 6.34 (dd, 1H, J = 16, 10 Hz), 5.79 (dt, 1H, J = 17.1, 10.3 Hz), 5.01 (d, 1H, J = 2.4 Hz), 4.99 (d, 1H, J = 2.7 Hz), 4.69 (d, 1H, J = 16 Hz). ^{13}C{^{1}H}-NMR (C_6D_6, 125 MHz): δ (ppm) 150.0, 134.3, 125.9, 117.8, 100.2. IR (neat): (cm^{-1}) 3054 (w), 2218 (m), 1629 (w), 1589 (m), 1417 (w), 1292 (w), 1258 (w), 1001 (s), 955 (m), 932 (m), 835 (m), 475 (w). HRMS (ESI) *m/z*: $[M+H]^+$ Calcd for C_5H_6N: 80.0495. Found: 80.0494.

(*Z*)-1-Cyano-1,3-butadiene (*Z*-1) ((*Z*)-2,4-Pentadienenitrile). Potassium cyanide (9.88 g, 152 mmol, 3 equiv) and 18-crown-6 (6.66 g, 25 mmol, 50 mol%) were dissolved in 20 mL of deionized H_2O in a 100 mL three-neck round-bottom flask. Hydroquinone (110 mg, 1 mmol) was

added to the flask to inhibit polymerization of the product. The flask was purged with N_2 and sealed with rubber septa. The vessel was heated to 50 ºC in an oil bath. Under positive N_2 pressure, one septum was removed from the reaction vessel and solid (*E*)-1,4-dibromo-2-butene (***E*-10**) (10.72 g, 50.1 mmol, 1 equiv) was added in ~2 g increments to the vigorously stirring KCN/18-crown-6 solution over the course of 15 min. The reaction mixture darkened to a reddish-brown color during the addition of ***E*-10**. The reaction was cooled to room temperature and rinsed into a separatory funnel with 10 mL diethyl ether and 10 mL deionized H_2O. The organic layer was separated, and the aqueous layer was extracted with diethyl ether (4 × 25 mL). The combined organic layers were washed with sat. aq. NaCl (1 × 25 mL) and dried over anhydrous $CaCl_2$. The drying agent was removed by gravity filtration and the ethereal solvent was removed by fractional distillation at atmospheric pressure (45 cm glass bead packed column). The product was purified by vacuum distillation through the same apparatus to yield 1-cyano-1,3-butadiene (**1**) (34%, 2:3 *E*:*Z*) as a colorless oil (bp 75 ºC, 100 Torr). Subsequent fractional distillations through the same apparatus can be performed to further separate ***Z*-1** from ***E*-1**. Compound ***Z*-1** exhibits greater thermal stability than ***E*-1**, presumably due to lower reactivity with respect to dimerization or polymerization. ^{1}H-NMR (C_6D_6, 500 MHz): δ (ppm) ***Z*-1**: 6.58 (dt, 1H, J = 16.8, 10.6 Hz), 5.98 (t, 1H, J = 10.9 Hz), 5.02 (d, 1H, J = 16.8 Hz), 5.0 (d, 1H, J = 10.2 Hz), 4.48 (d, 1H, J = 10.7 Hz). ^{13}C{^{1}H}-NMR (C_6D_6, 125 MHz): δ (ppm) 148.7, 132.7, 126.2, 115.9, 98.4. IR (neat): (cm^{-1}) 3071 (w), 2216 (m), 1628 (w), 1574 (m), 1428 (w), 1359 (w), 1296 (w), 1229 (w), 1001 (m), 934 (s), 778 (m), 667 (s), 487 (w), 444 (w). HRMS (ESI) *m/z*: $[M+H]^+$ Calcd for C_5H_6N: 80.0495. Found: 80.0494.

4-Chloro-2-butyne-1-ol (7). In a slight modification to literature procedures:[129-132] 59.75 g (0.69 mol, 1 equiv) 2-butyne-1,4-diol (**6**), 70 mL dry dichloromethane, and 62 mL (770 mmol,

1.1 equiv) dry pyridine were added to a 1-L flame-dried three-neck round-bottom flask under an N_2 atmosphere. The stirring reaction vessel was cooled to 0 ºC on ice, and 56 mL (92 g, 772 mmol) $SOCl_2$ was added dropwise over a time of 4 h *via* pressure-equalizing addition funnel. A white precipitate formed over the course of the $SOCl_2$ addition. The reaction was then poured onto 200 mL of ice water, and subsequently extracted with dichloromethane (3 × 150 mL). The combined organic layers were washed with saturated aqueous $NaHCO_3$ (1 × 100 mL), saturated aqueous NaCl (1 × 100 mL), and dried over anhydrous Na_2SO_4. After removal of the drying agent by gravity filtration, dichloromethane was removed *in vacuo* to yield a deep red oil. The crude product was purified by vacuum distillation using a short path apparatus to yield 42.32 g (58%) of colorless 4-chloro-2-butyne-1-ol (**7**), bp 50 ºC (0.5 Torr). **CAUTION: 4-chloro-2-butyne-1-ol is highly explosive and a powerful skin irritant – care must be used when handling.**[133] ^{1}H-NMR ($CDCl_3$, 500 MHz): δ (ppm) 4.33 (t, 2H, $^5J = 2$ Hz), 4.19 (t, 2H, $^5J = 2$ Hz). $^{13}C\{^1H\}$-NMR ($CDCl_3$, 125 MHz): δ (ppm) 84.6, 80.5, 51.1, 30.3. HRMS (ESI) *m/z*: $[M+H]^+$ Calcd for C_4H_5ClO; [^{35}Cl]-isotopologue; Calcd: 105.0107. Found: 105.0102; [^{37}Cl]-isotopologue; Calcd: 107.0078. Found: 107.0072.

1,2-Butadien-4-ol (8). Early Method:[130-131] Lithium aluminum hydride (6.0902 g, 16 mmol) and dry diethyl ether (80 mL) was added to a flame-dried 250 mL three-neck round-bottom flask fitted with a dry ice condenser under an N_2 atmosphere and stirred to generate a slurry. 4-Chloro-2-butyne-1-ol (**7**) (4.19 g, 40 mmol) was diluted with 16 mL dry diethyl ether and delivered dropwise *via* syringe to the stirring LAH slurry at a rate sufficient to maintain a gentle reflux. After the addition of **7**, the reaction was stirred for 30 min at 25 ºC. The reaction was cooled to 0 ºC on ice and the septa were removed. The reaction was quenched *via* Fieser workup: (slow addition of 6 mL deionized H_2O, then 6 mL 15% aqueous NaOH, and finally 18 mL deionized H_2O). A scoop

of anhydrous Na_2SO_4 was added to promote aggregation of the precipitated aluminum salts and the vessel was stirred overnight at 25 ºC. The reaction mixture was filtered and the organic layer was separated. The aqueous layer was extracted with diethyl ether (3 × 25 mL). The combined organic extracts were then dried over anhydrous Na_2SO_4, filtered, and the solvent was removed *in vacuo*. The crude product was purified by vacuum distillation using a short path apparatus to yield 1.99 g (71%) of colorless 1,2-butadien-4-ol (**8**), bp 60 ºC (40 Torr).

Primary method:[115, 133] A flame-dried 5 L three-neck round-bottom flask was equipped with a reflux condenser (open to air), thermometer, and mechanical stirrer. To this vessel were added CuI (115.37 g, 605 mmol, 50 mol%), paraformaldehyde (59.53 g, 1.98 mol, 1.6 equiv) and 2.4 L dry THF. The mechanical stirrer was started, and dry diisopropylamine (240 mL, 1.71 mol, 1.4 eq.) was added – the reaction mixture appeared faint green. Propargyl alcohol (**13**) (74 g, 76 mL, 1.3 mol) was added to the reaction mixture. The addition of propargyl alcohol resulted in an immediate exotherm (increase from 20 ºC to 30 ºC) and the reaction color changed to bright orange. The reaction was heated with a mantle to reflux for 24 h. After cooling to 25 ºC, most of the THF solvent was removed *via* rotary evaporation. The concentrated reaction mixture was slowly added to a stirred, cooled (0 ºC) solution of diethyl ether (1 L) and 12 N HCl (120 mL), resulting in the formation of a viscous brown precipitate. The stirring was stopped and the mixture was allowed to separate. The supernatant ether was decanted, and the brown precipitate was extracted with diethyl ether (2 × 1 L). The combined ether extracts were filtered through a silica plug (ø = 80 mm × 50 mm), dried over anhydrous Na_2SO_4, and concentrated *in vacuo*. The crude product was purified by vacuum-distillation using a short path apparatus to yield 47.2 g (52%) of colorless 1,2-butadien-4-ol (**8**), bp 60 ºC (40 Torr). ^{1}H-NMR ($CDCl_3$, 500 MHz): δ (ppm) complex

spin system, 5.34 (apparent quint, 1H, J = 6.4 Hz), 4.85 (m, 2H, J = 3 Hz), 4.14 (m, 2H, J = 3 Hz), 2.4 (br s, 1H). $^{13}C\{^{1}H\}$-NMR ($CDCl_3$, 125 MHz): δ (ppm) 207.9, 90.8, 77.0, 60.2.

4-Chloro-1,2-butadiene (9)[113, 129, 131] 16.97 g $SOCl_2$ (10.4 mL, 143 mmol, 1.25 eq.), 11.28 g dry pyridine (11.5 mL, 143 mmol, 1.25 eq.) and 50 mL dry diethyl ether were added to a flame-dried, three-neck 500 mL round-bottom flask equipped with a pressure-equalizing addition funnel and reflux condenser under an N_2 atmosphere. The vessel was cooled to 0 ºC on an ice bath. A solution of 1,2-butadien-4-ol (**8**) (7.97 g, 114 mmol, 1 eq.) in 70 mL dry diethyl ether was delivered dropwise to the stirring reaction *via* addition funnel over 15 min. A white precipitate formed over the course of the addition. The reaction was heated to reflux in an oil bath for 2 h. The reaction was cooled to room temperature and quenched *via* addition of 15 mL deionized H_2O. The organic layer was separated and the aqueous layer was extracted with diethyl ether (3 × 15 mL). The combined organic layers were dried over anhydrous Na_2SO_4 and filtered. The ethereal solvent was removed by fractional distillation at atmospheric pressure (45 cm Vigreux column). The fractionating column was removed and the product was purified by distillation at atmospheric pressure using a short path apparatus to yield 6.10 g (60%) of 4-chloro-1,2-butadiene (**9**) as a colorless oil. bp 88 ºC (760 Torr). ^{1}H-NMR ($CDCl_3$, 500 MHz): δ (ppm) complex spin system, 5.36 (m, 1H, J = 7.7, 6.6 Hz), 4.91 (dt, 2H, J = 6.6, 2.2 Hz), 4.08 (dt, 2H, J = 7.7, 2.2 Hz). $^{13}C\{^{1}H\}$-NMR ($CDCl_3$, 125 MHz): δ (ppm) 209.5, 89.0, 77.5, 66.0.

4-Bromo-1,2-butadiene (12)[131] 21.6 g PBr_3 (10.4 mL, 80 mmol), 7.89 g dry pyridine (8 mL, 100 mmol), and 20 mL dry diethyl ether were added to a flame-dried, single-neck 250 mL round-bottom flask equipped with a pressure-equalizing addition funnel under an N_2 atmosphere. The vessel was cooled to 0 ºC on an ice bath. A solution of 1,2-butadien-4-ol (**8**) (14.01 g, 200 mmol, 1 eq.) in 20 mL dry diethyl ether was delivered dropwise over 15 min to the stirring reaction

via addition funnel and stirring was continued for 24 h. The reaction was allowed to warm to room temperature and quenched with 100 mL deionized H_2O. The layers were separated, and the aqueous layer was extracted with diethyl ether (4 × 75 mL). The combined organic extracts were washed with saturated aqueous NaCl (1 × 75 mL) and dried over anhydrous Na_2SO_4. After removal of the drying agent by filtration, the solvent was removed *in vacuo*. The crude product was purified by vacuum-distillation using a short path apparatus to yield 17.73 g (67%) of colorless 4-Bromo-1,2-butadiene (**12**), bp 62 °C (100 Torr). ^{1}H-NMR ($CDCl_3$, 500 MHz): δ (ppm) complex spin system, 5.45 (m, 1H, J = 8.1, 6.5 Hz), 4.93 (dt, 2H, J = 6.6, 2.2 Hz), 3.96 (dt, 2H, J = 8.2, 2.0 Hz). ^{13}C{^{1}H}-NMR ($CDCl_3$, 125 MHz): δ (ppm) 209.8, 89.5, 77.5, 30.1.

4-Cyano-1,2-butadiene (3) (2,3-Pentadienenitrile). 3.38 g (25.4 mmol) 4-Bromo-1,2-butadiene (**12**), was added to a flame-dried 100 mL single-neck round-bottom flask. The reaction vessel was then sealed with a septum and purged with N_2 *via* syringe needle inlet. Dry acetonitrile (10 mL) was added *via* syringe and the stirring vessel was cooled to 0 ºC on ice. A solution of 6.70 g (24.99 mmol) tetrabutylammonium cyanide (TBAC) in 15 mL dry acetonitrile was delivered dropwise to the vigorously stirring reaction over 1 h *via* syringe pump. The reaction was allowed to stir at 0 ºC for 15 min after the TBAC addition had completed. The ^{1}H-NMR spectrum of a reaction aliquot showed complete conversion of **3** with minimal (< 2%) isomerization to ***E*-1** and ***Z*-1**. The reaction was then rinsed into a separatory funnel with 50 mL diethyl ether and 30 mL cold deionized H_2O (0 ºC). The organic layer was separated, and the aqueous layer was extracted with diethyl ether (3 × 25 mL). The combined organic layers were washed with deionized H_2O (5 × 25 mL), saturated aqueous NaCl (1 × 25 mL), and dried over anhydrous Na_2SO_4. After removal of the drying agent by gravity filtration, the ethereal solvent was removed by fractional distillation at atmospheric pressure *via* short path apparatus. From the resulting concentrate, 4-cyano-1,2-

butadiene (**3**) was purified either by flash column chromatography (SiO_2, 3:1 *n*-pentane:Et_2O, R_f = 0.5) or by distillation (bp 94 ºC, 100 Torr). Isolated yield: 62%. ^{1}H-NMR ($CDCl_3$, 500 MHz): δ (ppm) complex spin system; 5.13 (apparent quint, 1H, J = 6.4 Hz), 4.97 (m, 2H, J = 3.3 Hz), 3.09 (m, 2H, J = 3.3 Hz). ^{13}C{^{1}H}-NMR ($CDCl_3$, 125 MHz): δ (ppm) 209.0, 117.3, 81.2, 78.6, 17.5. IR (neat): (cm^{-1}) 2252 (w), 1960 (w), 1417 (w), 913 (w), 852 (s), 731 (w), 678 (w), 521 (w), 467 (w). HRMS (ESI) *m/z*: $[M+H]^+$ Calcd for C_5H_6N: 80.0495. Found: 80.0495.

3-Hydroxy-2-methylenebutanenitrile (17). Acrylonitrile (**16**) (13.64 g, 257 mmol, 1 equiv), acetaldehyde (11.4 g, 259 mmol, 1 equiv) and 1,4-diazabicyclo[2.2.2]octane (DABCO) (5.64 g, 50 mmol, 20 mol%) were added to a 250 mL single-neck round-bottom flask. The vessel was sealed with a septum and stirred for 96 h. The ^{1}H-NMR spectrum of a reaction aliquot showed complete conversion after 96 h. The crude product was put on a vacuum line (~100 Torr) to remove any unreacted acrylonitrile and acetaldehyde and the crude 3-hydroxy-2-methylenebutanenitrile (**17**) was used in the next synthetic step without further purification (clear amber liquid). ^{1}H-NMR ($CDCl_3$, 500 MHz): δ (ppm) 6.0 (d, 1H, J = 1.4 Hz), 5.94 (s, 1H), 4.38 (qt, 1H, J = 6.4, 1.2 Hz), 3.90 (brs, 1H), 1.41 (d, 3H, J = 6.5 Hz). ^{13}C{^{1}H}-NMR ($CDCl_3$, 125 MHz): δ (ppm) 128.9, 128.4, 117.3, 68.0, 22.3.

2-Cyano-1,3-butadiene (2). K_2CO_3 (0.19 g, 1.4 mmol, 1.8 mol%) and 1.2 mL deionized H_2O were added to a 50 mL round-bottom flask containing the crude 3-hydroxy-2-methylene-butanitrile (**17**) from the preceding synthetic step. Hydroquinone (20 mg) was added to the mixture to inhibit polymerization during the subsequent distillation. The vessel was connected to a short path distillation apparatus and a vacuum of 100 Torr was applied to the system. The boiling flask was immersed in an oil bath at 100 ºC and the reaction was stirred vigorously to break the surface tension. The distillation head temperature increased to 52 ºC as colorless distillate immediately

started condensing as a biphasic mixture. A total 8.6 g of biphasic distillate was collected over 1 h. Over the elapsed collection time, the contents of the boiling flask darkened to a dark red color and the collection rate slowed. The colorless product (the organic layer of the distillate) was separated and dried over anhydrous Na_2SO_4 /activated charcoal. The drying and decolorizing agents were removed by filtration through a fine glass frit to yield 3.21 g (51%) of 2-cyano-1,3-butadiene (**2**) as a colorless oil. When stabilized with hydroquinone, **2** can be purified *via* vacuum distillation (bp 55 ºC, 100 Torr). Compound **2** is prone to undergo polymerization, even at –20 ºC. ^{1}H-NMR ($CDCl_3$, 500 MHz): δ (ppm) 6.35 (dd, 1H, J = 17.2, 10.4 Hz), 5.94 (s, 1H), 5.86 (s, 1H), 5.73 (d, 1H, J = 17.2 Hz), 5.47 (d, 1H, J = 10.4 Hz). ^{13}C{^{1}H}-NMR ($CDCl_3$, 125 MHz): δ (ppm) 132.2, 130.5, 122.5, 120.7, 115.9. IR (neat): (cm^{-1}) 2986 (w), 2233 (w), 1736 (m), 1582 (w), 1378 (m), 1244 (m), 1045 (w), 983 (m), 924 (s), 492 (m). HRMS (ESI) *m/z*: $[M+H]^+$ Calcd for C_5H_6N: 80.0495. Found: 80.0494.

References

1. Endres, C. P.; Schlemmer, S.; Schilke, P.; Stutzki, J.; Müller, H. S. P., The Cologne Database for Molecular Spectroscopy, CDMS, in the Virtual Atomic and Molecular Data Centre, VAMDC. *J. Mol. Spectrosc.* **2016,** *327*, 95-104.

2. Müller, H. S. P.; Schlöder, F.; Stutzki, J.; Winnewisser, G., The Cologne Database for Molecular Spectroscopy, CDMS: A Useful Tool for Astronomers and Spectroscopists. *J. Mol. Struct.* **2005,** *742* (1), 215-227.

3. Sagan, C.; Khare, B. N., Tholins: Organic Chemistry of Interstellar Grains and Gas. *Nature* **1979,** *277* (5692), 102-107.

4. Herbst, E., Chemistry in the Interstellar Medium. *Annu. Rev. Phys. Chem.* **1995,** *46* (1), 27-54.

5. Garrod, R. T.; Widicus Weaver, S. L.; Herbst, E., Complex Chemistry in Star-Forming Regions: An Expanded Gas-Grain Warm-Up Chemical Model. *Astrophys. J.* **2008,** *682*, 283-302.

6. Costes, M.; Naulin, C., Studies of Reactions Relevant to Astrochemistry. *Annu. Rev. Phys. Chem. C* **2013,** *109* (0), 189-210.

7. Agúndez, M.; Wakelam, V., Chemistry of Dark Clouds: Databases, Networks, and Models. *Chem. Rev.* **2013,** *113* (12), 8710-8737.

8. Cumper, C. W. N.; Dev, S. K.; Landor, S. R., Electric Dipole Moments of Acrylonitriles, Allyl Cyanides, and Alicyclic Nitriles. *J. Chem. Soc., Perkin Trans. 2* **1973,** (5), 537-540.

9. Hannay, N. B.; Smyth, C. P., The Dipole Moments and Structures of Ketene and of Several Polar Molecules Containing Conjugated Systems. *J. Am. Chem. Soc.* **1946,** *68*, 1357-1360.

10. Soundararajan, S., Charge Distribution, Electric Dipole Moments, and Molecular Structure of Nitriles. *Indian J. Chem.* **1963,** *1* (12), 503-506.

11. McGuire, B. A.; Burkhardt, A. M.; Kalenskii, S. V.; Shingledecker, C. N.; Remijan, A. J.; Herbst, E.; McCarthy, M. C., Detection of the Aromatic Molecule Benzonitrile (*c*-C_6H_5CN) in the Interstellar Medium. *Science* **2018,** *359* (6372), 202-205.

12. Zeng, S.; Quénard, D.; Jiménez-Serra, I.; Martín-Pintado, J.; Rivilla, V. M.; Testi, L.; Martín-Doménech, R., First Detection of the Pre-Biotic Molecule Glycolonitrile ($HOCH_2CN$) in the Interstellar Medium. *Mon Not R Astron Soc., Lett.* **2019,** *484* (1), L43-L48.

13. Cernicharo, J.; Agúndez, M.; Velilla Prieto, L.; Guélin, M.; Pardo, J. R.; Kahane, C.; Marka, C.; Kramer, C.; Navarro, S.; Quintana-Lacaci, G.; Fonfría, J. P.; Marcelino, N.; Tercero, B.; Moreno, E.; Massalkhi, S.; Santander-García, M.; McCarthy, M. C.; Gottlieb, C. A.; Alonso, J. L., Discovery of Methyl Silane and Confirmation of Silyl Cyanide in IRC +10216. *Astron. Astrophys.* **2017,** *606*, L5.

14. Avery, L. W.; Broten, N. W.; MacLeod, J. M.; Oka, T.; Kroto, H. W., Detection of the Heavy Interstellar Molecule Cyanodiacetylene. *Astrophys. J., Lett.* **1976,** *205* (3), L173-L175.

15. Broten, N. W.; Oka, T.; Avery, L. W.; MacLeod, J. M.; Kroto, H. W., The Detection of Cyanooctatetrayne (HC_9N) in Interstellar Space. *Astrophys. J., Lett.* **1978,** *223* (2), L105-L107.

16. Kroto, H. W.; Kirby, C.; Walton, D. R. M.; Avery, L. W.; Broten, N. W.; MacLeod, J. M.; Oka, T., The Detection of Cyanohexatriyne, $H(C{\equiv}C)_3CN$, in Heiles's Cloud 2. *Astrophys. J.* **1978,** *219* (3), L133-L137.

17. Snyder, L. E.; Buhl, D., Radio Emission from Interstellar Hydrogen Cyanide. *Astrophys. J.* **1971,** *163*, L47-L52.

18. Walmsley, C. M.; Winnewisser, G.; Toelle, F., Cyanoacetylene and Cyanodiacetylene in Interstellar Clouds. *Astron. Astrophys.* **1980,** *81*, 245-50.

19. Loomis, R. A.; Burkhardt, A. M.; Shingledecker, C. N.; Charnley, S. B.; Cordiner, M. A.; Herbst, E.; Kalenskii, S.; Lee, K. L. K.; Willis, E. R.; Xue, C.; Remijan, A. J.; McCarthy, M. C.; McGuire, B. A., An investigation of spectral line stacking techniques and application to the detection of $HC_{11}N$. *Nat. Astron.* **2021,** *5*, 188-196.

20. Broten, N. W.; MacLeod, J. M.; Avery, L. W.; Irvine, W. M.; Hoeglund, B.; Friberg, P.; Hjalmarson, A., The Detection of Interstellar Methylcyanoacetylene. *Astrophys. J.* **1984,** *276* (1, Pt. 2), L25-L29.

21. Snyder, L. E.; Hollis, J. M.; Jewell, P. R.; Lovas, F. J.; Remijan, A., Confirmation of Interstellar Methylcyanodiacetylene (CH_3C_5N). *Astrophys. J.* **2006,** *647* (1), 412-417.

22. Gardner, F. F.; Winnewisser, G., Detection of Interstellar Vinyl Cyanide (Acrylonitrile). *Astrophys. J.* **1975,** *195* (3, Pt. 2), L127-L130.

23. Lovas, F. J.; Remijan, A. J.; Hollis, J. M.; Jewell, P. R.; Snyder, L. E., Hyperfine Structure Identification of Interstellar Cyanoallene Toward TMC-1. *Astrophys. J., Lett.* **2006,** *637* (1), L37-L40.

24. Solomon, P. M.; Jefferts, K. B.; Penzias, A. A.; Wilson, R. W., Detection of Millimeter Emission Lines from Interstellar Methyl Cyanide. *Astrophys. J.* **1971,** *168* (3)(Pt. 2), L107-L110.

25. Belloche, A.; Garrod, R. T.; Müller, H. S. P.; Menten, K. M.; Comito, C.; Schilke, P., Increased Complexity in Interstellar Chemistry: Detection and Chemical Modeling of Ethyl Formate and n-Propyl Cyanide in Sagittarius B2(N). *Astron. Astrophys.* **2009,** *499* (1), 215-232.

26. Belloche, A.; Garrod, R. T.; Müller, H. S. P.; Menten, K. M., Detection of a Branched Alkyl Molecule in the Interstellar Medium: *iso*-Propyl Cyanide. *Science* **2014,** *345* (6204), 1584-1587.

27. McCarthy, M. C.; Lee, K. L. K.; Loomis, R. A.; Burkhardt, A. M.; Shingledecker, C. N.; Charnley, S. B.; Cordiner, M. A.; Herbst, E.; Kalenskii, S.; Willis, E. R.; Xue, C.; Remijan, A. J.; McGuire, B. A., Interstellar detection of the highly polar five-membered ring cyanocyclopentadiene. *Nat. Astron.* **2021,** *5*, 176–180.

28. McGuire, B. A.; Loomis, R. A.; Burkhardt, A. M.; Lee, K. L. K.; Shingledecker, C. N.; Charnley, S. B.; Cooke, I. R.; Cordiner, M. A.; Herbst, E.; Kalenskii, S.; Siebert, M. A.; Willis, E. R.; Xue, C.; Remijan, A. J.; McCarthy, M. C., Detection of two interstellar polycyclic aromatic hydrocarbons via spectral matched filtering. *Science* **2021,** *371*, 1265–1269.

29. McCarthy, M. C.; McGuire, B. A., Aromatics and Cyclic Molecules in Molecular Clouds: A New Dimension of Interstellar Organic Chemistry. *J. Phys. Chem. A* **2021,** *125* (16), 3231–3243.

30. Halter, R. J.; Fimmen, R. L.; McMahon, R. J.; Peebles, S. A.; Kuczkowski, R. L.; Stanton, J. F., Microwave Spectra and Molecular Structures of (Z)-Pent-2-en-4-ynenitrile and Maleonitrile. *J. Am. Chem. Soc.* **2001,** *123* (49), 12353-12363.

31. Charnley, S. B.; Kuan, Y.-J.; Huang, H.-C.; Botta, O.; Butner, H. M.; Cox, N.; Despois, D.; Ehrenfreund, P.; Kisiel, Z.; Lee, Y.-Y.; Markwick, A. J.; Peeters, Z.; Rodgers, S. D., Astronomical Searches for Nitrogen Heterocycles. *Adv. Space Res.* **2005,** *36* (2), 137-145.

32. McCarthy, M. C.; Lee, K. L. K.; Carroll, P. B.; Porterfield, J. P.; Changala, P. B.; Thorpe, J. H.; Stanton, J. F., Exhaustive Product Analysis of Three Benzene Discharges by Microwave Spectroscopy. *J. Phys. Chem. A* **2020,** *124* (25), 5170-5181.

33. Mishra, P.; Fritz, S. M.; Herbers, S.; Mebel, A. M.; Zwier, T. S., Gas-Phase Pyrolysis of *trans* 3-Pentenenitrile: Competition between Direct and Isomerization-Mediated Dissociation. *Phys. Chem. Chem. Phys.* **2021,** *23*, 6462–6471.

34. Tsukamoto, A.; Lichtin, N. N., Reactions of Active Nitrogen with Organic Substrates. I. The Monomeric Products of the Reaction with 1,3-Butadiene. *J. Am. Chem. Soc.* **1962,** *84* (9), 1601-1605.

35. Sun, B. J.; Huang, C. H.; Chen, S. Y.; Chen, S. H.; Kaiser, R. I.; Chang, A. H. H., Theoretical Study on Reaction Mechanism of Ground-State Cyano Radical with 1,3-Butadiene: Prospect of Pyridine Formation. *J. Phys. Chem. A* **2014,** *118* (36), 7715-7724.

36. Morales, S. B.; Bennett, C. J.; Le Picard, S. D.; Canosa, A.; Sims, I. R.; Sun, B. J.; Chen, P. H.; Chang, A. H. H.; Kislov, V. V.; Mebel, A. M.; Gu, X.; Zhang, F.; Maksyutenko, P.; Kaiser, R. I., A Crossed Molecular Beam, Low-Temperature Kinetics, And Theoretical Investigation Of The Reaction Of The Cyano Radical (CN) With 1,3-Butadiene (C_4H_6). A Route To Complex Nitrogen-Bearing Molecules In Low-Temperature Extraterrestrial Environments. *Astrophys. J.* **2011,** *742* (1), 26.

37. McKellar, A., Evidence for the Molecular Origin of Some Hitherto Unidentified Interstellar Lines. *Publ. Astron. Soc. Pac.* **1940,** *52*, 187.

38. Baraban, J. H.; Martin-Drumel, M.-A.; Changala, P. B.; Eibenberger, S.; Nava, M.; Patterson, D.; Stanton, J. F.; Ellison, G. B.; McCarthy, M. C., The Molecular Structure of gauche-1,3-Butadiene: Experimental Establishment of Non-planarity. *Angew. Chem., Int. Ed.* **2018,** *57* (7), 1821-1825.

39. Balucani, N.; Asvany, O.; Huang, L. C. L.; Lee, Y. T.; Kaiser, R. I.; Osamura, Y.; Bettinger, H. F., Formation of Nitriles in the Interstellar Medium *via* Reactions of Cyano Radicals, $CN(X\,^2\Sigma^+)$, with Unsaturated Hydrocarbons. *Astrophys. J.* **2000,** *545* (2), 892-906.

40. Jamal, A.; Mebel, A. M., Theoretical Investigation of the Mechanism and Product Branching Ratios of the Reactions of Cyano Radical with 1- and 2-Butyne and 1,2-Butadiene. *J. Phys. Chem. A* **2013,** *117* (4), 741-755.

41. Zdanovskaia, M. A.; Esselman, B. J.; Kougias, S. M.; Patel, A. R.; Woods, R. C.; McMahon, R. J., The 130-360 GHz rotational spectrum of *syn*-2-cyano-1,3-butadiene (C_5H_5N) - a molecule of astrochemical relevance. *Mol. Phys.* **2021,** *119* (21-22), e1964629.

42. Sagan, C.; Thompson, W. R.; Khare, B. N., Titan: a laboratory for prebiological organic chemistry. *Acc. Chem. Res.* **1992,** *25* (7), 286-292.

43. Waite, J. H.; Niemann, H.; Yelle, R. V.; Kasprzak, W. T.; Cravens, T. E.; Luhmann, J. G.; McNutt, R. L.; Ip, W.-H.; Gell, D.; De La Haye, V.; Müller-Wordag, I.; Magee, B.; Borggren, N.; Ledvina, S.; Fletcher, G.; Walter, E.; Miller, R.; Scherer, S.; Thorpe, R.; Xu, J.; Block, B.; Arnett, K., Ion Neutral Mass Spectrometer Results from the First Flyby of Titan. *Science* **2005,** *308* (5724), 982.

44. Waite, J. H.; Young, D. T.; Cravens, T. E.; Coates, A. J.; Crary, F. J.; Magee, B.; Westlake, J., The Process of Tholin Formation in Titan's Upper Atmosphere. *Science* **2007,** *316* (5826), 870.

45. Desai, R. T.; Coates, A. J.; Wellbrock, A.; Vuitton, V.; Crary, F. J.; González-Caniulef, D.; Shebanits, O.; Jones, G. H.; Lewis, G. R.; Waite, J. H., Carbon chain anions and the growth of complex organic molecules in Titan's ionosphere. *Astrophys. J., Lett.* **2017,** *844* (2), L18.

46. McGuigan, M.; Waite, J. H.; Imanaka, H.; Sacks, R. D., Analysis of Titan tholin pyrolysis products by comprehensive two-dimensional gas chromatography–time-of-flight mass spectrometry. *J. Chromatogr. A* **2006,** *1132* (1), 280-288.

47. Morisson, M.; Szopa, C.; Carrasco, N.; Buch, A.; Gautier, T., Titan's organic aerosols: Molecular composition and structure of laboratory analogues inferred from pyrolysis gas chromatography mass spectrometry analysis. *Icarus* **2016,** *277*, 442-454.

48. Nixon, C. A.; Thelen, A. E.; Cordiner, M. A.; Kisiel, Z.; Charnley, S. B.; Molter, E. M.; Serigano, J.; Irwin, P. G.; Teanby, N. A.; Kuan, Y.-J., Detection of Cyclopropenylidene on Titan with ALMA. *Astrophys. J.* **2020,** *160* (5), 205.

49. Thompson, W. R.; Henry, T. J.; Schwartz, J. M.; Khare, B. N.; Sagan, C., Plasma discharge in $N_2 + CH_4$ at low pressures: Experimental results and applications to Titan. *Icarus* **1991,** *90* (1), 57-73.

50. Guillemin, J. C.; Ferris, J. P., Photochemistry of unsaturated nitriles on Titan. *Eur. Space Agency, Spec. Publ.* **1992,** *ESA SP-338* (Proc. - Symp. Titan, 1991), 177-81.

51. Ferris, J. P.; Guillemin, J. C., Photochemical cycloaddition reactions of cyanoacetylene and dicyanoacetylene. *J. Org. Chem.* **1990,** *55* (21), 5601-6.

52. Gale, D. M., Mechanistic aspects of the photochemistry of unsaturated nitriles. *J. Org. Chem.* **1970,** *35* (4), 970-2.

53. Sarner, S. F.; Gale, D. M.; Hall, H. K., Jr.; Richmond, A. B., Gas-phase thermolysis kinetics of small ring nitriles. *J. Phys. Chem.* **1972,** *76* (20), 2817-19.

54. Gale, D. M.; Cherkofsky, S. C., Dehydrocyanation of dinitriles. Preparation of 1-cyclobutenecarbonitrile by direct dehydrocyanation of 1,2-cyclobutanedicarbonitrile. *J. Org. Chem.* **1973,** *38* (3), 475-8.

55. Cyanopyridine isomers represent alternate proxies for pyridine.

56. Dorman, P. M.; Esselman, B. J.; Park, J. E.; Woods, R. C.; McMahon, R. J., Millimeter-wave spectrum of 4-cyanopyridine in its ground state and lowest-energy vibrationally excited states, ν_{20} and ν_{30}. *J. Mol. Spectrosc.* **2020,** *369*, 111274.

57. Dorman, P. M.; Esselman, B. J.; Woods, R. C.; McMahon, R. J., An analysis of the rotational ground state and lowest-energy vibrationally excited dyad of 3-

cyanopyridine: Low symmetry reveals rich complexity of perturbations, couplings, and interstate transitions. *J. Mol. Spectrosc.* **2020,** *373*, 111373.

58. Raffaelli, N., Nicotinamide Coenzyme Synthesis: A Case of Ribonucleotide Emergence or a Byproduct of the RNA World? . In *Origins of Life: The Primal Self-Organization*, Egel, R.; Lankenau, D.-H.; Mulkidjanian, A. Y., Eds. Springer-Verlag: Heidelberg, 2011; p 191.

59. McMurtry, B. M.; Turner, A. M.; Saito, S. E. J.; Kaiser, R. I., On the formation of niacin (vitamin B3) and pyridine carboxylic acids in interstellar model ices. *Chem. Phys.* **2016,** *472*, 173-184.

60. Pizzarello, S.; Huang, Y., The deuterium enrichment of individual amino acids in carbonaceous meteorites: A case for the presolar distribution of biomolecule precursors. *Geochim. Cosmochim. Acta* **2005,** *69* (3), 599-605.

61. Pizzarello, S.; Huang, Y.; Fuller, M., The carbon isotopic distribution of Murchison amino acids. *Geochim. Cosmochim. Acta* **2004,** *68* (23), 4963-4969.

62. Parker, D. S. N.; Kaiser, R. I., On the formation of nitrogen-substituted polycyclic aromatic hydrocarbons (NPAHs) in circumstellar and interstellar environments. *Chem. Soc. Rev.* **2017,** *46* (2), 452-463.

63. Zdanovskaia, M. A.; Dorman, P. M.; Orr, V. L.; Owen, A. N.; Kougias, S. M.; Esselman, B. J.; Woods, R. C.; McMahon, R. J., Rotational Spectra of Three Cyanobutadiene Isomers (C_5H_5N) of Relevance to Astrochemistry and Other Harsh Reaction Environments. *J. Am. Chem. Soc.* **2021,** *143* (25), 9551-9564.

64. Kougias, S. M.; Knezz, S. N.; Owen, A. N.; Sanchez, R. A.; Hyland, G. E.; Lee, D. J.; Patel, A. R.; Esselman, B. J.; Woods, R. C.; McMahon, R. J., Synthesis and Characterization of Cyanobutadiene Isomers—Molecules of Astrochemical Significance. *J. Org. Chem.* **2020,** *85* (9), 5787-5798.

65. Carothers, W. H.; Kirby, J. E.; Collins, A. M., Acetylene Polymers and their Derivatives. V. The Polymerization of Bromoprene (Third Paper on New Synthetic Rubbers). *J. Am. Chem. Soc.* **1933,** *55* (2), 789-795.

66. Carothers, W. H.; Berchet, G. J., Acetylene polymers and their derivatives. X. The chlorination of the hydrochlorides of vinylacetylene. *J. Am. Chem. Soc.* **1933,** *55*, 1628-31.

67. Carothers, W. H.; Berchet, G. J., Acetylene Polymers and their Derivatives. XV. Halo-4-butadienes-1,2. The mechanism of 1,4-Addition and of α,γ-Rearrangement. *J. Am. Chem. Soc.* **1933,** *55*, 2807-2813.

68. Carothers, W. H.; Berchet, G. J. Butadienyl Compounds. U.S. Patent 2073363, 1937.

69. Coffman, D. D., Acetylene Polymers and their Derivatives. XXIII. 4-Cyano-1,3-butadiene. *J. Am. Chem. Soc.* **1935,** *57*, 1981-4.

70. Carothers, W. H.; Berchet, G. J. Reaction Products From a 4-Halo-1,2-butadiene and Alkaline Earth or Alkali Metal Compounds. U.S. Patent 2136178, 1938.

71. Snyder, H. R.; Stewart, J. M.; Myers, R. L., 1-Cyano-1,3-butadienes: *cis*, *trans*-Isomers of 1-Cyano-1,3-butadiene. *J. Am. Chem. Soc.* **1949,** *71*, 1055-1056.

72. Snyder, H. R.; Poos, G. L., 1-Cyano-1,3-butadiene. III. The Dimer of 1-Cyano-1,3-butadiene. *J. Am. Chem. Soc.* **1949,** *71*, 1395-1396.

73. Snyder, H. R.; Poos, G. I., 1-Cyano-1,3-butadienes. IV. Diels-Alder Reactions with Dienes. *J. Am. Chem. Soc.* **1950,** *72*, 4096-4103.

74. Snyder, H. R.; Murdock, K. C.; Marvel, C. S., 1-Cyano-1,3-butadienes. VI. Copolymerization of the *cis*- and *trans*-1-cyano-1,3-butadienes with Butadiene. *J. Am. Chem. Soc.* **1953,** *75*, 4742-4746.

75. Bissinger, W. E.; Fredenburg, R. H.; Kadesch, R. G.; Kung, F.; Langston, J. H.; Stevens, H. C.; Strain, F., Some Reactions of Butadiene Monochlorohydrin, 1-Chloro-3-buten-2-ol. *J. Am. Chem. Soc.* **1947,** *69*, 2955-2961.

76. Wise, P. H. 1-Cyano-1,3-butadiene. U.S. Patent 2473486, 1949.

77. Gudgeon, H.; Hill, R.; Isaacs, E., Preparation of Some Substituted Butadienes. *J. Chem. Soc.* **1951**, 1926-1928.

78. Daessle, C.; Tarlton, E. J.; McKay, A. F., *trans*-1-Cyano-4-chloro-2-butene. *Can. J. Chem.* **1959,** *37*, 629-631.

79. Lambert, A.; Makinson, G. K.; Hill, A. 1-Cyano-1,3-butadiene. British Patent GB1040308, 1966.

80. Descotes, G.; Robbe, P., Synthesis of Unsaturated Nitriles Structurally Related to Butadiene and Isoprene. *Bull. Soc. Chim. Fr.* **1969,** (4), 1349-55.

81. Wei, P. E.; Milliman, G. E., Synthesis and Polymerization of 1- and 2-Cyano-1,3-butadienes. *J. Polym. Sci., Part A-1: Polym. Chem.* **1969,** *7* (8), 2305-2317.

82. Ikawa, T.; Nishizawa, T.; Suzuki, H.; Maurata, A., Preparation of 1-Cyano-1,3-butadiene by Ammoxidation of 1,3-Pentadiene. *Sekiyu Gakkai Shi* **1972,** *15* (11), 941-943.

83. Katagiri, T.; Nito, T.; Takabe, K.; Tanaka, J., Derivatives of Isoprene. IV. Synthesis of Cyanodienes and their Photosensitized Dimerization. *Nippon Kagaku Kaishi* **1974,** (12), 2370-2374.

84. Fischer, R.; Weitz, H. M.; Kempe, U. 1-Cyano-1,3-butadiene. German Patent DE2745873A1, 1979.

85. Braun, M.; Mroß, S.; Schwarz, I., Mild and Stereoconvergent Palladium-Catalyzed Carbonyl Alkenylation Reaction of α,β-Unsaturated Aldehydes. *Synthesis* **1998,** (1), 83-88.

86. Clary, K. N.; Back, T. G., Preparation of Unsaturated Aminonitriles from the Aza-Morita-Baylis-Hillman Reactions of Aldimines with Penta-2,4-dienenitrile. *Synlett* **2007,** (19), 2995-2998.

87. Banert, K., The Chemistry of Unusually Functionalized Azides. *Synthesis* **2016,** *48* (15), 2361-2375.

88. Co., F. T. R. Improvements in or relating to stabilized rubber compositions and method of producing same. 1951.

89. Carter, A. S.; Johnson, F. W. 2-Cyano-1,3-butadiene. GB569036, 1945.

90. Carter, A. S.; Johnson, F. W. 2-Cyano-1,3-butadiene. US2205239, 1940.

91. Grasselli, R. K.; Greene, J. L.; Gray, N. R. 2-Cyanobutadienes. US3347902, 1967.

92. Nonaka, Y.; Kihara, K.; Hironaka, T.; Oda, Y. 2-Cyano-1,3-alkadienes. JP53037618A, 1978.

93. Nonaka, Y.; Kihara, K.; Hironaka, T.; Oda, Y., A novel synthesis of 2-cyano-1, 3-butadiene. *Toyo Soda Kenkyu Hokoku* **1976,** *20* (1), 9-11.

94. Nonaka, Y.; Kihara, K.; Hironaka, T.; Oda, Y. 2-Cyano-1,3-butadiene. JP51029443A, 1976.

95. Nonaka, Y.; Kihara, K.; Hironaka, T.; Oda, Y. Conjugated dienenitrile. DE2456126A1, 1975.

96. Rickborn, B., The retro-Diels-Alder reaction. Part I. C-C dienophiles. *Org. React.* **1998,** *52*, No pp. given.

97. Maciagiewicz, I.; Dybowski, P.; Skowronska, A., A general one-post synthesis of vinyl-thiiranes and conjugated dienes. *Pol. J. Chem.* **2005,** *79* (3), 515-523.

98. Maciagiewicz, I.; Dybowski, P.; Skowronska, A., A general one-pot synthesis of vinylthiiranes and conjugated dienes. *Tetrahedron Lett.* **1999,** *40* (19), 3791-3794.

99. Marvel, C. S.; Brace, N. O., Dimer of 2-cyano-1,3-butadiene. *J. Am. Chem. Soc.* **1949,** *71*, 37-40.

100. Marvel, C. S.; Brace, N. O., Allylic rearrangement in the pyrolysis of 3-acetoxy-3-cyano-1-butene. *J. Am. Chem. Soc.* **1948,** *70*, 1775-6.

101. Lichty, J. G. Cyano diolefins. US2301131, 1942.

102. Tanaka, M.; Nishimura, T.; Murata, N., Synthesis of 2-cyano-1,3-butadiene. I. *Kogyo Kagaku Zasshi* **1957,** *60*, 435-6.

103. Tanaka, M.; Murata, N., Synthesis of 2-cyano-1,3-butadiene. II. *Kogyo Kagaku Zasshi* **1957,** *60*, 437-8.

104. Tanaka, M., Emulsion polymerization of 2-cyano-1,3-butadiene. *Kogyo Kagaku Zasshi* **1958,** *61*, 1370-4.

105. Tanaka, M., Block polymerization of 2-cyano-1,3-butadiene. *Kogyo Kagaku Zasshi* **1958,** *61*, 1367-9.

106. Buono, G., New pathway to α-allenic ketones, esters, and nitriles. *Tetrahedron Lett.* **1972,** (32), 3257-9.

107. Chalchat, J. C.; Theron, F., Nucleophilic substitution of carbon-carbon double bonds. XI. α-Methyl-β-halocrotononitriles and esters. Reactions with sulfide and oxide nucleophiles. *Bull. Soc. Chim. Fr.* **1974,** (5-6, Pt. 2), 953-7.

108. Brandsma, L.; Verkruijsse, H. D., *Studies in Organic Chemistry, Vol. 8: Synthesis of Acetylenes, Allenes and Cumulenes: A laboratory Manual*. Elsevier: 1981; p 276.

109. Smith, L. I.; Swenson, J. S., Synthesis and properties of an allenic nitrile. *J. Am. Chem. Soc.* **1957,** *79*, 2962-6.

110. Reddy, G. S.; Mandell, L.; Goldstein, J. H., Synthesis and proton magnetic resonance spectrum of propargyl cyanide. *J. Am. Chem. Soc.* **1961,** *83*, 4729-31.

111. Carles, S.; Moellendal, H.; Trolez, Y.; Guillemin, J. C., Rotational spectrum of 4-methylcyanoallene ($CH_3CH=C=CH-CN$) a chiral molecule of potential astrochemical interest. *Astron. Astrophys.* **2014,** *564* (Pt. 2), A82/1-A82/5.

112. Naidu, V. R.; Posevins, D.; Volla, C. M. R.; Bäckvall, J.-E., Selective Cascade Reaction of Bisallenes via Palladium-Catalyzed Aerobic Oxidative Carbocyclization-Borylation and Aldehyde Trapping. *Angew. Chem., Int. Ed.* **2017,** *56* (6), 1590-1594.

113. Wright, M. W.; Smalley Jr, T. L.; Welker, M. E.; Rheingold, A. L., Synthesis of Cobalt-Substituted 1,3-Diene Complexes with Unusual Structures and their *exo*-Selective Diels-Alder Reactions. *J. Am. Chem. Soc.* **1994,** *116* (15), 6777-6791.

114. Pedersen, C. J., Cyclic Polyethers and their Complexes with Metal Salts. *J. Am. Chem. Soc.* **1967,** *89* (26), 7017-7036.

115. Luo, H.; Ma, S., CuI-Catalyzed Synthesis of Functionalized Terminal Allenes from 1-Alkynes. *Eur. J. Org. Chem.* **2013,** (15), 3041-3048.

116. Tayama, E.; Sugai, S., A Facile Method for the Stereoselective Preparation of (1*Z*,3*E*)-Dienyl Ethers *via* 1,4-Elimination of 1,4-Dialkoxy-(2*Z*)-alkenes with *n*-Butyllithium. *Synlett* **2006,** (06), 849-852.

117. Tayama, E.; Sugai, S., A facile method for the stereoselective preparation of (1*E*,3*E*)-4-substituted-1-amino-1,3-dienes *via* 1,4-elimination. *Tetrahedron Lett.* **2007,** *48* (35), 6163-6166.

118. Tayama, E.; Toma, Y., Stereoselective preparation of (1*Z*)- and (1*E*)-*N*-Boc-1-amino-1,3-dienes by stereospecific base-promoted 1,4-elimination. *Tetrahedron* **2015,** *71* (4), 554-559.

119. Appel, R., Tertiary Phosphane/Tetrachloromethane, a Versatile Reagent for Chlorination, Dehydration, and P-N Linkage. *Angew. Chem., Int. Ed. Engl.* **1975,** *14* (12), 801-811.

120. Wise, K. V., Physical Properties of *cis*-1-Cyano-1,3-butadiene. *J. Am. Chem. Soc.* **1954,** *76*, 3094-3096.

121. Seeman, J. I., Effect of Conformational Change on Reactivity in Organic Chemistry. Evaluations, Applications, and Extensions of Curtin-Hammett Winstein-Holness Kinetics. *Chem. Rev.* **1983,** *83* (2), 83-134.

122. Shestakov, G. K.; Airyan, S. M.; Bel'skii, F. I.; Temkin, O. N., Kinetics and mechanism of the isomerization of 4-chloro-1,2-butadiene to 2-chloro-1,3-butadiene. *Zh. Org. Khim.* **1976,** *12* (10), 2053-2057.

123. Strub, D. J.; Garbos, A.; Lochynski, S., Synthesis, lipase catalyzed kinetic resolution, and determination of the absolute configuration of enantiomers of the Morita-Baylis-Hillman adduct 3-hydroxy-2-methylenebutanenitrile. *Arkivoc* **2017,** (2), 313-323.

124. McEwen, C. N.; McKay, R. G.; Larsen, B. S., Analysis of solids, liquids, and biological tissues using solids probe introduction at atmospheric pressure on commercial LC/MS instruments. *Anal. Chem.* **2005,** *77*, 7826-7831.

125. Knezz, S. A. Synthesis, Spectroscopy, and Photochemistry of Reactive Organic Molecules. Ph.D. Dissertation, University of Wisconsin-Madison, Madison, WI, 2016.

126. Keegstra, M. A.; Verkruijsse, H. D.; Andringa, H.; Brandsma, L., Efficient procedures for 1-bromo-1,3-butadiene and 2-bromo-1,3-butadiene. *Synth. Commun.* **1991,** *21* (5), 721-726.

127. Musilek, K.; Holas, O.; Kuca, K.; Jun, D.; Dohnal, V.; Opletalova, V.; Dolezal, M., Novel series of bispyridinium compounds bearing a (*Z*)-but-2-ene linker. Synthesis and evaluation of their reactivation activity against tabun and paraoxon-inhibited acetylcholinesterase. *Bioorg. Med. Chem. Lett.* **2007,** *17* (11), 3172-3176.

128. Efskind, J.; Benneche, T.; Undheim, K., Stereoselective synthesis of alkenyl α,α'-bridged bis(glycines) using palladium promoted substitution in the bridge. *Acta Chem. Scand.* **1997,** *51* (9), 942-952.

129. Streit, U.; Birbaum, F.; Quattropani, A.; Bochet, C. G., Photocycloaddition of Arenes and Allenes. *J. Org. Chem.* **2013,** *78* (14), 6890-6910.

130. Lehrich, F.; Hopf, H.; Grunenberg, J., The Preparation and Structures of Several Cross-Conjugated Allenes ("Allenic Dendralenes"). *Eur. J. Org. Chem.* **2011,** (14), 2705-2718.

131. Molander, G. A.; Cormier, E. P., Ketyl−Allene Cyclizations Promoted by Samarium(II) Iodide. *J. Org. Chem.* **2005,** *70* (7), 2622-2626.

132. Bailey, W. J.; Fujiwara, E., Acetylenes. I. Mixed dihalides and halohydrins from butynediol. *J. Am. Chem. Soc.* **1955,** *77*, 165-166.

133. Luo, H.; Ma, D.; Ma, S., Buta-2,3-dien-1-ol. *Org. Synth.* **2017,** *94*, 153-170.

Supporting Information for Chapter 1:
Synthesis of Cyanobutadiene (C_5H_5N) Isomers – Molecules of Astrochemical Relevance.

Spectroscopic Characterization and Assignments

Mass Spectrometry: Characterization of the diene was complicated in the initial stages. Because the ^{1}H-NMR did not agree with the published values and there were unidentified side products upon initial reaction, the mass spectrometry data were crucial. Because of the size and volatility of the compound, GC-MS was the initial approach. GC-MS analysis is often complicated with products as small and volatile as cyanobutadiene because of potential interactions with the column. In addition, it is often difficult to find a solvent to dilute the sample that does not elute with the compound of interest (a similar issue to that encountered in the workup). Indeed, most elution solvents had elution times that overlapped with cyanobutadiene (**1**). In acetonitrile, however, a method was developed where the *E* and *Z* cyanobutadiene peaks were visible and resolved. Solvent mass spectral features were subtracted out to reveal an EI mass spectrum that agrees well with the NIST library spectrum for cyanobutadiene (**1**) (Figure S1.1).[1]

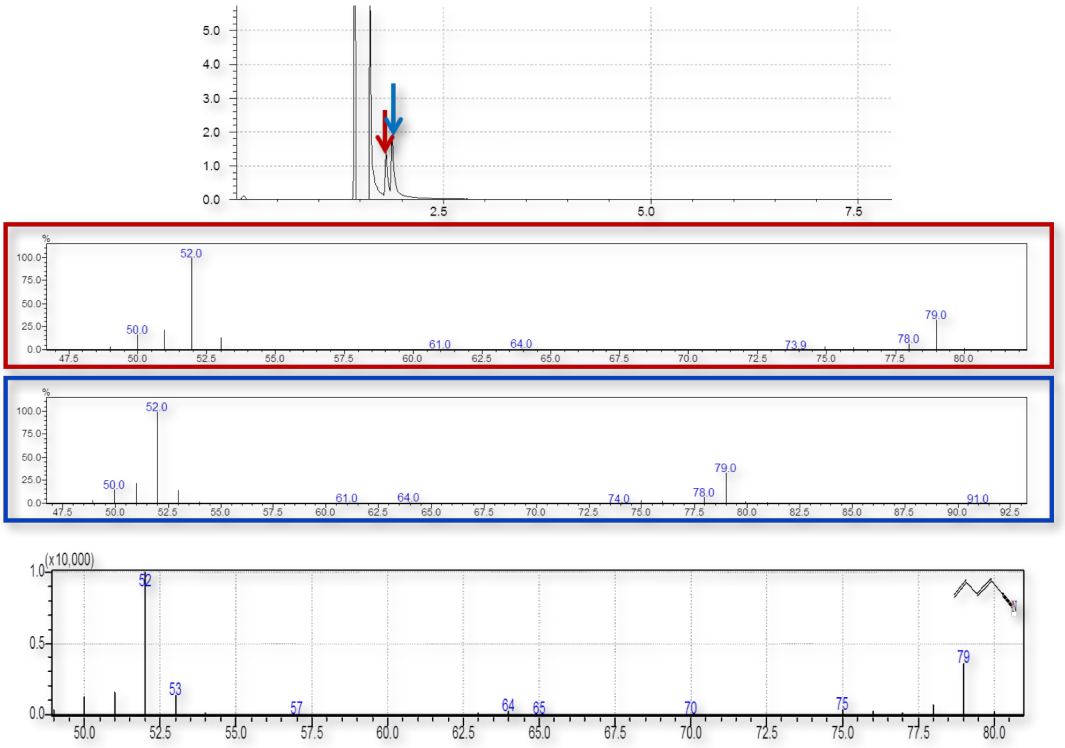


Figure S1.1. GC-MS analysis of *E* and *Z* 1-cyano-1,3-butadiene (***E*-1** and ***Z*-1**) crude reaction mixture in acetonitrile. Top: GC trace with *Z* (red arrow) and *E* (blue arrow) cyanobutadiene. Middle: Mass spectra of the indicated GC peaks with solvent subtraction. Bottom: NIST library spectrum for cyanobutadiene ***E*-1**.

It was with this information that the degradation of cyanobutadiene on the silica column was confirmed. By establishing the presence of cyanobutadiene in the crude product and its absence in purified product, it became obvious which ^{1}H-NMR signals corresponded to cyanobutadiene, and the aforementioned modifications led to progress toward purification. In order to obtain a high-resolution exact mass for the structure, we turned to a fairly new method of ionization commonly referred to as ASAP-MS (Atmospheric Solids Analysis Probe Mass Spectrometry).[2] Most high-resolution exact mass measurements are acquired by electrospray ionization. Unfortunately, many compounds, such as small hydrocarbons and alcohols, cannot be easily ionized by electrospray. The ASAP analysis works quite well for these compounds. Using

the same instrument as the ESI, the ASAP works by simply exposing the sample at the closed end of a glass capillary tube to a corona discharge. Using this method, the mass was identified within 2.5 ppm (calculated $[M+H]^+$ 80.0495, found 80.0493). In addition to providing an exact mass to four decimal places, ASAP on the Q-Exactive also provides MS/MS data. The MS/MS of **1** shows loss of CN as the major fragment (calculated 53.0386, found 53.0388), providing compelling evidence that the compound has been correctly identified (Figure S1.2).

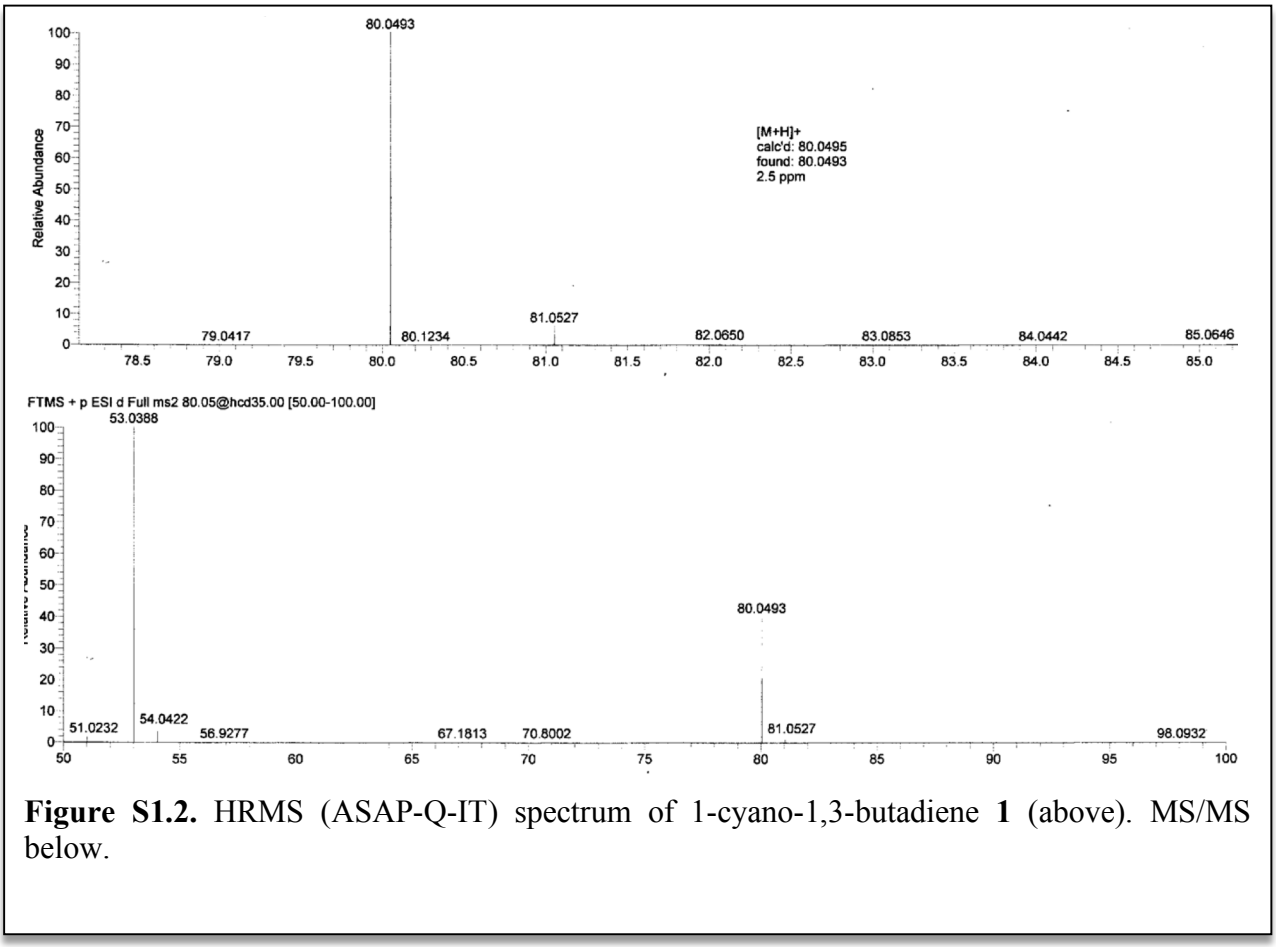


Figure S1.2. HRMS (ASAP-Q-IT) spectrum of 1-cyano-1,3-butadiene **1** (above). MS/MS below.

^{1}H-NMR Spectroscopy: One of the most challenging aspects of the characterization of **1** was the assignment of its ^{1}H-NMR spectrum. In addition to the incomplete assignment from the literature, the coupling patterns present are clearly second order and require a more sophisticated treatment for assignment. Each isomer displays the ABX characteristic of vinyl protons with the addition of coupling from the protons on the second alkene moiety. The initial spectrum in $CDCl_3$ is shown in the bottom panel of Figure S1.3. One way to get around complicated second order effects is to use NMR solvents that cause significant upfield shifts, such as benzene-*d*$_6$.[3] It is often the case with alkenes in $CDCl_3$ that two or more of the protons are nearly superimposed, and the remaining protons that are coupled to them appear as complex multiplets. By spreading out the signals in the spectrum, the degree of overlap can be significantly reduced, and the spectrum can be interpreted as first order. The upfield shift in C_6D_6 aids in the elucidation of the downfield signals, but the signals further upfield remained somewhat overlapping (Figure S1.3, top panel). As the figure shows, in order to get a clear picture of all signals in the spectrum, multiple NMR solvents (C_6D_6 – top, CD_3CN – middle, $CDCl_3$ – bottom) are required.

Using the C_6D_6 spectrum, the protons of ***E*-1** and ***Z*-1** 1-cyano-1,3-butadiene were assigned (Figure S1.4). Signals in the downfield region (top panel of Figure S1.4) are more spread out and allow for identification of coupling constants in each isomer. Relative intensities reveal which signals belong to which isomer, and from there protons in similar environments can be identified by their coupling patterns. Using the coupling constants identified in the downfield region, the overlapping signals in the upfield region can be teased apart and assigned. Some coupling in these signals is still unclear, but the assignment given is logical and consistent with expectations for a compound of this type.

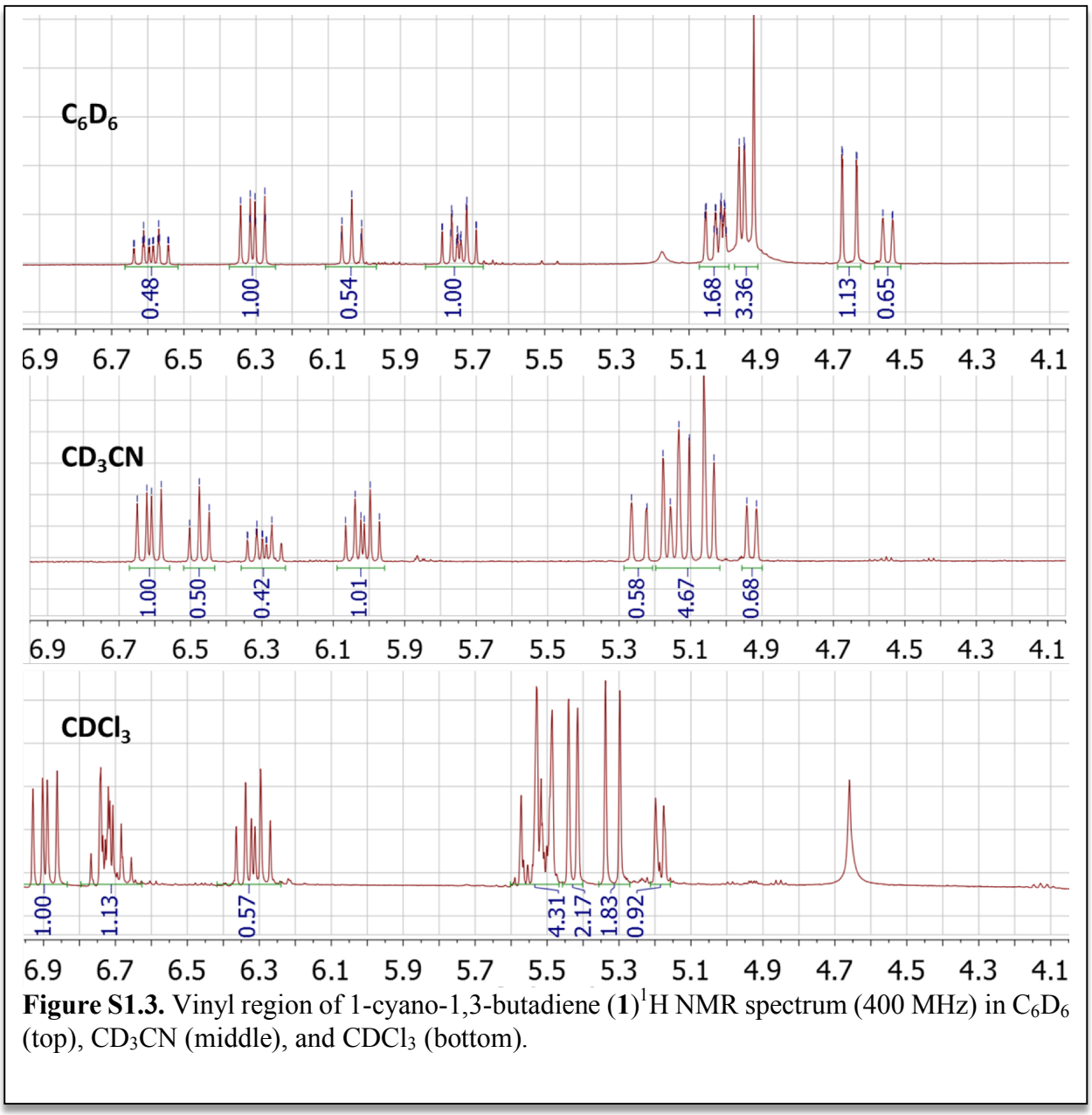


Figure S1.3. Vinyl region of 1-cyano-1,3-butadiene (**1**) ^{1}H NMR spectrum (400 MHz) in C_6D_6 (top), CD_3CN (middle), and $CDCl_3$ (bottom).

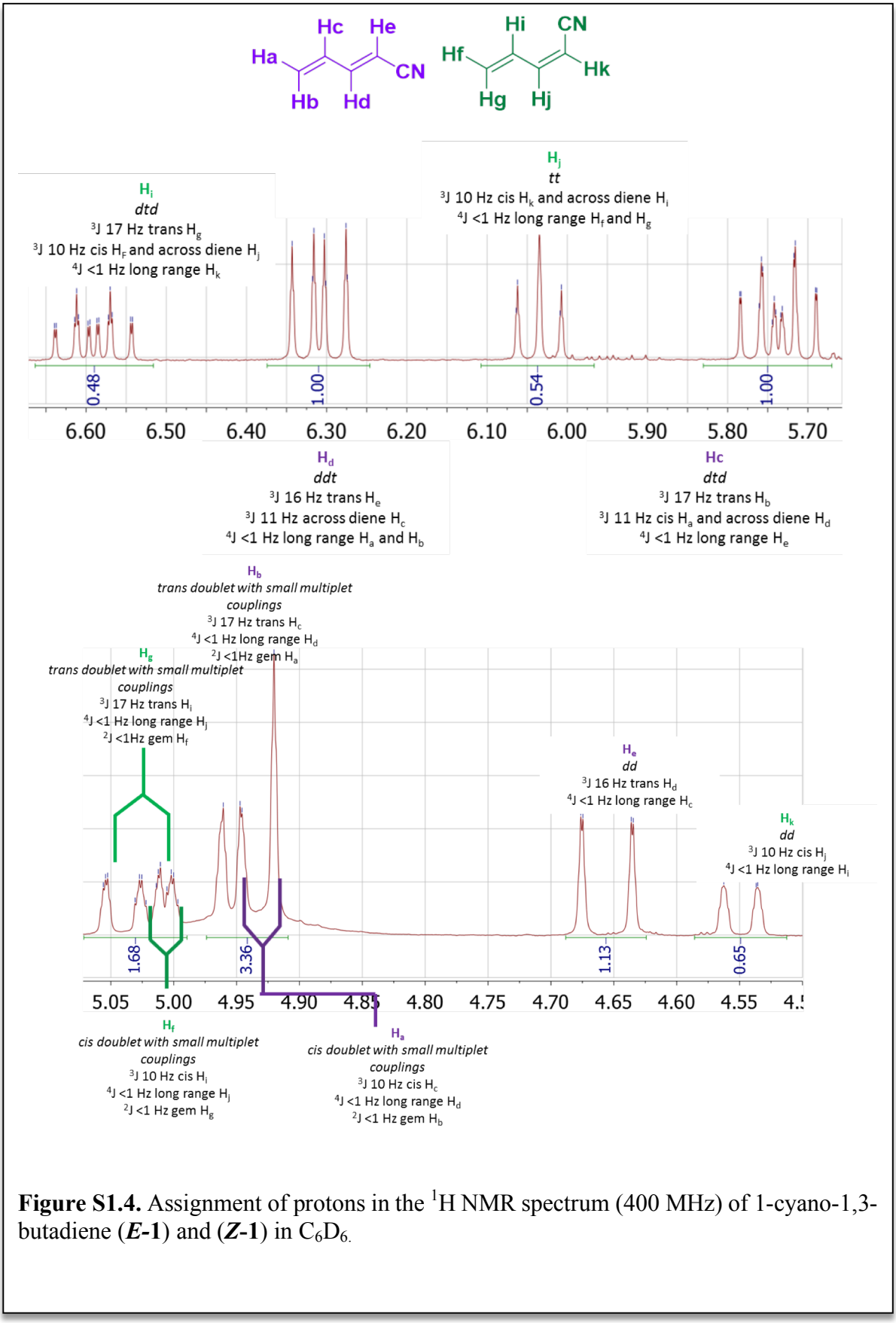


Figure S1.4. Assignment of protons in the ^{1}H NMR spectrum (400 MHz) of 1-cyano-1,3-butadiene (***E*-1**) and (***Z*-1**) in C_6D_6.

Table S1.1 shows a comparison of the previously reported ^{1}H-NMR spectrum with the current interpretation of the spectrum.[4] The analysis was done on the spectrum in $CDCl_3$ to maintain consistency between the two, even though some of the couplings are subject to second order effects. By understanding the spectrum in C_6D_6, the spectrum in $CDCl_3$ is much more navigable, and the overlapping signals can be more easily distinguished. It is clear that the agreements between the two reports differ, but because the ^{1}H-NMR spectrum from the previous report is not available, it is difficult to determine the source of the discrepancy.

Table S1.1. ^{1}H NMR signal assignments of *E*-1 and *Z*-1 in $CDCl_3$ previously reported and found in this work. Estimated coupling constants affected by second order effects. For more accurate coupling constants, see data from spectrum in C_6D_6 (Figure S1.4).

(*E*-1) Clary	(*E*-1) this work	(*Z*-1) Clary	(*Z*-1) this work
7.00 dd, *J* = 15.9, 10.8 Hz	6.90 dd, *J* = 16.1, 10.8 Hz	7.24 d, *J* = 6.7 Hz	
6.42 dt, *J* = 16.9, 10.8 Hz	6.32 dt, *J* = 16.9, 10.6 Hz	7.17 d, *J* = 7.2 Hz	
5.61 d, *J* = 16.9 Hz	5.51 d, *J* = 16.9 Hz	6.83 dt, *J* = 10.3, 5.1 Hz	
5.55 d, *J* = 10.2 Hz	5.43 d, *J* = 10.1 Hz		6.73 dt, *J* = 13.3, 10.2
	5.32 *J* = 16.1 Hz		6.68 t, *J* = 10.6
			5.55 d, *J* = 17.6
			5.51 d, *J* = 9.6
			5.19 d, *J* = 9.0

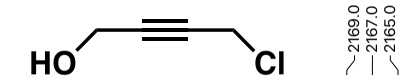
References

1. Mass Spectrometry Data Center; National Institute of Standards and Technology; https://chemdata.nist.gov/.

2. McEwen, C. N.; McKay, R. G.; Larsen, B. S., Analysis of solids, liquids, and biological tissues using solids probe introduction at atmospheric pressure on commercial LC/MS instruments. *Anal. Chem.* **2005**, *77*, 7826-7831.

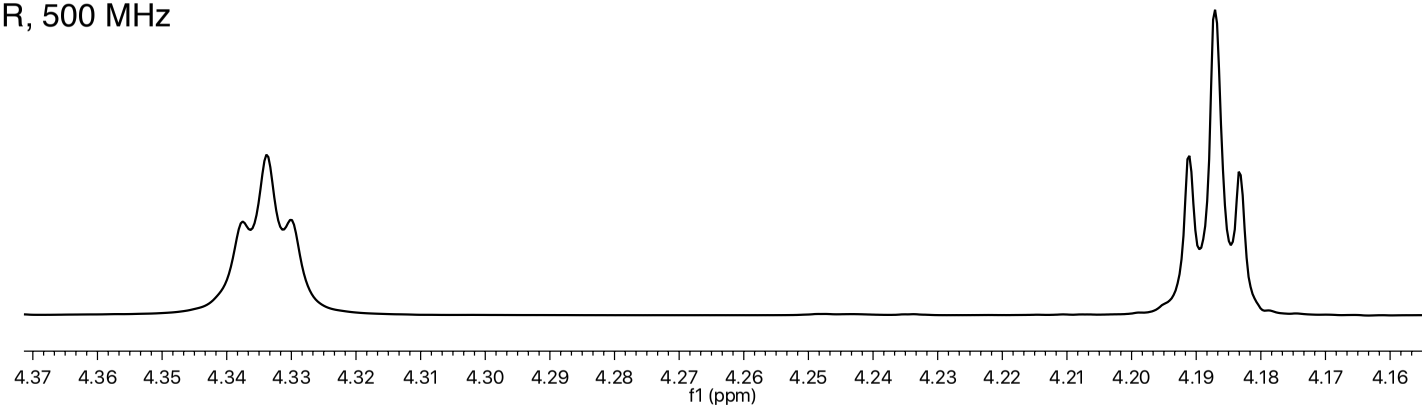
3. Reich, H. J., Structure Determination Using NMR - Chem 605; Section 5-HMR-02.7 Chemical Shift Effects - Aromatic Rings, https://www.chem.wisc.edu/areas/reich/nmr/index.htm.

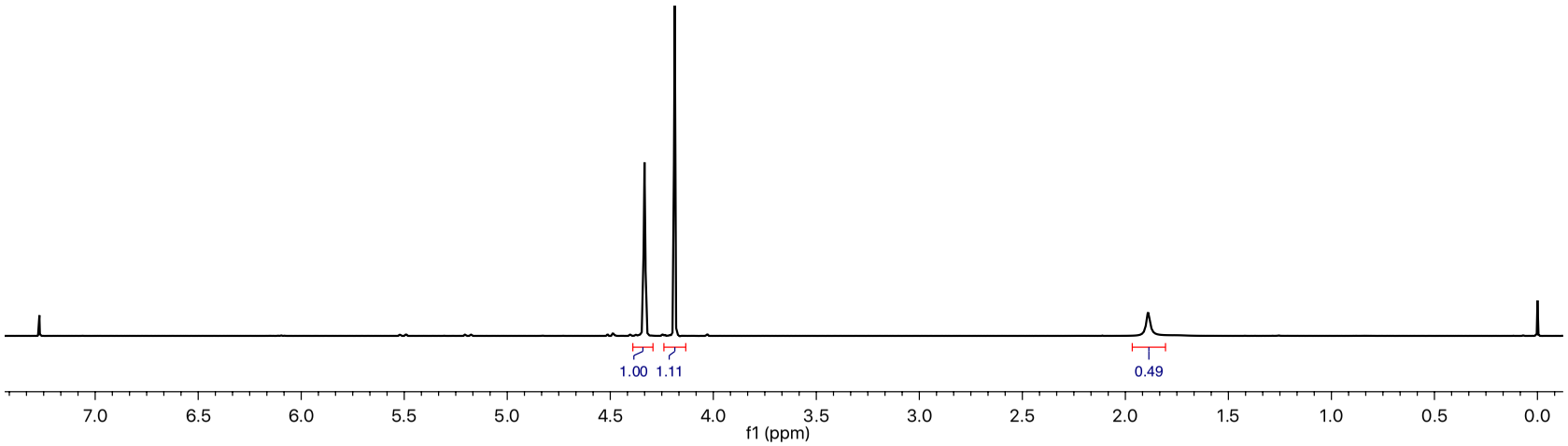
4. Clary, K. N.; Back, T. G., Preparation of Unsaturated Aminonitriles from the Aza-Morita-Baylis-Hillman Reactions of Aldimines with Penta-2,4-dienenitrile. *Synlett* **2007**, 2995-2998.



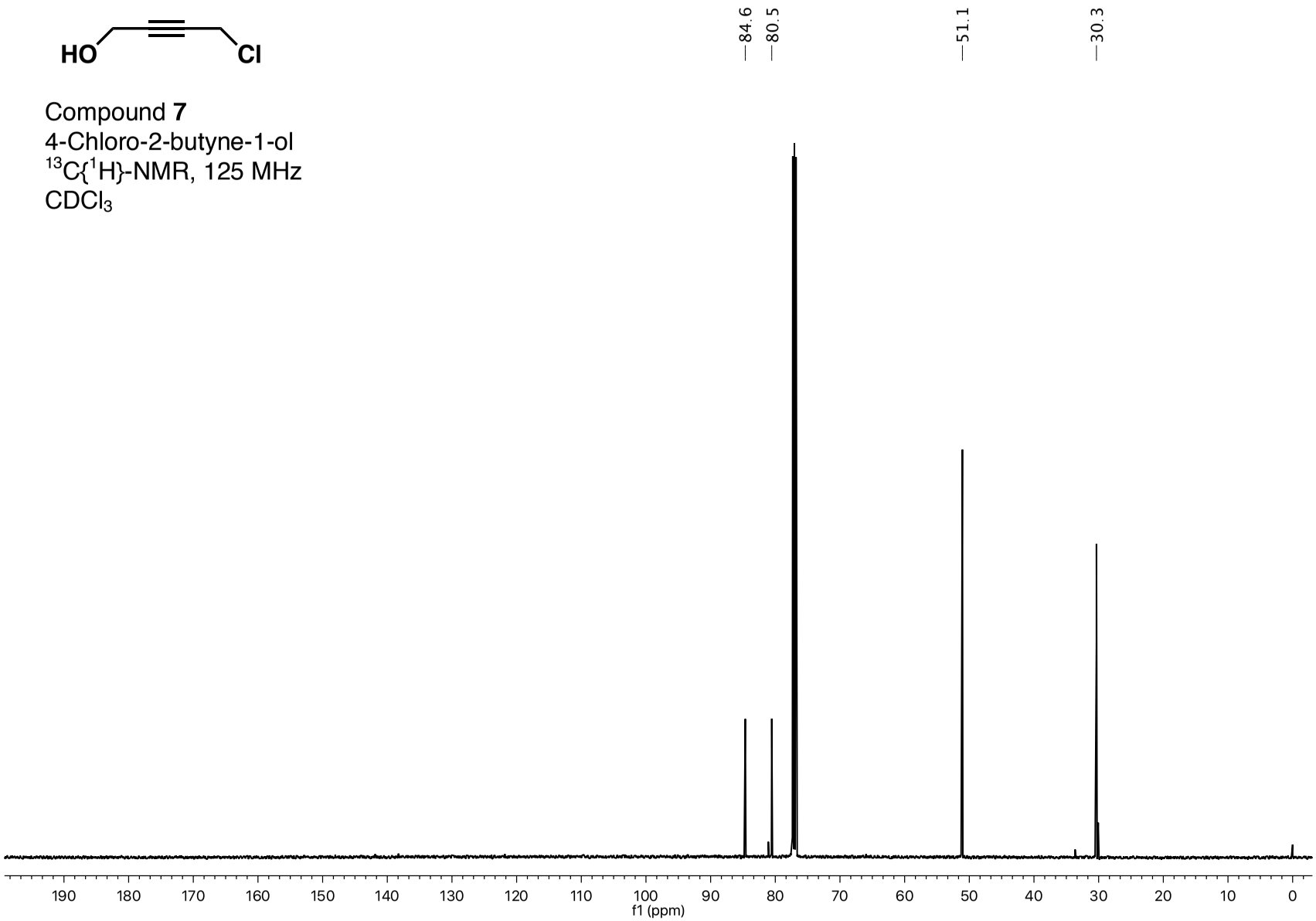


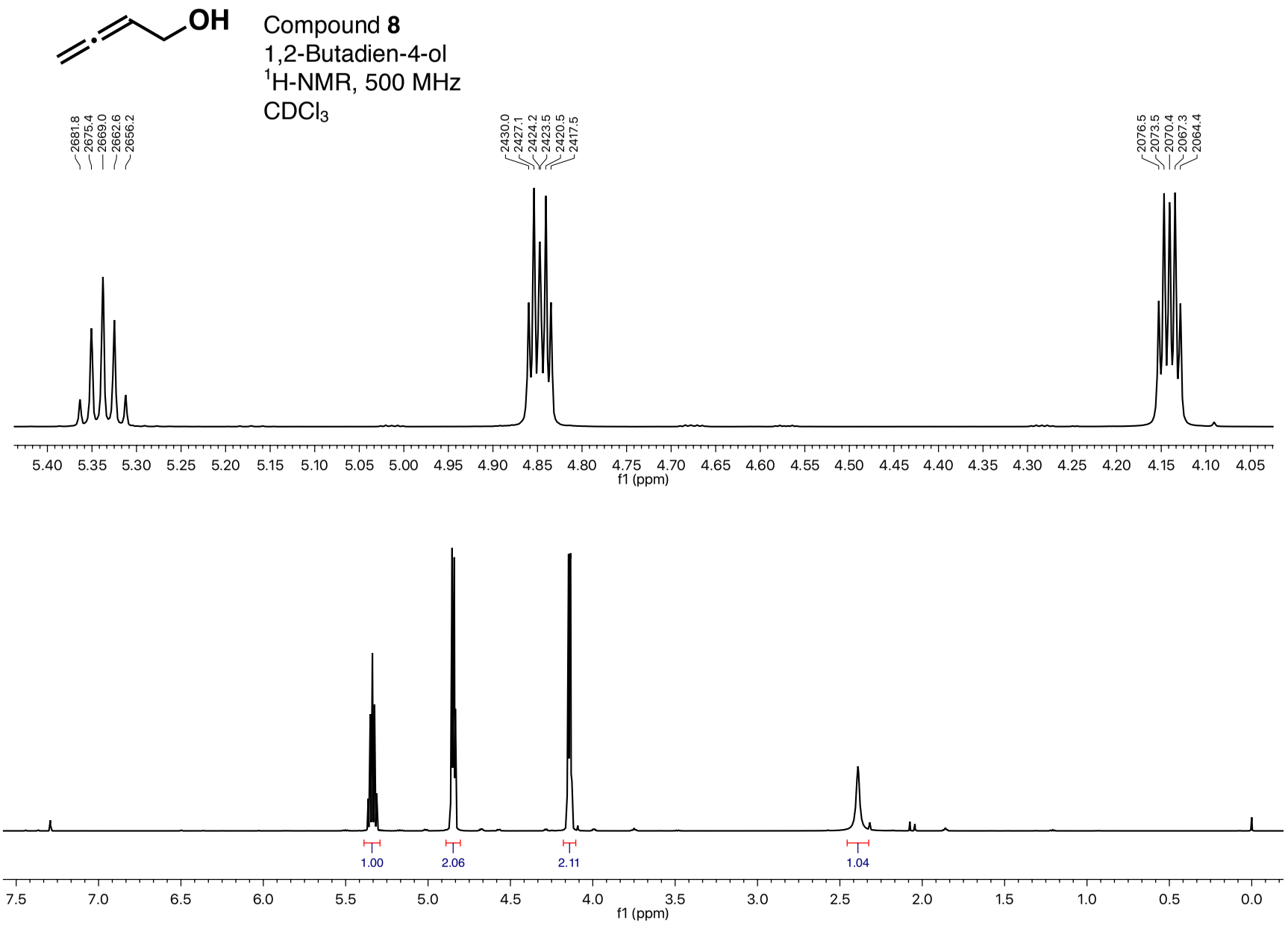
Compound **7**
4-Chloro-2-butyne-1-ol
^{1}H-NMR, 500 MHz
$CDCl_3$

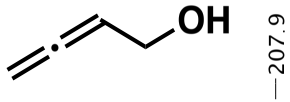




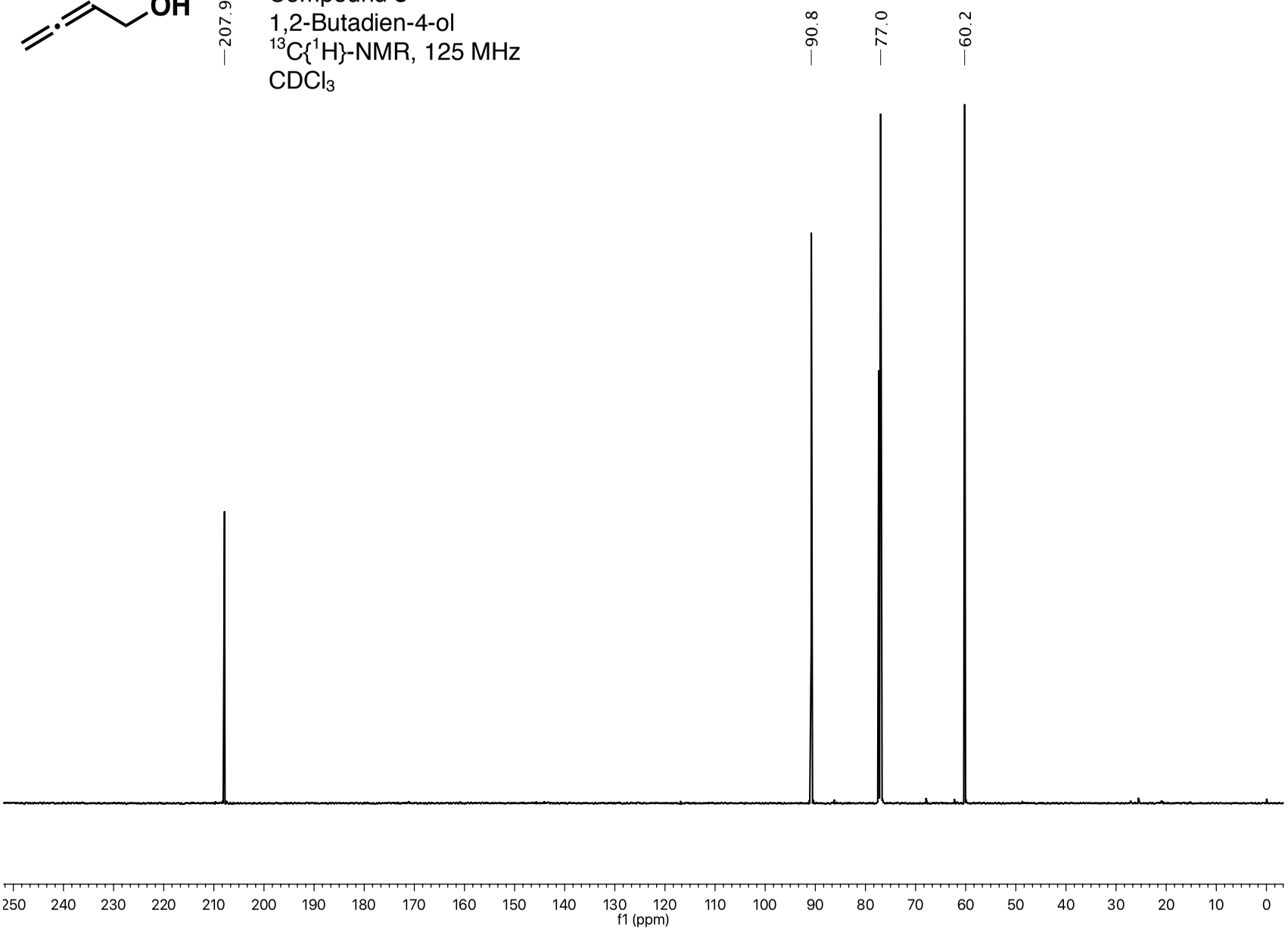
Compound **7**
4-Chloro-2-butyne-1-ol
$^{13}C\{^{1}H\}$-NMR, 125 MHz
$CDCl_3$

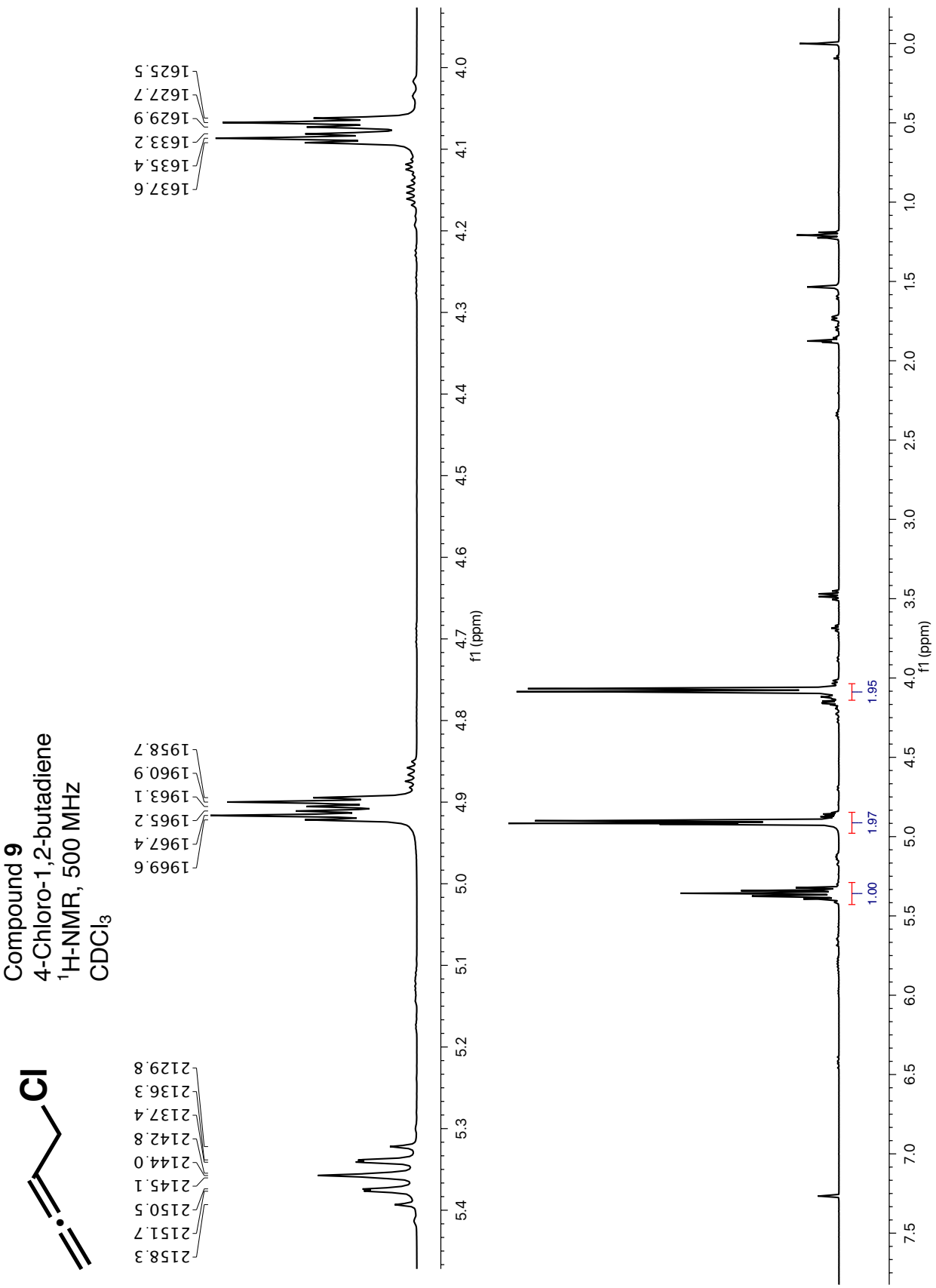


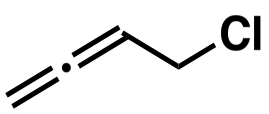

OH
Compound 8
1,2-Butadien-4-ol
1H-NMR, 500 MHz
CDCl3
2681.8
2675.4
2669.0
2662.6
2656.2
2430.0
2427.1
2424.2
2423.5
2420.5
2417.5
2076.5
2073.5
2070.4
2067.3
2064.4
f1 (ppm)
1.00
2.06
2.11
1.04
f1 (ppm)



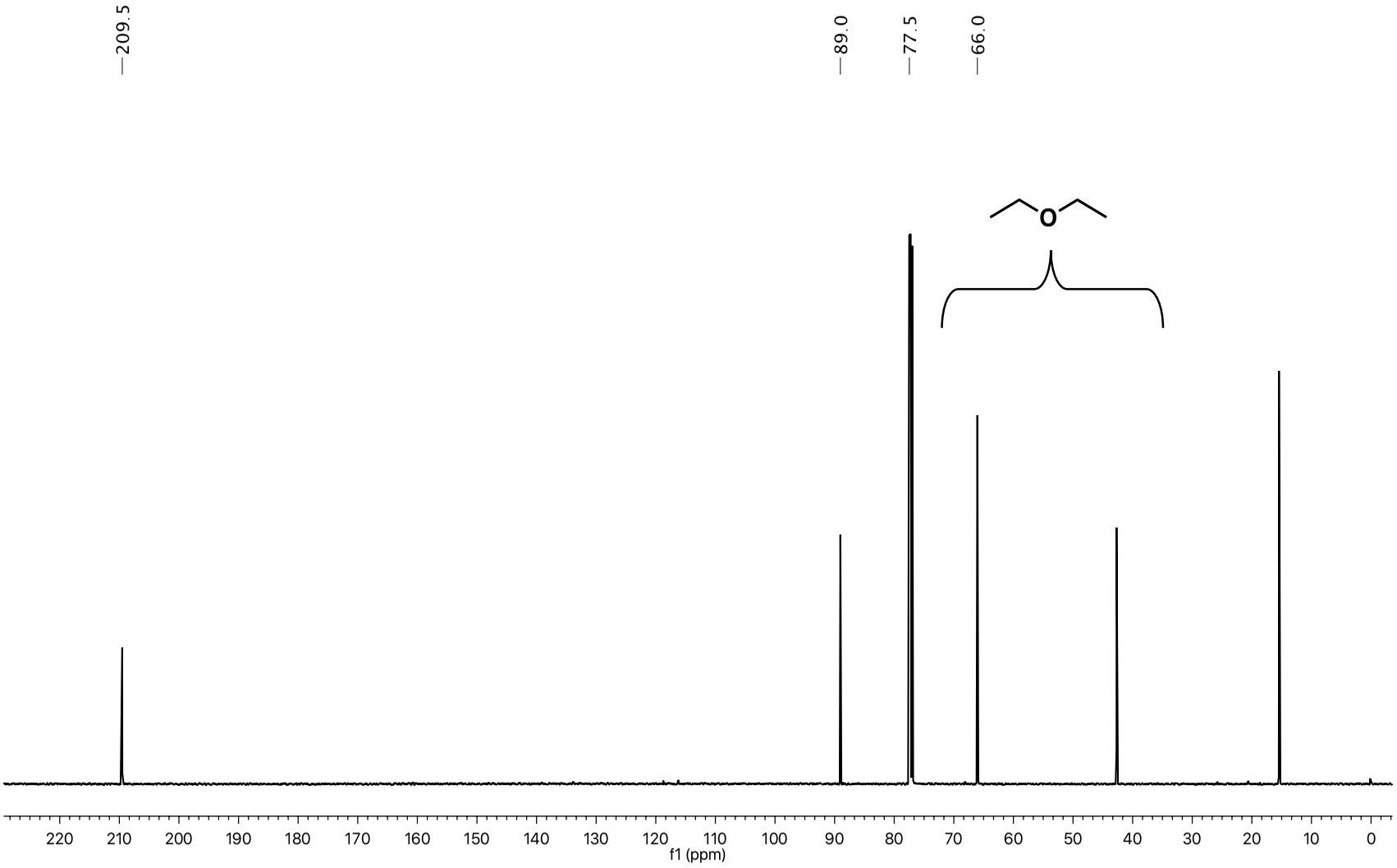
Compound **8**
1,2-Butadien-4-ol
$^{13}C\{^{1}H\}$-NMR, 125 MHz
$CDCl_3$

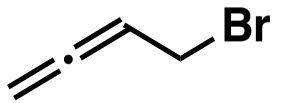



Compound 9
4-Chloro-1,2-butadiene
1H-NMR, 500 MHz
CDCl3
Cl
2158.3
2151.7
2150.5
2145.1
2144.0
2142.8
2137.4
2136.3
2129.8
1969.6
1967.4
1965.2
1963.1
1960.9
1958.7
1637.6
1635.4
1633.2
1629.9
1627.7
1625.5
f1 (ppm)
1.00
1.97
1.95
f1 (ppm)

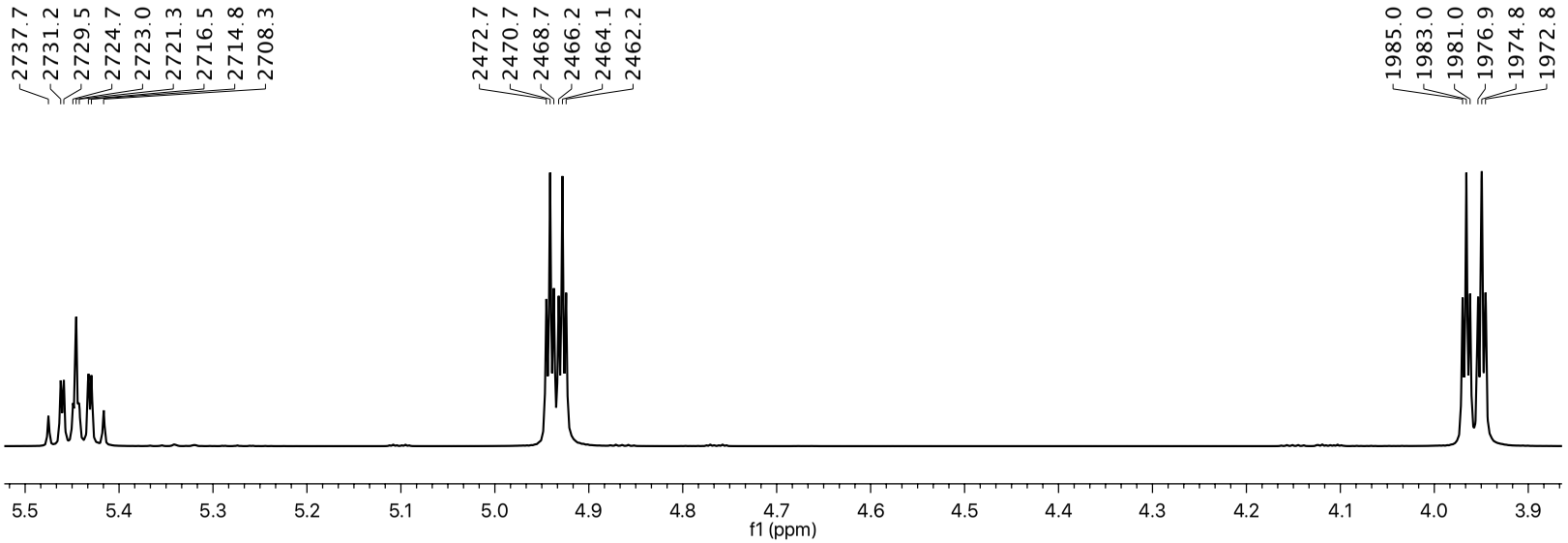


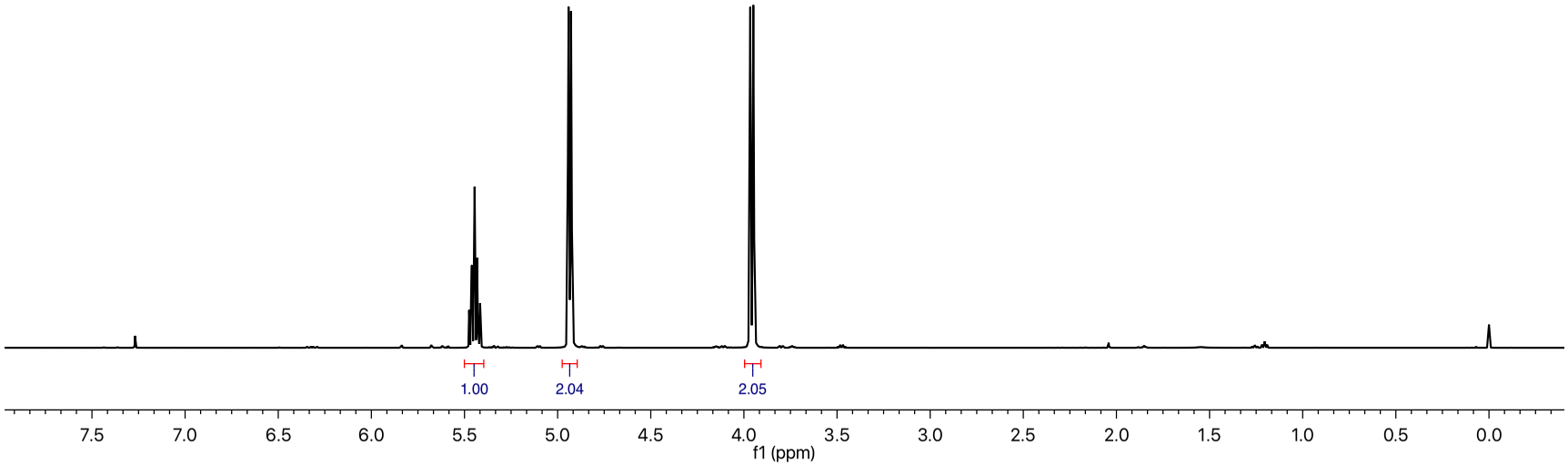
Compound **9**
4-Chloro-1,2-butadiene
$^{13}C\{^{1}H\}$-NMR, 125 MHz
$CDCl_3$

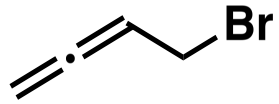




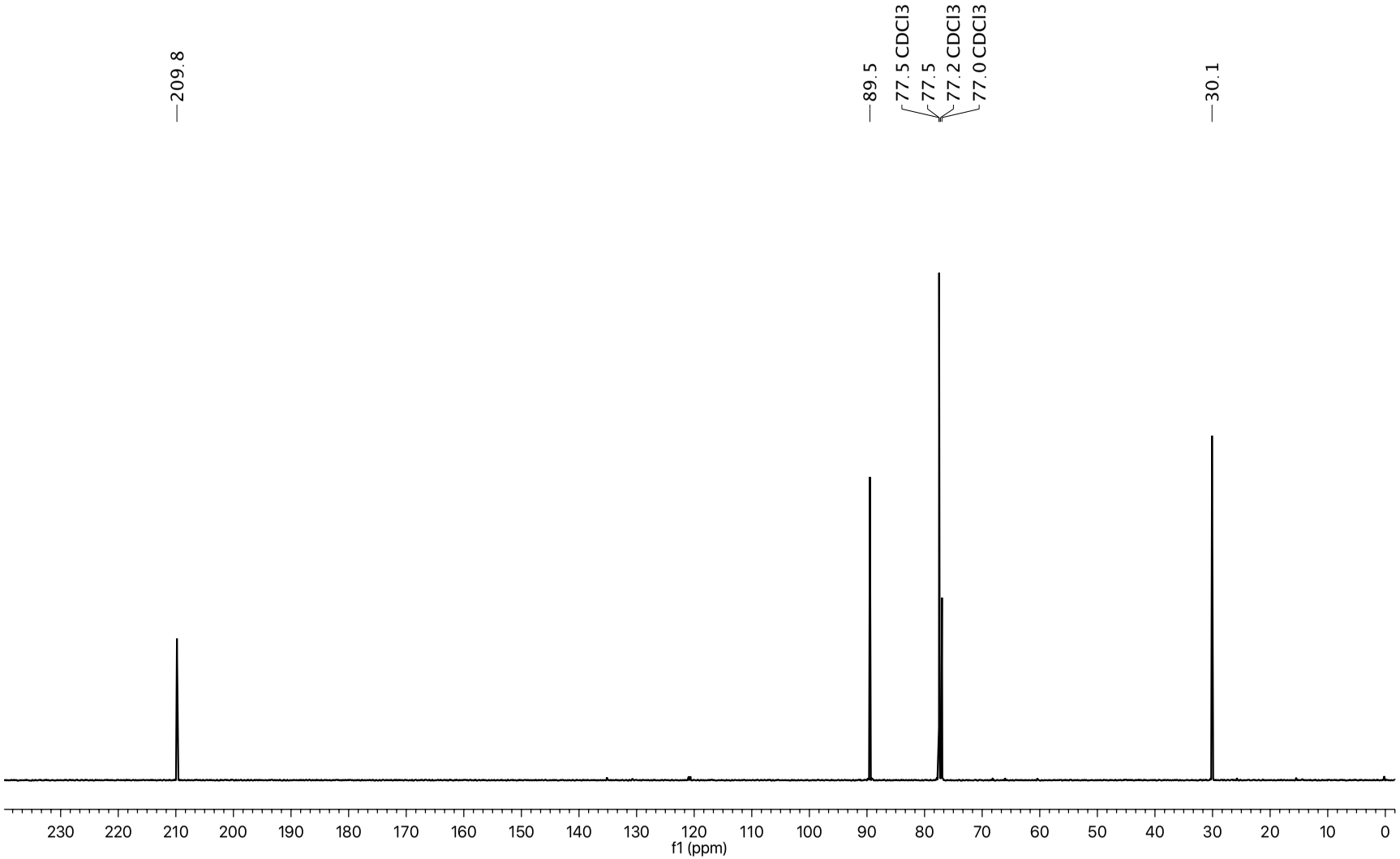
Compound **12**
4-Bromo-1,2-butadiene
^{1}H-NMR, 500 MHz
$CDCl_3$

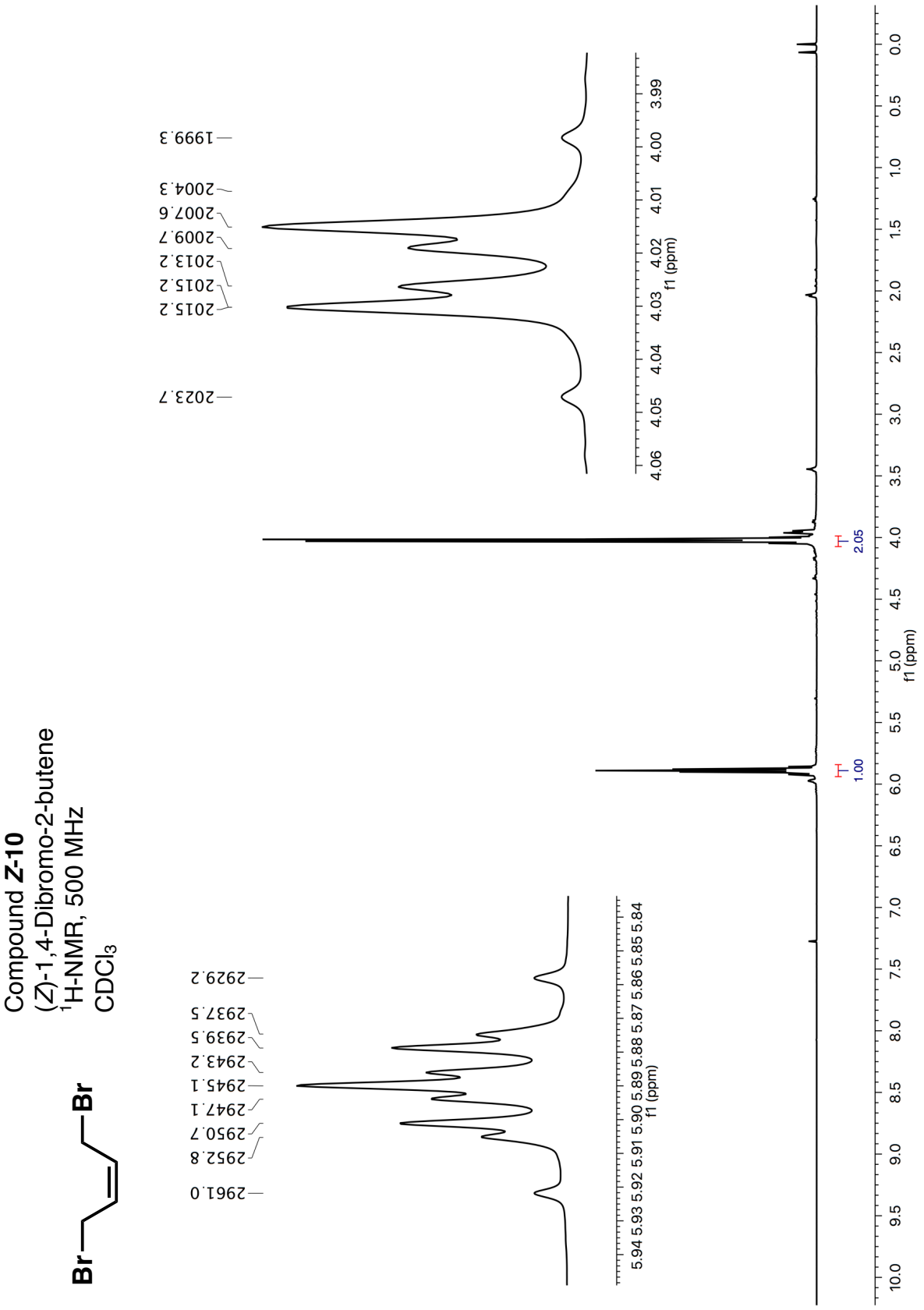


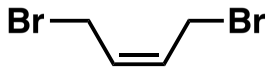




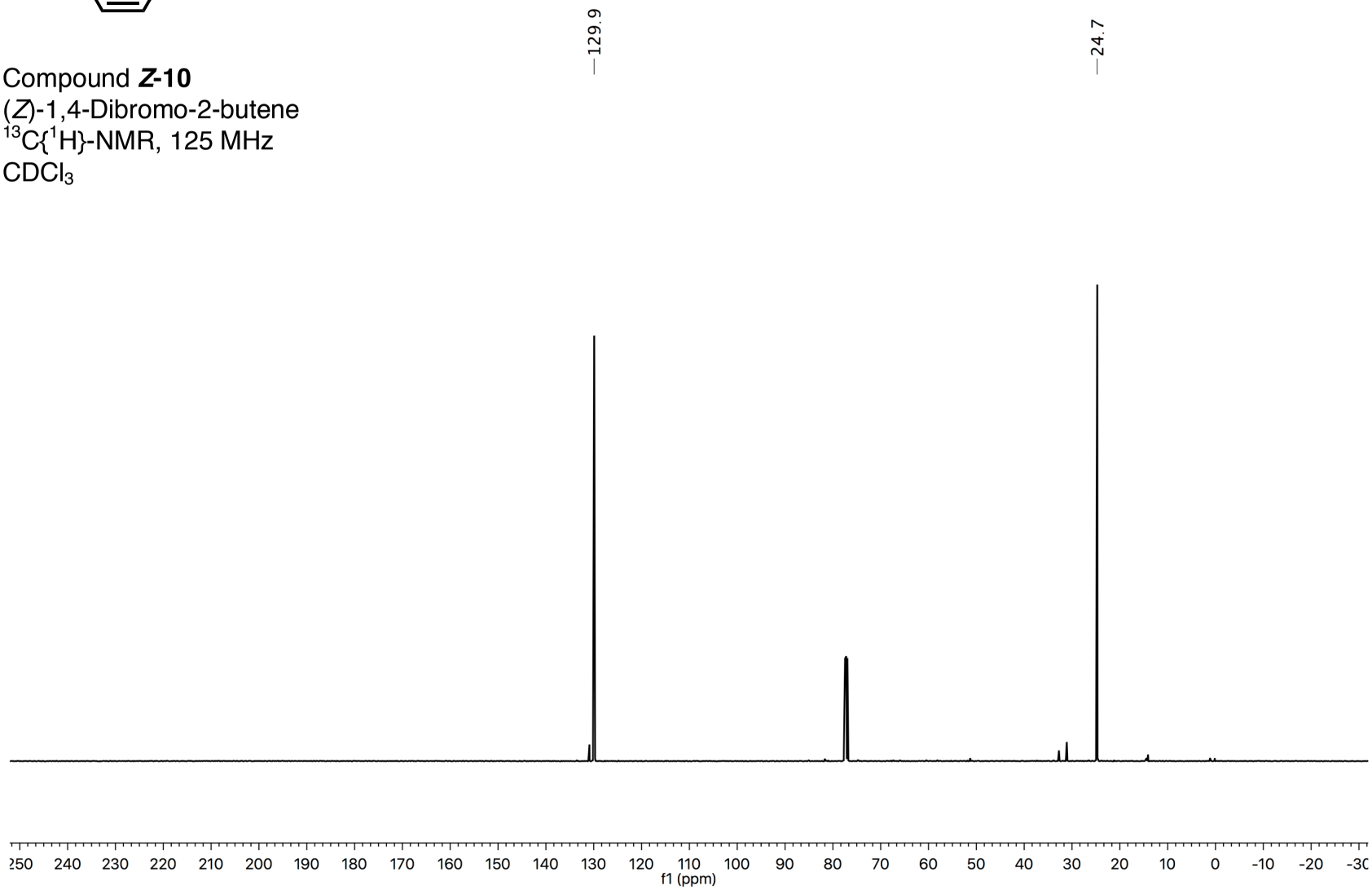
Compound **12**
4-Bromo-1,2-butadiene
$^{13}C\{^{1}H\}$-NMR, 125 MHz
$CDCl_3$

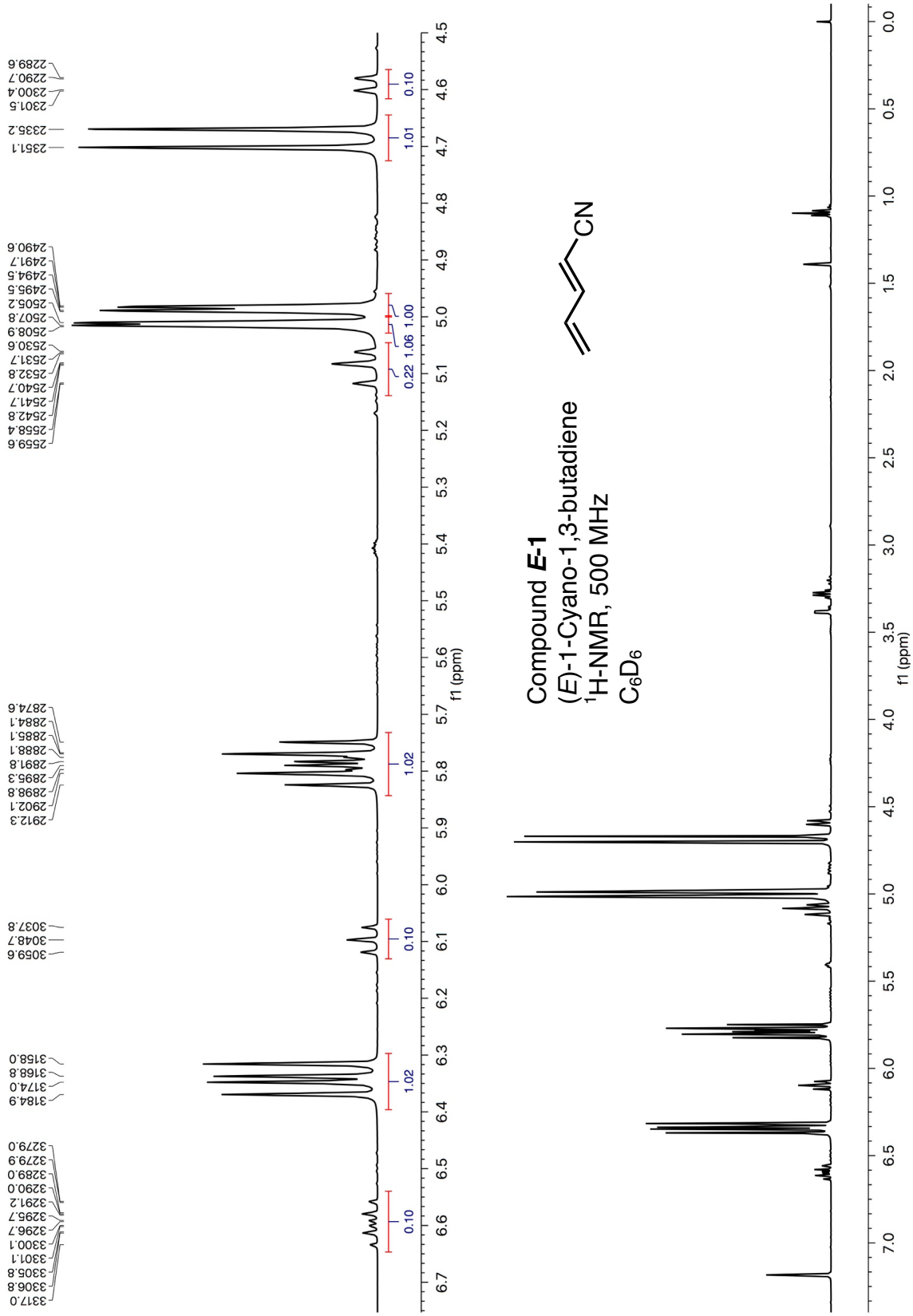


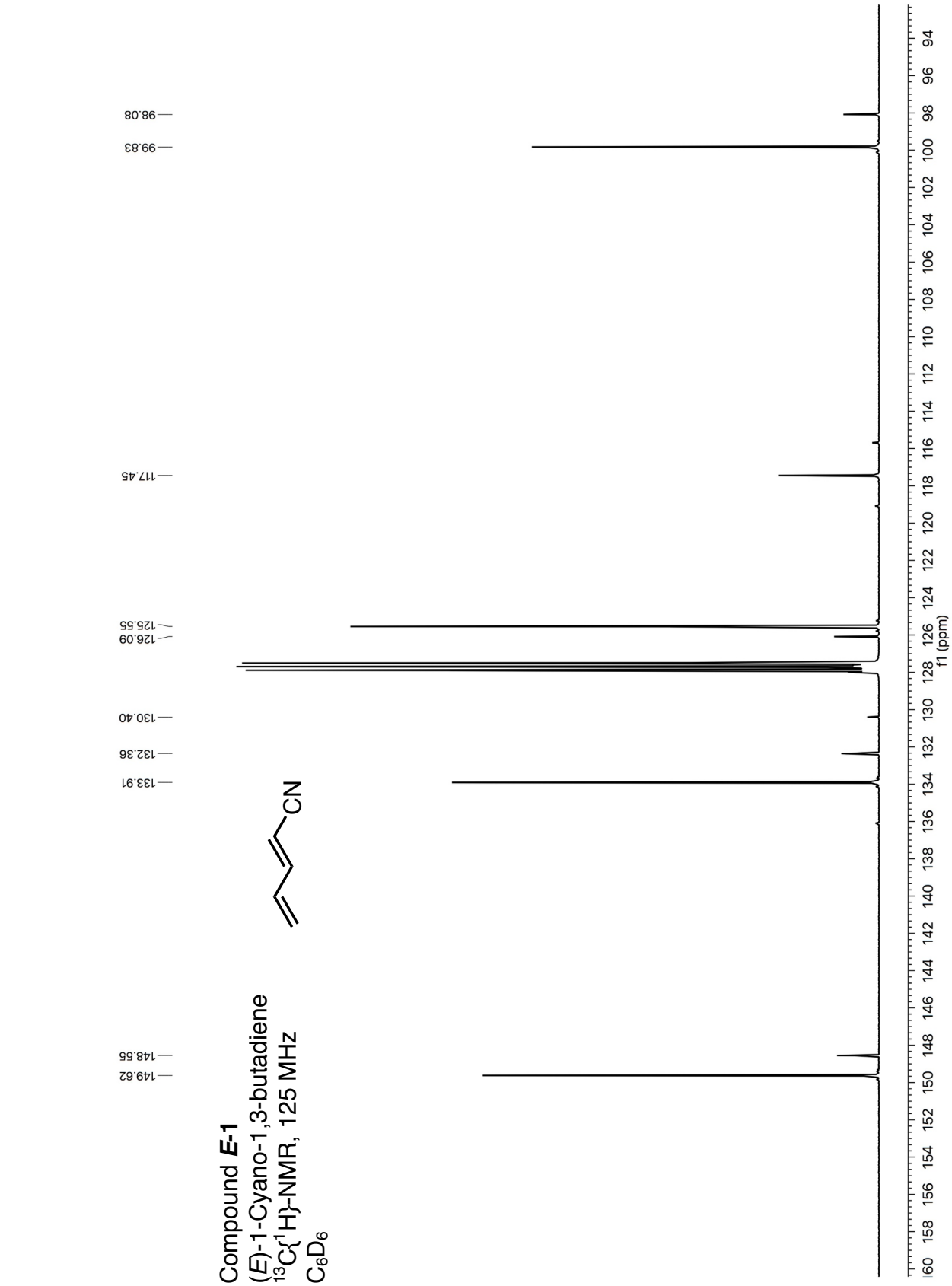

Compound Z-10
(Z)-1,4-Dibromo-2-butene
1H-NMR, 500 MHz
CDCl3
Br
Br
2961.0
2952.8
2950.7
2947.1
2945.1
2943.2
2939.5
2937.5
2929.2
2023.7
2015.2
2015.2
2013.2
2009.7
2007.6
2004.3
1999.3
5.94 5.93 5.92 5.91 5.90 5.89 5.88 5.87 5.86 5.85 5.84
f1 (ppm)
4.06 4.05 4.04 4.03 4.02 4.01 4.00 3.99
f1 (ppm)
1.00
2.05
10.0 9.5 9.0 8.5 8.0 7.5 7.0 6.5 6.0 5.5 5.0 4.5 4.0 3.5 3.0 2.5 2.0 1.5 1.0 0.5 0.0
f1 (ppm)



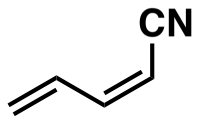
Compound ***Z*-10**
(*Z*)-1,4-Dibromo-2-butene
$^{13}C\{^{1}H\}$-NMR, 125 MHz
$CDCl_3$

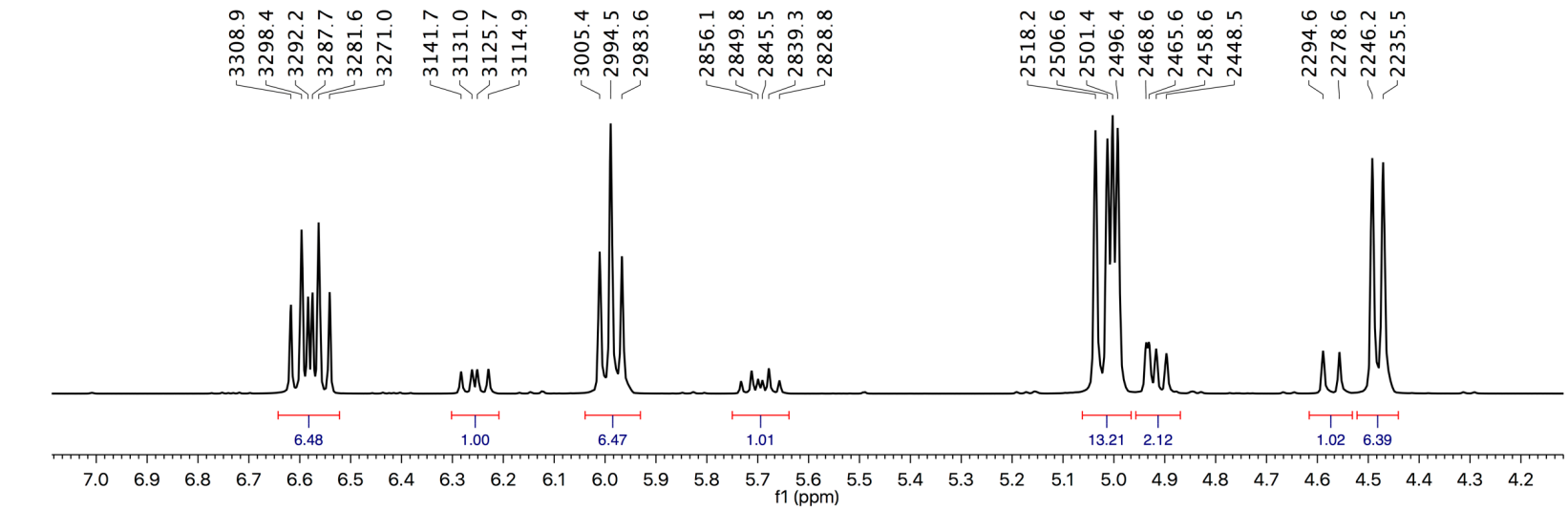


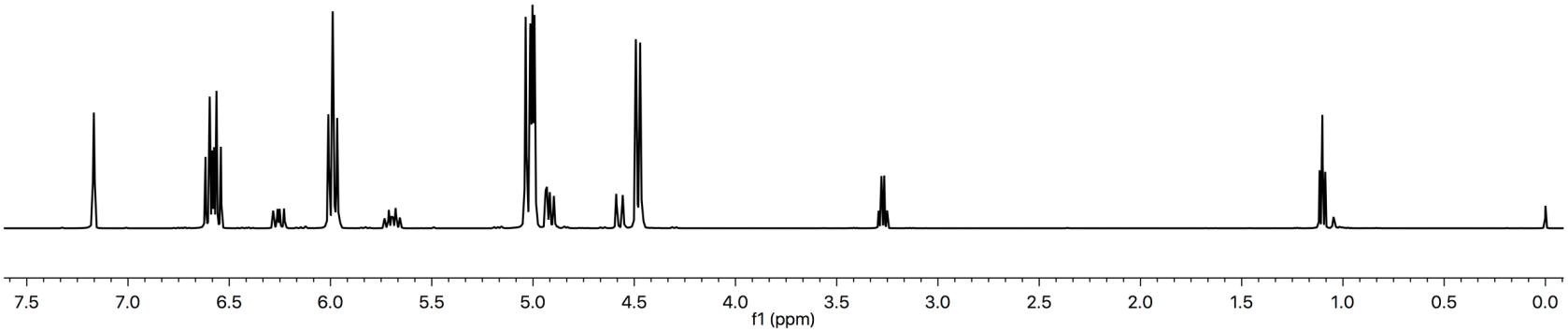

Compound E-1
(E)-1-Cyano-1,3-butadiene
1H-NMR, 500 MHz
C6D6
CN
f1 (ppm)
0.10
1.02
0.10
1.02
0.22
1.06
1.00
1.01
0.10


Compound *E*-1
(*E*)-1-Cyano-1,3-butadiene
$^{13}C\{^{1}H\}$-NMR, 125 MHz
C_6D_6
CN
149.62
148.55
133.91
132.36
130.40
126.09
125.55
117.45
99.83
98.08
f1 (ppm)

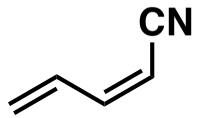
Compound ***Z*-1**
(*Z*)-1-Cyano-1,3-butadiene
^{1}H-NMR, 500 MHz
C_6D_6

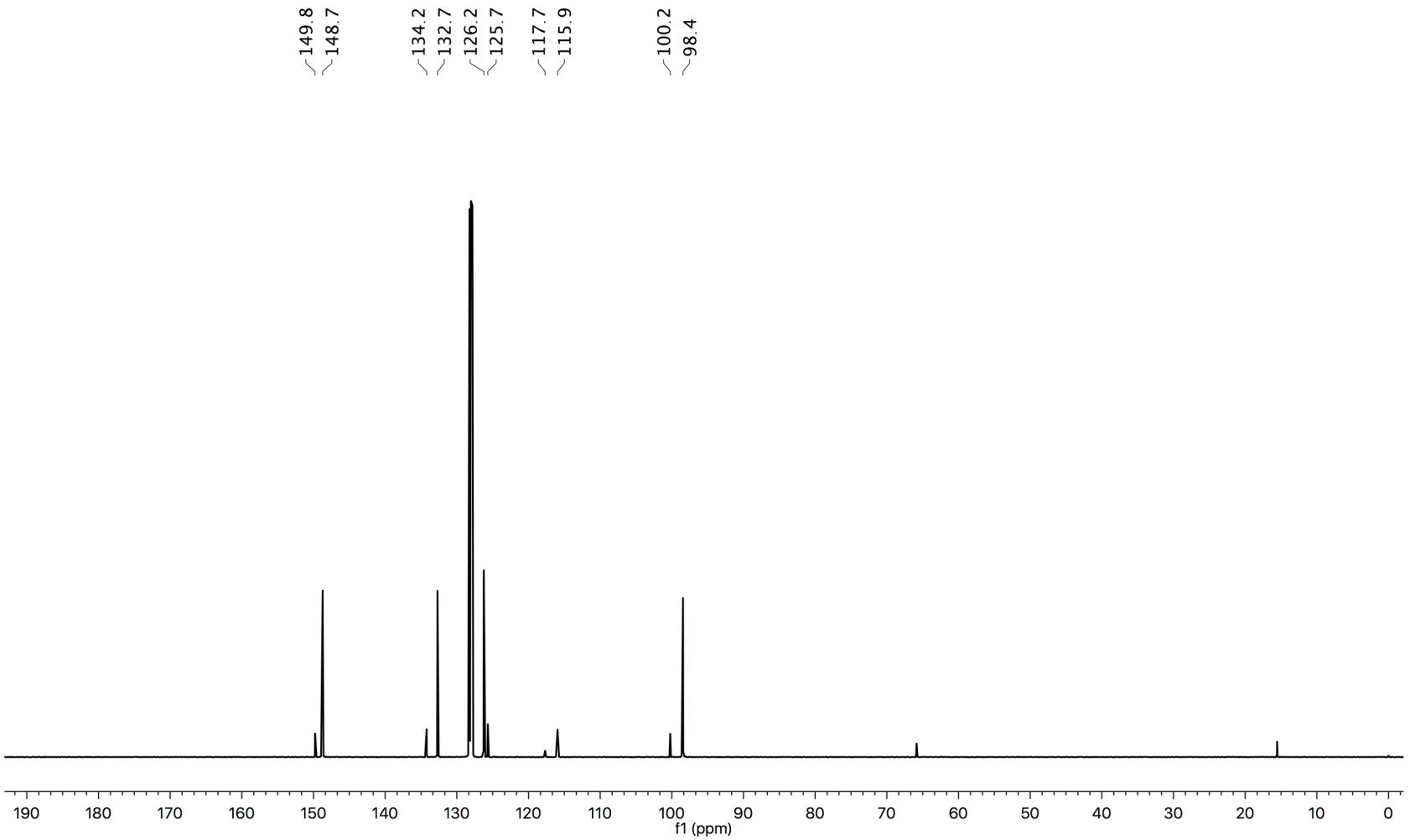


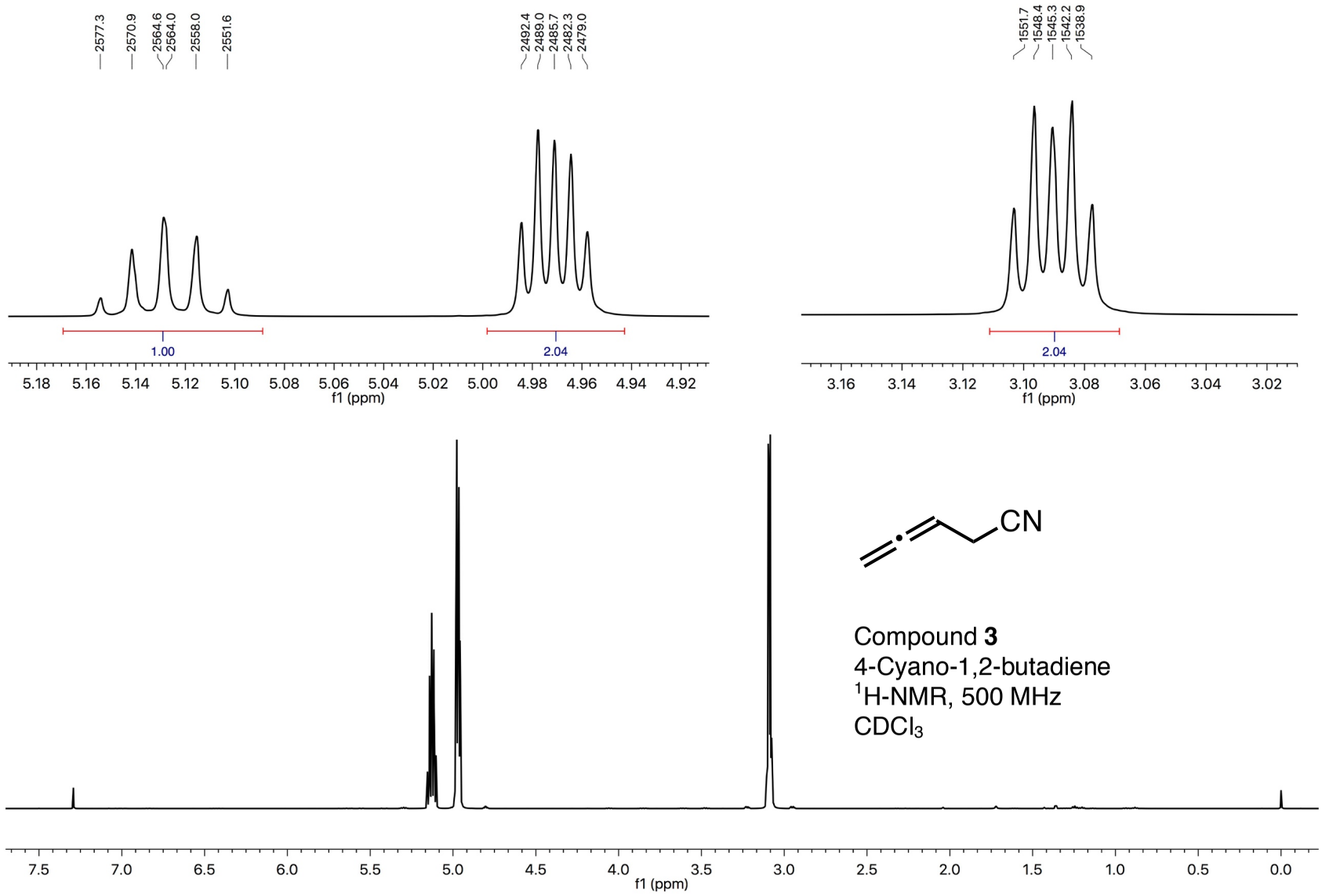


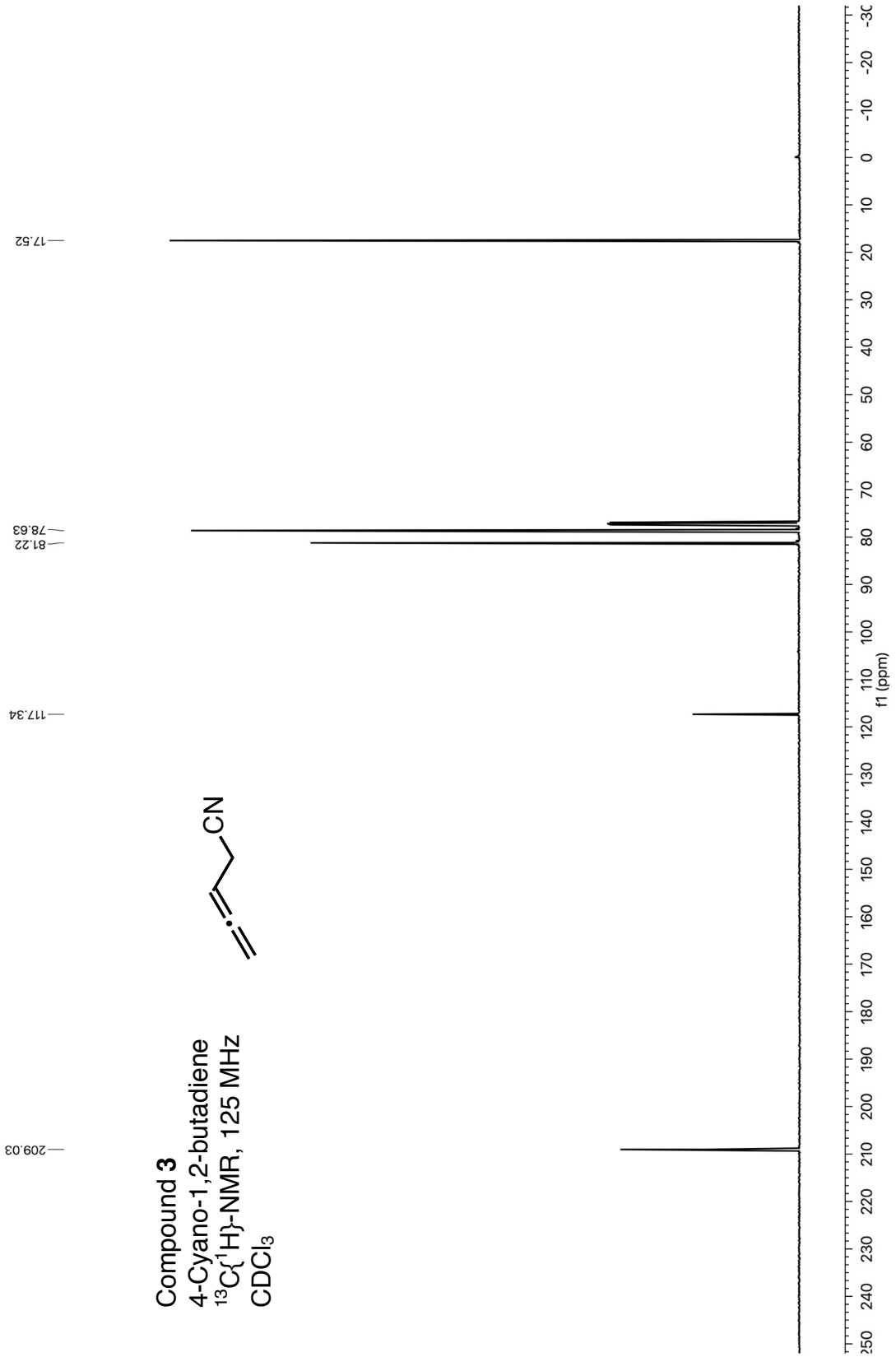


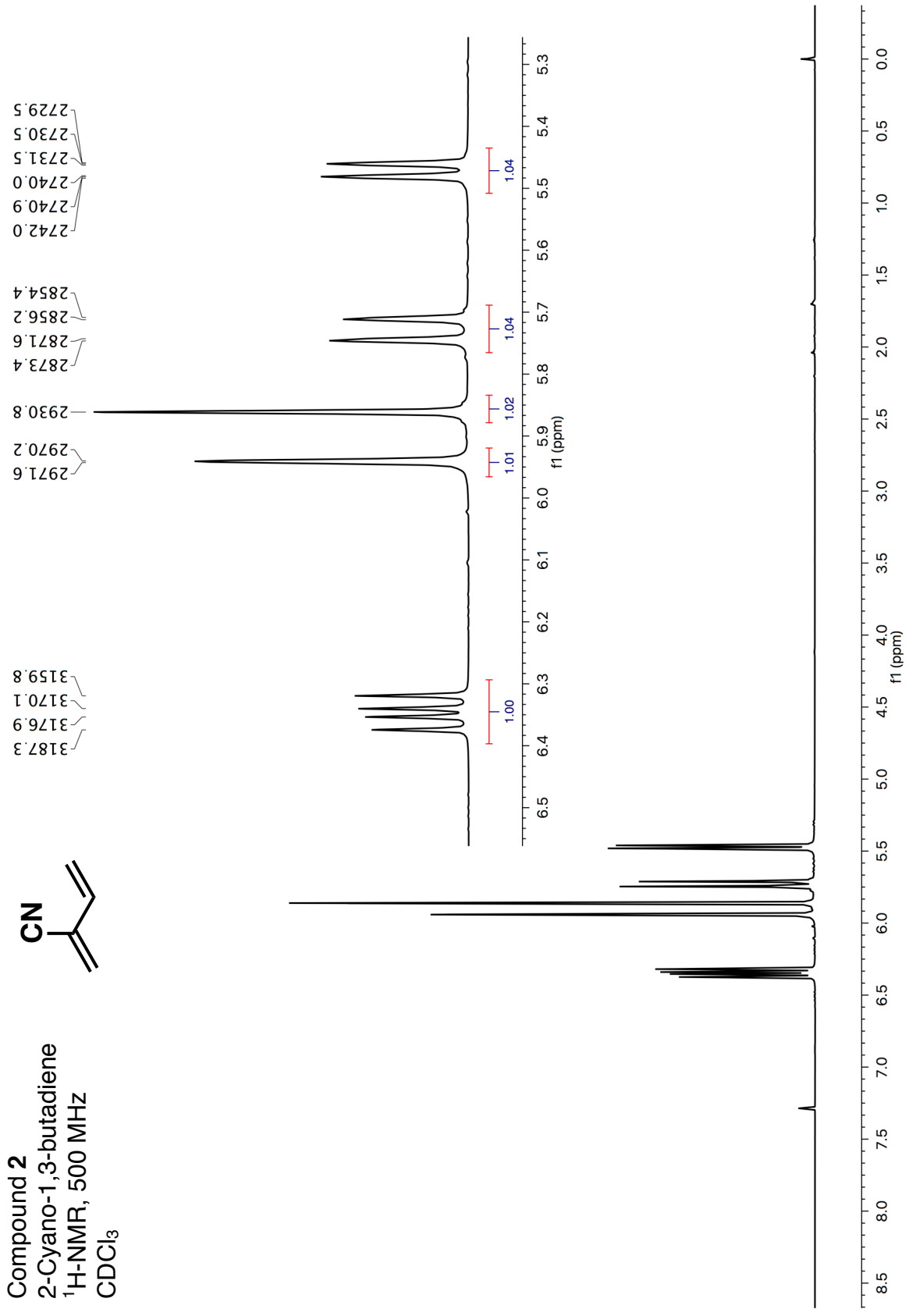
Compound ***Z*-1**
(*Z*)-1-Cyano-1,3-butadiene
$^{13}C\{^{1}H\}$-NMR, 125 MHz
C_6D_6



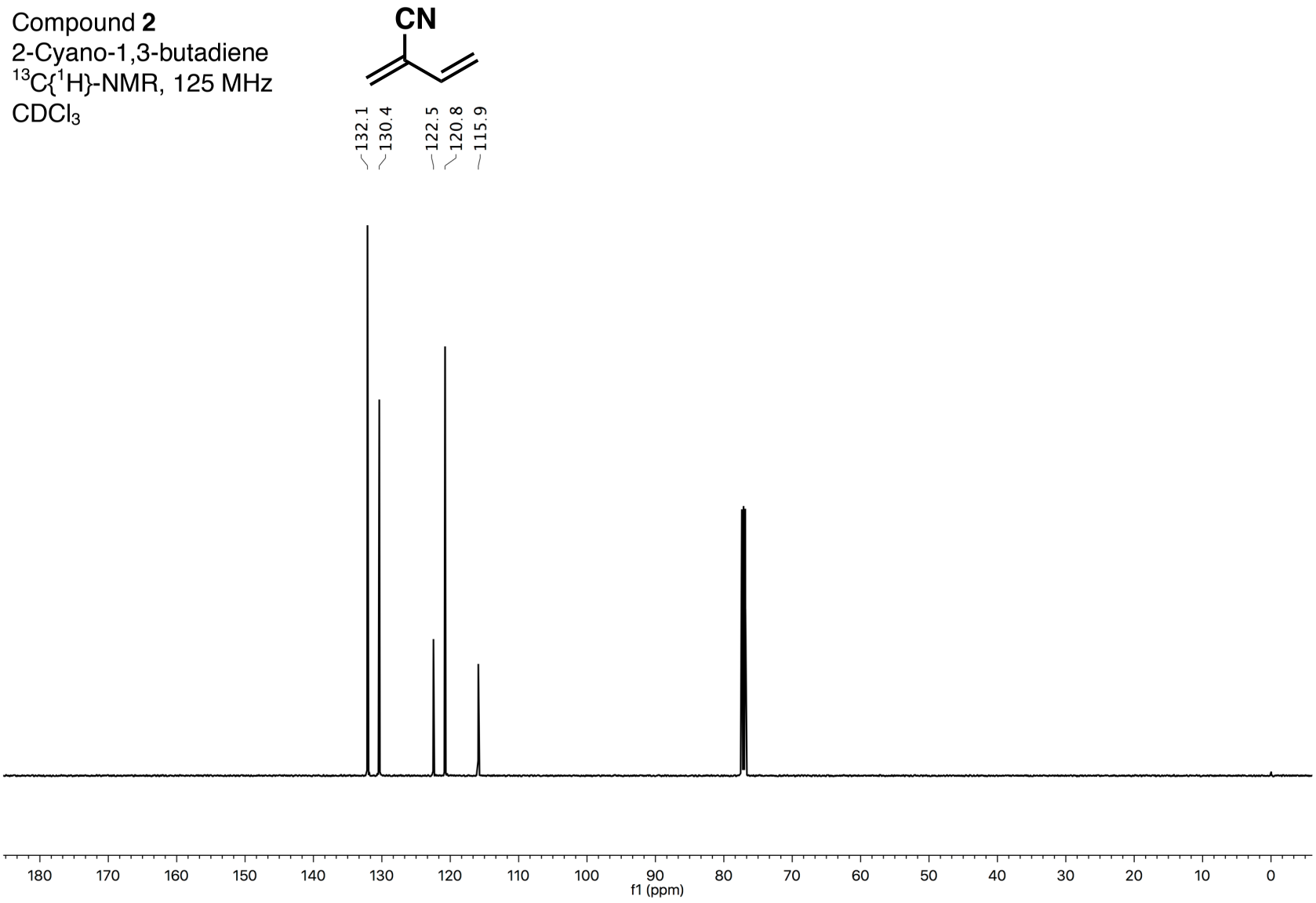


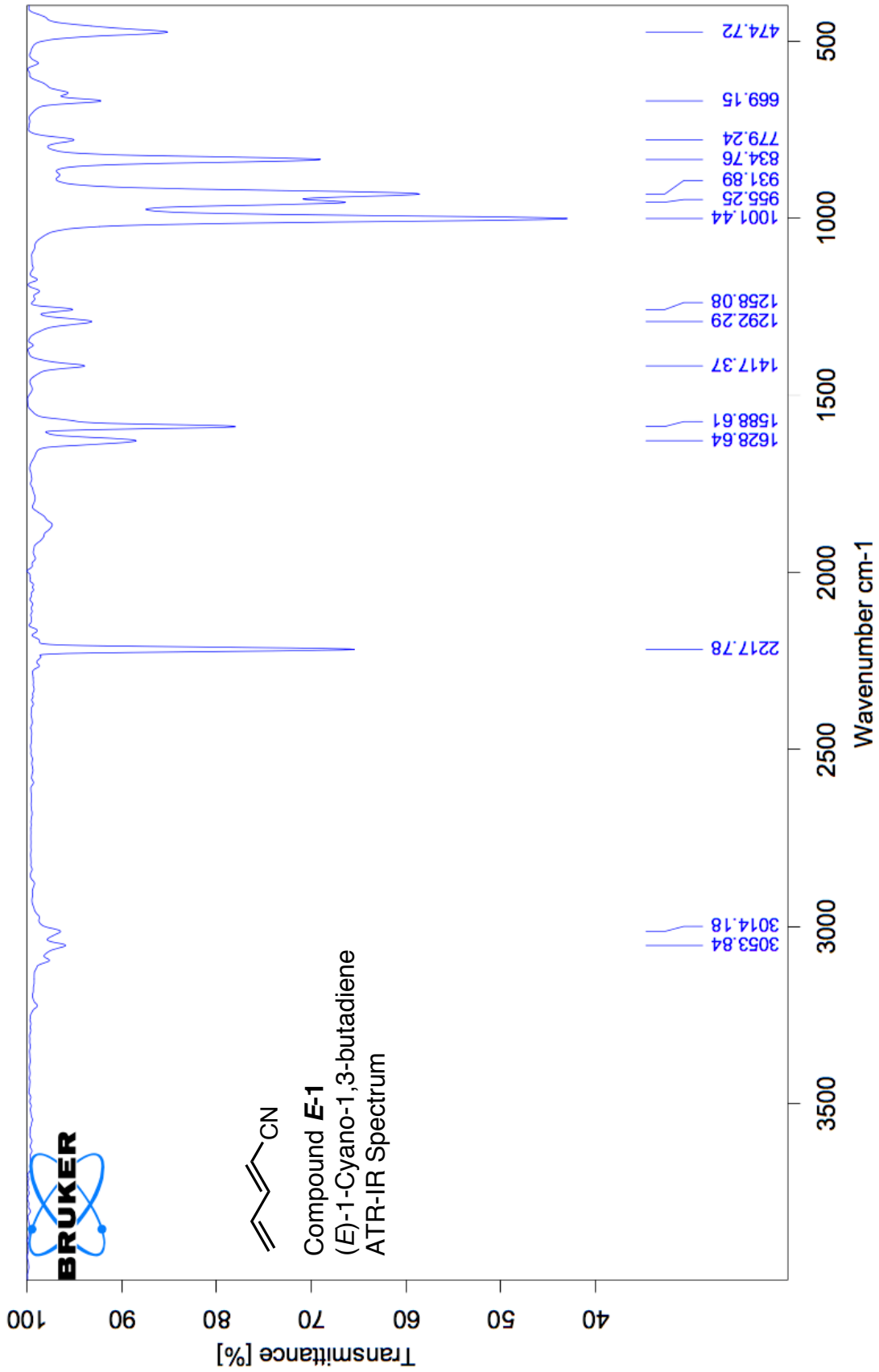

2577.3
2570.9
2564.6
2564.0
2558.0
2551.6
2492.4
2489.0
2485.7
2482.3
2479.0
1551.7
1548.4
1545.3
1542.2
1538.9
1.00
2.04
2.04
f1 (ppm)
f1 (ppm)
f1 (ppm)
CN
Compound 3
4-Cyano-1,2-butadiene
1H-NMR, 500 MHz
CDCl3

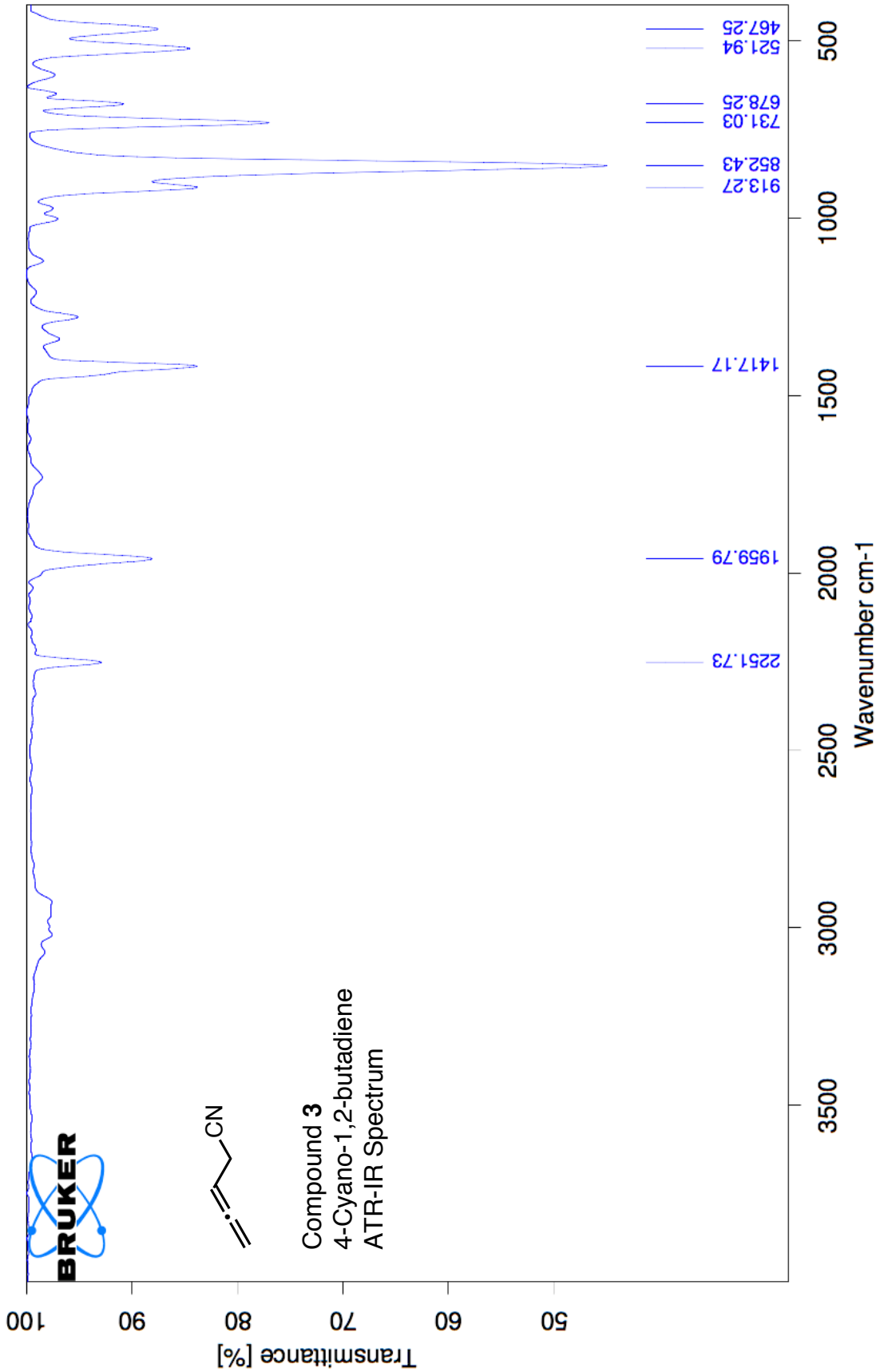

Compound 3
4-Cyano-1,2-butadiene
$^{13}C\{^{1}H\}$-NMR, 125 MHz
$CDCl_3$
CN
209.03
117.34
81.22
78.63
17.52
f1 (ppm)

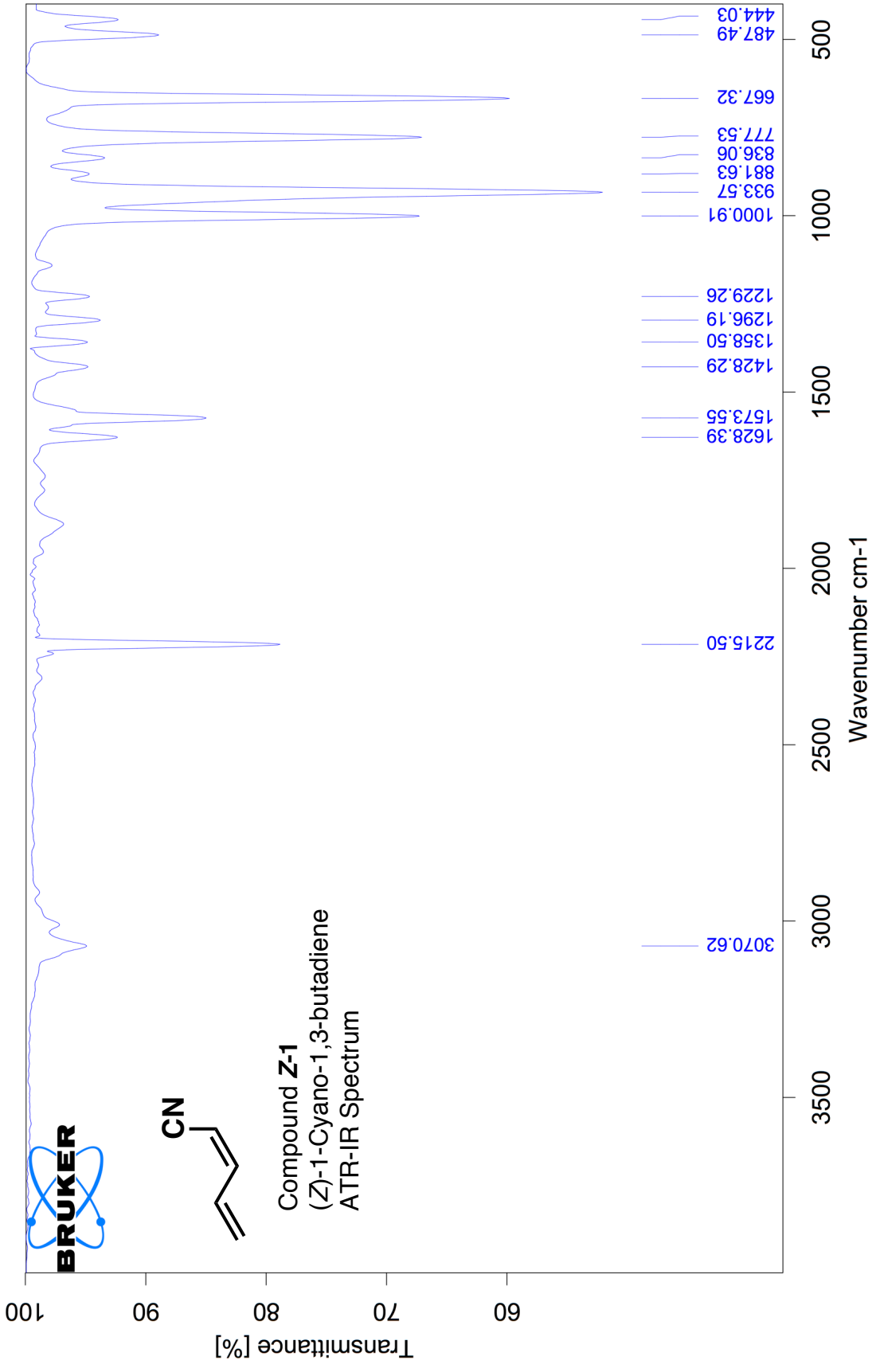

Compound 2
2-Cyano-1,3-butadiene
1H-NMR, 500 MHz
CDCl3
CN
3187.3
3176.9
3170.1
3159.8
2971.6
2970.2
2930.8
2873.4
2871.6
2856.2
2854.4
2742.0
2740.9
2740.0
2731.5
2730.5
2729.5
1.00
1.01
1.02
1.04
1.04
1.04
f1 (ppm)
f1 (ppm)

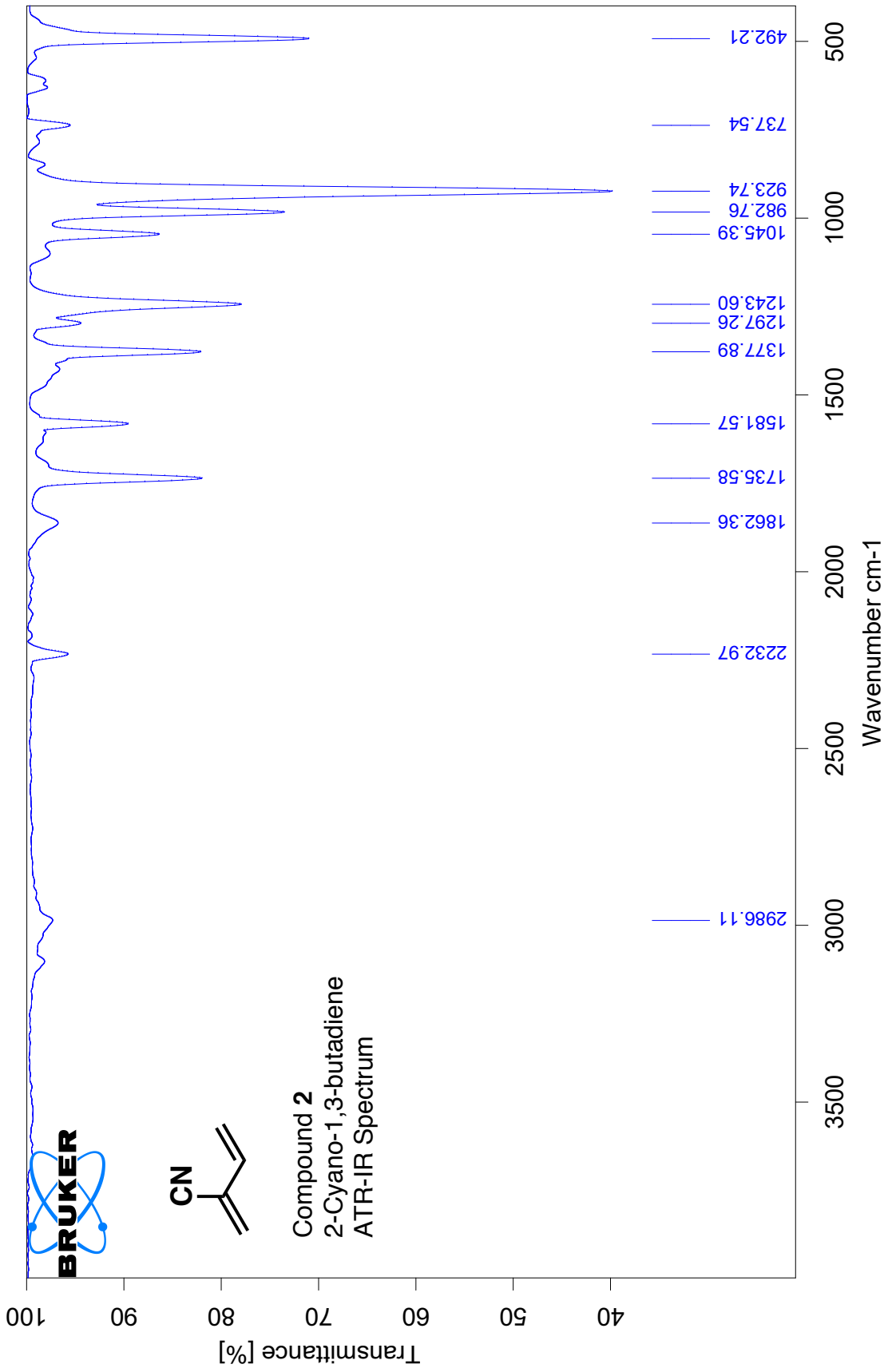
Compound **2**
2-Cyano-1,3-butadiene
$^{13}C\{^{1}H\}$-NMR, 125 MHz
$CDCl_3$

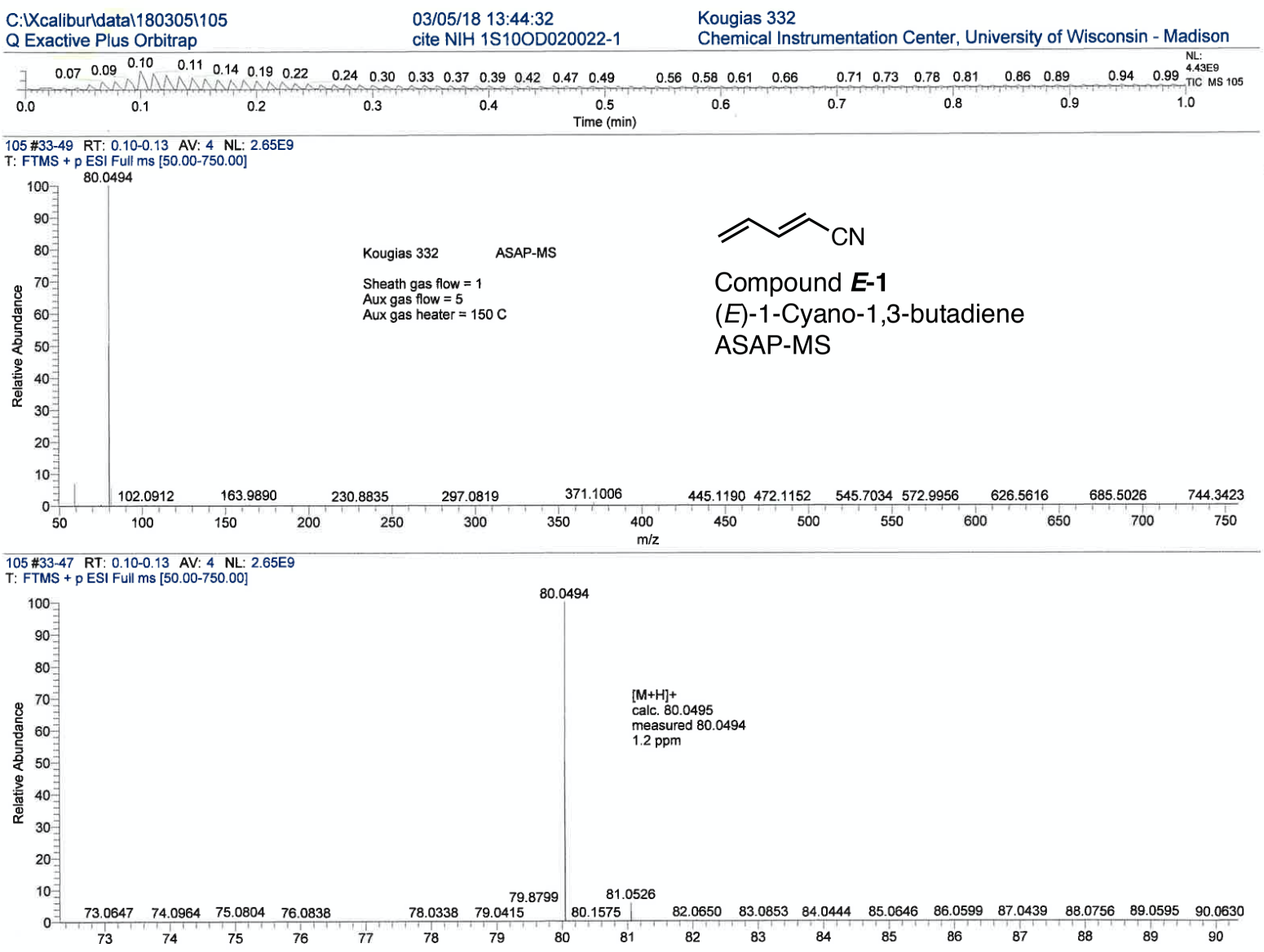


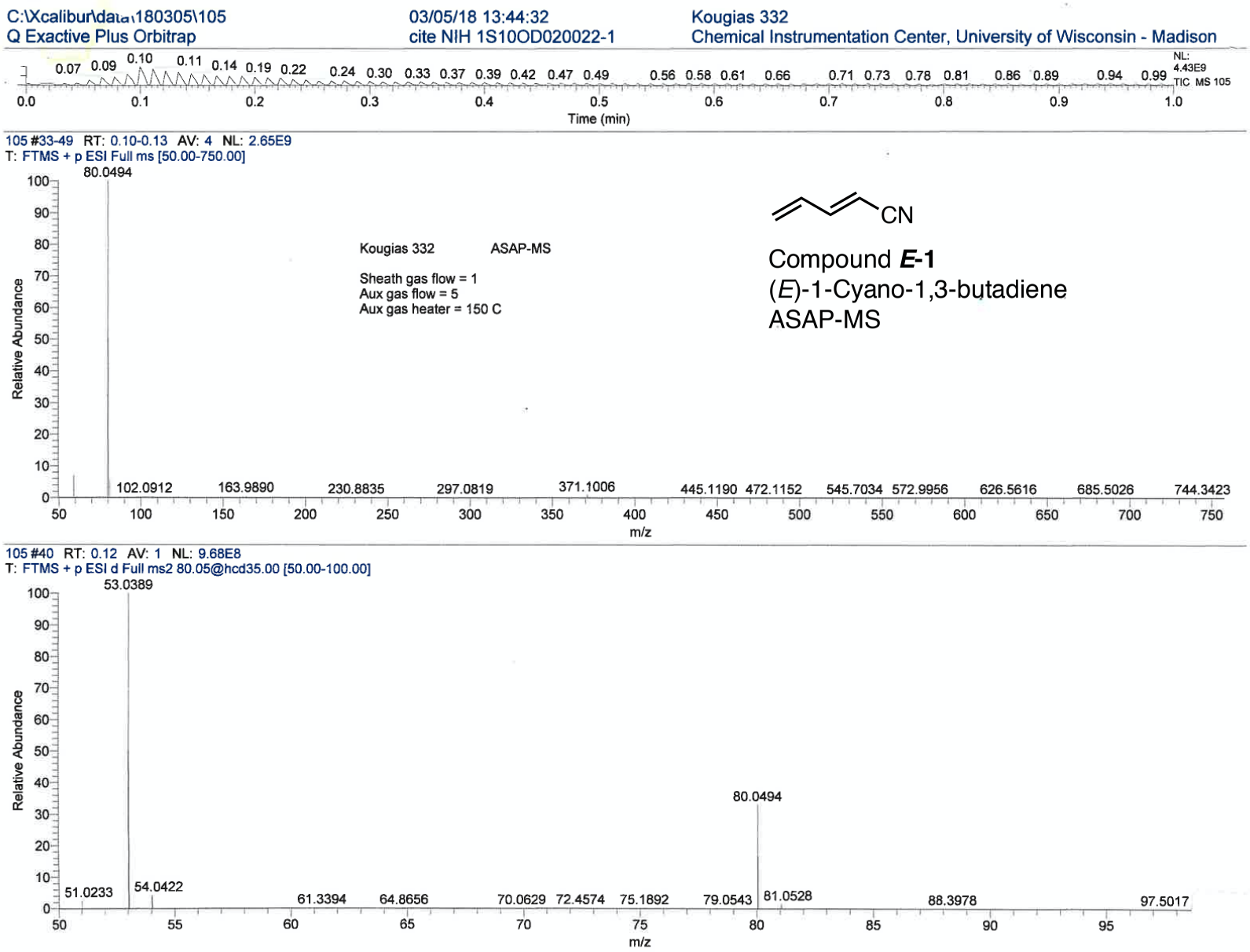

Transmittance [%]
100
90
80
70
60
50
40
Wavenumber cm-1
3500
3000
2500
2000
1500
1000
500
3053.84
3014.18
2217.78
1628.64
1588.61
1417.37
1292.29
1258.08
1001.44
955.25
931.89
834.76
779.24
669.15
474.72
BRUKER
CN
Compound E-1
(E)-1-Cyano-1,3-butadiene
ATR-IR Spectrum

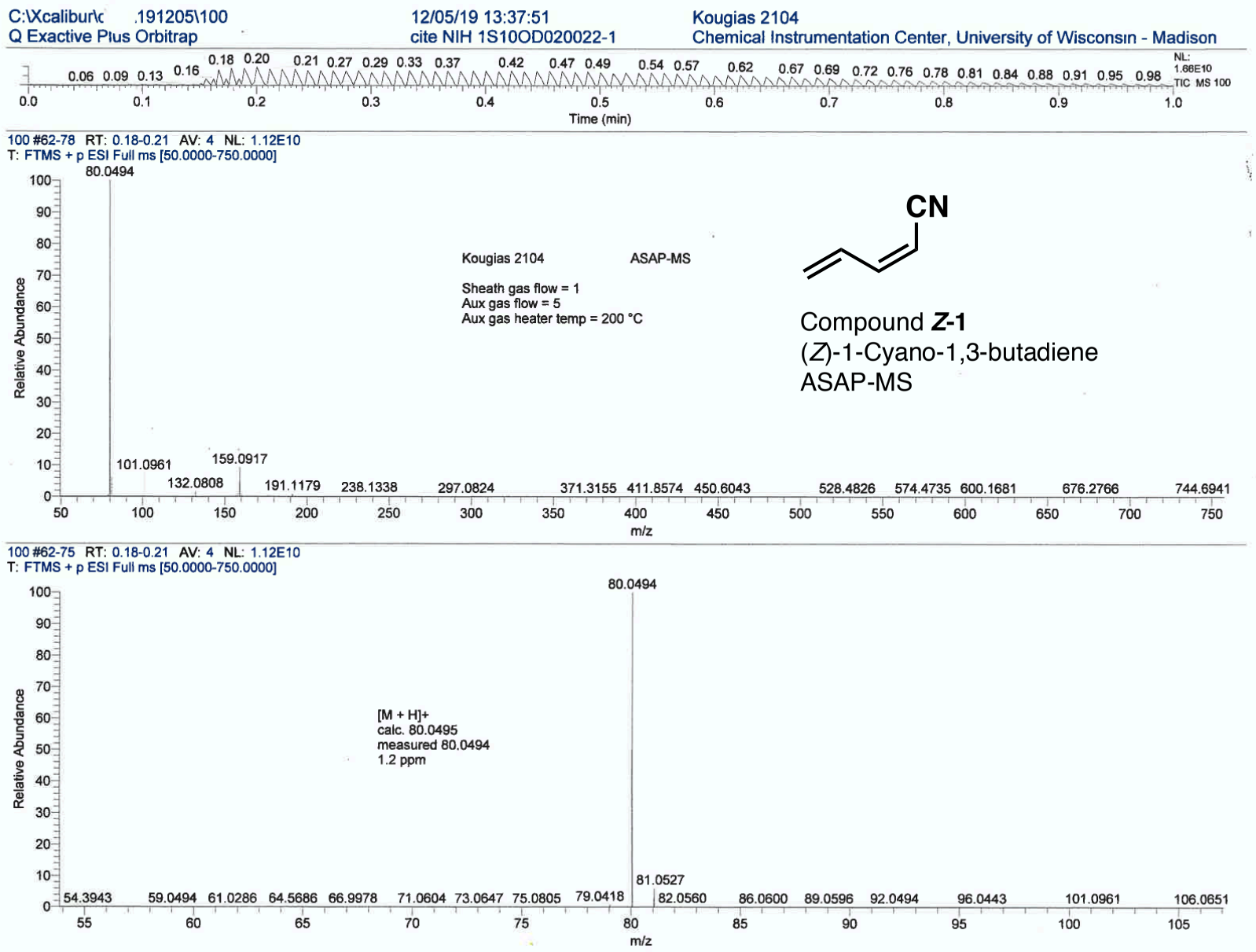

BRUKER
CN
Compound 3
4-Cyano-1,2-butadiene
ATR-IR Spectrum
Transmittance [%]
100
90
80
70
60
50
3500
3000
2500
2000
1500
1000
500
Wavenumber cm-1
2251.73
1959.79
1417.17
913.27
852.43
731.03
678.25
521.94
467.25

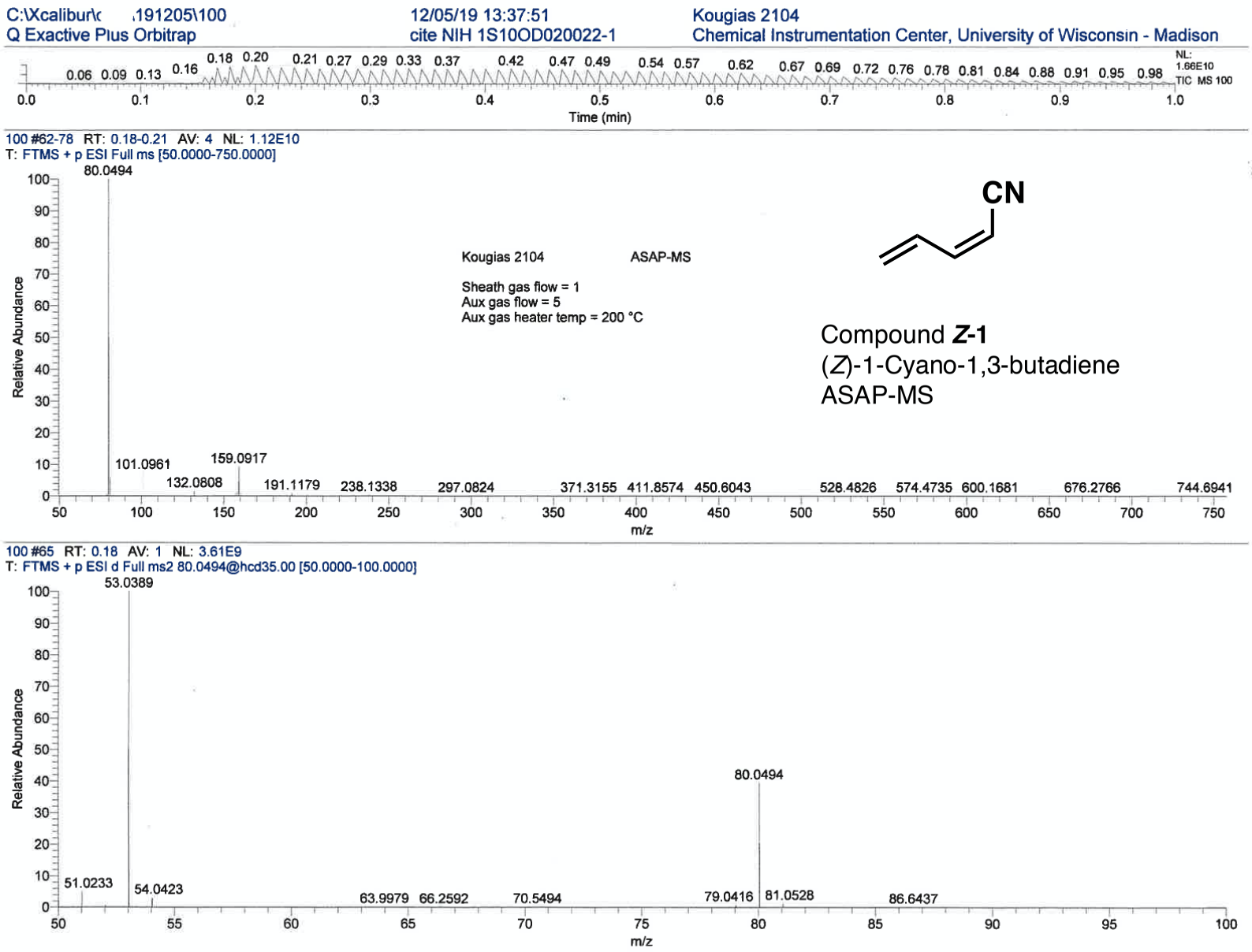

BRUKER
CN
Compound Z-1
(Z)-1-Cyano-1,3-butadiene
ATR-IR Spectrum
Transmittance [%]
100
90
80
70
60
3500
3000
2500
2000
1500
1000
500
Wavenumber cm-1
3070.62
2215.50
1628.39
1573.55
1428.29
1358.50
1296.19
1229.26
1000.91
933.57
881.63
836.06
777.53
667.32
487.49
444.03

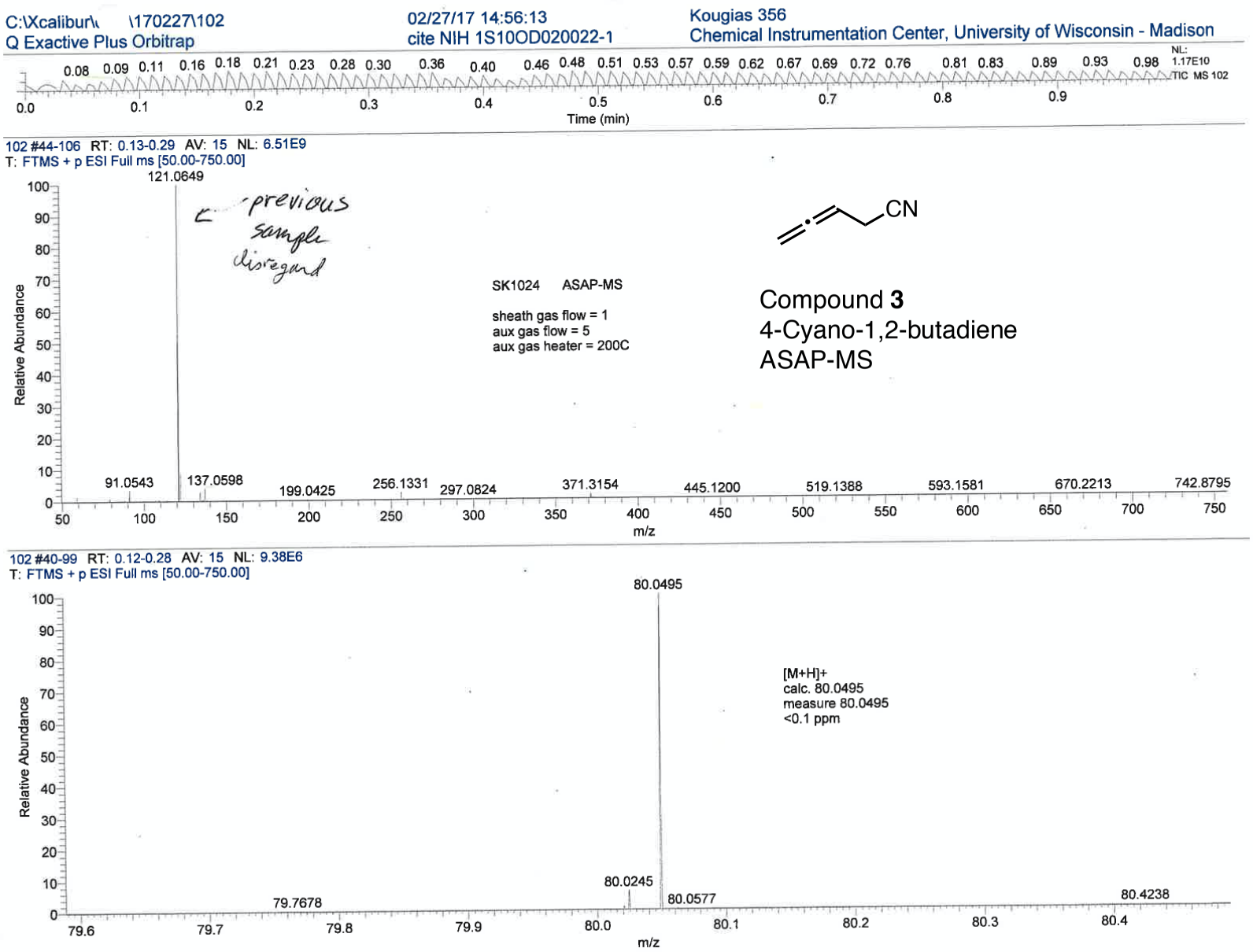

BRUKER
CN
Compound 2
2-Cyano-1,3-butadiene
ATR-IR Spectrum
Transmittance [%]
100
90
80
70
60
50
40
3500
3000
2500
2000
1500
1000
500
Wavenumber cm-1
2986.11
2232.97
1862.36
1735.58
1581.57
1377.89
1297.26
1243.60
1045.39
982.76
923.74
737.54
492.21

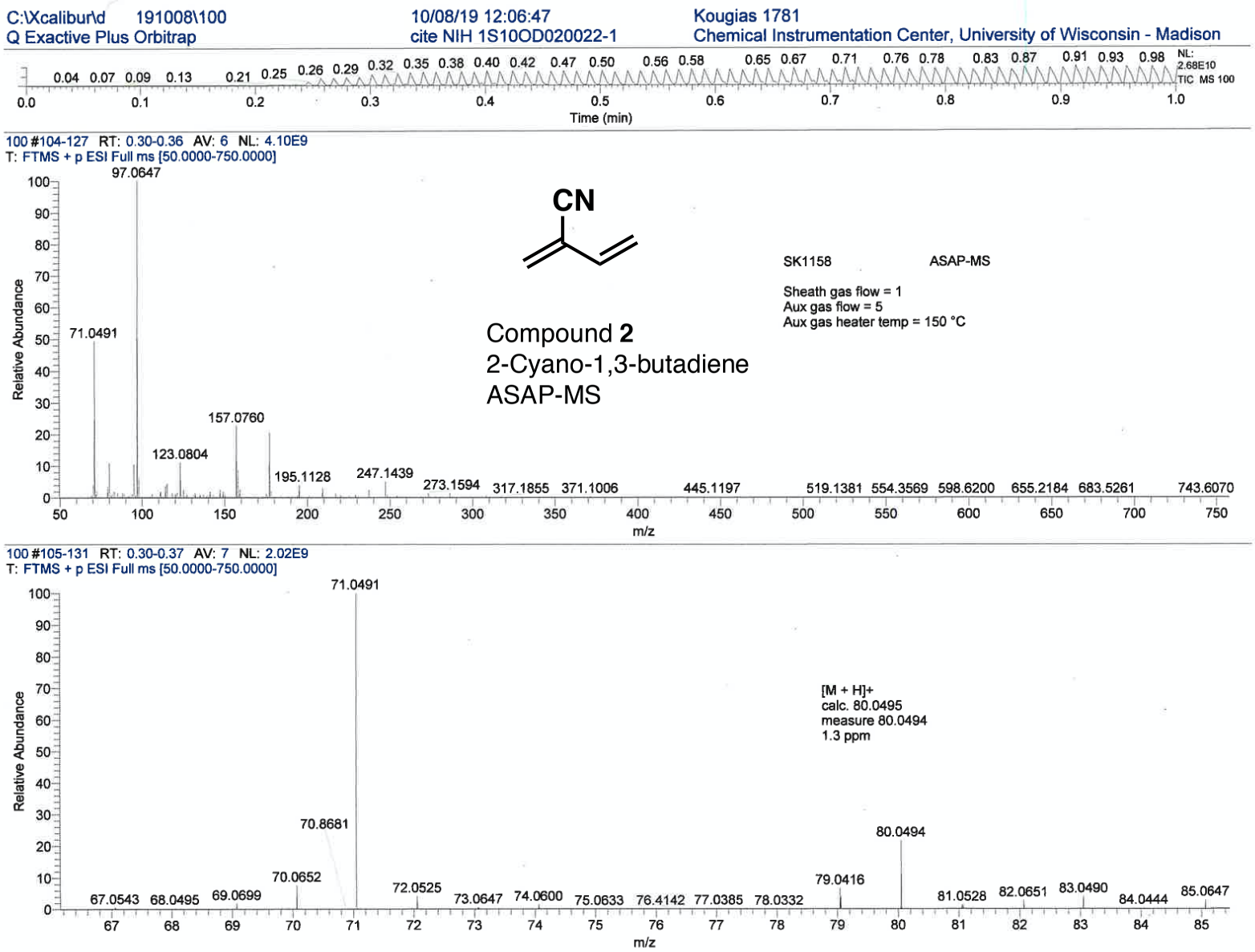

C:\Xcalibur\data\180305\105
Q Exactive Plus Orbitrap
03/05/18 13:44:32
cite NIH 1S10OD020022-1
Kougias 332
Chemical Instrumentation Center, University of Wisconsin - Madison
NL: 4.43E9 TIC MS 105
Time (min)
105 #33-49 RT: 0.10-0.13 AV: 4 NL: 2.65E9
T: FTMS + p ESI Full ms [50.00-750.00]
Relative Abundance
m/z
80.0494
Kougias 332 ASAP-MS
Sheath gas flow = 1
Aux gas flow = 5
Aux gas heater = 150 C
CN
Compound E-1
(E)-1-Cyano-1,3-butadiene
ASAP-MS
105 #33-47 RT: 0.10-0.13 AV: 4 NL: 2.65E9
T: FTMS + p ESI Full ms [50.00-750.00]
[M+H]+
calc. 80.0495
measured 80.0494
1.2 ppm


C:\Xcalibur\data\180305\105
Q Exactive Plus Orbitrap
03/05/18 13:44:32
cite NIH 1S10OD020022-1
Kougias 332
Chemical Instrumentation Center, University of Wisconsin - Madison
NL: 4.43E9 TIC MS 105
Time (min)
105 #33-49 RT: 0.10-0.13 AV: 4 NL: 2.65E9
T: FTMS + p ESI Full ms [50.00-750.00]
80.0494
Relative Abundance
m/z
Kougias 332 ASAP-MS
Sheath gas flow = 1
Aux gas flow = 5
Aux gas heater = 150 C
CN
Compound E-1
(E)-1-Cyano-1,3-butadiene
ASAP-MS
105 #40 RT: 0.12 AV: 1 NL: 9.68E8
T: FTMS + p ESI d Full ms2 80.05@hcd35.00 [50.00-100.00]
53.0389
80.0494
Relative Abundance
m/z


C:\Xcalibur\c .191205\100
Q Exactive Plus Orbitrap
12/05/19 13:37:51
cite NIH 1S10OD020022-1
Kougias 2104
Chemical Instrumentation Center, University of Wisconsin - Madison
NL: 1.66E10 TIC MS 100
Time (min)
100 #62-78 RT: 0.18-0.21 AV: 4 NL: 1.12E10
T: FTMS + p ESI Full ms [50.0000-750.0000]
80.0494
Relative Abundance
m/z
Kougias 2104 ASAP-MS
Sheath gas flow = 1
Aux gas flow = 5
Aux gas heater temp = 200 °C
CN
Compound Z-1
(Z)-1-Cyano-1,3-butadiene
ASAP-MS
100 #62-75 RT: 0.18-0.21 AV: 4 NL: 1.12E10
T: FTMS + p ESI Full ms [50.0000-750.0000]
[M + H]+
calc. 80.0495
measured 80.0494
1.2 ppm


C:\Xcalibur\c ,191205\100
Q Exactive Plus Orbitrap
12/05/19 13:37:51
cite NIH 1S10OD020022-1
Kougias 2104
Chemical Instrumentation Center, University of Wisconsin - Madison
NL: 1.66E10 TIC MS 100
Time (min)
100 #62-78 RT: 0.18-0.21 AV: 4 NL: 1.12E10
T: FTMS + p ESI Full ms [50.0000-750.0000]
80.0494
101.0961
159.0917
132.0808
191.1179
238.1338
297.0824
371.3155
411.8574
450.6043
528.4826
574.4735
600.1681
676.2766
744.6941
Relative Abundance
m/z
Kougias 2104 ASAP-MS
Sheath gas flow = 1
Aux gas flow = 5
Aux gas heater temp = 200 °C
CN
Compound Z-1
(Z)-1-Cyano-1,3-butadiene
ASAP-MS
100 #65 RT: 0.18 AV: 1 NL: 3.61E9
T: FTMS + p ESI d Full ms2 80.0494@hcd35.00 [50.0000-100.0000]
53.0389
80.0494
51.0233
54.0423
63.9979
66.2592
70.5494
79.0416
81.0528
86.6437
Relative Abundance
m/z


C:\Xcalibur\ \170227\102
Q Exactive Plus Orbitrap
02/27/17 14:56:13
cite NIH 1S10OD020022-1
Kougias 356
Chemical Instrumentation Center, University of Wisconsin - Madison
NL: 1.17E10 TIC MS 102
Time (min)
102 #44-106 RT: 0.13-0.29 AV: 15 NL: 6.51E9
T: FTMS + p ESI Full ms [50.00-750.00]
121.0649
previous sample disregard
SK1024 ASAP-MS
sheath gas flow = 1
aux gas flow = 5
aux gas heater = 200C
CN
Compound 3
4-Cyano-1,2-butadiene
ASAP-MS
Relative Abundance
m/z
102 #40-99 RT: 0.12-0.28 AV: 15 NL: 9.38E6
T: FTMS + p ESI Full ms [50.00-750.00]
80.0495
[M+H]+
calc. 80.0495
measure 80.0495
<0.1 ppm
80.0245
79.7678
80.0577
80.4238


C:\Xcalibur\d 191008\100
Q Exactive Plus Orbitrap
10/08/19 12:06:47
cite NIH 1S10OD020022-1
Kougias 1781
Chemical Instrumentation Center, University of Wisconsin - Madison
NL: 2.68E10 TIC MS 100
Time (min)
100 #104-127 RT: 0.30-0.36 AV: 6 NL: 4.10E9
T: FTMS + p ESI Full ms [50.0000-750.0000]
Relative Abundance
m/z
97.0647
71.0491
157.0760
123.0804
195.1128
247.1439
CN
Compound 2
2-Cyano-1,3-butadiene
ASAP-MS
SK1158 ASAP-MS
Sheath gas flow = 1
Aux gas flow = 5
Aux gas heater temp = 150 °C
100 #105-131 RT: 0.30-0.37 AV: 7 NL: 2.02E9
T: FTMS + p ESI Full ms [50.0000-750.0000]
71.0491
70.8681
70.0652
80.0494
79.0416
[M + H]+
calc. 80.0495
measure 80.0494
1.3 ppm

Computational Conformation Analysis of E2′ Reaction

The proposed 1-bromo-4-cyano-2-butene intermediates (***E*-11** and ***Z*-11**) of the reaction of 1,4-dibromo-2-butene (**10**) with excess cyanide have multiple conformations as a function of the bromo-methyl rotor and the cyano-methyl rotor. As discussed in the manuscript, the Curtin-Hammett principle was applied to the E2′ reaction to explain the observed diastereoselectivity. A key assumption of the Curtin-Hammett principle is that the outgoing transition states (in this case the E2′ transition states) have much larger barriers than the transition states for conversion between conformations of the starting materials. To ensure that this was the case, two-dimensional relaxed conformation scans at B3LYP/cc-pVTZ with PCM solvent corrections for water were conducted at 15° intervals of the dihedral angle for the bromo- and cyano-methyl rotors of ***E*-11** and ***Z*-11**. The results of the scan were used to obtain starting guesses for optimization of conformer stationary points reported herein. The results of these scans are depicted in Figures S1.5 and S1.6. Finally, the electronic and free energies of the stationary points are summarized in Tables S1.2 and S3.

The conformations of the ***E*-11** species are the *anti*-clinal and *syn*-periplanar positions of the bromomethyl rotor in various combinations with the *anti*-clinal and *syn*-periplanar positions of the cyanomethyl group. Thus, for ***E*-11** there are nine conformations consisting of four enantiomeric pairs of local minima and one unique local minimum. Interconnecting these conformations are eight enantiomeric pairs of transition states and two unique transition states. The 2D conformational surface is given in Figure S5 along with snapshots of the conformational local minima. Relative energies of each stationary point are provided under the molecule's designation. In addition, the approximate entrance channels to the E2′ transition states are provided based on the Intrinsic Reaction Coordinate (IRC) calculations. Most importantly, the

largest activation barrier for interconversion of any of the conformations is 4.2 kcal/mol (***E*-11y**), which is at least 10 kcal/mol lower in energy than any of the outgoing E2′ transition state barriers. Thus, should the reaction system have enough energy to surmount the E2′ barrier, the bromo- and cyano-methyl groups will act as free rotors, justifying the application of the Curtin-Hammett principle to the reaction of ***E*-11** to give **1**.

The conformations of the ***Z*-11** species are the possible combinations of the anti-clinal bromomethyl rotor with the *anti*-clinal cyanomethyl group, as the steric interactions of the bromo and cyano groups destabilize the *syn*-periplanar positions. Thus, for ***Z*-11** there are a total of four conformations consisting of two enantiomeric pairs of local minima. Interconnecting these conformations are four pairs of enantiomeric transition states. The 2-D conformational surface is given in Figure S1.6 along with snapshots of the conformational local minima. Relative energies of each stationary point are provided under the molecule's designation. In addition, the approximate entrance channels to the E2′ transition states are provided based on the Intrinsic Reaction Coordinate (IRC) calculations. Most importantly, the largest activation barrier for interconversion of any of the conformations is 5.5 kcal/mol (***Z*-11z**), which is at least 10 kcal/mol lower in energy than any of the outgoing E2′ transition state barriers. Thus, should the reaction system have enough energy to surmount the E2′ barrier, the bromo- and cyano-methyl groups will act as free rotors, justifying the application of the Curtin-Hammett principle to the reaction of the ***Z*-11** to give **1**.

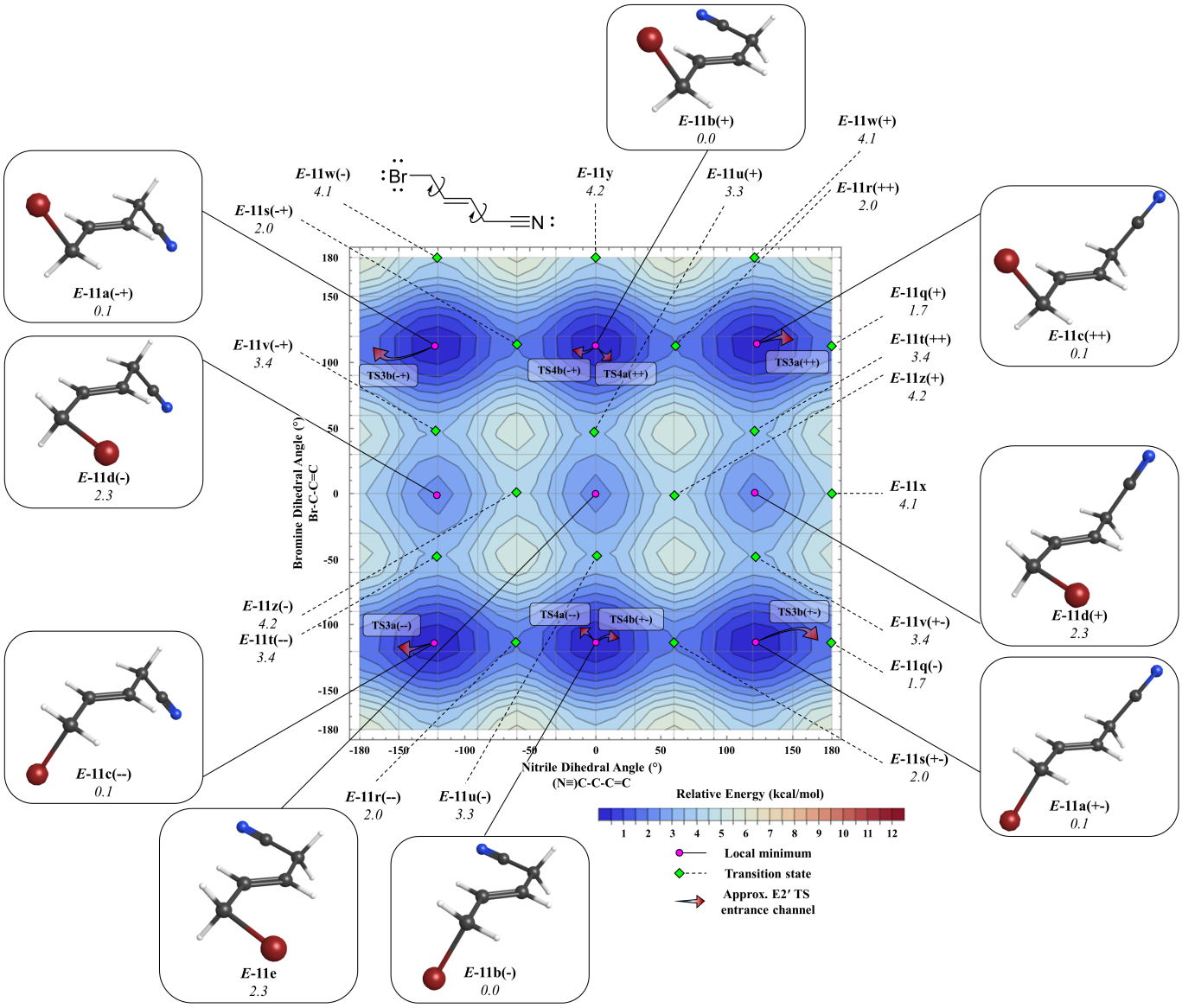


Figure S1.5. Relaxed 2-D conformational scan of (*E*)-1-bromo-4-cyano-2-butene (***E*-11**) using B3LYP/cc-pVTZ electronic energies with PCM solvent correction for water. Relative energies in kcal/mol.

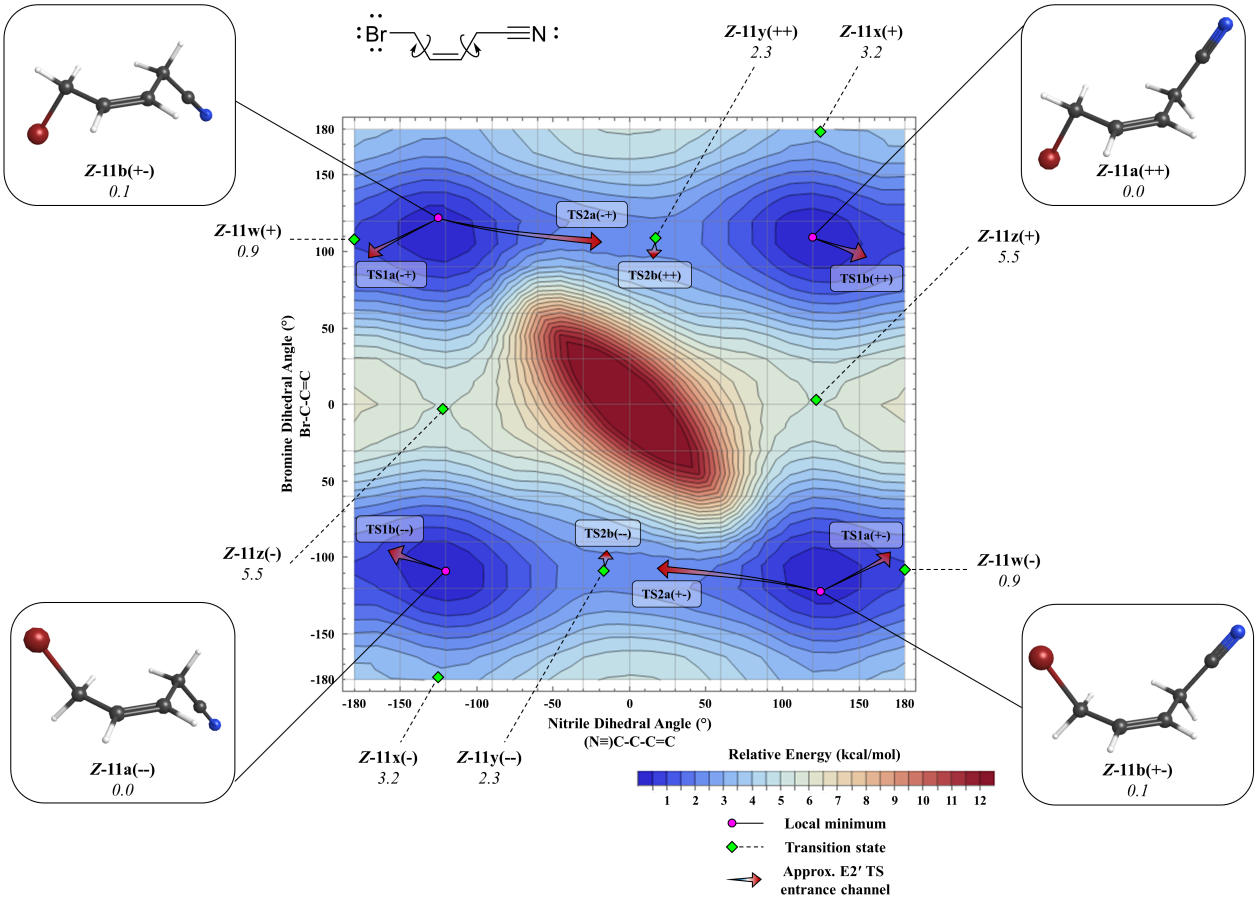


Figure S1.6. Relaxed 2-D conformational scan of (*Z*)-1-bromo-4-cyano-2-butene (***Z*-11**) using B3LYP/cc-pVTZ electronic energies with PCM solvent correction for water. Relative energies in kcal/mol.

Computed Intramolecular Isomerization Pathway of 4-Cyano-1,2-butadiene (2) to 1-Cyano-1,3-butadiene (1).

Following previous investigations of the isomerization of allenes to butadienes (antarafacial [1,3]-hydrogen shift), we briefly examined the isomerization pathway of 4-cyano-1,2-butadiene (**2**) to 1-cyano-1,3-butadiene (**1**). As illustrated in Figure S1.7, the neutral intramolecular isomerization proceeds through a high barrier (60 kcal/mol) to form a singlet carbene intermediate (**16**) that is endothermic by 50 kcal/mol *via* hydrogen transfer of the substituted terminal allene carbon to the internal unsaturated allene carbon. Lastly, one of the methylene hydrogens is transferred to the carbene to form ***E*-1** or ***Z*-1**. The high barrier of this pathway explains the stability of isolated **2** in the laboratory and emphasizes the importance of additional reagents for the efficient isomerization of **2** to **1** via an intermolecular process.

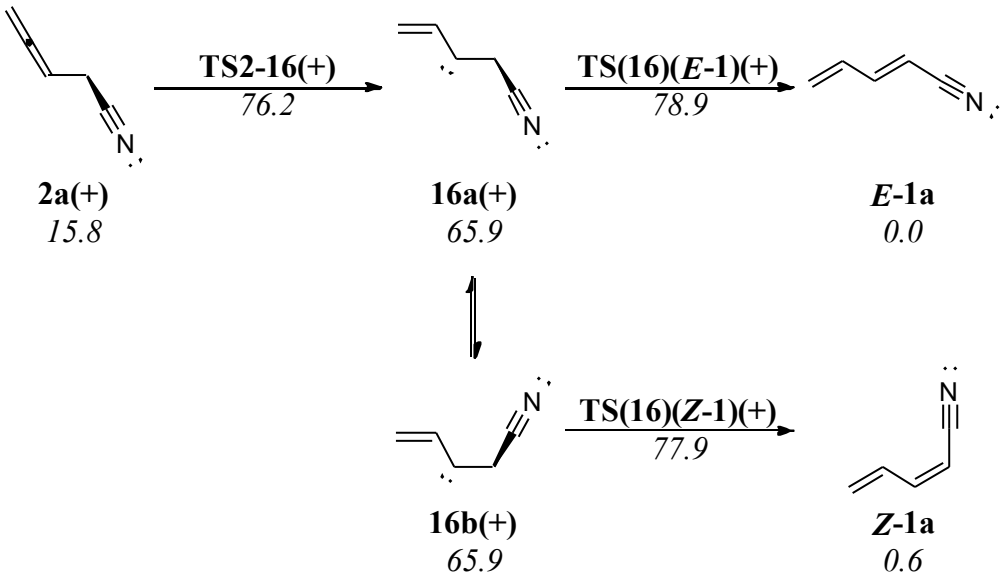


Figure S1.7. Free energies (kcal/mol) for the isomerization of 4-cyano-1,2-butadiene (**2**) to 1-cyano-1,3-butadiene (**1**) at B3LYP/cc-pVTZ with PCM (H_2O) at 298 K.

Table S1.2. Summary of Absolute Electronic and Free Energies Determined by B3LYP/cc-pVTZ with PCM(H_2O).

	Absolute Energies (Hartrees/Particle)				
Molecule	B3LYP/cc-PVTZ + PCM(H_2O)	Zero-Point Energy Correction	$\Delta G_{(273)}$	$\Delta G_{(298)}$	$\Delta G_{(323)}$
Br^-	-2574.418411	0.000000	-2574.418411	-2574.418411	-2574.418411
CN^-	-92.991754	0.004908	-93.004002	-93.005874	-93.007747
HBr	-2574.838558	0.005931	-2574.849968	-2574.851857	-2574.853746
HCN	-93.468406	0.016417	-93.469431	-93.471341	-93.473257
***E*-1a**	-248.340828	0.084356	-248.282958	-248.286009	-248.289100
***E*-1b**	-248.334771	0.084168	-248.277418	-248.280511	-248.283644
***E*-1y**	-248.334559	0.084012	-248.276615	-248.279577	-248.282573
***E*-1z**	-248.327279	0.083381	-248.270103	-248.273087	-248.276106
***Z*-1a**	-248.339893	0.084520	-248.281996	-248.285050	-248.288144
***Z*-1b**	-248.332893	0.084422	-248.275466	-248.278565	-248.281702
***Z*-1y**	-248.332731	0.084419	-248.274222	-248.277149	-248.280110
***Z*-1z**	-248.327168	0.083577	-248.269759	-248.272725	-248.275725
2a	-248.313392	0.083035		-248.260787	
2b	-248.313208	0.082958		-248.260535	
2y	-248.310685	0.082643		-248.257043	
2z	-248.311022	0.082826		-248.257424	
***E*-11a**	-2823.194404	0.098175	-2823.127395	-2823.131032	-2823.134719
***E*-11b**	-2823.194485	0.098159	-2823.127363	-2823.130984	-2823.134655
***E*-11c**	-2823.194389	0.098296	-2823.127250	-2823.130880	-2823.134561
***E*-11d**	-2823.190835	0.097896	-2823.124064	-2823.127694	-2823.131374
***E*-11e**	-2823.190824	0.097840	-2823.123940	-2823.127555	-2823.131221
***E*-11q**	-2823.191723	0.097771	-2823.124021	-2823.127493	-2823.131012
***E*-11r**	-2823.191330	0.097968	-2823.123583	-2823.127067	-2823.130597
***E*-11s**	-2823.191353	0.097961	-2823.123395	-2823.126859	-2823.130370
***E*-11t**	-2823.189099	0.097772	-2823.121718	-2823.125221	-2823.128771
***E*-11u**	-2823.189151	0.097699	-2823.121494	-2823.124965	-2823.128482
***E*-11v**	-2823.189058	0.097803	-2823.121467	-2823.124954	-2823.128487
***E*-11w**	-2823.187933	0.097626	-2823.120606	-2823.124104	-2823.127648
***E*-11x**	-2823.187932	0.097423	-2823.120623	-2823.124100	-2823.127624
***E*-11y**	-2823.187844	0.097561	-2823.120429	-2823.123910	-2823.127438
***E*-11z**	-2823.187776	0.097621	-2823.120196	-2823.123665	-2823.127180
***Z*-11a**	-2823.191453	0.098526	-2823.124487	-2823.128150	-2823.131863
***Z*-11b**	-2823.191333	0.098385	-2823.124717	-2823.128403	-2823.132138
***Z*-11w**	-2823.189959	0.098048	-2823.122111	-2823.125584	-2823.129102

Molecule	Absolute Energies (Hartrees/Particle) B3LYP/cc-PVTZ + PCM(H_2O)	Zero-Point Energy Correction	$\Delta G_{(273)}$	$\Delta G_{(298)}$	$\Delta G_{(323)}$
***Z*-11x**	-2823.186419	0.097900	-2823.119022	-2823.122526	-2823.126077
***Z*-11y**	-2823.187784	0.098354	-2823.119423	-2823.122869	-2823.126361
***Z*-11z**	-2823.182743	0.097987	-2823.115009	-2823.118484	-2823.122004
16a	-248.229912	0.080712		-248.180977	
16b	-248.230450	0.081184		-248.180942	
TS2-16	-248.212170	0.077561		-248.164655	
TS1a	-2916.168979	0.098350	-2916.111809	-2916.107383	-2916.116306
TS1b	-2916.168536	0.098410	-2916.106121	-2916.110469	-2916.114888
TS2a	-2916.166206	0.098627	-2916.103509	-2916.107845	-2916.112252
TS2b	-2916.165918	0.098570	-2916.103504	-2916.107866	-2916.112298
TS3a	-2916.170754	0.098139	-2916.108687	-2916.113050	-2916.117486
TS3b	-2916.170780	0.098076	-2916.108970	-2916.113357	-2916.117816
TS4a	-2916.170427	0.098153	-2916.108532	-2916.112916	-2916.117371
TS4b	-2916.170529	0.098102	-2916.108783	-2916.113178	-2916.117644
TS(16)(*E*-1)	-248.208169	0.078017		-248.160279	
TS(16)(*Z*-1)	-248.209734	0.078344		-248.161920	

Table S1.3. Summary of Relative Electronic and Free Energies Determined by B3LYP/cc-pVTZ with PCM(H_2O).

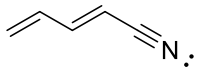
Molecule	Relative Energies (kcal/mol)[a]				
	B3LYP/cc-PVTZ + PCM(H_2O)	B3LYP/cc-PVTZ + PCM(H_2O) + ZPE	$\Delta G_{(273)}$	$\Delta G_{(298)}$	$\Delta G_{(323)}$
***E*-1a**	0.0	0.0	0.0	0.0	0.0
***E*-1b**	3.8	3.7	3.5	3.5	3.4
***E*-1y**	3.9	3.7	4.0	4.0	4.1
***E*-1z**	8.5	7.9	8.1	8.1	8.2
***Z*-1a**	0.6	0.7	0.6	0.6	0.6
***Z*-1b**	5.0	5.0	4.7	4.7	4.6
***Z*-1y**	5.1	5.1	5.5	5.6	5.6
***Z*-1z**	8.6	8.1	8.3	8.3	8.4
2a	17.2	16.4		15.8	
2b	17.3	16.5		16.0	
2y	18.9	17.8		18.2	
2z	18.7	17.7		17.9	
***E*-11a**	26.0	27.5	24.7	24.4	24.0
***E*-11b**	26.0	27.4	24.7	24.4	24.1
***E*-11c**	26.0	27.6	24.8	24.5	24.1
***E*-11d**	28.3	29.5	26.8	26.5	26.1
***E*-11e**	28.3	29.5	26.9	26.6	26.2
***E*-11q**	27.7	28.9	26.8	26.6	26.4
***E*-11r**	28.0	29.3	27.1	26.9	26.6
***E*-11s**	27.9	29.3	27.2	27.0	26.8
***E*-11t**	29.4	30.6	28.3	28.0	27.8
***E*-11u**	29.3	30.5	28.4	28.2	27.9
***E*-11v**	29.4	30.6	28.4	28.2	27.9
***E*-11w**	30.1	31.2	29.0	28.7	28.5
***E*-11x**	30.1	31.1	29.0	28.7	28.5
***E*-11y**	30.1	31.2	29.1	28.9	28.6
***E*-11z**	30.2	31.3	29.2	29.0	28.8
***Z*-11a**	27.9	29.6	26.6	26.2	25.8
***Z*-11b**	28.0	29.5	26.4	26.0	25.7
***Z*-11w**	28.8	30.2	28.0	27.8	27.6
***Z*-11x**	31.0	32.3	30.0	29.7	29.5
***Z*-11y**	30.2	31.7	29.7	29.5	29.3
***Z*-11z**	33.4	34.7	32.5	32.3	32.0
16a	69.6	67.3		65.9	
16b	69.3	67.3		65.9	

Molecule	Relative Energies (kcal/mol)[a]				
	B3LYP/cc-PVTZ + PCM(H_2O)	B3LYP/cc-PVTZ + PCM(H_2O) + ZPE	$\Delta G_{(273)}$	$\Delta G_{(298)}$	$\Delta G_{(323)}$
TS2-16	80.7	76.5		76.2	
TS1a	36.8	35.3	37.0	42.9	40.5
TS1b	37.1	35.6	40.6	41.0	41.3
TS2a	38.6	37.2	42.2	42.6	43.0
TS2b	38.7	37.4	42.2	42.6	43.0
TS3a	35.7	34.0	39.0	39.4	39.7
TS3b	35.7	34.0	38.8	39.2	39.5
TS4a	35.9	34.3	39.1	39.4	39.8
TS4b	35.8	34.2	38.9	39.3	39.6
TS(16)(*E*-1)	83.2	79.3		78.9	
TS(16)(*Z*-1)	82.3	78.5		77.9	

[a] Mass-balanced energies relative to ***E*-1a** on the $C_6H_6N_2Br^-$ surface

*Gray lines in many of the following Lewis structures indicate the plane of the internal carbon-carbon double bond.

***E*-1a**



s-trans-(E)-1-cyano-1,3-butadiene

Charge	Multiplicity	Theory/Basis Set	Full Point Group
0	1	RB3LYP/CC-pVTZ	C_S

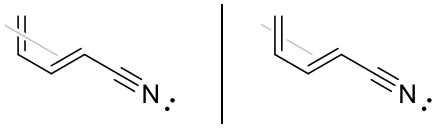
Zero-point Energy	Electronic Energy	Electronic and Zero-Point Energy	Dipole Moment (D)
0.084356	-248.340828	-248.256472	6.0956

$\Delta H_{(298)}$	$\Delta G_{(298)}$	(Energies in Hartrees/particle)
-248.249373	-248.286009	

$\Delta G_{(273)}$	$\Delta G_{(323)}$
-248.282958	-248.289100

Atom	Coordinates (Angstroms)		
	X	Y	Z
C	-0.246314	-0.883670	0.000000
C	0.000000	0.439151	0.000000
C	-1.037507	1.444586	0.000000
C	-0.777722	2.755394	0.000000
C	0.787336	-1.853471	0.000000
N	1.610852	-2.663595	0.000000
H	-1.259057	-1.266855	0.000000
H	1.026595	0.787920	0.000000
H	-2.064119	1.095075	0.000000
H	0.238374	3.129289	0.000000
H	-1.572519	3.487787	0.000000

***E*-1b(+) | *E*-1b(–)**



(+)-*s-gauche-(E)*-1-cyano-1,3-butadiene | (–)-*s-gauche-(E)*-1-cyano-1,3-butadiene

Charge	Multiplicity	Theory/Basis Set	Full Point Group
0	1	RB3LYP/CC-pVTZ	C_1
Zero-point Energy	**Electronic Energy**	**Electronic and Zero-Point Energy**	**Dipole Moment (D)**
0.084168	-248.334771	-248.250603	5.9748

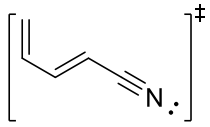
$\Delta H_{(298)}$	$\Delta G_{(298)}$
-248.243378	-248.280511

$\Delta G_{(273)}$	$\Delta G_{(323)}$
-248.277418	-248.283644

(Energies in Hartrees/particle)

Atom	Coordinates (Angstroms)		
	X	Y	Z
C	-0.515494	-0.346874	0.149330
C	0.366304	0.650251	-0.035464
C	1.815841	0.531436	0.060105
C	2.518577	-0.591642	-0.099950
C	-1.913959	-0.153959	0.015600
N	-3.057181	-0.022897	-0.084921
H	-0.200955	-1.346548	0.420411
H	-0.016985	1.639209	-0.257377
H	2.344033	1.459253	0.246448
H	2.050788	-1.537282	-0.341758
H	3.595770	-0.589618	-0.010995

***E*-1y**

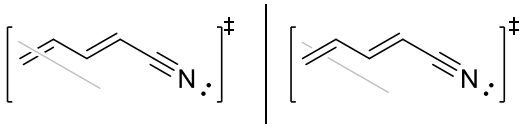


s-cis-(E)-1-cyano-1,3-butadiene

Charge	Multiplicity	Theory/Basis Set	Full Point Group
0	1	RB3LYP/CC-pVTZ	C_1
Zero-point Energy	**Electronic Energy**	**Electronic and Zero-Point Energy**	**Dipole Moment (D)**
0.084012	-248.334559	-248.250546	6.0537
$\Delta H_{(298)}$	$\Delta G_{(298)}$	(Energies in Hartrees/particle)	**Imaginary Frequency (cm^{-1})**
-248.244039	-248.279577		86.3171
$\Delta G_{(273)}$	$\Delta G_{(323)}$		
-248.276615	-248.282573		

Atom	Coordinates (Angstroms)		
	X	Y	Z
C	0.517039	-0.372573	0.000000
C	-0.361015	0.645876	0.000000
C	-1.815476	0.541312	0.000000
C	-2.533023	-0.584683	0.000000
C	1.917692	-0.156702	0.000000
N	3.063379	-0.007988	0.000000
H	0.203361	-1.408389	-0.000001
H	0.035391	1.653807	0.000000
H	-2.339269	1.489402	0.000000
H	-2.081190	-1.568077	0.000001
H	-3.613250	-0.550205	0.000000

***E*-1z(+) | *E*-1z(-)**

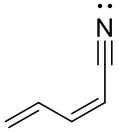


(+)-*s-skew-(E)*-1-cyano-1,3-butadiene | (–)-*s-skew-(E)*-1-cyano-1,3-butadiene

Charge	Multiplicity	Theory/Basis Set	Full Point Group
0	1	RB3LYP/CC-pVTZ	C_1
Zero-point Energy	**Electronic Energy**	**Electronic and Zero-Point Energy**	**Dipole Moment (D)**
0.083381	-248.327279	-248.243898	5.4938
$\Delta H_{(298)}$	**$\Delta G_{(298)}$**	(Energies in Hartrees/particle)	**Imaginary Frequency (cm^{-1})**
-248.237285	-248.273087		200.2876
$\Delta G_{(273)}$	**$\Delta G_{(323)}$**		
-248.270103	-248.276106		

Atom	Coordinates (Angstroms)		
	X	Y	Z
C	-0.616428	-0.266108	-0.425531
C	0.371929	-0.106936	0.459573
C	1.787955	-0.417756	0.173471
C	2.699538	0.483413	-0.169602
C	-1.973801	0.026278	-0.113611
N	-3.081702	0.256699	0.112203
H	-0.427401	-0.625411	-1.429211
H	0.131623	0.249912	1.456205
H	2.073355	-1.460827	0.277562
H	2.455139	1.532568	-0.276899
H	3.724039	0.193522	-0.358883

***Z*-1a**



s-trans-(Z)-1-cyano-1,3-butadiene

Charge	Multiplicity	Theory/Basis Set	Full Point Group
0	1	RB3LYP/CC-pVTZ	C_S

Zero-point Energy	Electronic Energy	Electronic and Zero-Point Energy	Dipole Moment (D)
0.084520	-248.339893	-248.255373	5.5887

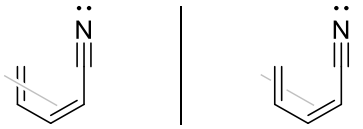
$\Delta H_{(298)}$	$\Delta G_{(298)}$
-248.248378	-248.28505

$\Delta G_{(273)}$	$\Delta G_{(323)}$
-248.281996	-248.288144

(Energies in Hartrees/particle)

Atom	Coordinates (Angstroms)		
	X	Y	Z
C	-1.218863	0.423579	0.000000
C	0.000000	0.996382	0.000000
C	1.266555	0.300483	0.000000
C	2.440012	0.939688	0.000000
C	-1.428194	-0.980405	0.000000
N	-1.628069	-2.118016	0.000000
H	-2.113271	1.031053	0.000000
H	0.038519	2.079386	0.000000
H	1.244039	-0.783378	0.000000
H	2.493942	2.021109	0.000000
H	3.376194	0.399584	0.000000

***Z*-1b(+) | *Z*-1b(–)**

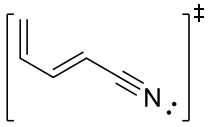


(+)-*s-gauche-(Z)*-1-cyano-1,3-butadiene | (–)-*s-gauche-(Z)*-1-cyano-1,3-butadiene

Charge	Multiplicity	Theory/Basis Set	Full Point Group
0	1	RB3LYP/CC-pVTZ	C_1
Zero-point Energy	**Electronic Energy**	**Electronic and Zero-Point Energy**	**Dipole Moment (D)**
0.084422	-248.332893	-248.248472	5.1069
$\Delta H_{(298)}$	**$\Delta G_{(298)}$**	(Energies in Hartrees/particle)	
-248.241369	-248.278565		
$\Delta G_{(273)}$	**$\Delta G_{(323)}$**		
-248.275466	-248.281702		

Atom	Coordinates (Angstroms)		
	X	Y	Z
C	0.641664	1.110847	0.100521
C	-0.701481	1.124285	0.022660
C	-1.630726	0.018690	-0.169965
C	-1.436248	-1.261582	0.154405
C	1.466219	-0.037319	-0.022662
N	2.182113	-0.938219	-0.122281
H	1.176637	2.039176	0.250630
H	-1.161539	2.103296	0.085734
H	-2.589088	0.306321	-0.587399
H	-0.528542	-1.614592	0.622640
H	-2.208825	-1.996198	-0.025385

***Z*-1y**

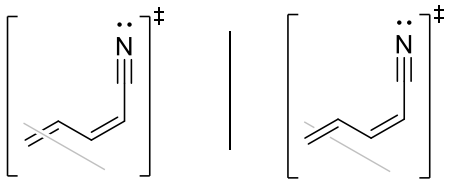


s-cis-(Z)-1-cyano-1,3-butadiene

Charge	Multiplicity	Theory/Basis Set	Full Point Group
0	1	RB3LYP/CC-pVTZ	C_1
Zero-point Energy	**Electronic Energy**	**Electronic and Zero-Point Energy**	**Dipole Moment (D)**
0.084419	-248.332731	-248.248312	5.0013
$\Delta H_{(298)}$	$\Delta G_{(298)}$	(Energies in Hartrees/particle)	**Imaginary Frequency (cm^{-1})**
-248.242033	-248.277149		51.8056
$\Delta G_{(273)}$	$\Delta G_{(323)}$		
-248.274222	-248.280110		

Atom	Coordinates (Angstroms)		
	X	Y	Z
C	-0.637556	1.122276	0.000001
C	0.709570	1.122512	0.000000
C	1.661582	0.019632	-0.000001
C	1.406720	-1.292668	0.000001
C	-1.472657	-0.022605	0.000000
N	-2.190240	-0.928048	-0.000001
H	-1.166165	2.066223	0.000002
H	1.164050	2.105556	0.000000
H	2.698326	0.334727	-0.000003
H	0.407553	-1.702191	0.000003
H	2.221957	-2.002859	0.000000

***Z*-1z(+) | *Z*-1z(–)**

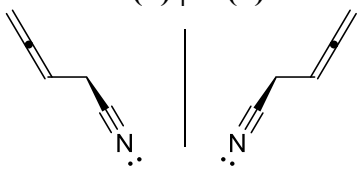


(+)-*s-skew-(Z)*-1-cyano-1,3-butadiene | (–)-*s-skew-(Z)*-1-cyano-1,3-butadiene

Charge	Multiplicity	Theory/Basis Set	Full Point Group
0	1	RB3LYP/CC-pVTZ	C_1
Zero-point Energy	**Electronic Energy**	**Electronic and Zero-Point Energy**	**Dipole Moment (D)**
0.083577	-248.327168	-248.243590	5.1811
$\Delta H_{(298)}$	**$\Delta G_{(298)}$**	(Energies in Hartrees/particle)	**Imaginary Frequency (cm^{-1})**
-248.23714	-248.272725		151.5822
$\Delta G_{(273)}$	**$\Delta G_{(323)}$**		
-248.269759	-248.275725		

Atom	Coordinates (Angstroms)		
	X	Y	Z
C	-0.795599	1.026193	-0.160230
C	0.521433	1.071014	0.064212
C	1.362270	-0.069360	0.482052
C	2.095535	-0.804693	-0.344193
C	-1.567571	-0.164555	-0.041363
N	-2.221859	-1.110820	0.047290
H	-1.341520	1.914438	-0.448840
H	1.009554	2.033546	-0.047787
H	1.374565	-0.282080	1.547458
H	2.114468	-0.620037	-1.410712
H	2.699536	-1.621723	0.025980

2a(+) | 2a(–)



(+)-*anti-clinal*-4-cyano-1,2-butadiene | (–)-*anti-clinal*-4-cyano-1,2-butadiene

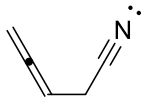
Charge	Multiplicity	Theory/Basis Set	Full Point Group
0	1	RB3LYP/CC-pVTZ	C_1

Zero-point Energy	Electronic Energy	Electronic and Zero-Point Energy	Dipole Moment (D)
0.083035	-248.313392	-248.230357	4.9760

$\Delta H_{(298)}$	$\Delta G_{(298)}$	(Energies in Hartrees/particle)
-248.222999	-248.260787	

Atom	Coordinates (Angstroms)		
	X	Y	Z
C	-0.673170	0.741549	-0.362192
C	0.458394	0.387409	0.584010
C	1.622571	-0.033155	0.182535
C	2.788534	-0.445357	-0.217962
H	3.586303	0.252523	-0.443395
H	3.002438	-1.500729	-0.338803
H	0.264552	0.514345	1.643425
C	-1.861416	-0.078506	-0.130842
N	-2.790988	-0.728603	0.062495
H	-0.962235	1.787397	-0.232899
H	-0.363617	0.615043	-1.399088

2b



syn-periplanar-4-cyano-1,2-butadiene

Charge	Multiplicity	Theory/Basis Set	Full Point Group
0	1	RB3LYP/CC-pVTZ	C_S

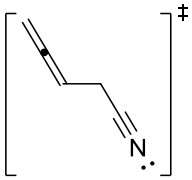
Zero-point Energy	Electronic Energy	Electronic and Zero-Point Energy	Dipole Moment (D)
0.082958	-248.313208	-248.230250	4.6967

$\Delta H_{(298)}$	$\Delta G_{(298)}$
-248.222894	-248.260535

(Energies in Hartrees/particle)

Atom	Coordinates (Angstroms)		
	X	Y	Z
C	1.326830	0.532630	0.000000
C	0.000000	1.266049	0.000000
C	-1.178461	0.715379	0.000000
C	-2.359400	0.171296	0.000000
H	-2.872118	-0.064728	0.925140
H	-2.872118	-0.064728	-0.925140
H	0.086630	2.347226	0.000000
C	1.209480	-0.919767	0.000000
N	1.119950	-2.066426	0.000000
H	1.913635	0.826846	-0.873964
H	1.913635	0.826846	0.873964

2y

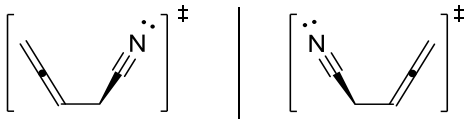


anti-periplanar-4-cyano-1,2-butadiene

Charge	Multiplicity	Theory/Basis Set	Full Point Group
0	1	RB3LYP/CC-pVTZ	C_1
Zero-point Energy	**Electronic Energy**	**Electronic and Zero-Point Energy**	**Dipole Moment (D)**
0.082643	-248.310685	-248.228043	5.0316
$\Delta H_{(298)}$	**$\Delta G_{(298)}$**	(Energies in Hartrees/particle)	**Imaginary Frequency (cm^{-1})**
-248.221394	-248.257043		71.0116

Atom	Coordinates (Angstroms)		
	X	Y	Z
C	-0.623578	0.642554	0.000002
C	0.435981	-0.453953	0.000004
C	1.713381	-0.205945	0.000001
C	2.989667	0.041520	-0.000003
H	3.544139	0.148210	0.925180
H	3.544136	0.148201	-0.925189
H	0.092224	-1.481807	0.000010
C	-1.981114	0.110756	-0.000001
N	-3.050359	-0.313582	-0.000003
H	-0.517003	1.285438	0.875781
H	-0.516999	1.285440	-0.875776

2z(+) | 2z(–)

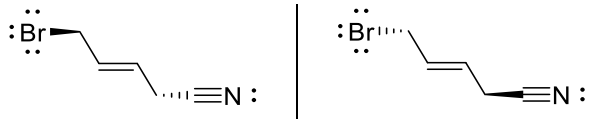


(+)-*syn-clinal*-4-cyano-1,2-butadiene | (–)-*syn-clinal*-4-cyano-1,2-butadiene

Charge	Multiplicity	Theory/Basis Set	Full Point Group
0	1	RB3LYP/CC-pVTZ	C_1
Zero-point Energy	**Electronic Energy**	**Electronic and Zero-Point Energy**	**Dipole Moment (D)**
0.082826	-248.311022	-248.228196	4.7999
$\Delta H_{(298)}$	**$\Delta G_{(298)}$**	(Energies in Hartrees/particle)	**Imaginary Frequency (cm^{-1})**
-248.221609	-248.257424		80.2687

Atom	Coordinates (Angstroms)		
	X	Y	Z
C	0.847201	0.981190	0.311493
C	-0.528247	0.975276	-0.347765
C	-1.451958	0.091027	-0.105580
C	-2.369793	-0.798118	0.131789
H	-3.093817	-0.663676	0.926870
H	-2.442657	-1.703975	-0.458728
H	-0.724676	1.776012	-1.050791
C	1.609697	-0.237297	0.055933
N	2.204078	-1.201607	-0.146822
H	1.429188	1.825148	-0.057508
H	0.762022	1.105263	1.392695

***E*-11a(+–) | *E*-11a(–+)**



(E)-1-((–)-*anti*-*clinal*-bromo)-4-((+)-*anti*-*clinal*-cyano)-2-butene |
(E)-1-((+)-*anti*-*clinal*-bromo)-4-((–)-*anti*-*clinal*-cyano)-2-butene

Charge	Multiplicity	Theory/Basis Set	Full Point Group
0	1	RB3LYP/CC-pVTZ	C_1

Zero-point Energy	Electronic Energy	Electronic and Zero-Point Energy	Dipole Moment (D)
0.098175	-2823.194404	-2823.096229	2.0861

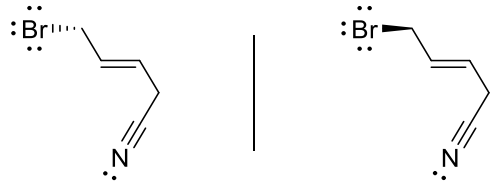
$\Delta H_{(298)}$	$\Delta G_{(298)}$
-2823.087344	-2823.131032

$\Delta G_{(273)}$	$\Delta G_{(323)}$
-2823.127395	-2823.134719

(Energies in Hartrees/particle)

Atom	Coordinates (Angstroms)		
	X	Y	Z
C	2.634131	-0.854615	-0.055435
C	1.432291	-0.026356	0.322579
C	0.397354	0.175931	-0.486006
C	-0.774353	0.994784	-0.108017
Br	-2.421607	-0.148556	0.056223
H	-0.672386	1.473083	0.858828
H	-1.051702	1.716692	-0.867977
H	0.389028	-0.255069	-1.480907
H	1.440926	0.402282	1.318225
C	3.879214	-0.091058	0.014801
N	4.853036	0.518806	0.074066
H	2.734760	-1.706725	0.622848
H	2.532536	-1.254559	-1.064802

***E*-11b(+) | *E*-11b(–)**



(E)-1-((+)-*anti-clinal*-bromo)-4-(*syn-periplanar*-cyano)-2-butene |
(E)-1-((–)-*anti-clinal*-bromo)-4-(*syn-periplanar*-cyano)-2-butene

Charge	Multiplicity	Theory/Basis Set	Full Point Group
0	1	RB3LYP/CC-pVTZ	C_1

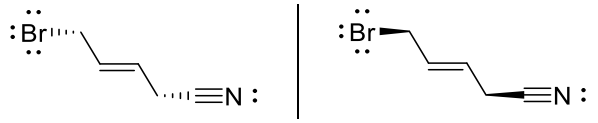
Zero-point Energy	Electronic Energy	Electronic and Zero-Point Energy	Dipole Moment (D)
0.098159	-2823.194485	-2823.096326	5.8649

$\Delta H_{(298)}$	$\Delta G_{(298)}$	(Energies in Hartrees/particle)
-2823.087491	-2823.130984	

$\Delta G_{(273)}$	$\Delta G_{(323)}$
-2823.127363	-2823.134655

Atom	Coordinates (Angstroms) X	Y	Z
C	2.850060	0.793412	-0.501990
C	1.425229	1.130914	-0.148617
C	0.568382	0.349272	0.499477
C	-0.805536	0.776028	0.838741
Br	-2.165855	-0.296053	-0.190145
H	-1.071546	0.578529	1.871081
H	-1.014618	1.806515	0.577393
H	0.861907	-0.642598	0.823366
H	1.119123	2.119053	-0.472474
C	3.288578	-0.529807	-0.075634
N	3.633191	-1.573951	0.262005
H	2.990052	0.866111	-1.584360
H	3.527383	1.532995	-0.065829

***E*-11c(++) | *E*-11c(--)**



(E)-1-((+)-*anti*-*clinal*-bromo)-4-((+)-*anti*-*clinal*-cyano)-2-butene |
(E)-1-((–)-*anti*-*clinal*-bromo)-4-((–)-*anti*-*clinal*-cyano)-2-butene

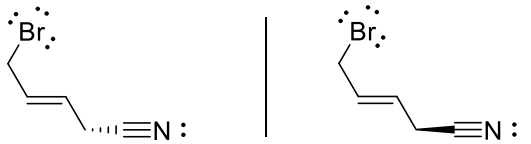
Charge	Multiplicity	Theory/Basis Set	Full Point Group
0	1	RB3LYP/CC-pVTZ	C_1
Zero-point Energy	**Electronic Energy**	**Electronic and Zero-Point Energy**	**Dipole Moment (D)**
0.098296	-2823.194389	-2823.096093	6.1826

$\Delta H_{(298)}$	$\Delta G_{(298)}$	(Energies in Hartrees/particle)
-2823.087272	-2823.13088	

$\Delta G_{(273)}$	$\Delta G_{(323)}$
-2823.127250	-2823.134561

Atom	Coordinates (Angstroms)		
	X	Y	Z
C	-2.803873	0.735233	-0.329228
C	-1.459776	0.804092	0.350609
C	-0.316475	0.982723	-0.302423
C	0.988632	1.117067	0.379702
Br	2.182391	-0.442750	-0.053342
H	1.563736	1.969506	0.035821
H	0.911737	1.115062	1.460466
H	-0.311048	1.058881	-1.384029
H	-1.465164	0.721169	1.431496
C	-3.506243	-0.514260	-0.039622
N	-4.050339	-1.500304	0.195965
H	-3.443969	1.555333	0.007880
H	-2.700203	0.829307	-1.410643

***E*-11d(+) | *E*-11d(–)**



(E)-1-(*syn-periplanar*-bromo)-4-((+)-*anti-clinal*-cyano)-2-butene |
(E)-1-(*syn-periplanar*-bromo)-4-((–)-*anti-clinal*-cyano)-2-butene

Charge	Multiplicity	Theory/Basis Set	Full Point Group
0	1	RB3LYP/CC-pVTZ	C_1

Zero-point Energy	Electronic Energy	Electronic and Zero-Point Energy	Dipole Moment (D)
0.097896	-2823.190835	-2823.092939	5.9936

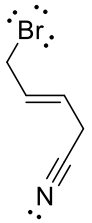
$\Delta H_{(298)}$	$\Delta G_{(298)}$
-2823.08409	-2823.127694

$\Delta G_{(273)}$	$\Delta G_{(323)}$
-2823.124064	-2823.131374

(Energies in Hartrees/particle)

Atom	Coordinates (Angstroms)		
	X	Y	Z
C	-2.584756	0.592985	0.609834
C	-1.112717	0.371201	0.361615
C	-0.330032	1.279861	-0.199781
C	1.132904	1.204133	-0.473797
Br	2.012774	-0.483439	0.059448
H	1.340474	1.304394	-1.536056
H	1.675230	1.982102	0.057356
H	-0.757047	2.227734	-0.519018
H	-0.709753	-0.579965	0.684694
C	-3.416624	-0.405824	-0.060630
N	-4.061024	-1.197696	-0.591487
H	-2.804814	0.534641	1.679386
H	-2.896651	1.581191	0.269928

***E*-11e**



(E)-1-(*syn-periplanar*-bromo)-4-(*syn-periplanar*-cyano)-2-butene

Charge	Multiplicity	Theory/Basis Set	Full Point Group
0	1	RB3LYP/CC-pVTZ	C_1

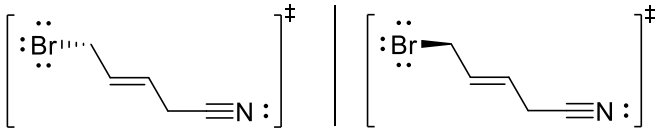
Zero-point Energy	Electronic Energy	Electronic and Zero-Point Energy	Dipole Moment (D)
0.097840	-2823.190824	-2823.092983	2.2658

$\Delta H_{(298)}$	$\Delta G_{(298)}$	(Energies in Hartrees/particle)
-2823.084126	-2823.127555	

$\Delta G_{(273)}$	$\Delta G_{(323)}$
-2823.123940	-2823.131221

Atom	Coordinates (Angstroms)		
	X	Y	Z
C	2.463141	-1.114307	-0.000020
C	1.037087	-0.622675	-0.000009
C	0.652046	0.643704	-0.000020
C	-0.735829	1.187591	-0.000024
Br	-2.181099	-0.162199	0.000009
H	-0.922961	1.794881	0.881767
H	-0.922970	1.794847	-0.881836
H	1.397973	1.434817	-0.000028
H	0.301787	-1.416833	0.000000
C	3.473032	-0.063098	0.000007
N	4.267351	0.769053	0.000034
H	2.638167	-1.750732	0.871851
H	2.638171	-1.750688	-0.871922

_E_-11q(+) | _E_-11q(–)



(E)-1-((+)-*anti-clinal*-bromo)-4-(*anti-periplanar*-cyano)-2-butene |
(E)-1-((–)-*anti-clinal*-bromo)-4-(*anti-periplanar*-cyano)-2-butene

Charge	Multiplicity	Theory/Basis Set	Full Point Group
0	1	RB3LYP/CC-pVTZ	C_1

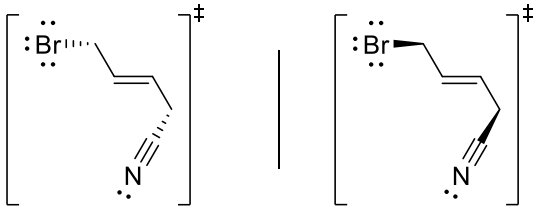
Zero-point Energy	Electronic Energy	Electronic and Zero-Point Energy	Dipole Moment (D)
0.097771	-2823.191723	-2823.093952	4.1689

$\Delta H_{(298)}$	$\Delta G_{(298)}$	(Energies in Hartrees/particle)	Imaginary Frequency (cm^{-1})
-2823.085792	-2823.127493		73.7049

$\Delta G_{(273)}$	$\Delta G_{(323)}$
-2823.124021	-2823.131012

Atom	Coordinates (Angstroms)		
	X	Y	Z
C	-2.688878	0.391034	-0.648253
C	-1.447318	0.310629	0.217032
C	-0.286509	0.856125	-0.130839
C	0.911729	0.809139	0.732057
Br	2.353848	-0.324453	-0.102538
H	1.396286	1.772432	0.844862
H	0.729468	0.353393	1.698040
H	-0.185971	1.381209	-1.074603
H	-1.536197	-0.215712	1.159564
C	-3.839223	-0.289242	-0.065419
N	-4.744487	-0.826364	0.398486
H	-2.972225	1.431265	-0.824657
H	-2.503438	-0.048298	-1.631232

_E_-11r(++) | _E_-11r(--)

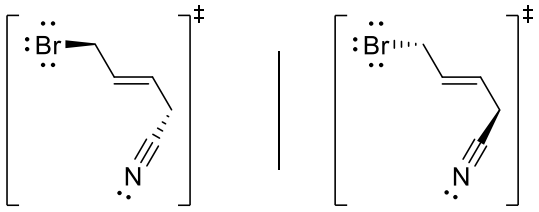


(E)-1-((+)-*anti-clinal*-bromo)-4-((+)-*syn-clinal*-cyano)-2-butene |
(E)-1-((−)-*anti-clinal*-bromo)-4-((−)-*syn-clinal*-cyano)-2-butene

Charge	Multiplicity	Theory/Basis Set	Full Point Group
0	1	RB3LYP/CC-pVTZ	C_1
Zero-point Energy	**Electronic Energy**	**Electronic and Zero-Point Energy**	**Dipole Moment (D)**
0.097968	-2823.191330	-2823.093362	6.9137
$\Delta H_{(298)}$	$\Delta G_{(298)}$	(Energies in Hartrees/particle)	**Imaginary Frequency (cm^{-1})**
-2823.085232	-2823.127067		89.9063
$\Delta G_{(273)}$	$\Delta G_{(323)}$		
-2823.123583	-2823.130597		

Atom	Coordinates (Angstroms)		
	X	Y	Z
C	-2.927896	-0.765245	-0.119204
C	-1.468437	-1.107148	-0.358399
C	-0.483250	-0.811376	0.482682
C	0.921179	-1.205370	0.244034
Br	2.073714	0.413631	-0.073229
H	1.385819	-1.671342	1.105743
H	1.051873	-1.815245	-0.641945
H	-0.685407	-0.272221	1.402029
H	-1.254114	-1.640746	-1.276114
C	-3.168878	0.670429	-0.002223
N	-3.353741	1.802415	0.090632
H	-3.543834	-1.140855	-0.935664
H	-3.294448	-1.241317	0.793186

***E*-11s(+–) | *E*-11s(–+)**



(E)-1-((–)-*anti-clinal*-bromo)-4-((+)-*syn-clinal*-cyano)-2-butene |
(E)-1-((+)-*anti-clinal*-bromo)-4-((–)-*syn-clinal*-cyano)-2-butene

Charge	Multiplicity	Theory/Basis Set	Full Point Group
0	1	RB3LYP/CC-pVTZ	C_1

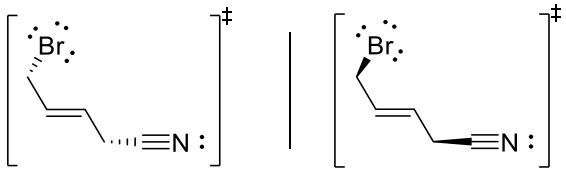
Zero-point Energy	Electronic Energy	Electronic and Zero-Point Energy	Dipole Moment (D)
0.097961	-2823.191353	-2823.093392	3.6263

$\Delta H_{(298)}$	$\Delta G_{(298)}$	(Energies in Hartrees/particle)	Imaginary Frequency (cm^{-1})
-2823.085254	-2823.126859		71.9978

$\Delta G_{(273)}$	$\Delta G_{(323)}$
-2823.123395	-2823.130370

Atom	Coordinates (Angstroms)		
	X	Y	Z
C	-2.706927	0.993123	-0.223173
C	-1.401517	0.733475	0.506430
C	-0.531134	-0.211668	0.168175
C	0.723225	-0.452276	0.912299
Br	2.323094	-0.007874	-0.224437
H	0.827425	0.171312	1.792229
H	0.880040	-1.496532	1.158608
H	-0.727613	-0.866321	-0.674137
H	-1.194268	1.384607	1.346701
C	-3.607352	-0.156600	-0.224537
N	-4.313757	-1.064981	-0.224771
H	-3.235854	1.829211	0.233129
H	-2.519487	1.271846	-1.263010

_E_-11t(++) | _E_-11t(--)

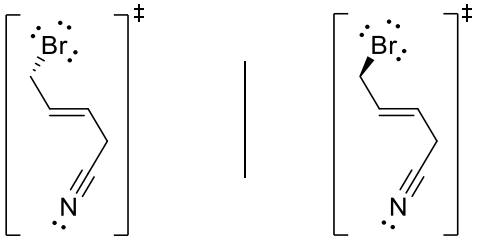


(E)-1-((+)-*syn*-*clinal*-bromo)-4-((+)-*anti*-*clinal*-cyano)-2-butene |
(E)-1-((−)-*syn*-*clinal*-bromo)-4-((−)-*anti*-*clinal*-cyano)-2-butene

Charge	Multiplicity	Theory/Basis Set	Full Point Group
0	1	RB3LYP/CC-pVTZ	C_1
Zero-point Energy	**Electronic Energy**	**Electronic and Zero-Point Energy**	**Dipole Moment (D)**
0.097772	-2823.189099	-2823.091327	6.6936
$\Delta H_{(298)}$	**$\Delta G_{(298)}$**	(Energies in Hartrees/particle)	**Imaginary Frequency (cm^{-1})**
-2823.083157	-2823.125221		103.1515
$\Delta G_{(273)}$	**$\Delta G_{(323)}$**		
-2823.121718	-2823.128771		

Atom	Coordinates (Angstroms)		
	X	Y	Z
C	-2.672722	0.776041	0.248465
C	-1.180624	0.646953	0.421824
C	-0.303316	1.312801	-0.317130
C	1.181157	1.296565	-0.148958
Br	1.962584	-0.532745	0.020302
H	1.687456	1.727503	-1.003772
H	1.508051	1.799603	0.755670
H	-0.660628	1.966388	-1.106585
H	-0.847404	-0.031884	1.198047
C	-3.310682	-0.504363	-0.056247
N	-3.802325	-1.517127	-0.293995
H	-3.129956	1.157556	1.165806
H	-2.914563	1.478832	-0.549485

***E*-11u(+) | *E*-11u(–)**



(E)-1-((+)-*syn-clinal*-bromo)-4-(*syn-periplanar*-cyano)-2-butene |
(E)-1-((–)-*syn-clinal*-bromo)-4-(*syn-periplanar*-cyano)-2-butene

Charge	Multiplicity	Theory/Basis Set	Full Point Group
0	1	RB3LYP/CC-pVTZ	C_1

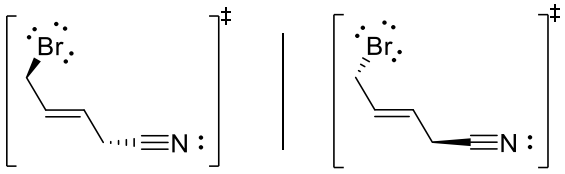
Zero-point Energy	Electronic Energy	Electronic and Zero-Point Energy	Dipole Moment (D)
0.097699	-2823.189151	-2823.091451	3.2868

$\Delta H_{(298)}$	$\Delta G_{(298)}$	(Energies in Hartrees/particle)	Imaginary Frequency (cm^{-1})
-2823.083282	-2823.124965		89.5655

$\Delta G_{(273)}$	$\Delta G_{(323)}$
-2823.121494	-2823.128482

Atom	Coordinates (Angstroms)		
	X	Y	Z
C	2.523169	1.079286	0.191861
C	1.104121	0.632857	0.431025
C	0.637195	-0.599514	0.286079
C	-0.759927	-1.045440	0.571082
Br	-2.172613	0.138905	-0.198386
H	-0.965604	-2.019464	0.144776
H	-0.990673	-1.060256	1.631686
H	1.302432	-1.392764	-0.038844
H	0.442335	1.436707	0.731024
C	3.439308	0.018235	-0.208324
N	4.160333	-0.820302	-0.524792
H	2.546219	1.855708	-0.578218
H	2.921216	1.547963	1.096287

***E*-11v(+–) | *E*-11v(–+)**



(E)-1-((–)-*syn*-*clinal*-bromo)-4-((+)-*anti*-*clinal*-cyano)-2-butene |
(E)-1-((+)-*syn*-*clinal*-bromo)-4-((–)-*anti*-*clinal*-cyano)-2-butene

Charge	Multiplicity	Theory/Basis Set	Full Point Group
0	1	RB3LYP/CC-pVTZ	C_1

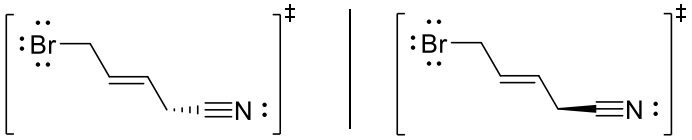
Zero-point Energy	Electronic Energy	Electronic and Zero-Point Energy	Dipole Moment (D)
0.097803	-2823.189058	-2823.091254	4.4212

$\Delta H_{(298)}$	$\Delta G_{(298)}$	(Energies in Hartrees/particle)	Imaginary Frequency (cm^{-1})
-2823.083083	-2823.124954		94.3808

$\Delta G_{(273)}$	$\Delta G_{(323)}$
-2823.121467	-2823.128487

Atom	Coordinates (Angstroms)		
	X	Y	Z
C	-2.540075	0.149094	0.845368
C	-1.178596	0.068711	0.201749
C	-0.371117	1.113288	0.077155
C	0.979212	1.111572	-0.562738
Br	2.164673	-0.379771	0.032722
H	0.933043	0.987775	-1.640229
H	1.536994	2.009446	-0.326986
H	-0.696726	2.083339	0.439313
H	-0.867371	-0.913625	-0.133503
C	-3.604488	-0.289815	-0.056371
N	-4.433767	-0.638647	-0.773678
H	-2.581635	-0.488647	1.732810
H	-2.761089	1.167128	1.168079

***E*-11w(+) | *E*-11w(–)**



(E)-1-(*anti-periplanar*-bromo)-4-((+)-*anti-clinal*-cyano)-2-butene |
(E)-1-(*anti-periplanar*-bromo)-4-((–)-*anti-clinal*-cyano)-2-butene

Charge	Multiplicity	Theory/Basis Set	Full Point Group
0	1	RB3LYP/CC-pVTZ	C_1

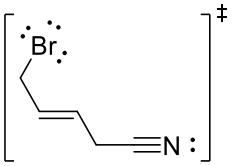
Zero-point Energy	Electronic Energy	Electronic and Zero-Point Energy	Dipole Moment (D)
0.097626	-2823.187933	-2823.090307	3.9493

$\Delta H_{(298)}$	$\Delta G_{(298)}$	(Energies in Hartrees/particle)	Imaginary Frequency (cm^{-1})
-2823.082102	-2823.124104		124.6095

$\Delta G_{(273)}$	$\Delta G_{(323)}$
-2823.120606	-2823.127648

Atom	Coordinates (Angstroms)		
	X	Y	Z
C	-2.817349	0.523427	-0.682642
C	-1.610795	0.671148	0.211663
C	-0.392964	0.284731	-0.143291
C	0.804378	0.465108	0.745208
Br	2.461761	-0.209278	-0.099915
H	1.009386	1.507799	0.965196
H	0.721839	-0.088667	1.674904
H	-0.231762	-0.178603	-1.108974
H	-1.787739	1.134112	1.176173
C	-3.865520	-0.292045	-0.069970
N	-4.683552	-0.933632	0.423251
H	-3.252547	1.501950	-0.903500
H	-2.542444	0.069337	-1.635340

E-11x



(E)-1-(*syn-periplanar*-bromo)-4-(*anti-periplanar*-cyano)-2-butene

Charge	Multiplicity	Theory/Basis Set	Full Point Group
0	1	RB3LYP/CC-pVTZ	C_1

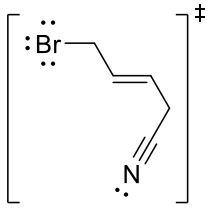
Zero-point Energy	Electronic Energy	Electronic and Zero-Point Energy	Dipole Moment (D)
0.097423	-2823.187932	-2823.090509	6.7710

$\Delta H_{(298)}$	$\Delta G_{(298)}$	(Energies in Hartrees/particle)	Imaginary Frequency (cm^{-1})
-2823.082339	-2823.1241		89.1381

$\Delta G_{(273)}$	$\Delta G_{(323)}$
-2823.120623	-2823.127624

Atom	Coordinates (Angstroms)		
	X	Y	Z
C	-2.607206	0.772754	0.000002
C	-1.118716	0.476051	0.000002
C	-0.202976	1.432113	0.000000
C	1.280852	1.293431	-0.000002
Br	1.961225	-0.562834	0.000000
H	1.721603	1.751311	-0.881860
H	1.721605	1.751314	0.881853
H	-0.515460	2.474287	-0.000002
H	-0.821232	-0.563765	0.000004
C	-3.428662	-0.432142	0.000000
N	-4.073418	-1.384953	-0.000002
H	-2.887610	1.363742	0.874820
H	-2.887609	1.363744	-0.874816

E-11y



(E)-1-(*anti-periplanar*-bromo)-4-(*syn-periplanar*-cyano)-2-butene

Charge	Multiplicity	Theory/Basis Set	Full Point Group
0	1	RB3LYP/CC-pVTZ	C_1

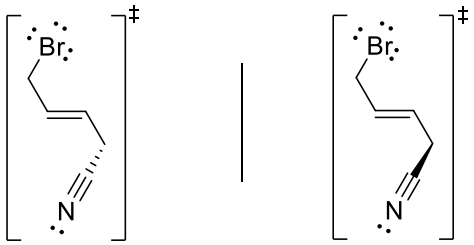
Zero-point Energy	Electronic Energy	Electronic and Zero-Point Energy	Dipole Moment (D)
0.097561	-2823.187844	-2823.090284	6.7439

$\Delta H_{(298)}$	$\Delta G_{(298)}$	(Energies in Hartrees/particle)	Imaginary Frequency (cm^{-1})
-2823.082102	-2823.12391		124.3362

$\Delta G_{(273)}$	$\Delta G_{(323)}$
-2823.120429	-2823.127438

Atom	Coordinates (Angstroms)		
	X	Y	Z
C	-3.086771	-0.751398	0.000013
C	-1.661727	-1.246458	0.000000
C	-0.573363	-0.489721	-0.000007
C	0.810716	-1.073370	-0.000015
Br	2.205561	0.331699	0.000003
H	1.016482	-1.666192	0.885349
H	1.016482	-1.666170	-0.885393
H	-0.656709	0.589858	-0.000005
H	-1.580062	-2.327696	-0.000002
C	-3.226030	0.699512	0.000000
N	-3.333037	1.844849	-0.000009
H	-3.618267	-1.142315	-0.872125
H	-3.618245	-1.142298	0.872171

E-11z(+) | *E*-11z(–)



(E)-1-(*syn-periplanar*-bromo)-4-((+)-*syn-clinal*-cyano)-2-butene |
(E)-1-(*syn-periplanar*-bromo)-4-((–)-*syn-clinal*-cyano)-2-butene

Charge	Multiplicity	Theory/Basis Set	Full Point Group
0	1	RB3LYP/CC-pVTZ	C_1

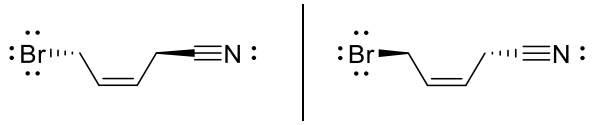
Zero-point Energy	Electronic Energy	Electronic and Zero-Point Energy	Dipole Moment (D)
0.097621	-2823.187776	-2823.090155	3.9118

$\Delta H_{(298)}$	$\Delta G_{(298)}$	(Energies in Hartrees/particle)	Imaginary Frequency (cm^{-1})
-2823.082008	-2823.123665		83.0746

$\Delta G_{(273)}$	$\Delta G_{(323)}$
-2823.120196	-2823.127180

Atom	Coordinates (Angstroms)		
	X	Y	Z
C	-2.519275	-0.857740	0.580470
C	-1.060699	-0.497921	0.353499
C	-0.561172	0.712609	0.548188
C	0.844569	1.174347	0.372620
Br	2.130121	-0.212188	-0.203503
H	0.913773	1.951205	-0.384617
H	1.251345	1.563706	1.302357
H	-1.214774	1.518302	0.876361
H	-0.421177	-1.306172	0.026686
C	-3.442307	-0.087852	-0.249068
N	-4.166186	0.522556	-0.903248
H	-2.684062	-1.913344	0.365841
H	-2.802739	-0.705679	1.624455

_Z_-11a(++) | _Z_-11a(--)



(Z)-1-((+)-*anti-clinal*-bromo)-4-((+)-*anti-clinal*-cyano)-2-butene |
(Z)-1-((−)-*anti-clinal*-bromo)-4-((−)-*anti-clinal*-cyano)-2-butene

Charge	Multiplicity	Theory/Basis Set	Full Point Group
0	1	RB3LYP/CC-pVTZ	C_1

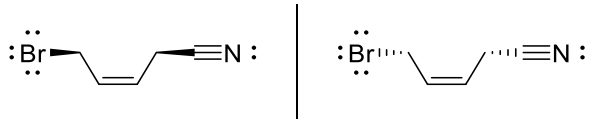
Zero-point Energy	Electronic Energy	Electronic and Zero-Point Energy	Dipole Moment (D)
0.098526	-2823.191453	-2823.092927	2.2651

$\Delta H_{(298)}$	$\Delta G_{(298)}$	(Energies in Hartrees/particle)
-2823.084153	-2823.12815	

$\Delta G_{(273)}$	$\Delta G_{(323)}$
-2823.124487	-2823.131863

Atom	Coordinates (Angstroms)		
	X	Y	Z
C	-2.144965	-0.458784	-0.577489
C	-1.454160	0.882427	-0.533492
C	-0.303507	1.167975	0.072844
C	0.521613	0.250444	0.889004
Br	2.217793	-0.228360	-0.080227
H	0.880428	0.718063	1.798682
H	0.061584	-0.702251	1.115368
H	0.078862	2.177280	-0.020501
H	-1.961292	1.673538	-1.071663
C	-3.478315	-0.406523	0.020542
N	-4.526055	-0.353143	0.492903
H	-2.265681	-0.774300	-1.617542
H	-1.578262	-1.240951	-0.075167

***Z*-11b(+–) | *Z*-11b(–+)**



(Z)-1-((–)-*anti*-*clinal*-bromo)-4-((+)-*anti*-*clinal*-cyano)-2-butene |
(Z)-1-((+)-*anti*-*clinal*-bromo)-4-((–)-*anti*-*clinal*-cyano)-2-butene

Charge	Multiplicity	Theory/Basis Set	Full Point Group
0	1	RB3LYP/CC-pVTZ	C_1

Zero-point Energy	Electronic Energy	Electronic and Zero-Point Energy	Dipole Moment (D)
0.098385	-2823.191333	-2823.092948	6.1423

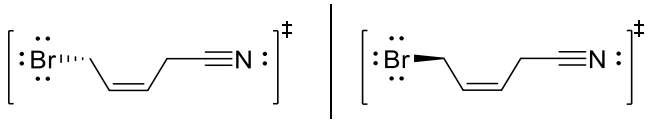
$\Delta H_{(298)}$	$\Delta G_{(298)}$
-2823.08414	-2823.128403

$\Delta G_{(273)}$	$\Delta G_{(323)}$
-2823.124717	-2823.132138

(Energies in Hartrees/particle)

Atom	Coordinates (Angstroms)		
	X	Y	Z
C	2.328098	0.503308	0.600038
C	1.518577	1.133250	-0.507012
C	0.203112	1.339107	-0.516813
C	-0.758671	1.000264	0.555364
Br	-1.986439	-0.475338	-0.043061
H	-0.317061	0.628989	1.470544
H	-1.439294	1.815618	0.772734
H	-0.224617	1.821318	-1.387603
H	2.095141	1.462024	-1.362691
C	3.121165	-0.625852	0.116560
N	3.743130	-1.511618	-0.273541
H	3.025080	1.237062	1.015018
H	1.710525	0.152676	1.425112

***Z*-11w(+) | *Z*-11w(–)**

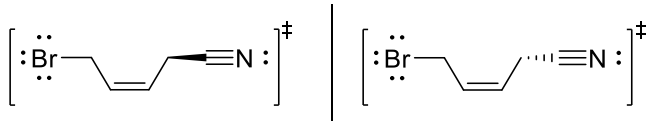


(Z)-1-((+)-*anti-clinal*-bromo)-4-(*anti-periplanar*-cyano)-2-butene |
(Z)-1-((–)-*anti-clinal*-bromo)-4-(*anti-periplanar*-cyano)-2-butene

Charge	Multiplicity	Theory/Basis Set	Full Point Group
0	1	RB3LYP/CC-pVTZ	C_1
Zero-point Energy	**Electronic Energy**	**Electronic and Zero-Point Energy**	**Dipole Moment (D)**
0.098048	-2823.189959	-2823.091911	4.1080
$\Delta H_{(298)}$	$\Delta G_{(298)}$	(Energies in Hartrees/particle)	**Imaginary Frequency (cm^{-1})**
-2823.083887	-2823.125584		60.3269
$\Delta G_{(273)}$	$\Delta G_{(323)}$		
-2823.122111	-2823.129102		

Atom	Coordinates (Angstroms)		
	X	Y	Z
C	-2.132387	-0.219639	0.434555
C	-1.467709	0.867633	-0.387070
C	-0.208055	1.272972	-0.242275
C	0.753652	0.762447	0.758669
Br	2.164009	-0.370499	-0.125628
H	1.329636	1.552046	1.227084
H	0.323321	0.113650	1.510860
H	0.158476	2.051624	-0.899438
H	-2.077938	1.338463	-1.146142
C	-3.520075	-0.447008	0.049098
N	-4.614536	-0.623105	-0.257743
H	-1.601422	-1.169496	0.331494
H	-2.123185	0.024487	1.499460

***Z*-11x(+) | *Z*-11x(–)**



(Z)-1-(*anti-periplanar*-bromo)-4-((+)-*anti-clinal*-cyano)-2-butene |
(Z)-1-(*anti-periplanar*-bromo)-4-((–)-*anti-clinal*-cyano)-2-butene

Charge	Multiplicity	Theory/Basis Set	Full Point Group
0	1	RB3LYP/CC-pVTZ	C_1

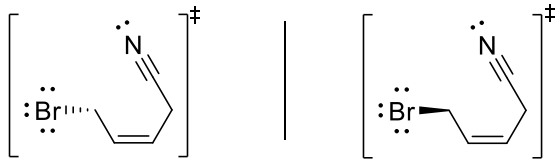
Zero-point Energy	Electronic Energy	Electronic and Zero-Point Energy	Dipole Moment (D)
0.097900	-2823.186419	-2823.088519	3.7270

$\Delta H_{(298)}$	$\Delta G_{(298)}$	(Energies in Hartrees/particle)	Imaginary Frequency (cm^{-1})
-2823.08045	-2823.122526		61.8042

$\Delta G_{(273)}$	$\Delta G_{(323)}$
-2823.119022	-2823.126077

Atom	Coordinates (Angstroms)		
	X	Y	Z
C	2.535821	0.126402	0.752780
C	1.620734	1.021197	-0.049389
C	0.314593	0.845173	-0.213566
C	-0.479386	-0.296182	0.353390
Br	-2.401831	-0.139409	-0.085089
H	-0.183198	-1.259548	-0.050881
H	-0.448656	-0.338682	1.437685
H	-0.229524	1.575400	-0.797597
H	2.091485	1.882622	-0.505650
C	3.669341	-0.348674	-0.038571
N	4.558631	-0.714048	-0.670604
H	2.941031	0.674050	1.608519
H	2.015895	-0.743703	1.152423

_Z_-11y(++) | _Z_-11y(--)



(Z)-1-((+)-*anti-clinal*-bromo)-4-((+)*syn-periplanar*-cyano)-2-butene |
(Z)-1-((−)-*anti-clinal*-bromo)-4-((−)*syn-periplanar*-cyano)-2-butene

Charge	Multiplicity	Theory/Basis Set	Full Point Group
0	1	RB3LYP/CC-pVTZ	C_1

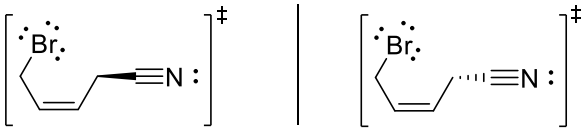
Zero-point Energy	Electronic Energy	Electronic and Zero-Point Energy	Dipole Moment (D)
0.098354	-2823.187784	-2823.089430	5.6308

$\Delta H_{(298)}$	$\Delta G_{(298)}$	(Energies in Hartrees/particle)	Imaginary Frequency (cm^{-1})
-2823.081485	-2823.122869		30.8817

$\Delta G_{(273)}$	$\Delta G_{(323)}$
-2823.119423	-2823.126361

Atom	Coordinates (Angstroms)		
	X	Y	Z
C	-2.588463	0.499260	-0.590992
C	-1.577974	1.504237	-0.094062
C	-0.404483	1.363941	0.521384
C	0.279133	0.123605	0.950187
Br	1.889763	-0.217413	-0.211589
H	0.708825	0.212331	1.941444
H	-0.302298	-0.782045	0.868188
H	0.134849	2.276897	0.745353
H	-1.890982	2.516781	-0.318429
C	-2.530751	-0.868060	-0.088811
N	-2.533016	-1.954320	0.290292
H	-3.589720	0.874783	-0.365534
H	-2.536028	0.453035	-1.683677

***Z*-11z(+) | *Z*-11z(−)**



(Z)-1-(*syn-periplanar*-bromo)-4-((+)-*anti-clinal*-cyano)-2-butene |
(Z)-1-(*syn-periplanar*-bromo)-4-((−)-*anti-clinal*-cyano)-2-butene

Charge	Multiplicity	Theory/Basis Set	Full Point Group
0	1	RB3LYP/CC-pVTZ	C_1

Zero-point Energy	Electronic Energy	Electronic and Zero-Point Energy	Dipole Moment (D)
0.097987	-2823.182743	-2823.084757	5.9140

$\Delta H_{(298)}$	$\Delta G_{(298)}$	(Energies in Hartrees/particle)	Imaginary Frequency (cm^{-1})
-2823.07676	-2823.118484		45.9418

$\Delta G_{(273)}$	$\Delta G_{(323)}$
-2823.115009	-2823.122004

Atom	Coordinates (Angstroms)		
	X	Y	Z
C	1.706701	-0.072053	0.751916
C	1.333135	1.321887	0.304249
C	0.171653	1.800951	-0.127618
C	-1.193848	1.261157	-0.387849
Br	-1.611395	-0.633172	0.018231
H	-1.928578	1.819116	0.186428
H	-1.440444	1.365048	-1.441526
H	0.173233	2.862167	-0.369621
H	2.150163	2.030962	0.364709
C	2.800204	-0.616996	-0.050008
N	3.659729	-1.039579	-0.688152
H	2.047497	-0.043850	1.790735
H	0.871796	-0.765044	0.704099

16a(+) | 16a(–)



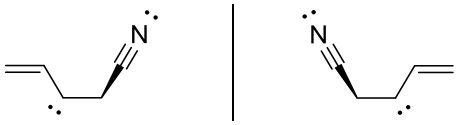
Charge	Multiplicity	Theory/Basis Set	Full Point Group
0	1	RB3LYP/CC-pVTZ	C_1

Zero-point Energy	Electronic Energy	Electronic and Zero-Point Energy	Dipole Moment (D)
0.080712	-248.229912	-248.149200	8.1592

$\Delta H_{(298)}$	$\Delta G_{(298)}$	(Energies in Hartrees/particle)
-248.141346	-248.180977	

Atom	Coordinates (Angstroms)		
	X	Y	Z
C	-0.677240	0.621661	-0.039175
C	0.464643	-0.334589	-0.166380
C	1.718781	0.326332	0.008321
C	2.832046	-0.434212	0.056617
H	2.757874	-1.504160	-0.084990
H	3.811007	-0.015412	0.254770
H	1.810590	1.404400	0.155608
C	-1.995517	-0.005667	0.020426
N	-3.032328	-0.500535	0.078248
H	-0.574762	1.330070	0.793327
H	-0.634692	1.247702	-0.945301

16b(+) | 16b(–)



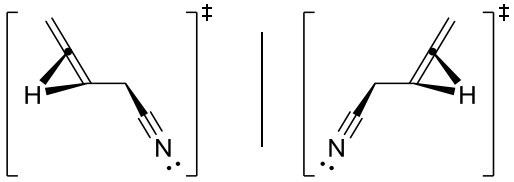
Charge	Multiplicity	Theory/Basis Set	Full Point Group
0	1	RB3LYP/CC-pVTZ	C_1

Zero-point Energy	Electronic Energy	Electronic and Zero-Point Energy	Dipole Moment (D)
0.081184	-248.230450	-248.149266	3.5851

$\Delta H_{(298)}$	$\Delta G_{(298)}$	(Energies in Hartrees/particle)
-248.141488	-248.180942	

Atom	Coordinates (Angstroms)		
	X	Y	Z
C	0.836937	1.087450	0.017217
C	-0.652018	0.972084	-0.042211
C	-1.193441	-0.345318	-0.085488
C	-2.531630	-0.473012	0.048406
H	-3.151046	0.409986	0.132804
H	-3.017738	-1.439761	0.097863
H	-0.587174	-1.247992	-0.170401
C	1.665108	-0.127850	0.019025
N	2.254218	-1.117426	0.016207
H	1.145230	1.730424	-0.815605
H	1.081462	1.689198	0.900199

TS2-16(+) | TS2-16(–)



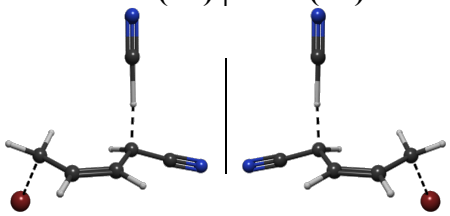
Charge	Multiplicity	Theory/Basis Set	Full Point Group
0	1	RB3LYP/CC-pVTZ	C_1

Zero-point Energy	Electronic Energy	Electronic and Zero-Point Energy	Dipole Moment (D)
0.077561	-248.212170	-248.134609	5.8239

$\Delta H_{(298)}$	$\Delta G_{(298)}$	(Energies in Hartrees/particle)	Imaginary Frequency (cm^{-1})
-248.127312	-248.164655		511.1469

Atom	Coordinates (Angstroms)		
	X	Y	Z
C	-0.643216	0.601876	0.100314
C	0.402784	-0.339635	-0.431530
C	1.669733	-0.211716	-0.007458
C	2.972931	0.012516	0.054179
H	3.582818	-0.413668	0.833922
H	3.440188	0.643136	-0.688427
H	1.139975	-1.002174	0.707298
C	-2.003287	0.067092	0.041832
N	-3.073556	-0.351932	0.010414
H	-0.451990	0.988871	1.104289
H	-0.589774	1.466551	-0.574007

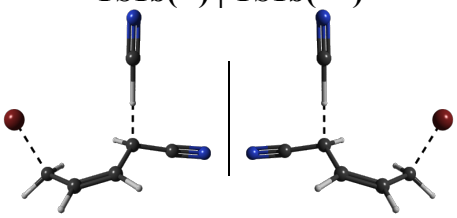
TS1a(–+) | TS1a(+–)



Charge	Multiplicity	Theory/Basis Set	Full Point Group
-1	1	RB3LYP/CC-pVTZ	C_1
Zero-point Energy	**Electronic Energy**	**Electronic and Zero-Point Energy**	**Dipole Moment (D)**
0.098350	-2916.168979	-2916.070629	11.7098
$\Delta H_{(298)}$	$\Delta G_{(298)}$	(Energies in Hartrees/particle)	**Imaginary Frequency (cm^{-1})**
-2916.058584	-2916.111809		-1430.2003
$\Delta G_{(273)}$	$\Delta G_{(323)}$		
-2916.107383	-2916.116306		

Atom	Coordinates (Angstroms)		
	X	Y	Z
C	1.567002	0.680311	-0.127416
C	0.877258	0.554071	1.145654
C	-0.220400	-0.188581	1.414756
C	-0.957547	-0.974036	0.435769
H	-0.427784	-1.206367	-0.477998
H	-1.450428	-1.848936	0.837868
H	-0.595346	-0.200342	2.429993
H	1.345982	1.051372	1.988421
C	2.485566	1.754325	-0.267068
N	3.292452	2.577726	-0.390560
H	0.962708	0.542638	-1.021344
H	2.362696	-0.490937	-0.193066
C	3.073561	-1.688753	-0.289262
N	3.683957	-2.661848	-0.442787
Br	-2.628152	0.054783	-0.331573

TS1b(--) | TS1b(++)



Charge	Multiplicity	Theory/Basis Set	Full Point Group
-1	1	RB3LYP/CC-pVTZ	C_1

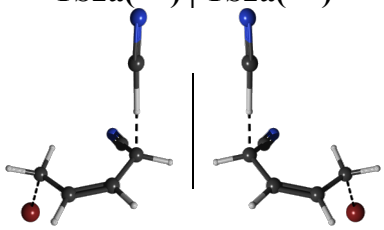
Zero-point Energy	Electronic Energy	Electronic and Zero-Point Energy	Dipole Moment (D)
0.098410	-2916.168536	-2916.070126	12.6560

$\Delta H_{(298)}$	$\Delta G_{(298)}$	(Energies in Hartrees/particle)	Imaginary Frequency (cm^{-1})
-2916.058173	-2916.110469		-1440.4762

$\Delta G_{(273)}$	$\Delta G_{(323)}$
-2916.106121	-2916.114888

Atom	Coordinates (Angstroms)		
	X	Y	Z
C	1.757036	-0.562228	-0.303214
C	1.093232	-1.202441	0.819388
C	-0.208882	-1.551098	0.928760
C	-1.183448	-1.503353	-0.151923
H	-0.769734	-1.501682	-1.152137
H	-1.987855	-2.220913	-0.059998
H	-0.564036	-1.908197	1.886939
H	1.710095	-1.351925	1.699924
C	3.154788	-0.780475	-0.440005
N	4.306345	-0.873626	-0.537754
H	1.240909	-0.598209	-1.260066
H	1.695195	0.833524	-0.023729
C	1.636763	2.208756	0.212187
N	1.614979	3.354193	0.387102
Br	-2.293451	0.277956	-0.183644

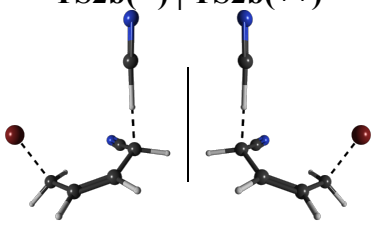
TS2a(–+) | TS2a(+–)



Charge	Multiplicity	Theory/Basis Set	Full Point Group
-1	1	RB3LYP/CC-pVTZ	C_1
Zero-point Energy	**Electronic Energy**	**Electronic and Zero-Point Energy**	**Dipole Moment (D)**
0.098627	-2916.166206	-2916.067580	10.1355
$\Delta H_{(298)}$	$\Delta G_{(298)}$	(Energies in Hartrees/particle)	**Imaginary Frequency (cm^{-1})**
-2916.055697	-2916.107845		-1426.9554
$\Delta G_{(273)}$	$\Delta G_{(323)}$		
-2916.103509	-2916.112252		

Atom	Coordinates (Angstroms)		
	X	Y	Z
C	-1.757385	-0.455069	1.132746
C	-0.984516	0.759916	1.345381
C	0.002740	1.344633	0.628937
C	0.625945	0.830424	-0.583643
H	0.122763	0.002840	-1.062493
H	0.903651	1.594029	-1.298511
H	0.373243	2.298756	0.982945
H	-1.345359	1.337854	2.190000
C	-1.242942	-1.557502	0.400717
N	-0.907778	-2.463773	-0.240459
H	-2.285484	-0.788566	2.023073
H	-2.830858	-0.020742	0.300965
C	-3.864927	0.397944	-0.533171
N	-4.773531	0.709079	-1.181706
Br	2.518792	-0.001811	-0.215047

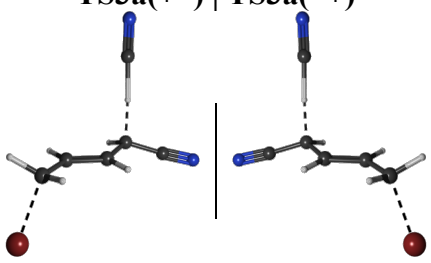
TS2b(--) | TS2b(++)



Charge	Multiplicity	Theory/Basis Set	Full Point Group
-1	1	RB3LYP/CC-pVTZ	C_1
Zero-point Energy	**Electronic Energy**	**Electronic and Zero-Point Energy**	**Dipole Moment (D)**
0.098570	-2916.165918	-2916.067348	10.5126
$\Delta H_{(298)}$	$\Delta G_{(298)}$	(Energies in Hartrees/particle)	**Imaginary Frequency (cm^{-1})**
-2916.055409	-2916.107866		-1443.1183
$\Delta G_{(273)}$	$\Delta G_{(323)}$		
-2916.103504	-2916.112298		

Atom	Coordinates (Angstroms)		
	X	Y	Z
C	-1.984937	-1.065155	-0.333073
C	-1.020201	-1.182390	-1.415295
C	0.332942	-1.197041	-1.440069
C	1.232770	-1.223949	-0.295344
H	0.799258	-1.534191	0.643921
H	2.176467	-1.718832	-0.483220
H	0.807673	-1.185088	-2.413499
H	-1.497717	-1.187530	-2.389958
C	-1.653334	-1.372266	1.013509
N	-1.429857	-1.549288	2.137400
H	-2.965981	-1.459546	-0.591332
H	-2.287900	0.325717	-0.271116
C	-2.615452	1.682552	-0.193993
N	-2.943541	2.792703	-0.137938
Br	1.938036	0.691573	0.214130

TS3a(+–) | TS3a(–+)



Charge	Multiplicity	Theory/Basis Set	Full Point Group
-1	1	RB3LYP/CC-pVTZ	C_1

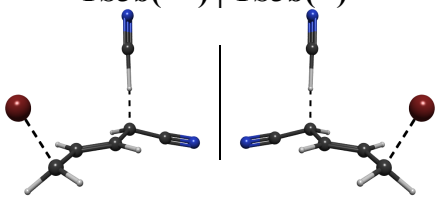
Zero-point Energy	Electronic Energy	Electronic and Zero-Point Energy	Dipole Moment (D)
0.098139	-2916.170754	-2916.072615	12.7954

$\Delta H_{(298)}$	$\Delta G_{(298)}$	(Energies in Hartrees/particle)	Imaginary Frequency (cm^{-1})
-2916.060561	-2916.11305		-1434.7207

$\Delta G_{(273)}$	$\Delta G_{(323)}$
-2916.108687	-2916.117486

Atom	Coordinates (Angstroms)		
	X	Y	Z
C	-1.257867	-0.966995	0.469638
C	-0.123082	-0.528803	-0.321586
C	0.829808	0.293787	0.166536
C	2.058055	0.660556	-0.512984
C	2.752343	1.811550	-0.055423
N	3.382015	2.702541	0.337276
H	2.030631	0.590963	-1.599097
H	0.720465	0.641987	1.190173
H	-0.059187	-0.885021	-1.343935
H	-1.188014	-0.748439	1.527629
H	-1.592724	-1.979360	0.286519
H	2.934238	-0.418168	-0.232845
C	3.773810	-1.514341	-0.025422
N	4.536961	-2.375428	0.113461
Br	-3.042190	0.056392	-0.037376

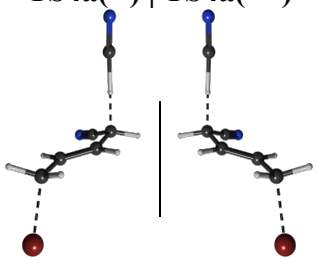
TS3b(++) | TS3b(--)



Charge	Multiplicity	Theory/Basis Set	Full Point Group
-1	1	RB3LYP/CC-pVTZ	C_1
Zero-point Energy	**Electronic Energy**	**Electronic and Zero-Point Energy**	**Dipole Moment (D)**
0.098076	-2916.170780	-2916.072704	13.0624
$\Delta H_{(298)}$	**$\Delta G_{(298)}$**	(Energies in Hartrees/particle)	**Imaginary Frequency (cm^{-1})**
-2916.060593	-2916.113357		-1442.0677
$\Delta G_{(273)}$	**$\Delta G_{(323)}$**		
-2916.108970	-2916.117816		

Atom	Coordinates (Angstroms)		
	X	Y	Z
C	1.451809	-1.395412	0.183896
C	0.168510	-1.034247	0.756277
C	-0.971189	-1.018669	0.032873
C	-2.277784	-0.610983	0.515329
C	-3.419865	-1.095858	-0.176568
N	-4.369318	-1.410715	-0.762922
H	-2.403942	-0.632406	1.596470
H	-0.903692	-1.270710	-1.022113
H	0.144148	-0.782114	1.810775
H	1.402615	-1.830147	-0.806436
H	2.115718	-1.946830	0.836349
H	-2.319140	0.790802	0.295167
C	-2.357810	2.179613	0.144126
N	-2.449454	3.328872	0.025867
Br	2.689533	0.288504	-0.179612

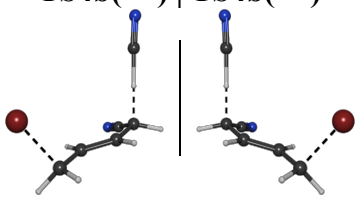
TS4a(--) | TS4a(++)



Charge	Multiplicity	Theory/Basis Set	Full Point Group
-1	1	RB3LYP/CC-pVTZ	C_1
Zero-point Energy	**Electronic Energy**	**Electronic and Zero-Point Energy**	**Dipole Moment (D)**
0.098153	-2916.170427	-2916.072274	12.1263
$\Delta H_{(298)}$	$\Delta G_{(298)}$	(Energies in Hartrees/particle)	**Imaginary Frequency (cm^{-1})**
-2916.06019	-2916.112916		-1446.0593
$\Delta G_{(273)}$	$\Delta G_{(323)}$		
-2916.108532	-2916.117371		

Atom	Coordinates (Angstroms)		
	X	Y	Z
C	-1.149533	-1.022434	-0.413633
C	-0.009467	-0.129750	-0.327381
C	0.831919	-0.129332	0.729022
C	2.074190	0.605872	0.881832
C	2.300048	1.739248	0.055961
N	2.541684	2.619991	-0.657791
H	2.384179	0.767935	1.911208
H	0.619529	-0.820961	1.539418
H	0.150497	0.555334	-1.152337
H	-1.167699	-1.814254	0.324371
H	-1.386073	-1.386221	-1.404679
H	3.074631	-0.305262	0.428246
C	4.055525	-1.178059	-0.037201
N	4.907749	-1.884906	-0.379284
Br	-2.983920	-0.041584	0.008049

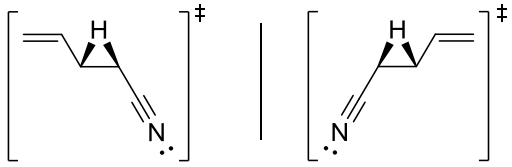
TS4b(–+) | TS4b(+–)



Charge	Multiplicity	Theory/Basis Set	Full Point Group
-1	1	RB3LYP/CC-pVTZ	C_1
Zero-point Energy	**Electronic Energy**	**Electronic and Zero-Point Energy**	**Dipole Moment (D)**
0.098102	-2916.170529	-2916.072428	12.3466
$\Delta H_{(298)}$	$\Delta G_{(298)}$	(Energies in Hartrees/particle)	**Imaginary Frequency (cm^{-1})**
-2916.060321	-2916.113178		-1451.6409
$\Delta G_{(273)}$	$\Delta G_{(323)}$		
-2916.108783	-2916.117644		

Atom	Coordinates (Angstroms)		
	X	Y	Z
C	-1.472170	-1.213970	0.568359
C	-0.074041	-1.195820	0.184463
C	0.902729	-0.796535	1.027224
C	2.324396	-0.675481	0.758406
C	2.857481	-1.325926	-0.386774
N	3.303517	-1.783442	-1.353748
H	2.963497	-0.780209	1.632144
H	0.605983	-0.463253	2.017767
H	0.172579	-1.530135	-0.816926
H	-1.657870	-1.070807	1.625260
H	-2.060124	-2.024378	0.158598
H	2.518556	0.704537	0.450621
C	2.731507	2.046617	0.136551
N	2.944467	3.163851	-0.085844
Br	-2.568512	0.413373	-0.249134

TS(16)(*E*-1)(+) | TS(16)(*E*-1)(–)



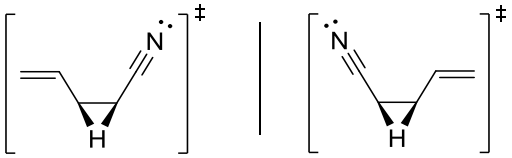
Charge	Multiplicity	Theory/Basis Set	Full Point Group
0	1	RB3LYP/CC-pVTZ	C_1

Zero-point Energy	Electronic Energy	Electronic and Zero-Point Energy	Dipole Moment (D)
0.078017	-248.208169	-248.130152	6.0169

$\Delta H_{(298)}$	$\Delta G_{(298)}$	(Energies in Hartrees/particle)	Imaginary Frequency (cm^{-1})
-248.122876	-248.160279		-1214.5494

Atom	Coordinates (Angstroms)		
	X	Y	Z
C	0.665270	0.514592	0.080393
C	-0.439677	-0.342983	-0.034651
C	-1.726153	0.338470	-0.074170
C	-2.864418	-0.360815	-0.018512
H	-2.843427	-1.438253	0.079673
H	-3.832788	0.119849	-0.067767
H	-1.774729	1.423050	-0.186707
H	0.235322	-0.136927	1.098181
C	2.014314	0.006293	0.001227
N	3.101611	-0.358385	-0.099786
H	0.608333	1.607639	0.049402

TS(16)(*Z*-1)(+) | TS(16)(*Z*-1)(–)



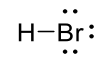
Charge	Multiplicity	Theory/Basis Set	Full Point Group
0	1	RB3LYP/CC-pVTZ	C_1

Zero-point Energy	Electronic Energy	Electronic and Zero-Point Energy	Dipole Moment (D)
0.078344	-248.209734	-248.131390	2.5699

$\Delta H_{(298)}$	$\Delta G_{(298)}$	(Energies in Hartrees/particle)	Imaginary Frequency (cm^{-1})
-248.124151	-248.16192		-1225.3607

Atom	Coordinates (Angstroms)		
	X	Y	Z
C	-0.791126	1.036247	-0.023718
C	0.606911	0.958326	-0.147951
C	1.215427	-0.361158	-0.128163
C	2.530090	-0.491854	0.083316
H	3.151176	0.379578	0.244258
H	3.009135	-1.461843	0.113886
H	0.618687	-1.257600	-0.299864
H	-0.076359	1.336571	0.969461
C	-1.694509	-0.102562	0.006346
N	-2.373108	-1.032119	0.051646
H	-1.291645	1.994130	-0.128239

HBr



hydrobromic acid

Charge	Multiplicity	Theory/Basis Set	Full Point Group
0	1	RB3LYP/CC-pVTZ	C_{*V}

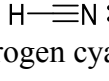
Zero-point Energy	Electronic Energy	Electronic and Zero-Point Energy	Dipole Moment (D)
0.005931	-2574.838558	-2574.832627	1.1716

$\Delta H_{(298)}$	$\Delta G_{(298)}$	(Energies in Hartrees/particle)
-2574.829322	-2574.851857	

$\Delta G_{(273)}$	$\Delta G_{(323)}$
-2574.849968	-2574.853746

Atom	Coordinates (Angstroms)		
	X	Y	Z
H	0.000000	0.000000	-1.387576
Br	0.000000	0.000000	0.039645

HCN



hydrogen cyanide

Charge	Multiplicity	Theory/Basis Set	Full Point Group
0	1	RB3LYP/CC-pVTZ	C_{*V}

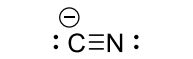
Zero-point Energy	Electronic Energy	Electronic and Zero-Point Energy	Dipole Moment (D)
0.016417	-93.468406	-93.451988	3.6120

$\Delta H_{(298)}$	$\Delta G_{(298)}$	(Energies in Hartrees/particle)
-93.448521	-93.471341	

$\Delta G_{(273)}$	$\Delta G_{(323)}$
-93.469431	-93.473257

Atom	Coordinates (Angstroms)		
	X	Y	Z
C	0.000000	0.000000	-0.496782
H	0.000000	0.000000	-1.564729
N	0.000000	0.000000	0.649346

CN^-

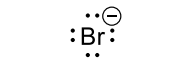


cyanide anion

Charge	Multiplicity	Theory/Basis Set	Full Point Group
-1	1	RB3LYP/CC-pVTZ	C_{*V}
Zero-point Energy	**Electronic Energy**	**Electronic and Zero-Point Energy**	**Dipole Moment (D)**
0.004908	-92.991754	-92.986846	0.6109
$\Delta H_{(298)}$	$\Delta G_{(298)}$	(Energies in Hartrees/particle)	
-92.983541	-93.005874		
$\Delta G_{(273)}$	$\Delta G_{(323)}$		
-93.004002	-93.007747		

Atom	Coordinates (Angstroms)		
	X	Y	Z
C	0.000000	0.000000	-0.629136
N	0.000000	0.000000	0.539260

Br^-



bromide anion

Charge	Multiplicity	Theory/Basis Set	Full Point Group
-1	1	RB3LYP/CC-pVTZ	O_H
Zero-point Energy	**Electronic Energy**	**Electronic and Zero-Point Energy**	**Dipole Moment (D)**
0.000000	-2574.418411	-2574.418411	0.0000
$\Delta H_{(298)}$	$\Delta G_{(298)}$	(Energies in Hartrees/particle)	
-2574.418411	-2574.418411		
$\Delta G_{(273)}$	$\Delta G_{(323)}$		
-2574.418411	-2574.418411		

Chapter 2: Synthesis and Characterization of C_5H_5N Carbocycle-Containing Carbonitriles

Some content contained in this section has been submitted and accepted for publication. Contributions to the content in this section have been made by Brian J. Esselman, Daniel Lee and Aatmik Patel.

Introduction

Upon the isolation of the cyanobutadiene isomers, it became clear to our research team that the C_5H_5N nitriles were intrinsically linked to each other through isomerization reactions, and to other smaller nitrile-containing molecules already detected in interstellar environments *via* photolysis reactions. Given the diverse structural arrangements possible using the C_5H_5N formula, the linear cyanobutadiene isomers represented only a fraction of potential astromolecules isomeric to pyridine. Of the enormous number of possible C_5H_5N structural isomers, our research team was particularly interested in studying isomers that contained a nitrile group. The synthesis and spectroscopic characterization of additional nitrile isomers would not only be valuable for enabling radioastronomical searches, but also in gaining insight regarding the reactivity of such compounds in astrochemical environments *via* laboratory matrix isolation/photolysis and electrical discharge experiments. This thesis chapter is focused on our research regarding the synthesis and rotational spectroscopy of C_5H_5N nitrile isomers with a cyclic backbone. While structural isomers containing three-, four-, five-or six-membered rings are entirely possible using the formula of pyridine (C_5H_5N), only three-membered or four-membered cyclic configurations are possible with a concurrent nitrile functional group. In this thesis chapter, we report the synthesis, purification and characterization of three carbocycle-containing C_5H_5N nitrile isomers: 3-cyano-3-methylcyclopropene (**1**), (cyanomethylene)cyclopropane (**2**), and 1-cyanocyclobutene (**9**). Additional carbocycle-containing C_5H_5N nitrile isomers are discussed to provide context and to build a foundation for future synthetic and spectroscopic endeavors within the McMahon/Woods group.

C_5H_5N Carbonitriles Containing Three-Membered Carbocycles

The family of C_5H_5N nitrile isomers that contain a three-membered carbocycle exhibits eight individual structural arrangements, and is the largest sub-classification of the C_5H_5N nitrile isomers (Figure 2.1). Like the cyanobutadiene species, the nitrile isomers presented in Figure 2.1 share structural features to molecules or ions detected in the cosmos, and are of considerable interest to the field of radioastronomy.

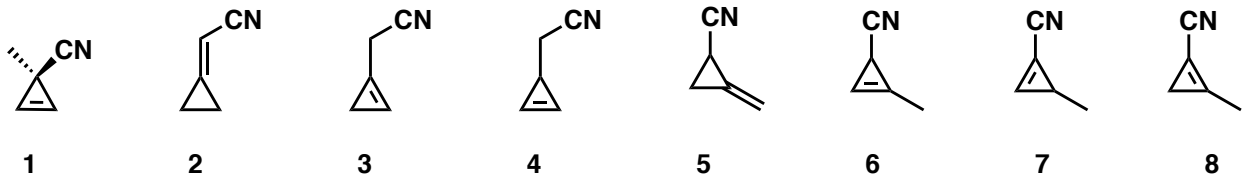


Figure 2.1. C_5H_5N Nitrile Isomers Containing a Three-Membered Carbocycle: 3-Cyano-3-methylcyclopropene (**1**), (Cyanomethylene)cyclopropane (**2**), 1-Cyanomethylcyclopropene (**3**), 3-Cyanomethylcyclopropene (**4**), 2-Methylenecyclopropanecarbonitrile (**5**), 3-Cyano-1-methylcyclopropene (**6**), 1-Cyano-3-methylcyclopropene (**7**) and 1-Cyano-2-methylcyclopropene (**8**).

At the core of each molecule presented in Figure 2.1 is a three-membered carbocycle paired with either an endocyclic or exocyclic olefin. The inherent strain energy of three-membered rings notwithstanding, four known interstellar molecules include this structural motif (with differing degrees of unsaturation): cyclopropenylidene (c-C_3H_2),[1] cyclopropenone (C_3H_2O),[2] ethylene oxide (c-C_2H_4O),[3] and propylene oxide ($CH_3C_2H_3O$).[4] Additionally, species **2**, **6** and **8** contain an α,β–unsaturated nitrile moiety, which is similar to the known interstellar species vinyl cyanide (H_2C=CHCN; acrylonitrile),[5] cyanoallene (H_2C=C=CHCN),[6] and methylcyano-acetylene (CH_3C≡CCN).[7]

Despite their relevance to the astrochemical community, the species shown in Figure 2.1 have received little attention as potential astromolecules. In contrast to the other structural families of C_5H_5N nitrile isomers, there is a notable absence of literature reports (both theoretical and

experimental) regarding the spectroscopic characterization and gas phase reactivity of the species shown in Figure 2.1. The chemical mechanisms describing the formation of the species in Figure 2.1 and their role in the formation or destruction of pyridine (or other species) in cosmic environments remain a matter of conjecture, but we are continuing our investigations of the reaction chemistry of **2** under a variety of harsh conditions.

C_5H_5N Carbonitriles Containing Four-Membered Carbocycles

In the series of isomeric C_5H_5N nitriles, there are four unique possible structural arrangements that contain a four-membered ring (Figure 2.2). The four-membered carbocycle is present either as a cyclobutenyl moiety present in 1-cyanocyclobutene (**9**) and 3-cyanocyclobutene (**11**) or as a fused bicyclic structure observed in 1-cyanobicyclo[1.1.0]butane (**10**) and 2-cyanobicyclo[1.1.0]butane (**12**). The two isomers containing fused bicyclic structures (**10** and **12**) exist exclusively as *cis* stereoisomers. Currently, only compounds **9** and **10** have reported synthesis and have been experimentally isolated. Compounds **11** and **12** have been the subject of multiple theoretical studies,[8-16] but there are no reports regarding the synthesis and characterization of these compounds.

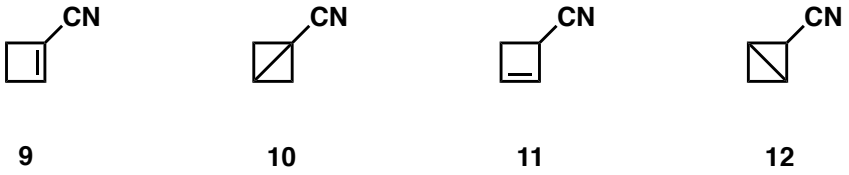


Figure 2.2. C_5H_5N Nitrile Isomers Containing a Four-Membered Ring: 1-Cyanocyclobutene (**9**), 1-Cyanobicyclo[1.1.0]butane (**10**), 3-Cyanocyclobutene (**11**), and 2-Cyanobicyclo[1.1.0]butane (**12**)

The nitriles presented in Figure 2.2 are all potential candidates for astrochemical detection.[17-18] 1-Cyanocyclobutene (**9**) is a particularly attractive candidate for astrochemical searches due to its relationship to species already detected in extraterrestrial environments and to

other C_5H_5N nitriles. Ferris *et al.* demonstrated the photochemical formation of 1-cyanocyclobutene (**9**) from species already detected (or highly likely present) in the atmosphere of Titan.[19-20] Irradiation of gaseous mixtures consisting of cyanoacetylene and ethylene with 185 nm UV radiation generates 1-cyanocyclobutene (**9**) *via* [2+2] photocycloaddition (Figure 2.3a). 1-Cyanocyclobutene (**9**) is closely related to its cyclic isomer, 2-cyano-1,3-butadiene (**13**) through several reactions. In comparison to the reaction in Figure 2.3a, the irradiation of gaseous cyanoacetylene and ethylene with lower energy 254 nm UV radiation yields 2-cyano-1,3-butadiene (**13**) as the primary product instead of 1-cyanocyclobutene (**9**) (Figure 2.3b).[19-20] Direct irradiation of 2-cyano-1,3-butadiene (**13**) with 254 nm UV radiation also yields 1-cyanocyclobutene (**9**) (in the presence of an inorganic metal catalyst).[21] The ring cleavage/isomerization of 1-cyanocyclobutene (**9**) to 2-cyano-1,3-butadiene (**13**) occurs readily *via* thermolysis (Figure 2.3c).[22-23] The relationship between cyanobutadiene species and their cyclic isomers and may indicate the possible presence of multiple C_5H_5N nitrile isomers in an environment where one is detected.

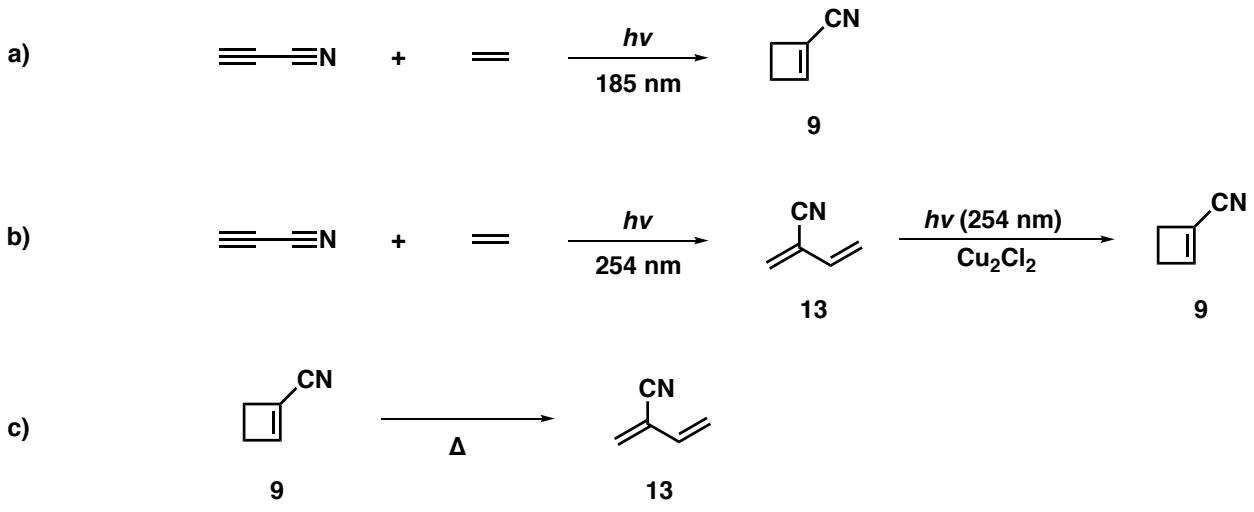


Figure 2.3. Gas-phase Synthesis of 1-Cyanocyclobutene (**9**) *via* Photochemical [2+2] Cycloaddition of Cyanoacetylene and Ethylene.

The structural features present in 1-cyanocyclobutene (**9**) make it an ideal candidate for rotational spectroscopy and radioastronomical searches. 1-Cyanocyclobutene (**9**) contains an α,β–unsaturated nitrile moiety, which is similar to the known interstellar species acrylonitrile,[5] cyanoallene,[6] and methylcyano-acetylene.[7] The polar nitrile moiety imparts a relatively large molecular dipole moment; making its detection and assignment more facile and the rigid cyclobutene moiety results in a simplified rotational spectrum with only *a*- and *b*- type rotational transitions and no conformational isomers or internal rotors. The π bond within the ring enforces the planarity of the ring by greatly restricting the ability of the carbon atoms to move out-of-plane. Structurally similar, four-membered ring molecules with π-conjugated substituents have been studied by rotational spectroscopy, *e.g.*, β-propiolactone (**16**)[24-26] and diketene (**17**) (Figure 2.4).[27]

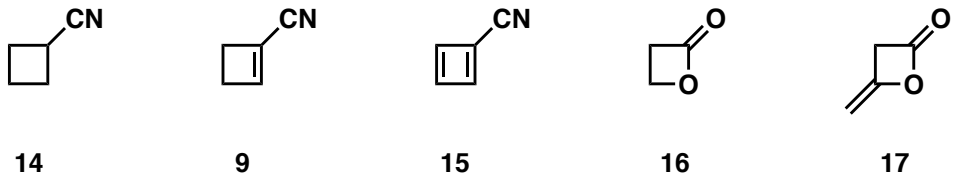


Figure 2.4. Structurally Similar Four-membered Ring Species: Cyanocyclobutane (**14**), 1-Cyanocyclobutene (**9**), Cyano-1,3-cyclobutadiene (**15**), β–Propiolactone (**16**), and Diketene (**17**).

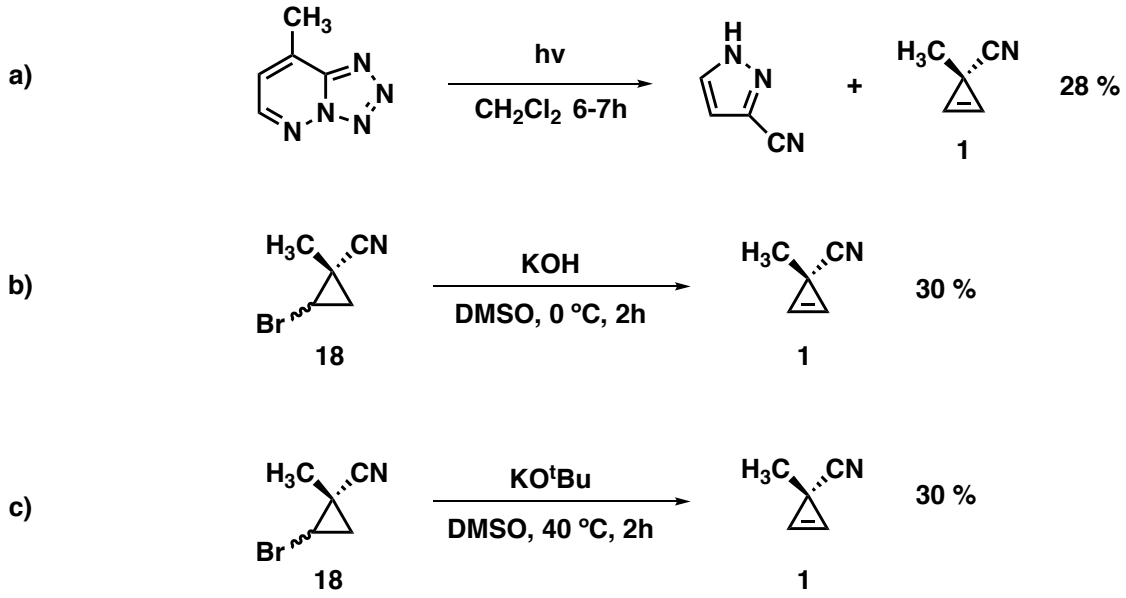
Each of these species, like cyanocyclobutene, has a planar ring due to the presence of sp^2-hybridized carbon atoms in the ring or conjugation between ring atoms and substituents. Unlike the molecules mentioned above, rotational or vibrational spectra of 1-cyanocyclobutene (**9**) have not been reported in the literature. Cyanocyclobutane (**14**), due to its fully saturated ring, exhibits two non-planar conformers (−CN equatorial or axial), which have been well-studied by rotational and vibrational spectroscopy.[28-32] While the fully unsaturated cyanocyclobutadiene (**15**) has been generated and characterized under matrix-isolation conditions,[33] it has not been analyzed *via* gas-phase spectroscopy. Exploration of the spectroscopy and structures of these similar compounds allows meaningful comparisons to be made of these strained four-membered ring systems.

Background

3-Cyano-3-methylcyclopropene (1)

Of the species presented in Figure 2.1, the structure of 3-cyano-3-methylcyclopropene (**1**) stands out as a particularly unique example amongst the other isomers. 3-Cyano-3-methylcyclopropene (**1**) contains a strained cyclopropene core and a quaternary sp^3 hybridized carbon – which results in the highest calculated relative energy of the C_5H_5N isomers synthesized in this thesis. Three synthetic methods have been reported to produce 3-cyano-3-methylcyclopropene (**1**). Tsuchiya *et al.* first reported 3-cyano-3-methylcyclopropene (**1**) as a product resulting from the photolysis of matrix-isolated and solution-phase samples of 4-methyltetrazolo[1,5-b]pyridazine (Scheme 2.1a).[34-35] Nine years later, Latypova *et al.* reported the synthesis of 3-cyano-3-methylcyclopropene (**1**) *via* base-promoted elimination of 2-bromo-1-methylcyclopropanecarbonitrile (**18**) (Scheme 2.1b).[36] A similar base-promoted elimination was reported by Bolesov *et al.* using potassium *tert*-butoxide (Scheme 2.1c).[37] Although the methods presented in Scheme 2.1 have comparable yields, the method reported by Latypova is the most widely-used synthetic route for producing 3-cyano-3-methylcyclopropene (**1**) in subsequent studies of the molecule. The precursor species, 2-bromo-1-methylcyclopropanecarbonitrile (**18**), was synthesized in two steps *via* initial [1+2] cycloaddition of dibromocarbene and methacrylonitrile to yield 2,2-dibromo-1-methylcyclopropanecarbonitrile. Subsequent reductive monodehalogenation of the intermediate geminal dibromocyclopropane using a Grignard/organolithium reagent and water quench yields (**18**) as a mixture of diastereomers.[36]

Scheme 2.1. Previous Syntheses of 3-Cyano-3-methylcyclopropene (1).



(a) Tsuchiya *et al.*[34-35] (b) Latypova *et al.*[36] (c) Bolesov *et al.*[37]

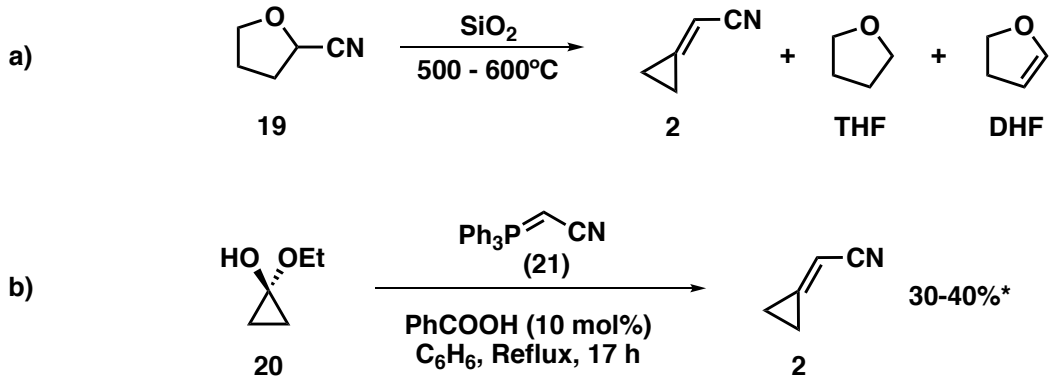
Much of the interest surrounding 3-cyano-3-methylcyclopropene (**1**) in other publications is concerned with using the molecule as a substrate in Diels-Alder or Alder-ene type reactions.[36, 38-44] Although the $^{1}H/^{13}C$-NMR chemical shifts and IR spectroscopy data for 3-cyano-3-methylcyclopropene (**1**) were reported by Latypova *et al.*[36] and Zinin *et al.*[45] details concerning the physical properties and rotational spectroscopy of **1** remain incomplete at the current time.

(Cyanomethylene)cyclopropane (2)

(Cyanomethylene)cyclopropane (**2**) is an attractive candidate for astronomical searches, being a nitrile-containing structural isomer of pyridine (C_s, C_5H_5N) and a highly prolate, asymmetric top ($\kappa = -0.96$) with a strong dipole ($\mu_a = 4.4$ D, $\mu_b = 1.2$ D, MP2/6-311+G(2d,p)). This molecule has been generated only twice, previously,[19-20] and the characterization data are quite limited compared to other simple organic nitriles. In 1945, Wilson first reported **2** as the

principle product resulting from the high-temperature pyrolysis of 2-cyanotetrahydrofuran (**19**) at 500-600°C on silica with co-production of tetrahydrofuran and dihydrofuran (Scheme 2.2a).[46] This early report predated the widespread utility of NMR and IR spectroscopy for structure elucidation in organic synthesis, and identifies **2** only *via* its empirical formula and likely formation routes. Wilson's description of **2** was rather simple, it was a non-basic liquid with an atmospheric boiling point of 130 – 140 ºC and had an odor reminiscent of an aliphatic nitrile. While effective, the pyrolysis reported by Wilson is not an ideal synthetic approach for studying the rotational spectrum of **2** due to the concurrent generation of volatile byproducts, with permanent dipole moments, as sample contaminants.

Scheme 2.2. Previous Syntheses of (Cyanomethylene)cyclopropane (2)



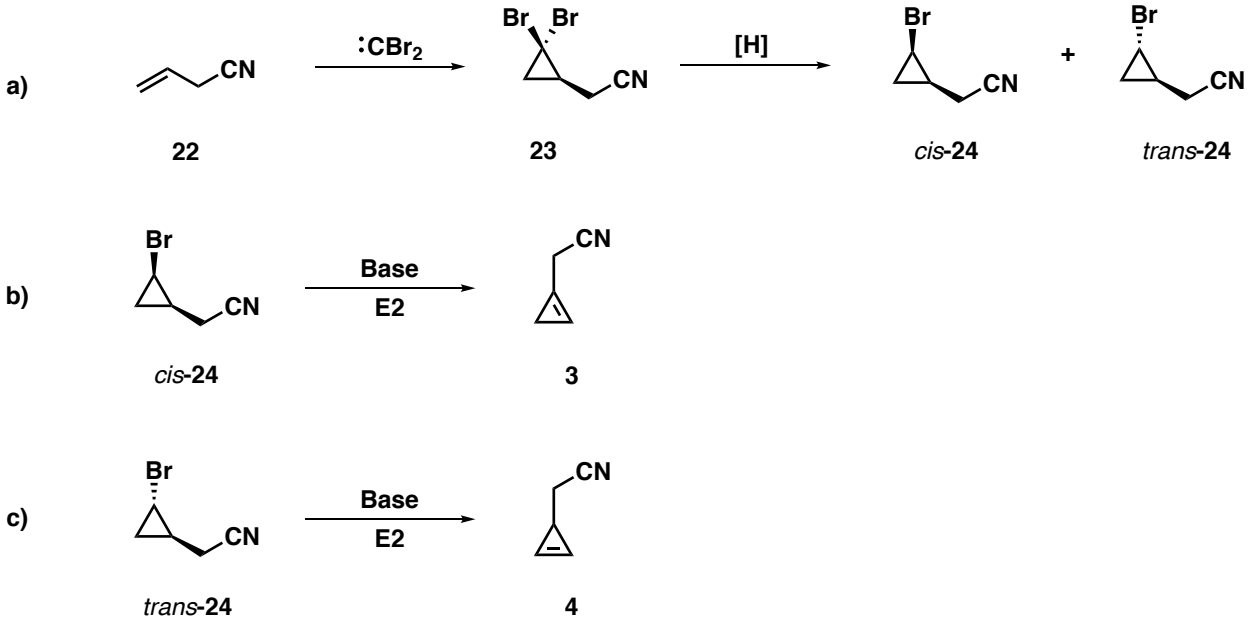
(a) Wilson.[46] (b) Mauduit *et al.*[47] *yield approximated *via* ^{1}H-NMR

More recently, **2** attracted interest as a useful dipolarophile or dienophile in [2+3] cycloadditions used in natural product synthesis. Mauduit *et al*. reported a facile, gram-scale synthesis of **2** *via* a Wittig reaction of 1-ethoxycyclopropanol (**20**) with (cyanomethylene)triphenylphosphorane (**21**) (Scheme 2.2b).[47] This synthesis is ideal for analysis by rotational spectroscopy, as it produces the desired product, in significant quantity, without volatile, polar solvents or byproducts.

1-Cyanomethylcyclopropene (3) and 3-Cyanomethylcyclopropene (4)

Currently there appear to be no reports describing the synthesis and characterization of 1-cyanomethylcyclopropene (**3**) and 3-cyanomethylcyclopropene (**4**). However, synthetic methodology used to prepare and isolate related cyclopropene congeners could likely be applied in developing a procedure for isolating both 1-cyanomethylcyclopropene (**3**) and 3-cyanomethylcyclopropene (**4**) from a single feedstock (Scheme 2.3).

Scheme 2.3. Proposed Synthesis of 1-Cyanomethylcyclopropene (3) and 3-Cyanomethylcyclopropene (4).



Our proposed approach for the novel synthesis of 1-cyanomethylcyclopropene (**3**) and 3-cyanomethylcyclopropene (**4**) involves a sequence of reactions similar to the processes used to prepare 3-cyano-3-methylcyclopropene (**1**) from methacrylonitrile (**35**). 2,2-Dibromocyclopropaneacetonitrile (**23**) is produced *via* cyclopropanation of allyl cyanide (**22**) with dibromocarbene and subsequent reductive monodehalogenation of **23** can be accomplished using a variety of conditions (diethyl phosphite, zinc dust, metal-halogen exchange/protic quench) to

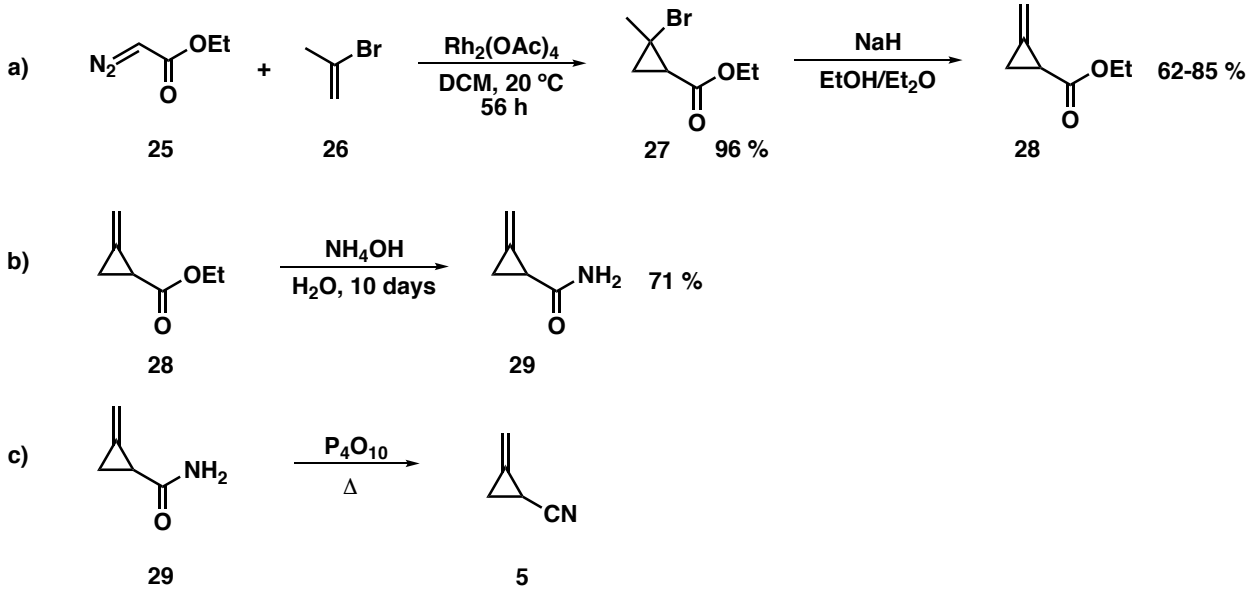
yield the *cis* and *trans* diastereomers of 2-bromocyclopropylacetonitrile (**24**) (Scheme 2.3a). Separation of the *cis* and *trans* diastereomers of **24** should be possible through conventional flash chromatography. Treatment of each isolated diastereomer with a strong base should result in the formation of a separate C_5H_5N nitrile isomer due specificity of the E2 mechanism. Treatment of racemic *cis*-**24** with a strong base should yield **3** as the primary product (with the minor co-formation of the anti-Zaitzev isomer, **4**) (Scheme 2.3a), and treatment of *trans*-**24** with a strong base should exclusively yield **4** as the product (Scheme 2.3b).

2-Methylenecyclopropanecarbonitrile (5)

Like many of its related isomers, 2-methylenecyclopropanecarbonitrile (**5**) is another structurally unique C_5H_5N nitrile specimen that has received little attention and has no published reports pertaining to its synthesis or characterization. In the eyes of the McMahon/Woods group, 2-methylenecyclopropanecarbonitrile (**5**) is a particularly attractive species as it may be a potential product resulting from the photolysis of matrix-isolated (cyanomethylene)cyclopropane (**2**). While the analysis of spectroscopic evidence obtained from our matrix isolation experiments indicates that **5** is a likely product resulting from the photolysis of **2**, preparation and spectroscopic characterization of an authentic sample of **5** provides concrete evidence to confirm its presence in such experiments. Further, the isolation of a sample of **5** would permit the collection and assignment of its gas-phase rotational spectrum for the first time, and ultimately provide the spectroscopic data required for radioastronomical searches. Although a method for the synthesis of **5** has not been reported in literature, methods for the synthesis of related 2-methylenecyclo-propyl-substituted carboxylic acid derivatives have been published and serve as an important foundation for the proposed route of accessing **5** (Scheme 2.4).[48-49] Considering that small nitrile species are easily obtained *via* dehydration of the corresponding amide, we propose that **5** could

easily be accessed *via* treatment of the known 2-methylenecyclopropanecarboxamide (**29**) with phosphorus pentoxide (Scheme 2.4c). The nature of such dehydration reactions is ideal for our intended purposes since such solid-phase reactions use no solvents, and the distilled product is frequently collected at very high purity.

Scheme 2.4. Proposed Synthesis of 2-Methylenecyclopropanecarbonitrile (5).



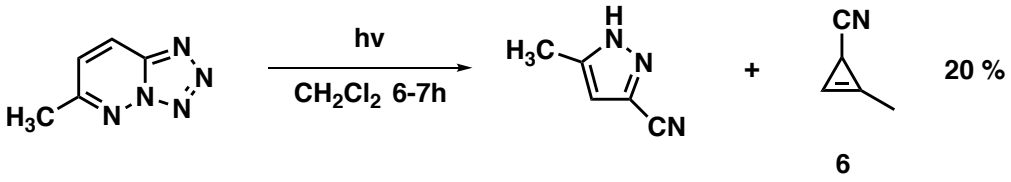
(a) Scott *et al.*[48] (b) Nishimura *et al.*[49]

The requisite starting materials can be prepared as follows: the initial production of ethyl 2-methylenecyclopropanecarboxylate (**28**) can be accomplished using the 2-step procedure reported by Scott *et al.* (Scheme 2.4a).[48] The catalyzed addition of ethyldiazoacetate (**25**) and 2-bromopropene (**26**) affords ethyl 2-bromo-2-methyl-cyclopropanecarboxylate (**27**), which is used in a subsequent elimination step to produce **28** in fair yields. Conversion of the ester (**28**) to the respective amide (29) can be accomplished using aqueous ammonia in accord with the procedure reported by Nishimura *et al.* (Scheme 2.4b).[49]

3-Cyano-1-methylcyclopropene (6) and 1-Cyano-3-methylcyclopropene (7)

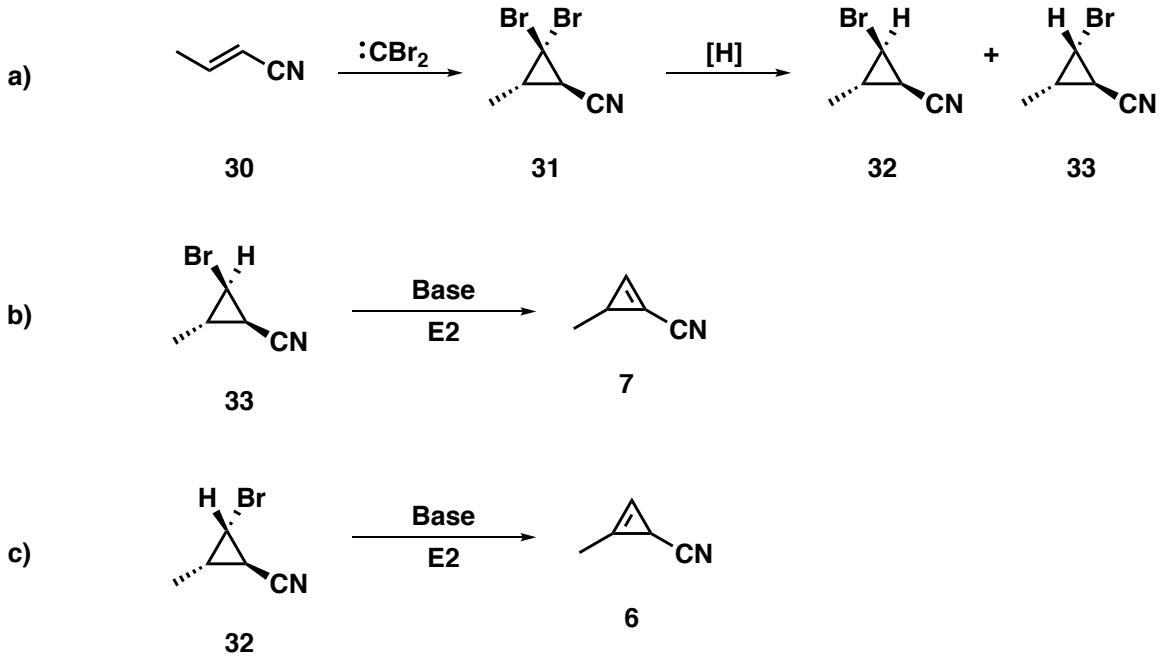
3-Cyano-1-methylcyclopropene (**6**) appears in only one published article. Tsuchiya *et al.* first reported **6** as a product resulting from the photolysis of solution-phase 4-methyltetrazolo[1,5-b]pyridazine (Scheme 2.5).[34-35] While this report includes basic characterization of **6** *via* NMR, IR and mass spectrometry, the detailed spectroscopic characterization of **6** has yet to be reported.

Scheme 2.5. Previous Synthesis of 3-Cyano-1-methylcyclopropene (6) by Tsuchiya *et al.*[34-35]



No reports regarding the synthesis or spectroscopic characterization of 1-cyano-3-methylcyclopropene (**7**) have been published. Considering that both **6** and **7** are mutual regioisomers, both **6** and **7** can likely be prepared from the same starting material by leveraging the specificity of an E2 reaction during the formation of the alkene. In the proposed synthetic route presented in Scheme 2.6, cyclopropanation is performed on *E*-crotonitrile (**30**) using dibromocarbene to generate the intermediate geminal dibromide (**31**) as a racemic mixture. Subsequent reductive dehalogenation can be performed *via* subjection of **31** to several reagent combinations to yields 2-bromo-3-methylcyclopropanecarbonitrile as two diastereomers (**32** and **33**) (Scheme 2.6a). Since **32** and **33** are diastereomers, their separation should be feasible *via* conventional flash chromatography. Each diastereomer should react with a strong base to form a separate product regioisomer due to the specificity of the E2 elimination mechanism. Upon subjection to a strong base, **33** should react to form **7** (Scheme 2.6b) and **32** should react to form **6** (Scheme 2.6c).

Scheme 2.6. Proposed Synthesis of 3-Cyano-1-methylcyclopropene (6) and 1-Cyano-3-methylcyclopropene (7) from (*E*)-Crotonitrile (30).



1-Cyano-2-methylcyclopropene (8)

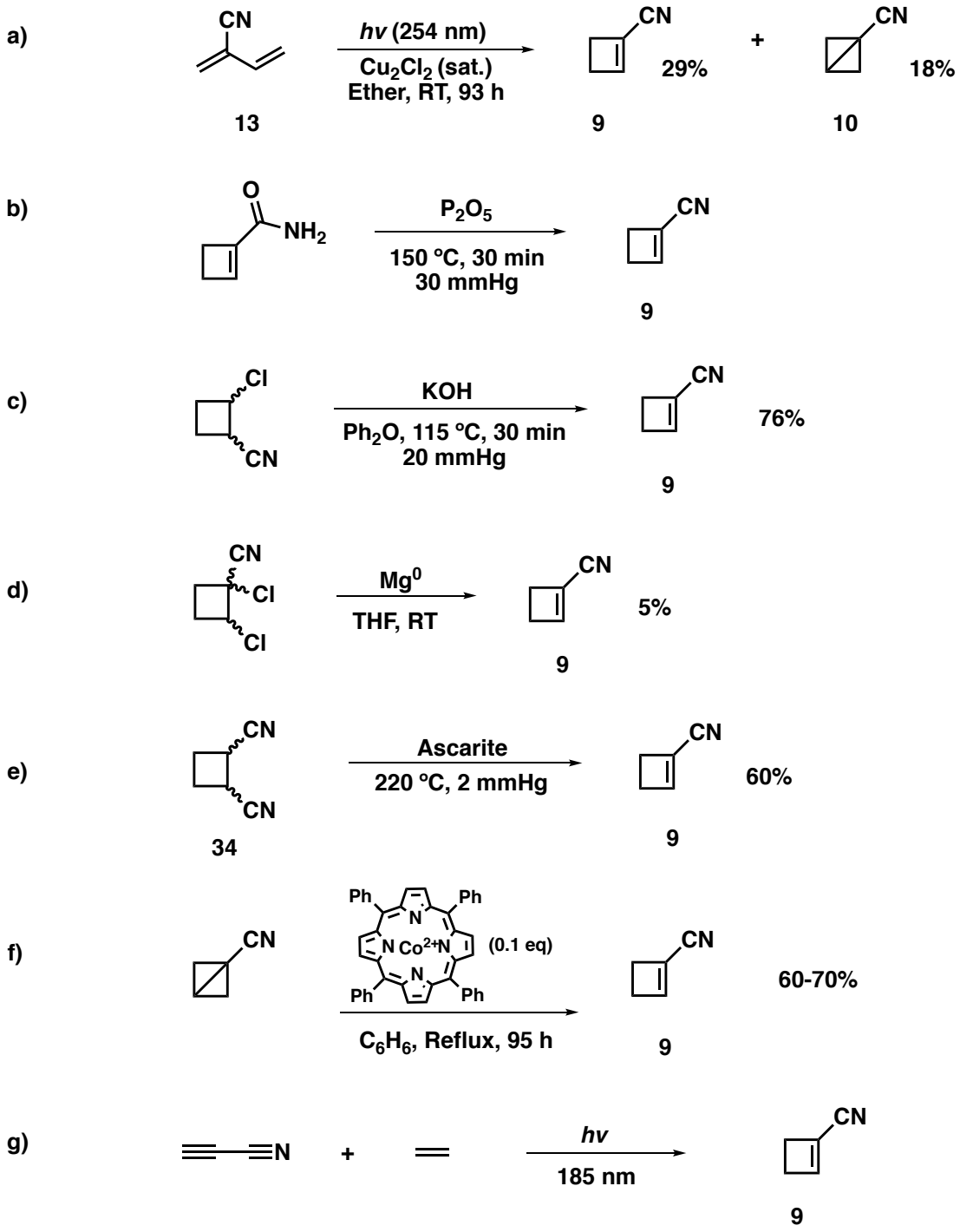
No reports regarding the synthesis or spectroscopic characterization of 1-cyano-2-methylcyclopropene (**8**) have been published. As a synthetic target, 1-cyano-2-methylcyclopropene is a slightly more challenging structure to produce (using cyclopropanation reactions with crotonitrile and dibromocarbene) since the alkene is positioned between the two carbons in the ring that carry substituents. Structurally, **8** is closely related to its regioisomers **5**, **6** and **7** and shares a similar general connectivity of its carbon skeleton. Presumably, it may be possible to access **8** *via* isomerization of either **5**,**6** or **7**.

1-Cyanocyclobutene (9)

Multiple synthetic routes leading to **9** have been described previously,[19-21, 23, 50-55] yet no experimental rotational spectrum has been reported prior to our investigation. Like many of the

isomeric cyanobutadiene species, **9** was initially made and studied by DuPont researchers as a valuable monomer/comonomer unit.[51] Because of the early interest in **9** for industrial purposes, several methods leading to **9** have been published, and many have related patents (Scheme 2.7). The overwhelming amount of research regarding the synthesis of **9** and its description as a monomer was performed by David Gale at Dupont.[21, 23, 51-54] In 1969, Gale *et al.* first reported the synthesis of 1-cyanocyclobutene (**9**) *via* photo-induced 4π electrocyclization from 2-cyano-1,3-butadiene (**13**) (Scheme 2.7a).[54] Gale *et al.* also indicated that **9** could be made *via* dehydration of 1-cyclobutene-1-carboxamide (Scheme 2.7b).[54] Within a month, Tietz *et al.* (DuPont) patented the dehydration method.[50] Three years later, Gale *et al.* patented a series of processes for the preparation of chlorinated cyclobutanecarbonitriles resulting from the photo-induced cycloaddition of vinyl chloride and acrylonitrile.[53] The conclusion of this patent demonstrated that the chlorinated cyclobutanecarbonitrile species could be used to ultimately produce **9** *via* the base-promoted elimination from 1-chloro-2-cyanocyclobutane (Scheme 2.7c) and base-promoted elimination from 1,2-dichloro-1-cyanocyclobutane (Scheme 2.7d).[53] Within two months, Gale and co-workers published and patented a method for the preparation of **9** *via* base-promoted dehydrocyanation of 1,2-dicyanocyclobutane (**34**) (Scheme 2.7e).[23, 52] Since its publication in 1972, the dehydrocyanation method remains the primary means of producing **9** in subsequent works. In 1986, Miki *et al.* demonstrated the preparation of **9** *via* cobalt(II) porphyrin-catalyzed isomerization/ring expansion of 1-cyanobicyclo[1.1.0]butane (**10**) (Scheme 2.7f).[55] Most recently, Ferris *et al.* reported that **9** could be made *via* photocatalyzed [2+2] cycloaddition of cyanoacetylene and ethylene (Scheme 2.7g).[19-20] Although 1-cyanocyclobutene (**9**) has attracted significant interest over the years, details concerning its modern spectroscopic characterization and structure were incomplete.

Scheme 2.7. Previous Syntheses of 1-Cyanocyclobutene (9)

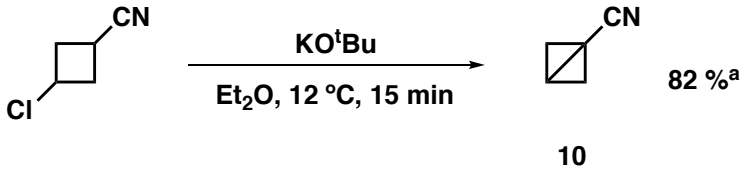


(a) Gale *et al.*[54] (b) Gale[54] and Tietz[50] (c) Gale *et al.*[53] (d) Gale *et al.*[53] (e) Gale and Cherkovsky[23, 52] (f) Miki *et al.*[55] (g) Ferris *et al.*[19-20]

1-Cyanobicyclo[1.1.0]butane (10)

Prior to the work of our research group, 1-cyanobicyclo[1.1.0]butane (**10**) was the only carbocycle-containing C_5H_5N isomer with an experimentally-measured and assigned rotational spectrum. Taylor *et al.* reported the microwave spectrum, dipole moment and proposed structure of **10** in 1991.[17] For the preparation of a sample of **10** to use in their studies, Taylor and co-workers used the synthetic procedure reported by Hall *et al.* (Scheme 2.8)[56] that involves the treatment of a mixture of *cis* and *trans* (85:15) 3-chlorocyclobutanecarbonitrile with potassium *tert*-butoxide in diethyl ether. Along with the procedure for the synthesis and purification of **10**, Hall *et al.* also provided its spectroscopic characterization *via* ^{1}H-NMR and FT-IR.[56]

Scheme 2.8. Previous Synthesis of 1-Cyanobicyclo[1.1.0]butane (10)



[a]Hall *et al.*[56], Isolated Yield

Methodology targeting the synthesis and isolation of 3-cyanocyclobutene (**11**), and 2-cyanobicyclo[1.1.0]butane (**12**) remains undefined at this time. While both species are certainly of interest to the field as potential astromolecules, their syntheses are significantly more challenging due to the likelihood that most synthetic methods and conditions would favor the formation of **9**.

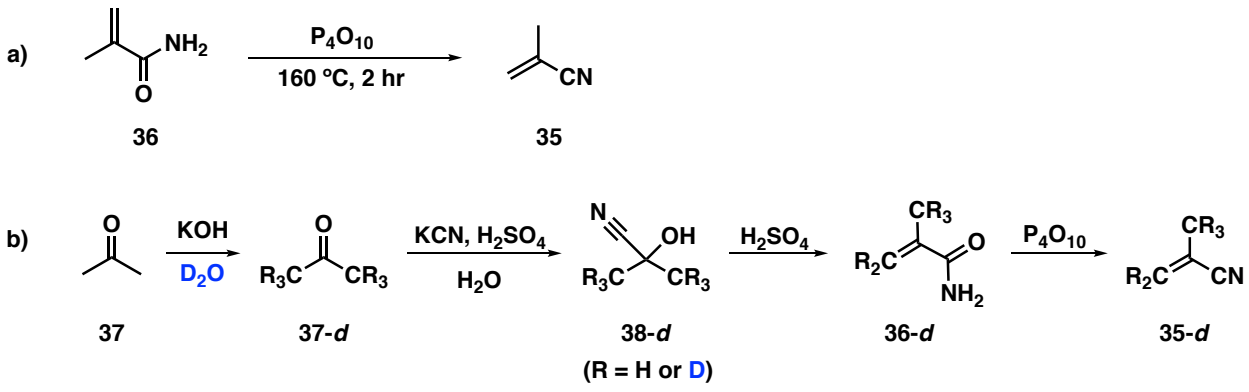
Results and Discussion

Methacrylonitrile (35)[57]

Methacrylonitrile (**35**) plays a critical role as one of the starting materials needed to generate the 3-membered carbocycle structure in 3-cyano-3-methylcyclobutene (**1**). Although it is not an isomer of pyridine, methacrylonitrile (**35**) itself shares structural similarity to the known

interstellar molecule acrylonitrile, and captivated the attention of our group as another low-molecular weight unsaturated nitrile that is highly likely to be present in the cosmos. Aside from using methcrylonitrile (**35**) as a starting material for producing **1**, we sought to study the rotational spectrum of **35** in depth to provide the detailed structural and spectroscopic characterization data necessary to search for **35** in the cosmos. In the past, methacrylonitrile (**35**) used to be a commercially available substance. Recently, suppliers have stopped stocking **35** due to environmental safety concerns. For the preparation of **35**, we followed two general routes depending on if we desired deuterium enrichment in the product (Scheme 2.9). For the preparation of methacrylonitrile (**35**) without deuterium enrichment, we found that methacrylonitrile (**35**) could be easily distilled in high purity *via* the dehydration of methacrylamide (**36**) (Scheme 2.9a). This process involves the mixing of both reagents (which are solids) and heating the mixture to 160 ºC. Methacrylonitrile (**35**) is then distilled into a dry ice or liquid nitrogen receiving flask.[58]

Scheme 2.9. Methods for Producing Methacrylonitrile (35) (a), and Deuterium-enriched Methacrylonitrile (35-*d*) (b).



To provide a comprehensive structural/spectroscopic characterization of methacrylonitrile (**35**), the synthesis of isotopologues was necessary. For the preparation of deuterium-enriched samples of methacrylonitrile (**35-*d***), an extended synthetic route was followed starting from acetone (Scheme 2.9b). In this method, acetone (**37**) is subjected to a strong base in the presence

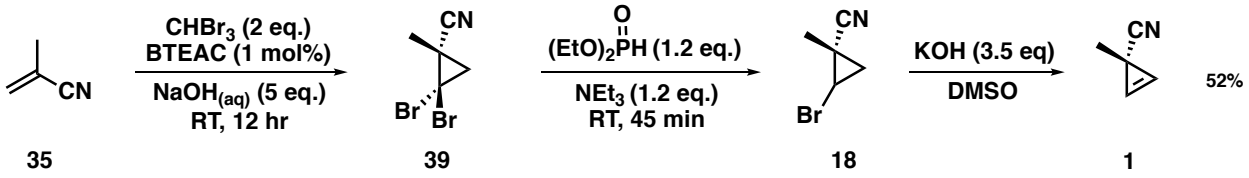
of D_2O, leading to deuterium enrichment through base-catalyzed tautomerization. Deuterium-enriched acetone (**37-*d***) is converted to deuterium-enriched acetone cyanohydrin (**38-*d***) *via* addition of potassium cyanide under acidic conditions. We attempted to directly convert deuterium-enriched acetone cyanohydrin (**38-*d***) to deuterium-enriched methacrylonitrile (**35-*d***), however some amount of hydrolysis of the carbonitriles group was always observed. We found that stepwise approach was more practical (Scheme 2.9b): acetone cyanohydrin (**38**) is first converted to deuterium-enriched methacrylamide (**36-*d***) using sulfuric acid followed by dehydration with phosphorus pentoxide to yield deuterium-enriched methacrylonitrile (**35-*d***).

The method for producing deuterium-enriched samples yielded samples of varying deuterium incorporation, and proved to be very useful for the spectroscopic/structural characterization of methacrylonitrile (**35**). Using samples prepared using the synthetic methods presented in Scheme 2.9, we obtained the rotational spectrum of methacrylonitrile (**35**) and several of its isotopologues from 6 – 40 GHz and 130 – 500 GHz. In total, 23 isotopologues including the main isotopologue have been analyzed with a varying number of transitions assigned. The main isotopologue ground state has been least-squares fit to a sextic Hamiltonian accounting for internal rotation splitting, and the resulting spectroscopic constants compare well with previous literature. The increase in the frequency range measured has allowed for improvement in the determination of centrifugal distortion constants, and thus enhances the possibility of detection *via* radioastronomy. Additionally, a semi-experimental equilibrium structure (r_e^{SE}) for methacrylonitrile (**35**) is sought due to its small molecular size and accessibility to a wide range of isotopologues. We have analyzed the spectra from 6 – 40 GHz and 130 –360 GHz of all singly-substituted heavy-atom isotopologues (^{13}C and ^{15}N), which were detectable at natural abundance, and least-squares fit them to sextic Hamiltonians accounting for internal rotation.

3-Cyano-3-Methylcyclobutene (1)

For the preparation of a sample of 3-cyano-3-methylcyclopropene (**1**) suited for rotational spectroscopy, the synthetic route presented in Scheme 2.10 was developed using the existing preparation reported by Latypova *et al*.[36] However, some modifications were made for the incorporation of different methodology for the second step (reductive dehalogenation). Methacrylonitrile (**35**) (generated using the method presented in Scheme 2.9a), is reacted with *in situ* generated dibromocarbene to yield 2,2-dibromo-1-methylcyclopropanecarbonitrile (**39**). Reductive monodehalogenation of **39** using diethyl phosphite under basic conditions yields 2-bromo-1-methylcyclopropanecarbonitrile (**18**). Treatment of **18** with KOH yields 3-cyano-3-methylcyclopropene (**1**).

Scheme 2.10. Preparation of 3-Cyano-3-methylcyclopropene (1).



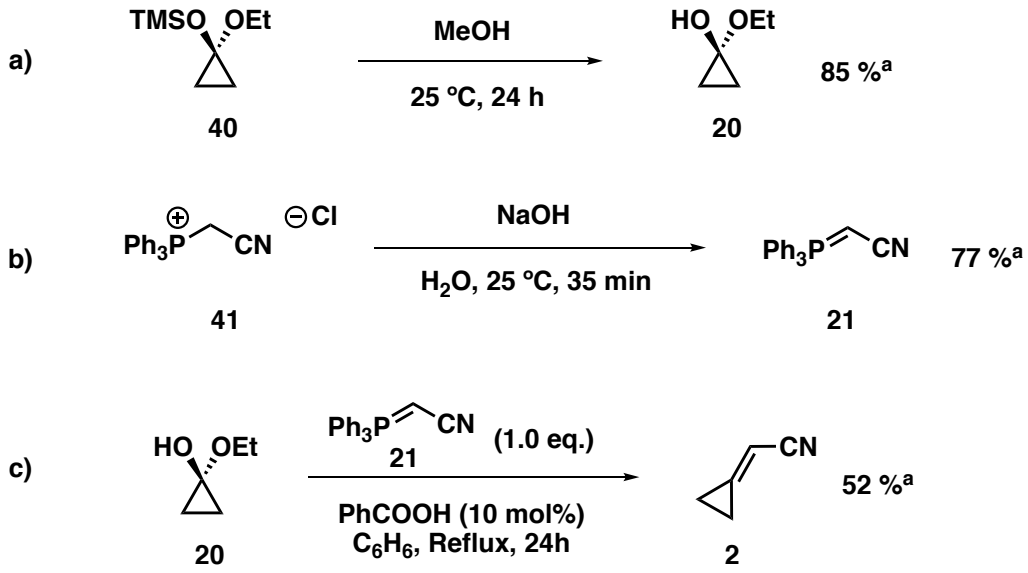
The rotational spectrum of 3-cyano-3-methylcyclopropene (**1**) was collected from 130 to 230 and from 235 to 360 GHz. Analysis of its rotational spectrum and assignment of its spectroscopic constants are currently underway and are being actively studied in our group.

(Cyanomethylene)Cyclopropane (2)[59]

Our synthetic approach to (cyanomethylene)cyclopropane (**2**) is based upon the previous work of Mauduit *et al*.[47] as shown in Scheme 2.2b. The desired compound was obtained in three relatively simple steps, with sufficient quantity and purity to enable the spectroscopic investigation (Scheme 2.11). A commercial sample of (1-ethoxycyclopropoxy)trimethylsilane (**40**) was deprotected by stirring in methanol for 24 h to reveal the required hemiketal **20** in 85% yield.[60]

Ylide **21** was prepared in 93% yield from a commercial sample of (cyanomethyl)triphenylphosphonium chloride (**41**) by stirring in basic solution for 35 min. Subsequently, **20** and **21** were allowed to react in refluxing benzene with catalytic benzoic acid to generate (cyanomethylene)cyclopropane (**2**) which was isolated as a pure substance, for the first time, in 52% yield. As previously reported,[47] this reaction could be carried out in a variety of non-polar organic solvents. Benzene was selected, in this case, because it does not possess a permanent dipole moment, and any residual benzene would not be observed in the rotational spectrum. After distillation, this sample was used to collect the rotational spectrum of (cyanomethylene)cyclopropane (**2**).

Scheme 2.11. Modified Synthesis of (Cyanomethylene)cyclopropane (2).



[a]Isolated yields.

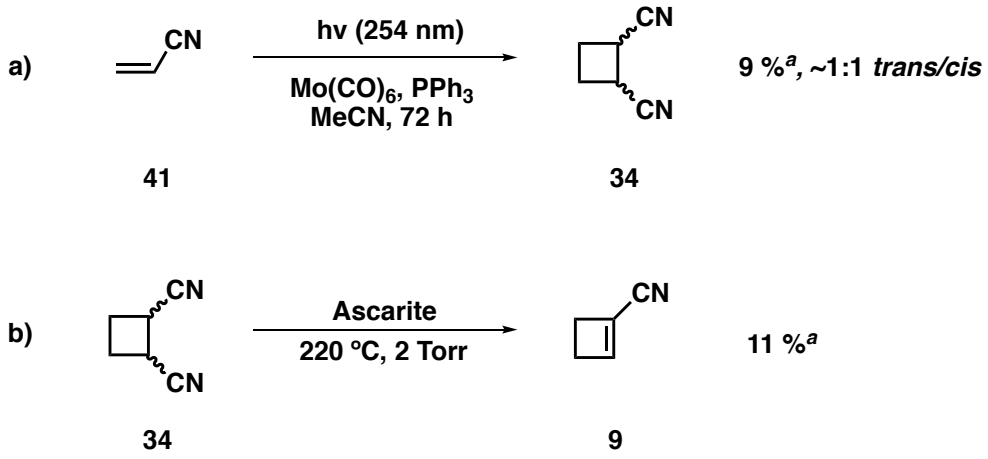
The rotational spectra of the ground state and two vibrationally excited states were observed, analyzed, and least-squares fit from 130 to 360 GHz.[59] Over 3900 R-, P-, and Q-branch, ground-state rotational transitions were fit to low-error, partial octic, A- and S-reduced Hamiltonians, providing precise determinations of the spectroscopic constants. The two lowest-

energy vibrationally excited states, ν_{17} and ν_{27}, form a Coriolis-coupled dyad displaying small *a*- and *b*-type resonances. Transitions for these two states were measured and least-squares fit to a two-state, partial octic, A-reduced Hamiltonian in the I^r representation with nine Coriolis coupling terms (G_a, G_a^J, G_a^K, G_a^{JJ}, F_{bc}, F_{bc}^J, F_{bc}^K, G_b, and G_b^J).[59]

1-Cyanocyclobutene (9)[61]

For the preparation of a sample intended for rotational spectroscopy, the method utilizing the gas-phase base-promoted dehydrocyanation of 1,2-dicyanocyclobutane (**34**) developed by Gale *et. al* [23, 52, 62] was the most attractive since it could generate **9** on a multi-gram scale with excellent purity, free of other C_5H_5N nitriles. The requisite starting material, 1,2-dicyanocyclobutane (**34**) was formerly available as the "acrylonitrile cyclodimer" from numerous commercial reagent distributors decades ago.[62-63] Although compound **34** has been discontinued as a commercially available reagent in recent years, multiple methods describing the thermally or photochemically promoted dimerization of acrylonitrile have been described previously,[64-75]and that **34** could be easily made in sufficiently large batches in our lab *via* dimerization of readily available acrylonitrile (**41**). Depending on the reaction conditions, this dimerization can produce predominantly the *trans* stereoisomer 1,2-dicyanocyclobutane[76] or a mixture (58:42) of *trans* and *cis* (1,2-dicyanocyclobutane) isomers.[77] Additionally, methods for the isomerization of *cis*-1,2-dicyanocyclobutane to *trans*-1,2-dicyanocyclobutane have been reported.[78] We prepared **34** using the methodology patented by Hughes *et. al.*[73] Acrylonitrile (**41**) was photo-dimerized to generate 1,2-dicyanocyclobutane (**34**) *via* [2+2] cycloaddition in 9% yield using $Mo(CO)_6$ as a photosensitizer.

Scheme 2.12. Synthesis of 1,2-Dicyanocyclobutane (34) and 1-Cyanocyclobutene (9).[73]



[a]Isolated yields.

As evidenced by ^{1}H-NMR data, our reaction yielded approximately a 1:1 mixture of the cis and trans diastereomers of **34**. The sample of 1,2-dicyanocyclobutane stereoisomers (**34**) was used without separation, as the dehydrocyanation of both stereoisomers results in the generation of the desired compound, 1-cyanocyclobutene (**9**). Dehydrocyanation of the mixture of 1,2-dicyanocyclobutane isomers (**34**) was performed by passing through a heated quartz tube packed with Ascarite (NaOH supported on granular silica), and afforded the desired compound, 1-cyanocyclobutene (**9**) in 11% yield. After isolation of **9** by vacuum distillation, the product was characterized and analyzed by ^{1}H-NMR, ^{13}C-NMR, IR, and MS, and this sample was then used to measure the rotational spectrum of 1-cyanocyclobutene (**9**).

The rotational spectrum of 1-cyanocyclobutene was collected from 130 to 360 GHz. Over 2500 *a*-type, R-branch transitions of the ground state were least-squares fit to low-error with partial-octic A- and S-reduced Hamiltonians, providing precise determinations of the corresponding spectroscopic constants. In both reductions, computed spectroscopic constants are in close agreement with their experimentally determined counterparts. Two vibrationally excited states (ν_{27} and ν_{17}) form a Coriolis-coupled dyad, displaying many *a*-type and *b*-type local

resonances and related nominal interstate transitions. Somewhat unexpectedly, despite the very small permanent *b*-axis dipole moment, a number of *b*-type transitions could be observed for the ν_{17} state; this is explained in terms of state mixing by the Coriolis perturbations. Over 2200 transitions for each of these states were least-squares fit to a low-error, two-state, partial-octic, A-reduced Hamiltonian with nine Coriolis-coupling terms (G_a, G_a^J, G_a^K, G_a^{JJ}, F_{bc}, F_{bc}^K, G_b, G_b^J, and F_{ac}).

Conclusions

We describe the synthesis and isolation of three carbocycle-containing C_5H_5N nitrile isomers: 3-cyano-3-methylcyclopropene (**1**), (cyanomethylene)cyclopropane (**2**)[59] and 1-cyanocyclobutene (**9**).[61] We also describe the synthesis of methacrylonitrile (**35**) and its deuterium-labelled isotopologues.[57] These molecules are of considerable significance to the field of astrochemistry, as possible constituents of both planetary atmospheres and interstellar space. The preparation of pure samples of these molecules has enabled the measurement of their laboratory rotational spectra. Our group has analyzed, assigned and characterized the rotational spectra of **2**, **9** and **35**. Our published works[57, 59, 61] describing the spectroscopic characterization of these species has provided the critical data needed to search for these species in space by radioastronomy. The rotational constants of the ground vibrational state for each species are very well determined and should accurately predict the rotational transitions at frequencies used for an astronomical search, even for transitions well outside the range explored by our group.

Experimental Section

General Experimental Methods. All commercial reagents were purchased from Sigma-Aldrich, Acros, and Oakwood and used as received without further purification, unless otherwise noted. ^{1}H-NMR spectra (400 or 500 MHz) and ^{13}C{^{1}H}-NMR spectra (100 or 125 MHz) were obtained in $CDCl_3$, CD_3CN, or C_6D_6 on a Bruker 400 MHz Avance III or Bruker 500 MHz DCH Avance III spectrometer; chemical shifts (δ) are reported as ppm downfield from internal standard $SiMe_4$. Mass spectra were acquired using electrospray ionization (ESI) or Atmospheric Solids Analysis Probe (ASAP)[79] on a Thermo Scientific Q-Exactive Plus™ mass spectrometer. GC/MS analysis was performed on a Shimadzu GCMS-2010S. IR spectra were obtained on a Bruker Tensor FTIR instrument as neat samples using an attenuated total reflectance accessory (Bruker Platinum ATR).

Synthetic Procedures & Information

1,2-Dicyanocyclobutane (34). ***Note:*** *Exposure of the reaction mixture to short-wavelength UV-C (254 nm) is critical, and necessitates the use of a quartz reaction vessel or immersion probe.* Photolyses were carried out in an immersion-type quartz photochemical reactor (Ace Glass # 7861-250) having an inner annular volume of 500 mL and equipped with a magnetic stirrer. In the water-cooled quartz immersion probe was inserted a centrally positioned 450 W medium-pressure mercury arc lamp (Hanovia # 679A36, 122 mm arc length). The quartz lamp chamber was continuously purged with a slow, steady stream of dry N_2 to prevent ozone generation/damage during lamp operation. Molybdenum hexacarbonyl ($Mo(CO)_6$, 5.43 g, 20.6 mmol), triphenylphosphine (PPh_3, 5.42 g, 20.7 mmol), hydroquinone (350 mg, 3.2 mmol), acrylonitrile (**41**) (195 mL, 160 g, 3 mol) and acetonitrile (143 mL) were added to the annular reactor compartment and stirred until most of the solids were dissolved. The reaction mixture was purged

of atmosphere under a steady stream of dry N_2 for 5 minutes. The reactor vessel was then sealed under vented N_2 pressure. With the immersion probe coolant flowing, the lamp was ignited, and the stirred reaction temperature was maintained at 55-60 ºC by the heat of the mercury lamp throughout the course of the photolysis. Any remaining undissolved reactants dissolved within minutes of igniting the lamp as the reaction temperature increased. The reaction progress was monitored *via* ^{1}H-NMR over the 72-hour photolysis. After the irradiation time had elapsed, the photolysis was halted, and the reaction vessel was cooled to room temperature. The amber-colored reactor contents were filtered through a coarse glass fritted funnel and concentrated *in vacuo* to remove acetonitrile and acrylonitrile. The resulting deep-red oil was purified *via* short path vacuum distillation to afford a mixture of 1,2-dicyanocyclobutane stereoisomers (**34**) as a viscous amber oil that solidified upon cooling to room temperature (14.6 g, 0.138 mmol, 9%, bp = 110–125 ºC at 2 Torr). ^{1}H-NMR ($CDCl_3$, 500 MHz): δ (ppm) 3.42 - 3.60 (m, 2H), 2.42 – 2.62 (m, 4H). *trans:* $^{13}C\{^1H\}$-NMR ($CDCl_3$, 125 MHz): δ (ppm) 118.6, 26.6, 24.8. *cis*: $^{13}C\{^1H\}$-NMR ($CDCl_3$, 125 MHz): δ (ppm) 118.3, 26.7, 24.8. IR (neat): (cm^{-1}) 2969 (m), 2242 (s), 1444 (m), 1244 (w), 1205 (m), 751 (w), 492 (w). HRMS (ASAP-MS) *m/z*: $[M+H]^+$ Calcd for $C_6H_6N_2$: 107.0604. Found: 107.0604.

1-Cyanocyclobutene (9). A vertical quartz tube 50 cm long and 2.5 cm in diameter, packed 20 cm of its length with Ascarite (Aldrich, 20-30 mesh) was heated in a 40 cm long cylindrical tube furnace to 200 ºC for 2 hours under a steady stream of dry N_2 to remove any water or absorbed gases from the Ascarite bed. A stoppered pressure-equilibrated dropping funnel containing 1,2-dicyanocyclobutane (**34**) (9.95 g, 94 mmol) was connected to the top of the quartz reactor tube and bottom was connected to a vacuum manifold thru a series of three dry ice/acetone cooled traps. The temperature of the tube furnace was set to 225 ºC, and the system was evacuated to a vacuum of 500 mTorr. The dropping funnel at the top of the reactor was lightly heated until the 1,2-

dicyanocyclobutane (**34**) was thoroughly melted and degassed. The 1,2-dicyanocyclobutane melt was added dropwise to the heated reaction tube. The exact rate of addition was sufficient to maintain an internal vacuum pressure below 2 Torr. The complete dropwise delivery of molten **34** to the heated reactor bed was achieved over a course of 2 hours. A total of 1.56 grams of hazy, colorless liquid was recovered from the traps after the addition of **34** was completed. The collected distillate was cooled to 0 ºC on ice and allowed to separate. The clear organic supernatant layer was separated and dried over granular anhydrous Na_2SO_4 to yield 1-cyanocyclobutene (**9**) as a colorless oil (834 mg, 10.6 mmol, 11%). ^{1}H-NMR ($CDCl_3$, 500 MHz): δ (ppm) 6.78 (t, J = 1.4 Hz, 1H), 2.84 (dd, J = 3.4 Hz, 2H), 2.63 (ddd, J = 3.4 Hz, 3.2 Hz, 1.4 Hz, 2H) ^{13}C{^{1}H}-NMR ($CDCl_3$, 125 MHz): δ (ppm) 153.0, 117.2, 113.9, 32.4, 30.3. IR (neat): (cm^{-1}) 2978 (w), 2937 (m), 2835 (w), 2218 (m), 1584 (w), 1425 (w), 1252 (m), 1213 (w), 1162 (w), 1073 (w), 936 (w), 910 (m), 867 (m), 757 (m), 684 (w), 584 (w), 516 (s). HRMS (ASAP-MS) *m/z*: $[M+H]^+$ Calcd for $C_6H_6N_2$: 80.0495. Found: 80.0494.

1-Ethoxycyclopropanol (20). A solution of (1-ethoxycyclopropoxy)trimethylsilane (**40**, 9.98 g, 57 mmol) in methanol (25 mL) was stirred at room temperature for 24 hours. The reaction was monitored *via* ^{1}H-NMR and TLC. A reaction aliquot taken at 24 hours showed complete deprotection of the TMS group. The methanol solvent was subsequently removed *in vacuo* to afford a clear, colorless oil. The crude oil was then purified *via* short-path distillation to yield 1-ethoxycyclopropanol (**20**) (bp = 88-90 ºC at 100 Torr) as a colorless oil (5.0 g, 48.5 mmol, 85%). TLC: R_f = 0.3 (Hexane : EtOAc, 4:1; $KMnO_4$). ^{1}H-NMR ($CDCl_3$, 500 MHz): δ (ppm) 4.37 (brs, 1H), 3.77 (q, J = 7.2 Hz, 2H), 1.21 (t, J = 7.1 Hz, 4H), 0.98 – 0.87 (m, 4H).^{13}C-NMR ($CDCl_3$, 125 MHz): δ (ppm) 85.5, 62.0, 15.4, 14.2. IR (neat): (cm^{-1}) 3386 (m), 2978 (w), 1734 (m), 1460 (w), 1298 (m), 1225 (m), 1052 (m), 943 (m), 487 (w). HRMS (ESI) *m/z*: $[M+H]^+$ Calcd for $C_5H_{10}O_2$: 103.0754. Found: 103.0753.

Triphenylcyanomethylenephosphorane (21). To a stirred solution of cyanomethyltriphenylphosphonium chloride (**41**) (10.0 g, 30 mmol) in water was added dropwise at room temperature an aqueous solution of sodium hydroxide (50% *w/w*, 5.0 mL) over a course of 5 minutes. The addition resulted in the formation of a white precipitate and the reaction was stirred for an additional 30 minutes. The resulting white solids were filtered *via* coarse glass fritted filter and dried *in vacuo* for 24 hours to yield cyanomethylene triphenylphosphorane (**21**) (7.02 g, 23.25 mmol, 77%). ^{1}H-NMR ($CDCl_3$, 500 MHz): δ (ppm) 7.43-7.71 (*m*, 15H), 1.60 (*s*, 1H) ^{13}C-NMR (125 MHz, $CDCl_3$) δ 132.80 (d, J = 10.1 Hz), 132.57 (d, J = 3.0 Hz), 132.11 (d, J = 9.8 Hz), 129.08 (d, J = 12.4 Hz), 128.50 (d, J = 12.1 Hz), 127.43 (d, J = 91.8 Hz).

(Cyanomethylene)cyclopropane (2). To a flame-dried 250 mL single-necked round bottom flask (cooled under a stream of N_2) was added cyanomethylene triphenylphosphorane (**21**, 6.01 g, 20 mmol), 1-ethoxycyclopropanol (**20**, 2.07 g, 20.3 mmol), benzoic acid (243 mg, 2 mmol, 10 mol%) and 115 mL benzene. The reaction vessel was fitted with a water-cooled reflux condenser (with N_2 vent) and heated to reflux for 24 hours. After cooling to room temperature, the flask was fitted with a fractionating column (23 cm, glass bead-packed) and most the benzene was fractionated away at atmospheric pressure. 100 mL pentane was added to the remaining liquid (~40 mL) in the boiling flask, and was cooled on ice to precipitate the triphenylphosphine oxide byproduct. The resulting mixture was filtered through a fine glass frit into a separate boiling flask, and the pentane was fractionated away at atmospheric pressure leaving the crude product as a bright yellow liquid. The crude product was purified *via* short-path vacuum distillation to yield (cyanomethylene)cyclopropane (**2**) (bp = 88 ºC at 100 Torr) as a colorless oil (820 mg, 52%). The odor of cyanomethylene cyclopropane is highly reminiscent of 4-cyano-1,2-butadiene. ^{1}H-NMR ($CDCl_3$, 500 MHz): δ (ppm) 5.80 (m, 1H), 1.44 (d, J = 7.2 Hz, 4H). ^{13}C-NMR ($CDCl_3$, 125 MHz):

δ (ppm) 151.9, 116.8, 90.5, 5.2, 4.2. IR (neat): (cm^{-1}) 3023 (w), 2987 (w), 2221 (m), 1745 (w), 1722 (m), 1403 (w), 1278 (m), 1002 (m), 939 (m), 913 (m), 760 (s), 723 (m), 683 (m). HRMS (ESI) *m/z*: $[M+H]^+$ Calcd for C_5H_6N: 80.0495. Found: 80.0494.

Methacrylonitrile (35). In a flame-dried, single-necked 500 mL round bottom flask (cooled under a stream of N_2) was added 10.15 g (119.2 mmol) methacrylamide (**36**) and 25.21 g (178 mmol) P_2O_5. The reaction flask was shaken to homogenize the solid reactants. The flask was then connected to a short path distillation apparatus with the receiving flask cooled to -78 ºC in a dry ice/acetone bath. The system was purged with N_2 for 5 minutes, and then heated to 160 ºC *via* heating mantle. At approximately 130 ºC, the solid reactants will begin to expand and the distillate will begin to collect in the receiving flask as solid crystals. A heat gun was periodically used to warm exposed portions of the distillation flask to move any remaining distillate to the receiving flask. 5.22 g methacrylonitrile (**35**) (65%) was collected over a course of 2 hours as a colorless oil. ^{1}H-NMR ($CDCl_3$, 500 MHz): δ (ppm) 5.83 (*p*, 1H, *J* = 1 Hz), 5.74 (*qd*, 1H, *J* = 1.7, 1 Hz), 2.0 (*dd*, 3H *J*= 1.7, 1 Hz). ^{13}C-NMR ($CDCl_3$, 125 MHz): δ (ppm) 131.2, 119.1, 118.0, 20.7. HRMS (ASAP-MS) *m/z*: $[M+H]^+$ Calcd for C_4H_6N: 68.0495. Found: 68.0496.

Deuterium-Enriched Acetone (37-*d*). In an oven-dried, single-necked 150 mL round bottom flask was added acetone (37) (11.6546 g, 200 mmol), KOH (1.2275 g, 21.8 mmol), and D_2O (4.0642 g, 203 mmol). The flask was sealed with a rubber septum and stirred at room temperature for 24 hours. The reaction was quenched *via* addition of 2M HCl (5.5 mL). Distillation of the resulting mixture at atmospheric pressure through a short-path distillation rig fitted with a 20-cm helix-packed fractionating column yielded **37-*d*** (bp = 56 ºC at 1 atm) as a volatile, colorless liquid (10.9382 g). Analysis of the product *via* HRMS (ASAP-MS) showed the presence of acetone at varying levels of deuteration. HRMS (ASAP-MS) *m/z*: $[M+H]^+$ Calcd for C_3H_6DO: 60.0554.

Found: 60.0556. Calcd for $C_3H_5D_2O$: 61.0617. Found: 61.0618. Calcd for $C_3H_4D_3O$: 62.0680. Found: 62.0681. Calcd for $C_3H_3D_4O$: 63.0743. Found: 63.0743. Calcd for $C_3H_2D_5O$: 64.0805. Found: 64.0806. Calcd for C_3HD_6O: 65.0868. Found: 65.0869.

Deuterium-Enriched Acetone Cyanohydrin (38-*d*). ***Note:*** *This procedure must be performed in an efficient fume hood due to the generation of HCN gas.* In an oven-dried, single-necked 250 mL round bottom flask was added **37-*d*** (12.7936 g, approx. 200 mmol), KCN (13.6674 g, 210 mmol), and DI H_2O (50 mL). The flask was fitted with a 150-mL pressure-equalizing addition funnel and cooled to 0 ºC on an ice bath. An aqueous solution of sulfuric acid (4.4 M, 100 mL) was added to the addition funnel. The neck of the addition funnel was fitted with a gas inlet adaptor and connected to a gas washing bottle containing dilute aqueous KOH. The sulfuric acid solution was added dropwise to the stirring reaction vessel over the course of 15 minutes. White vapor was observed outgassing from the reaction upon addition of the sulfuric acid solution. The reaction was stirred for an additional 45 minutes at 0 ºC after the addition of the sulfuric acid solution was complete. The resulting pale yellow mixture was filtered, extracted with diethyl ether (3 × 50 mL), washed with saturated aqueous $NaHCO_3$ (30 mL), dried over anhydrous $MgSO_4$, filtered, and the solvent was removed *in vacuo* to yield **38-*d*** as a colorless oil (12.3246 g). ^{1}H-NMR ($CDCl_3$, 500 MHz): δ (ppm) 1.63 (*s*, 3H), 3.24 (*brs*, 1H).

Deuterium-Enriched Methacrylamide (36-*d*). In an oven-dried, single-necked 250 mL round bottom flask was added concentrated (95-98%) sulfuric acid (20.81 g). The flask was fitted with a 50-mL pressure-equalizing addition funnel, and was heated to 80 ºC on an oil bath. Deuterium-enriched acetone cyanohydrin (**38-*d***) (12.3246 g, 145 mmol) was added to the addition funnel and delivered dropwise to the stirring sulfuric acid. After the addition was completed, the reaction temperature was increased to 145 ºC, and stirred for 15 minutes. The reaction vessel was

removed from heat and cooled to 0 ºC on an ice bath. A solution of saturated aqueous $NaHCO_3$ (25 mL) was slowly added to the chilled reaction vessel, and resulted in effervescence. The reaction mixture was transferred to a separatory funnel and extracted with ethyl acetate (5 × 50 mL). The combined organic extracts were dried over anhydrous $MgSO_4$, filtered, and the solvent was removed *in vacuo via* rotary evaporation to yield **36-*d*** as a white crystalline solid (7.6857 g, 62 %).

Deuterium-Enriched Methacrylonitrile (35-*d*). In a flame-dried, single-necked 100 mL round bottom flask (cooled under a stream of N_2) was added 2.1410 g (25.2 mmol) deuterium-enriched methacrylamide (**36-*d***) and 5.0 g (35.2 mmol) P_2O_5. The reaction flask was shaken to homogenize the solid reactants. The flask was then connected to a short path distillation apparatus with the receiving flask cooled to -78 ºC in a dry ice/acetone bath. The system was purged with N_2 for 5 minutes, and then heated to 160 ºC *via* heating mantle. At approximately 130 ºC, the solid reactants will begin to expand and the distillate will begin to collect in the receiving flask as solid crystals. A heat gun was periodically used to warm exposed portions of the distillation flask to move any remaining distillate to the receiving flask. Deuterium-enriched methacrylonitrile (**35-*d***) was collected over a course of 2 hours as a colorless oil (610 mg, 36%). ^{1}H-NMR ($CDCl_3$, 500 MHz): δ (ppm) 5.83 (*p*, 1H, J = 1 Hz), 5.74 (*qd*, 1H, J = 1.7, 1 Hz), 2.0 (*dd*, 3H J= 1.7, 1 Hz). ^{13}C-NMR ($CDCl_3$, 125 MHz): δ (ppm) 131.2, 119.1, 118.0, 20.7. HRMS (ASAP-MS) *m/z*: $[M+H]^+$ Calcd for C_4H_6N: 68.0495. Found: 68.0496. Calcd for C_4H_5DN: 69.0558. Found: 69.0559. Calcd for $C_4H_4D_2N$: 70.0620. Found: 70.0621. Calcd for $C_4H_3D_3N$: 71.0683. Found: 71.0683. Calcd for $C_4H_2D_4N$: 72.0746. Found: 72.0746.

Acetone Cyanohydrin-d$_6$ (38-*d*$_6$). ***Note:*** *This procedure must be performed in an efficient fume hood due to the generation of HCN gas.* In an oven-dried, single-necked 250 mL round

bottom flask was added acetone-d_6 (**37-*d*$_6$**) (Aldrich, 99.9 atom percent D) (12.3954 g, 193 mmol), KCN (12.5865 g, 193 mmol), and DI H_2O (50 mL). The flask was fitted with a 150-mL pressure-equalizing addition funnel and cooled to 0 ºC on an ice bath. An aqueous solution of sulfuric acid (4.4 M, 100 mL) was added to the addition funnel. The neck of the addition funnel was fitted with a gas inlet adaptor and connected to a gas washing bottle containing dilute aqueous KOH. The sulfuric acid solution was added dropwise to the stirring reaction vessel over the course of 15 minutes. White vapor was observed outgassing from the reaction upon addition of the sulfuric acid solution. The reaction was stirred for an additional 45 minutes at 0 ºC after the addition of the sulfuric acid solution was complete. The resulting pale yellow mixture was filtered, extracted with diethyl ether (3 × 50 mL), washed with saturated aqueous $NaHCO_3$ (30 mL), dried over anhydrous $MgSO_4$, filtered, and the solvent was removed *in vacuo* to yield **38-*d*** as a colorless oil (13.5802 g, 149 mmol, 77%).

Methacrylamide-d$_5$ (36-*d*$_5$). In an oven-dried, single-necked 250 mL round bottom flask was added concentrated (95-98%) sulfuric acid (21.9407 g). The flask was fitted with a 50-mL pressure-equalizing addition funnel, and was heated to 80 ºC on an oil bath. Acetone cyanohydrin-d_6 (**38-*d*$_6$**) (13.5802 g, 149.13 mmol) was added to the addition funnel and delivered dropwise to the stirring sulfuric acid. After the addition was completed, the reaction temperature was increased to 145 ºC, and stirred for 15 minutes. The reaction vessel was removed from heat and cooled to 0 ºC on an ice bath. A solution of saturated aqueous $NaHCO_3$ (25 mL) was slowly added to the chilled reaction vessel, and resulted in effervescence. The reaction mixture was transferred to a separatory funnel and extracted with ethyl acetate (5 × 50 mL). The combined organic extracts were dried over anhydrous $MgSO_4$, filtered, and the solvent was removed *in vacuo via* rotary evaporation to yield **36-*d*$_5$** as a white crystalline solid (5.7187 g, 63,5 mmol, 42 %).

Methacrylonitrile-d_5 (35-*d_5*). In a flame-dried, single-necked 100 mL round bottom flask (cooled under a stream of N_2) was added 5.7187 g (63.49 mmol) methacrylamide-d_5 (**36-*d_5***) and 12.8433 g (90.5 mmol) P_2O_5. The reaction flask was shaken to homogenize the solid reactants. The flask was then connected to a short path distillation apparatus with the receiving flask cooled to -78 ºC in a dry ice/acetone bath. The system was purged with N_2 for 5 minutes, and then heated to 160 ºC *via* heating mantle. At approximately 130 ºC, the solid reactants will begin to expand and the distillate will begin to collect in the receiving flask as solid crystals. A heat gun was periodically used to warm exposed portions of the distillation flask to move any remaining distillate to the receiving flask. Methacrylonitrile-d_5 (**35-*d_5***) was collected over a course of 2 hours as a colorless oil (931 mg, 13 mmol, 20%). HRMS (ASAP-MS) *m/z*: $[M+H]^+$ Calcd for $C_4H_4D_2N$: 70.0620. Found: 70.0621. Calcd for $C_4H_3D_3N$: 71.0683. Found: 71.0683. Calcd for $C_4H_2D_4N$: 72.0746. Found: 72.0746. C_4HD_5N: 73.0809. Found: 73.0808.

2,2-Dibromo-1-methylcyclopropane-1-carbonitrile (39). A solution of methacrylonitrile (**35**) (6.12 g, 90 mmol) and benzyltriethylammonium chloride (2.0 g, 8.7mmol) in bromoform (46.5 g, 183 mmol) was prepared in 250 mL single-necked round bottom flask. A pressure-equalizing dropping funnel was connected to the reaction flask and 37.2 g NaOH solution (50% *w/w*) was added to the dropping funnel. The NaOH solution was then added dropwise to the rapidly stirring bromoform mixture over a course of 20 minutes at room temperature. Over the course of the addition, the reaction darkened significantly. The reaction was left stirring for 12 hours at room temperature. The reaction was quenched *via* addition of 10 mL saturated aqueous ammonium chloride, then extracted with methylene chloride (5 × 50 mL). The organic extract was then dried over anhydrous Na_2SO_4, filtered, and the solvent was removed *via* rotary evaporation. The crude isolate was then purified *via* short-path distillation (bp = 70-75 ºC, 0.1 Torr) to yield 2,2-dibromo-1-methylcyclopropane-1-carbonitrile (**39**) as a colorless oil (14.27 g, 66%). ^{1}H-NMR ($CDCl_3$, 500

MHz): δ (ppm) 2.26 (*d*, 1H, *J* = 8.08 Hz), 1.81 (*d*, 1H, *J* = 8.08 Hz), 1.70 (*s*, 3H). ^{13}C-NMR ($CDCl_3$, 125 MHz): δ (ppm) 119.3, 35.3, 26.8, 22.0, 21.2. HRMS (ASAP-MS) *m/z*: $[M+H]^+$ Calcd for $C_5H_6Br_2N$: 237.8862. Found: 237.8862.

2-Bromo-1-methylcyclopropane-1-carbonitrile (18). In a flame-dried, single-necked 250 mL round bottom flask (cooled under a stream of N_2) was added 9.57 g (40 mmol, 1 eq.) 2,2-dibromo-1-methylcyclopropane-1-carbonitrile (**39**) and 8.28 g (60 mmol, 1.5 eq.) diethylphosphite. The flask was sealed with a rubber septum and purged with N_2. Triethylamine (6.1 g, 60 mmol, 1.5 eq.) was added dropwise to the stirring reaction mixture over the course of 5 minutes *via* syringe pump. The addition of triethylamine resulted in a noticeable exotherm as the reaction mixture turned dark red and viscous. The reaction was stirred for an additional 45 minutes. The resulting mixture was rinsed through a coarse fritted glass funnel with 100 mL diethyl ether (to remove the solid $NH(Et)_3Br$ byproduct). An additional 100 mL diethyl ether was added, and the resulting organic extract was washed with water (3 × 50 mL) then with saturated $NaHCO_{3(aq)}$. The organic extract was then dried over anhydrous Na_2SO_4, filtered, and the solvent removed *in vacuo* to yield 2-bromo-1-methylcyclopropane-1-carbonitrile (**18**) as a pale-yellow oil (3.53 g, 55%). ^{1}H-NMR ($CDCl_3$, 500 MHz): δ (ppm) 3.47 (*dd*, 1H, J = 8.3 Hz, 5.7 Hz), 1.88 (*dd*, 1H, J = 8.3 Hz, 6.9 Hz), 1.56 (*s*, 3H), 1.10 (*dd*, 1H, J = 6.9 Hz, 5.7 Hz). ^{13}C-NMR ($CDCl_3$, 125 MHz): δ (ppm) 121.6, 25.6, 23.6, 18.4, 9.7. HRMS (ASAP-MS) *m/z*: $[M+H]^+$ Calcd for C_5H_7BrN: 159.9756. Found: 159.9756.

3-Cyano-3-methylcyclopropene (1). In an oven-dried 100 mL round bottomed flask was added under an atmosphere of dry N_2 potassium hydroxide (4.4720 g, 80 mmol) and DMSO (11.75 mL). The reaction flask was sealed with a rubber septum, degassed/backfilled with N_2 (3×), and stirred at room temperature until the solid KOH had fully dissolved. In a separate dry flask 2-

bromo-1-methylcyclopropane-1-carbonitrile (**18**) (3.572 g, 22.3 mmol) was dissolved in 5 mL DMSO and drawn into a syringe. The solution of **18** was delivered to the stirring solution of KOH over the course of 1 hour *via* syringe pump. The reaction mixture turned blood-red upon addition of 2-bromo-1-methylcyclopropane-1-carbonitrile (**18**). After the addition was complete, the reaction was stirred for an additional 2 hours. After the reaction time had elapsed, the reaction mixture was poured over 40 mL H_2O and rinsed into a separatory funnel with 20 mL DCM. The organic layer was separated, and the mixture was extracted with 10 mL DCM (2×). The combined organic extracts were washed with DI H_2O (5 × 10 mL), dried over $MgSO_4$, filtered, and the solvent was removed *in vacuo* to yield the crude product as an orange oil. The crude product was further *via* vacuum distillation (bp = 50-60 ºC at 100 Torr) to yield 3-cyano-3-methylcyclopropene (**1**) as a colorless oil (194 mg, 2.45 mmol, 11%). ^{1}H-NMR ($CDCl_3$, 500 MHz): δ (ppm) 5.30 (s, 2H), 1.45 (s, 3H). ^{13}C-NMR ($CDCl_3$, 125 MHz): δ (ppm) 124.7, 111.9, 23.8, 8.1. IR (neat): (cm^{-1}) 3154 (w), 3114 (m), 2970 (w), 2931 (w), 2222 (m), 1653 (m), 1452 (m), 1382 (w), 1201 (w), 1156 (m), 997 (m), 916 (m), 678 (s), 622 (s), 568 (s). HRMS (ASAP-MS) *m/z*: $[M+H]^+$ Calcd for C_5H_6N: 80.0495. Found: 80.0494.

Notes and References

1. Thaddeus, P.; Vrtilek, J. M.; Gottlieb, C. A., Laboratory and Astronomical Identification of Cyclopropenylidene, C_3H_2. *Astrophys. J.* **1985,** *299*, L63-L66.

2. Hollis, J. M.; Remijan, A. J.; Jewell, P. R.; Lovas, F. J., Cyclopropenone (*c*-H_2C_3O): A New Interstellar Ring Molecule. *Astrophys. J.* **2006,** *642* (2), 933-939.

3. Dickens, J. E.; Irvine, W. M.; Ohishi, M.; Ikeda, M.; Ishikawa, S.; Nummelin, A.; Hjalmarson, Å., Detection of Interstellar Ethylene Oxide (*c*-C_2H_4O). *Astrophys. J.* **1997,** *489*, 753-757.

4. McGuire, B. A.; Carroll, P. B.; Loomis, R. A.; Finneran, I. A.; Jewell, P. R.; Remijan, A. J.; Blake, G. A., Discovery of the Interstellar Chiral Molecule Propylene Oxide (CH_3CHCH_2O). *Science* **2016,** *352*, 1449-1452.

5. Gardner, F. F.; Winnewisser, G., The Detection of Interstellar Vinyl Cyanide (Acrylonitrile). *Astrophys. J.* **1975,** *195*, L127-L130.

6. Lovas, F. J.; Remijan, A. J.; Hollis, J. M.; Jewell, P. R.; Snyder, L. E., Hyperfine Structure Identification of Interstellar Cyanoallene toward TMC-1. *Astrophys. J.* **2006,** *637* (1), L37-L40.

7. Broten, N. W.; MacLeod, J. M.; Avery, L. W.; Irvine, W. M.; Hoglund, B.; Friberg, P.; Hjalmarson, A., The Detection of Interstellar Methylcyanoacetylene. *Astrophys. J.* **1984,** *276*, L25-L29.

8. Niwayama, S.; Kallel, E. A.; Spellmeyer, D. C.; Sheu, C.; Houk, K. N., Substituent Effects on Rates and Stereoselectivities of Conrotatory Electrocyclic Reactions of Cyclobutenes. A Theoretical Study. *J. Org. Chem.* **1996,** *61* (8), 2813-25.

9. Nakamura, K.; Houk, K. N., Substituent Effects on Torquoselectivity. Computational Investigations of the Thermal Ring Openings of Cyclobutenes Fused to Substituted Cyclohexenes. *J. Org. Chem.* **1995,** *60* (3), 686-91.

10. Spellmeyer, D. C.; Houk, K. N.; Rondan, N. G.; Miller, R. D.; Franz, L.; Fickes, G. N., Experimental and theoretical studies of substituent effects on an orbital-symmetry-forbidden electrocyclization. *J. Am. Chem. Soc.* **1989,** *111* (14), 5356-67.

11. Sheikh, N. S., Captodative substitution induced acceleration effect towards 4π electrocyclic ring-opening of substituted cyclobutenes. *RSC Adv.* **2016,** *6* (30), 25503-25510.

12. Rudolf, K.; Spellmeyer, D. C.; Houk, K. N., Prediction and experimental verification of the stereoselective electrocyclization of 3-formylcyclobutene. *J. Org. Chem.* **1987,** *52* (16), 3708-10.

13. Yasui, M.; Naruse, Y.; Inagaki, S., An Orbital Phase Theory for the Torquoselectivity of the Ring-Opening Reactions of 3-Substituted Cyclobutenes: Geminal Bond Participation. *J. Org. Chem.* **2004,** *69* (21), 7246-7249.

14. Richtsmeier, S. C.; Gassman, P. G.; Dixon, D. A., A theoretical evaluation of substituent effects on the ionization potential of bicyclo[1.1.0]butane. *J. Org. Chem.* **1985,** *50* (3), 311-17.

15. Arnaud, R.; Subra, R.; Barone, V., A theoretical study of substituent effects on the structure of isolated and condensed three-membered rings. A comparison between radicals and parent hydrocarbons. *Theor. Chem. Acc.* **1998,** *99* (6), 411-419.

16. Sella, A.; Basch, H.; Hoz, S., Reactivity of Strained Compounds: Is Ground State Destabilization the Major Cause for Rate Enhancement? *J. Am. Chem. Soc.* **1996,** *118* (2), 416-20.

17. Taylor, W. H.; Harmony, M. D.; Staley, S. W., Microwave spectrum, dipole moment, and a proposed structure for 1-cyanobicyclo[1.1.0]butane. *Struct. Chem.* **1991,** *2* (2), 167-73.

18. Anicich, V. G.; Wilson, P. F.; McEwan, M. J., An ICR study of ion-molecules reactions relevant to Titan's atmosphere: an investigation of binary hydrocarbon mixtures up to 1 micron. *J. Am. Soc. Mass Spectrom.* **2006,** *17* (4), 544-561.

19. Guillemin, J. C.; Ferris, J. P., Photochemistry of unsaturated nitriles on Titan. *Eur. Space Agency, Spec. Publ.* **1992,** *ESA SP-338* (Proc. - Symp. Titan, 1991), 177-81.

20. Ferris, J. P.; Guillemin, J. C., Photochemical cycloaddition reactions of cyanoacetylene and dicyanoacetylene. *J. Org. Chem.* **1990,** *55* (21), 5601-6.

21. Gale, D. M., Mechanistic aspects of the photochemistry of unsaturated nitriles. *J. Org. Chem.* **1970,** *35* (4), 970-2.

22. Sarner, S. F.; Gale, D. M.; Hall, H. K., Jr.; Richmond, A. B., Gas-phase thermolysis kinetics of small ring nitriles. *J. Phys. Chem.* **1972,** *76* (20), 2817-19.

23. Gale, D. M.; Cherkofsky, S. C., Dehydrocyanation of dinitriles. Preparation of 1-cyclobutenecarbonitrile by direct dehydrocyanation of 1,2-cyclobutanedicarbonitrile. *J. Org. Chem.* **1973,** *38* (3), 475-8.

24. Kwak, N.; Simmons, J. W.; Goldstein, J. H., Microwave Spectrum of Propiolactone. *J. Chem. Phys* **1955,** *23* (12), 2450-2450.

25. Boone, D. W.; Britt, C. O.; Boggs, J. E., Microwave Spectrum, Dipole Moment, and Ring-Puckering Vibration of β-Propiolactone. *J. Chem. Phys* **1965,** *43* (4), 1190-1194.

26. Chen, Z.; van Wijngaarden, J., A Combined *Ab Initio*, Fourier Transform Microwave and Fourier Transform Infrared Spectroscopic Investigation of β-Propiolactone: The ν_8 and ν_{12} bands. *J. Mol. Spectrosc.* **2009,** *257* (2), 164-169.

27. Orr, V. L.; Esselman, B. J.; Dorman, P. M.; Amberger, B. K.; Guzei, I. A.; Woods, R. C.; McMahon, R. J., Millimeter-wave Spectroscopy, X-ray Crystal Structure, and Quantum Chemical Studies of Diketene – Resolving Ambiguities Concerning the Structure of the Ketene Dimer. *J. Phys. Chem. A* **2016,** *120* (39), 7753-7763.

28. Durig, J. R.; Carreira, L. A.; Lafferty, W. J., Spectra and Structure of Small Ring Compounds. Microwave Spectrum of Cyanocyclobutane. *J. Mol. Spectrosc.* **1973,** *46* (2), 187-193.

29. Fong, M. Y.; Harmony, M. D., Microwave Spectrum, Dipole Moment, Quadrupole Coupling Constants, and Conformation of Cyanocyclobutane. *J. Chem. Phys* **1973,** *58* (10), 4260-4264.

30. Caminati, W.; Velino, B.; Della Valle, R. G., Rotational Spectra of Several Vibrational Excited States of Axial and Equatorial Cyanocyclobutane and Potential Energy Function of the Ring Puckering. *J. Mol. Spectrosc.* **1988,** *129* (2), 284-292.

31. Durig, J. R.; Ganguly, A.; Klaassen, J. J.; Guirgis, G. A., The r_0 Structural Parameters, Conformational Stability, and Vibrational Assignment of Equatorial and Axial Cyanocyclobutane. *J. Mol. Struct.* **2009,** *923* (1), 28-38.

32. Caminati, W.; Velino, B.; Dakkouri, M.; Schäfer, L.; Siam, K.; Ewbank, J. D., Reinvestigation of the Microwave Spectrum of Cyanocyclobutane: Assignment of the Axial Conformer. *J. Mol. Spectrosc.* **1987,** *123* (2), 469-475.

33. Menke, J. L.; McMahon, R. J., Photochemistry of matrix-isolated 5-cyano-2*H*-pyran-2-one (δ-cyano-α-pyrone) and cyanocyclobuta-1,3-diene. *Can. J. Chem.* **2011,** *89* (2), 186-194.

34. Tsuchiya, T.; Arai, H.; Igeta, H., Photolysis of tetrazolo[1,5-b]pyridazines. Formation of cyanocyclopropenes. *J. Chem. Soc., Chem. Commun.* **1972,** (19), 1059.

35. Tsuchiya; Arai; Igeta, Photochemistry. X. Photolysis of tetrazolo[1,5 b]pyridazines. *Chem. Pharm. Bull.* **1973,** *21* (11), 2517 - 2520.

36. Latypova, M. M.; Plemenkov, V. V.; Kalinina, V. N.; Bolesov, I. G., Synthesis, structure, and reactivity of cyclopropanes and cyclopropenes. XVIII. 3-Methyl-3-cyanocyclopropene in a Diels-Alder reaction. *Zh. Org. Khim.* **1984,** *20* (3), 542-8.

37. Bolesov, I. G.; Ignatchenko, A. V.; Bovin, N. V.; Prudchenko, I. A.; Surmina, L. S.; *et al.*, Selectivity In The Reactions Of 3,3-Disubstituted Cyclopropenes With Nitrile Oxides. *Russ. J. Org. Chem.* **1990,** *26* (1.2), 87 - 100.

38. Lodochnikova, O. A.; Ashirov, R. V.; Appolonova, S. A.; Litvinov, I. A.; Plemenkov, V. V., 1-Methyl-2-cyclopropene-1-carbonitrile in tandem Alder-ene and Diels-Alder reactions. *Russ. J. Org. Chem.* **2010,** *46* (1), 49-53.

39. Ashirov, R. V.; Shamov, G. A.; Lodochnikova, O. A.; Litvynov, I. A.; Appolonova, S. A.; Plemenkov, V. V., Tetramerization of 3-Methyl-cyclopropene-3-carbonitrile: A Novel CN-Alder-ene Reaction. *J. Org. Chem.* **2008,** *73* (15), 5985-5988.

40. Ashirov, R. V.; Balandina, A. A.; Kharlamov, S. V.; Appolonova, S. A.; Figadere, B.; Latypov, S. K.; Plemenkov, V. V., Alder-ene reaction of 3-methyl-3-cyanocyclopropene with monoterpenes. *Lett. Org. Chem.* **2006,** *3* (9), 670-673.

41. Ashirov, R. V.; Appolonova, S. A.; Plemenkov, V. V., Diels-Alder modification of monoterpenes and Alder-ene synthesis involving 3-methyl-3-cyanocyclopropene. *Chem. Nat. Compd.* **2006,** *42* (4), 434-438.

42. Plemenkov, V. V.; Ashirov, R. V.; Lodochnikova, O. A.; Litvinov, I. A.; Zagidullin, R. N., Diels-Alder reaction of 1-methylcycloprop-2-ene-1-carbonitrile with methyl 2-oxo-2*H*-pyran-5-carboxylate. *Russ. J. Org. Chem.* **2006,** *42* (7), 969-972.

43. Rul, S. V.; Plemenkov, V. V.; Gubaidullin, A. T.; Litvinov, I. A.; Kataeva, O. N.; Apollonova, S. A., Stereochemistry of Diels-Alder addition of 3-methyl-3-cyanocyclopropene to 1,4-disubstituted butadienes. exo-syn-orientation. *Russ. J. Org. Chem.* **1999,** *35* (8), 1121-1126.

44. Plemenkov, V. V.; Rul, S. V.; Khaliullin, R. R., Diels-Alder condensation with 3-methyl-3-cyanocyclopropene as a method of synthesis of 3-carene-type terpenoids. *Zh. Org. Khim.* **1994,** *30* (9), 1331-4.

45. Zinin, V. N.; Il'yasov, A. V.; Plemenkov, V. V., Proton and carbon-13 NMR spectra of 3-cyano-3-methylcyclopropene and 3-methyl-3-phenylcyclopropene. *Izv. Akad. Nauk SSSR, Ser. Khim.* **1985,** (6), 1405-8.

46. Wilson, C. L., 17. Reactions of Furan compounds. Part IV. High-Temperature Decomposition of the Vapours of Tetrahydrofuronitrile and Methyl Tetrahydrofuroate to Give 2,3-Dihydrofuran and Cyclopropanealdehyde. *J. Chem. Soc.* **1945,** (0), 58-61.

47. Mauduit, M.; Kouklovsky, C.; Langlois, Y., Cyanomethylene Cyclopropane, a Useful Dipolarophile and Dienophile in [2+3] and [2+4] Cycloadditions. *Tetrahedron Lett.* **1998,** *39* (38), 6857-6860.

48. Scott, M. E.; Tseng, N.-W.; Lautens, M., 2-methylenecyclopropanecarboxylic acid ethyl ester. *Org. Synth.* **2008,** *85*, 172-178.

49. Nishimura, A.; Ohta, M.; Kato, H., Deamination of methylenecyclopropylcarbinylamine. The formation of a vinyl cation by carbon-carbon bond cleavage. *Bull. Chem. Soc. Jap.* **1970,** *43* (5), 1530-4.

50. Tietz, R. F.; Kenyon, W. G. 1-Cyanocyclobutene monomer and polymer and their preparation. US3468861A, 1969.

51. Gale, D. M. Film- and fiber-forming cyclobutene homopolymers and copolymers. US3696080A, 1972.

52. Gale, D. M. Catalytic preparation of 1-cyanocyclobutene from 1,2-dicyanocyclobutane. US3657313A, 1972.

53. Gale, D. M. Mono- and dichlorocyclobutanecarbonitriles by cycloaddition of vinyl chloride and an acrylonitrile. US3642859A, 1972.

54. Gale, D. M. 1-Cyanobicyclo[1.1.0]butane and 1-cyanocyclobutene by photolysis of 2-cyano-1,3-butadiene. US3459647A, 1969.

55. Miki, S.; Matsumura, S.; Ohno, T.; Yoshida, Z., Cobalt(II) porphyrin-catalyzed isomerization of bicyclobutanecarbonitrile. *Tetrahedron Lett.* **1986,** *27* (31), 3669-72.

56. Hall, H. K., Jr.; Blanchard, E. P., Jr.; Cherkofsky, S. C.; Sieja, J. B.; Sheppard, W. A., Synthesis and polymerization of 1-bicyclobutanecarbonitriles. *J. Amer. Chem. Soc.* **1971,** *93* (1), 110-20.

57. Smith, H. H.; Kougias, S. M.; Lee, D. J.; Esselman, B. J.; Woods, R. C.; McMahon, R. J. In *Semi-Experimental Equilibrium Structure (r_e^{SE}) of Methacrylonitrile (C_4H_5N)*, International Symposium on Molecular Spectroscopy, 2021/06/1; 2021.

58. Ruhland, K.; Haase, N.; Fischer, A., Detailed examination of nitrile stretching vibrations relevant for understanding the behavior of thermally treated polyacrylonitrile. *J. Appl. Polym. Sci.* **2017,** *134* (29), n/a.

59. Esselman, B. J.; Kougias, S. M.; Zdanovskaia, M. A.; Woods, R. C.; McMahon, R. J., Synthesis, Purification, and Rotational Spectroscopy of (Cyanomethylene)Cyclopropane-An Isomer of Pyridine. *J. Phys. Chem. A* **2021,** *125* (25), 5601-5614.

60. Kleinbeck, F.; Toste, F. D., Gold(I)-Catalyzed Enantioselective Ring Expansion of Allenylcyclopropanols. *J. Am. Chem. Soc.* **2009,** *131* (26), 9178-9179.

61. Smith, H. H.; Kougias, S. M.; Esselman, B. J.; Woods, R. C.; McMahon, R. J., Synthesis, Purification, and Rotational Spectroscopy of 1-Cyanocyclobutene (C_5H_5N). *J. Phys. Chem. A* **2022,** *126* (12), 1980-1993.

62. Wilson, S. R.; Phillips, L. R.; Pelister, Y.; Huffman, J. C., Cyclobutene derivatives as isoprene equivalents in terpene synthesis. 3. Bicyclo[2.2.0]hexanes. *J. Am. Chem. Soc.* **1979,** *101* (24), 7373-9.

63. Grubbs, R. H.; Miyashita, A., Carbon-carbon bond cleavage reactions in the decomposition of metallacycles. *J. Am. Chem. Soc.* **1978,** *100* (23), 7418-7420.

64. Coyner, E. C.; Hillman, W. S., The thermal dimerization of acrylonitrile. *J. Am. Chem. Soc.* **1949,** *71*, 324-6.

65. Sennewald, K.; Gotz, A.; Kallrath, G. 1,2-Dicyanocyclobutane. US3099680, 1960.

66. Idol, J. D., Jr.; Greene, J. L.; Gray, N. R. 1,2-Dicyanocyclobutanes. US3275675, 1966.

67. Idol, J. D., Jr.; Greene, J. L.; Gray, N. R. Preparation of cyclobutane-1,2-dicyanide from acrylonitrile. US3202697, 1965.

68. Lehn, W. L.; Nacci, G. R. Acrylonitrile dimerization. US3265723, 1966.

69. Runge, J.; Kache, R., Photocyclodimerization of acrylonitrile. *Z. Chem.* **1968,** *8* (10), 382b-3.

70. Runge, J.; Kache, R. Cyclobutane-1,2-dinitrile. GB1095849, 1967.

71. Hosaka, S.; Wakamatsu, S., Photodimerization of acrylonitrile. *Tetrahedron Lett.* **1968,** (2), 219-20.

72. Sato, T.; Hasui, H. 1,2-Dicyanocyclobutane. JP43022979B, 1968.

73. Hughes, W. B. Photodimerization of acrylonitrile to 1,2-dicyanocyclobutane. US3623966A, 1971.

74. Seko, M., Electrohydrodimerization of acrylonitrile. *Nikkakyo Geppo* **1975,** *28* (6), 309-15.

75. Beresis, R. T.; Panek, J. S. In *1,2-Dicyanocyclobutene*, John Wiley & Sons, Ltd.: 2001; pp 1-2.

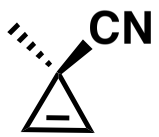
76. Miyashita, A.; Ikezu, S.; Nohira, H., Stereospecific Photodimerization of Unsaturated Compounds Induced by Nickel Complexes. *Chem. Lett.* **1985,** *14* (8), 1235-1238.

77. Hosaka, S.; Wakamatsu, S., Photodimerization of Acrylonitrile. *Tetrahedron Lett.* **1968,** *9* (2), 219-220.

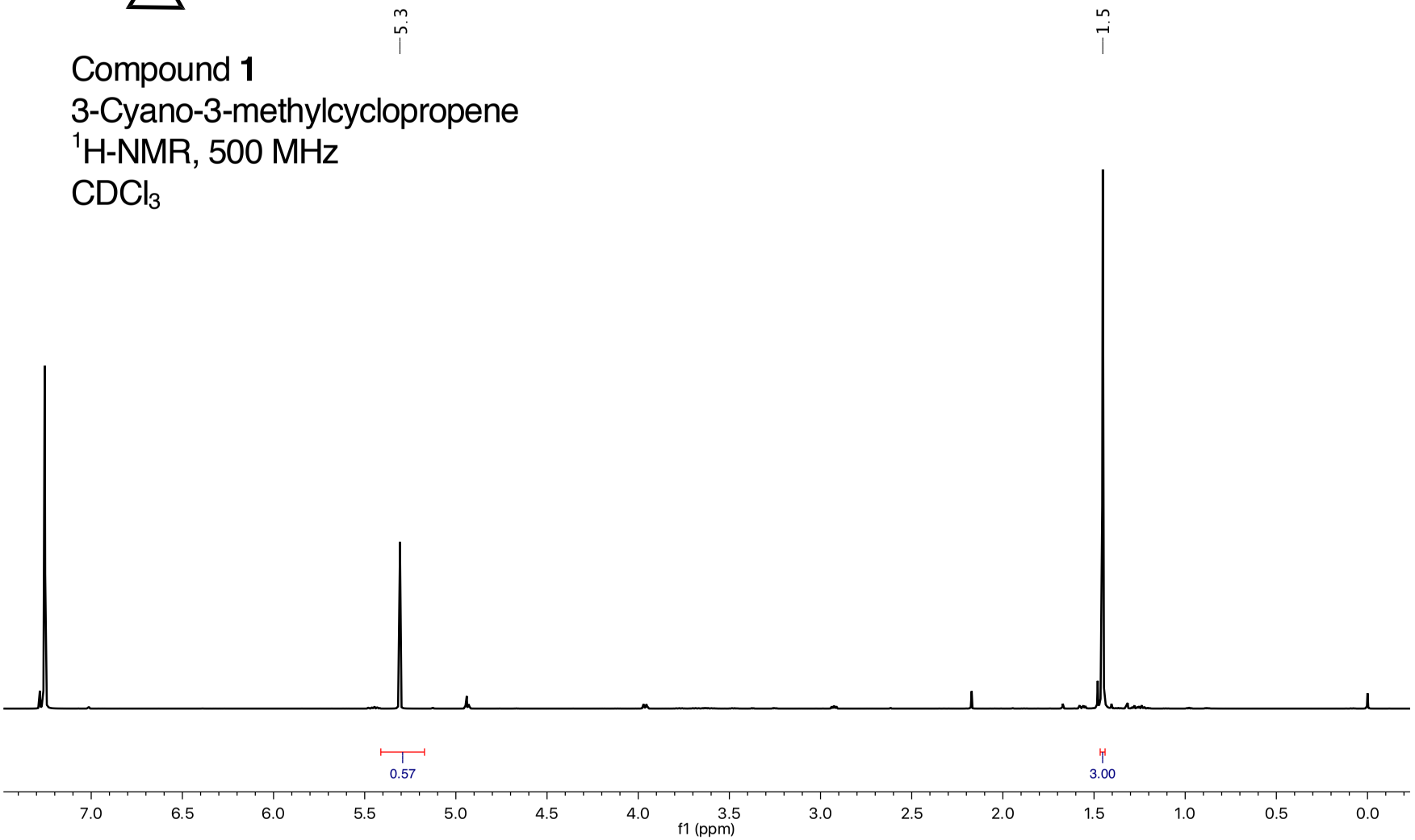
78. Schreyer, R. C. *trans*-1,2-Bis(aminomethyl)cyclobutane and its copolymerization with dicarboxylic acids. US3192262, 1965.

79. McEwen, C. N.; McKay, R. G.; Larsen, B. S., Analysis of solids, liquids, and biological tissues using solids probe introduction at atmospheric pressure on commercial LC/MS instruments. *Anal. Chem.* **2005,** *77*, 7826-7831.

Supporting Information for Chapter 2:
Synthesis and Characterization of C_5H_5N Carbocycle-Containing Carbonitriles

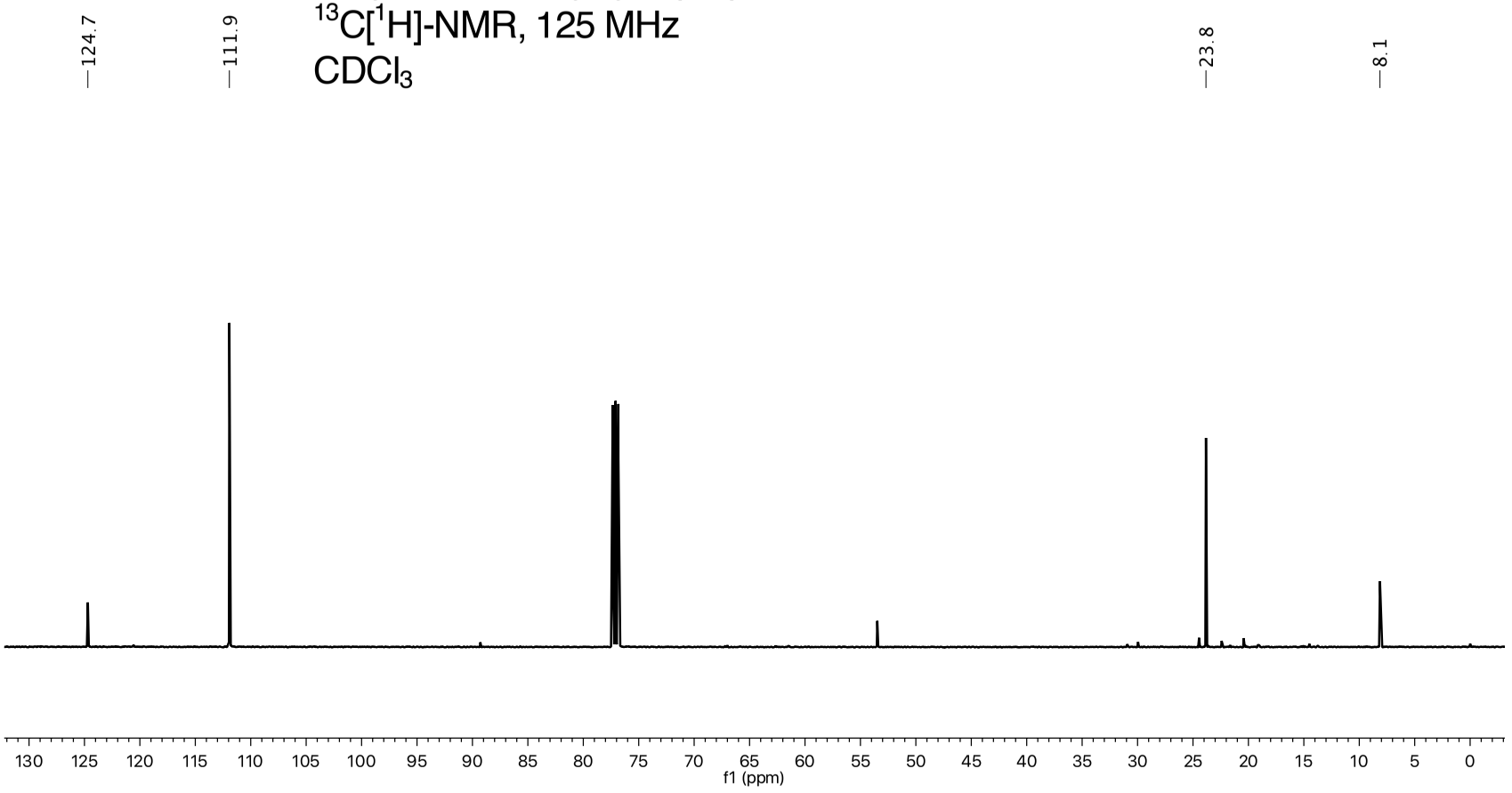


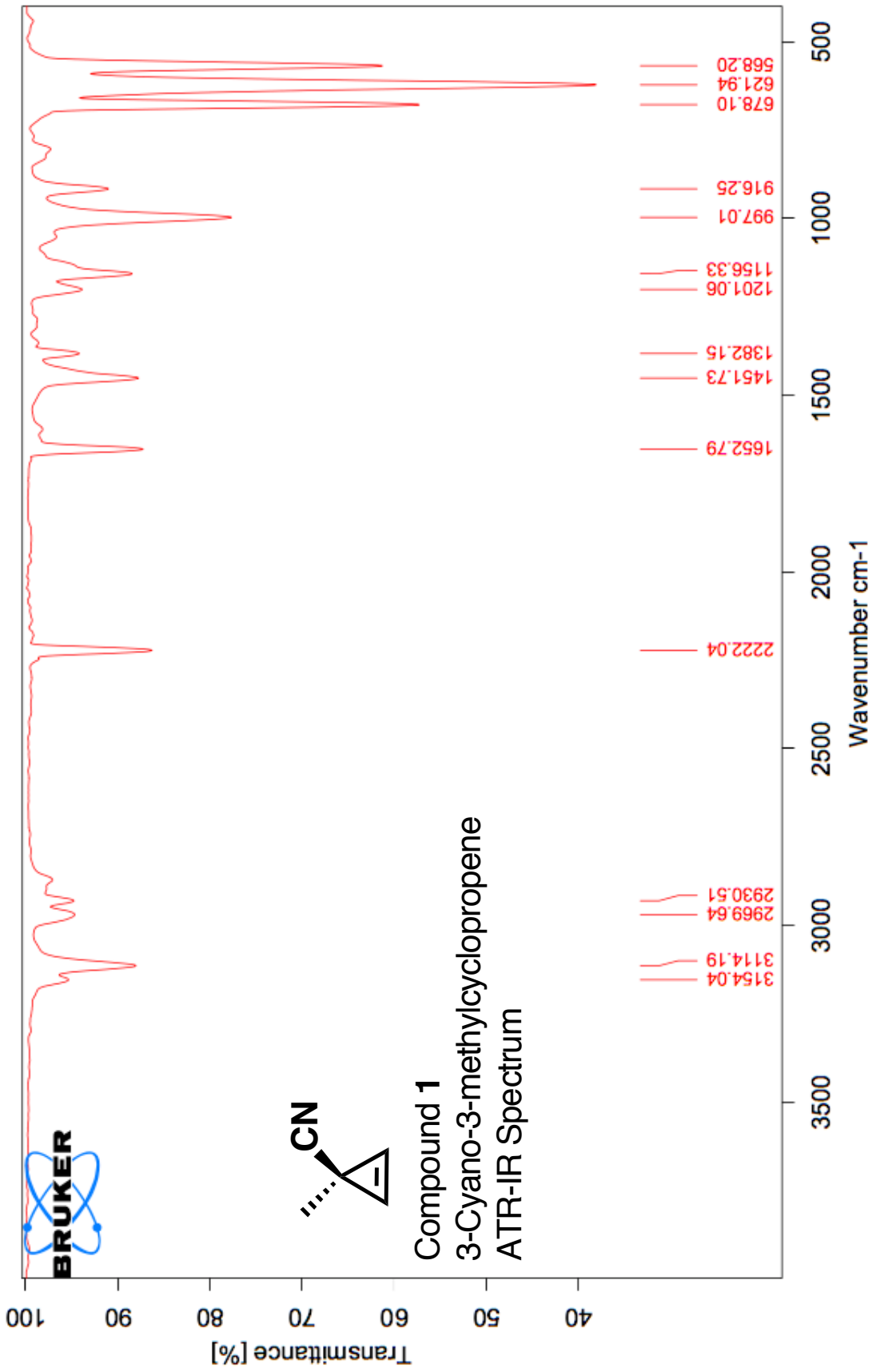
Compound **1**
3-Cyano-3-methylcyclopropene
^{1}H-NMR, 500 MHz
$CDCl_3$

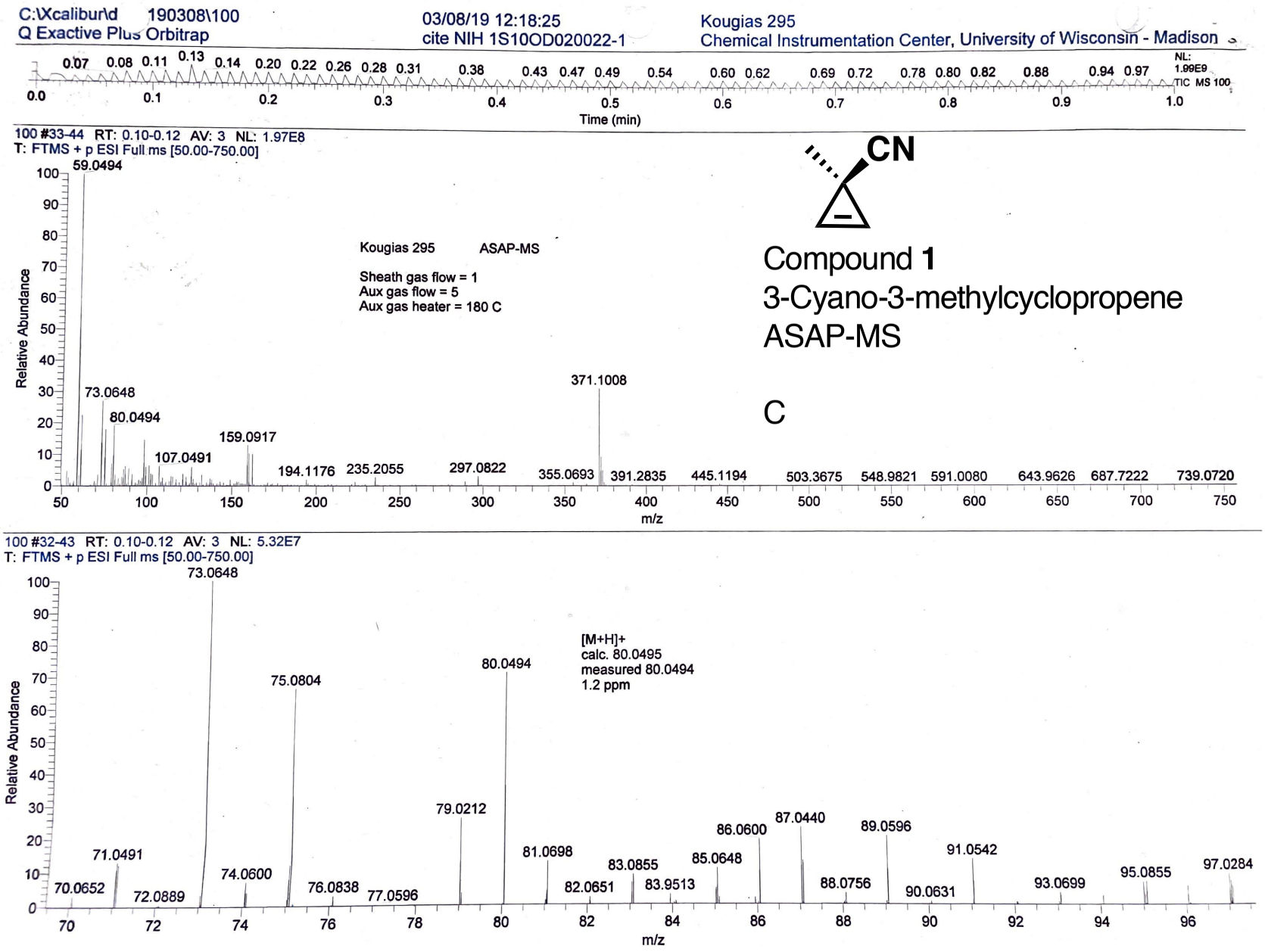


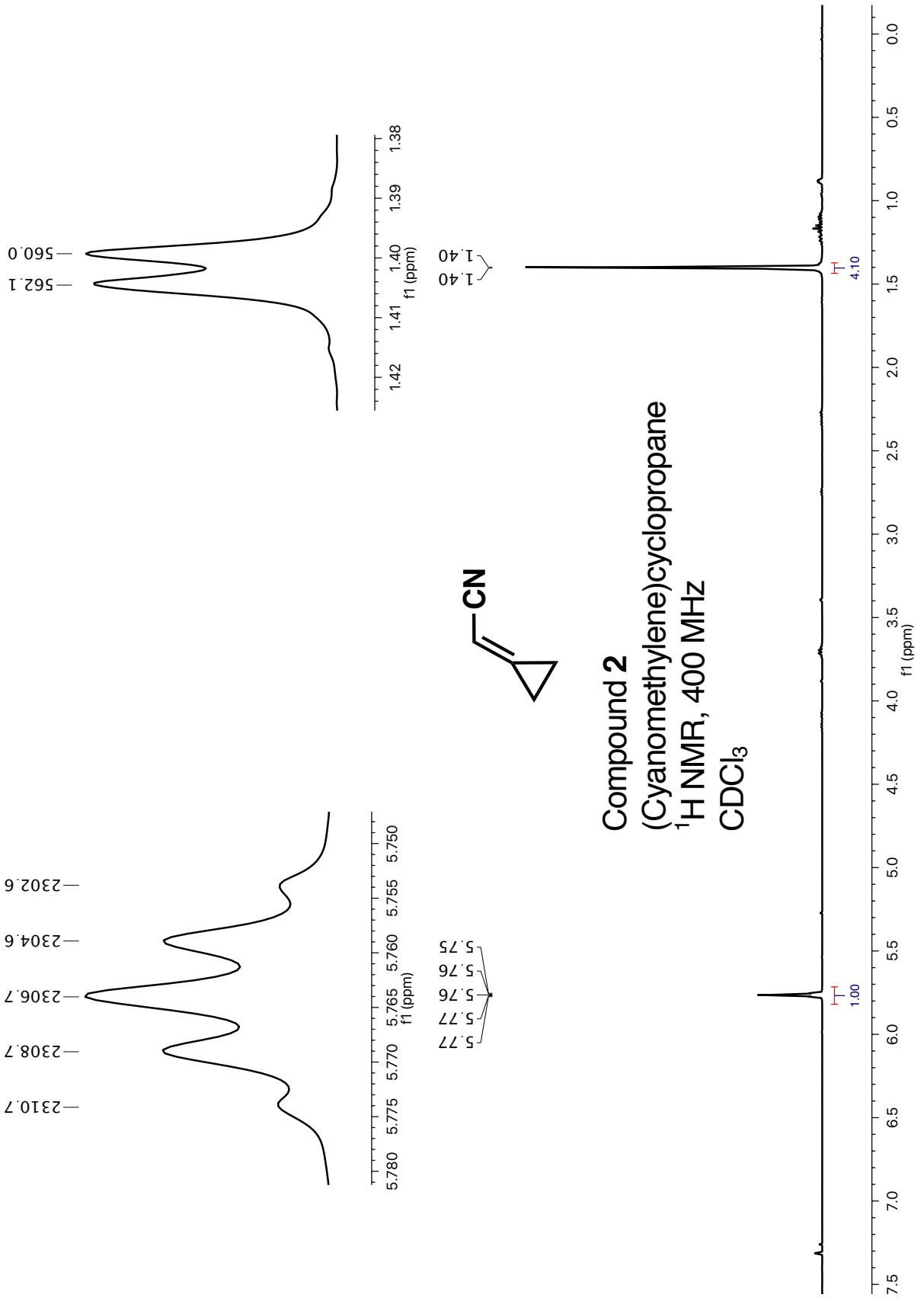


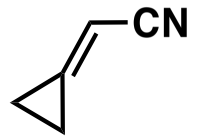
Compound **1**
3-Cyano-3-methylcyclopropene
$^{13}C[^{1}H]$-NMR, 125 MHz
$CDCl_3$



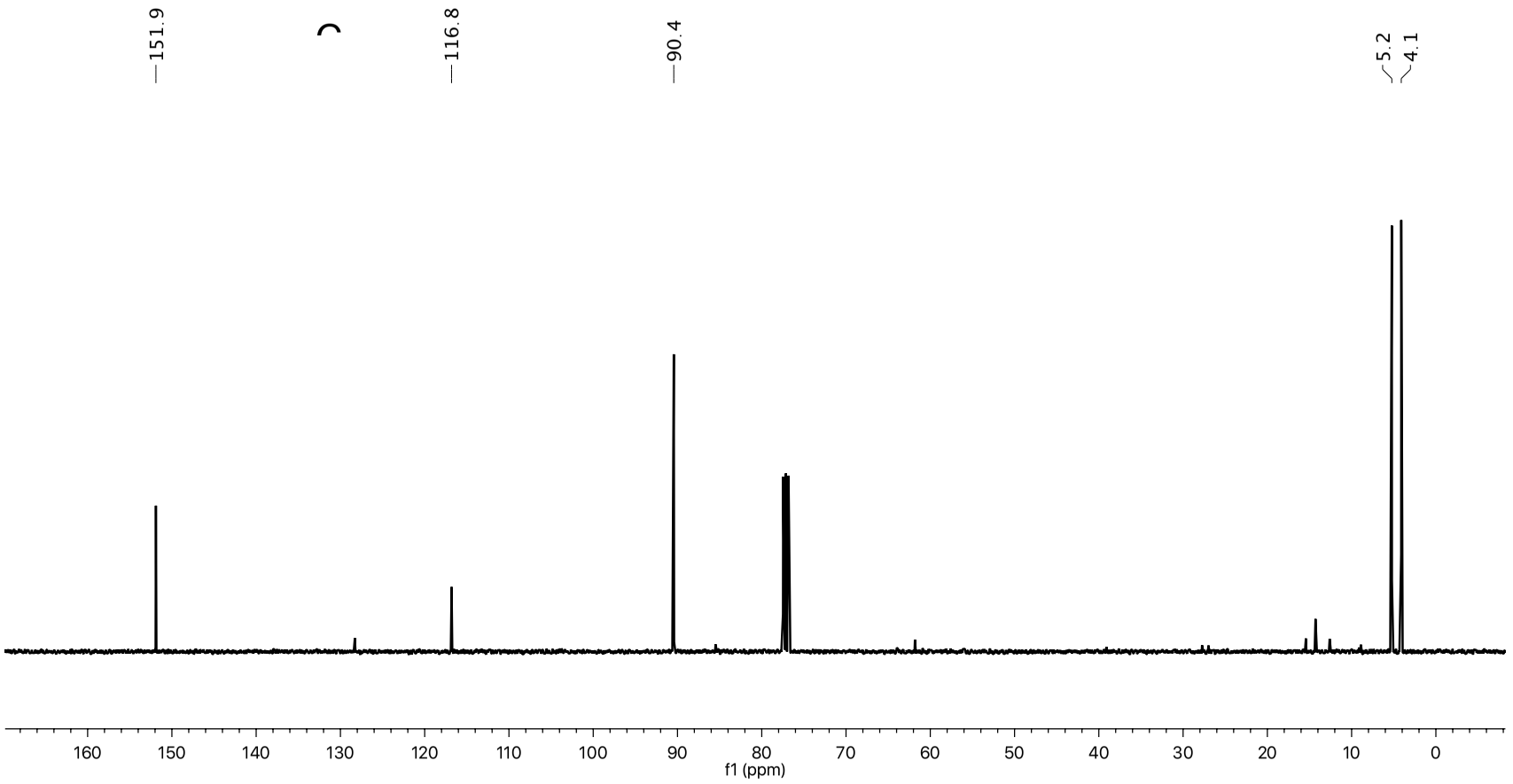

BRUKER
CN
Compound 1
3-Cyano-3-methylcyclopropene
ATR-IR Spectrum
Transmittance [%]
100
90
80
70
60
50
40
3500
3000
2500
2000
1500
1000
500
Wavenumber cm-1
3154.04
3114.19
2969.64
2930.51
2222.04
1652.79
1451.73
1382.15
1201.06
1156.33
997.01
916.25
678.10
621.94
568.20

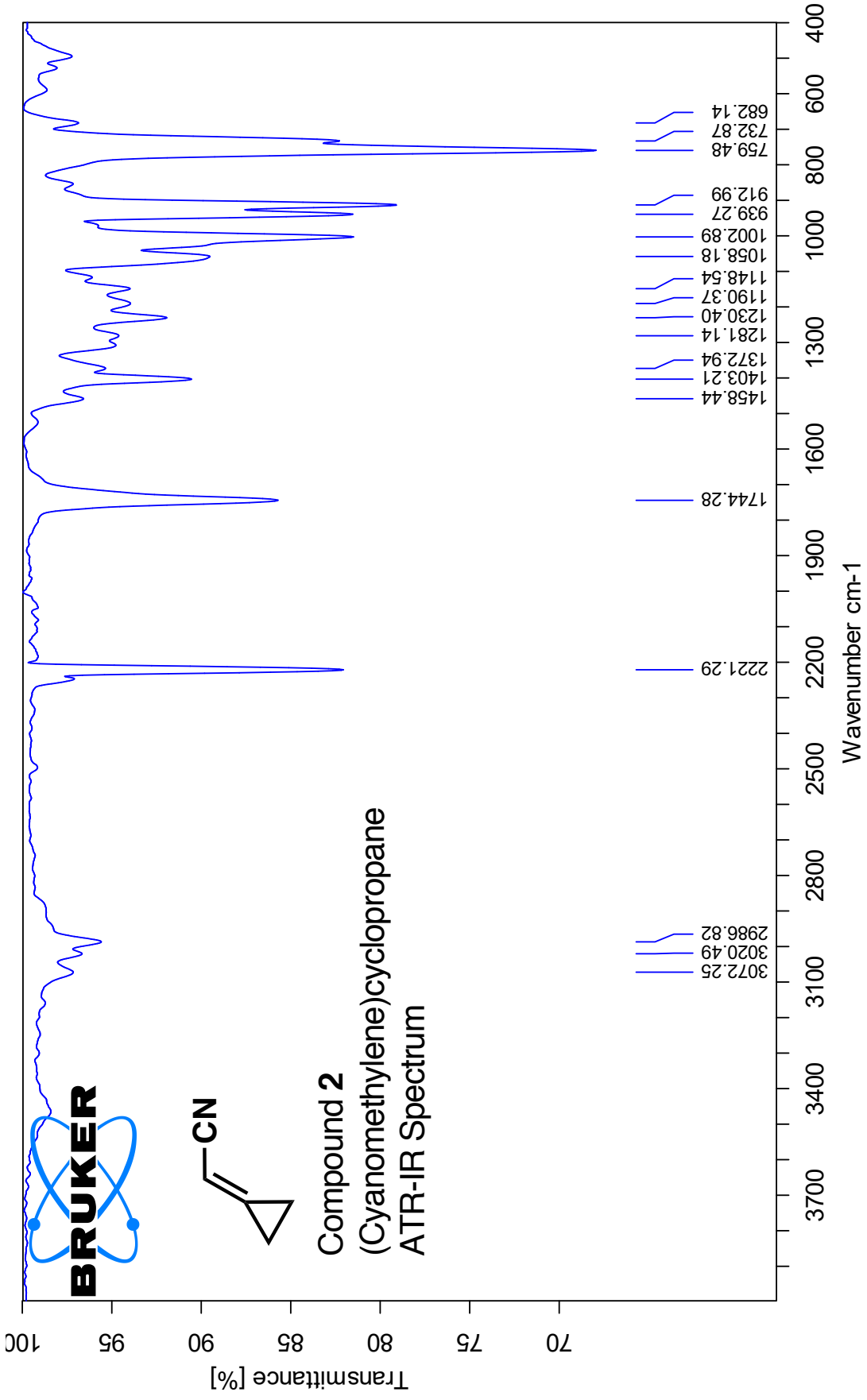

C:\Xcalibur\d 190308\100
Q Exactive Plus Orbitrap
03/08/19 12:18:25
cite NIH 1S10OD020022-1
Kougias 295
Chemical Instrumentation Center, University of Wisconsin - Madison
NL: 1.99E9 TIC MS 100
Time (min)
100 #33-44 RT: 0.10-0.12 AV: 3 NL: 1.97E8
T: FTMS + p ESI Full ms [50.00-750.00]
Kougias 295 ASAP-MS
Sheath gas flow = 1
Aux gas flow = 5
Aux gas heater = 180 C
Relative Abundance
m/z
CN
Compound 1
3-Cyano-3-methylcyclopropene
ASAP-MS
C
100 #32-43 RT: 0.10-0.12 AV: 3 NL: 5.32E7
T: FTMS + p ESI Full ms [50.00-750.00]
[M+H]+
calc. 80.0495
measured 80.0494
1.2 ppm
Relative Abundance
m/z

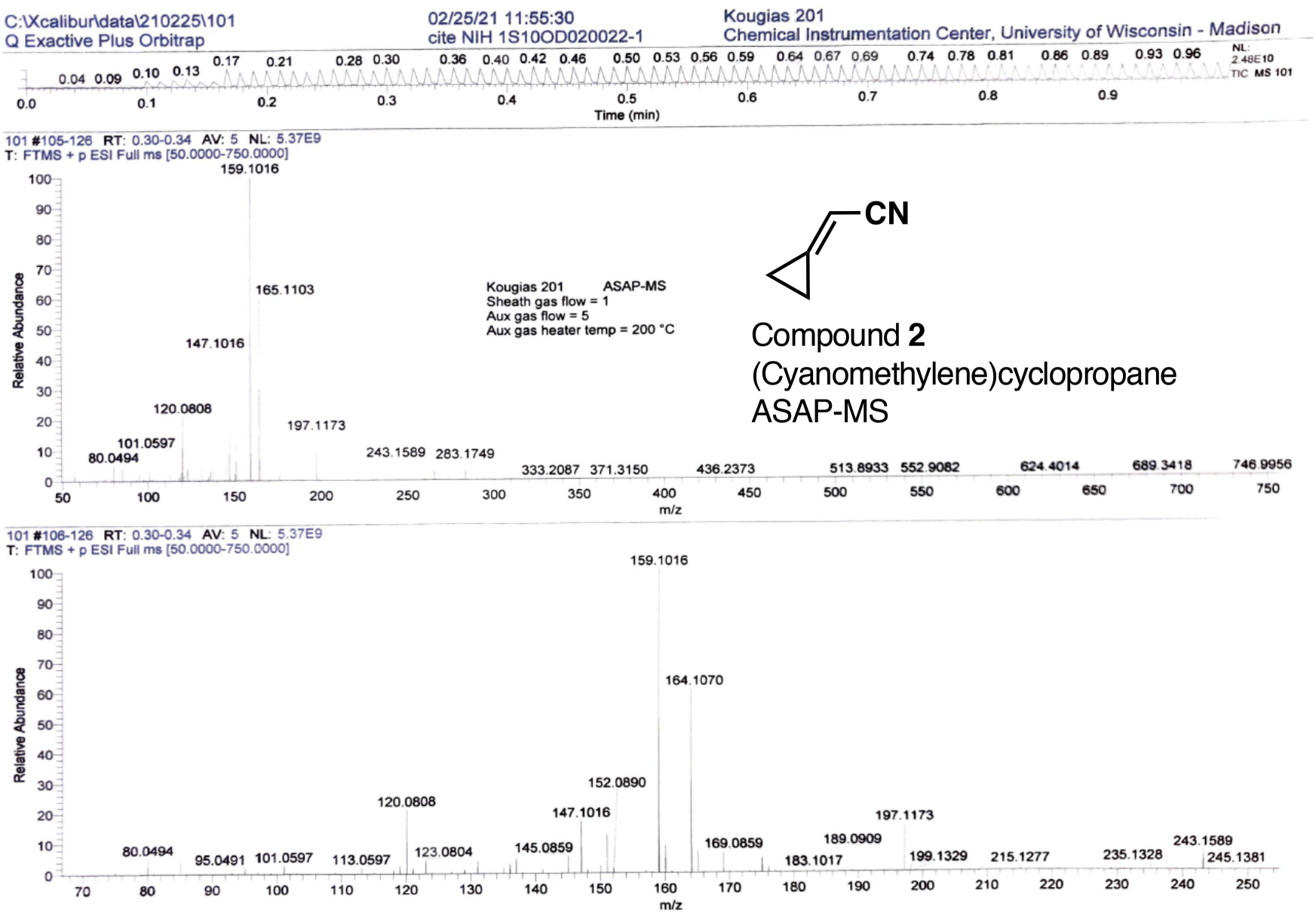

Compound 2
(Cyanomethylene)cyclopropane
^{1}H NMR, 400 MHz
$CDCl_3$
CN
1.00
4.10
f1 (ppm)
1.40
1.40
f1 (ppm)
5.77
5.76
5.76
5.75
5.77
f1 (ppm)
562.1
560.0
2310.7
2308.7
2306.7
2304.6
2302.6

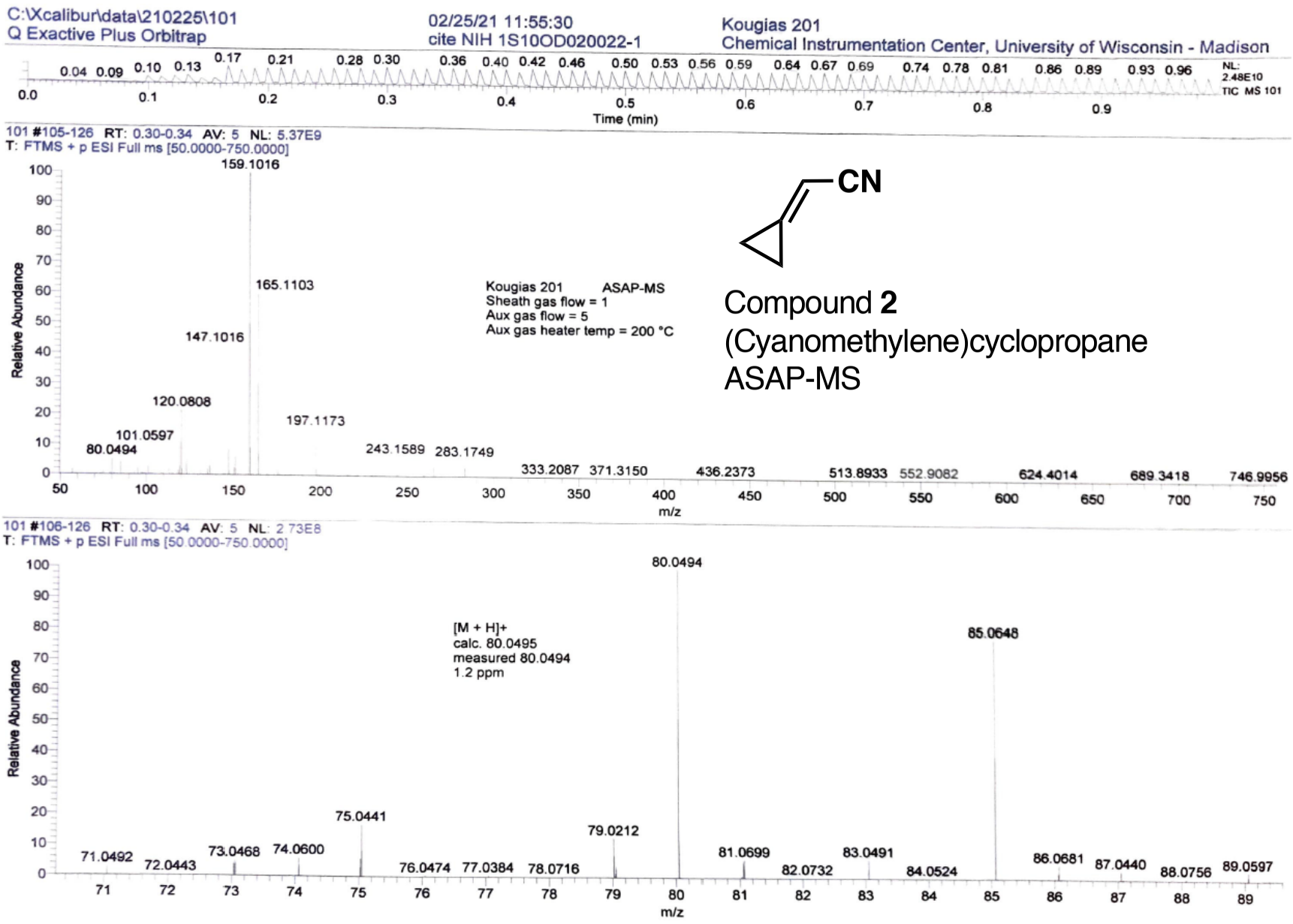


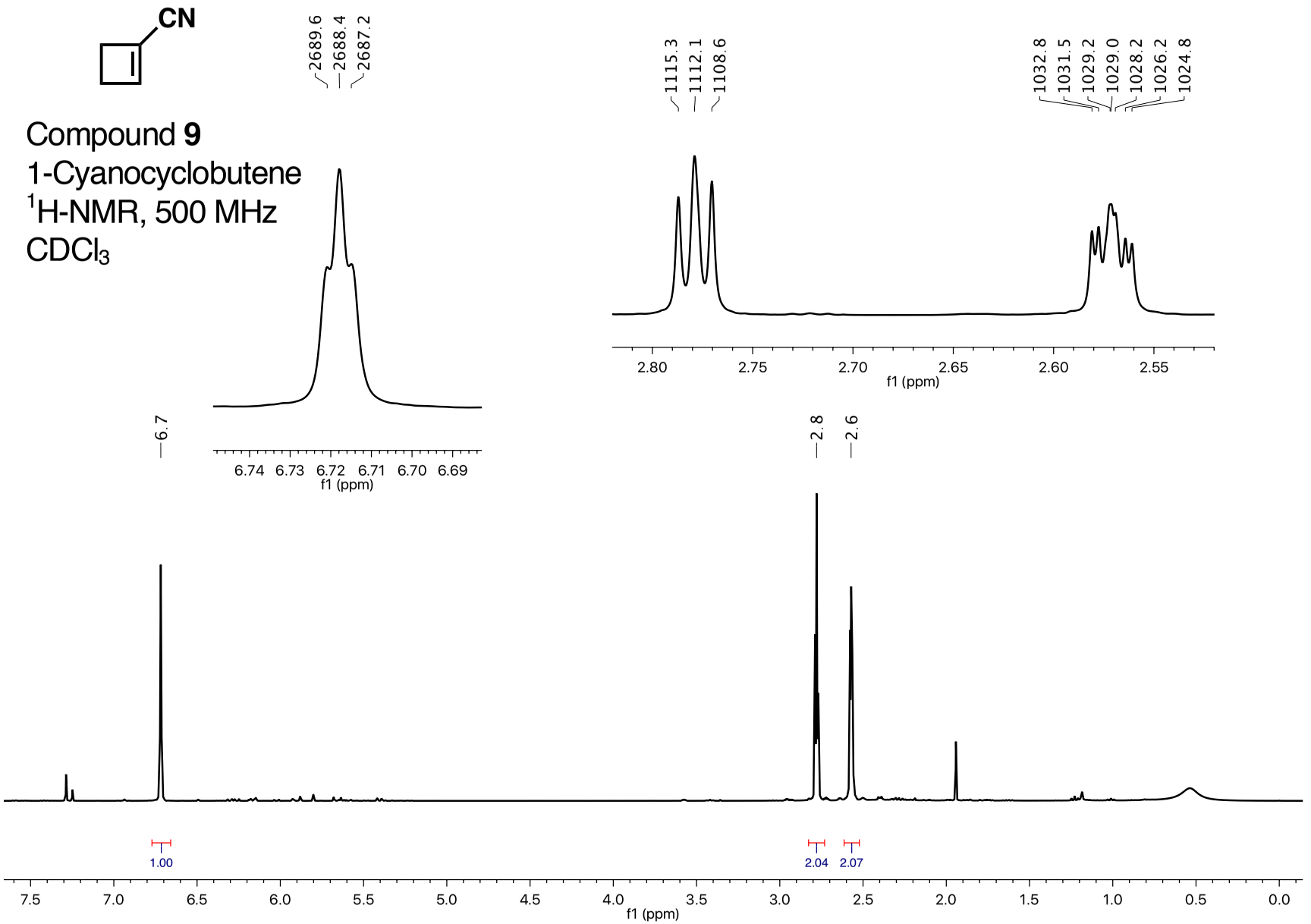
Compound **2**
(Cyanomethylene)cyclopropane
$^{13}C\{^{1}H\}$-NMR, 100 MHz
$CDCl_3$

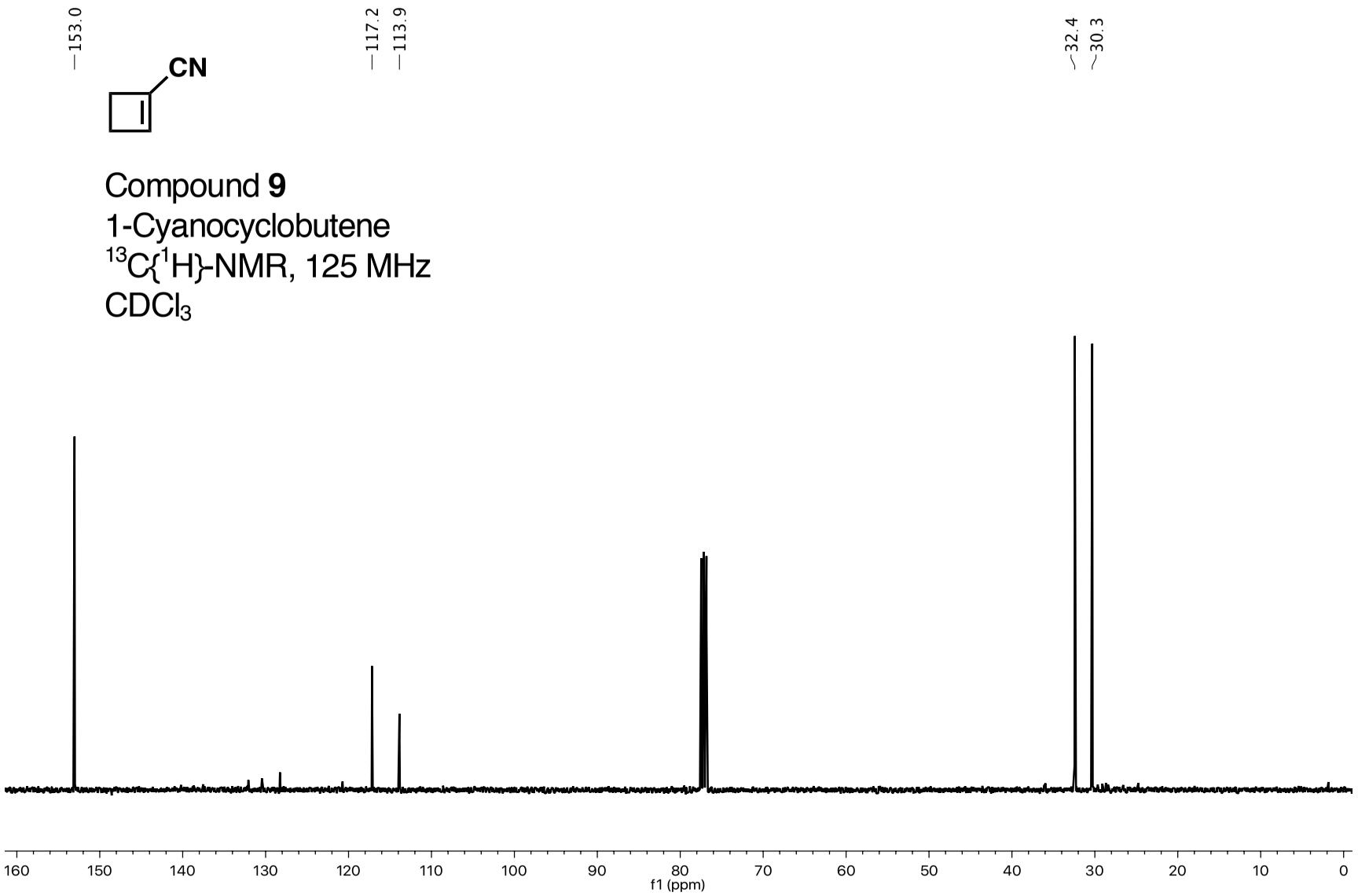


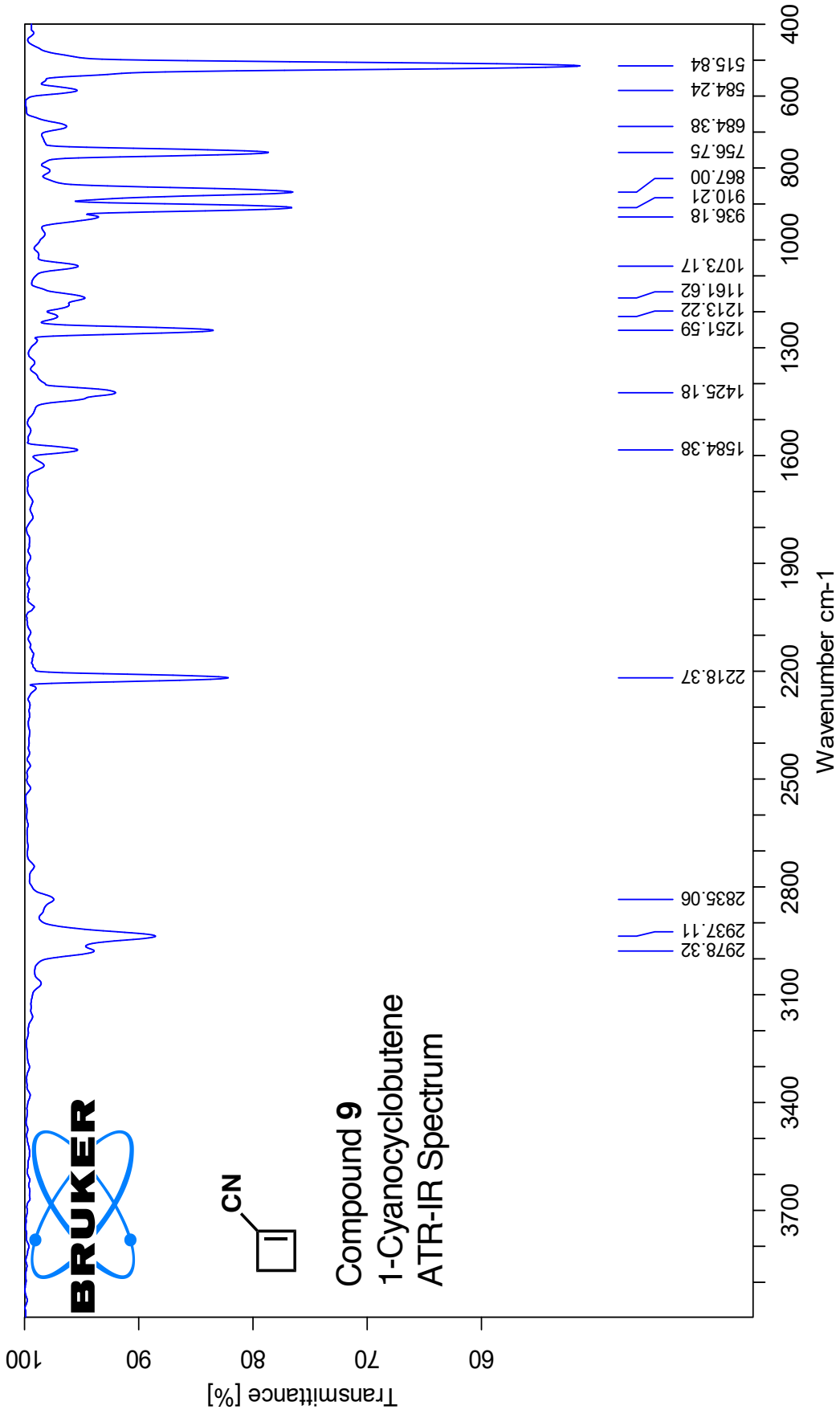

BRUKER
CN
Compound 2
(Cyanomethylene)cyclopropane
ATR-IR Spectrum
Transmittance [%]
100
95
90
85
80
75
70
Wavenumber cm-1
3700
3400
3100
2800
2500
2200
1900
1600
1300
1000
800
600
400
3072.25
3020.49
2986.82
2221.29
1744.28
1458.44
1403.21
1372.94
1281.14
1230.40
1190.37
1148.54
1058.18
1002.89
939.27
912.99
759.48
732.87
682.14

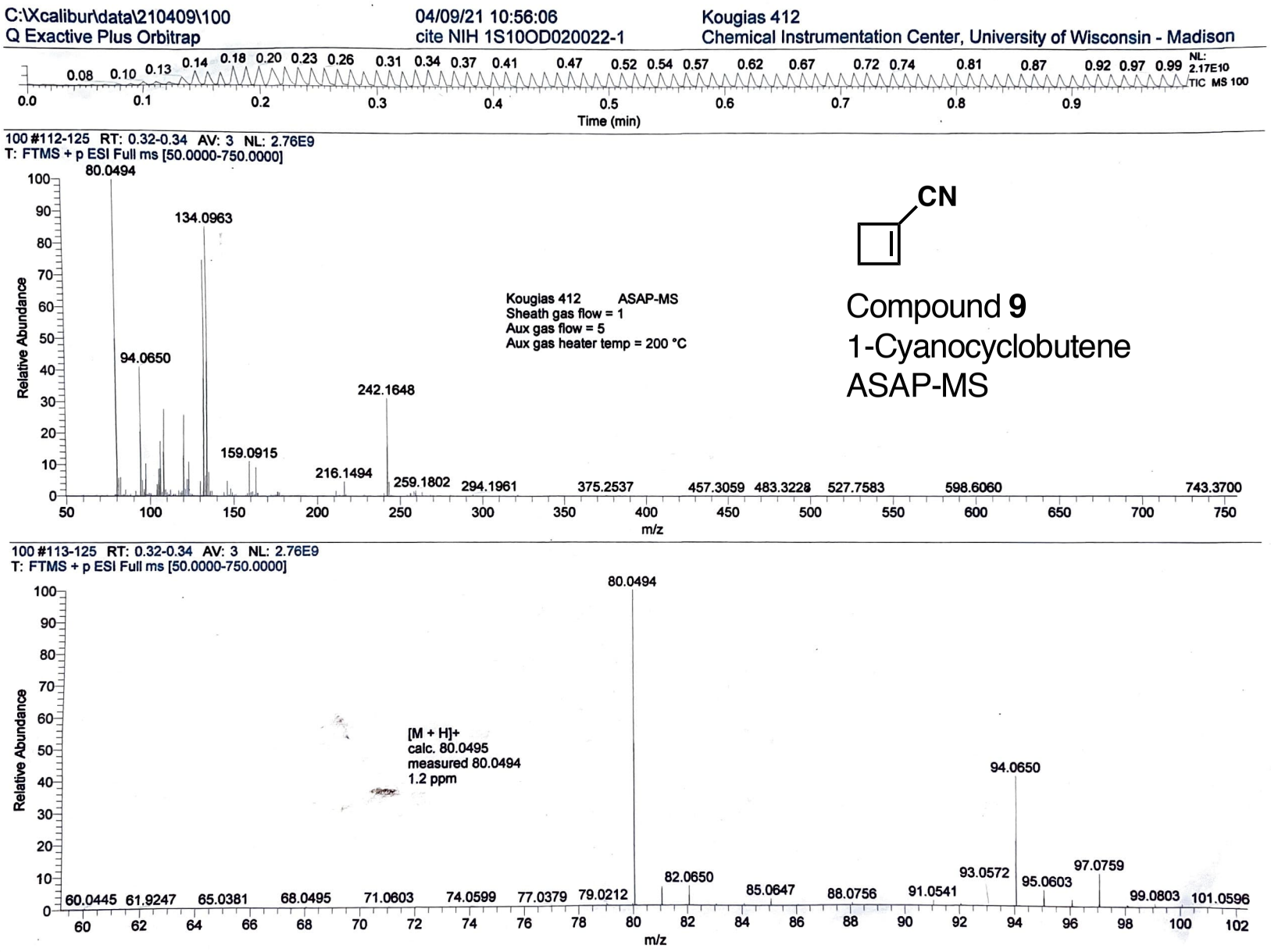

C:\Xcalibur\data\210225\101
Q Exactive Plus Orbitrap
02/25/21 11:55:30
cite NIH 1S10OD020022-1
Kougias 201
Chemical Instrumentation Center, University of Wisconsin - Madison
NL: 2.48E10 TIC MS 101
Time (min)
101 #105-126 RT: 0.30-0.34 AV: 5 NL: 5.37E9
T: FTMS + p ESI Full ms [50.0000-750.0000]
Relative Abundance
m/z
Kougias 201 ASAP-MS
Sheath gas flow = 1
Aux gas flow = 5
Aux gas heater temp = 200 °C
CN
Compound 2
(Cyanomethylene)cyclopropane
ASAP-MS
101 #106-126 RT: 0.30-0.34 AV: 5 NL: 5.37E9
T: FTMS + p ESI Full ms [50.0000-750.0000]
Relative Abundance
m/z

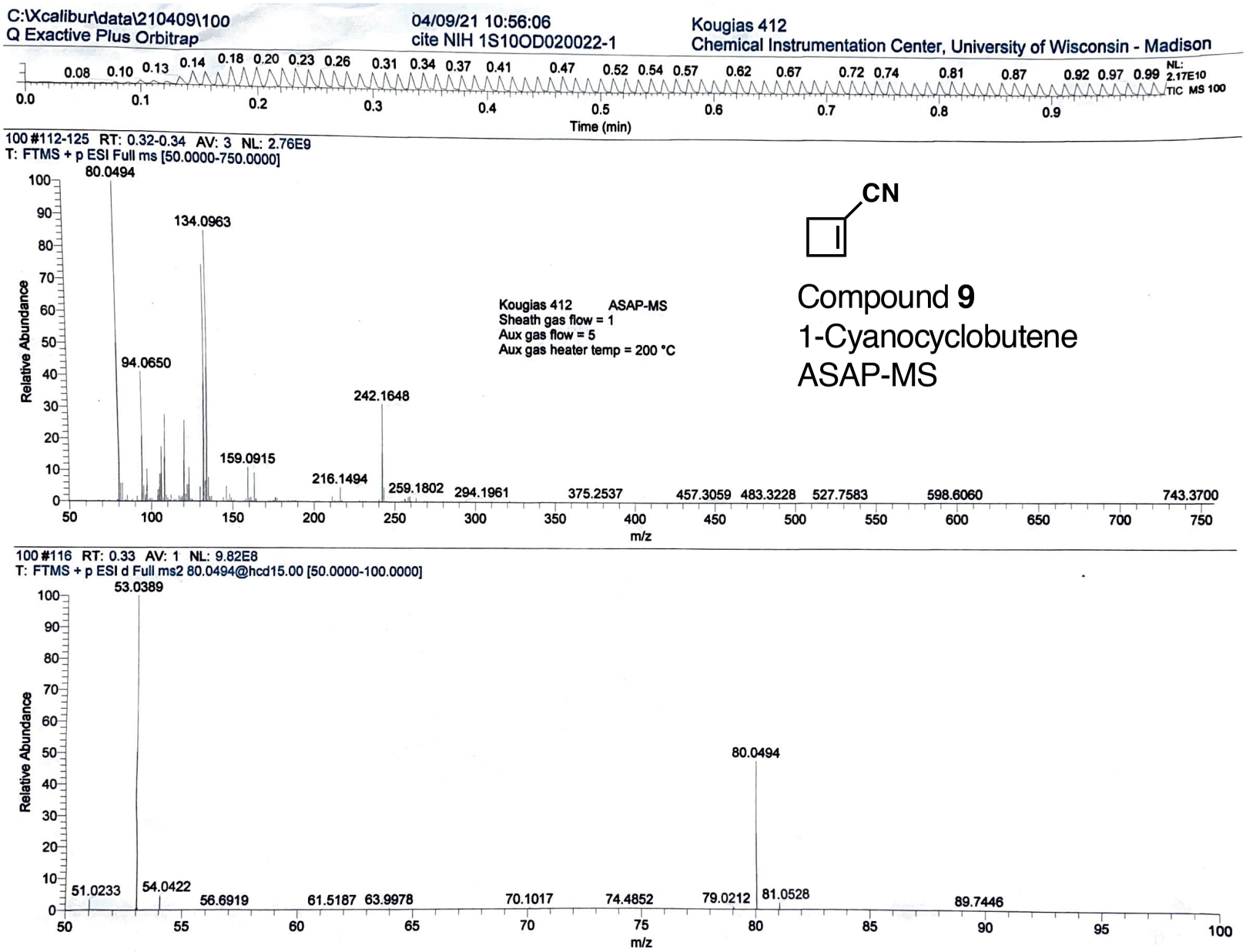

C:\Xcalibur\data\210225\101
Q Exactive Plus Orbitrap
02/25/21 11:55:30
cite NIH 1S10OD020022-1
Kougias 201
Chemical Instrumentation Center, University of Wisconsin - Madison
Time (min)
NL: 2.48E10 TIC MS 101
101 #105-126 RT: 0.30-0.34 AV: 5 NL: 5.37E9
T: FTMS + p ESI Full ms [50.0000-750.0000]
Relative Abundance
m/z
159.1016
165.1103
147.1016
120.0808
197.1173
101.0597
80.0494
243.1589
283.1749
333.2087
371.3150
436.2373
513.8933
552.9082
624.4014
689.3418
746.9956
Kougias 201 ASAP-MS
Sheath gas flow = 1
Aux gas flow = 5
Aux gas heater temp = 200 °C
CN
Compound 2
(Cyanomethylene)cyclopropane
ASAP-MS
101 #106-126 RT: 0.30-0.34 AV: 5 NL: 2.73E8
T: FTMS + p ESI Full ms [50.0000-750.0000]
[M + H]+
calc. 80.0495
measured 80.0494
1.2 ppm
80.0494
85.0648
75.0441
79.0212
71.0492
72.0443
73.0468
74.0600
76.0474
77.0384
78.0716
81.0699
82.0732
83.0491
84.0524
86.0681
87.0440
88.0756
89.0597

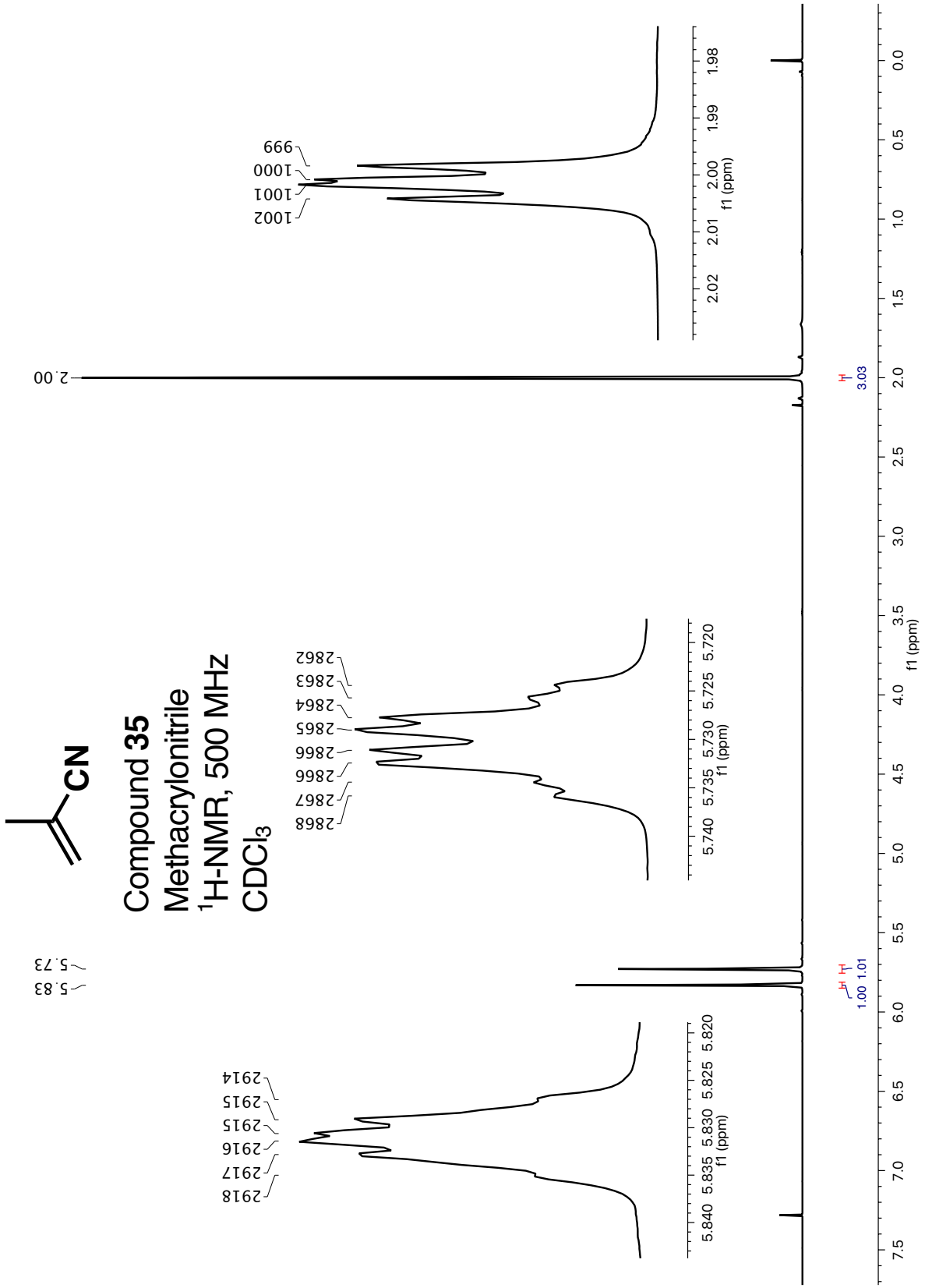

CN
Compound 9
1-Cyanocyclobutene
1H-NMR, 500 MHz
CDCl3
2689.6
2688.4
2687.2
1115.3
1112.1
1108.6
1032.8
1031.5
1029.2
1029.0
1028.2
1026.2
1024.8
6.7
2.8
2.6
6.74 6.73 6.72 6.71 6.70 6.69
f1 (ppm)
2.80 2.75 2.70 2.65 2.60 2.55
f1 (ppm)
1.00
2.04
2.07
7.5 7.0 6.5 6.0 5.5 5.0 4.5 4.0 3.5 3.0 2.5 2.0 1.5 1.0 0.5 0.0
f1 (ppm)

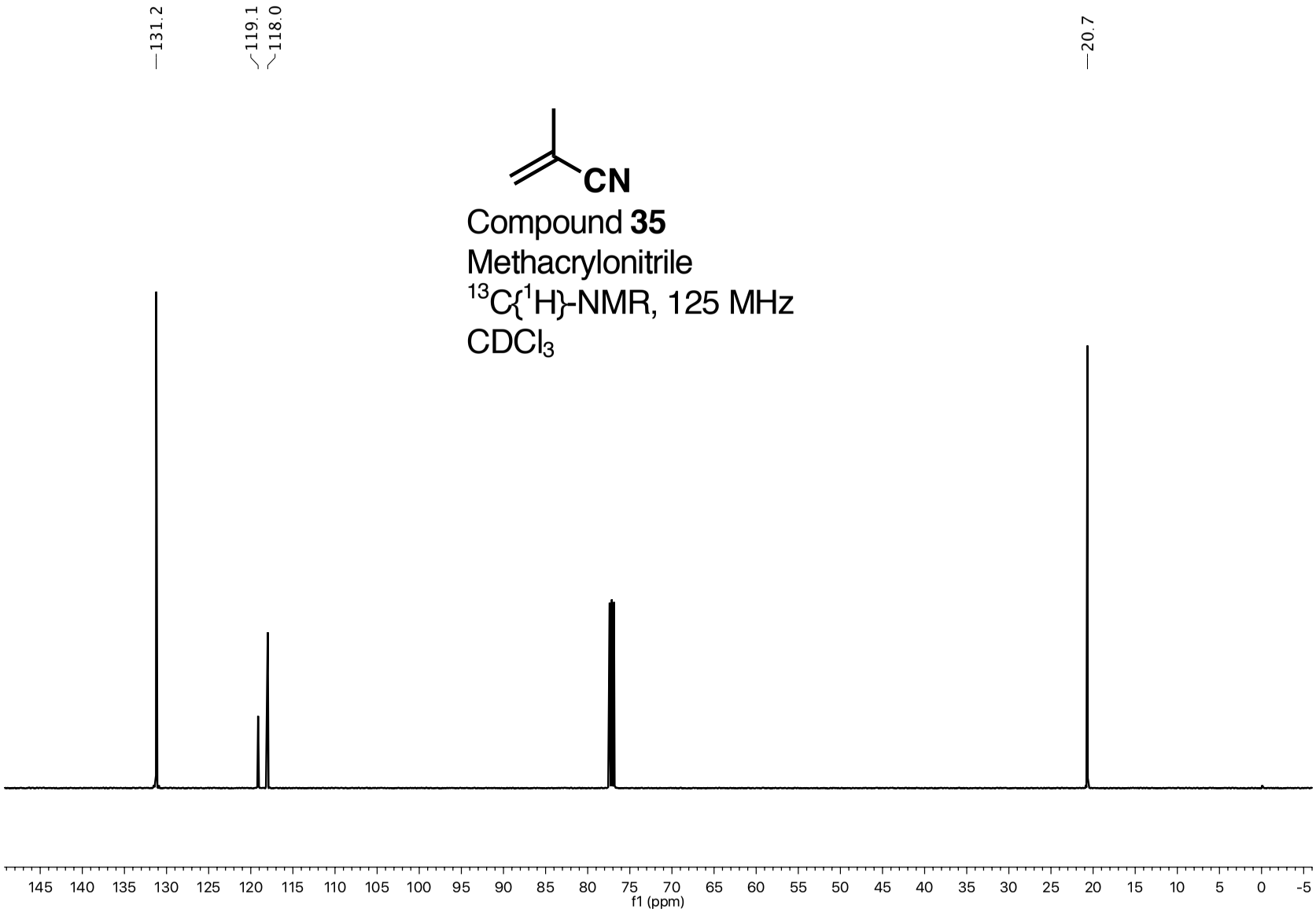

153.0
117.2
113.9
32.4
30.3
CN
Compound 9
1-Cyanocyclobutene
13C{1H}-NMR, 125 MHz
CDCl3
160
150
140
130
120
110
100
90
80
70
60
50
40
30
20
10
0
f1 (ppm)

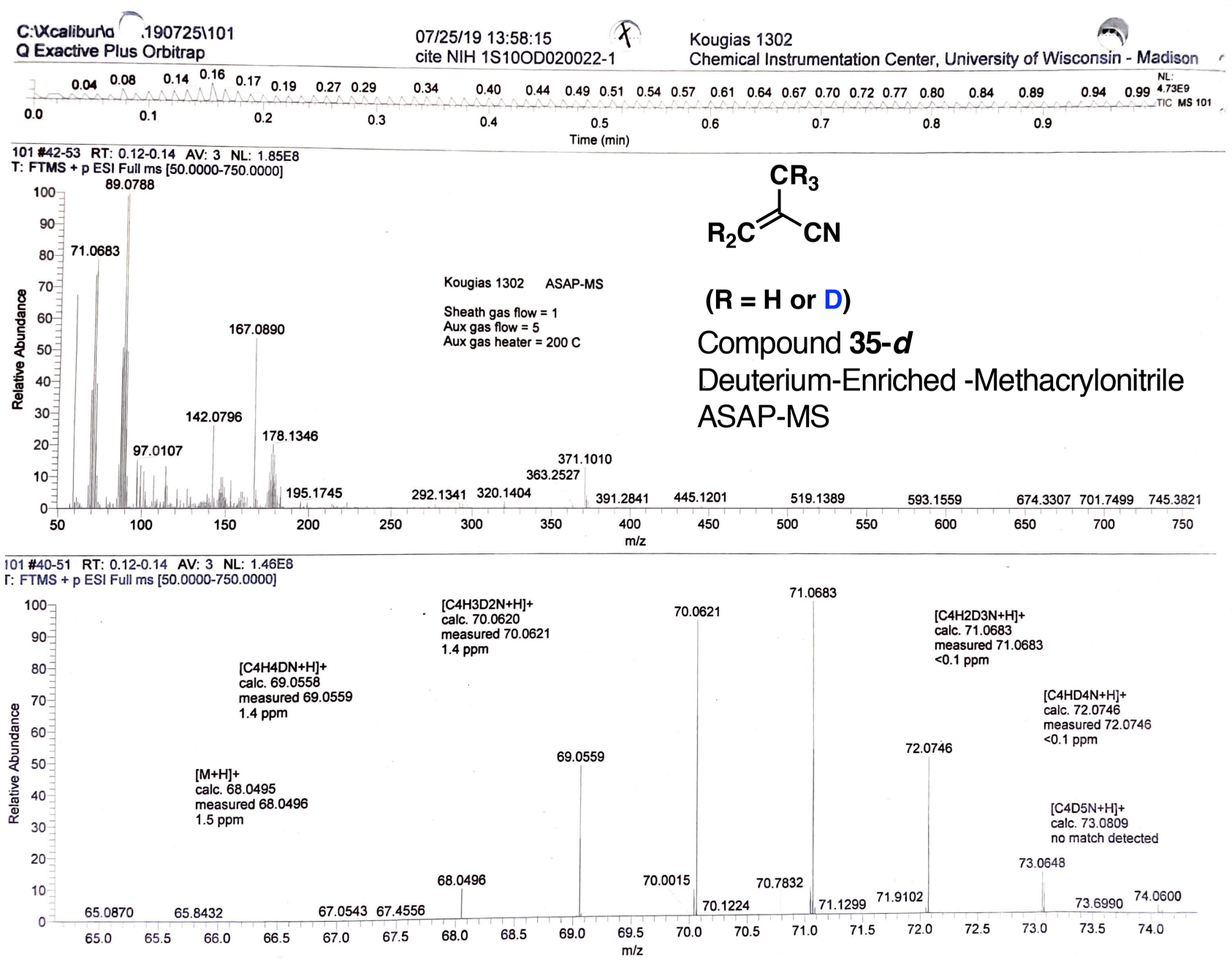

Transmittance [%]
100
90
80
70
60
Wavenumber cm-1
3700
3400
3100
2800
2500
2200
1900
1600
1300
1000
800
600
400
2978.32
2937.11
2835.06
2218.37
1584.38
1425.18
1251.59
1213.22
1161.62
1073.17
936.18
910.21
867.00
756.75
684.38
584.24
515.84
Compound 9
1-Cyanocyclobutene
ATR-IR Spectrum
CN
BRUKER

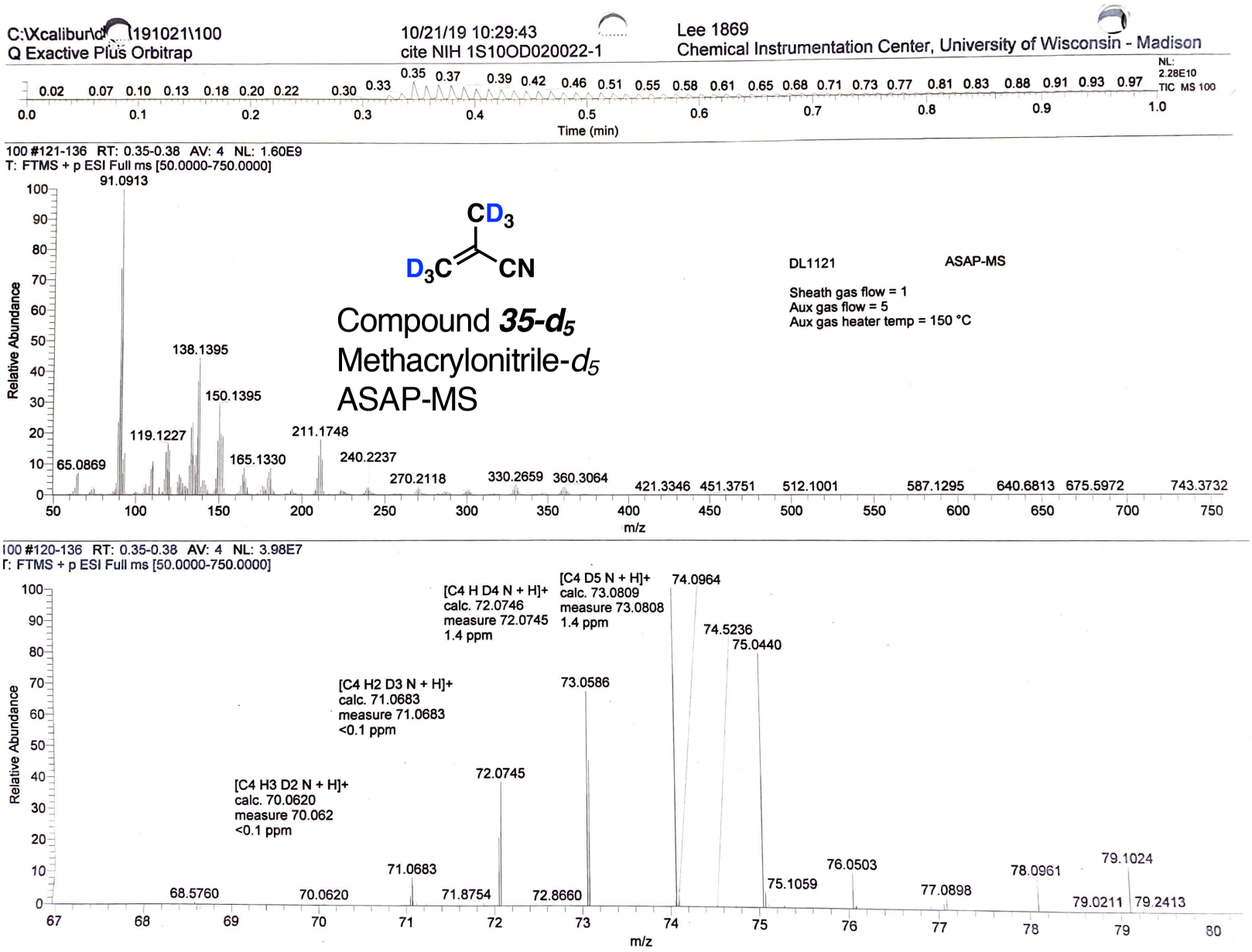

C:\Xcalibur\data\210409\100
Q Exactive Plus Orbitrap
04/09/21 10:56:06
cite NIH 1S10OD020022-1
Kougias 412
Chemical Instrumentation Center, University of Wisconsin - Madison
Time (min)
NL: 2.17E10 TIC MS 100
100 #112-125 RT: 0.32-0.34 AV: 3 NL: 2.76E9
T: FTMS + p ESI Full ms [50.0000-750.0000]
Relative Abundance
m/z
80.0494
134.0963
94.0650
242.1648
159.0915
216.1494
259.1802
294.1961
375.2537
457.3059
483.3228
527.7583
598.6060
743.3700
Kougias 412 ASAP-MS
Sheath gas flow = 1
Aux gas flow = 5
Aux gas heater temp = 200 °C
CN
Compound 9
1-Cyanocyclobutene
ASAP-MS
100 #113-125 RT: 0.32-0.34 AV: 3 NL: 2.76E9
T: FTMS + p ESI Full ms [50.0000-750.0000]
[M + H]+
calc. 80.0495
measured 80.0494
1.2 ppm
80.0494
94.0650
82.0650
93.0572
97.0759
95.0603
99.0803
101.0596
85.0647
88.0756
91.0541
60.0445
61.9247
65.0381
68.0495
71.0603
74.0599
77.0379
79.0212


C:\Xcalibur\data\210409\100
Q Exactive Plus Orbitrap
04/09/21 10:56:06
cite NIH 1S10OD020022-1
Kougias 412
Chemical Instrumentation Center, University of Wisconsin - Madison
Time (min)
NL: 2.17E10 TIC MS 100
100 #112-125 RT: 0.32-0.34 AV: 3 NL: 2.76E9
T: FTMS + p ESI Full ms [50.0000-750.0000]
80.0494
134.0963
94.0650
242.1648
159.0915
216.1494
259.1802
294.1961
375.2537
457.3059
483.3228
527.7583
598.6060
743.3700
Relative Abundance
m/z
Kougias 412 ASAP-MS
Sheath gas flow = 1
Aux gas flow = 5
Aux gas heater temp = 200 °C
CN
Compound 9
1-Cyanocyclobutene
ASAP-MS
100 #116 RT: 0.33 AV: 1 NL: 9.82E8
T: FTMS + p ESI d Full ms2 80.0494@hcd15.00 [50.0000-100.0000]
53.0389
80.0494
51.0233
54.0422
56.6919
61.5187
63.9978
70.1017
74.4852
79.0212
81.0528
89.7446
Relative Abundance
m/z


CN
Compound 35
Methacrylonitrile
1H-NMR, 500 MHz
CDCl3
5.83
5.73
2.00
3.03
1.00 1.01
f1 (ppm)


131.2
119.1
118.0
20.7
CN
Compound 35
Methacrylonitrile
13C{1H}-NMR, 125 MHz
CDCl3
145 140 135 130 125 120 115 110 105 100 95 90 85 80 75 70 65 60 55 50 45 40 35 30 25 20 15 10 5 0 -5
f1 (ppm)


C:\Xcalibur\d .190725\101
Q Exactive Plus Orbitrap
07/25/19 13:58:15
cite NIH 1S10OD020022-1
Kougias 1302
Chemical Instrumentation Center, University of Wisconsin - Madison
NL: 4.73E9 TIC MS 101
Time (min)
101 #42-53 RT: 0.12-0.14 AV: 3 NL: 1.85E8
T: FTMS + p ESI Full ms [50.0000-750.0000]
Relative Abundance
m/z
Kougias 1302 ASAP-MS
Sheath gas flow = 1
Aux gas flow = 5
Aux gas heater = 200 C
89.0788
71.0683
167.0890
142.0796
178.1346
97.0107
371.1010
363.2527
195.1745
292.1341
320.1404
391.2841
445.1201
519.1389
593.1559
674.3307
701.7499
745.3821
CR_3
R_2C
CN
(R = H or D)
Compound 35-d
Deuterium-Enriched -Methacrylonitrile
ASAP-MS
101 #40-51 RT: 0.12-0.14 AV: 3 NL: 1.46E8
T: FTMS + p ESI Full ms [50.0000-750.0000]
[C4H4DN+H]+
calc. 69.0558
measured 69.0559
1.4 ppm
[C4H3D2N+H]+
calc. 70.0620
measured 70.0621
1.4 ppm
[C4H2D3N+H]+
calc. 71.0683
measured 71.0683
<0.1 ppm
[C4HD4N+H]+
calc. 72.0746
measured 72.0746
<0.1 ppm
[M+H]+
calc. 68.0495
measured 68.0496
1.5 ppm
[C4D5N+H]+
calc. 73.0809
no match detected
71.0683
70.0621
69.0559
72.0746
68.0496
70.0015
70.7832
70.1224
71.1299
71.9102
73.0648
73.6990
74.0600
65.0870
65.8432
67.0543
67.4556


C:\Xcalibur\d...\191021\100
Q Exactive Plus Orbitrap
10/21/19 10:29:43
cite NIH 1S10OD020022-1
Lee 1869
Chemical Instrumentation Center, University of Wisconsin - Madison
NL: 2.28E10 TIC MS 100
Time (min)
100 #121-136 RT: 0.35-0.38 AV: 4 NL: 1.60E9
T: FTMS + p ESI Full ms [50.0000-750.0000]
Relative Abundance
m/z
Compound 35-d5
Methacrylonitrile-d5
ASAP-MS
DL1121
ASAP-MS
Sheath gas flow = 1
Aux gas flow = 5
Aux gas heater temp = 150 °C
91.0913
138.1395
150.1395
119.1227
211.1748
65.0869
165.1330
240.2237
270.2118
330.2659
360.3064
421.3346
451.3751
512.1001
587.1295
640.6813
675.5972
743.3732
100 #120-136 RT: 0.35-0.38 AV: 4 NL: 3.98E7
T: FTMS + p ESI Full ms [50.0000-750.0000]
[C4 H D4 N + H]+
calc. 72.0746
measure 72.0745
1.4 ppm
[C4 D5 N + H]+
calc. 73.0809
measure 73.0808
1.4 ppm
74.0964
74.5236
75.0440
[C4 H2 D3 N + H]+
calc. 71.0683
measure 71.0683
<0.1 ppm
73.0586
72.0745
[C4 H3 D2 N + H]+
calc. 70.0620
measure 70.062
<0.1 ppm
71.0683
68.5760
70.0620
71.8754
72.8660
75.1059
76.0503
77.0898
78.0961
79.1024
79.0211
79.2413

Chapter 3: C_5H_5N Alkynyl Nitrile Isomers.

Some content contained in this section has been submitted and accepted for publication. Contributions to the content in this section have been made by P. Matisha Dorman and Brian J. Esselman.

Introduction

Perhaps one of the most well-recognized classes of organic molecules detected in cosmic environments are the cyanopolyynes. The cyanopolyynes, H–(C≡C)$_n$–CN (n = 0–5), are a homologous family of highly unsaturated nitrogenous species that are prolific in the interstellar medium (ISM) and other astrochemical environments. In unsymmetrical species, cyanopolyynes have prominent dipole moments and correspondingly intense rotational transitions, making them ideal targets for detection *via* radioastronomy. The existence of organic nitriles in the ISM is relevant not only to our understanding of the chemical processes in the ISM, but also to our understanding of the origin of aromatic species, heterocyclic molecules, amino acids, nucleotides, and prebiotic compounds that are found in terrestrial carbon-based life. Cyanopolyynes are important radioastronomical target species due to their relevance to prebiotic chemistry, and are considered to be likely precursors to primitive amino acids.[1-2] The simplest cyanopolyyne, cyanoacetylene, H–C≡C–CN, has been known for decades as a component of the ISM.[3] More recently, cyanoacetylene has been detected in the tail of comet 1995 O1 (Hale-Bopp),[4] and in the nitrogen-rich atmosphere of Saturn's largest moon, Titan.[5] Cyanoacetylene is considered to be a versatile starting material for the synthesis of nitrogen containing species of prebiotic relevance, and is one of many molecules produced in the iconic Miller-Urey experiment.[6] Aqueous solutions of cyanoacetylene have been shown to react with ammonia and potassium cyanate to produce aspartic acid, asparagine, and cytosine.[7] The ubiquity of cyanopolyynes in the cosmos and their relevance to prebiotic organic chemistry has made them one of the hottest species studied by radioastronomers and astrochemists. Coincidentally, combustion of dicyanoacetylene (aka. carbon subnitride, C_4N_2), a molecule impossible to detect in the gaseous ISM due to its inherent lack of

dipole moment, produces the hottest known flame (>6000 K, 5730 ºC) when burnt in the presence of ozone.[8]

The diverse array of nitrogenous organic species in the cosmos does not exclusively consist of fully-unsaturated species such as the cyanopolyynes – open-chain nitriles of varying chain lengths have been observed in varying degrees of unsaturation in different regions of the hydrogen-rich ISM.[9] [10-21] Of the H_nC_3N series, cyanoacetylene (HC_3N), acrylonitrile (H_3C_3N), and propionitrile (ethyl cyanide, H_5C_3N) have each been detected in the ISM *via* radioastronomy.[22-24] The radioastronomical search for partially-hydrogenated species derived from larger cyanopolyyne series (H_nC_5N and above), is largely dependent on the availability of experimentally collected rotational spectra. The McMahon/Woods group has been keenly interested on open-chain nitriles as well as partially-hydrogenated congeners of astrochemically detected cyanopolyyne species for some time. Along with further understanding the reactivity of these molecules, our goal is to expand the list of detected astromolecules by providing the critical spectroscopic characterization required for radioastronomical searches.

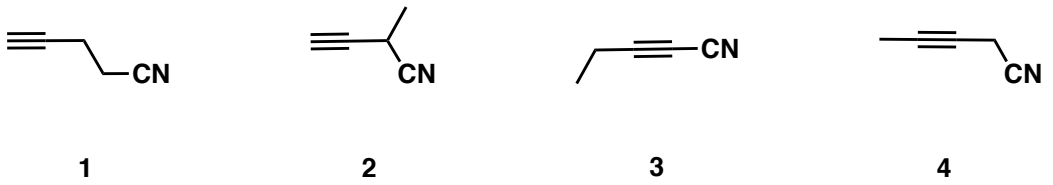


Figure 3.1. C_5H_5N Nitrile Isomers Containing an Alkynyl Moiety: 4-Cyano-1-butyne (**1**), 2-Methyl-3-butynenitrile (**2**), 2-Pentynenitrile (**3**), and 3-Pentynenitrile (**4**).

This thesis chapter discusses our current research regarding the series of four isomeric (C_5H_5N) open-chain nitriles that contain a concurrent alkynyl moiety: 4-cyano-1-butyne (**1**), 2-methyl-3-butynenitrile (**2**), 2-pentynenitrile (1-cyano-1-butyne, ethyl cyanoacetylene) (**3**), and 3-pentynenitrile (methylpropargyl cyanide) (**4**) (Figure 3.1). Methods and techniques used for the synthesis, purification and characterization of each isomer are provided to serve as a guide for

producing samples that are critical for the detailed spectroscopic characterization of these astrochemically relevant species, and to build the foundation for future synthetic and spectroscopic investigations within our group.

The nitriles presented in Figure 3.1 reside at the intersection of several interests of our group and of the astrochemical community in general. Each species is a nitrile-containing acyclic isomer of pyridine, an aromatic heterocycle of prebiotic relevance that has yet to be detected in cosmic environments. Given the formula of pyridine (C_5H_5N) contains four units of unsaturation, isomers with a nitrile functional group have two remaining units of unsaturation. Consolidation of the two units of unsaturation in the form of a C≡C triple bond results in four possible structural arrangements containing concurrent nitrile and alkynyl groups (Figure 3.1). Computational and experimental studies of complex chemical reactions in the ISM are ongoing, and open-chain nitriles are emerging as attractive candidates for a possible mechanistic connection to aromatic species.[25-27] Recently, the first examples of five- and six-membered ring systems, ubiquitous in organic chemistry, were discovered in the ISM as their nitrile-substituted derivatives: benzonitrile,[28] 1- and 2-cyanonaphthalene,[29] and 1- and 2-cyano-1,3-cyclopentadiene.[30-31] These detections represent a dramatic advance in our understanding of interstellar organic chemistry, yet it remains unclear if these ring systems are formed through decomposition of larger polycyclic species or are generated from smaller precursors. In a recent study, several open-chain nitriles and a few nitrile-substituted five- and six-membered rings were generated and detected in a benzene/nitrogen discharge.[32] Detection of any of these nitriles in the cosmos would provide additional motivation to detect pyridine and other aromatic heterocycles.

The four isomers presented in Figure 3.1 each exhibit structural features that are similar to species known to be present in the ISM, and can be classified based on their respective structural

arrangement. The two propargylic nitriles isomers, 2-methyl-3-butynenitrile (**2**, 2º propargylic) and 3-pentynenitrile (**4**, 1º propargylic), vary based on the placement of the methyl group at either the propargylic or acetylenic sites relative to the alkynyl moiety. 2-Methyl-3-butynenitrile (**2**) is the only species within the alkyne-containing C_5H_5N nitrile family that exhibits chirality and is the only structural arrangement with "branched" carbon connectivity. 2-Pentynenitrile (**3**) is the only C_5H_5N isomer with a cyano group at the acetylenic position. 4-Cyano-1-butene (**1**) is the only isomer within the alkyne-containing C_5H_5N nitrile family where the cyano group is not present at either the propargylic or acetylenic positions.

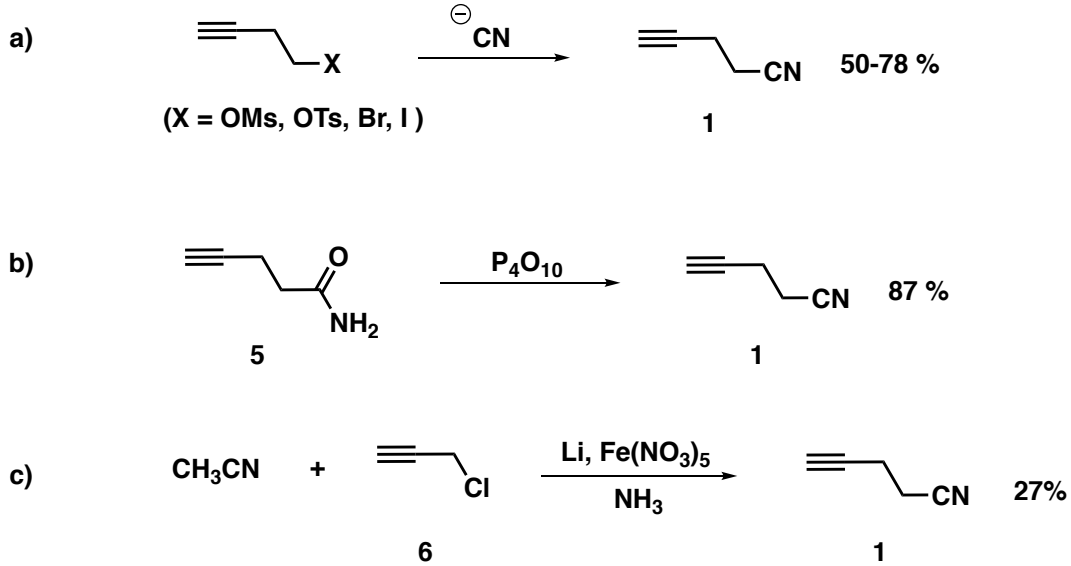
4-Cyano-1-butyne (**1**), is a partially-hydrogenated congener of the known interstellar species C_5N (cyanobutadiynyl radical) and HC_5N (cyanodiacetylene) and is an ethynyl-substituted derivative of the known interstellar molecule, CH_3CH_2CN (cyanoethane). The rotational spectrum of the corresponding isonitrile (4-isocyano-1-butyne) was studied previously from 12 − 70 GHz,[33] resulting in spectroscopic constants for its *anti* and *gauche* forms. The rotational constants of **1** have been previously predicted, along with a collection of cyanodiacetylene-derived nitriles, to facilitate astronomical detection.[34] Our group has recently published[35] an analysis of the rotational spectrum of *anti*- and *gauche*-4-cyano-1-butyne (**1**) that covers a larger frequency range (8 – 38 GHz and 130 – 360 GHz) than previously reported. Details concerning the rotational spectroscopy of (**1**) performed by our group are presented in this chapter and are provided in greater detail in Appendix A.

Background

4-Cyano-1-butyne (**1**) has been synthetically produced through three general techniques (Scheme 3.1). In 1954, Shaw *et al.* first reported the synthesis of 4-cyano-1-butyne (**1**) resulting

from the treatment of homopropargyl tosylate with potassium cyanide.[36] Several similar methods were reported for the production of 4-cyano-1-butyne (**1**) *via* S_N2 metathesis of homopropargyl halides or sulfonate esters and alkali metal cyanides (Scheme 3.1a).[37-44] Sun *et al.* reported the synthesis of 4-cyano-1-butyne (**1**) through the dehydration of 4-pentynamide (**5**) with phosphorus pentoxide (Scheme 3.1b).[45] Compagnon *et al.* showed that 4-cyano-1-butyne (**1**) could be made in lower yields *via* base-promoted addition of acetonitrile to propargyl chloride (**6**) (Scheme 3.1c).[46] Aside from rotational spectroscopy, characterization of 4-cyano-1-butyne (**1**) is rather complete. The physical properties of 4-cyano-1-butyne (**1**) have been well described,[36, 43, 46-47] and the molecule has been characterized *via* several spectroscopic techniques (NMR, IR, vibrational spectroscopy and mass spectrometry).[40, 47-50]

Scheme 3.1. Previous Syntheses of 4-Cyano-1-butyne (1)

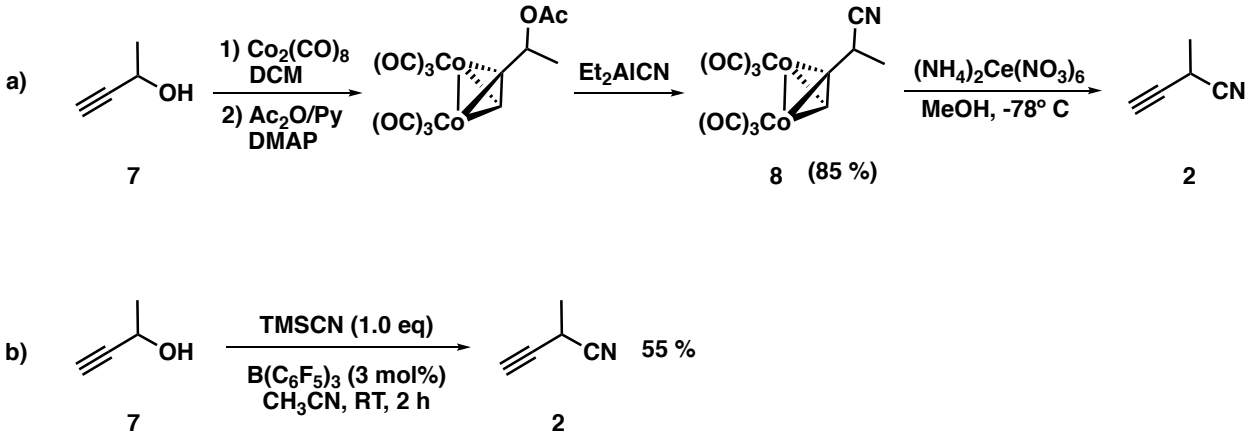


(a) Shaw *et al.*;[36] Gautier *et al.*;[43] Messer *et al.*;[44] Guzman-Duran *et al.*;[40] Mukherjee *et al.*;[41] Li *et al.*;[42] Bennett *et al.*;[39] Fu *et al.*;[38] Safar *et al.*[37] (b) Sun *et al.*[45] (c) Compagnon *et al.*[46]

2-Methyl-3-butynenitrile (**2**) has only appeared in four reports in the literature,[51-53] and does not currently have an experimentally-collected rotational spectrum. 2-Methyl-3-butynenitrile

(**2**) has appeared in two publications reporting new synthetic methodology for the conversion of propargyl (or benzylic) alcohols to nitriles, and appears in a list of products demonstrating the substrate scope of the published methodology (Scheme 3.2). In 1989, Stuart *et al.* reported the cobalt-mediated coupling of propargyl alcohols with diethylaluminum cyanide to yield propargyl nitriles free of allenic derivatives resulting from undesirable isomerization (Scheme 3.2a).[53] This communication reports the successful conversion of 3-butyn-2-ol (**7**) to a complex of **2** with dicobalt hexacarbonyl (**8**) and documents the spectroscopic characterization data of the cobalt-nitrile complex species. However, the procedure for the cleavage of the cobalt-nitrile complex with ceric ammonium nitrate to yield the free propargyl nitrile was only demonstrated once with a different substrate complex. While the authors indicate that the reported methodology could be applied to produce **2** as a free molecule, the isolation and characterization of **2** was not explicitly reported in this communication. In 2009, Rajagopal *et al.* reported methodology for the synthesis of α-aryl nitriles *via* $B(C_6F_5)_3$-catalyzed direct cyanation of α-aryl alcohols and thiols using trimethylsilyl cyanide.[54] While the list of substrates covered in this report largely consists of α–aryl alcohols/thiols, the process was successfully applied to one propargyl alcohol substrate, 3-butyn-2-ol (**7**), and was reported to produce 2-methyl-3-butynenitrile (**2**) in moderate yields (Scheme 3.2b). Although the $^{1}H/^{13}C$-NMR chemical shifts and HRMS data for 2-methyl-3-butynenitrile (**2**) were reported by Rajagopal *et al.*, details concerning the physical properties, purification, and IR spectroscopy of **2** remains incomplete at the current time.

Scheme 3.2. Previous Syntheses of 2-Methyl-3-butynenitrile (2)

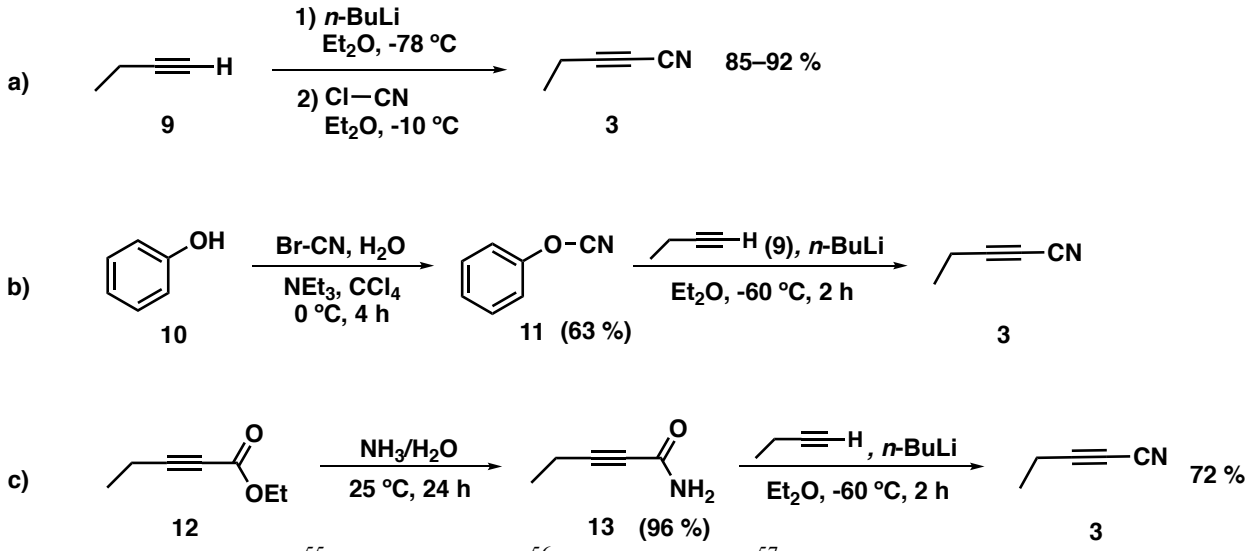


(a) Stuart *et al.*[53] (b) Rajagopal *et al.*[54]

Van der Welle *et al.* first reported the efficient synthesis of 2-pentynenitrile (**3**) *via* generation of the 1-butynyl lithium from 1-butyne (**9**) and subsequent treatment with cyanogen chloride at low temperatures (Scheme 3.3a).[55] Later, Huard *et al.* reported an improved method for the synthesis of **3** that mitigates the use of gaseous cyanogen chloride. In the methodology reported by Huard *et al.*, phenol (**10**) is treated with cyanogen bromide (a solid reagent) to generate phenyl cyanate (**11**) as a liquid cyanating agent. Subsequent S_N2 displacement with *in situ* generated 1-butynyl lithium yielded a solution of 2-pentynenitrile (**3**) (Scheme 3.3b).[56] In both methods reported by Van der Welle *et al.* and Huard *et al.*, the authors generated **3** as an intermediate reagent for the synthesis of heterocyclic compounds, and did not report spectroscopic characterization of isolated **3**. The gas-phase rotational spectrum of 2-pentynenitrile (**3**) between 13 and 116 GHz was been reported by Carles *et al.* in 2013.[57] Seeking to avoid the hazardous synthesis and handling of highly toxic cyanogen chloride, Carles *et al.* generated **3** in good yields *via* dehydration of 2-pentynamide (**13**) produced from commercially-available ethyl pent-2-ynoate (**12**) (Scheme 3.3c).[57-58] Although Carles *et al.* reported the gas-phase rotational spectrum, the $^1H/^{13}C$-NMR chemical shifts, and the *J*–coupling frequencies of 2-pentynenitrile (**3**), details

concerning the characterization of **3** *via* IR spectroscopy and high-resolution mass spectrometry remains incomplete at the current time.

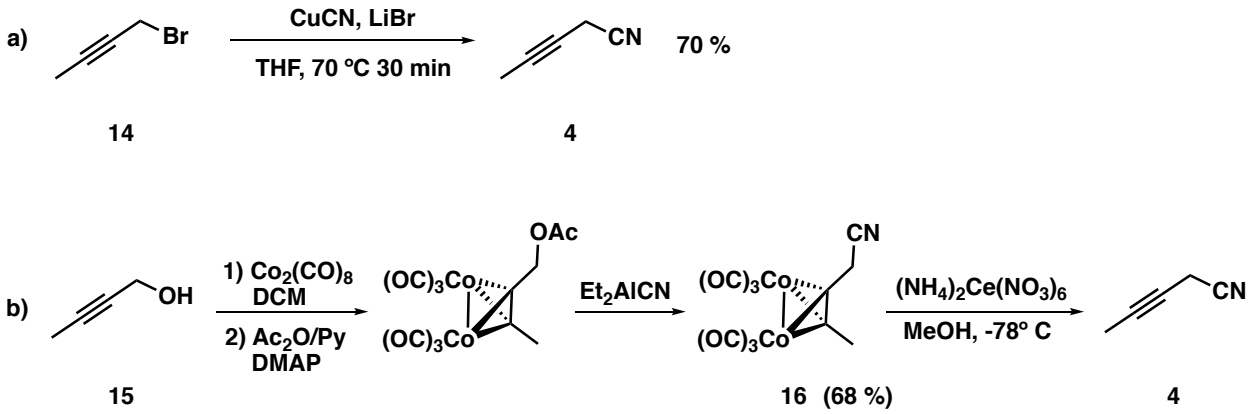
Scheme 3.3. Previous Syntheses of 2-Pentynenitrile (3)



(a) Van der Welle *et al.*[55] (b) Huard *et al.*[56] (c) Carles *et al.*[57]

Although multiple reports have been published describing the synthesis and isolation of 3-pentynenitrile (**4**), no data describing the gas-phase rotational spectrum of **4** have been published. The earliest method for the synthesis of 3-pentynenitrile (**4**) was reported by Schulke *et al.* in 1954, and involves the treatment of 1-bromo-2-butyne (**14**) with cuprous cyanide.[59-60] This methodology was later improved by Brandsma *et al.* to include the physical characterization of **4**, and remains the most widely used procedure for isolating **4** in its pure state (Scheme 3.4a).[61-62] Samples later prepared by Marson *et al.* using this methodology were characterized by ^{1}H-NMR spectroscopy.[63] A separate route reported by Stuart *et al.* shows that **4** can likely be isolated from the corresponding complex with dicobalt hexacarbonyl (**16**) generated *via* cobalt-mediated coupling of 2-butyn-1-ol (**15**) with diethylaluminum cyanide (Scheme 3.4b).[53] However, much like in the case of 2-methyl-3-pentynenitrile (**2**), this Stuart *et al.* only reported the isolation and spectral characterization of the propargyl nitrile-cobalt complex (**16**), and did not fully isolate or characterize **4**.

Scheme 3.4. Previous Syntheses of 3-Pentynenitrile (4)



(a) Brandsma *et al*.[61-63] (b) Stuart *et al*.[53]

Aside from ^{1}H-NMR chemical shifts, the complete spectroscopic characterization of **4** remains incomplete at the current time. In addition to an experimentally-collected gas-phase rotational spectrum, any data regarding the spectroscopic characterization of **4** *via* ^{13}C-NMR, UV-Vis, or IR spectroscopy or mass spectrometry has yet to be reported.

Results and Discussion

Conveniently, we found that 4-cyano-1-butyne (**1**) is a commercially available substance stocked by a reputable chemical supplier (Sigma-Aldrich, 97% purity). A sample of 4-cyano-1-butyne (**1**) was purchased commercially, analyzed *via* ^{1}H-NMR, ^{13}C-NMR, and ATR-IR spectroscopy, and found to be sufficiently pure to be used without further refinement. A sample of 4-cyano-1-butyne (**1**) maintained at room temperature and a pressure of 6 mTorr was used to collect the 130 – 230 GHz and 235 – 360 GHz broadband spectra (Figure 3.2). Transitions for the ground vibrational states of both conformational isomers, *anti* and *gauche*, were observed in the 8 – 38 GHz and 130 – 360 GHz frequency ranges and fit to effective sextic distorted-rotor Hamiltonians with low uncertainty (σ_{fit} < 50 kHz), allowing for their potential detection by radioastronomy or in harsh reaction environments. [35]

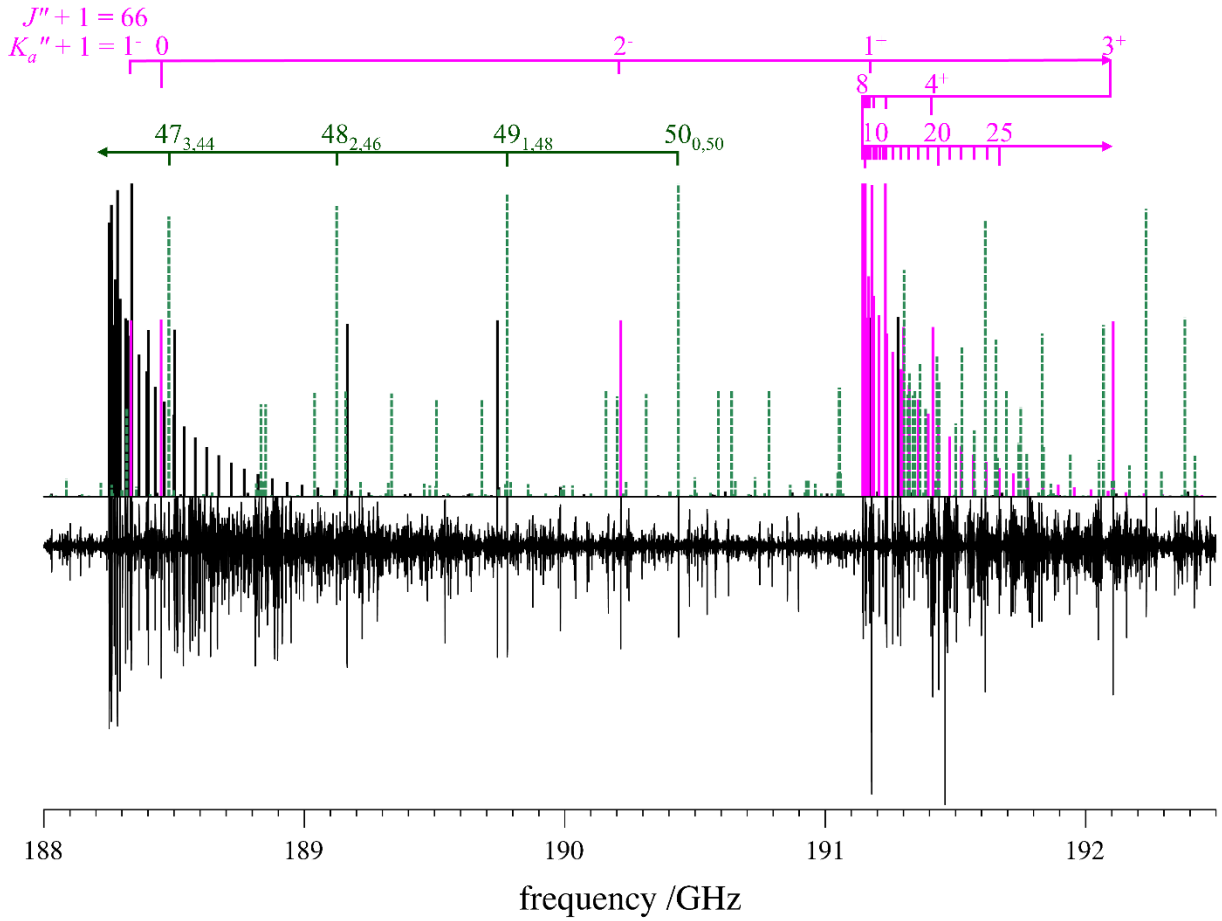


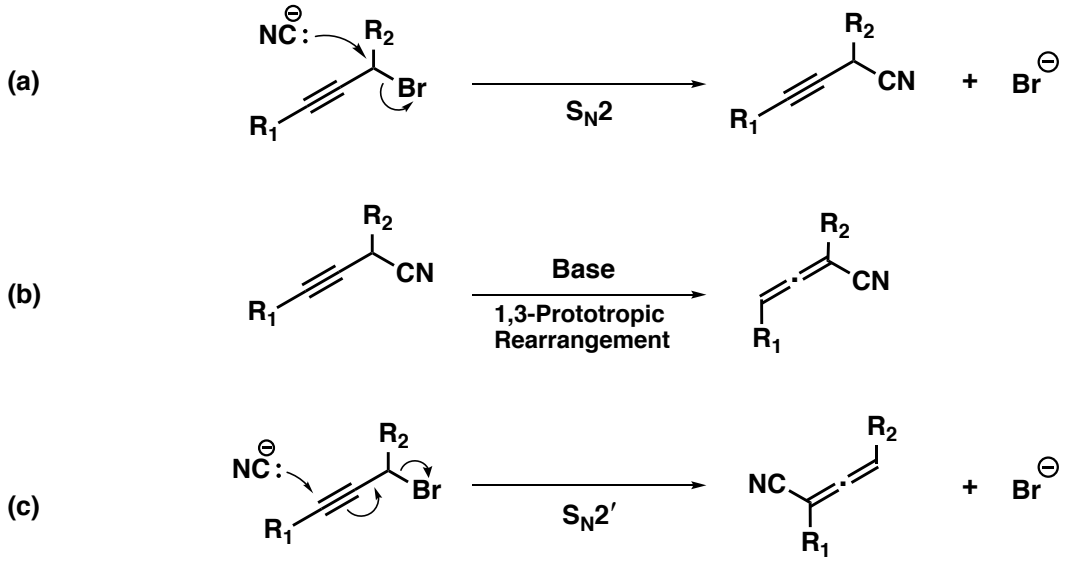
Figure 3.2. Rotational spectrum of 4-cyano-1-butyne (**1**) from 188.0 GHz to 192.5 GHz (bottom) and stick spectrum of the ground vibrational states (top). Dashed green lines mark transitions of *gauche*-4-cyano-1-butyne, and solid-colored lines mark transitions of anti-4-cyano-1-butyne. Solid lines highlighted in magenta belong to the J″ + 1 = 66 series of *anti*-4-cyano-1-butyne, and the corresponding K_a'' + 1 values are marked above. Many transitions belonging to other vibrational satellites are also visible in the experimental spectrum.

The microwave region includes hyperfine-split transitions for both conformers, allowing for the experimental determination of the χ_{aa}, χ_{bb}, and χ_{cc} quadrupole coupling constants. In the millimeter-wave region, not every observable ground-state transition could be satisfactorily addressed by a single-state Hamiltonian due to Coriolis coupling with the low-energy vibrationally excited states. Thus, effective single-state fits of the ground states were obtained by including only K_a series transitions without obviously perturbed energy levels. Importantly, the effective fit does include the most intense transitions throughout the observed frequency ranges. The predicted

values (MP2/cc-pVTZ) are in close agreement with the experimental spectroscopic constants. These data provide a sufficient foundation for the identification of *anti*- and *gauche*-4-cyano-1-butyne (**1**) in the interstellar medium by radioastronomy.[35]

Of the four individual isomers presented in Figure 3.1, the two propargylic nitrile isomers, 2-methyl-3-butynenitrile (**2**) and 3-pentynenitrile (**4**) are the only remaining species without published gas-phase rotational spectra. Neither 2-methyl-3-butynenitrile (**2**) and 3-pentynenitrile (**4**) are commercially-available substances and thus require samples be synthetically produced in house. The primary challenge associated with the synthesis and purification of propargylic nitrile species arises from the competitive formation of isomeric cyanoallene derivatives under the reaction conditions. The synthesis of propargyl nitriles is typically accomplished *via* 1,1-substitution (S_N2 displacement) of the corresponding propargyl bromide with a metal cyanide salt (Scheme 3.5a). The formation of the isomeric cyanoallene derivative can occur *via* base-catalyzed 1,3-protropic rearrangement of the propargyl nitrile (Scheme 3.5b). Alternatively, nucleophilic attack can occur at the distal *sp*-hybridized carbon in the propargylic bromide to form the cyanoallene isomer through 1,3-substitution (S_N2') (Scheme 3.5c). The extent of the cyanoallene formation/isomerization is largely dependent on the substitution of the propargyl bromide, the metal cyanide salt, and the reaction conditions. Sterically large substituents at the propargylic site, and the presence of catalytic or stoichiometric transition metal salts (such as copper) tends to favor the 1,3-substitution mechanism, while the 1,1-substitution pathway prevails in the absence of both factors. For the preparation of primary propargyl nitriles, such as 3-pentynenitrile (**4**), the use of copper (I) cyanide as the cyanide source has been shown to effectively accomplish 1,1-substitution of primary propargyl bromides without being sufficiently basic to facilitate substantial isomerization of the product nitrile *via* 1,3-prototropic rearrangement.

Scheme 3.5. Propargylic Substitution and Rearrangement Mechanisms



The reaction mechanisms presented in Scheme 3.5 and the factors that influence the mode of substitution effectively describe the difficulty of obtaining secondary propargyl nitriles *via* conventional methodology. Substituents at the propargyl site with added steric bulk will restrict nucleophilic attack at that site *via* S_N2 metathesis. Secondary propargyl bromides will typically undergo substitution with metal cyanides *via* S_N2' to yield a cyanoallene derivative. As a result of the mechanistic constraints posed by the conventional methods, specialized methodologies such as those highlighted by Stuart[53] and Rajagopal *et al.*[54] have been developed for the synthesis of secondary propargyl nitriles. For the synthesis of a sample of 2-methyl-3-butynenitrile (**2**) for rotational spectroscopy, the procedure reported by Rajagopal *et al.*[54] appeared to be the best approach due to its relatively facile process.[54] However, our attempts to replicate the conditions reported by Rajagopal *et al.*[54] failed to produce any quantity of 2-methyl-3-butynenitrile (**2**) detectable by ^{1}H-NMR or HRMS. Replicate reactions were performed using acetonitrile or CH_2Cl_2 as solvents, using brand new reagents/catalysts, and under rigorously dry conditions. In each trial, the reaction progress was monitored *via* thin layer chromatography, and showed the clean

conversion of the substrate, 3-butyn-2-ol (**7**), to a single product with a significantly higher R_f value relative to 3-butyn-2-ol (**7**). Purification and isolation of the unknown product *via* flash chromatography yielded a clear colorless oil. The ^{1}H-NMR of the isolated product showed similar signal numbers and splitting patterns indicative of a 3-substituted 1-butyne (much like 3-butyn-2-ol) but at different chemical shifts compared to the values reported for **7** and the anticipated nitrile product (**2**). Analysis of the same product *via* HRMS showed no detectable signal at the accurate mass of **2** (79.04 *m/z*). Spectroscopic evidence indicates that the isolated product is likely TMS protected 3-butyn-2-ol. Our current efforts are focused on troubleshooting this reaction for the preparation of a sample of **2.** Details concerning the experimental procedures attempted for the synthesis of 2-methyl-3-butynenitrile (**2**), and spectra of the obtained product are provided in the supporting information section for this chapter.

Conclusions

We describe our ongoing research regarding the series of four isomeric (C_5H_5N) open-chain nitriles that contain a concurrent alkynyl moiety: 4-cyano-1-butyne (**1**), 2-methyl-3-butynenitrile (**2**), 2-pentynenitrile (**3**), and 3-pentynenitrile (**4**). These molecules are of considerable significance to the field of astrochemistry, as possible constituents of both planetary atmospheres and interstellar space. The analysis of the rotational spectrum of 4-cyano-1-butyne (**1**), an open-chain isomer of pyridine, is published for the first time by our group.[35] Transitions for the ground vibrational states of both conformational isomers, *anti* and *gauche*, were observed in the 8 – 38 GHz and 130 – 360 GHz frequency ranges. In our publication, we generated effective fits for *anti*- and *gauche*-4-cyano-1-butyne and expect the constants presented above to enable those seeking either of these C_5H_5N conformers in harsh interstellar environments to identify them using the most intense transitions at frequencies up to 360 GHz.[35] Research involving the synthesis,

characterization and rotational spectroscopy of 2-methyl-3-butynenitrile (**2**) and 3-pentynenitrile (**4**) are currently ongoing.

Notes and References

1. Taniguchi, K.; Saito, M.; Hirota, T.; Ozeki, H.; Miyamoto, Y.; Kaneko, H.; Minamidani, T.; Shimoikura, T.; Nakamura, F.; Dobashi, K., Observations of Cyanopolyynes toward Four High-mass Star-forming Regions Containing Hot Cores. *Astrophys. J.* **2017,** *844*, 68.

2. Jaber Al-Edhari, A.; Ceccarelli, C.; Kahane, C.; Viti, S.; Balucani, N.; Caux, E.; Faure, A.; Lefloch, B.; Lique, F.; Mendoza, E.; Quenard, D.; Wiesenfeld, L., History of the solar-type protostar IRAS 16293–2422 as told by the cyanopolyynes. *Astron. Astrophys.* **2017,** *597*.

3. Turner, B. E., Detection of Interstellar Cyanoacetylene. *Astrophys. J.* **1971,** *163*, L35.

4. Bockelée-Morvan, D.; Lis, D. C.; Wink, J. E.; Despois, D.; Crovisier, J.; Bachiller, R.; Benford, D.; Biver, N.; Colom, P.; Davies, J.; Gérard, E.; Germain, B.; Houde, M.; Mehringer, D.; Moreno, R.; Phillips, T.; Paubert, G.; Rauer, H., New molecules found in comet C/1995 O1 (Hale-Bopp) Investigating the link between cometary and interstellar material. *Astron. Astrophys.* **1999,** *353*, 1103-1114.

5. Niemann, H. B.; Atreya, S. K.; Bauer, S. J.; Carignan, G. R.; Demick, J. E.; Frost, R. L.; Gautier, D.; Haberman, J. A.; Harpold, D. N.; Hunten, D. M.; Israel, G.; Lunine, J. I.; Kasprzak, W. T.; Owen, T. C.; Paulkovich, M.; Raulin, F.; Raaen, E.; Way, S. H., The abundances of constituents of Titan's atmosphere from the GCMS instrument on the Huygens probe. *Nature* **2005,** *438* (7069), 779-784.

6. McCollom, T. M., Miller-Urey and Beyond: What Have We Learned About Prebiotic Organic Synthesis Reactions in the Past 60 Years? *Annu. Rev. Earth Planet. Sci.* **2013,** *41* (1), 207-229.

7. Sanchez, R. A.; Ferris, J. P.; Orgel, L. E., Cyanoacetylene in Prebiotic Synthesis. *Science* **1966,** *154* (3750), 784-785.

8. Kirshenbaum, A. D.; Grosse, A. V., The Combustion of Carbon Subnitride, C_4N_2, and a Chemical Method For The Production of Continuous Temperatures In The Range of 5000-6000°K. *J. Am. Chem. Soc.* **1956,** *78* (9), 2020-2020.

9. Halter, R. J.; Fimmen, R. L.; McMahon, R. J.; Peebles, S. A.; Kuczkowski, R. L.; Stanton, J. F., Microwave Spectra and Molecular Structures of (*Z*)-Pent-2-en-4-ynenitrile and Maleonitrile. *J. Am. Chem. Soc.* **2001,** *123* (49), 12353-12363.

10. Avery, L. W.; Broten, N. W.; MacLeod, J. M.; Oka, T.; Kroto, H. W., Detection of the Heavy Interstellar Molecule Cyanodiacetylene. *Astrophys. J.* **1976,** *205* (3), L173-L175.

11. Broten, N. W.; Oka, T.; Avery, L. W.; MacLeod, J. M.; Kroto, H. W., The Detection of Cyanooctatetrayne (HC_9N) in Interstellar Space. *Astrophys. J.* **1978,** *223* (2), L105-L107.

12. Kroto, H. W.; Kirby, C.; Walton, D. R. M.; Avery, L. W.; Broten, N. W.; MacLeod, J. M.; Oka, T., The Detection of Cyanohexatriyne, $H(C{\equiv}C)_3CN$, in Heiles's Cloud 2. *Astrophys. J.* **1978,** *219* (3), L133-L137.

13. Walmsley, C. M.; Winnewisser, G.; Toelle, F., Cyanoacetylene and Cyanodiacetylene in Interstellar Clouds. *Astron. Astrophys.* **1980,** *81*, 245-50.

14. Broten, N. W.; MacLeod, J. M.; Avery, L. W.; Irvine, W. M.; Hoeglund, B.; Friberg, P.; Hjalmarson, A., The Detection of Interstellar Methylcyanoacetylene. *Astrophys. J.* **1984,** *276* (1, Pt. 2), L25-L29.

15. Gardner, F. F.; Winnewisser, G., Detection of Interstellar Vinyl Cyanide (Acrylonitrile). *Astrophys. J.* **1975,** *195* (3, Pt. 2), L127-L130.

16. Snyder, L. E.; Hollis, J. M.; Jewell, P. R.; Lovas, F. J.; Remijan, A., Confirmation of Interstellar Methylcyanodiacetylene (CH_3C_5N). *Astrophys. J.* **2006,** *647* (1), 412-417.

17. Lovas, F. J.; Remijan, A. J.; Hollis, J. M.; Jewell, P. R.; Snyder, L. E., Hyperfine Structure Identification of Interstellar Cyanoallene Toward TMC-1. *Astrophys. J.* **2006,** *637* (1), L37-L40.

18. Solomon, P. M.; Jefferts, K. B.; Penzias, A. A.; Wilson, R. W., Detection of Millimeter Emission Lines from Interstellar Methyl Cyanide. *Astrophys. J.* **1971,** *168* (3)(Pt. 2), L107-L110.

19. Belloche, A.; Garrod, R. T.; Müller, H. S. P.; Menten, K. M., Detection of a Branched Alkyl Molecule in the Interstellar Medium: *iso*-Propyl Cyanide. *Science* **2014,** *345* (6204), 1584-1587.

20. Belloche, A.; Garrod, R. T.; Müller, H. S. P.; Menten, K. M.; Comito, C.; Schilke, P., Increased Complexity in Interstellar Chemistry: Detection and Chemical Modeling of Ethyl Formate and *n*-Propyl Cyanide in Sagittarius B2(N). *Astron. Astrophys.* **2009,** *499* (1), 215-232.

21. Loomis, R. A.; Burkhardt, A. M.; Shingledecker, C. N.; Charnley, S. B.; Cordiner, M. A.; Herbst, E.; Kalenskii, S.; Lee, K. L. K.; Willis, E. R.; Xue, C.; Remijan, A. J.; McCarthy, M. C.; McGuire, B. A., An investigation of spectral line stacking techniques and application to the detection of $HC_{11}N$. *Nat. Astron.* **2021,** *5* (2), 188-196.

22. Gardner, F. F.; Winnewisser, G., The detection of interstellar vinyl cyanide (acrylonitrile). *Astrophys. J. Lett.* **1975,** *195* (3), L127-L130.

23. Johnson, D. R.; Lovas, F. J.; Gottlieb, C. A.; Gottlieb, E. W.; Litvak, M. M.; Guelin, M.; Thaddeus, P., Detection of interstellar ethyl cyanide. *Astrophys. J.* **1977,** *218*, 370-376.

24. Matthews, H. E.; Sears, T. J., The detection of vinyl cyanide in TMC-1. *Astrophys. J.* **1983,** *272*, 149-153.

25. McCarthy, M. C.; McGuire, B. A., Aromatics and Cyclic Molecules in Molecular Clouds: A New Dimension of Interstellar Organic Chemistry. *J. Phys. Chem. A* **2021,** *125* (16), 3231-3243.

26. Lee, K. L. K.; McGuire, B. A.; McCarthy, M. C., Gas-phase synthetic pathways to benzene and benzonitrile: a combined microwave and thermochemical investigation. *Phys. Chem. Chem. Phys.* **2019,** *21* (6), 2946-2956.

27. Cernicharo, J.; Agúndez, M.; Cabezas, C.; Tercero, B.; Marcelino, N.; Pardo, J. R.; de Vicente, P., Pure hydrocarbon cycles in TMC-1: Discovery of ethynyl cyclopropenylidene, cyclopentadiene, and indene. *Astron. Astrophys.* **2021,** *649*, L15.

28. McGuire, B. A.; Burkhardt, A. M.; Kalenskii, S. V.; Shingledecker, C. N.; Remijan, A. J.; Herbst, E.; McCarthy, M. C., Detection of the Aromatic Molecule Benzonitrile (*c*-C_6H_5CN) in the Interstellar Medium. *Science* **2018,** *359* (6372), 202-205.

29. McGuire, B. A.; Loomis, R. A.; Burkhardt Andrew, M.; Lee, K. L. K.; Shingledecker, C. N.; Charnley, S. B.; Cooke, I. R.; Cordiner, M. A.; Herbst, E.; Kalenskii, S.; Siebert Mark, A.; Willis Eric, R.; Xue, C.; Remijan, A. J.; McCarthy, M. C., Detection of two interstellar polycyclic aromatic hydrocarbons via spectral matched filtering. *Science* **2021,** *371* (6535), 1265-1269.

30. McCarthy, M. C.; Lee, K. L. K.; Loomis, R. A.; Burkhardt, A. M.; Shingledecker, C. N.; Charnley, S. B.; Cordiner, M. A.; Herbst, E.; Kalenskii, S.; Willis, E. R.; Xue, C.; Remijan, A. J.; McGuire, B. A., Interstellar detection of the highly polar five-membered ring cyanocyclopentadiene. *Nat. Astron.* **2021,** *5* (2), 176-180.

31. Lee, K. L. K.; Changala, P. B.; Loomis, R. A.; Burkhardt, A. M.; Xue, C.; Cordiner, M. A.; Charnley, S. B.; McCarthy, M. C.; McGuire, B. A., Interstellar Detection of 2-Cyanocyclopentadiene, C_5H_5CN, a Second Five-membered Ring toward TMC-1. *Astrophys. J.* **2021,** *910*, L2.

32. McCarthy, M. C.; Lee, K. L. K.; Carroll, P. B.; Porterfield, J. P.; Changala, P. B.; Thorpe, J. H.; Stanton, J. F., Exhaustive Product Analysis of Three Benzene Discharges by Microwave Spectroscopy. *J. Phys. Chem. A* **2020,** *124* (25), 5170-5181.

33. Samdal, S.; Møllendal, H.; Guillemin, J.-C., Microwave Spectrum and Conformational Properties of 4-Isocyano-1-butyne ($HC{\equiv}CCH_2CH_2N{\equiv}C$). *J. Phys. Chem. A* **2013,** *117* (40), 10304-10310.

34. Moreno, R.; Silla, E.; Tunon, I.; Arnau, A., *Ab initio* rotational constants of the nitriles derived from cyanodiacetylene (HC_4CN). *Astrophys. J.* **1994,** *437* (1, Pt. 1), 532-9.

35. Dorman, P. M.; Esselman, B. J.; Changala, P. B.; Kougias, S. M.; McCarthy, M. C.; Woods, R. C.; McMahon, R. J., Rotational spectrum of *anti*- and *gauche*-4-cyano-1-butyne (C_5H_5N) - An open-chain isomer of pyridine. *J. Mol. Spectrosc.* **2022,** *385*, 111604.

36. Shaw, B. L.; Whiting, M. C., Polyenes. I. Synthesis of corticrocin. *J. Chem. Soc.* **1954**, 3217-21.

37. Safar, P.; Marchalin, S.; Soral, M.; Moncol, J.; Daich, A., Structure and Mechanism Revision of a Catalyzed Cyclization of Benzaldehyde Bearing Alkyne-Nitrile. *Org. Lett.* **2017,** *19* (18), 4742-4745.

38. Fu, J.; Lee, P.; Madera, A. M.; Sweeney, Z. K. Preparation of oxazolidinone hydroxamic acid compounds for the treatment of bacterial infections. WO2015066413A1, 2015.

39. Bennett, M. K.; Gross, M. I.; Bromley, S. D.; Li, J.; Chen, L.; Goyal, B.; Laidig, G.; Stanton, T. F.; Sjogren, E. B. Preparation of heterocyclic inhibitors of glutaminase. WO2014089048A1, 2014.

40. Guzman-Duran, A.; Guzman, E.; Pannell, K. H.; Lloyd, W. D., Synthesis of (*E,Z*)-5-Bromo-1,1-dimethoxy-5-trimethylsilyl-4-pentene, an Upper Chain Allenic Prostaglandin Building Block. *Synth. Commun.* **2003,** *33* (19), 3271-3283.

41. Mukherjee, A.; Liu, R.-S., Chemoselectivities in the Platinum-Catalyzed Hydrative Carbocyclizations of Oxo-Alkyne-Nitrile Functionalities. *Org. Lett.* **2011,** *13* (4), 660-663.

42. Li, J.; Chen, L.; Goyal, B.; Laidig, G.; Stanton, T. F.; Sjogren, E. B. Oxadiazoles, thiadiazoles and pyridazines as inhibitors of glutaminase and their preparation. WO2013078123A1, 2013.

43. Gautier, J. A.; Miocque, M.; Mascrier-Demagny, L., Acetylenic aryl aliphatic ketones. I. Preparation. *Bull. Soc. Chim. Fr.* **1967,** (5), 1551-4.

44. Messer, W. S., Jr.; Abuh, Y. F.; Liu, Y.; Periyasamy, S.; Ngur, D. O.; Edgar, M. A. N.; El-Assadi, A. A.; Sbeih, S.; Dunbar, P. G.; Roknich, S.; Rho, T.; Fang, Z.; Ojo, B.; Zhang, H.; Huzl, J. J., III; Nagy, P. I., Synthesis and Biological Characterization of 1,4,5,6-Tetrahydropyrimidine and 2-Amino-3,4,5,6-tetrahydropyridine Derivatives as Selective M1 Agonists. *J. Med. Chem.* **1997,** *40* (8), 1230-1246.

45. Sun, H.; Wei, Y.; Gao, Y.; Chen, X.; Miao, J.; Li, N.; Kan, L.; Bai, J.; Chen, S.; Yang, A.; Xu, Y. A process for manufacturing of nitrile and the corresponding amine. CN104557610A, 2015.

46. Compagnon, P. L.; Miocque, M., Preparation of 4-pentynonitrile from acetonitrile. *Bull. Soc. Chim. Fr.* **1968,** (5), 2105-6.

47. Cullen, M. D.; Deng, B.-L.; Hartman, T. L.; Watson, K. M.; Buckheit, R. W., Jr.; Pannecouque, C.; De Clercq, E.; Cushman, M., Synthesis and Biological Evaluation of Alkenyldiarylmethane HIV-1 Non-Nucleoside Reverse Transcriptase Inhibitors That Possess Increased Hydrolytic Stability. *J. Med. Chem.* **2007,** *50* (20), 4854-4867.

48. Klaeboe, P.; Moneeb, M.; Torneng, E.; Hopf, H.; Boehm, I.; Cyvin, B. N.; Cyvin, S. J., The conformation and vibrational spectra of 1-cyano-3-butyne. *Z. Naturforsch., A* **1980,** *35A* (5), 537-48.

49. Klaeboe, P., High-pressure vibrational spectroscopy and conformational analysis. *Opt. Pura Apl.* **1978,** *11* (3), 137-42.

50. Klaeboe, P., Study of conformational equilibria and hydrogen bonding by high-pressure vibrational spectroscopy. *Kem. Kozl.* **1984,** *61* (1), 57-74.

51. Jamal, A.; Mebel, A. M., Theoretical Investigation of the Mechanism and Product Branching Ratios of the Reactions of Cyano Radical with 1- and 2-Butyne and 1,2-Butadiene. *J. Phys. Chem. A* **2013,** *117* (4), 741-755.

52. Rablen, P. R.; McLarney, B. D.; Karlow, B. J.; Schneider, J. E., How Alkyl Halide Structure Affects E2 and S_N2 Reaction Barriers: E2 Reactions Are as Sensitive as S_N2 Reactions. *J. Org. Chem.* **2014,** *79* (3), 867-879.

53. Stuart, J. G.; Nicholas, K. M., Cobalt-mediated synthesis of propyargyl nitriles and α-alkoxy propargyl nitriles. *Synthesis* **1989,** (6), 454-5.

54. Rajagopal, G.; Kim, S. S., Synthesis of α-aryl nitriles through $B(C_6F_5)_3$-catalyzed direct cyanation of α-aryl alcohols and thiols. *Tetrahedron* **2009,** *65* (22), 4351-4355.

55. Van der Welle, R. A.; Brandsma, L., Preparation of 5-cyano-2*H*-thiopyrans and 4-cyano-2-methylthiophenes by thermal rearrangement of the adducts from 2-propynethiol and cyanoalkynes. *Recl. Trav. Chim. Pays-Bas* **1973,** *92* (5), 667-72.

56. Huard, K.; Ahn, K.; Amor, P.; Beebe, D. A.; Borzilleri, K. A.; Chrunyk, B. A.; Coffey, S. B.; Cong, Y.; Conn, E. L.; Culp, J. S.; Dowling, M. S.; Gorgoglione, M. F.; Gutierrez, J. A.; Knafels, J. D.; Lachapelle, E. A.; Pandit, J.; Parris, K. D.; Perez, S.; Pfefferkorn, J. A.; Price, D. A.; Raymer, B.; Ross, T. T.; Shavnya, A.; Smith, A. C.; Subashi, T. A.; Tesz, G. J.; Thuma, B. A.; Tu, M.; Weaver, J. D.; Weng, Y.; Withka, J. M.; Xing, G.;

Magee, T. V., Discovery of Fragment-Derived Small Molecules for in Vivo Inhibition of Ketohexokinase (KHK). *J. Med. Chem.* **2017,** *60* (18), 7835-7849.

57. Carles, S.; Moellendal, H.; Guillemin, J. C., Rotational spectrum of ethyl cyanoacetylene (C_2H_5CCCN), a compound of potential, astrochemical interest. *Astron. Astrophys.* **2013,** *558* (Pt. 1), A6/1-A6/12.

58. Struebing, D.; Neumann, H.; Klaus, S.; Huebner, S.; Beller, M., A facile and efficient synthesis of enyne-reaction precursors by multicomponent reactions. *Tetrahedron* **2005,** *61* (48), 11333-11344.

59. Schulte, K. E.; Reiss, K. P., Zur Kenntnis der Acetylencarbonsäuren, II. Mitteil.): Die Darstellung der Hexinsäure, Pentin-(4)-säure und Heptadiin-(1.6)-carbonsäure-(4. *Chemische Berichte* **1954,** *87* (7), 964-970.

60. Haruki, E.; Hirai, Y.; Imoto, E., Synthesis of some substituted heterocyclic compounds from propargyl cyanide and methylpropargyl cyanide. *Bull. Chem. Soc. Jap.* **1968,** *41* (1), 267.

61. Brandsma, L.; Verkruijsse, H. D., *Studies in Organic Chemistry, Vol. 8: Synthesis of Acetylenes, Allenes and Cumulenes: A laboratory Manual*. Elsevier: 1981; p 276

62. Subramanian, L. R., Introduction of the cyano group by substitution of a halogen. *Sci. Synth.* **2004,** *19*, 173-195.

63. Marson, C. M.; Grabowska, U.; Walsgrove, T.; Eggleston, D. S.; Baures, P. W., Stereocontrolled construction of condensed γ-lactam ring systems by cationic cyclizations. Rearrangement of a γ-lactam to a δ-lactam. *J. Org. Chem.* **1994,** *59* (2), 284-90.

Supporting Information Section for Chapter 3:
C_5H_5N Alkynyl Nitrile Isomers.

Attempted Synthesis of 2-Methyl-3-butynenitrile (2):

General Notes

3-Butyn-2-ol (**7**) is a commercially-available substance. Two 125-mL bottles of **7** were already in our reagent inventory at the outset of our experimental trials. The quality of the **7** contained in each bottle was assessed *via* ^{1}H-NMR, and confirmed to be of good purity. TMSCN is also a commercially-available substance. The bottle of TMSCN in our chemical inventory was deep red in color and of questionable quality. A new bottle of TMSCN was purchased for our experiments and was stored in a desiccator cabinet. The catalyst, tris(pentafluorophenyl)borane ($B(C_6F_5)_3$) is also a commercially available product. Samples of $B(C_6F_5)_3$ were obtained in glass ampoules sealed under an inert atmosphere. The ampoules of $B(C_6F_5)_3$ were only opened immediately before being used. The $B(C_6F_5)_3$ used in our experimental trials only came from freshly-opened ampoules. Excess $B(C_6F_5)_3$ from opened ampoules was not used in this synthesis, but were stored in vials under dry conditions without noticeable decomposition.

Synthetic Procedure[1]

In an oven-dried 50-mL round bottom flask (cooled under dry N_2) was added: 3-butyn-2-ol (**7**) (1.75 g, 25 mmol), $B(C_6F_5)_3$ (350 mg, 2.7 mol %) and dry acetonitrile (20 mL). The flask was capped with a rubber septum and purged with dry N_2 for 5 minutes at room temperature. Trimethylsilyl cyanide (TMSCN) (2.50 g, 25.2 mmol) was delivered dropwise to the stirred reaction flask over a course of 3 minutes *via* syringe needle. A slight exotherm was observed upon addition of the TMSCN to the stirred reaction. The reaction was stirred at room temperature for 2 hours. After 2 hours has elapsed, the progress of the reaction was assessed *via* TLC: (hexane : EtOAc, 9:1 – UV visualization). Developed plates showed two spots at approximately equal intensity: R_f = 0.26 (3-butyn-2-ol (**7**)) and R_f = 0.87 (an unknown product). Reassessment of the

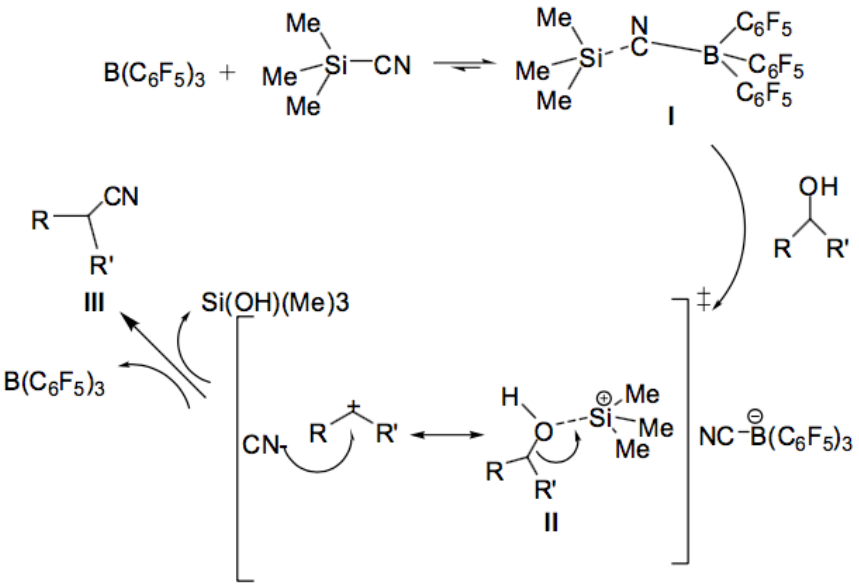
reaction progress after stirring for an additional 12 hours at room temperature showed no further conversion of the starting material. An additional 1.0 g (10.1 mmol) of TMSCN was added dropwise to the stirred reaction. After stirring for 20 minutes, evaluation of the reaction *via* TLC showed nearly complete conversion of the starting material. The reaction mixture was rinsed into a separatory funnel with 40 mL diethyl ether and washed with water (8 × 10 mL) to remove the acetonitrile solvent. The organic layer was washed with brine (15 mL), dried over anhydrous $MgSO_4$ and filtered. The ether solvent was removed *in vacuo via* rotary evaporation to yield the crude product as an amber oil. The crude product was purified by vacuum distillation using a short path apparatus to yield 2.1 g of colorless oil (bp = 48 ºC at 100 Torr).

At this juncture, the identity of the collected product was still unknown. The procedure reported by Rajagopal *et al.* did not provide TLC conditions, retention factors, or a boiling point for identifying **2** in the product mixture. ^{1}H and ^{13}C-NMR data obtained from the collected distillate did not match the NMR data reported by Rajagopal *et al.*[1] for compound **2**. The ^{13}C-NMR spectrum of the collected distillate showed no signals at a chemical shift representative of a nitrile functional group. Signals in the ^{1}H-NMR spectrum of the collected distillate closely resembled those observed in the ^{1}H-NMR spectrum of 3-butyn-2-ol (**7**) with the notable addition of a singlet at 0.2 ppm that integrated to 9H with respect to the other signals. Although there are no published authentic NMR spectra for comparison, the evidence from our NMR spectra indicated that the collected distillate was likely TMS-protected **7**. This hypothesis is consistent with the high R_f (0.87) observed during TLC of the reaction mixture/product using a largely nonpolar eluent (hexane : EtOAc, 9:1). HRMS data obtained from the collected distillate did not show any signals matching the mass of **2**, **7**, or TMS-**7**. The base peak detected in the HRMS (*m/z* = 114.9366)

appears to represent an unknown ion fragment. ^{1}H and ^{13}C-NMR spectra of the collected distillate and alcohol **7** are included later in the supporting info section for this chapter.

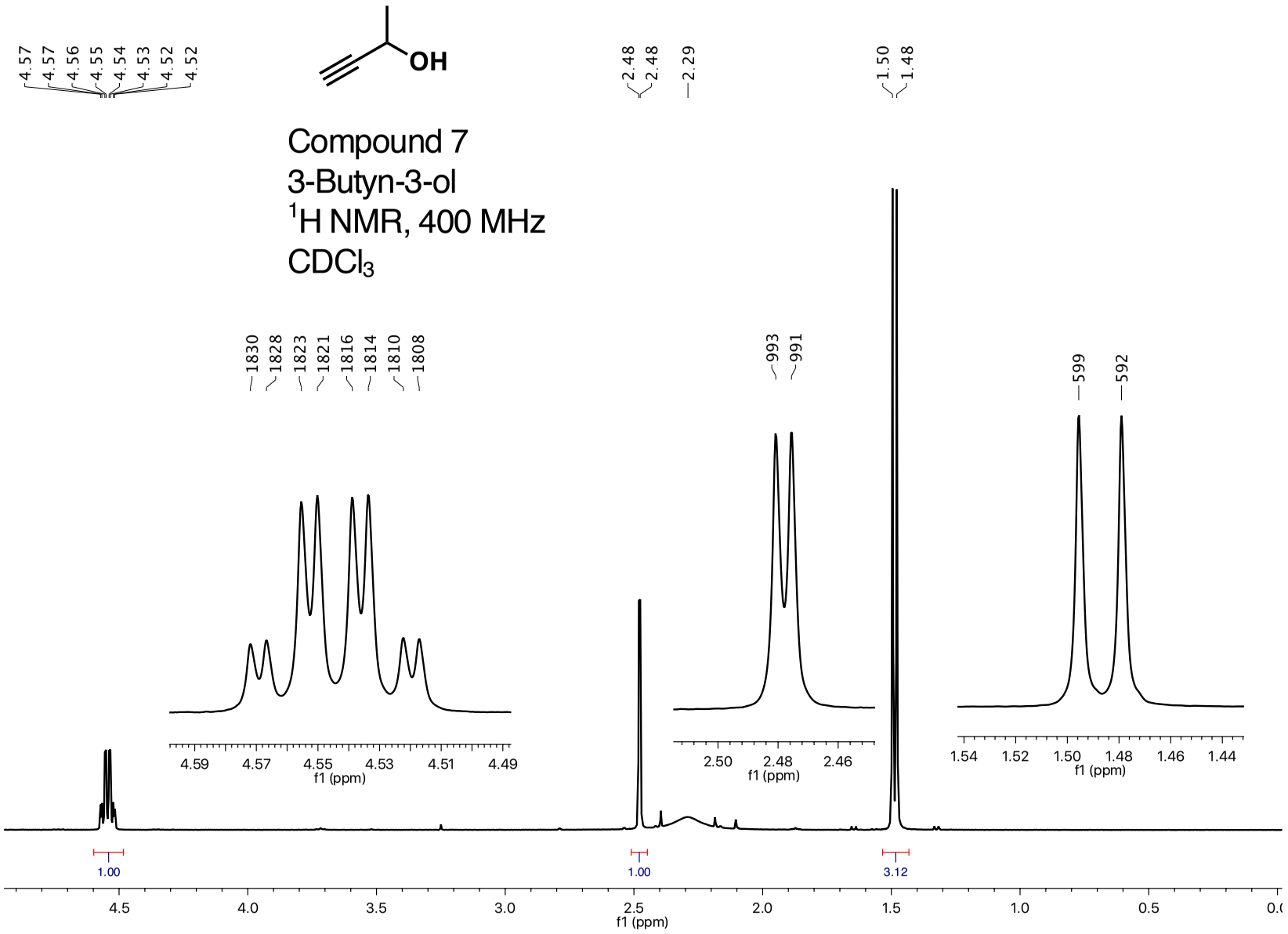
Based on the evidence provided from NMR data and experimental observations, it appears that TMS- **7** is the product we obtained from our attempts to produce **2** using the methodology reported by Rajagopal *et al.*[1] The reaction pathway proposed by Rajagopal *et al.* shows the formation of TMS-**7** as a reaction intermediate (shown in its protonated form) (Scheme S3.1).[1] Factors influencing the displacement of TMS-OH from the intermediate by cyanide are currently being considered by our group.

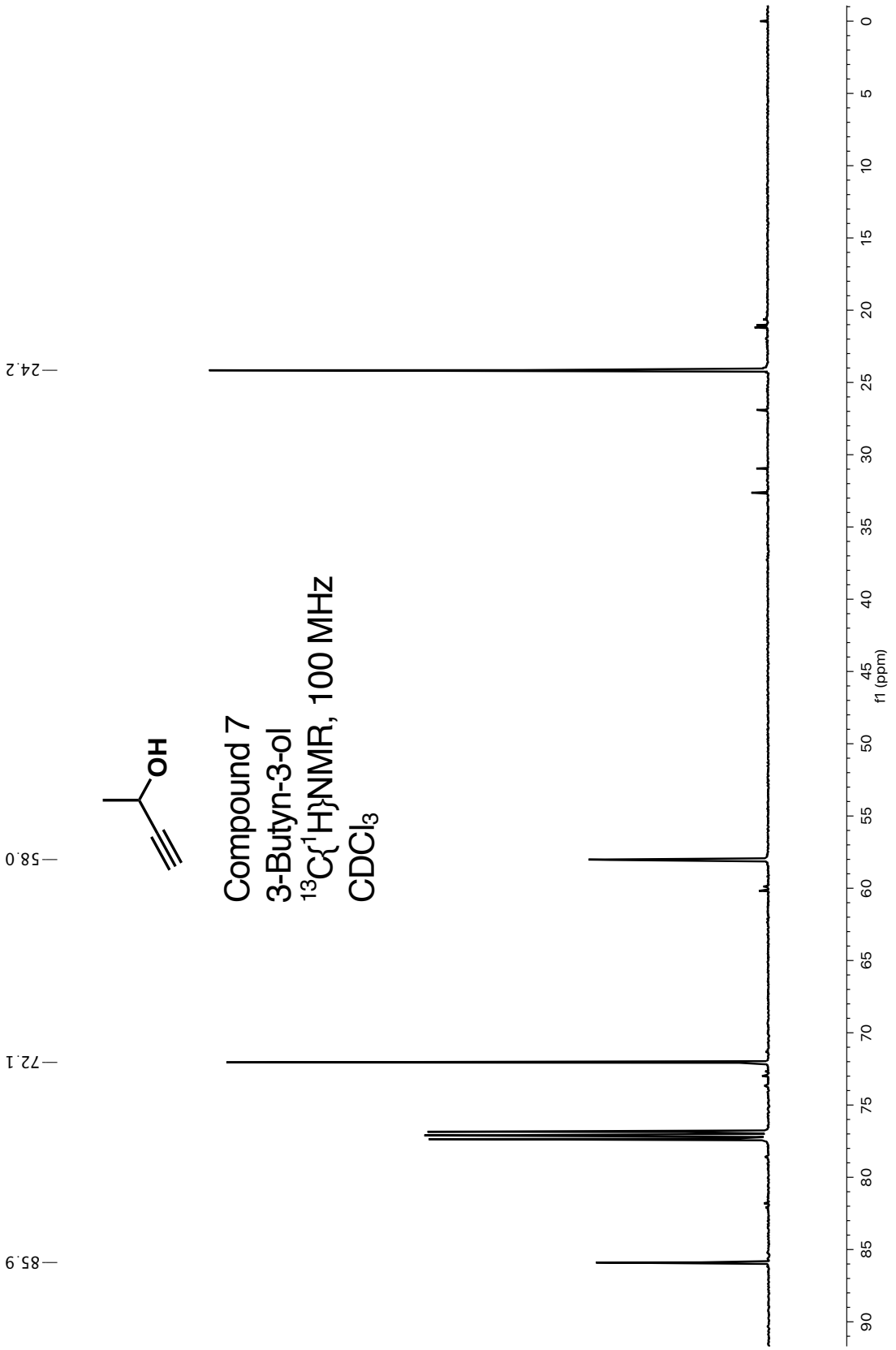
Scheme S3.1. Reaction Pathway for the Direct Cyanation of α-Aryl, and 2°-Propargyl Alcohols proposed by Rajagopal *et al.*[1]

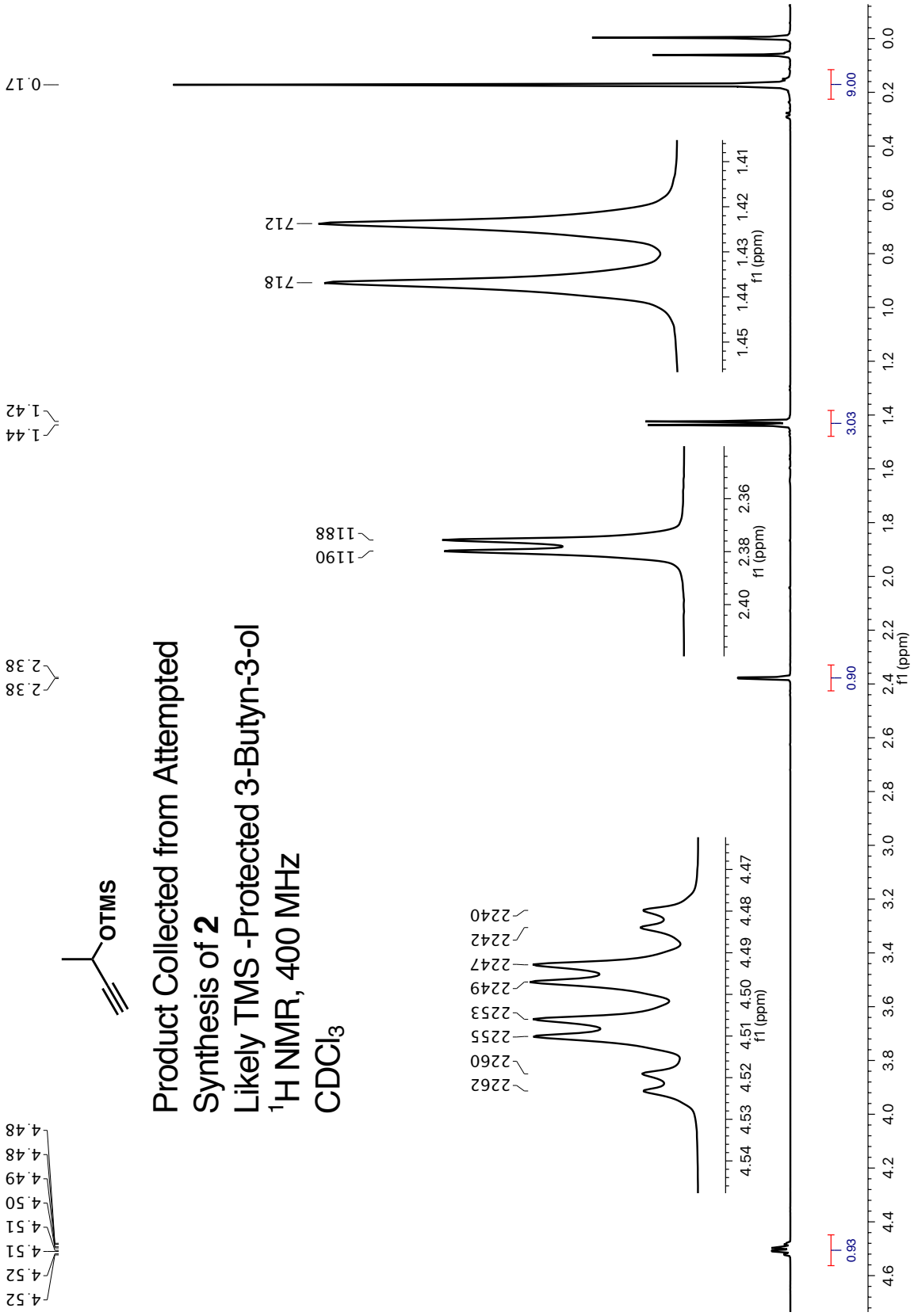


References

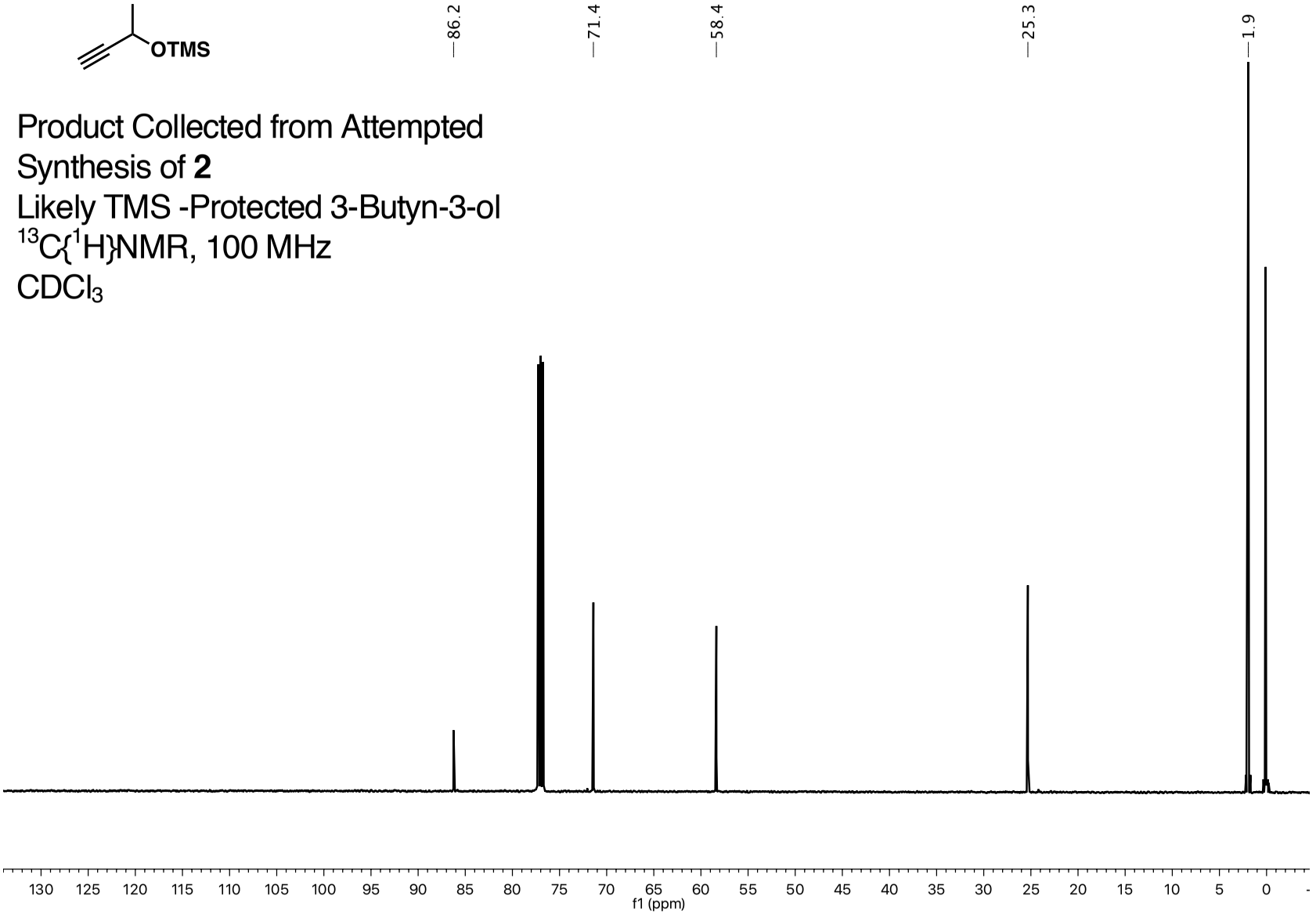
1. Rajagopal, G.; Kim, S. S., Synthesis of α-aryl nitriles through $B(C_6F_5)_3$-catalyzed direct cyanation of α-aryl alcohols and thiols. *Tetrahedron* **2009,** *65* (22), 4351-4355.

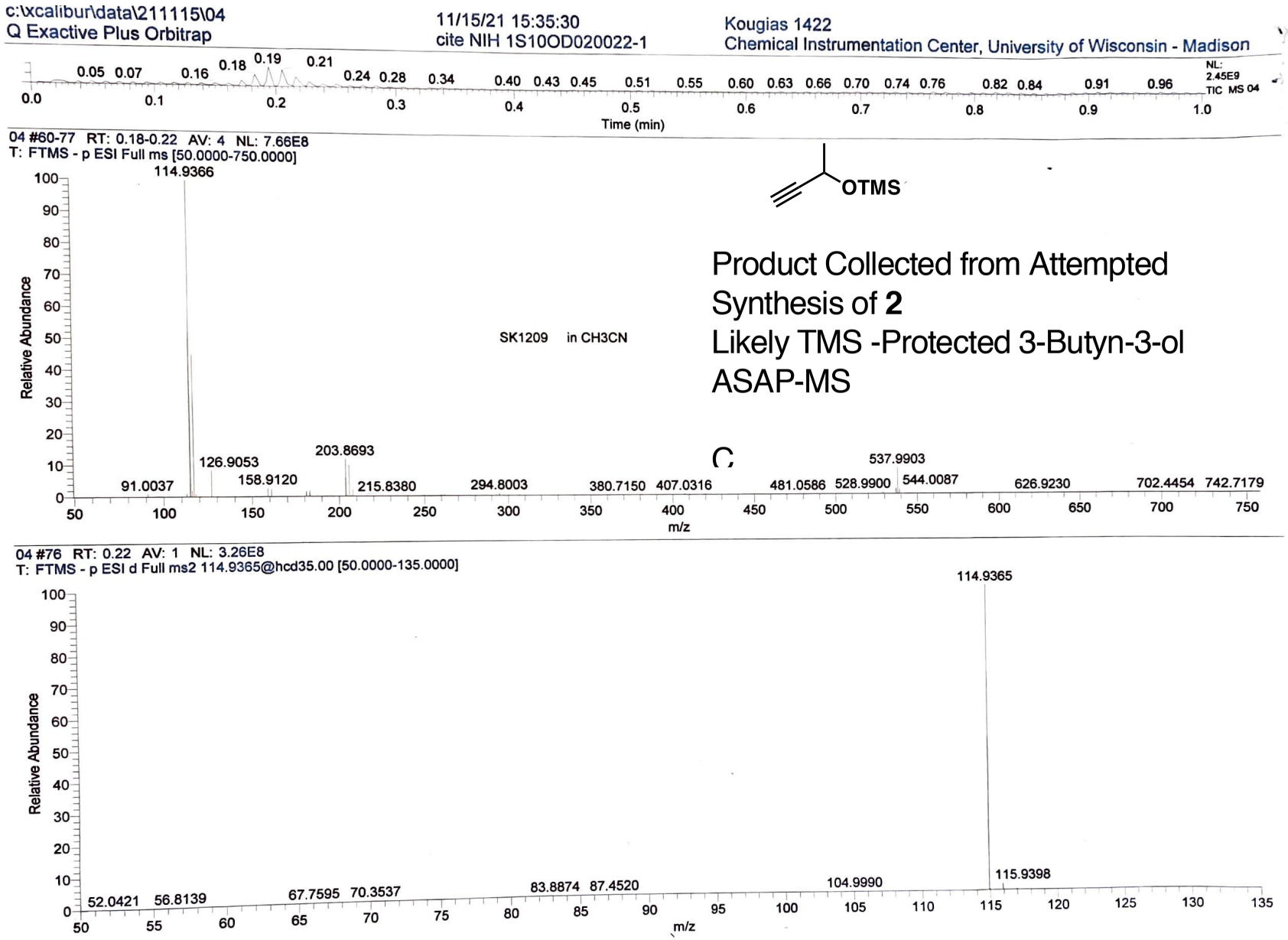

4.57
4.57
4.56
4.55
4.54
4.53
4.52
4.52
OH
2.48
2.48
2.29
1.50
1.48
Compound 7
3-Butyn-3-ol
1H NMR, 400 MHz
CDCl3
1830
1828
1823
1821
1816
1814
1810
1808
993
991
599
592
4.59
4.57
4.55
4.53
4.51
4.49
f1 (ppm)
2.50
2.48
2.46
f1 (ppm)
1.54
1.52
1.50
1.48
1.46
1.44
f1 (ppm)
1.00
1.00
3.12
4.5
4.0
3.5
3.0
2.5
2.0
1.5
1.0
0.5
f1 (ppm)

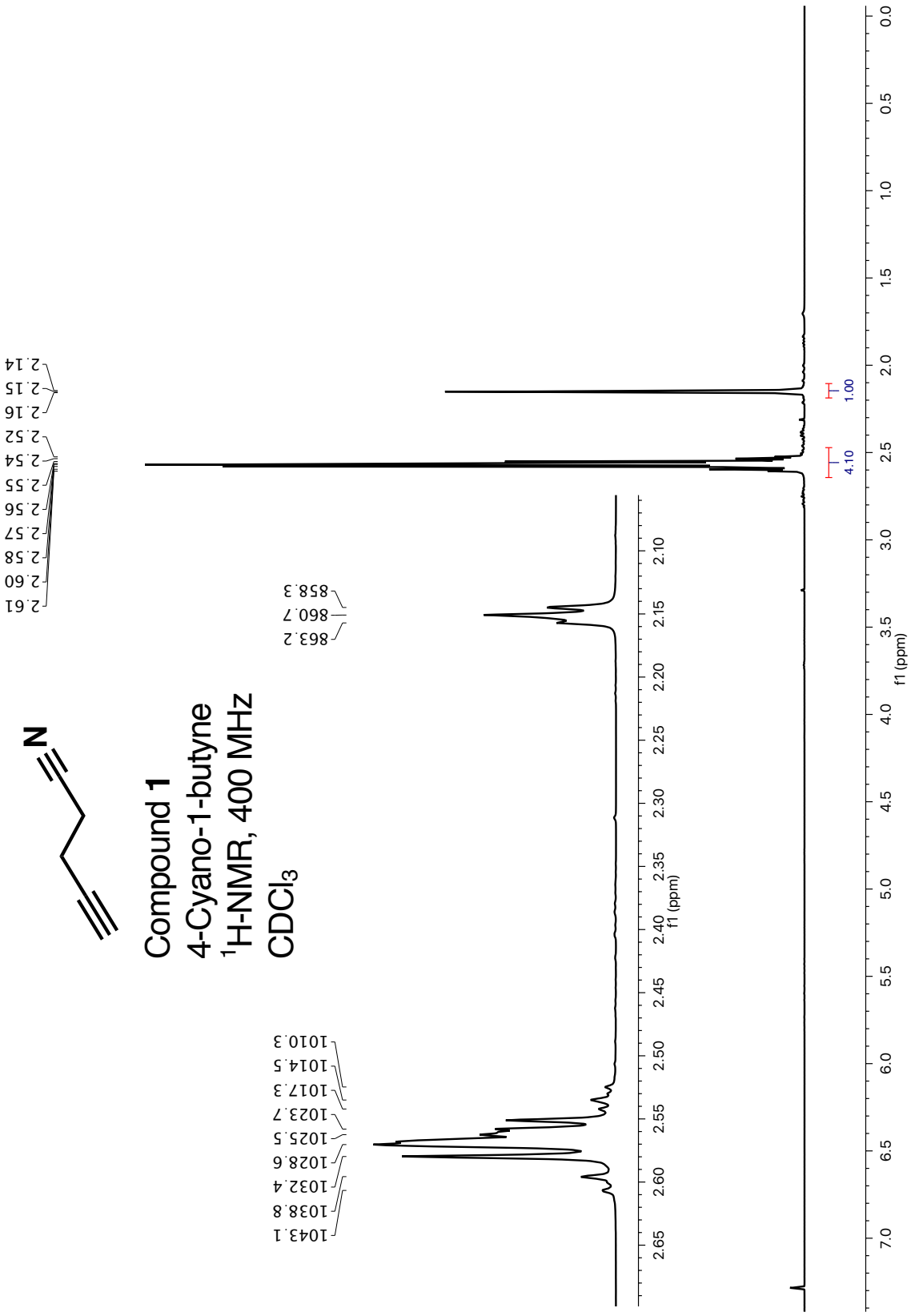

Compound 7
3-Butyn-3-ol
$^{13}C\{^{1}H\}$NMR, 100 MHz
$CDCl_3$
OH
85.9
72.1
58.0
24.2
f1 (ppm)

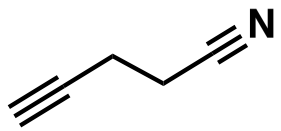

Product Collected from Attempted Synthesis of 2
Likely TMS -Protected 3-Butyn-3-ol
1H NMR, 400 MHz
CDCl3
OTMS
4.52
4.52
4.51
4.51
4.50
4.49
4.48
4.48
2.38
2.38
1.44
1.42
0.17
2262
2260
2255
2253
2249
2247
2242
2240
1190
1188
718
712
f1 (ppm)
0.93
0.90
3.03
9.00

Product Collected from Attempted Synthesis of **2**
Likely TMS -Protected 3-Butyn-3-ol
$^{13}C\{^{1}H\}$NMR, 100 MHz
$CDCl_3$

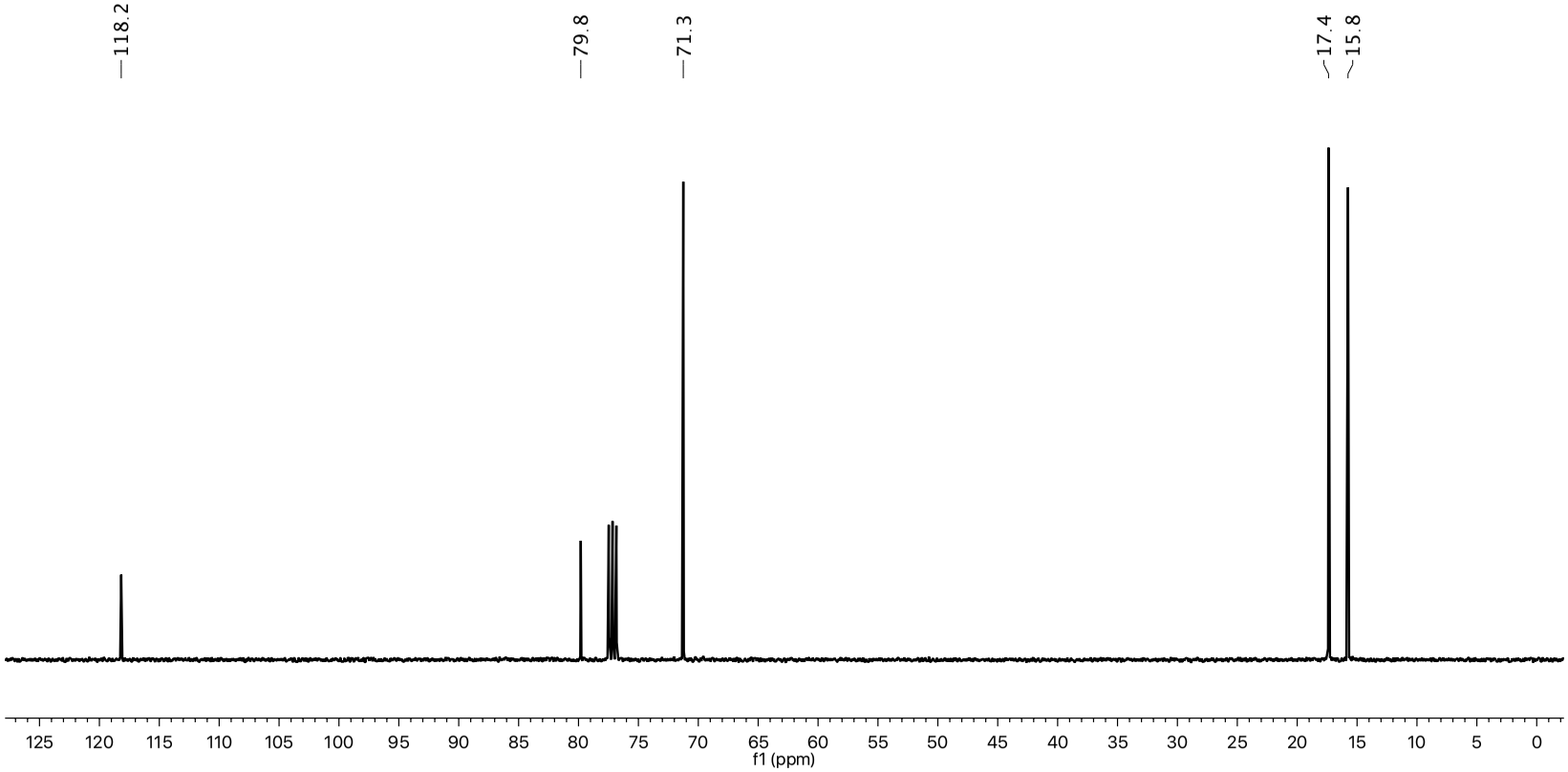


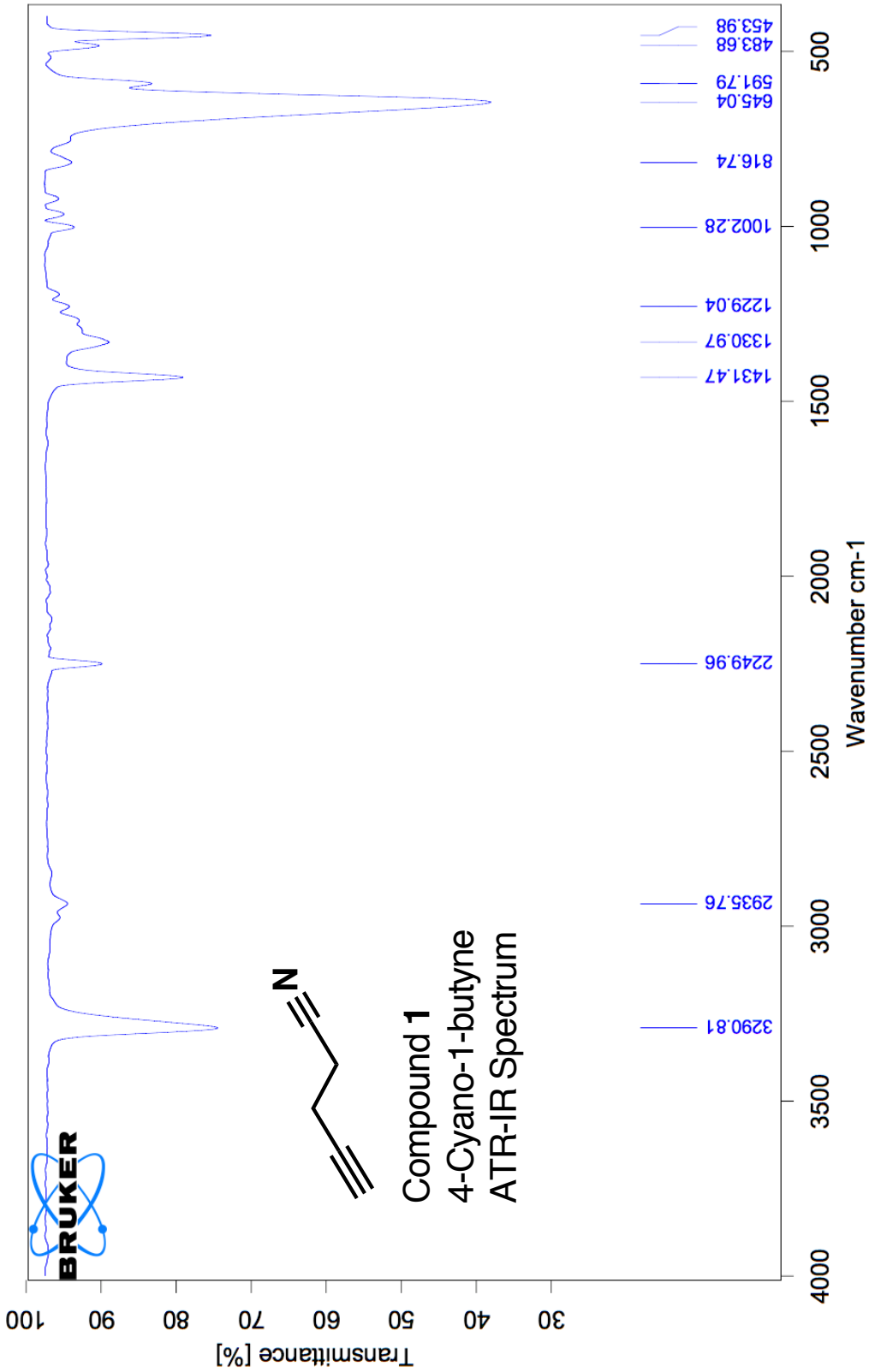

c:\xcalibur\data\211115\04
Q Exactive Plus Orbitrap
11/15/21 15:35:30
cite NIH 1S10OD020022-1
Kougias 1422
Chemical Instrumentation Center, University of Wisconsin - Madison
NL: 2.45E9 TIC MS 04
Time (min)
04 #60-77 RT: 0.18-0.22 AV: 4 NL: 7.66E8
T: FTMS - p ESI Full ms [50.0000-750.0000]
114.9366
Relative Abundance
SK1209 in CH3CN
OTMS
Product Collected from Attempted Synthesis of 2
Likely TMS -Protected 3-Butyn-3-ol
ASAP-MS
C
91.0037
126.9053
158.9120
203.8693
215.8380
294.8003
380.7150
407.0316
481.0586
528.9900
537.9903
544.0087
626.9230
702.4454
742.7179
m/z
04 #76 RT: 0.22 AV: 1 NL: 3.26E8
T: FTMS - p ESI d Full ms2 114.9365@hcd35.00 [50.0000-135.0000]
114.9365
52.0421
56.8139
67.7595
70.3537
83.8874
87.4520
104.9990
115.9398
m/z

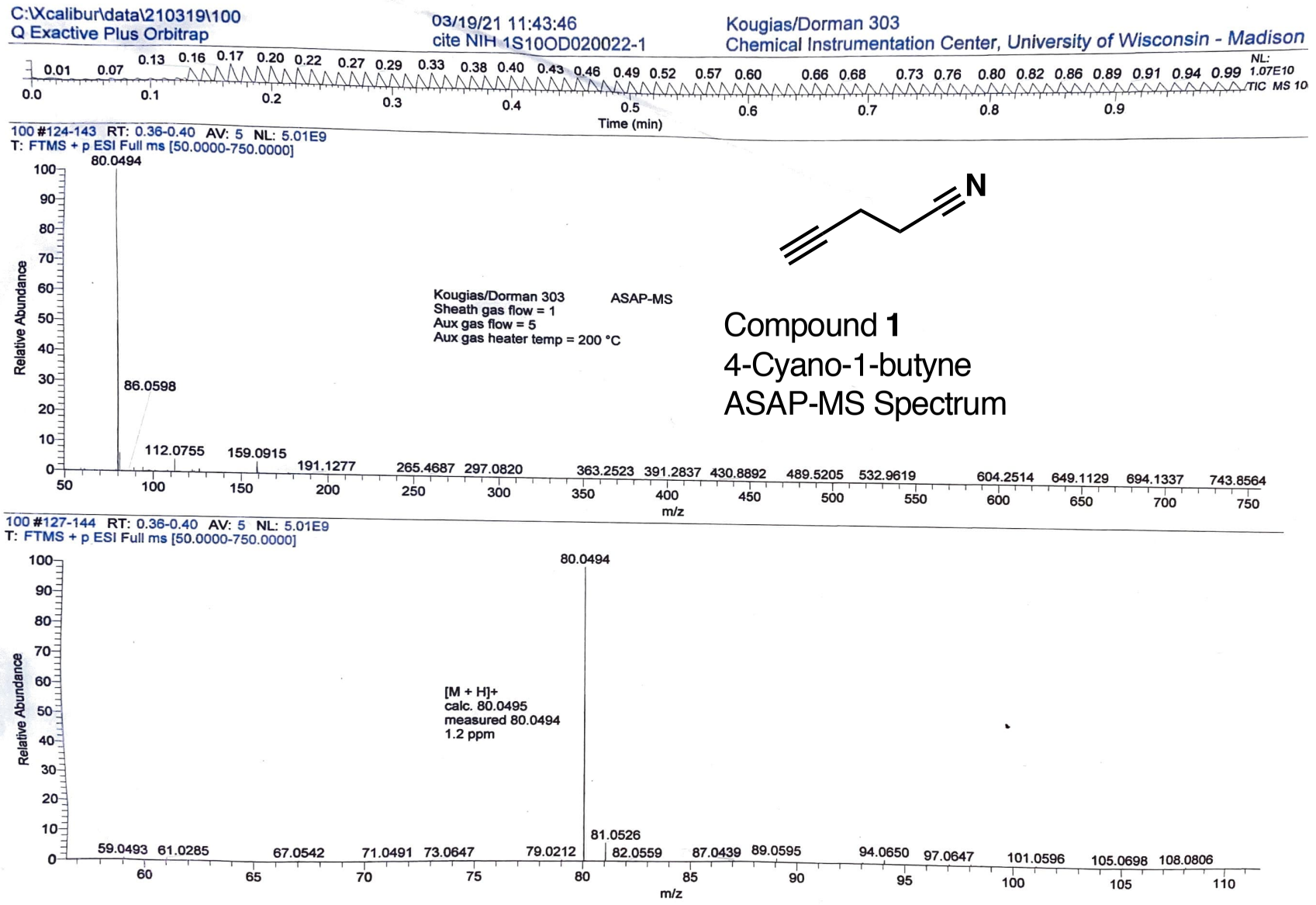

Compound 1
4-Cyano-1-butyne
1H-NMR, 400 MHz
CDCl3
N
2.14
2.15
2.16
2.52
2.54
2.55
2.56
2.57
2.58
2.60
2.61
858.3
860.7
863.2
1010.3
1014.5
1017.3
1023.7
1025.5
1028.6
1032.4
1038.8
1043.1
4.10
1.00
f1 (ppm)

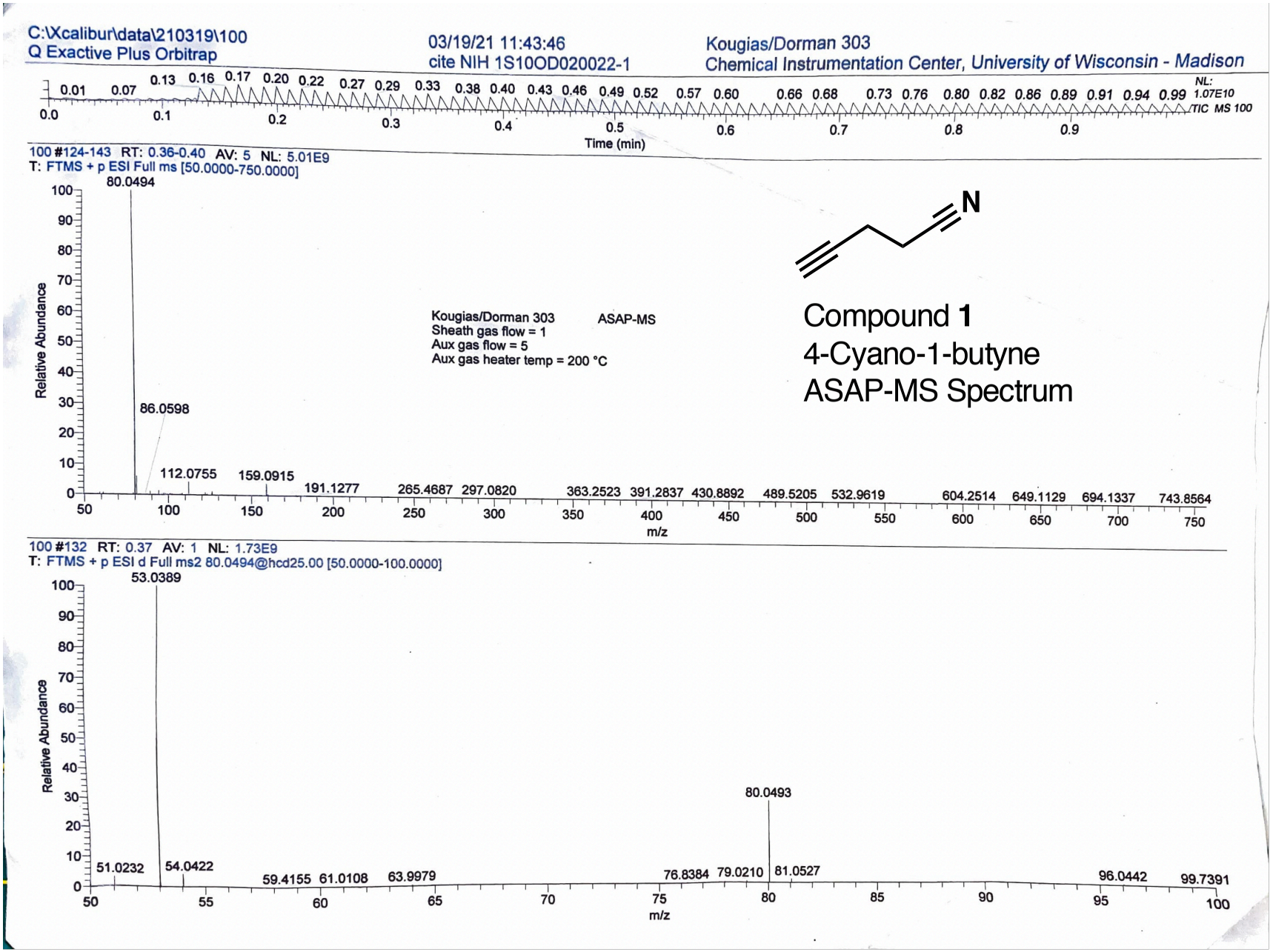


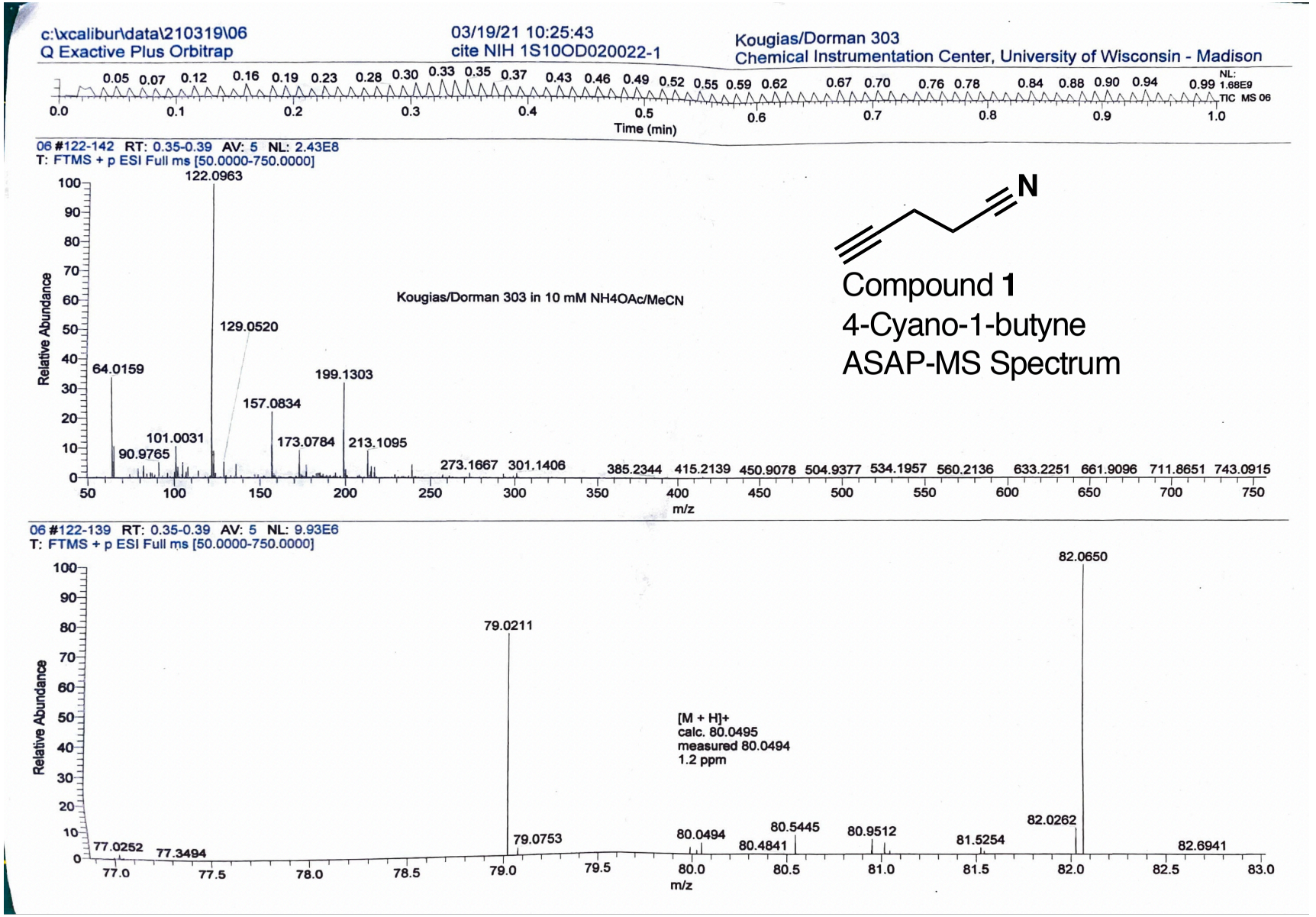
Compound **1**
4-Cyano-1-butyne
$^{13}C\{^{1}H\}$-NMR, 100 MHz
$CDCl_3$




Compound 1
4-Cyano-1-butyne
ATR-IR Spectrum
N
BRUKER
Transmittance [%]
100
90
80
70
60
50
40
30
Wavenumber cm-1
4000
3500
3000
2500
2000
1500
1000
500
3290.81
2935.76
2249.96
1431.47
1330.97
1229.04
1002.28
816.74
645.04
591.79
483.68
453.98


C:\Xcalibur\data\210319\100
Q Exactive Plus Orbitrap
03/19/21 11:43:46
cite NIH 1S10OD020022-1
Kougias/Dorman 303
Chemical Instrumentation Center, University of Wisconsin - Madison
Time (min)
NL: 1.07E10 TIC MS 10
100 #124-143 RT: 0.36-0.40 AV: 5 NL: 5.01E9
T: FTMS + p ESI Full ms [50.0000-750.0000]
80.0494
86.0598
112.0755
159.0915
191.1277
265.4687
297.0820
363.2523
391.2837
430.8892
489.5205
532.9619
604.2514
649.1129
694.1337
743.8564
Relative Abundance
m/z
Kougias/Dorman 303
Sheath gas flow = 1
Aux gas flow = 5
Aux gas heater temp = 200 °C
ASAP-MS
N
Compound 1
4-Cyano-1-butyne
ASAP-MS Spectrum
100 #127-144 RT: 0.36-0.40 AV: 5 NL: 5.01E9
T: FTMS + p ESI Full ms [50.0000-750.0000]
80.0494
[M + H]+
calc. 80.0495
measured 80.0494
1.2 ppm
59.0493
61.0285
67.0542
71.0491
73.0647
79.0212
81.0526
82.0559
87.0439
89.0595
94.0650
97.0647
101.0596
105.0698
108.0806
Relative Abundance
m/z


C:\Xcalibur\data\210319\100
Q Exactive Plus Orbitrap
03/19/21 11:43:46
cite NIH 1S10OD020022-1
Kougias/Dorman 303
Chemical Instrumentation Center, University of Wisconsin - Madison
NL: 1.07E10 TIC MS 100
Time (min)
100 #124-143 RT: 0.36-0.40 AV: 5 NL: 5.01E9
T: FTMS + p ESI Full ms [50.0000-750.0000]
Relative Abundance
m/z
Kougias/Dorman 303 ASAP-MS
Sheath gas flow = 1
Aux gas flow = 5
Aux gas heater temp = 200 °C
Compound 1
4-Cyano-1-butyne
ASAP-MS Spectrum
100 #132 RT: 0.37 AV: 1 NL: 1.73E9
T: FTMS + p ESI d Full ms2 80.0494@hcd25.00 [50.0000-100.0000]
Relative Abundance
m/z


c:\xcalibur\data\210319\06
Q Exactive Plus Orbitrap
03/19/21 10:25:43
cite NIH 1S10OD020022-1
Kougias/Dorman 303
Chemical Instrumentation Center, University of Wisconsin - Madison
Time (min)
NL: 1.68E9 TIC MS 06
06 #122-142 RT: 0.35-0.39 AV: 5 NL: 2.43E8
T: FTMS + p ESI Full ms [50.0000-750.0000]
Relative Abundance
m/z
Kougias/Dorman 303 in 10 mM NH4OAc/MeCN
122.0963
129.0520
64.0159
199.1303
157.0834
101.0031
90.9765
173.0784
213.1095
273.1667
301.1406
385.2344
415.2139
450.9078
504.9377
534.1957
560.2136
633.2251
661.9096
711.8651
743.0915
N
Compound 1
4-Cyano-1-butyne
ASAP-MS Spectrum
06 #122-139 RT: 0.35-0.39 AV: 5 NL: 9.93E6
T: FTMS + p ESI Full ms [50.0000-750.0000]
82.0650
79.0211
[M + H]+
calc. 80.0495
measured 80.0494
1.2 ppm
77.0252
77.3494
79.0753
80.0494
80.4841
80.5445
80.9512
81.5254
82.0262
82.6941

Chapter 4: Synthesis of Isotopically – Labeled Heterocyclic Molecules for Detailed Equilibrium Structure Determinations
"Heavy Heterocycles"

Some content contained in this section has been submitted and accepted for publication. Contributions to the content in this section have been made by Vanessa Orr, Maria Zdanovskaia, Hayley Bunn, Madison Fellows, Brian J. Esselman, and Aatmik Patel.

Introduction

Rotational spectroscopy is an indispensable technique for understanding the chemistry of the cosmos. Characterization of a molecular candidate through the assignment of transitions in its rotational spectrum yields the critical data, a proverbial "fingerprint", used by radioastronomers to search and identify such species in the cosmos. Rotational spectroscopy is also an extremely powerful technique used in highly precise structural characterizations of gas-phase molecules through the determination of rotational constants. Analysis of rotational spectra yields the semi-experimental equilibrium (r_e^{SE}) structure, which combines experimentally determined rotational constants obtained from multiple isotopologues with computational corrections that account for electron mass, vibrational-rotational interactions, and relativistic effects. Semi-experimental structure (r_e^{SE})[1-5] determinations were pioneered in 1978[5] and have been applied to various heterocycles.[1-4, 6-9] Recent works on heteroaromatic compounds[10-13] have set a new standard for the determination of accurate and precise semi-experimental equilibrium (r_e^{SE}) structures. The methodology employs well-determined rotational constants for as many isotopologues as practical, but far exceeding the minimal requirement, and CCSD(T) corrections to determine the semi-experimental equilibrium structure. This method results in accurate structural parameters where typical 2σ uncertainty is less than 0.0005 Å for bond distances and 0.05° for angles.

The initial step in a semi-experimental equilibrium (r_e^{SE}) structure determination involves the careful least-squares fitting of the ground state isotopologues visible in the experimentally collected rotational spectrum. The number of individual isotopologues that can be least-squares fit contributes to the accuracy of the resulting r_e^{SE} structure. Although numerous isotopologues may be theoretically possible for a given molecular structure, successful application of a least squares fit depends on the strength of the representative signals in the rotational spectrum. Isotopologues

composed of isotopes that are low in natural abundance may fall below detectable limits or yield fits with greater error.

The McMahon|Woods group has been interested in rotational spectroscopy and detailed structural determination of aromatic/heterocyclic species for some time.[10-12, 14-19] Our group has a powerful combination of specialized skills (computational chemists, physical organic chemists, rotational spectroscopists, synthetic chemists) that permit the highly-precise determination of structural parameters. Unique amongst groups studying molecular structure though rotational spectroscopy, our group possesses the ability to synthetically produce authentic samples of specific organic molecules tailored for rotational spectroscopy studies. When applied in detailed structural determination projects, the synthesis of isotopically-tagged organic species provides a massive advantage by permitting the measurement, analysis and inclusion of data from a large library of isotopologues that could not be analyzed or detected in samples consisting of natural isotopic abundance. The synthesis of isotopologues, however, is only one component of structural determination investigations: i) chemical synthesis and purification of a family of isotopologues, ii) measurement, assignment, and fitting of the high-resolution rotational spectrum of each isotopologue, iii) computationally demanding calculations involving electronic structure, vibration-rotation coupling, corrections for electron mass distribution, and iv) theoretical methods for providing a "best theoretical estimate" (BTE) of the molecular structure. Integration of this data affords a highly precise semi-experimental structure (r_e^{SE}) for the analyte molecule.

Aside from structural characterization, the synthesis of isotopically-labelled organic molecules is a highly important component of drug development,[20-21] radiopharmaceuticals,[22] pharmokinetic assays,[23-24] and metabolic compound tracing within living systems. Significant focus has been placed on isotopic labelling of heterocyclic molecules.[25-28] Because of its broad

applications and importance, several specialized techniques and methodologies have been developed specifically for the isotopic enrichment of organic species.

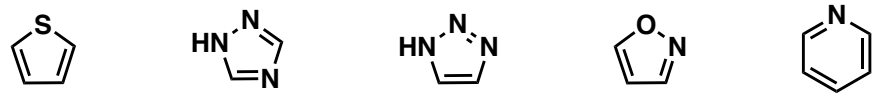


Figure 4.1. Aromatic heterocycles described in this chapter for isotopologue synthesis and detailed structural determination: thiophene, 1,2,4-triazole, 1,2,3-triazole, isoxazole, and pyridine.

This thesis chapter describes part of the research in our group regarding the synthesis of isotopically-labelled aromatic heterocycles for spectroscopic evaluation and precise structural characterization. Specifically, this chapter covers methods and research regarding the deuterium-tagging of five heterocyclic organic compounds: thiophene, 1,2,4-triazole, 1,2,3-triazole, isoxazole, and pyridine (Figure 4.1). Background regarding previous spectroscopic studies, and our spectroscopic contributions are discussed to provide context. Although the production of isotopologues has produced data included in multiple published works describing the structure of the species shown in Figure 4.1,[13, 29] several additional studies concerning the spectroscopy of these molecules are currently in progress within our group.

Background.

Thiophene.[13]

The five-membered, aromatic ring of thiophene (C_4H_4S, C_{2v}) is a fundamental molecular structural moiety in organic chemistry and is prevalent in pharmaceuticals[30] and organic electronic materials.[31-32] Thiophenes can be found naturally on Earth and have been detected on Mars.[33-34] Thiophene itself has been proposed to be present in the interstellar medium,[35] and unsaturated

carbon-chain molecules containing sulfur have been detected.[36-37] The rotational and vibrational spectroscopy of thiophene have been of interest for over a century. The first infrared absorption spectrum was reported in 1905 by Coblentz,[38] and other Raman and infrared studies were reported in the 1930's and 40's.[39-42] In 1965, a low-resolution infrared study of liquid and vapor phase thiophene and all of its deuterio isotopologues (mono- through tetra-deuterio, except [2,4-^{2}H]-thiophene) was published including assignment of their fundamental vibrations.[43] The vibrational assignments were later reaffirmed,[44] and the rotationally resolved IR spectrum of the ν_{13} band was reported by G. Winnewisser and co-workers.[45] The rotationally resolved IR spectrum has subsequently been analyzed for ν_{14}, ν_8, ν_7 (400 – 750 cm^{-1}),[46-47] and ν_{13}, ν_7, ν_6, ν_5, and ν_{19} (600 – 1200 cm^{-1}).[48] These studies provided the rotational and centrifugal distortion constants for each of these vibrationally excited states, along with their precise vibrational frequencies. More recently, Raman and resonance Raman spectra of thiophene, neat and in solution (cyclohexane, dimethyl sulfoxide, and methanol), have also been reported.[49-50] Analysis of the fundamental, combination, and overtone vibrational states using rotational spectroscopy is on-going and will be the subject of a future work.

The dipole moment of thiophene (0.55 ± 0.01 D)[51] permits its observation by rotational spectroscopy. Bak *et al*. provided the rotational constants for the normal isotopologue of thiophene, four deuterated isotopologues,[52] the ^{34}S, and the two ^{13}C isotopologues based upon microwave spectral data from 12 – 30 GHz.[53] Using Kraitchman's equations,[54] they determined the first substitution structure of thiophene (r_s) from the parent and five mono-substituted isotopologues.[53] This early microwave data was combined with electron diffraction and liquid-crystal NMR data to determine the r_α structure.[55] Later the microwave, electron diffraction, and vibrational spectroscopy were combined with computational methods to find a mixed-method,

semi-experimental equilibrium structure (r_e^{SE}).[56] The work of Bak *et al.*[52-53] was used to determine a subsequent semi-experimental equilibrium structure (r_e^{SE}) with corrections for vibration-rotation interaction constants and the electron-mass distributions from DFT methods.[6, 57] Though not utilized in the previous thiophene structure determinations, additional rotational transitions of the normal isotopologue have been reported in later works,[58-61] as well as transitions for the ^{33}S and ^{34}S isotopologues.[61]

Recently, a very satisfying level of agreement was achieved for pyrimidine between the semi-experimental equilibrium (r_e^{SE}) parameters and the highest practical level of theoretical calculation available – differences no more than 0.0004 Å in bond distances and no more than 0.01° in the bond angles.[10] That result raises the question of whether or not such a level of agreement is possible in parallel treatments of other similarly sized molecules. While we have begun the study of similar species consisting of carbon, nitrogen, and hydrogen, we have also chosen to explore the impact of including third-row atoms on this methodology. Heavier atoms inherently present additional challenges regarding the computational level of theory and basis set, but also may impact the ability of the theory to adequately treat the corrections to the rotational constants. The present study of thiophene was undertaken with the primary goal of attempting to answer that question for a prototypical sulfur-containing aromatic ring. The method steps beyond the traditional Kraitchman analysis of structure determination by single-atom isotopic substitution and validates the ability of modern experimental and computational methods to establish the structure of an organic heterocyclic molecule containing a third-row element.

The Triazoles: 1*H*-1,2,4-Triazole, 1*H*-1,2,3-Triazole and their Respective Tautomers.

Triazoles ($C_2H_3N_3$) are a family of five-membered nitrogenous heterocycles that are highly

prevalent species in the photochemical, materials, pharmaceutical[62-65] and agrochemical industries, and have multiple applications due to their antifungal,[66-69] antibacterial,[70] and antiviral[71] properties. In total, four individual isomers of triazole exist (Figure 4.2), and are divided into two sets of regioisomers (1,2,4 triazole and 1,2,3-triazole) that differ in the arrangement of the nitrogen and carbon atoms in the aromatic ring structure. Each regioisomer consists of an equilibrium mixture of two tautomers that differ by which nitrogen atom is bound to hydrogen.

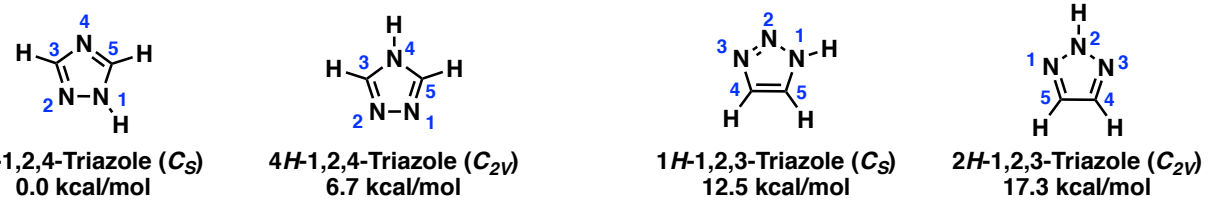


Figure 4.2. Tautomers of 1,2,3- and 1,2,4-Triazole with Conventional Numbering of Ring Atoms and Relative Energies Calculated at B3LYP/6311G**.

1,2,4-Triazole.[72]

The 1,2,4-triazole tautomers, where one nitrogen atom is separated from the other two by interstitial carbon atoms, are more stable than the 1,2,3- triazole tautomers where all three nitrogen atoms are adjacent. 1,2,4-Triazole exists as 1*H*-1,2,4-triazole (C_s) and 4*H*-1,2,4-triazole (C_{2v}), where the asymmetric 1*H*-tautomer is the energetically-favored isomer by 6.7 kcal/mol.[73] All previous spectroscopic studies of 1,2,4-triazole have only reported detection of the more stable 1*H*-tautomer. The first gas-phase microwave study of 1,2,4-triazole was reported in 1975 by Bolton *et al*.,[74-75] including analysis of the structure and nuclear quadrupole coupling. Low resolution gas-phase infrared[76-77] and Raman[77] spectra have been reported between approximately 500 and 4000 cm for 1*H*-1,2,4-triazole, providing reliable estimates of the vibrational band origins. The structure of 1,2,4-triazole has been the focus of multiple studies involving X-ray crystallography,[78-79] microwave spectroscopy,[74] electron diffraction,[80] and computational

methods.[81-83] The rotational constants reported in the gas-phase microwave work were only determined for three isotopologues,[74] which did not provide sufficient information to adequately determine its structural parameters. 1*H*-1,2,4-Triazole has 13 independent structural parameters, which require a minimum of 7 isotopologues to provide a sufficient quantity of independent moments of inertia for a comprehensive structure determination.[72] The structure was further analyzed by use of electron diffraction,[80] resulting in additional experimentally determined structural parameters to a 3σ uncertainty of 0.004 - 0.01 Å for bond distances and 0.5 – 1.3º for bond angles. In that work, not all parameters could be satisfactorily determined, so several of them had to be constrained to computational predictions or values from similar molecules.

In our work, we have determined a precise semi-experimental structure (r_e^{SE}) for 1*H*-1,2,4-triazole that compares quite well to its CCSD(T) equilibrium structure (r_e) and previous studies. In order to more accurately determine the structure of 1*H*-1,2,4-triazole and to provide accurate frequencies to guide observational studies, the millimeter/submillimeter spectrum has been collected from 70-700 GHz. The experiment, spectral analysis, and structural determination are presented here. The extension of the spectral range observed in previous work has allowed for the further refinement of rotational constants for three previously reported isotopologues[74] and spectroscopic constants for an additional 23 isotopologues.[72] A semi-experimental structure (r_e^{SE}) has been determined using 50 independent moments of inertia (excluding one isotopologue, *vide infra*) including isotopic substitution of all atoms in multiple isotopologues.

The transition frequencies and spectroscopic constants reported in this work can be reliably used to predict the spectrum up to 1 THz and used to guide the search of 1*H*-1,2,4-triazole in Titan's atmosphere and in the interstellar medium (ISM). The experimental characterization of Titan aerosols investigating the formation of tholins by electric discharge resulted in the detection

of multiple organic nitrogen-containing species, including 1*H*-1,2,4-triazole.[84] The aerosols in this study were composed of 95% N_2 and 5% CH_4, to match the atmosphere of Titan. Ultraviolet photo processing of Titans atmosphere primarily results in HCN and more complex nitrogen-containing species, such as methylcyanoacetylene (CH_3C_3N) that was recently reported using the ALMA (Atacama Large Millimeter/submillimeter Array) telescope.[85] The formation of ring-containing species, such as 1,2,4-triazole, have been predicted to form known Titan atmospheric components *via* formation of HCN and NH_3.[86-89] Thus, 1*H*-1,2,4-triazole is a prime target for detection in the atmosphere of Titan and other extraterrestrial environments that are rich in nitrogen and carbon.

1*H*-1,2,3-Triazole.[29]

1*H*- and 2*H*-1,2,3-Triazole ($C_2H_3N_3$, Figure 4.2) are near-oblate, asymmetric rotors (κ = 0.94, C_s and 0.82 C_{2v}, respectively). The tautomers, as well as a few of their isotopologues, have been studied using ultraviolet,[90] infrared (IR),[77, 90-92] Raman,[77] and microwave[75, 93-95] spectroscopy. The 1*H*/2*H* tautomerism and equilibrium has received a fair amount of interest.[81, 93, 95-101] Both of the tautomers are present in the solid,[98] liquid,[81, 92, 97, 99] and gas[93, 96-97, 99-101] phases. Although 1*H*-1,2,3-triazole is preferentially stabilized in polar solvents,[81] the 2*H*-1,2,3-triazole tautomer is estimated to be more stable by *ca*. 3.5 – 4.5 kcal/mol in the gas phase.[93, 96-97, 99] Despite the greater abundance of the 2*H* tautomer in the gas phase, its smaller dipole moment (μ_b = 0.10 D) relative to that of the 1*H* tautomer (μ_a = 4.2 D, μ_b = 0.77 D) results in both molecules being observable in the gas-phase by millimeter-wave spectroscopy at room temperature.

While the structures of the triazoles have been computed at a variety of levels of theory[77, 102-103] and there has been a crystal-structure determination,[98] there has been only a single attempt to determine a gas-phase, equilibrium structure of 1,2,3-triazole. Begtrup *et al.*[93] used electron

diffraction and microwave spectroscopy data to approximate an equilibrium structure for 2*H*-1,2,3-triazole. That structure determination, however, used microwave data from only three isotopologues. To date, there have been no attempts to determine the gas-phase structure of 1*H*-1,2,3-triazole. Following the pioneering work of Pulay, Meyer, and Boggs,[5] semi-experimental structure (r_e^{SE}) determination has evolved into a powerful method for establishing gas-phase molecular structure.[10, 104] Semi-experimental structures for a variety of small heterocyclic compounds have been reported using a density functional theory version of the method.[105] Recently, we used coupled-cluster computations to achieve high-accuracy and high-precision semi-experimental equilibrium structure (r_e^{SE}) determinations of pyrimidine,[10] pyridazine,[11] thiophene,[13] thiazole,[12] and benzene.[18] We therefore sought to determine semi-experimental equilibrium structures for the 1,2,3-triazoles.

In our recent studies of structures of the six-membered ring molecules (which include only first- and second-row elements), the r_e^{SE} structures displayed exceptional agreement with the purely computational, "best theoretical estimate" (BTE) structures. Structures of two sulfur-containing, five-membered ring molecules, however, had BTE parameters that did not uniformly fall within the r_e^{SE} parameter uncertainties. Those discrepancies were plausibly ascribed to the proximity of certain atoms to principal axes,[12-13, 106] combined with the inability to shift those atoms from the principal axes upon isotopic substitution (because the heavy sulfur atom essentially set the axes' orientation). 2*H*-1,2,3-Triazole offers the possibility to examine the above assertion – one nitrogen atom and one hydrogen atom lie directly on the *a*-axis, but the principal axes are easily rotated upon isotopic substitution. The ability to obtain well-determined parameters involving the on-axis atoms would support the idea that the near-axis sulfur atom was the culprit in previously examined five-membered ring structures.

The precise determination of spectroscopic constants of the 1,2,3-triazoles achieved in the current study – particularly the determination of the centrifugal distortion constants – enables accurate prediction of the high-intensity transitions across a large range of frequencies for possible search in the interstellar medium (ISM) or in other harsh environments, such as Saturn's moon, Titan. There is considerable current interest in identifying aromatic molecules[107] and nitrogen heterocycles[108-109] in these environments, and such studies may be particularly relevant to the nitrogen-rich atmosphere of Titan, where the structurally related molecule, 1*H*-1,2,4-triazole, has been suggested as a likely tholin component.[84, 110] Although these molecules are not believed to be naturally occurring on Earth, they have been found to act as effective mimics in a variety of biological applications[111-112] with beneficial properties, such that 1,2,3-triazole-containing species are now widely targeted pharmaceuticals.[113] In terms of organic chemistry, 1*H*-1,2,3-triazole is the stable product of the Huisgen cycloaddition (a 1,3-dipolar cycloaddition) between hydrazoic acid and acetylene.[114] This is a quintessential example of "Click chemistry" where two small molecules generate an aromatic product in a highly exothermic reaction.[115-116] Acetylene has been detected in the ISM[117-118] and on Titan.[119] Amberger *et al.* assigned the rotational spectrum of hydrazoic acid,[120] allowing for its search and potential identification. The detection (or not) of these molecules could be informative regarding the chemistry in various environments.

Isoxazole

Isoxazole (C_3H_3NO, C_s) is a five-membered azole species that exhibits biological activity and is of interest to the radioastronomical community. A unique structural feature observed in isoxazole is the relatively weak N—O bond that is part of an aromatic ring, and that most of the reactivity observed with isoxazole involves the cleavage of the N—O bond. The isoxazole structural motif occurs naturally in plant based insecticides and pigments, and is regarded as a

potent pharmacophore with appearances in numerous pharmaceuticals[121] and agrochemicals.[122] In terms of astrochemical significance, isoxazole derivatives such as 2- and 3-aminoisoxazole have attracted significant interest as a prebiotic precursor of ribonucleotides, and has led to the spectroscopic characterization of such compounds to facilitate radioastronomical searches.[123-125] Ultraviolet photolysis of matrix-isolated isoxazole has been shown to yield ketene and hydrogen cyanide, both of which have been detected in the ISM.[126]

Isoxazole and some of its isotopologues have been studied using solution- and gas-phase infrared (IR) and Raman spectroscopy, leading to the vibrational assignment of isoxazole and its trideuterio isotopologue.[95, 127-132] The rotational spectrum of isoxazole has been studied using nuclear quadrupole resonance (NQR),[133-134] and microwave spectroscopy.[58, 135-137] The rotational spectrum of complexes of isoxazole with water,[138-139] carbon monoxide,[140] and argon[141] have also been studied by microwave spectroscopy. The electronic and molecular structure of isoxazole have been the subject of multiple studies involving microwave spectroscopy[142-143] and computational methods.[144-146] Previous reports of the microwave spectroscopy were only performed in the low-frequency region. To assist in the radioastronomical search for isoxazole, it is desirable to collect its rotational spectrum in higher frequencies to match those used by radiotelescope facilities.

Pyridine[147-148]

Pyridine is an oblate, asymmetric top ($\kappa = 0.85$). Unsurprisingly, given the importance of pyridine (C_5H_5N, C_{2v}), previous work on the molecule is fairly extensive[58, 149-162] – from the first microwave study in 1953 by Bak *et al*. to the more recent 2005 works of Ye *et al.* in the millimeter and submillimeter region and the high-resolution infrared (IR) study by Albert *et al*. in 2007. Ye *et al*. were able to determine all of the quartic centrifugal distortion constants and even several of the sextic terms.[149] To improve the accuracy of transition frequencies predicted on the basis of

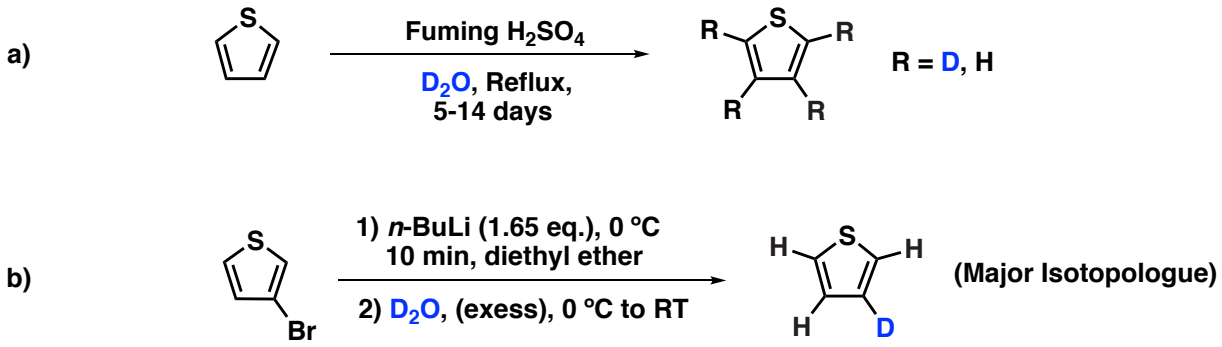
experimentally measured spectroscopic constants (into frequency regions that may not have been studied, but are used by various radiotelescopes), it is beneficial to complete the set of sextic constants by either determining them using additional spectroscopic data or by holding those that cannot be constant to computed values (an option that has become available only more recently). Ye *et al.* also examined several vibrational states of pyridine, although some uncertainty remained in the assignments. Four structure determinations have also been carried out for the molecule,[57, 153, 163-164] including three semi-experimental equilibrium (r_e^{SE}) structures. The most recent of these works, however, only used the minimal set of isotopologues (substituting each unique atom one time),[57] while the other used 10 isotopologues.[163] Recent analysis on the effect of number of isotopologues used for r_e^{SE} determination has shown that some molecules require more than the minimal set of isotopologues to accurately determine the structural parameters and it is not known *a priori* how many isotopologues are necessary.[10-13, 18] Combined with the fact that some of the spectroscopic work used in the previous structure determinations had been completed some time ago, we expected that we could improve the quality of the experimental spectroscopic constants used in the r_e^{SE} determination, as well as the number of isotopologues. Additionally, we expected to improve both the computational corrections and best theoretical estimate of the equilibrium structure by using higher levels of theory than those utilized previously (B3LYP and CCSD(T)/CBS+CV).

Results and Discussion

Thiophene[13, 165]

The synthetic approach of deuterium enrichment, *via* isotopic exchange of an existing heterocycle species, is ideal for rotational spectroscopy, enabling the broadband spectra of all isotopologues to be obtained in a single experiment. The characteristics of thiophene's rotational spectrum cause the transitions of each isotopologue to be relatively distinct, thereby minimizing problems with the identification and assignment of transitions because of overlapping signals from multiple species. The ability to prepare and measure a single sample containing multiple species represents a dramatic savings in time and effort, relative to an alternative approach involving the chemical synthesis and measurement of each isotopologue, individually. Deuterium-containing isotopologues of thiophene were prepared in a manner analogous to the incorporation of deuterium in other 5-membered heteroaromatic ring compounds and previous efforts on thiophene itself.[166-169] The acid-catalyzed reaction involved refluxing thiophene, D_2O, and fuming sulfuric acid at 100 °C for five days (Scheme 4.1a).

Scheme 4.1. Synthesis of Deuterium-Containing Isotopologues of Thiophene.



The duration of reflux may be varied to control the level of deuterium-hydrogen exchange. The five-day reaction time generated a mixture containing all nine of the possible deuterium-

containing isotopologues of the normal isotopologue of thiophene. To shift the distribution of isotopologues toward those with a higher level of deuterium incorporation, the same reaction was conducted with refluxing extended over two weeks, with the addition of more H_2SO_4 and D_2O after seven days. This procedure yielded a small sample consisting of mostly tetra-deuterio thiophene, which provided transitions for the [2,3,4,5-^{2}H, ^{34}S] isotopologue. While the extended time for reflux and replenishing the deuterium source did increase the amount of deuterium incorporation, this method is not sufficient for obtaining a sample that has only the tetra-deuterio isotopologue present.

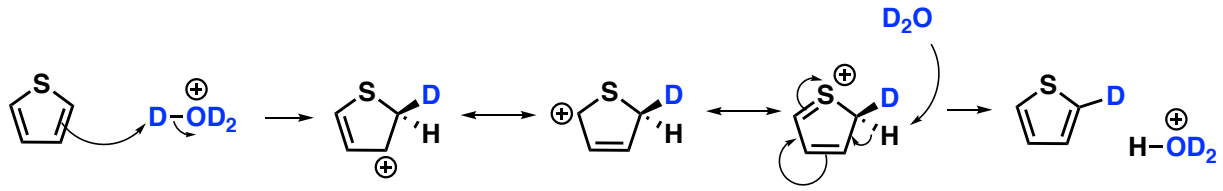


Figure 4.3. Deuteration of Thiophene *via* Deuteration/Deprotonation at the C2 Site.

The deuterium-hydrogen exchange reactions proceed *via* deuteriation / deprotonation at each carbon atom in the ring (Figure 4.3). The preference for D/H exchange at C2 over C3 is consistent with the relative energies of the thiolium cation intermediates (Figure 4.4). The 9.1 kcal/mol energy difference (B3LYP/6-311G+(2d,p)+ZPVE) is rationalized by delocalization of positive charge over more atoms *via* π conjugation when the H/D$^+$ is attached to C2, as is shown in the accompanying resonance structures. A similar stabilization is not afforded when the H/D$^+$ is bonded to C3. This interpretation is drawn from the highest-contributing resonance structures from the Natural Resonance Theory analysis and the Natural Population Analysis charges of each thiolium displayed in Figure 4.4. The differential rate of exchange leads to the dominance of [2-^{2}H]-, [2,5-^{2}H]-, and [2,3,5-^{2}H]-thiophene in the rotational spectrum of the deuterium-enriched

sample (after 5 days reflux), while the lowest-abundance thiophene-d_x species in the spectrum (excluding heavy-atom sulfur or carbon isotopologues) is [3,4-^{2}H]-thiophene.

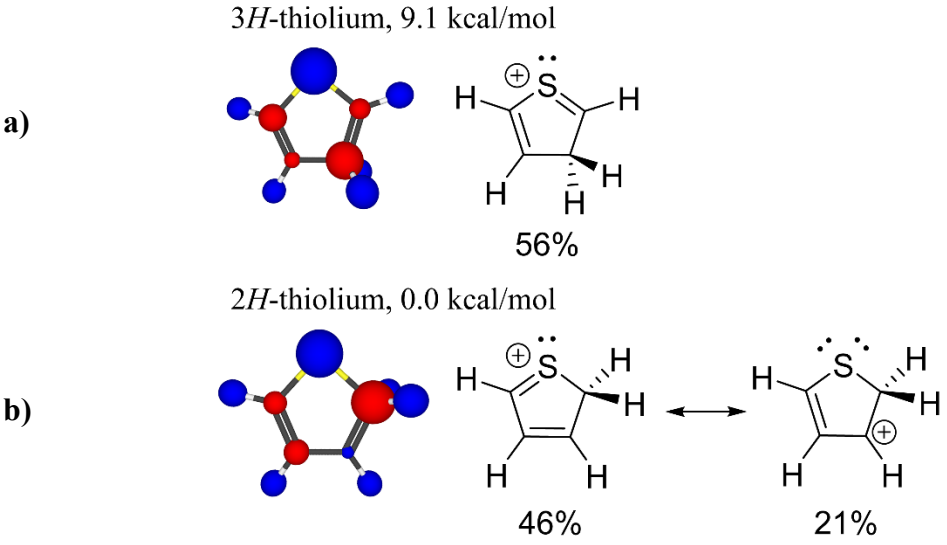


Figure 4.4. 3*H*-thiolium (a) and 2*H*-Thiolium (b) with their relative energies (B3LYP/6-311G+(2d,p)+ZPVE), the Natural Population Analysis (NPA) charges as spheres whose size correspond to the magnitude of the local charge (blue for positive and red for negative), and relevant resonance structures from the Natural Resonance Theory analysis.

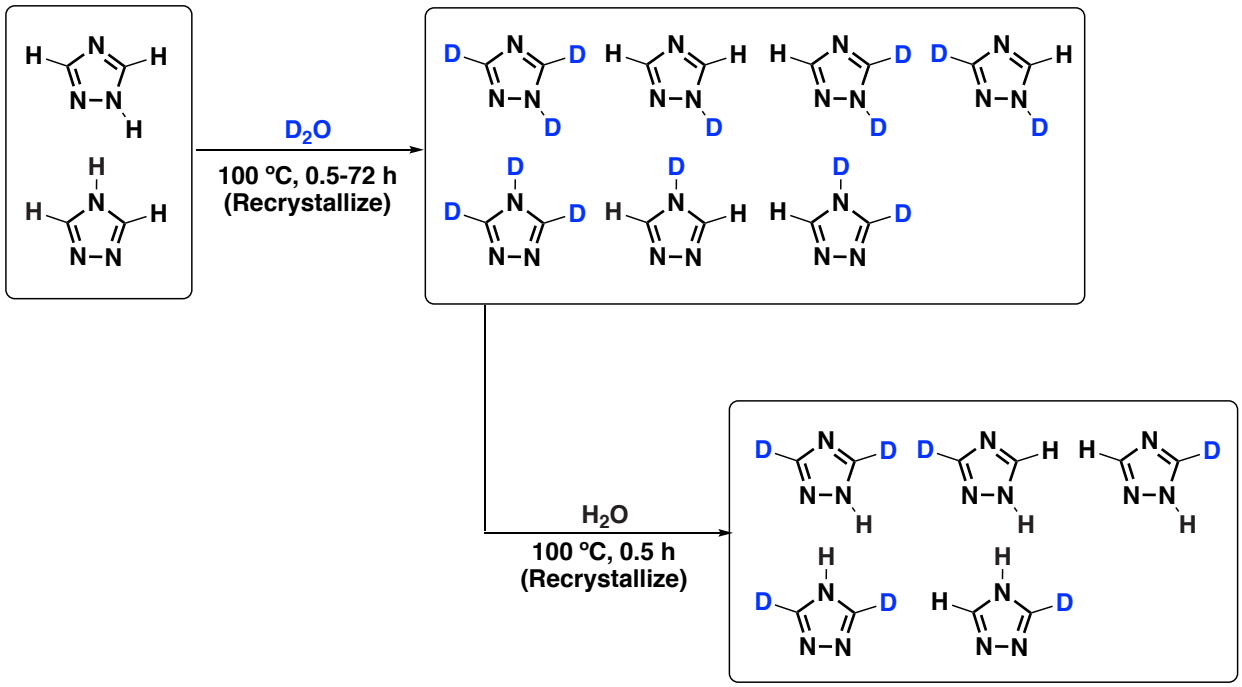
An alternate synthetic route was adapted to generate [3-^{2}H]-thiophene,[170] because that isotopologue cannot be prepared in high abundance using acid-catalyzed H/D exchange. A sample of [3-^{2}H]-thiophene was generated from 3-bromothiophene by lithium-halogen exchange, followed by quenching with D_2O (Scheme 4.1b). The resultant sample was primarily [3-^{2}H]-thiophene, but the reaction did contain some [2-^{2}H]-thiophene, along with other combinations of di- and tri-deuterio isotopologues (though in substantially smaller amounts than generated by acid-catalyzed H/D exchange). The rearranged and poly-deuteriated thiophenes presumably result from base-catalyzed H/D exchange in the strongly basic conditions. The reaction described in Scheme 1b allowed for the assignment of more transitions for the [3-^{2}H] isotopologue and permitted the observation of sulfur and carbon heavy-atom isotopologues of [3-^{2}H] thiophene. We have

extended the number of isotopologues for which rotational constants are available to 26 isotopologues. Of these, 24 were included in the determination of the semi-experimental equilibrium structure (r_e^{SE}) published by our group. We have systematically investigated the extent to which additional isotopologues are valuable in reducing the statistical errors of the r_e^{SE} structural parameters.

1*H*-1,2,4-Triazole

Deuteration of both the nitrogen and carbon atoms of 1*H*-1,2,4-triazole is remarkably facile compared to other aromatic heterocycles, e.g., pyridazine, pyrimidine, thiazole, due to its amphoteric nature. The pK_{a_1} of 1,2,4-triazolium (N-protonated 1,2,4-triazole) is 2.45 and the pK_{a_2} of 1,2,4-triazole is 10.26.[171] The acidity and basicity of 1*H*-1,2,4-triazole allow easy exchange of the H-atoms with D_2O, even at moderate pHs. The exchange at the N-atom is most rapid, but exchange at both the C- and N-atoms can be observed by simple a recrystallization of 1,2,4-triazole in D_2O. It is presumed that exchange at the carbon atoms proceeds by an addition-elimination mechanism *via* a zwitterionic intermediate similar to that described for thiazole.[12, 172-173] The deuteration of 1*H*-1,2,4-triazole was performed using the methodology reported by Bolton *et al.* and Bougeard *et al.* (Scheme 4.2).[74, 76] Two separate deuteration trials were performed with different reaction durations to generate samples containing different levels of deuterium enrichment. Deuterated samples from each trial were recrystallized again in proteo-water (H_2O) to specifically access deuterated isotopologues of 1*H*-1,2,4-triazole protonated at the nitrogen site.

Scheme 4.2. Recrystallizations of 1,2,4-Triazole in D_2O/H_2O for Accessing all Deuterated Isotopologue Combinations.



Taking advantage of the differential rate of exchange between N—H and C—H and the choice of solvent (D_2O or H_2O), four different deuterium- enriched samples were prepared with different species as the main isotopologue. This allowed for the observation of all deuterated 1H - 1,2,4-triazoles as well as many of their ^{13}C- and ^{15}N-isotopologues in natural abundance. The spectral ranges collected for the deuterium-enriched samples were limited to 90 to 335 GHz for sample two and 225 GHz to 335 GHz for the remainder.

1*H*-1,2,3-Triazole

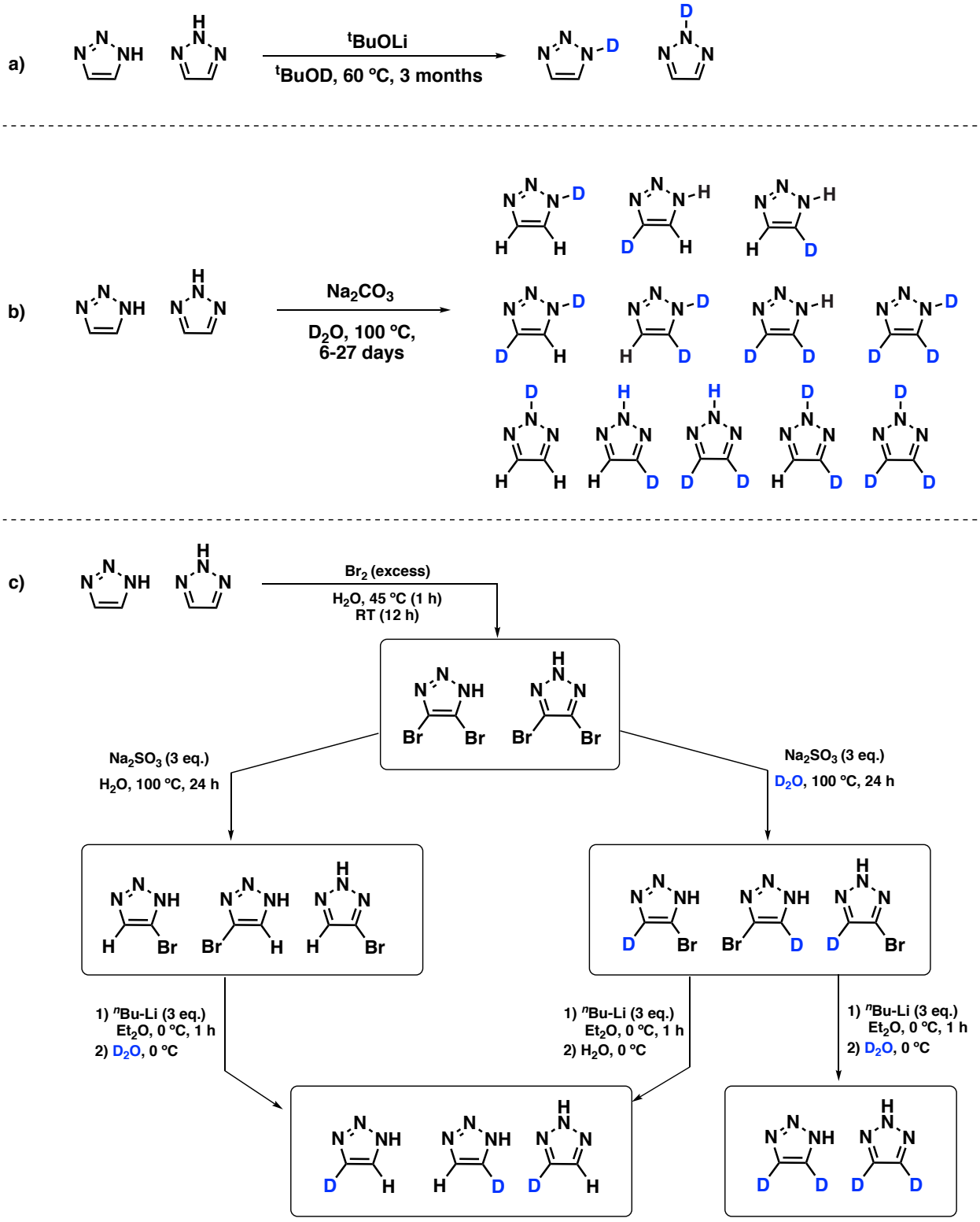
The preparation of deuterium-containing isotopologues of 1,2,3-triazole was not as straightforward as for thiophene, 1,2,4-triazole, pyridine, pyridazine[14] and pyrimidine.[10] H/D exchange using a strong base (*t*-BuOLi / *t*-BuOD), was attempted, but only produced a detectable quantity of only the *N*-deuteriated species (Scheme 4.3a). Alternate synthetic routes involving the

metalation of halogenated triazole species using Grignard or organolithium reagents were considered. The reaction sequence presented in Scheme 4.3b was developed and is comprised of three steps: bromination of 1,2,3-triazole, reductive monodehalogenation using Na_2SO_3 in H_2O or D_2O, and lithium-halogen exchange followed by quenching with H_2O or D_2O. Although the crude product was not as clean as that obtained by the procedure in Scheme 4.3c, this method afforded [4-^{2}H]-2*H*-1,2,3-triazole or [4,5-^{2}H]-2*H*-1,2,3-triazole in high abundance. This, in turn, enabled the detection of some [^{13}C] isotopologues of the deuterium-containing species. The third step of this sequence, involving treatment of bromo-triazole with excess *n*-BuLi followed by D_2O, does not lead to H/D exchange at nitrogen. Control experiments, in which unsubstituted triazole is subjected to similar reaction conditions, do not lead to recovery of triazole. This observation suggests that the dianion of triazole either does not form or undergoes decomposition. In the case of bromo-triazole, it is possible that rapid metal-halogen exchange precludes deprotonation at nitrogen. Although the apparent lack of exchange is not well understood, the identity of the species observed by rotational spectroscopy is unambiguous.

During the course of attempting to generate singly carbon-deuteriated 1,2,3-triazole using a set of steps similar to those in Scheme 4.3b, we were intrigued by the ability of Na_2SO_3 to perform reductive monodehalogenation of dibromotriazole under mild conditions, and were interested if complete dehalogenation could be achieved. We learned that subjection of dibromotriazole to inorganic weak bases, such as carbonate, resulted in exchange of both bromine and hydrogen/deuterium at the carbon atoms. The weak base-catalyzed exchange between hydrogen and deuterium was also active when no halogens were present on the triazole core. This observation led us to develop the reaction in Scheme 4.3c where deuterium exchange at each position of 1,2,3-triazole is achieved *via* subjection to sodium carbonate in D_2O. The crude product

obtained by this method was reasonably clean and the isotopic composition of the sample could be straightforwardly varied by changing the reaction time. This method ultimately provided every possible deuterium-containing isotopologue of 1*H*- and 2*H*-1,2,3-triazole, although some were observed in very small abundance. The other preparative methods were important in providing some of the isotopologues in higher abundance. The deuterium-enriched isotopologues synthesized using the methods presented in Scheme 4.3 were evaluated using millimeter-wave rotational spectroscopy in the 130 – 375 GHz frequency range. In total, the spectroscopic constants for thirteen 1*H*-1,2,3-triazole and sixteen 2*H*-1,2,3-triazole isotopologues were measured and included in the determination of the semi-experimental equilibrium structures (r_e^{SE}) published by our group.

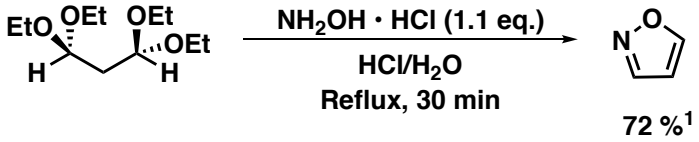
Scheme 4.3. Deuterium incorporation in 1*H*- and 2*H*-1,2,3-triazoles: (a) *N*-deuteriation by strong base, (b) C-deuteriation by weak base, (c) three-step sequence to achieve a high level of deuterium content at C-4 and C-5.



Isoxazole

Our initial approach for the synthesis of deuterium-enriched isoxazole isotopologues involved a series of reaction conditions that had been successfully used to deuterium-enrich other heterocyclic molecules. Several methods were employed unsuccessfully. Subjecting isoxazole to highly acidic or basic conditions in the presence of D_2O ultimately resulted in no deuterium enrichment or the decomposition of isoxazole itself. Our attempts at lithiating bromoisoxazole at low temperatures (-78 ºC) also resulted in the decomposition of the parent heterocycle. Since methods involving the treatment of an existing isoxazole molecule/core were unsuccessful, we were interested in processes that permitted the *de novo* generation of the heterocycle from a precursor that could easily be deuterium-enriched. The cyclization described by Wakefield *et al.*[174] was found to be the most practical approach for producing deuterium-enriched isotopologues of isoxazole (Scheme 4.4). This method involves the *in-situ* generation of malondialdehyde *via* acid-catalyzed hydrolysis of 1,1,3,3-tetraethoxypropane and its subsequent cyclization with hydroxylamine hydrochloride to generate isoxazole.

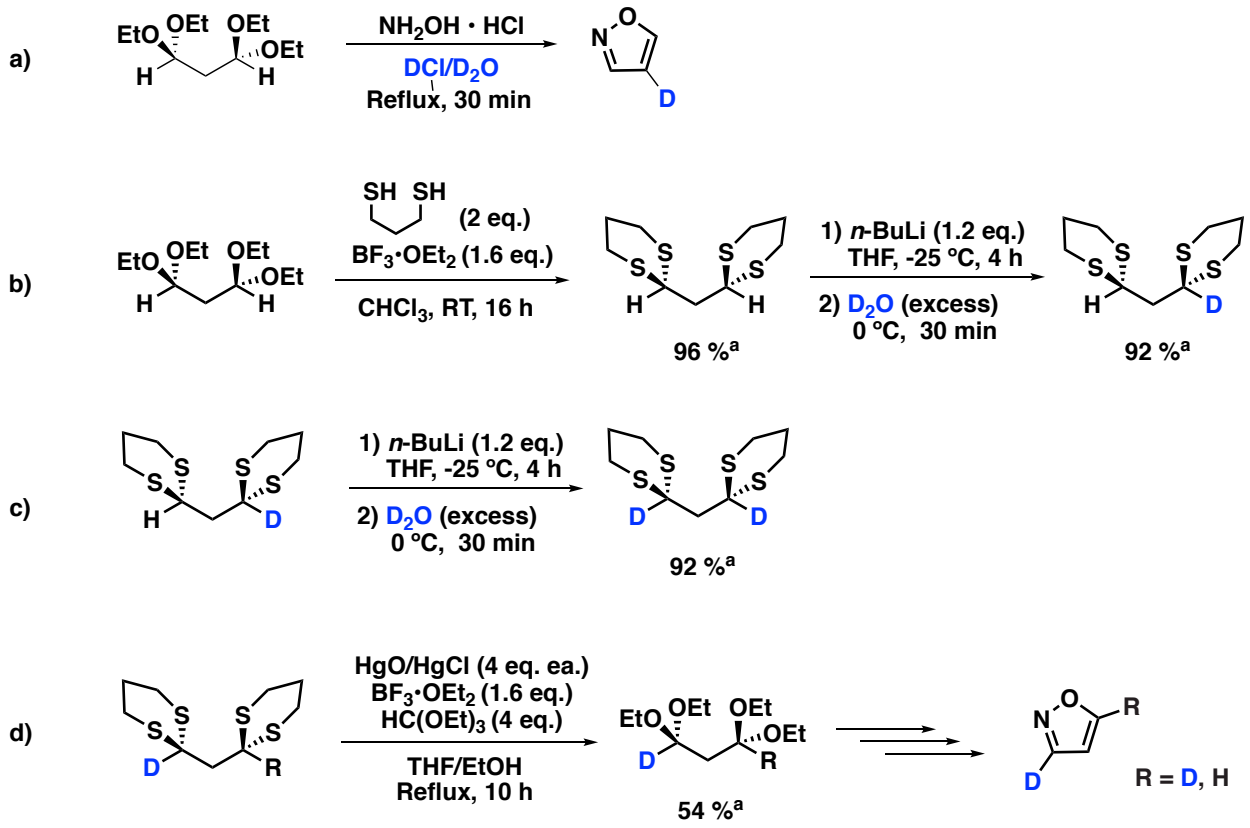
Scheme 4.4. Synthesis of Isoxazole from 1,1,3,3-Tetraethoxypropane and Hydroxylamine Reported by Wakefield *et al.*[174]



Using the reaction in Scheme 4.4 as a primary synthetic route, we proposed that deuterium enrichment at each of the three carbon atoms is possible *via* modification of 1,1,3,3-tetraethoxypropane (Scheme 4.5). Considering that malondialdehyde is a toxic, naturally occurring compound that results from oxidative stress in mammals, significant research has been focused on understanding the deleterious effects of malondialdehyde on living systems and how it reacts with

proteins or nucleic acids. Since such research is facilitated by the availability of isotopically-labeled malondialdehyde, detailed methodology describing the deuterium enrichment of malondialdehyde and its parent compound 1,1,3,3-tetraethoxypropane has been well-documented.[175-176]

Scheme 4.5. Proposed Methods for Accessing Each Deuterated Isotopologue of Isoxazole via Modification of 1,1,3,3-Tetraethoxypropane.



In our proposed route, the simplest case of deuterium enrichment in isoxazole is obtained by performing the cyclization of 1,1,3,3-tetraethoxypropane with hydroxylamine in D_2O as the reaction solvent (Scheme 4.5a). Deuterium enrichment of *in situ*-generated malondialdehyde occurs rapidly *via* acid-catalyzed tautomerization in the presence of D_2O, and results in deuterium enrichment at carbon 4 in the product heterocycle. We propose that the amount of deuterium

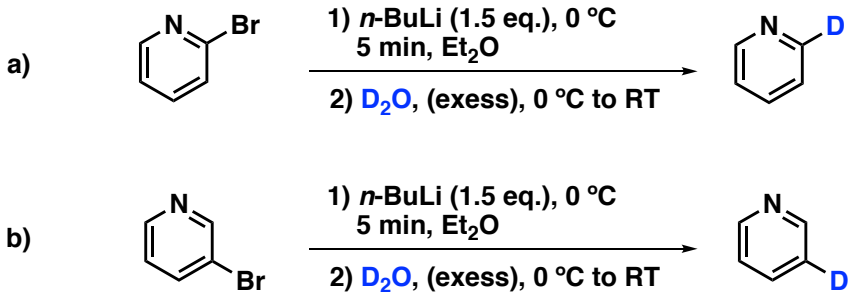
enrichment could likely be increased by pre-treating 1,1,3,3-tetraethoxypropane with acidified D_2O prior to its addition with hydroxylamine.

To install deuterium at the 3 and/or 5 positions of isoxazole requires deuterium enrichment of the aldehydic position(s) of malondialdehyde, and can be achieved *via* Corey-Seebach reaction. 1,1,3,3-Tetraethoxypropane can be directly converted to 2,2′-methylenebis-1,3-dithiane, lithiated with *n*-BuLi, and quenched with D_2O in a very efficient manner (Scheme 4.5b). Deprotection of the resulting product yields [1-^{2}H]-malondialdehyde (as [1-^{2}H]-1,1,3,3-tetraethoxypropane), and ultimately yields a mixture of [3-^{2}H]-isoxazole and [5-^{2}H]-isoxazole when used in the cyclization (Scheme 4.5d, R = H). Alternatively, prior to deprotection, the Seebach umpolung process can be repeated (Scheme 4.5c) to produce [1,3-^{2}H]-malondialdehyde (as [1,3-^{2}H]-1,1,3,3-tetraethoxypropane), and ultimately yielding [3,5-^{2}H]-isoxazole when used in the cyclization (Scheme 4.5d, R = D). Deuterium enrichment at the aldehydic positions of malondialdehyde in combination with the selection of D_2O or H_2O as the solvent for the final cyclization with hydroxylamine hydrochloride allows for controlled access to each mono/polydeuterated isotopologue of isoxazole. Performing the cyclization reaction using the shown in Scheme 4.5a generated the anticipated [4-^{2}H]-isoxazle in good yield and purity. Analysis of the product *via* HRMS, and rotational spectroscopy showed excellent enrichment of deuterium at C4 in the isoxazole structure. The 130 - 360 GHz rotational spectrum of the synthesized [4-^{2}H]-isoxazle was collected (as well as isoxazole at natural isotopic abundance). Analysis of the obtained rotational spectra has led to the assignment of several isotopologues and the analysis of several vibrationally excited states. Synthesis of additional isotopologues *via* the reactions shown in Scheme 4.5b/c/d and the complete semi-experimental equilibrium structural (r_e^{SE}) determination of isoxazole are currently being investigated in our group.

Pyridine

A sample of fully-deuterated pyridine (pyridine-d_5) was obtained from a commercial source and used without purification. Two monodeuterated isotopologues of pyridine were synthesized in our lab (Scheme 4.6). Samples of [2-^{2}H]-pyridine (Scheme 4.6a) and [3-^{2}H]-pyridine (Scheme 4.6b) were prepared *via* lithiation of 2-bromopyridine or 3-bromopyridine respectively using *n*-BuLi and subsequent quenching with D_2O.

Scheme 4.6. Preparation of 2- and 3-deuteropyridine *via* lithiation/D_2O quench of 2- and 3-bromopyridines.



Preparation of [4-^{2}H]-pyridine was briefly investigated, but issues were encountered with the requisite 4-bromopyridine polymerizing prior to its treatment with *n*-BuLi. These issues were concurrent with the re-opening of the laboratories after the initial COVID-19 lockdown (July, 2020). During this period, humid conditions caused multiple problems with our laboratory freezers, and obtaining/maintaining the dry solvents requisite for lithium/halogen exchange reactions. Currently, the 130-360 GHz rotational spectrum has been obtained using samples of the three isotopologues and a sample at natural isotopic abundance. Fitting of the ground state and the vibrationally excited state is currently underway for each isotopologue.

Conclusions

The work presented in this chapter is a representation of the ongoing studies within our group to determine high-accuracy equilibrium structures of aromatic species. The production of

deuterium-tagged aromatic species for each of the heterocyclic molecules shown in Figure 4.1 has permitted the detailed analysis of their respective rotational spectrum and the determination of their semi-experimental equilibrium structure (r_e^{SE}) at unprecedented levels of accuracy. The synthetic work described in this chapter has contributed to several published works[13, 29, 72, 147] within our group and in collaboration with other elite spectroscopists regarding the spectroscopic characterization of the heterocyclic species in Figure 4.1. The measured frequencies, constants and other characterization data determined by our combined efforts builds the foundation for the search of these aromatic heterocycles in the cosmos.

Experimental Section

General Experimental Methods

All commercial reagents were purchased from Sigma-Aldrich, Acros, and Oakwood and used as received without further purification, unless otherwise noted. ^{1}H-NMR spectra (500 MHz), ^{2}H-NMR spectra (500 MHz) and ^{13}C{^{1}H}-NMR spectra (125 MHz) were obtained in D_2O or H_2O, Bruker 500 MHz DCH Avance III spectrometer; chemical shifts (δ) are reported as ppm and referenced versus the solvent residual signal. Mass spectra were acquired using electrospray ionization (ESI) or Atmospheric Solids Analysis Probe (ASAP)[177] on a Thermo Scientific Q-Exactive Plus™ mass spectrometer.

Thiophene.

Method 1: *mono- through tetra-deuterio-thiophene isotopologues via isotopic exchange of thiophene [166] (Scheme 4.1a; 5-day reaction)***.**

In a slight modification to literature procedure: In a 250-mL single-neck, round-bottom flask, 12.43 g (6.8 mL, 127 mmol) of fuming sulfuric acid (H_2SO_4 w/ 18% dissolved SO_3) was

slowly added to 20 mL (22.2 g, 1.1 mol) of D_2O. Thiophene (10.61 g, 10 mL, 126 mmol) was added to the H_2SO_4/D_2O mixture and a reflux condenser was attached to the reaction vessel. The reaction was then heated to reflux (100-105 ºC) and stirred for 5 days. The reaction progress was monitored *via* mass spectrometry of reaction aliquots. After 5 days of reflux, the reaction was cooled to room temperature and extracted with diethyl ether (3 × 20 mL). The combined organic extracts were washed with saturated $NaHCO_{3(aq)}$ (1 × 20 mL), H_2O (3 × 20 mL), and brine (1 × 20 mL). The organic extract was dried over anhydrous $MgSO_4$ and then filtered. The majority of the ether solvent was evaporated *in vacuo*. The residual ether was removed by fractional distillation using a short-path distillation apparatus at ambient pressure. The product was then distilled through the same apparatus to yield 3.8 g of colorless oil (bp = 82 ºC, 1 atm). The resulting oil consisted of multiple deuterium-containing thiophene isotopologues. ^{2}H-NMR ($CHCl_3$, 500 MHz): δ (ppm) 7.35 (s), 7.12 (s). HRMS (ASAP-MS) *m/z*: $[M+H]^+$ Calcd for C_4H_5S: 85.0107. Found: 85.0106. Calcd for C_4H_4DS: 86.0169. Found: 86.0169. Calcd for $C_4H_3D_2S$: 87.0232. Found: 87.0232. Calcd for $C_4H_2D_3S$: 88.0295. Found: 88.0294. Calcd for C_4HD_4S: 89.0358. Found: 89.0358.

Method 2: *mono- through tetra-deuterio-thiophene isotopologues via isotopic exchange of thiophene [166] (Scheme 4.1a; 14-day reaction).*

In a 250-mL single-neck, round-bottom flask, 12.43 g (6.8 mL, 127 mmol) of fuming sulfuric acid (H_2SO_4 w/ 18% dissolved SO_3) was slowly added to 20 mL (22.2 g, 1.1 mol) of D_2O. Thiophene (10.6 g, 10 mL, 125 mmol) was added to the H_2SO_4/D_2O mixture and a reflux condenser was attached to the reaction vessel. The reaction was then heated to reflux (100-105 ºC) and stirred for 7 days. After 7 days, the reaction was cooled to room temperature and an additional 6.8 mL of fuming H_2SO_4 and 20 mL D_2O were added, and the reaction was heated to reflux for an additional 7 days. The second addition of H_2SO_4 and extended reflux time resulted in some

charring of the reaction mixture. After cooling to room temperature, the reaction mixture was extracted with diethyl ether (3 × 20 mL). The combined organic extracts were washed with saturated $NaHCO_{3(aq)}$ (1 × 20 mL), H_2O (3 × 20 mL), and brine (1 × 20 mL). The organic extract was dried over anhydrous $MgSO_4$ and then filtered. The majority of the ether solvent was then evaporated *in vacuo*. The residual ether was removed by fractional distillation using a short-path distillation apparatus at ambient pressure. The product was then distilled through the same apparatus to yield 1.83 g of pale-yellow oil (bp = 82-84 ºC, 1 atm). The isolated distillate consisted of multiple poly-deuterium-containing thiophene isotopologues. ^{1}H-NMR ($CDCl_3$, 500 MHz): δ (ppm) 7.31 (m, 1H), 7.10 (m, 3H). HRMS (ASAP-MS) *m/z*: $[M+H]^+$ Calcd for C_4H_4DS: 86.0169. Found: 86.0168. Calcd for $C_4H_3D_2S$: 87.0232. Found: 87.0231. Calcd for $C_4H_2D_3S$: 88.0295. Found: 88.0294. Calcd for C_4HD_4S: 89.0358. Found: 89.0356.

Method 3: *[3-^{2}H]-Thiophene (and other isotopologues)[170] (Scheme 4.1b).*

3-Bromothiophene (16.3502 g, 100 mmol, 1 eq.) and 100 mL dry diethyl ether were added to a 250 mL flame-dried, single-neck, round-bottom flask under nitrogen atmosphere. The stirred reaction was cooled to 0 ºC on ice and 15 mL (165 mmol) *n*-BuLi (11.0 M in hexanes) was then added dropwise *via* syringe over a time of 10 min. The reaction mixture turned cloudy and gradually turned pale yellow over the course of the *n*-BuLi addition. The reaction was stirred at 0 ºC an additional 10 min after the addition of *n*-BuLi was complete. D_2O (10 mL, 550 mmol) was slowly added dropwise to the reaction mixture, and the reaction mixture was allowed to warm to room temperature. The crude reaction mixture was stirred over $MgSO_4$ and then filtered through a Celite plug (5 cm). The ethereal solvent was removed by fractional distillation at atmospheric pressure (short-path apparatus with a 15 cm Vigreux column). The product was then distilled

through the same apparatus (1 atm) to yield thiophene (8.9 g) as a colorless oil consisting of multiple deuterium-containing isotopologues (primarily [3-^{2}H]-thiophene). b.p. 86-89 ºC (1 atm). ^{1}H-NMR ($CDCl_3$, 500 MHz): δ (ppm) 7.35 (m, 1H), 7.14 (m, 1H). ^{2}H-NMR ($CHCl_3$, 500 MHz): δ (ppm) 7.35 (s), 7.12 (s). HRMS (ASAP-MS) *m/z*: $[M+H]^+$ Calcd for C_4H_4DS: 86.0169. Found: 86.0166. Calcd for $C_4H_3D_2S$: 87.0232. Found: 87.0229. Calcd for $C_4H_2D_3S$: 88.0295. Found: 88.0293.

1*H*-1,2,4-Triazole.

The commercially available sample of 1,2,4-triazole (97%) was used without further purification. 1,2,4-Triazole is a while solid with very low volatility at room temperature compared to other heteroaromatics studied previously.[10-13] Therefore, it was necessary to employ a cell that could be operated at high temperatures. The sample was introduced into a 2 m long stainless steel cell with a base pressure of 15 mTorr. The cell was equipped with a millimeter/submillimeter spectrometer, described previously.[178] In brief, the spectrometer is composed of a microwave synthesizer (Agilent Technologies, E8257D PSG), Virginia Diodes Inc. frequency multipliers with varying doublers and triplers to cover the frequency region from 70 to 700 GHz, an InSb Hot electron bolometer (QMC Ltd. model QFI/2BI with a closed-cycle He chiller) and a lock-in ampli er (Standford Research Systems SR830 DSP). The cell was heated to a temperature of ~100 °C and the spectrum was acquired with a total cell pressure of approximately 30 mTorr. A single sweep of the spectrum was collected at a step size of 0.1 MHz.

Trial 1: *Recrystallization of 1,2,4-triazole from D_2O.*

1*H*-1,2,4-triazole (17 g, 246 mmol) and 10 mL D_2O were added to a 100 mL Erlenmeyer flask. The stirred contents of the flask were heated on a ceramic hot plate until boiling, and the

complete dissolution of solids was observed. The flask was slowly cooled to room temperature. During the slow cooling process, colorless needle-like crystals formed. The flask was then further cooled to 0 ºC on ice to promote complete crystallization of the product. The solids were collected *via* vacuum filtration through a fine fritted funnel and dried *in vacuo* to yield 15 grams of 1,2,4-triazole as colorless crystals. Analysis of the resulting product *via* high resolution mass spectrometry (ASAP-MS) showed the majority of the sample had been mono-deuterated. ^{1}H-NMR (D_2O, 500 MHz): δ (ppm) 8.3 (s, 2H). $^{13}C\{^{1}H\}$-NMR (D_2O, 125 MHz): δ (ppm) 146.1. ^{2}H-NMR (H_2O, 500 MHz): δ (ppm) 8.3 (s, 2H). HRMS (ASAP-MS) *m/z*: $[M]^+$ Calcd for $C_2H_2DN_3$: 70.0384. Found: 70.0399.

Trial 2: *3-day reflux of 1,2,4-triazole in D_2O, and subsequent recrystallization.*

1*H*-1,2,4-triazole (5.23 g, 76 mmol) and 15 mL D_2O was added to a 100 mL round bottom flask. The flask was fitted with a water-cooled reflux condenser, connected to an N_2 line *via* gas inlet, and purged of atmosphere through three vacuum/N_2 backfill cycles. The stirred reaction was heated to reflux in an oil bath for three days. Reaction aliquots were taken at the 24, 48 and 72 hour marks to monitor the deuterium enrichment *via* high resolution mass spectrometry. After 72 hours of refluxing, the vessel was removed from heat, and allowed to cool to room temperature without stirring. During the slow cooling process, colorless needle-like crystals formed. The flask was then further cooled to 0 ºC on ice to promote complete crystallization of the product. The solids were collected *via* vacuum filtration through a fine fritted funnel and dried *in vacuo* to yield 3.3 grams of 1,2,4-triazole as colorless crystals. Analysis of the resulting product *via* high resolution mass spectrometry (ASAP-MS) showed the majority of the sample had been double deuterated with an approximate ratio of 1:3 ($C_2DH_2N_3$ to $C_2D_2HN_3$) ^{1}H-NMR (D_2O, 500 MHz): δ

(ppm) 8.4 (s, 2H). $^{13}C\{^{1}H\}$-NMR (D_2O, 125 MHz): δ (ppm) 146.1. ^{2}H-NMR (H_2O, 500 MHz): (ppm) 8.3 (s, 2D). HRMS (ASAP-MS) *m/z*: $[M+H]^+$ Calcd for $C_2H_3DN_3$: 71.0463. Found: 71.0463. Calcd for $C_2H_2D_2N_3$: 72.0525. Found: 72.0524. δ (ppm) 8.3 (s, 2D). HRMS (ASAP-MS) *m/z*: $[M+H]^+$ Calcd for $C_2H_3DN_3$: 71.0463. Found: 71.0463. Calcd for $C_2H_2D_2N_3$: 72.0525. Found: 72.0524.

1*H*-1,2,3-Triazole.

Method 1: *H/D exchange by strong base.*

N-deuteriated samples of 1*H*- and 2*H*-1,2,3-triazole were obtained by H/D exchange using strong base (*t*-BuOLi / *t*-BuOD), adapted from Esselman *et al.* and depicted in Scheme 4.3a. All glassware was oven dried. In a round-bottom flask equipped with a magnetic stir bar, 0.5 mL 1,2,3-triazole was combined with 198 mg *t*-BuOLi and 1.2 mL *t*-BuOD. The mixture was stirred at 60 ºC for three months in an unsuccessful attempt to force deuterium into the C-H positions.[14] The reaction mixture was extracted using anhydrous diethyl ether, dried over $MgSO_4$, and the solvent removed *in vacuo*. Analysis of the crude product by millimeter-wave rotational spectroscopy established that the sample consisted of [1-^{2}H]-1*H*-1,2,3-triazole and [2-^{2}H]-2*H*-1,2,3-triazole.

Method 2: *H/D exchange by weak base.*

C-deuteriated samples of 1*H*- and 2*H*-1,2,3-triazole were obtained by a weakly nucleophilic base-catalyzed exchange (Na_2CO_3 / D_2O) and depicted in Scheme S2. In a beaker, 9.2 g Na_2CO_3 was dissolved in 50 mL D_2O. This solution was subsequently added to a round-

bottom flask containing a magnetic stir bar and 2.1 g 1,2,3-triazole. The solution was stirred at ~100 °C between 6 and 27 days (for varying levels of deuterium incorporation and due to several fume hood exhaust malfunctions). Conversion to deuteriated triazole was monitored by taking aliquots for analysis by mass spectrometry at ~ 1-week intervals. Once the desired proportion of deuteriated triazole was achieved, the solution was cooled to room temperature and neutralized to pH ~7 – 6 using P_2O_5 in D_2O. Triazole was extracted using anhydrous diethyl ether, dried over Na_2SO_4, and ether was removed by rotary evaporation.

The crude product obtained by this method was reasonably clean and the isotopic composition of the sample could be straightforwardly varied by changing the reaction time. This method ultimately provided all of the possible deuterium-containing isotopologues of 1*H*- and 2*H*-1,2,3-triazole, although some were observed in very small abundance. The other preparative methods were important in providing some of the isotopologues in higher abundance.

Method 3: *Three-step deuteriation.*

The first step followed the procedure of Iddon *et al.*[179] 1*H*-1,2,3-Triazole (15.30 g, 222 mmol) and 100 mL of deionized H_2O were combined in a 250 mL round-bottom flask with magnetic stir bar. A 100 mL pressure-equalizing addition funnel was connected to the flask with the inlet open to air. Into the funnel were added 15 mL of liquid Br_2, which was delivered dropwise to the stirring reaction mixture. A white precipitate appeared with concurrent disappearance of brownish-red bromine color. After the addition was complete, the stirring reaction was heated to 45 ºC for one hour, during which time additional precipitate formed. The reaction was cooled to room temperature and vacuum filtered. The filtrate was transferred back to the round-bottom flask, to which an additional 10 mL of Br_2 were added and left stirring overnight at room temperature to

yield a second batch of yellow-white solid. The filtered solids were combined, washed with cold water (3 × 50 mL), recrystallized from hot MeOH/H_2O, and dried *in vacuo* to yield 4,5-dibromo 1*H*- and 2*H*-1,2,3-triazoles as white crystals (41.8 g, 84% yield). HRMS (ASAP-MS), *m/z*: $[M+H]^+$ Calcd for $C_2H_2[^{79}Br]_2N_3$: 225.8610. Found: 225.8613. Isotopic pattern consistent with dibromo compound: $[^{79}Br]_2$, $[^{79}Br][^{81}Br]$, $[^{81}Br]_2$.

The second transformation utilized a procedure modified from Sakurada *et al*.[180] To an oven-dried round-bottom flask equipped with stir bar and condenser were added 7.0 g (931 mmol) of the di-brominated triazoles, 11.6 g of Na_2SO_3 (92.0 mmol, 3 equiv.), and 50 mL of D_2O. The system was capped with a septum and connected to a nitrogen purge *via* syringe needle. The flask was heated to ~ 100 °C and stirred for one day. After this time, the reaction was cooled to room temperature, and the aqueous and organic layers were separated. The aqueous layer was extracted with ethyl acetate (5 × 50 mL). The combined organic layers were dried over Na_2SO_4, vacuum filtered, and dried *in vacuo*, yielding 4.5 g of mono-brominated, mono-deuteriated 1,2,3-triazoles as white crystals (97% yield). HRMS (ASAP-MS), *m/z*: $[M+H]^+$ Calcd for $C_2H_2D[^{79}Br]N_3$: 148.9568. Found: 148.9567. Isotopic pattern consistent with mono-bromo compound: $[^{79}Br]$, $[^{81}Br]$. An analogous procedure was carried out using H_2O instead of D_2O to acquire the mono-brominated, un-deuteriated 1,2,3-triazoles.

The final transformation is based the metal-halogen exchange procedure of Wang *et al.*[181] Into a dried, 250 mL round-bottom flask were added 4.4g (29.7 mmol) of the mono-brominated, mono-deuteriated 1,2,3-triazoles. The flask was sealed with a septum and evacuated of air and backfilled with nitrogen three times. To the flask was added 60 mL of dry diethyl ether. The components were stirred and cooled using an ice-water bath. Then, dropwise over the course of

several minutes, 36 mL (90 mmol) of 2.5 M *n*-butyl lithium was added to the stirring reagents. Over this time, a white precipitate formed. After complete addition of *n*-butyl lithium, the reaction was stirred at ~ 0 °C for an hour. Again, dropwise over the course of several minutes was added 12 mL of D_2O, taking care to avoid a vigorous reaction. The reaction was allowed to warm to room temperature, while continuing to stir for one hour. The pH of the flask contents was adjusted to ~ 7 – 5 using $HCl_{(aq)}$. Much of the white precipitate dissolved, and the organic and aqueous layers were separated. The aqueous layer was extracted with ethyl acetate (5 × 50 mL). The combined organic layers were dried over Na_2SO_4 and dried *in vacuo*, yielding a clear, yellow oil. The oil was purified using flash chromatography (60 μ SiO_2, pentane → diethyl ether gradient elution) and collected over fifteen 8 mL fractions. The eluent was removed *in vacuo*, giving 1.5 g of the 4,5-deuteriated 1,2,3-triazoles as a clear colorless oil (72% yield). Analysis of the crude product by millimeter-wave rotational spectroscopy established that the sample consisted primarily of [4,5-^{2}H]-1*H*-1,2,3-triazole and [4,5-^{2}H]-2*H*-1,2,3-triazole. An analogous reaction using the non-deuteriated, mono-brominated triazoles or using H_2O instead of D_2O can be used generate mono-deuteriated triazoles.

Isoxazole.

4-^{2}H-isoxazole Enrichment.

In a slight modification to the procedure reported by Wakefield *et al.*[174], concentrated HCl (0.4 mL) was added to a solution of malonaldehyde diethyl acetal (22 g, 0.1 mol) in deuterium oxide (5 mL) and stirred at room temperature for 15 minutes. The mixture was then added to a 100-mL round bottom flask containing a heated (50 ºC) solution of hydroxylamine hydrochloride (7.73 g, 0.11 mmol) in deuterium oxide (50 mL). A water-cooled reflux condenser was fitted to

the flask, and the reaction mixture was heated to 100 ºC on a boiling water bath for 30 minutes. The reflux condenser was switched with a short-path distillation rig and the reaction was distilled into a receiving flask containing a solution of $CdCl_2$ (29 g, 0.16 mol) in water (25 mL). Contact between the distillate and the $CdCl_2$ solution resulted in the formation of a white precipitate in the receiving vessel. The precipitate was collected *via* vacuum filtration through a fine glass fritted funnel, washed with saturated aqueous $CdCl_2$ (5 mL), and transferred to a 50-mL round bottom flask with 25 mL water. A short path distillation rig was connected to the flask, and the mixture was steam distilled under atmospheric pressure. The collected distillate was saturated with NaCl, and the crude product was separated. The crude product was dried over anhydrous $CaCl_2$, filtered, and redistilled under atmospheric pressure (bp = 94 ºC) to give isoxazole (3.1 g, 44 %) as a colorless liquid. HRMS (ASAP-MS) *m/z*: $[M+H]^+$ Calcd for C_3H_3DNO: 71.0350. Found: 71.0350.

Pyridine.

[2-^{2}H]-Pyridine.

In an oven-dried 100 mL round bottom flask (cooled and maintained under an atmosphere of dry N_2), 2-bromopyridine (8.0104 g, 50.6 mmol) was added in 35 mL dry diethyl ether. The mixture was cooled to 0 ºC on an ice bath, and *n*-BuLi (11.0 M in hexanes, 7 mL, 77 mmol, 1.5 equiv.) was added dropwise to the stirred reaction. The reaction turned rust-colored as the *n*-BuLi was added. After the addition was completed, the reaction was stirred at 0 ºC for an additional 5 minutes. Deuterium oxide (8.0 mL, 8.8 g, 440 mmol) was added dropwise to the stirred reaction flask at 0 ºC. The addition of D_2O results in an exotherm, the rate of addition was performed sufficiently slow to maintain the 0 ºC reaction temperature. After the addition of D_2O was complete, the reaction vessel was removed from the cooling bath and allowed to warm to room

temperature. The reaction was extracted with diethyl ether (4 × 15 mL), the organic extract was dried over anhydrous $MgSO_4$, and filtered. The volume of the dried extract was reduced to approximately 25 mL by rotary evaporation. The remaining solvent was distilled away using a short path distillation rig at atmospheric pressure. The product ([2-^{2}H]-pyridine) was distilled at atmospheric pressure (bp = 100-115 ºC) as a colorless oil (937 mg, 23 %). HRMS (ASAP-MS) *m/z*: $[M+H]^+$ Calcd for C_5H_5DN: 81.0558. Found: 81.0556.

[3-^{2}H]-Pyridine.

In an oven-dried 100 mL round bottom flask (cooled and maintained under an atmosphere of dry N_2), 2-bromopyridine (8.3335 g, 52.7 mmol) was added in 35 mL dry diethyl ether. The mixture was cooled to 0 ºC on an ice bath, and *n*-BuLi (11.0 M in hexanes, 7 mL, 77 mmol, 1.5 equiv.) was added dropwise to the stirred reaction. The reaction turned rust-colored as the *n*-BuLi was added. After the addition was completed, the reaction was stirred at 0 ºC for an additional 5 minutes. Deuterium oxide (8.0 mL, 8.8 g, 440 mmol) was added dropwise to the stirred reaction flask at 0 ºC. The addition of D_2O results in an exotherm, the rate of addition was performed sufficiently slow to maintain the 0 ºC reaction temperature. After the addition of D_2O was complete, the reaction vessel was removed from the cooling bath and allowed to warm to room temperature. The reaction was extracted with diethyl ether (4 × 15 mL), the organic extract was dried over anhydrous $MgSO_4$, and filtered. The volume of the dried extract was reduced to approximately 25 mL by rotary evaporation. The remaining solvent was distilled away using a short path distillation rig at atmospheric pressure. The product ([3-^{2}H]-pyridine) was distilled at atmospheric pressure (bp = 100-115 ºC) as a colorless oil (725 mg, 17 %). HRMS (ASAP-MS) *m/z*: $[M+H]^+$ Calcd for C_5H_5DN: 81.0558. Found: 81.0556.

Notes and References

1. Demaison, J., Experimental, semi-experimental and *ab initio* equilibrium structures. *Mol. Phys.* **2007,** *105* (23-24), 3109-3138.

2. Liévin, J.; Demaison, J.; Herman, M.; Fayt, A.; Puzzarini, C., Comparison of the experimental, semi-experimental and *ab initio* equilibrium structures of acetylene: Influence of relativisitic effects and of the diagonal Born–Oppenheimer corrections. *J. Chem. Phys.* **2011,** *134* (6), 064119.

3. Mendolicchio, M.; Penocchio, E.; Licari, D.; Tasinato, N.; Barone, V., Development and Implementation of Advanced Fitting Methods for the Calculation of Accurate Molecular Structures. *J. Chem. Theory Comput.* **2017,** *13* (6), 3060-3075.

4. Puzzarini, C.; Barone, V., Diving for Accurate Structures in the Ocean of Molecular Systems with the Help of Spectroscopy and Quantum Chemistry. *Acc. Chem. Res.* **2018,** *51* (2), 548-556.

5. Pulay, P.; Meyer, W.; Boggs, J. E., Cubic force constants and equilibrium geometry of methane from Hartree–Fock and correlated wavefunctions. *J. Chem. Phys.* **1978,** *68* (11), 5077-5085.

6. Penocchio, E.; Piccardo, M.; Barone, V., Semiexperimental Equilibrium Structures for Building Blocks of Organic and Biological Molecules: The B2PLYP Route. *J. Chem. Theory Comput.* **2015,** *11* (10), 4689-4707.

7. Penocchio, E.; Mendolicchio, M.; Tasinato, N.; Barone, V., Structural features of the carbon-sulfur chemical bond: a semi-experimental perspective. *Can. J. Chem.* **2016,** *94 12*, 1065-1076.

8. Puzzarini, C., Accurate molecular structures of small- and medium-sized molecules. *Int. J. Quantum Chem.* **2016,** *116* (21), 1513-1519.

9. Piccardo, M.; Penocchio, E.; Puzzarini, C.; Biczysko, M.; Barone, V., Correction to Semi-Experimental Equilibrium Structure Determinations by Employing B3LYP/SNSD Anharmonic Force Fields: Validation and Application to Semirigid Organic Molecules. *J. Phys. Chem. A* **2016,** *120* (20), 3754-3754.

10. Heim, Z. N.; Amberger, B. K.; Esselman, B. J.; Stanton, J. F.; Woods, R. C.; McMahon, R. J., Molecular structure determination: Equilibrium structure of pyrimidine (*m*-$C_4H_4N_2$) from rotational spectroscopy (r_e^{SE}) and high-level ab initio calculation (r_e) agree within the uncertainty of experimental measurement. *J. Chem. Phys.* **2020,** *152* (10), 104303.

11. Owen, A. N.; Zdanovskaia, M. A.; Esselman, B. J.; Stanton, J. F.; Woods, R. C.; McMahon, R. J., Semi-Experimental Equilibrium (r_e^{SE}) and Theoretical Structures of Pyridazine (*o*-$C_4H_4N_2$). *J. Phys. Chem. A* **2021,** *125* (36), 7976-7987.

12. Esselman, B. J.; Zdanovskaia, M. A.; Owen, A. N.; Stanton, J. F.; Woods, R. C.; McMahon, R. J., Precise equilibrium structure of thiazole (c-C_3H_3NS) from twenty-four isotopologues. *J. Chem. Phys.* **2021,** *155* (5), 054302.

13. Orr, V. L.; Ichikawa, Y.; Patel, A. R.; Kougias, S. M.; Kobayashi, K.; Stanton, J. F.; Esselman, B. J.; Woods, R. C.; McMahon, R. J., Precise equilibrium structure determination of thiophene (*c*-C_4H_4S) by rotational spectroscopy—Structure of a five-membered heterocycle containing a third-row atom. *J. Chem. Phys.* **2021,** *154* (24), 244310.

14. Esselman, B. J.; Amberger, B. K.; Shutter, J. D.; Daane, M. A.; Stanton, J. F.; Woods, R. C.; McMahon, R. J., Rotational Spectroscopy of Pyridazine and its Isotopologs from 235-360 GHz: Equilibrium Structure and Vibrational Satellites. *J. Chem. Phys.* **2013,** *139* (22), 224304/1-224304/13.

15. Zdanovskaia, M. A.; Esselman, B. J.; Lau, H. S.; Bates, D. M.; Woods, R. C.; McMahon, R. J.; Kisiel, Z., The 103 – 360 GHz Rotational Spectrum of Benzonitrile, the First Interstellar Benzene Derivative Detected by Radioastronomy. *J. Mol. Spectrosc.* **2018,** *351*, 39-48.

16. Higgins, P. M.; Esselman, B. J.; Zdanovskaia, M. A.; Woods, R. C.; McMahon, R. J., Millimeter-wave Spectroscopy of the Chlorine Isotopologues of Chloropyrazine and Twenty-two of their Vibrationally Excited States. *J. Mol. Spectrosc.* **2019,** *364,* 111179.

17. Esselman, B. J.; Zdanovskaia, M. A.; Woods, R. C.; McMahon, R. J., Millimeter-wave Spectroscopy of the Chlorine Isotopologues of 2-Chloropyridine and Twenty-three of Their Vibrationally Excited States. *J. Mol. Spectrosc.* **2019,** *365*, 111206.

18. Esselman, B. J.; Zdanovskaia, M. A.; Owen, A. N.; Stanton, J. F.; Woods, R. C.; McMahon, R. J., Precise Equilibrium Structure of Benzene from Eleven Isotopologues. *Unpublished Work* **2021**.

19. Zdanovskaia, M. A.; Esselman, B. J.; Woods, R. C.; McMahon, R. J., The 130 - 370 GHz Rotational Spectrum of Phenyl Isocyanide (C_6H_5NC). *J. Chem. Phys.* **2019,** *151*.

20. Elmore, C. S.; Bragg, R. A., Isotope chemistry; a useful tool in the drug discovery arsenal. *Bioorg. Med. Chem. Lett.* **2015,** *25* (2), 167-171.

21. Molga, K.; Dittwald, P.; Grzybowski, B. A., Computational design of syntheses leading to compound libraries or isotopically labelled targets. *Chem. Sci.* **2019,** *10* (40), 9219-9232.

22. Dahl, K.; Halldin, C.; Schou, M., New methodologies for the preparation of carbon-11 labeled radiopharmaceuticals. *Clin. Transl. Imaging* **2017,** *5* (3), 275-289.

23. Pedersen, A. K.; Fitzgerald, G. A., Preparation and analysis of deuterium-labeled aspirin: Application to pharmacokinetic studies. *J. Pharm. Sci.* **1985,** *74* (2), 188-192.

24. Barrish, A.; Olah, T. V.; Gatto, G. J.; Dobrinska, M. R.; Gilbert, J. D., The Use of Stable Isotope Labeling and Liquid Chromatography/Tandem Mass Spectrometry Techniques to Study the Pharmacokinetics and Bioavailability of the Antimigraine Drug, MK-0462 (Rizatriptan) in Dogs. *Rapid Commun. Mass Spectrom.* **1996,** *10* (9), 1033-1037.

25. Del Vecchio, A.; Destro, G.; Taran, F.; Audisio, D., Recent developments in heterocycle labeling with carbon isotopes. *J. Label. Compd. Radiopharm.* **2018,** *61* (13), 988-1007.

26. Calf, G. E.; Garnett, J. L., Isotopic Hydrogen Labeling of Heterocyclic Compounds by One-Step Methods. In *Adv. Heterocycl. Chem.*, Katritzky, A. R.; Boulton, A. J., Eds. Academic Press: 1973; Vol. 15, pp 137-185.

27. Burton, A. J.; Wadsworth, A. H., Stable isotopic labelling of heterocyclic compounds. *J. Label. Compd. Radiopharm.* **2007,** *50* (5-6), 273-276.

28. Levernier, E.; Tatoueix, K.; Garcia-Argote, S.; Pfeifer, V.; Kiesling, R.; Gravel, E.; Feuillastre, S.; Pieters, G., Easy-to-Implement Hydrogen Isotope Exchange for the Labeling of N-Heterocycles, Alkylkamines, Benzylic Scaffolds, and Pharmaceuticals. *JACS Au* **2022,** *2* (4), 801-808.

29. Zdanovskaia, M. A.; Esselman, B. J.; Kougias, S. M.; Amberger, B. K.; Stanton, J. F.; Woods, R. C.; McMahon, R. J. , Precise Equilibrium Structures of 1*H*- and 2*H*-1,2,3-Triazoles ($C_2H_3N_3$) by Millimeter-wave Spectroscopy. *J. Chem. Phys.* **2022,** *157*, 084305

30. Singh, A.; Singh, G.; Bedi, P. M. S., Thiophene derivatives: A potent multitargeted pharmacological scaffold. *J. Heterocycl. Chem.* **2020,** *57* (7), 2658-2703.

31. Amna, B.; Siddiqi, H. M.; Hassan, A.; Ozturk, T., Recent developments in the synthesis of regioregular thiophene-based conjugated polymers for electronic and optoelectronic applications using nickel and palladium-based catalytic systems. *RSC Adv.* **2020,** *10* (8), 4322-4396.

32. Barbarella, G.; Melucci, M.; Sotgiu, G., The Versatile Thiophene: An Overview of Recent Research on Thiophene-Based Materials. *Adv. Mater.* **2005,** *17* (13), 1581-1593.

33. Heinz, J.; Schulze-Makuch, D., Thiophenes on Mars: Biotic or Abiotic Origin? *Astrobiology* **2020,** *20* (4), 552-561.

34. Eigenbrode, J. L.; Summons, R. E.; Steele, A.; Freissinet, C.; Millan, M.; Navarro-González, R.; Sutter, B.; McAdam, A. C.; Franz, H. B.; Glavin, D. P.; Archer, P. D.; Mahaffy, P. R.; Conrad, P. G.; Hurowitz, J. A.; Grotzinger, J. P.; Gupta, S.; Ming, D. W.; Sumner, D. Y.; Szopa, C.; Malespin, C.; Buch, A.; Coll, P., Organic matter preserved in 3-billion-year-old mudstones at Gale crater, Mars. *Science* **2018,** *360* (6393), 1096.

35. Lattelais, M.; Ellinger, Y.; Matrane, A.; Guillemin, J. C., Looking for heteroaromatic rings and related isomers as interstellar candidates. *Phys. Chem. Chem. Phys.* **2010,** *12* (16), 4165-4171.

36. Agúndez, M.; Cernicharo, J.; Guélin, M., New molecules in IRC +10216: confirmation of C_5S and tentative identification of MgCCH, NCCP, and SiH_3CN. *Astron. Astrophys.* **2014,** *570*.

37. Cernicharo, J.; Guelin, M.; Hein, H.; Kahane, C., Sulfur in IRC +10216. *Astron. Astrophys.* **1987,** *181*, L9-L12.

38. Coblentz, W. W., *Investigations of Infrared Spectra Part 1 - Infra-Red Absorption Spectra*. Carnegie Institution of Washington: 1905.

39. Thompson, H. W.; Temple, R. B., The infra-red spectra of furan and thiophene. *Trans. Faraday Soc.* **1945,** *41*, 27-34.

40. Barnes, R.; Liddel, U.; Williams, V., Infrared Spectroscopy. Industrial Applications. *Ind. Eng. Chem., Anal. Ed* **1943,** *15* (11), 659-709.

41. Barnes, R. B.; Brattain, R. R., The Near Infrared Spectrum of Benzene-d_6. *J. Chem. Phys.* **1935,** *3* (8), 446-449.

42. Bonino, G. B.; Manzoni-Ansidei, R., The Raman Spectra of Thiophenes and Furans and a few of their derivatives. *Z. Physik. Chem.* **1934,** *B25*, 327-347.

43. Rico, M.; Orza, J. M.; Morcillo, J., Fundamental vibrations of thiophene and its deuterated derivatives. *Spectrochim. Acta A* **1965,** *21* (4), 689-719.

44. Klots, T. D.; Chirico, R. D.; Steele, W. V., Complete vapor phase assignment for the fundamental vibrations of furan, pyrrole and thiophene. *Spectrochim. Acta A* **1994,** *50* (4), 765-795.

45. Pankoke, B.; Yamada, K. M. T.; Winnewisser, G., High resolution IR-spectra of furan and thiophene. *Z. Naturforsch., A: Phys. Sci.* **1994,** *48* (12), 1193-202.

46. van Wijngaarden, J.; Van Nest, S. J.; van Dijk, C. W.; Tokaryk, D. W., Rovibrational spectrum and analysis of the ν_8 band of thiophene using infrared synchrotron radiation. *J. Mol. Spectrosc.* **2010,** *259* (1), 56-59.

47. van Wijngaarden, J.; Tokaryk, D. W., High resolution synchrotron-based study and analysis of the ν_{14} band of thiophene. *J. Mol. Spectrosc.* **2008,** *251* (1), 365-368.

48. Hegelund, F.; Wugt Larsen, R.; Palmer, M. H., The high-resolution infrared spectrum of thiophene between 600 and 1200cm^{-1}: A spectroscopic and theoretical study of the fundamental bands ν_6, ν_7, ν_{13}, and the *c*-Coriolis interacting dyad ν_5, ν_{19}. *J. Mol. Spectrosc.* **2008,** *247* (1), 100-114.

49. Wu, X.-F.; Zheng, X.; Wang, H.-G.; Zhao, Y.-Y.; Guan, X.; Phillips, D. L.; Chen, X.; Fang, W., A resonance Raman spectroscopic and CASSCF investigation of the Franck–Condon region structural dynamics and conical intersections of thiophene. *J. Chem. Phys.* **2010,** *133* (13), 134507.

50. Singh, D. K.; Srivastava, S. K.; Ojha, A. K.; Asthana, B. P., Vibrational study of thiophene and its solvation in two polar solvents, DMSO and methanol by Raman spectroscopy combined with ab initio and DFT calculations. *J. Mol. Struct.* **2008,** *892* (1), 384-391.

51. Ogata, T.; Kozima, K., Microwave spectrum, barrier height to internal rotation of methyl group of 3-methylthiophene, and dipole moments of 3-methylthiophene and thiophene. *J. Mol. Spectrosc.* **1972,** *42* (1), 38-46.

52. Bak, B.; Christensen, D.; Rastrup-Andersen, J.; Tannenbaum, E., Microwave Spectra of Thiophene, 2- and 3-Monodeutero, 3,3′-Dideutero, and Tetradeuterothiophene. Structure of the Thiophene Molecule. *J. Chem. Phys.* **1956,** *25* (5), 892-896.

53. Bak, B.; Christensen, D.; Hansen-Nygaard, L.; Rastrup-Andersen, J., The structure of thiophene. *J. Mol. Spectrosc.* **1961,** *7* (1), 58-63.

54. Kraitchman, J., Determination of Molecular Structure from Microwave Spectroscopic Data. *Am. J. Phys.* **1953,** *21* (1), 17-24.

55. Liescheski, P. B.; Rankin, D. W. H., Determination of the r_α structure of thiophene by combined analysis of electron diffraction, liquid crystal NMR and rotational data. *J. Mol. Struct.* **1988,** *178*, 227-241.

56. Kochikov, I. V.; Tarasov, Y. I.; Spiridonov, V. P.; Kuramshina, G. M.; Rankin, D. W. H.; Saakjan, A. S.; Yagola, A. G., The equilibrium structure of thiophene by the combined use of electron diffraction, vibrational spectroscopy and microwave spectroscopy guided by theoretical calculations. *J. Mol. Struct.* **2001,** *567-568*, 29-40.

57. Piccardo, M.; Penocchio, E.; Puzzarini, C.; Biczysko, M.; Barone, V., Semi-Experimental Equilibrium Structure Determinations by Employing B3LYP/SNSD Anharmonic Force Fields: Validation and Application to Semirigid Organic Molecules. *J. Phys. Chem. A* **2015,** *119*, 2058-2082.

58. White, W. F. *Microwave Spectra of Some Sulfur and Nitrogen Compounds*; NASA: Hampton, VA, 1974; pp 99-100.

59. Pozdeev, N. M.; Gunderova, L. N., Microwave spectra of thiophane and thiophene. *Khim. Seraorg. Soedin., Soderzh. Neftyakh Nefteprod.* **1972,** *9*, 101-6.

60. Pozdeev, N. M.; Panikovskaya, L. I.; Lisovskaya, L. N.; Mamleev, A. K. In *Rotation constants and dipole moment of thiophene*, Primen. Mol. Spektrosk. Khim., Sb. Dokl. Sib. Soveshch., 3rd, Krasnoyarsk, USSR, 1966; pp 26-7.

61. Kretschmer, U.; Stahl, W.; Dreizler, H., The Rotational Spectra of the ^{32}S-, ^{33}S-, and ^{34}S-Isotopomers of Thiophene. *Z. Naturforsch., A: Phys. Sci.* **1993,** *48* (5-6), 733-736.

62. Kumari, M.; Tahlan, S.; Narasimhan, B.; Ramasamy, K.; Lim, S. M.; Shah, S. A. A.; Mani, V.; Kakkar, S., Synthesis and biological evaluation of heterocyclic 1,2,4-triazole scaffolds as promising pharmacological agents. *BMC Chem.* **2021,** *15* (1), 5.

63. Kumar, S.; Khokra, S. L.; Yadav, A., Triazole analogues as potential pharmacological agents: a brief review. *Future J. Pharm. Sci.* **2021,** *7* (1), 106.

64. Kharb, R.; Sharma, P. C.; Yar, M. S., Pharmacological significance of triazole scaffold. *J. Enzyme Inhib. Med. Chem.* **2011,** *26* (1), 1-21.

65. Dheer, D.; Singh, V.; Shankar, R., Medicinal attributes of 1,2,3-triazoles: Current developments. *Bioorg. Chem.* **2017,** *71*, 30-54.

66. Saag, M. S.; Dismukes, W. E., Azole antifungal agents: emphasis on new triazoles. *Antimicrob. Agents Chemother.* **1988,** *32* (1), 1-8.

67. Lass-Flörl, C., Triazole Antifungal Agents in Invasive Fungal Infections. *Drugs* **2011,** *71* (18), 2405-2419.

68. Bailey, E. M.; Krakovsky, D. J.; Rybak, M. J., The Triazole Antifungal Agents: A Review of Itraconazole and Fluconazole. *Pharmacotherapy* **1990,** *10* (2), 146-153.

69. Peyton, L.; Gallagher, S.; Hashemzadeh, M., Triazole antifungals: a review. *Drugs Today* **2015,** *51* (12), 705-718.

70. Gao, F.; Wang, T.; Xiao, J.; Huang, G., Antibacterial activity study of 1,2,4-triazole derivatives. *Eur. J. Med. Chem.* **2019,** *173*, 274-281.

71. Zhou, L.; Amer, A.; Korn, M.; Burda, R.; Balzarini, J.; De Clercq, E.; Kern, E. R.; Torrence, P. F., Synthesis and Antiviral Activities of 1,2,3-triazole Functionalized Thymidines: 1,3-dipolar Cycloaddition for Efficient Regioselective Diversity Generation. *Antivir. Chem. Chemother.* **2005,** *16* (6), 375-383.

72. Bunn, H. A.; Esselman, B.J.; Kougias, S.M.; Franke, P.R.; Stanton, J.F.; Woods, R.C.; McMahon, R.J.; Widicus Weaver, S.L., Millimeter/Submillimeter Wave Spectroscopy and Semi-Experimental Equilibrium (r_e^{SE}) Structure of 1*H*-1,2,4-Triazole (c-$C_2H_3N_3$). *J. Phys. Chem.* **2022**, *Manuscript Submitted*

73. Lu, Y. L. X.-D., G.; Ju, G.F. X. H.M., Xue-Hai; Ji Structures and Properties of 1,2,3-Triazoles and 1,2,4-Triazoles. . *Chin. J. Struc. Chem.* **2006,** *5*, 582-588.

74. Bolton, K.; Brown, R. D.; Burden, F. R.; Mishra, A., The microwave spectrum and structure of 1,2,4-triazole. *J. Mol. Struct.* **1975,** *27*, 261-266.

75. Blackman, G. L.; Brown, R. D.; Burden, F. R.; Garland, W., Nuclear quadrupole coupling in the microwave spectrum of 1,2,3-triazole. *J. Mol. Spectrosc.* **1977,** *65* (2), 313-318.

76. Bougeard, D.; Le Calvé, N.; Roch, B. S.; Novak, A., 1,2,4-Triazole: Vibrational spectra, normal coordinate calculations, and hydrogen bonding. *J. Chem. Phys.* **1976,** *64* (12), 5152-5164.

77. Billes, F.; Endrédi, H.; Keresztury, G., Vibrational spectroscopy of triazoles and tetrazole. *J. Mol. Struct.* **2000,** *530* (1), 183-200.

78. Deuschl, H., X-ray structure analysis of 1, 2, 4-triazole. *Ber. Bunseges. Phys. Chem.* **1965,** *69*, 550-557.

79. Goldstein, P.; Ladell, J.; Abowitz, G., Refinement of the crystal and molecular structure of 1,2,4-triazole ($C_2H_3N_3$) at low temperature. *Acta. Crystallogr. B. Struct. Sci. Cryst. Eng. Mater.* **1969,** *25*, 135-143.

80. Chiang, J. F.; Lu, K. C., Molecular structure of 1,2,4-triazole. *J. Mol. Struct.* **1977,** *41* (2), 223-229.

81. Cox, J. R.; Woodcock, S.; Hillier, I. H.; Vincent, M. A., Tautomerism of 1,2,3- and 1,2,4-triazole in the gas phase and in aqueous solution: a combined ab initio quantum mechanics and free energy perturbation study. *J. Phys. Chem. A* **1990,** *94* (14), 5499-5501.

82. Aziz, S. G.; Elroby, S. A.; Alyoubi, A.; Osman, O. I.; Hilal, R., Experimental and theoretical assignment of the vibrational spectra of triazoles and benzotriazoles. Identification of IR marker bands and electric response properties. *J. Mol. Model* **2014,** *20* (3), 2078.

83. Abdulov, K. S.; Mulloev, N. U.; Tabarov, S. K.; Khodiev, M. K., Quantum Chemical Determination of the Molecular Structure of 1,2,4-Triazole and the Calculation of its Infrared Spectrum. *J. Struct. Chem.* **2020,** *61* (4), 510-514.

84. He, C.; Smith, M. A., Identification of nitrogenous organic species in Titan aerosols analogs: Nitrogen fixation routes in early atmospheres. *Icarus* **2013,** *226* (1), 33-40.

85. Thelen, A. E.; Cordiner, M. A.; Nixon, C. A.; Vuitton, V.; Kisiel, Z.; Charnley, S. B.; Palmer, M. Y.; Teanby, N. A.; Irwin, P. G. J., Detection of CH_3C_3N in Titan's Atmosphere. *Astrophys. J.* **2020,** *903* (1), L22.

86. Teanby, N.; Irwin, P.; de Kok, R.; Nixon, C.; Coustenis, A.; Bezard, B.; Calcutt, S.; Bowles, N.; Flasar, F.; Fletcher, L.; Howett, C.; Taylor, F., Latitudinal variations of HCN, HC_3N, and C_2N_2 in Titan's stratosphere derived from cassini CIRS data. *Icarus* **2016,** *181* (1), 243-255.

87. Teanby, N. A.; Irwin, P. G. J.; de Kok, R.; Vinatier, S.; Bézard, B.; Nixon, C. A.; Flasar, F. M.; Calcutt, S. B.; Bowles, N. E.; Fletcher, L.; Howett, C.; Taylor, F. W., Vertical profiles of HCN, HC_3N, and C_2H_2 in Titan's atmosphere derived from Cassini/CIRS data. *Icarus* **2007,** *186* (2), 364-384.

88. Vuitton, V.; Yelle, R. V.; Anicich, V. G., The Nitrogen Chemistry of Titan's Upper Atmosphere Revealed. *Astrophys. J.* **2006,** *647* (2), L175-L178.

89. Cui, J.; Yelle, R. V.; Vuitton, V.; Waite, J. H.; Kasprzak, W. T.; Gell, D. A.; Niemann, H. B.; Müller-Wodarg, I. C. F.; Borggren, N.; Fletcher, G. G.; Patrick, E. L.; Raaen, E.; Magee, B. A., Analysis of Titan's neutral upper atmosphere from Cassini Ion Neutral Mass Spectrometer measurements. *Icarus* **2009,** *200* (2), 581-615.

90. Hartzel, L. W.; Benson, F. R., Synthesis of 4-Alkyl-v-triazoles from Acetylenic Compounds and Hydrogen Azide. *J. Am. Chem. Soc.* **1954,** *76* (3), 667-670.

91. Borello, E.; Zecchina, A.; Guglielminotti, E., A vibrational assignment for 1,2,3-triazole. *J. Chem. Soc. B* **1969,** (0), 307-311.

92. Aziz, S.; Elroby, S.; Alyoubi, A.; Osman, O.; Hilal, R., Experimental and theoretical assignment of the vibrational spectra of triazoles and benzotriazoles. Identification of IR marker bands and electric response properties. *J. Mol. Model* **2014,** *20* (3), 1-15.

93. Begtrup, M.; Nielsen, C. J.; Nygaard, L.; Samdal, S.; Sjørgen, C. E.; Sørensen, G. O., The Molecular Structure and Tautomer Equilibrium of Gaseous 1,2,3-Triazole Studied by Microwave Spectroscopy, Electron Diffraction and *Ab Initio* Calculations. *Acta Chem. Scand.* **1988,** *A 42*, 500-514.

94. Sorensen, G. O.; Nygaard, L.; Begtrup, M., Microwave spectrum of 1-deuterio-1,2,3-triazole. *J. Chem. Soc., Chem. Commun.* **1974,** (15), 605-606.

95. Stiefvater, O. L.; Jones, H.; Sheridan, J., Double-resonance-double-search assignment of the microwave spectrum of 1,2,3-triazole. *Spectrochim. Acta A* **1970,** *26* (4), 825-833.

96. Zhou, Z.; Liu, R.; Wang, J.; Li, S.; Liu, M.; Brédas, J.-L., Intra- and Intermolecular Proton Transfer in 1*H* (2*H*)-1,2,3-Triazole Based Systems. *J. Phys. Chem. A* **2006,** *110* (7), 2322-2324.

97. Abboud, J.-L. M.; Foces-Foces, C.; Notario, R.; Trifonov, R. E.; Volovodenko, A. P.; Ostrovskii, V. A.; Alkorta, I.; Elguero, J., Basicity of N-H- and N-Methyl-1,2,3-triazoles in the Gas Phase, in Solution, and in the Solid State − An Experimental and Theoretical Study. *Eur. J. Org. Chem.* **2001,** *2001* (16), 3013-3024.

98. Goddard, R.; Heinemann, O.; Kruger, C., Pyrrole and a Co-crystal of 1*H*- and 2*H*-1,2,3-Triazole. *Acta Crystallogr. C Struct. Chem.* **1997,** *53* (12), 1846-1850.

99. Tomas, F.; Abboud, J. L. M.; Laynez, J.; Notario, R.; Santos, L.; Nilsson, S. O.; Catalan, J.; Claramunt, R. M.; Elguero, J., Tautomerism and aromaticity in 1,2,3-triazoles: the case of benzotriazole. *J. Am. Chem. Soc.* **1989,** *111* (19), 7348-7353.

100. Catalán, J.; Sánchez-Cabezudo, M.; De Paz, J. L. G.; Elguero, J.; Taft, R. W.; Anvia, F., The tautomerism of 1,2,3-triazole, 3(5)-methylpyrazole and their cations. *J. Comput. Chem.* **1989,** *10* (3), 426-433.

101. Palmer, M. H.; Simpson, I.; Findlay, R. H., ^{14}N Nuclear Quadrupole Coupling in Heterocyclic Compounds, Part 2. A Comparison of *ab initio* Calculations and Experimental Results for the Azoles and Azines. *Z. Naturforsch., A: Phys. Sci.* **1980,** *36 A*, 34-50.

102. Törnkvist, C.; Bergman, J.; Liedberg, B., Correlated *ab initio* geometries and vibrations of 1*H*- and 2*H*-1,2,3-triazole. *J. Phys. Chem. A* **1991,** *95* (8), 3123-3128.

103. Lu, Y.-L.; Gong, X.-D.; Ju, X.-H.; Ji, G.-F.; Xiao, H.-M., Structures and Properties of 1,2,3-Triazoles and 1,2,4-Triazoles. *Chin. J. Struc. Chem.* **2006,** (5), 582-588.

104. Puzzarini, C.; Bloino, J.; Tasinato, N.; Barone, V., Accuracy and Interpretability: The Devil and the Holy Grail. New Routes across Old Boundaries in Computational Spectroscopy. *Chem. Rev.* **2019,** *119* (13), 8131-8191.

105. Császár, A. G.; Demaison, J.; Rudolph, H. D., Equilibrium Structures of Three-, Four-, Five-, Six-, and Seven-Membered Unsaturated N-Containing Heterocycles. *J. Phys. Chem. A* **2015,** *119* (9), 1731-1746.

106. Nygaard, L.; Asmussen, E.; Høg, J. H.; Maheshwari, R. C.; Nielsen, C. H.; Petersen, I. B.; Rastrup-Andersen, J.; Sørensen, G. O., Microwave Spectra of Isotopic Thiazoles. Molecular Structure ^{14}N Quadrupole Coupling Constants of Thiazole. *J. Mol. Struct.* **1971,** *8* (1), 225-233.

107. Cernicharo, J.; Heras, A. M.; Tielens, A. G. G. M.; Pardo, J. R.; Herpin, F.; Guelin, M.; Waters, L. B. F. M., Infrared space observatory's discovery of C_4H_2, C_6H_2, and benzene in CRL 618. *Astrophys. J.* **2001,** *546* (2), L123-L126.

108. Charnley, S. B.; Kuan, Y.-J.; Huang, H.-C.; Botta, O.; Butner, H. M.; Cox, N.; Despois, D.; Ehrenfreund, P.; Kisiel, Z.; Lee, Y.-Y.; Markwick, A. J.; Peeters, Z.; Rodgers, S. D., Astronomical searches for nitrogen heterocycles. *Adv. Space Res.* **2005,** *36*, 137-145.

109. Kuan, Y.-J.; Yan, C.-H.; Charnley, S. B.; Kisiel, Z.; Ehrenfreund, P.; Huang, H.-C., A search for interstellar pyrimidine. *Mon. Notices Royal Astron. Soc.* **2003,** *345*, 650-656.

110. Cunha de Miranda, B.; Garcia, G. A.; Gaie-Levrel, F.; Mahjoub, A.; Gautier, T.; Fleury, B.; Nahon, L.; Pernot, P.; Carrasco, N., Molecular Isomer Identification of Titan's Tholins Organic Aerosols by Photoelectron/Photoion Coincidence Spectroscopy Coupled to VUV Synchrotron Radiation. *J. Phys. Chem. A* **2016,** *120* (33), 6529-6540.

111. Bonandi, E.; Christodoulou, M. S.; Fumagalli, G.; Perdicchia, D.; Rastelli, G.; Passarella, D., The 1,2,3-triazole ring as a bioisostere in medicinal chemistry. *Drug Discov. Today* **2017,** *22* (10), 1572-1581.

112. Valverde, I. E.; Bauman, A.; Kluba, C. A.; Vomstein, S.; Walter, M. A.; Mindt, T. L., 1,2,3-Triazoles as Amide Bond Mimics: Triazole Scan Yields Protease-Resistant Peptidomimetics for Tumor Targeting. *Angew. Chem. Int. Ed.* **2013,** *52* (34), 8957-8960.

113. Bozorov, K.; Zhao, J.; Aisa, H. A., 1,2,3-Triazole-containing hybrids as leads in medicinal chemistry: A recent overview. *Bioorg. Med. Chem.* **2019,** *27* (16), 3511-3531.

114. Huisgen, R., Kinetics and Mechanism of 1,3-Dipolar Cycloadditions. *Angew. Chem., Int. Ed. Engl.* **1963,** *2* (11), 633-645.

115. Kolb, H. C.; Finn, M. G.; Sharpless, K. B., Click Chemistry: Diverse Chemical Function from a Few Good Reactions. *Angew. Chem. Int. Ed.* **2001,** *40*, 2004-2021.

116. Devaraj, N. K.; Finn, M. G., Introduction: Click Chemistry *Chem. Rev. (Washington, D. C.)* **2021,** *121*, 6697−6698.

117. Lahuis, F.; Dishoeck, E. F. V., ISO–SWS spectroscopy of gas–phase C_2H_2 and HCN toward massive young stellar objects. *Astron. Astrophys.* **2000,** *355*, 699-712.

118. Sonnentrucker, P.; González-Alfonso, E.; Neufeld, D. A., Detection of Acetylene toward Cepheus A East with Spitzer. *Astrophys. J.* **2007,** *671* (1), L37-L40.

119. Singh, S.; McCord, T. B.; Combe, J. P.; Rodriguez, S.; Cornet, T.; Mouélic, S. L.; Clark, R. N.; Maltagliati, L.; Chevrier, V. F., Acetylene on Titan's Surface. *Astrophys. J.* **2016,** *828* (1), 55.

120. Amberger, B. K.; Esselman, B. J.; Stanton, J. F.; Woods, R. C.; McMahon, R. J., Precise Equilibrium Structure Determination of Hydrazoic Acid (HN_3) by Millimeter-wave Spectroscopy. *J. Chem. Phys.* **2015,** *143* (10), 104310/1-104310/9.

121. Zhu, J.; Mo, J.; Lin, H.-z.; Chen, Y.; Sun, H.-p., The recent progress of isoxazole in medicinal chemistry. *Bioorg. Med. Chem.* **2018,** *26* (12), 3065-3075.

122. Lamberth, C., Oxazole and Isoxazole Chemistry in Crop Protection. *J. Heterocycl. Chem.* **2018,** *55* (9), 2035-2045.

123. Møllendal, H.; Konovalov, A., Microwave Spectrum of 2-Aminooxazole, a Compound of Potential Prebiotic and Astrochemical Interest. *J. Phys. Chem. A* **2010,** *114* (5), 2151-2156.

124. Melli, A.; Melosso, M.; Lengsfeld, K. G.; Bizzocchi, L.; Rivilla, V. M.; Dore, L.; Barone, V.; Grabow, J.-U.; Puzzarini, C., Spectroscopic Characterization of 3-Aminoisoxazole, a Prebiotic Precursor of Ribonucleotides. *Molecules* **2022,** *27* (10), 3278.

125. Maté, B.; Carrasco-Herrera, R.; Timón, V.; Tanarro, I.; Herrero, V.; Carrascosa, H.; Caro, G.; Gonzalez Diaz, C.; Jiménez-Serra, I., *2-aminooxazole in astrophysical environments: IR spectra and destruction cross sections for energetic processing*. 2021.

126. Nunes, C. M.; Reva, I.; Pinho e Melo, T. M. V. D.; Fausto, R., UV-Laser Photochemistry of Isoxazole Isolated in a Low-Temperature Matrix. *J. Org. Chem.* **2012,** *77* (19), 8723-8732.

127. Hegelund, F.; Wugt Larsen, R.; Nicolaisen, F. M.; Palmer, M. H., The high-resolution infrared spectrum of isoxazole vapor between 800 and 1700cm−1. *J. Mol. Spectrosc.* **2005,** *229* (2), 244-256.

128. Palmer, M. H.; Wugt Larsen, R.; Hegelund, F., The Infrared Spectrum of Isoxazole in the Range 600–1400 cm^{-1}, Including a High-Resolution Study of the ν_7 (A′) Band at 1370.9 cm^{-1} and the ν_{16} (A″) band at 764.9 cm^{-1}, Together with *Ab Initio* Studies of the Full Spectrum. *Mol. Phys.* **2004,** *102* (14-15), 1569-1581.

129. Califano, S.; Piacenti, F.; Speroni, G., Infrared and Raman spectra of isoxazole: the vibrational assignment. *Spectrochim. Acta A* **1959,** *15*, 86-94.

130. Katritzky, A. B.; Boulton, A. J., Infra-red absorption of heteroaromatic, five-membered, monocyclic nuclei—III: Isoxazoles. *Spectrochim. Acta A* **1961,** *17* (3), 238-247.

131. Adembri, G.; Speroni, G.; Califano, S., Vibrational assignment of isoxazole-d_3. *Spectrochim. Acta A* **1963,** *19* (7), 1145-1152.

132. Robertson, E. G., Vibrational assignment of isoxazole aided by rovibrational data and density functional theory. *J. Mol. Spectrosc.* **2005,** *231* (1), 50-56.

133. Sauer, E. G.; Oja, T., Nitrogen-14 nuclear quadrupole resonance in isoxazole. *J. Chem. Phys.* **1973,** *58* (6), 2650-2651.

134. Lowe, S. E.; Sheridan, J., Nuclear quadrupole coupling tensor of 14N in isoxazole from the microwave spectrum of isoxazole-4D. *Chem. Phys. Lett.* **1978,** *58* (1), 79-82.

135. Mackrodt, W. C.; Wardley, A.; Curnuck, P. A.; Owen, N. L.; Sheridan, J., Microwave spectra of oxazole and isoxazole. *Chem. Commun. (London)* **1966,** (19), 692-693.

136. Dias, N.; Joalland, B.; Ariyasingha, N. M.; Suits, A. G.; Broderick, B. M., Direct versus Indirect Photodissociation of Isoxazole from Product Branching: A Chirped-Pulse Fourier Transform mm-Wave Spectroscopy/Pulsed Uniform Flow Investigation. *J. Phys. Chem. A* **2018,** *122* (38), 7523-7531.

137. Kobayashi, K.; Tsunekawa, S. In *Microwave Spectroscopy of Oxazole and Isoxazole*, 2019/06/1.

138. McGlone, S.; Moreschini, P.; Ha, T. K.; Bauder, A., Microwave spectra and structure of an isoxazole-water complex. *Mol. Phys.* **2001,** *99* (16), 1353-1364.

139. Roy, T. K.; Chatterjee, K.; Khatri, J.; Schwaab, G.; Havenith, M., Stepwise Microhydration of Isoxazole: Infrared Spectroscopy of Isoxazole-$(H_2O)_2$ Clusters in Helium Nanodroplets. *J. Phys. Chem. A* **2021,** *125* (22), 4766-4774.

140. McGlone, S.; Bauder, A., Microwave spectra and structure of an isoxazole-CO Van der Waals complex. *J. Chem. Phys.* **1998,** *109* (13), 5383-5392.

141. Spoerel, U.; Dreizler, H.; Stahl, W.; Kraka, E.; Cremer, D., Intermolecular Forces in van der Waals Complexes between Argon and Aromatic Molecules: Rotational Spectrum and ab Initio Investigation of Isoxazole-Argon. *J. Phys. Chem.* **1996,** *100* (34), 14298-14309.

142. Stiefvater, O. L., The complete structure of isoxazole from naturally occurring isotopic forms by double resonance modulated microwave spectroscopy. *J. Chem. Phys.* **1975,** *63* (6), 2560-2569.

143. Stiefvater, O. L.; Nösberger, P.; Sheridan, J., Microwave spectrum and structure of isoxazole. *Chem. Phys.* **1975,** *9* (3), 435-444.

144. El-Bakali Kassimi, N.; Doerksen, R. J.; Thakkar, A. J., Polarizabilities of Oxazoles: Ab Initio Calculations and Simple Models. *J. Phys. Chem. A* **1996,** *100* (21), 8752-8757.

145. Palmer, M. H.; Findlay, R. H.; Egdell, R. G., The electronic structure of heteroaromatic molecules; ab initio calculations and photoelectron spectra for the isomeric-oxazoles and some -oxadiazoles. *J. Mol. Struct.* **1977,** *40* (2), 191-210.

146. Ha, T. K., A theoretical study of the electronic structure and properties of some five-membered heterocyclic compounds: pyrazole, imidazole, furan, isoxazole, 1,2,5-oxadiazole and 1,3,4-oxadiazole. *J. Mol. Struct.* **1979,** *51*, 87-98.

147. Zdanovskaia, M. A.; Esselman, B. J.; Kougias, S. M.; Woods, R. C.; McMahon, R. J., Vibrational and Structural Analysis of Pyridine using Millimeter-wave Spectroscopy. *To Be Submitted* **2022**.

148. Zdanovskaia, M. A. Rotational Spectroscopy of Nitrogen-Containing Molecules (and Some with Heavier Elements). Ph.D. Dissertation. University of Wisconsin - Madison, 2022.

149. Ye, E.; Bettens, R. P. A.; De Lucia, F. C.; Petkie, D. T.; Albert, S., Millimeter and submillimeter wave rotational spectrum of pyridine in the ground and excited vibrational states. *J. Mol. Spectrosc.* **2005,** *232* (1), 61-65.

150. Bettens, R. P. A.; Bauder, A., The microwave spectrum and structure of the pyridine–CO complex. *J. Chem. Phys.* **1995,** *102* (4), 1501-1509.

151. Heineking, N.; Dreizler, H.; Schwarz, R., Nitrogen and deuterium hyperfine structure in the rotational spectra of pyridine and [4-D]pyridine. *Z. Naturforsch., A: Phys. Sci.* **1986,** *41A* (10), 1210-13.

152. Mata, F.; Quintana, M. J.; Sørensen, G. O., Microwave spectra of pyridine and monodeuterated pyridines. Revised molecular structure of pyridine. *J. Mol. Struct.* **1977,** *42*, 1-5.

153. Sharma, S. D.; Doraiswamy, S., Effect of substitution on the pyridine ring geometry - a microwave spectroscopic study. *Chem. Phys. Lett.* **1976,** *41* (1), 192-198.

154. Sørensen, G. O.; Mahler, L.; Rastrup-Andersen, N., Microwave spectra of [^{15}N] and [^{13}C] pyridines, quadrupole coupling constants, dipole moment and molecular structure of pyridine. *J. Mol. Struct.* **1974,** *20* (1), 119-126.

155. Sørensen, G. O., Centrifugal distortion analysis of microwave spectra of asymmetric top molecules. The microwave spectrum of pyridine. *J. Mol. Spectrosc.* **1967,** *22* (1), 325-346.

156. Bak, B.; Hansen-Nygaard, L.; Rastrup-Andersen, J., Complete determination of the structure of pyridine by microwave spectra. *J. Mol. Spectrosc.* **1958,** *2* (1), 361-368.

157. McCulloh, K. E.; Pollnow, G. F., An Investigation of the Microwave Spectrum of Pyridine. *J. Chem. Phys.* **1954,** *22* (4), 681-682.

158. DeMore, B. B.; Wilcox, W. S.; Goldstein, J. H., Microwave Spectrum and Dipole Moment of Pyridine. *J. Chem. Phys.* **1954,** *22* (5), 876-877.

159. Bak, B.; Hansen, L.; Rastrup-Anderson, J., Microwave Spectrum of Pyridine. *J. Chem. Phys.* **1954,** *22* (3), 565-565.

160. Bak, B.; Rastrup-Andersen, J., Microwave Investigation of Pyridine. *J. Chem. Phys.* **1953,** *21* (7), 1305-1306.

161. Albert, S.; Quack, M., High Resolution Rovibrational Spectroscopy of Chiral and Aromatic Compounds. *ChemPhysChem* **2007,** *8* (9), 1271-1281.

162. Stidham, H. D.; Dilella, D. P., Vibrational spectra of C_{2v} deuterium substituted pyridines. 4-pyridine-2,3,5,6-d_4 and pyridine-d_5. *J. Raman Spectrosc.* **1980,** *9* (4), 247-256.

163. Csaszar, A. G.; Demaison, J.; Rudolph, H. D., Equilibrium Structures of Three-, Four-, Five-, Six-, and Seven-Membered Unsaturated N-Containing Heterocycles. *J. Phys. Chem. A* **2015,** *119*, 1731-1746.

164. Demaison, J.; Jahn, M. K.; Cocinero, E. J.; Lesarri, A.; Grabow, J.-U.; Guillemin, J.-C.; Rudolph, H. D., Accurate Semiexperimental Structure of 1,3,4-Oxadiazole by the Mixed Estimation Method. *J. Phys. Chem. A* **2013,** *117* (10), 2278-2284.

165. Orr, V. L. Rotational and Vibrational Spectroscopy and Structure Determination of Organic Molecules of Astrochemical Relevance. Ph.D. Dissertation. University of Wisconsin - Madison, 2021.

166. Lin, S.; Herbert, D. E.; Velian, A.; Day, M. W.; Agapie, T., Dipalladium(I) Terphenyl Diphosphine Complexes as Models for Two-Site Adsorption and Activation of Organic Molecules. *J. Am. Chem. Soc.* **2013,** *135* (42), 15830-15840.

167. Leis, H. J.; Fauler, G.; Windischhofer, W., Stable isotope labeled target compounds: preparation and use as internal standards in quantitative mass spectrometry. *Curr. Org. Chem.* **1998,** *2* (2), 131-144.

168. Burton, A. G.; Forsythe, P. P.; Johnson, C. D.; Katritzky, A. R., The kinetics and mechanism of the electrophilic substitution of heteroaromatic compounds. Part XXVII. The nitration and hydrogen exchange of 1,3,5-trimethylpyrazole, 3,5-dimethylisoxazole, and 3,5-dimethylisothiazole. *J. Chem. Soc. B* **1971**, 2365-2371.

169. Roussel, P.; Metzger, J., Synthesis and infrared spectral study of the deuteriothiazoles. *Bull. Soc. Chim. Fr.* **1962**, 2075-2078.

170. Alonso, B.; Ocejo, M.; Carrillo, L.; Vicario, J. L.; Reyes, E.; Uria, U., Using Heteroaryl-lithium Reagents as Hydroxycarbonyl Anion Equivalents in Conjugate Addition Reactions with (S,S)-(+)-Pseudoephedrine as Chiral Auxiliary; Enantioselective Synthesis of 3-Substituted Pyrrolidines. *J. Org. Chem.* **2013,** *78* (2), 614-627.

171. Katritzky, A. R. R. C. W. S. E. F. V., *Comprehensive heterocyclic chemistry II : a review of the literature 1982-1995 : the structure, reactions, synthesis, and uses of heterocyclic compounds*. Pergamon: Oxford; New York, 1996.

172. Belen'kii, L. I.; Nesterov, I. D.; Chuvylkin, N. D., Quantum chemical studies of azoles 13. Specific solvation effect on the calculated energetic parameters of the electrophilic substitution mechanism in thiazole *via* elimination–addition schemes. *Russ. Chem. Bull.* **2018,** *67* (11), 1971-1977.

173. Olofson, R. A.; Landesberg, J. M.; Houk, K. N.; Michelman, J. S., The Deprotonation of Thiazole and Related Bases. *J. Am. Chem. Soc.* **1966,** *88* (18), 4265-4266.

174. Wakefield, B. J., Product class 9: isoxazoles. *Sci. Synth.* **2002,** *11*, 229-288.

175. Basu, A. K.; Marnett, L. J., Synthesis of malondialdehyde-1-^{2}H and malondialdehyde-1,3-$^{2}H_2$. *J. Labelled Compd. Radiopharm.* **1985,** *22* (11), 1175-9.

176. Chuaqui-Offermanns, N.; Chuaqui, C. A., Studies on the reactivity of malondialdehyde. I. Effects of acid concentration and solvent composition on deuterium exchange reactions. *Chem. Phys. Lipids* **1983,** *33* (3), 215-21.

177. McEwen, C. N.; McKay, R. G.; Larsen, B. S., Analysis of solids, liquids, and biological tissues using solids probe introduction at atmospheric pressure on commercial LC/MS instruments. *Anal. Chem.* **2005,** *77*, 7826-7831.

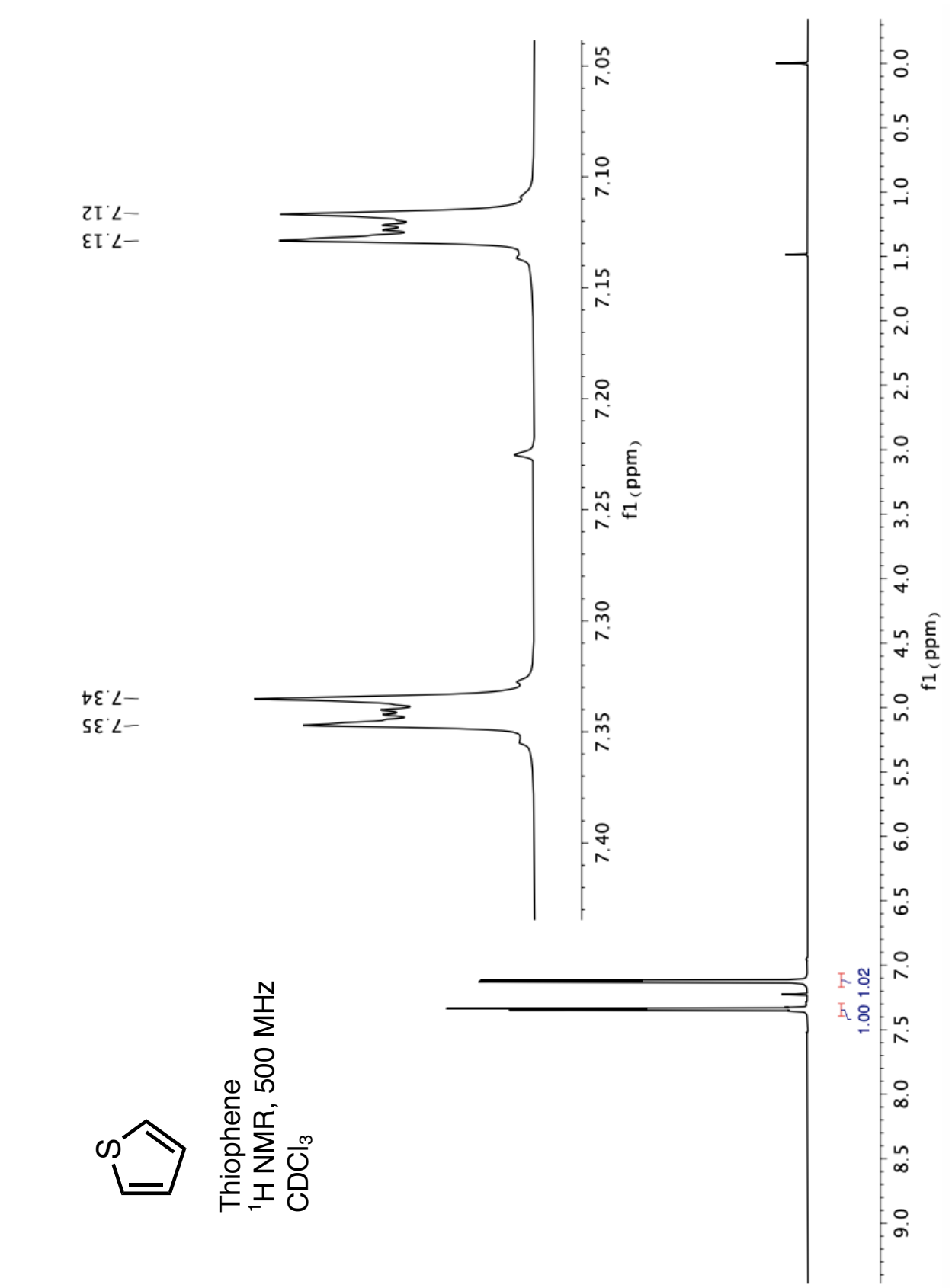
178. Wright, C. J.; Smith, R. N.; Kroll, J. A.; Shipman, S. T.; Widicus Weaver, S. L., Extending the Millimeter/Submillimeter Wave Spectrum of Ground State Pyruvic Acid for Comparison to Astronomical Data. *ACS Earth Space Chem.* **2022,** *6* (3), 482-495.

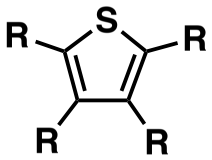
179. Iddon, B.; Nicholas, M., Azoles. Part 13. Synthesis and bromine → lithium exchange reactions of some 1-substituted 4,5-dibromo-1*H*-1,2,3-triazoles and 2-substituted 4,5-dibromo-2*H*-1,2,3-triazoles. *J. Chem. Soc., Perkin Trans. 1* **1996,** (12), 1341-1347.

180. Sakurada, I., Facile synthesis of bromo- and iodo-1,2,3-triazoles. *Tetrahedron Lett.* **2017,** *58* (32), 3188-3190.

181. Wang, X.-j.; Zhang, L.; Krishnamurthy, D.; Senanayake, C. H.; Wipf, P., General Solution to the Synthesis of *N*-2-Substituted 1,2,3-Triazoles. *Org. Lett.* **2010,** *12* (20), 4632-4635.

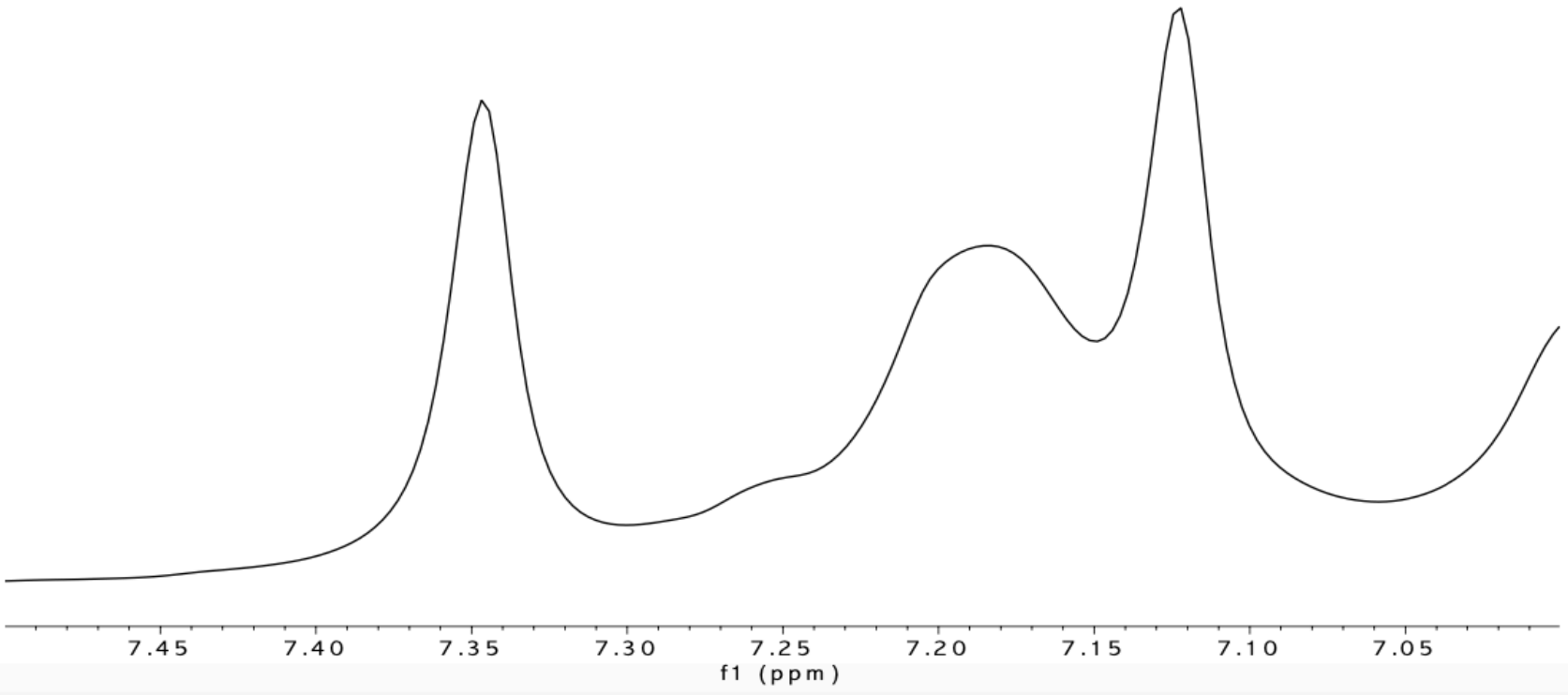
Supporting Information for Chapter 4:
Synthesis of Isotopically – Labeled Heterocyclic Molecules for Detailed Equilibrium Structure Determinations
"Heavy Heterocycles"

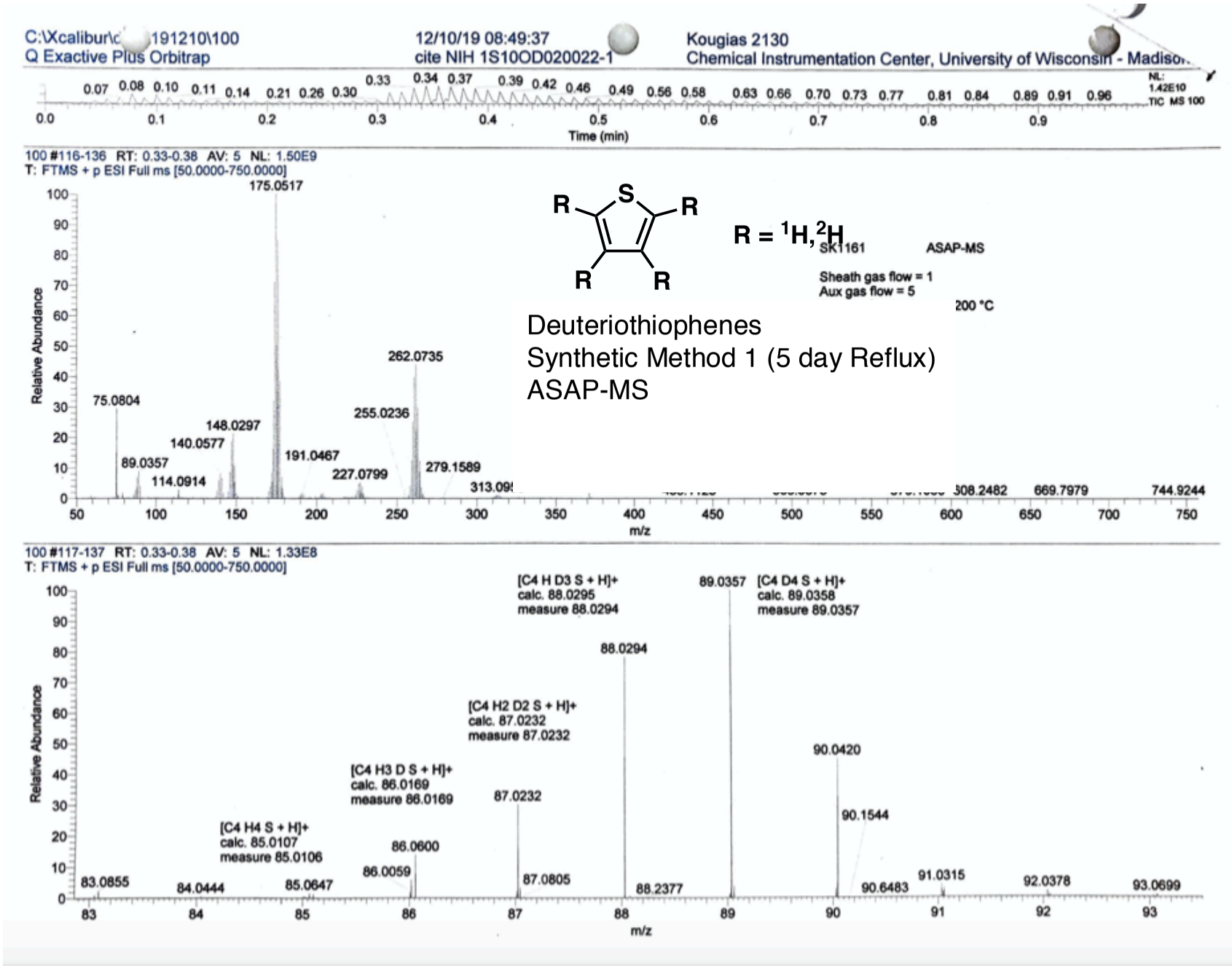

Thiophene
^{1}H NMR, 500 MHz
$CDCl_3$
7.35
7.34
7.13
7.12
1.00 1.02
f1 (ppm)
f1 (ppm)

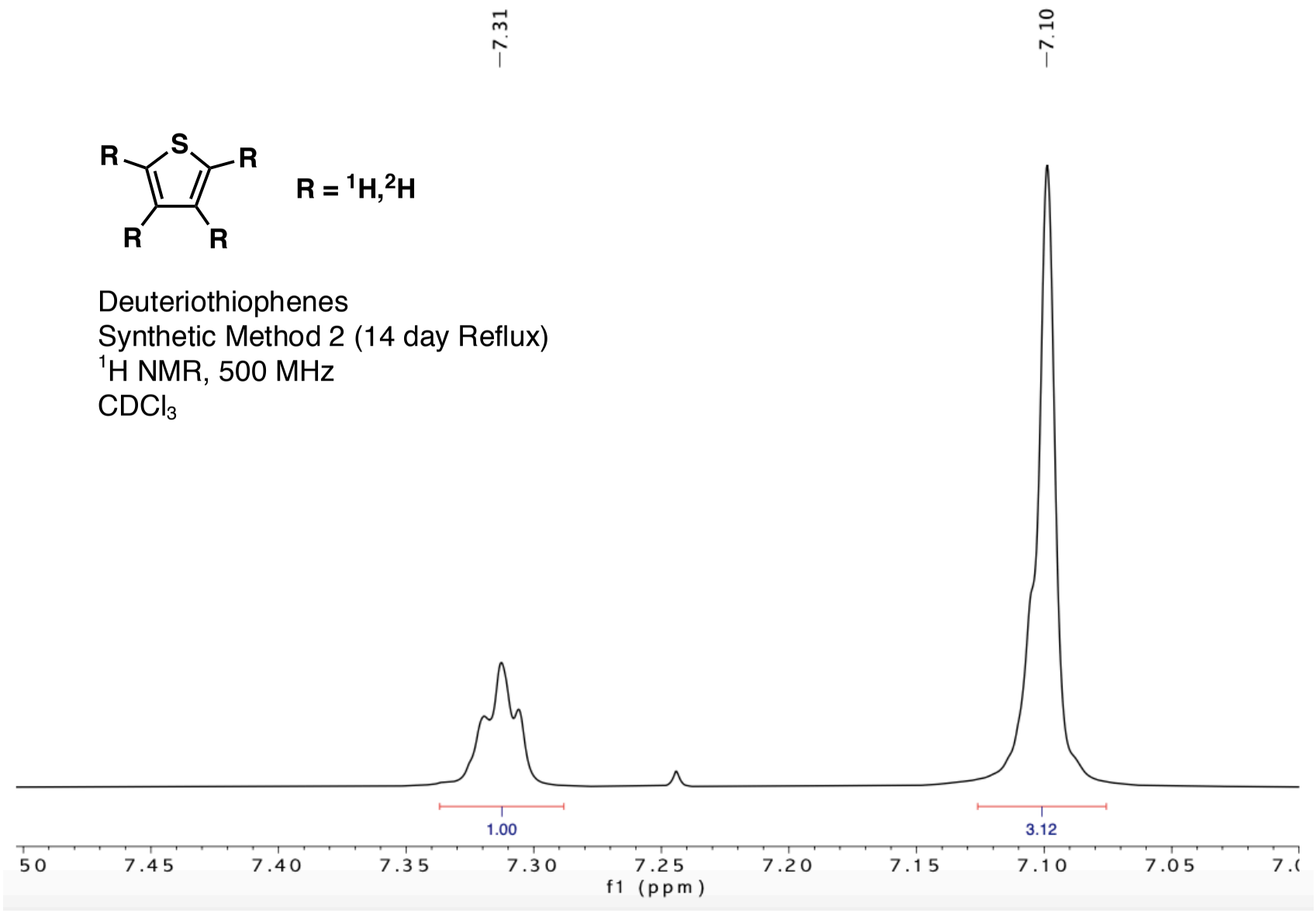


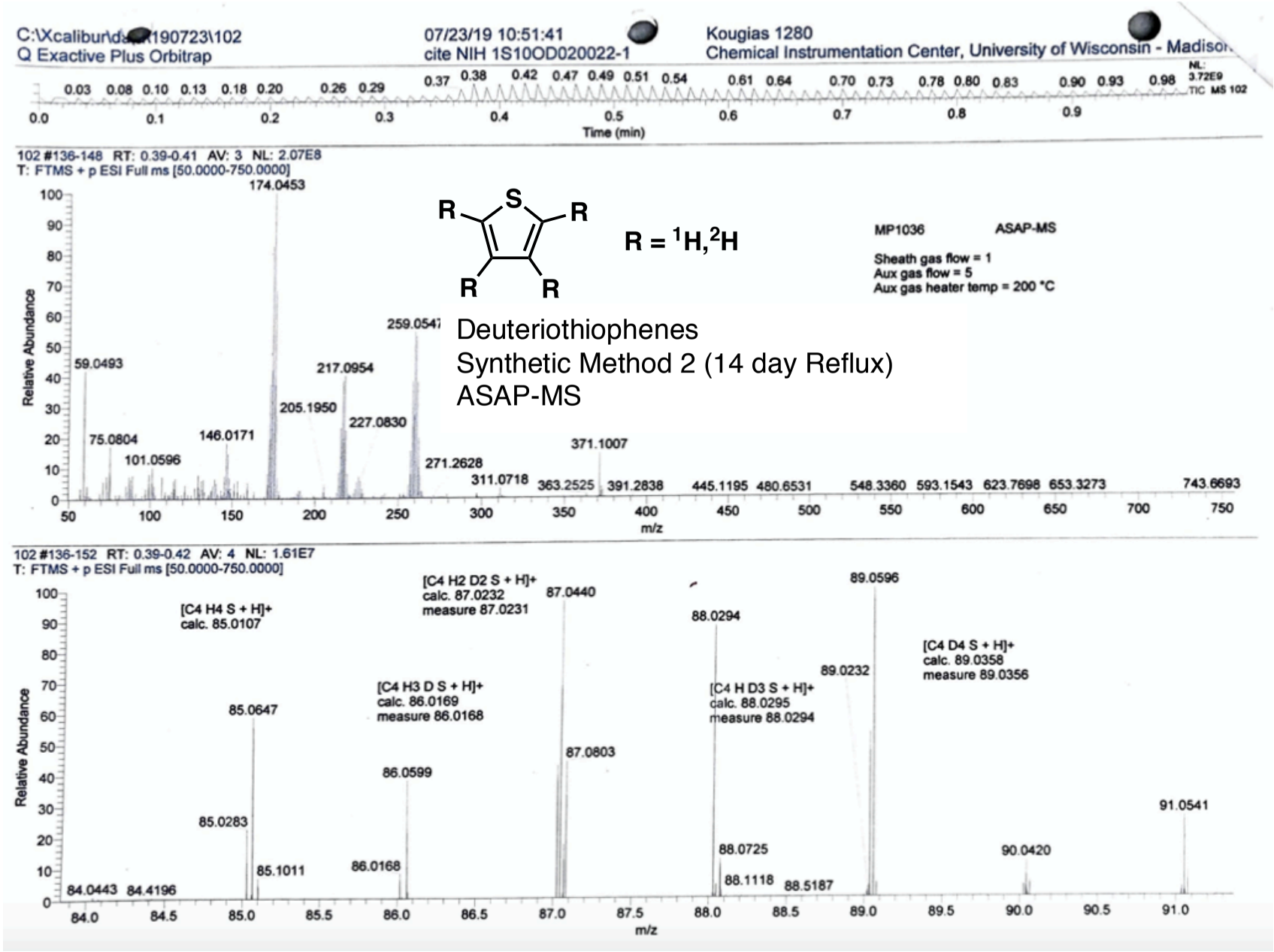
R = $^{1}H,^{2}H$

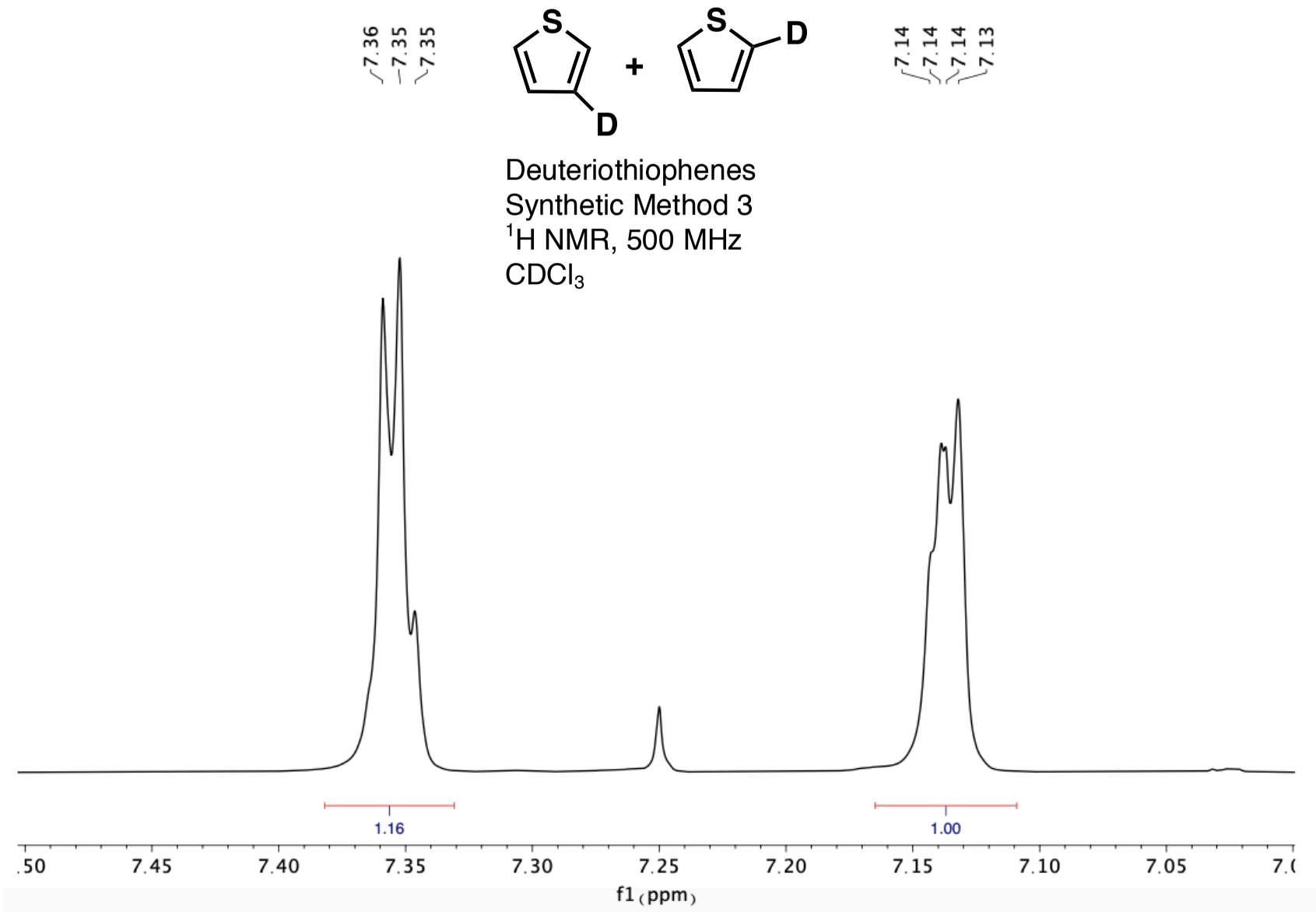
Deuteriothiophenes
Synthetic Method 1 (5 day Reflux)
^{2}H NMR, 500 MHz
$CHCl_3$

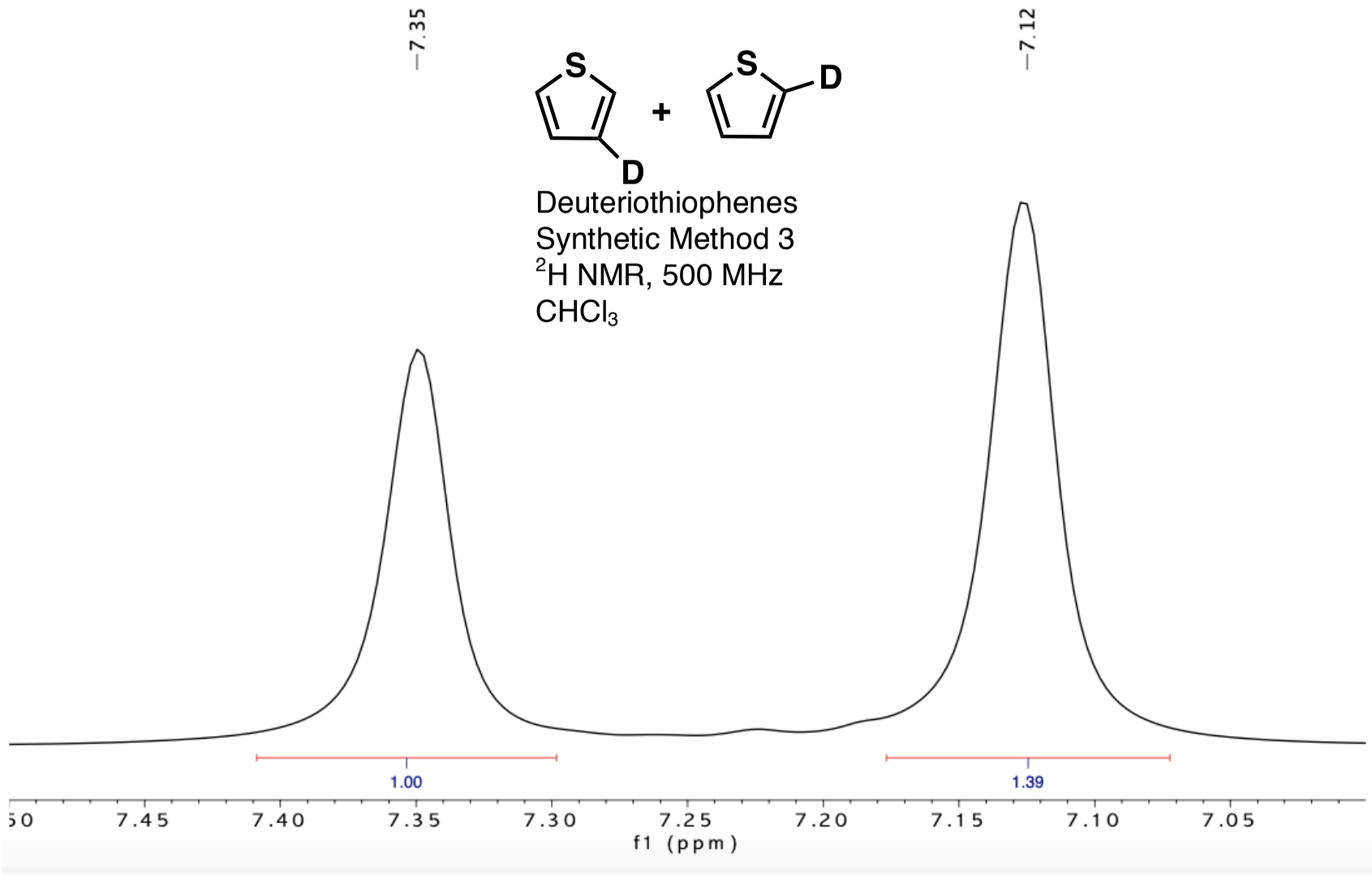


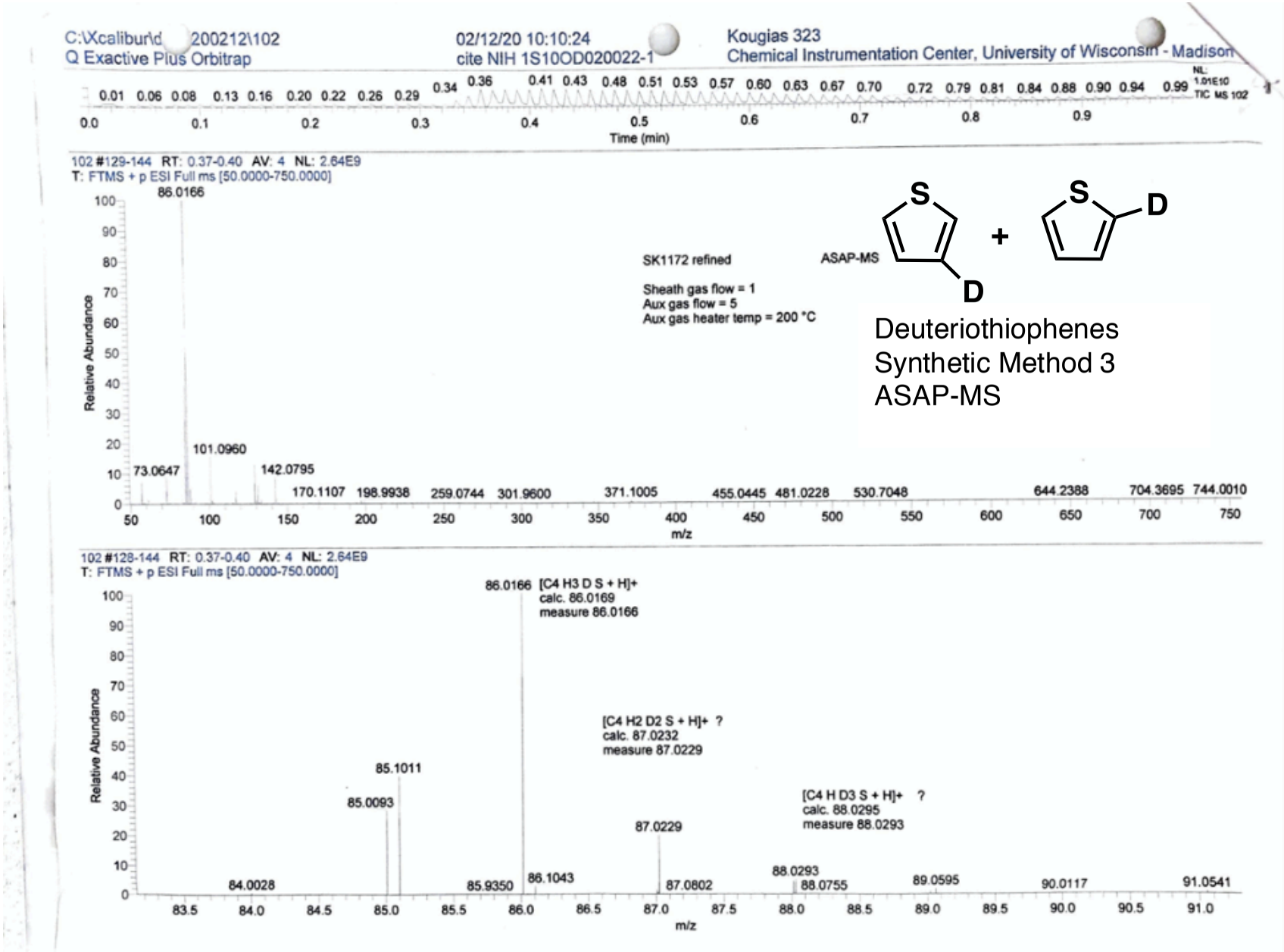

C:\Xcalibur\d 191210\100
Q Exactive Plus Orbitrap
12/10/19 08:49:37
cite NIH 1S10OD020022-1
Kougias 2130
Chemical Instrumentation Center, University of Wisconsin - Madiso
NL: 1.42E10 TIC MS 100
Time (min)
100 #116-136 RT: 0.33-0.38 AV: 5 NL: 1.50E9
T: FTMS + p ESI Full ms [50.0000-750.0000]
Relative Abundance
m/z
R = 1H,2H
SK1161
ASAP-MS
Sheath gas flow = 1
Aux gas flow = 5
200 °C
Deuteriothiophenes
Synthetic Method 1 (5 day Reflux)
ASAP-MS
100 #117-137 RT: 0.33-0.38 AV: 5 NL: 1.33E8
T: FTMS + p ESI Full ms [50.0000-750.0000]
[C4 H D3 S + H]+ calc. 88.0295 measure 88.0294
[C4 D4 S + H]+ calc. 89.0358 measure 89.0357
[C4 H2 D2 S + H]+ calc. 87.0232 measure 87.0232
[C4 H3 D S + H]+ calc. 86.0169 measure 86.0169
[C4 H4 S + H]+ calc. 85.0107 measure 85.0106

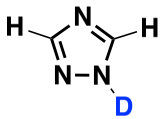

R
S
R
R
R
R = $^{1}H,^{2}H$
Deuteriothiophenes
Synthetic Method 2 (14 day Reflux)
^{1}H NMR, 500 MHz
$CDCl_3$
7.31
7.10
1.00
3.12
50
7.45
7.40
7.35
7.30
7.25
7.20
7.15
7.10
7.05
f1 (ppm)


C:\Xcalibur\data\190723\102
Q Exactive Plus Orbitrap
07/23/19 10:51:41
cite NIH 1S10OD020022-1
Kougias 1280
Chemical Instrumentation Center, University of Wisconsin - Madison
TIC MS 102
Time (min)
102 #136-148 RT: 0.39-0.41 AV: 3 NL: 2.07E8
T: FTMS + p ESI Full ms [50.0000-750.0000]
R = 1H,2H
MP1036 ASAP-MS
Sheath gas flow = 1
Aux gas flow = 5
Aux gas heater temp = 200 °C
Deuteriothiophenes
Synthetic Method 2 (14 day Reflux)
ASAP-MS
Relative Abundance
m/z
102 #136-152 RT: 0.39-0.42 AV: 4 NL: 1.61E7
T: FTMS + p ESI Full ms [50.0000-750.0000]
[C4 H4 S + H]+
calc. 85.0107
[C4 H2 D2 S + H]+
calc. 87.0232
measure 87.0231
[C4 H3 D S + H]+
calc. 86.0169
measure 86.0168
[C4 H D3 S + H]+
calc. 88.0295
measure 88.0294
[C4 D4 S + H]+
calc. 89.0358
measure 89.0356

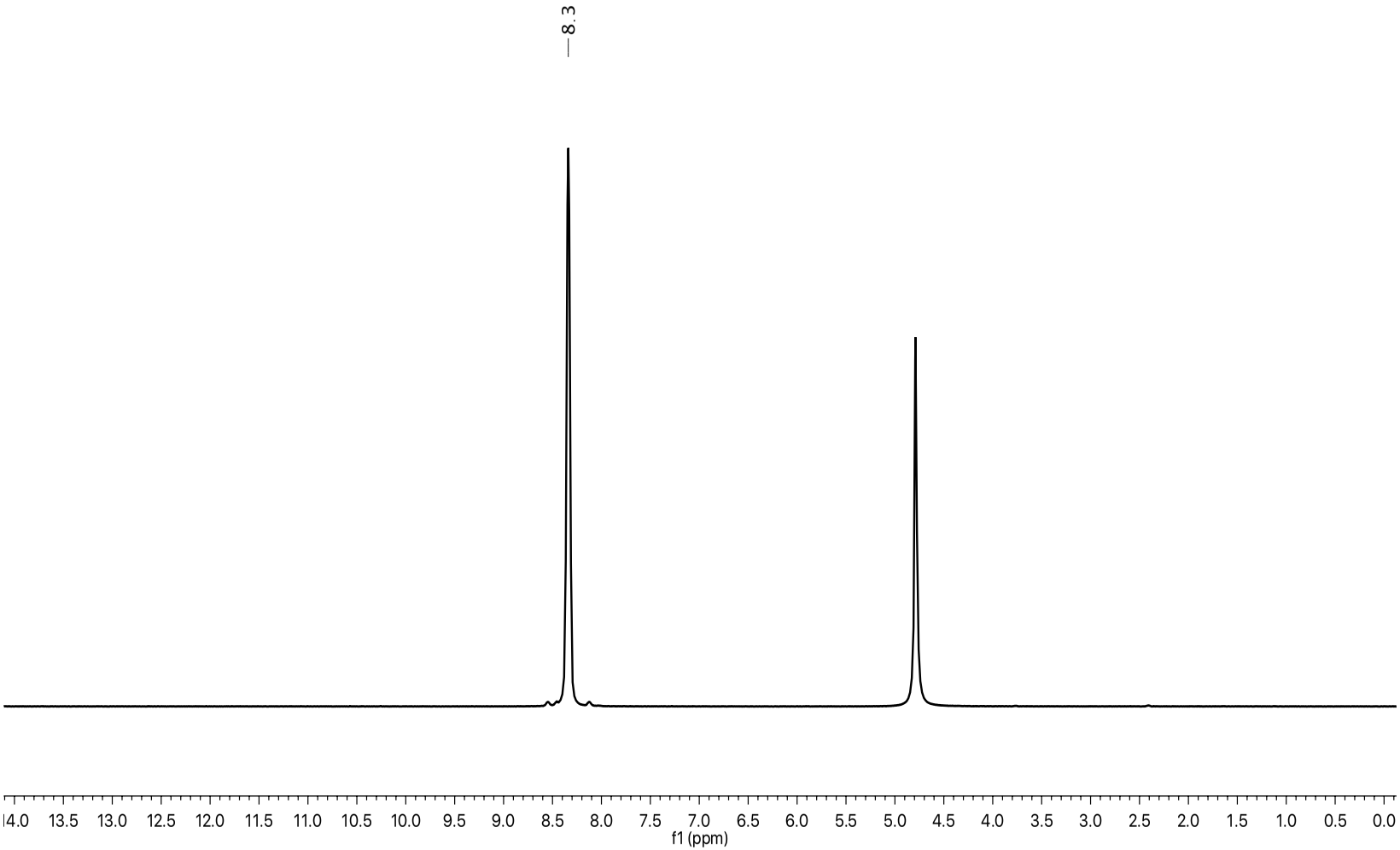

7.36
7.35
7.35
S
D
+
S
D
7.14
7.14
7.14
7.13
Deuteriothiophenes
Synthetic Method 3
1H NMR, 500 MHz
CDCl3
1.16
1.00
.50
7.45
7.40
7.35
7.30
7.25
7.20
7.15
7.10
7.05
f1 (ppm)

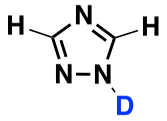

7.35
7.12
S
S
D
+
D
Deuteriothiophenes
Synthetic Method 3
2H NMR, 500 MHz
CHCl3
1.00
1.39
50
7.45
7.40
7.35
7.30
7.25
7.20
7.15
7.10
7.05
f1 (ppm)


C:\Xcalibur\d 200212\102
Q Exactive Plus Orbitrap
02/12/20 10:10:24
cite NIH 1S10OD020022-1
Kougias 323
Chemical Instrumentation Center, University of Wisconsin - Madison
Time (min)
102 #129-144 RT: 0.37-0.40 AV: 4 NL: 2.64E9
T: FTMS + p ESI Full ms [50.0000-750.0000]
86.0166
101.0960
73.0647
142.0795
SK1172 refined
Sheath gas flow = 1
Aux gas flow = 5
Aux gas heater temp = 200 °C
ASAP-MS
Deuteriothiophenes
Synthetic Method 3
ASAP-MS
Relative Abundance
m/z
102 #128-144 RT: 0.37-0.40 AV: 4 NL: 2.64E9
T: FTMS + p ESI Full ms [50.0000-750.0000]
86.0166 [C4 H3 D S + H]+
calc. 86.0169
measure 86.0166
[C4 H2 D2 S + H]+ ?
calc. 87.0232
measure 87.0229
[C4 H D3 S + H]+ ?
calc. 88.0295
measure 88.0293
85.1011
85.0093
87.0229
84.0028
85.9350
86.1043
87.0802
88.0293
88.0755
89.0595
90.0117
91.0541

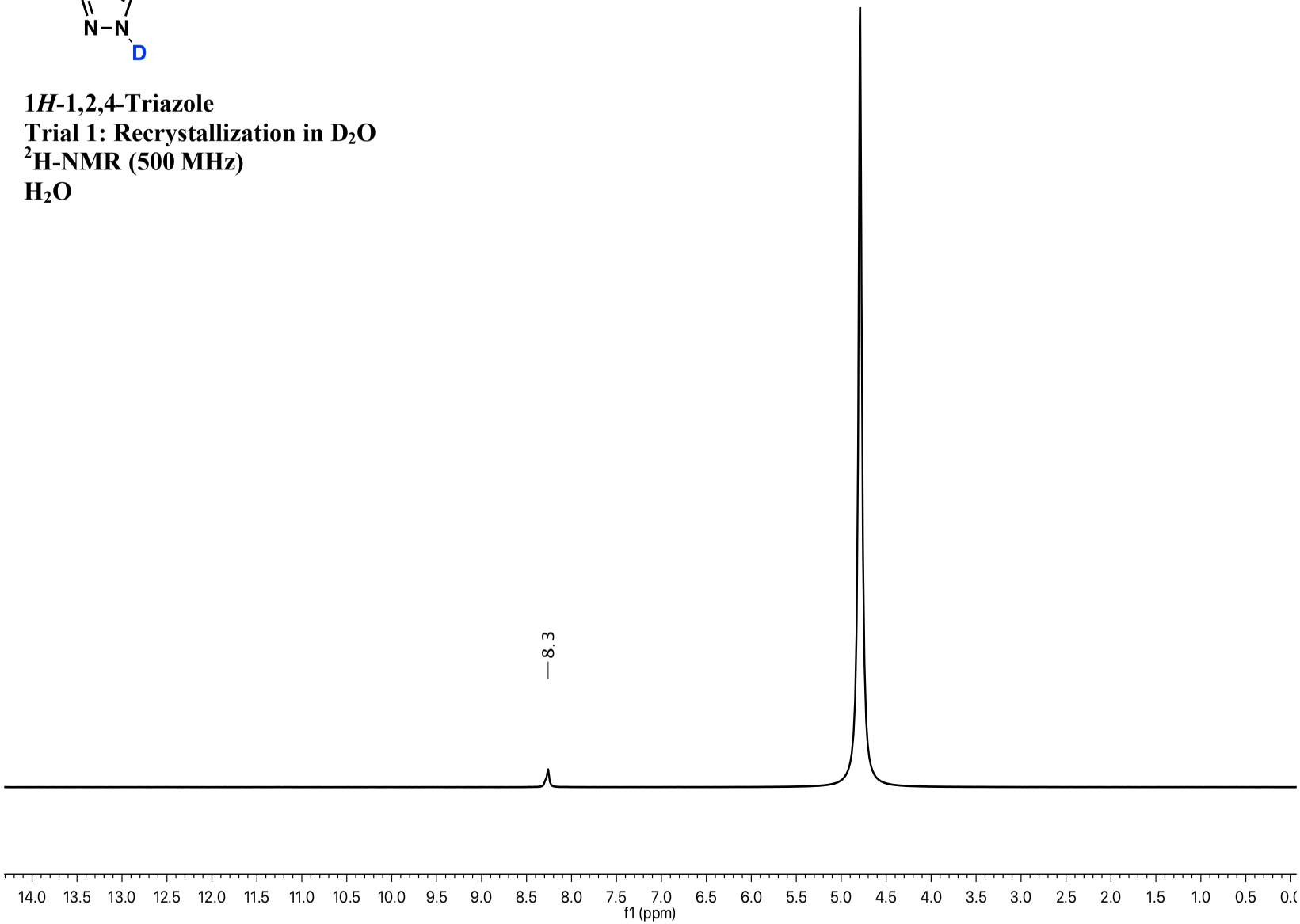


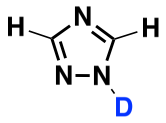
Deuterated 1*H*-1,2,4-Triazole
Trial 1: Recrystallization in D_2O
^{1}H-NMR (500 MHz)
D_2O



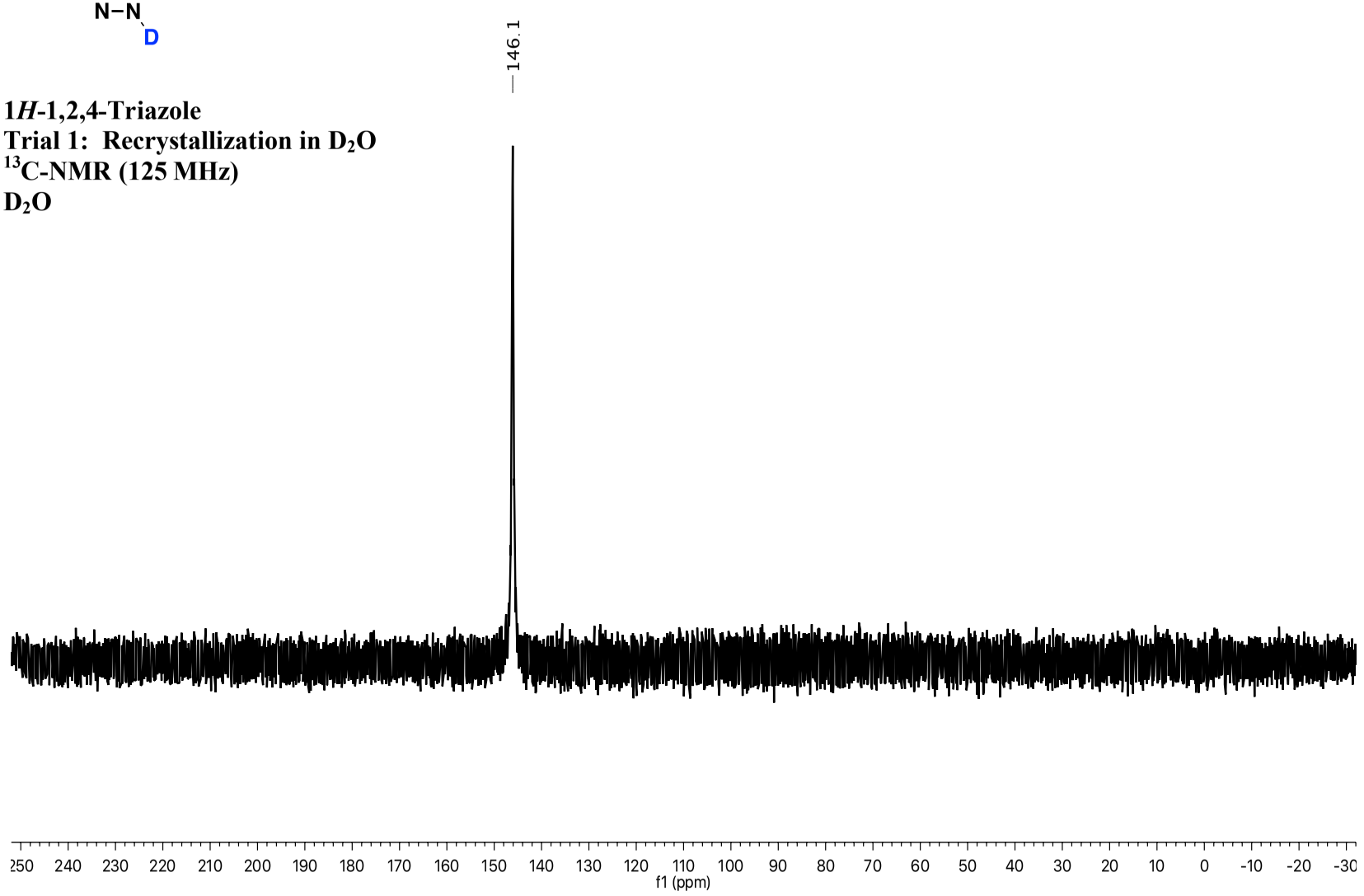


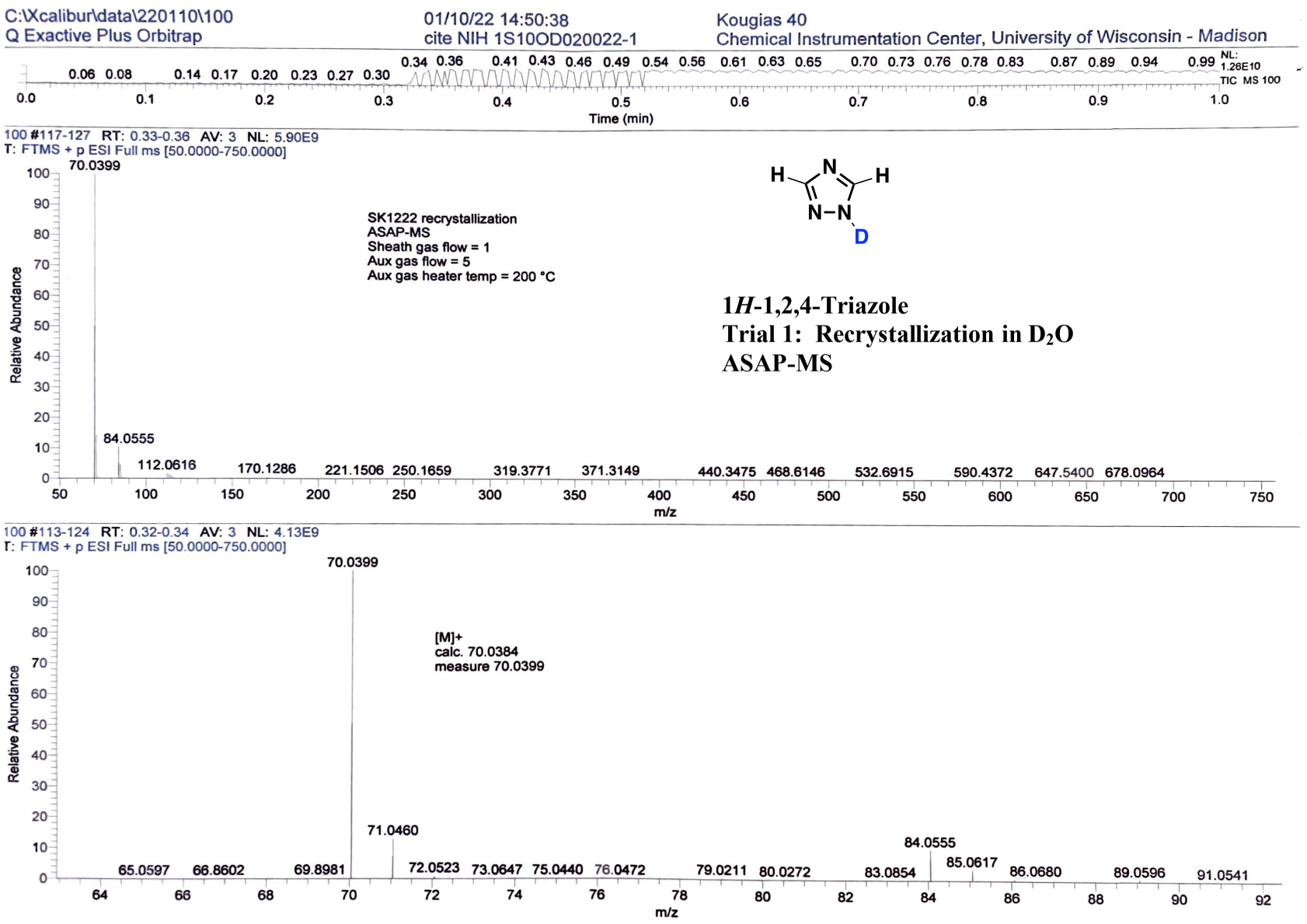
1*H*-1,2,4-Triazole
Trial 1: Recrystallization in D_2O
^{2}H-NMR (500 MHz)
H_2O

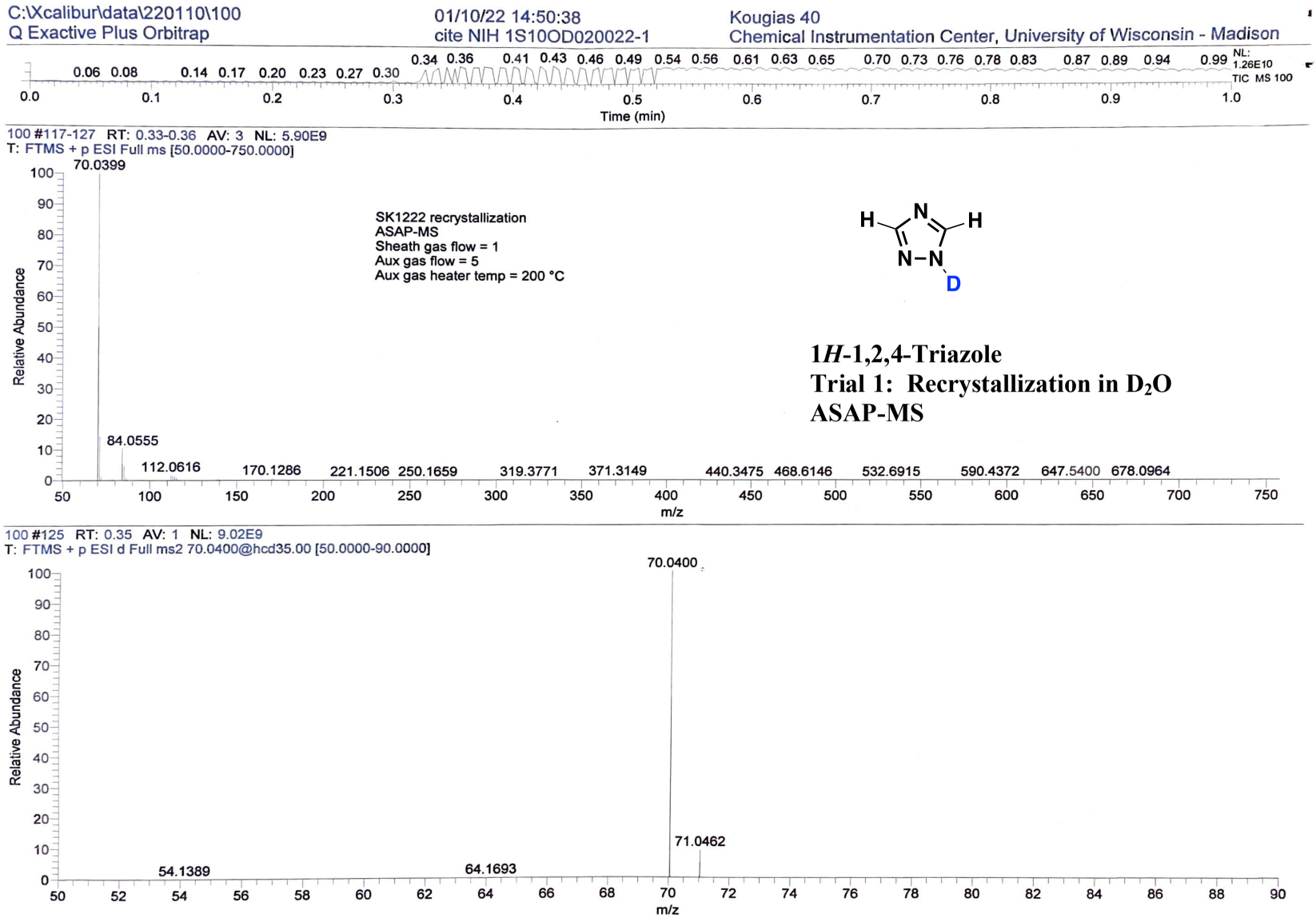


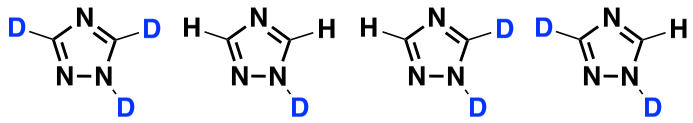


1*H*-1,2,4-Triazole
Trial 1: Recrystallization in D_2O
^{13}C-NMR (125 MHz)
D_2O



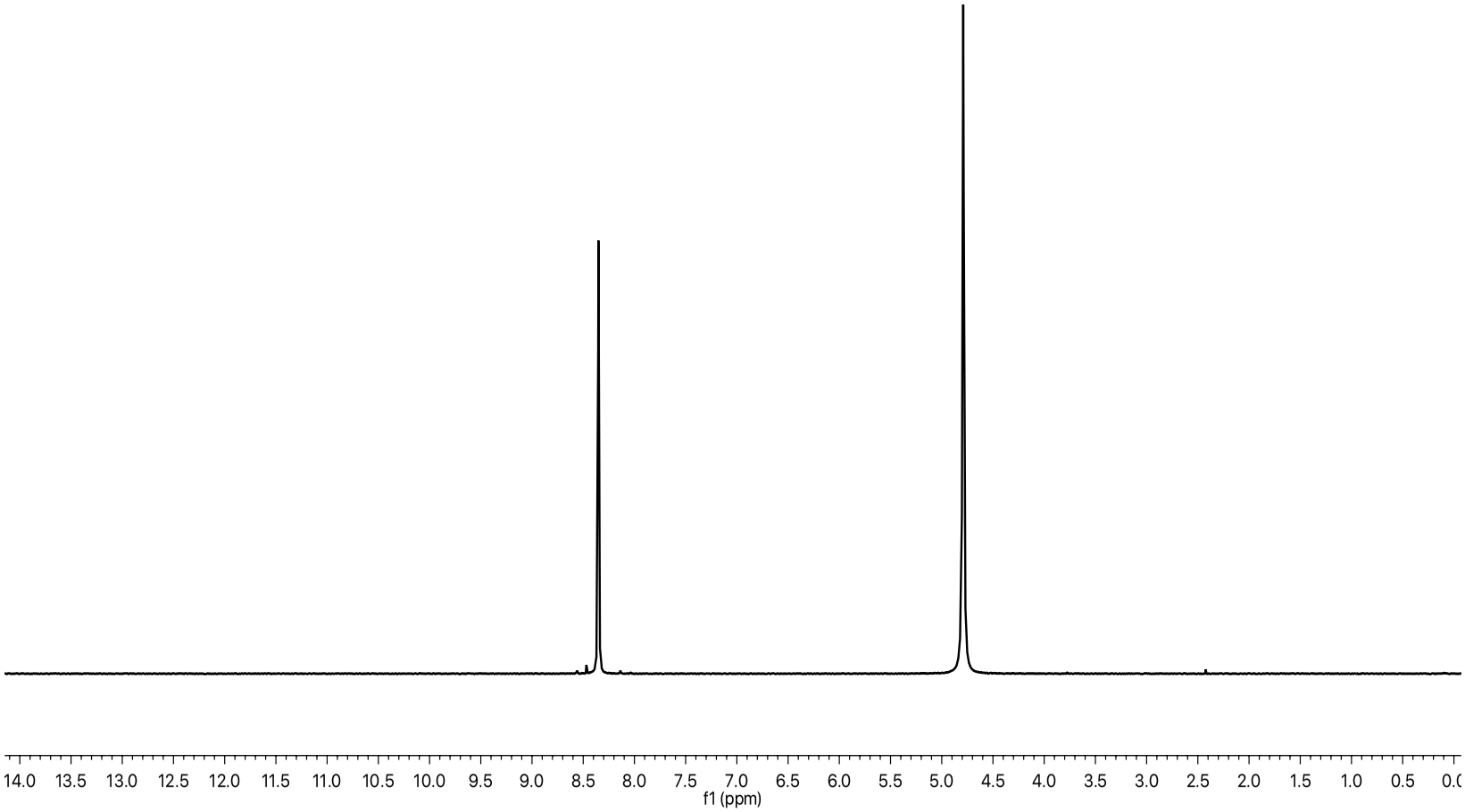

C:\Xcalibur\data\220110\100
Q Exactive Plus Orbitrap
01/10/22 14:50:38
cite NIH 1S10OD020022-1
Kougias 40
Chemical Instrumentation Center, University of Wisconsin - Madison
NL: 1.26E10 TIC MS 100
Time (min)
100 #117-127 RT: 0.33-0.36 AV: 3 NL: 5.90E9
T: FTMS + p ESI Full ms [50.0000-750.0000]
70.0399
SK1222 recrystallization
ASAP-MS
Sheath gas flow = 1
Aux gas flow = 5
Aux gas heater temp = 200 °C
Relative Abundance
m/z
84.0555
112.0616
170.1286
221.1506
250.1659
319.3771
371.3149
440.3475
468.6146
532.6915
590.4372
647.5400
678.0964
1H-1,2,4-Triazole
Trial 1: Recrystallization in D2O
ASAP-MS
100 #113-124 RT: 0.32-0.34 AV: 3 NL: 4.13E9
T: FTMS + p ESI Full ms [50.0000-750.0000]
70.0399
[M]+
calc. 70.0384
measure 70.0399
71.0460
65.0597
66.8602
69.8981
72.0523
73.0647
75.0440
76.0472
79.0211
80.0272
83.0854
84.0555
85.0617
86.0680
89.0596
91.0541

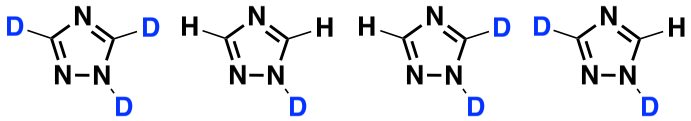

C:\Xcalibur\data\220110\100
Q Exactive Plus Orbitrap
01/10/22 14:50:38
cite NIH 1S10OD020022-1
Kougias 40
Chemical Instrumentation Center, University of Wisconsin - Madison
NL: 1.26E10 TIC MS 100
Time (min)
100 #117-127 RT: 0.33-0.36 AV: 3 NL: 5.90E9
T: FTMS + p ESI Full ms [50.0000-750.0000]
SK1222 recrystallization
ASAP-MS
Sheath gas flow = 1
Aux gas flow = 5
Aux gas heater temp = 200 °C
1H-1,2,4-Triazole
Trial 1: Recrystallization in D2O
ASAP-MS
Relative Abundance
m/z
100 #125 RT: 0.35 AV: 1 NL: 9.02E9
T: FTMS + p ESI d Full ms2 70.0400@hcd35.00 [50.0000-90.0000]



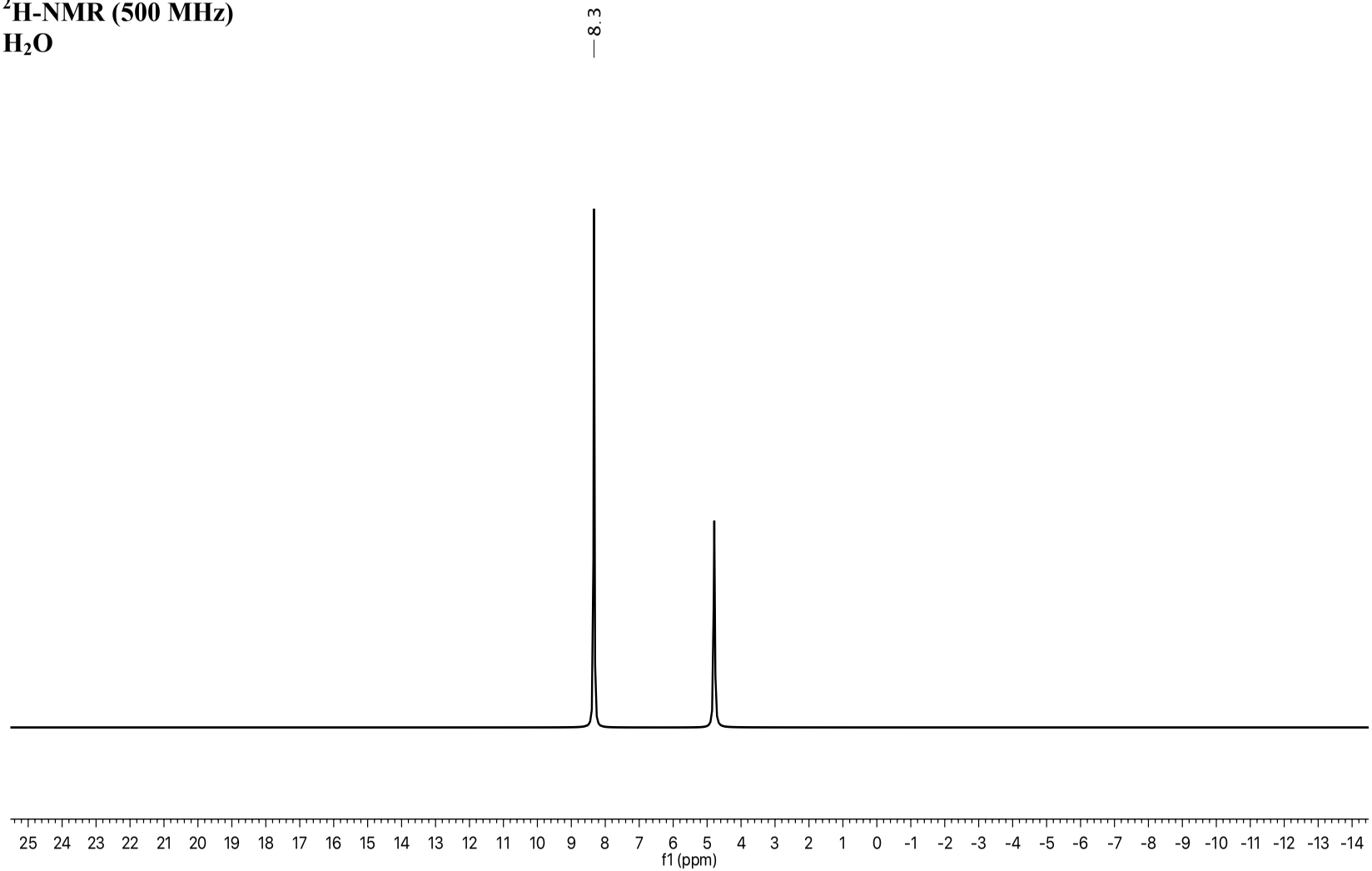
1*H*-1,2,4-Triazole
Trial 2: 72 hour reflux in D_2O/Recrystallization
^{1}H-NMR (500 MHz)
D_2O

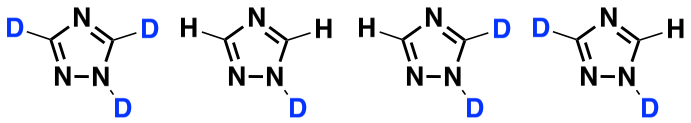
8.4



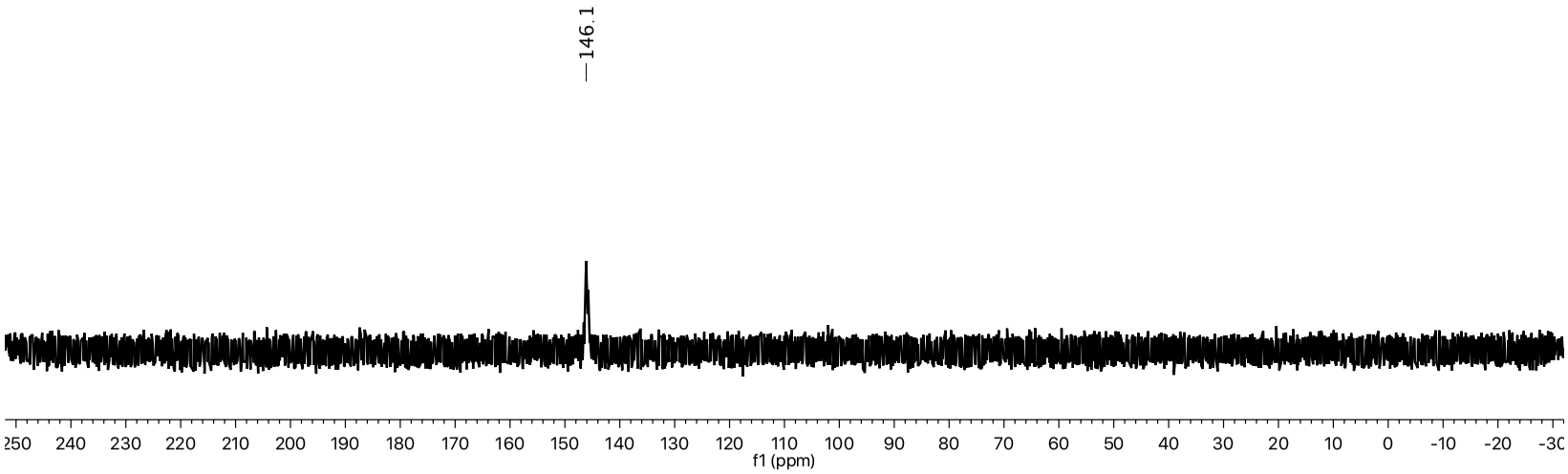


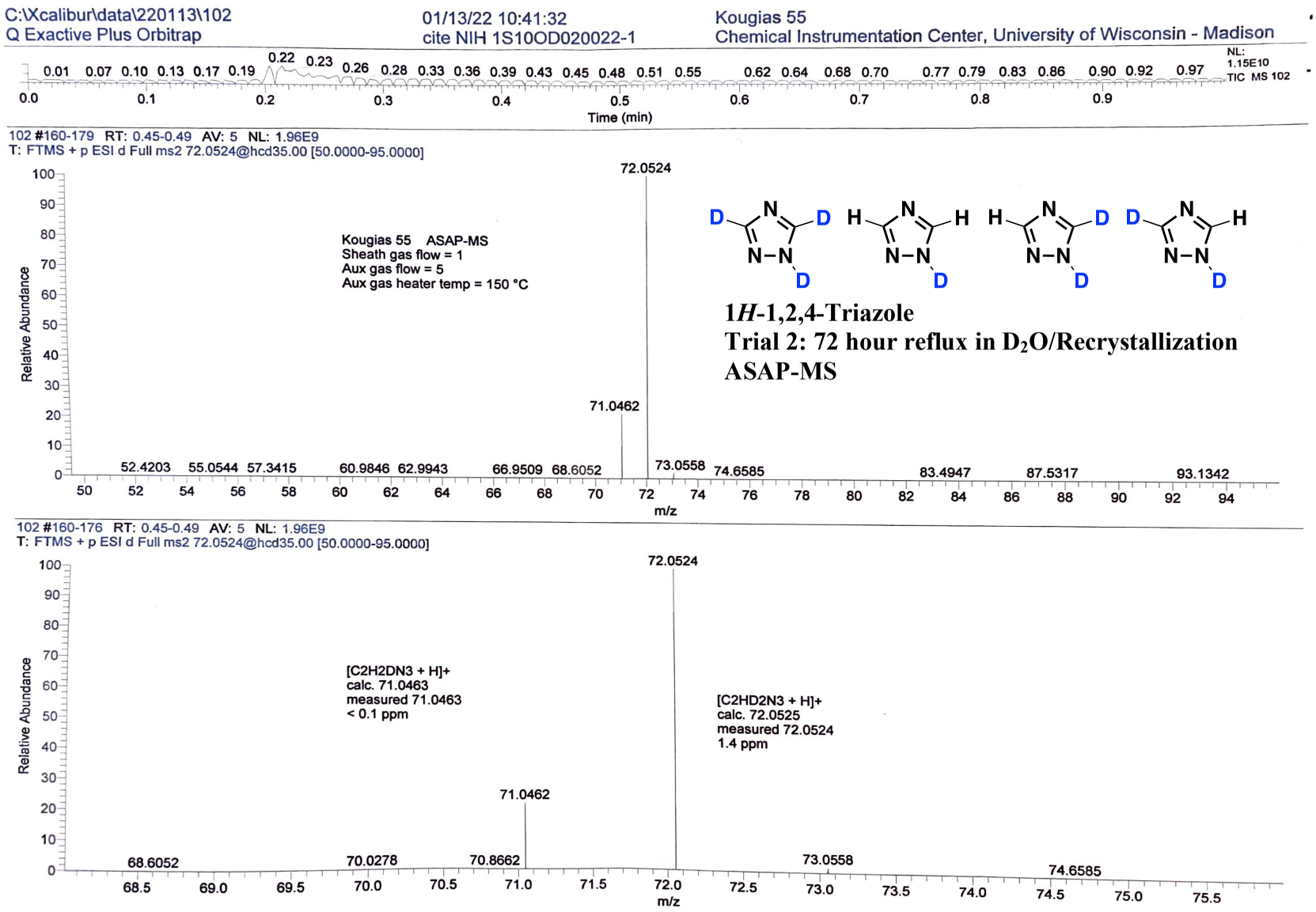
1*H*-1,2,4-Triazole
Trial 2: 72 hour reflux in D_2O/Recrystallization
^{2}H-NMR (500 MHz)
H_2O

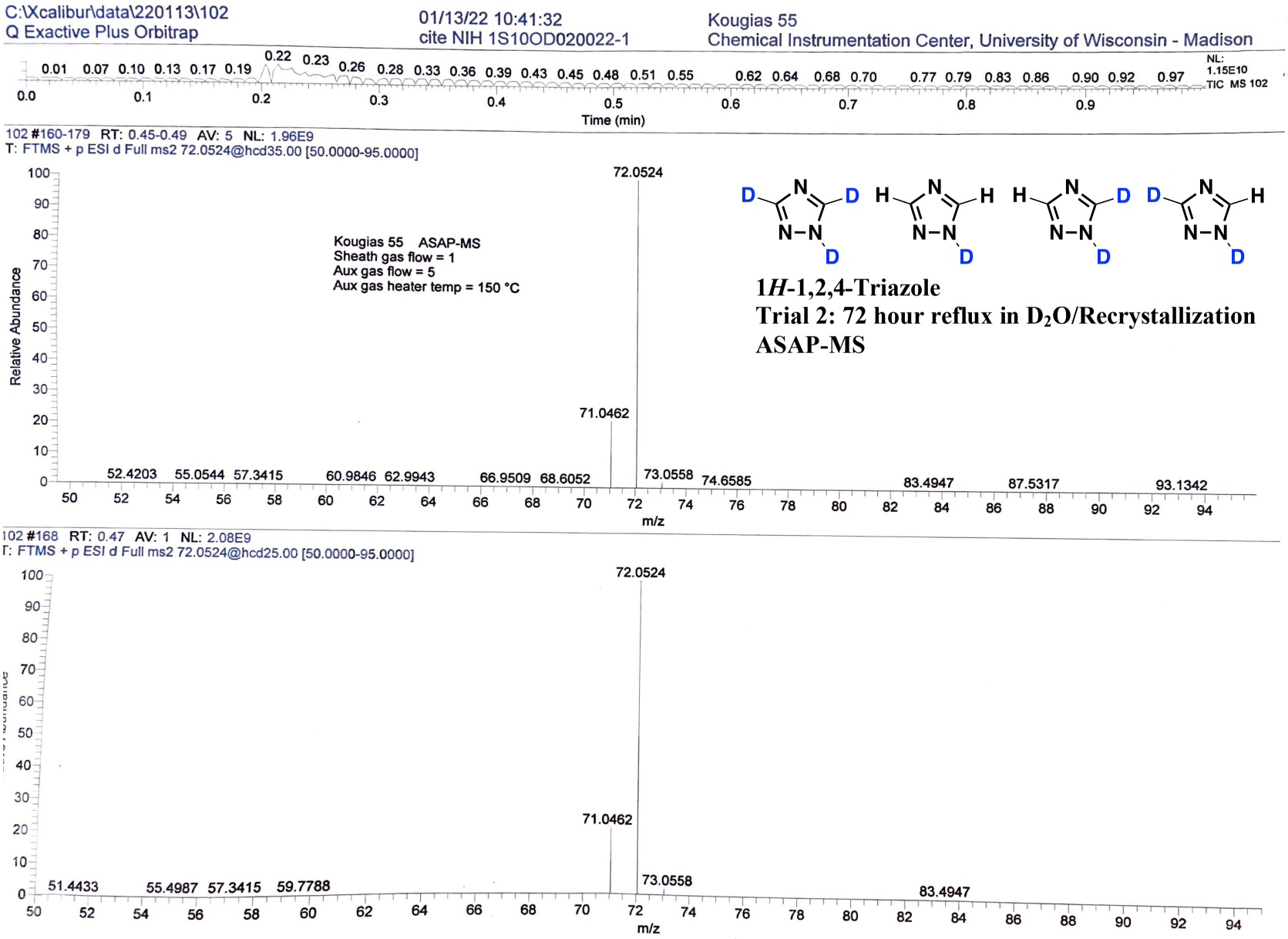


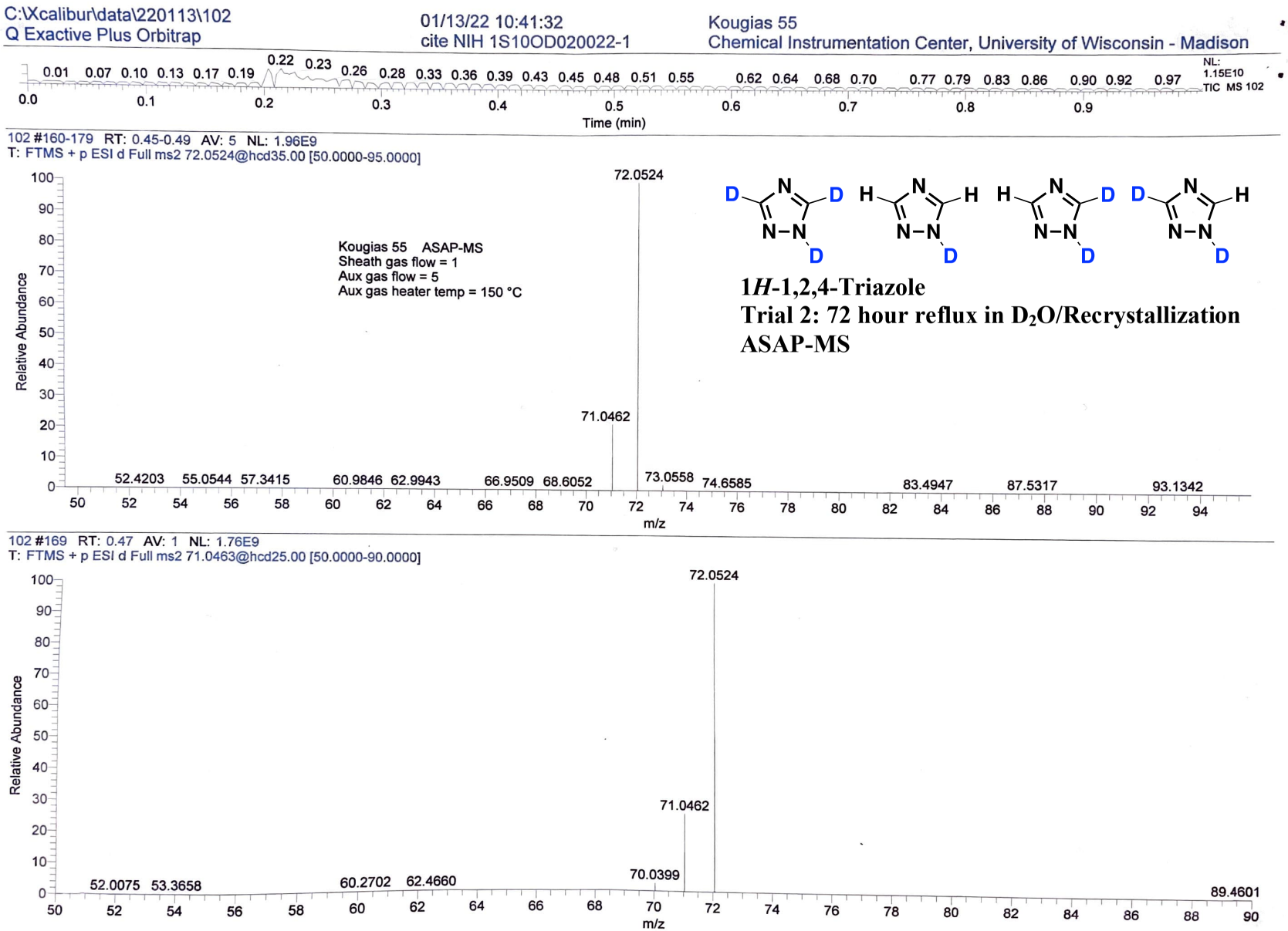


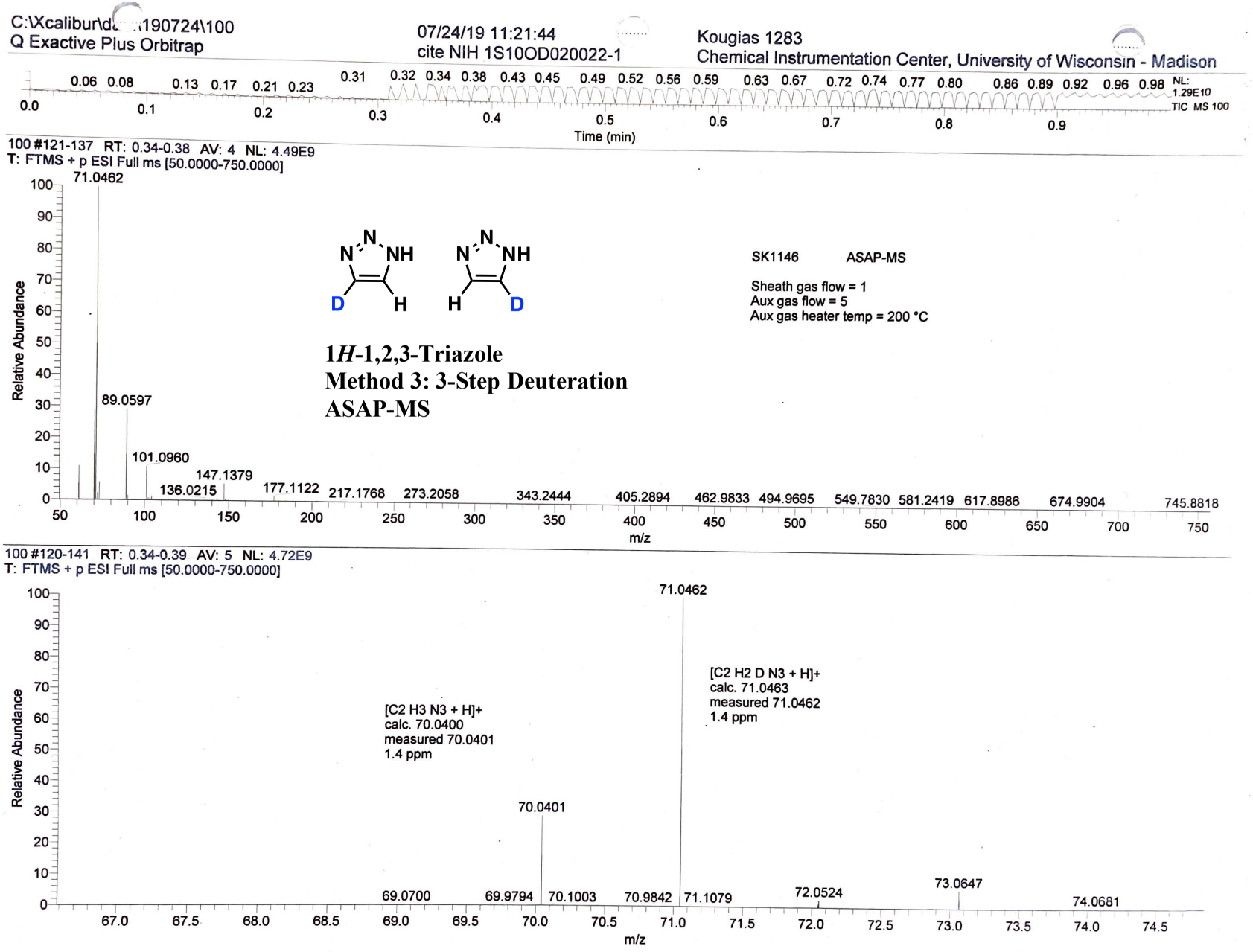
1*H*-1,2,4-Triazole
Trial 2: 72 hour reflux in D_2O/Recrystallization
^{13}C-NMR (125 MHz)
D_2O

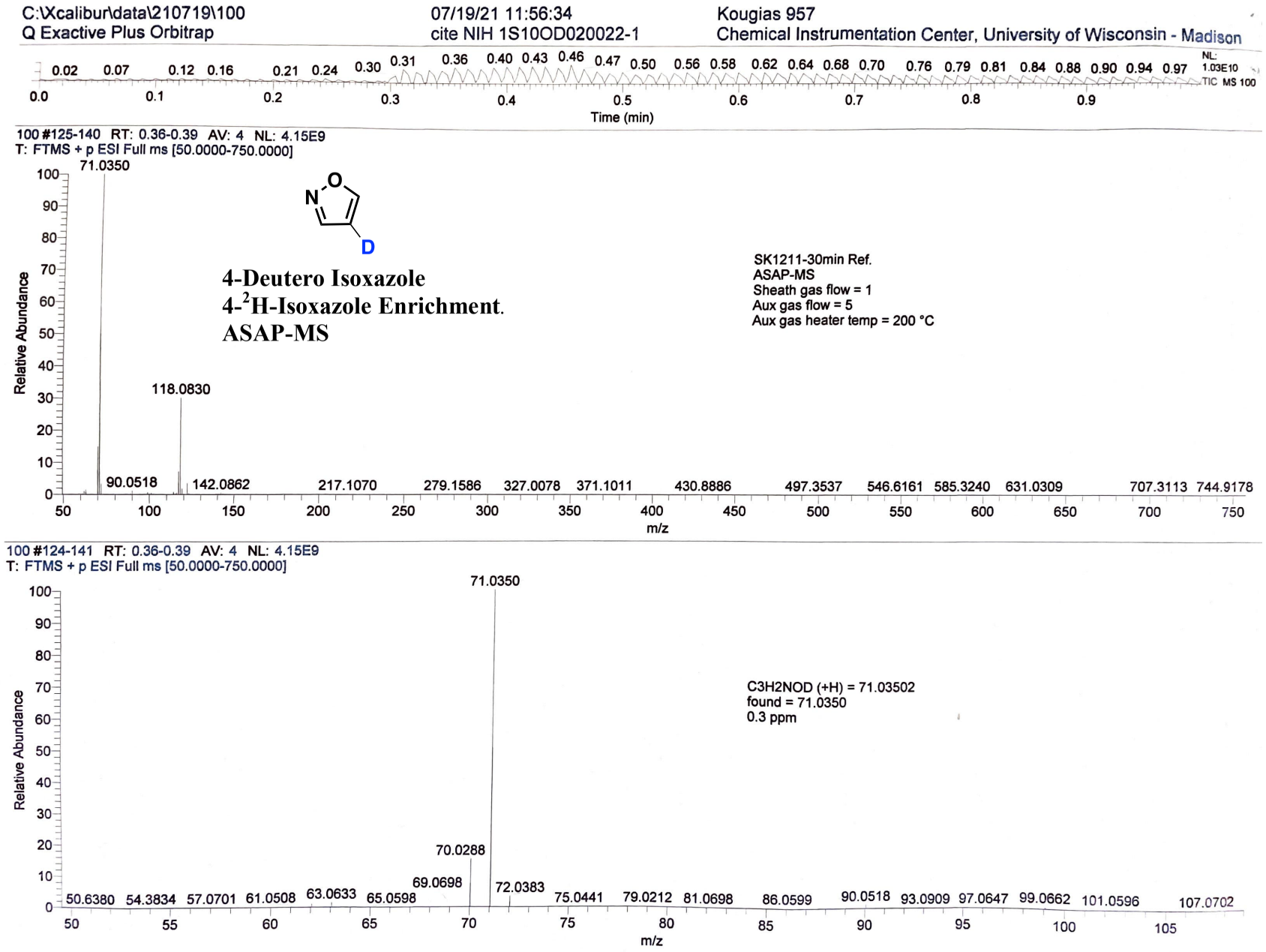


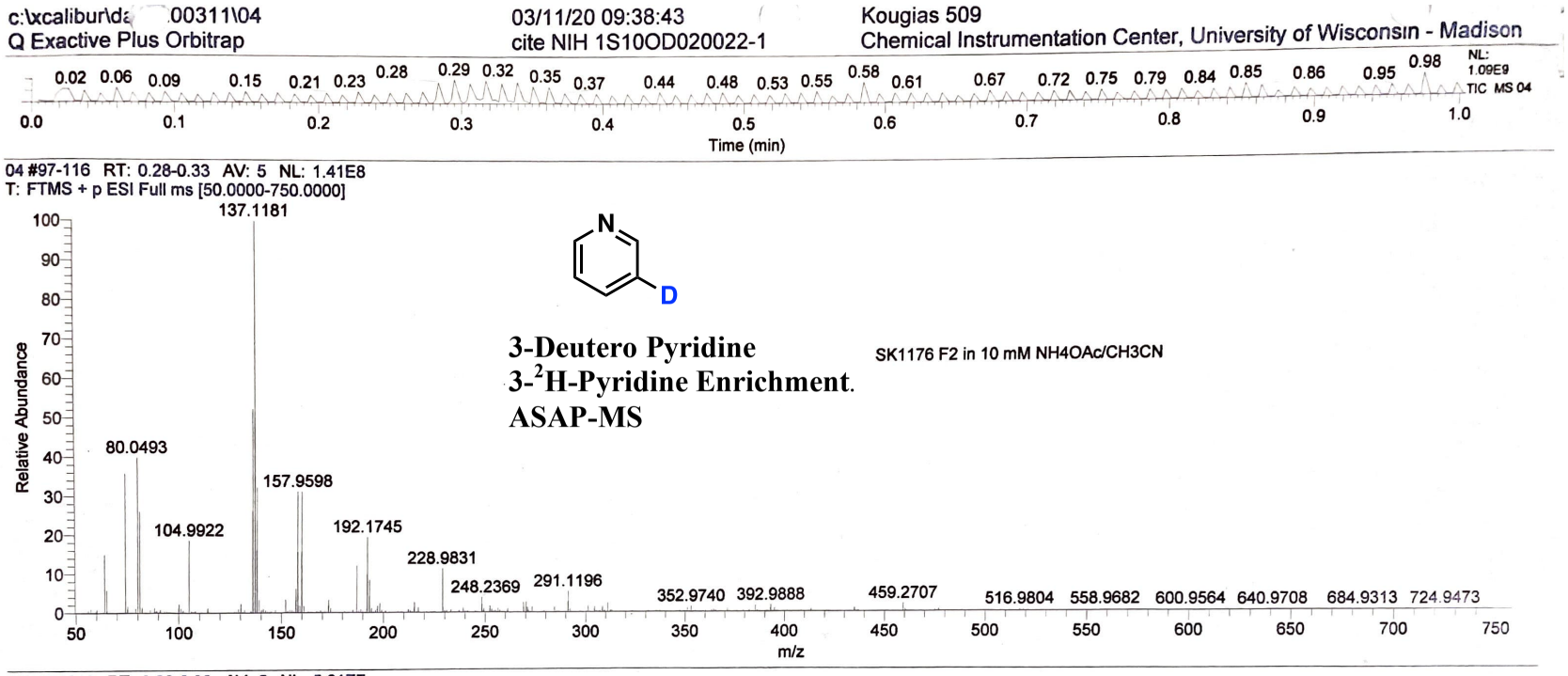

C:\Xcalibur\data\220113\102
Q Exactive Plus Orbitrap
01/13/22 10:41:32
cite NIH 1S10OD020022-1
Kougias 55
Chemical Instrumentation Center, University of Wisconsin - Madison
NL: 1.15E10 TIC MS 102
Time (min)
102 #160-179 RT: 0.45-0.49 AV: 5 NL: 1.96E9
T: FTMS + p ESI d Full ms2 72.0524@hcd35.00 [50.0000-95.0000]
Kougias 55 ASAP-MS
Sheath gas flow = 1
Aux gas flow = 5
Aux gas heater temp = 150 °C
1H-1,2,4-Triazole
Trial 2: 72 hour reflux in D2O/Recrystallization
ASAP-MS
Relative Abundance
m/z
102 #160-176 RT: 0.45-0.49 AV: 5 NL: 1.96E9
T: FTMS + p ESI d Full ms2 72.0524@hcd35.00 [50.0000-95.0000]
[C2H2DN3 + H]+
calc. 71.0463
measured 71.0463
< 0.1 ppm
[C2HD2N3 + H]+
calc. 72.0525
measured 72.0524
1.4 ppm


C:\Xcalibur\data\220113\102
Q Exactive Plus Orbitrap
01/13/22 10:41:32
cite NIH 1S10OD020022-1
Kougias 55
Chemical Instrumentation Center, University of Wisconsin - Madison
NL: 1.15E10 TIC MS 102
Time (min)
102 #160-179 RT: 0.45-0.49 AV: 5 NL: 1.96E9
T: FTMS + p ESI d Full ms2 72.0524@hcd35.00 [50.0000-95.0000]
Kougias 55 ASAP-MS
Sheath gas flow = 1
Aux gas flow = 5
Aux gas heater temp = 150 °C
Relative Abundance
m/z
72.0524
71.0462
52.4203
55.0544
57.3415
60.9846
62.9943
66.9509
68.6052
73.0558
74.6585
83.4947
87.5317
93.1342
1H-1,2,4-Triazole
Trial 2: 72 hour reflux in D2O/Recrystallization
ASAP-MS
102 #168 RT: 0.47 AV: 1 NL: 2.08E9
T: FTMS + p ESI d Full ms2 72.0524@hcd25.00 [50.0000-95.0000]
72.0524
71.0462
51.4433
55.4987
57.3415
59.7788
73.0558
83.4947


C:\Xcalibur\data\220113\102
Q Exactive Plus Orbitrap
01/13/22 10:41:32
cite NIH 1S10OD020022-1
Kougias 55
Chemical Instrumentation Center, University of Wisconsin - Madison
NL: 1.15E10 TIC MS 102
Time (min)
102 #160-179 RT: 0.45-0.49 AV: 5 NL: 1.96E9
T: FTMS + p ESI d Full ms2 72.0524@hcd35.00 [50.0000-95.0000]
Kougias 55 ASAP-MS
Sheath gas flow = 1
Aux gas flow = 5
Aux gas heater temp = 150 °C
Relative Abundance
m/z
1H-1,2,4-Triazole
Trial 2: 72 hour reflux in D2O/Recrystallization
ASAP-MS
102 #169 RT: 0.47 AV: 1 NL: 1.76E9
T: FTMS + p ESI d Full ms2 71.0463@hcd25.00 [50.0000-90.0000]


C:\Xcalibur\d...190724\100
Q Exactive Plus Orbitrap
07/24/19 11:21:44
cite NIH 1S10OD020022-1
Kougias 1283
Chemical Instrumentation Center, University of Wisconsin - Madison
Time (min)
NL: 1.29E10 TIC MS 100
100 #121-137 RT: 0.34-0.38 AV: 4 NL: 4.49E9
T: FTMS + p ESI Full ms [50.0000-750.0000]
Relative Abundance
m/z
71.0462
89.0597
101.0960
147.1379
136.0215
177.1122
217.1768
273.2058
343.2444
405.2894
462.9833
494.9695
549.7830
581.2419
617.8986
674.9904
745.8818
SK1146 ASAP-MS
Sheath gas flow = 1
Aux gas flow = 5
Aux gas heater temp = 200 °C
1H-1,2,3-Triazole
Method 3: 3-Step Deuteration
ASAP-MS
100 #120-141 RT: 0.34-0.39 AV: 5 NL: 4.72E9
T: FTMS + p ESI Full ms [50.0000-750.0000]
[C2 H3 N3 + H]+
calc. 70.0400
measured 70.0401
1.4 ppm
[C2 H2 D N3 + H]+
calc. 71.0463
measured 71.0462
1.4 ppm
70.0401
69.0700
69.9794
70.1003
70.9842
71.1079
72.0524
73.0647
74.0681


C:\Xcalibur\data\210719\100
Q Exactive Plus Orbitrap
07/19/21 11:56:34
cite NIH 1S10OD020022-1
Kougias 957
Chemical Instrumentation Center, University of Wisconsin - Madison
NL: 1.03E10 TIC MS 100
Time (min)
100 #125-140 RT: 0.36-0.39 AV: 4 NL: 4.15E9
T: FTMS + p ESI Full ms [50.0000-750.0000]
Relative Abundance
m/z
4-Deutero Isoxazole
4-2H-Isoxazole Enrichment.
ASAP-MS
SK1211-30min Ref.
ASAP-MS
Sheath gas flow = 1
Aux gas flow = 5
Aux gas heater temp = 200 °C
71.0350
118.0830
90.0518
142.0862
217.1070
279.1586
327.0078
371.1011
430.8886
497.3537
546.6161
585.3240
631.0309
707.3113
744.9178
100 #124-141 RT: 0.36-0.39 AV: 4 NL: 4.15E9
T: FTMS + p ESI Full ms [50.0000-750.0000]
C3H2NOD (+H) = 71.03502
found = 71.0350
0.3 ppm
70.0288
69.0698
72.0383
50.6380
54.3834
57.0701
61.0508
63.0633
65.0598
75.0441
79.0212
81.0698
86.0599
90.0518
93.0909
97.0647
99.0662
101.0596
107.0702


c:\xcalibur\da 00311\04
Q Exactive Plus Orbitrap
03/11/20 09:38:43
cite NIH 1S10OD020022-1
Kougias 509
Chemical Instrumentation Center, University of Wisconsin - Madison
NL: 1.09E9 TIC MS 04
Time (min)
04 #97-116 RT: 0.28-0.33 AV: 5 NL: 1.41E8
T: FTMS + p ESI Full ms [50.0000-750.0000]
Relative Abundance
m/z
3-Deutero Pyridine
3-2H-Pyridine Enrichment.
ASAP-MS
SK1176 F2 in 10 mM NH4OAc/CH3CN
04 #97-116 RT: 0.28-0.33 AV: 5 NL: 5.61E7
T: FTMS + p ESI Full ms [50.0000-750.0000]
[C5 H5 N + H]+
calc. 80.0495
measure 80.0493
[C5 H4 D N + H]+
calc. 81.0558
measure 81.0556

Chapter 5: Mediated Electrocatalytic Ammoxidation of Methyl Arenes

Contributions to the content in this section have been made by Dr. Damian Hruszkewycz and Dr. Kelsey Miles.

Introduction

On terrestrial Earth, the nitrile remains an important structural moiety present is countless materials, agrochemicals, pharmaceuticals and advanced technologies. In the materials industry, nitrile containing compounds appear in a diverse array of applications. Synthetic rubbers, specialty polymers, adhesives, coatings, and liquid crystal optics frequently contain molecules with nitrile groups or are synthesized from nitrile containing feedstocks (Figure 5.1a). Nitrile-containing ingredients are also an important component of numerous insecticides, herbicides and fungicides used throughout the agrochemical industry to protect crops and permit higher yields per harvested acre (Figure 5.1b).

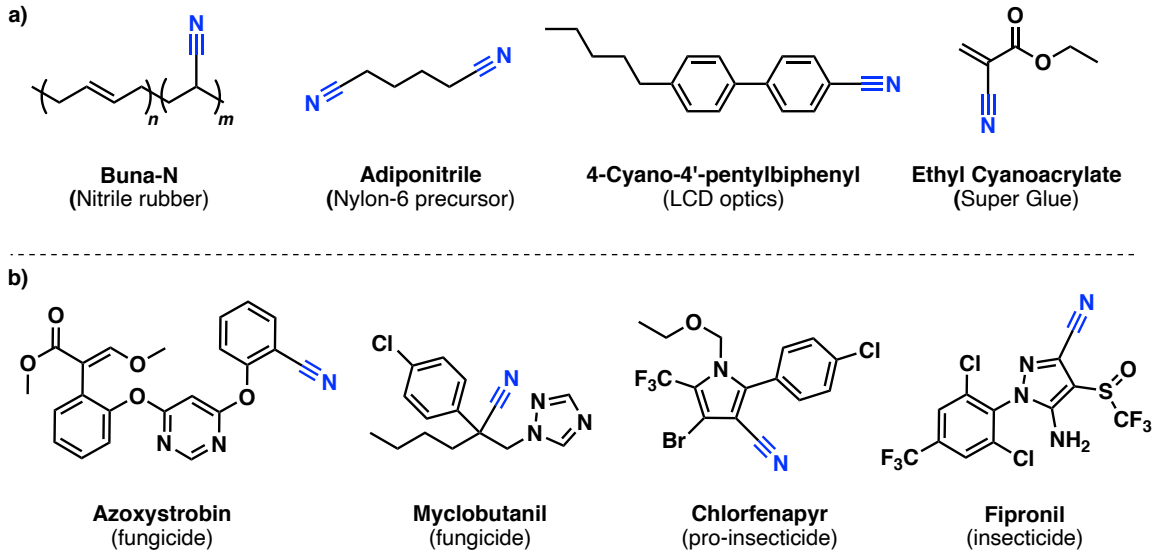


Figure 5.1. Nitrile-Containing Compounds Produced in the Materials (a) and Agrochemical (b) Industries.

In the pharmaceutical industry, the nitrile is a highly prevalent functional group present in various pharmaceuticals used in the treatment of multiple ailments or diseases (Figure 5.2). Currently, over 30 prescription drugs on the market contain the nitrile pharmacophore, and more than 20 are currently in clinical development.[12] The prevalence

of aryl nitriles in pharmaceuticals is due to the metabolic stability imparted by the nitrile moiety. The nitrile group is a polarized, compact hydrogen bond acceptor that reduces the susceptibility of aromatic rings being oxidatively metabolized and extends the metabolic half-life of pharmaceuticals in living systems.

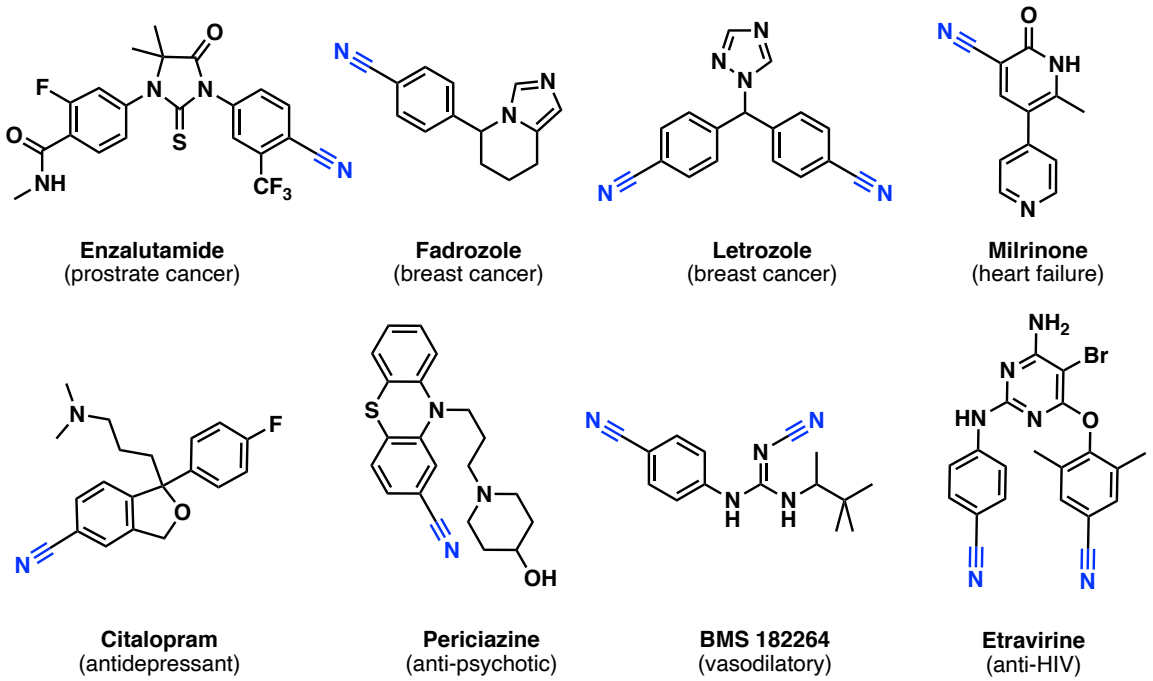


Figure 5.2. Modern Pharmaceuticals Containing the Nitrile Pharmacophore

Due to the outstanding prevalence of aryl nitriles in modern technology, a diverse array of synthetic methodologies have been developed for the installation of nitrile groups using various existing functionalities. Using conventional (non-electrochemical) synthetic methods, aromatic nitriles are frequently prepared *via* the oxidation of various existing benzylic functional groups,[16,17] metal catalyzed cyanation of aryl halides,[14,15] or *via* ammoxidation of *alpha*-aryl C-H bonds (frequently benzylic C-H bonds).[13] The major disadvantage of synthesizing aryl nitriles using conventional synthetic organic methodologies comes from the substantial health/safety risks and environmental impact posed by performing such techniques. Harsh oxidants, poisonous metal cyanides and

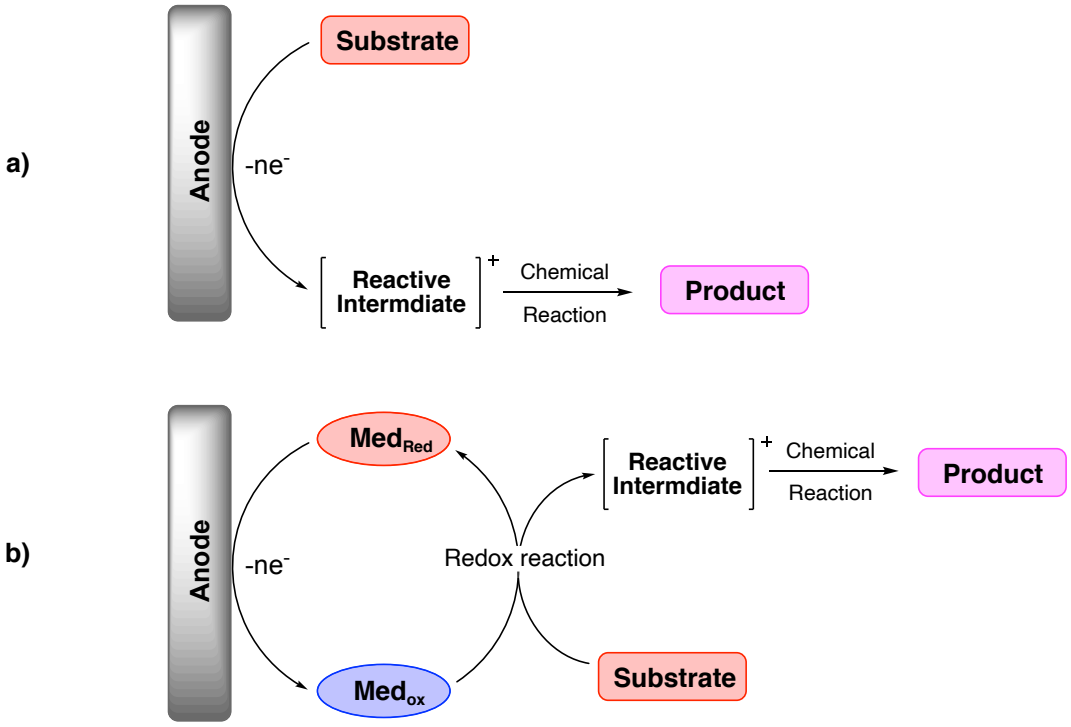
expensive noble metal-containing catalysts are often required in modern synthetic methods, and stoichiometric equivalents of hazardous waste are often produced as a result. Due to an ever-increasing focus on developing environmentally friendly chemical processes, designing safe and efficient methods for accomplishing challenging cyanation reactions is indeed desirable for any scale of preparative organic synthesis.

The application of electrochemical processes for synthesizing organic compounds is a highly attractive avenue of advancing the efficiency of synthetic organic methodology while simultaneously reducing the negative environmental/safety issues encountered with conventional synthetic techniques. Electrosynthetic processes are advantageous in that they allow for the replacement of toxic reagents with a working electrode and can be easily controlled *via* management of the applied voltage and regulated amperage.[3] Hazardous or unstable reagents can be generated *in situ* at the electrode surface in controlled amounts – allowing for reactions to be carried out under more mild conditions while reducing the direct handling of hazardous reagents in bulk quantities. Since the generation of reactants or reactive intermediates can be controlled by an applied potential, electrochemical methods also offer better control over the reaction rate compared to conventional synthetic methods and can be halted upon removal of the applied electromotive potential.

Electrochemical reactions are classified in two general modes of operation depending on how electrons are transferred between the working electrode and the substrate (Scheme 5.1). Direct electrolysis conditions (Scheme 5.1a) involve the direct transfer of electrons between the electrode and the substrate at the surface of the working electrode. Indirect electrolysis conditions (Scheme 5.1b) implement electrocatalytic

compounds called redox mediators to effectively shuttle electrons between the electrode surface and the substrate molecules.

Scheme 5.1. Direct (a) and Indirect (b) Anodic Oxidation Configurations.

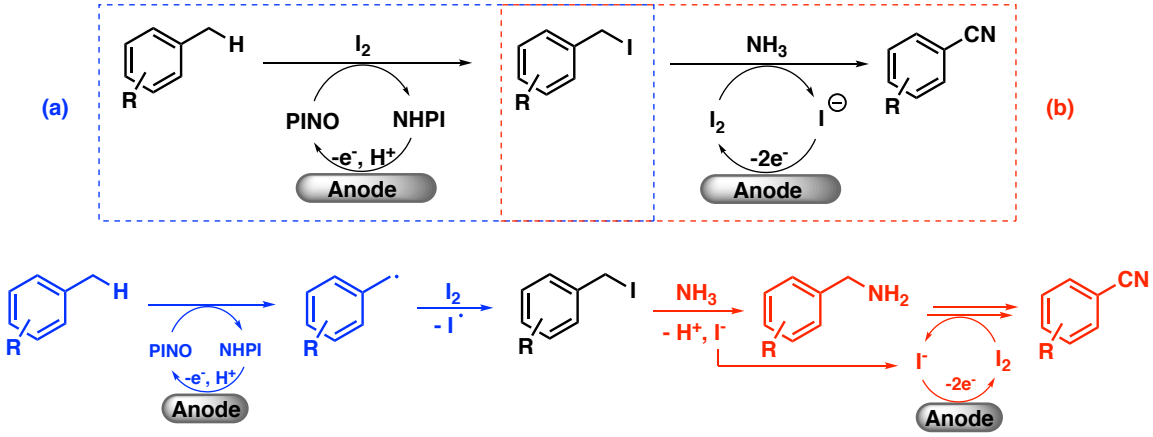


The use of redox mediators in indirect electrochemical redox reactions offers several advantages compared to direct electrolysis methods. Redox mediators offer more facile redox reactions at the electrode surface relative to the substrate. Kinetic inhibition between the electrode surface and the substrate can be minimized - allowing indirect electrolysis methods to proceed at significantly lower applied potentials compared to direct electrochemical redox reactions. Direct contact between the substrate and electrode surfaces is minimized and results in less passivation (fouling) of the electrode surfaces. Additionally, the use of redox mediators in indirect electrolysis techniques offers enhanced selectivity compared to direct electrolysis or conventional stoichiometric chemical oxidants.[4]

Project Goals

The general goal of this project is to develop a technique for the mediated electrochemical oxidation of methyl arenes to the corresponding benzonitriles *via* activation of relatively weak benzylic C-H bonds. Conventionally, the conversion of unsaturated hydrocarbons to nitriles *via* leveraging weak C-H bonds is known as ammoxidation (a chemical process developed by Standard Oil that uses oxygen and ammonia under high pressures and temperatures for the conversion of weak C-H bonds to nitriles). Our proposed plan for performing electrochemical "ammoxidation" is divided into two separate indirect electrochemical oxidation processes (Scheme 5.2). The first electrochemical process is designed to perform benzylic C-H activation of the methyl arene substrate to yield a benzyl iodide intermediate (Scheme 5.2a). The subsequent process is designed to perform amination of the benzyl iodide using aqueous ammonia and then electrochemically oxidize/dehydrogenate the generated benzylic amine to the respective benzonitrile (Scheme 5.2b). This chapter is organized to discuss the background, goals, technical considerations and results from the two indirect electrochemical steps separately.

Scheme 5.2. Proposed Two-Step Indirect Electrochemical Ammoxidation Process for the Conversion of Methyl Arenes to the Corresponding Aryl Nitriles.



Part 1: Electrocatalytic Benzylic Iodination of Methyl Arenes Using *N*-Hydroxypthalimide (NHPI).

Background

Benzylic C-H functionalization is a synthetically powerful process that is frequently used as a means of accessing a plethora of complex chemical moieties from relatively weak benzylic C-H bonds.[1] In particular, the direct halogenation of *alpha* C-H bonds in aromatic compounds is an important and widely used reaction in organic synthesis. Organic halides appear in multiple pharmaceuticals, agrochemicals and bulk chemicals. Further, organic halides are key reagents in essential C-C bond forming reactions such as Grignard reactions, organolithium reactions, and palladium-catalyzed cross coupling reactions.

Traditionally, benzylic bromides and chlorides are accessed through the radical addition of harsh elemental bromine or chlorine. Other methods, such as the classic Wohl-Ziegler bromination, utilize more easily-handled *N*-halosuccinimides as the halogen radical source.[2] A major disadvantage of conventional radical halogenations is that they use stoichiometric amounts of elemental halogens or *N*-halosuccinimides, have particularly harsh reaction conditions, and operate on a narrow substrate scope.



***N*-Hydroxypthalimide (NHPI)** **Phthalimido-*N*-oxyl (PINO)**

Figure 5.3. Structures of *N*-Hydroxypthalimide (NHPI) (a) and Phthalimido-*N*-Oxyl (PINO) (b).

N-hydroxyphthalimide (NHPI) has been used in multiple C-H abstraction reactions as an organocatalyst (Figure 5.3a).[5,6] NHPI has excellent availability, low cost, low toxicity, and is easily synthesized from hydroxylamine and phthalic anhydride. NHPI is the precursor of the phthalimido-*N*-oxyl (PINO) radical (Figure 5.3b), which serves as a hydrogen atom-abstracting agent in C-H activation reactions. For the abstraction of benzylic C-H bonds (along with several other relatively weak C-H bonds), PINO exhibits higher reactivity relative to peroxyl radicals ($k_{PINO}/k_{R\text{-}OO\bullet} > 1$ for the hydrogen abstraction step).[7] The enhanced reactivity of PINO results from a polar effect in the transition state during hydrogen atom abstraction. The two adjacent carbonyl moieties in the structure of PINO effectively enhance the electrophilicity of the nitroxyl radical and are the origin of the increased reactivity of PINO (Figure 5.4).

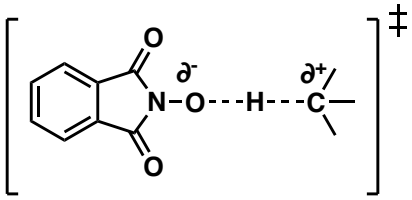
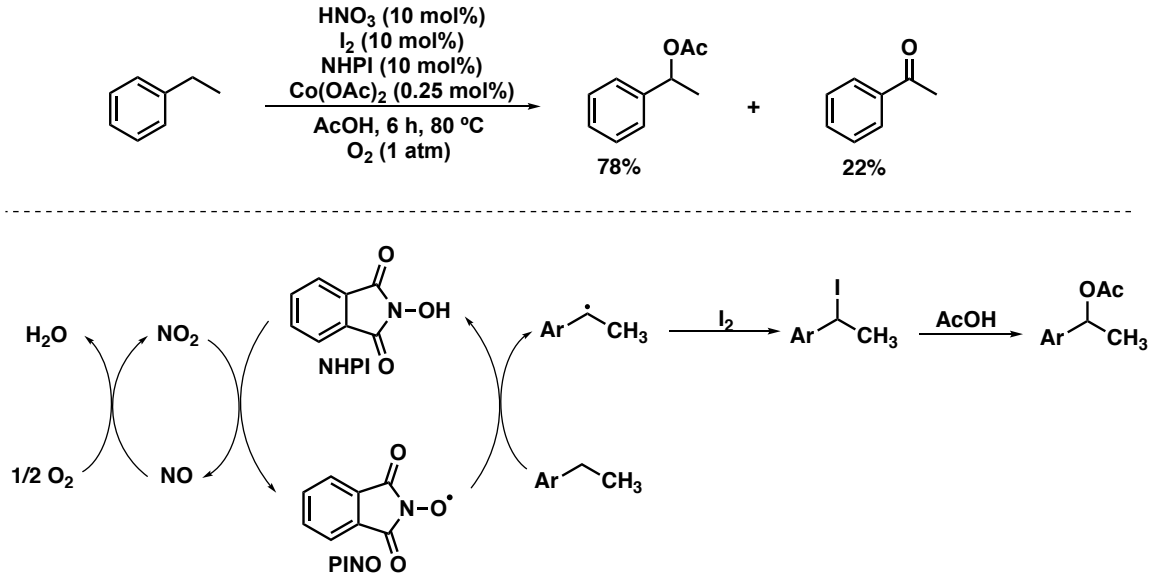


Figure 5.4. Polar Effect Observed in the Stabilized Transition State of C-H Abstraction Events Involving PINO

Interestingly, the polar effect observed in C-H abstraction events involving PINO can be "tuned" *via* modification of the electronic structure of the nitroxyl radical. Substitution of electron withdrawing groups on the aryl ring in PINO further enhances the rate of hydrogen atom transfer from the substrate.[8] The basis of using NHPI as an electrocatalyst for functionalizing benzylic C-H bonds was of interest to the members of the Stahl group since methods of electrochemically generating PINO from NHPI have also been well described in literature sources.[9]

As a C-H activation catalyst, NHPI has been used for accessing carbon-based radicals in free radical halogenations. Minisci *et al.* have reported conditions for the free-radical chlorination and bromination of alkanes using NHPI as a catalytic hydrogen-abstracting agent.[10] Minisci and co-workers have also reported conditions for benzylic iodination *via* trapping of benzylic radicals with molecular iodine.[11] This work was part of a larger scheme for accomplishing aerobic benzylic acetoxylation using NHPI/PINO as the hydrogen atom abstracting agent in conjunction with a NO_x co-catalyst (Scheme 5.3).

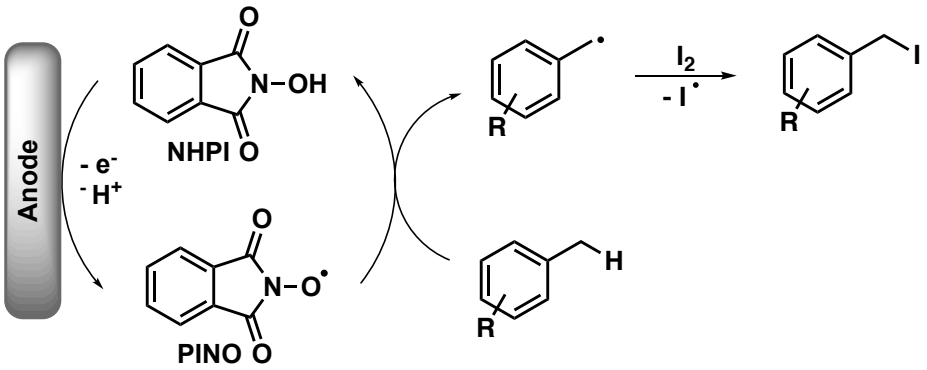
Scheme 5.3. NHPI/NOx Catalyzed Aerobic Benzylic Halogenation/Acetoxylation Methodology Described by Minisci *et al.*[10,11]



Building from the conditions developed by Minisci and co-workers, the initial hypothesis was that gaseous oxygen could potentially be replaced by an electrode as the terminal oxidant and benzylic iodination of methyl arenes could be driven electrochemically *via* generation of PINO directly at an anodic surface from NHPI. As an electrocatalytic mediator, PINO would perform selective C-H abstraction at the benzylic position of the of a methyl arene substrate to yield a transient carbon-based benzylic

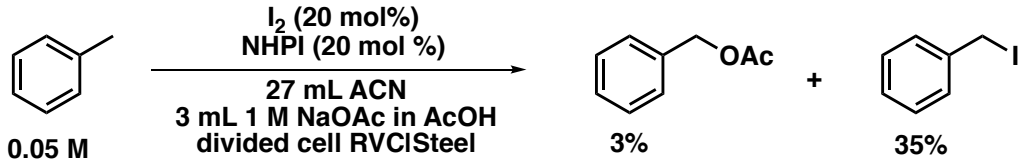
radical. Rapid trapping of the benzylic radical with molecular iodine would yield a benzyl iodide (Scheme 5.4).

Scheme 5.4. Proposed Method of Accessing Benzyl Iodides *via* NHPI/PINO Mediated Electrocatalytic Benzylic C-H Activation.



The design of the electrochemical adaptation of Minisci's benzylic C-H activation/iodination was performed by Dr. Damian Hruszkewycz, a fellow post-doctoral researcher in the Stahl group. The initial objective was to develop electrolysis conditions allowing access to benzylic radicals *via* anodic generation of PINO. The preliminary electrolysis conditions presented in Scheme 5.5 were developed using experimental parameters described in Minisci's aerobic acetoxylation methodology. The use of a divided electrochemical cell was necessary to prevent unwanted reduction of iodine to iodide at the cathode. Reticulated vitreous carbon (RVC) was used as the working electrode material (anode) with steel mesh as the counter electrode (cathode).

Scheme 5.5. Preliminary Bulk Electrolysis for Benzylic Iodination Conditions Derived from Minisci's Acetoxylation Methodology.



Analysis of the product mixture resulting from the electrochemical conditions shown in Scheme 5.5 indicated the presence of benzyl iodide and that C-H activation had

successfully occurred under the preliminary conditions. The resulting benzyl iodide showed remarkable stability in the presence of the acetate buffer present in the electrolytic solvent. However, further use of the acetate buffer in future electrolysis experiments was discontinued to prevent any undesirable solvolysis of the benzyl iodide from occurring. Further, the elimination of the acidic acetate buffer would allow for the more facile generation of PINO under slightly basic conditions in later experiments.

The presence of a weak base in the electrolyte allows for more facile oxidation of NHPI to PINO *via* application of lower overpotentials. The pKa of NHPI is approximately 7. At pH levels below 7, the anodic oxidation of NHPI to PINO proceeds through proton-coupled electron transfer (PCET). However, when the pH of the electrolyte is above 7, NHPI exists in a deprotonated form, and can be oxidized *via* simple single electron transfer (SET) at lower applied overpotentials.[9] The effect of pH on the oxidation potential of NHPI can be observed *via* cyclic voltammetry (CV). Figure 5.5 shows a series of cyclic voltammogram traces collected of a solution of NHPI with varying levels of base (2,6-lutidine). In the absence of 2,6-lutidine (black trace), NHPI undergoes anodic oxidation through PCET at a halfway potential of approximately 1.1 Volts vs. $Ag/AgNO_3$. The addition of substoichiometric levels of 2,6-lutidine results in the appearance of an anodic wave at a halfway potential of approximately 0.4 Volts vs. $Ag/AgNO_3$ as deprotonated NHPI undergoes facile SET at the anodic surface. As the equivalents of added base approaches unity, the percentage of deprotonated NHPI in the electrolyte becomes dominant resulting in the disappearance of the PCET anodic wave and the corresponding growth of the SET anodic wave. While illustrating the importance of an added base for the facile generation of PINO at lower overpotentials, cyclic voltammetry also indicates the

ideal electromotive potential that should be applied to obtain optimal catalytic performance and was used as a routine diagnostic tool when determining voltage settings for bulk electrolysis in these experiments.

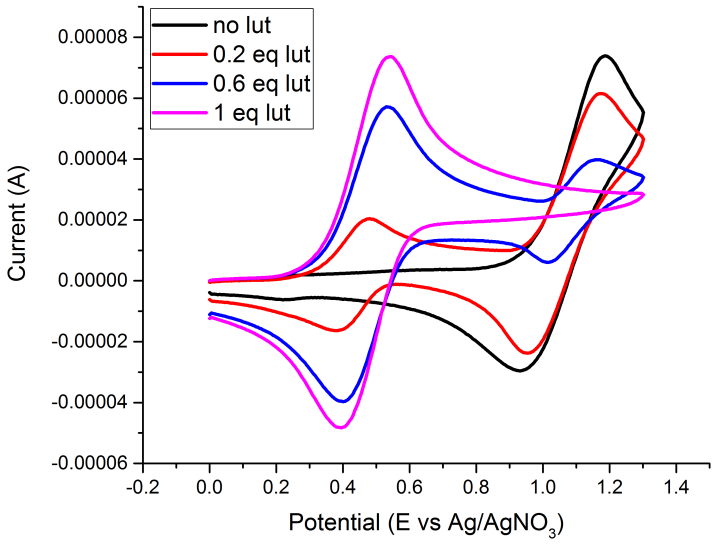


Figure 5.5. Cyclic voltammograms of 0.01 M NHPI in acetonitrile (with 0.1 M $LiClO_4$ supporting electrolyte) at different concentrations of an added organic base, 2,6-lutidine (50 mV/s scan rate).

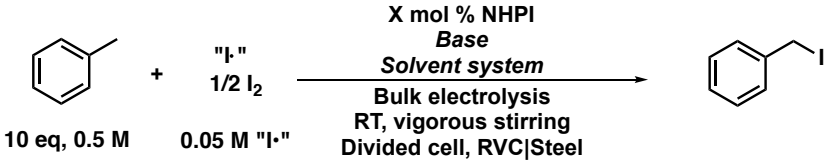
To determine electrolysis conditions optimal for the generation of PINO under basic conditions, a series of different organic bases and solvent combinations were screened (Table 5.1). The Coulombic efficiency (charge efficiency, $Q_{eff,}$ Equation 5.1) represents the percentage of passed charge (Q_{passed}) that resulted in the formation of product, and is calculated using the product yield, the number of electrons required per redox event, and Faraday's constant (***F***, 96,485 C • mol $^{-1}$).

$$Q_{eff} = \left(\frac{yield(mol) \cdot F \cdot ne^{-}}{Q_{passed}} \right) \bullet 100 \qquad \textbf{(Eq. 5.1)}$$

Low yields of benzyl iodide were observed when pyridine was used as the added base (Table 5.1, entries 3 and 5). Pyridine was likely reacting with the benzyl iodide to form

pyridinium salts. 2,6-Lutidine (2,6-dimethylpyridine) was found to be an effective non-nucleophilic organic base for use in this electrolysis. The use of 2,6-lutidine also allowed for efficient catalysis using lower NHPI loadings (Table 5.1, entry 7). It was hypothesized that the loading of lutidine could be reduced to catalytic amounts if it could be regenerated by sacrificial inorganic base. Addition of 1.1 equivalents of $KHCO_3$ was found to be sufficient for maintaining a basic pH in the anolyte and allowed for the concentration of 2,6-lutidine to be reduced to 0.01 M (Table 5.1, entry 9). Similar results were also obtained using catalytic acridine as an alternative non-nucleophilic organic base lacking potentially abstractable benzylic C-H bonds (Table 5.1, entry 10).

Table 5.1. Evaluation of Bulk Electrolysis Solvent/Base Systems for Benzylic Iodinations.



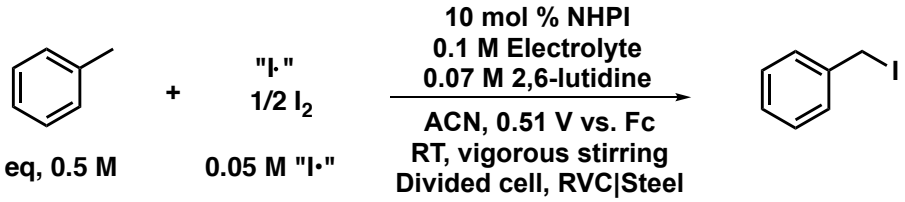
entry	NHPI	base	solvent system	yield[a]	Q_{eff}[b]
1	20 mol%	NaOAc (0.1 M)	9:1 ACN:AcOH	**46%**	93%
2	20 mol%	NaTFA (0.1 M)	0.1 M TFA in ACN	**10%**	14%
3	20 mol%	Pyrdine (0.1 M)	0.1 M TBAP in ACN	**16%**	68%
4	20 mol%	Lutidine (0.1 M + aliquots)	0.1 M TBAP in ACN	**68%**	73%
5	20 mol%	Pyridine (0.07 M)	0.1 M TBAP in ACN	**3%**	4%
6	20 mol%	Lutidine (0.07 M)	0.1 M TBAP in ACN	**56%**	86%
7	10 mol%	Lutidine (0.07 M)	0.1 M TBAP in ACN	**74%**	73%
8	10 mol%	Lutidine (0.07 M)	0.1 M KPF_6 in ACN	**94%**	84%
9	10 mol%	Lutidine (0.01 M), $KHCO_3$ (1.1 eq)	0.1 M KPF_6 in ACN	**86%**	80%
10	10 mol%	Acridine (0.01 M), $KHCO_3$ (1.1 eq)	0.1 M KPF_6 in ACN	**77%**	74%

[a] Yield determined *via* HPLC using benzonitrile as internal standard
[b] Charge efficiency

Having determined a suitable solvent/base system for the reaction, the supporting electrolyte was further screened. Previously, tetrabutylammonium perchlorate (TBAP) had shown to be an effective supporting electrolyte for this electrolysis. However, TBAP is

difficult to separate during product purification and is relatively expensive compared to other ionic electrolytes. To determine if a more ideal supporting electrolyte could be used, several supporting electrolytes were evaluated using replicate conditions (Table 5.2). Of the electrolytes evaluated, KPF_6 was ultimately chosen to be a more effective (and inexpensive) alternative to TBAP.

Table 5.2. Optimization of the supporting electrolyte

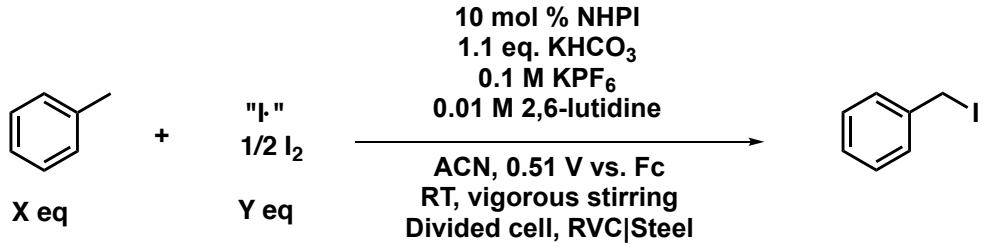


entry	electrolyte	yield[a]	Q_{eff}[b]
1	TBAP	**74%**	73%
2	KPF_6	**94%**	84%
3	$LiClO_4$	**74%**	76%
4	$NaClO_4$	**51%**	83%
5	$NaBF_4$	**64%**	68%

[a] Yield determined *via* HPLC using benzonitrile as internal standard
[b] Charge efficiency

Using the electrolysis conditions developed to this point, benzyl iodide is obtained in good yields and with excellent current efficiencies when toluene is used in a tenfold excess with respect to iodine (Table 5.3, entry 1). As the loading of toluene is decreased (Table 5.3, entries 2-5), the charge efficiency (Q_{eff}) and the yield of benzyl iodide decrease drastically. A common problem encountered when electrolyses were performed at lower toluene ratios is the complete decay of current before the required amount of charge passes.

Table 5.3. Evaluating Effect of Toluene : Iodine Ratio on Charge Efficiency and Yield.

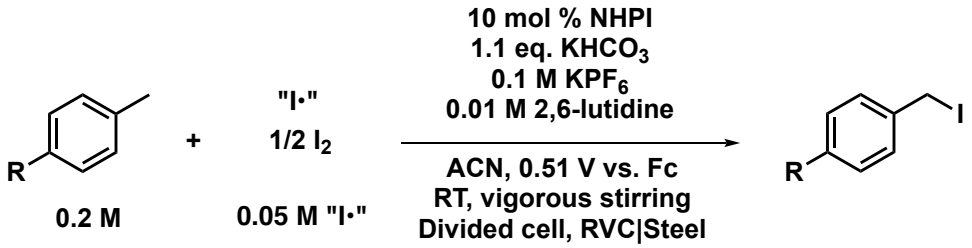


entry	Toluene eq. : I• eq.	[Toluene]	[I•]	yield[a]	Q_{eff}[b]
1	10 : 1	0.5 M	0.05 M	**86%**	80%
2	4 : 1	0.2 M	0.05 M	**73%**	69%
3	2 : 1	0.1 M	0.05 M	**59%**	55%
4	1.1 : 1	0.055 M	0.05 M	**45%**	38%
5	1 : 2	0.05 M	0.1 M	**31%**	31%

[a] Yield determined *via* HPLC using benzonitrile as internal standard
[b] Charge efficiency

The substrate scope was explored using a fourfold excess of methyl arene relative to iodine. Under the conditions presented in Table 5.4, toluene, 4-bromotoluene and 4-*tert*-butyltoluene can be converted to the corresponding benzyl iodide in good yields and charge efficiencies. Electrolysis of highly electron rich or poor methyl arenes (Table 5.4, entries 4 and 5) encountered difficulty passing sufficient charge and generated low yields of product.

Table 5.4. Substrate Scope and Yields of Electrochemical Iodination Using a Fourfold Excess of Methyl Arene Substrates.



entry	R	MA : I•	charge	yield[a]	Q_{eff}[b]
1	H	4 : 1	103 C	**73%**	69%
2	Br	4 : 1	120 C	**74%**	60%
3	^{t}Bu	4 : 1	124 C	**73%**	57%
4	SO_2NH_2	4 : 1	87 C	**8%**	9%
5	OMe	4 : 1	67 C	**4%**	6%

[a] Yield determined *via* ^{1}H-NMR using diphenylmethane as internal standard
[b] Charge efficiency
MA = *methyl arene*

Table 5.4 shows the best yields are obtained when the methyl arene substrate is used in large excess relative to iodine. While the method presented in Table 5.4 could potentially be used in the electrochemical ammoxidation project as a means of accessing benzyl iodides, the overall efficiency, practicality, and impact of the process would be improved if good yields were also obtained when the methyl arene is the limiting reagent.

Results and Discussion

Upon joining the electrochemical benzylic iodination project, my first objective was investigating how to achieve efficient catalysis when the methyl arene substrate is the limiting reagent. A problem encountered in previous experiments was the decay of electrolytic currents before the prescribed amount of charge had passed or before the reaction was complete. Cyclic voltammetry of stalled electrolyses revealed that NHPI was

still present in the anolyte solution, but application of the appropriate voltage in a bulk electrolysis yielded essentially no current through the cell. During bulk electrolysis experiments, the evolution of gas bubbles was observed at the cathode surface. Further, we observed an increase in sustained current when additional $KHCO_3$ was added to the anolyte of stalled bulk electrolyses. It appeared as if the $KHCO_3$ in the anolyte was being consumed before the electrolysis reached completion, causing a drop in the pH of the anolyte, and the electrolysis currents. The nature of the corresponding reduction occurring at the cathode was unclear considering that there are no easily reduced species in the catholyte. In the electrolysis conditions used to this point, the catholyte consisted only of 0.1 M KPF_6 and 0.01 M 2,6-lutidine in acetonitrile. Often reactions occurring at the counter electrode are ignored, however we speculated that some of the dissolved bicarbonate ions may diffuse through the frit into the catholyte where the reduction of hydrogen from bicarbonate would yield insoluble carbonate (Figure 5.6).

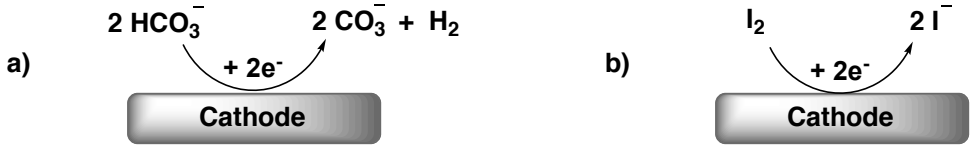
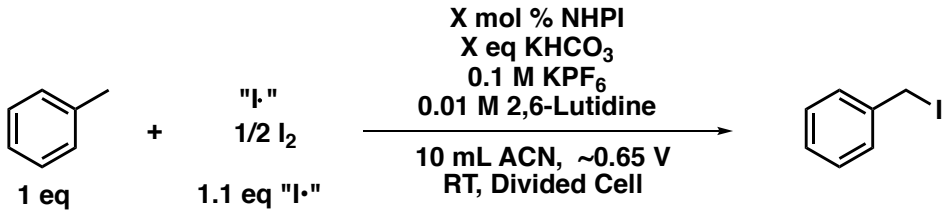


Figure 5.6. Potential Reduction of Bicarbonate (a) or Iodine (b) Occurring at the Cathodic Surface During Bulk Electrolyses

To remedy this issue, and to provide an easily oxidized species to the cathodic compartment of the cell, $KHCO_3$ and I_2 were added to the catholyte at various amounts to serve as a sacrificial oxidant (Table 5.5). The addition of one equivalent of iodine to the catholyte (Table 5.5, entry 3) appeared to be the most effective. As experienced in earlier trials, reducing the amount of base in the anolyte by half caused the electrolysis currents to stall, and resulted in lower yields (Table 5.5, entry 1). We also noticed that performing

electrolysis at higher concentrations resulted in lower yield of product as well (Table 5.5, entry 7).

Table 5.5. Optimization of Catholytic Sacrificial Oxidants for Benzylic Iodination Bulk Electrolyses



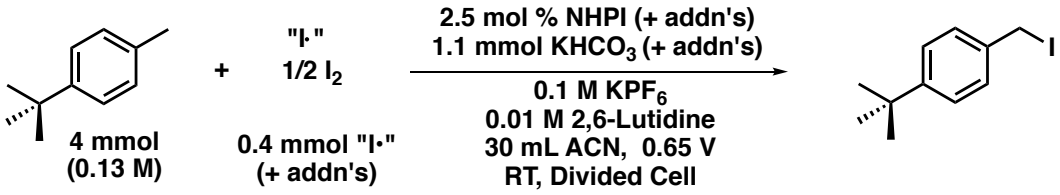
	Anolyte			Catholyte			
entry	**[Toluene]**	**NHPI**	**eq. $KHCO_3$**	**eq I•**	**eq. $KHCO_3$**	**yield[a]**	**Q_{eff}[b]**
1	0.165 M	10 mol%	0.55	0	0	30%	54%
2	0.165 M	10 mol%	1.1	0	1.1	40%	42%
3	0.165 M	10 mol%	1.1	1.1	0	42%	39%
4	0.165 M	10 mol%	1.1	2.2	0	38%	30%
5	0.165 M	10 mol%	1.1	3.3	0	39%	36%
6	0.165 M	20 mol%	1.1	1.1	0	40%	39%
7	2.0 M	10 mol%	2.2	1.1	0	26%	22%

[a] Yield determined *via* ^{1}H-NMR using diphenylmethane as internal standard
[b] Charge efficiency

We observed an interesting effect of the reaction concentration on the efficiency of the electrolysis when 4-*tert*-butyltoluene was used as a substrate. Electrolysis performed using a 1:1 ratio of 4-*tert*-butyltoluene to iodine performed poorly at a concentration of 0.1 M, ultimately yielding only 10% of the desired benzyl iodide. Increasing the concentration to 0.165 M only further decreased the yield. Similar experiments where the equivalent of iodine was slowly delivered to the anolyte *via* syringe pump showed a small increase in yield to 19%. We were intrigued by the prospect of running electrolysis where the iodine concentration is maintained at low levels. We directed our focus to investigating if effective catalysis could be obtained by maintaining low iodine concentrations through small, incremental additions of solid I_2.

A time course evaluation of the electrolysis shown in Table 5.6 was set up to further understand the conditions where the most efficient catalysis occurs and if optimal conditions could be maintained.

Table 5.6. Charge Course Evaluation of the Anodic Iodination on 4-*tert*-Butyltoluene with Incremental Additions of I_2, NHPI, and $KHCO_3$.



entry	charge (C)	current (mA)	mmol I• added	yield[a] w.r.t. MA	yield[a] w.r.t. I•	Q_{eff}[b]
1	0	0	0.4	0.7%	**7%**	0%
2	15	27	0.4	3%	**31%**	79%
3	45	28	0.4	7%	**71%**	61%
Addition #1: 0.4 mmol of iodine added						
4	75	26	0.8	11%	**55%**	57%
5	105	17	0.8	14%	**70%**	51%
Addition #2: 0.4 mmol of iodine, 2.5 mol % NHPI, 1.1 mmol $KHCO_3$ added						
6	135	30	1.2	18%	**60%**	51%
7	190	23	1.2	22%	**74%**	45%
Addition #3: 0.4 mmol of iodine added						
8	220	14	1.6	24%	**59%**	41%
Addition #4: 2.5 mol % NHPI, 1.1 mmol $KHCO_3$ added						
9	250	29	1.6	26%	**66%**	40%
10	290	21	1.6	29%	**72%**	38%

[a] Yield determined *via* HPLC using benzonitrile as internal standard
[b] Charge efficiency

In this experiment, the initial concentration of the methyl arene substrate (4-*tert*-butyltoluene) was set at 10 times the starting concentration of iodine, and the initial NHPI electrocatalyst loading was set at 2.5 mol % (with respect to the methyl arene). As the electrolysis was conducted, the progress of the reaction was monitored *via* HPLC of reaction aliquots. Consistent earlier electrolyses, the best charge efficiencies were observed early in the electrolysis when the concentration of the methyl arene was still relatively high.

As the relative concentration of methyl arene was consumed, the charge efficiency steadily declined. Addition of iodine to the anolyte showed little or no change to the electrolysis amperage even when the currents were steadily decaying. However, a revival of sustained current was observed whenever NHPI and $KHCO_3$ were added to the anolyte. Figure 5.7 presents a time plot of the amperage measured through the electrolysis with points of addition marked according to the addition numbers presented in Table 5.6. Additions were performed when the amperage was noticeably decreasing.

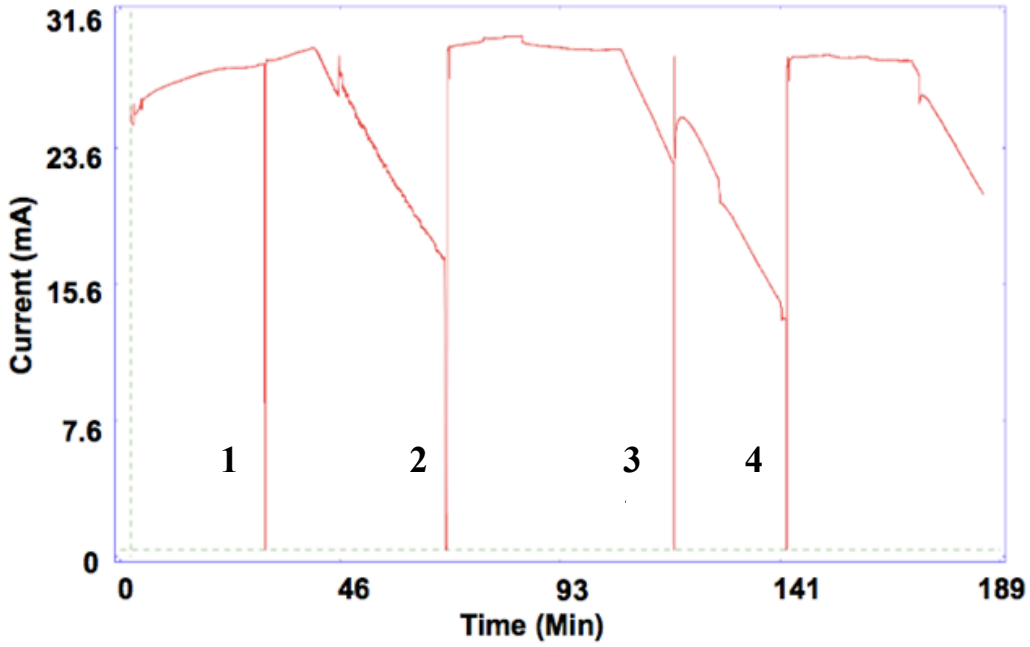


Figure 5.7. Trace of the currents observed in the electrolysis presented in Table 5.6. Points where additions were made are numbered in the order shown in Table 5.6.

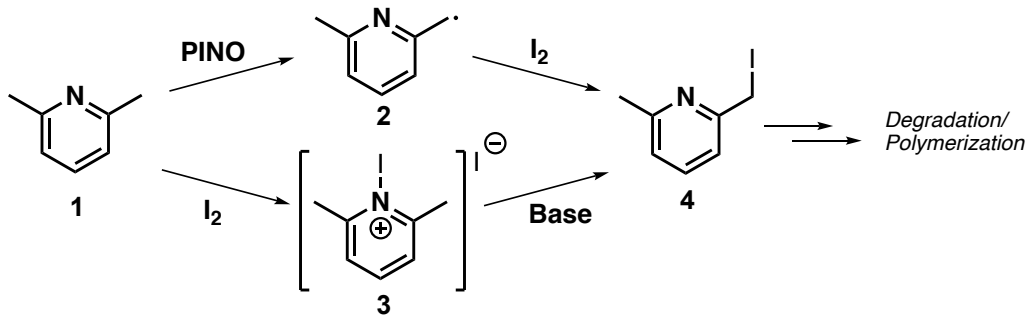
CVs collected of the anolyte prior to each NHPI addition (Figure 5.7, points 2 & 4) showed that much of the NHPI in the anolyte had decomposed over the course of the electrolysis. Interestingly, it appears that after each addition of iodine, the yield of the benzyl iodide (with respect to the total amount of iodine added) approached a value of approximately 70%. A similar timecourse evaluation was conducted where the initial concentration of 4-*tert*-butyltoluene was only fourfold the relative starting concentration

of iodine. The results of this experiment were similar to those shown in Table 5.6 with the exception being that the yield of the benzyl iodine (with respect to the total mmol iodine added) approached a value of about 50% after each iodine addition.

Additionally, it appears that the generation of product is the most efficient when the concentration of iodine in the anolyte is low. Our hypothesis is that maintaining even lower concentration of iodine in the anolyte will result in a higher terminal yield of the product between each smaller, more frequent additions of solid iodine. Future experiments would involve performing timecourse evaluations of electrolyses where the iodine concentration is started and maintained at a lower value relative to the experiment shown in Table 5.6. If higher terminal yields of the product are observed between additions, it may be possible to deliver iodine to the anolyte at slower, more consistent rates *via* use of a syringe pump.

When NHPI is used as an electrocatalyst, the presence of a weak base during the electrolysis is imperative for the electrooxidation of NHPI at low overpotentials. The steric congestion of 2,6-lutidine effectively reduces the loss of benzyl iodide *via* S_N2 side-reactions with the base. Although the methyl substituents on 2,6-lutidine effectively reduce the nucleophilicity of the heterocycle, they also provide a site where PINO can perform C-H abstraction. This reaction ultimately leads to the degradation of the base (Scheme 5.6). While the best yields were obtained in reactions using 2,6-lutidine as the non-nucleophilic base, it is possible that C-H abstraction at the methyl groups on 2,6-lutidine may become more problematic when the concentration of methyl arene drops below a certain level.

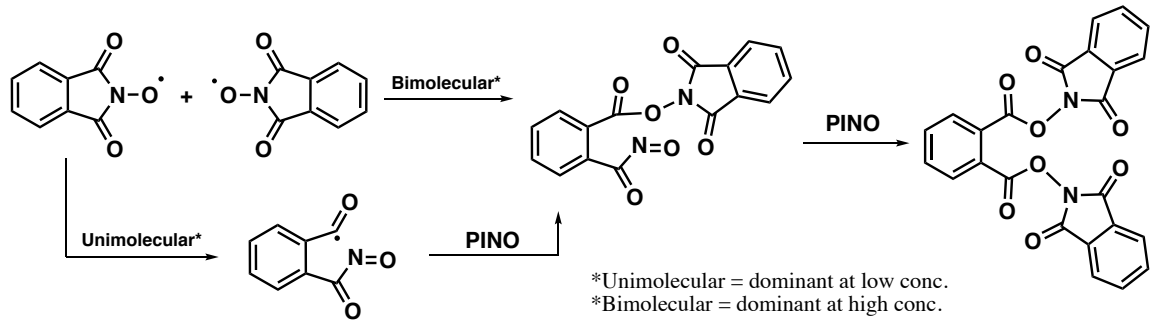
Scheme 5.6. Degradation Routes of 2,6-Lutidine (1) in the Presence of I_2 or PINO Through the Formation of Benzylic Radicals (2) or Unstable Complexes (3).



An additional issue associated with using 2,6-lutidine is the formation of unstable charge-transfer complexes (**3**) in the presence of molecular iodine. Popov *et al.* has reported the synthesis and isolation of molecular complexes of pyridine, 2-picoline and 2,6-lutidine with iodine and iodine halides.[37,38] Of the substrates synthesized, Popov was unable to isolate the 2,6-lutidine-iodine complex (**3**) due to the inherent instability of the complex. Hackley and co-workers proposed that complex **3** undergoes rearrangement to yield a transient benzylic halide that may further degrade.[39] Due to the low stability of these bases in the presence of iodine, future work will likely involve screening for a more stable base that is relatively unreactive with iodine, PINO or other radicals. Although acridine could be used as a non-nucleophilic base that lacks potentially reactive benzylic C-H bonds, the use of other heterocyclic bases is unlikely - Brivio and co-workers reported the trapping of benzyl radicals with heterocyclic bases to form cross-coupled products.[40]

Although the electrochemical synthesis of benzylic halides shows several advantages over conventional radical halogenation techniques, the use of PINO as a hydrogen abstraction electrocatalyst is limited primarily by its own stability during anodic generation. Whenever PINO is being generated at the anode surface, there are two primary routes where PINO undergoes self-annihilation (Scheme 5.7).

Scheme 5.7. Unimolecular and Bimolecular Degradation Routes of PINO



The first order rate constant for which PINO undergoes decay has been reported at $k_d = 0.1$ s^{-1}.[7] The second order rate constant for which PINO undergoes decay in acetonitrile has been reported at $k_d = 0.6$ $M^{-1}s^{-1}$.[7] Both rates reported for the decomposition of PINO are comparative to the rate which PINO performs hydrogen atom abstraction from toluene ($k = 0.127$ $M^{-1}s^{-1}$).[7] Since the decay of PINO results in the steady decrease of electrolysis current, and since the decomposition shrapnel is destructive to NHPI (and possibly benzyl iodides), methods minimizing the decomposition of PINO are indeed desirable. Future experiments will focus on determining strategies for maximizing the catalytic lifespan of PINO under electrochemical conditions.

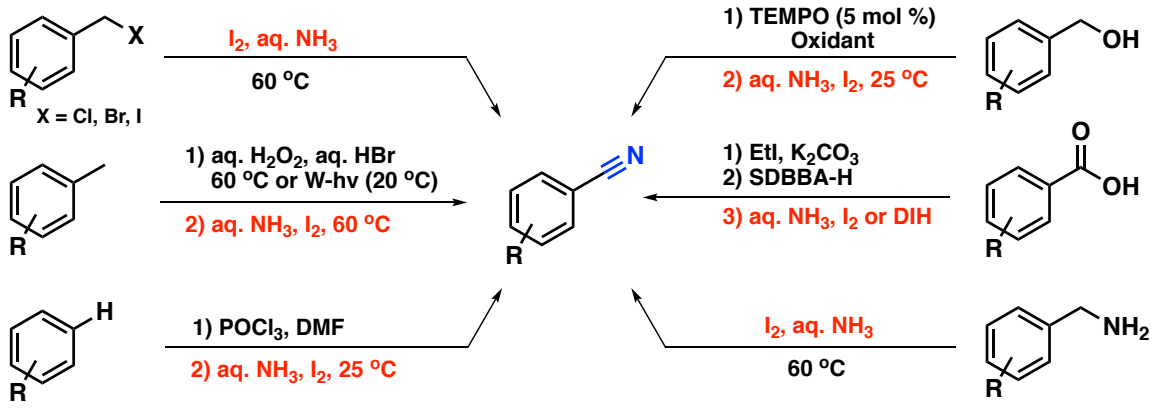
A possible engineering solution for prolonging the catalytic lifespan of PINO is to use RVC with larger porosity for anode material. When the porosity of the anode material is small, the circulation of electrolyte/substrate through the anode is restricted. This results in "pockets" of electrolyte where the local concentration of PINO is high – promoting the bimolecular degradation pathway of PINO. Using RVC with larger porosity will permit free flow of the anolyte through the anode and reduce the buildup of areas where the local PINO concentration is high. An additional strategy is to reduce the amount of PINO generated at the surface of the electrode by conducting electrolysis at lower overpotentials.

Part 2: Iodine-Mediated Electrochemical Oxidation of Benzyl Iodides to Benzonitriles

Background

In organic synthesis, iodine has been used extensively in various reactions.[18] Iodine can be used for the introduction of or removal of protecting groups, and as a catalyst in oxidative coupling reactions.[19,20] Iodine is also used as a mild, environmentally benign oxidant. Misono *et al.* has presented an effective oxidation system consisting of elemental iodine in aqueous ammonia and its application in oxidation of aromatic aldehydes to nitriles.[21-24] Although mixtures of iodine and ammonia have been known to produce explosive NI_3, the combination can also be used to successfully (and safely) oxidize a variety of benzylic and aliphatic moieties to the corresponding nitriles in good yields. Togo has also demonstrated the oxidation benzylic amines, halides, alcohols, and carboxylic acids to the corresponding nitriles using similar variations of the aqueous ammonia/iodine oxidation system (Scheme 5.8).[25-31]

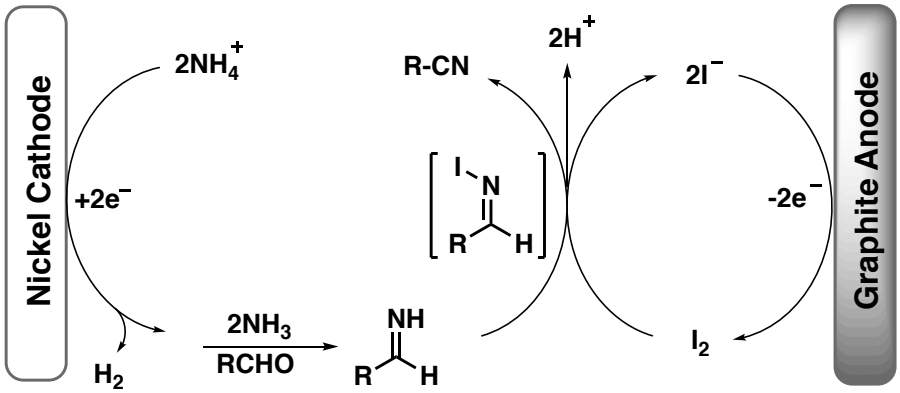
Scheme 5.8. Methodologies Reported by Togo *et al.* for Conversion of Multiple Benzylic Groups to Benzonitriles Using the NH_3/I_2 Oxidation System.[25-31]



The use of iodine as a mild oxidant and the broad substrate scope of Togo's oxidation conditions were attractive features to our group as a potential method to synthesize nitriles

using iodide generated *in situ* through an electrochemical process. Electrochemical methods for the generation of halogen oxidants *in situ* have been well described in literature as a route to access nitriles.[32,33] Qu and co-workers recently reported the iodine-mediated electrooxidation of aromatic aldehydes to the corresponding benzonitriles *via* the synergistic *in situ* generation of NH_3 and I_2 from the NH_4I supporting electrolyte (Scheme 5.9).[34]

Scheme 5.9. Electrochemical Method Reported by Qu *et al.* for the Anodic Oxidation of Aldehydes *via in situ* Generation of I_2 from the Supporting Electrolyte.



In the mechanism proposed for this reaction, ammonia is produced *via* two-electron reduction of ammonium at the cathodic surface and proceeds to react with the aldehyde substrate to yield an aldimine intermediate. Simultaneously, a two-electron oxidation of iodide at the anode yields the iodine oxidant. Reaction between iodine and the aldimine yields an *N*-iodoaldimine intermediate that undergoes rapid elimination of HI to yield the nitrile. A potential drawback to this technique is the use of DMSO as the primary solvent – which may be difficult to eliminate during work-up and purification of the product.

Our vision is to combine features from the research done by Qu and Togo into a method for the one-pot electrochemical oxidation of benzyl iodides to nitriles. The goal is to

perform the electrolysis of the benzyl iodide in an aqueous ammonia solution without any added supporting electrolyte. S_N2 displacement of iodide from the substrate will generate ammonium iodide – which will serve as both the supporting electrolyte and the precursor for electrochemical generation of the iodine oxidant.

Results and Discussion

The initial objective was to investigate the feasibility of using the ammonium iodide byproduct as both the supporting electrolyte and the precursor for electrochemical generation of iodine. Cyclic voltammetry of solutions containing potassium iodide showed an oxidative signal and a clear generation of reddish-brown iodine at the anodic surface. For a model substrate when designing reaction conditions, 4-methylbenzyl iodide was selected due to easy synthesis from 4-methylbenzyl chloride. Procedures for the synthesis and isolation of benzyl iodides *via* Finkelstein conditions are presented in the experimental section. The initial experiment design involved the electrolysis of 4-methylbenzyl iodide in 30% aqueous ammonia at 60 ºC. Electrolysis performed under these conditions generated low currents (~1.5 mA), and a passed total of 20 Coulombs of charge over three hours of electrolysis. Analysis of the product showed low conversion of the benzyl iodide starting material to the corresponding amine, and failure to produce any of the target nitrile. It was hypothesized that the low currents observed resulted from low levels of supporting electrolyte (NH_4I) liberated from the starting material. Further, it was also hypothesized that the low conversion to the amine resulted from the escape of ammonia gas from the cell upon heating. Using a sealed electrochemical cell would maintain the required ammonia levels in the electrolyte necessary to drive the displacement of iodine to completion.

We speculated that a pre-electrolysis reaction of the benzyl iodide and aqueous ammonia in a sealed cell would allow for the maximum liberation of NH_4I before the electrolysis was started. Doing so would allow for optimal currents once a potential was applied. A ^{1}H-NMR timecourse evaluation of the pre-electrolysis reaction showed that the displacement of iodide was complete after 30 minutes of reacting with aqueous ammonia at 60 ºC in a gastight vial.

Having determined the pre-electrolysis conditions, another electrolysis was performed where the 4-methylbenzyl iodide was allowed to react with aqueous ammonia in a gas-tight undivided cell for 30 minutes at 60 ºC. Significantly greater currents (~25 mA) were observed throughout the electrolysis allowing for a total of 1000 Coulombs to pass. As the electrolysis proceeded, the solution gained a reddish-brown tint showing that iodine was indeed being generated at the anode. Analysis of the product showed 23% of the target benzonitrile had formed and 34% of the intermediate amine remained.

We further speculated that residual ammonia in the electrolyte perturbs the efficiency of the electrolysis by interfering with the anodic generation of iodine. Gao and co-workers reported that iodide could be electrochemically oxidized to iodate when electrolysis is performed under moderately basic conditions (Equation 5.2).[35]

$$I^- + 6OH^- \longrightarrow IO_3^- + 3H_2O + 6e^- \qquad \textbf{(Eq. 5.2)}$$

We hypothesized that removing excess ammonia after the 30-minute pre-electrolysis reaction would further enhance the yield and efficiency of the electrolysis by minimizing the loss of iodide *via* the oxidation pathway presented by Gao. We found that

applying a mild vacuum after the pre-electrolysis reaction was the most effective method of removing excess ammonia gas from the reaction prior to electrolysis. The effect of removing excess ammonia from the electrolyte on the redox potentials of iodine was evaluated by cyclic voltammetry (Figure 5.8).

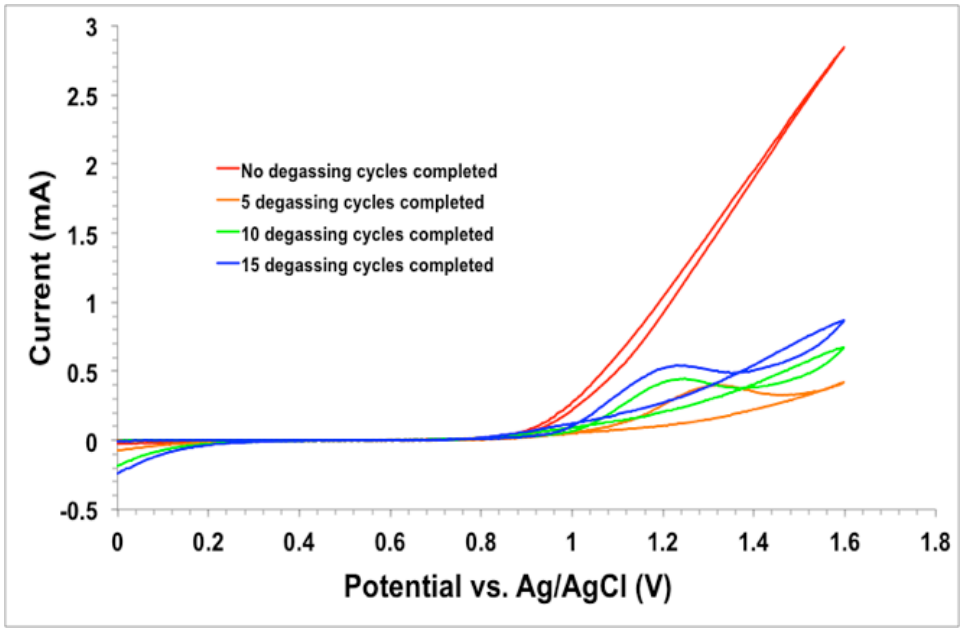


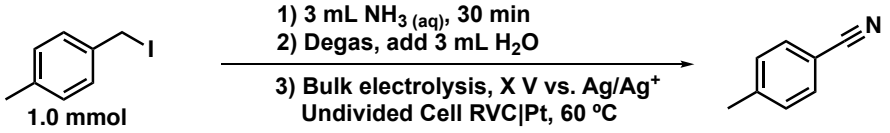
Figure 5.8. Cyclic Voltammograms Collected of the Benzyl Iodide/Ammonia Reaction Mixture after every Five Degassing Cycles for Ammonia Removal (scan rate: 50 mV/s).

The CV traces presented in Figure 5.8 were collected after an increasing number of degassing cycles had been completed. The CVs show that as the ammonia is removed by vacuum, the $2I^- \rightarrow I_2$ oxidation wave appears at approximately 1.2 V vs. Ag/Ag^+ and continues to shift to lower potentials as more ammonia is removed. Additionally, as more ammonia is removed from the electrolyte, the corresponding $I_2 \rightarrow 2I^-$ reduction wave appears and begins to shift to more positive potentials.

When electrolysis was performed after the degassing cycles had been completed, the electrolysis proceeded smoothly at a steady current (Table 5.7, entry 3). Analysis of the product showed that 63% of the target benzonitrile had formed at a charge efficiency of

32%. The pH of the electrolyte after the mild degassing procedure was measured to be approximately 10.5. Electrolysis performed at this pH seemed to operate most efficiently. If the pH of the electrolyte was too low (Table 5.7, entry 6), the electrolysis current decays and low conversion of the benzylamine intermediate to product was observed.

Table 5.7. Evaluation of the Voltage Applied During Bulk Electrolysis of 4-Methylbenzyl Iodide to *p*-tolunitrile



entry	set voltage	pH	time	avg. current	yield[a]	MB[d]	Q_{eff}[b]
1	0.9 V	10.5	18.6 h	13 mA	**65%**	70%	33%
2	1.0 V	10.5	9.2 h	25 mA	**52%**	52%	26%
3	1.1 V	10.5	4.3 h	60 mA	**63%**	63%	32%
4	1.4 V	10.5	3.8 h	55 mA	**70%**	70%	35%
5	1.7 V	10.5	3.7 h	66 mA	**76%**	76%	37%
6	1.1 V	9.5	4.6 h	varied[c]	**44%**	37%	22%

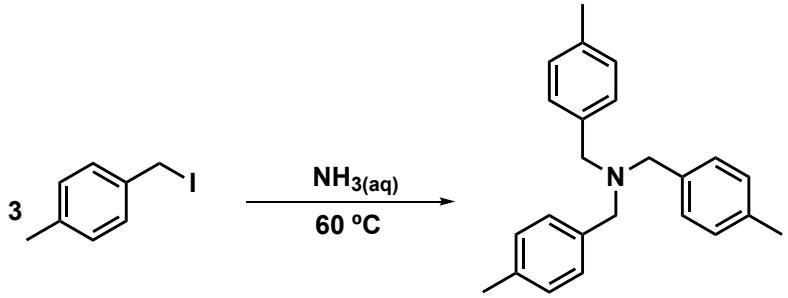
[a] Yield determined *via* ^{1}H-NMR using trimethyl(phenyl)silane as an internal standard
[b] Charge efficiency
[c] Currents started at approx 50 mA, decayed to approx 15 mA
[d] MB = Mass balance

Table 5.7 also shows experiments where the applied electrolysis voltage was varied. We found performing the electrolysis at higher voltages allows for greater currents and shorter reaction times. Additionally, the yield of product increases slightly as the applied voltage increases. However, it is possible that direct, unmediated oxidation of the substrate occurs at the anode surface when a large overpotential is applied (Table 5.7, entry 4 & 5). To prevent direct oxidation of the substrate, we elected to use an applied voltage of 1.2 - 1.2 V for future electrolysis.

At this juncture, the identity of the benzylamine intermediate had not yet been verified. Previously, we had assumed that after treatment with aqueous ammonia, the benzyl iodide forms a mixture of primary, secondary and tertiary benzylamines or

quaternary benzylammonium salts. Considering that a large amount of the mass balance was not accounted in the reactions presented in Table 5.7, we were concerned that the formation of quaternary benzylammonium salts would reduce the yield and mass balance of these reactions. We decided to isolate the intermediate after the benzyl iodide was treated with aqueous ammonia. Analysis of the product *via* ^{1}H-NMR, ^{13}C-NMR and high-resolution mass spectrometry showed that the tertiary tribenzylamine forms as the *only* product after reacting with excess aqueous ammonia (Scheme 5.10).

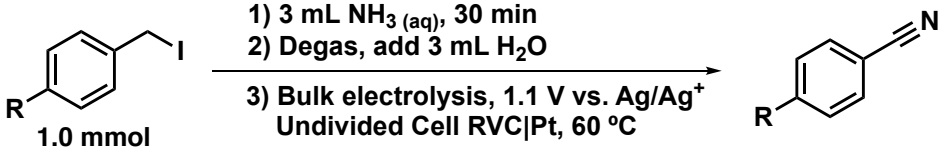
Scheme 5.10. Formation of tris(4-Methylbenzyl)amine as the Only Product of Reacting 4-Methylbenzyliodide with Aqueous Ammonia.



Although the tribenzylamine forms as the only intermediate, we were still able to obtain yields near 75% when electrolysis was performed – showing that the conversion of the tribenzylamine to the nitrile was still possible under our electrolysis conditions. Togo and co-workers presented the direct oxidative conversion of primary, secondary and tertiary amines to the corresponding nitriles in good yields using similar conditions used in their previous publications (I_2/NH_3).[36] In this publication, Togo mentions that the conversion of secondary and tertiary amines to nitriles proceeds poorly in the absence of aqueous ammonia – indicating that ammonia is necessary for the conversion of tertiary amines to nitriles under the described conditions.

Table 5.8 shows an evaluation of different substituted benzyl iodide substrates using the currently optimized conditions. Decent yields are obtained with 4-chloro, 4-methyl and 4-*tert*-butylbenzyl iodides. The electron-poor 4-trifluoromethyl benzyl iodide showed low conversion from the tertiary amine intermediate to the nitrile.

Table 5.8. Substrate Scope of the Electrochemical Conversion of Benzyl Iodides to Benzonitriles.



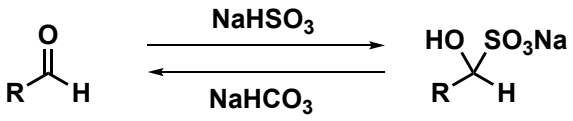
entry	R	charge	yield[a]	MB[c]	Q_{eff}[b]
1	Cl	800 C	**83%**	83%	41%
2	CH_3	800 C	**76%**	76%	37%
3	^tBu	800 C	**70%**	83%	35%
4	CF_3	800 C	**27%**	78%	13%

[a] Yield determined *via* ^{1}H-NMR using trimethyl(phenyl)silane as internal standard
[b] Charge efficiency
[c] MB = Mass Balance

When analyzing the product of the benzyl iodide oxidation reactions, the target benzonitrile is obtained usually in a nearly pure state. In many cases, the mass balance is equivalent to the percent yield of the nitrile (Table 5.8). However, in nearly every reaction, a large part of the mass balance remained unaccounted for. Since the electrolysis is being performed in a basic aqueous environment, we hypothesized that part of the mass balance ended up being converted to aldehydes. Since the oxidation of one equivalent of amine intermediate yields four equivalents of HI, and since additional ammonia is required for the conversion of the tertiary amine intermediate into individual primary aldimine fragments, it is possible that as the electrolysis proceeds, the amount of free ammonia in the reaction depletes completely. When the free ammonia is consumed, and the pH of the solution continues to decrease from the production of HI, there is a possibility that the

hydrolysis of imine intermediates results in the formation of the corresponding benzaldehydes. The first step of the work-up for this reaction is to quench the excess iodine with aqueous sodium bisulfite (a large excess of iodine is still present in the cell at the end of the bulk electrolysis). Aldehydes have been reported to form insoluble adducts with the bisulfite ion (Scheme 5.11). Considering that the work-up mixture is filtered after the drying process, the low mass balance observed in the benzyl iodide oxidation reactions may be resulting from the removal of aldehyde-adduct side-products during the work-up of the product.

Scheme 5.11. Formation and Cleavage of Aldehyde/Bisulfite Adducts.



Future experiments focused on this half of the reaction will investigate the presence of benzaldehyde in the reaction after the electrolysis has concluded. To prevent the loss of the aldehyde during work up, addition of potassium bicarbonate after the bisulfite quench will effectively convert any aldehyde/bisulfite adduct back into the pure aldehyde. The presence of aldehyde in the product in the organic extraction could then be easily verified *via* ^{1}H-NMR spectroscopy or *via* gas chromatography. If aldehyde is observed, it may be possible to rectify the mass balance anomaly by metering how much ammonia is removed during the degassing cycles to maintain an optimal pH during the electrolysis so imine hydrolysis becomes less prevalent during the I_2 oxidation.

Apparatus Design

Sealable Undivided and Divided Cells. An important technological aspect of electroorganic chemistry is the design of effective electrochemical cells that can be easily used in the organic laboratory. Although commercially manufactured electrochemical cells are available, there are few cell designs that support the use of large working electrodes while still providing a sealable design for working under a controlled atmosphere. We have designed a series of divided/undivided cells that have features useful for performing commonly used synthetic organic reactions and practices (Figure 5.9).

Our new design of electrochemical cells feature interchangeable glass lids that include an O-ring joint designed to form a seal with the cell base when compressed by an external clamp or spring clips. Additionally, the lids are fitted with a standard 14/20 taper joint for accommodating standard rubber septa. The airtight seal of electrode wires exiting the cell can be easily accomplished by inserting the wires through the rubber septum with the assistance of a standard syringe needle. The cell base is cylindrical in shape to easily support working electrodes made from shaped pieces of reticulated vitreous carbon (RVC).

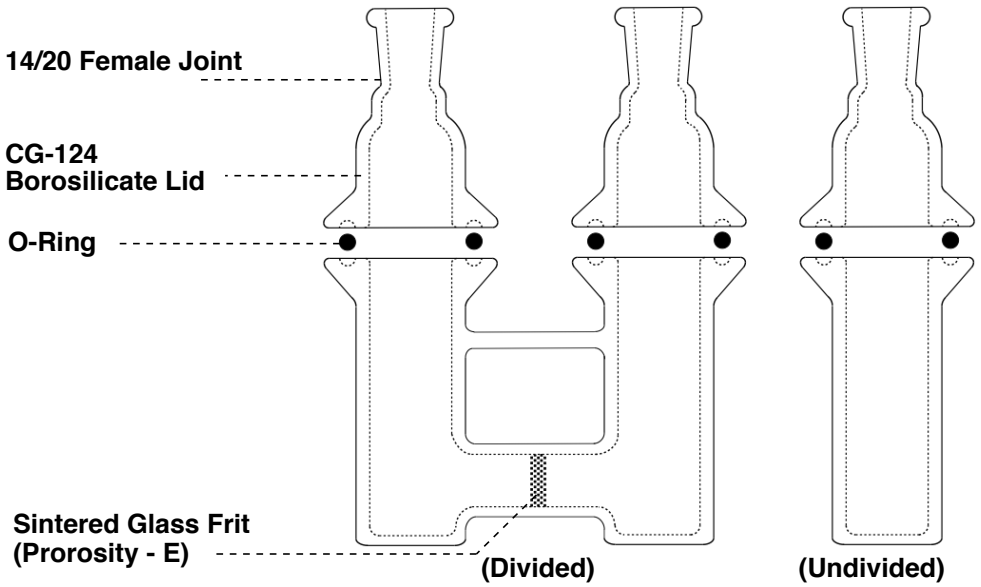


Figure 5.9. Divided and Undivided Electrochemical Cells Designed for Electroorganic Reactions. Sealable Design allows for Frequently-used Practices in Organic Synthesis (Application of Vacuum, Controlled Atmospheres, etc.).

Platinum Counter Electrodes. An issue encountered frequently during our early experiments resulted from the task of inserting three separate electrodes (the RVC working electrode, the silver reference electrode, and the platinum counter electrode) into the confined space of one of our new undivided cells. Due to the restriction of space inside the cell, the electrodes had to be assembled as close as possible to each other, and contact between the exposed platinum coil of the counter electrode and the surface of the RVC working electrode (a short circuit) was a frequently encountered problem. A simple solution to this problem would be to protect the platinum coil with a glass shield to prevent accidental contact with other electrodes. However, the evolution of gas resulting from the reduction of hydrogen is a common occurrence at the surface of a platinum counter electrode. If the platinum coil is covered, the escape of gas bubbles from the electrode is restricted – which leads to a significant reduction in current since gas bubbles effectively block contact between the platinum wire and the solution.

To solve this problem, we designed a simple, yet effective type of counter electrode that prevents accidental contact with the working electrode and allows gas to easily escape the electrode surface while maintaining a low space profile (Figure 5.10). In this design, the platinum wire is wound in a helix about a thin glass spool at the terminal of the working electrode. At the top and bottom of the thin spool, raised glass surfaces were added to the electrode profile to generate a recessed region containing the platinum helix. One end of the platinum wire was pulled through the molten glass during manufacturing to provide a solid anchor point and to allow access to the solder joint. A copper wire was soldered to end of the platinum wire fused in the glass to serves as the wire connection terminal. A protective glass sleeve was added to shield the copper wire from contact with the electrolyte.

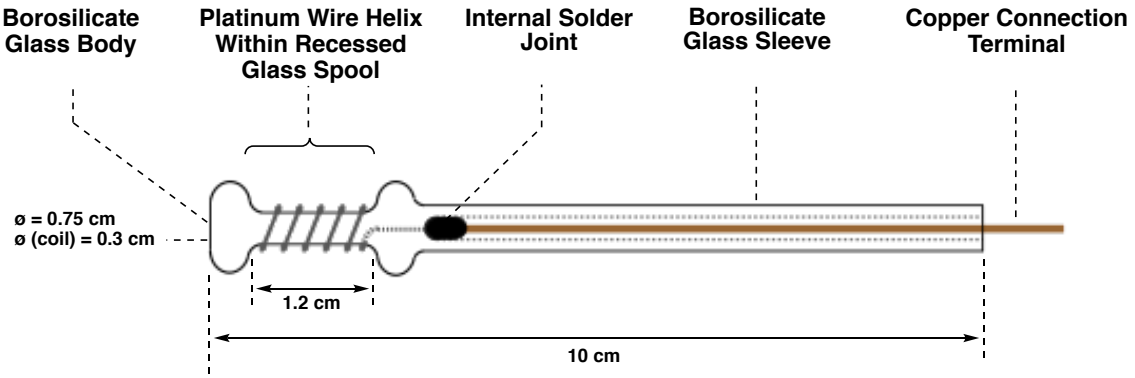


Figure 5.10. Low-Profile Short-Resistant Platinum Counter Electrode Design.

This design of the counter electrode proved to be very effective – the recessed platinum coil proved to be nearly inaccessible to the relatively flat surface of the RVC working electrode. Further, electrochemically generated gas could easily escape the platinum surface when the electrode was operating under substantial currents (~100 mA).

Conclusions

We reported a new technique for the mediated electrochemical conversion of methyl arenes to benzyl iodides and the mediated electrochemical oxidation of benzyl iodides to benzonitriles. Methodology for the benzylic iodination of methyl arenes was found to be most efficient when the substrate was used in large excess relative to iodine and was largely limited to the stability of NHPI as an electrocatalyst. Methodology for the electrochemical conversion of benzyl iodides to benzonitriles was successfully developed and applied to a small substrate scope of simple species. Specialized electrochemical cells and counter electrodes were designed for being used in electrosynthetic methods in the organic laboratory.

Experimental Section

General Experimental Methods. All commercial reagents were purchased from Sigma-Aldrich, Acros, and Oakwood and used as received without further purification, unless otherwise noted. ^{1}H-NMR spectra (400 or 500 MHz) and $^{13}C\{^{1}H\}$-NMR spectra (100 or 125 MHz) were obtained in $CDCl_3$, CD_3CN, or C_6D_6 on a Bruker 400 MHz Avance III or Bruker 500 MHz DCH Avance III spectrometer; chemical shifts (δ) are reported as ppm downfield from internal standard ($SiMe_4$). Mass spectra were acquired using electrospray ionization (ESI) on a Thermo Scientific Q-Exactive Plus™ mass spectrometer. GC/MS analysis was performed on a Shimadzu GCMS-2010S. IR spectra were obtained on a Bruker Tensor FTIR instrument as neat samples using an attenuated total reflectance accessory (Bruker Platinum ATR). Electrolyses were conducted in borosilicate cells made in-house. Electrochemical experiments were performed either with a Pine Wavenow™ or BASI Epsilon™ potentiostat.

Synthetic Procedures & Information

Finkelstein Conditions for Large-Scale Synthesis of Benzyl Iodides from Benzyl Chlorides. To a 50 mL round bottom flask was added 4-methylbenzyl chloride (1.70 g, 12 mmol), 20 mL of acetone and a Teflon stir bar. Under stirring, sodium iodide (2.02 g, 13.5 mmol) was added to the solution in the round bottom flask. The flask was then capped and left stirring at 23 ºC for 20 hours. The solution was diluted with 25 mL of deionized water and transferred to a 125 mL separatory funnel. The reaction was extracted with hexanes (5 × 25 mL) and washed with water (1 × 30 mL). The combined organic extracts were dried over $MgSO_4$, filtered, and the solvent was removed *in vacuo via* rotary evaporation to yield yellow crystals of 4-methylbenzyl iodide (2.73 g, 11.75 mmol, 98%) in a nearly pure state.

General Procedure for the Electrochemical Iodination of Methyl Arenes. To each half of a 60 mL, 25 mm divided electrochemical cell was added 30 mL of 0.1 M KPF_6, 0.01 M 2,6-lutidine solution in acetonitrile. To the anode compartment was added 4-*tert*-butyltoluene (691 μL, 4.0 mmol), I_2 (0.128 g, 0.5 mmol), $KHCO_3$ (0.440 g, 4 mmol) and NHPI (16.3 mg, 0.1 mmol) with a Teflon-coated stir bar. To the cathode compartment was added I_2 (0.128 g, 0.5 mmol) as a sacrificial oxidant. For the collection of the preliminary CV, a glassy carbon working electrode and an $Ag/AgNO_3$ non-aqueous reference electrode were immersed in the anolyte and stainless-steel mesh cathode was immersed in the catholyte. A CV was collected to determine the peak anodic oxidation potential of NHPI. The working electrode was switched with a shaped piece of RVC for the bulk electrolysis. Bulk electrolysis was performed at an overpotential of 0.15 V vs. $Ag/AgNO_3$. The electrodes were removed and rinsed into the anolyte with acetone. For the quantification

of product, diphenylmethane (167 μL, 1.0 mmol) was added to the anolyte as an internal standard and the anolyte was homogenized. An aliquot of the anolyte was removed, and the solvent was removed *in vacuo via* rotary evaporation. The remaining material was dissolved in $CDCl_3$, and a characterized *via* ^{1}H-NMR spectroscopy.

General Procedure for the Electrochemical Oxidation of Benzyl Iodides to Benzonitriles. To a 10 mL, 20 mm undivided electrochemical cell with a sealable lid was added 4-methylbenzyl iodide (0.232 g, 1.00 mmol) and 3 mL of 28-30% aqueous ammonia solution and a Teflon stir bar. The cell was then sealed with the corresponding lid (fitted with a standard rubber septum) and clamped shut with spring clamps. The cell was then placed in a 60 ºC heating bath for 30 minutes under rapid stirring. The cell was removed from heat and allowed to cool to room temperature. The cell was connected to a Schlenk line *via* syringe needle, and vacuum was gently applied to the contents of the flask to remove excess ammonia. Vacuum was applied until 400 microns was measured to assure the removal of most free ammonia. Wires connecting the shaped RVC working electrode, platinum counter electrode and Ag/AgCl reference electrode were pulled through the rubber septum in the lid. The electrodes were inserted into the base of the cell, the sealed lid was secured, and the electrode wires were connected to the potentiostat. The cell was placed back in the 60 ºC heating bath. Bulk electrolysis of the solution was then initiated via application of 1.1 V vs. Ag/AgCl. Electrolysis was performed until 800 C of charge was passed. After the prescribed charge had been passed, the cell was removed from the heating bath and cooled to room temperature. The electrodes were rinsed into the flask with approximately 5 mL of diethyl ether. Excess iodine was quenched *via* addition of 5 mL saturated aqueous sodium bisulfite solution to the crude reaction mixture, and the reaction

mixture was transferred to a separatory funnel. The reaction was extracted with diethyl ether (3 × 20 mL) and washed with brine (1 × 20 mL). The combined organic extracts were dried over anhydrous $MgSO_4$, filtered, and the solvent was removed *in vacuo via* rotary evaporation to yield *p*-tolunitrile in a nearly pure state.

References

1) Vanjari, R.; Singh, K. N., Utilization of methylarenes as versatile building blocks in organic synthesis. *Chem. Soc. Rev.* **2015,** *44* (22), 8062-8096.

2) Wang Z. Wohl-Ziegler Bromination. Comprehensive Organic Name Reactions and Reagents: John Wiley & Sons, Inc.; **2010**.

3) Frontana-Uribe, B. A.; Little, R. D.; Ibanez, J. G.; Palma, A.; Vasquez-Medrano, R., Organic electrosynthesis: a promising green methodology in organic chemistry. *Green Chem.* **2010,** *12* (12), 2099-2119.

4) Francke, R.; Little, R. D., Redox catalysis in organic electrosynthesis: basic principles and recent developments. *Chem Soc Rev* **2014,** *43* (8), 2492-521

5) Gambarotti, C.; Punta, C.; Recupero, F.; Sammis, G.; Zlotorzynska, M. In *N-Hydroxyphthalimide*, *John Wiley & Sons Ltd.*: **2013**; pp 307-316.

6) Melone, L.; Punta, C., Metal-free aerobic oxidations mediated by N-hydroxyphthalimide. A concise review. *Beilstein J. Org. Chem.* **2013,** *9*, 1296-1310, No. 146.

7) Recupero, F.; Punta, C., Free Radical Functionalization of Organic Compounds Catalyzed by N-Hydroxyphthalimide. *Chem. Rev. (Washington, DC, U. S.)* **2007,** *107* (9), 3800-3842.

8) Annunziatini, C.; Gerini, M. F.; Lanzalunga, O.; Lucarini, M., Aerobic Oxidation of Benzyl Alcohols Catalyzed by Aryl Substituted N-Hydroxyphthalimides. Possible Involvement of a Charge-Transfer Complex. *J. Org. Chem*. **2004**, 69 (10), 3431-3438.

9) Rafiee, M.; Karimi, B.; Alizadeh, S. Mechanistic Study of the Electrocatalytic Oxidation of Alcohols by TEMPO and NHPI. *ChemElectroChem* **2014**, 1, 455–462.

10) Minisci, F.; Porta, O.; Recupero, F.; Gambarotti, C.; Paganelli, R.; Pedulli, G. F.; Fontana, F., New free-radical halogenations of alkanes, catalysed by N-hydroxyphthalimide. Polar and enthalpic effects on the chemo- and regioselectivity. *Tetrahedron Lett.* **2004,** *45* (8), 1607-1609.

11) Minisci, F.; Recupero, F.; Gambarotti, C.; Punta, C.; Paganelli, R., Selective functionalization of hydrocarbons by nitric acid and aerobic oxidation catalyzed by N-hydroxyphthalimide and iodine under mild conditions. *Tetrahedron Lett.* **2003,** *44* (36), 6919-6922.

12) Fleming, F. F.; Yao, L.; Ravikumar, P. C.; Funk, L.; Shook, B. C., Nitrile-Containing Pharmaceuticals: Efficacious Roles of the Nitrile Pharmacophore. *Journal of medicinal chemistry* **2010,** *53* (22), 7902-7917.

13) Luecke, B.; Narayana, K. V.; Martin, A.; Jaehnisch, K., Oxidation and ammoxidation

of aromatics. *Adv. Synth. Catal.* **2004,** *346* (12), 1407-1424.

14) Sundermeier, M.; Zapf, A.; Beller, M., Palladium-catalyzed cyanation of aryl halides. Recent developments and perspectives. *Eur. J. Inorg. Chem.* **2003,** (19), 3513-3526.

15) Schareina, T.; Beller, M. In *Copper-catalyzed cyanations of aryl halides and related compounds*, John Wiley & Sons, Inc.: 2014; pp 313-334.

16) Mowry, D. T., The Preparation of Nitriles. *Chemical Reviews* **1948,** *42* (2), 189-283.

17) Hodgson, H. H., The Sandmeyer Reaction. *Chemical Reviews* **1947,** *40* (2), 251-277.

18) Togo, H.; Iida, S., Synthetic use of molecular iodine for organic synthesis. *Synlett* **2006,** (14), 2159-2175.

19) Liu, D.; Lei, A., Iodine-Catalyzed Oxidative Coupling Reactions Utilizing C-H and X-H as Nucleophiles. *Chem. - Asian J.* **2015,** *10* (4), 806-823.

20) Finkbeiner, P.; Nachtsheim, B. J., Iodine in modern oxidation catalysis. *Synthesis* **2013,** *45* (8), 979-999.

21) Misono, A.; Osa, T.; Koda, S., Synthesis of nitriles from aldehydes. *Bull. Chem. Soc. Jpn.* **1966,** *39* (4), 854.

22) Misono, A.; Osa, T.; Koda, S.; Sato, Y., Synthesis of nitriles from aldehydes. *Bull. Chem. Soc. Jpn.* **1967,** *40* (6), 1553.

23) Misono, A.; Osa, T.; Koda, S., Formation of benzonitrile from benzaldehyde and ammonia. II. Iodine as an oxidant. *Bull. Chem. Soc. Jap.* **1967,** *40* (12), 2875-84.

24) Misono, A.; Osa, T.; Koda, S., The formation of benzonitrile from benzaldehyde and ammonia. III. A role of the existing base. *Bull. Chem. Soc. Jap.* **1968,** *41* (3), 735-6.

25) Shimojo, H.; Moriyama, K.; Togo, H., Simple one-pot conversion of alcohols into nitriles. *Synthesis* **2013,** *45* (15), 2155-2164.

26) Kawagoe, Y.; Moriyama, K.; Togo, H., One-pot transformation of methylarenes into aromatic nitriles with inorganic metal-free reagents. *Eur. J. Org. Chem.* **2014,** *2014* (19), 4115-4122.

27) Miyagi, K.; Moriyama, K.; Togo, H., One-Pot Transformation of Carboxylic Acids into Nitriles. *Eur. J. Org. Chem.* **2013,** *2013* (26), 5886-5892.

28) Iida, S.; Ohmura, R.; Togo, H., Direct oxidative conversion of alkyl halides into nitriles with molecular iodine and 1,3-diiodo-5,5-dimethylhydantoin in aq ammonia. *Tetrahedron* **2009,** *65* (31), 6257-6262.

29) Ushijima, S.; Moriyama, K.; Togo, H., Practical one-pot transformation of electron-rich aromatics into aromatic nitriles with molecular iodine and aqueous NH3 using Vilsmeier-Haack reaction. *Tetrahedron* **2012,** *68* (24), 4588-4595.

30) Ushijima, S.; Togo, H., Metal-free one-pot conversion of electron-rich aromatics into aromatic nitriles. *Synlett* **2010,** (7), 1067-1070.

31) Ishii, G.; Harigae, R.; Moriyama, K.; Togo, H., Practical one-pot conversion of aryl bromides and β-bromostyrenes into aromatic nitriles and cinnamonitriles. *Tetrahedron* **2013,** *69* (5), 1462-1469.

32) Shono, T.; Matsumura, Y.; Inoue, K., Electroorganic chemistry. 87. Indirect electrooxidation of amines to nitriles using halogen ions as mediators. *J. Am. Chem. Soc.* **1984,** *106* (20), 6075-6.

33) Okimoto, M.; Chiba, T., Electrochemical transformations of aldehydes into methyl carboxylates and nitriles. *J. Org. Chem.* **1988,** *53* (1), 218-19.

34) Qu, Q.; Gao, X.; Gao, J.; Yuan, G., A highly efficient electrochemical route for the conversion of aldehydes to nitriles. *Sci. China: Chem.* **2015,** *58* (4), 747-750.

35) Gao, X.; Yuan, G.; Chen, H.; Jiang, H.; Li, Y.; Qi, C., Efficient conversion of CO2 with olefins into cyclic carbonates via a synergistic action of I2 and base electrochemically generated in situ. *Electrochem. Commun.* **2013,** *34*, 242-245.

36) Iida, S.; Togo, H., Direct and facile oxidative conversion of primary, secondary, and tertiary amines to their corresponding nitriles. *Synlett* **2006,** (16), 2633-2635.

37) Popov, A. I.; Rygg, R. H., The chemistry of halogens and of polyhalides. XI. Molecular complexes of pyridine, 2-picoline, and 2,6-lutidine with iodine and iodine halides. *J. Am. Chem. Soc.* **1957,** *79*, 4622-5.

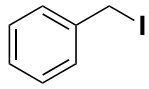
38) Popov, A. I.; Pflaum, R. T., Studies on the chemistry of halogens and polyhalides. X. The reactions of iodine monochloride with pyridine and 2,2'-bipyridine. *J. Am. Chem. Soc.* **1957,** *79*, 570-2.

39) Markovac, A.; Stevens, C. L.; Ash, A. B.; Hackley, B. E., Jr., Synthesis of oximes. III. Iodine dimethyl sulfoxide reaction with methylpyridines. *J. Org. Chem.* **1970,** *35* (3), 841-3.

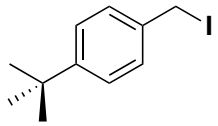
40) Brivio, L.; Caronna, T.; Fontana, F.; Gambarotti, C.; Mele, A.; Sora, I. N.; Punta, C.; Recupero, F., Reactivity of benzyl radicals: The trapping of primary, secondary and tertiary benzyl radicals with heterocyclic bases. *J. Photochem. Photobiol., A* **2010,** *214* (1), 112-114.

Supporting Information for Chapter 5:
Mediated Electrocatalytic Ammoxidation of Methyl Arenes

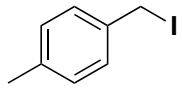
^{1}H-NMR and ^{13}C-NMR Characterization of Products



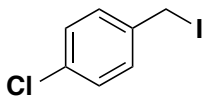
Benzyl iodide: ^{1}H-NMR (500 MHz, $CDCl_3$): δ 7.37 (d, J = 7 Hz, 2H), 7.29 (t, J = 7 Hz, 2H), 7.23 (t, J = 7 Hz, 1H), 4.45 (s, 2H); ^{13}C {1H} NMR (126 MHz, $CDCl_3$): δ 139.2, 128.8, 128.7, 127.8, 5.73



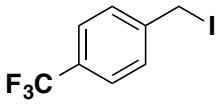
4-tert-Butylbenzyl iodide: ^{1}H-NMR (500 MHz, $CDCl_3$): δ 7.30 (s, 4H), 4.44 (s, 2H), 1.29 (s, 9H); ^{13}C {^{1}H} NMR (126 MHz, $CDCl_3$): δ 148.7, 133.9, 126.2, 123.5, 29.0, 3.8



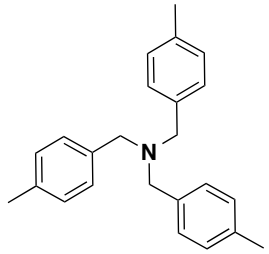
4-methylbenzyl iodide: ^{1}H-NMR (500 MHz, $CDCl_3$): δ 7.28 (d, J = 7.8 Hz, 2H), 7.10 (d, J = 7.8 Hz 2H), 4.45 (s, 2H), 2.31 (s, 3H); ^{13}C {^{1}H} NMR (126 MHz, $CDCl_3$): δ 137.8, 136.3, 129.5, 128.6, 21.2, 6.15



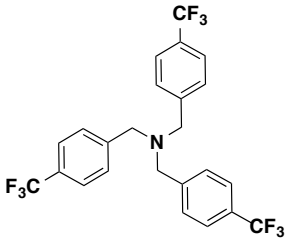
4-chlorobenzyl iodide: ^{1}H-NMR (500 MHz, $CDCl_3$): δ 7.31 (d, J = 8.5 Hz, 2H), 7.26 (d, J = 8.5 Hz 2H), 4.41 (s, 2H); ^{13}C {^{1}H} NMR (126 MHz, $CDCl_3$): δ 137.8, 133.6, 130.0, 129.0, 4.20



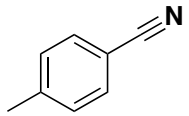
4-trifluoromehylbenzyl iodide: ^{1}H-NMR (500 MHz, $CDCl_3$): δ 7.55 (d, *J* = 8.1 Hz, 2H), 7.48 (d, *J* = 8.1 Hz 2H), 4.45 (s, 2H); ^{13}C {^{1}H} NMR (126 MHz, $CDCl_3$): δ 143.3, 129.9 (q, *J* = 32.6 Hz,), 129.0, 125.8 (q, *J* = 3.8 Hz,), 123.9 (q, *J* = 272 Hz,), 3.24



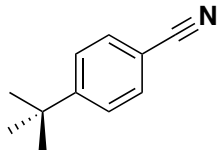
tris(4-methylbenzyl)amine: ^{1}H-NMR (500 MHz, $CDCl_3$): δ 7.27 (d, *J* = 7.7 Hz, 6H), 7.11 (d, *J* = 7.7 Hz 6H), 3.49 (s, 6H), 2.32 (s, 9H); ^{13}C {^{1}H} NMR (126 MHz, $CDCl_3$): δ 136.6, 136.2, 128.8, 128.7, 57.3, 21.1. [M+H] = 330 M/Z



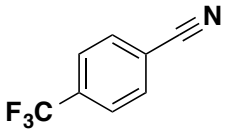
tris(4-trifluoromethylbenzyl)amine: ^{1}H-NMR (400 MHz, $CDCl_3$): δ 7.58 (d, *J* = 8.1 Hz, 6H), 7.49 (d, *J* = 8.1 Hz 6H), 3.61 (s, 6H)



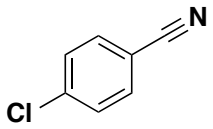
4-Methylbenzonitrile: ^{1}H-NMR (500 MHz, $CDCl_3$): δ 7.51 (d, *J* = 8 Hz, 2H), 7.24 (d, *J* = 8 Hz 2H), 2.40 (s, 3H)



4-*tert*-Butylbenzonitrile: ^{1}H-NMR (500 MHz, $CDCl_3$): δ 7.57 (d, *J* = 8.5 Hz, 2H), 7.47 (d, *J* = 8.5 Hz 2H), 1.33 (s, 9H)



4-Trifluoromethylbenzonitrile: ^{1}H-NMR (400 MHz, $CDCl_3$): δ 7.77 (d, *J* = 8.4 Hz, 2H), 7.72 (d, *J* = 8.5 Hz 2H)



4-Chlorobenzonitrile: ^{1}H-NMR (400 MHz, $CDCl_3$): δ 7.58 (d, *J* = 8.6 Hz, 2H), 7.44 (d, *J* = 8.6 Hz 2H)

Appendix A
Synthesis and Characterization of Cyanobutadiene Isomers –Molecules of Astrochemical Significance

Samuel M. Kougias
Stephanie N. Knezz
Andrew N. Owen
Rodrigo A. Sanchez
Grace E. Hyland
Daniel J. Lee
Aatmik R. Patel
Brian J. Esselman
R. Claude Woods
Robert J. McMahon

The Journal of Organic Chemistry, 2020, *85*, 5787-5798

JOC The Journal of Organic Chemistry

pubs.acs.org/joc Article

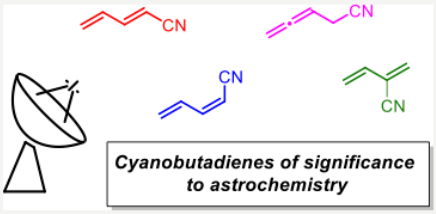
Synthesis and Characterization of Cyanobutadiene Isomers—Molecules of Astrochemical Significance

Samuel M. Kougias, Stephanie N. Knezz, Andrew N. Owen, Rodrigo A. Sanchez, Grace E. Hyland, Daniel J. Lee, Aatmik R. Patel, Brian J. Esselman, R. Claude Woods, and Robert J. McMahon*

Cite This: J. Org. Chem. 2020, 85, 5787−5798 Read Online

ACCESS | Metrics & More | Article Recommendations | Supporting Information

ABSTRACT: Four cyanobutadiene isomers of considerable interest to the organic chemistry, molecular spectroscopy, and astrochemistry communities were synthesized in good yields and isolated as pure compounds: (*E*)-1-cyano-1,3-butadiene (***E*-1**), (*Z*)-1-cyano-1,3-butadiene (***Z*-1**), 4-cyano-1,2-butadiene (**2**), and 2-cyano-1,3-butadiene (**3**). A diastereoselective synthesis was developed to generate (*E*)-1-cyano-1,3-butadiene (**1**) (10:1 *E*/*Z*) *via* tandem S_N2 and E2′ reactions. The potential energy surfaces of the E2′ reactions leading to (*E*)- and (*Z*)-1-cyano-1,3-butadiene (**1**) were analyzed by density functional theory calculations, and the observed diastereoselectivity was rationalized in the context of the Curtin−Hammett principle. The preparation of pure samples of these reactive compounds enables measurement of their laboratory rotational spectra, which are the critical data needed to search for these species in space by radioastronomy.



INTRODUCTION

Over 200 different molecules have been detected in the interstellar medium (ISM) or circumstellar shells[1,2] and are theorized to be involved in complex reaction networks.[3−7] The vast majority of these detections have been made *via* radioastronomy, through observation and assignment of rotational spectra. Because of their large dipole moments,[8−10] which confer intense rotational transitions, and composition of relatively abundant elements, nitriles (R−CN) represent realistic targets for detection by radioastronomy. Approximately 10% of the known interstellar molecules are nitriles, including recently detected benzonitrile,[11] hydroxyacetonitrile,[12] and silyl cyanide.[13] Interstellar nitriles are observed in varying degrees of hydrogenation, from highly unsaturated cyanopolyynes, $RC_{2n+1}N$ (R = H, n = 1−4; R = CH_3, n = 1, 2),[14−20] to vinyl and phenyl derivatives (vinyl cyanide (acrylonitrile),[21] cyanoallene,[22] and benzonitrile[11]), to compounds with fully saturated backbones (acetonitrile,[23] hydroxyacetonitrile,[12] propyl cyanide,[24] and isopropyl cyanide[25]). Spectroscopic data for the organic nitriles described herein—(*E*)-1-cyano-1,3-butadiene (***E*-1**), (*Z*)-1-cyano-1,3-butadiene (***Z*-1**), 4-cyano-1,2-butadiene (**2**), and 2-cyano-1,3-butadiene (**3**) (Figure 1)—would enable radioastronomical searches for these compounds. Each of these nitriles has been proposed as a likely component of the ISM.[26−30] Additionally, these nitriles are acyclic isomers of the aromatic heterocycle, pyridine, which has yet to be identified in the ISM.[31] Detection of any of these nitriles would provide additional motivation to detect pyridine and other aromatic heterocycles. The existence of organic nitriles in the ISM is relevant not only to our understanding of the chemical processes in the ISM but also to our understanding of the origin of amino acids, nucleotides, and other prebiotic compounds that are critical for life on Earth.

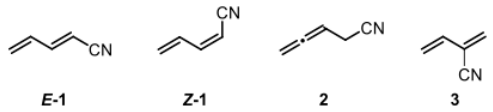


Figure 1. Cyanobutadiene isomers: (*E*)-1-cyano-1,3-butadiene (***E*-1**), (*Z*)-1-cyano-1,3-butadiene (***Z*-1**), 4-cyano-1,2-butadiene (**2**), and 2-cyano-1,3-butadiene (**3**).

Organic nitriles have also been detected in the nitrogen-rich atmosphere of Saturn's largest moon, Titan. Titan has been of interest as a possible analogue to prebiotic Earth[26] and has been visited by the Cassini−Huygens probe.[32] Small organic nitriles (up to four carbon atoms) and their corresponding anions were detected in Titan's atmosphere.[33] Electric discharge experiments performed on various gaseous mixtures (*e.g.* N_2, CH_4, C_2H_6, NH_3, H_2O, and H_2S) simulating the atmosphere of Titan produce a myriad of nitrile-containing small molecules.[3,34,35] It is plausible that the nitriles in Figure 1 are components of Titan's atmosphere.

Despite the sophistication of modern synthetic chemistry, the synthesis, purification, and isolation of the simple organic

Received: December 16, 2019
Published: April 17, 2020



ACS Publications © 2020 American Chemical Society

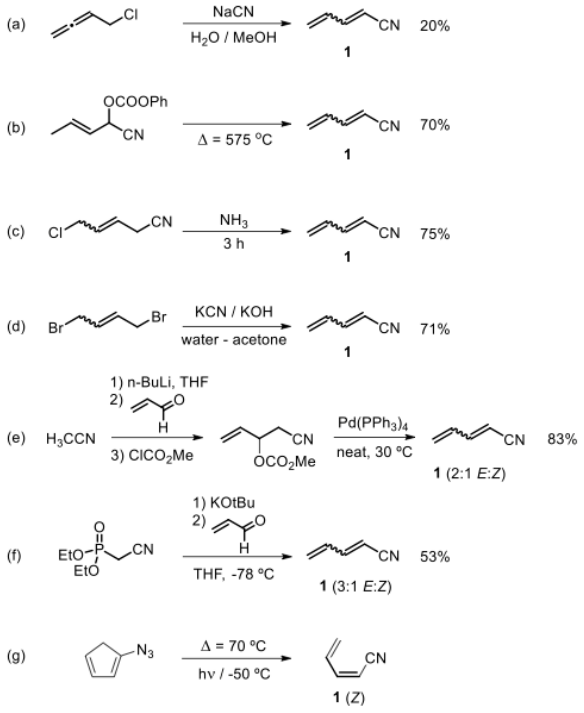
https://dx.doi.org/10.1021/acs.joc.9b03388
J. Org. Chem. 2020, 85, 5787−5798

nitriles shown in Figure 1 remain a challenge at the current time. The new procedures reported in this work enable detailed studies of the high-resolution rotational spectroscopy of the four cyanobutadiene isomers (Figure 1).[36] The rotational spectrum of each of these compounds is very complex; having a pure sample, for which spectral features are not obscured by impurities, is critical to achieve a sophisticated analysis of the complex spectrum. In measuring gas-phase spectra, volatile impurities are especially problematic. Our procedures have been designed to minimize, or eliminate, these troubling contaminants. This work provides the foundation for the ultimate detection of nitriles ***E*-1**, ***Z*-1**, **2**, and **3** in extraterrestrial environments. With their relevance in the atmospheric chemistry of Titan and interstellar chemistry, the improved isolation of these nitriles allows new spectroscopic measurements of broad interest to the chemistry community.

BACKGROUND

1-Cyano-1,3-butadiene (2,4-pentadienenitrile) (**1**; mixture of *E* and *Z* isomers) was originally isolated and studied at DuPont as a potential monomer unit by Carothers and co-workers (Scheme 1a).[37−40] Snyder *et al.* prepared **1** by flash vacuum pyrolysis (Scheme 1b), separated the *E* and *Z* isomers by careful fractional distillation,[41] and investigated the reactivity of **1** in trapping, dimerization, and polymerization reactions.[42−44] These early investigations contain a wealth of useful data describing the synthesis and physical properties of ***E*-1** and ***Z*-1**, but the experimental procedures for synthesis, purification, and isolation were designed for a relatively large scale, and these reports predate modern methods for spectroscopic characterization.[45−54]

Scheme 1. Previous Syntheses of 1-Cyano-1,3-butadiene (1)[a]



[a](a) Carothers and Berchet;[38] Coffman.[39] (b) Snyder *et al.*[41] (c) Daessle *et al.*[48] (d) Katagiri *et al.*[53] (e) Braun *et al.*[55] (f) Clary and Back.[56] (g) Banert.[57]

An efficient, selective synthesis of (*E*)-1-cyano-1,3-butadiene (***E*-1**) has not been described, although modern synthetic procedures for producing a mixture of diastereomers (***E*-1** and ***Z*-1**) have been reported (Scheme 1e−g). The preparation reported by Braun *et al.*[55] (Scheme 1e) involves the reaction of the acetonitrile anion with acrolein and subsequent protection/elimination steps to yield diastereomers ***E*-1** and ***Z*-1** in a 2:1 ratio. The procedure described by Clary and Back[56] (Scheme 1f) combines diethylcyanomethyl-phosphonate ylide with acrolein in a Horner−Wadsworth−Emmons olefination to afford diastereomers ***E*-1** and ***Z*-1** in a 3:1 ratio. Banert[57] reported the selective preparation of ***Z*-1** by thermolysis or photolysis of 1-azido-cyclopentadiene (Scheme 1g). These various procedures notwithstanding, details concerning both purification and characterization of ***E*-1** and ***Z*-1** remain incomplete because of the sensitivity and high reactivity of these compounds under a variety of conditions.

The literature does not include any reports describing the synthesis of 4-cyano-1,2-butadiene (**2**) or the determination of its physical properties. 2-Cyano-1,3-butadiene (**3**) has been prepared, typically *via* synthetic routes that involve a pyrolysis reaction.[51,58−60] As with the 1-cyano isomers, details concerning both purification and characterization of 2-cyano-1,3-butadiene (**3**) remain incomplete.

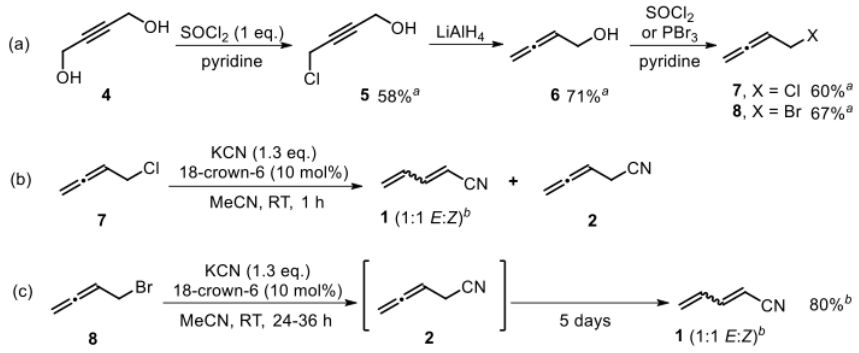
RESULTS AND DISCUSSION

1-Cyano-1,3-butadiene (1). From the time of the earliest interest in 1-cyano-1,3-butadiene (**1**) (Scheme 1),[37−44] it has been evident that *generating* this compound has not been the obstacle to further study. Rather, the sensitivity of **1** to undergo reaction (dimerization, polymerization) or degradation (heat, light, strong bases, and silica/alumina gels) greatly complicates the task of purifying and characterizing **1**. Our attempts to replicate the procedure reported by Braun *et al.*[55] (Scheme 1e) failed to produce an isolable amount of the expected mixture of diastereomers. In our hands, the procedure described by Clary and Back[56] (Scheme 1f) afforded ***E*-1** and ***Z*-1** as components in a rather complex mixture of products. Analysis of the crude ^{1}H NMR spectrum revealed the presence of suspected polymeric byproducts generated through addition reactions between ***E*-1**/***Z*-1** and the strong base used to generate the phosphonate ylide. Thus, we sought alternate synthetic strategies to facilitate isolation, purification, and characterization of compound **1**.

We replicated the conditions for the synthesis of 1-cyano-1,3-butadiene (**1**) reported by the DuPont group (Scheme 1a).[38,39] To prepare the requisite starting material, 4-chloro-1,2-butadiene (**7**), we employed the sequence depicted in Scheme 2a. 2-Butyne-1,4-diol (**4**) was monochlorinated with $SOCl_2$ to produce 4-chloro-2-butyn-1-ol (**5**), and subsequent reduction of **5** with $LiAlH_4$ produced 1,2-butadien-4-ol (**6**).[61] Chlorination of **6** with $SOCl_2$ produced 4-chloro-1,2-butadiene (**7**),[62] which was isolated and subjected to the reaction conditions described by Coffman (Scheme 1a).[39] Analysis of the resulting product mixture *via* ^{1}H NMR spectroscopy revealed the presence of both ***E*-1** and ***Z*-1** along with several methoxy-substituted species resulting from the addition of methanol across one (or both) of the double bonds present in **1**, as noted previously.[39] We suspected that the mixed solvent

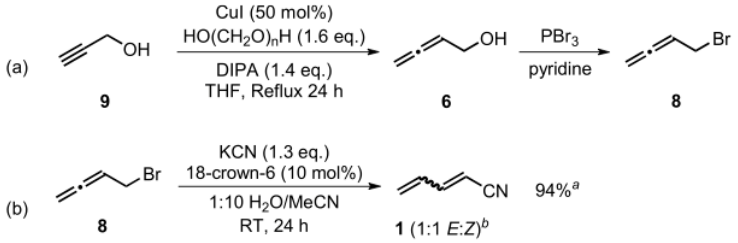
https://dx.doi.org/10.1021/acs.joc.9b03388
J. Org. Chem. 2020, 85, 5787−5798

Scheme 2. Initial Synthetic Route to 1-Cyano-1,3-butadiene (1) from 2-Butyne-1,4-diol (4)



[a]Isolated (gravimetric) yield. [b]Yield and diastereomeric ratio determined *via* ^{1}H NMR.

Scheme 3. Improved Synthetic Route to 1-Cyano-1,3-butadiene (Mixture *E*-1 and *Z*-1) from Propargyl Alcohol (9)



[a]Reaction yield determined *via* ^{1}H NMR using phenyltrimethylsilane (Ph-TMS) as an internal standard. [b]Diastereomeric ratio determined *via* ^{1}H NMR.

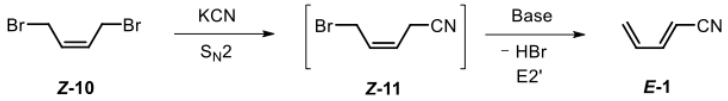
system (H_2O/MeOH) in Scheme 1a was used in an attempt to optimize the solubility of the ionic and the organic reactants (sodium cyanide and 4-chloro-1,2-butadiene (**7**), respectively), but the formation of methanol adducts is clearly problematic.

We changed the reaction solvent to acetonitrile, which seemed to be a more appropriate solvent for an S_N2 reaction. The solubility of alkali-metal cyanides in most polar aprotic organic solvents is low, so a crown ether (18-crown-6)[63] was used as a phase-transfer catalyst. Although a solution of KCN and 18-crown-6 in acetonitrile was not completely homogenous, the increased solubility of cyanide was apparently sufficient that the reaction mixture rapidly became a turbid, dark brown color as the reaction progressed (Scheme 2b). The $^{13}C\{^1H\}$NMR spectrum of the crude reaction mixture contained three signals characteristic of an allenic sp-hybridized ^{13}C atom, indicating the presence of alcohol **6**, chloride **7**, and a previously unreported allene derivative. Further analysis *via* two-dimensional NMR spectroscopy (HMBC/HSQC) showed correlation of the new allenic ^{13}C signal to three ^1H signals sharing a very similar coupling pattern as observed in alcohol **6** and chloride **7**, but with different *J*-coupling frequencies and chemical shifts. We suspected that the unassigned ^{13}C signal was due to 4-cyano-1,2-butadiene (**2**), the presumed product of initial S_N2 substitution in chloro compound **7**, prior to rearrangement to 1-cyano-1,3-butadiene (**1**). This suspicion was later confirmed to be true. Details concerning the optimization of reaction conditions, isolation, and spectroscopic characterization of 4-cyano-1,2-butadiene (**2**) are discussed below.

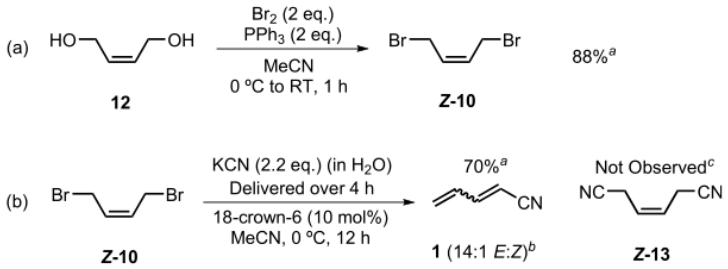
Along with 4-cyano-1,2-butadiene (**2**), smaller amounts of 1-cyano-1,3-butadiene (***E*-1** and ***Z*-1**) were formed in this reaction, and the product mixture also included a large amount of unreacted starting material **7**. Extending the reaction time to 4 h resulted in the formation of a polymeric material and complete loss of both ***E*-1** and ***Z*-1**—yet, there was still unreacted **7** present (evident *via* NMR). The same reaction sequence employing the corresponding 4-bromo-1,2-butadiene (**8**) afforded a better result. 4-Bromo-1,2-butadiene (**8**) was prepared in two steps from propargyl alcohol (**9**) (Scheme 3a).[61,64] When treated with the same reaction conditions as allenic chloride **7**, allenic bromide **8** reacted in a more controlled, clean manner, yielding significantly less of the brown polymeric material. The reaction of allenic bromide **8** to form **2** and the subsequent isomerization of **2** to **1** were unexpectedly slow; at room temperature and under anhydrous conditions, isomerization of 4-cyano-1,2-butadiene (**2**) to 1-cyano-1,3-butadiene (**1**) took 5 days (80% yield; approximately 1:1 mixture of ***E*-1** and ***Z*-1**) (Scheme 2c). Despite the use of a phase-transfer catalyst, the reaction in acetonitrile was not homogenous. The addition of water (~10% v/v) to the reaction mixture increased the solubility of KCN and decreased the reaction time to approximately 24 h (Scheme 3b). The optimal conditions for producing a 1:1 mixture of ***E*-1** and ***Z*-1** with minimal byproducts are reported in Scheme 3b. Even though the reaction efficiently produced ***E*-1** and ***Z*-1**, we were confounded in our efforts to separate, purify, and isolate these isomers, as prepared using this procedure. Difficulties included the inability to remove small amounts of acetonitrile and propensity for dimerization and/or polymerization. Requiring pure, neat materials in order to obtain their rotational spectra, we turned to other synthetic strategies that might afford a measure of selectivity in the preparation of ***E*-1** and ***Z*-1**.

https://dx.doi.org/10.1021/acs.joc.9b03388
J. Org. Chem. 2020, 85, 5787−5798

Scheme 4. Strategy for Diastereoselective Synthesis of (*E*)-1-Cyano-1,3-butadiene (*E*-1)



Scheme 5. Diastereoselective Synthesis of (*E*)-1-Cyano-1,3-butadiene (*E*-1) from (*Z*)-1,2-Dibromo-2-butene (*Z*-10)



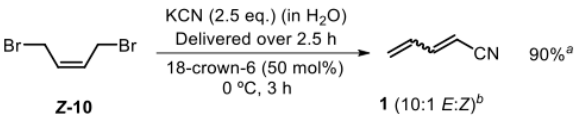
[a]Isolated (gravimetric) yield. [b]Diastereomeric ratio determined *via* ^{1}H NMR. [c]1,4-Dicyano-2-butene (*Z*-13) not observed *via* ^{1}H NMR.

(E)-1-Cyano-1,3-butadiene (E-1). Daessle *et al.* demonstrated that 1-cyano-1,3-butadiene (**1**) can be accessed *via* an E2′ (1,4-elimination) reaction of a mixture of 1-chloro-4-cyano-2-butenes with anhydrous ammonia (Scheme 1c).[48] Katagiri *et al.* demonstrated that **1** can be produced in a one-pot synthesis involving the treatment of a mixture of 1,4-dibromo-2-butenes (**10**) with alkali-metal cyanides under basic conditions (Scheme 1d).[53] Although the diastereoselectivity of these reactions was not previously investigated, we saw an opportunity to influence the diastereoselectivity of the reaction to favor the formation of *E*-**1** over *Z*-**1** *via* the stereochemistry of the 1,4-dibromo-2-butene precursor *Z*-**10** or *E*-**10** (Scheme 4). Consistent with similar precedents,[65−67] we hypothesized that E2′ reaction of (*Z*)-1-bromo-4-cyano-2-butene (*Z*-**11**) would favor the formation of *E*-**1** over *Z*-**1** because of a steric preference for the cyano group to be rotated away from the *cis* $-CH_2Br$ group in the transition state for the elimination reaction. In fact, selectivity in favor of *E*-**1** was observed, and a computational analysis of the basis for the selectivity is described later in this article.

(*Z*)-1,4-Dibromo-2-butene (*Z*-**10**), prepared from (*Z*)-2-buten-1,4-diol (**12**) *via* Appel conditions,[68] readily reacts with two equivalents of KCN through tandem S_N2/E2′ reactions to form 1-cyano-1,3-butadiene (**1**; *E*/*Z* ratio 14:1) without the addition of an exogenous base (Scheme 5). The best results were observed using binary acetonitrile/water solvent systems. Reactions performed in pure acetonitrile (*via* the addition of solid KCN to the stirring reaction) proceeded slowly and never to full conversion—likely because of the low solubility of KCN in acetonitrile. Several other polar aprotic solvents were investigated for use in these reactions [dimethylformamide (DMF), tetrahydrofuran (THF), glyme, diethyl ether, polyethylene glycol (PEG), and dimethyl sulfoxide (DMSO)], although the cleanest reactions were observed with the acetonitrile/water solvent system. DMF and DMSO accelerated the reaction to the point of a rapid exotherm, which resulted in degradation of the product, likely because of the high concentration of cyanide in these solvents. We found that the best diastereoselectivity was observed (with near-complete conversion) in experiments where aqueous KCN was added slowly to a solution of *Z*-**10** and 18-crown-6 in acetonitrile at 0 °C. Evaluation of the reaction progress *via* ^{1}H NMR spectroscopy showed the rapid formation of *E*-**1**/*Z*-**1** upon the addition of KCN to *Z*-**10**. Signals corresponding to (*Z*)-1-bromo-4-cyano-2-butene (*Z*-**11**) or (*Z*)-1,4-dicyano-2-butene (*Z*-**13**), a potential byproduct resulting from a second S_N2 displacement in *Z*-**11**, were not observed in the ^{1}H NMR spectrum as the reaction progressed. The rapid formation of *E*-**1**/*Z*-**1** and the absence of observable *Z*-**11** and *Z*-**13** signals in the ^{1}H NMR evaluation suggest that the product-forming E2′ reaction occurs more rapidly than either of these competing reactions. The drawback of this procedure was the difficulty of removing the residual acetonitrile solvent from the product *E*-**1**.

The following procedure was developed with the goal of optimizing the isolation and purification of the target compound (*E*)-1-cyano-1,3-butadiene (*E*-**1**). The addition of *Z*-**10** to 50 mol % of 18-crown-6 resulted in a eutectic mixture, which remained a liquid when cooled to 0 °C. Slow addition of aqueous KCN to a rapidly stirring eutectic mixture of *Z*-**10**/18-crown-6 at 0 °C proceeded to full conversion, while retaining good diastereoselectivity to produce *E*-**1**. Subsequent extraction with diethyl ether and fractional distillation of the product mixture yielded 1-cyano-1,3-butadiene (**1**) in 90% isolated yield (*E*/*Z* ratio 10:1) (Scheme 6).

Scheme 6. Modified Reaction Conditions for Efficient Synthesis and Purification of (*E*)-1-Cyano-1,3-butadiene (*E*-1)[a]



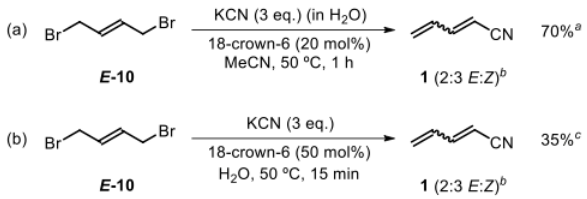
[a]Isolated (gravimetric) yield. [b]Diastereomeric ratio determined *via* ^{1}H NMR.

(Z)-1-Cyano-1,3-butadiene (Z-1). A selective route to produce (*Z*)-1-cyano-1,3-butadiene (*Z*-**1**) has been reported,[57] although details of the experimental procedure and spectroscopic properties are not readily available. Multiple studies describe the separation, isolation, and physical properties of *Z*-**1**.[41,69] As a counterpart to our development of a selective process for the preparation of *E*-**1** from *Z*-1,4-dibromo-2-

https://dx.doi.org/10.1021/acs.joc.9b03388
J. Org. Chem. 2020, 85, 5787−5798

butene (**Z-10**), we observed that subjecting ***E*-10** to the reaction conditions shown in Scheme 7 resulted in a mildly

Scheme 7. Modified Reaction Conditions for Semi-selective Preparation of (*Z*)-1-Cyano-1,3-butadiene (*Z*-1) from (*E*)-1,4-Dibromo-2-butene (*E*-10)



[a]Reaction yield determined *via* ^{1}H NMR. [b]Diastereomeric ratio determined *via* ^{1}H NMR. [c]Isolated (gravimetric) yield.

selective formation of **Z-1**. Although this procedure utilizes acetonitrile as the solvent, which was problematic in the isolation and purification of ***E*-1**, the slightly higher volatility of **Z-1** enables its separation from ***E*-1** and acetonitrile in a straightforward fashion. Iterative fractional distillation of the product mixture increased the relative concentration of **Z-1** in the distillate, resulting in a reasonably pure sample of **Z-1** after three distillations. Purity was sufficient that the ratio of *E* to *Z* by rotational spectroscopy was observed to be approximately 1:8 (***E*-1**/**Z-1**).

Computational Analysis of Diastereoselectivity in the Formation of 1-Cyano-1,3-butadiene (E-1/Z-1). The reaction to form (*E*)-1-cyano-1,3-butadiene (***E*-1**) from (*Z*)-1,4-dibromo-2-butene (**Z-10**) is hypothesized to proceed through (*Z*)-1-bromo-4-cyano-2-butene (**Z-11**), which, once formed, reacts with another equivalent of cyanide to eliminate HBr in a concerted 1,4-elimination mechanism (E2′ mechanism). Given that the *E* and *Z* diastereomers of 1-cyano-1,3-butadiene (**1**) are predicted to be very similar in energy (within 1 kcal/mol) and the reactions of different precursor stereoisomers lead to different product ratios, it is clear that a kinetically controlled reaction is responsible for the observed diastereoselectivity. Thus, the E2′ transition state barriers leading to each diastereomer of **10** must be responsible for the selectivity, or lack thereof, in the formation of ***E*-1** and **Z-1**.

The proposed E2′ substrates, (*Z*)- and (*E*)-1-bromo-4-cyano-2-butene (**11**), exhibit multiple conformational isomers, which are analyzed in detail (see Supporting Information). The isomerization barriers for all conformations of both diastereomers are less than 6 kcal/mol. Contour plots and the detailed analysis of the complete conformational potential energy surfaces of **Z-11** and ***E*-11** are provided in the Supporting Information. For the reaction of each diastereomer (**Z-11** or ***E*-11**) with cyanide ion, calculations predict two pairs of E2′ transition states leading to products (***E*-1** and **Z-1**) (Figures 2 and 3). In each of the transition state geometries, an acidic hydrogen atom at C-4 is perpendicular to the plane of the adjacent alkene unit. The bromide leaving group at C-1 can be in an *anti* or *syn* orientation with respect to the acidic hydrogen atom at C-4. The cyano substituent at C-4 may occupy a *syn*-periplanar conformation relative to the alkene moiety, which leads to the formation of (*Z*)-1-cyano-1,3-butadiene (**Z-1**), or an antiperiplanar conformation, which leads to the formation of (*E*)-1-cyano-1,3-butadiene (***E*-1**). Each transition state was verified to connect one diastereomer

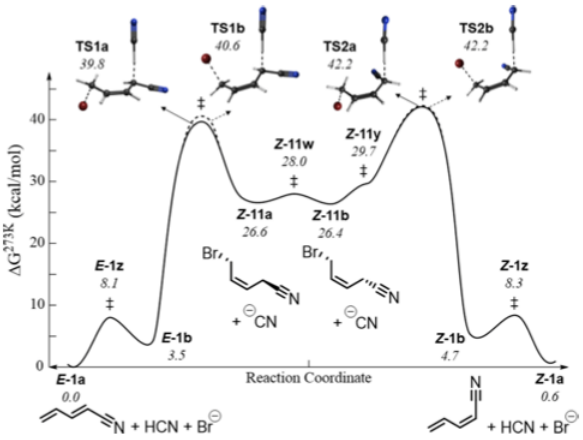


Figure 2. Computed reaction coordinate diagram for E2′ reaction of (*Z*)-1-bromo-4-cyano-2-butene (**Z-11**) with cyanide in water. Gibbs free energies at B3LYP/cc-pVTZ with the polarized continuum model for the solvent (H_2O) at 273 K (0 °C). Solid line: lower energy transition state. Dashed line: higher energy transition state.

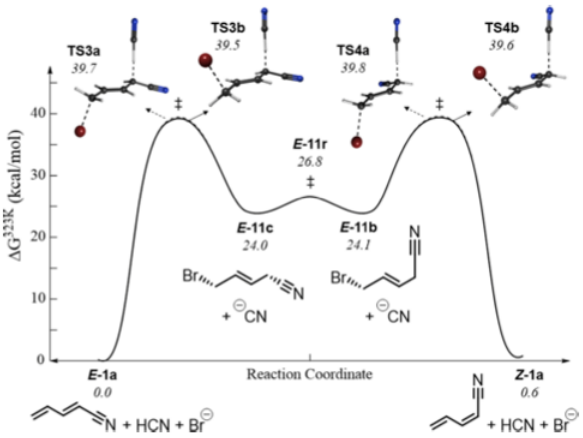


Figure 3. Computed reaction coordinate diagram for E2′ reaction of (*E*)-1-bromo-4-cyano-2-butene (***E*-11**) with cyanide in water. Gibbs free energies at B3LYP/cc-pVTZ with the polarized continuum model for the solvent (H_2O) at 323 K (50 °C). Solid line: lower energy transition state. Dashed line: higher energy transition state.

of the starting material (**11**) to one diastereomer of the product (**1**), using an intrinsic reaction coordinate (IRC) calculation. Attempts to explore a stepwise pathway beginning with deprotonation of **Z-11** or ***E*-11** failed to obtain an anionic intermediate as a stationary point. Therefore, a stepwise mechanism was not considered further.

For either diastereomer of 1-bromo-4-cyano-2-butene (***E*-11** or **Z-11**), the computed activation barriers of the E2′ transition states are significantly higher (by 7−14 kcal/mol) than the activation barriers for conformational interconversion. Thus, the diasteroselectivity in the elimination reaction is interpreted in terms of the Curtin−Hammett principle.[70] Product selectivity is governed by the difference in energy between the competing product-forming transition states ($\Delta\Delta G^{\ddagger}$); conformational equilibrium in the starting materials is rapid and does not govern the composition of products. As such, the potential energy surfaces for the E2′ reactions shown in Figures 2 and 3 contain a simplified surface for the

https://dx.doi.org/10.1021/acs.joc.9b03388
J. Org. Chem. 2020, 85, 5787−5798

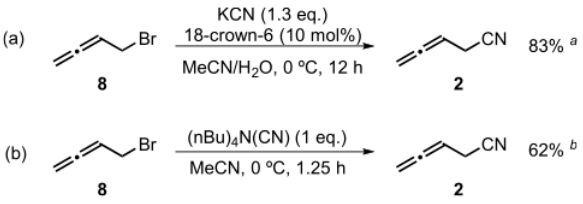
conformational isomerization of each 1-bromo-4-cyano-2-butene (*E*-**11** or *Z*-**11**).

In the E2′ reaction of (*Z*)-1-bromo-4-cyano-2-butene (*Z*-**11**) with cyanide in water at 273 K (0 °C) (Figure 2), the transition states **TS2a** and **TS2b** that lead to (*Z*)-1-cyano-1,3-butadiene (*Z*-**1**) are higher in energy than the transition states **TS1a** and **TS1b** that lead to (*E*)-1-cyano-1,3-butadiene (*E*-**1**). Thus, the computational analysis is in qualitative accordance with the experimental observation of diastereoselectivity favoring the formation of (*E*)-1-cyano-1,3-butadiene (*E*-**1**). The difference in transition state energies ($\Delta\Delta G^{\ddagger}$) appears to arise from a steric interaction in the transition states involving the $-CH_2CN$ group. Both transition states leading to *Z*-**1** (**TS2a** and **TS2b**) have a larger interaction between −CN and $-CH_2Br$, relative to the transition states leading to *E*-**1** (**TS1a** and **TS1b**). The small energy difference between the *E*-**1**-forming transition states **TS1a** and **TS1b** (0.8 kcal/mol) is likely due to a subtle difference in electrostatic interactions (repulsion) between the bromo and cyano substituents in the *anti* versus *syn* E2′ elimination pathways. Natural bond orbital (NBO) analysis of each transition state did not reveal any obvious hyperconjugation contribution to the energy differences among **TS1a**, **TS1b**, **TS2a**, and **TS2b**. Assuming that this potential energy surface reasonably models this reaction, the *E*-**1**/*Z*-**1** ratio derived from the $\Delta\Delta G^{\ddagger}$ between **TS1a** and **TS2a** (2.4 kcal/mol) is expected to be ca. 60:1. This result is in qualitative agreement with the experimental observation of an *E*-**1**/*Z*-**1** ratio of 10:1. This does indicate, however, that the computational prediction of $\Delta\Delta G^{\ddagger}$ is larger than its true value by about 1 kcal/mol.

In a similar fashion, the potential energy surface of the E2′ reaction of (*E*)-1-bromo-4-cyano-2-butene (*E*-**11**) with cyanide in water at 323 K (50 °C) is presented in Figure 3. Unlike the reaction of the isomeric system (*Z*-**11**), the transition states for the E2′ reaction of *E*-**11** leading to (*E*)- and (*Z*)-1-cyano-1,3-butadiene (**1**) are computed to be virtually isoergic ($\Delta\Delta G^{\ddagger}$ = 0.1 kcal/mol favoring the formation of *E*-**1**). With the $-CH_2CN$ and $-CH_2Br$ groups in a *trans* orientation in the ground state of *E*-**11**, there is no significant preference for the −CN substituent to adopt one conformation over the other. This situation is also manifested in the transition states (**TS3a**, **TS3b**, **TS4a**, and **TS4b**); the relative energies of the transition states reveal no preference for the stereochemical course of the reaction. Thus, the rates of product formation would be expected to afford a diastereomeric ratio of nearly 1:1. This prediction is consistent with the experimentally observed product ratio of *E*-**1**/*Z*-**1** (*E*/*Z* ratio 2:3). The deviation of the experimental ratio from 1:1 reveals that there is a slight energetic preference (<1 kcal/mol) for the transition states leading to the *Z* diastereomer. Our computational model is not expected to be of sufficient accuracy to account for such a small energetic difference.

4-Cyano-1,2-butadiene (2). As described earlier, we observed 4-cyano-1,2-butadiene (**2**) as an intermediate during the preparation of 1-cyano-1,3-butadiene (**1**) from 4-halo-1,2-butadienes (**7** or **8**) (Scheme 2). In order to optimize conditions for the preparation and isolation of **2**, it was necessary to avoid the isomerization of **2** to **1**—a process that is typically observed under conditions that utilize both water and cyanide (a weak base) at ambient temperature. When the reaction of 4-bromo-1,2-butadiene (**8**) is performed under anhydrous conditions (dry solvent, vacuum-dried crown ether, and vacuum-dried KCN), bromide **8** undergoes slow S_N2 reaction; minimal isomerization of **2** is observed. The rate of substitution, however, is too slow to be useful. The addition of water to the reaction mixture increases the solubility of cyanide, increases the rate of substitution, and increases the rate of isomerization of **2** to **1**. (Ultimately, the rate becomes very rapid and results in a noticeable exotherm.) At a reaction temperature of 0 °C, the isomerization is slow enough such that 4-cyano-1,2-butadiene (**2**) can be isolated (Scheme 8a). In

Scheme 8. Preparation of 4-Cyano-1,2-butadiene (2)

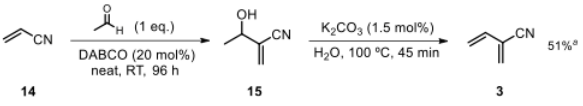


[a]Reaction yield determined *via* ^{1}H NMR. [b]Isolated (gravimetric) yield.

the absence of aqueous acidic or basic conditions, **2** is stable when isolated. The slow addition of an organic-soluble cyanide source [tetrabutylammonium cyanide (TBAC)], under anhydrous conditions, allows for an efficient S_N2 reaction and isolation of pure **2** without significant isomerization (Scheme 8b). Once the cyanide is consumed, exposure to water in the subsequent extraction (to remove the polar aprotic solvent) does not promote significant isomerization of **2**. In fact, neat **2** can be left at ambient conditions for weeks without observable isomerization. Nitrile **2** is sufficiently stable that it can be distilled under a relatively low vacuum (100 Torr) without noticeable degradation. In contrast to the regioselectivity exhibited in the rearrangement of the corresponding allenic halides,[71] the isomerization of allenic nitrile **2** yields exclusively 1-cyano-1,3-butadiene (**1**). 2-Cyano-1,3-butadiene (**3**) is not observed, which is attributable to the absence of cyanide dissociation/recombination previously observed for the corresponding allenic halides.

2-Cyano-1,3-butadiene (3). Although 2-cyano-1,3-butadiene (**3**) has been prepared previously, synthetic routes often involve a pyrolysis reaction as the last step.[51,58−60] Preferring to avoid a pyrolysis reaction, we prepared 2-cyano-1,3-butadiene (**3**) using a combination of literature procedures from Strub *et al.*[72] and Nonaka *et al.*[73−75] (Scheme 9).

Scheme 9. Preparation of 2-Cyano-1,3-butadiene (3)



[a]Isolated (gravimetric) yield.

Morita−Baylis−Hillman addition of acrylonitrile (**14**) and acetaldehyde using catalytic 1,4-diazabicyclo[2.2.2]octane (DABCO) afforded 3-hydroxy-2-methylenebutanenitrile (**15**) in quantitative yield.[72] Subsequent dehydration of **15** was performed using catalytic K_2CO_3. The resulting 2-cyano-1,3-butadiene (**3**) was distilled from the reaction mixture under vacuum and collected as an aqueous emulsion that separated upon cooling. Compound **3** is prone to undergo polymerization, even at −20 °C.

https://dx.doi.org/10.1021/acs.joc.9b03388
J. Org. Chem. 2020, 85, 5787−5798

SUMMARY

We describe the synthesis, isolation, purification, and spectroscopic characterization of four cyano-butadiene isomers: (*E*)-1-cyano-1,3-butadiene (***E*-1**), (*Z*)-1-cyano-1,3-butadiene (***Z*-1**), 4-cyano-1,2-butadiene (**2**), and 2-cyano-1,3-butadiene (**3**). These molecules are of considerable significance to the field of astrochemistry, as possible constituents of both planetary atmospheres and interstellar space. Because of the general experimental difficulties in handling these reactive compounds, the literature data concerning the spectroscopic characterization [NMR, IR, and mass spectrometry (MS)] of these simple organic molecules are remarkably sparse. Our new procedures enable isolation and purification of these compounds, affording high quality NMR, IR, and MS data, for the first time. The preparation of pure samples of these molecules enables the measurement of their laboratory rotational spectra—the critical data needed to search for these species in space by radioastronomy.

COMPUTATIONAL METHODS

Geometry optimizations and harmonic frequency calculations were conducted with density functional theory using the B3LYP functional[76,77] and the cc-pVTZ basis set,[78] correcting for water as a solvent by employing the polarizable continuum model as implemented in Gaussian 16.[79] Thermally corrected Gibbs free energies for all species were obtained from the harmonic frequency calculations at 273, 298, and 323 K and are summarized in the Supporting Information. Conformational analyses of the local minima are included in the Supporting Information along with the Cartesian coordinates of the optimized stationary points. Additional calculations were conducted for the E2′ (1,4-elimination) transition states: IRC calculations verified that each transition state smoothly connects one diastereomer of the starting material to one diastereomer of the product. Natural Bond Orbital (NBO) and Natural Resonance Theory (NRT) calculations[80] were used to analyze the electronic structure, bonding, hyperconjugation, and relative energies of energy minima and transition states on the potential energy surfaces.

EXPERIMENTAL SECTION

General Experimental Methods. All commercial reagents were purchased from Sigma-Aldrich, Acros, or Oakwood and used as received, unless otherwise noted. ^{1}H NMR spectra (400 or 500 MHz) and ^{13}C{^{1}H}-NMR spectra (100 or 125 MHz) were obtained in $CDCl_3$, CD_3CN, or C_6D_6 on a Bruker 400 MHz AVANCE III or Bruker 500 MHz DCH AVANCE III spectrometer; chemical shifts (δ) are reported as ppm downfield from internal standard $SiMe_4$. Mass spectra were acquired using electrospray ionization (ESI) or the atmospheric solids analysis probe (ASAP)[81] on a Thermo Scientific Q-Exactive Plus mass spectrometer. GC/MS analysis was performed on a Shimadzu GCMS-2010S. IR spectra were obtained on a Bruker TENSOR Fourier transform infrared instrument as neat samples using an attenuated total reflectance accessory (Bruker PLATINUM ATR).

*1-Cyano-1,3-butadiene (**1**).* Our preliminary studies concerning the preparation, isolation, and identification of 1-cyano-1,3-butadiene (**1**) provide some context for the experimental difficulties encountered and detail concerning the spectroscopic assignments.[82]

Following the procedure of Clary and Back:[56] to a suspension of sodium hydride (2.88 g, 120 mmol) in freshly distilled THF (500 mL) was added diethyl cyanomethylphosphonate (8.1 mL, 50.1 mmol) dropwise *via* a syringe at 0 °C. After stirring for 1 h, freshly distilled acrolein (3.6 mL, 53.9 mmol) was added dropwise. The reactants were stirred for 5 h at 0 °C, warmed to room temperature, and quenched with saturated aqueous NH_4Cl solution. The solution was extracted with diethyl ether, washed with saturated aqueous NaCl, and dried over $MgSO_4$. After removal of the drying agent by filtration, ether was removed under reduced pressure at room temperature, and the resulting mixture was fractionally distilled (collection flask cooled to −78 °C and distillation flask cooled to 0 °C). The distillate consisted of a mixture of *E* and *Z* isomers of 1-cyano-1,3-butadiene (**1**) in a ratio of 2:1 in addition to residual THF.

^{1}H NMR (400 MHz, $CDCl_3$): ***E*-isomer** δ 6.31 (ddt, 1H, J = 16, 11, <1 Hz), 5.74 (tt, 1H, J = 10, <1 Hz), 4.94 (dm, 1H, J = 17, <1, <1 Hz), 4.93 (dm, 1H, J = 10, <1, <1 Hz), 4.65 (dd, 1H, J = 16, <1 Hz) ppm; ***Z*-isomer** δ 6.59 (dtd, 1H, J = 17, 10, <1 Hz), 6.03 (tt, 1H, J = 10, <1 Hz), 5.03 (dm, 1H, J = 17, <1, <1 Hz), 5.02 (dm, 1H, J = 10, <1, <1 Hz), 4.55 (dd, 1H, J = 10, <1 Hz). HRMS (ASAP-Q-IT)[81] m/z: $[M + H]^+$ calcd for C_5H_6N, 80.0495; found, 80.0493.

The procedure involves the formation of a phosphonate ylide followed by reaction with acrolein in a Horner−Wadsworth−Emmons-type olefination.[56] Although this reaction appears to be straightforward, the resulting ^{1}H NMR spectrum does not agree with that described in the literature.[56] Upon closer investigation, the previously reported ^{1}H NMR data do not account for all hydrogen atoms in the molecule. Although each isomer (***E*-1** and ***Z*-1**) should have five signals in the spectrum, the *E*-isomer (***E*-1**) has four reported signals and the *Z*-isomer (***Z*-1**) has only three.[56] Additionally, the reaction inherently undergoes a side reaction, and not all signals in the crude spectrum are attributable to **1**. The combination of the two issues combined with challenges encountered in purification created confusion in characterization and complicated the optimization and troubleshooting processes. These issues are discussed in greater detail in the Supporting Information section.

*Isolation of E- and Z-Isomers of 1-Cyano-1,3-butadiene (**1**).* One of the challenges encountered during the isolation of neat ***E*-1**/***Z*-1** originates from its volatility and its tendency to form azeotropes with acetonitrile. The complete removal of acetonitrile was necessary for obtaining accurate spectra and isolated yields of the product. Solvent removal *via* rotary evaporation drastically reduced product yields because of the azeotropic losses. We found that most acetonitrile could be removed through aqueous washes of the crude ethereal extract during reaction workup. Remaining traces of acetonitrile could be fully removed from the products by low-temperature vacuum distillation (~100−500 mTorr, 0 °C). Attempts to remove acetonitrile *via* careful vacuum fractional distillation were marginally effective, as a small amount of acetonitrile always codistilled with the product diastereomers. We found that highly volatile solvents (such as the diethyl ether used during the biphasic extraction of the reaction mixture) were more easily removed *via* fractional distillation through a packed column under atmospheric pressure without codistilling any ***E*-1** and ***Z*-1**. Additionally, product losses resulting from polymerization of ***E*-1** and ***Z*-1** during the distillation process were minimized *via* the addition of a phenolic polymerization inhibitor. We found that hydroquinone was ideal for our purposes because its high boiling point and extremely low volatility prevented its codistillation with ***E*-1** and ***Z*-1** during the final purification.

*(Z)-1,4-Dibromo-2-butene (**Z*-10).* In a modification of literature procedures,[83−85] 52.55 g (200 mmol) of PPh_3 was added to 300 mL of acetonitrile in a 500 mL round-bottom flask equipped with a 100 mL dropping funnel. The reaction vessel was sealed with a septum and cooled to 0 °C on ice. The reaction vessel and contents were subjected to three vacuum pump/N_2 purge cycles. Br_2 (10.2 mL, 197.8 mmol) was added dropwise to the stirring PPh_3 suspension *via* the dropping funnel. (*Z*)-2-Buten-1,4-diol (**12**) (9.04 g, 103 mmol) was rapidly added to the stirring suspension *via* a syringe. The cooling bath was removed, and the reactants were stirred for 1 h. After the elapsed reaction time, approximately half of the acetonitrile solvent was removed by rotary evaporation. The resulting triphenylphosphine oxide precipitate was removed *via* vacuum filtration. The filtrate was then evaporated to dryness. The resulting orange solids were dissolved in 50 mL of 1:4 EtOAc/*n*-hexane and filtered through a silica plug (5 cm) to remove any remaining triphenylphosphine oxide. The solvent was removed *in vacuo* to yield 18.07 g (88%) of (*Z*)-1,4-dibromo-2-butene (***Z*-10**) as a pale-yellow oil. **CAUTION**: (*Z*)-1,4-Dibromo-2-butene is a potent lachrymator and vesicant and must be handled with caution. Samples of (*Z*)-1,4-dibromo-2-butene will isomerize upon heating and should be stored in a freezer (−20 °C).

^{1}H NMR ($CDCl_3$, 500 MHz):δ (ppm) complex spin system, 5.89 (m,

https://dx.doi.org/10.1021/acs.joc.9b03388
J. Org. Chem. 2020, 85, 5787−5798

2H), 4.02 (m, 4H). $^{13}C\{^1H\}$-NMR ($CDCl_3$, 125 MHz): δ (ppm) 129.9, 24.7.

(E)-1-Cyano-1,3-butadiene (E-1) ((E)-2,4-Pentadienenitrile). (*Z*)-1,4-Dibromo-2-butene (**Z-10**; 5.38 g, 25.2 mmol), 3.36 g (12.7 mmol) of 18-crown-6, and 57 mg (0.52 mmol) of hydroquinone were added to a 50 mL single-neck round-bottom flask. The reaction vessel was sealed with a septum and purged with N_2 *via* a syringe needle inlet. The vessel was then cooled to 0 °C on ice. Potassium cyanide (4.09 g, 62.8 mmol) was dissolved in 10 mL of deionized H_2O and delivered to the cooled reaction dropwise *via* a syringe pump over the course of 2 h with vigorous stirring. As the addition completed, the reaction became biphasic with an orange top organic layer and a tan bottom aqueous layer. The reactants were stirred for an additional 15 min at 0 °C after the addition was complete and then allowed to warm to room temperature. The reaction mixture was rinsed into a separatory funnel with 10 mL of diethyl ether and 10 mL of deionized H_2O, the organic layer was separated, and the aqueous layer was extracted with diethyl ether (4 × 10 mL). The combined organic layers were washed with 10 mL of saturated aqueous NaCl and dried over anhydrous $CaCl_2$. After removal of the drying agent by gravity filtration, hydroquinone (97 mg) was added to the filtrate and the ethereal solvent was removed by fractional distillation at atmospheric pressure (45 cm Vigreux column). The crude product was cooled to room temperature, and a vacuum of ∼400 Torr was applied to remove residual ether. The remaining yellow concentrate was purified *via* bulb-to-bulb (Kugelrohr) distillation to yield 1.80 g of 1-cyano-1,3-butadiene (**1**) (90%, 10:1 *E*/*Z*) as a colorless oil. Compound ***E*-1** is indefinitely stable as a neat substance at −80 °C or in a dilute solution of diethyl ether with the hydroquinone inhibitor to prevent polymerization. ^1H NMR (C_6D_6, 500 MHz): δ (ppm) ***E*-1**: 6.34 (dd, 1H, J = 16, 10 Hz), 5.79 (dt, 1H, J = 17.1, 10.3 Hz), 5.01 (d, 1H, J = 2.4 Hz), 4.99 (d, 1H, J = 2.7 Hz), 4.69 (d, 1H, J = 16 Hz). $^{13}C\{^1H\}$-NMR (C_6D_6, 125 MHz): δ (ppm) 150.0, 134.3, 125.9, 117.8, 100.2. IR (neat): (cm^{-1}) 3054 (w), 2218 (m), 1629 (w), 1589 (m), 1417 (w), 1292 (w), 1258 (w), 1001 (s), 955 (m), 932 (m), 835 (m), 475 (w). HRMS (ESI) *m*/*z*: $[M + H]^+$ calcd for C_5H_6N, 80.0495; found, 80.0494.

(Z)-1-Cyano-1,3-butadiene (Z-1) ((Z)-2,4-Pentadienenitrile). Potassium cyanide (9.88 g, 152 mmol, 3 equiv) and 18-crown-6 (6.66 g, 25 mmol, 50 mol %) were dissolved in 20 mL of deionized H_2O in a 100 mL three-neck round-bottom flask. Hydroquinone (110 mg, 1 mmol) was added to the flask to inhibit polymerization of the product. The flask was purged with N_2 and sealed with rubber septa. The vessel was heated to 50 °C in an oil bath. Under positive N_2 pressure, one septum was removed from the reaction vessel and solid (*E*)-1,4-dibromo-2-butene (***E*-10**) (10.72 g, 50.1 mmol, 1 equiv) was added in ∼2 g increments to the vigorously stirring KCN/18-crown-6 solution over the course of 15 min. The reaction mixture darkened to a reddish-brown color during the addition of ***E*-10**. The reaction was cooled to room temperature and rinsed into a separatory funnel with 10 mL of diethyl ether and 10 mL of deionized H_2O. The organic layer was separated, and the aqueous layer was extracted with diethyl ether (4 × 25 mL). The combined organic layers were washed with saturated aqueous NaCl (1 × 25 mL) and dried over anhydrous $CaCl_2$. The drying agent was removed by gravity filtration, and the ethereal solvent was removed by fractional distillation at atmospheric pressure (45 cm glass bead packed column). The product was purified by vacuum distillation through the same apparatus to yield 1-cyano-1,3-butadiene (**1**) (34%, 2:3 *E*/*Z*) as a colorless oil (bp 75 °C, 100 Torr). Subsequent fractional distillations through the same apparatus can be performed to further separate ***Z*-1** from ***E*-1**. Compound ***Z*-1** exhibits greater thermal stability than ***E*-1**, presumably because of lower reactivity with respect to dimerization or polymerization. ^1H NMR (C_6D_6, 500 MHz): δ (ppm) ***Z*-1**: 6.58 (dt, 1H, J = 16.8, 10.6 Hz), 5.98 (t, 1H, J = 10.9 Hz), 5.02 (d, 1H, J = 16.8 Hz), 5.0 (d, 1H, J = 10.2 Hz), 4.48 (d, 1H, J = 10.7 Hz). $^{13}C\{^1H\}$-NMR (C_6D_6, 125 MHz): δ (ppm) 148.7, 132.7, 126.2, 115.9, 98.4. IR (neat): (cm^{-1}) 3071 (w), 2216 (m), 1628 (w), 1574 (m), 1428 (w), 1359 (w), 1296 (w), 1229 (w), 1001 (m), 934 (s), 778 (m), 667 (s), 487 (w), 444 (w). HRMS (ESI) *m*/*z*: $[M + H]^+$ calcd for C_5H_6N, 80.0495; found, 80.0494.

4-Chloro-2-butyne-1-ol (5). In a slight modification of literature procedures,[86−89] 59.75 g (0.69 mol, 1 equiv) of 2-butyne-1,4-diol (**4**), 70 mL of dry dichloromethane, and 62 mL (770 mmol, 1.1 equiv) of dry pyridine were added to a 1 L flame-dried three-neck round-bottom flask under a N_2 atmosphere. The stirring reaction vessel was cooled to 0 °C on ice, and 56 mL (92 g, 772 mmol) of $SOCl_2$ was added dropwise over a time of 4 h *via* a pressure-equalizing addition funnel. A white precipitate formed over the course of the $SOCl_2$ addition. The reactants were then poured onto 200 mL of ice water and subsequently extracted with dichloromethane (3 × 150 mL). The combined organic layers were washed with saturated aqueous $NaHCO_3$ (1 × 100 mL) and saturated aqueous NaCl (1 × 100 mL) and dried over anhydrous Na_2SO_4. After removal of the drying agent by gravity filtration, dichloromethane was removed *in vacuo* to yield a deep red oil. The crude product was purified by vacuum distillation using a short-path apparatus to yield 42.32 g (58%) of colorless 4-chloro-2-butyne-1-ol (**5**), bp 50 °C (0.5 Torr). **CAUTION**: 4-chloro-2-butyne-1-ol is highly explosive and a powerful skin irritant—care must be taken when handling.[90] ^1H NMR ($CDCl_3$, 500 MHz): δ (ppm) 4.33 (t, 2H, ^5J = 2 Hz), 4.19 (t, 2H, ^5J = 2 Hz). $^{13}C\{^1H\}$-NMR ($CDCl_3$, 125 MHz): δ (ppm) 84.6, 80.5, 51.1, 30.3. HRMS (ESI) *m*/*z*: $[M + H]^+$ calcd for C_4H_5ClO; [^{35}Cl]-isotopologue calcd, 105.0107; found, 105.0102; [^{37}Cl]-isotopologue calcd, 107.0078; found, 107.0072.

1,2-Butadien-4-ol (6). Early Method.[87,88] Lithium aluminum hydride (6.09 g, 16 mmol) and dry diethyl ether (80 mL) were added to a flame-dried 250 mL three-neck round-bottom flask fitted with a dry ice condenser under a N_2 atmosphere and stirred to generate a slurry. 4-Chloro-2-butyne-1-ol (**5**) (4.19 g, 40 mmol) was diluted with 16 mL of dry diethyl ether and delivered dropwise *via* a syringe to the stirring LAH slurry at a rate sufficient to maintain a gentle reflux. After the addition of **5**, the reactants were stirred for 30 min at 25 °C. The reaction was cooled to 0 °C on ice, and the septa were removed. The reaction was quenched *via* Fieser workup: (slow addition of 6 mL of deionized H_2O, then 6 mL of 15% aqueous NaOH, and finally 18 mL of deionized H_2O). A scoop of anhydrous Na_2SO_4 was added to promote aggregation of the precipitated aluminum salts, and the vessel was stirred overnight at 25 °C. The reaction mixture was filtered, and the organic layer was separated. The aqueous layer was extracted with diethyl ether (3 × 25 mL). The combined organic extracts were then dried over anhydrous Na_2SO_4 and filtered, and the solvent was removed *in vacuo*. The crude product was purified by vacuum distillation using a short-path apparatus to yield 1.99 g (71%) of colorless 1,2-butadien-4-ol (**6**), bp 60 °C (40 Torr).

Primary Method.[64,90] A flame-dried 5 L three-neck round-bottom flask was equipped with a reflux condenser (open to air), thermometer, and mechanical stirrer. To this vessel were added CuI (115.37 g, 605 mmol, 50 mol %), paraformaldehyde (59.53 g, 1.98 mol, 1.6 equiv), and 2.4 L of dry THF. The mechanical stirrer was started, and dry diisopropylamine (240 mL, 1.71 mol, 1.4 equiv) was added—the reaction mixture appeared faint green. Propargyl alcohol (**9**) (74 g, 76 mL, 1.3 mol) was added to the reaction mixture. The addition of propargyl alcohol resulted in an immediate exotherm (increase from 20 to 30 °C), and the reaction color changed to bright orange. The reaction was heated with a mantle to reflux for 24 h. After cooling to 25 °C, most of the THF solvent was removed *via* rotary evaporation. The concentrated reaction mixture was slowly added to a stirred, cooled (0 °C) solution of diethyl ether (1 L) and 12 N HCl (120 mL), resulting in the formation of a viscous brown precipitate. The stirring was stopped, and the mixture was allowed to separate. The supernatant ether was decanted, and the brown precipitate was extracted with diethyl ether (2 × 1 L). The combined ether extracts were filtered through a silica plug (ø = 80 mm × 50 mm), dried over anhydrous Na_2SO_4, and concentrated *in vacuo*. The crude product was purified by vacuum distillation using a short-path apparatus to yield 47.2 g (52%) of colorless 1,2-butadien-4-ol (**6**), bp 60 °C (40 Torr). ^1H NMR ($CDCl_3$, 500 MHz): δ (ppm) complex spin system,

https://dx.doi.org/10.1021/acs.joc.9b03388
J. Org. Chem. 2020, 85, 5787−5798

5.34 (apparent quint, 1H, J = 6.4 Hz), 4.85 (m, 2H, J = 3 Hz), 4.14 (m, 2H, J = 3 Hz), 2.4 (br s, 1H). $^{13}C\{^1H\}$-NMR ($CDCl_3$, 125 MHz): δ (ppm) 207.9, 90.8, 77.0, 60.2.

4-Chloro-1,2-butadiene (7).[62,86,88] $SOCl_2$ (16.97 g, 10.4 mL, 143 mmol, 1.25 equiv), 11.28 g of dry pyridine (11.5 mL, 143 mmol, 1.25 equiv) and 50 mL of dry diethyl ether were added to a flame-dried, three-neck 500 mL round-bottom flask equipped with a pressure-equalizing addition funnel and reflux condenser under a N_2 atmosphere. The vessel was cooled to 0 °C on an ice bath. A solution of 1,2-butadien-4-ol (**6**) (7.97 g, 114 mmol, 1 equiv) in 70 mL of dry diethyl ether was delivered dropwise to the stirring reaction *via* an addition funnel over 15 min. A white precipitate formed over the course of the addition. The reaction was heated to reflux in an oil bath for 2 h. The reaction was cooled to room temperature and quenched *via* the addition of 15 mL of deionized H_2O. The organic layer was separated, and the aqueous layer was extracted with diethyl ether (3 × 15 mL). The combined organic layers were dried over anhydrous Na_2SO_4 and filtered. The ethereal solvent was removed by fractional distillation at atmospheric pressure (45 cm Vigreux column). The fractionating column was removed, and the product was purified by distillation at atmospheric pressure using a short-path apparatus to yield 6.10 g (60%) of 4-chloro-1,2-butadiene (**7**) as a colorless oil. bp 88 °C (760 Torr). ^1H NMR ($CDCl_3$, 500 MHz): δ (ppm) complex spin system, 5.36 (m, 1H, J = 7.7, 6.6 Hz), 4.91 (dt, 2H, J = 6.6, 2.2 Hz), 4.08 (dt, 2H, J = 7.7, 2.2 Hz). $^{13}C\{^1H\}$-NMR ($CDCl_3$, 125 MHz): δ (ppm) 209.5, 89.0, 77.5, 66.0.

4-Bromo-1,2-butadiene (8).[88] PBr_3 (21.6 g, 10.4 mL, 80 mmol), 7.89 g of dry pyridine (8 mL, 100 mmol), and 20 mL of dry diethyl ether were added to a flame-dried, single-neck 250 mL round-bottom flask equipped with a pressure-equalizing addition funnel under a N_2 atmosphere. The vessel was cooled to 0 °C on an ice bath. A solution of 1,2-butadien-4-ol (**6**) (14.01 g, 200 mmol, 1 equiv) in 20 mL of dry diethyl ether was delivered dropwise over 15 min to the stirring reaction *via* an addition funnel, and stirring was continued for 24 h. The reaction was allowed to warm to room temperature and quenched with 100 mL of deionized H_2O. The layers were separated, and the aqueous layer was extracted with diethyl ether (4 × 75 mL). The combined organic extracts were washed with saturated aqueous NaCl (1 × 75 mL) and dried over anhydrous Na_2SO_4. After removal of the drying agent by filtration, the solvent was removed *in vacuo*. The crude product was purified by vacuum distillation using a short-path apparatus to yield 17.73 g (67%) of colorless 4-bromo-1,2-butadiene (**8**), bp 62 °C (100 Torr). ^1H NMR ($CDCl_3$, 500 MHz): δ (ppm) complex spin system, 5.45 (m, 1H, J = 8.1, 6.5 Hz), 4.93 (dt, 2H, J = 6.6, 2.2 Hz), 3.96 (dt, 2H, J = 8.2, 2.0 Hz). $^{13}C\{^1H\}$-NMR ($CDCl_3$, 125 MHz): δ (ppm) 209.8, 89.5, 77.5, 30.1.

4-Cyano-1,2-butadiene (2) (2,3-Pentadienenitrile). 4-Bromo-1,2-butadiene (**8**; 3.38 g; 25.4 mmol), was added to a flame-dried 100 mL single-neck round-bottom flask. The reaction vessel was then sealed with a septum and purged with N_2 *via* the syringe needle inlet. Dry acetonitrile (10 mL) was added *via* a syringe, and the stirring vessel was cooled to 0 °C on ice. A solution of 6.70 g (24.99 mmol) of tetrabutylammonium cyanide (TBAC) in 15 mL of dry acetonitrile was delivered dropwise to the vigorously stirring reaction over 1 h *via* a syringe pump. The reaction was allowed to stir at 0 °C for 15 min after the TBAC addition had completed. The ^1H NMR spectrum of a reaction aliquot showed complete conversion of **2** with minimal (<2%) isomerization to ***E*-1** and ***Z*-1**. The reaction was then rinsed into a separatory funnel with 50 mL of diethyl ether and 30 mL of cold deionized H_2O (0 °C). The organic layer was separated, and the aqueous layer was extracted with diethyl ether (3 × 25 mL). The combined organic layers were washed with deionized H_2O (5 × 25 mL) and saturated aqueous NaCl (1 × 25 mL) and dried over anhydrous Na_2SO_4. After removal of the drying agent by gravity filtration, the ethereal solvent was removed by fractional distillation at atmospheric pressure *via* a short-path apparatus. From the resulting concentrate, 4-cyano-1,2-butadiene (**2**) was purified either by flash column chromatography (SiO_2, 3:1 *n*-pentane/Et_2O, R_f = 0.5) or by distillation (bp 94 °C, 100 Torr). Isolated yield: 62%. ^1H NMR ($CDCl_3$, 500 MHz): δ (ppm) complex spin system; 5.13 (apparent quint, 1H, J = 6.4 Hz), 4.97 (m, 2H, J = 3.3 Hz), 3.09 (m, 2H, J = 3.3 Hz). $^{13}C\{^1H\}$-NMR ($CDCl_3$, 125 MHz): δ (ppm) 209.0, 117.3, 81.2, 78.6, 17.5. IR (neat): (cm^{-1}) 2252 (w), 1960 (w), 1417 (w), 913 (w), 852 (s), 731 (w), 678 (w), 521 (w), 467 (w). HRMS (ESI) m/z: $[M + H]^+$ calcd for C_5H_6N, 80.0495; found, 80.0495.

3-Hydroxy-2-methylenebutanenitrile (15). Acrylonitrile (**14**) (13.64 g, 257 mmol, 1 equiv), acetaldehyde (11.4 g, 259 mmol, 1 equiv), and 1,4-diazabicyclo[2.2.2]octane (DABCO) (5.64 g, 50 mmol, 20 mol %) were added to a 250 mL single-neck round-bottom flask. The vessel was sealed with a septum and stirred for 96 h. The ^1H NMR spectrum of a reaction aliquot showed complete conversion after 96 h. The crude product was put on a vacuum line (~100 Torr) to remove unreacted acrylonitrile and acetaldehyde, and the crude 3-hydroxy-2-methylenebutanenitrile (**15**) was used in the next synthetic step without further purification (clear amber liquid). ^1H NMR ($CDCl_3$, 500 MHz): δ (ppm) 6.0 (d, 1H, J = 1.4 Hz), 5.94 (s, 1H), 4.38 (qt, 1H, J = 6.4, 1.2 Hz), 3.90 (br s, 1H), 1.41 (d, 3H, J = 6.5 Hz). $^{13}C\{^1H\}$-NMR ($CDCl_3$, 125 MHz): δ (ppm) 128.9, 128.4, 117.3, 68.0, 22.3.

2-Cyano-1,3-butadiene (3). K_2CO_3 (0.19 g, 1.4 mmol, 1.8 mol %) and 1.2 mL of deionized H_2O were added to a 50 mL round-bottom flask containing the crude 3-hydroxy-2-methylene-butanenitrile (**15**) from the preceding synthetic step. Hydroquinone (20 mg) was added to the mixture to inhibit polymerization during the subsequent distillation. The vessel was connected to a short-path distillation apparatus, and a vacuum of 100 Torr was applied to the system. The boiling flask was immersed in an oil bath at 100 °C, and the reactants were stirred vigorously to break the surface tension. The distillation-head temperature increased to 52 °C as the colorless distillate immediately started condensing as a biphasic mixture. A total of 8.6 g of biphasic distillate was collected over 1 h. Over the elapsed collection time, the contents of the boiling flask darkened to a dark red color and the collection rate slowed. The colorless product (the organic layer of the distillate) was separated and dried over anhydrous Na_2SO_4/activated charcoal. The drying and decolorizing agents were removed by filtration through a fine glass frit to yield 3.21 g (51%) of 2-cyano-1,3-butadiene (**3**) as a colorless oil. When stabilized with hydroquinone, **3** can be purified *via* vacuum distillation (bp 55 °C, 100 Torr). Compound **3** is prone to undergo polymerization, even at −20 °C. ^1H NMR ($CDCl_3$, 500 MHz): δ (ppm) 6.35 (dd, 1H, J = 17.2, 10.4 Hz), 5.94 (s, 1H), 5.86 (s, 1H), 5.73 (d, 1H, J = 17.2 Hz), 5.47 (d, 1H, J = 10.4 Hz). $^{13}C\{^1H\}$-NMR ($CDCl_3$, 125 MHz): δ (ppm) 132.2, 130.5, 122.5, 120.7, 115.9. IR (neat): (cm^{-1}) 2986 (w), 2233 (w), 1736 (m), 1582 (w), 1378 (m), 1244 (m), 1045 (w), 983 (m), 924 (s), 492 (m). HRMS (ESI) m/z: $[M + H]^+$ calcd for C_5H_6N, 80.0495; found, 80.0494.

■ ASSOCIATED CONTENT

Supporting Information

The Supporting Information is available free of charge at https://pubs.acs.org/doi/10.1021/acs.joc.9b03388.

Computational details and ^1H- and $^{13}C\{^1H\}$-NMR, IR, and mass spectra for all compounds (PDF)

■ AUTHOR INFORMATION

Corresponding Author

Robert J. McMahon − *Department of Chemistry, University of Wisconsin−Madison, Madison, Wisconsin 53706-1322, United States;* orcid.org/0000-0003-1377-5107; Email: robert.mcmahon@wisc.edu

Authors

Samuel M. Kougias − *Department of Chemistry, University of Wisconsin−Madison, Madison, Wisconsin 53706-1322, United States;* orcid.org/0000-0002-9877-0817

https://dx.doi.org/10.1021/acs.joc.9b03388
J. Org. Chem. 2020, 85, 5787−5798

Stephanie N. Knezz − *Department of Chemistry, University of Wisconsin−Madison, Madison, Wisconsin 53706-1322, United States;* orcid.org/0000-0001-9445-2953
Andrew N. Owen − *Department of Chemistry, University of Wisconsin−Madison, Madison, Wisconsin 53706-1322, United States*
Rodrigo A. Sanchez − *Department of Chemistry, University of Wisconsin−Madison, Madison, Wisconsin 53706-1322, United States*
Grace E. Hyland − *Department of Chemistry, University of Wisconsin−Madison, Madison, Wisconsin 53706-1322, United States*
Daniel J. Lee − *Department of Chemistry, University of Wisconsin−Madison, Madison, Wisconsin 53706-1322, United States*
Aatmik R. Patel − *Department of Chemistry, University of Wisconsin−Madison, Madison, Wisconsin 53706-1322, United States*
Brian J. Esselman − *Department of Chemistry, University of Wisconsin−Madison, Madison, Wisconsin 53706-1322, United States*
R. Claude Woods − *Department of Chemistry, University of Wisconsin−Madison, Madison, Wisconsin 53706-1322, United States*

Complete contact information is available at: https://pubs.acs.org/10.1021/acs.joc.9b03388

Notes

The authors declare no competing financial interest.

■ ACKNOWLEDGMENTS

We gratefully acknowledge the National Science Foundation for support of this project (CHE-1664912, CHE-1362264). We thank the following organizations and individuals for support of shared departmental facilities: departmental computing resources (NSF CHE-0840494), Bruker AVANCE 400 NMR spectrometer (NSF CHE-1048642), Bruker AVANCE 500 NMR spectrometer (gift from Paul J. and Margaret M. Bender), and Thermo Scientific Q Exactive Plus mass spectrometer (NIH 1S10 OD020022-1). We thank Dr. Timothy S. Zwier for stimulating discussions.

■ REFERENCES

(1) Endres, C. P.; Schlemmer, S.; Schilke, P.; Stutzki, J.; Müller, H. S. P. The Cologne Database for Molecular Spectroscopy, CDMS, in the Virtual Atomic and Molecular Data Centre, VAMDC. *J. Mol. Spectrosc.* **2016**, *327*, 95−104.
(2) Müller, H. S. P.; Schlöder, F.; Stutzki, J.; Winnewisser, G. The Cologne Database for Molecular Spectroscopy, CDMS: A Useful Tool for Astronomers and Spectroscopists. *J. Mol. Struct.* **2005**, *742*, 215−227.
(3) Sagan, C.; Khare, B. N. Tholins: Organic Chemistry of Interstellar Grains and Gas. *Nature* **1979**, *277*, 102−107.
(4) Herbst, E. Chemistry in the Interstellar Medium. *Annu. Rev. Phys. Chem.* **1995**, *46*, 27−54.
(5) Garrod, R. T.; Widicus Weaver, S. L.; Herbst, E. Complex Chemistry in Star-Forming Regions: An Expanded Gas-Grain Warm-Up Chemical Model. *Astrophys. J.* **2008**, *682*, 283−302.
(6) Costes, M.; Naulin, C. Studies of Reactions Relevant to Astrochemistry. *Annu. Rep. Prog. Chem., Sect. C: Phys. Chem.* **2013**, *109*, 189−210.
(7) Agúndez, M.; Wakelam, V. Chemistry of Dark Clouds: Databases, Networks, and Models. *Chem. Rev.* **2013**, *113*, 8710−8737.
(8) Cumper, C. W. N.; Dev, S. K.; Landor, S. R. Electric Dipole Moments of Acrylonitriles, Allyl Cyanides, and Alicyclic Nitriles. *J. Chem. Soc., Perkin Trans. 2* **1973**, 537−540.
(9) Hannay, N. B.; Smyth, C. P. The Dipole Moments and Structures of Ketene and of Several Polar Molecules Containing Conjugated Systems. *J. Am. Chem. Soc.* **1946**, *68*, 1357−1360.
(10) Soundararajan, S. Charge Distribution, Electric Dipole Moments, and Molecular Structure of Nitriles. *Indian J. Chem.* **1963**, *1*, 503−506.
(11) McGuire, B. A.; Burkhardt, A. M.; Kalenskii, S.; Shingledecker, C. N.; Remijan, A. J.; Herbst, E.; McCarthy, M. C. Detection of the Aromatic Molecule Benzonitrile (*c*-C_6H_5CN) in the Interstellar Medium. *Science* **2018**, *359*, 202−205.
(12) Zeng, S.; Quénard, D.; Jiménez-Serra, I.; Martín-Pintado, J.; Rivilla, V. M.; Testi, L.; Martín-Doménech, R. First Detection of the Pre-Biotic Molecule Glycolonitrile ($HOCH_2CN$) in the Interstellar Medium. *Mon. Not. R. Astron. Soc.: Lett.* **2019**, *484*, L43−L48.
(13) Cernicharo, J.; Agúndez, M.; Velilla Prieto, L.; Guélin, M.; Pardo, J. R.; Kahane, C.; Marka, C.; Kramer, C.; Navarro, S.; Quintana-Lacaci, G.; Fonfría, J. P.; Marcelino, N.; Tercero, B.; Moreno, E.; Massalkhi, S.; Santander-García, M.; McCarthy, M. C.; Gottlieb, C. A.; Alonso, J. L. Discovery of Methyl Silane and Confirmation of Silyl Cyanide in IRC+10216. *Astron. Astrophys.* **2017**, *606*, L5.
(14) Walmsley, C. M.; Winnewisser, G.; Toelle, F. Cyanoacetylene and Cyanodiacetylene in Interstellar Clouds. *Astron. Astrophys.* **1980**, *81*, 245−250.
(15) Snyder, L. E.; Buhl, D. Radio Emission from Interstellar Hydrogen Cyanide. *Astrophys. J.* **1971**, *163*, L47−L52.
(16) Avery, L. W.; Broten, N. W.; MacLeod, J. M.; Oka, T.; Kroto, H. W. Detection of the Heavy Interstellar Molecule Cyanodiacetylene. *Astrophys. J., Lett.* **1976**, *205*, L173−L175.
(17) Kroto, H. W.; Kirby, C.; Walton, D. R. M.; Avery, L. W.; Broten, N. W.; MacLeod, J. M.; Oka, T. The Detection of Cyanohexatriyne, $H(C{\equiv}C)_3CN$, in Heiles's Cloud 2. *Astrophys. J.* **1978**, *219*, L133−L137.
(18) Broten, N. W.; Oka, T.; Avery, L. W.; MacLeod, J. M.; Kroto, H. W. The Detection of Cyanooctatetrayne (HC_9N) in Interstellar Space. *Astrophys. J.* **1978**, *223*, L105−L107.
(19) Broten, N. W.; MacLeod, J. M.; Avery, L. W.; Friberg, P.; Hjalmarson, A.; Hoglund, B.; Irvine, W. M. The Detection of Interstellar Methylcyanoacetylene. *Astrophys. J.* **1984**, *276*, L25−L29.
(20) Snyder, L. E.; Hollis, J. M.; Jewell, P. R.; Lovas, F. J.; Remijan, A. Confirmation of Interstellar Methylcyanodiacetylene (CH_3C_5N). *Astrophys. J.* **2006**, *647*, 412−417.
(21) Gardner, F. F.; Winnewisser, G. Detection of Interstellar Vinyl Cyanide (Acrylonitrile). *Astrophys. J.* **1975**, *195*, L127−L130.
(22) Lovas, F. J.; Remijan, A. J.; Hollis, J. M.; Jewell, P. R.; Snyder, L. E. Hyperfine Structure Identification of Interstellar Cyanoallene Toward TMC-1. *Astrophys. J.* **2006**, *637*, L37−L40.
(23) Solomon, P. M.; Jefferts, K. B.; Penzias, A. A.; Wilson, R. W. Detection of Millimeter Emission Lines from Interstellar Methyl Cyanide. *Astrophys. J.* **1971**, *168*, L107−L110.
(24) Belloche, A.; Garrod, R. T.; Müller, H. S. P.; Menten, K. M.; Comito, C.; Schilke, P. Increased Complexity in Interstellar Chemistry: Detection and Chemical Modeling of Ethyl Formate and *n*-Propyl Cyanide in Sagittarius B2(N). *Astron. Astrophys.* **2009**, *499*, 215−232.
(25) Belloche, A.; Garrod, R. T.; Muller, H. S. P.; Menten, K. M. Detection of a Branched Alkyl Molecule in the Interstellar Medium: *iso*-Propyl Cyanide. *Science* **2014**, *345*, 1584−1587.
(26) Sagan, C.; Thompson, W. R.; Khare, B. N. Titan: A Laboratory for Prebiological Organic Chemistry. *Acc. Chem. Res.* **1992**, *25*, 286−292.
(27) Moreno, R.; Silla, E.; Tunon, I.; Arnau, A. Ab Initio Rotational Constants of the Nitriles Derived from Cyanodiacetylene (HC_4CN). *Astrophys. J.* **1994**, *437*, 532−539.
(28) Sun, B. J.; Huang, C. H.; Chen, S. Y.; Chen, S. H.; Kaiser, R. I.; Chang, A. H. H. Theoretical Study on Reaction Mechanism of

Ground-state Cyano Radical with 1,3-Butadiene: Prospect of Pyridine Formation. *J. Phys. Chem. A* **2014**, *118*, 7715−7724.
(29) Jamal, A.; Mebel, A. M. Theoretical Investigation of the Mechanism and Product Branching Ratios of the Reactions of Cyano Radical with 1- and 2-Butyne and 1,2-Butadiene. *J. Phys. Chem. A* **2013**, *117*, 741−755.
(30) Morales, S. B.; Bennett, C. J.; Le Picard, S. D.; Canosa, A.; Sims, I. R.; Sun, B. J.; Chen, P. H.; Chang, A. H. H.; Kislov, V. V.; Mebel, A. M.; Gu, X.; Zhang, F.; Maksyutenko, P.; Kaiser, R. I. A Crossed Molecular Beam, Low-Temperature Kinetics, and Theoretical Investigation of the Reaction of the Cyano Radical (CN) with 1,3-Butadiene (C_4H_6). a Route to Complex Nitrogen-Bearing Molecules in Low-Temperature Extraterrestrial Environments. *Astrophys. J.* **2011**, *742*, 26.
(31) Charnley, S. B.; Kuan, Y.-J.; Huang, H.-C.; Botta, O.; Butner, H. M.; Cox, N.; Despois, D.; Ehrenfreund, P.; Kisiel, Z.; Lee, Y.-Y.; Markwick, A. J.; Peeters, Z.; Rodgers, S. D. Astronomical Searches for Nitrogen Heterocycles. *Adv. Space Res.* **2005**, *36*, 137−145.
(32) Cassini Titan Science; NASA Planetary Data System (PDS); National Aeronautics and Space Administration , https://atmos.nmsu.edu/data_and_services/atmospheres_data/Cassini/sci-titan.html#huygens (accessed 2020).
(33) Desai, R. T.; Coates, A. J.; Wellbrock, A.; Vuitton, V.; Crary, F. J.; González-Caniulef, D.; Shebanits, O.; Jones, G. H.; Lewis, G. R.; Waite, J. H.; Cordiner, M.; Taylor, S. A.; Kataria, D. O.; Wahlund, J.-E.; Edberg, N. J. T.; Sittler, E. C. Carbon Chain Anions and the Growth of Complex Organic Molecules in Titan's Ionosphere. *Astrophys. J.* **2017**, *844*, L18.
(34) Thompson, W. R.; Henry, T. J.; Schwartz, J. M.; Khare, B. N.; Sagan, C. Plasma Discharge in N_2 + CH_4 at Low Pressures: Experimental Results and Applications to Titan. *Icarus* **1991**, *90*, 57−73.
(35) Cable, M. L.; Hörst, S. M.; Hodyss, R.; Beauchamp, P. M.; Smith, M. A.; Willis, P. A. Titan Tholins: Simulating Titan Organic Chemistry in the Cassini-Huygens Era. *Chem. Rev.* **2012**, *112*, 1882−1909.
(36) Dorman, P. M.; Orr, V. L.; Zdanovskaia, M. A.; Esselman, B. J.; Kougias, S. M.; Woods, R. C.; McMahon, R. J., manuscripts in preparation.
(37) Carothers, W. H.; Berchet, G. J. Acetylene Polymers and their Derivatives. XV. Halo-4-butadienes-1,2. The mechanism of 1,4-Addition and of α,γ-Rearrangement. *J. Am. Chem. Soc.* **1933**, *55*, 2807−2813.
(38) Carothers, W. H.; Berchet, G. J. Butadienyl compounds and processes for preparing same. U.S. Patent 2,073,363 A, March 9, 1937.
(39) Coffman, D. D. Acetylene Polymers and their Derivatives. XXIII. 4-Cyano-1,3-butadiene. *J. Am. Chem. Soc.* **1935**, *57*, 1981−1984.
(40) Carothers, W. H.; Berchet, G. J. Aliphatic unsaturated compounds and the process of preparing them. U.S. Patent 2,136,178A, Nov 8, 1938.
(41) Snyder, H. R.; Stewart, J. M.; Myers, R. L. 1-Cyano-1,3-butadienes: *cis, trans*-Isomers of 1-Cyano-1,3-butadiene. *J. Am. Chem. Soc.* **1949**, *71*, 1055−1056.
(42) Snyder, H. R.; Poos, G. I. 1-Cyano-1,3-butadiene. III. The Dimer of 1-Cyano-1,3-butadiene. *J. Am. Chem. Soc.* **1949**, *71*, 1395−1396.
(43) Snyder, H. R.; Poos, G. I. 1-Cyano-1,3-butadienes. IV. Diels-Alder Reactions with Dienes. *J. Am. Chem. Soc.* **1950**, *72*, 4096−4103.
(44) Snyder, H. R.; Murdock, K. C.; Marvel, C. S. 1-Cyano-1,3-butadienes. VI. Copolymerization of the *cis*- and *trans*-1-Cyano-1,3-butadienes with Butadiene. *J. Am. Chem. Soc.* **1953**, *75*, 4742−4746.
(45) Bissinger, W. E.; Fredenburg, R. H.; Kadesch, R. G.; Kung, F.; Langston, J. H.; Stevens, H. C.; Strain, F. Some Reactions of Butadiene Monochlorohydrin, 1-Chloro-3-buten-2-ol. *J. Am. Chem. Soc.* **1947**, *69*, 2955−2961.
(46) Wise, P. H. Preparation of 1-cyano-1,3-butadiene. U.S. Patent 2,473,486 A, June 14, 1949.
(47) Gudgeon, H.; Hill, R.; Isaacs, E. Preparation of Some Substituted Butadienes. *J. Chem. Soc.* **1951**, 1926−1928.
(48) Daessle, C.; Tarlton, E. J.; McKay, A. F. Preparation and Chemistry of *Trans* 1-Cyano-4-Chloro-2-Butene. *Can. J. Chem.* **1959**, *37*, 629−631.
(49) Lambert, A.; Makinson, G. K.; Hill, A. Manufacture of 1-cyano-1, 3-butadiene. GB 1040308 A, Aug 24, 1966.
(50) Descotes, G.; Robbe, P. Synthesis of Unsaturated Nitriles Structurally Related to Butadiene and Isoprene. *Bull. Soc. Chim. Fr.* **1969**, 1349−1355.
(51) Wei, P. E.; Milliman, G. E. Synthesis and Polymerization of 1- and 2-Cyano-1,3-butadienes. *J. Polym. Sci., Part A-1: Polym. Chem.* **1969**, *7*, 2305−2317.
(52) Ikawa, T.; Nishizawa, T.; Suzuki, H.; Maurata, A. Preparation of 1-Cyano-1,3-butadiene by Ammoxidation of 1,3-Pentadiene. *Sekiyu Gakkaishi* **1972**, *15*, 941−943.
(53) Katagiri, T.; Nito, T.; Takabe, K.; Tanaka, J. Derivatives of Isoprene. IV. Synthesis of Cyanodienes and their Photosensitized Dimerization. *Nippon Kagaku Kaishi* **1974**, *1974*, 2370−2374.
(54) Fischer, R.; Weitz, H. M.; Kempe, U. 1-Cyano-1,3-butadiene prepn. useful as polymer starting material - by gas phase pyrolysis of 1-cyano-4-acyloxy-2-butene esp. the 4-acetoxy cpd. DE 2745873 A1, April 19, 1979.
(55) Braun, M.; Mroß, S.; Schwarz, I. Mild and Stereoconvergent Palladium-Catalyzed Carbonyl Alkenylation Reaction of α,β-Unsaturated Aldehydes. *Synthesis* **1998**, *1998*, 83−88.
(56) Clary, K. N.; Back, T. G. Preparation of Unsaturated Aminonitriles from the Aza-Morita-Baylis-Hillman Reactions of Aldimines with Penta-2,4-dienenitrile. *Synlett* **2007**, *2007*, 2995−2998.
(57) Banert, K. The Chemistry of Unusually Functionalized Azides. *Synthesis* **2016**, *48*, 2361−2375.
(58) Marvel, C. S.; Brace, N. O. An Allylic Rearrangement in the Pyrolysis of 3-Acetoxy-3-cyano-1-butene1. *J. Am. Chem. Soc.* **1948**, *70*, 1775−1776.
(59) Marvel, C. S.; Brace, N. O. The Dimer of 2-Cyano-1,3-butadiene. *J. Am. Chem. Soc.* **1949**, *71*, 37−40.
(60) Inukai, T.; Kojima, T. Aluminum Chloride Catalyzed Diene Condensation. VI. Partial Rate Factors of 2-Phenyl-, 2-Chloro-, 2-Trifluoromethyl, and 2-Cyanobutadienes in Reactions with Methyl Acrylate. A Differential Hammett Correlation. *J. Org. Chem.* **1971**, *36*, 924−928.
(61) Naidu, V. R.; Posevins, D.; Volla, C. M. R.; Bäckvall, J. E. Selective Cascade Reaction of Bisallenes via Palladium-Catalyzed Aerobic Oxidative Carbocyclization-Borylation and Aldehyde Trapping. *Angew. Chem., Int. Ed.* **2017**, *56*, 1590−1594.
(62) Wright, M. W.; Smalley, T. L., Jr.; Welker, M. E.; Rheingold, A. L. Synthesis of Cobalt-Substituted 1,3-Diene Complexes with Unusual Structures and their exo-Selective Diels-Alder Reactions. *J. Am. Chem. Soc.* **1994**, *116*, 6777−6791.
(63) Pedersen, C. J. Cyclic Polyethers and their Complexes with Metal Salts. *J. Am. Chem. Soc.* **1967**, *89*, 7017−7036.
(64) Luo, H.; Ma, S. CuI-Catalyzed Synthesis of Functionalized Terminal Allenes from 1-Alkynes. *Eur. J. Org. Chem.* **2013**, *2013*, 3041−3048.
(65) Tayama, E.; Sugai, S. A Facile Method for the Stereoselective Preparation of (1*Z*,3*E*)-Dienyl Ethers via 1,4-Elimination of 1,4-Dialkoxy-(2*Z*)-alkenes with n-Butyllithium. *Synlett* **2006**, *2006*, 849−852.
(66) Tayama, E.; Sugai, S. A facile method for the stereoselective preparation of (1*E*,3*E*)-4-substituted-1-amino-1,3-dienes via 1,4-elimination. *Tetrahedron Lett.* **2007**, *48*, 6163−6166.
(67) Tayama, E.; Toma, Y. Stereoselective preparation of (1*Z*)- and (1*E*)-*N*-Boc-1-amino-1,3-dienes by stereospecific base-promoted 1,4-elimination. *Tetrahedron* **2015**, *71*, 554−559.
(68) Appel, R. Tertiary Phosphane/Tetrachloromethane, a Versatile Reagent for Chlorination, Dehydration, and P-N Linkage. *Angew. Chem., Int. Ed. Engl.* **1975**, *14*, 801−811.

https://dx.doi.org/10.1021/acs.joc.9b03388
J. Org. Chem. 2020, 85, 5787−5798

(69) Wise, K. V. Physical Properties of *cis*-1-Cyano-1,3-butadiene. *J. Am. Chem. Soc.* **1954**, *76*, 3094−3096.
(70) Seeman, J. I. Effect of Conformational Change on Reactivity in Organic Chemistry. Evaluations, Applications, and Extensions of Curtin-Hammett Winstein-Holness Kinetics. *Chem. Rev.* **1983**, *83*, 83−134.
(71) Shestakov, G. K.; Airyan, S. M.; Bel'skii, F. I.; Temkin, O. N. Kinetics and mechanism of the isomerization of 4-chloro-1,2-butadiene to 2-chloro-1,3-butadiene. *Zh. Org. Khim.* **1976**, *12*, 2053−2057.
(72) Strub, D. J.; Garboś, A.; Lochyński, S. Synthesis, lipase catalyzed kinetic resolution, and determination of the absolute configuration of enantiomers of the Morita-Baylis-Hillman adduct 3-hydroxy-2-methylenebutanenitrile. *ARKIVOC* **2017**, *2017*, 313−323.
(73) Nonaka, Y.; Kihara, K.; Hironaka, T.; Oda, Y. A process for producing a conjugated diene with a cyano group. DE 2456126 A1, May 28, 1975.
(74) Nonaka, Y.; Kihara, K.; Hironaka, T.; Oda, Y. 2-Cyano-1,3-butadiene. Jpn. Kokai Tokkyo Koho JP 51029443 A, Mar 12, 1976.
(75) Nonaka, Y.; Kihara, K.; Hironaka, T.; Oda, Y. A novel synthesis of 2-cyano-1,3-butadiene. *Toyo Soda Kenkyu Hokoku* **1976**, *20*, 9−11.
(76) Becke, A. D. Density-Functional Thermochemistry. III. The Role of Exact Exchange. *J. Chem. Phys.* **1993**, *98*, 5648−5652.
(77) Lee, C.; Yang, W.; Parr, R. G. Development of the Colle-Salvetti Correlation-Energy Formula into a Functional of the Electron Density. *Phys. Rev. B: Condens. Matter Mater. Phys.* **1988**, *37*, 785−789.
(78) Dunning, T. H. Gaussian-Basis Sets for Use in Correlated Molecular Calculations. I. The Atoms Boron Through Neon and Hydrogen. *J. Chem. Phys.* **1989**, *90*, 1007−1023.
(79) Frisch, M. J.; Trucks, G. W.; Schlegel, H. B.; Scuseria, G. E.; Robb, M. A.; Cheeseman, J. R.; Scalmani, G.; Barone, V.; Petersson, G. A.; Nakatsuji, H.; Li, X.; Caricato, M.; Marenich, A. V.; Bloino, J.; Janesko, B. G.; Gomperts, R.; Mennucci, B.; Hratchian, H. P.; Ortiz, J. V.; Izmaylov, A. F.; Sonnenberg, J. L.; Williams-Young, D.; Ding, F.; Lipparini, F.; Egidi, F.; Goings, J.; Peng, B.; Petrone, A.; Henderson, T.; Ranasinghe, D.; Zakrzewski, V. G.; Gao, J.; Rega, N.; Zheng, G.; Liang, W.; Hada, M.; Ehara, M.; Toyota, K.; Fukuda, R.; Hasegawa, J.; Ishida, M.; Nakajima, T.; Honda, Y.; Kitao, O.; Nakai, H.; Vreven, T.; Throssell, K.; Montgomery, J. A., Jr.; Peralta, J. E.; Ogliaro, F.; Bearpark, M. J.; Heyd, J. J.; Brothers, E. N.; Kudin, K. N.; Staroverov, V. N.; Keith, T. A.; Kobayashi, R.; Normand, J.; Raghavachari, K.; Rendell, A. P.; Burant, J. C.; Iyengar, S. S.; Tomasi, J.; Cossi, M.; Millam, J. M.; Klene, M.; Adamo, C.; Cammi, R.; Ochterski, J. W.; Martin, R. L.; Morokuma, K.; Farkas, O.; Foresman, J. B.; Fox, D. J. *Gaussian 16*, Revision B.01; Gaussian, Inc.: Wallingford, CT, USA, 2016.
(80) Glendening, E. D.; Badenhoop, J. K.; Reed, A. E.; Carpenter, J. E.; Bohmann, J. A.; Morales, C. M.; Landis, C. R.; Weinhold, F. *NBO 6.0*; Theoretical Chemistry Institute, University of Wisconsin−Madison: Madison, WI, 2013.
(81) McEwen, C. N.; McKay, R. G.; Larsen, B. S. Analysis of solids, liquids, and biological tissues using solids probe introduction at atmospheric pressure on commercial LC/MS instruments. *Anal. Chem.* **2005**, *77*, 7826−7831.
(82) Knezz, S. A. Synthesis, Spectroscopy, and Photochemistry of Reactive Organic Molecules. Ph.D. Dissertation, University of Wisconsin-Madison, Madison, WI, 2016.
(83) Keegstra, M. A.; Verkruijsse, H. D.; Andringa, H.; Brandsma, L. Efficient procedures for 1-bromo-1,3-butadiene and 2-bromo-1,3-butadiene. *Synth. Commun.* **1991**, *21*, 721−726.
(84) Musilek, K.; Holas, O.; Kuca, K.; Jun, D.; Dohnal, V.; Opletalova, V.; Dolezal, M. Novel series of bispyridinium compounds bearing a (*Z*)-but-2-ene linker. Synthesis and evaluation of their reactivation activity against tabun and paraoxon-inhibited acetylcholinesterase. *Bioorg. Med. Chem. Lett.* **2007**, *17*, 3172−3176.
(85) Efskind, J.; Benneche, T.; Undheim, K.; Husebye, S.; Moreno, J. M.; Romerosa, A.; Robinson, W. T.; Roos, B. O.; Vallance, C.; Wood, B. R. Stereoselective synthesis of alkenyl α,α'-bridged bis(glycines) using palladium promoted substitution in the bridge. *Acta Chem. Scand.* **1997**, *51*, 942−952.
(86) Streit, U.; Birbaum, F.; Quattropani, A.; Bochet, C. G. Photocycloaddition of Arenes and Allenes. *J. Org. Chem.* **2013**, *78*, 6890−6910.
(87) Lehrich, F.; Hopf, H.; Grunenberg, J. The Preparation and Structures of Several Cross-Conjugated Allenes ("Allenic Dendralenes"). *Eur. J. Org. Chem.* **2011**, *2011*, 2705−2718.
(88) Molander, G. A.; Cormier, E. P. Ketyl−Allene Cyclizations Promoted by Samarium(II) Iodide. *J. Org. Chem.* **2005**, *70*, 2622−2626.
(89) Bailey, W. J.; Fujiwara, E.; Acetylenes, I. Mixed dihalides and halohydrins from butynediol. *J. Am. Chem. Soc.* **1955**, *77*, 165−166.
(90) Luo, H.; Ma, D.; Ma, S. Buta-2,3-dien-1-ol. *Org. Synth.* **2017**, *94*, 153−166.

https://dx.doi.org/10.1021/acs.joc.9b03388
J. Org. Chem. 2020, 85, 5787−5798

Appendix B

Synthesis, Purification and Rotational Spectroscopy of (Cyanomethylene)Cyclopropane– An Isomer of Pyridine

Brian J. Esselman
Samuel M. Kougias
Maria A. Zdanovskaia
R. Claude Woods
Robert J. McMahon

The Journal of Physical Chemistry A, 2021, *125*, 5601-5614

THE JOURNAL OF PHYSICAL CHEMISTRY A
A JOURNAL OF THE AMERICAN CHEMICAL SOCIETY

pubs.acs.org/JPCA Article

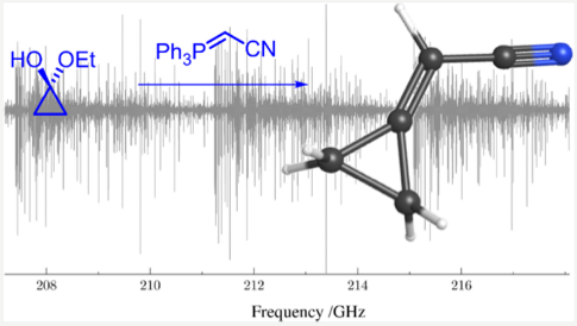
Synthesis, Purification, and Rotational Spectroscopy of (Cyanomethylene)Cyclopropane—An Isomer of Pyridine

Brian J. Esselman, Samuel M. Kougias, Maria A. Zdanovskaia, R. Claude Woods,* and Robert J. McMahon*

Cite This: J. Phys. Chem. A 2021, 125, 5601−5614 Read Online

ACCESS | Metrics & More | Article Recommendations | Supporting Information

ABSTRACT: The gas-phase rotational spectrum of (cyanomethylene)cyclopropane, $(CH_2)_2C{=}CHCN$, generated by a Wittig reaction between the hemiketal of cyclopropanone and (cyanomethylene)triphenylphosphorane, is presented for the first time. This small, highly polar nitrile is a cyclopropyl-containing structural isomer of pyridine. The rotational spectra of the ground state and two vibrationally excited states were observed, analyzed, and least-squares fit from 130 to 360 GHz. Over 3900 R-, P-, and Q-branch, ground-state rotational transitions were fit to low-error, partial octic, A- and S-reduced Hamiltonians, providing precise determinations of the spectroscopic constants. The two lowest-energy vibrationally excited states, ν_{17} and ν_{27}, form a Coriolis-coupled dyad displaying small *a*- and *b*-type resonances. Transitions for these two states were measured and least-squares fit to a two-state, partial octic, A-reduced Hamiltonian in the I^r representation with nine Coriolis-coupling terms (G_a, G_a^J, G_a^K, G_a^{JJ}, F_{bc}, F_{bc}^J, F_{bc}^K, G_b, and G_b^J). The observation of many resonant transitions and nine nominal interstate transitions enabled a very accurate and precise energy difference between ν_{17} and ν_{27} to be determined: $\Delta E_{17,27}$ = 29.8975453 (33) cm^{-1}. The spectroscopic constants presented herein provide the foundation for future astronomical searches for (cyanomethylene)cyclopropane.



INTRODUCTION

Organic nitriles occupy a significant place in the field of astrochemistry and are well represented in the list of ~220 species detected in space.[1,2] Their large molecular dipole moments, due to the cyano moiety, result in intense rotational transitions that facilitate identification of these species by radioastronomy. We have been keenly interested in measuring spectroscopic constants of organic nitriles in two groups: aryl nitriles/isonitriles[3−6] and nitrile-containing isomers of pyridine.[7−9] The former group was inspired by the potential of these aryl species to serve as tracers for their parent compounds (*e.g.*, benzene, pyridine, pyridazine, pyrimidine, and pyrazine). While pyridine, pyridazine, and pyrimidine possess a permanent dipole moment and have been sought in the interstellar medium unsuccessfully,[10] benzene and pyrazine do not and thus cannot be detected by radioastronomy. Recent detections of benzonitrile,[11] 1- and 2-cyanonaphthalene,[12] and 1-cyano-1,3-cyclopentadiene[13] represent a dramatic breakthrough in the field and have further inspired our spectroscopy of related compounds. The latter group of molecules that we have been studying are nitrile-containing structural isomers of pyridine (C_5H_5N) (Figure 1). Several of these species are likely to be involved in complex, astrochemically relevant processes[14,15] and have been detected in harsh reaction

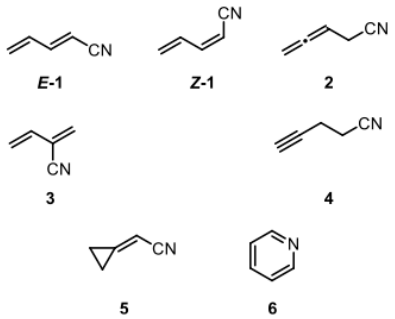
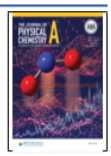


Figure 1. C_5H_5N isomers studied by rotational spectroscopy: (*E*)-1-cyano-1,3-butadiene (***E*-1**), (*Z*)-1-cyano-1,3-butadiene (***Z*-1**), 4-cyano-1,2-butadiene (**2**), 2-cyano-1,3-butadiene (**3**), 4-cyano-1-butyne (**4**), (cyanomethylene)cyclopropane (**5**), and pyridine (**6**).

Received: April 10, 2021
Revised: May 28, 2021
Published: June 21, 2021



ACS Publications © 2021 American Chemical Society

https://doi.org/10.1021/acs.jpca.1c03246
J. Phys. Chem. A 2021, 125, 5601−5614

environments.[16−18] Expanding the family of pyridine isomers facilitates future investigations of the reactivity of these small molecules and astronomical searches for these species in extraterrestrial environments. Astronomical detections of any of the molecules from either group would be of fundamental interest and could illuminate new astrochemical pathways toward complex aromatic species.

(Cyanomethylene)cyclopropane (**5**) (2-cyclopropylidene-acetonitrile) is a structurally intriguing molecule (Figure 2).

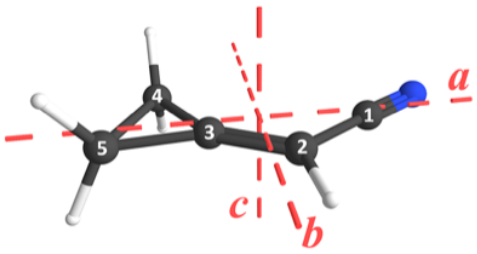
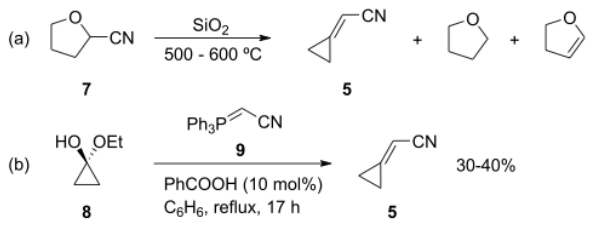


Figure 2. (Cyanomethylene)cyclopropane (**5**) (C_s, C_5H_5N) structure with principal inertial axes (μ_a = 4.4 D, μ_b = 1.2 D).

It is substantially higher in energy than its isomer, pyridine [*ca.* 50 kcal/mol, B3LYP/6-311+G(2d,p)] due to the absence of aromaticity and the presence of a strained, three-membered cyclopropyl ring with the exocyclic π bond. The inherent strain energy of three-membered rings notwithstanding, four interstellar molecules include this structural motif (with differing degrees of unsaturation): cyclopropenylidene (*c*-C_3H_2),[19] cyclopropenone (C_3H_2O),[20] ethylene oxide (*c*-C_2H_4O),[21] and propylene oxide ($CH_3C_2H_3O$).[22] Additionally, **5** contains an α,β-unsaturated nitrile moiety, which is similar to the known interstellar species vinyl cyanide ($H_2C{=}CHCN$; acrylonitrile),[23] cyanoallene ($H_2C{=}C{=}CHCN$),[24] and methylcyano-acetylene ($CH_3C{\equiv}CCN$).[25] The role of (cyanomethylene)cyclopropane (**5**) in the chemical mechanisms of formation or destruction of pyridine (**6**) remains a matter of conjecture, but we are continuing our investigations of the reaction chemistry of **5** under a variety of harsh conditions.

(Cyanomethylene)cyclopropane (**5**) is an attractive candidate for astronomical search, being a nitrile-containing structural isomer of pyridine (C_s, C_5H_5N) and a highly prolate, asymmetric top (κ = −0.96) with a strong dipole [μ_a = 4.4 D, μ_b = 1.2 D, MP2/6-311+G(2d,p)]. This molecule has been generated only twice previously,[19,20] and the characterization data are quite limited compared to other simple organic nitriles. As shown in Scheme 1a, Wilson first generated **5** in

Scheme 1. Previous Syntheses of (Cyanomethylene)cyclopropane (5)[a]



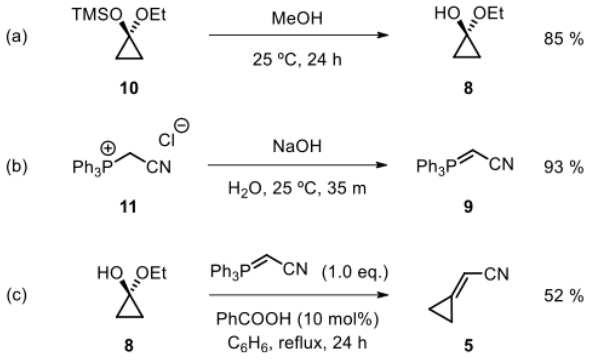
[a]Yield estimated by NMR.

1945 by pyrolysis of 2-cyanotetrahydrofuran (**7**) at 500−600 °C on silica with coproduction of tetrahydrofuran and dihydrofuran.[26] While effective at generating the desired compound, it is not an ideal synthetic approach for studying its rotational spectrum due to the generation of volatile byproducts with permanent dipole moments as sample contaminants. More recently, Mauduit *et al.* reported a facile, gram-scale synthesis of **5** *via* a Wittig reaction of 1-ethoxycyclopropanol (**8**) with (cyanomethylene)-triphenylphosphorane (**9**) (Scheme 1b).[27] This synthesis is ideal for analysis by rotational spectroscopy as it produces the desired product in significant quantity without volatile, polar solvents or byproducts. A slightly modified version of this synthetic procedure, along with improved procedures for isolation of **5**, provided the foundation of this spectroscopic investigation.

EXPERIMENTAL AND THEORETICAL METHODS

Synthesis. Our synthetic approach to (cyanomethylene)-cyclopropane (**5**) is based upon previous work of Mauduit *et al.*[27] as shown in Scheme 1b. The desired compound was obtained in three relatively simple steps with sufficient quantity and purity to enable the spectroscopic investigation (Scheme 2). A commercial sample of (1-ethoxycyclopropoxy)-

Scheme 2. Modified Synthesis of (Cyanomethylene)cyclopropane (5)[a]



[a]Isolated yields.

trimethylsilane (**10**) was deprotected by stirring in methanol for 24 h to reveal the required hemiketal **8** in 85% yield.[28] Ylide **9** was prepared in 93% yield from a commercial sample of (cyanomethyl)triphenylphosphonium chloride (**11**) by stirring in basic solution for 35 min. Subsequently, **8** and **9** were allowed to react in refluxing benzene with catalytic benzoic acid to generate (cyanomethylene)cyclopropane (**5**), which was isolated as a pure substance, for the first time, in 52% yield. As previously reported,[27] this reaction could be carried out in a variety of nonpolar organic solvents. Benzene was selected, in this case, because it does not possess a permanent dipole moment, and any residual benzene would not be observed in the rotational spectrum. After distillation, this sample was used to measure the rotational spectrum of (cyanomethylene)cyclopropane (**5**). Detailed experimental procedures and characterization data are provided below for each compound.

Spectroscopy. Using a millimeter-wave spectrometer that has been previously described,[29,30] the rotational spectrum of

https://doi.org/10.1021/acs.jpca.1c03246
J. Phys. Chem. A 2021, 125, 5601−5614

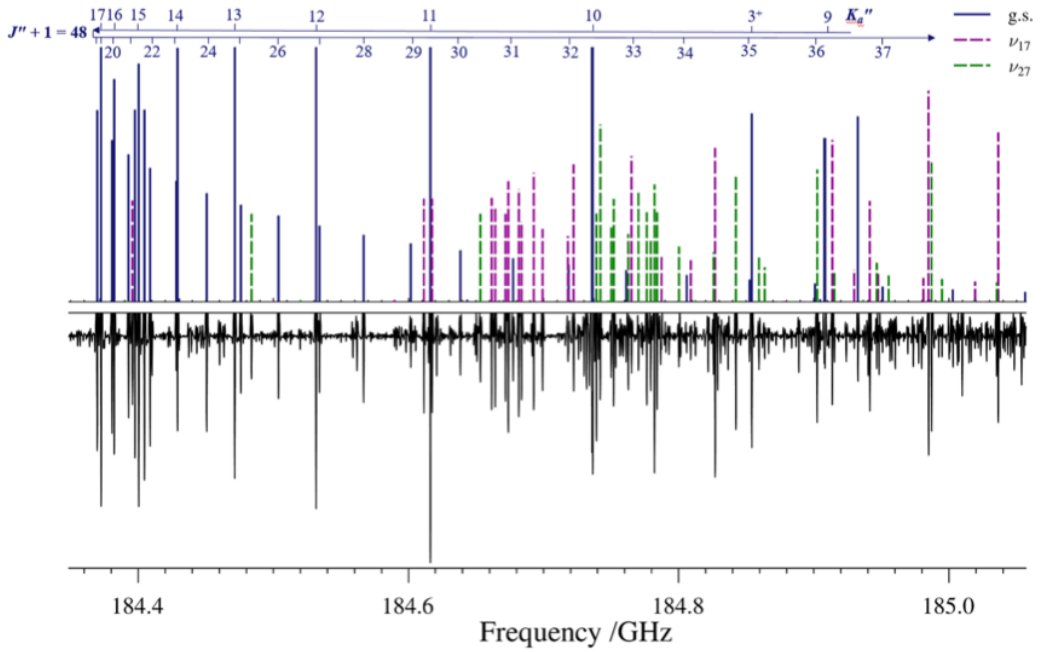


Figure 3. Predicted (top) and experimental (bottom) rotational spectrum of (cyanomethylene)cyclopropane (**5**) from 184.35 to 185.05 GHz. Ground-state transitions for the $J'' + 1 = 48$ band in dark blue, ν_{17} in purple, and ν_{27} in green.

(cyanomethylene)cyclopropane (**5**) was collected from 130 to 230 and from 235 to 360 GHz in a continuous flow at room temperature with a sample pressure of 4 mTorr. The separate spectral segments were combined into a single broadband spectrum using Kisiel's Assignment and Analysis of Broadband Spectra software.[31,32] Pickett's SPFIT/SPCAT[33] and Kisiel's ASFIT/ASROT[31,32] were used for least-squares fits and spectral predictions, along with the PIFORM, PMIXC, PLANM, and AC programs for analysis.[34] A uniform frequency measurement uncertainty of 0.050 MHz was assumed for all measurements.

Computation. Electronic structure calculations were carried out with Gaussian 16[35] using the WebMO interface[36] to obtain theoretical spectroscopic constants. Optimized geometries at the B3LYP/6-311+(2d,p) and MP2/6-311+(2d,p) levels were obtained using "verytight" convergence criteria and an "ultrafine" integration grid, and subsequent anharmonic vibrational frequency calculations were carried out. The B3LYP predictions of the spectroscopic constants, which were sufficient to begin the analysis, did not have the expected agreement with the experimental spectroscopic constants. Thus, MP2 calculations were performed which had slightly closer agreement with the experimental constants. All computational output files can be found in the Supporting Information.

■ RESULTS AND DISCUSSION

Ground Vibrational State. (Cyanomethylene)-cyclopropane (**5**) is a highly prolate, asymmetric top molecule ($\kappa = -0.96$) with strong dipole moments along its *a*- and *b*-principal axes ($\mu_a = 4.4$ D, $\mu_b = 1.2$ D, MP2). As shown in Figure 3, its rotational spectrum in the 130 to 360 GHz region is dominated by intense $^aR_{0,1}$ transitions that appear in clearly observable bands of transitions sharing a single J value. At low values of K_a, the plus- and minus-symmetry $^aR_{0,1}$ transitions are nondegenerate and located far from these obvious bands. As the K_a value increases, the plus- and minus-symmetry transitions become degenerate and progress to lower frequency before experiencing a turnaround and forming the recognizable bandhead. As expected for the spectrum of a highly prolate molecule, these bands are separated by approximately $B + C$ (~3.8 GHz). The transitions progress to higher frequency away from the bandhead with further increasing K_a until the transitions are lost in the spectral confusion limit. Much lower intensity *b*-type ($^bR_{1,1}$ and $^bR_{-1,1}$) transitions are observable with low values of K_a, some of which become degenerate with the much more intense $^aR_{0,1}$ transitions in this frequency range. Transitions from 11 $^bQ_{1,-1}$ branch series with constant K_a are also visible across our observed frequency range. They increase in J and intensity as they progress to higher frequency, forming an identifiable band structure, turn around, and progress to lower frequency with further increasing J. Eventually, the degenerate transitions separate to form pairs of plus- and minus-symmetry $^bQ_{1,-1}$ transitions. Finally, a limited number of low-intensity, degenerate $^bP_{1,-1}$ and $^bP_{1,-3}$ transitions are also included in the data set. Due to the relatively high values of J and K for the transitions observed in this work, nuclear quadrupole splitting was not resolved and thus not treated in the data analysis.

Due to the high spectral density shown in Figure 3, the detection limit for transitions of all species in the observed spectrum is due to spectral confusion, rather than the signal-to-noise ratio. Because this sample was prepared by an intentional synthesis, purified by vacuum distillation, and characterized by other spectroscopic techniques (MS and NMR), we are confident that the vast majority of the spectral features are from **5** and not an impurity. The ground and vibrationally excited states of **5** each contribute a few thousand transitions to the rotational spectrum from 130 to 360 GHz. This spectral density makes accurate measurement of low-intensity tran-

https://doi.org/10.1021/acs.jpca.1c03246
J. Phys. Chem. A 2021, 125, 5601−5614

Table 1. Spectroscopic Constants for the Ground Vibrational State of (Cyanomethylene)cyclopropane (5) (S- and A-Reduced Hamiltonian, I^r Representation)[e]

	S Reduction, I^r representation			A Reduction, I^r representation	
	Experimental	MP2 [a]		Experimental	MP2 [a]
A_0 (MHz)	12644.00265 (20)	12527	A_0 (MHz)	12644.00216 (20)	12527
B_0 (MHz)	2038.861622 (59)	2014	B_0 (MHz)	2038.866459 (58)	2014
C_0 (MHz)	1797.034263 (54)	1776	C_0 (MHz)	1797.029487 (53)	1776
D_J (kHz)	0.561813 (18)	0.540	Δ_J (kHz)	0.575343 (17)	0.552
D_{JK} (kHz)	−7.547487 (70)	−7.43	Δ_{JK} (kHz)	−7.629007 (69)	−7.51
D_K (kHz)	63.1448 (11)	63.1	Δ_K (kHz)	63.2116 (10)	63.2
d_1 (kHz)	−0.1207251 (70)	−0.115	δ_J (kHz)	0.1207298 (69)	0.115
d_2 (kHz)	−0.00676037 (56)	−0.00618	δ_K (kHz)	2.40341 (20)	2.25
H_J (Hz)	0.0009849 (25)	0.000857	Φ_J (Hz)	0.0010541 (25)	0.000913
H_{JK} (Hz)	−0.020207 (12)	−0.0184	Φ_{JK} (Hz)	−0.012678 (39)	−0.0117
H_{KJ} (Hz)	0.052221 (75)	0.0364	Φ_{KJ} (Hz)	0.02518 (15)	0.0130
H_K (Hz)	0.6080 (19)	0.686	Φ_K (Hz)	0.6261 (18)	0.702
h_1 (Hz)	0.0003513 (12)	0.000304	ϕ_J (Hz)	0.0003565 (11)	0.000309
h_2 (Hz)	0.000033184 (83)	0.0000279	ϕ_{JK} (Hz)	0.005722 (30)	0.00418
h_3 (Hz)	0.000005436 (25)	0.00000487	ϕ_K (Hz)	0.4541 (22)	0.413
L_J (μHz)	−0.00200 (12)		L_J (μHz)	−0.00220 (11)	
L_{JJK} (μHz)	0.07038 (76)		L_{JJK} (μHz)	0.05070 (75)	
L_{JK} (μHz)	−1.1331 (47)		L_{JK} (μHz)	1.2714 (46)	
L_{KKJ} (μHz)	−2.134 (31)		L_{KKJ} (μHz)	−1.169 (32)	
L_K (μHz)	[0.0]		L_K (μHz)	[0.0]	
l_1 (μHz)	−0.000984 (64)		l_J (μHz)	−0.000978 (63)	
l_2 (μHz)	[0.0]		l_{JK} (μHz)	[0.0]	
l_3 (μHz)	[0.0]		l_{KJ} (μHz)	[0.0]	
l_4 (μHz)	[0.0]		l_K (μHz)	[0.0]	
Δ_i (uÅ^2) [b,c]	−6.613509 (11)	−6.716	Δ_i (uÅ^2) [b,c]	−6.612175 (11)	−6.716
N_{lines} [d]	3933		N_{lines} [d]	3933	
σ_{fit} (MHz)	0.031		σ_{fit} (MHz)	0.031	

[a]Evaluated with the 6-311+G(2d,p) basis set. [b]Inertial defect, $\Delta_i = I_c - I_a - I_b$. [c]Calculated using PLANM from the B_0 constants. [d]Number of fitted transition frequencies. [e]Values in square brackets held fixed in least-squares fit.

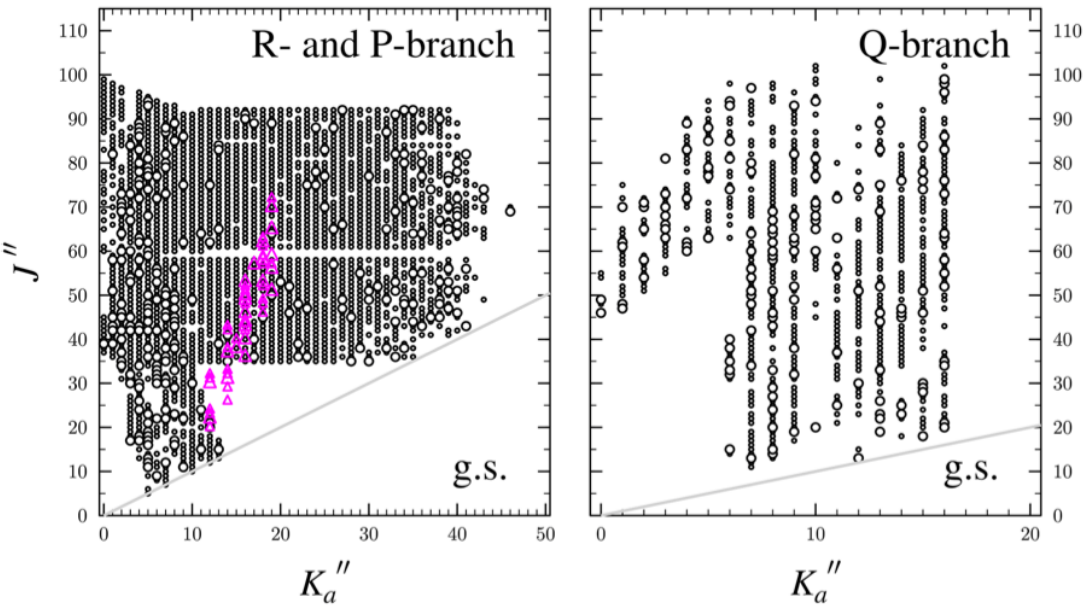


Figure 4. Data distribution plots for the least-squares fit of spectroscopic data for the vibrational ground state of (cyanomethylene)cyclopropane (**5**). R-branch and Q-branch transitions are represented by black circles. P-branch transitions are represented as pink triangles. The size of the symbol is proportional to the value of $|(f_{obs.} - f_{calc.})/\delta f|$, where δf is the frequency measurement uncertainty.

https://doi.org/10.1021/acs.jpca.1c03246
J. Phys. Chem. A 2021, 125, 5601−5614

sitions challenging due to coincidental overlapping transitions from other vibrational states. It also makes observation of the [^{13}C]- or [^{15}N]-isotopologues at their natural abundances particularly difficult, as there are a few dozen vibrationally excited states with transitions of higher intensity. Using standard methods of predicting the spectra of these isotopologues from the spectroscopic constants of the main isotopologue and computed constants for the main and heavy atom isotopologues, none of these species were observable in the experimental spectrum. Thus, the spectral analysis presented in this work is limited to the ground and two lowest-energy vibrationally excited states.

A total of over 3900 ground-state transitions were observed, measured, and least-squares fit to partial octic, distorted rotor A- and S-reduced Hamiltonians in the I^r representation (σ_{fit} = 0.031 MHz). The resulting values of the spectroscopic constants and their theoretical counterparts are provided in Table 1. The MP2 predictions of the rotational constants are within about 1% of their experimentally determined values. The B3LYP values provided in Table S1 are in slightly worse agreement, with errors in B_0 and C_0 of 1.9 and 1.6%, respectively. While these predictions are quite reasonable and of the expected quality, the absolute error in the predicted spectrum resulting from them is substantial. As mentioned, the most recognizable features of the rotational spectrum are the $^aR_{0,1}$ bands ranging from J = 35 to 93 across the observed frequency range. With these bands separated by approximately $B + C$ and the sum of these constants predicted to be too small (66 MHz with B3LYP and 46 MHz with MP2), the initial predictions of each band's location were off by 2.3−6.1 GHz (B3LYP) and 1.6−4.3 GHz (MP2). The large relative errors of the computed $B + C$ compared to the experimental value of 3835.895885 (80) MHz, however, did not substantially hinder the assignment of transitions.

The large number of measured transition and the diversity of J (5 to 102) and K_a (0 to 46) values in the data set (Figure 4) enabled the quartic and sextic centrifugal distortion constants to be very well determined. The experimental quartic centrifugal distortion constants should be very reliable, given the inclusion of a full set of sextic centrifugal distortion constants. For both reductions, the MP2 quartic centrifugal distortion constants are within 9% of their experimental values. In particular, there is remarkable agreement for the D_K and Δ_K constants, where the predicted values are nearly identical to the experimental values. Both values are quite large (>60 kHz) due to the very prolate ($\kappa = -0.96$) nature of **5**, which is consistent with other highly prolate species.[29,37] Due, in part, to the incomplete set of octic centrifugal distortion terms included in the Hamiltonian, the determination of the sextic centrifugal distortion terms is less reliable. All MP2 values of the constants are of the correct sign and magnitude, though some differ by as much as 50% from their experimental values. No method is currently implemented in Gaussian (or other commonly available computational software) for estimating the octic centrifugal distortion constants, so no comparison can be made between experiment and theory. This absence of a prediction also reduces the physical meaningfulness of those parameters that are varied in the least-squares fit, as remaining constants that cannot be satisfactorily determined cannot be held constant at a theoretical value and must instead be held constant at zero. Nevertheless, it appears that the centrifugal distortion constants for the ground state are sufficiently well determined (particularly the octic and sextic ones) that they can be used with confidence for any distortion constants of the vibrationally excited states that cannot be determined in their least-squares fits.

Fundamental Vibrational States ν_{27} and ν_{17}. The vibrationally excited states of (cyanomethylene)cyclopropane (**5**) below 500 cm^{-1} consist of a Coriolis-coupled dyad of its two lowest-energy fundamentals and a complex polyad of several higher-energy vibrationally excited states (Figure 5).

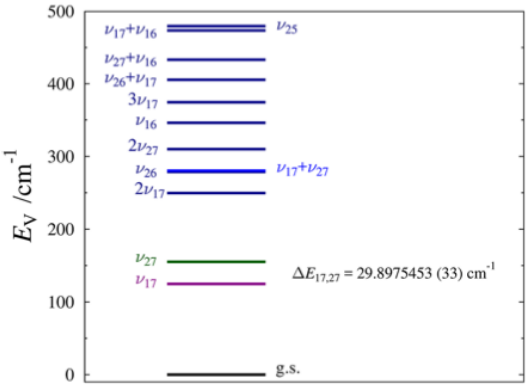


Figure 5. Vibrational energy levels of (cyanomethylene)cyclopropane (**5**) below 500 cm^{-1} from the computed fundamental frequencies (MP2/6-311+G(2d,p)). The value of $\Delta E_{17,27}$ results from the experimental perturbation analysis of ν_{17} and ν_{27} in this work.

The lowest-energy fundamental, ν_{17} (A', 125 cm^{-1}), is an in-plane bend of the nitrile and cyclopropyl groups with respect to C2 and C3. The second-lowest energy fundamental, ν_{27} (A'', 155 cm^{-1}), is a symmetric, out-of-plane bend of the nitrile and a CH_2 of the cyclopropyl with respect to the ethylene. The two lowest-energy fundamentals are expected to show strong interactions between their energy levels due to the large values of A_v, their moderate predicted energy difference of 30 cm^{-1} (MP2), the large predicted Coriolis ζ values, and the range of J values observed in this work. As expected, the transitions of these vibrationally excited states are not adequately treated by single-state, distorted-rotor Hamiltonians. A two-state partial octic, A-reduced Hamiltonian with nine terms treating the coupling between states was used to successfully least-squares fit the transitions for the ν_{17} and ν_{27} dyad. The final data set includes over 2600 transitions for each fundamental state and is least-squares fit to a low statistical error (σ_{fit} < 0.039 MHz). As shown in Figure 6, the range of J (6 to 99) and K_a (0 to 37) values represented is still quite extensive, albeit reduced from the ground-state data set. Due to the lower intensity of these two vibrationally excited states, substantially fewer Q-branch transitions could be measured and included in the least-squares fit. No P-branch transitions could be measured or included for these lower-intensity states.

The resulting spectroscopic constants for ν_{17} and ν_{27} (Table 2) include a complete set of well-determined rotational and quartic centrifugal distortion constants. The least well-determined rotational constants, A_{17} and A_{27}, have statistical uncertainties of about 0.01% the magnitude of their values. The A_v constants are hardest to determine for a molecule such as (cyanomethylene)cyclopropane (**5**), given that the majority of observed transitions are *a*-type and relatively few are *b*-type. This is true for the ground state as well as the excited

https://doi.org/10.1021/acs.jpca.1c03246
J. Phys. Chem. A 2021, 125, 5601−5614

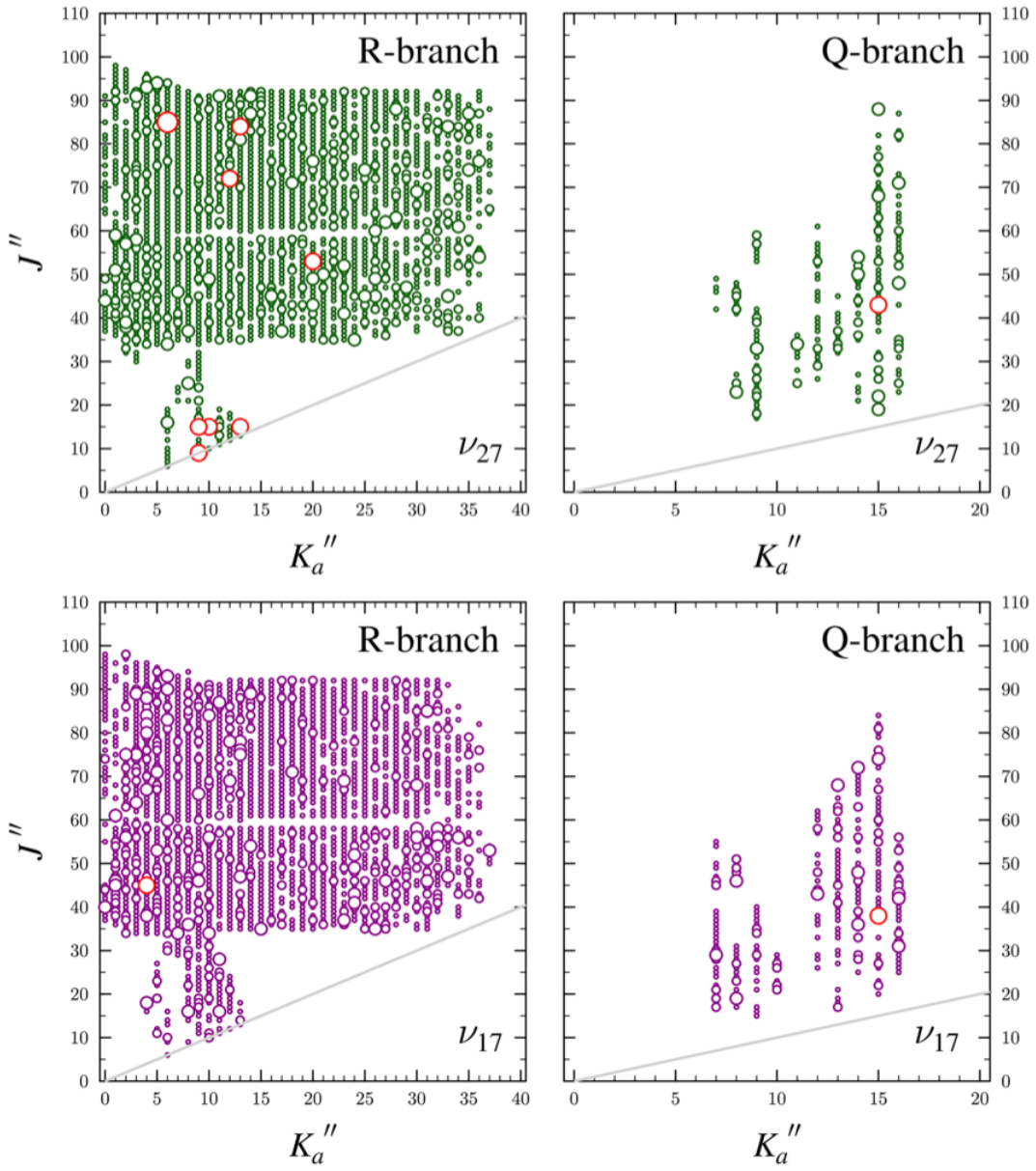


Figure 6. Data distribution plots for the coupled fit of measured transitions in the two lowest-energy excited vibrational states in (cyanomethylene)cyclopropane (**5**). The size of the plotted symbol is proportional to the value of $|(f_{obs.} - f_{calc.})/\delta f|$, where δf is the frequency measurement uncertainty (50 kHz). Values for which this relative error is >3 shown in red.

vibrational states. Even more problematic, the $A\nu$ constants are also the most correlated with the large *a*-type Coriolis-coupling constants and are therefore generally more poorly determined in the fit of a coupled dyad. Only a few *J*-dependent sextic constants (Φ_J Φ_{JK}, and ϕ_J) could be determined, and all other centrifugal distortion constants were held constant at their ground-state values. With no method currently implemented to obtain theoretical values for the quartic distortion constants of these fundamentals, only a comparison to their ground-state counterparts is possible. With a complete set of quartic distortion constants, but only an incomplete set of sextic distortion constants, the quartic distortion constants provide the more reliable estimation of how well the least-squares fit is treating the perturbations between ν_{17} and ν_{27}. The relatively small deviations (<10%) of all quartic constants from their ground-state counterparts suggest that the coupling is being sufficiently treated and that these values are physically meaningful. None of these constants bears a clear sign of absorbing untreated coupling between the states, which would typically cause large deviations in some spectroscopic constants in opposite directions relative to the ground-state constants.

https://doi.org/10.1021/acs.jpca.1c03246
J. Phys. Chem. A 2021, 125, 5601−5614

Table 2. Spectroscopic Constants for Vibrationally Excited States ν_{17} and ν_{27} of (Cyanomethylene)cyclopropane (5) (A-Reduced Hamiltonian, I^r Representation)[e]

	Ground state	ν_{17} (A', 125 cm^{-1}) [a]	ν_{27} (A', 155 cm^{-1}) [a]
A_v (MHz)	12644.00216 (20)	12725.8 (12)	12570.5 (12)
B_v (MHz)	2038.866459 (58)	2044.336 (18)	2041.600 (18)
C_v (MHz)	1797.029487 (53)	1799.526614 (64)	1800.078788 (50)
Δ_J (kHz)	0.575343 (17)	0.577820 (28)	0.578479 (28)
Δ_{JK} (kHz)	−7.629007 (69)	−7.6499 (17)	−7.5923 (17)
Δ_K (kHz)	63.2116 (10)	63.021 (32)	63.649 (32)
δ_J (kHz)	0.1207298 (69)	0.122045 (15)	0.121117 (15)
δ_K (kHz)	2.40341 (20)	2.6318 (11)	2.3490 (10)
Φ_J (Hz)	0.0010541 (25)	0.00103342 (48)	0.00107110 (49)
Φ_{JK} (Hz)	−0.012678 (39)	−0.013792 (83)	−0.010726 (84)
Φ_{KJ} (Hz)	0.02518 (15)	[0.02518]	[0.02518]
Φ_K (Hz)	0.6261 (18)	[0.6261]	[0.6261]
ϕ_J (Hz)	0.0003565 (11)	0.00034856 (48)	0.00036235 (42)
ϕ_{JK} (Hz)	0.005722 (30)	[0.005722]	[0.005722]
ϕ_K (Hz)	0.4541 (22)	[0.4541]	[0.4541]
ΔE		896305.858 (98) MHz / 29.8975453 (33) cm^{-1}	
G_a (MHz)		16023. (32)	
G_a^J (MHz)		0.012739 (88)	
G_a^K (MHz)		−0.3961 (60)	
G_a^{JJ} (MHz)		−0.0000000919 (20)	
F_{bc} (MHz)		0.6737 (19)	
F_{bc}^J (MHz)		−0.000000374 (19)	
F_{bc}^K (MHz)		0.00034376 (81)	
G_b (MHz)		1371.4 (59)	
G_b^J (MHz)		−0.002270 (25)	
Δ_i (uÅ^2) [b,c]	−6.613509 (11)	−6.06823 (43)	−6.9904 (44)
N_{lines} [d]	3933	2789	2666
σ_{fit} (MHz)	0.031	0.038	0.039

[a]Fundamental frequencies calculated using MP2/6-311+G(2d,p). [b]Inertial defect, $\Delta_i = I_c - I_a - I_b$. [c]Calculated using PLANM from the B_0 constants. [d]Number of fitted transition frequencies. [e]Values in square brackets held fixed in least-squares fit.

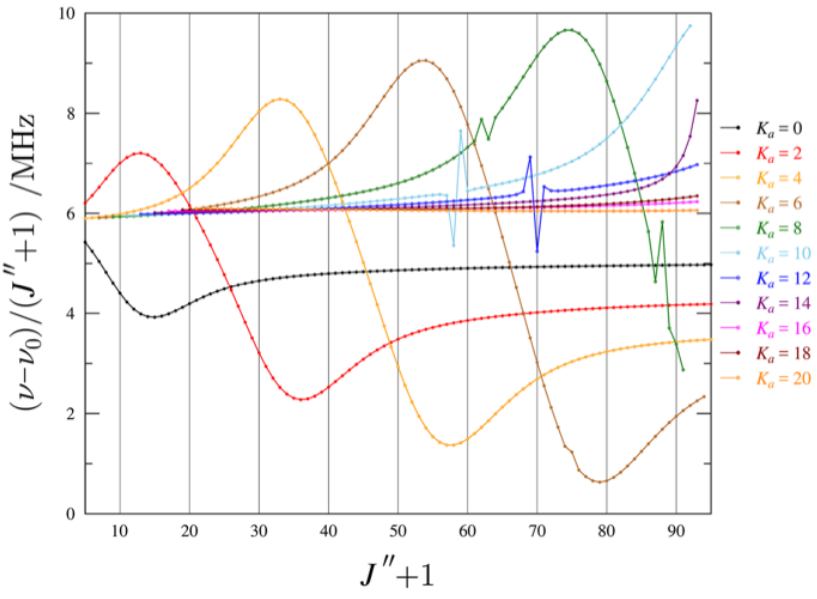


Figure 7. Superimposed resonance plots of ν_{17} for $^aR_{0,1}$ K_a^+ series with even values of K_a^+ between 0 and 30 for (cyanomethylene)cyclopropane (5). Measured transitions are omitted for clarity, but they are indistinguishable from the plotted values on this scale. The plotted values are frequency differences between excited-state transitions and their ground-state counterparts, scaled by (J'' + 1).

https://doi.org/10.1021/acs.jpca.1c03246
J. Phys. Chem. A 2021, 125, 5601−5614

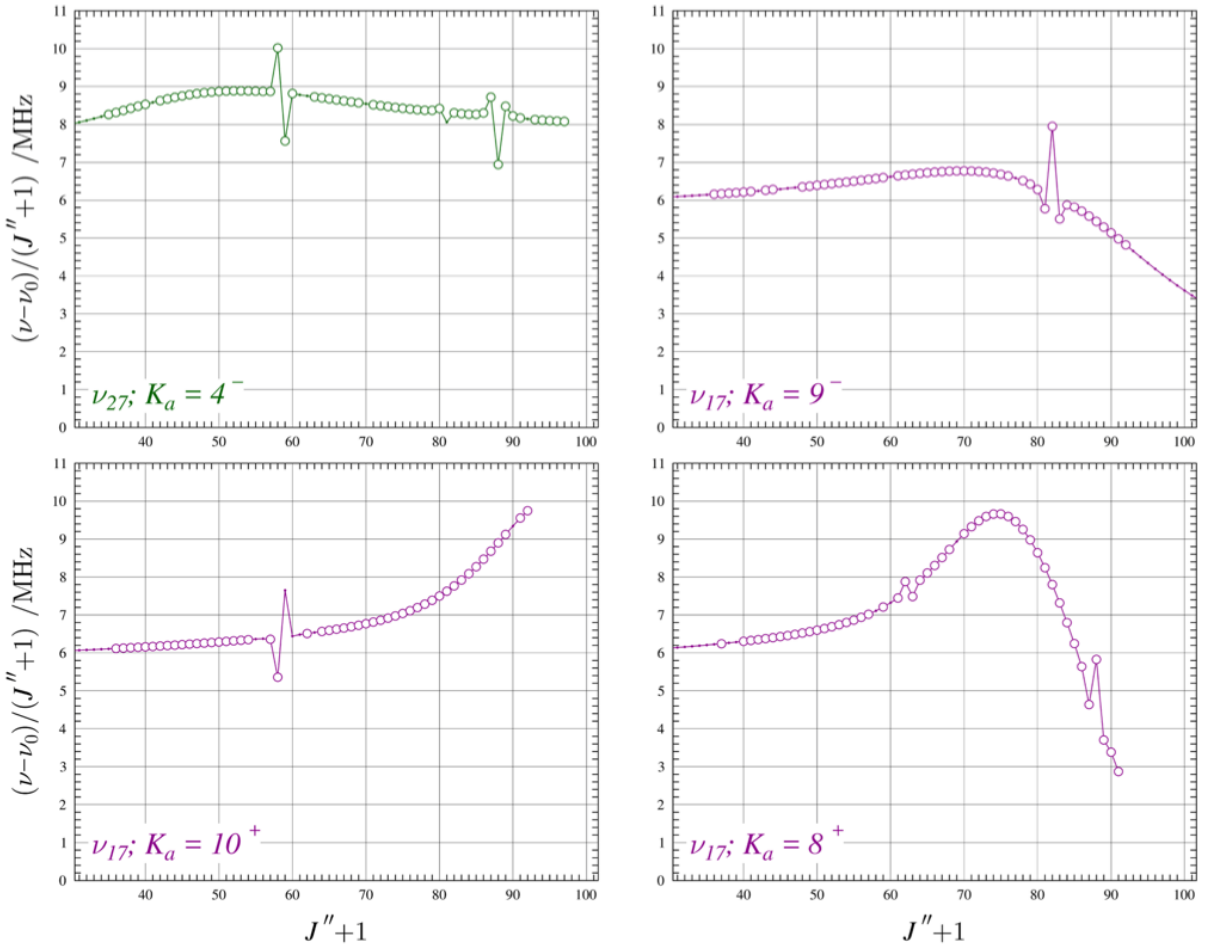


Figure 8. Resonance plots for (cyanomethylene)cyclopropane (**5**) showing the $K_a = 4^-$ series for ν_{27} and $K_a = 9^-$, 10^+, and 8^+ series for ν_{17}. Examples of resonances conforming to the $\Delta K_a = 5$ and $\Delta K_a = 6$, 4 selection rules for *b*- and *a*-type resonances, respectively. The plotted values are frequency differences between excited-state transitions and their ground-state counterparts, scaled by $(J'' + 1)$ in order to make the plots more horizontal. Measured transitions are represented by circles: ν_{17} (purple); ν_{27} (green). There are no measured transitions with $|(f_{obs.} - f_{calc.})/\delta f| > 3$. Predictions from the final coupled fit are represented by a solid, colored line.

Coriolis-Coupling Analysis. The satisfactory treatment and least-squares fitting of the coupled dyad between ν_{17} and ν_{27} provide a highly precise and accurate energy difference [$\Delta E_{17,27}$ = 896305.858 (98) MHz or 29.8975453 (33) cm^{-1}] between these fundamentals. Both the MP2 (30.4 cm^{-1}) and B3LYP (29.5 cm^{-1}) energy differences are in unexpectedly close agreement with the experimentally determined value. The precision of the experimentally determined energy difference is dependent upon the inclusion of many transitions involved in global interactions between the fundamentals, transitions whose energy levels are impacted by energy level crossings (causing sharp local resonances), and related formally forbidden interstate transitions. The energy difference is very sensitive to, and well-determined by, the last two kinds of frequency data.

In the initial fitting process, the global perturbations between states can be seen as the undulations or curvature of the resonance plots for the K_a series of R-branch transitions. Several example series are shown in Figures 7 and 8 for ν_{17} and ν_{27}. As the quantum number value of K_a increases, the peak and trough of the undulation progress rapidly toward higher *J* values. By $K_a = 12$ for ν_{17}, the undulations of the series have largely passed out of the observed range of *J*, and the K_a series appear to be much flatter. These curving series of ν_{17}, combined with the mirrored undulations in the resonance plots of the low-K_a series of ν_{27}, allow for an initial fitting and refinement of the Coriolis-coupling terms and $\Delta E_{17,27}$. Once there is a preliminary treatment of the global interaction, the local resonances (Figures 7 and 8) can be assigned and included in the least-squares fit data set. These intense interactions become visibly noticeable at $K_a \sim 6$ for ν_{17} (lower K_a for ν_{27}) and provide critical refinement of the energy and coupling coefficients. Eventually, these global undulations and local resonances allow for a precise determination of the Coriolis-coupling coefficients and $\Delta E_{17,27}$ and should result in rotational and centrifugal distortion constants that are relatively free of the impact of untreated coupling between states.

The different symmetries of fundamentals ν_{17} (A', 125 cm^{-1}) and ν_{27} (A'', 155 cm^{-1}) permit Coriolis couplings along both their *a*- and *b*-principal axes. Both of the resulting types of *a*- and *b*-type resonances (ΔK_a = even and ΔK_a = odd,

https://doi.org/10.1021/acs.jpca.1c03246
J. Phys. Chem. A 2021, 125, 5601−5614

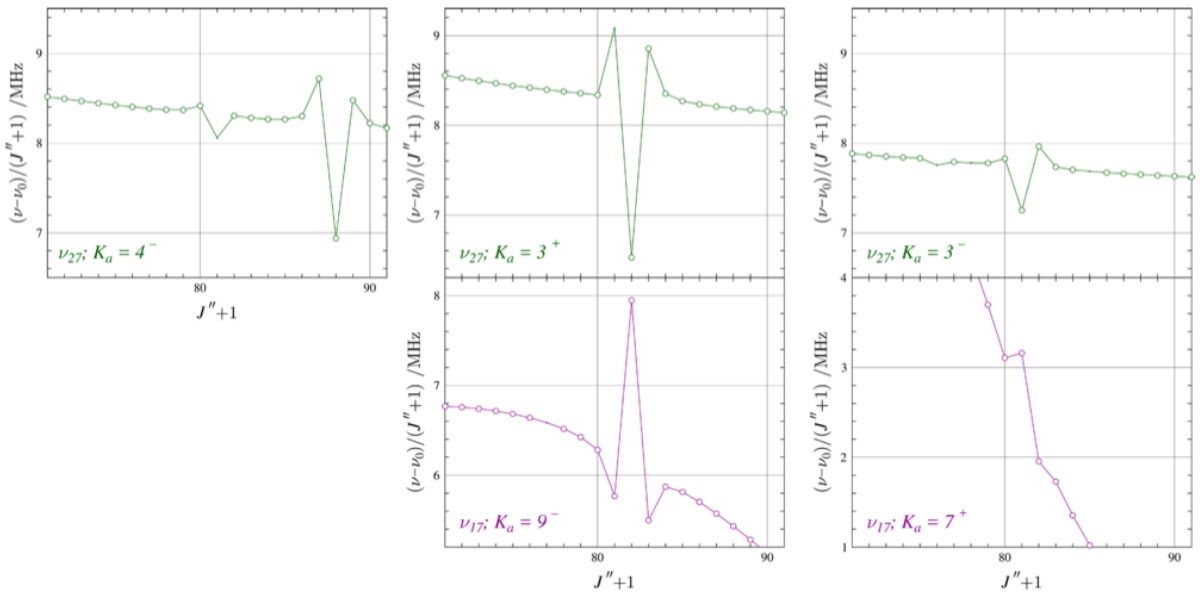


Figure 9. Resonance plots for (cyanomethylene)cyclopropane (**5**) showing the $K_a = 4^-$, 3^+, and 3^- series for ν_{27} and the $K_a = 9^-$ and 7^+ series for ν_{17}. All of these series have transitions affected by perturbation at $J'' + 1 = 81$. The plotted values are frequency differences between excited-state transitions and their ground-state counterparts, scaled by $(J'' + 1)$ in order to make the plots more horizontal. Measured transitions are represented by circles: ν_{17} (purple); ν_{27} (green). There are no measured transitions with $|(f_{obs.} - f_{calc.})/\delta f| > 3$. Predictions from the final coupled fit are represented by a solid, colored line.

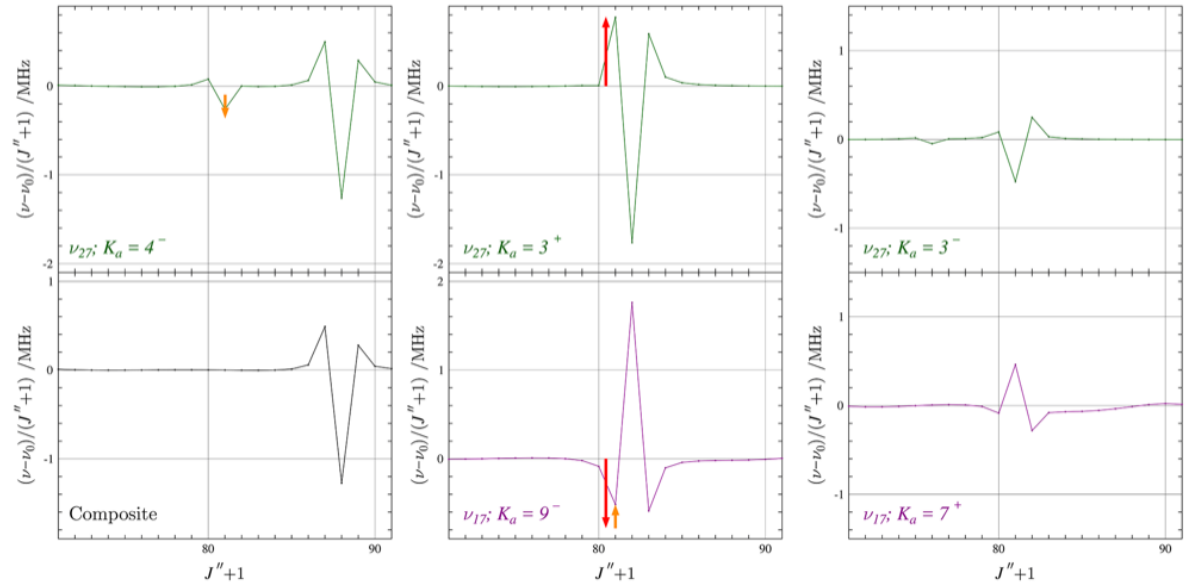


Figure 10. Baseline-flattened resonance plots for (cyanomethylene)cyclopropane (**5**) showing the $K_a = 4^-$, 3^+, and 3^- series for ν_{27} and the $K_a = 9^-$ and 7^+ series for ν_{17}, as well as a composite plot of ν_{27} $K_a = 4^-$, ν_{27} $K_a = 3^+$, and ν_{17} $K_a = 9^-$. All of these series have transitions affected by perturbation at $J'' + 1 = 81$. Measured transitions are omitted for clarity, but they are indistinguishable from the plotted values on this scale. Red arrows denote the magnitude of frequency displacement due to the *a*-type interaction between transitions of ν_{27} $K_a = 3^+$ and ν_{17} $K_a = 9^-$ at $J'' + 1 = 81$, and orange arrows denote the magnitude of frequency displacement due to the *b*-type interaction between transitions of ν_{27} $K_a = 4^-$ and ν_{17} $K_a = 9^-$ at $J'' + 1 = 81$.

respectively) are observed between ν_{17} and ν_{27}. An informative example is shown in Figure 7, involving resonances between the $K_a = 4^-$ series of ν_{27} and the $K_a = 9^-$, 10^+, and 8^+ series of ν_{17}. These resonances showcase the two possible appearances of resonances, with either a single highly displaced transition or with two highly displaced transitions in opposite directions. The former occurs when the energy crossing of the vibrational states occurs at or very near to a single J quantum number. The

https://doi.org/10.1021/acs.jpca.1c03246
J. Phys. Chem. A 2021, 125, 5601−5614

latter occurs when the exact energy level crossing of the vibrational states occurs midway between two different J quantum numbers. The first of the three small resonances (J'' + 1 = 58, 59) in the $K_a = 4^-$ series of ν_{27} is the result of an a-type interaction with the $K_a = 10^+$ series of ν_{27} ($\Delta K_a = 6$). Due to both of these resonances occurring at relatively flat regions of the curving series, the mirroring of these resonances is visually apparent with both plots using the same y-axis scale. The absent resonant transition of the ν_{27} series is excluded due to its near-degeneracy with a $K_a = 2$ transition from the ground state, preventing an accurate measurement of either transition. The second of the three small resonances (J'' + 1 = 81) is the result of a complicated interaction with the $K_a = 9^-$ series of ν_{17} ($\Delta K_a = 5$) (*vide infra*). The ν_{27} transition of this resonance is not included in the data set due to a significant loss of intensity to its related nominal interstate transition, combined with an incidental overlap with two significantly more intense transitions. The final resonance (J'' + 1 = 88) is due to a second a-type interaction with the $K_a = 8^+$ series of ν_{17} (ΔK_a = 4). The $K_a = 8^+$ series of ν_{17} has a second small resonance (J'' + 1 = 62, 63) with the $K_a = 2^-$ series (resonance plot not shown) of ν_{27} ($\Delta K_a = 6$).

It is not readily apparent from Figure 8 that the ν_{27} transition at J'' + 1 = 81 is involved in a b-type, $\Delta K_a = 5$ interaction with a transition in the $K_a = 9^-$ series of ν_{17} because these two features appear quite unsymmetrical. It so happens that five different K_a series (two of ν_{17} and three of ν_{27}) contain transitions affected by resonances at J'' + 1 = 81; these series are depicted in Figure 9. Upon first inspection, the magnitudes of transition displacement match between the ν_{27} $K_a = 3^+$ and ν_{17} $K_a = 9^-$ series, and it visually appears that the shape of displacement in the ν_{17} $K_a = 7^+$ plot resembles that of the ν_{27} $K_a = 4^-$, J'' + 1 = 81 displacement, perhaps affected by the steep slope on which the former is found. Such an interaction, however, is symmetry disallowed for this Coriolis-coupled system as a $\Delta K_a = 3$ (odd), $\Delta K_c = 4$ (even) interaction should only occur with a c-type Coriolis interaction.

To elucidate the appearance of local perturbations in the resonance plots, we modeled the baseline curvature of each resonance plot with a polynomial of appropriate order, excluding the highly perturbed transitions. This baseline model was subtracted from the corresponding resonance plots in Figure 9, and the resultant, baseline-flattened resonance plots are provided in Figure 10 with all x- and y-axes set at the same scale. Once the baseline is flattened, it becomes apparent that the displacements in the ν_{27} $K_a = 3^-$ and ν_{17} $K_a = 7^+$ series at J'' + 1 = 81 are involved in an a-type interaction with $\Delta K_a = 4$. The expected a-type interaction between the ν_{27} $K_a = 3^+$ and ν_{17} $K_a = 9^-$ series ($\Delta K_a = 6$) is also confirmed. Upon closer inspection, however, the displacements of transitions in these two series near J'' + 1 = 81 do not perfectly mirror one another. The red arrows in Figure 10 show the magnitude of displacement at J'' + 1 = 81 due to the a-type interaction between ν_{27} $K_a = 3^+$ and ν_{17} $K_a = 9^-$. This perturbation coincides with the b-type interaction at J'' + 1 = 81 between ν_{27} $K_a = 4^-$ and ν_{17} $K_a = 9^-$ (represented by the orange arrows). The confirmation of this interaction is provided in the "Composite," bottom-left panel in Figure 10, which shows the sum of the three resonance plots (ν_{27} $K_a = 4^-$, ν_{27} $K_a = 3^+$, and ν_{17} $K_a = 9^-$). In this plot, the displacements of all transitions involved in interactions near J'' + 1 = 81 have cancelled out, and the only remaining feature is the unrelated set of resonant transitions at J'' + 1 = 87−89.

If the experimental least-squares fit or the computational deperturbation treatment is not adequately addressing the coupling between states, the values of the vibration−rotation interaction constants (α_i) typically show characteristic large, equal, and opposite deviations for ν_{17} and ν_{27}, relative to their corresponding ground-state values. Whether or not the experimental $A_0 - A_v$ values are displaying such behavior is ambiguous in the present dyad (Table 3). The $A_0 - A_v$ values

Table 3. Vibration−Rotation Interaction and Coriolis-Coupling Constants of (Cyanomethylene)cyclopropane (5)

	Experimental	B3LYP	MP2
$A_0 - A_{17}$ (MHz)	−81.8 (12)	203	186
$B_0 - B_{17}$ (MHz)	−5.470 (18)	−2.06	−2.34
$C_0 - C_{17}$ (MHz)	−2.497127 (83)	−1.69	−1.77
$A_0 - A_{27}$ (MHz)	73.5 (12)	−230	−212
$B_0 - B_{27}$ (MHz)	−2.734 (0.018)	−3.51	−3.51
$C_0 - C_{27}$ (MHz)	−3.049301 (73)	−2.24	−2.33
$\frac{(A_0 - A_{17}) + (A_0 - A_{27})}{2}$ (MHz)	−4.1 (17)	−13.28	−13.17
$\frac{(B_0 - B_{17}) + (B_0 - B_{27})}{2}$ (MHz)	−4.102 (25)	−2.79	−2.93
$\frac{(C_0 - C_{17}) + (C_0 - C_{27})}{2}$ (MHz)	−2.77321 (11)	−1.97	−2.05
$\zeta^a_{17,27}$ (MHz)	0.633	0.584	0.578
$\zeta^b_{17,27}$ (MHz)	0.054	0.035	0.035

are large and of opposite sign, making it unclear whether this is a physically meaningful set of vibration−rotation interaction constants or if there is some residual, unaddressed a-axis coupling. It is much more apparent that the theoretical values for $A_0 - A_v$ have equal and opposite discrepancies of approximately 300 MHz, relative to their experimental counterparts using either level of theory. This indicates that whatever deperturbation treatment may have been included in the computational prediction is not sufficient for these two states. As can be seen for the $B_0 - B_v$ and $C_0 - C_v$ values as well as the average of the ν_{17} and ν_{27} vibration−rotation interaction constants, these two states are also more poorly modeled than is typically expected for both theoretical treatments.

The Coriolis coupling along the a- and b-axes cannot be modeled by simply using the first-order G_a and G_b constants. The Coriolis-coupling spectroscopic constants G_a and G_b are related to the Coriolis-coupling constant ζ values by eq 1.

$$G_x = \frac{\omega_{17} + \omega_{27}}{\sqrt{\omega_{17} \times \omega_{27}}} \zeta^x_{17,27} B^x_e \approx 2\zeta^x_{17,27} B^x_e \quad (1)$$

This relation between G and ζ is approximate in its dependence upon the harmonic frequencies of each state, in the estimate of the equilibrium rotational constants, and in the neglect of higher-order coupling terms. The experimentally estimated ζ values and their computed counterparts are presented in Table 3. Both of the theoretical values of $\zeta^a_{17,27}$ and $\zeta^b_{17,27}$ are somewhat smaller than the corresponding experimental estimates. It cannot be determined from this work whether the discrepancies in the computed and experimental values are due to incomplete theoretical treatment or an incomplete resolution of the G_a and G_b contributions to the resonances and global perturbations.

When the state mixing is sufficient to create these resonances, formally *forbidden* simultaneous transitions involving changes in both rotational and vibrational quantum numbers become allowed. Due to the relatively weak resonances of ν_{17} (A', 125 cm^{-1}) and ν_{27} (A'', 155 cm^{-1}),

https://doi.org/10.1021/acs.jpca.1c03246
J. Phys. Chem. A 2021, 125, 5601−5614

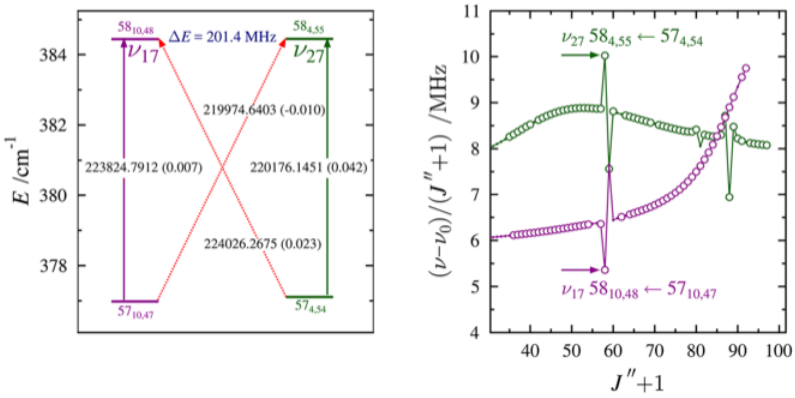


Figure 11. Energy diagram (left) depicting a representative matched pair of nominal rotation−vibration transitions between the ν_{27} (purple) and ν_{17} (green) vibrational states of (cyanomethylene)cyclopropane (**5**). Standard $^aR_{0,1}$ transitions within vibrational states are denoted by vertical arrows. The diagonal, dashed arrows indicate nominal interstate transitions that are formally forbidden but become allowed as a result of rotational energy level mixing. Values printed on each of the arrows are the corresponding transition frequency (in MHz) with its *obs.* − *calc.* value in parentheses. The marked energy separation is the energy separation between the two strongly interacting rotational energy levels. Resonance plots (right) of the K_a series of ν_{17} and ν_{27} contain the corresponding resonant transitions labeled with their quantum numbers and marked by colored arrows.

only a small number of these *forbidden* nominal interstate transitions were visible. Interstate transitions were included in the data set when they could be confidently assigned due to their intensity or in comparison to their corresponding intravibrational state transitions. In total, only nine nominal interstate transitions were included in the data set. One set of nominal interstate transitions and their intrastate counterparts are shown in Figure 11. The measured frequency of each transition and its *obs.* − *calc.* value are provided for all four transitions. All four transitions were close to their predicted intensities, and the sum of the intrastate and interstate transition frequencies differ by only 28 kHz. The low error in each individual transition and their energetic consistency provides confidence that all four transitions are properly assigned and accurately measured. The two corresponding resonant transitions are the $(J'' + 1 = 58)$ transitions from the $K_a = 4^-$ series of ν_{27} and $K_a = 10^+$ series of ν_{17} shown in Figure 8, and their resonance plots are redisplayed in Figure 11 to highlight the relation between the resonant transitions and the nominal interstate transitions. The mixing occurs with $\Delta K_a = 6$ due to the large vibrational energy difference of 30 cm^{-1} and the requirement for the rotational energy levels of the lower-energy vibrational state (ν_{17}) to catch up with the rotational energy levels of the higher-energy vibrational state (ν_{27}). For example, the $58_{10,48}$ energy level of ν_{17} and the $58_{4,55}$ energy level of ν_{27} are sufficiently close to one another (0.006720 cm^{-1} or 201.4 MHz) that strong state-mixing becomes possible. The result of the least-squares fitting of transitions involving strongly interacting energy levels results in the very accurate value determination of the energy separation between these two vibrationally excited states.

■ CONCLUSIONS

The first isolation of (cyanomethylene)cyclopropane (**5**) as a pure compound allowed an investigation of its gas-phase, pure rotational spectrum. The rotational constants of the ground vibrational state are very well determined and should accurately predict the rotational transitions at frequencies lower than in this work. Transitions at slightly higher frequencies than 360 GHz should also be reasonably well predicted, though with reduced accuracy as the frequency increases. These transitions provide the foundational work needed for further investigation of this molecule *via* rotational spectroscopy or radioastronomy.

The analysis of the experimentally determined spectroscopic constants in this work and many others is incomplete due to the lack of theoretical values available for comparison. The ground-state spectroscopic constants require an octic treatment of the centrifugal distortion, but there is insufficient data in the transitions measured to determine a complete set of these constants. A broader frequency range that includes transitions of higher J and K values would be necessary to reliably determine all of the octic terms. Given the present inability of theoretical methods to predict octic centrifugal distortion constants, their values in this work cannot be evaluated for their physical meaningfulness. The tactic of setting some of the octic constants to a value of 0 inherently distorts the remaining octic constants and, to a lesser extent, the sextic centrifugal distortion constants.

The impact of a lack of theoretical spectroscopic constants is more profound for the vibrationally excited states. With no method currently available to address the vibration−rotation interaction for the centrifugal distortion constants, values for these constants that cannot be sufficiently determined must be held constant at their corresponding ground-state values. In this work, computational quartic constants for ν_{17} and ν_{27} would have assisted in the initial stages of least-squares fitting by using values closer to their true values than the ground-state constants. Given the complexity of modeling the centrifugal distortion and Coriolis coupling in the same least-squares fit, computational centrifugal distortion values would allow the coupling to be addressed more efficiently early in the fitting process. To further complicate matters, the majority of the Coriolis-coupling terms cannot be predicted in a straightforward manner. In the final analysis of the spectroscopic constants, computational values of either the centrifugal distortion or Coriolis-coupling beyond those currently available would greatly expedite the fitting process and

https://doi.org/10.1021/acs.jpca.1c03246
J. Phys. Chem. A 2021, 125, 5601−5614

improve the confidence in the experimental values obtained by least-squares fitting transitions of coupled dyads and polyads.

Independent of the ambiguities with the higher-order centrifugal distortion constants and Coriolis-coupling terms, this work provides a highly accurate and precise energy difference between these two vibrationally excited states, ν_{17} and ν_{27}. Pure rotational spectroscopy, however, cannot directly determine the individual energy values of these states. Due to their isolation from the ground vibrational state, high-resolution IR spectroscopy would be necessary for accurate measurement of the energy of these fundamentals. The experimental measurement of $\Delta E_{17,27}$ serves as a benchmark for future computational estimations and, combined with the spectroscopic constants determined for (cyanomethylene)-cyclopropane (**5**) in this work, makes the fitting of the high-resolution IR spectra of ν_{17} and ν_{27} a one-variable problem.

General Experimental Methods. All commercial reagents were purchased from Sigma-Aldrich or Oakwood Chemical and used as received, unless otherwise noted. ^{1}H NMR spectra (400 or 500 MHz) and ^{13}C{^{1}H}-NMR spectra (100 or 125 MHz) were obtained in $CDCl_3$ on a Bruker 400 MHz AVANCE III or Bruker 500 MHz DCH AVANCE III spectrometer; chemical shifts (δ) are reported as ppm downfield from internal standard $SiMe_4$ or referenced to residual solvent signals. Mass spectra were acquired using electrospray ionization (ESI) or the atmospheric solids analysis probe (ASAP) on a Thermo Scientific Q-Exactive Plus mass spectrometer. IR spectra were obtained on a Bruker TENSOR Fourier transform IR instrument as neat samples using an attenuated total reflectance accessory (Bruker PLATINUM ATR).

*1-Ethoxycyclopropanol (**8**).*[28] A solution of (1-ethoxycyclopropoxy)trimethylsilane (**10**, 9.98 g, 57 mmol) in methanol (25 mL) was stirred at room temperature for 24 h. The reaction was monitored *via* ^{1}H NMR and TLC, which confirmed complete deprotection of the trimethylsilane group at 24 h. The methanol solvent was subsequently removed *in vacuo* to afford a clear, colorless oil. The crude oil was purified *via* short-path distillation to yield 1-ethoxycyclopropanol (**8**, bp = 88−90 °C at 100 Torr) as a colorless oil (5.0 g, 48.5 mmol, 85%). TLC: R_f = 0.3 (hexane/EtOAc, 4:1; $KMnO_4$). ^{1}H NMR ($CDCl_3$, 500 MHz): δ (ppm) 4.37 (br s, 1H), 3.77 (q, J = 7.2 Hz, 2H), 1.21 (t, J = 7.1 Hz, 3H), 0.98−0.87 (m, 4H). ^{13}C{^{1}H}-NMR ($CDCl_3$, 125 MHz): δ (ppm) 85.5, 62.0, 15.4, 14.2. IR (neat): (cm^{-1}) 3386 (m), 2978 (w), 1734 (m), 1460 (w), 1298 (m), 1225 (m), 1052 (m), 943 (m), 487 (w). HRMS (ESI) m/z: [M + H]$^+$ calcd for $C_5H_{11}O_2$, 103.0754; found, 103.0753.

*(Cyanomethylene)triphenylphosphorane (**9**).*[27] To a stirred solution of (cyanomethyl)triphenylphosphonium chloride (**11**, 120.4 g, 60.5 mmol) in 200 mL of deionized water was added, dropwise, an aqueous solution of sodium hydroxide (50% w/w, 10.0 mL) over 5 min at room temperature. The addition resulted in the formation of a white precipitate, and the mixture was stirred for an additional 30 min. The resulting white solid was isolated by filtration *via* a coarse glass fritted filter and dried *in vacuo* for 24 h to yield (cyanomethylene)-triphenylphosphorane (**9**, 17.0 g, 56.5 mmol, 93%). ^{1}H NMR ($CDCl_3$, 500 MHz): δ (ppm) 7.43−7.71 (m, 15H), 1.60 (s, 1H). ^{13}C{^{1}H}-NMR (125 MHz, $CDCl_3$): δ (ppm) 132.80 (d, J = 10.1 Hz), 132.57 (d, J = 3.0 Hz), 132.11 (d, J = 9.8 Hz), 129.08 (d, J = 12.4 Hz), 128.50 (d, J = 12.1 Hz), 127.43 (d, J = 91.8 Hz). Chemical shifts are consistent with previous reports.[38]

*(Cyanomethylene)cyclopropane (**5**).* To a flame-dried 250 mL single-neck round-bottom flask (cooled under a stream of N_2) was added 1-ethoxycyclopropanol (**8**, 2.07 g, 20.3 mmol), (cyanomethylene)triphenylphosphorane (**9**, 6.01 g, 20 mmol), benzoic acid (243 mg, 2 mmol, 10 mol %), and 115 mL of benzene. The reaction vessel was fitted with a water-cooled reflux condenser (with N_2 vent) and heated to reflux for 24 h. After cooling to room temperature, the flask was fitted with a fractionating column (23 cm, glass bead-packed) and a short-path distillation apparatus. Most of the benzene was removed by distillation at atmospheric pressure. To the remaining liquid (~40 mL) in the boiling flask, 100 mL of pentane was added, and the solution was cooled on ice to precipitate triphenylphosphine oxide. The resulting mixture was filtered through a fine glass frit into a separate boiling flask, and pentane was removed by short-path distillation with a fractionating column at atmospheric pressure, leaving the crude product as a bright yellow liquid. The crude product was purified *via* short-path vacuum distillation to yield (cyanomethylene)cyclopropane (**5**) (bp = 88 °C at 100 Torr) as a colorless oil (820 mg, 52%). TLC: R_f = 0.5 (pentane/diethyl ether, 6:1; $KMnO_4$). ^{1}H NMR ($CDCl_3$, 400 MHz): δ (ppm) 5.76 (p, J = 2 Hz, 1H), 1.40 (d, J = 2 Hz, 4H). ^{13}C{^{1}H}-NMR ($CDCl_3$, 100 MHz): δ (ppm) 151.9, 116.8, 90.4, 5.2, 4.1 IR (neat): (cm^{-1}) 3072 (w), 3020 (w), 2987 (w), 2221 (m), 1744 (w), 1403 (w), 1230 (w), 1058 (m), 1003 (m), 939 (m), 913 (m), 760 (s), 732 (m), 682 (m). HRMS (ESI) m/z: [M + H]$^+$ calcd for C_5H_6N, 80.0495; found, 80.0494.

■ ASSOCIATED CONTENT

Supporting Information

The Supporting Information is available free of charge at https://pubs.acs.org/doi/10.1021/acs.jpca.1c03246.

Experimental IR, ^{1}H NMR, ^{13}C NMR, and mass spectra of all compounds (PDF)

Computational chemistry output files, least-squares fitting output files from ASFIT and SPFIT (ZIP)

■ AUTHOR INFORMATION

Corresponding Authors

Robert J. McMahon − *Department of Chemistry, University of Wisconsin−Madison, Madison, Wisconsin 53706-1322, United States;* orcid.org/0000-0003-1377-5107; Email: robert.mcmahon@wisc.edu

R. Claude Woods − *Department of Chemistry, University of Wisconsin−Madison, Madison, Wisconsin 53706-1322, United States;* Email: rcwoods@wisc.edu

Authors

Brian J. Esselman − *Department of Chemistry, University of Wisconsin−Madison, Madison, Wisconsin 53706-1322, United States;* orcid.org/0000-0002-9385-8078

Samuel M. Kougias − *Department of Chemistry, University of Wisconsin−Madison, Madison, Wisconsin 53706-1322, United States;* orcid.org/0000-0002-9877-0817

Maria A. Zdanovskaia − *Department of Chemistry, University of Wisconsin−Madison, Madison, Wisconsin 53706-1322, United States;* orcid.org/0000-0001-5167-8573

Complete contact information is available at:

https://pubs.acs.org/10.1021/acs.jpca.1c03246

Notes

The authors declare no competing financial interest.

■ ACKNOWLEDGMENTS

We gratefully acknowledge the National Science Foundation for support of this project (CHE-1664912 and CHE-1954270). We thank Michael McCarthy for the loan of an amplification−multiplication chain and the Harvey Spangler Award (to B.J.E.) for support of the purchase of the corresponding zero-bias detector. We thank the following organizations and individuals for support of shared departmental facilities: Bruker AVANCE 400 NMR spectrometer (NSF CHE-1048642), Bruker AVANCE 500 NMR spectrometer (gift from Paul J. and Margaret M. Bender), and Thermo Scientific Q Exactive Plus mass spectrometer (NIH 1S10 OD020022-1).

■ REFERENCES

(1) Müller, H. S. P.; Schlöder, F.; Stutzki, J.; Winnewisser, G. The Cologne Database for Molecular Spectroscopy, CDMS: a Useful Tool for Astronomers and Spectroscopists. *J. Mol. Struct.* **2005**, *742*, 215−227.

(2) Müller, H. S. P.; Thorwirth, S.; Roth, D. A.; Winnewisser, G. The Cologne Database for Molecular Spectroscopy. *Astron. Astrophys.* **2001**, *370*, L49−L52.

(3) Zdanovskaia, M. A.; Esselman, B. J.; Lau, H. S.; Bates, D. M.; Woods, R. C.; McMahon, R. J.; Kisiel, Z. The 103 − 360 GHz Rotational Spectrum of Benzonitrile, the First Interstellar Benzene Derivative Detected by Radioastronomy. *J. Mol. Spectrosc.* **2018**, *351*, 39−48.

(4) Zdanovskaia, M. A.; Esselman, B. J.; Woods, R. C.; McMahon, R. J. The 130 − 370 GHz Rotational Spectrum of Phenyl Isocyanide (C_6H_5NC). *J. Chem. Phys.* **2019**, *151*, 024301.

(5) Dorman, P. M.; Esselman, B. J.; Woods, R. C.; McMahon, R. J. An Analysis of the Rotational Ground State and Lowest-energy Vibrationally Excited Dyad of 3-Cyanopyridine: Low Symmetry Reveals Rich Complexity of Perturbations, Couplings, and Interstate Transitions. *J. Mol. Spectrosc.* **2020**, *373*, 111373.

(6) Dorman, P. M.; Esselman, B. J.; Park, J. E.; Woods, R. C.; McMahon, R. J. Millimeter-Wave Spectrum of 4-Cyanopyridine in its Ground State and Lowest-Energy Vibrationally Excited States, ν_{20} and ν_{30}. *J. Mol. Spectrosc.* **2020**, *369*, 111274.

(7) Kougias, S. M.; Knezz, S. N.; Owen, A. N.; Sanchez, R. A.; Hyland, G. E.; Lee, D. J.; Patel, A. R.; Esselman, B. J.; Woods, R. C.; McMahon, R. J. Synthesis and Characterization of Cyanobutadiene Isomers—Molecules of Astrochemical Significance. *J. Org. Chem.* **2020**, *85*, 5787−5798.

(8) Zdanovskaia, M. A.; Dorman, P. M.; Orr, V. L.; Owen, A. N.; Kougias, S. M.; Esselman, B. J.; Woods, R. C.; McMahon, R. J. Rotational Spectra of Three Cyanobutadiene Isomers (C_5H_5N) of Relevance to Astrochemistry and Other Harsh Reaction Environments. *J. Am. Chem. Soc.*, in press.

(9) Zdanovskaia, M. A.; Esselman, B. J.; Kougias, S. M.; Patel, A. R.; Woods, R. C.; McMahon, R. J. The 130 − 370 GHz Rotational Spectrum of 2-Cyano-1,3-Butadiene − A Molecule of Astrochemical Relevance. Manuscript submitted.

(10) Charnley, S. B.; Kuan, Y.-J.; Huang, H.-C.; Botta, O.; Butner, H. M.; Cox, N.; Despois, D.; Ehrenfreund, P.; Kisiel, Z.; Lee, Y.-Y.; et al. Astronomical Searches for Nitrogen Heterocycles. *Adv. Space Res.* **2005**, *36*, 137−145.

(11) McGuire, B. A.; Burkhardt, A. M.; Kalenskii, S.; Shingledecker, C. N.; Remijan, A. J.; Herbst, E.; McCarthy, M. C. Detection of the Aromatic Molecule Benzonitrile (*c*-C_6H_5CN) in the Interstellar Medium. *Science* **2018**, *359*, 202−205.

(12) McGuire, B. A.; Loomis, R. A.; Burkhardt, A. M.; Lee, K. L. K.; Shingledecker, C. N.; Charnley, S. B.; Cooke, I. R.; Cordiner, M. A.; Herbst, E.; Kalenskii, S.; et al. Detection of Two Interstellar Polycyclic Aromatic Hydrocarbons via Spectral Matched Filtering. *Science* **2021**, *371*, 1265−1269.

(13) McCarthy, M. C.; Lee, K. L. K.; Loomis, R. A.; Burkhardt, A. M.; Shingledecker, C. N.; Charnley, S. B.; Cordiner, M. A.; Herbst, E.; Kalenskii, S.; Willis, E. R.; et al. Interstellar Detection of the Highly Polar Five-Membered Ring Cyanocyclopentadiene. *Nat. Astron.* **2021**, *5*, 176−180.

(14) Sun, B. J.; Huang, C. H.; Chen, S. Y.; Chen, S. H.; Kaiser, R. I.; Chang, A. H. H. Theoretical Study on Reaction Mechanism of Ground-State Cyano Radical with 1,3-Butadiene: Prospect of Pyridine Formation. *J. Phys. Chem. A* **2014**, *118*, 7715−7724.

(15) Morales, S. B.; Bennett, C. J.; Le Picard, S. D.; Canosa, A.; Sims, I. R.; Sun, B. J.; Chen, P. H.; Chang, A. H. H.; Kislov, V. V.; Mebel, A. M.; et al. A Crossed Molecular Beam, Low-Temperature Kinetics, and Theoretical Investigation of the Reaction of the Cyano Radical (CN) with 1,3-Butadiene (C_4H_6). A Route to Complex Nitrogen-Bearing Molecules in Low-Temperature Extraterrestrial Environments. *Astrophys. J.* **2011**, *742*, 26.

(16) Mishra, P.; Fritz, S. M.; Herbers, S.; Mebel, A. M.; Zwier, T. S. Gas-phase Pyrolysis of *trans* 3-Pentenenitrile: Competition Between Direct and Isomerization-Mediated Dissociation. *PCCP Phys. Chem. Chem. Phys.* **2021**, *23*, 6462−6471.

(17) McCarthy, M. C.; Lee, K. L. K.; Carroll, P. B.; Porterfield, J. P.; Changala, P. B.; Thorpe, J. H.; Stanton, J. F. Exhaustive Product Analysis of Three Benzene Discharges by Microwave Spectroscopy. *J. Phys. Chem. A* **2020**, *124*, 5170−5181.

(18) Tsukamoto, A.; Lichtin, N. N. Reactions of Active Nitrogen with Organic Substrates. I. The Monomeric Products of the Reaction with 1,3-Butadiene. *J. Am. Chem. Soc.* **1962**, *84*, 1601−1605.

(19) Thaddeus, P.; Vrtilek, J. M.; Gottlieb, C. A. Laboratory and Astronomical Identification of Cyclopropenylidene, C_3H_2. *Astrophys. J.* **1985**, *299*, L63−L66.

(20) Hollis, J. M.; Remijan, A. J.; Jewell, P. R.; Lovas, F. J. Cyclopropenone (*c*-H_2C_3O): A New Interstellar Ring Molecule. *Astrophys. J.* **2006**, *642*, 933−939.

(21) Dickens, J. E.; Irvine, W. M.; Ohishi, M.; Ikeda, M.; Ishikawa, S.; Nummelin, A.; Hjalmarson, Å. Detection of Interstellar Ethylene Oxide (*c*-C_2H_4O). *Astrophys. J.* **1997**, *489*, 753−757.

(22) McGuire, B. A.; Carroll, P. B.; Loomis, R. A.; Finneran, I. A.; Jewell, P. R.; Remijan, A. J.; Blake, G. A. Discovery of the Interstellar Chiral Molecule Propylene Oxide (CH_3CHCH_2O). *Science* **2016**, *352*, 1449−1452.

(23) Gardner, F. F.; Winnewisser, G. The Detection of Interstellar Vinyl Cyanide (Acrylonitrile). *Astrophys. J.* **1975**, *195*, L127−L130.

(24) Lovas, F. J.; Remijan, A. J.; Hollis, J. M.; Jewell, P. R.; Snyder, L. E. Hyperfine Structure Identification of Interstellar Cyanoallene toward TMC-1. *Astrophys. J.* **2006**, *637*, L37−L40.

(25) Broten, N. W.; MacLeod, J. M.; Avery, L. W.; Friberg, P.; Hjalmarson, A.; Hoglund, B.; Irvine, W. M. The Detection of Interstellar Methylcyanoacetylene. *Astrophys. J.* **1984**, *276*, L25−L29.

(26) Wilson, C. L. 17. Reactions of Furan compounds. Part IV. High-Temperature Decomposition of the Vapours of Tetrahydrofuronitrile and Methyl Tetrahydrofuroate to Give 2,3-Dihydrofuran and Cyclopropanealdehyde. *J. Chem. Soc.* **1945**, 58−61.

(27) Mauduit, M.; Kouklovsky, C.; Langlois, Y. Cyanomethylene Cyclopropane, a Useful Dipolarophile and Dienophile in [2+3] and [2+4] Cycloadditions. *Tetrahedron Lett.* **1998**, *39*, 6857−6860.

(28) Kleinbeck, F.; Toste, F. D. Gold(I)-Catalyzed Enantioselective Ring Expansion of Allenylcyclopropanols. *J. Am. Chem. Soc.* **2009**, *131*, 9178−9179.

(29) Amberger, B. K.; Esselman, B. J.; Stanton, J. F.; Woods, R. C.; McMahon, R. J. Precise Equilibrium Structure Determination of Hydrazoic Acid (HN_3) by Millimeter-wave Spectroscopy. *J. Chem. Phys.* **2015**, *143*, 104310.

(30) Esselman, B. J.; Amberger, B. K.; Shutter, J. D.; Daane, M. A.; Stanton, J. F.; Woods, R. C.; McMahon, R. J. Rotational Spectroscopy

of Pyridazine and its Isotopologs from 235−360 GHz: Equilibrium Structure and Vibrational Satellites. *J. Chem. Phys.* **2013**, *139*, 224304.
(31) Kisiel, Z.; Pszczółkowski, L.; Drouin, B. J.; Brauer, C. S.; Yu, S.; Pearson, J. C.; Medvedev, I. R.; Fortman, S.; Neese, C. Broadband Rotational Spectroscopy of Acrylonitrile: Vibrational Energies from Perturbations. *J. Mol. Spectrosc.* **2012**, *280*, 134−144.
(32) Kisiel, Z.; Pszczółkowski, L.; Medvedev, I. R.; Winnewisser, M.; De Lucia, F. C.; Herbst, E. Rotational Spectrum of *trans*−*trans* Diethyl Ether in the Ground and Three Excited Vibrational States. *J. Mol. Spectrosc.* **2005**, *233*, 231−243.
(33) Pickett, H. M. The Fitting and Prediction of Vibration-rotation Spectra with Spin Interactions. *J. Mol. Spectrosc.* **1991**, *148*, 371−377.
(34) Kisiel, Z. PROSPE—Programs for ROtational SPEctroscopy. http://info.ifpan.edu.pl/?kisiel/prospe.htm (accessed March 04, 2021).
(35) Frisch, M. J.; Trucks, G. W.; Schlegel, H. B.; Scuseria, G. E.; Robb, M. A.; Cheeseman, J. R.; Scalmani, G.; Barone, V.; Petersson, G. A.; Nakatsuji, H.; et al. *Gaussian 16*, rev C.01, Gaussian, Inc.: Wallingford, CT, USA, 2016.
(36) Schmidt, J. R.; Polik, W. F. *WebMO Enterprise*, version 20.0; WebMO LLC: Madison, WI, USA, 2020; http://www.webmo.net (accessed April 2021).
(37) Amberger, B. K.; Esselman, B. J.; Woods, R. C.; McMahon, R. J. Millimeter-wave Spectroscopy of Carbonyl Diazide, $OC(N_3)_2$. *J. Mol. Spectrosc.* **2014**, *295*, 15−20.
(38) Aitken, R. A.; Al-Awadi, N. A.; El-Dusouqui, O. M. E.; Farrell, D. M. M.; Kumar, A. Synthesis, Thermal Reactivity, and Kinetics of Stabilized Phosphorus Ylides. Part 2: [(Arylcarbamoyl)(cyano)-methylene]Triphenylphosphoranes and Their Thiocarbamoyl Analogues. *Int. J. Chem. Kinet.* **2006**, *38*, 496−502.

https://doi.org/10.1021/acs.jpca.1c03246
J. Phys. Chem. A 2021, 125, 5601−5614

Appendix C

Rotational Spectra of Three Cyanobutadiene Isomers (C_5H_5N) of Relevance to Astrochemistry and Other Harsh Reaction Environments

Maria A. Zdanovskaia
P. Matisha Dorman
Vanessa L. Orr
Andrew N. Owen
Samuel M. Kougias
Brian J. Esselman
R. Claude Woods
Robert J. McMahon

Journal of the American Chemical Society, 2021, *143*, 9551-9564

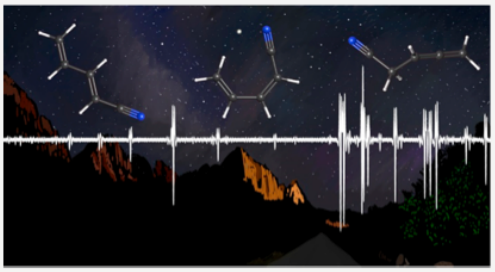
JACS
JOURNAL OF THE AMERICAN CHEMICAL SOCIETY
pubs.acs.org/JACS
Article

Rotational Spectra of Three Cyanobutadiene Isomers (C_5H_5N) of Relevance to Astrochemistry and Other Harsh Reaction Environments

Maria A. Zdanovskaia, P. Matisha Dorman, Vanessa L. Orr, Andrew N. Owen, Samuel M. Kougias, Brian J. Esselman, R. Claude Woods,* and Robert J. McMahon*

Cite This: J. Am. Chem. Soc. 2021, 143, 9551−9564
Read Online
ACCESS | Metrics & More | Article Recommendations | Supporting Information

ABSTRACT: Three cyanobutadiene isomers have been synthesized and their rotational spectra analyzed in the 130−375 GHz frequency range. These species, which are close analogues of known interstellar molecules and are isomers of the heterocyclic aromatic molecule pyridine (C_5H_5N), offer the opportunity of revealing important insights concerning the chemistry in astronomical environments. The *s-trans* conformers of *E*-1-cyano-1,3-butadiene and *Z*-1-cyano-1,3-butadiene are observed, while both the *anti-clinal* and *syn-periplanar* conformers of 4-cyano-1,2-butadiene are evident in the rotational spectra. Over 1000 transitions for *s-trans-Z*-1-cyano-1,3-butadiene and for *syn-periplanar*-4-cyano-1,2-butadiene are fit to an octic, distorted-rotor Hamiltonian with low uncertainty (<50 kHz). Although neither *s-trans-E*-1-cyano-1,3-butadiene nor *anti-clinal*-4-cyano-1,2-butadiene can be fully treated with a distorted-rotor Hamiltonian in this frequency range, we provide herein minimally perturbed, single-state least-squares fits of over 1000 transitions for each species, yielding sets of spectroscopic constants that are expected to enable accurate prediction of high-intensity transitions at frequencies up to 370 GHz for both isomers. The assigned transitions and spectroscopic constants for these cyanobutadienes have already enabled the identification of two isomers in harsh reaction environments and should be sufficient to enable their identification in astronomical environments by radio astronomy.



INTRODUCTION

Organic nitriles occupy a significant place in the field of astrochemistry. Their large molecular dipole moments confer rotational transitions with significant intensity, which facilitates identification of these species by radio astronomy. Recent detections of benzonitrile, the cyano-1,3-cyclopentadienes, and the cyanonaphthalenes represent a dramatic breakthrough in the field,[1−3] revealing a glimpse of simple aromatic compounds in astronomical environments.[4] We have been keenly interested in both structural and chemical relationships between open-chain organic nitriles and their cyclic counterparts for some time.[5] In the current investigation, we report millimeter-wave rotational spectra of three isomers of cyanobutadiene, which are also isomers of the heterocyclic aromatic molecule pyridine (C_5H_5N).

Radio astronomy is the primary method of detecting molecules and ions in the interstellar medium (ISM) and circumstellar shells.[6,7] With their large dipole moments, nitriles (R−CN) are well represented in the list of ∼220 species detected in space. The isomeric isocyanides/isonitriles (R−NC) are also polar, and many have been detected in the ISM despite being higher in energy by ∼21 kcal/mol. The list of astronomically detected nitriles reveals variety in chain length[8−12] −from hydrogen cyanide (HCN)[11] to cyanodecapentayne ($HC_{11}N$)[13] −as well as a variety in the level of saturation.[14−20] Of particular interest to the current work are vinyl cyanide (C_3H_3N; acrylonitrile),[15] cyanoallene (C_4H_3N),[17] and cyanodiacetylene (HC_5N),[8] which share structural elements with the cyanobutadiene isomers (C_5H_5N) of interest: *E*-1-cyano-1,3-butadiene, *Z*-1-cyano-1,3-butadiene, and 4-cyano-1,2-butadiene (Figure 1).

The structural similarity, and the fact that both smaller and larger carbon-chain nitriles are known in extraterrestrial environments, suggest that the cyanobutadiene isomers described in this work represent plausible targets for detection in the ISM. Recent studies examined potential routes to their formation. McCarthy *et al.* analyzed the products generated by electrical discharge of benzene and molecular nitrogen and identified both *E*- and *Z*-1-cyano-1,3-butadiene isomers in the product spectra (Figure 2a).[21] Zwier and co-workers

Received: April 9, 2021
Published: June 22, 2021



ACS Publications
© 2021 American Chemical Society

https://doi.org/10.1021/jacs.1c03777
J. Am. Chem. Soc. 2021, 143, 9551−9564

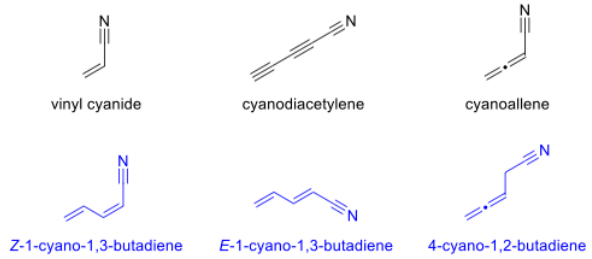


Figure 1. Molecules studied in this work (blue): *Z*-1-cyano-1,3-butadiene, *E*-1-cyano-1,3-butadiene, and 4-cyano-1,2-butadiene. Nitriles with similar structures that have been detected in the interstellar medium (black): vinyl cyanide, cyanodiacetylene, and cyanoallene.

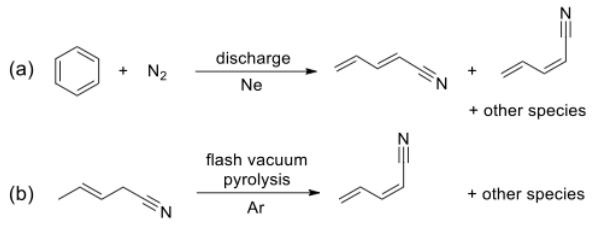


Figure 2. (a) Discharge of benzene and nitrogen produces *E*-1-cyano-1,3-butadiene and *Z*-1-cyano-1,3-butadiene.[21] (b) Pyrolysis of 1-cyano-2-butene produces *Z*-1-cyano-1,3-butadiene.[22]

investigated the gas-phase pyrolysis of *trans*-3-pentenenitrile, which results in dehydrogenation to afford *Z*-1-cyano-1,3-butadiene, among many products (Figure 2b). Notably, pyridine was not detected, despite being lower in energy than the detected cyanobutadiene isomer.[22] The spectroscopic assignments in both of these experiments were made on the basis of data reported herein. Much earlier, Tsukamoto and Lichtin observed *E*- and *Z*-1-cyano-1,3-butadiene as products in a reaction between 1,3-butadiene and nitrogen activated via microwave discharge.[23] They noted the possibility that this reaction involves cyano radical as the primary intermediate. More recent theoretical and experimental studies indicate the reaction between cyano radical and 1,3-butadiene produces *E*-1-cyano-1,3-butadiene, despite the open-chain molecule being less thermodynamically favorable than pyridine.[24,25] Although the cyano radical has been known in the ISM for decades,[26] 1,3-butadiene has not been detected. The predominant *s-trans* conformer does not possess a dipole moment, while the small dipole moment in the higher energy *syn* conformation makes it a difficult astronomical target.[27] Balucani *et al.* suggested that the reaction of cyano radical with an unsaturated hydrocarbon species is a highly plausible route to formation of the nitriles in the ISM, and that the detection of a particular unsaturated hydrocarbon can be used to predict the presence of the corresponding nitrile.[28] Given the small dipole moment of 1,3-butadiene, however, it seems that the detection of the 1-cyano-1,3-butadiene isomers could better serve as potential tracers for 1,3-butadiene. A theoretical study by Jamal and Mebel[29] suggested that reaction of cyano radical with 1,2-butadiene would preferentially form 2-cyano-1,3-butadiene (C_5H_5N),[30] 1-cyano-3-propyne (C_4H_3N), or cyanoallene (C_4H_3N) and not 4-cyano-1,2-butadiene. This does not preclude, however, generation of 4-cyano-1,2-butadiene by other reaction pathways.

The ISM is not the only location where detection of the cyanobutadiene isomers could be informative. Saturn's largest moon, Titan, possesses a nitrogen atmosphere with complex atmospheric chemistry and photochemistry. The atmospheric chemistry of Titan has been suggested to be relevant to prebiotic Earth.[31] Small neutral nitriles, as well as their anions, have been detected in Titan's atmosphere and are implicated in the formation of tholins,[32−34] the organic polymers responsible for the reddish haze of various bodies in our solar system and suggested as potential prebiotic precursors in the presence of water. Pyrolysis of tholin analogues produces 1-cyano-1,3-butadiene.[35,36] Data from the Cassini−Huygens probe also suggests the presence of benzene,[32,33] and data from the Atacama Large Millimeter Array (ALMA) recently revealed the presence of cyclopropenylidene.[37] It is likely that other aromatics like pyridine or its isomers could be detected in this environment.

With respect to astrochemistry, electrical discharge, or other harsh reaction environments, the cyanobutadiene isomers (Figure 1) are important in that they may be considered proxies for pyridine. Pyridine is an aromatic molecule of substantial astrochemical interest that has thus far eluded detection in the ISM.[38] The cyanobutadiene isomers are more polar (μ = 3.7−4.7 D), and therefore more readily detectable, than pyridine (μ = 2.2 D). Mechanistically, it is not known whether the cyanobutadiene isomers might represent precursors to pyridine or decomposition products of pyridine, but the detection of any isomer of pyridine (C_5H_5N) would represent a significant observation in astrochemistry.[39−41] Pyridine is nearly 23.2 kcal/mol lower in energy than *E*-1-cyano-1,3-butadiene, which itself is 0.3 and 16.3 kcal/mol lower in energy than *Z*-1-cyano-1,3-butadiene and 4-cyano-1,2-butadiene (B3LYP/6-311+G(2d,p)), respectively. Pyridine is a building block of nicotinic acid (vitamin B3) and nicotinamide, which are precursors to a key coenzyme used in metabolism, nicotinamide adenine dinucleotide (NAD).[42] A possible route to interstellar formation of nicotinic acid from pyridine has been suggested,[43] and nicotinic acid of interstellar origin has been detected on the Murchison meteorite.[44,45] Identification of extraterrestrial pyridine could assist our understanding of prebiotic chemistry occurring in extreme environments as well as our understanding of formation of nitrogen-containing polycyclic aromatic hydrocarbons (NPAHs), in which pyridine has been suggested as a precursor.[46]

Herein, we present a detailed analysis of the rotational spectra of the ground vibrational states of *E*-1-cyano-1,3-butadiene, *Z*-1-cyano-1,3-butadiene, and 4-cyano-1,2-butadiene in the 130−375 GHz frequency range. These experimental studies are predicated on the availability of pure samples of the neat materials, which is not an inconsequential matter.[47] These laboratory measurements provide the foundation for spectroscopic studies of astronomical and other harsh reaction environments. Interstellar detection involves astronomical measurement of either (i) transitions that have been directly measured in the laboratory or (ii) transitions that have been predicted, with high precision, on the basis of experimentally determined spectroscopic constants. The transition frequencies and spectroscopic constants determined in the current investigation provide a sufficient basis for radio astronomy searches for these species from radio- to millimeter-wave frequencies.

https://doi.org/10.1021/jacs.1c03777
J. Am. Chem. Soc. 2021, 143, 9551−9564

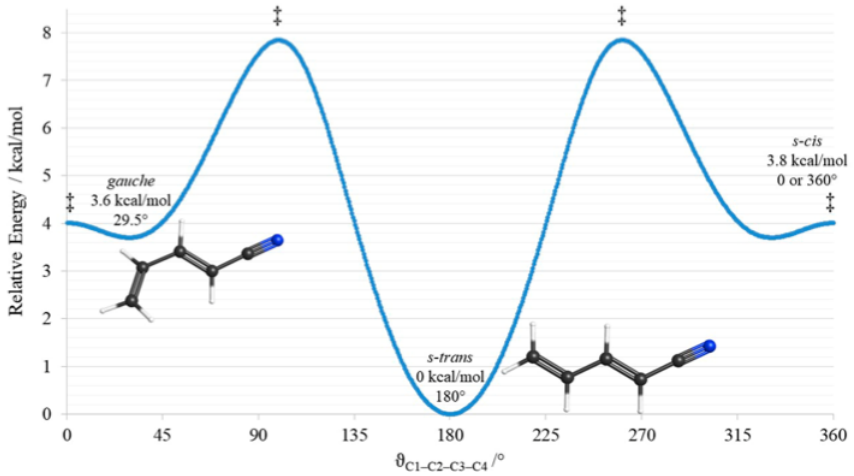


Figure 3. Computed conformational potential energy surface of *E*-1-cyano-1,3-butadiene (B3LYP/6-311+G(2d,p)).

MATERIALS AND METHODS

Experimental Methods. The cyanobutadiene isomers were synthesized in our lab as described previously.[47] Spectra were collected on a broadband spectrometer using 3−13 mTorr sample pressures in a flow system at 0 to −50 °C. Liquid samples of all three cyanobutadiene isomers were kept in ice−water baths to minimize sample degradation. The (high) purity of each sample was established on the basis of ^{1}H NMR and mass spectra.[47] No impurities were evident in the rotational spectra. Transitions observed in the rotational spectra are associated with the designated molecule (ground state, vibrationally excited states, isotopologues detectable in natural abundance, and minor conformational isomers). The 130−230 and 235−375 GHz spectra were collected by using an instrument described previously[48,49] and two separate Virginia Diodes amplification and multiplication chains and zero-bias detectors. The spectra were combined into a single broadband spectrum by using Assignment and Analysis of Broadband Spectra (AABS) software.[50,51] Pickett's SPFIT/SPCAT programs[52] and Kisiel's ASFIT/ASROT[50,51] were used to conduct least-squares fitting and spectral prediction. PIFORM, PLANM, and AC programs[53] were used for data analysis, file formatting, and generating various plots and graphics.

In our least-squares fits, we assume a uniform frequency measurement uncertainty of 50 kHz for our data. Transitions from McCarthy *et al.*[21] use an uncertainty of 2 kHz, and those from Mishra *et al.*[22] use 60 kHz.

Computational Methods. Computations were performed at the B3LYP/6-311+G(2d,p) level of theory by using Gaussian 16.[54] Optimized geometries were obtained by using "verytight" convergence criteria and an "ultrafine" integration grid for each of the energy-minimized conformers of *E*-1-cyano-1,3-butadiene, *Z*-1-cyano-1,3-butadiene, and 4-cyano-1,2-butadiene. Anharmonic vibrational frequency calculations provided predictions of vibration−rotation interaction constants and quartic and sextic centrifugal distortion constants, as well as fundamental frequencies of the vibrationally excited states. Coordinate scans for rotation about the C2−C3 bond for the 1-cyano-1,3-butadiene isomers and the C3−C4 bond for 4-cyano-1,2-butadiene were computed at the same level of theory. Computational output files are provided in the Supporting Information.

RESULTS AND DISCUSSION

Analysis of Rotational Spectra. *E-1-Cyano-1,3-butadiene.* *E*-1-Cyano-1,3-butadiene exhibits two low-energy conformations: *s-trans* and *gauche*, depicted on the conformational potential energy surface in Figure 3. The latter conformer has a predicted C1−C2−C3−C4 dihedral angle of 29.5°, which is reasonably close to the corresponding dihedral angle experimentally determined for 1,3-butadiene (33.8 ± 1.3°).[27] *s-trans-E*-1-Cyano-1,3-butadiene is favored by ∼3.6 kcal/mol or 1259 cm^{-1} (B3LYP/6-311+G(2d,p)) and is observed in the rotational spectrum. The predicted energy difference in the conformers indicates that the *gauche* conformer is ∼0.3% as abundant as the *s-trans* at room temperature. Although the transition intensity of the *gauche* conformer would be statistically doubled by the presence of enantiomers, the small energy barrier between the two conformations (0.2 kcal/mol or 70 cm^{-1}; B3LYP) would possibly result in tunneling splitting, diminishing the transition intensity. These factors, taken together with the similar dipole moments of the *gauche* (μ_a = 4.6 D, μ_b = 0.2 D, μ_c = 0.2 D) and the *s-trans* (μ_a = 4.6 D, μ_b = 1.0 D) conformer and the very dense spectrum of *s-trans-E*-1-cyano-1,3-butadiene, make it unsurprising that *gauche-E*-1-cyano-1,3-butadiene was not observed in the rotational spectrum.

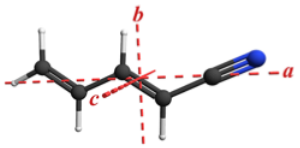


Figure 4. *s-trans-E*-1-Cyano-1,3-butadiene structure with principal inertial axes (μ_a = 4.6 D, μ_b = 1.0 D).

The *s-trans* conformer of *E*-1-cyano-1,3-butadiene, depicted in Figure 4, is a planar (C_s), prolate (κ = −0.99), asymmetric top with its dipole moment predominantly along the *a* principal axis. The lowest-energy vibrationally excited state is predicted to be 137 cm^{-1} higher in energy than the ground state and is close in energy to the second-lowest energy vibrationally excited state (141 cm^{-1}).

The rotational spectrum of *s-trans-E*-1-cyano-1,3-butadiene in the 130−370 GHz region is dominated by $^aR_{0,1}$ transitions that appear in clusters of transitions sharing a single *J* value. A small portion of the spectrum is shown in Figure 5. Such a band structure is typical for a highly prolate, asymmetric top, and bands throughout our spectral region follow the same pattern. Although the K_a = 0 and 1 transitions of the J'' + 1 = 119 series appear near the middle of this region, and several

https://doi.org/10.1021/jacs.1c03777
J. Am. Chem. Soc. 2021, 143, 9551−9564

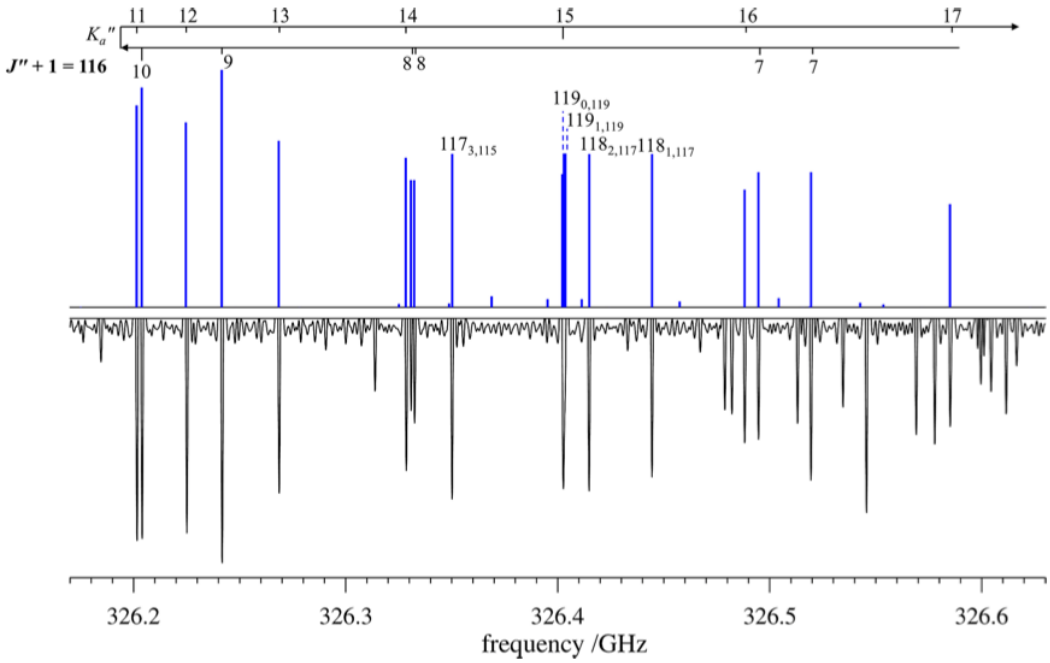


Figure 5. Rotational spectrum of *s-trans-E*-1-cyano-1,3-butadiene from 326.17 to 326.63 GHz (bottom) and stick spectrum of the ground vibrational state transitions (top). The upper state J (*i.e.*, $J'' + 1$) value for most transitions in this region is 116; K_a values for this series are denoted at the top. The upper state quantum numbers of the five $^aR_{0,1}$ transitions not belonging to the $J'' + 1 = 116$ series are marked immediately above their stick spectrum positions. Many transitions belonging to other vibrational satellites are also visible in the experimental spectrum.

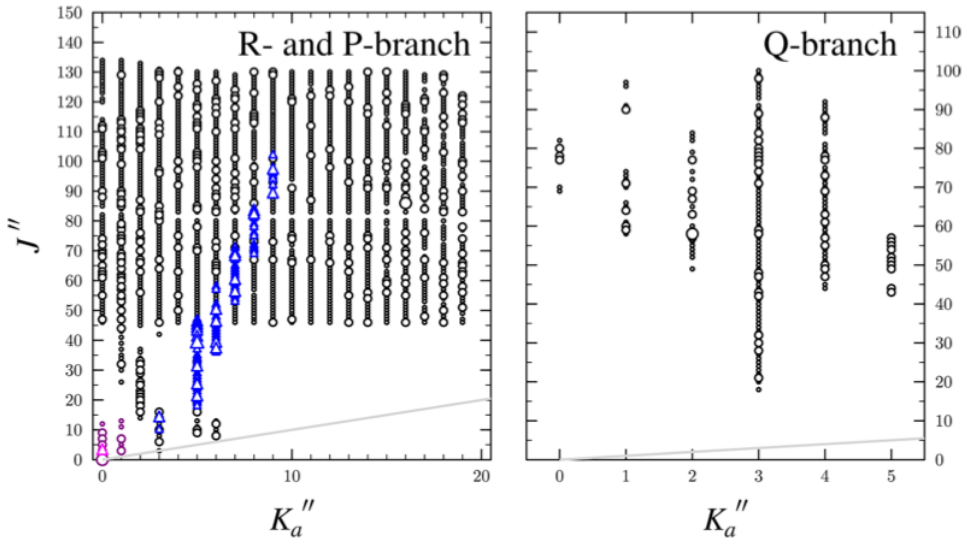


Figure 6. Data distribution plot for the minimally perturbed least-squares fit of spectroscopic data from the current work (black and blue) and measurements from McCarthy *et al.*[21] (purple and magenta) for the vibrational ground state of *s-trans-E*-1-cyano-1,3-butadiene. Circles indicate Q- and R-branch transitions. Triangles indicate P-branch transitions. The size of the plotted symbol is proportional to the value of $|(f_{obs} - f_{calc})/\delta f|$, where δf is the frequency measurement uncertainty; all values shown are smaller than 3.

transitions with increasing values of K_a and decreasing J are present, the majority of the transitions in the cluster have a value of $J'' + 1 = 116$. The $K_a = 0$ transition of the $J'' + 1 = 116$ series appears ~8 GHz lower in frequency than the depicted spectral region and is not degenerate with any other transition. With increasing values of K_a, transitions appear at higher frequencies up to ~329.5 GHz, which marks a turnaround at $K_a = 4$. Transitions sharing the same values of J and K_a, but with values of K_c differing by one, become degenerate at $K_a = 9$ for the given series. Another turnaround, which appears in the depicted spectral region, occurs at $K_a = 11$. Other bands in our frequency region follow a similar pattern. Though they are less intense than the *a*-type transitions, *b*-type R-branch transitions are also observed. Q-branch transitions, which occur in clusters

https://doi.org/10.1021/jacs.1c03777
J. Am. Chem. Soc. 2021, 143, 9551−9564

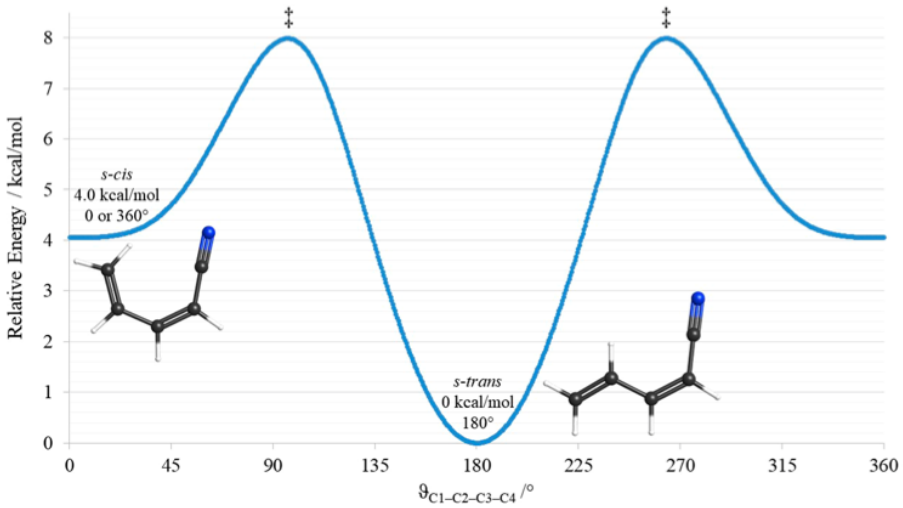


Figure 7. Computed conformational potential energy surface of *Z*-1-cyano-1,3-butadiene (B3LYP/6-311+G(2d,p)).

Table 1. Experimental and Computational Spectroscopic Constants for the Ground Vibrational State of *s-trans-E*-1-Cyano-1,3-butadiene (C_5H_5N) (S-Reduced Hamiltonian, I^r Representation)

	B3LYP[a]	experimental[b,c]
A_0 (MHz)	27003	26243.02934 (59)
B_0 (MHz)	1437	1443.620880 (19)
C_0 (MHz)	1364	1368.119206 (18)
D_J (kHz)	0.11	0.1208886 (39)
D_{JK} (kHz)	−14.9	−15.71829 (18)
D_K (kHz)	1107.1	1106.785 (15)
d_1 (kHz)	−0.016	−0.01794561 (99)
d_2 (kHz)	−0.00029	−0.00041621 (28)
H_J (Hz)	0.000068	0.00008551 (35)
H_{JK} (Hz)	−0.015	−0.017117 (23)
H_{KJ} (Hz)	−0.199	−0.0618 (14)
H_K (Hz)	73.1	69.63 (11)
h_1 (Hz)	0.000021	0.000024998 (45)
h_2 (Hz)	0.00000068	0.000001168 (28)
h_3 (Hz)	0.00000038	0.000000544 (15)
L_J (μHz)		−0.000129 (10)
L_{JJK} (μHz)		0.02058 (75)
L_{JK} (μHz)		−2.594 (47)
L_{KKJ} (μHz)		−238.5 (39)
χ_{aa} (MHz)	−3.7[d]	−3.329 (19)
χ_{bb} (MHz)	1.5[d]	1.280 (25)
Δ_i (uÅ^2)[e,f]		0.061888 (7)
N_{lines}[g]		2644
σ_{fit} (MHz)		0.036

[a]Evaluated with the 6-311+G(2d,p) basis set. [b]Global fit to the present minimally perturbed millimeter wave measurements (2600 independent transitions) and the available literature data (44 independent transitions from McCarthy *et al.*[21]). [c]Constants not shown explicitly were held fixed at a value of zero. [d]Constants converted from the field gradient axis system to the inertial moment axis system. [e]Inertial defect, $\Delta_i = I_c - I_a - I_b$. [f]Calculated by using PLANM from the B_0 constants. [g]Number of fitted transition frequencies.

sharing the same K_a value, and widely spaced P-branch transitions are also observed in the spectrum.

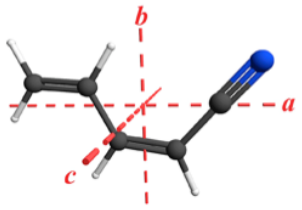


Figure 8. *s-trans-Z*-1-Cyano-1,3-butadiene structure with principal inertial axes (μ_a = 3.6 D, μ_b = 2.3 D).

Although the rotational spectrum of *s-trans-E*-1-cyano-1,3-butadiene appears well-behaved at low K_a, those series near K_a = 20 appear curved in Loomis–Wood plots and increasingly deviate from predicted frequencies at higher values of *J*. While many such series of R-, Q-, and P-branch transitions can be assigned, it is clear that their energy levels are perturbed and thus not amenable to a single-state least-squares fit. Many of these assignable, but highly perturbed transitions are excluded from the data set provided here (*vide infra*). Assigned transitions in the data set provided here include R-branch transitions ranging in J'' from 3 to 134 and in K_a'' from 0 to 19, Q-branch transitions with values of J'' from 18 to 100 and K_a'' from 0 to 5, and P-branch transitions with values of J'' from 3 to 102 and K_a'' from 3 to 9. Although this is not a complete transition list and transitions could certainly be added if the spectrum were properly analyzed with a Hamiltonian addressing the coupling, the most intense transitions—those that would be most useful to anyone seeking this molecule in a reaction or extraterrestrial spectrum—are assigned and included in the data provided here. A coupled-state least-squares fit is in progress. In an attempt to acquire minimally perturbed, reasonably realistic constants, we excluded all transitions with $K_a'' \geq 20$, numerous transitions with $K_a'' > 15$ at high *J*, and transitions with error greater than 0.1 MHz. A data distribution plot demonstrating the breadth of data included in this minimally perturbed least-squares fit is presented in Figure 6.

In this work, we provide a set of spectroscopic constants that includes a full set of quartic and sextic centrifugal distortion constants, along with a partial set of octic constants, for *s-trans-*

https://doi.org/10.1021/jacs.1c03777
J. Am. Chem. Soc. 2021, 143, 9551−9564

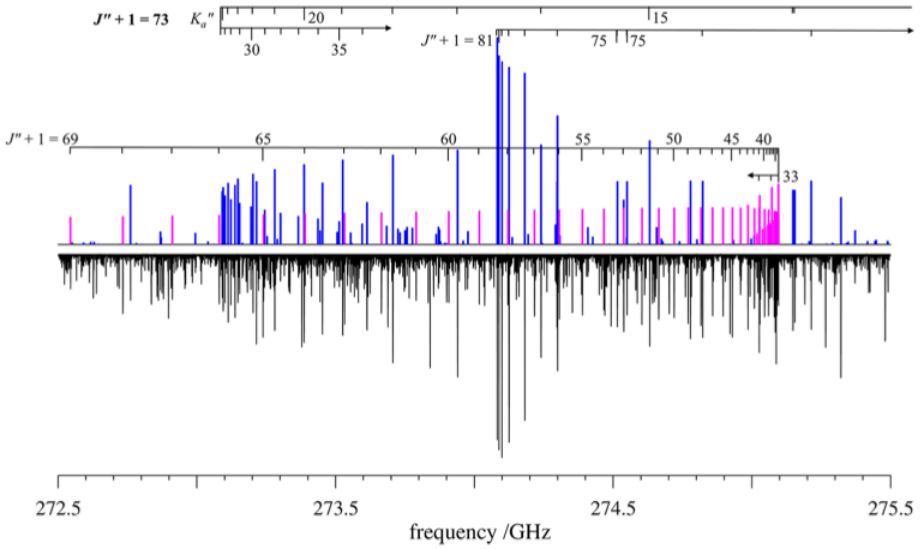


Figure 9. Rotational spectrum of *s-trans-Z*-1-cyano-1,3-butadiene from 272.50 to 275.50 GHz (bottom) and stick spectrum of the ground vibrational state transitions (top). Blue transitions denote R-branch transitions, while magenta transitions belong to the Q-branch. The upper state J (*i.e.*, J'' + 1) values are marked immediately above their stick spectrum positions. Many transitions belonging to other vibrational satellites are also visible in the experimental spectrum.

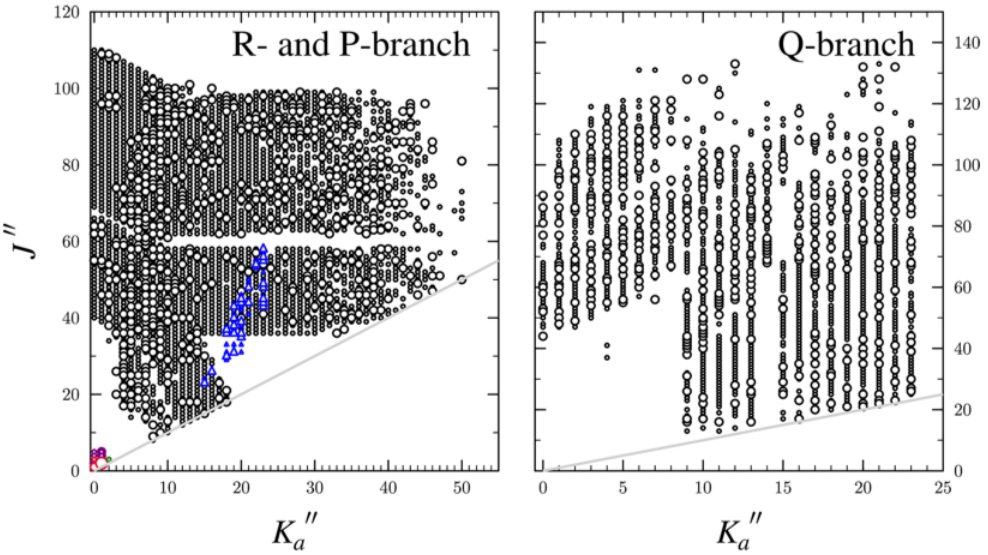


Figure 10. Data distribution plot for the least-squares fit of spectroscopic data from the current work (black and blue), measurements from McCarthy *et al.*[21] (purple and red, due to the high relative error), and measurements from Mishra *et al.*[22] (green) for the vibrational ground state of *s-trans-Z*-1-cyano-1,3-butadiene. Circles indicate Q- and R-branch transitions. Triangles indicate P-branch transitions. The size of the plotted symbol is proportional to the value of $|(f_{obs} - f_{calc})/\delta f|$, where δf is the frequency measurement uncertainty. For several precisely measured low-J'' and low-K_a transitions, the relative error is greater than 3 (red).

E-1-cyano-1,3-butadiene, fit with low error (σ_{fit} = 0.036 MHz). Although this least-squares fit does not address the coupling observed in our frequency range, we expect that the constants are minimally affected by perturbation and physically meaningful. A comparison of the predicted rotational and distortion constants with those from the minimally perturbed least-squares fit is provided in Table 1, and the resultant fit file is provided in the Supporting Information. The predicted rotational constants are within 3% of the minimally perturbed fit constants, and the quartic distortion constants, with the exception of d_2, are within 11%. Meanwhile, d_2 deviates from the experimental value by 31%, but its value is also quite small—100× smaller than the next smallest quartic distortion constant. As a result, it is correspondingly difficult to predict its value with a small relative error. This situation is, in fact, very similar to that observed for *syn*-2-cyano-1,3-butadiene.[30] The sextic distortion constants are also well predicted and within 42% of the effective fit values, except H_{KJ}, which is about 3 times larger than its experimental value. The predicted constants are in good agreement with those determined

https://doi.org/10.1021/jacs.1c03777
J. Am. Chem. Soc. 2021, 143, 9551−9564

Table 2. Experimental and Computational Spectroscopic Constants for the Ground Vibrational State of *s-trans-Z*-1-Cyano-1,3-butadiene (C_5H_5N) (S-Reduced Hamiltonian, I^r Representation)

	B3LYP[a]	experimental[b]
A_0 (MHz)	10155	9759.44594 (25)
B_0 (MHz)	1983	2039.686938 (29)
C_0 (MHz)	1658	1686.177389 (28)
D_J (kHz)	0.75	0.8175616 (81)
D_{JK} (kHz)	−12.3	−11.904999 (55)
D_K (kHz)	78.0	68.8804 (15)
d_1 (kHz)	−0.22	−0.2426311 (30)
d_2 (kHz)	−0.0090	−0.01140453 (74)
H_J (Hz)	0.000799	0.0007551 (11)
H_{JK} (Hz)	0.0027	0.0076984 (74)
H_{KJ} (Hz)	−0.385	−0.390414 (51)
H_K (Hz)	2.45	2.1490 (35)
h_1 (Hz)	0.000395	0.00039284 (36)
h_2 (Hz)	0.000058	0.00007271 (15)
h_3 (Hz)	0.0000113	0.000014285 (32)
L_J (μHz)		0.000709 (46)
L_{JJK} (μHz)		−0.08232 (29)
L_{JK} (μHz)		−0.0230 (43)
L_{KKJ} (μHz)		13.293 (17)
L_K (μHz)		−97.1 (2.8)
l_1 (μHz)		0.000237 (13)
l_2 (μHz)		−0.0002057 (77)
l_3 (μHz)		−0.0000505 (28)
l_4 (μHz)		−0.00001450 (55)
χ_{aa} (MHz)	−0.8[c]	−0.3586 (55)
χ_{bb} (MHz)	−1.4[c]	−1.651 (15)
Δ_i (uÅ^2)[d,e]		0.162360 (6)
N_{lines}[f]		5531
σ_{fit} (MHz)		0.038

[a]Evaluated with the 6-311+G(2d,p) basis set. [b]Global fit to the present millimeter wave measurements (5495 independent transitions) and the available literature data (34 independent transitions from McCarthy *et al.*[21] and 2 independent transitions from Mishra *et al.*[22]). [c]Constants converted from the field gradient axis system to the inertial moment axis system. [d]Inertial defect, $\Delta_i = I_c - I_a - I_b$. [e]Calculated by using PLANM from the B_0 constants. [f]Number of fitted transition frequencies.

experimentally. There are no computational or previously determined octic centrifugal distortion constants to serve as an external reference, but we believe the octic constants determined here do not serve as strictly empirical corrections, nor do they absorb unaddressed perturbations because of the previously described efforts to avoid effects of perturbation.

The quadrupole coupling constants presented in Table 1 are obtained by including the low-frequency, hyperfine-resolved data from McCarthy *et al.*[21] in our least-squares fit. No new hyperfine-resolved transitions were added in the current work, as transitions affected by the nitrogen quadrupole are not resolvable in our frequency range. The values reported here vary somewhat from those based solely on the lower-frequency data due to our more accurate determination of the distortion constants, which decreases the convolution of quadrupole coupling and distortion in the least-squares fit. The small, but nonzero, value of the inertial defect (Δ_i) is within the range expected for a planar molecule. Although the inertial defect derived from the *equilibrium* rotational constants of a planar molecule should be precisely zero, the *measured* rotational constants reported in Table 1 are affected by vibration−rotation interaction and the electron-mass distribution in the molecule.

Z-1-Cyano-1,3-butadiene. *Z*-1-Cyano-1,3-butadiene is predicted to exhibit two low-energy conformations: *s-trans* and *s-cis*, depicted on the conformational potential energy surface in Figure 7. It is well established that B3LYP calculations tend to overestimate stabilization due to π conjugation, so it is conceivable that the *s-cis* conformation may actually be a transition state separating enantiomeric *gauche* conformers, in a situation analogous to that predicted for the *E*-isomer and observed for 1,3-butadiene.[27] The *s-cis* conformer is 4.0 kcal/mol (1399 cm^{-1}) higher in energy than the *s-trans* conformer, which would make the former ∼0.1% the abundance of the latter at room temperature. Considering also the comparable dipole moment of the *s-cis* conformer (μ_a = 3.7, μ_b = 2.4) relative to the *s-trans* (μ_a = 3.6 D, μ_b = 2.3 D) and the possibility of tunneling splitting if the *s-cis* conformer is indeed a transition state, it is not surprising that the *s-trans* conformer is the only species observed in the rotational spectrum.

s-trans-Z-1-Cyano-1,3-butadiene, depicted in Figure 8, is a prolate (κ = −0.91), asymmetric top with C_s symmetry. The lowest-energy vibrationally excited state is predicted to be 129 cm^{-1} higher in energy than the ground state and is close in energy to the second-lowest-energy vibrationally excited state (135 cm^{-1}).

In our frequency region, the most intense rotational transitions in the ground vibrational state are part of the oblate-structure R-branch bandhead, where *a*- and *b*-type transitions ($^aR_{0,1}$, $^bR_{1,1}$, and $^bR_{1,-1}$) with the same value of K_c are quadruply degenerate. An example of such a bandhead is provided in Figure 9. Near the bandhead, transitions with increasing values of K_a occur at higher frequency and become nondegenerate. Because of the substantial *a*- and *b*-dipole moments, both types of transitions are observed, even when they are nondegenerate. Eventually, $^aR_{0,1}$ transitions with the same value of K_a become degenerate and coalesce into rolate series with the same values of J, as do $^bR_{1,1}$ with $^bR_{1,-1}$ transitions. Such a prolate ^{a}R-branch series for $J'' + 1 = 73$ is also apparent in the spectrum in Figure 9. Q-branch and P-branch transitions are visible across our spectral region as well.

Notably different between the *s-trans* conformers of *Z*- and *E*-1-cyano-1,3-butadiene is the apparent lack of coupling in the ground state of the *Z* isomer. The ground-state rotational spectrum of *s-trans-Z*-1-cyano-1,3-butadiene was successfully fit to a full octic, distorted-rotor Hamiltonian with low error (σ_{fit} = 0.039 MHz). A total of 5495 new independent transitions were assigned in the 130−375 GHz frequency region. The full data set, including recently reported transitions from McCarthy *et al.*[21] and Mishra *et al.*,[22] encompasses R-branch transitions with K_a values ranging from 0 to 50 and J'' values from 1 to 110 with no evidence of perturbation. Numerous *a*- and *b*-type Q-branch series, with J'' values from 13 to 133 and K_a values from 0 to 23, were fit, along with a few weak P-branch transitions with J'' values ranging from 23 to 58 and K_a values from 15 to 23. The data distribution plot for transitions of *s-trans-Z*-1-cyano-1,3-butadiene fit in this work is provided in Figure 10.

The current work provides spectroscopic constants, including full sets of sextic and octic centrifugal distortion constants, for *s-trans-Z*-1-cyano-1,3-butadiene (Table 2; S reduction, I^r representation). The resultant fit files and a comparison of A reduction constants to those recently

https://doi.org/10.1021/jacs.1c03777
J. Am. Chem. Soc. 2021, 143, 9551−9564

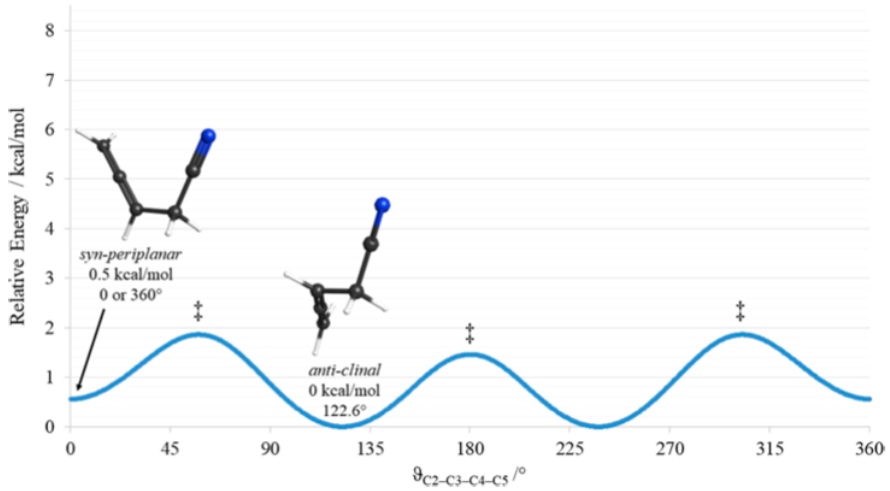


Figure 11. Computed conformational potential energy surface of 4-cyano-1,2-butadiene (B3LYP/6-311+G(2d,p)).

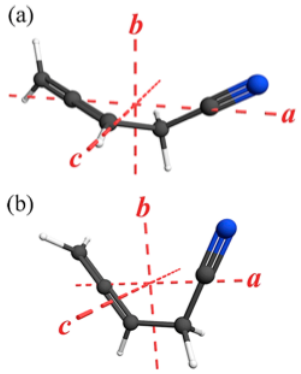


Figure 12. 4-Cyano-1,2-butadiene structures with principal inertial axes: (a) *anti-clinal* (μ_a = 3.6 D, μ_b = 1.9 D, μ_c = 0.6 D) and (b) *syn-periplanar* (μ_a = 2.0 D, μ_b = 3.1 D).

published by McCarthy *et al.*[21] are provided in the Supporting Information. The experimentally determined distortion constants are expected to be physically meaningful and accurate in view of the very large number of transitions and lack of observed perturbation. Overall, the spectroscopic constants predicted by the B3LYP anharmonic calculation are reasonably good estimates of the experimental constants. The predicted rotational constants are within 4.2% of the experimentally determined values. The quartic centrifugal distortion constants are predicted within 21.4%, which is the error on the smallest of the constants, and the sextic constants are predicted to within 65% of their experimentally determined values. Again, no computational software currently predicts the octic centrifugal distortion constants, and no published data are available that would provide an external comparison. Data for the quadrupole coupling constants are based on the hyperfine-resolved transitions measured by McCarthy *et al.*[21] These values are very close to those based solely on the lower-frequency data (in fact, these values are within the uncertainty of the previous values), and the slight difference can be attributed to the improved determination of the distortion constants in this work. The value of the inertial defect (Δ_i) for the *Z* isomer is reasonable for a planar molecule. The difference between the inertial defects for the *Z* and *E* isomers (~0.1 uÅ^2) is likely due to differences in vibration−rotation interactions and is not indicative of structural differences, *i.e.*, degree of deviation from planarity.

4-Cyano-1,2-butadiene. 4-Cyano-1,2-butadiene exhibits two low-energy conformations: *syn-periplanar* (*syn-*) and *anti-clinal* (*anti-*), depicted on the conformational potential energy surface in Figure 11. The computed energy difference between the two conformers is quite small; the *syn-periplanar* conformer is only ~0.5 kcal/mol (175 cm^{-1}) higher in energy than the *anti-clinal* conformer—a value that is within the uncertainty of the level of theory employed. As a consequence of the small energy difference and the low barriers to internal rotation, both conformers are expected to be observable in the room temperature rotational spectrum. The transition intensities of *anti*-4-cyano-1,2-butadiene benefit from statistical doubling due to the presence of enantiomeric forms.

anti-4-Cyano-1,2-butadiene (Figure 12a) is a prolate (κ = −0.99), asymmetric top with C_1 symmetry and substantial dipole moment components along both the *a* and *b* principal axes (μ_a = 3.6 D, μ_b = 1.9 D, μ_c = 0.6 D). The lowest-energy vibrationally excited state (the torsion) is predicted to be only 53 cm^{-1} higher in energy than the ground vibrational state. *syn*-4-Cyano-1,2-butadiene (Figure 12b) is a less prolate (κ = −0.60), asymmetric top with C_s symmetry and substantial dipole moment components along both the *a* and *b* principal axes (μ_a = 2.0 D, μ_b = 3.1 D). The lowest-energy vibrationally excited state (also the torsion) is predicted to be 86 cm^{-1} higher in energy than the ground vibrational state.

The 130−375 GHz rotational spectrum of 4-cyano-1,2-butadiene reveals the presence of both *anti* and *syn* conformers. The most intense rotational transitions in the spectrum are the ^{a}R transitions of the *anti* conformer (Figure 13). The K_a = 0 and 1 transitions are nondegenerate in our frequency region, although the two *a*-type transitions with the same value of K_c become near-degenerate at the top of the observed frequency region. Transitions of individual bands at low K_a are spread sufficiently far that it is difficult to discern the pattern, but transitions sharing the same value of *J* and the same value of K_a become degenerate near K_a = 6. At this point, a clear band structure becomes distinguishable. Lower-intensity, *b*-type R-branch transitions and Q-branch transitions are also observable

https://doi.org/10.1021/jacs.1c03777
J. Am. Chem. Soc. 2021, 143, 9551−9564

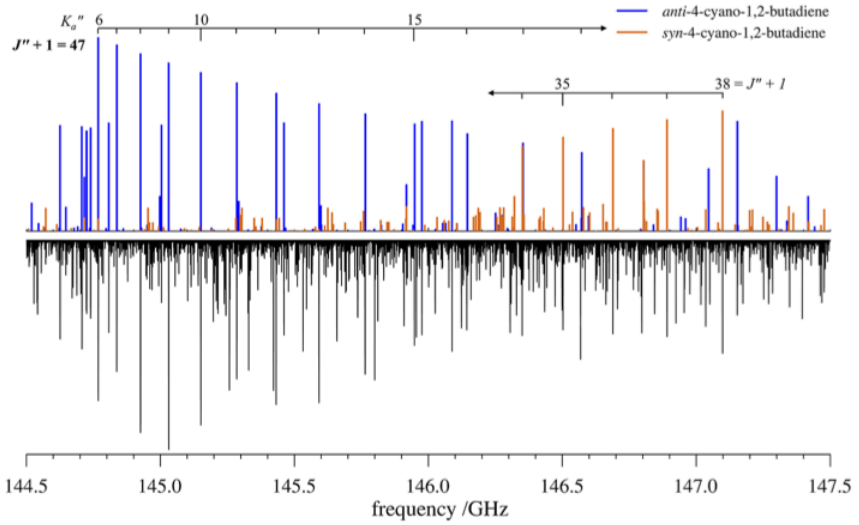


Figure 13. Rotational spectrum of 4-cyano-1,2-butadiene from 144.50 to 147.50 GHz (bottom) and stick spectrum of the ground vibrational state transitions (top). Blue lines mark transitions of *anti*-4-cyano-1,2-butadiene, and copper lines mark transitions of *syn*-4-cyano-1,2-butadiene. Many transitions belonging to other vibrational satellites are also visible in the experimental spectrum.

in the spectrum. The rotational transitions of the *syn* conformer exhibit a more regular spectral pattern (Figure 13). R-branch bandheads of the *syn* conformer begin quadruply degenerate (two $^{a}R_{0,1}$ transitions, $^{b}R_{1,1}$, $^{b}R_{-1,1}$) at $K_a = 0$ and 1 with all same values of K_c. Transitions proceed to lower frequency with increasing K_a, undergo a turnaround, and lose degeneracy. At higher values of K_a, the two *a*-type transitions with the same value of K_a become degenerate and the two *b*-type transitions with the same value of K_a become degenerate. Numerous Q-branch transitions are also observed in the spectrum of the *syn* conformer.

The ground vibrational state of the *anti* conformer of 4-cyano-1,2-butadiene exhibits coupling in our spectral range. Most noticeably, $^{a}R_{0,1}$ transitions of the $K_a = 18$ series exhibit deviation from their distorted-rotor-predicted frequencies in a manner that does not follow a consistent pattern across values of J. During initial fitting, transitions of this series appeared well-predicted at $J'' + 1 = 50$, deviated to increasingly lower frequencies with increasing J, and reached a maximum deviation at $J'' + 1 = 93$. At even higher values of J, the transitions reapproached their predicted frequencies and appeared reasonably predicted near $J'' + 1 = 115$. Such a pattern of deviations cannot be addressed by including more distortion constants in the least-squares fit. As was done for *s-trans-E*-1-cyano-1,3-butadiene, transitions that were evidently perturbed or had quantum-number values proximate to those of clearly perturbed transitions (all $K_a > 12$) were excluded from the data set presented here to acquire minimally perturbed spectroscopic constants. The resultant data set includes R-branch transitions ranging in J'' from 5 to 123 and K_a'' from 0 to 12, as well as Q-branch transitions that range in J'' from 21 to 67 and K_a'' from 6 to 8. The corresponding data distribution plot is provided in Figure 14a. The ground vibrational state of the *syn* conformer, on the other hand, appears to behave as a distorted rotor in the same frequency range. R-branch transitions assigned for this conformer range in J'' from 11 to 94 and K_a'' from 0 to 29 and Q-branch transitions range in J'' from 23 to 69 and K_a'' from 1 to 30. The data distribution plot for the *syn*-4-cyano-1,2-butadiene ground vibrational state is provided in Figure 14b.

These data represent the first millimeter-wave observation and analysis of 4-cyano-1,2-butadiene. The ground vibrational states of both the *anti* and *syn* conformers are fit to partial octic, distorted-rotor Hamiltonians with low error ($\sigma_{fit} < 0.05$ MHz). Their spectroscopic constants are presented in Table 3. Although the least-squares fit for the *anti* conformer does not address the coupling observed in our frequency range, we expect that the constants are minimally affected by perturbation and physically meaningful (*vide infra*). A comparison of the predicted rotational and distortion constants with those from the minimally perturbed least-squares fit is provided in Table 3, and the resultant fit files are provided in the Supporting Information. As with the other isomers, the spectroscopic constants predicted by the B3LYP anharmonic calculation are reasonably good estimates of the experimental constants. The A_0 rotational constant of the *anti* conformer is predicted within 2.2% of the value determined in the minimally perturbed least-squares fit; the values of B_0 and C_0 are within 1%. The quartic centrifugal distortion constants are predicted within 24% of the values obtained in the experimental fit, and the sextic centrifugal distortion constants are within 61% of the experimental values. Overall, these discrepancies between predicted and experimental constants are within the expected ranges, lending credence to the idea that most effects of perturbation have been minimized or avoided. This conclusion is reinforced by the fact that the predicted vs. experimental discrepancies for the *anti* conformer are *smaller* than those for the *syn* conformer, which was amenable to a single-state least-squares fit without indications of perturbation. The rotational constants of *syn*-4-cyano-1,2-butadiene are within 2.8%−5.5% of their experimental values. The quartic centrifugal distortion constants are predicted within 27%, and the sextic constants are predicted within 61% of the experimentally determined values, with the exception of H_{JK}, which is predicted to be a little over 3 times larger than its fitted value. The large values of inertial defect for the *anti* and *syn* conformers (−23.9 and −6.3 uÅ^2, respectively; Table 3)

https://doi.org/10.1021/jacs.1c03777
J. Am. Chem. Soc. 2021, 143, 9551−9564

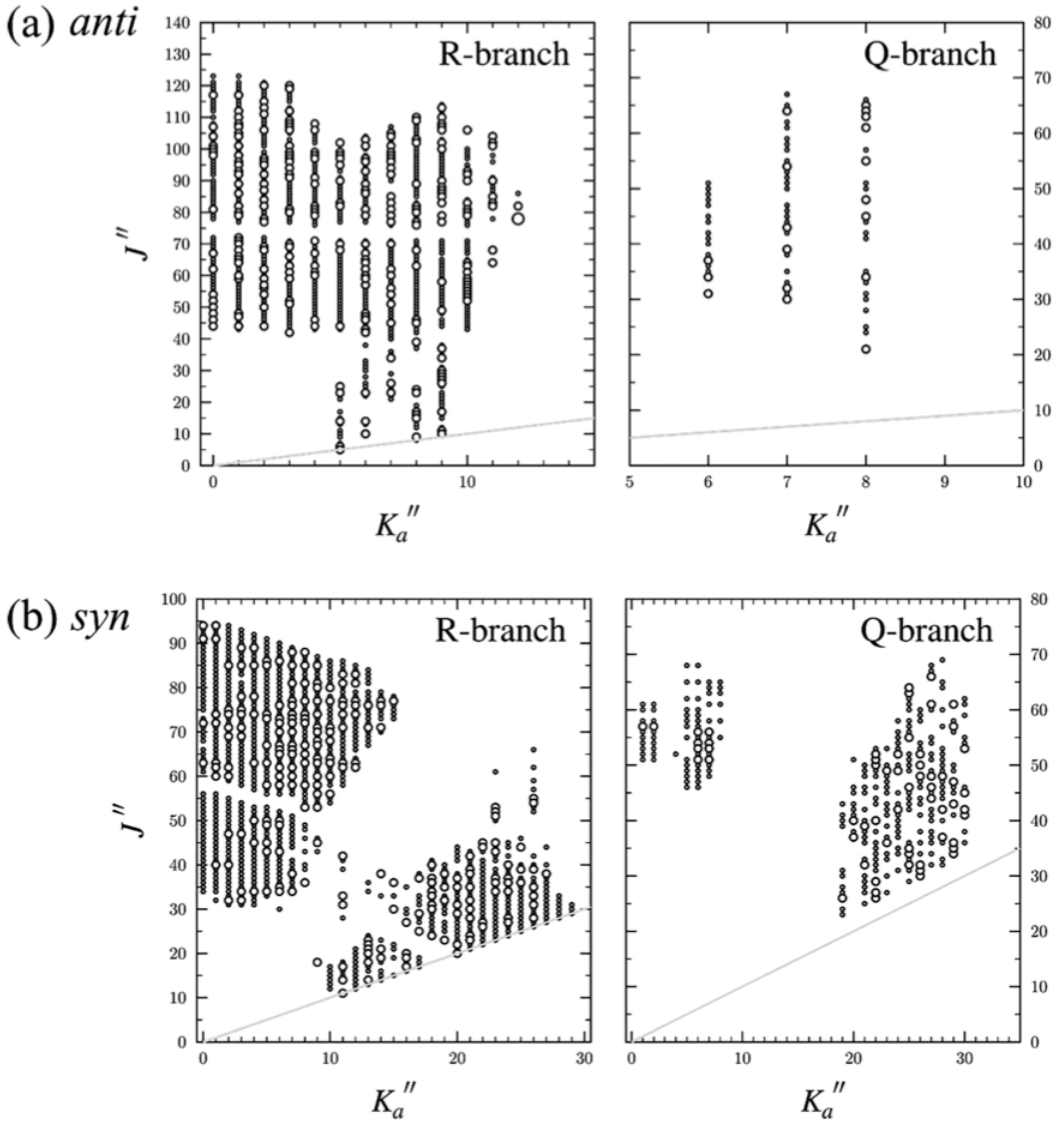


Figure 14. Data distribution plots for the least-squares fits of spectroscopic data for the vibrational ground state of (a) *anti*-4-cyano-1,2-butadiene and (b) *syn*-4-cyano-1,2-butadiene. Circles indicate Q- and R-branch transitions. The size of the plotted symbol is proportional to the value of $|(f_{obs} - f_{calc})/\delta f|$, where δf is the frequency measurement uncertainty (50 kHz); all values shown are smaller than 3.

are indicative of the nonplanarity of both species, as well as the significant structural differences between the two conformers.

Structural and Spectroscopic Comparisons. The cyanobutadiene isomers discussed in this work reveal interesting, and perhaps unanticipated, facets of the oftentimes complex relationships between structural and spectroscopic properties within a closely related family of molecules. In terms of molecular structure, the *E*- and *Z*-1-cyano-1,3-butadienes are quite similar: the connectivity of their atoms is the same, the conformational potential energy surfaces resemble one another in form and energetics, and the electronic distribution is similar, resulting in similar NMR and IR spectra.[47] All of these features are distinct from those of 4-cyano-1,2-butadiene. In terms of molecular spectroscopy, however, the comparisons cut in a different direction. The rotational spectra of the *E*- and *Z*-1-cyano-1,3-butadienes are distinctly different because of differing values of the asymmetry parameter ($\kappa = -0.99$ vs -0.91, respectively). The rotational spectra of the *anti*- and *syn*-4-cyano-1,2-butadienes are even more different, for the same reason ($\kappa = -0.99$ vs -0.60, respectively). The highly prolate character of *s-trans-E*-1-cyano-1,3-butadiene and *anti*-4-cyano-1,2-butadiene ($\kappa = -0.99$) sets these molecules apart from *s-trans-Z*-1-cyano-1,3-butadiene and *syn*-4-cyano-1,2-butadiene. Even within a closely related family of isomers, differences in molecular shape may lead to a disparate set of rotational spectra and spectroscopic constants (Table 4).

One significant difference among the rotational spectra in this study involves whether the rotational ground states are "isolated" (*i.e.*, not coupled to other states) in the observed frequency range or whether they exhibit coupling. Coupling becomes evident when rotational energies of one vibrational state are close to those of another vibrational state. For a

https://doi.org/10.1021/jacs.1c03777
J. Am. Chem. Soc. 2021, 143, 9551−9564

Table 3. Experimental and Computational Spectroscopic Constants for the Ground Vibrational States of *anti*- and *syn*-4-Cyano-1,2-butadiene (C_5H_5N) (S-Reduced Hamiltonian, I^r Representation)[e]

	anti-4-cyano-1,2-butadiene		*syn*-4-cyano-1,2-butadiene	
	B3LYP[a]	experimental	B3LYP[a]	experimental
A_0 (MHz)	14798	14498.4293 (34)	6187	5967.20395 (62)
B_0 (MHz)	1552	1567.06312 (17)	2575	2722.54115 (25)
C_0 (MHz)	1503	1515.78726 (13)	1860	1914.200040 (81)
D_J (kHz)	0.94	1.071171 (27)	2.7	3.278037 (57)
D_{JK} (kHz)	−64	−73.5948 (19)	−13.4	−14.49348 (57)
D_K (kHz)	1394	1611.957 (57)	23	22.1617 (23)
d_1 (kHz)	−0.195	−0.227538 (19)	−1.03	−1.305350 (30)
d_2 (kHz)	−0.0050	−0.006534 (10)	−0.062	−0.0849150 (95)
H_J (Hz)	0.0043	0.0070148 (28)	0.0123	0.0110340 (76)
H_{JK} (Hz)	−0.13	−0.31896 (19)	−0.048	−0.015533 (94)
H_{KJ} (Hz)	−12	−11.206 (28)	−0.069	−0.17240 (99)
H_K (Hz)	362	397.33 (30)	0.27	0.3383 (33)
h_1 (Hz)	0.0019	0.0030023 (21)	0.00653	0.0062572 (45)
h_2 (Hz)	0.00019	0.0003851 (15)	0.00094	0.0011238 (21)
h_3 (Hz)	0.000012	0.00002934 (38)	0.00016	0.00020095 (51)
L_J (μHz)		−0.05251 (10)		[0.0]
L_{JJK} (μHz)		3.4508 (96)		−0.237 (11)
L_{JK} (μHz)		−81.34 (99)		[0.0]
L_{KKJ} (μHz)		6390 (150)		4.94 (57)
L_K (μHz)		[0.0]		−7.4 (1.7)
l_1 (μHz)		−0.025404 (85)		[0.0]
l_2 (μHz)		−0.004564 (63)		[0.0]
l_3 (μHz)		−0.000833 (25)		[0.0]
l_4 (μHz)		[0.0]		[0.0]
Δ_i (uÅ^2)[b,c]		−23.947986 (46)		−6.304674 (22)
N_{lines}[d]		1147		1172
σ_{fit} (MHz)		0.043		0.038

[a]Evaluated with the 6-311+G(2d,p) basis set. [b]Inertial defect, $\Delta_i = I_c - I_a - I_b$. [c]Calculated by using PLANM from the B_0 constants. [d]Number of fitted transition frequencies. [e]Values in square brackets held fixed in least-squares fit.

Table 4. Summary of Rotational Constants and Two Lowest-Energy Fundamentals for *s-trans-E*-1-Cyano-1,3-butadiene, *s-trans-Z*-1-Cyano-1,3-butadiene, *anti*-4-Cyano-1,2-butadiene, and *syn*-4-Cyano-1,2-butadiene (S-Reduced Hamiltonian, I^r Representation)

molecule	A_0 (MHz)	B_0 (MHz)	C_0 (MHz)	lowest-energy fundamentals[a]
s-trans-E-1-cyano-1,3-butadiene	26243.02934 (59)	1443.620880 (18)	1368.119206 (18)	ν_{19} (A′, 138 cm^{-1}, 141 cm^{-1})
				ν_{27} (A″, 141 cm^{-1}, 137 cm^{-1})
s-trans-Z-1-cyano-1,3-butadiene	9759.44594 (25)	2039.686938 (29)	1686.177389 (28)	ν_{19} (A′, 127 cm^{-1}, 129 cm^{-1})
				ν_{27} (A″, 140 cm^{-1}, 135 cm^{-1})
anti-4-cyano-1,2-butadiene	14498.4293 (34)	1567.06312 (17)	1515.78726 (13)	ν_{27} (A, 56 cm^{-1}, 53 cm^{-1})
				ν_{26} (A, 173 cm^{-1}, 170 cm^{-1})
syn-4-cyano-1,2-butadiene	5967.20395 (62)	2722.54115 (25)	1914.200040 (81)	ν_{27} (A″, 95 cm^{-1}, 86 cm^{-1})
				ν_{17} (A′, 105 cm^{-1}, 103 cm^{-1})

[a]B3LYP/6-311+G(2d,p). First value is energy from harmonic frequency calculation; second value is energy from anharmonic frequency calculation.

molecule with a given symmetry, the triple direct product of the irreducible representations of the interacting vibrations and the coupling interaction must equal the totally symmetric representation. In a C_s molecule, Fermi and *c*-type Coriolis coupling transform like the A′ irreducible representation, while *a*- and *b*-type Coriolis coupling transform like the A″ irreducible representation.[55,56] For a molecule with no symmetry, all types of coupling are possible between any interacting states. The matter of whether or not coupling is observed is not just a detail of the spectroscopy; it is fundamental to the proper understanding of laboratory spectra and the use of these spectra as a basis for assigning species in astronomical or other harsh reaction environments. The differing observations of coupling in our frequency range (absent for *s-trans-Z*-1-cyano-1,3-butadiene and *syn*-4-cyano-1,2-butadiene; present for *s-trans-E*-1-cyano-1,3-butadiene and *anti*-4-cyano-1,2-butadiene) result from several interacting factors. One factor that plays into the observation of coupling is the magnitude of the coupling constant(s). Even without predicting the coupling constants, however, the magnitudes of each molecule's A_0 and C_0 constants and the energy separations between states make it possible to rationalize the different spectroscopic behaviors (Table 4). A smaller energy separation between vibrational states increases the likelihood of proximity between their rotational levels. In the case of *anti*-4-cyano-1,2-butadiene, the lowest-energy vibrationally excited

https://doi.org/10.1021/jacs.1c03777
J. Am. Chem. Soc. 2021, 143, 9551−9564

state is predicted to be only 53 cm^{-1} above the ground state—less than half of the predicted energy separation in either *E*- or *Z*-1-cyano-1,3-butadiene. Although the energy separation between *syn*-4-cyano-1,2-butadiene and its lowest-energy fundamental is 86 cm^{-1}, which is also smaller than the predicted energy separation of either 1-cyano-1,3-butadiene ground state and fundamental, the lack of observed coupling can be rationalized by the magnitudes of the rotational constants. The larger the value of A_0, the more widely spread the rotational energy levels for different K values of a vibrational state, and therefore the rotational energy levels of the lower-energy vibrational state approach those of the higher-energy state at lower K_a values. At the same time, the smaller the value of C_0, the more closely spaced the rotational levels for different J values. As a result, higher values of J, which are more likely to exhibit coupling, are observed in a given frequency region. Indeed, of the isomers examined here, *s-trans-E*-1-cyano-1,3-butadiene exhibits the largest value of A_0, the smallest value of C_0, and observed R-branch transitions with the highest value of J (J'' = 134). *anti*-4-Cyano-1,2-butadiene has the second-largest A_0, second-smallest C_0, and observed R-branch transitions with the second-highest value of J (J'' = 123). As a result, it is reasonable that these molecules exhibit coupling in our observed frequency region. Ground vibrational state coupling is not unfamiliar in rotational spectroscopy; other highly prolate molecules such as hydrazoic acid (HN_3)[57,58] and vinyl cyanide (C_3H_3N)[50,59] also show coupling between their ground and vibrationally excited states. These molecules similarly have large values of A_0: 611 034.132 (29) MHz for hydrazoic acid[60] and 49 850.69655 (43) MHz for vinyl cyanide.[50]

CONCLUSIONS

In this work, we present a detailed analysis of the millimeter-wave rotational spectra of *E*-1-cyano-1,3-butadiene, *Z*-1-cyano-1,3-butadiene, and 4-cyano-1,2-butadiene. Each of the observed conformers of these molecules has been fit to an octic, distorted-rotor Hamiltonian, and the resultant spectroscopic constants may be used for identification of these species in spectra of extraterrestrial sources and other harsh environments. Transitions for *Z*-1-cyano-1,3-butadiene and *syn*-4-cyano-1,2-butadiene, which do not exhibit coupling in their ground states, are expected to be accurately predicted to 370 GHz for the entire range of quantum numbers observed in this work. Despite evidence of coupling in the ground states of *s-trans-E*-1-cyano-1,3-butadiene and *anti*-4-cyano-1,2-butadiene, the spectroscopic constants provided for these two molecules are expected to be minimally perturbed and sufficiently precise for detection of these molecules up to 370 GHz. For *anti*-4-cyano-1,2-butadiene, it is expected that R-branch transitions with K_a up to 10 within this frequency range are well-predicted by the spectroscopic constants presented above. For *s-trans-E*-1-cyano-1,3-butadiene, this limit is slightly higher, such that R-branch transitions with K_a values up to 15 are expected to be predicted within experimental accuracy by using the constants provided above. Indeed, the predicted spectra resulting from this work have already enabled identification of the *s-trans* conformers of *E*- and *Z*-1-cyano-1,3-butadiene as products in reaction spectra.[21,22]

ASSOCIATED CONTENT

Supporting Information

The Supporting Information is available free of charge at https://pubs.acs.org/doi/10.1021/jacs.1c03777.

Directory of files; comparison of A reduction constants for *s-trans-Z*-1-cyano-1,3-butadiene, as determined in this work and in the work of McCarthy *et al.*[21] (PDF)

Least-squares fitting files of *E*-1-cyano-1,3-butadiene, *Z*-1-cyano-1,3-butadiene, and 4-cyano-1,2-butadiene; output files from computational studies (ZIP)

AUTHOR INFORMATION

Corresponding Authors

Robert J. McMahon − *Department of Chemistry, University of Wisconsin−Madison, Madison, Wisconsin 53706, United States*; orcid.org/0000-0003-1377-5107; Email: robert.mcmahon@wisc.edu

R. Claude Woods − *Department of Chemistry, University of Wisconsin−Madison, Madison, Wisconsin 53706, United States*; Email: rcwoods@wisc.edu

Authors

Maria A. Zdanovskaia − *Department of Chemistry, University of Wisconsin−Madison, Madison, Wisconsin 53706, United States*; orcid.org/0000-0001-5167-8573

P. Matisha Dorman − *Department of Chemistry, University of Wisconsin−Madison, Madison, Wisconsin 53706, United States*; orcid.org/0000-0003-3802-6719

Vanessa L. Orr − *Department of Chemistry, University of Wisconsin−Madison, Madison, Wisconsin 53706, United States*

Andrew N. Owen − *Department of Chemistry, University of Wisconsin−Madison, Madison, Wisconsin 53706, United States*

Samuel M. Kougias − *Department of Chemistry, University of Wisconsin−Madison, Madison, Wisconsin 53706, United States*; orcid.org/0000-0002-9877-0817

Brian J. Esselman − *Department of Chemistry, University of Wisconsin−Madison, Madison, Wisconsin 53706, United States*; orcid.org/0000-0002-9385-8078

Complete contact information is available at: https://pubs.acs.org/10.1021/jacs.1c03777

Author Contributions

M.A.Z., P.M.D., and V.L.O. contributed equally to the spectroscopic analyses described in this work.

Notes

The authors declare no competing financial interest.

ACKNOWLEDGMENTS

We gratefully acknowledge funding from the National Science Foundation for support of this project (CHE-1664912 and CHE-1954270). P.M.D. thanks the University of Wisconsin−Madison Graduate School for support as an Advanced Opportunity Fellow. We thank Michael McCarthy for the loan of an Amplification-Multiplication Chain (WR5.1 AMC 530). We thank the Harvey Spangler Award (to B.J.E.) for the funding that supported the purchase of the Virginia Diodes Zero-Bias Detector (WR5.1ZBD 140−220 GHz). We thank Michael McCarthy, Kelvin Lee, Timothy Zwier, and Piyush Mishra for stimulating discussions.

REFERENCES

(1) McGuire, B. A.; Burkhardt, A. M.; Kalenskii, S. V.; Shingledecker, C. N.; Remijan, A. J.; Herbst, E.; McCarthy, M. C. Detection of the Aromatic Molecule Benzonitrile (*c*-C_6H_5CN) in the Interstellar Medium. *Science* **2018**, *359*, 202−205.

(2) McCarthy, M. C.; Lee, K. L. K.; Loomis, R. A.; Burkhardt, A. M.; Shingledecker, C. N.; Charnley, S. B.; Cordiner, M. A.; Herbst, E.; Kalenskii, S.; Willis, E. R.; Xue, C.; Remijan, A. J.; McGuire, B. A. Interstellar detection of the highly polar five-membered ring cyanocyclopentadiene. *Nat. Astron.* **2021**, *5*, 176−180.

(3) McGuire, B. A.; Loomis, R. A.; Burkhardt, A. M.; Lee, K. L. K.; Shingledecker, C. N.; Charnley, S. B.; Cooke, I. R.; Cordiner, M. A.; Herbst, E.; Kalenskii, S.; Siebert, M. A.; Willis, E. R.; Xue, C.; Remijan, A. J.; McCarthy, M. C. Detection of two interstellar polycyclic aromatic hydrocarbons via spectral matched filtering. *Science* **2021**, *371*, 1265−1269.

(4) McCarthy, M. C.; McGuire, B. A. Aromatics and Cyclic Molecules in Molecular Clouds: A New Dimension of Interstellar Organic Chemistry. *J. Phys. Chem. A* **2021**, *125*, 3231−3243.

(5) Halter, R. J.; Fimmen, R. L.; McMahon, R. J.; Peebles, S. A.; Kuczkowski, R. L.; Stanton, J. F. Microwave Spectra and Molecular Structures of (Z)-Pent-2-en-4-ynenitrile and Maleonitrile. *J. Am. Chem. Soc.* **2001**, *123*, 12353−12363.

(6) Müller, H. S. P.; Schlöder, F.; Stutzki, J.; Winnewisser, G. The Cologne Database for Molecular Spectroscopy, CDMS: a Useful Tool for Astronomers and Spectroscopists. *J. Mol. Struct.* **2005**, *742*, 215−227.

(7) Endres, C. P.; Schlemmer, S.; Schilke, P.; Stutzki, J.; Müller, H. S. P. The Cologne Database for Molecular Spectroscopy, CDMS, in the Virtual Atomic and Molecular Data Centre. *J. Mol. Spectrosc.* **2016**, *327*, 95−104.

(8) Avery, L. W.; Broten, N. W.; MacLeod, J. M.; Oka, T.; Kroto, H. W. Detection of the Heavy Interstellar Molecule Cyanodiacetylene. *Astrophys. J.* **1976**, *205*, L173−L175.

(9) Broten, N. W.; Oka, T.; Avery, L. W.; MacLeod, J. M.; Kroto, H. W. The Detection of Cyanooctatetrayne (HC_9N) in Interstellar Space. *Astrophys. J.* **1978**, *223*, L105−L107.

(10) Kroto, H. W.; Kirby, C.; Walton, D. R. M.; Avery, L. W.; Broten, N. W.; MacLeod, J. M.; Oka, T. The Detection of Cyanohexatriyne, $H(C{\equiv}C)_3CN$, in Heiles's Cloud 2. *Astrophys. J.* **1978**, *219*, L133−L137.

(11) Snyder, L. E.; Buhl, D. Radio Emission from Interstellar Hydrogen Cyanide. *Astrophys. J.* **1971**, *163*, L47−L52.

(12) Walmsley, C. M.; Winnewisser, G.; Toelle, F. Cyanoacetylene and Cyanodiacetylene in Interstellar Clouds. *Astron. Astrophys.* **1980**, *81*, 245−50.

(13) Loomis, R. A.; Burkhardt, A. M.; Shingledecker, C. N.; Charnley, S. B.; Cordiner, M. A.; Herbst, E.; Kalenskii, S.; Lee, K. L. K.; Willis, E. R.; Xue, C.; Remijan, A. J.; McCarthy, M. C.; McGuire, B. A. An investigation of spectral line stacking techniques and application to the detection of $HC_{11}N$. *Nat. Astron.* **2021**, *5*, 188−196.

(14) Broten, N. W.; MacLeod, J. M.; Avery, L. W.; Irvine, W. M.; Hoeglund, B.; Friberg, P.; Hjalmarson, A. The Detection of Interstellar Methylcyanoacetylene. *Astrophys. J.* **1984**, *276*, L25−L29.

(15) Gardner, F. F.; Winnewisser, G. Detection of Interstellar Vinyl Cyanide (Acrylonitrile). *Astrophys. J.* **1975**, *195*, L127−L130.

(16) Snyder, L. E.; Hollis, J. M.; Jewell, P. R.; Lovas, F. J.; Remijan, A. Confirmation of Interstellar Methylcyanodiacetylene (CH_3C_5N). *Astrophys. J.* **2006**, *647*, 412−417.

(17) Lovas, F. J.; Remijan, A. J.; Hollis, J. M.; Jewell, P. R.; Snyder, L. E. Hyperfine Structure Identification of Interstellar Cyanoallene Toward TMC-1. *Astrophys. J.* **2006**, *637*, L37−L40.

(18) Solomon, P. M.; Jefferts, K. B.; Penzias, A. A.; Wilson, R. W. Detection of Millimeter Emission Lines from Interstellar Methyl Cyanide. *Astrophys. J.* **1971**, *168*, L107−L110.

(19) Belloche, A.; Garrod, R. T.; Müller, H. S. P.; Menten, K. M. Detection of a Branched Alkyl Molecule in the Interstellar Medium: *iso*-Propyl Cyanide. *Science* **2014**, *345*, 1584−1587.

(20) Belloche, A.; Garrod, R. T.; Müller, H. S. P.; Menten, K. M.; Comito, C.; Schilke, P. Increased Complexity in Interstellar Chemistry: Detection and Chemical Modeling of Ethyl Formate and *n*-Propyl Cyanide in Sagittarius B2(N). *Astron. Astrophys.* **2009**, *499*, 215−232.

(21) McCarthy, M. C.; Lee, K. L. K.; Carroll, P. B.; Porterfield, J. P.; Changala, P. B.; Thorpe, J. H.; Stanton, J. F. Exhaustive Product Analysis of Three Benzene Discharges by Microwave Spectroscopy. *J. Phys. Chem. A* **2020**, *124*, 5170−5181.

(22) Mishra, P.; Fritz, S. M.; Herbers, S.; Mebel, A. M.; Zwier, T. S. Gas-Phase Pyrolysis of *trans* 3-Pentenenitrile: Competition between Direct and Isomerization-Mediated Dissociation. *Phys. Chem. Chem. Phys.* **2021**, *23*, 6462−6471.

(23) Tsukamoto, A.; Lichtin, N. N., Reactions of Active Nitrogen with Organic Substrates. I. The Monomeric Products of the Reaction with 1,3-Butadiene. *J. Am. Chem. Soc.* **1962**, *84*, 1601−1605.

(24) Sun, B. J.; Huang, C. H.; Chen, S. Y.; Chen, S. H.; Kaiser, R. I.; Chang, A. H. H. Theoretical Study on Reaction Mechanism of Ground-State Cyano Radical with 1,3-Butadiene: Prospect of Pyridine Formation. *J. Phys. Chem. A* **2014**, *118*, 7715−7724.

(25) Morales, S. B.; Bennett, C. J.; Le Picard, S. D.; Canosa, A.; Sims, I. R.; Sun, B. J.; Chen, P. H.; Chang, A. H. H.; Kislov, V. V.; Mebel, A. M.; Gu, X.; Zhang, F.; Maksyutenko, P.; Kaiser, R. I. A Crossed Molecular Beam, Low-Temperature Kinetics, And Theoretical Investigation Of The Reaction Of The Cyano Radical (CN) With 1,3-Butadiene (C_4H_6). A Route To Complex Nitrogen-Bearing Molecules In Low-Temperature Extraterrestrial Environments. *Astrophys. J.* **2011**, *742*, 26.

(26) McKellar, A. Evidence for the Molecular Origin of Some Hitherto Unidentified Interstellar Lines. *Publ. Astron. Soc. Pac.* **1940**, *52*, 187.

(27) Baraban, J. H.; Martin-Drumel, M.-A.; Changala, P. B.; Eibenberger, S.; Nava, M.; Patterson, D.; Stanton, J. F.; Ellison, G. B.; McCarthy, M. C. The Molecular Structure of *gauche*-1,3-Butadiene: Experimental Establishment of Non-planarity. *Angew. Chem., Int. Ed.* **2018**, *57*, 1821−1825.

(28) Balucani, N.; Asvany, O.; Huang, L. C. L.; Lee, Y. T.; Kaiser, R. I.; Osamura, Y.; Bettinger, H. F. Formation of Nitriles in the Interstellar Medium via Reactions of Cyano Radicals, $CN(X\ ^2\Sigma^+)$, with Unsaturated Hydrocarbons. *Astrophys. J.* **2000**, *545*, 892−906.

(29) Jamal, A.; Mebel, A. M. Theoretical Investigation of the Mechanism and Product Branching Ratios of the Reactions of Cyano Radical with 1- and 2-Butyne and 1,2-Butadiene. *J. Phys. Chem. A* **2013**, *117*, 741−755.

(30) Esselman, B. J.; Zdanovskaia, M. A.; Kougias, S. M.; Patel, A. R.; Woods, R. C.; McMahon, R. J. The 130−360 GHz Rotational Spectrum of *syn*-2-Cyano-1,3-Butadiene (C_5H_5N) − A Molecule of Astrochemical Relevance, manuscript submitted.

(31) Sagan, C.; Thompson, W. R.; Khare, B. N. Titan: a laboratory for prebiological organic chemistry. *Acc. Chem. Res.* **1992**, *25*, 286−292.

(32) Waite, J. H.; Niemann, H.; Yelle, R. V.; Kasprzak, W. T.; Cravens, T. E.; Luhmann, J. G.; McNutt, R. L.; Ip, W.-H.; Gell, D.; De La Haye, V.; Müller-Wordag, I.; Magee, B.; Borggren, N.; Ledvina, S.; Fletcher, G.; Walter, E.; Miller, R.; Scherer, S.; Thorpe, R.; Xu, J.; Block, B.; Arnett, K. Ion Neutral Mass Spectrometer Results from the First Flyby of Titan. *Science* **2005**, *308*, 982−986.

(33) Waite, J. H.; Young, D. T.; Cravens, T. E.; Coates, A. J.; Crary, F. J.; Magee, B.; Westlake, J. The Process of Tholin Formation in Titan's Upper Atmosphere. *Science* **2007**, *316*, 870−875.

(34) Desai, R. T.; Coates, A. J.; Wellbrock, A.; Vuitton, V.; Crary, F. J.; González-Caniulef, D.; Shebanits, O.; Jones, G. H.; Lewis, G. R.; Waite, J. H.; Cordiner, M.; Taylor, S. A.; Kataria, D. O.; Wahlund, J.-E.; Edberg, N. J. T.; Sittler, E. C. Carbon chain anions and the growth of complex organic molecules in Titan's ionosphere. *Astrophys. J., Lett.* **2017**, *844*, L18.

(35) McGuigan, M.; Waite, J. H.; Imanaka, H.; Sacks, R. D. Analysis of Titan tholin pyrolysis products by comprehensive two-dimensional

gas chromatography−time-of-flight mass spectrometry. *J. Chromatogr. A* **2006**, *1132*, 280−288.
(36) Morisson, M.; Szopa, C.; Carrasco, N.; Buch, A.; Gautier, T. Titan's organic aerosols: Molecular composition and structure of laboratory analogues inferred from pyrolysis gas chromatography mass spectrometry analysis. *Icarus* **2016**, *277*, 442−454.
(37) Nixon, C. A.; Thelen, A. E.; Cordiner, M. A.; Kisiel, Z.; Charnley, S. B.; Molter, E. M.; Serigano, J.; Irwin, P. G.; Teanby, N. A.; Kuan, Y.-J. Detection of Cyclopropenylidene on Titan with ALMA. *Astron. J.* **2020**, *160*, 205.
(38) Charnley, S. B.; Kuan, Y.-J.; Huang, H.-C.; Botta, O.; Butner, H. M.; Cox, N.; Despois, D.; Ehrenfreund, P.; Kisiel, Z.; Lee, Y.-Y.; Markwick, A. J.; Peeters, Z.; Rodgers, S. D. Astronomical Searches for Nitrogen Heterocycles. *Adv. Space Res.* **2005**, *36*, 137−145.
(39) Cyanopyridine isomers represent alternate proxies for pyridine.
(40) Dorman, P. M.; Esselman, B. J.; Park, J. E.; Woods, R. C.; McMahon, R. J. Millimeter-wave spectrum of 4-cyanopyridine in its ground state and lowest-energy vibrationally excited states, ν_{20} and ν_{30}. *J. Mol. Spectrosc.* **2020**, *369*, 111274.
(41) Dorman, P. M.; Esselman, B. J.; Woods, R. C.; McMahon, R. J. An analysis of the rotational ground state and lowest-energy vibrationally excited dyad of 3-cyanopyridine: Low symmetry reveals rich complexity of perturbations, couplings, and interstate transitions. *J. Mol. Spectrosc.* **2020**, *373*, 111373.
(42) Raffaelli, N. Nicotinamide Coenzyme Synthesis: A Case of Ribonucleotide Emergence or a Byproduct of the RNA World?. In *Origins of Life: The Primal Self-Organization*; Egel, R., Lankenau, D.-H., Mulkidjanian, A. Y., Eds.; Springer-Verlag: Heidelberg, 2011; p 191.
(43) McMurtry, B. M.; Turner, A. M.; Saito, S. E. J.; Kaiser, R. I. On the formation of niacin (vitamin B3) and pyridine carboxylic acids in interstellar model ices. *Chem. Phys.* **2016**, *472*, 173−184.
(44) Pizzarello, S.; Huang, Y. The deuterium enrichment of individual amino acids in carbonaceous meteorites: A case for the presolar distribution of biomolecule precursors. *Geochim. Cosmochim. Acta* **2005**, *69*, 599−605.
(45) Pizzarello, S.; Huang, Y.; Fuller, M. The carbon isotopic distribution of Murchison amino acids. *Geochim. Cosmochim. Acta* **2004**, *68*, 4963−4969.
(46) Parker, D. S. N.; Kaiser, R. I. On the formation of nitrogen-substituted polycyclic aromatic hydrocarbons (NPAHs) in circumstellar and interstellar environments. *Chem. Soc. Rev.* **2017**, *46*, 452−463.
(47) Kougias, S. M.; Knezz, S. N.; Owen, A. N.; Sanchez, R. A.; Hyland, G. E.; Lee, D. J.; Patel, A. R.; Esselman, B. J.; Woods, R. C.; McMahon, R. J. Synthesis and Characterization of Cyanobutadiene Isomers−Molecules of Astrochemical Significance. *J. Org. Chem.* **2020**, *85*, 5787−5798.
(48) Esselman, B. J.; Amberger, B. K.; Shutter, J. D.; Daane, M. A.; Stanton, J. F.; Woods, R. C.; McMahon, R. J. Rotational Spectroscopy of Pyridazine and its Isotopologs from 235−360 GHz: Equilibrium Structure and Vibrational Satellites. *J. Chem. Phys.* **2013**, *139*, 224304.
(49) Zdanovskaia, M. A.; Esselman, B. J.; Woods, R. C.; McMahon, R. J. The 130 − 370 GHz Rotational Spectrum of Phenyl Isocyanide (C_6H_5NC). *J. Chem. Phys.* **2019**, *151*, No. 024301.
(50) Kisiel, Z.; Pszczółkowski, L.; Drouin, B. J.; Brauer, C. S.; Yu, S.; Pearson, J. C.; Medvedev, I. R.; Fortman, S.; Neese, C. Broadband rotational spectroscopy of acrylonitrile: Vibrational energies from perturbations. *J. Mol. Spectrosc.* **2012**, *280*, 134−144.
(51) Kisiel, Z.; Pszczółkowski, L.; Medvedev, I. R.; Winnewisser, M.; De Lucia, F. C.; Herbst, E. Rotational spectrum of *trans*−*trans* diethyl ether in the ground and three excited vibrational states. *J. Mol. Spectrosc.* **2005**, *233*, 231−243.
(52) Pickett, H. M. The fitting and prediction of vibration-rotation spectra with spin interactions. *J. Mol. Spectrosc.* **1991**, *148*, 371−377.
(53) Kisiel, Z. PROSPE - Programs for ROtational SPEctroscopy; http://info.ifpan.edu.pl/~kisiel/prospe.htm (accessed 2020-01-22).
(54) Frisch, M. J.; Trucks, G. W.; Schlegel, H. B.; Scuseria, G. E.; Robb, M. A.; Cheeseman, J. R.; Scalmani, G.; Barone, V.; Petersson, G. A.; Nakatsuji, H.; Li, X.; Caricato, M.; Marenich, A. V.; Bloino, J.; Janesko, B. G.; Gomperts, R.; Mennucci, B.; Hratchian, H. P.; Ortiz, J. V.; Izmaylov, A. F.; Sonnenberg, J. L.; Williams-Young, D.; Ding, F.; Lipparini, F.; Egidi, F.; Goings, J.; Peng, B.; Petrone, A.; Henderson, T.; Ranasinghe, D.; Zakrzewski, V. G.; Gao, J.; Rega, N.; Zheng, G.; Liang, W.; Hada, M.; Ehara, M.; Toyota, K.; Fukuda, R.; Hasegawa, J.; Ishida, M.; Nakajima, T.; Honda, Y.; Kitao, O.; Nakai, H.; Vreven, T.; Throssell, K.; Montgomery, J. A., Jr.; Peralta, J. E.; Ogliaro, F.; Bearpark, M. J.; Heyd, J. J.; Brothers, E. N.; Kudin, K. N.; Staroverov, V. N.; Keith, T. A.; Kobayashi, R.; Normand, J.; Raghavachari, K.; Rendell, A. P.; Burant, J. C.; Iyengar, S. S.; Tomasi, J.; Cossi, M.; Millam, J. M.; Klene, M.; Adamo, C.; Cammi, R.; Ochterski, J. W.; Martin, R. L.; Morokuma, K.; Farkas, O.; Foresman, J. B.; Fox, D. J. *Gaussian 16*, Revision C.01; Gaussian, Inc.: Wallingford, CT, 2019.
(55) Wilson, E. B., Jr.; Decius, J. C.; Cross, P. C. *Molecular Vibrations*; Dover: New York, 1980.
(56) Gordy, W.; Cook, R. L. *Microwave Molecular Spectra*, 3rd ed.; Wiley-Interscience: New York, 1984.
(57) Amberger, B. K. Millimeter-wave Spectroscopy of Highly Nitrogenous Molecules of Potential Astrochemical Interest. Ph.D. Thesis, University of Wisconsin−Madison, Madison, WI, 2015.
(58) Vávra, K.; Kania, P.; Koucký, J.; Kisiel, Z.; Urban, Š. Rotational spectra of hydrazoic acid. *J. Mol. Spectrosc.* **2017**, *337*, 27−31.
(59) Kisiel, Z.; Martin-Drumel, M.-A.; Pirali, O. Lowest vibrational states of acrylonitrile from microwave and synchrotron radiation spectra. *J. Mol. Spectrosc.* **2015**, *315*, 83−91.
(60) Amberger, B. K.; Esselman, B. J.; Stanton, J. F.; Woods, R. C.; McMahon, R. J. Precise Equilibrium Structure Determination of Hydrazoic Acid (HN_3) by Millimeter-wave Spectroscopy. *J. Chem. Phys.* **2015**, *143*, 104310.

https://doi.org/10.1021/jacs.1c03777
J. Am. Chem. Soc. 2021, 143, 9551−9564

Appendix D

Precise Equilibrium Structure Determination of Thiophene (*c*-C_4H_4S) by Rotational Spectroscopy–Structure of a Five-Membered Heterocycle Containing a Third-Row Atom

Vanessa L. Orr
Yotaro Ichikwa
Aatmik R. Patel
Samuel M. Kougias
Kaori Kobayashi
John F. Stanton
Brian J. Esselman
R. Claude Woods
Robert J. McMahon

The Journal of Chemical Physics, 2021, *154*, 244310

The Journal of Chemical Physics ARTICLE scitation.org/journal/jcp

Precise equilibrium structure determination of thiophene (*c*-C_4H_4S) by rotational spectroscopy—Structure of a five-membered heterocycle containing a third-row atom

Cite as: J. Chem. Phys. 154, 244310 (2021); doi: 10.1063/5.0055267
Submitted: 27 April 2021 • Accepted: 7 June 2021 •
Published Online: 29 June 2021

View Online Export Citation CrossMark

Vanessa L. Orr,[1] Yotaro Ichikawa,[2] Aatmik R. Patel,[1] Samuel M. Kougias,[1] Kaori Kobayashi,[2] John F. Stanton,[3] Brian J. Esselman,[1] R. Claude Woods,[1,a)] and Robert J. McMahon[1,a)]

AFFILIATIONS

[1] Department of Chemistry, University of Wisconsin–Madison, 1101 University Avenue, Madison, Wisconsin 53706-1322, USA
[2] Department of Physics, University of Toyama, 3190 Gofuku, Toyama 930-8555, Japan
[3] Quantum Theory Project, Departments of Physics and Chemistry, University of Florida, Gainesville, Florida 32611, USA

[a)] **Authors to whom correspondence should be addressed:** rcwoods@wisc.edu and robert.mcmahon@wisc.edu

ABSTRACT

The rotational spectrum of thiophene (*c*-C_4H_4S) has been collected between 8 and 360 GHz. Samples of varying deuterium-enrichment were synthesized to yield all possible deuterium-substituted isotopologues of thiophene. A total of 26 isotopologues have been measured and least-squares fit using A- and S-reduced distorted-rotor Hamiltonians in the I^r representation. The resultant rotational constants (A_0, B_0, and C_0) from each reduction were converted to determinable constants (A'', B'', and C'') to remove the impact of centrifugal distortion. The computed vibrational and electron mass corrections [CCSD(T)/cc-pCVTZ] were applied to the determinable constants to obtain semi-experimental equilibrium rotational constants (A_e, B_e, and C_e) for 24 isotopologues. A precise semi-experimental equilibrium (r_e^{SE}) structure has been achieved from a least-squares fit of the equilibrium moments of inertia. The combination of the expanded isotopologue rotational data with high-level computational work establishes a precise r_e^{SE} structure for this sulfur-containing heterocycle. The CCSD(T)/cc-pCV5Z structure has been obtained and corrected for the extrapolation to the complete basis set, electron correlation beyond CCSD(T), relativistic effects, and the diagonal Born–Oppenheimer correction. The precise r_e^{SE} structure is compared to the resulting "best theoretical estimate" structure. Several of the best theoretical r_e structural parameters fall within the narrow statistical limits (2σ) of the r_e^{SE} results. The possible origin of the discrepancies for the computed parameters that fall outside the statistical uncertainties is discussed.

Published under an exclusive license by AIP Publishing. https://doi.org/10.1063/5.0055267

INTRODUCTION

Recently, a very satisfying level of agreement was achieved for pyrimidine between the semi-experimental equilibrium (r_e^{SE}) parameters and the highest practical level of theoretical calculation available—differences no more than 0.0004 Å in bond distances and no more than 0.01° in bond angles.[1] That result raises the question of whether or not such a level of agreement is possible in parallel treatments of other similarly sized molecules. While we have begun the study of similar species consisting of carbon, nitrogen, and hydrogen, we have also chosen to explore the impact of including third-row atoms in this methodology. Heavier atoms not only inherently present additional challenges regarding the computational level of theory and basis set but also may impact the ability of the theory to adequately treat the corrections to the rotational constants. The present study of thiophene was undertaken with the primary goal of attempting to answer that question for a prototypical sulfur-containing aromatic ring. Each component of this investigation represents a challenging undertaking: (i) chemical synthesis and purification of a substantial family of isotopologues of thiophene; (ii) measurement, assignment, and fitting of the high-resolution rotational spectrum of each isotopologue;

Published under an exclusive license by AIP Publishing

The Journal of Chemical Physics ARTICLE scitation.org/journal/jcp

(iii) computationally demanding calculations involving electronic structure, vibration–rotation coupling, and corrections for electron mass distribution; and (iv) theoretical methods for providing a "best theoretical estimate" (BTE) of the molecular structure. Integration of all of these data affords a highly precise semi-experimental structure (r_e^{SE}) for thiophene. The method steps beyond the traditional Kraitchman analysis of structure determination by single-atom isotopic substitution and validates the ability of modern experimental and computational methods to establish the structure of an organic heterocyclic molecule containing a third-row element.

The five-membered, aromatic ring of thiophene (c-C_4H_4S, Fig. 1, C_{2v}) is a fundamental molecular structural moiety in organic chemistry and is prevalent in pharmaceuticals[2] and organic electronic materials.[3,4] Thiophenes are naturally occurring on the Earth and have been detected on Mars.[5,6] Thiophene itself has been proposed to be present in the interstellar medium,[7] and unsaturated carbon-chain molecules containing sulfur have been detected.[8,9] The rotational and vibrational spectroscopies of thiophene have been of interest for over a century. The first infrared absorption spectrum was reported in 1905 by Coblentz,[10] and other Raman and infrared studies were reported in the 1930s and 1940s.[11–14] In 1965, a low-resolution infrared study of liquid and vapor phase thiophenes and all its deuterio isotopologues (mono- through tetra-deuterio, except [2,4-^{2}H]-thiophene) was published, including the assignment of their fundamental vibrations.[15] The vibrational assignments were later reaffirmed,[16] and the rotationally resolved IR spectrum of the ν_{13} band was reported by Pankoke *et al.*[17] The rotationally resolved IR spectrum has subsequently been analyzed for ν_{14}, ν_8, and ν_7 (400–750 cm^{-1})[18,19] and ν_{13}, ν_7, ν_6, ν_5, and ν_{19} (600–1200 cm^{-1}).[20] These studies provided the rotational and centrifugal distortion constants for each of these vibrationally excited states, along with their precise vibrational frequencies. More recently, Raman and resonance Raman spectra of thiophenes, neat and in solution (cyclohexane, dimethyl sulfoxide, and methanol), have also been reported.[21,22] Analysis of the fundamental, combination, and overtone vibrational states using rotational spectroscopy is on-going and will be the subject of a future work.

The dipole moment of thiophene (0.55 ± 0.01 D)[23] permits its observation by rotational spectroscopy. Bak *et al.* provided the rotational constants for the normal isotopologue of thiophene, four deuterated isotopologues,[24] the ^{34}S, and the two ^{13}C isotopologues based on microwave spectral data from 12 to 30 GHz.[25]

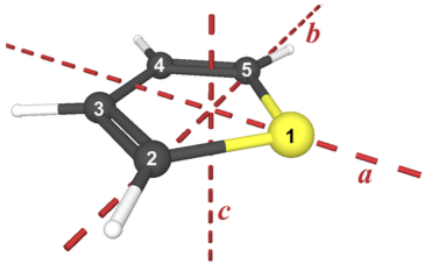


FIG. 1. Thiophene (c-C_4H_4S, μ_a = 0.55 D) with its principal axes and numerical atom designations.

Using Kraitchman's equations,[26] they determined the first substitution structure of thiophene (r_s) from the normal and five monosubstituted isotopologues.[25] These early microwave data were combined with electron diffraction and liquid-crystal nuclear magnetic resonance (NMR) data to determine the r_α structure.[27] Later, the microwave, electron diffraction, and vibrational spectroscopy were combined with computational methods to find a mixed-method, semi-experimental equilibrium structure (r_e^{SE}).[28] The work of Bak *et al.*[24,25] was used to determine a subsequent semi-experimental equilibrium structure (r_e^{SE}) with corrections for vibration–rotation interaction constants and electron mass distributions from density functional theory (DFT) methods.[29,30] Although not utilized in the previous thiophene structure determinations, additional rotational transitions of the normal isotopologue have been reported in later works,[31–34] as well as transitions for the ^{33}S and ^{34}S isotopologues.[34] We have extended the number of isotopologues for which rotational constants are available to 26 isotopologues. Of these, 24 were included in the determination of the semi-experimental equilibrium structure (r_e^{SE}) presented in this work. We have systematically investigated the extent to which additional isotopologues are valuable in reducing the statistical errors of the r_e^{SE} structural parameters.

METHODS

Spectroscopy methods

Rotational spectra of thiophene were collected at room temperature using three different spectrometers. The spectrum of thiophene was collected at the University of Toyama using two different instruments. The spectrum was collected between 40 and 121.5 GHz at sample pressures of 30–50 mTorr using instrumentation described previously.[35,36] Additional transitions were measured between 8 and 18 GHz with a CP-FTMW spectrometer, based on the design of McJunkins and Brown,[37] with a chirp span of 50–150 or 50–200 MHz, at sample pressures of 9–13 mTorr, with 10 000–50 000 molecular signal acquisitions. The broadband spectra of thiophene and its deuterium-containing isotopologues were collected at the University of Wisconsin–Madison from 130 to 230 and 235–360 GHz with a pressure of 5 mTorr using instrumentation described previously.[38,39] The spectrum of the sample containing primarily tetradeuterio thiophene was collected only from 130 to 230 GHz. Spectral segments were combined into a single broadband spectrum using Kisiel's Assignment and Analysis of Broadband Spectra (AABS) software package.[40,41] ASFIT/ASROT were used for least-squares fits and spectral predictions,[40,41] along with PLAN and AC programs for analysis.[42] Measured transitions for each isotopologue were least-squares fit in the I^r representation and the A and S reductions. The ground state of the normal isotopologue has also been fit in both reductions in the III^r representation. With the exception of a few new CP-FTMW measurements with 30 kHz uncertainties, all new measurements assume an experimental uncertainty of 50 kHz; all previously reported measurements use the uncertainty that was provided in either the original publication or a related publication using the same instrument.

Computational methods

Density functional theory calculations were performed using Gaussian 16[43] with the WebMO interface.[44] The optimized

Published under an exclusive license by AIP Publishing

The Journal of Chemical Physics ARTICLE scitation.org/journal/jcp

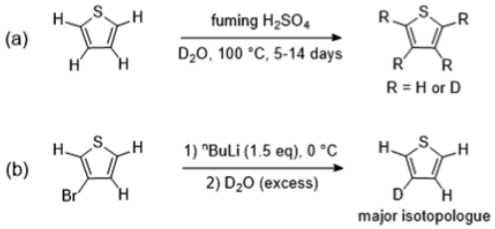
geometries were calculated at the B3LYP/6-311G+(2d,p) level utilizing a "verytight" convergence criterion and an "ultrafine" integration grid. An anharmonic frequency calculation was performed to obtain the quartic and sextic centrifugal distortion constants for the normal isotopologue. Natural population analysis and Natural Bond Orbital (NBO)/Natural Resonance Theory (NRT) analysis of thiolium cations (C-atom protonated thiophenes) were performed with NBO 7.0.8.[45]

Coupled-cluster calculations with single, double, and perturbative triple excitations [CCSD(T)] were performed using CFOUR.[46] Geometry optimizations were performed at the CCSD(T) level with the cc-pCVXZ basis set where X = D, T, Q, and 5. The structure computed at CCSD(T)/cc-pCVTZ was subsequently used for a second-order vibrational perturbation (VPT2) anharmonic frequency calculation by evaluating the cubic force constants using analytical second derivatives at displaced points.[47–49] The VPT2 calculation was used to obtain anharmonic frequencies for each isotopologue and provide vibration–rotation interaction constants (α_i), along with quartic and sextic distortion terms (in both the A and S reductions and I^r representation). The structure computed at the CCSD(T)/cc-pCVTZ level was also used for magnetic calculations to obtain the electron mass corrections to the rotational constants.[50] Additional computational corrections to the CCSD(T)/cc-pCV5Z structure are used to determine the best theoretical structure. These corrections were performed following the method prescribed by Heim *et al.*[1] and are specified below. The *xrefit* module of CFOUR was utilized to obtain the semi-experimental r_e^{SE} structure by least-squares fitting of the isotopologue equilibrium moments of inertia.

SYNTHESIS OF DEUTERIO THIOPHENES

The synthetic approach to deuterium incorporation, via isotopic exchange, is ideal for rotational spectroscopy, enabling the broadband spectra of all isotopologues to be obtained in a single experiment. The characteristics of thiophene's rotational spectrum cause the transitions of each isotopologue to be relatively distinct, thereby minimizing problems with the identification and assignment of transitions because of overlapping signals from multiple species. The ability to prepare and measure a single sample containing multiple species represents dramatic savings in time and effort, relative to an alternative approach involving the chemical synthesis and measurement of each isotopologue, individually.

Deuterium-containing isotopologues of thiophene were prepared in a manner analogous to the incorporation of deuterium in other five-membered heteroaromatic ring compounds and previous efforts on thiophene itself.[51–54] The acid-catalyzed reaction involved refluxing thiophene, D_2O, and fuming sulfuric acid at 100 °C for five days [Scheme 1(a)]. The duration of reflux may be varied to control the level of deuterium–hydrogen exchange. The five-day reaction time generated a mixture containing all nine of the possible deuterium-containing isotopologues of the normal isotopologue of thiophene. To shift the distribution of isotopologues toward those with a higher level of deuterium incorporation, the same reaction was conducted with refluxing extended over two weeks, with the addition of more H_2SO_4 and D_2O after seven days. This procedure yielded a small sample consisting of



SCHEME 1. Synthesis of deuterium-containing isotopologues of thiophene.

mostly tetra-deuterio thiophene, which provided transitions for the [2,3,4,5-^{2}H, ^{34}S] isotopologue. While the extended time for reflux and replenishing the deuterium source did increase the amount of deuterium incorporation, this method is not sufficient for obtaining a sample that has only the tetra-deuterio isotopologue present.

The deuterium–hydrogen exchange reactions proceed via deuteriation/deprotonation at each carbon atom in the ring [Scheme 1(a)]. The preference for D/H exchange at C2 over C3 is consistent with the relative energies of the thiolium cation intermediates (Fig. 2). The 9.1 kcal/mol energy difference [B3LYP/6-311G+(2d,p)+ZPVE] is rationalized by delocalization of positive charge over more atoms via π conjugation when H/D^+ is attached to C2, as shown in the accompanying resonance structures. A similar stabilization is not afforded when H/D^+ is bonded to C3. This interpretation is drawn from the highest-contributing resonance structures from the natural resonance theory analysis and the natural population analysis charges of each thiolium ion, as displayed in Fig. 2. The differential rate of exchange leads to the dominance of [2-^{2}H]-, [2,5-^{2}H]-, and [2,3,5-^{2}H]-thiophene in the rotational spectrum of the deuterium-enriched sample (after five days reflux), while the lowest-abundance thiophene-d_x species in the spectrum

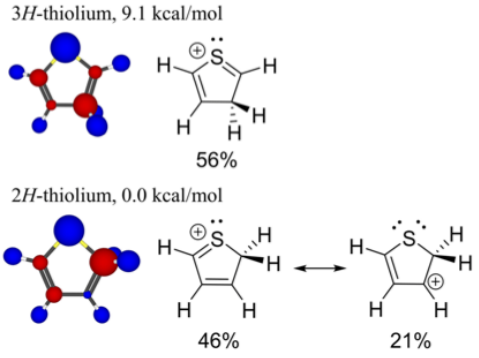


FIG. 2. 2H-thiolium and 3H-thiolium with their relative energies [B3LYP/6-311G+(2d,p)+ZPVE], the natural population analysis charges as spheres whose size corresponds to the magnitude of the local charge (blue for positive and red for negative), and relevant resonance structures from the natural resonance theory analysis.

Published under an exclusive license by AIP Publishing

The Journal of Chemical Physics ARTICLE scitation.org/journal/jcp

(excluding heavy-atom sulfur or carbon isotopologues) is [3,4-^{2}H]-thiophene.

An alternate synthetic route was adapted to generate [3-^{2}H]-thiophene[55] because that isotopologue cannot be prepared in high abundance using acid-catalyzed H/D exchange. A sample of [3-^{2}H]-thiophene was generated from 3-bromothiophene by lithium–halogen exchange, followed by quenching with D_2O [Scheme 1(b)]. The resultant sample was primarily [3-^{2}H]-thiophene, but the reaction did contain some [2-^{2}H]-thiophene, along with other combinations of di- and tri-deuterio isotopologues (although in substantially smaller amounts than generated by acid-catalyzed H/D exchange). The rearranged and poly-deuteriated thiophenes presumably result from base-catalyzed H/D exchange in the strongly basic conditions. The reaction described in Scheme 1(b) allowed for the assignment of more transitions for the [3-^{2}H] isotopologue and permitted the observation of sulfur and carbon heavy-atom isotopologues of [3-^{2}H]-thiophene. Synthetic details and relevant NMR and mass spectra are included in the supplementary material.

ANALYSIS OF ROTATIONAL SPECTRA

Normal isotopologue, ground vibrational state

The rotational spectrum of the ground vibrational state of the normal isotopologue of thiophene has been greatly expanded from previous works (5–40 GHz)[24,31–34] to include 40–360 GHz, along with some additional transitions between 12 and 18 GHz. The spectrum of thiophene, which includes the normal isotopologue and four heavy-atom isotopologues at natural abundance, is shown in Fig. 3. The distinct bands in the spectrum are due to $^aR_{0,1}$ transitions that are degenerate with respect to K_c and decrease in J as they increase in K_a progressing toward higher frequency. As K_a continues to increase, these transitions lose degeneracy near K_a = 10 and eventually become degenerate with respect to K_a around K_a = 20. With the inclusion of transitions previously reported,[31,32,34] the dataset contains 3270 transitions with a J'' range from 1 to 93 and K_a'' range from 0 to 38; this is depicted in the data distribution plot provided in the supplementary material. Least-squares fitting of this large dataset requires a full sextic, distorted-rotor Hamiltonian (A and S reductions and I^r and III^r representations all employed) to obtain a low-error fit (σ = 0.022 MHz) with physically meaningful spectroscopic constants. The experimental κ value of −0.0917 indicates the highly asymmetric, barely prolate nature of thiophene and suggests the I^r representation to be somewhat more appropriate than III^r. The III^r representation, which is more appropriate to oblate asymmetric tops, has commonly been used in previous studies of thiophene. To allow for comparison with previous work, the A-reduced, I^r and III^r spectroscopic constants from this work are presented in Table I along with computational values and previously determined values from high-resolution IR studies.[18,20] The computed and experimental spectroscopic constants display excellent agreement. Compared to the experimentally determined spectroscopic constants (A-reduced, I^r representation), the computed rotational constants [CCSD(T)/cc-pCVTZ] are within 0.8%, the quartic distortion constants are within 2%, and the sextic constants are within 10%. This agreement provides excellent indication that the experimental constants (A reduction and I^r representation) are physically meaningful. Constants from the S-reduced Hamiltonian in the I^r representation are presented in Table II, and constants in the III^r representation least-squares fit are presented in Table SI. With the exception of H_K in the S reduction, I^r representation, all quartic and sextic constants were satisfactorily determined in both representations and in both reductions.

Heavy-atom isotopologues: [2-^{13}C]-, [3-^{13}C]-, [^{34}S]-, and [^{33}S]-thiophene

Clearly visible in the spectrum at natural abundance are two sulfur isotopologues ([^{34}S] and [^{33}S]) and two ^{13}C isotopologues ([2-^{13}C] and [3-^{13}C]) of thiophene (Fig. 3). Transitions for each of these isotopologues from 40 to 360 GHz were combined with transitions from the literature (when within two times their reported experimental uncertainty)[25,34] and least-squares fit to a

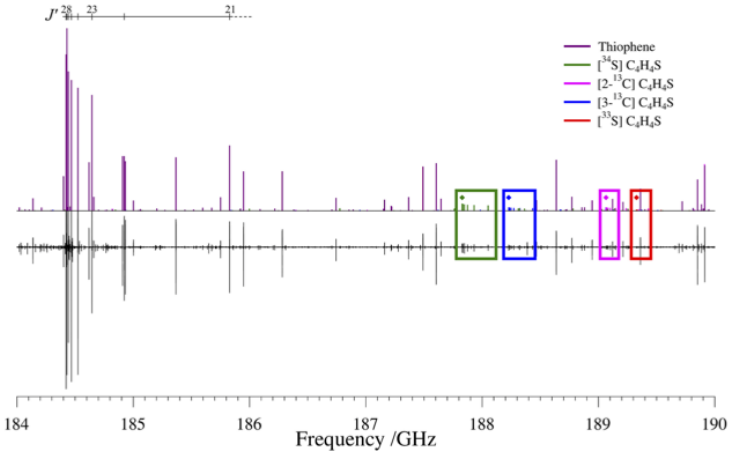


FIG. 3. Experimental rotational spectrum of thiophene (below) and predicted stick spectra (above) for the vibrational ground states (G.S.) of the normal (purple), [^{34}S] (green), [2-^{13}C] (pink), [3-^{13}C] (blue), and [^{33}S] (red) isotopologues of thiophene from 184 to 190 GHz. The J' = 29, K_a' = 0$^+$, 1$^-$ degenerate transition for each heavy-atom isotopologue is denoted with a diamond marker in the respective color. Major transitions for the normal isotopologue are labeled with the J' value of the upper energy-level quantum number.

Published under an exclusive license by AIP Publishing

The Journal of Chemical Physics ARTICLE scitation.org/journal/jcp

TABLE I. Computed and experimental spectroscopic constants for the vibrational ground state of the normal isotopologue of thiophene (A-reduced Hamiltonian, I^r and III^r representations).

		Experimental			Experimental	
	CCSD(T)/cc-pCVTZ	Rotational	IR[20,a]	CCSD(T)/cc-pCVTZ	Rotational	IR[18,a]
Representation	I^r	I^r	I^r	III^r	III^r	III^r
$A_0^{(A)}$ (MHz)	7 999	8 041.594 988 (44)	8 041.643 (13)	7 999	8 041.594 596 (44)	8 041.595 67 (25)
$B_0^{(A)}$ (MHz)	5 376	5 418.264 739 (36)	5 418.201 5 (33)	5 376	5 418.265 640 (36)	5 418.265 78 (11)
$C_0^{(A)}$ (MHz)	3 213	3 235.779 214 (39)	3 235.776 3 (36)	3 213	3 235.778 713 (39)	3 235.778 71 (10)
Δ_J (kHz)	0.823	0.837 865 (26)	0.830 (24)	2.155	2.176 349 (46)	2.178 2 (14)
Δ_{JK} (kHz)	−0.269	−0.272 860 (41)	−0.25 (11)	−4.263	−4.288 32 (15)	−4.299 (54)
Δ_K (kHz)	2.32	2.326 48 (10)	2.32 (10)	2.320	2.326 54 (11)	2.337 2 (42)
δ_J (kHz)	0.306	0.311 642 9 (36)	0.307 (12)	0.360	0.357 595 (20)	0.359 42 (69)
δ_K (kHz)	0.901	0.917 685 (27)	0.909 (81)	−1.372	−1.367 59 (11)	−1.376 6 (45)
Φ_J (Hz)	0.000 294	0.000 299 0 (53)		0.001 01	0.000 967 (41)	
Φ_{JK} (Hz)	−0.000 984	−0.000 951 (14)		−0.005 85	−0.005 59 (30)	
Φ_{KJ} (Hz)	−0.001 33	−0.001 477 (44)		0.007 73	0.007 30 (54)	
Φ_K (Hz)	0.003 45	0.003 42 (11)		−0.002 89	−0.002 68 (28)	
ϕ_J (Hz)	0.000 151	0.000 153 71 (80)		0.000 208	0.000 180 (20)	
ϕ_{JK} (Hz)	−0.000 093 7	−0.000 085 9 (99)		−0.003 36	−0.003 20 (17)	
ϕ_K (Hz)	0.003 11	0.003 184 (21)		0.001 19	0.001 00 (23)	
$N_{\text{lines MW}}$		3 270[b]	6		3 270[b]	25
$N_{\text{lines IR}}$		0	3 971[c]		0	10 725[c]
σ (MHz)		0.022			0.022	
κ[d]	−0.096 5	−0.091 7	−0.091 8	−0.096 5	−0.091 7	−0.091 7
Δ_i (μÅ^2)[e]	0.076 4	0.065 799 1 (20)	0.065 23 (21)	0.076 4	0.065 835 7 (20)	0.065 846 5 (56)

[a]Converted from cm^{-1}.
[b]Number of independent frequencies in the fit, including transitions from previous works.[31,32,34]
[c]Total number of transitions in the fit.
[d]$\kappa = (2B - A - C)/(A - C)$, experimental values calculated using PLAN.
[e]$\Delta_i = I_c - I_b - I_a$, experimental values calculated using PLAN.

sextic, distorted-rotor Hamiltonian in the S reduction and I^r representation. For the ^{13}C isotopologues (2.2% of the intensity of the normal isotopologue), over 960 distinct transitions were included in the least-squares fits. More than 1250 distinct transitions were least-squares fits for the [^{34}S] isotopologue (4.3% natural abundance), and over 250 transitions were least-squares fits for the much less abundant [^{33}S] isotopologue (0.75% natural abundance). No sextic distortion constants were able to be determined for the [^{33}S] isotopologue, unlike for the other three heavy-atom isotopologues, where each has some sextic distortion constants determined. The spectroscopic constants for all rare thiophene isotopologues are presented in Table II in the S reduction and I^r representation. All isotopologues have also been fit to a sextic, distorted-rotor Hamiltonian in the A reduction and I^r representation, which are presented in the supplementary material (Table SII), along with the data distribution plots for all other isotopologues (A reduction and I^r representation). Distortion constants that were not able to be experimentally determined were held constant to the predicted values [CCSD(T)/cc-pCVTZ]. The ^{36}S-isotopologue was sought using the rotational constants derived from the r_e^{SE} structure, but not identified due to its low natural abundance (0.01%).

Deuterium-enriched isotopologues

Previously, rotational transitions of both mono-deuterio-, one di-deuterio ([3,4-^{2}H])-, and tetra-deuteriothiophene isotopologues were reported.[24] The synthesis outlined in Scheme 1(a), after five days of reflux, resulted in a sample containing all possible mono-, di-, tri-, and tetra-deuterio isotopologues. A number of ^{34}S and ^{13}C variants of these deuterium-enriched isotopologues were also observed at their natural abundances. In total, 15 isotopologues of thiophene, including 11 that were previously unreported, were observed from this sample. For each isotopologue, rotational transitions were least-squares fits to a sextic, distorted-rotor Hamiltonian in the A and S reductions and the I^r representation (S reduction in Table II and A reduction in the supplementary material, Table SII). The deuterio isotopologues follow a similar spectral pattern to the normal isotopologue, with strong $^aR_{0,1}$ bands; a portion of the spectrum of the deuterium-containing isotopologues is displayed in Fig. 4. The band structure of thiophene is such that the spacing

Published under an exclusive license by AIP Publishing

The Journal of Chemical Physics ARTICLE scitation.org/journal/jcp

TABLE II. Spectroscopic constants for isotopologues of thiophene (S-reduced Hamiltonian, I^r representation).[a]

Isotopologue	C_4H_4S[b]	[2-^{13}C][b]	[3-^{13}C][b]	[^{34}S][b]	[^{33}S][b]	[2-^{2}H][b]
$A_0^{(S)}$ (MHz)	8 041.595 658 (44)	7 852.775 54 (31)	7 981.280 38 (34)	8 041.715 07 (20)	8 041.651 5 (20)	7 437.197 29 (20)
$B_0^{(S)}$ (MHz)	5 418.262 629 (36)	5 418.405 62 (10)	5 319.305 933 (98)	5 274.184 579 (69)	5 344.297 61 (59)	5 413.721 571 (84)
$C_0^{(S)}$ (MHz)	3 235.780 781 (39)	3 204.806 550 (87)	3 190.618 898 (88)	3 183.843 198 (67)	3 209.258 34 (13)	3 131.815 069 (83)
D_J (kHz)	0.703 074 (26)	0.699 151 (61)	0.675 952 (59)	0.680 947 (46)	0.691 62 (14)	0.681 599 (56)
D_{JK} (kHz)	0.535 835 (27)	0.506 44 (37)	0.551 34 (32)	0.510 05 (19)	0.521 62 (77)	0.444 81 (26)
D_K (kHz)	1.652 637 (67)	1.583 22 (56)	1.611 09 (65)	1.699 58 (45)	1.665 9 (33)	1.269 81 (35)
d_1 (kHz)	−0.3116416 (36)	−0.313 237 (19)	−0.298 436 (19)	−0.297 537 (19)	−0.304 257 (86)	−0.313 542 (24)
d_2 (kHz)	−0.067 394 2 (18)	−0.068 193 (11)	−0.064 8635 (97)	−0.062 968 7 (79)	−0.065 028 (28)	−0.069 745 1 (78)
H_J (Hz)	0.000 212 5 (54)	0.000 218 (14)	0.000 203 (14)	0.000 197 (12)	[0.000 212]	0.000 225 (17)
H_{JK} (Hz)	−0.001668 (10)	−0.001 54 (18)	−0.001 48 (15)	[−0.001 66]	[−0.001 69]	−0.001 82 (18)
H_{KJ} (Hz)	0.002 158 (32)	0.003 03 (51)	0.001 79 (36)	0.002 09 (20)	[0.002 18]	0.00247 (37)
H_K (Hz)	[0.000 672]	[0.000 597]	[0.000 672]	[0.000 759]	[0.000 716]	[0.000 387]
h_1 (Hz)	0.000 131 05 (73)	[0.000 128]	[0.000 121]	0.000 122 0 (61)	[0.000 126]	0.000 122 4 (73)
h_2 (Hz)	0.000 043 05 (56)	[0.000 0360]	[0.000 038 6]	0.000 041 4 (25)	[0.000 036 7]	0.000 032 9 (50)
h_3 (Hz)	0.000 022 52 (14)	[0.000 0221]	[0.000 020 3]	0.000 021 08 (86)	[0.000 020 5]	0.000 021 9 (10)
N_{lines}[c]	3 270	965	983	1262	258	1350
σ (MHz)	0.022	0.030	0.029	0.024	0.029	0.028
κ[d]	−0.917	−0.047 5	−0.111	−0.139	−0.116	0.060 0
Δ_i (μÅ^2)[e]	0.065 692 3 (20)	0.066 543 0 (53)	0.066 298 4 (55)	0.066 441 0 (39)	0.065 992 (20)	0.064 984 2 (49)

Isotopologue	[3-^{2}H][b]	[2,3-^{2}H]	[2,4-^{2}H]	[2,5-^{2}H]	[3,4-^{2}H]	[2,3,4-^{2}H]
$A_0^{(S)}$ (MHz)	7 855.997 58 (11)	7 277.001 30 (27)	7 288.383 17 (21)	6 903.426 58 (12)	7 616.557 (16)	7 072.276 05 (33)
$B_0^{(S)}$ (MHz)	5 138.229 854 (63)	5 137.627 501 (97)	5 124.657 587 (77)	5 410.698 544 (68)	4 914.679 4 (78)	4 909.469 19 (10)
$C_0^{(S)}$ (MHz)	3 105.222 733 (72)	3 010.350 104 (87)	3 007.831 223 (83)	3 032.130 273 (70)	2 986.054 60 (18)	2 896.801 160 (94)
D_J (kHz)	0.606 648 (43)	0.592 435 (59)	0.578 844 (46)	0.666 346 (46)	0.537 95 (23)	0.520 247 (60)
D_{JK} (kHz)	0.567 38 (10)	0.457 48 (34)	0.538 407 (90)	0.326 19 (15)	[0.531]	0.469 51 (35)
D_K (kHz)	1.524 38 (13)	1.178 63 (53)	1.142 75 (32)	1.001 64 (15)	[1.40]	1.075 91 (53)
d_1 (kHz)	−0.265 109 (10)	−0.268 999 (28)	−0.262 829 (14)	−0.316 194 (18)	−0.233 02 (18)	−0.234 458 (26)
d_2 (kHz)	−0.058 206 4 (36)	−0.060 220 (10)	−0.060 718 8 (32)	−0.070 902 5 (42)	−0.050 945 (68)	−0.053 293 1 (94)
H_J (Hz)	0.000 146 5 (92)	0.000 142 (21)	0.000 120 9 (96)	0.000 236 (10)	[0.000 123]	0.000 123 (19)
H_{JK} (Hz)	−0.001 063 (43)	−0.001 10 (18)	[−0.000 752]	−0.001 619 (44)	[−0.000 972]	−0.000 80 (11)
H_{KJ} (Hz)	0.001 17 (10)	0.001 43 (38)	[0.000 762]	0.002 274 (91)	[0.001 29]	0.001 23 (28)
H_K (Hz)	[0.000 920]	[0.000 530]	[0.000 791]	[0.000 116]	[0.000 696]	[0.000 472]
h_1 (Hz)	0.000 096 4 (20)	0.000 084 (10)	[0.000 087 8]	0.000 122 2 (46)	[0.000 079 4]	0.000 082 1 (97)
h_2 (Hz)	0.000 038 5 (12)	0.000 030 7 (52)	[0.000 040 1]	[0.000 030 9]	[0.000 029 3]	[0.000 029 2]
h_3 (Hz)	0.000 016 76 (26)	0.000 018 1 (12)	[0.000 016 8]	0.000 025 05 (58)	[0.000 013 6]	0.000 015 9 (14)
N_{lines}[c]	1 880	1 187	1 171	1 651	203	1 049
σ (MHz)	0.029	0.030	0.030	0.027	0.038	0.032
κ[d]	−0.144 1	−0.002 8	−0.011 0	0.228 8	−0.167 0	−0.036 0
Δ_i (μÅ^2)[e]	0.064 312 3 (41)	0.063 507 3 (58)	0.063 593 3 (53)	0.063 937 3 (43)	0.063 22 (22)	0.062 244 6 (70)

Published under an exclusive license by AIP Publishing

The Journal of Chemical Physics ARTICLE scitation.org/journal/jcp

TABLE II. (*Continued.*)

Isotopologue	[2,3,5-^{2}H]	[2,3,4,5-^{2}H]	[2,5-^{2}H, ^{34}S]	[2,3,5-^{2}H, ^{34}S]	[2,3,4,5-^{2}H, ^{34}S][f]	[2,5-^{2}H, 2-^{13}C]
$A_0^{(S)}$ (MHz)	6 775.849 57(12)	6 587.731 79(20)	6 903.535 0(11)	6 773.399 56(92)	6 588.36(32)	6 763.947(25)
$B_0^{(S)}$ (MHz)	5 124.449 058(64)	4 905.808 107(85)	5 268.343 08(37)	4 992.253 90(32)	4 777.72(18)	5 410.781(17)
$C_0^{(S)}$ (MHz)	2 916.731 610(66)	2 810.897 843(77)	2 986.906 70(30)	2 872.969 11(23)	2 768.492 1(18)	3 004.929 39(26)
D_J (kHz)	0.567 721(40)	0.507 404(48)	0.645 38(15)	0.552 89(13)	0.487 0(65)	0.667 44(43)
D_{JK} (kHz)	0.418 49(19)	0.377 71(25)	0.317 68(78)	0.376 2(24)	[0.348]	[0.271]
D_K (kHz)	0.888 63(18)	0.843 81(29)	1.035 4(14)	0.964 8(52)	[0.882]	[0.996]
d_1 (kHz)	−0.266 630(16)	−0.236 303(23)	−0.302 494(66)	−0.255 757(61)	−0.222 5(45)	−0.318 45(33)
d_2 (kHz)	−0.062 119 2(50)	−0.054 507 4(35)	−0.066 729(35)	−0.057 659(83)	−0.050 3(12)	−0.070 65(11)
H_J (Hz)	0.000 151(12)	0.000 144(17)	0.000 237(30)	0.000 111(16)	[0.000 116]	[0.000 229]
H_{JK} (Hz)	−0.000 862(70)	−0.000 906(94)	−0.001 27(36)	[−0.000 792]	[−0.000 780]	[−0.001 54]
H_{KJ} (Hz)	[0.000 857]	[0.001 05]	[0.001 85]	[0.000 895]	[0.001 01]	[0.002 03]
H_K (Hz)	[0.000 474]	[0.000 270]	[0.000 173]	[0.000 473]	[0.000 301]	[0.000 068 2]
h_1 (Hz)	0.000 093 6(52)	0.000 080 2(86)	[0.000 116]	[0.000 084 3]	[0.000 071 7]	[0.000 121]
h_2 (Hz)	0.000 037 9(16)	[0.000 027 0]	[0.000 029 2]	[0.000 032 8]	[0.000 024 9]	[0.000 027 3]
h_3 (Hz)	0.000 017 90(55)	0.000 015 52(66)	[0.000 021 0]	[0.000 015 8]	[0.000 013 1]	[0.000 023 6]
N_{lines}[c]	1672	1 349	420	458	39	165
σ (MHz)	0.027	0.031	0.042	0.039	0.039	0.044
κ[d]	0.144 2	0.109 3	0.165 0	0.086 7	0.052 0	0.280 0
Δ_i (μÅ^2)[e]	0.062 470 0(44)	0.061 092 5(58)	0.064 788(22)	0.063 317(19)	0.060 8(56)	0.064 52(41)

Isotopologue	[2,5-^{2}H, 3-^{13}C]	[2-^{2}H, ^{34}S]	[3-^{2}H, 2-^{13}C]	[3-^{2}H, 3-^{13}C]	[3-^{2}H, 4-^{13}C]	[3-^{2}H, 5-^{13}C]
$A_0^{(S)}$ (MHz)	6 860.081(23)	7 436.863(16)	7 681.747(50)	7 816.981(61)	7 775.956(56)	7 671.947(41)
$B_0^{(S)}$ (MHz)	5 310.447(15)	5 270.700 0(92)	5 137.725(24)	5 045.949(27)	5 060.889(25)	5 138.103(19)
$C_0^{(S)}$ (MHz)	2 992.158 23(26)	3 083.341 37(19)	3 077.431 02(28)	3 065.287 40(28)	3 064.440 94(27)	3 075.993 25(24)
D_J (kHz)	0.641 97(37)	0.663 89(23)	0.605 49(44)	0.585 84(48)	0.588 84(51)	0.602 06(37)
D_{JK} (kHz)	[0.329]	[0.404]	[0.520]	[0.563]	[0.552]	[0.534]
D_K (kHz)	[0.989]	[1.33]	[1.47]	[1.51]	[1.49]	[1.46]
d_1 (kHz)	−0.303 29(28)	−0.301 28(18)	−0.267 33(34)	−0.254 28(37)	−0.256 68(39)	−0.265 54(28)
d_2 (kHz)	−0.067 76(10)	−0.065 200(70)	−0.058 59(13)	−0.055 59(14)	−0.056 13(14)	−0.058 44(11)
H_J (Hz)	[0.000 200]	[0.000 203]	[0.000 151]	[0.000 134]	[0.000 144]	[0.000 147]
H_{JK} (Hz)	[−0.001 31]	[−0.001 48]	[−0.001 14]	[−0.000 949]	[−0.001 09]	[−0.001 08]
H_{KJ} (Hz)	[0.001 71]	[0.001 89]	[0.001 39]	[0.001 05]	[0.001 39]	[0.001 24]
H_K (Hz)	[0.000 166]	[0.000 450]	[0.000 827]	[0.000 979]	[0.000 771]	[0.000 901]
h_1 (Hz)	[0.000 114]	[0.000 119]	[0.000 095 9]	[0.000 090 4]	[0.000 0931]	[0.000 095 3]
h_2 (Hz)	[0.000 032 9]	[0.000 034 0]	[0.000 034 6]	[0.000 036 8]	[0.000 0346]	[0.000 036 0]
h_3 (Hz)	[0.000 021 6]	[0.000 020 3]	[0.000 016 9]	[0.000 015 5]	[0.000 0159]	[0.000 016 8]
N_{lines}[c]	174	237	133	112	113	143
σ (MHz)	0.045	0.039	0.046	0.041	0.041	0.040
κ[d]	0.198 7	0.004 9	−0.105 1	−0.166 3	−0.152 5	−0.102 6
Δ_i (μÅ^2)[e]	0.064 70(38)	0.065 73(23)	0.065 19(64)	0.064 83(75)	0.064 95(69)	0.065 15(52)

Published under an exclusive license by AIP Publishing

The Journal of Chemical Physics ARTICLE scitation.org/journal/jcp

TABLE II. (*Continued.*)

Isotopologue	[3-^{2}H, ^{34}S]	[3-^{2}H, ^{33}S][f]
$A_0^{(S)}$ (MHz)	7 854.541 26(65)	7 854.84(47)
$B_0^{(S)}$ (MHz)	5 003.229 49(16)	5 069.12(20)
$C_0^{(S)}$ (MHz)	3 055.165 94(14)	3079.662 92(44)
D_J (kHz)	0.588 513 (76)	0.595 8 (15)
D_{JK} (kHz)	0.537 56 (46)	[0.534]
D_K (kHz)	1.570 5 (12)	[1.56]
d_1 (kHz)	−0.253 387 (27)	−0.257 1 (11)
d_2 (kHz)	−0.054 331 (10)	−0.054 93 (42)
H_J (Hz)	0.000 157 (17)	[0.000 146]
H_{JK} (Hz)	−0.001 03 (16)	[−0.001 103]
H_{KJ} (Hz)	[0.001 26]	[0.001 28]
H_K (Hz)	[0.000 964]	[0.000 942]
h_1 (Hz)	[0.000 092 2]	[0.000 094 3]
h_2 (Hz)	[0.000 033 0]	[0.000 034 5]
h_3 (Hz)	[0.000 015 0]	[0.000 015 7]
N_{lines}[c]	664	57
σ (MHz)	0.035	0.045
κ[d]	−0.188 2	−0.166 7
Δ_i (μÅ^2)[e]	0.065 030 5(99)	0.064 8 (56)

[a]Values in square brackets held fixed at the CCSD(T)/cc-pCVTZ predicted value in the least-squares fit.
[b]Includes previously reported transitions.[24,25,31,32,34]
[c]Number of independent frequencies in the fit.
[d]$\kappa = (2B - A - C)/(A - C)$, calculated using PLAN.
[e]$\Delta_i = I_c - I_b - I_a$, calculated using PLAN.
[f]Shaded columns indicate that the isotopologue is not included in structure determination.

between bands and the transitions within the bands allows for clear visibility of each of the various isotopologues. While the [2,3,4,5-^{2}H, ^{34}S] species was observed in the original five-day deuterium-enriched sample, the measured transitions reported in Table II come from the sample containing primarily tetra-deuterio thiophene (14-day sample). Transitions from previous microwave work[24] of the [2-^{2}H] and [3-^{2}H] isotopologues that agreed to within 2σ of their experimental uncertainty were included in their respective

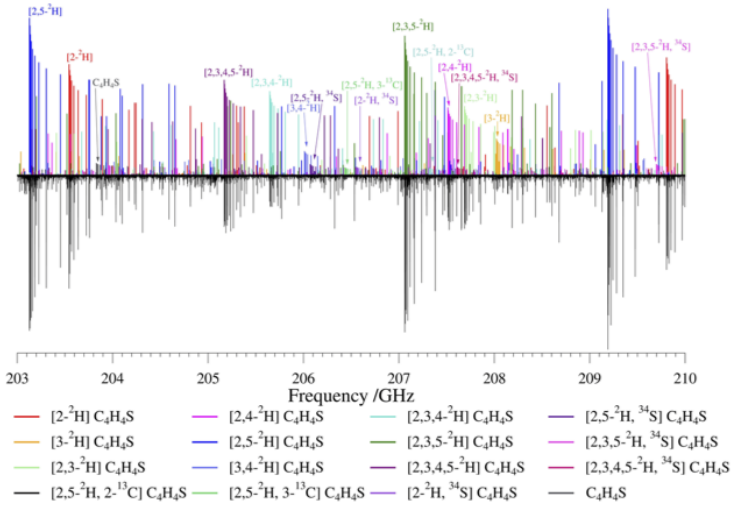


FIG. 4. Experimental rotational spectrum of deuterium-enriched thiophene (below) and the predicted stick spectra (above) for the vibrational ground states of thiophene isotopologues from 203 to 210 GHz.

Published under an exclusive license by AIP Publishing

The Journal of Chemical Physics ARTICLE scitation.org/journal/jcp

datasets (data distribution plots provided in the supplementary material).

In the [3-^{2}H]-enriched sample [Scheme 1(b)], [3-^{2}H, ^{34}S]-thiophene was the most abundant heavy-atom isotopologue, and its enhanced intensity allowed for the measurement of 664 distinct transitions. The presence of deuterium at the three-position breaks the C_{2v} symmetry, which results in four unique mono-^{13}C isotopologues (1.1% the intensity of the [3-^{2}H] isotopologue). Over 100 transitions were measured and least-squares fit for each [3-^{2}H, ^{13}C] isotopologue. The incomplete specificity of the reaction also resulted in deuterium incorporation at the two and five positions and provided additional transitions for the [2-^{2}H, ^{34}S] isotopologue. Inasmuch as ^{33}S is the least naturally abundant isotope observed, only 57 transitions for [3-^{2}H, ^{33}S]-thiophene were able to be included in its least-squares fit. Like with the [2,3,4,5-^{2}H, ^{34}S] isotopologue, the small number of transitions and relatively large error in A_0 and B_0 means that the spectroscopic constants of [3-^{2}H, ^{33}S] are not confidently determined. Therefore, neither of these isotopologues were included in the determination of the structure.

STRUCTURE DETERMINATION

The semi-experimental equilibrium structural parameters (r_e^{SE}) of thiophene were determined by least-squares fitting of the equilibrium moments of inertia. The experimental rotational constants (B_0) of 24 isotopologues provide 72 moments of inertia to determine eight independent structural parameters (due to the C_{2v} symmetry of thiophene). The B_0 constants from both the A- and S-reductions (I^r representations) were converted to their determinable constants (B'') to remove effects of centrifugal distortion using Eqs. (S1)–(S6) (see the supplementary material)[56] and then averaged. The very close agreement of the B'' constants (Table SIII) confirms that each isotopologue transition dataset is well treated by both the A- and S-reduced Hamiltonians, which produce physically meaningful spectroscopic constants. The averaged B'' constants from the A and S reductions were further corrected to their equilibrium rotational constants by applying the computational vibration–rotation corrections (half the sum of the vibration–rotation interaction constants, α_i) and the computational electron mass corrections, as described in Eq. (1).[1,30] The electron mass corrections are obtained from the diagonal elements of the electronic contribution to the rotational g-tensor, $g^{\beta\beta}$, multiplied by the electron–proton mass ratio (m_e/M_P) and the computed equilibrium rotational constant [$B^{\beta}{}_{CCSD(T)}$], where $\beta = a$, b, or c,[1,30]

$$B_e^{\beta} = B''^{\beta} + \frac{1}{2}\sum_i \alpha_i^{\beta} - \frac{m_e}{M_P} g^{\beta\beta} B^{\beta}_{CCSD(T)}. \quad (1)$$

The deviation in the experimentally determined inertial defect ($\Delta_i = I_c - I_a - I_b$) from the ideal inertial defect value of zero for a planar molecule is much reduced by the inclusion of these computational corrections. The effect of each of the corrections on the inertial defect is shown in Table III for each isotopologue included in the structure. Table III includes $\Delta_i\ r_0$, the inertial defects from only the experimental B'' values relating to an r_0 structure, $\Delta_i\ r_e^{SE}$ (vib. corr. only), the inertial defects from the B'' values applying the vibration–rotation corrections only, and $\Delta_i\ r_e^{SE}$, the inertial defects calculated from the B'' values applying the vibration–rotation and electron mass corrections. The averages ($\bar{x}$) of these respective

TABLE III. Inertial defects (Δ_i in μÅ^2) of isotopologues of thiophene from various determinations of the moments of inertia.

Isotopologue	$\Delta_i\ r_0$	$\Delta_i\ r_e^{SE}$ (vib. corr. only)	$\Delta_i\ r_e^{SE}$
Normal	0.065 61	−0.009 02	0.001 28
[2-^{13}C]	0.066 45	−0.009 00	0.001 30
[3-^{13}C]	0.066 21	−0.009 01	0.001 29
[^{34}S]	0.066 36	−0.008 98	0.001 32
[^{33}S]	0.065 91	−0.009 08	0.001 22
[2-^{2}H]	0.064 90	−0.009 21	0.001 09
[3-^{2}H]	0.064 23	−0.009 03	0.001 28
[2,3-^{2}H]	0.063 42	−0.009 19	0.001 12
[2,4-^{2}H]	0.063 51	−0.009 22	0.001 09
[2,5-^{2}H]	0.063 85	−0.009 38	0.000 93
[3,4-^{2}H]	0.063 13	−0.008 89	0.001 42
[2,3,4-^{2}H]	0.062 16	−0.009 17	0.001 14
[2,3,5-^{2}H]	0.062 38	−0.009 37	0.000 94
[2,3,4,5-^{2}H]	0.061 01	−0.009 33	0.000 98
[2,5-^{2}H, ^{34}S]	0.064 70	−0.009 34	0.000 96
[2,3,5-^{2}H, ^{34}S]	0.063 23	−0.009 30	0.001 00
[2,5-^{2}H, 2-^{13}C]	0.064 43	−0.009 40	0.000 91
[2,5-^{2}H, 3-^{13}C]	0.064 60	−0.009 18	0.001 13
[2-^{2}H, ^{34}S]	0.065 65	−0.009 23	0.001 08
[3-^{2}H, 2-^{13}C]	0.065 10	−0.008 88	0.001 43
[3-^{2}H, 3-^{13}C]	0.064 76	−0.008 99	0.001 31
[3-^{2}H, 4-^{13}C]	0.064 87	−0.009 00	0.001 30
[3-^{2}H, 5-^{13}C]	0.065 06	−0.009 05	0.001 26
[3-^{2}H, ^{34}S]	0.064 95	−0.009 00	0.001 31
Average ($\bar{x}$)	0.064 44	−0.009 14	0.001 17
Std. dev. (s)	0.001 39	0.000 16	0.000 16

inertial defects, as well as the individual values for each isotopologue, indicate that both the vibrational and electronic corrections are needed to bring Δ_i closer to the ideal value of zero and obtain the best possible equilibrium constants (B_e). It is further clear that, including both corrections, the inertial defects are highly systematic and fairly constant. The low sample standard deviations (s) strongly indicate the high level of precision in the equilibrium moments of inertia used to calculate $\Delta_i\ r_e^{SE}$ and that the remaining deviations from zero are due to a yet unidentified systematic effect. Any random errors in the rotational constants (including in the vibration–rotation corrections) larger than a few tens of kHz would cause the value of s to be greater than what is observed. The ratio of $\bar{x}/s$ in the last column (Δ_i with both corrections applied) is ~7. It is also notable that all the shifts due to the electron mass correction are +0.010 30 or +0.010 31, even though the corresponding shifts in the individual rotational constants vary with isotopologue. The constancy in this shift is, of course, reflected in the standard deviation being the same in the two corresponding columns.

The averaged B'' values and computational corrections for each isotopologue are submitted to the *xrefit* module in CFOUR,[46] which least-squares fits the semi-experimental equilibrium moments of inertia and determines the structural parameters. The r_e^{SE} structural parameters are presented in Fig. 5(a) and in Table IV, alongside the computed structural parameters [CCSD(T)/cc-pCV5Z] and

Published under an exclusive license by AIP Publishing

The Journal of Chemical Physics ARTICLE scitation.org/journal/jcp

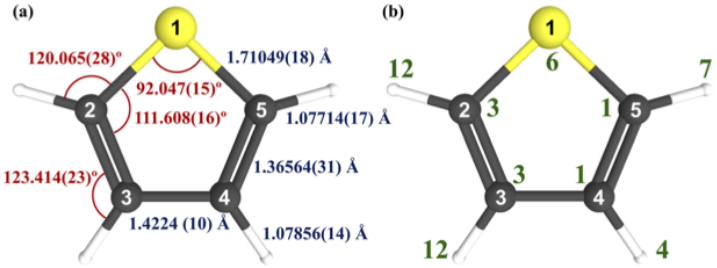


FIG. 5. (a) Semi-experimental equilibrium structure (r_e^{SE}) of thiophene and (b) the number of isotopic substitutions at each position included in the structure determined from the least-squares fit of 24 isotopologues.

experimental structural parameters determined previously.[25,27,28,30] Figure 5(b) presents the number of isotopologues with substitution(s) at the designated position used in the least-squares fit of the structure from 24 isotopologues. (For example, 3 at the C2 position indicates that its substitution is present in three isotopologues: [2-^{13}C], [2,5-^{2}H, 2-^{13}C], and [3-^{2}H, 2-^{13}C].) The structural parameters are presented graphically in Fig. 6.

To provide the best comparison to the semi-experimental equilibrium structure, the following four computational corrections to the CCSD(T)/cc-pCV5Z structure have been implemented to address residual error in the computational structure:

1. Residual basis set effects beyond cc-pCV5Z.
2. Residual electron correlation effects beyond the CCSD(T) treatment.
3. Effects of scalar (mass–velocity and Darwin) relativistic effects.
4. The diagonal Born–Oppenheimer correction (DBOC).

These four corrections are obtained in a manner similar to pyrimidine[1] using Eqs. (2)–(8), as described below.

1. To estimate the correction needed to approach the infinite basis set limit, equilibrium structural parameters obtained with the cc-pCVXZ (X = T, Q, and 5) basis sets were extrapolated using the empirical exponential[58]

$$R(x) = R(\infty) + Ae^{-Bx}, \tag{2}$$

where R(x) are the values of the parameters obtained using the largest three basis sets (x = 3, 4, and 5) and R(∞) is the desired basis set limit estimate. Using these three basis sets, Eq. (2) can be expressed as follows:

$$R(\infty) = -\frac{R(4)^2 - R(3)R(5)}{R(3) + R(5) - 2R(4)}. \tag{3}$$

The correction to the structure due to a finite basis set is then estimated by the following equation:

$$\Delta R(\text{basis}) = R(\infty) - R(\text{CCSD(T)/cc-pCV5Z}). \tag{4}$$

TABLE IV. Experimental and computational structural parameters of thiophene.

	r_e^{SE} [a,b]	CCSD(T)[c]	r_e^{SE} [d] Ref. 30	r_s Ref. 25	r_e [e] Ref. 28	r_α [f] Ref. 27
R_{S1-C2} (Å)	**1.710 49 (18)**	**1.709 44**	1.7126 (5)	1.7140 (14)	1.704 (2)	1.7136 (11)
R_{C2-C3} (Å)	**1.365 64 (31)**	**1.366 32**	1.3622 (8)	1.3696 (17)	1.372 (3)	1.3783 (15)
R_{C2-H} (Å)	**1.077 14 (17)**	**1.076 33**	1.0771 (5)	1.0776 (15)	1.085 (5)	1.0688 (6)
R_{C3-H} (Å)	**1.078 56 (14)**	**1.078 60**	1.0794 (3)	1.0805 (14)	1.088	1.0812 (11)
R_{C3-C4} (Å)	**1.422 4 (10)**[g]	**1.422 16**	1.4233 (21)	1.4232 (23)	1.421 (4)	1.4274 (11)
1/2 $A_{C2-S1-C5}$ (deg)	**46.024 (7)**	**46.051**	45.94 (2)	46.09 (5)	46.2 (1)	46.28 (4)
$A_{S1-C2-C3}$ (deg)	**111.608 (16)**	**111.596**	111.66 (3)	111.49 (24)	111.6	111.34 (7)
$A_{S1-C2-H}$ (deg)	**120.065 (28)**	**120.286**	120.11 (10)	119.89 (82)	119.9 (3)	120.24 (8)
$A_{C2-C3-H}$ (deg)	**123.414 (23)**	**123.416**	123.46 (7)	123.25 (7)	123.4	123.56 (8)
$A_{C2-S1-C5}$ (deg)	**92.047 (15)**[g]	**92.101**	91.88 (4)	92.17 (10)	92.4 (2)	92.56 (8)
$N_{isotopologues}$	**24**		8	6		

[a]Uncertainty reported is 2σ.
[b]Vibration–rotation and electron mass corrections at CCSD(T)/cc-pCVTZ.
[c]Evaluated using the cc-pCV5Z basis set.
[d]Vibration–rotation and electron mass corrections at B2PLYP/VTZ.
[e]Combined electron diffraction, microwave, vibrational, and computational data.
[f]Combined electron diffraction, microwave, and liquid-crystal NMR data.
[g]Parameter calculated from r_e^{SE} with propagated error; see Ref. 57.

Published under an exclusive license by AIP Publishing

The Journal of Chemical Physics ARTICLE scitation.org/journal/jcp

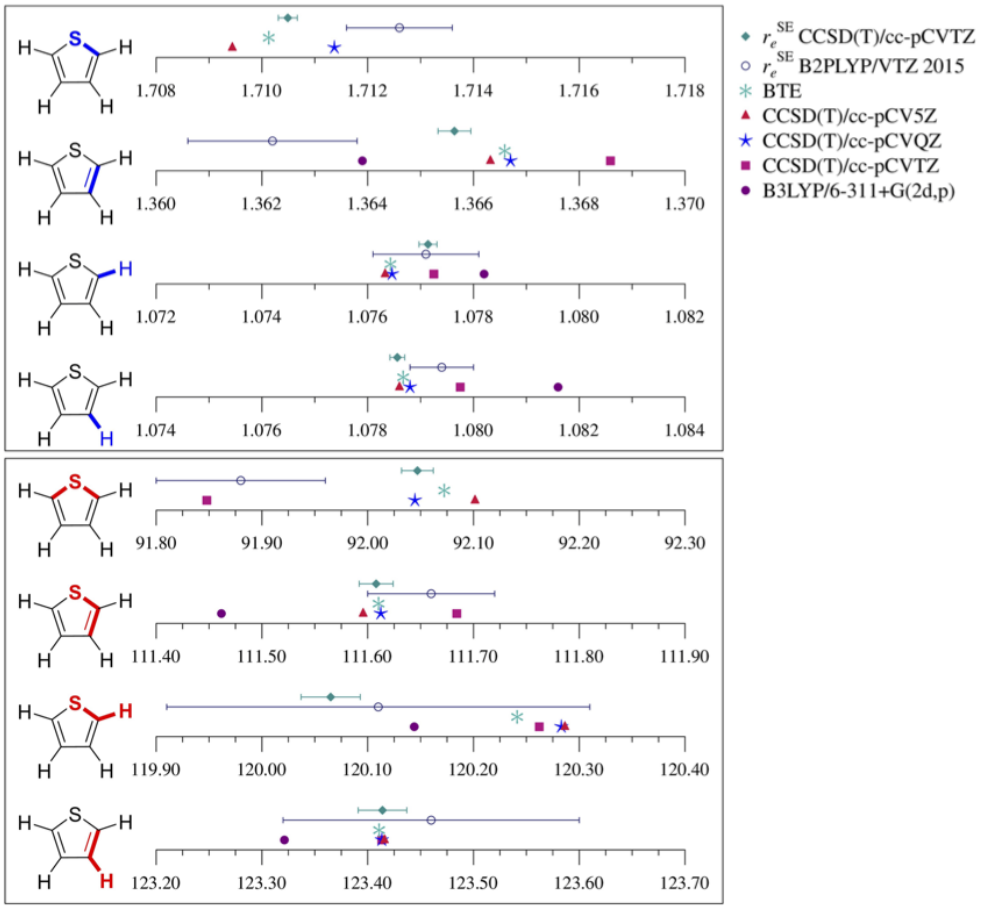


FIG. 6. Graphical comparison of the thiophene structural parameters with bond distances in angstrom (Å, blue) and angles in degree (°, red). All errors shown are 2σ.

2. Residual correlation effects are assessed by optimizing geometries at the CCSDT(Q) level[59] and then estimating the correlation correction as in the following equation:

$$\Delta R(\text{cor}) = R(\text{CCSDT(Q)}) - R(\text{CCSD(T)}). \quad (5)$$

Due to the expense of calculations at the CCSDT(Q) level, the cc-pVDZ basis in the frozen-core approximation is used for these calculations.

3. Relativistic corrections are obtained by subtraction of the parameters with a standard non-relativistic calculation from the equilibrium structure obtained with the X2C-1e variant of coupled-cluster theory,[60–62] as in the following equation:

$$\Delta R(\text{rel}) = R(\text{CCSD(T)/cc-pCVTZ})_{\text{SFX2C-1e}} - R(\text{CCSD(T)/cc-pCVTZ})_{NR}. \quad (6)$$

4. The diagonal Born–Oppenheimer correction (DBOC)[63,64] is obtained from the following equation:

$$\Delta R(\text{DBOC}) = R(\text{SCF/cc-pVTZ})_{DBOC} - R(\text{SCF/cc-pVTZ})_{NR}. \quad (7)$$

Here, the first value is obtained by minimizing the DBOC-corrected SCF energy with respect to nuclear positions, and the latter is again the traditional calculation.

The sum of these corrections is used to obtain the best equilibrium structural parameters, given by the following equation:

$$\Delta R(\text{best}) = \Delta R(\text{basis}) + \Delta R(\text{cor}) + \Delta R(\text{rel}) + \Delta R(\text{DBOC}). \quad (8)$$

Published under an exclusive license by AIP Publishing

The Journal of Chemical Physics ARTICLE scitation.org/journal/jcp

TABLE V. Corrections for the best theoretical estimate (BTE) of the equilibrium structure (r_e) of thiophene and comparison with the r_e^{SE} structure.

	Basis set correction [Eq. (4)]	Correlation correction [Eq. (5)]	Relativistic correction [Eq. (6)]	DBOC [Eq. (7)]	Sum of corrections [Eq. (8)]	CCSD(T)/cc-pCV5Z	BTE	r_e^{SE} [a]
R_{S1-C2} (Å)	−0.000 756	0.001 481	−0.000 052	0.000 009	0.000 682	1.709 44	**1.710 13**	**1.710 49 (18)**
R_{C2-C3} (Å)	−0.000 093	0.000 705	−0.000 355	0.000 012	0.000 269	1.366 32	**1.366 59**	**1.365 64 (31)**
R_{C2-H} (Å)	−0.000 026	0.000 090	−0.000 100	0.000 135	0.000 099	1.076 33	**1.076 43**	**1.077 14 (17)**
R_{C3-H} (Å)	−0.000 055	0.000 103	−0.000 111	0.000 130	0.000 067	1.078 60	**1.078 67**	**1.078 56 (14)**
1/2 $A_{C2-S1-C5}$ (deg)	0.011 523	−0.015 291	−0.011 943	0.001 172	−0.014 540	46.051	**46.036**	**46.024 (7)**
$A_{S1-C2-C3}$ (deg)	−0.005 025	0.005 053	0.015 810	−0.001 276	0.014 561	111.596	**111.610**	**111.608 (16)**
$A_{S1-C2-H}$ (deg)	0.000 635	−0.015 990	−0.031 264	0.001 444	−0.045 175	120.286	**120.241**	**120.065 (28)** [b]
$A_{C2-C3-H}$ (deg)	−0.002 507	−0.005 022	0.003 706	−0.001 211	−0.005 033	123.416	**123.411**	**123.414 (23)**
$A_{C2-S1-C5}$ (deg)	0.023 045	−0.030 583	−0.023 887	0.002 345	−0.029 079	92.101	**92.072**	**92.047 (15)** [c]

[a] Uncertainty reported is 2σ.
[b] $A_{S1-C2-H}$ has the greatest discrepancy between theory and experiment.
[c] Parameter calculated from r_e^{SE} with propagated error.

The values of each correction, ΔR(best), are applied to the CCSD(T)/cc-pCV5Z structural parameters and are presented in Table V and Fig. 6. We will refer to them as the "best theoretical estimate" (BTE) parameters.

DISCUSSION

In the r_e^{SE} structure of thiophene, the largest computed statistical (2σ) bond distance uncertainty is in R_{C2-C3} (0.000 31 Å), and the largest bond angle uncertainty is in $A_{S1-C2-H}$ (0.028°). Exactly how reliable these error estimates are, however, is a more subtle question. Comparing current r_e^{SE} to the previously published r_e^{SE} structure (Table IV), which applied vibration–rotation and electron mass corrections computed using DFT methods[30] to the rotational constants of eight isotopologues,[25] none of the previous parameters fall within the 2σ error bars of our current r_e^{SE} structure except for the R_{C2-H} distance. For most parameters, the earlier r_e^{SE} structure[30] is not in close agreement with our BTE structure, either. The differences between the two r_e^{SE} structures are presumably due to a combination of the incorporation of the precisely determined moments of inertia for more isotopologues and to differences in computational treatment.

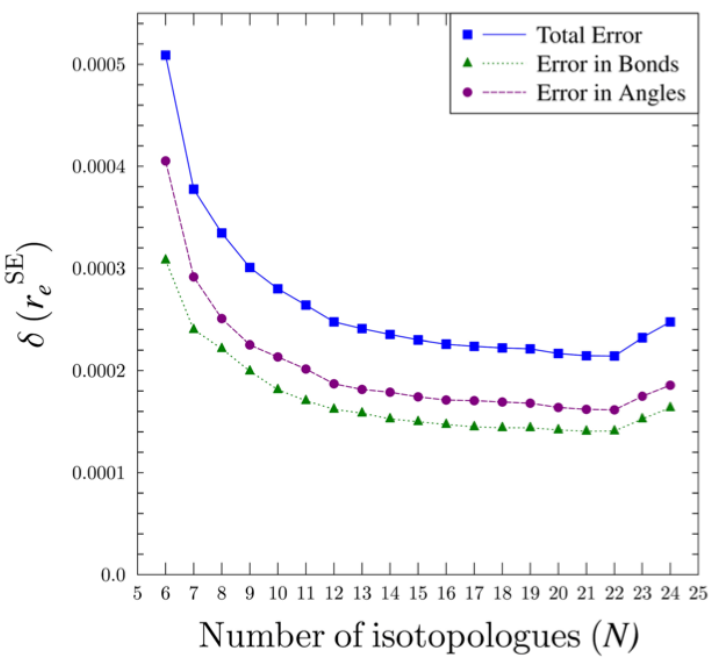
The large number of isotopologues incorporated in our current studies poses some new challenges with respect to analysis and interpretation of data. Therefore, our group developed a new method to analyze the contribution and importance of each isotopologue to the r_e^{SE} structure determination. A traditional substitution structure (r_s) from a Kraitchman analysis[26] relies on single isotopic substitution, which is sufficient to determine the structure.[25] Originally, this calculation employed ground-state constants (B_0), but it can also be applied to equilibrium rotational constants. The success of the Kraitchman analysis demonstrates that there is, at least, in principle, sufficient information content in the value of the rotational constants for the normal form and the singly substituted forms to locate every atom in the molecule. We have found, however, that the use of multiply substituted isotopologues provides useful additional structural information.[1,38] The parameters become highly over-determined, and the experimental uncertainty can be pushed well below the value achievable with smaller datasets, i.e., single substitutions. The analysis of isotopologue incorporation was performed with an iterative analysis, where we began with the normal isotopologue and five mono-substituted isotopologues ([2-^{13}C], [3-^{13}C], [^{34}S], [2-^{2}H], and [3-^{2}H]) as the "core set" and then added each of the remaining isotopologues, one-at-a-time, to the least-squares fit of the structure in *xrefit*. The value of the square root of the sum of the squared relative errors, which we call the $\delta(r_e^{SE})$, was determined for each isotopologue addition by using the following equation:

$$\delta(r_e^{SE}) = \sqrt{\sum_p \left(\frac{\sigma_p}{P}\right)^2}, \tag{9}$$

where P is each structural parameter determined by *xrefit* and σ_p is the respective (1σ) error of each parameter. The isotopologue that results in the lowest value of the $\delta(r_e^{SE})$ for the extended set is then incorporated into the structure determination for a total of seven isotopologues. The procedure repeats again, testing each

Published under an exclusive license by AIP Publishing

The Journal of Chemical Physics ARTICLE scitation.org/journal/jcp



N	Isotopologue Added
6	Core Set
7	[2,3,5-^{2}H, ^{34}S]
8	[2,5-^{2}H, 2-^{13}C]
9	[2,5-^{2}H, ^{34}S]
10	[2,5-^{2}H, 3-^{13}C]
11	[2,3,4,5-^{2}H]
12	[3-^{2}H, 4-^{13}C]
13	[2,3,5-^{2}H]
14	[3-^{2}H, ^{34}S]
15	[2,5-^{2}H]
16	[2,3,4-^{2}H]
17	[2-^{2}H, ^{34}S]
18	[^{33}S]
19	[3-^{2}H, 5-^{13}C]
20	[3-^{2}H, 3-^{13}C]
21	[3-^{2}H, 2-^{13}C]
22	[3,4-^{2}H]
23	[2,3-^{2}H]
24	[2,4-^{2}H]

FIG. 7. Plot of $\delta(r_e^{SE})$ vs the number of isotopologues (N) incorporated into the structure determination. The total error [$\delta(r_e^{SE})$, blue squares], the error in bond distances [green triangles], and the error in angles [purple circles] are presented. The isotopologue numbering scheme is presented explicitly in the accompanying legend, at the right.

remaining isotopologue and incorporating the one that gives the smallest δ (r_e^{SE}) into the fit, for a new total of eight isotopologues. This procedure repeats until all 24 isotopologues are incorporated. As this iterative process could be tedious, a program, *xrefiteration*, has been written to automate it. The code will be discussed in more detail in a publication on the improved semi-experimental equilibrium structure determination of pyridazine.[65] The resultant $\delta(r_e^{SE})$ values from each iteration are plotted in Fig. 7, along with $\delta(r_e^{SE})$ for the bond distances and the angles individually.

Upon examination of the *xrefiteration* results, we observe that the addition of the [2,3-^{2}H] and [2,4-^{2}H] isotopologues (the last two) causes $\delta(r_e^{SE})$ with 24 isotopologues to increase to nearly the same as $\delta(r_e^{SE})$ with 12 isotopologues. In an attempt to understand this behavior, we excluded data from the last two isotopologues ([2,3-^{2}H] and [2,4-^{2}H]) and determined a new semi-experimental equilibrium structure, labeled r_e^{SE} (r_{22}), which is provided in the supplementary material (Table SIV) alongside the r_e^{SE} structure. Despite the modest increase in the uncertainties obtained by including the last two isotopologues, the structural parameters themselves [r_e^{SE} vs r_e^{SE} (r_{22})] are hardly changed at all. The most substantial impact of the final two isotopologues, beyond raising $\delta(r_e^{SE})$, is to move the r_e^{SE} values of R_{C2-H} and $A_{S1-C2-H}$ closer to their BTE values (Fig. 8). This suggests that these isotopologues are providing important structural information about the locations of C2 (and C5) that is not contained in the isotopologue dataset from the previous 22 isotopologues.

A comparison of the various correction terms for the best theoretical estimate of the equilibrium structure for thiophene (Table V) to equivalent data for pyrimidine[1] shows that values for thiophene are somewhat larger, but not by a great deal. This leads us to suspect that the BTE results for thiophene might be of comparable accuracy to those obtained previously for pyrimidine. Referring to the last two columns of Table V or to Figs. 6 and 8, we observe that, for several structural parameters of thiophene, the BTE values are within 2σ of the r_e^{SE} values, or nearly so, and the corresponding residuals are similar in magnitude to those found in pyrimidine. In contrast to pyrimidine, Fig. 8 shows that for two of the bond distances (R_{C2-C3} and R_{C2-H}) and one of the angles in thiophene ($A_{S1-C2-H}$), the BTE values are well outside 2σ of their corresponding r_e^{SE} values. It is easily seen that all the offending parameters involve C2 and the H atom on that carbon. We suspect that this problem arises because these two atoms lie close to the b principal axis, a classically problematic issue in using moments of inertia to determine structures.[25] In a planar molecule, the atom a axis coordinates determine I_b and the b axis coordinates determine I_a. An atom being near the b axis will hinder determination of its a axis coordinate and conversely. The uncertainties in atom coordinates are typically

Published under an exclusive license by AIP Publishing

The Journal of Chemical Physics ARTICLE scitation.org/journal/jcp

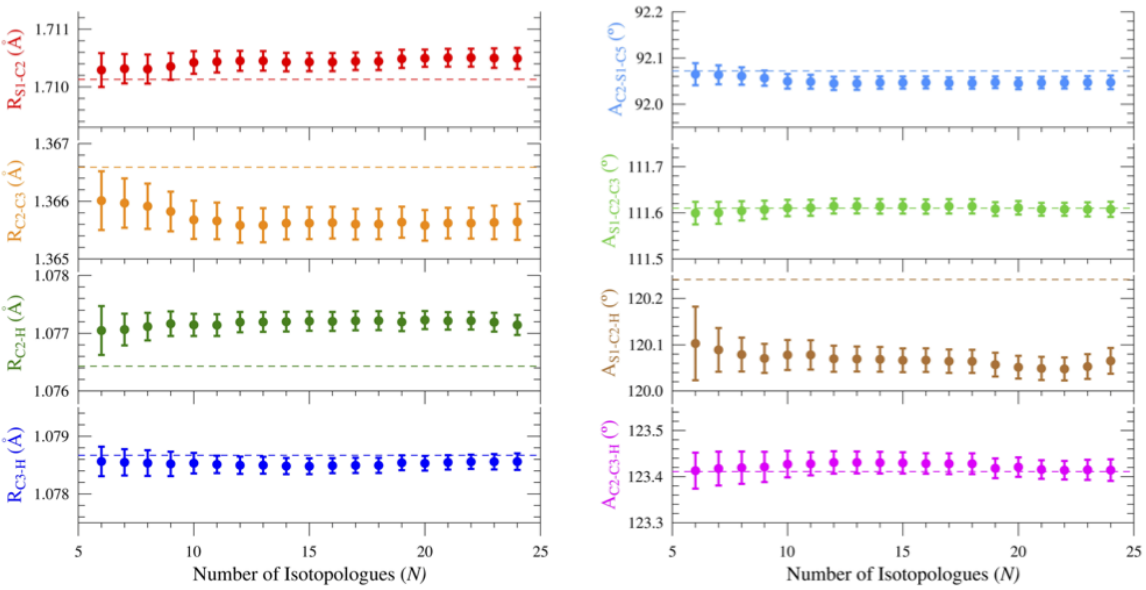


FIG. 8. Plots of the thiophene structural parameters as a function of the number of isotopologues (N) and their 2σ uncertainties with consistent scales for each distance and for each angle. The dashed line represents the BTE value of the parameter. The isotopologue ordering along the x axis is the same as that in Fig. 7.

magnified when those atoms lie near any principal axis, but not on it. Sometimes, the principal axes can be substantially rotated by isotopic substitution to move such atoms away from the axis and greatly mitigate this problem. Not much rotation can occur in thiophene, however, because the heavy sulfur atom must always be very near the a axis.

To obtain a better understanding of the origin of the structural errors in thiophene, we expressed the various structure types in a new coordinate system shown in Table VI. We use rectangular coordinates aligned with the symmetry axis, but with the sulfur atom at the origin. There are four unique a axis coordinates and four unique b axis coordinates. We find that the agreement between BTE and r_e^{SE} for all b axis coordinates is excellent. The a axis coordinate residuals for C3 and H3 are fairly small (especially considering that the values themselves are large), but the a axis coordinate residuals for C2 (0.000 52 Å) and, especially, H2 (−0.002 63 Å) are clearly where the problem lies. Because there is no reason to believe that the BTE value of the a axis coordinates would be less accurate than that of the b axis coordinates, it seems reasonable that any accuracy problems in the present thiophene r_e^{SE} determination trace back to the proximity of the C2 and H2 atoms to the b principal axis, for which we have not yet found a satisfactory solution.

TABLE VI. Rectangular coordinates for thiophene structure with the sulfur atom centered at the origin (0,0).[a]

	r_e^{SE}		CCSD(T)/cc-pCV5Z		Best theoretical estimate	
	a	b	a	b	a	b
S	0.000 00	0.000 00	0.000 00	0.000 00	0.000 00	0.000 00
C2	−1.187 70	1.23092	−1.186 39	1.230 72	−1.187 18	1.230 91
C5	−1.187 70	−1.230 92	−1.186 39	−1.230 72	−1.187 18	−1.230 91
C3	−2.450 58	0.711 20	−2.450 04	0.711 08	−2.451 08	0.711 17
C4	−2.450 58	−0.711 20	−2.450 04	−0.711 08	−2.451 08	−0.711 17
H2	−0.891 55	2.266 55	−0.893 97	2.266 57	−0.894 18	2.266 70
H5	−0.891 55	−2.266 55	−0.893 97	−2.266 57	−0.894 18	−2.266 70
H3	−3.342 46	1.317 70	−3.341 80	1.317 82	−3.342 85	1.318 03
H4	−3.342 46	−1.317 70	−3.341 80	−1.317 82	−3.342 85	−1.318 03

[a] a axis and b axis coordinates in Å

Published under an exclusive license by AIP Publishing

The Journal of Chemical Physics ARTICLE scitation.org/journal/jcp

CONCLUSION

The current study explores the limits of how accurately and precisely an r_e^{SE} structure can be determined by rotational spectroscopy with CCSD(T) corrections. Despite obtaining an r_e^{SE} structure for thiophene that is a substantial improvement on previous structure determinations for molecules containing sulfur, the agreement found for some parameters is somewhat problematic compared to the outstanding agreement found for r_e^{SE} of pyrimidine. For pyrimidine, all structural parameters of best theoretical CCSD(T) r_e are within the statistical uncertainties of semi-experimental r_e^{SE} with CCSD(T) corrections. For thiophene, this is not the case, despite a substantial over-determination of its geometry with moments of inertia from 24 isotopologues. Our analysis indicates that the proximity of C2 and H2 to the *b* principal axis is the source of the problem, preventing the locations of those atoms from being determined to sufficient accuracy. It was not possible in this study to overcome the problem by the inclusion of isotopologues that cause a large rotation of the principal axes. The large mass of the sulfur atom in thiophene prevents any isotopic substitution from causing the necessary large rotation of the principal axes. Given the accuracy of the determination of all atom positions except those near the *b* axis, this study provides strong evidence that satisfactory agreement between r_e^{SE} and the best computed parameters is as likely for a molecule containing a third-row atom, as for the one which does not. Future investigations of other molecules with third-row atoms (Si, P, S, Cl, etc.), but without any atoms lying near a principal axis, would provide an opportunity to confirm this assertion.

SUPPLEMENTARY MATERIAL

See the supplementary material for least-squares fitting files for all thiophene isotopologues, spectroscopic constants in the A-reduction, data distribution plots for isotopologues, determinable constant equations, determinable constants from the A and S reductions, output files from computations, output files from the structure fitting programs (*xrefit* and *xrefiteration*), synthetic details, and characterization data.

ACKNOWLEDGMENTS

We acknowledge funding from the National Science Foundation (Grant Nos. RJM CHE-1664912, CHE-1954270, and JFS CHE-1664325). We also acknowledge funding from the National Institutes of Health for the support of the shared UW-Madison departmental mass spectrometry instruments (Grant No. NIH 1S10 OD020022-1). K.K. thanks KAKENHI, Grants in-Aid for Scientific Research by the Ministry of Education, Culture, Sports, Science, and Technology of Japan (Grant Nos. 26108507, 15H03646, and 19H05074), and the National Astronomical Observatory of Japan. We acknowledge Michael McCarthy for the loan of an amplification multiplication chain. We thank the Harvey Spangler Award (to B.J.E.) for the funding that supported the purchase of a zero-bias detector. We thank Maria A. Zdanovskaia and Andrew N. Owen for their assistance and thoughtful conversations.

DATA AVAILABILITY

The data that support the findings of this study are available within the article and its supplementary material.

REFERENCES

[1]Z. N. Heim, B. K. Amberger, B. J. Esselman, J. F. Stanton, R. C. Woods, and R. J. McMahon, "Molecular structure determination: Equilibrium structure of pyrimidine (m-$C_4H_4N_2$) from rotational spectroscopy (r_e^{SE}) and high-level *ab initio* calculation (r_e) agree within the uncertainty of experimental measurement," J. Chem. Phys. **152**, 104303 (2020).
[2]A. Singh, G. Singh, and P. M. S. Bedi, "Thiophene derivatives: A potent multitargeted pharmacological scaffold," J. Heterocycl. Chem. **57**, 2658–2703 (2020).
[3]B. Amna, H. M. Siddiqi, A. Hassan, and T. Ozturk, "Recent developments in the synthesis of regioregular thiophene-based conjugated polymers for electronic and optoelectronic applications using nickel and palladium-based catalytic systems," RSC Adv. **10**, 4322–4396 (2020).
[4]G. Barbarella, M. Melucci, and G. Sotgiu, "The versatile thiophene: An overview of recent research on thiophene-based materials," Adv. Mater. **17**, 1581–1593 (2005).
[5]J. Heinz and D. Schulze-Makuch, "Thiophenes on Mars: Biotic or abiotic origin?," Astrobiology **20**, 552–561 (2020).
[6]J. L. Eigenbrode, R. E. Summons, A. Steele, C. Freissinet, M. Millan, R. Navarro-González, B. Sutter, A. C. McAdam, H. B. Franz, D. P. Glavin, P. D. Archer, P. R. Mahaffy, P. G. Conrad, J. A. Hurowitz, J. P. Grotzinger, S. Gupta, D. W. Ming, D. Y. Sumner, C. Szopa, C. Malespin, A. Buch, and P. Coll, "Organic matter preserved in 3-billion-year-old mudstones at Gale crater, Mars," Science **360**, 1096 (2018).
[7]M. Lattelais, Y. Ellinger, A. Matrane, and J.-C. Guillemin, "Looking for heteroaromatic rings and related isomers as interstellar candidates," Phys. Chem. Chem. Phys. **12**, 4165–4171 (2010).
[8]M. Agúndez, J. Cernicharo, and M. Guélin, "New molecules in IRC +10216: Confirmation of C_5S and tentative identification of MgCCH, NCCP, and SiH_3CN," Astron. Astrophys. **570**, A45 (2014).
[9]J. Cernicharo, M. Guelin, H. Hein, and C. Kahane, "Sulfur in IRC +10216," Astron. Astrophys. **181**, L9–L12 (1987).
[10]W. W. Coblentz, *Investigations of Infrared Spectra Part 1: Infra-Red Absorption Spectra* (Carnegie Institution of Washington, 1905).
[11]H. W. Thompson and R. B. Temple, "The infra-red spectra of furan and thiophen," Trans. Faraday Soc. **41**, 27–34 (1945).
[12]R. Barnes, U. Liddel, and V. Williams, "Infrared spectroscopy. Industrial applications," Ind. Eng. Chem. Anal. Ed. **15**, 659–709 (1943).
[13]R. B. Barnes and R. R. Brattain, "The near infrared spectrum of benzene-d_6," J. Chem. Phys. **3**, 446–449 (1935).
[14]G. B. Bonino and R. Manzoni-Ansidei, "The Raman spectra of thiophenes and furans and a few of their derivatives," Z. Phys. Chem. **B25**, 327–347 (1934).
[15]M. Rico, J. M. Orza, and J. Morcillo, "Fundamental vibrations of thiophene and its deuterated derivatives," Spectrochim. Acta **21**, 689–719 (1965).
[16]T. D. Klots, R. D. Chirico, and W. V. Steele, "Complete vapor phase assignment for the fundamental vibrations of furan, pyrrole and thiophene," Spectrochim. Acta, Part A **50**, 765–795 (1994).
[17]B. Pankoke, K. M. T. Yamada, and G. Winnewisser, "High resolution IR-spectra of furan and thiophene," Z. Naturforsch., A **48**, 1193–1202 (1994).
[18]J. van Wijngaarden, S. J. Van Nest, C. W. van Dijk, and D. W. Tokaryk, "Rovibrational spectrum and analysis of the ν_8 band of thiophene using infrared synchrotron radiation," J. Mol. Spectrosc. **259**, 56–59 (2010).
[19]J. van Wijngaarden and D. W. Tokaryk, "High resolution synchrotron-based study and analysis of the ν_{14} band of thiophene," J. Mol. Spectrosc. **251**, 365–368 (2008).
[20]F. Hegelund, R. Wugt Larsen, and M. H. Palmer, "The high-resolution infrared spectrum of thiophene between 600 and 1200 cm^{-1}: A spectroscopic and theoretical study of the fundamental bands ν_6, ν_7, ν_{13}, and the *c*-Coriolis interacting dyad ν_5, ν_{19}," J. Mol. Spectrosc. **247**, 100–114 (2008).

Published under an exclusive license by AIP Publishing

The Journal of Chemical Physics ARTICLE scitation.org/journal/jcp

[21]X.-F. Wu, X. Zheng, H.-G. Wang, Y.-Y. Zhao, X. Guan, D. L. Phillips, X. Chen, and W. Fang, "A resonance Raman spectroscopic and CASSCF investigation of the Franck–Condon region structural dynamics and conical intersections of thiophene," J. Chem. Phys. **133**, 134507 (2010).
[22]D. K. Singh, S. K. Srivastava, A. K. Ojha, and B. P. Asthana, "Vibrational study of thiophene and its solvation in two polar solvents, DMSO and methanol by Raman spectroscopy combined with ab initio and DFT calculations," J. Mol. Struct. **892**, 384–391 (2008).
[23]T. Ogata and K. Kozima, "Microwave spectrum, barrier height to internal rotation of methyl group of 3-methylthiophene, and dipole moments of 3-methylthiophene and thiophene," J. Mol. Spectrosc. **42**, 38–46 (1972).
[24]B. Bak, D. Christensen, J. Rastrup-Andersen, and E. Tannenbaum, "Microwave spectra of thiophene, 2- and 3-monodeutero, 3,3′-dideutero, and tetradeuterothiophene. Structure of the thiophene molecule," J. Chem. Phys. **25**, 892–896 (1956).
[25]B. Bak, D. Christensen, L. Hansen-Nygaard, and J. Rastrup-Andersen, "The structure of thiophene," J. Mol. Spectrosc. **7**, 58–63 (1961).
[26]J. Kraitchman, "Determination of molecular structure from microwave spectroscopic data," Am. J. Phys. **21**, 17–24 (1953).
[27]P. B. Liescheski and D. W. H. Rankin, "Determination of the r_α structure of thiophene by combined analysis of electron diffraction, liquid crystal NMR and rotational data," J. Mol. Struct. **178**, 227–241 (1988).
[28]I. V. Kochikov, Y. I. Tarasov, V. P. Spiridonov, G. M. Kuramshina, D. W. H. Rankin, A. S. Saakjan, and A. G. Yagola, "The equilibrium structure of thiophene by the combined use of electron diffraction, vibrational spectroscopy and microwave spectroscopy guided by theoretical calculations," J. Mol. Struct. **567-568**, 29–40 (2001).
[29]M. Piccardo, E. Penocchio, C. Puzzarini, M. Biczysko, and V. Barone, "Semi-experimental equilibrium structure determinations by employing B3LYP/SNSD anharmonic force fields: Validation and application to semirigid organic molecules," J. Phys. Chem. A **119**, 2058–2082 (2015).
[30]E. Penocchio, M. Piccardo, and V. Barone, "Semiexperimental equilibrium structures for building blocks of organic and biological molecules: The B2PLYP route," J. Chem. Theory Comput. **11**, 4689–4707 (2015).
[31]W. F. White, *Microwave Spectra of Some Sulfur and Nitrogen Compounds*, NASA Technical Note, NASA TN D-7450, National Aeronautics and Space Administration, Washington, DC, 1974.
[32]N. M. Pozdeev and L. N. Gunderova, "Microwave spectra of thiophane and thiophene," Khim. Seraorg. Soedin., Soderzh. Neftyakh Nefteprod. **9**, 101–106 (1972).
[33]N. M. Pozdeev, L. I. Panikovskaya, L. N. Lisovskaya, and A. K. Mamleev, *Primenenie Molekulyarnoi Spektroskopii v Khimii, Sbornik Dokladov na Sibirskom Soveshchanii po Spektroskopii*, 3rd ed. (Krasnoyarsk, USSR, 1966), pp. 26–27.
[34]U. Kretschmer, W. Stahl, and H. Dreizler, "The rotational spectra of the ^{32}S-, ^{33}S-, and ^{34}S-isotopomers of thiophene," Z. Naturforsch., A **48**, 733–736 (1993).
[35]K. Kobayashi, K. Takamura, Y. Sakai, S. Tsunekawa, H. Odashima, and N. Ohashi, "The microwave spectroscopy of methyl formate in the second torsional excited state," Astrophys. J., Suppl. Ser. **205**, 9 (2013).
[36]Y. Fukuyama, H. Odashima, K. Takagi, and S. Tsunekawa, "The microwave spectrum of propionitrile (C_2H_5CN) in the frequency range from 8 to 200 GHz," Astrophys. J., Suppl. Ser. **104**, 329 (1996).
[37]A. McJunkins and G. G. Brown, "An inexpensive room-temperature chirped-pulse fourier transform microwave (RT-CP-FTMW) spectrometer," J. Undergrad. Chem. Res. **10**, 158–161 (2011).
[38]B. J. Esselman, B. K. Amberger, J. D. Shutter, M. A. Daane, J. F. Stanton, R. C. Woods, and R. J. McMahon, "Rotational spectroscopy of pyridazine and its isotopologs from 235–360 GHz: Equilibrium structure and vibrational satellites," J. Chem. Phys. **139**, 224304 (2013).
[39]M. A. Zdanovskaia, B. J. Esselman, R. C. Woods, and R. J. McMahon, "The 130–370 GHz rotational spectrum of phenyl isocyanide (C_6H_5NC)," J. Chem. Phys. **151**, 024301 (2019).
[40]Z. Kisiel, L. Pszczółkowski, B. J. Drouin, C. S. Brauer, S. Yu, J. C. Pearson, I. R. Medvedev, S. Fortman, and C. Neese, "Broadband rotational spectroscopy of acrylonitrile: Vibrational energies from perturbations," J. Mol. Spectrosc. **280**, 134–144 (2012).
[41]Z. Kisiel, L. Pszczółkowski, I. R. Medvedev, M. Winnewisser, F. C. De Lucia, and E. Herbst, "Rotational spectrum of *trans–trans* diethyl ether in the ground and three excited vibrational states," J. Mol. Spectrosc. **233**, 231–243 (2005).
[42]PROSPE, Programs for ROtational SPEctroscopy, http://info.ifpan.edu.pl/~kisiel/prospe.htm.
[43]M. J. Frisch, G. W. Trucks, H. B. Schlegel, G. E. Scuseria, M. A. Robb, J. R. Cheeseman, G. Scalmani, V. Barone, G. A. Petersson, H. Nakatsuji, X. Li, M. Caricato, A. V. Marenich, J. Bloino, B. G. Janesko, R. Gomperts, B. Mennucci, H. P. Hratchian, J. V. Ortiz, A. F. Izmaylov, J. L. Sonnenberg, D. Williams-Young, F. Ding, F. Lipparini, F. Egidi, J. Goings, B. Peng, A. Petrone, T. Henderson, D. Ranasinghe, V. G. Zakrzewski, J. Gao, N. Rega, G. Zheng, W. Liang, M. Hada, M. Ehara, K. Toyota, R. Fukuda, J. Hasegawa, M. Ishida, T. Nakajima, Y. Honda, O. Kitao, H. Nakai, T. Vreven, K. Throssell, J. A. Montgomery, Jr., J. E. Peralta, F. Ogliaro, M. J. Bearpark, J. J. Heyd, E. N. Brothers, K. N. Kudin, V. N. Staroverov, T. A. Keith, R. Kobayashi, J. Normand, K. Raghavachari, A. P. Rendell, J. C. Burant, S. S. Iyengar, J. Tomasi, M. Cossi, J. M. Millam, M. Klene, C. Adamo, R. Cammi, J. W. Ochterski, R. L. Martin, K. Morokuma, O. Farkas, J. B. Foresman, and D. J. Fox, Gaussian 16, Revision C.01 (Gaussian, Inc., Wallingford, CT, 2016).
[44]J. Schmidt and W. Polik, WebMO Enterprise, WebMO LLC, Holland, MI, 2013.
[45]NBO 7.0.8 (11 February 2020) NBO 7.0, E. D. Glendening, J. K. Badenhoop, A. E. Reed, J. E. Carpenter, J. A. Bohmann, C. M. Morales, P. Karafiloglou, C. R. Landis, and F. Weinhold, Theoretical Chemistry Institute, University of Wisconsin, Madison, WI, 2018.
[46]J. F. Stanton, L. Cheng, M. E. Harding, D. A. Matthews, and P. G. Szalay, CFOUR, coupled-cluster techniques for computational chemistry, with contributions from A. A. Auer, R. J. Bartlett, U. Benedikt, C. Berger, D. E. Bernholdt, S. Blaschke, Y. J. Bomble, S. Burger, O. Christiansen, D. Datta, F. Engel, R. Faber, J. Greiner, M. Heckert, O. Heun, M. Hilgenberg, C. Huber, T.-C. Jagau, D. Jonsson, J. Jusélius, T. Kirsch, K. Klein, G. M. Kopper, W. J. Lauderdale, F. Lipparini, T. Metzroth, L. A. Mück, T. Nottoli, D. P. O'Neill, D. R. Price, E. Prochnow, C. Puzzarini, K. Ruud, F. Schiffmann, W. Schwalbach, C. Simmons, S. Stopkowicz, A. Tajti, J. Vázquez, F. Wang, and J. D. Watts, the integral packages MOLECULE J. Almlöf and P. R. Taylor, PROPS P. R. Taylor, ABACUS T. Helgaker, H. J. Aa. Jensen, P. Jørgensen, and J. Olsen, and ECP routines by A. V. Mitin and C. van Wüllen, http://www.cfour.de.
[47]I. M. Mills, "Vibration-rotation structure in asymmetric- and symmetric-top molecules," in *Molecular Spectroscopy: Modern Research*, edited by K. N. Rao and C. W. Mathews (Academic Press, New York, 1972), Vol. 1, pp. 115–140.
[48]W. Schneider and W. Thiel, "Anharmonic force fields from analytic second derivatives: Method and application to methyl bromide," Chem. Phys. Lett. **157**, 367–373 (1989).
[49]J. F. Stanton, C. L. Lopreore, and J. Gauss, "The equilibrium structure and fundamental vibrational frequencies of dioxirane," J. Chem. Phys. **108**, 7190–7196 (1998).
[50]W. H. Flygare, "Magnetic interactions in molecules and an analysis of molecular electronic charge distribution from magnetic parameters," Chem. Rev. **74**, 653–687 (1974).
[51]S. Lin, D. E. Herbert, A. Velian, M. W. Day, and T. Agapie, "Dipalladium(I) terphenyl diphosphine complexes as models for two-site adsorption and activation of organic molecules," J. Am. Chem. Soc. **135**, 15830–15840 (2013).
[52]H. J. Leis, G. Fauler, and W. Windischhofer, "Stable isotope labeled target compounds: Preparation and use as internal standards in quantitative mass spectrometry," Curr. Org. Chem. **2**, 131–144 (1998).
[53]A. G. Burton, P. P. Forsythe, C. D. Johnson, and A. R. Katritzky, "The kinetics and mechanism of the electrophilic substitution of heteroaromatic compounds. Part XXVII. The nitration and hydrogen exchange of 1,3,5-trimethylpyrazole, 3,5-dimethylisoxazole, and 3,5-dimethylisothiazole," J. Chem. Soc. B **1971**, 2365–2371.
[54]P. Roussel and J. Metzger, "Synthesis and infrared spectral study of the deuteriothiazoles," Bull. Soc. Chim. Fr. **1962**, 2075–2078.
[55]B. Alonso, M. Ocejo, L. Carrillo, J. L. Vicario, E. Reyes, and U. Uria, "Using heteroaryl-lithium reagents as hydroxycarbonyl anion equivalents in conjugate addition reactions with (*S,S*)-(+)-pseudoephedrine as chiral auxiliary; enantioselective synthesis of 3-substituted pyrrolidines," J. Org. Chem. **78**, 614–627 (2013).

Published under an exclusive license by AIP Publishing

The Journal of Chemical Physics ARTICLE scitation.org/journal/jcp

[56]W. Gordy and R. Cook, *Microwave Molecular Spectra*, 3rd ed. (Wiley-Interscience, New York, 1984).
[57]E. O. Lebigot, Uncertainties: A Python package for calculations with uncertainties, v 3.1.5.
[58]C. Puzzarini, J. Bloino, N. Tasinato, and V. Barone, "Accuracy and interpretability: The devil and the holy grail. New routes across old boundaries in computational spectroscopy," Chem. Rev. **119**, 8131–8191 (2019).
[59]Y. J. Bomble, J. F. Stanton, M. Kállay, and J. Gauss, "Coupled-cluster methods including noniterative corrections for quadruple excitations," J. Chem. Phys. **123**, 054101 (2005).
[60]L. Cheng and J. Gauss, "Analytic energy gradients for the spin-free exact two-component theory using an exact block diagonalization for the one-electron Dirac Hamiltonian," J. Chem. Phys. **135**, 084114 (2011).
[61]W. Liu and D. Peng, "Exact two-component Hamiltonians revisited," J. Chem. Phys. **131**, 031104 (2009).
[62]K. G. Dyall, "Interfacing relativistic and nonrelativistic methods. II. Investigation of a low-order approximation," J. Chem. Phys. **109**, 4201–4208 (1998).
[63]N. C. Handy, Y. Yamaguchi, and H. F. Schaefer, "The diagonal correction to the Born–Oppenheimer approximation: Its effect on the singlet–triplet splitting of CH_2 and other molecular effects," J. Chem. Phys. **84**, 4481–4484 (1986).
[64]M. Born and K. Huang, *Dynamical Theory of Crystal Lattices* (Oxford University Press, New York, 1956).
[65]A. N. Owen, M. A. Zdanovskaia, B. J. Esselman, J. F. Stanton, R. C. Woods, and R. J. McMahon, "The semi-experimental equilibrium (r_eSE) and theoretical structures of pyridazine (o-$C_4H_4N_2$)" (unpublished).

Published under an exclusive license by AIP Publishing

Appendix E

The 130–360 GHz Rotational Spectrum of *syn*-2-Cyano-1,3-Butadiene(C_5H_5N) – A Molecule of Astrochemical Relevance

Maria A. Zdanovskaia
Brian J. Esselman
Samuel M. Kougias
Aatmik R. Patel
R. Claude Woods
Robert J. McMahon

Molecular Physics, 2021, *119*, e1964629

MOLECULAR PHYSICS
2021, VOL. 119, NOS. 21–22, e1964629 (14 pages)
https://doi.org/10.1080/00268976.2021.1964629

Taylor & Francis
Taylor & Francis Group

JOHN STANTON SPECIAL ISSUE: THEORY MEETS EXPERIMENT

Check for updates

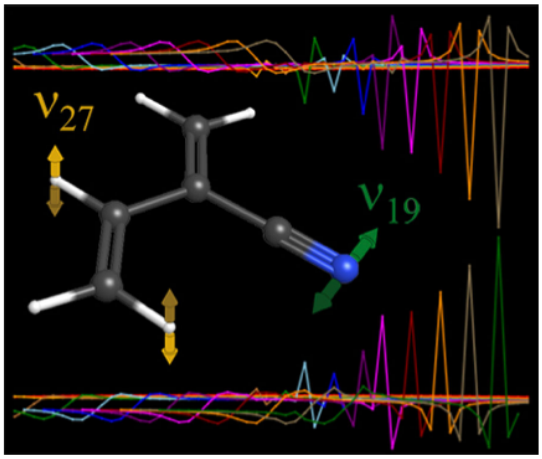
The 130–360 GHz rotational spectrum of *syn*-2-cyano-1,3-butadiene (C_5H_5N) – a molecule of astrochemical relevance

Maria A. Zdanovskaia, Brian J. Esselman, Samuel M. Kougias, Aatmik R. Patel, R. Claude Woods and Robert J. McMahon

Department of Chemistry, University of Wisconsin–Madison, Madison, WI, USA

ABSTRACT

The analysis of *syn*-2-cyano-1,3-butadiene (C_5H_5N, $\mu_a = 3.2$ D, $\mu_b = 2.3$ D) in its ground vibrational state and two lowest-energy excited vibrational states, ν_{27} (A″, 144 cm^{-1}) and ν_{19} (A′, 163 cm^{-1}), in the 130–360 GHz frequency region has been completed. Nearly 4200 rotational transitions have been measured in the ground vibrational state for the first time, resulting in the determination of the spectroscopic constants for a complete octic Hamiltonian with low error. Analysis of the two lowest-energy, Coriolis-coupled fundamentals reported herein, each containing circa 3000 transitions, yielded two possible least-squares fitting solutions. Both solutions address perturbation between the two vibrational states, including resonances and several nominal interstate transitions, using four *a*-type and five *b*-type Coriolis coupling terms (G_a, G_a^J, G_a^K, F_{bc}, G_b, G_b^K, F_{ac}, and F_{ac}^K, with or without F_{ac}^J). The energy separation between the two states, $\Delta E_{27,19} = 12.307065$ (2) cm^{-1}, agrees between the two solutions within their statistical uncertainties, giving confidence that this value is accurate despite the differing Coriolis-coupling terms. The precise rotational and distortion constants determined in this work provide the foundation for an astronomical search for *syn*-2-cyano-1,3-butadiene across the radio band.



ARTICLE HISTORY
Received 29 May 2021
Accepted 29 July 2021

KEYWORDS
Astrochemistry; Coriolis coupling; rotational spectroscopy; pyridine isomer; Titan atmosphere

Introduction

More than 200 molecules have been detected in the interstellar medium (ISM) or in circumstellar shells – the majority of these detections *via* radioastronomy [1,2]. Approximately ten percent of the detected species are organic nitriles, including recent detections of benzonitrile [3], 1- and 2-cyanonaphthalene [4], hydroxyacetonitrile [5], and silyl cyanide [6]. Due to their characteristically strong dipole moments and composition of relatively abundant elements, nitriles (R–CN) represent

CONTACT Robert J. McMahon robert.mcmahon@wisc.edu Department of Chemistry, University of Wisconsin–Madison, Madison, WI 53706, USA

Supplemental data for this article can be accessed here https://doi.org/10.1080/00268976.2021.1964629

© 2021 Informa UK Limited, trading as Taylor & Francis Group

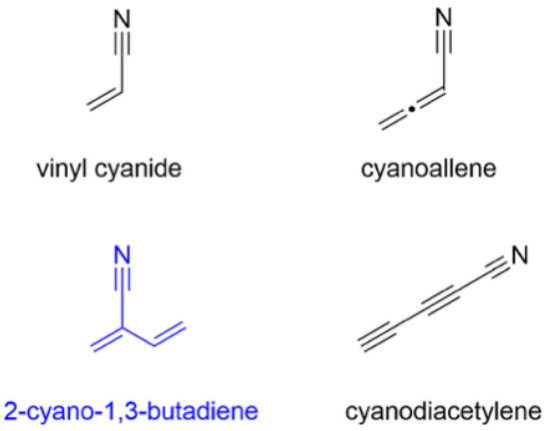


Figure 1. Nitriles detected in the ISM (vinyl cyanide, cyanoallene, and cyanodiacetylene) with structures similar to 2-cyano-1,3-butadiene.

inviting targets for additional radioastronomical detections. A series of highly unsaturated nitrile-containing carbon chains ($HC_{2n+1}N$ with $n = 0–5$) have been detected [7–12], as well as several partially unsaturated [13–16] and fully saturated [17–19] organic nitriles. Specifically, the known interstellar molecules vinyl cyanide (C_3H_3N) [14], cyanoallene (C_4H_3N) [16], and cyanodiacetylene (C_5HN) [7] exhibit structural similarities to the molecule of interest in the current work: 2-cyano-1,3-butadiene (C_5H_5N) (Figure 1). Our group synthesised and characterised several astrochemically relevant nitriles and isonitriles in order to analyse their rotational spectra [20–23]. Although neither McCarthy *et al.*, who examined the electrical discharge of benzene with molecular nitrogen [24], nor Zwier and coauthors, who examined the gas-phase pyrolysis of 3-pentenenitrile [25], detected 2-cyano-1,3-butadiene among their products, it may nevertheless be considered a likely interstellar molecule. Irradiation of cyanoacetylene with ethylene with 254 nm light, for example, produces 2-cyano-1,3-butadiene [26]. A theoretical study suggested that 2-cyano-1,3-butadiene is a predominant product in the reactions of cyano radical with 1,2-butadiene and cyano radical with 1-butyne [27]. There are, however, no published spectroscopic data available to enable a radioastronomical search for this nitrile.

An additional reason for targeting the cyano-butadiene isomers is that they share the same molecular formula as pyridine (C_5H_5N, $\mu = 2.19$ D). Pyridine, along with several other nitrogen heterocycles, is an aromatic molecule of substantial astrochemical interest. Not only has pyridine been implicated as a building block for nitrogen-substituted polycyclic aromatic hydrocarbons (NPAHs) [28], but it is also a building block of nicotinic acid (Vitamin B3) and nicotinamide. These pyridine-based moieties are precursors to nicotinamide adenine dinucleotide (NAD), a key coenzyme in metabolism [29]. Nicotinic acid of interstellar origin has been detected on the Murchison meteorite [30,31], and a possible route to interstellar formation from pyridine has also been suggested [32]. Detection of extraterrestrial pyridine could shed light on the chemistry occurring in extreme, prebiotic environments. To date, however, pyridine has eluded detection in the ISM [33]. This work on 2-cyano-1,3-butadiene could enable its detection in the ISM and an exploration of the chemistry of C_5H_5N species in that environment.

Materials and methods

Experimental

As described recently, 2-cyano-1,3-butadiene was prepared from acrylonitrile and acetaldehyde and purified by distillation [22]. Rotational spectra were collected on a broadband spectrometer with a pressure of 3 mTorr at room temperature. The 130–360 GHz spectrum was collected using the instrument described previously [21,34], using two separate Virginia Diodes amplification and multiplication chains and Virginia Diodes Zero-Bias Detectors for the 130–230 GHz and 235–360 GHz frequency segments. In each region of the spectrum, we assume a uniform frequency measurement uncertainty of 0.05 MHz. The spectra were combined into a single broadband spectrum using Assignment and Analysis of Broadband Spectra (AABS) software [35,36]. Pickett's SPFIT and SPCAT programs [37] were used to conduct least-squares fitting and spectral prediction, respectively. Kisiel's PIFORM, PMIXC, PLANM, and AC programs were used to analyse data, reformat output files, and generate various plots [38].

Computational

Density functional theory computations were performed at the B3LYP/6-311+G(2d,p) level of theory using Gaussian 16 software [39] and the WebMO [40] user interface. Optimised geometries for *syn-* and *gauche-*2-cyano-1,3-butadiene were obtained using 'very tight' convergence criteria and an 'ultrafine' integration grid (opt = verytight int = grid = ultrafine). Anharmonic vibrational frequency calculations provided the fundamental vibrations, the vibration-rotation interaction constants ($A_0–A_v$), and the Coriolis coupling (ζ) constants. A relaxed coordinate scan of rotation about the central C–C bond for 2-cyano-1,3-butadiene was also performed. An optimisation and anharmonic vibrational

frequency calculation using the above-described criteria were also performed for the *syn-syn-cis* (SSC) conformer of glycolic acid [41] to enable direct comparison of computational accuracies. Computational output files are provided in the supplemental material.

Results

Conformational analysis of 2-cyano-1,3-butadiene

Like 1,3-butadiene [42], 2-cyano-1,3-butadiene has two low-energy conformations – *syn* and *gauche*. The *syn* conformation is a planar, C_s structure that allows effective π conjugation throughout the molecule. The higher-energy *gauche* conformations are an enantiomeric pair of nonplanar, C_1 structures, in which steric interactions between the methylene groups create a twist around the central C–C bond. The computed dihedral angle between the two terminal carbon atoms of *gauche*-2-cyano-1,3-butadiene is 33.3°, a value similar to that determined for 1,3-butadiene (33.8 (13)°) [42]. The computed energy difference between the *syn* and *gauche* conformers is 3.1 kcal/mol or 1080 cm^{-1} (including ZPVE). The barrier to conformational exchange (Figure 2) is only 6.5 kcal/mol, which allows these species to interconvert readily at room temperature. Even if assuming the statistical doubling due to two enantiomeric forms of the *gauche* conformer, the energy difference of ca. 3 kcal/mol results in an equilibrium population of the *gauche* conformational isomer of only 1.0% of the total for 2-cyano-1,3-butadiene at the temperature the spectrum was collected (298 K). This low population makes the detection of the *gauche* conformation unlikely, due to the high spectral density of the *syn* conformation. Detection of the *gauche* conformer is further complicated by its possible tunnelling splitting, which would nullify the statistical doubling in intensity and make the distorted rotor prediction insufficient to assign its transitions. The *syn* conformer of 2-cyano-1,3-butadiene is only about 1 kcal/mol higher in energy than the *E*-1-cyano isomer, but approximately 23 kcal/mol (CCSD(T)/cc-pVTZ//B3LYP/cc-pVTZ) higher in energy than pyridine [43].

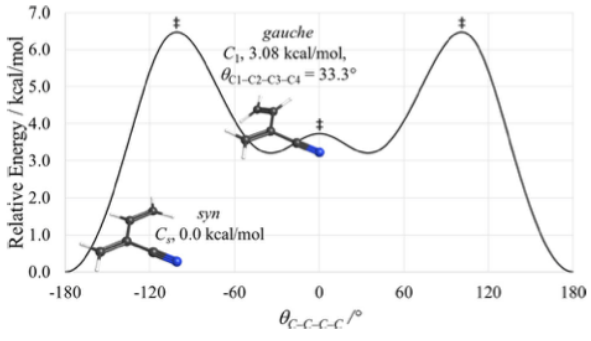


Figure 2. Computed conformational potential energy surface of 2-cyano-1,3-butadiene (B3LYP/6-311+G(2d,*p*)).

Analysis of rotational spectra

As expected – based upon the conformational analysis, the comparable dipole moments (B3LYP/6-311+(2d,p)) of the *syn* (μ_a = 3.2 D, μ_b = 2.3 D) and *gauche* (μ_a = 3.9 D, μ_b = 1.6 D, μ_c = 0.1 D) conformers, and the very dense spectrum of the *syn* conformer – only the *syn* conformer (Figure 3) was observed in the spectrum. The spectral density of thousands of observable transitions for each of the three lowest-energy vibrational states in this frequency range is compounded by the fact that there are many additional vibrational states with transitions more intense than the *gauche* conformer (1080 cm^{-1}). Figure 4 shows the manifold of 16 vibrationally excited states with energies less than 500 cm^{-1}. The ground state is separated from the lowest-energy excited vibrational state, ν_{27}, by 144 cm^{-1} and was thus



Figure 3. *syn*-2-Cyano-1,3-butadiene structure with principal inertial axes.

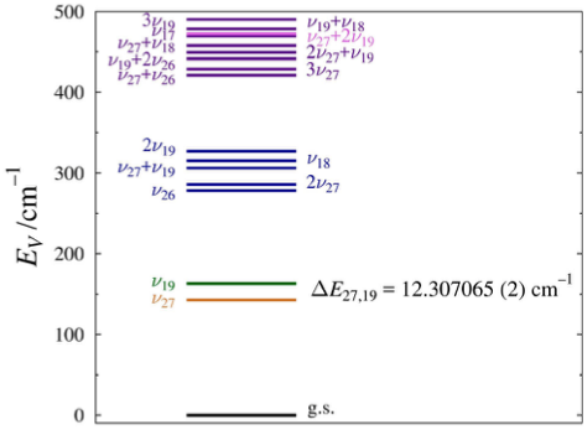


Figure 4. Vibrational energy levels of *syn*-2-cyano-1,3-butadiene below 500 cm^{-1} from computed fundamental frequencies (B3LYP/6-311+G(2d,*p*)). The value of $\Delta E_{27,19}$ results from the experimental perturbation analysis of ν_{27} and ν_{19} in this work.

expected to behave as a distorted rotor. The first two fundamentals ν_{27} (A″, 144 cm^{-1}) and ν_{19} (A′, 163 cm^{-1}) are much closer in energy (19 cm^{-1}) and were expected to require a coupled-dyad treatment. Centred around 300 cm^{-1}, there is a pentad of the first overtone states ($2\nu_{27}$ and $2\nu_{19}$), first combination state ($\nu_{27}+\nu_{19}$), and third and fourth fundamentals (ν_{26} and ν_{18}). While higher-energy vibrational states are also visible in the spectrum, the assignment and least-squares fitting of their spectra is not addressed in the current work.

Ground state

syn-2-Cyano-1,3-butadiene is a highly asymmetric oblate-top molecule (C_s, $\kappa = 0.187$) with large *a*-axis and *b*-axis dipole moments. Its rotational spectrum is dominated by clearly distinguishable R-branch bands comprised of strong, degenerate $^{a}R_{0,1}$, $^{b}R_{-1,1}$, and $^{b}R_{1,1}$ transitions. While these transitions are easily assignable in the early stages of fitting, the Q-branch transitions are much more spread out than the R-branch transitions, making the Q-branch transitions difficult to visibly discern before a fairly predictive least-squares fit is established. A portion of the experimental spectrum in the region near 167.65 GHz is provided in Figure 5, which depicts a typical R-branch series near its bandhead. We did not observe hyperfine-resolved transitions due to N-quadrupole coupling in our frequency range. Strong transitions of vibrationally excited states are also clearly visible in Figure 5, many of which can be attributed to the two lowest-energy states, ν_{27} and ν_{19}.

Transitions for the ground state of *syn*-2-cyano-1,3-butadiene were fit to a distorted-rotor Hamiltonian with octic centrifugal distortion terms (A-reduced, I^r representation and S-reduced, III^r representation). The resulting spectroscopic parameters are presented in Table 1, along with their corresponding computational values for the S-reduced, III^r representation. Due to the large *a*-axis and *b*-axis dipole moments, the broad spectral range, and the large number of transitions ($>$ 4000) included in the least-squares fit, all octic centrifugal distortion terms were satisfactorily determined in a fit with low statistical error (0.033 MHz). The predicted quartic and sextic centrifugal distortion constants, with the exception of d_1, are in good agreement with the experimental values. The predicted rotational constants are within 2% and all of the distortion constants agree to within 12%, with the clear exception of d_1. While it may initially seem surprising that d_1 is predicted to have the opposite sign from that determined experimentally, it is likely due to the very small magnitude of d_1 – almost 50× smaller than the next smallest quartic distortion constant. A slight underprediction of the near-zero d_1 value leads to a negative value. Although it would be highly desirable to

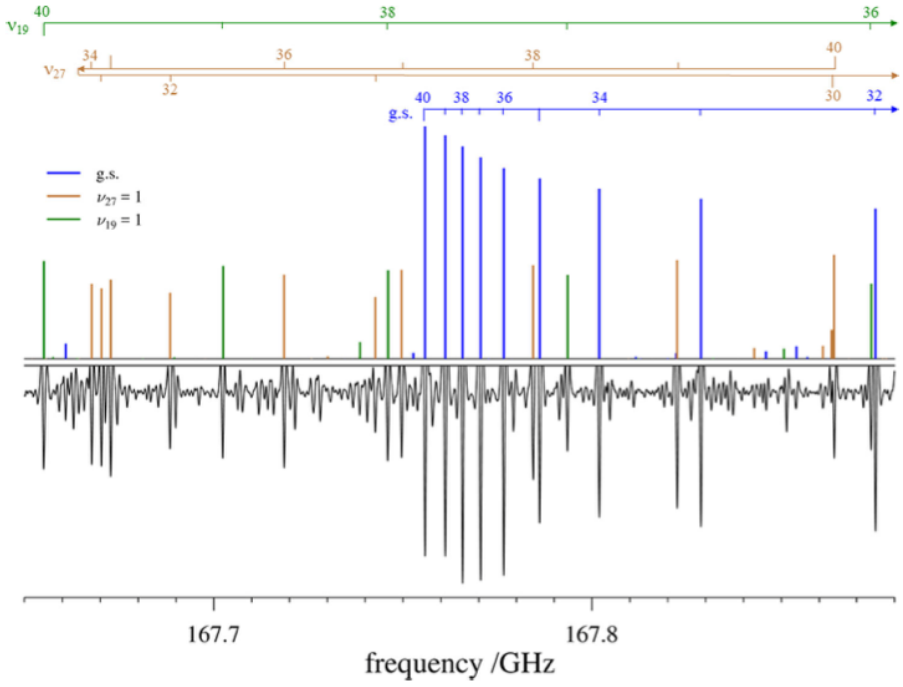


Figure 5. 2-Cyano-1,3-butadiene rotational spectrum from 167.65 to 167.88 GHz (bottom) and stick spectra for the ground vibrational state, ν_{27}, and ν_{19} of the *syn* conformer (top). Values on the numberlines at the top indicate the $J'' + 1$ values of the corresponding transitions.

Table 1. Experimental and computational spectroscopic constants for the ground vibrational state of *syn*-2-cyano-1,3-butadiene.

S Reduction, III^r representation				A Reduction, I^r representation		
	Experimental[a]		B3LYP		Experimental	
A_0 (MHz)	4773.019689	(77)	4819.	A_0 (MHz)	4773.011589	(78)
B_0 (MHz)	3665.214370	(55)	3607.	B_0 (MHz)	3665.217803	(55)
C_0 (MHz)	2071.623950	(66)	2061.	C_0 (MHz)	2071.626692	(66)
D_J (kHz)	2.883776	(44)	2.73	Δ_J (kHz)	2.506066	(32)
D_{JK} (kHz)	−5.075865	(77)	−4.73	Δ_{JK} (kHz)	−9.656771	(82)
D_K (kHz)	2.375684	(42)	2.18	Δ_K (kHz)	11.89902	(10)
d_1 (kHz)	0.020027	(25)	−0.0510	δ_J (kHz)	1.161226	(11)
d_2 (kHz)	−0.9523601	(95)	−0.923	δ_K (kHz)	−0.181326	(43)
H_J (Hz)	0.010119	(12)	0.00918	Φ_J (Hz)	0.0069441	(76)
H_{JK} (Hz)	−0.036931	(26)	−0.0331	Φ_{JK} (Hz)	−0.030943	(37)
H_{KJ} (Hz)	0.044472	(24)	0.0396	Φ_{KJ} (Hz)	0.006032	(62)
H_K (Hz)	−0.017681	(10)	−0.0157	Φ_K (Hz)	0.044383	(51)
h_1 (Hz)	0.001990	(10)	0.00192	ϕ_J (Hz)	0.0034811	(28)
h_2 (Hz)	0.0050266	(64)	0.00468	ϕ_{JK} (Hz)	−0.010379	(16)
h_3 (Hz)	0.0011408	(12)	0.00104	ϕ_K (Hz)	0.029736	(20)
L_J (μHz)	−0.0435	(12)		L_J (μHz)	−0.01135	(59)
L_{JJK} (μHz)	0.2024	(31)		L_{JJK} (μHz)	0.0542	(52)
L_{JK} (μHz)	−0.3960	(40)		L_{JK} (μHz)	−0.178	(11)
L_{KKJ} (μHz)	0.3488	(31)		L_{KKJ} (μHz)	0.504	(13)
L_K (μHz)	−0.1112	(12)		L_K (μHz)	−0.5463	(96)
l_1 (μHz)	−0.0259	(12)		l_J (μHz)	−0.00586	(24)
l_2 (μHz)	−0.0282	(10)		l_{JK} (μHz)	0.0353	(21)
l_3 (μHz)	−0.01357	(36)		l_{KJ} (μHz)	0.1162	(36)
l_4 (μHz)	−0.001241	(68)		l_K (μHz)	−0.4869	(51)
Δ_i (uÅ^2)[b]	0.185363	(8)	0.228	Δ_i (uÅ^2)[b]	0.184990	(8)
N_{lines}[c]	4185			N_{lines}[c]	4185	
σ_{fit} (MHz)	0.033			σ_{fit} (MHz)	0.033	

[a]Converted from III^l representation by applying opposite sign to all odd-numbered, off-diagonal distortion constants.
[b]Inertial defect, $\Delta_i = I_c - I_a - I_b$. Calculated using PLANM from the B_0 constants.
[c]Number of fitted transition frequencies.

compare the experimentally determined octic centrifugal distortion constants with their theoretically predicted values, current computational chemistry software packages cannot perform these calculations, because they require the implementation of higher-order vibrational perturbation theory. Data distribution plots for measured R- and Q-branch transitions are provided in Figure 6, demonstrating the breadth of data. Q-branch transitions cover a range of K_a values from 0 to 60 and J'' values from 33 to 100. R-branch transitions cover a range of K_a values from 0 to 55 and J'' values from 13 to 85.

The lowest-energy vibrationally excited states ν_{27} and ν_{19}

The two lowest-energy vibrationally excited states, ν_{27} (A″, 144 cm^{-1}) and ν_{19} (A′, 163 cm^{-1}), are an *a*-type and *b*-type Coriolis-coupled dyad. The lowest-energy vibration (ν_{27}) is a torsion about the C2–C3 bond, while ν_{19} is an in-plane wag of the cyano group. The data distribution plots for ν_{27} and ν_{19} are provided in Figure 7. The measured transitions cover a narrower range of quantum numbers than the ground state, as would be expected due to the lower intensity of the vibrationally excited states. The data distribution plots for ν_{27} and ν_{19} look similar to one another, as well as to the ground-state plot, with regard to the distribution of larger errors, indicating no obvious systematic error in the coupled-state treatment.

Both *a*- and *b*-types of Coriolis coupling have a discernable effect on the spectra of ν_{27} and ν_{19} as a result of the C_s symmetry of *syn*-2-cyano-1,3-butadiene, its large *a*- and *b*-type dipole moments, and its substantial Coriolis-coupling constants ($\zeta^a_{27,19}$ and $\zeta^b_{27,19}$). These Coriolis-coupling constants are directly related to the spectroscopic constants G_a and G_b through Eq. (1), where ω is the harmonic vibrational frequency of the corresponding mode, and x is the corresponding inertial axis [44].

$$G_x = \frac{\omega_{27} + \omega_{19}}{\sqrt{\omega_{27} \times \omega_{19}}} \zeta^x_{27,19} B^x_e \approx 2\zeta^x_{27,19} B^x_e \qquad (1)$$

The initial least-squares fitting of ν_{27} and ν_{19} was remarkably straightforward, using the predicted G_a and G_b values, the predicted energy difference, and the ground-state distortion constants. The values of C_v were predicted using the experimental C_0 value and the corresponding computed vibration-rotation interaction constants,

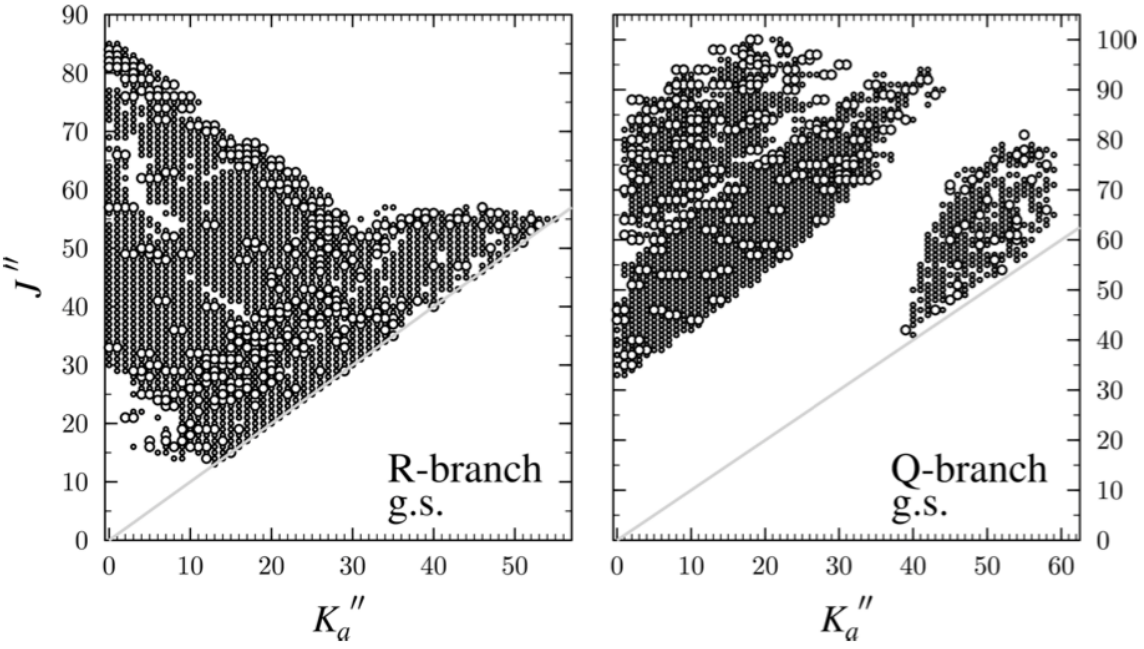


Figure 6. Data distribution plot for the least-squares fit of spectroscopic data for the vibrational ground state of *syn*-2-cyano-1,3-butadiene. The size of the plotted symbol is proportional to the value of $|(f_{obs.}-f_{calc.})/\delta f\ |$, where δf is the frequency measurement uncertainty (0.05 MHz), and all values shown are smaller than 3.

while the values of A_v and B_v were set to corresponding experimental ground-state values. As the first dozen R-branch K_a series were added to the least-squares fit, it became possible to fit G_b and the interaction between the states could be relatively well modelled. Adding higher K_a series enabled inclusion of G_a and higher-order coupling terms. Fitting of the available R- and Q-branch transitions, including resonances and nominal interstate transitions, resulted in a low-error (0.040 MHz) least-squares fit with a well-determined energy separation and several coupling coefficients. While the value of G_b and the energy separation remained relatively stable throughout the fitting process, the value of G_a was volatile. In the end, two different solutions, labelled Fit I and Fit II, were able to model the spectra with the same energy difference, $\Delta E_{27,19} = 12.307065\ (2)\ cm^{-1}$. Table 2 presents the ground-state spectroscopic constants in the A reduction, I^r representation, along with two sets of spectroscopic constants for the ν_{27}:ν_{19} dyad. The octic centrifugal distortion constants, not shown explicitly in the table, are held constant at their corresponding ground-state values.

Fit I and Fit II are both presented here because it is unclear which set of spectroscopic constants is more physically meaningful. Fit I and Fit II are distinguished by the inclusion (Fit I) or exclusion (Fit II) of F_{ac}^J in the Hamiltonian. Inclusion of this coupling term has a relatively small impact on the rotational and distortion constants, but a relatively large impact on G_a and other Coriolis coupling terms. Between the two least-squares fits, the values of the corresponding states' rotational constants differ by less than 0.01%. The quartic distortion constants agree within 0.25% between fits, with the exception of δ_K. The latter differs by 1.8% for ν_{27} and 2.5% for ν_{19} upon exclusion of F_{ac}^J. This difference does not, however, appear to be substantial, considering that δ_K changes by approximately 14% and 35% upon excitation from the ground state to ν_{27} and ν_{19}, respectively. Similarly, Φ_J and ϕ_J for both states change by 2.0-2.5% between the two fits, the values of Φ_{JK} are within 1.2% for both states, and the other fitted sextic distortion constants are within 0.45%. In contrast, the value of G_a in Fit I increases by 40.2% in Fit II. As might be expected, the other F_{ac} terms are also impacted substantially by inclusion or exclusion of F_{ac}^J. Importantly, however, the energy separation between the two least-squares fits is nearly unaffected by the inclusion or absence of F_{ac}^J, and the two values fall within the experimental error of one another – determined to the millionth of a wavenumber digit. The experimentally determined value ($12.307065\ (2)\ cm^{-1}$) is approximately two-thirds of the predicted value (19.605 cm^{-1}).

In order to discern the better, or more physically meaningful, of the two least-squares fits, one might compare the experimentally determined values to those predicted computationally. The B3LYP prediction of G_b is 1918 MHz, which is approximately 11% different from

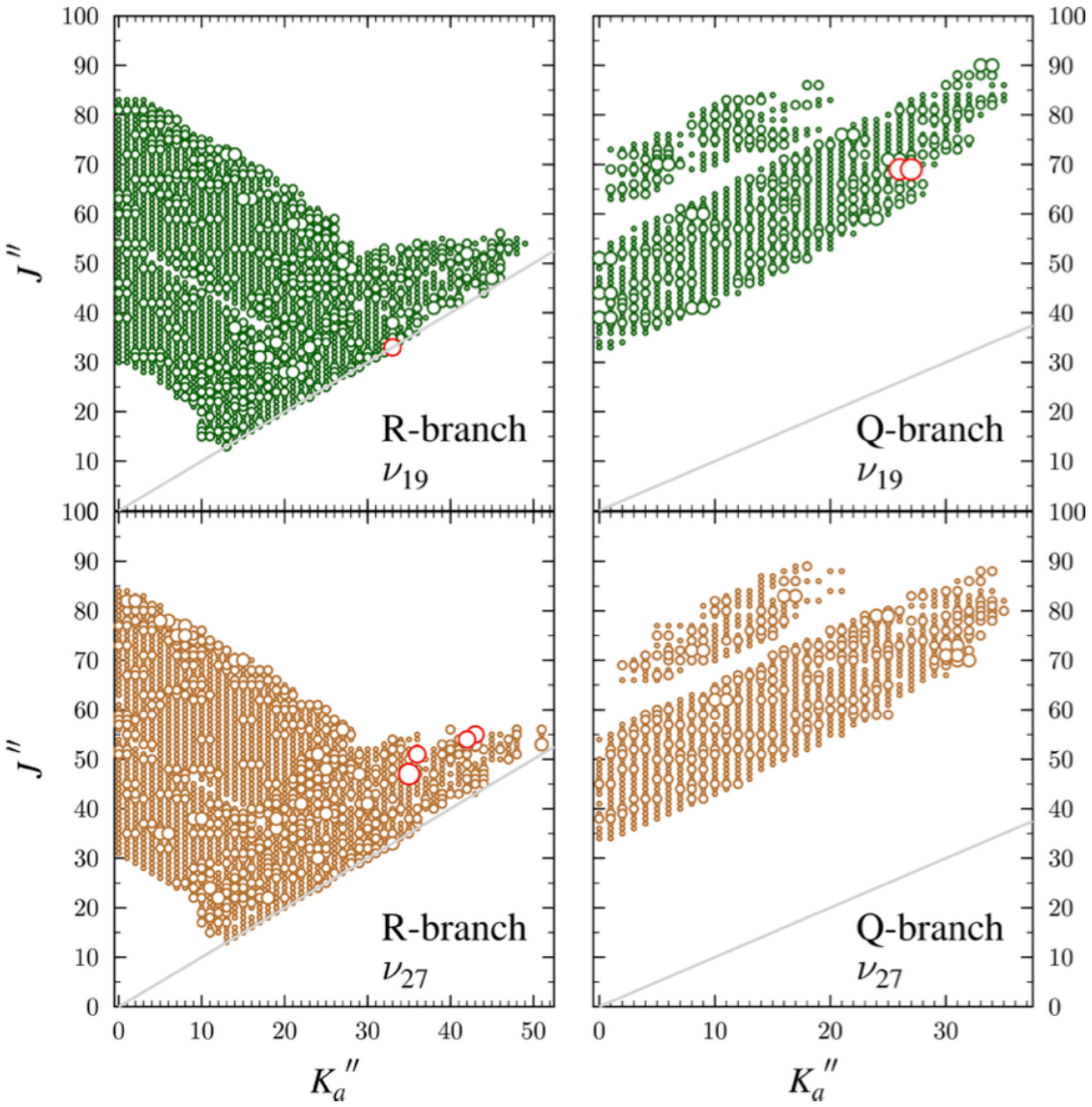


Figure 7. Data distribution plots for the coupled fit (Fit I, *vide infra*) of measured transitions in the two lowest-energy excited vibrational states in *syn*-2-cyano-1,3-butadiene. The size of the plotted symbol is proportional to the value of of $|(f_{obs.}-f_{calc.})/\delta f|$, where δf is the frequency measurement uncertainty (50 kHz). Values for which this relative error is $>$ 3 are plotted in red.

1731.9 (10) MHz in Fit I and 12% different from the 1708.65 (70) MHz in Fit II. The value of G_a, however, is predicted to be 1025.44 MHz. This value is nearly an order of magnitude larger than the value determined in Fit I (135.1 (19) MHz), and the value in Fit II is only 54 MHz closer to the prediction. Since predictions of additional coupling terms – their values or even which terms are necessary to properly address coupling between perturbing states – are not readily available, computational predictions do not offer an effective way to suggest which of the two sets of constants is more physically meaningful. The two least-squares fits do agree on the energy separation between ν_{27} and ν_{19} within the error of the energy (368956.53 (5) MHz). The errors of the fits and comparison of the spectroscopic constants to their ground-state values do not provide a clear answer, either. Inclusion of an additional coupling term could affect the extent of state mixing, and therefore change the predicted intensities of various transitions. None of the observed transitions' predicted intensities, however, differ sufficiently between Fit I and Fit II to enable a choice based on transition intensities. The fact that Fit I enabled the fitting of 81 more transitions than Fit II appears to be the only indication that Fit I is better able to model

Table 2. Experimentally determined parameters for ν_{27} and ν_{19} excited vibrational states of *syn*-2-cyano-1,3-butadiene compared to those for the ground state (A-reduced Hamiltonian, I^r representation).[a]

			Fit I				Fit II			
	ground state		ν_{27} (A'', 144 cm^{-1})		ν_{19} (A', 163 cm^{-1})		ν_{27} (A'', 144 cm^{-1})		ν_{19} (A', 163 cm^{-1})	
A_v (MHz)	4773.011589	(78)	4777.0079	(15)	4791.5856	(13)	4777.0574	(17)	4791.5398	(16)
B_v (MHz)	3665.217803	(55)	3649.663	(10)	3665.811	(10)	3649.4474	(65)	3666.0288	(65)
C_v (MHz)	2071.626692	(66)	2073.14036	(11)	2069.96427	(11)	2073.137345	(69)	2069.961582	(89)
Δ_J (kHz)	2.506066	(32)	2.48463	(22)	2.45624	(22)	2.47990	(15)	2.46104	(14)
Δ_{JK} (kHz)	−9.656771	(82)	−9.67560	(49)	−9.37343	(49)	−9.66066	(15)	−9.38847	(17)
Δ_K (kHz)	11.89902	(10)	11.91046	(18)	11.77140	(19)	11.90831	(17)	11.77322	(18)
δ_J (kHz)	1.161226	(11)	1.14949	(10)	1.13712	(10)	1.147151	(73)	1.139456	(73)
δ_K (kHz)	−0.181326	(43)	−0.15618	(29)	−0.11757	(29)	−0.15896	(28)	−0.11469	(28)
Φ_J (Hz)	0.0069441	(76)	0.0070293	(80)	0.0062762	(89)	0.0068778	(65)	0.0064332	(75)
Φ_{JK} (Hz)	−0.030943	(37)	−0.031698	(21)	−0.028573	(26)	−0.031361	(20)	−0.028907	(25)
Φ_{KJ} (Hz)	0.006032	(62)	[0.006032]		[0.006032]		[0.006032]		[0.006032]	
Φ_K (Hz)	0.044383	(51)	0.045319	(64)	0.044718	(82)	0.045369	(70)	0.044513	(83)
ϕ_J (Hz)	0.0034811	(28)	0.0035287	(39)	0.0031480	(42)	0.0034552	(32)	0.0032223	(36)
ϕ_{JK} (Hz)	−0.010379	(16)	−0.010658	(11)	−0.010148	(11)	−0.010624	(12)	−0.010181	(11)
ϕ_K (Hz)	0.029736	(20)	[0.029736]		[0.029736]		[0.029736]		[0.029736]	
ΔE (MHz)			368956.534	(49)			368956.516	(50)		
ΔE (cm^{-1})			12.3070652	(16)			12.3070646	(17)		
G_a (MHz)			135.1	(19)			189.4	(16)		
G_a^J (MHz)			−0.027244	(60)			−0.026539	(64)		
G_a^K (MHz)			0.005204	(57)			0.004510	(60)		
F_{bc} (MHz)			−4.106	(24)			−3.450	(21)		
G_b (MHz)			1731.9	(10)			1708.65	(70)		
G_b^K (MHz)			0.024318	(92)			0.021749	(43)		
F_{ac} (MHz)			1.598	(14)			2.0219	(44)		
F_{ac}^J (MHz)			0.00001080	(34)			[0.0]			
F_{ac}^K (MHz)			−0.00002339	(43)			−0.00001578	(37)		
Δ_i (uÅ^2) [b]	0.184990	(8)	−0.49221	(38)	0.81366	(38)	−0.49894	(25)	0.82117	(25)
N_{lines} [c]			3039		3013		2994		2977	
σ (MHz)			0.040		0.039		0.040		0.040	

[a] Values in square brackets held fixed at the specified value in the least-squares fit.
[b] Inertial defect, $\Delta_i = I_c - I_a - I_b$. Calculated using PLANM from the B_0 constants.
[c] Number of fitted transition frequencies.

the rotational spectra of ν_{27} and ν_{19}. While there is no evident commonality between these 81 lines, a number of them are affected by resonances. Attempts to fit additional distortion constants or coupling terms resulted in either non-convergence of the least-squares fit, or constants that were not well-fit and did not meaningfully improve the least-squares fit.

Since our group has not previously encountered a case where a coupling term, such as G_a, has been so poorly predicted, we attempted to find a third least-squares fit with a G_a value closer to that predicted. It is evident that *a*- and *b*-type Coriolis coupling terms interplay with one another. We thus considered that, while it may appear reasonable to attempt to fit the zeroth-order coupling terms (*i.e.* G_a and G_b) first, followed by the higher-order terms, perhaps it is necessary to first fit one set (*e.g.* all *b*-type terms) before fitting the other, to prevent convolution of their effects. Fit III was attempted in this manner – by first fitting the *b*-type Coriolis coupling terms. At early stages and throughout the fitting process, we attempted to fit G_a in order to observe its effect. At these early stages, however, the least-squares fit failed to converge when G_a was allowed to vary, and there was nearly no effect on the overall error of the least-squares fit. This seemed to indicate both that there was not sufficient data to address G_a, and that G_a was not the most important term for addressing perturbation in low K_a series. Addition of G_b addressed the global perturbation observed in low K_a series and allowed *b*-type resonances to be fit, along with additional *b*-type coupling terms, while the *a*-type resonances continued to be poorly predicted. Around $K_a = 16$–20, a curvature resembling a global perturbation became evident in Loomis-Wood plots. No distortion terms were able to address this curvature and, after addition of several such series, the least-squares fit failed to converge. At this point, inclusion of G_a enabled convergence and substantially decreased the overall error of the least-squares fit. The spectral prediction using the resulting constants eliminated the curvature previously observed in Loomis-Wood plots and began to bring

a-type resonances closer to fitting. Through this procedure, however, the value of G_a dropped from 1025 to ~300 MHz. It is expected that further fitting and refinement would lead to Fits I and II, and not result in a G_a value closer to the computational prediction. To further test the sensitivity of G_a to the inclusion or omission of other, higher-order Coriolis terms, we also attempted a least-squares fit of the spectroscopic data with F_{bc} arbitrarily set to zero. The fitting procedure did converge, and in fact, the value of G_a did increase to 453 MHz. This value, however, remains far from the predicted value. Moreover, this fit was inferior to Fits I and II in several respects, including its inability to fit many resonances, and was therefore not considered further.

As it appears that Fit I better models the rotational spectra of ν_{27} and ν_{19}, all discussion henceforth refers to Fit I. In comparison to the ground state, the rotational and distortion constants of ν_{27} and ν_{19} appear to be reasonably determined, physically meaningful values. The values of the rotational constants for both vibrationally excited states are within 0.5% of the corresponding ground-state constant. Upon excitation to ν_{27}, the largest change occurs in the value of B_{27}, whereas the largest change upon excitation to ν_{19} occurs in A_{19}. Among the distortion constants, δ_K displays the largest changes from the ground state by 13.9% for ν_{27} and 35.2% for ν_{19}. Although the percent change of δ_K for ν_{19} is the largest of any of the constants, it may parallel the large change in A_{19} from the ground-state value. Since the values of δ_K for the two vibrationally excited states do not diverge from the ground-state value (shift of equal magnitude, but opposite direction), we do not expect that they are absorbing perturbation. Moreover, δ_K does not appear in the table of most strongly correlated values (correlation matrix provided in the fitting output file and in the supplemental material). All of the fitted sextic distortion constants for ν_{27} are within 3% of the corresponding ground-state values, with the values of Φ_{JK} and ϕ_{JK} having the greatest change upon excitation. Upon excitation to ν_{19}, the greatest change is observed in Φ_J and ϕ_J, which both change by approximately 9.6% from the ground state.

Interpretation and analysis of the resonances

The resonance landscape of ν_{27} and ν_{19} is dominated, both in quantity and in size, by a-type resonances, *i.e.* resonances that have an even number value of ΔK_a between the near-resonant ν_{19} and ν_{27} states. Such a-type resonances observed in ${}^{a}R_{0,1}$ branch transitions in this work have perturbing interactions between opposite-symmetry states. That is, one series exhibiting resonance behaviour involves transitions with quantum numbers where $K_a + K_c = J$ (denoted with a superscript '+' over the K_a value), and the corresponding series in the other perturbing state involves transitions between levels with quantum numbers $K_a + K_c = J+1$ (denoted with a superscript '−' over the value of K_a). An example of such a pair of resonance plots is provided in Figure 8, where the selection rule for this particular set of resonances is $\Delta K_a = 2$. This set of transitions displays one of the most substantial displacements observed in the current work, appearing approximately 6.3 GHz away from the frequency that would be expected absent the local perturbation. In general, a-type resonances within the quantum number range of the work presented here are predicted to appear up to 7.8 GHz away from their expected location without perturbation, although the transitions with the largest displacements fall just outside of the spectral range in which we can measure them. All of the a-type resonances we observed conform to a $\Delta K_a = 2$ or 4 selection rule. The b-type resonances (ΔK_a = odd number selection rule) in our spectral region tend to exhibit smaller displacements than the a-type resonances. An example is depicted in Figure 9, where $\Delta K_a = 5$ and the maximum local perturbation is less than 0.5 GHz from the expected location absent local perturbation. Unlike the a-type resonances, perturbing states involved in b-type resonances have the same symmetry.

The Coriolis coefficient G_b is much larger than G_a, while the a-type resonances dominate the observed spectral region both in quantity and magnitude. A set of resonance progression plots, presented in Figure 10, display both a set of ${}^{a}R_{0,1}$ branch, K_a series and a set of ${}^{b}R_{1,1}$ branch, K_a series (even values of K_a only). In these plots, the y-axis displays the difference between the ν_{27} transition frequency and its corresponding 'deperturbed' transition frequency, scaled by $J''+1$. The deperturbed frequency is that predicted using the same spectroscopic constants as in the coupled-state fit, but excluding all coupling terms, enabling a visualisation of the effect of the Coriolis coupling. Patterns observed in other Coriolis-coupled states of planar molecules [1,45–49], such as the presence and progression of a global undulation and an increase in resonance magnitude with increasing J, appear in these plots, as well.

For *syn*-2-cyano-1,3-butadiene, the resonance plots for the a-type, R-branch transitions (Figure 10, top panel) and for the b-type, R-branch transitions (Figure 10, bottom panel) are identical at higher values of $J''+1$. The prominent resonances occur in that high-J region, where the a- and b-type transitions are degenerate. At lower values of $J''+1$, however, the a- and b-type transitions are non-degenerate, and the global perturbation behaviour observed differs significantly between the two sets of

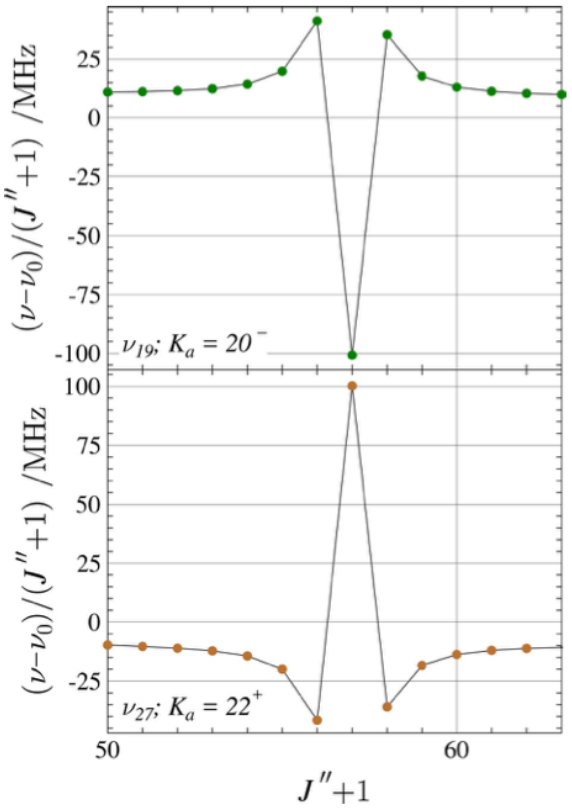


Figure 8. Resonance plots for *syn*-2-cyano-1,3-butadiene showing the $K_a = 22^+$ series for ν_{27} and $K_a = 20^-$ series for ν_{19}, an example of resonances conforming to the $\Delta K_a = 2$ selection rule. The plotted values are frequency differences between excited-state transitions and their ground-state counterparts, scaled by $(J''+1)$ in order to make the plots more horizontal. Measured transitions are represented by circles: ν_{27} (copper), ν_{19} (green). There are no measured transitions with $|(f_{obs.}-f_{calc.})/\delta f| > 3$. Predictions from the final coupled fit are represented by a solid, black line. The two resonances are mirror images of one another, confirming the K_a assignment of these resonance partners.

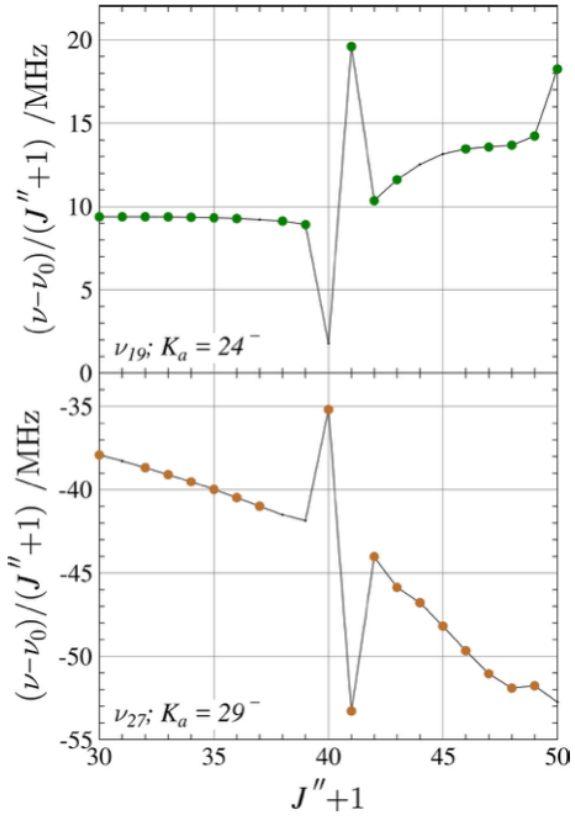


Figure 9. Resonance plots for *syn*-2-cyano-1,3-butadiene showing the $K_a = 29^-$ series for ν_{27} and $K_a = 24^-$ series for ν_{19}, an example of resonances conforming to the $\Delta K_a = 5$ selection rule. The plotted values are frequency differences between excited-state transitions and their ground-state counterparts, scaled by $(J''+1)$ in order to make the plots more horizontal. Measured transitions are represented by circles: ν_{27} (copper), ν_{19} (green). The missing data point at $J''+1 = 40$ in the plot of ν_{19} was not included, due to overlap with a ground-state transition. There are no measured transitions with $|(f_{obs.}-f_{calc.})/\delta f| > 3$. Predictions from the final coupled fit are represented by a solid, black line. The features of the two resonance plots are mirror images of one another, confirming the K_a assignment of these resonance partners.

transition types. While the undulation in the *a*-type plot has a serpentine shape whose amplitude increases only slightly with increasing K_a (Figure 10, top panel), the shape of the undulation in the *b*-type plot is akin to a hill shape whose amplitude increases more rapidly (Figure 10, bottom panel).

Figure 11 shows the same ${}^{b}R_{1,1}$ resonance progression plot for *syn*-2-cyano-1,3-butadiene as in Figure 10, but over a smaller set of $J''+1$ values and such that each K_a series is vertically staggered to better elucidate the shape of resonances. The large resonances in K_a series 6 through 16 are somewhat inconsistent in shape and do not increase in position by a steady value of J, indicating that the energy-level crossings responsible for these resonances occur at variable intervals between J values. After $K_a = 16$, the resonances of the ν_{27}:ν_{19} dyad of *syn*-2-cyano-1,3-butadiene take on a more regular shape and J progresses in regular steps of three.

As part of the coupled-state analysis, 16 matched pairs of nominal interstate transitions are included in Fit I. The formally forbidden, simultaneous vibrational and rotational transitions are enabled by substantial energy-level mixing between the two states. An example of a matched pair is depicted in Figure 12. In order for a pair of nominal interstate transitions to be a matched pair, their quantum numbers must describe two real, within-state transitions when either the upper or the lower energy levels are swapped between the nominal interstate transitions.

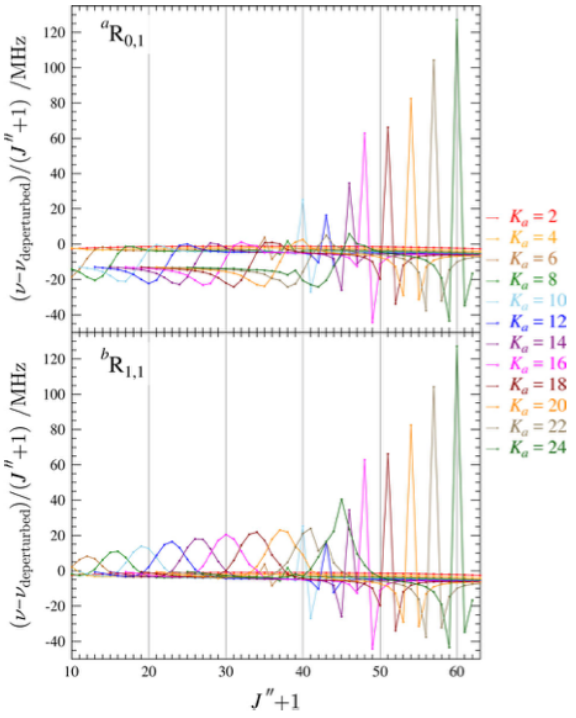


Figure 10. Superimposed resonance plots of ν_{27} for $^{a}R_{0,1}$ $K_a{}^{+}$ (top) and $^{b}R_{1,1}$ (bottom) series with even values of K_a between 2 and 24 for *syn*-2-cyano-1,3-butadiene. Measured transitions are omitted for clarity, but they are indistinguishable from the plotted values on this scale. The plotted values are frequency differences between excited-state transitions and their deperturbed counterparts, scaled by $(J''+1)$. The *x*- and *y*-axes are set to the same scale for each of the resonance plots.

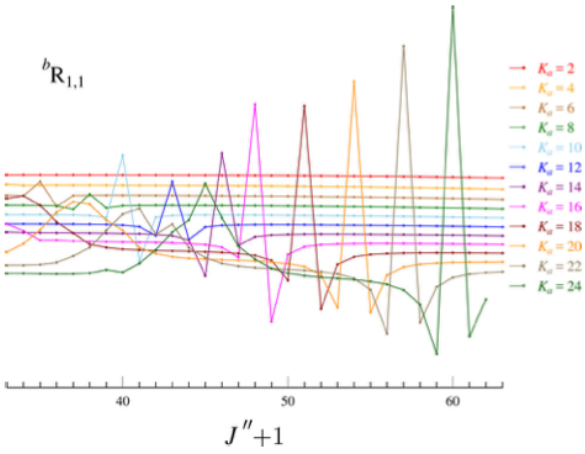


Figure 11. Superimposed resonance plots of ν_{27} for $^{b}R_{1,1}$ series with even values of K_a between 2 and 24 for *syn*-2-cyano-1,3-butadiene, vertically offset to simplify viewing individual plots. Measured transitions are omitted for clarity, but they are indistinguishable from the plotted values on this scale. The plotted values are frequency differences between excited state transitions and their deperturbed counterparts, scaled by $(J''+1)$.

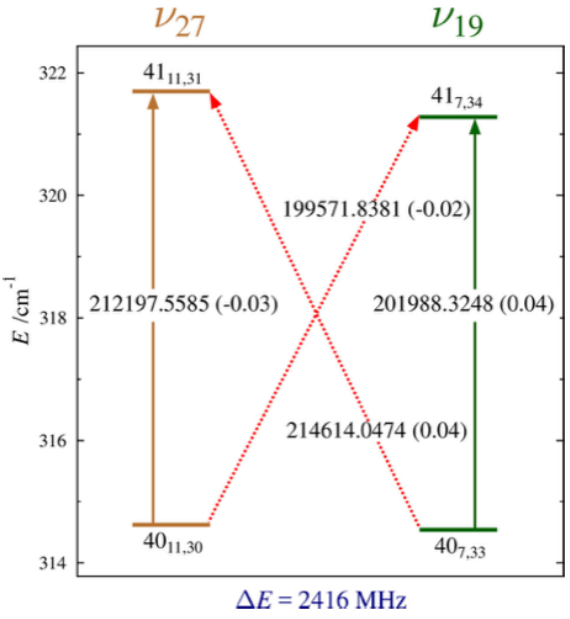


Figure 12. Energy diagram depicting a representative matched pair of nominal rotation-vibration transitions between ν_{27} (copper) and ν_{19} (green) vibrational states of *syn*-2-cyano-1,3-butadiene. Standard $^{a}R_{0,1}$ transitions within vibrational states are denoted by vertical arrows. The diagonal, dashed arrows indicate nominal interstate transitions that are formally forbidden, but enabled as a result of vibrational-rotational state mixing. Values printed on each of the arrows are the corresponding transition frequency (in MHz) with its *obs.* – *calc.* value in parentheses. The marked energy separation is the energy separation between the two strongly interacting rotational energy levels.

Matched pairs of nominal interstate transitions, therefore, have the same J values and their frequencies are typically predicted equally well. The average frequency of the within-state transitions and the average frequency of the matched nominal interstate transitions must be the same, within experimental error. In the example presented in Figure 12, these averages are 0.001 MHz apart, well within the experimental error of frequency measurement. A list of the measured nominal interstate transitions along with their average frequency analysis is provided in the supplemental material.

Comparison with computational estimates

The successful analysis of perturbed vibrationally excited states is reliant upon the ability to identify and assign their transitions in an initial fit. To this end, computational predictions of the vibration-rotation interaction constants are of particular utility. A comparison of the predicted and experimental vibration-rotation interaction constants is provided in Table 3. As expected, the C_0–C_v values are quite well predicted, with the value for

Table 3. Vibration-rotation interaction constants for ν_{27} and ν_{19} of *syn*-2-cyano-1,3-butadiene.

	Experimental	B3LYP/6-311+(2*d*,*p*)
	ν_{27}	
A_0–A_{27} (MHz)	−4.00	−6.51
B_0–B_{27} (MHz)	15.55	14.36
C_0–C_{27} (MHz)	−1.51	−1.39
	ν_{19}	
A_0–A_{19} (MHz)	−18.57	−15.34
B_0–B_{19} (MHz)	−0.59	−0.86
C_0–C_{19} (MHz)	1.66	1.68
	average	
$(A_0–A_\nu)_{ave}$ (MHz)	−11.29	−10.92
$(B_0–B_\nu)_{ave}$ (MHz)	7.84	6.75
$(C_0–C_\nu)_{ave}$ (MHz)	0.075	0.14

ν_{19} remarkably close to its experimental value. The theoretical A_0–A_ν and B_0–B_ν values are also in generally good agreement with the experimentally determined values. For ν_{27}, the largest discrepancy is in the value of A_0–A_ν, which is over-predicted by half its experimental value. For ν_{19}, it is the B_0–B_ν value whose magnitude is too large by a little over one-third of the experimental value. When, however, the average of the vibration-rotation interaction constants is examined (to balance out any potentially unaddressed perturbation factors in the theoretical treatment), the A_0–A_ν and B_0–B_ν averages fall within 10% of their experimental counterparts.

Discussion

The coupled-state analysis presented here provides an example of a Coriolis-coupled dyad, adding to the small body of data available on such dyads involving both *a*- and *b*-type Coriolis coupling. While most of the computational predictions for both the ground and vibrationally excited states are in good agreement with the experimental data, the present dyad analysis produces a value of G_a that is in poor agreement with the theoretical prediction. This discrepancy is unexpected, given the many previously studied coupled states (particularly those containing an aromatic ring and those of propionitrile) [21,45,46,48–50], where G_a was quite well computationally predicted. Our efforts to reduce this disagreement by modifying the least-squares fit have been unsuccessful. This turns out, however, to not be the first such example [41], as one of the predicted Coriolis-coupling coefficients for ν_{14}:ν_{20} dyad of SSC-glycolic acid ($G_a^{14,20}$ = 2599.36 MHz, B3LYP/6-311+G(2d,p)) is significantly different (76%) from the corresponding experimentally determined value (1477 (22) MHz). The predicted value of $G_b^{14,20}$ (2382.82 MHz), on the other hand, is only 8% different from the experimentally determined value of 2585.0 (95) MHz. It appears, based on the limited data available, that while the Coriolis-coupling coefficients (G_x) for substituted cyclic species are predicted quite well, computing those for acyclic species accurately is not always so straightforward. Attributing this problem to inaccuracies in the calculation of the Coriolis zeta constant is difficult to justify, because this parameter only depends on the normal coordinate analysis (the structure and harmonic force field), and computed results are not at all sensitive to basis set and correlation treatment. As discussed earlier, omitting the F_{bc} term does not fully address the discrepancy between the predicted and experimental values of G_a. Perhaps the omission of some higher-order (anharmonic) term in the spectroscopic Hamiltonian is responsible for the problem, but we have not been able to identify that term so far. It is alternatively possible that the issue arises from the determination of G_a and G_b from the spectral data, as the two terms interact strongly in the observed resonances, making the accuracy of the smaller constants highly affected by any errors in the larger constant.

The ground-state rotational spectrum of *syn*-2-cyano-1,3-butadiene has been measured and analysed here for the first time, resulting in a set of spectroscopic constants that include all of the octic centrifugal distortion constants. The experimental data provide the basis for an astronomical search for this highly polar species in the interstellar medium using high-frequency data (a low-frequency search would additionally require values of the N-quadrupole coupling terms, which can be reasonably well predicted theoretically). In terms of astrochemistry, this molecule represents a significant target for detection in its own right and because it is an isomer of the long-sought heterocyclic aromatic molecule, pyridine.

Supplemental material

See supplemental material for least-squares fitting files of 2-cyano-1,3-butadiene, output files from computations, computed vibration-rotation interaction constants, computed vibrational frequencies and infrared intensities, and nominal interstate transitions for the ν_{27} and ν_{19} dyad with their corresponding within-state transitions. These files may be found at https://doi.org/10.1080/00268976.2021.1964629.

Disclosure statement

No potential conflict of interest was reported by the author(s).

Funding

This work was supported by the National Science Foundation under Grants CHE-1954270 and CHE-1664912. We thank Michael McCarthy for the loan of an Amplification-Multiplication Chain and the Harvey Spangler Award (to B.J.E.) for the funding that supported the purchase of the corresponding Virginia Diodes Zero-Bias Detector (WR5.1ZBD 140 – 220 GHz). Current and former members of our research team thank Prof. John Stanton for his friendship and for sharing scientific insights through collaborative research over many, many years.

ORCID

Maria A. Zdanovskaia http://orcid.org/0000-0001-5167-8573
Brian J. Esselman http://orcid.org/0000-0002-9385-8078
Samuel M. Kougias http://orcid.org/0000-0002-9877-0817
Aatmik R. Patel http://orcid.org/0000-0001-8835-0870
R. Claude Woods http://orcid.org/0000-0003-0865-4693
Robert J. McMahon http://orcid.org/0000-0003-1377-5107

References

[1] C.P. Endres, S. Schlemmer, P. Schilke, J. Stutzki and H.S.P. Müller. J. Mol. Spectrosc. **327**, 95 (2016). doi:10.1016/j.jms.2016.03.005
[2] H.S.P. Müller, F. Schlöder, J. Stutzki and G. Winnewisser. J. Mol. Struct. **742**, 215 (2005). doi:10.1016/j.molstruc.2005.01.027
[3] B.A. McGuire, A.M. Burkhardt, S.V. Kalenskii, C.N. Shingledecker, A.J. Remijan, E. Herbst and M.C. McCarthy. Science. **359**, 202 (2018). doi:10.1126/science.aao4890
[4] B.A. McGuire, R.A. Loomis, A.M. Burkhardt, K.L.K. Lee, C.N. Shingledecker, S.B. Charnley, I.R. Cooke, M.A. Cordiner, E. Herbst, S. Kalenskii, M.A. Siebert, E.R. Willis, C. Xue, A.J. Remijan and M.C. McCarthy. Science. **371**, 1265 (2021). doi:10.1126/science.abb7535
[5] S. Zeng, D. Quénard, I. Jiménez-Serra, J. Martín-Pintado, V.M. Rivilla, L. Testi and R. Martín-Doménech. Mon. Not. R. Astron. Soc.: Letters. **484**, L43 (2019). doi:10.1093/mnrasl/slz002
[6] J. Cernicharo, M. Agúndez, L. Velilla Prieto, M. Guélin, J.R. Pardo, C. Kahane, C. Marka, C. Kramer, S. Navarro, G. Quintana-Lacaci, J.P. Fonfría, N. Marcelino, B. Tercero, E. Moreno, S. Massalkhi, M. Santander-García, M.C. McCarthy, C.A. Gottlieb and J.L. Alonso. Astron. Astrophys. **606**, L5 (2017). doi:10.1051/0004-6361/201731672
[7] L.W. Avery, N.W. Broten, J.M. MacLeod, T. Oka and H.W. Kroto. Astrophys J, Lett. **205**, L173 (1976). doi:10.1086/182117
[8] N.W. Broten, T. Oka, L.W. Avery, J.M. MacLeod, and H.W. Kroto, Astrophys. J. Lett. **223** L105 (1978). doi:10.1086/182739
[9] H.W. Kroto, C. Kirby, D.R.M. Walton, L.W. Avery, N.W. Broten, J.M. MacLeod and T. Oka. Astrophys. J. **219**, L133 (1978). doi:10.1086/182623
[10] L.E. Snyder and D. Buhl. Astrophys. J. **163**, L47 (1971). doi:10.1086/180664
[11] C.M. Walmsley, G. Winnewisser and F. Toelle. Astron. Astrophys. **81**, 245 (1980).
[12] R.A. Loomis, A.M. Burkhardt, C.N. Shingledecker, S.B. Charnley, M.A. Cordiner, E. Herbst, S. Kalenskii, K.L.K. Lee, E.R. Willis, C. Xue, A.J. Remijan, M.C. McCarthy and B.A. McGuire. Nat. Astron. **5**, 188 (2021). doi:10.1038/s41550-020-01261-4
[13] N.W. Broten, J.M. MacLeod, L.W. Avery, W.M. Irvine, B. Hoeglund, P. Friberg and A. Hjalmarson. Astrophys. J. **276**, L25 (1984). doi:10.1086/184181
[14] F.F. Gardner and G. Winnewisser. Astrophys. J. **195**, L127 (1975). doi:10.1086/181726
[15] L.E. Snyder, J.M. Hollis, P.R. Jewell, F.J. Lovas and A. Remijan. Astrophys. J. **647**, 412 (2006). doi:10.1086/505323
[16] F.J. Lovas, A.J. Remijan, J.M. Hollis, P.R. Jewell and L.E. Snyder. Astrophys. J. Lett. **637**, L37 (2006). doi:10.1086/500431
[17] P.M. Solomon, K.B. Jefferts, A.A. Penzias and R.W. Wilson. Astrophys. J. **168**, L107 (1971). doi:10.1086/180794
[18] A. Belloche, R.T. Garrod, H.S.P. Müller and K.M. Menten. Science. **345**, 1584 (2014). doi:10.1126/science.1256678
[19] A. Belloche, R.T. Garrod, H.S.P. Müller, K.M. Menten, C. Comito and P. Schilke Astron. Astrophys. **499**, 215 (2009). doi:10.1051/0004-6361/200811550
[20] R.J. Halter, R.L. Fimmen, R.J. McMahon, S.A. Peebles, R.L. Kuczkowski and J.F. Stanton. J. Am. Chem. Soc. **123**, 12353 (2001). doi:10.1021/ja011195t
[21] M.A. Zdanovskaia, B.J. Esselman, R.C. Woods and R.J. McMahon. J. Chem. Phys. **151**, 024301 (2019). doi:10.1063/1.5100805
[22] S.M. Kougias, S.N. Knezz, A.N. Owen, R.A. Sanchez, G.E. Hyland, D.J. Lee, A.R. Patel, B.J. Esselman, R.C. Woods and R.J. McMahon. J. Org. Chem. **85**, 5787 (2020). doi:10.1021/acs.joc.9b03388
[23] M.A. Zdanovskaia, P.M. Dorman, V.L. Orr, A.N. Owen, S.M. Kougias, B.J. Esselman, R.C. Woods and R.J. McMahon. J. Am. Chem. Soc. **143**, 9551 (2021). doi:10.1021/jacs.1c03777
[24] M.C. McCarthy, K.L.K. Lee, P.B. Carroll, J.P. Porterfield, P.B. Changala, J.H. Thorpe and J.F. Stanton. J. Phys. Chem. A. **124**, 5170 (2020). doi:10.1021/acs.jpca.0c02919
[25] P. Mishra, S.M. Fritz, S. Herbers, A.M. Mebel, and T.S. Zwier. PCCP **23** 6462 (2021). doi:10.1039/D1CP00104C
[26] J.P. Ferris and J.C. Guillemin. J. Org. Chem. **55**, 5601 (1990). doi:10.1021/jo00308a017
[27] A. Jamal and A.M. Mebel. J. Phys. Chem. A. **117**, 741 (2013). doi:10.1021/jp3091045
[28] D.S.N. Parker and R.I. Kaiser. Chem. Soc. Rev. **46**, 452 (2017). doi:10.1039/C6CS00714G
[29] N. Raffaelli, in *Origins of Life: The Primal Self-Organization*, edited by Richard Egel, Dirk-Henner Lankenau, and Armen Y. Mulkidjanian (Springer-Verlag, Heidelberg, 2011), Chap. 9, pp. 191.
[30] S. Pizzarello, Y. Huang and M. Fuller. Geochim. Cosmochim. Acta. **68**, 4963 (2004). doi:10.1016/j.gca.2004.05.024
[31] S. Pizzarello and Y. Huang. Geochim. Cosmochim. Acta. **69**, 599 (2005). doi:10.1016/j.gca.2004.07.031
[32] B.M. McMurtry, A.M. Turner, S.E.J. Saito and R.I. Kaiser. Chem. Phys. **472**, 173 (2016). doi:10.1016/j.chemphys.2016.03.010
[33] S.B. Charnley, Y.-J. Kuan, H.-C. Huang, O. Botta, H.M. Butner, N. Cox, D. Despois, P. Ehrenfreund, Z. Kisiel,

Y.-Y. Lee, A.J. Markwick, Z. Peeters and S.D. Rodgers. Adv. Space Res. **36**, 137 (2005). doi:10.1016/j.asr.2005.09.005

[34] B.J. Esselman, B.K. Amberger, J.D. Shutter, M.A. Daane, J.F. Stanton, R.C. Woods and R.J. McMahon. J. Chem. Phys. **139**, 224304 (2013). doi:10.1063/1.4832899

[35] Z. Kisiel, L. Pszczółkowski, I.R. Medvedev, M. Winnewisser, F.C. De Lucia and E. Herbst. J. Mol. Spectrosc. **233**, 231 (2005). doi:10.1016/j.jms.2005.07.006

[36] Z. Kisiel, L. Pszczółkowski, B.J. Drouin, C.S. Brauer, S. Yu, J.C. Pearson, I.R. Medvedev, S. Fortman and C. Neese. J. Mol. Spectrosc. **280**, 134 (2012). doi:10.1016/j.jms.2012.06.013

[37] H.M. Pickett. J. Mol. Spectrosc. **148**, 371 (1991). doi:10.1016/0022-2852(91)90393-O

[38] Z. Kisiel, in *Spectroscopy from Space*, edited by J. Demaison, K. Sarka, E.A. Cohen (Kluwer Academic Publishers, Dordrecht, 2001), pp. 91–106. < http://www.ifpan.edu.pl/ kisiel/prospe.htm > .

[39] M.J. Frisch, G.W. Trucks, H.B. Schlegel, G.E. Scuseria, M.A. Robb, J.R. Cheeseman, G. Scalmani, V. Barone, G.A. Petersson, H. Nakatsuji, X. Li, M. Caricato, A.V. Marenich, J. Bloino, B.G. Janesko, R. Gomperts, B. Mennucci, H.P. Hratchian, J.V. Ortiz, A.F. Izmaylov, J.L. Sonnenberg, D. Williams-Young, F. Ding, F. Lipparini, F. Egidi, J. Goings, B. Peng, A. Petrone, T. Henderson, D. Ranasinghe, V.G. Zakrzewski, J. Gao, N. Rega, G. Zheng, W. Liang, M. Hada, M. Ehara, K. Toyota, R. Fukuda, J. Hasegawa, M. Ishida, T. Nakajima, Y. Honda, O. Kitao, H. Nakai, T. Vreven, K. Throssell, J.A. Jr. Montgomery, J.E. Peralta, F. Ogliaro, M.J. Bearpark, J.J. Heyd, E.N. Brothers, K.N. Kudin, V.N. Staroverov, T.A. Keith, R. Kobayashi, J. Normand, K. Raghavachari, A.P. Rendell, J.C. Burant, S.S. Iyengar, J. Tomasi, M. Cossi, J.M. Millam, M. Klene, C. Adamo, R. Cammi, J.W. Ochterski,R.L. Martin, K. Morokuma, O. Farkas, J.B. Foresman and D.J. Fox, *Gaussian 16 rev C.01* (Gaussian, Inc., Wallingford, CT, 2016).

[40] J.R. Schmidt and W.F. Polik, WebMO Enterprise, version 19.0; WebMO LLC: Madison, WI, USA, 2019; http://www.webmo.net (accessed August, 2019).

[41] Z. Kisiel, L. Pszczółkowski, E. Białkowska-Jaworska and S.B. Charnley. J. Mol. Spectrosc. **321**, 13 (2016). doi:10.1016/j.jms.2016.01.014

[42] J.H. Baraban, M.-A. Martin-Drumel, P.B. Changala, S. Eibenberger, M. Nava, D. Patterson, J.F. Stanton, G.B. Ellison and M.C. McCarthy. Angew. Chem. Int. Ed. **57**, 1821 (2018). doi:10.1002/anie.201709966

[43] B.J. Sun, C.H. Huang, S.Y. Chen, S.H. Chen, R.I. Kaiser and A.H.H. Chang. J. Phys. Chem. A. **118**, 7715 (2014). doi:10.1021/jp5056864

[44] D. Papoušek and M.R. Aliev, *Molecular Vibrational-Rotational Spectra* (Elsevier Scientific Publishing Company, Prague, 1982), **Vol. 17**, p. 323.

[45] P.M. Dorman, B.J. Esselman, J.E. Park, R.C. Woods and R.J. McMahon. J. Mol. Spectrosc. **369**, 111274 (2020). doi:10.1016/j.jms.2020.111274

[46] M.A. Zdanovskaia, B.J. Esselman, H.S. Lau, D.M. Bates, R.C. Woods, R.J. McMahon and Z. Kisiel. J. Mol. Spectrosc. **351**, 39 (2018). doi:10.1016/j.jms.2018.06.004

[47] O. Pirali, Z. Kisiel, M. Goubet, S. Gruet, M.A. Martin-Drumel, A. Cuisset, F. Hindle and G. Mouret. J. Chem. Phys. **142**, 104310 (2015). doi:10.1063/1.4913750

[48] Z. Kisiel and A. Kraśnicki. J. Mol. Spectrosc. **262**, 82 (2010). doi:10.1016/j.jms.2010.05.007

[49] Z. Kisiel, E. Białkowska-Jaworska and L. Pszczółkowski. J. Mol. Spectrosc. **232**, 47 (2005). doi:10.1016/j.jms.2005.02.006

[50] Z. Kisiel, C.A. Nixon, M.A. Cordiner, A.E. Thelen and S.B. Charnley. J. Mol. Spectrosc. **372**, 111324 (2020). doi:10.1016/j.jms.2020.111324

Appendix F

Synthesis, Purification, and Rotational Spectroscopy of 1-Cyanocyclobutene (C_5H_5N)

Houston H. Smith
Samuel M. Kougias
Brian J. Esselman
R. Claude Woods
Robert J. McMahon

The Journal of Physical Chemistry A, 2022, *126*, 1980-1993

THE JOURNAL OF PHYSICAL CHEMISTRY A
A JOURNAL OF THE AMERICAN CHEMICAL SOCIETY

pubs.acs.org/JPCA Article

Synthesis, Purification, and Rotational Spectroscopy of 1-Cyanocyclobutene (C_5H_5N)

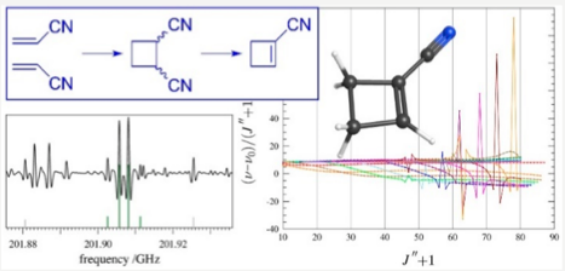
Published as part of The Journal of Physical Chemistry virtual special issue "10 Years of the ACS PHYS Astrochemistry Subdivision".

Houston H. Smith, Samuel M. Kougias, Brian J. Esselman, R. Claude Woods,* and Robert J. McMahon*

Cite This: *J. Phys. Chem. A* 2022, 126, 1980−1993 Read Online

ACCESS | Metrics & More | Article Recommendations | Supporting Information

ABSTRACT: The rotational spectrum of 1-cyanocyclobutene from 130 to 360 GHz has been observed, assigned, and least-squares fit for the ground state and the two lowest-energy vibrationally excited states. Synthesis by UV photochemical dimerization of acrylonitrile and subsequent base-catalyzed dehydrocyanation affords a highly pure sample, yielding several thousand observable rotational transitions for this small organic nitrile. Over 2500 *a*-type, R-branch transitions of the ground state have been least-squares fit to low error with partial-octic A- and S-reduced Hamiltonians, providing precise determinations of the corresponding spectroscopic constants. In both reductions, computed spectroscopic constants are in close agreement with their experimentally determined counterparts. Two vibrationally excited states (ν_{27} and ν_{17}) form a Coriolis-coupled dyad, displaying many *a*-type and *b*-type local resonances and related nominal interstate transitions. Somewhat unexpectedly, despite the very small permanent *b*-axis dipole moment, a number of *b*-type transitions could be observed for the ν_{17} state; this is explained in terms of state mixing by the Coriolis perturbations. Over 2200 transitions for each of these states have been least-squares fit to a low-error, two-state, partial-octic, A-reduced Hamiltonian with nine Coriolis-coupling terms (G_a, G_a^J, G_a^K, G_a^{JJ}, F_{bc}, F_{bc}^K, G_b, G_b^J, and F_{ac}). The availability of so many observed rotational transitions, including resonant transitions and nominal interstate transitions, enables a very accurate and precise determination of the energy difference ($\Delta E_{27,17}$ = 14.0588093 (43) cm^{-1}) between ν_{27} and ν_{17}. The spectroscopic constants presented herein provide a starting point for future astronomical searches for 1-cyanocyclobutene.



INTRODUCTION

The interstellar medium (ISM) and circumstellar shells are known to contain complex and diverse chemical environments, with almost 250 molecules currently detected, including many new detections in the past few years.[1,2] Organic nitriles comprise an important subset of interstellar molecules because of their chemical relationship to molecules of prebiotic relevance, *e.g.*, pyridine. The cyano moiety is prevalent among organic species detected in the ISM because the typically large permanent dipole moments lead to a higher likelihood that molecules containing this functional group may be detected via radioastronomy, relative to other functionalities. The assignment of laboratory rotational spectra of organic nitriles is highly desirable to facilitate the detection of new molecules in the ISM. We have been interested in expanding two areas of organic nitrile assignments: aryl nitriles/isonitriles[3−6] and nitrile-containing isomers of pyridine.[7−10] The aryl nitriles/isonitriles are of interest as possible tracer molecules for molecular species, e.g., benzene, pyridine, pyrimidine, pyrazine, and pyridazine. While pyridine, pyrimidine, and pyridazine have permanent dipole moments, they have been sought unsuccessfully in the ISM.[11] The addition of the cyano substituent could be beneficial by significantly increasing the dipole moment, allowing the substituted species to serve as a tracer molecule for the parent species. Benzene and pyrazine do not have a permanent dipole, while the former has been detected by infrared spectroscopy, tracer molecules are necessary for their existence in the ISM to be inferred by radioastronomy. The recent detections of benzonitrile,[12] 1- and 2-cyanoaphthalene,[13] and 1-cyano-1,3-cyclopentadiene[14] signify great advances utilizing this technique and encourage further studies of the laboratory rotational spectra of nitrile-containing tracer molecules.

Nitrogen-containing isomers of pyridine (C_5H_5N) provide similar motivation as tracers of pyridine's presence in various environments. Importantly, the detection, or lack thereof, of

Received: January 17, 2022
Revised: February 24, 2022
Published: March 22, 2022



ACS Publications © 2022 American Chemical Society

https://doi.org/10.1021/acs.jpca.2c00384
J. Phys. Chem. A 2022, 126, 1980−1993

particular C_5H_5N isomers could help elucidate the reaction chemistry of small organic nitriles and/or pathways for formation of aromatic molecules such as pyridine. We have recently investigated seven structural isomers of pyridine (including the present case) that are shown in Figure 1, several

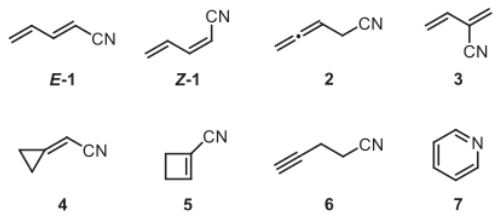


Figure 1. C_5H_5N isomers that have been studied by rotational spectroscopy: (*E*)-1-cyano-1,3-butadiene (*E*-**1**), (*Z*)-1-cyano-1,3-butadiene (*Z*-**1**), 4-cyano-1,2-butadiene (**2**), 2-cyano-1,3-butadiene (**3**), (cyanomethylene)cyclopropane (**4**), 1-cyanocyclobutene (**5**), 4-cyano-1-butyne (**6**), and pyridine (**7**).

of which are proposed to be a part of complex, astrochemically relevant processes.[15−17] Two derivatives, *E*- and *Z*-1-cyano-1,3-butadiene (*E*-**1**, *Z*-**1**) have recently been detected *via* laboratory rotational spectroscopy in various chemical environments.[18,19] Another 1,3-butadiene derivative, 2-cyano-1,3-butadiene (**3**), has been generated by UV irradiation of cyanoacetylene and ethylene.[20] In terms of potential relevance to astrochemistry, 1-cyanocyclobutene (**5**) has been generated by photolysis of 2-cyano-1,3-butadiene,[21] and the reverse transformation can be achieved by thermolysis.[22,23] Due to their proposed importance and recent detection in reactive environments, the astronomical search for these isomers seems warranted.

1-Cyanocyclobutene (**5**), the pyridine isomer presented in this work, has a planar, four-membered ring. The π bond within the ring enforces the planarity of the ring by greatly restricting the ability of the carbon atoms to move out-of-plane. Structurally similar, four-membered ring molecules with π-conjugated substituents have been studied by rotational spectroscopy, *e.g.*, β-propiolactone (**10**)[24−26] and diketene (**11**) (Figure 2).[27] Each of these species, like cyanocyclobutene,

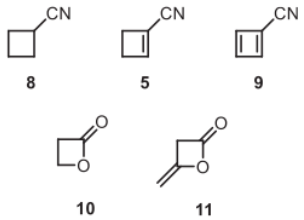


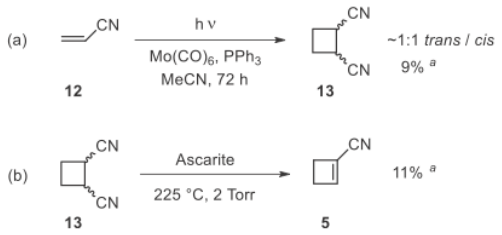
Figure 2. Structurally similar four-membered ring species: cyanocyclobutane (**8**), 1-cyanocyclobutene (**5**), cyano-1,3-cyclobutadiene (**9**), β-propiolactone (**10**), and diketene (**11**).

has a planar ring due to the presence of sp^2-hybridized carbon atoms in the ring or conjugation between ring atoms and substituents. Unlike the molecules mentioned above, rotational or vibrational spectra of 1-cyanocyclobutene (**5**) have not been reported in the literature. Cyanocyclobutane (**8**), due to its fully saturated ring, exhibits two nonplanar conformers (−CN equatorial or axial), which have been well-studied by rotational and vibrational spectroscopy.[28−32] While the fully unsaturated cyanocyclobutadiene (**9**) has been generated and characterized under matrix-isolation conditions,[33] it has not been analyzed *via* gas-phase spectroscopy. Exploration of the spectroscopy and structures of these similar compounds allows meaningful comparisons to be made of these strained four-membered ring systems.

EXPERIMENTAL AND THEORETICAL METHODS

Synthesis. 1-Cyanocyclobutene (**5**) has been prepared *via* a number of synthetic methods: photoinduced 4π electrocyclization from 2-cyano-1,3-butadiene (**3**),[21] ring expansion from 1-cyano-bicyclo[1.1.0]butane,[34] base-induced elimination from 1-chloro-2-cyanocyclobutane[22,35] or 1,2-dicyanocyclobutane,[22,35] dehydration of 1-cyclobutene-1-carboxamide,[36] or photochemical [2 + 2] cycloaddition of ethylene and cyanoacetylene.[37] To prepare a sample for analysis *via* rotational spectroscopy, the base-induced elimination of 1,2-dicyanocyclobutane described by Gale and Cherkofsky[22] was utilized. By this route, 1-cyanocyclobutene (**5**) could be selectively obtained on multigram scale in a two-step synthesis starting from acrylonitrile and isolated from the 1,2-dicyanocyclobutanes by distillation. As shown in Scheme 1, acrylonitrile (**12**) was

Scheme 1. Syntheses of 1,2-Dicyanocyclobutane (13) and 1-Cyanocyclobutene (5)



[a]Isolated yield.

photodimerized to generate 1,2-dicyanocyclobutane (**13**) *via* a [2 + 2] cycloaddition in 9% yield using $Mo(CO)_6$ as a photosensitizer.[38] Depending on the reaction conditions, this dimerization produces predominantly the *trans* stereoisomers of 1,2-dicyanocyclobutane[39] or a mixture (58:42) of *trans*- and *cis*-(1,2-dicyanocyclobutane) isomers.[40] As evidenced by the ^{1}H NMR data provided in the Supporting Information, our reaction yielded an approximately 1:1 mixture of the *trans* and *cis* diastereomers. Dehydrocyanation of the mixture of 1,2-dicyanocyclobutane isomers (**13**) by passing through a heated quartz tube packed with Ascarite afforded the desired compound, 1-cyanocyclobutene (**5**), in 11% yield.

Spectroscopy. Using a millimeter-wave spectrometer previously described,[4,41] the rotational spectrum of 1-cyanocyclobutene was collected from 130 to 230 GHz and from 235 to 360 GHz, in a continuous flow at room temperature, with a sample pressure of 4 mTorr. The separate spectral segments were combined into a single broadband spectrum using Kisiel's Assignment and Analysis of Broadband Spectra (AABS) software.[42,43] Pickett's SPFIT/SPCAT[44] was used for least-squares fits and spectral predictions, along with the PIFORM, PLANM, and AC programs for analysis.[45,46] A uniform frequency measurement uncertainty of 50 kHz was assumed for all measurements.

Computation. Electronic structure calculations were carried out with Gaussian 16[47] using the WebMO[48] interface to obtain predicted values for various spectroscopic constants. Optimized

https://doi.org/10.1021/acs.jpca.2c00384
J. Phys. Chem. A 2022, 126, 1980−1993

geometries at the B3LYP/6-311+G(2d,p) and the MP2/6-311+G(2d,p) levels were obtained using "verytight" convergence criteria and an "ultrafine" integration grid, and subsequent anharmonic vibrational frequency calculations were carried out. Although the B3LYP predictions of the spectroscopic constants were adequate to begin the analysis, they did not have the expected agreement with the experimental spectroscopic constants. Thus, MP2 calculations were performed, and these had slightly closer agreement with the experimental constants. All computational output files can be found in the Supporting Information.

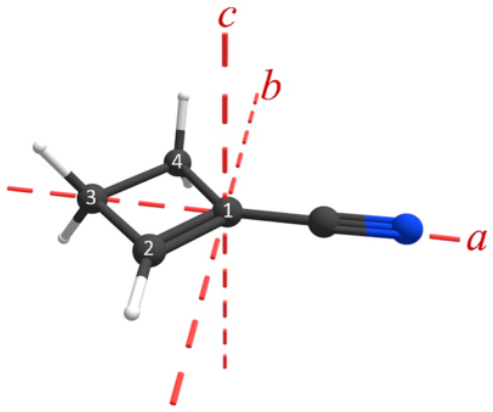


Figure 3. 1-Cyanocyclobutene (**S**, C_s, C_5H_5N) structure with principal inertial axes (μ_a = 4.2 D, μ_b = 0.07 D, MP2/6-311+G(2d,p)).

RESULTS AND DISCUSSION

Ground Vibrational State. 1-Cyanocyclobutene (Figure 3) is a highly prolate, asymmetric top molecule ($\kappa = -0.94$) with a strong dipole moment along its *a*-principal axis (μ_a = 4.2 D, MP2) and much weaker *b*-component (μ_b = 0.07 D, MP2). The experimental spectrum from 130−360 GHz is dominated by $^aR_{0,1}$ transitions that appear in clearly observable bands sharing a single *J* value (Figure 4). In this frequency range, the (+) and (−) symmetry $^aR_{0,1}$ transitions are degenerate for the initial series, $K_a = 0^+$ and $K_a = 1^-$ but lose degeneracy at higher K_a. The (+) and (−) symmetry transitions become degenerate at different *J* values depending on the particular band. As the K_a quantum number increases, transitions of the two symmetries attain K_a degeneracy. The transitions in the series shown in Figure 4 become prolate (K_a) degenerate at $K_a = 10$. This series continues to even lower frequency as the K_a value increases until the transitions become too weak to be observed. These bands are separated by approximately $B_0 + C_0$ (~4.5 GHz). Transitions for the singly substituted heavy isotopologues, ^{13}C and ^{15}N, could not be detected at their natural abundance. We attribute this to the spectral density arising from the ground and vibrationally excited states of the main isotopologue. Thus, the work presented herein addresses only the analysis of the ground vibrational state and first two vibrationally excited states of the normal species.

Over 2500 transitions, represented in Figure 5, have been measured and least-squares fit to partial-octic, distorted-rotor Hamiltonians in the I^r representation for both the A (σ_{fit} = 0.024 MHz) and S reductions (σ_{fit} = 0.024 MHz). The resulting values of the spectroscopic constants are shown in Table 1, along with their computational counterparts. The computed rotational constants (MP2/6-311+G(2d,p)) are within 1% of the experimental values. Even with this relatively small difference, the predicted sum of $B_0 + C_0$ is approximately 37 MHz too small, which results in $^aR_{0,1}$ band locations off by 1.3−4.1 GHz with $J'' + 1$ ranging from 32 to 87. While line assignments inside these obvious bands are initially challenging from computational predictions, the R-branch $K_a = 0$ series, which are outside of these bands and have spacing that mainly depends on C_0, are the first targets for assignment. This series has been readily identified *via* a Loomis−Wood plot and subsequent assignment and least-squares fitting has been straightforward. The computed quartic centifugal distortion constants agree quite well with the experimental values, the largest discrepancies being in δ_J (5%) and in d_2 (6%) for the A and S reductions, respectively. Likewise, there is satisfactory agreement between the computed and experimental sextic distortion constants, with the largest discrepancies being in φ_J (32%) and in h_3 (9%) for the A and S reductions, respectively. The transitions included in the final data set are insufficient to satisfactorily determine the sextic constants Φ_K, Hk, or h_1. These constants are held at their computed values, in a manner similar to that in previous works where there were only *a*-type transitions across a similar range of *J* and *K* values.[4,5] Even with the inability to determine a complete set of sextic distortion constants, three octic centrifugal distortion constants, L_{JJK}, L_{JK}, and L_{KKJ}, have been satisfactorily determined and their inclusion improves the σ_{fit}. Presently, no commonly available computational software is able to predict octic centrifugal distortion constants, so the octic constants that are not determined have been held at zero in the least-squares fit. This likely affects the reported octic distortion constants and somewhat reduces their physical meaningfulness compared to the well-determined quartic and sextic distortion constants.

Fundamental Vibrational States ν_{27} and ν_{17}. The vibrational energy manifold of 1-cyanocyclobutene below 550 cm^{-1} (Figure 6) consists of the ground state and three sets of vibrationally excited states. The first set is a Coriolis-coupled dyad of the two lowest-energy vibrationally excited states (ν_{27} and ν_{17}). The next-lowest-energy set of vibrational states consists of a likely Coriolis-, Fermi-, and Darling−Dennison-coupled tetrad of the corresponding two-quanta vibrational states ($2\nu_{27}$, $\nu_{27} + \nu_{17}$, and $2\nu_{17}$) and fundamental ν_{26}. Near 500 cm^{-1}, the three-quanta states of ν_{27} and ν_{17} form a complex polyad with $\nu_{27} + \nu_{26}$, $\nu_{17} + \nu_{26}$, ν_{25}, and ν_{16}. While all of these states are sufficiently intense to be observed in the current spectral data, this work strictly focuses on the Coriolis-coupled dyad of ν_{27} and ν_{17} at ca. 165 cm^{-1}. The lowest-energy fundamental state, ν_{27} (A″, 159 cm^{-1}), is an out-of-plane bend of the cyano substituent, with a simultaneous distortion of the cyclobutene ring by a large motion of the $C(3)H_2$ group with respect to C(1). The second-lowest-energy fundamental state, ν_{17} (A′, 173 cm^{-1}), is an in-plane bend of the cyano substituent, combined with some in-plane distortion of the cyclobutene ring. The two lowest-energy vibrational states are expected to have strong interactions, due to the small predicted energy separation (14 cm^{-1}) and the combination of relatively large A_v rotational constants, Coriolis ζ values, and *J* values observed in this frequency range. As expected, a single-state model cannot adequately predict or fit the transitions observed for either vibrationally excited state. Therefore, a two-state, partial-octic, A-reduced Hamiltonian has been employed to model ν_{27} and ν_{17} in a manner similar to that in our previous work on (cyanomethylene)cyclopropane.[10] The least-squares fit incor-

https://doi.org/10.1021/acs.jpca.2c00384
J. Phys. Chem. A 2022, 126, 1980−1993

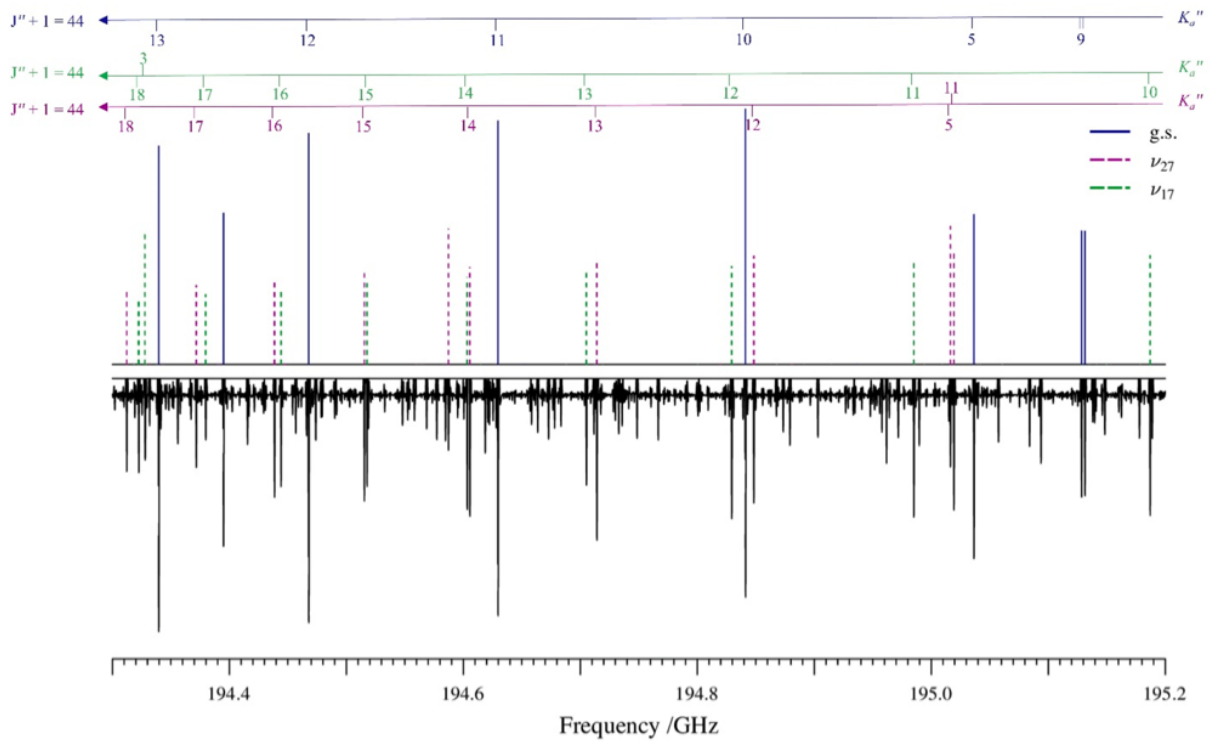


Figure 4. Predicted (top) and experimental (bottom) rotational spectra of 1-cyanocyclobutene (**5**) from 194.3 to 195.2 GHz. Ground-state transitions for the $J'' + 1 = 44$ band appear in dark blue, ν_{27} in purple, and ν_{17} in green. The complete frequency spectrum from 130 to 360 GHz was obtained automatically over approximately 6 days given these experimental parameters: 0.6 MHz/s sweep rate, 10 ms time constant, and 50 kHz AM and 500 kHz FM modulation in a tone burst design.

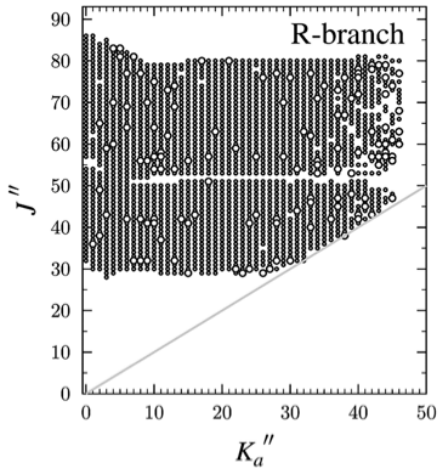


Figure 5. Data distribution plots for the least-squares fit of spectroscopic data for the vibrational ground state of 1-cyanocyclobutene (**5**). R-branch transitions are represented by black circles. The size of the symbol is proportional to the value of $|(f_{obs} - f_{calc})/\delta f|$, where δf is the frequency measurement uncertainty, and all values are smaller than 3.

porates at least 2200 transitions for each vibrationally excited state and has a low statistical error (σ_{fit} = 0.031 MHz). The wide range of J (28−87) and K_a (0−46 and 43 for ν_{27} and ν_{17}, respectively) quantum numbers recorded is illustrated in the data set distribution plot (Figure 7). This distribution of least-squares fit transitions is only slightly diminished in comparison to the vibrational ground state, due to the low energy (and thus high population) of these vibrationally excited states.

The spectroscopic constants resulting from the final least-squares fit (Table 2) include a precise determination of the rotational constants for each vibrational state. The rotational constants are well determined for each state, and the largest experimental uncertainty appears in the values of the A_v constants, whose relative statistical uncertainties are only 0.003% of their values. The near-absence of *b*-type transitions (*vide infra*), due to the very small μ_b value, contributes to this diminished precision of A_v, as in the ground state. As has been shown for similar cases,[3−5,49] the Coriolis-coupled dyad increases the uncertainty in the A_v rotational constants somewhat, due to the high correlation between A_v and the *a*-type Coriolis parameters. A full set of quartic distortion constants and a few (Φ_J, Φ_{JK}, and Φ_{KJ}) sextic distortion constants have been determined for each vibrational state. All distortion constants that cannot be determined in the fit have been held constant at their corresponding ground-state values. There are no clear signs of Coriolis coupling being absorbed by the quartic distortion constants, and all are within expected deviations from the ground state (<10%, except Δ_K at 15% for ν_{27}).

Coriolis-Coupling Analysis. The least-squares fit determines a precise energy separation ($\Delta E_{27,17}$ = 421472.50 (13) MHz; 14.0588093 (43) cm^{-1}) between ν_{27} and ν_{17}. The computed energy difference (13.8 cm^{-1}; MP2) agrees very well

https://doi.org/10.1021/acs.jpca.2c00384
J. Phys. Chem. A 2022, 126, 1980−1993

Table 1. Spectroscopic Constants for the Ground Vibrational State of 1-Cyanocyclobutene (S- and A-Reduced Hamiltonian, I^r Representation)

	S Reduction, I^r representation			A Reduction, I^r representation	
	Experimental	MP2 [a]		Experimental	MP2 [a]
A_0 (MHz)	12492.5719 (78)	12418	A_0 (MHz)	12492.5807 (81)	12418
B_0 (MHz)	2364.413212 (66)	2344	B_0 (MHz)	2364.41929 (11)	2344
C_0 (MHz)	2038.935375 (72)	2022	C_0 (MHz)	2038.929419 (99)	2022
D_J (kHz)	0.112235 (11)	0.108	Δ_J (kHz)	0.135307 (18)	0.129
D_{JK} (kHz)	5.513431 (92)	5.39	Δ_{JK} (kHz)	5.37497 (12)	5.26
D_K (kHz)	3.046 (74)	3.18	Δ_K (kHz)	3.252 (75)	3.28
d_1 (kHz)	−0.0204606 (23)	−0.0194	δ_J (kHz)	0.020490 (11)	0.0194
d_2 (kHz)	−0.0115338 (69)	−0.0108	δ_K (kHz)	2.9188 (18)	2.80
H_J (Hz)	−0.00004395 (77)	−0.0000441	Φ_J (Hz)	0.0000146 (19)	0.0000103
H_{JK} (Hz)	0.011349 (15)	0.0109	Φ_{JK} (Hz)	0.01604 (32)	0.0155
H_{KJ} (Hz)	−0.070845 (85)	−0.0718	Φ_{KJ} (Hz)	−0.0875 (11)	−0.0880
H_K (Hz)	[0.0710]	0.071	Φ_K (Hz)	[0.0825]	0.0825
h_1 (Hz)	[−0.000000621]	−0.000000621	ϕ_J (Hz)	0.00000622 (99)	0.00000417
h_2 (Hz)	0.00002895 (78)	0.0000272	ϕ_{JK} (Hz)	0.00802 (20)	0.00774
h_3 (Hz)	0.00000527 (33)	0.00000479	ϕ_K (Hz)	0.163 (14)	0.165
L_{JJK} (μHz)	−0.0000326 (12)		L_{JJK} (μHz)	−0.0000387 (12)	
L_{JK} (μHz)	0.0004759 (53)		L_{JK} (μHz)	0.000300 (16)	
L_{KKJ} (μHz)	−0.005681 (28)		L_{KKJ} (μHz)	−0.005089 (57)	
Δ_i (uÅ^2) [b,c]	−6.334144 (27)		Δ_i (uÅ^2) [b,c]	−6.332842 (31)	
N_{lines} [d]	2529		N_{lines} [d]	2529	
σ_{fit} (MHz)	0.024		σ_{fit} (MHz)	0.024	

[a]Evaluated with the 6-311+G(2d,p) basis set. [b]Inertial defect, $\Delta_i = I_c - I_a - I_b$. [c]Calculated using PLANM from the B_0 constants. [d]Number of fitted transition frequencies

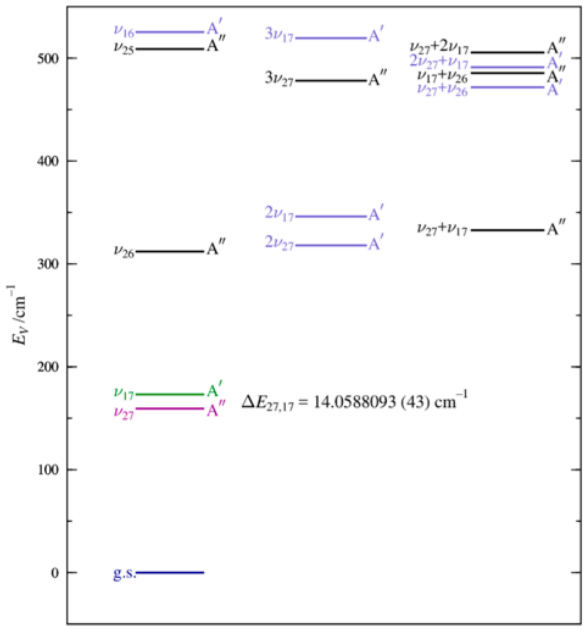


Figure 6. Vibrational energy levels of 1-cyanocyclobutene (**5**) below 550 cm^{-1} from computed fundamental frequencies (MP2/6-311+G(2d,p)). The value of $\Delta E_{27,17}$ results from the experimental perturbation analysis of ν_{27} and ν_{17} in this work.

with the experimentally determined value. The B3LYP computed value (17.9 cm^{-1}) is slightly overpredicted (ca. 5 cm^{-1}), as is the case in several similar works involving coupled dyads.[3−6,9] The high precision of the experimental value of $\Delta E_{27,17}$ arises because the data set includes all of the following: (i) numerous rotational transitions involved in global interactions between the two fundamentals, (ii) rotational transitions involved in local resonances occurring from energy-level crossings, and (iii) (formally forbidden) interstate transitions that involve changes in both rotational and vibrational quantum numbers. The symmetries of the two fundamentals, ν_{27} (A″, 159 cm^{-1}) and ν_{17} (A′, 173 cm^{-1}), allow for both *a*- and *b*-type Coriolis coupling between the states. The final least-squares fit requires incorporation of nine Coriolis-coupling terms (G_a , G_a^J, G_a^K, G_a^{JJ}, F_{bc} , F_{bc}^K, G_b , G_b^J, F_{ac}) to quantitatively account for both of these types of coupling across the observed spectrum.

The initial fitting process of the first several K_a series for each vibrational state has been accomplished by varying the energy separation and the G_a value to account for, and adequately predict, the global undulation that is present for each series. This global undulation in Figure 8 appears to be small relative to the magnitude of the local resonances at higher J and K_a. Figures 9 and 10, however, better illustrate the substantial impact of the global undulation on several K_a series. The undulation is observed at low J for low K_a series and progresses higher in J as K_a increases until approximately $K_a = 20$ for ν_{27} (lower for ν_{17}) where the position of the global undulation has increased to J values beyond the range investigated in this experiment. The values of J for a particular K_a at which the global undulation is most apparent are always those that correspond to the changeover from oblate asymmetric top behavior at low J to prolate-like at high J. During fitting, if any local resonances are predicted in the K_a series, transitions involved in the resonance, along with several transitions at lower and higher J values, are omitted from the fit until the global undulation is treated well. Once the global perturbation is well predicted, the local

https://doi.org/10.1021/acs.jpca.2c00384
J. Phys. Chem. A 2022, 126, 1980−1993

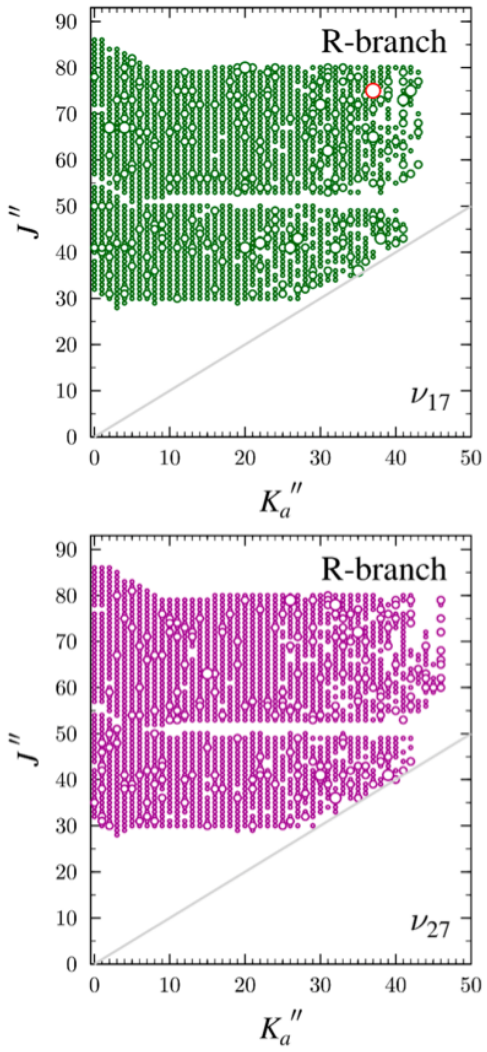


Figure 7. Data distribution plot for data in the two-state fit of ν_{27} and ν_{17} of 1-cyanocyclobutene (**5**). The size of the plotted symbol is proportional to the value of $|(f_{obs} - f_{calc})/\delta f|$, where δf is frequency measurement uncertainty, and values greater than or equal to 3 are marked in red.

resonances can be more readily assigned. As more transitions are incorporated into the least-squares fit, additional coupling terms are needed to account for the complex interactions between the two fundamental states. During the fitting process, all centrifugal distortion constants are monitored for signs of absorbed Coriolis perturbation or unfavorable correlations between distortion and coupling constants. This iterative process allows for a fully predictive fit to be achieved, which in turn makes it possible to perform a final frequency sweep measuring and recording every visible transition for each fundamental. Lastly, the nominal interstate transitions are measured and included in the least-squares fit in all cases where confident assignments can be made (*vide infra*).

Figure 8 illustrates the regularity of the *a*-type local resonances, which begin at $K_a = 4^-$ at $J = 48$ and subsequently increase in J by five until the end of the measured frequency range. As the local resonances progress to higher J, their magnitude increases with the largest resonance occurring at $K_a = 10^-$. This most displaced transition at $J = 78$ is approximately 9 GHz away from its unperturbed predicted position. A significant number of resonances (~40) are observed, with the majority being *a*-type resonances. The *a*-type resonances are also significantly larger in magnitude than *b*-type resonances, as can be seen in Figures 9 and 10.

A few *a*-type resonances are shown in Figure 9a; the $K_a = 1^-$ series of ν_{17} has two *a*-type resonances, at $J = 37$ and 47, with $\Delta K_a = 4$ and 2 selection rules, respectively. The paired resonance at $J = 37$ is in Figure 9c with the $K_a = 5^+$ ($\Delta K_a = 4$) series of ν_{27} and is obscured by the global undulation. The magnitude of the resonance and J value are exactly the same in the two series, although the different scale factors in the plots make this more difficult to see in the figure. The second paired local resonance at $J = 47$ is shown in Figure 9b with the $K_a = 3^+$ ($\Delta K_a = 2$) series of ν_{27}, and in this case the symmetry is more visually obvious. Figure 9d containing the $K_a = 3^-$ series of ν_{17} is included because it shows another paired resonance for the $K_a = 5^+$ series of ν_{27} at $J = 58$. The $K_a = 3^-$ series of ν_{17} has a second resonance at $J = 43$, which is paired with the $K_a = 7^+$ series of ν_{27} (not shown). An example of a *b*-type local resonance at $J = 72,73$ is shown in Figure 10, between the $K_a = 9^+$ series of ν_{17} and the $K_a = 12^+$ series of ν_{27} ($\Delta K_a = 3$). The ΔK_a selection rule is always even for *a*-type and odd for *b*-type resonances; in addition, there is a change in symmetry for *a*-type and no change in symmetry for *b*-type coupling.

An additional indication of unaddressed Coriolis coupling would be if the vibration–rotation interaction constants for ν_{27} and ν_{17} exhibit large, equal and opposite values. The $B_0 - B_v$ and $C_0 - C_v$ values presented in Table 3 are relatively small in magnitude, exhibit the same sign, and show excellent agreement between experiment and theory. These observations support the interpretation that these values are physically meaningful and that their corresponding rotational constants are well determined and likely free of residual Coriolis-coupling effects. The experimental and computational $A_0 - A_v$ values are in quite poor agreement and are much larger in magnitude than the $B_0 - B_v$ or $C_0 - C_v$ values for each vibrational state. It is unclear to what extent these large values of $A_0 - A_v$ and the disagreement between their theoretical and experimental values are caused by residual unaddressed Coriolis coupling or by poorly estimated $A_0 - A_v$ values. A similar observation was made for the $A_0 - A_v$ values in the analogous Coriolis-coupled dyad of (cyanomethylene)cyclopropane.[10] The discrepancy is larger for 1-cyanocyclobutene (**5**), but, for both molecules, the computed values for these interactions are of opposite sign than the fitted ones. Given the close agreement in the averages of these values, at least some untreated coupling must be manifest in the experimental and/or theoretical values. The very large data sets and the overall quality of the least-squares fits, however, make it possible that A_{27} and A_{17} are close to their true values, despite the discrepancy with the theoretical calculations.

The lowest-order spectroscopic Coriolis coupling parameters, G_a and G_b can be predicted, given the Coriolis constant ζ, by eq 1, where ω is the harmonic vibrational frequency of the corresponding mode and x is the corresponding inertial axis.

$$G_x = \frac{\omega_{27} + \omega_{17}}{\sqrt{\omega_{27} \times \omega_{17}}} \zeta^x_{27,17} B^x_e \approx 2\zeta^x_{27,17} B^x_e \quad (1)$$

The experimental ζ values in Table 3 are calculated from eq 1 using harmonic frequencies computed by MP2, the exper-

https://doi.org/10.1021/acs.jpca.2c00384
J. Phys. Chem. A 2022, 126, 1980−1993

Table 2. Spectroscopic Constants for Vibrationally Excited States ν_{27} and ν_{17} of 1-Cyanocyclobutene (5) (A-Reduced Hamiltonian, I^r Representation)

	Ground State	ν_{27} (A", 159 cm^{-1})[a,b]	ν_{17} (A', 173 cm^{-1})[a,b]
A_0 (MHz)	12492.5807 (81)	12576.09 (31)	12402.39 (31)
B_0 (MHz)	2364.41929 (11)	2367.99024 (40)	2370.86901 (39)
C_0 (MHz)	2038.929419 (99)	2043.148392 (65)	2041.224377 (62)
Δ_J (kHz)	0.135307 (18)	0.138684 (12)	0.139633 (12)
Δ_{JK} (kHz)	5.37497 (12)	5.53104 (59)	5.16909 (58)
Δ_K (kHz)	3.252 (75)	3.744 (25)	3.233 (29)
δ_J (kHz)	0.020490 (11)	0.0205743 (24)	0.0219861 (20)
δ_K (kHz)	2.9188 (18)	2.92104 (42)	2.99398 (54)
Φ_J (Hz)	0.0000146 (19)	0.00002013 (98)	0.0000183 (10)
Φ_{JK} (Hz)	0.01604 (32)	0.016545 (44)	0.015331 (43)
Φ_{KJ} (Hz)	−0.0875 (11)	−0.10018 (25)	−0.06685 (23)
Φ_K (Hz)	[0.0825]	[0.0825]	[0.0825]
ϕ_J (Hz)	0.00000622 (99)	[0.00000622]	[0.00000622]
ϕ_{JK} (Hz)	0.00802 (20)	[0.00802]	[0.00802]
ϕ_K (Hz)	0.163 (14)	[0.163]	[0.163]
ΔE		421472.50 (13) MHz / 14.0588093 (43) cm^{-1}	
G_a (MHz)		19993.0 (33)	
G_a^J (MHz)		−0.016787 (14)	
G_a^K (MHz)		−0.2226 (14)	
G_a^{JJ} (MHz)		0.00000003739 (26)	
F_{bc} (MHz)		−0.1191 (29)	
F_{bc}^K (MHz)		−0.00010156 (99)	
G_b (MHz)		97.09 (85)	
G_b^J (MHz)		−0.780 (57)	
F_{ac} (MHz)		−0.0004476 (74)	
Δ_i (uÅ^2)[c,d]	−6.332842 (31)	−6.25371 (99)	−6.3242 (10)
N_{lines}[e]	2529	2300	2233
σ_{fit} (MHz)	0.024	0.030	0.032

[a]Fundamental frequencies calculated using MP2/6-311+G(2d,p). [b]Octic centrifugal distortion constants (not shown) were held constant at their ground-state values. [c]Inertial defect, $\Delta_i = I_c - I_a - I_b$. [d]Calculated using PLANM from the B_0 constants. [e]Number of fitted transition frequencies.

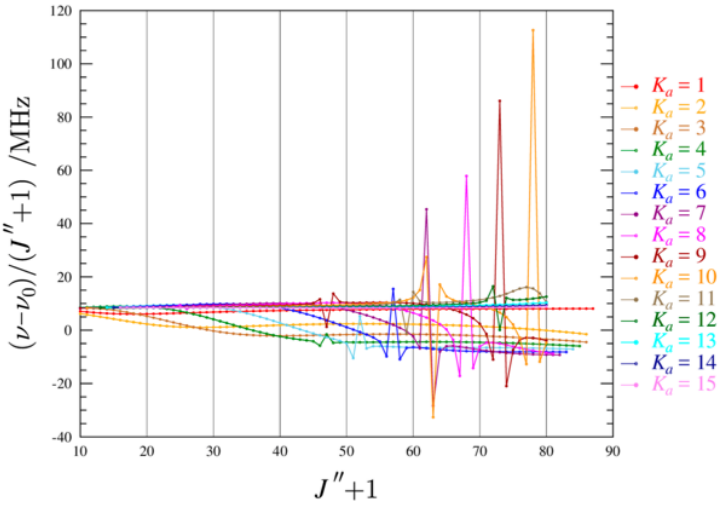


Figure 8. Superimposed resonance plots of ν_{27} for $^qR_{0,1}$ K_a^- series from 1 to 15 for 1-cyanocyclobutene (**5**). Measured transitions are omitted for clarity, but they are indistinguishable from the plotted values on this scale. The plotted values are frequency differences between excited-state transitions and their ground-state counterparts, scaled by (J'' + 1).

imentally determined G_x, and rotational constants corrected by half the sum of the corresponding MP2 vibration−rotation interaction constants for all vibrations. The experimental value of $\zeta^a_{27,17}$ is slightly greater than the computational predictions, while the experimental value of $\zeta^b_{27,17}$ is smaller by a similar magnitude.

The observed resonances are a result of state mixing between ν_{27} and ν_{17}. This state mixing can result in interstate transitions, where simultaneous changes in rotational and vibrational quantum numbers occur. The energy separation in the Coriolis-coupled dyad, ν_{27} and ν_{17} (14.0588093 (43) cm^{-1}), is small enough to cause intense local resonances and state mixing,

https://doi.org/10.1021/acs.jpca.2c00384
J. Phys. Chem. A 2022, 126, 1980−1993

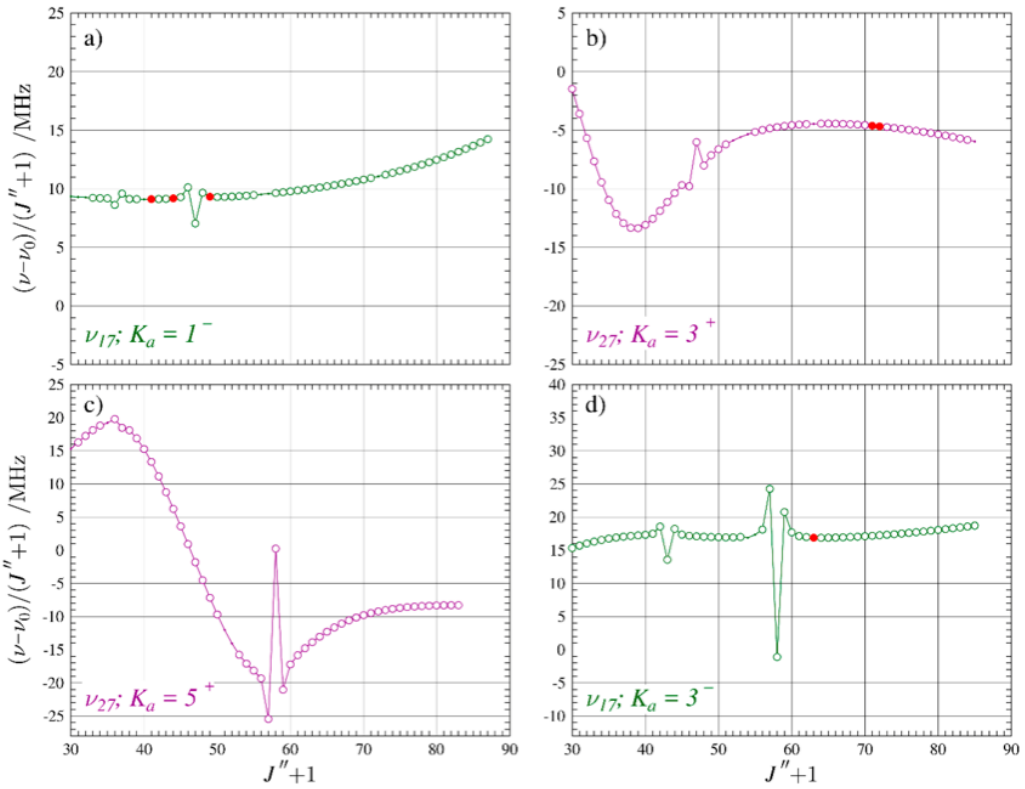


Figure 9. Resonance plots for 1-cyanocyclobutene (**5**) showing the $K_a = 1^-$ and 3^- series for ν_{17} and $K_a = 3^+$ and 5^+ series for ν_{27}. These are examples of resonances conforming to the $\Delta K_a = 2$ or 4 selection rules for *a*-type resonances. The plotted values are frequency differences between excited-state transitions and their ground-state counterparts, scaled by $(J'' + 1)$ in order to make the plots more horizontal. Measured transitions are represented by circles: ν_{27} (purple), ν_{17} (green). The measured transitions with $|(f_{obs} - f_{calc})/\delta f| > 3$ are marked in red. Predictions from the final coupled fit are represented by a solid, colored line.

and this allows a significant number (57) of nominal interstate transitions to be assigned. These transitions are assigned by comparison of the experimental and predicted frequencies, as well as by comparison of the observed average frequencies, which should ideally be exactly the same for matched sets of corresponding inter- and intrastate transitions. Two nominal interstate transitions, along with their corresponding intrastate transitions, are shown in Figure 11. Each measured transition includes its *obs.*−*calc.* value in parentheses. The average frequencies of the inter- and intrastate transitions shown in Figure 11 differ by only 62 kHz, illustrating the accuracy of the measurements and the correctness of the assignments. The corresponding intrastate resonances ($J'' + 1 = 73$) from the $K_a = 9^-$ series of ν_{27} and the $K_a = 5^+$ series of ν_{17} are displayed in Figure 11 to illustrate that the resonances and observable interstate transitions occur at the same J values, as a result of significant state mixing. For example, the smallest energy separation, $\Delta E = 8984$ MHz, occurs between $73_{9,65}$ for ν_{27} and $73_{5,68}$ for ν_{17}, which corresponds to the intrastate transitions most shifted in frequency for each vibrational state.

A rarely reported type of intensity enhancement by state mixing has been found in this spectrum. 1-Cyanocyclobutene has a quite small *b*-type dipole moment ($\mu_a = 4.2$ D, $\mu_b = 0.07$ D, MP2), which prevents observation of any *b*-type transitions in the ground state or in ν_{27}. Due to the Coriolis-coupling between ν_{27} and ν_{17}, however, indirect state mixing enhances the intensity of approximately 35 *b*-type transitions for ν_{17} sufficiently that they become measurable and are included in the least-squares fit of the coupled dyad. As exemplified in the Loomis−Wood plot in Figure 12, many of these intense *b*-type transitions occur near the *J*-levels where degeneracy of the $^aR_{0,1}$ K_a^+ and K_a^- series is established, and also near, but not necessarily exactly coincident with, *J* values where local resonances are observed between the two vibrational states. In most K_a^+/K_a^- series for ν_{17}, the rigid-rotor asymmetry splitting results in only the expected doublet at low *J* values. In the case of the $K_a^+/K_a^- = 1$ and 2 series shown, however, the two transitions involving the $J = 48$ level both exhibit the formation of a quartet that includes observably intense *b*-type transitions. At lower *J*-levels, the *b*-type transitions disappear, and the series progresses with the expected doublet pattern. Due to strong, local perturbation, transitions in the $J'' + 1 = 50-53$ range are nondegenerate but do not exhibit a clear doublet structure. The $K_a^+/K_a^- = 1$ and 2 series become degenerate after the resonances at $J'' + 1 = 57$. These *b*-type transitions are allowed, to a negligible extent, due to the small *b*-type dipole moment component. They are much more intense, however, due to intensity borrowing from *a*-type transitions with the same *J* values. Although the closest relevant resonance with ν_{27} is at $J = 51$, this is still a *J* region of significant state mixing with ν_{27}, which has the effect of perturbing the energy levels of ν_{17}. The perturbation causes two of the ν_{17} energy levels to cross at or near the *J* value where the observed *b*-type transitions are most intense. In some of the observed cases, the mixing is sufficiently strong that SPFIT and SPCAT reverse the labels of

https://doi.org/10.1021/acs.jpca.2c00384
J. Phys. Chem. A 2022, 126, 1980−1993

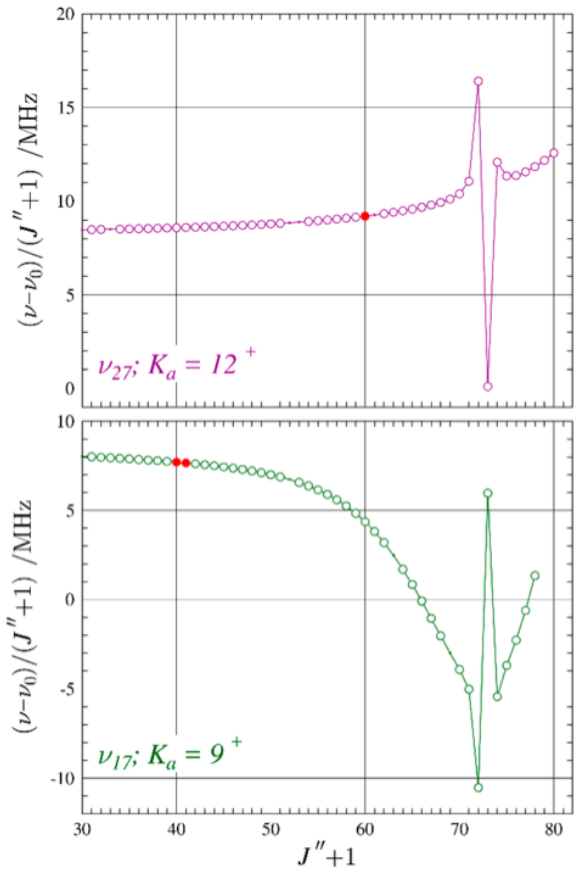


Figure 10. Resonance plots for 1-cyanocyclobutene (**5**) showing the $K_a = 9^+$ series for ν_{17} and $K_a = 12^+$ series for ν_{27}. These two resonances conform to the $\Delta K_a = 3$ selection rule for *b*-type resonances. The plotted values are frequency differences between excited-state transitions and their ground-state counterparts, scaled by $(J'' + 1)$ in order to make the plots more horizontal. Measured transitions are represented by circles: ν_{27} (purple), ν_{17} (green). The measured transitions with $|(f_{obs} - f_{calc})/\delta f| > 3$ are marked in red. Predictions from the final coupled fit are represented by a solid, colored line.

Table 3. Vibration–Rotation Interaction and Coriolis-Coupling Constants of 1-Cyanocyclobutene (5)

	Experimental	B3LYP [a]	MP2 [a]
$A_0 - A_{27}$ (MHz)	−83.41 (31)	17.8	17.4
$B_0 - B_{27}$ (MHz)	−3.57095 (41)	−3.42	−3.25
$C_0 - C_{27}$ (MHz)	−4.21897 (12)	−4.07	−3.94
$A_0 - A_{17}$ (MHz)	90.19 (31)	−11.1	−7.26
$B_0 - B_{17}$ (MHz)	−6.44972 (41)	−6.11	−6.29
$C_0 - C_{17}$ (MHz)	−2.29495 (12)	−2.14	−2.26
$\frac{(A_0-A_{27})+(A_0-A_{17})}{2}$ (MHz)	3.38 (22)	3.36	5.05
$\frac{(B_0-B_{27})+(B_0-B_{17})}{2}$ (MHz)	−5.01033 (29)	−4.77	−4.77
$\frac{(C_0-C_{27})+(C_0-C_{17})}{2}$ (MHz)	−3.256965 (83)	−3.10	−3.10
$\zeta^a_{27,17}$	0.807	0.751	0.744
$\zeta^b_{27,17}$	0.021	0.027	0.0227

[a]Evaluated with the 6-311+G(2d,p) basis set.

the mixed energy levels, resulting in an apparent exchange of the *a*-type and *b*-type identification of the transitions in the quartet. An example of that can be seen in the $J = 48–49$ transitions in Figure 12, where SPFIT and SPCAT misidentify the *a*- and *b*-type transitions. Because of this problem, we manually shifted this frequency segment in the Loomis–Wood plot by ~3 MHz to visually align all (lower-frequency) *a*-type transitions for clarity. In an extreme case of intensity borrowing, $J'' + 1 = 81$ for $K_a^+/K_a^- = 5$ and 6 transitions, almost all of the intensity is transferred from the *a*-type to *b*-type transitions. In all cases, SPCAT does accurately reproduce the observed pattern of the quartet, including the relative intensities. A summary listing of all *b*-type transitions included in the least-squares fit is provided in the Supporting Information.

There are several important clues to the quantum mechanical origin of the intensity enhancement of the nominally *b*-type transitions. First, this quartet phenomenon requires having both *a*- and *b*-type Coriolis coupling between ν_{27} and ν_{17}, which is easily confirmed by setting the *b*-type Coriolis parameters to zero in SPCAT, in which case the predicted intensities of the lines in question are not greater than they are in the ground-state spectrum, i.e., negligible. Second, unlike the local resonances observed between states, the enhancement effect is not present in the spectra of both vibrational levels; it is present only in ν_{17} (to be explained below). Finally, the frequency splittings of the quartets and the intensities of the "*b*-type" peaks are both highly dependent upon the energy-level splittings of the two near-degenerate rotational levels in ν_{17} and on the distance of these two levels from the Coriolis-connected rotational levels in ν_{27}, although not in a simply recognizable way. All these observations can be clearly understood by consideration of the diagonalization of the two-state Hamiltonian matrix for the J involved, focusing on the three or four vib-rotational levels of most interest. Figure 13 shows an example of four vib-rotational levels, where the $48_{1,47}$ and $48_{2,47}$ energy levels for ν_{17} are connected to the $48_{5,44}$ and $48_{4,44}$ energy levels, respectively, for ν_{27} through *a*-type Coriolis coupling. These ν_{17} energy levels are also connected to the other two rotational energy levels ($48_{1,47}$ to $48_{4,44}$ and $48_{2,47}$ to $48_{5,44}$) through *b*-type coupling (to a lesser extent). This double coupling in the matrix allows the $48_{1,47}$ and $48_{2,47}$ energy levels to indirectly mix with each other. The degree of this mixing is normally small, but it is greatly amplified when the two levels are very close to each other, i.e., near-degenerate, ultimately leading to the *b*-type transitions we have observed. In general, two connecting states in ν_{27}, *e.g.*, both $48_{5,44}$ and $48_{4,44}$ in the above instance, are not required for this effect, and cases of only one rotational energy level of ν_{27} interacting strongly with the two near-degenerate energy levels of ν_{17} are observed here. At first glance, one would suspect, from the symmetry of the interaction and the quantum number types involved, that the same phenomenon could be observed in ν_{27}. It must be remembered, however, that because ν_{27} has the lower vibrational energy, its resonances must always have the higher K_a value. The higher K_a value implies a greater oblate asymmetry (lower K_c) at any particular J value, which in turn yields much larger asymmetry splittings. This renders the indirect mixing of the two rotational states in ν_{27} inconsequential. An interesting aspect of the "*b*-type" intensities predicted by SPCAT is that they do, in fact, depend on the value of μ_b to a noticeable extent (about 10% when going from 0 to 0.07 D). This behavior is understood by considering that the intensities are proportional to the absolute square of a sum of (large) μ_a and (small) μ_b matrix elements. Thus, the cross term is more substantial than the square of the μ_b term (which leads to negligible intensity by itself) and does produce significant increases or decreases in predicted intensity. This example of a quantum interference

https://doi.org/10.1021/acs.jpca.2c00384
J. Phys. Chem. A 2022, 126, 1980–1993

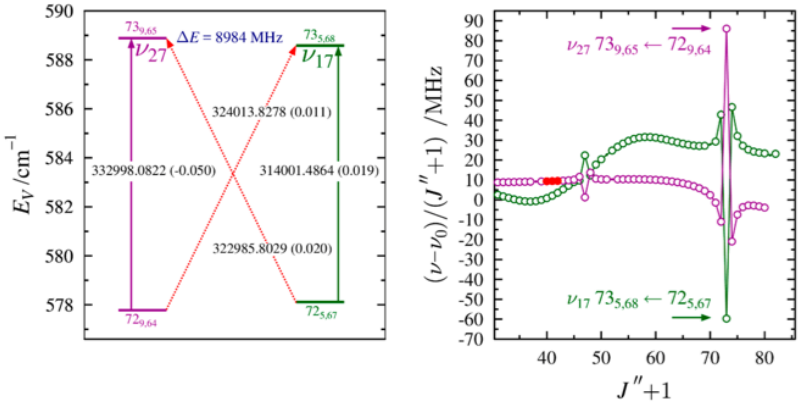


Figure 11. Energy diagram (left) depicting a representative matched pair of nominal interstate transitions between the ν_{27} (purple) and ν_{17} (green) vibrational states of 1-cyanocyclobutene (**5**). Standard $^aR_{0,1}$ transitions within vibrational states are denoted by vertical arrows. The diagonal, dashed arrows indicate nominal interstate transitions that are formally forbidden but enabled as a result of rotational energy level mixing. Values printed on each of the arrows are the corresponding transition frequency (in MHz) with its obs−calc value in parentheses. The marked energy separation is between the two strongly interacting rotational energy levels. Resonance plots (right) of the K_a series of ν_{27} and ν_{17} that contain the corresponding resonant transitions labeled with their quantum numbers and marked by colored arrows.

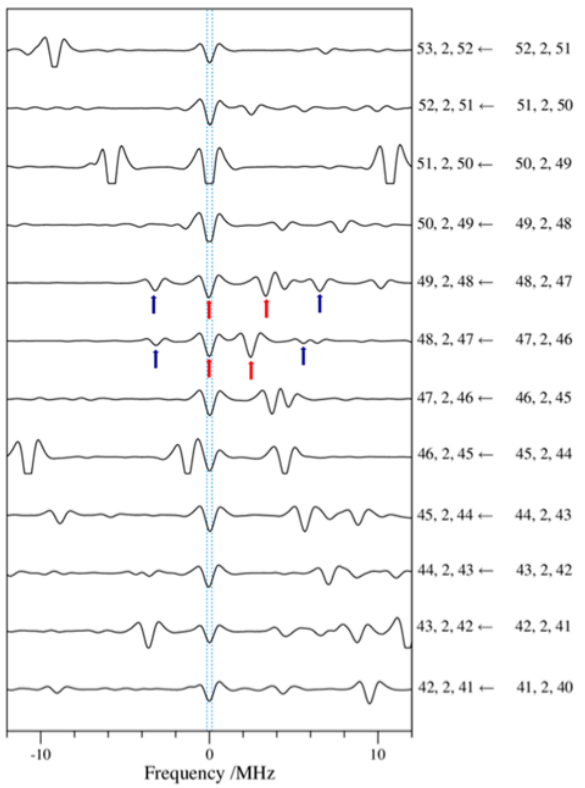


Figure 12. Loomis−Wood plot centered on the $K_a = 2^-$ series for ν_{17} ranging in $J'' + 1 = 42-53$. The $K_a = 1^+$ can be seen higher in frequency below $J'' + 1 = 47$ in a typical doublet pattern progressing further away in frequency as $J'' + 1$ decreases. A quartet of *a*-type (red) and *b*-type (blue) transitions is then observed for $J'' + 1 = 48$ and 49. The Loomis−Wood frequency segment corresponding to $J'' + 1 = 49$ was shifted lower in frequency by 3 MHz for this figure due to the SPCAT misassignment of the *a*- and *b*-type transitions.

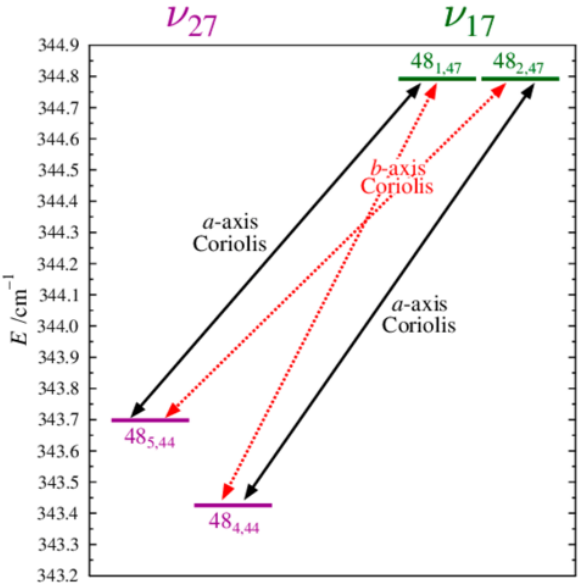


Figure 13. Four-state vib-rotational energy level diagram showing the states involved in creating an observable quartet in the $K_a^+/K_a^- = 1$ and 2 series. The red and black arrows indicate the *b*- and *a*-axis Coriolis interactions, respectively, that allow for state mixing between states.

effect may well be more important in other molecules with a somewhat larger μ_b. Meanwhile, this phenomenon is not possible in a molecule where the second dipole component is *exactly* zero, since the molecular symmetry that causes it will also mean that only one type of Coriolis coupling is allowed between any two vibrational states. Of course, if both dipole moment components are comparable in magnitude, the effects of the indirect coupling may not even be noticed.

Higher up the vibrational manifold, at approximately 330 cm^{-1}, the two-quanta vibrational states of ν_{27} (A″) and ν_{17} (A′) form a coupled tetrad with ν_{26}. This tetrad is expected to be well-isolated from other vibrationally excited states and of sufficient intensity that the rotational spectra of all four states can be measured, assigned, and least-squares fit, using the spectral data we have already acquired. Despite the complicating interaction

https://doi.org/10.1021/acs.jpca.2c00384
J. Phys. Chem. A 2022, 126, 1980−1993

with ν_{26} (A″), this tetrad can be addressed using the same general methodology recently employed with benzonitrile, where the triad consisting of the overtones and simple combination of the two lowest-lying states is analyzed very successfully.[50] In that study, the harmonic and anharmonic vibrational constants for the states involved are well predicted by the *xguinea* routine of CFOUR, as was the Darling−Dennison coupling term connecting the two overtone states. Furthermore, it has been found that the higher-order Coriolis coupling coefficients, *e.g.*, G_a^J or F_{bc}, for the triad scale rather closely as a factor of $\sqrt{2}$ from the corresponding ones of the dyad. Equivalent predictions and scaling for 1-cyanocyclobutene should greatly expedite assignment of the tetrad, and a successful fit would provide a further test of the accuracy of the predicted and scaled parameters. The ν_{26} fundamental should be coupled by anharmonic resonance to the combination state and by higher-order Coriolis interactions to all three triad states. Acquisition and analysis of the modestly strong ν_{17} band, its two hot bands, and possibly the weaker ν_{27} and ν_{26} bands, by high-resolution infrared spectroscopy, and a successful perturbation analysis of the tetrad, in addition to the results of this study, can potentially provide highly accurate absolute vibrational energies of the lowest six excited vibrational levels of 1-cyanocyclobutene.

■ CONCLUSION

The ground-state spectroscopic constants of 1-cyanocyclobutene (**5**) from this work should provide an excellent foundation for predicting frequencies for an astronomical search, even for transitions well outside the range explored here. In the lower microwave region and for the lower J transitions most often used in radioastronomy, these predictions would require inclusion of the effects of nuclear hyperfine structure. The needed quadrupole coupling constants can be well estimated computationally, or they could be much better determined by measuring and analyzing a few resolved hyperfine multiplets for low-J transitions occurring in the lower microwave region. Unlike several other C_5H_5N isomers,[8] the ground-state of 1-cyanocyclobutene (**5**) is well fit by a single-state Hamiltonian model, so the present centrifugal distortion analysis should provide accurate frequency estimates well above the current range. The accuracy is of course expected to degrade gradually as one encounters quantum number values further removed from those sampled in this study.

The experimentally well-determined higher-order Coriolis coupling parameters for interacting fundamental states in 1-cyanocyclobutene (**5**) contribute to a steadily growing list of organic molecules that have been analyzed in this level of detail. A similar statement can be made about the quartic centrifugal distortion constants for the two vibrationally excited states. Neither these higher-order Coriolis constants nor the changes between the ground-state and vibrationally excited-state centrifugal distortion constants, however, can be meaningfully estimated *via* any readily available computational software package. A practical computational approach to obtaining these constants thus remains a pressing challenge for theory. Not only would such computed values serve as a measure of quality for a least-squares fit, but they would also likely improve the initial predictions of excited-state rotational spectra and thereby facilitate the early stage of the fitting process. Incorporation of these computed values in the least-squares fit for all constants that could not be adequately determined should also improve the accuracy of those constants that can be varied and fit.

■ GENERAL EXPERIMENTAL METHODS

All commercial reagents were purchased from Sigma-Aldrich or Oakwood Chemical and used as received, unless otherwise noted. ^{1}H NMR spectra (400 or 500 MHz) and ^{13}C NMR spectra (100 or 125 MHz) were obtained in $CDCl_3$ on a Bruker 400 MHz AVANCE III or Bruker 500 MHz DCH AVANCE III spectrometer; chemical shifts (δ) are reported as ppm downfield from internal standard $SiMe_4$ or referenced to residual solvent signals. Mass spectra were acquired using electrospray ionization (ESI) or the atmospheric solids analysis probe (ASAP) on a Thermo Scientific Q-Exactive Plus mass spectrometer. GC/MS analysis was performed on a Shimadzu GCMS-2010S instrument. IR spectra were obtained on a Bruker TENSOR Fourier transform infrared instrument as neat samples using an attenuated total reflectance accessory (Bruker PLATINUM ATR).

Mixture of *trans*- and *cis*-1,2-Dicyanocyclobutane (13). ***Note:*** *Exposure of the reaction mixture to short-wavelength UV−C (254 nm) is critical and necessitates the use of a quartz reaction vessel or immersion probe.*

Photolyses were carried out in an immersion-type quartz photochemical reactor (Ace Glass # 7861-250) having an inner annular volume of 500 mL and equipped with a magnetic stirrer. Into the water-cooled quartz immersion probe was inserted a centrally positioned 450 W medium-pressure mercury arc lamp (Hanovia # 679A36, 122 mm arc length). The quartz lamp chamber was continuously purged with a slow, steady stream of dry N_2 to prevent ozone generation/damage during lamp operation. Molybdenum hexacarbonyl ($Mo(CO)_6$, 5.43 g, 20.6 mmol), triphenylphosphine (PPh_3, 5.42 g, 20.7 mmol), hydroquinone (350 mg, 3.2 mmol), acrylonitrile (195 mL, 160 g, 3 mol), and acetonitrile (143 mL) were added to the annular reactor compartment, and the mixture was stirred until most of the solids were dissolved. The reaction mixture was purged under a steady stream of dry N_2 for 5 min. The reactor vessel was then maintained under a nitrogen atmosphere. With the immersion probe coolant flowing, the lamp was ignited, and the temperature of the stirred reaction was maintained at 55−60 °C by the heat of the mercury lamp throughout the course of the photolysis. Any remaining undissolved reactants dissolved within minutes of igniting the lamp as the reaction temperature increased. The reaction progress was monitored *via* ^{1}H NMR over the 72 h photolysis. After the irradiation time had elapsed, the photolysis was halted, and the reaction vessel was cooled to room temperature. The amber-colored reactor contents were filtered through a coarse glass-fritted funnel and concentrated *in vacuo* to remove acetonitrile and acrylonitrile. The resulting deep-red oil was purified *via* short-path vacuum distillation to afford a mixture of 1,2-dicyanocyclobutane stereoisomers (**13**) as a viscous amber oil that solidified upon cooling to room temperature (14.6 g, 0.138 mol, 9%, bp = 110−125 °C at 2 Torr). ^{1}H NMR ($CDCl_3$, 500 MHz): δ (ppm) 3.42−3.60 (m, 2H), 2.42−2.62 (m, 4H). *trans* ^{13}C{^{1}H}-NMR ($CDCl_3$, 125 MHz): δ (ppm) 118.6, 26.6, 24.8. *cis* ^{13}C{^{1}H}-NMR ($CDCl_3$, 125 MHz): δ (ppm) 118.3, 26.7, 24.8. IR (neat): (cm^{-1}) 2969 (m), 2242 (s), 1444 (m), 1244 (w), 1205 (m), 751 (w), 492 (w). HRMS (ASAP-MS), m/z: $[M + H]^+$ Calcd for $C_6H_7N_2$: 107.0604. Found: 107.0604.

1-Cyanocyclobutene (5). A vertical quartz tube 50 cm long and 2.5 cm in diameter, with 20 cm of its length packed with

https://doi.org/10.1021/acs.jpca.2c00384
J. Phys. Chem. A 2022, 126, 1980−1993

Ascarite (Aldrich, 20−30 mesh), was heated in a 40 cm long cylindrical tube furnace to 200 °C for 2 h under a steady stream of dry N_2 to remove water or absorbed gases from the Ascarite bed. A stoppered pressure-equalizing dropping funnel containing 1,2-dicyanocyclobutane (**13**, 9.95 g, 94 mmol) was connected to the top of the quartz reactor tube and the bottom was connected to a vacuum manifold through a series of three dry ice/acetone cooled traps. The temperature of the tube furnace was set to 225 °C, and the system was evacuated to a pressure of 500 mTorr. The dropping funnel at the top of the reactor was lightly heated with a heat gun until the 1,2-dicyanocyclobutane was thoroughly melted and degassed. The 1,2-dicyanocyclobutane melt was added dropwise to the heated reaction tube. The rate of addition was sufficient to maintain an internal pressure below 2 Torr. The complete dropwise delivery of molten **13** to the heated reactor bed was achieved over a course of 2 h. A total of 1.56 g of hazy, colorless liquid was recovered from the traps after the addition of **13** was completed. The collected distillate was cooled to 0 °C on ice and allowed to separate. The clear organic supernatant layer was separated and dried over granular anhydrous Na_2SO_4 to yield 1-cyanocyclobutene (**5**) as a colorless oil (834 mg, 10.6 mmol, 11%). ^{1}H NMR ($CDCl_3$, 500 MHz): δ (ppm) 6.78 (t, J = 1.4 Hz, 1H), 2.84 (dd, J = 3.4 Hz, 2H), 2.63 (ddd, J = 3.4 Hz, 3.2 Hz, 1.4 Hz, 2H). ^{13}C{^{1}H}-NMR ($CDCl_3$, 125 MHz): δ (ppm) 153.0, 117.2, 113.9, 32.4, 30.3. IR (neat): (cm^{-1}) 2978 (w), 2937 (m), 2835 (w), 2218 (m), 1584 (w), 1425 (w), 1252 (m), 1213 (w), 1162 (w), 1073 (w), 936 (w), 910 (m), 867 (m), 757 (m), 684 (w), 584 (w), 516 (s). HRMS (ASAP-MS), m/z: $[M+H]^+$ Calcd for C_5H_6N: 80.0495. Found: 80.0494.

■ ASSOCIATED CONTENT

Supporting Information

The Supporting Information is available free of charge at https://pubs.acs.org/doi/10.1021/acs.jpca.2c00384.

Table of *b*-type transitions observed in ν_{17} paired with the corresponding *a*-type transitions; experimental IR, ^{1}H NMR, ^{13}C NMR, and mass spectra of all compounds (PDF)

Computational chemistry output files and least-squares fitting output files from SPFIT (ZIP)

■ AUTHOR INFORMATION

Corresponding Authors

R. Claude Woods − *Department of Chemistry, University of Wisconsin−Madison, Madison, Wisconsin 53706-1322, United States;* orcid.org/0000-0003-0865-4693; Email: rcwoods@wisc.edu

Robert J. McMahon − *Department of Chemistry, University of Wisconsin−Madison, Madison, Wisconsin 53706-1322, United States;* orcid.org/0000-0003-1377-5107; Email: robert.mcmahon@wisc.edu

Authors

Houston H. Smith − *Department of Chemistry, University of Wisconsin−Madison, Madison, Wisconsin 53706-1322, United States;* orcid.org/0000-0002-3762-1842

Samuel M. Kougias − *Department of Chemistry, University of Wisconsin−Madison, Madison, Wisconsin 53706-1322, United States;* orcid.org/0000-0002-9877-0817

Brian J. Esselman − *Department of Chemistry, University of Wisconsin−Madison, Madison, Wisconsin 53706-1322, United States;* orcid.org/0000-0002-9385-8078

Complete contact information is available at: https://pubs.acs.org/10.1021/acs.jpca.2c00384

Notes

The authors declare no competing financial interest.

■ ACKNOWLEDGMENTS

We gratefully acknowledge the National Science Foundation for support of this project (CHE-1954270). We thank Michael McCarthy for the loan of an amplification-multiplication chain and Aatmik R. Patel for stimulating discussions regarding the synthesis of 1-cyanocyclobutene precursors and the assessment of synthetic routes. We thank the following organizations and individuals for support of shared departmental facilities: Bruker AVANCE 400 NMR spectrometer (NSF CHE-1048642), Bruker AVANCE 500 NMR spectrometer (gift from Paul J. and Margaret M. Bender), and Thermo Scientific Q Exactive Plus mass spectrometer (NIH 1S10 OD020022-1).

■ REFERENCES

(1) Müller, H. S. P.; Schlöder, F.; Stutzki, J.; Winnewisser, G. The Cologne Database for Molecular Spectroscopy, CDMS: a Useful Tool for Astronomers and Spectroscopists. *J. Mol. Struct.* **2005**, *742*, 215−227.

(2) Müller, H. S. P.; Thorwirth, S.; Roth, D. A.; Winnewisser, G. The Cologne Database for Molecular Spectroscopy, CDMS. *Astron. Astrophys.* **2001**, *370*, L49−L52.

(3) Zdanovskaia, M. A.; Esselman, B. J.; Lau, H. S.; Bates, D. M.; Woods, R. C.; McMahon, R. J.; Kisiel, Z. The 103 - 360 GHz Rotational Spectrum of Benzonitrile, the First Interstellar Benzene Derivative Detected by Radioastronomy. *J. Mol. Spectrosc.* **2018**, *351*, 39−48.

(4) Zdanovskaia, M. A.; Esselman, B. J.; Woods, R. C.; McMahon, R. J. The 130 - 370 GHz Rotational Spectrum of Phenyl Isocyanide (C_6H_5NC). *J. Chem. Phys.* **2019**, *151*, 024301.

(5) Dorman, P. M.; Esselman, B. J.; Park, J. E.; Woods, R. C.; McMahon, R. J. Millimeter-Wave Spectrum of 4-Cyanopyridine in its Ground State and Lowest-Energy Vibrationally Excited States, ν_{20} and ν_{30}. *J. Mol. Spectrosc.* **2020**, *369*, 111274.

(6) Dorman, P. M.; Esselman, B. J.; Woods, R. C.; McMahon, R. J. An Analysis of the Rotational Ground State and Lowest-energy Vibrationally Excited Dyad of 3-Cyanopyridine: Low Symmetry Reveals Rich Complexity of Perturbations, Couplings, and Interstate Transitions. *J. Mol. Spectrosc.* **2020**, *373*, 111373.

(7) Kougias, S. M.; Knezz, S. N.; Owen, A. N.; Sanchez, R. A.; Hyland, G. E.; Lee, D. J.; Patel, A. R.; Esselman, B. J.; Woods, R. C.; McMahon, R. J. Synthesis and Characterization of Cyanobutadiene Isomers—Molecules of Astrochemical Significance. *J. Org. Chem.* **2020**, *85*, 5787−5798.

(8) Zdanovskaia, M. A.; Dorman, P. M.; Orr, V. L.; Owen, A. N.; Kougias, S. M.; Esselman, B. J.; Woods, R. C.; McMahon, R. J. Rotational Spectra of Three Cyanobutadiene Isomers (C_5H_5N) of Relevance to Astrochemistry and Other Harsh Reaction Environments. *J. Am. Chem. Soc.* **2021**, *143*, 9551−9564.

(9) Zdanovskaia, M. A.; Esselman, B. J.; Kougias, S. M.; Patel, A. R.; Woods, R. C.; McMahon, R. J. The 130−360 GHz rotational spectrum of *syn*-2-cyano-1,3-butadiene (C_5H_5N) - a molecule of astrochemical relevance. *Mol. Phys.* **2021**, *119*, No. e1964629.

(10) Esselman, B. J.; Kougias, S. M.; Zdanovskaia, M. A.; Woods, R. C.; McMahon, R. J. Synthesis, Purification, and Rotational Spectroscopy of (Cyanomethylene)Cyclopropane—An Isomer of Pyridine. *J. Phys. Chem. A* **2021**, *125*, 5601−5614.

(11) Charnley, S. B.; Kuan, Y.-J.; Huang, H.-C.; Botta, O.; Butner, H. M.; Cox, N.; Despois, D.; Ehrenfreund, P.; Kisiel, Z.; Lee, Y.-Y.; et al.

Astronomical Searches for Nitrogen Heterocycles. *Adv. Space Res.* **2005**, *36*, 137−145.
(12) McGuire, B. A.; Burkhardt, A. M.; Kalenskii, S. V.; Shingledecker, C. N.; Remijan, A. J.; Herbst, E.; McCarthy, M. C. Detection of the Aromatic Molecule Benzonitrile (*c*-C_6H_5CN) in the Interstellar Medium. *Science* **2018**, *359*, 202−205.
(13) McGuire, B. A.; Loomis, R. A.; Burkhardt, A. M.; Lee, K. L. K.; Shingledecker, C. N.; Charnley, S. B.; Cooke, I. R.; Cordiner, M. A.; Herbst, E.; Kalenskii, S.; et al. Detection of Two Interstellar Polycyclic Aromatic Hydrocarbons via Spectral Matched Filtering. *Science* **2021**, *371*, 1265−1269.
(14) McCarthy, M. C.; Lee, K. L. K.; Loomis, R. A.; Burkhardt, A. M.; Shingledecker, C. N.; Charnley, S. B.; Cordiner, M. A.; Herbst, E.; Kalenskii, S.; Willis, E. R.; et al. Interstellar Detection of the Highly Polar Five-Membered Ring Cyanocyclopentadiene. *Nat. Astron.* **2021**, *5*, 176−180.
(15) Morales, S. B.; Bennett, C. J.; Le Picard, S. D.; Canosa, A.; Sims, I. R.; Sun, B. J.; Chen, P. H.; Chang, A. H. H.; Kislov, V. V.; Mebel, A. M.; et al. A Crossed Molecular Beam, Low-Temperature Kinetics, and Theoretical Investigation of the Reaction of the Cyano Radical (CN) with 1,3-Butadiene (C_4H_6). A Route to Complex Nitrogen-Bearing Molecules in Low-Temperature Extraterrestrial Environments. *Astrophys. J.* **2011**, *742*, 26.
(16) Sun, B. J.; Huang, C. H.; Chen, S. Y.; Chen, S. H.; Kaiser, R. I.; Chang, A. H. H. Theoretical Study on Reaction Mechanism of Ground-State Cyano Radical with 1,3-Butadiene: Prospect of Pyridine Formation. *J. Phys. Chem. A* **2014**, *118*, 7715−7724.
(17) Jamal, A.; Mebel, A. M. Theoretical Investigation of the Mechanism and Product Branching Ratios of the Reactions of Cyano Radical with 1- and 2-Butyne and 1,2-Butadiene. *J. Phys. Chem. A* **2013**, *117*, 741−755.
(18) Mishra, P.; Fritz, S. M.; Herbers, S.; Mebel, A. M.; Zwier, T. S. Gas-phase Pyrolysis of *Trans* 3-Pentenenitrile: Competition Between Direct and Isomerization-Mediated Dissociation. *Phys. Chem. Chem. Phys.* **2021**, *23*, 6462−6471.
(19) McCarthy, M. C.; Lee, K. L. K.; Carroll, P. B.; Porterfield, J. P.; Changala, P. B.; Thorpe, J. H.; Stanton, J. F. Exhaustive Product Analysis of Three Benzene Discharges by Microwave Spectroscopy. *J. Phys. Chem. A* **2020**, *124*, 5170−5181.
(20) Guillemin, J. C.; Ferris, J. P. Photochemistry of Unsaturated Nitriles on Titan. *Symposium on Titan*; ESA, 1992; pp 177−181.
(21) Gale, D. M. 1-Cyanobicyclo[1.1.0]butane and 1-cyanocyclobutene by photolysis of 2-cyano-1,3-butadiene. Patent number 3459647, 1969.
(22) Gale, D. M.; Cherkofsky, S. C. Dehydrocyanation of Dinitriles. Preparation of 1-Cyclobutenecarbonitrile by Direct Dehydrocyanation of 1,2-Cyclobutanedicarbonitrile. *J. Org. Chem.* **1973**, *38*, 475−478.
(23) Sarner, S. F.; Gale, D. M.; Hall, H. K.; Richmond, A. B. Gas-phase Thermolysis Kinetics of Small Ring Nitriles. *J. Phys. Chem.* **1972**, *76*, 2817−2819.
(24) Kwak, N.; Simmons, J. W.; Goldstein, J. H. Microwave Spectrum of Propiolactone. *J. Chem. Phys.* **1955**, *23*, 2450−2450.
(25) Boone, D. W.; Britt, C. O.; Boggs, J. E. Microwave Spectrum, Dipole Moment, and Ring-Puckering Vibration of β-Propiolactone. *J. Chem. Phys.* **1965**, *43*, 1190−1194.
(26) Chen, Z.; van Wijngaarden, J. A Combined *ab Initio*, Fourier Transform Microwave and Fourier Transform Infrared Spectroscopic Investigation of β-Propiolactone: The ν_8 and ν_{12} bands. *J. Mol. Spectrosc.* **2009**, *257*, 164−169.
(27) Orr, V. L.; Esselman, B. J.; Dorman, P. M.; Amberger, B. K.; Guzei, I. A.; Woods, R. C.; McMahon, R. J. Millimeter-wave Spectroscopy, X-ray Crystal Structure, and Quantum Chemical Studies of Diketene - Resolving Ambiguities Concerning the Structure of the Ketene Dimer. *J. Phys. Chem. A* **2016**, *120*, 7753−7763.
(28) Durig, J. R.; Carreira, L. A.; Lafferty, W. J. Spectra and Structure of Small Ring Compounds. Microwave Spectrum of Cyanocyclobutane. *J. Mol. Spectrosc.* **1973**, *46*, 187−193.
(29) Fong, M. Y.; Harmony, M. D. Microwave Spectrum, Dipole Moment, Quadrupole Coupling Constants, and Conformation of Cyanocyclobutane. *J. Chem. Phys.* **1973**, *58*, 4260−4264.
(30) Caminati, W.; Velino, B.; Della Valle, R. G. Rotational Spectra of Several Vibrational Excited States of Axial and Equatorial Cyanocyclobutane and Potential Energy Function of the Ring Puckering. *J. Mol. Spectrosc.* **1988**, *129*, 284−292.
(31) Durig, J. R.; Ganguly, A.; Klaassen, J. J.; Guirgis, G. A. The r_0 Structural Parameters, Conformational Stability, and Vibrational Assignment of Equatorial and Axial Cyanocyclobutane. *J. Mol. Struct.* **2009**, *923*, 28−38.
(32) Caminati, W.; Velino, B.; Dakkouri, M.; Schäfer, L.; Siam, K.; Ewbank, J. D. Reinvestigation of the Microwave Spectrum of Cyanocyclobutane: Assignment of the Axial Conformer. *J. Mol. Spectrosc.* **1987**, *123*, 469−475.
(33) Menke, J. L.; McMahon, R. J. Photochemistry of matrix-isolated 5-cyano-2H-pyran-2-one (δ-cyano-α-pyrone) and cyanocyclobuta-1,3-diene. *Can. J. Chem.* **2011**, *89*, 186−194.
(34) Miki, S.; Matsumura, S.-i.; Ohno, T.; Yoshida, Z.-i. Co(II)-porphyrin Catalyzed Isomerization of Bicyclobutanecarbonitrile. *Tetrahedron Lett.* **1986**, *27*, 3669−3672.
(35) Gale, D. M., Mono- and Dichlorocyclobutanecarbonitriles by Cycloaddition of Vinyl Chloride and an Acrylonitrile. Patent number 3642859, 1972.
(36) Tietz, R. F.; Kenyon, W. G. 1-Cyanocyclobutene Monomer and Polymer and Their Preparation. Patent number 3468861, Sep 23, 1969.
(37) Ferris, J. P.; Guillemin, J. C. Photochemical Cycloaddition Reactions of Cyanoacetylene and Dicyanoacetylene. *J. Org. Chem.* **1990**, *55*, 5601−5606.
(38) Hughes, W. B. Photodimerization of Acrylonitrile. Patent number 3623966, Nov 30, 1971.
(39) Miyashita, A.; Ikezu, S.; Nohira, H. Stereospecific Photodimerization of Unsaturated Compounds Induced by Nickel Complexes. *Chem. Lett.* **1985**, *14*, 1235−1238.
(40) Hosaka, S.; Wakamatsu, S. Photodimerization of Acrylonitrile. *Tetrahedron Lett.* **1968**, *9*, 219−220.
(41) Esselman, B. J.; Amberger, B. K.; Shutter, J. D.; Daane, M. A.; Stanton, J. F.; Woods, R. C.; McMahon, R. J. Rotational Spectroscopy of Pyridazine and its Isotopologs from 235−360 GHz: Equilibrium Structure and Vibrational Satellites. *J. Chem. Phys.* **2013**, *139*, 224304.
(42) Kisiel, Z.; Pszczółkowski, L.; Drouin, B. J.; Brauer, C. S.; Yu, S.; Pearson, J. C.; Medvedev, I. R.; Fortman, S.; Neese, C. Broadband Rotational Spectroscopy of Acrylonitrile: Vibrational Energies from Perturbations. *J. Mol. Spectrosc.* **2012**, *280*, 134−144.
(43) Kisiel, Z.; Pszczółkowski, L.; Medvedev, I. R.; Winnewisser, M.; De Lucia, F. C.; Herbst, E. Rotational Spectrum of *Trans-Trans* Diethyl Ether in the Ground and Three Excited Vibrational States. *J. Mol. Spectrosc.* **2005**, *233*, 231−243.
(44) Pickett, H. M. The Fitting and Prediction of Vibration-rotation Spectra with Spin Interactions. *J. Mol. Spectrosc.* **1991**, *148*, 371−377.
(45) Kisiel, Z., PROSPE - Programs for ROtational SPEctroscopy; http://info.ifpan.edu.pl/~kisiel/prospe.htm (accessed April 3, 2021).
(46) Kisiel, Z. Assignment and Analysis of Complex Rotational Spectra. In *Spectroscopy from Space*, 1st ed.; Demaison, J., Sarka, K., Cohen, E. A., Eds.; Springer Netherlands: Dordrecht, 2001; pp 91−106.
(47) Frisch, M. J.; Trucks, G. W.; Schlegel, H. B.; Scuseria, G. E.; Robb, M. A.; Cheeseman, J. R.; Scalmani, G.; Barone, V.; Petersson, G. A.; Nakatsuji, H.; et al. *Gaussian 16*, rev C.01; Gaussian, Inc.: Wallingford, CT, USA, 2016.
(48) Schmidt, J. R.; Polik, W. F. *WebMO Enterprise, version 20.0*; WebMO LLC: Madison, WI, USA, 2020; http://www.webmo.net (accessed April 2021).
(49) Kisiel, Z.; Kraśnicki, A. The Millimetre-Wave Rotational Spectrum of Phenylacetylene. *J. Mol. Spectrosc.* **2010**, *262*, 82−88.
(50) Zdanovskaia, M. A.; Martin-Drumel, M.-A.; Kisiel, Z.; Pirali, O.; Esselman, B. J.; Woods, R. C.; McMahon, R. J. The eight lowest-energy vibrational states of benzonitrile: analysis of Coriolis and Darling-

https://doi.org/10.1021/acs.jpca.2c00384
J. Phys. Chem. A 2022, 126, 1980−1993

Dennison couplings by millimeter-wave and far-infrared spectroscopy.
J. Mol. Spectrosc. **2022**, *383*, 111568.

https://doi.org/10.1021/acs.jpca.2c00384
J. Phys. Chem. A 2022, 126, 1980−1993

Appendix G

Rotational Spectrum of *anti-* and *gauche*-4-Cyano-1-Butyne (C_5H_5N) – An Open-Chain Isomer of Pyridine

P. Matisha Dorman
Brian J. Esselman
P. Bryan Changala
Samuel M. Kougias
Michael C. McCarthy
R. Claude Woods
Robert J. McMahon

Journal of Molecular Spectroscopy, 2022, *385*, 111604

Journal of Molecular Spectroscopy 385 (2022) 111604

Contents lists available at ScienceDirect

Journal of Molecular Spectroscopy

journal homepage: www.elsevier.com/locate/yjmsp

Rotational spectrum of *anti*- and *gauche*-4-cyano-1-butyne (C_5H_5N) – An open-chain isomer of pyridine

P. Matisha Dorman [a], Brian J. Esselman [a], P. Bryan Changala [b], Samuel M. Kougias [a], Michael C. McCarthy [b,*], R. Claude Woods [a,*], Robert J. McMahon [a,*]

[a] Department of Chemistry, University of Wisconsin-Madison, 1101 University Avenue, Madison, WI 53706-1322, United States
[b] Center for Astrophysics, Harvard & Smithsonian, 60 Garden Street, Cambridge, MA 02138-1516, United States

ARTICLE INFO

Keywords:
Rotational spectroscopy
Microwave
Millimeter-wave
Astrochemistry
Centrifugal distorted rotor
Quadrupole coupling

ABSTRACT

The analysis of the rotational spectrum of 4-cyano-1-butyne, an open-chain isomer of pyridine, is presented herein for the first time. Transitions for the ground vibrational states of both conformational isomers, *anti* and *gauche*, were observed in the 8–38 GHz and 130–360 GHz frequency ranges and fit to effective sextic distorted-rotor Hamiltonians with low uncertainty (σ_{fit} < 50 kHz), allowing for their potential detection by radio-astronomy or in harsh reaction environments. The microwave region includes hyperfine-split transitions for both conformers, allowing for the experimental determination of the χ_{aa}, χ_{bb}, and χ_{cc} quadrupole coupling constants. In the millimeter-wave region, not every observable ground-state transition could be satisfactorily addressed by a single-state Hamiltonian due to Coriolis coupling with the low-energy vibrationally excited states. Thus, effective single-state fits of the ground states were obtained by including only K_a-series transitions without obviously perturbed energy levels. Importantly, the effective fit does include the most intense transitions throughout the observed frequency ranges. The predicted values (MP2/cc-pVTZ) are in close agreement with the experimental spectroscopic constants. These data provide a sufficient foundation for the identification of *anti*- and *gauche*-4-cyano-1-butyne in the interstellar medium by radioastronomy. The *gauche* conformer is estimated to lie 1.00 (5) kcal/mol higher in energy than the *anti* conformer, as determined using experimental transition intensities.

1. Introduction

Organic nitriles and isonitriles are well represented in the catalogue of >250 species detected in the interstellar medium (ISM) [1,2]. Because of the CN moiety, these groups typically have sizeable molecular dipole moments, resulting in intense rotational transitions detectable *via* radioastronomy. Recently, the first examples of five- and six-membered ring systems, ubiquitous in organic chemistry, were discovered in the ISM as their nitrile-substituted derivatives: benzonitrile [3], 1- and 2-cyanonaphthalene [4], and 1- and 2-cyano-1,3-cyclopentadiene [5,6]. These detections represent a dramatic advance in our understanding of interstellar organic chemistry, yet it remains unclear if these ring systems are formed through decomposition of larger polycyclic species or are generated from smaller precursors.

Computational and experimental studies of complex chemical reactions in the ISM are ongoing, and open-chain nitriles are emerging as attractive candidates for a possible mechanistic connection to aromatic species [7–9]. Combined with their prominent dipole moments (usually between 2 and 4 D), many nitriles possess observable hyperfine resolved transitions at low frequency that can also assist in their identification in the ISM. Open-chain nitriles of various chain lengths and levels of saturation have been detected in different regions of the ISM [10–21]. In a recent study, several open-chain nitriles and a few nitrile-substituted five- and six-membered rings were generated and detected in a benzene/nitrogen discharge [22]. Using spectral catalogues for known molecules, a complex mixture of many isomers with the same elemental formula were identified and assigned using microwave spectroscopy.

Organic nitriles and isonitriles have been of interest to our groups for some time due to their relevance to astrochemistry [3–5,23–27]. The Wisconsin group recently provided millimeter-wave rotational spectra of several pyridine (C_5H_5N) isomers (**1**–**6**) (Fig. 1) [28–32]. Unlike pyridine (**7**, a near-oblate, asymmetric top), these isomers are highly prolate asymmetric tops with intense rotational transitions. A defining characteristic in the rotational spectra of these C_5H_5N isomers is

* Corresponding authors.
E-mail addresses: mmccarthy@cfa.harvard.edu (M.C. McCarthy), rcwoods@wisc.edu (R.C. Woods), robert.mcmahon@wisc.edu (R.J. McMahon).

https://doi.org/10.1016/j.jms.2022.111604
Received 25 January 2022; Received in revised form 5 March 2022; Accepted 7 March 2022
Available online 18 March 2022
0022-2852/© 2022 Elsevier Inc. All rights reserved.

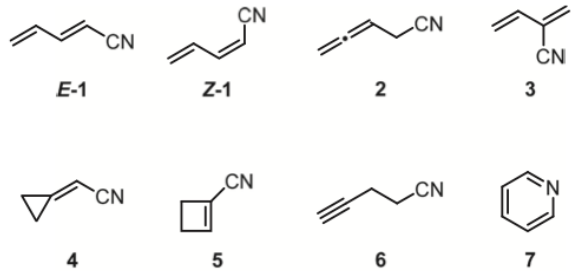


Fig. 1. C_5H_5N isomers that have been studied by rotational spectroscopy: (*E*)-1-cyano-1,3-butadiene (***E*-1**), (*Z*)-1-cyano-1,3-butadiene (***Z*-1**), 4-cyano-1,2-butadiene (**2**), 2-cyano-1,3-butadiene (**3**), (cyanomethylene)cyclopropane (**4**), 1-cyanocyclobutene (**5**), 4-cyano-1-butyne (**6**), and pyridine (**7**).

whether the vibrational ground state is 'isolated' in the frequency region of interest, which determines whether the system can be adequately fit to a single-state Hamiltonian model. Observable coupling between the ground and first fundamental states in the 130–360 GHz frequency range becomes increasingly likely when there is a vibrationally excited state that is close in energy and/or when a highly prolate species has a particularly large value of A_0 and low value of C_0. This creates a situation in which the 130–360 GHz rotational spectrum contains many transitions with very high J and K_a energy levels, allowing the ground-state energy levels to approach the vibrationally excited-state energy levels. The ground vibrational states of *s-trans-Z*-1-cyano-1,3-butadiene (***Z*-1**) [28], *syn*-2-cyano-1,3-butadiene (**3**) [31], (cyanomethylene) cyclopropane (**4**) [29], and 1-cyanocyclobutene (**5**) [32], are isolated and can be fit to a single-state, distorted-rotor Hamiltonian in the 130–360 GHz region with a low σ_{fit} value. In contrast, the ground-state rotational transitions of *s-trans-E*-1-cyano-1,3-butadiene (***E*-1**) and both conformers of 4-cyano-1,2-butadiene (**2**) [28] are not well fit by a single-state distorted rotor Hamiltonian. In the latter cases, the spectra were modeled with an effective Hamiltonian fit – a minimally perturbed, single-state, least-squares fit with exclusion of any transition frequencies that cannot be fit to a low-error distorted-rotor Hamiltonian (<50 kHz).

The open-chain isomer of pyridine presented herein, 4-cyano-1-butyne (4-pentynenitrile, **6**), has not been observed previously by rotational spectroscopy. This species is a hydrogenated version of the known interstellar molecules C_5N and HC_5N and is an ethynyl-substituted derivative of the known interstellar molecule CH_3CH_2CN. Its rotational constants were previously predicted, along with a collection of cyanodiacetylene-derived nitriles, to facilitate astronomical detection [33]. The rotational spectrum of the corresponding isonitrile (4-isocyano-1-butyne) was studied previously from 12 to 70 GHz [34], resulting in spectroscopic constants for its *anti* and *gauche* forms. The current rotational analysis of 4-cyano-1-butyne provides the first measurement, assignment, and least-squares fitting of this astrochemically intriguing species, facilitating an astronomical search and comparison to its isonitrile counterpart.

2. Computational methods

Initial electronic structure calculations of *anti*- and *gauche*-4-cyano-1-butyne were performed using Gaussian 16 [35] through the WebMO interface [36] at the B3LYP/6-311+G(2d,p) level of theory. Optimized geometries were obtained using "verytight" convergence criteria and an "ultrafine" integration grid for both energy-minimized conformers. Anharmonic vibrational frequency calculations were initially carried out using B3LYP. Although these spectroscopic constants were sufficiently accurate to begin analysis of the millimeter-wave spectrum of the *anti* conformer, they were not sufficiently accurate to begin assignment of the *gauche* conformer. (The millimeter-wave spectrum was assigned before the microwave spectrum became available). Thus, anharmonic vibrational frequency calculations were performed at the MP2/cc-pVTZ level, which provided spectroscopic constants that exhibit better agreement with the experimental constants of both conformers. A coordinate scan for the conformational analysis of the *gauche* and *anti* conformers was completed at the MP2/6-311+G(2d,p) level. A comparison of the spectroscopic constants across the B3LYP and MP2 calculations is provided in the Supplementary Material along with all other computational output files.

3. Experimental methods

A sample of 4-cyano-1-butyne was purchased commercially (Sigma-Aldrich, 97% purity), analyzed *via* ^{1}H NMR, $^{13}C\{^1H\}$-NMR, and ATR-IR spectroscopy (spectra available in Supplementary Material), and found to be sufficiently pure to be used without further refinement. A sample of 4-cyano-1-butyne at room temperature and a pressure of 6 mTorr was used to collect the 130–230 GHz and 235–360 GHz broadband spectra at the University of Wisconsin on a spectrometer described previously [24,37]. The 8–38 GHz region was collected using the same 4-cyano-1-butyne sample on a Fourier-transform microwave spectrometer at Harvard [38]. A sample of the nitrile diluted to a concentration of 0.05% in neon was supersonically expanded along the axis of a cavity-enhanced Fourier transform microwave spectrometer through a pulsed pinhole nozzle backed at 2.5 kTorr with a pulse length of 400 μs at a 6-Hz repetition rate. The spectrometer operates from 5 to 40 GHz with a line-center measurement accuracy of about 2 kHz. The large dipole moment of 4-cyano-1-butyne yielded a peak signal-to-noise ratio of the strongest transitions of about 10^2 for a 1-s integration time. The 8–38, 130–230, and 235–360 GHz segments were combined into a single broadband spectrum using Assignment and Analysis of Broadband Spectra (AABS) software [39,40]. Picket's SPFIT/SPCAT was used to conduct least-squares fitting and spectral prediction, while PIFORM, PLANM, and AC programs were used for analysis [41]. A uniform frequency measurement uncertainty of 2 kHz is assumed for all microwave measurements and 50 kHz for all millimeter-wave measurements.

4. Results

4.1. 4-Cyano-1-butyne (6)

anti-4-Cyano-1-butyne (Fig. 2a) is a highly prolate ($\kappa = -0.995$), asymmetric top (C_s) with dipole moment components predicted along the *a*- and *b*-principal axes ($\mu_a = 3.2$ D, $\mu_b = 0.84$ D; MP2/cc-pVTZ) giving rise to observable *a*- and weak *b*-type transitions. *gauche*-4-Cyano-1-butyne (Fig. 2b) is a prolate ($\kappa = -0.751$), asymmetric top (C_1) with dipole moment components predicted along each principal axis ($\mu_a = 2.0$ D, $\mu_b = 3.2$ D, $\mu_c = 0.68$ D; MP2/cc-pVTZ) creating potentially observable *a*-, *b*-, and weak *c*-type transitions. With no experimental spectroscopic constants available, the rotational constants (A_0, B_0, and C_0) of both conformers, along with their quartic and sextic centrifugal distortion constants, were calculated to facilitate initial transition assignments.

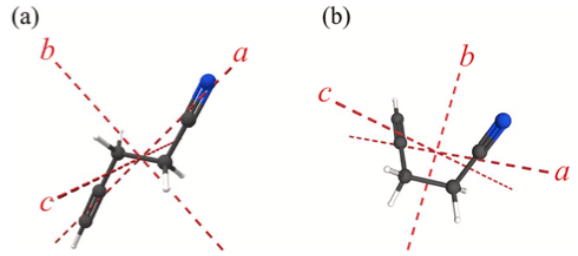


Fig. 2. 4-Cyano-1-butyne structures with principal inertial axes: (a) *anti* ($\mu_a = 3.2$ D, $\mu_b = 0.84$ D) and (b) *gauche* ($\mu_a = 2.0$ D, $\mu_b = 3.2$ D, $\mu_c = 0.68$ D).

The two energy-minimized conformations (*anti* and *gauche*) of 4-cyano-1-butyne are depicted on the conformational potential energy surface (MP2/6-311+G(2d,p)) in Fig. 3. The *gauche* conformer is predicted to be *ca.* 0.42 kcal/mol (147 cm^{-1}) higher in energy than the *anti* conformer (zero-point vibrational energy not included). This small energy difference is near the uncertainty of the level of theory employed. The rotational transition intensities of the *gauche* conformer benefit from statistical doubling due to its two enantiomeric forms. The barrier to rotation between the *gauche* and *anti* conformers (>3 kcal/mol) is sufficiently high that the transitions for each state are not expected to display observable tunneling splittings, which would increase spectral complexity and complicate the analysis. The vibrational spectra of 4-cyano-1-butyne (**6**) were observed by IR and Raman spectroscopy from 50 − 4000 cm^{-1} in the vapor, liquid, and solid states [42]. Klaeboe *et al.* note the appearance of two distinct crystalline solids at low temperature (90 K): one comprising purely the *gauche* conformers and the other purely the *anti* conformer.

4.2. Spectral analysis

Both conformations of 4-cyano-1-butyne were observed in the 8–360 GHz range with strong *a*-type R-branch bands from the *anti* conformation dominating the spectrum. The rotational spectrum of *anti*-4-cyano-1-butyne is composed of mainly $^{a}R_{0,1}$ transitions that demonstrate the typical band structure of a highly prolate, asymmetric top, in that clusters of transitions share a single *J* value. Fig. 4 shows the rotational spectrum in the 188.0–192.5 GHz range, where two such bands for the ground vibrational state of the *anti* conformer (all solid lines) can be distinguished. The $K_a = 0$ transition of the $J'' + 1 = 66$ band (magenta solid line) appears ~ 3 GHz lower in frequency within transitions of the $J'' + 1 = 65$ band. The $K_a = 1^+/1^-$ transitions are separated by 2.8 GHz, with the 1^- transition at lower frequency than $K_a = 0$ and the 1^+ transition at higher frequency. As the K_a value increases, the transitions progress to higher frequency until the first turnaround between $K_a = 2^+$ and 3^+. In this spectral window, the plus- and minus-symmetry series become degenerate at $K_a = 6$ (same values of *J* and K_a, but with values of K_c differing by one). Another turnaround is visible at $K_a = 8$, after which transitions progress to higher frequency until their transition intensities become too weak to measure. Throughout the entire frequency region, intense *b*-type R-branch transitions were observed, but only a few K_a series were of sufficient intensity to be included in the data set. No *a*-type Q- or P-branches were observed in either frequency regime, although a few sufficiently intense *b*-type, Q- and P-branch transitions were observed in the microwave region and included in the least squares fit.

The rotational spectrum of *gauche*-4-cyano-1-butyne exhibits a more typical prolate structure, wherein bands comprise transitions increasing in K_a with decreasing *J*. The bandheads are composed of quadruply degenerate *a*- and *b*-type R-branch transitions (two $^{a}R_{0,1}$ transitions, $^{b}R_{1,1}$, and $^{b}R_{-1,1}$) that share the same value of K_c. In the 188.0–192.5 GHz frequency region, transitions proceed to lower frequency as K_a increases and become non-degenerate at $K_a = 5$. The transitions progress to lower frequency and complete a turnaround many hundreds of MHz below the 188.0–192.5 GHz region. Eventually, two *a*-type transitions with the same value of K_a become a degenerate pair, while two *b*-type transitions form another set of quadruply degenerate R-branch transitions, this time with *c*-type transitions (two $^{c}R_{1,0}$ transitions, $^{b}R_{1,1}$, and $^{b}R_{1,-1}$). No *a*- or *b*-type P-branch transitions were observed for this conformer, although several series of *b*-type Q-branches were observed in the microwave region and included in the data set. No *a*-type Q branches were observed in either frequency regime.

4.3. anti-4-cyano-1-butyne ground state

The ground state of *anti*-4-cyano-1-butyne was least-squares fit to a sextic, distorted-rotor Hamiltonian with low error ($\sigma_{fit} < 50$ kHz). The experimental and predicted spectroscopic constants are reported in both

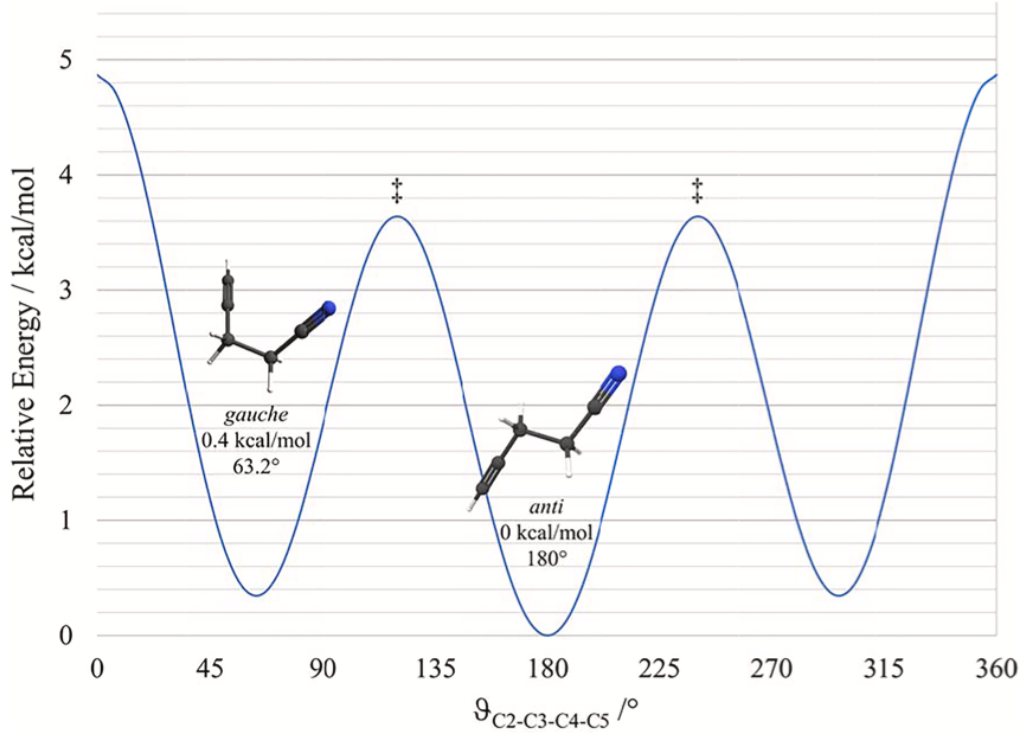


Fig. 3. Computed conformational potential energy surface of 4-cyano-1-butyne (MP2/6-311+G(2d,p)).

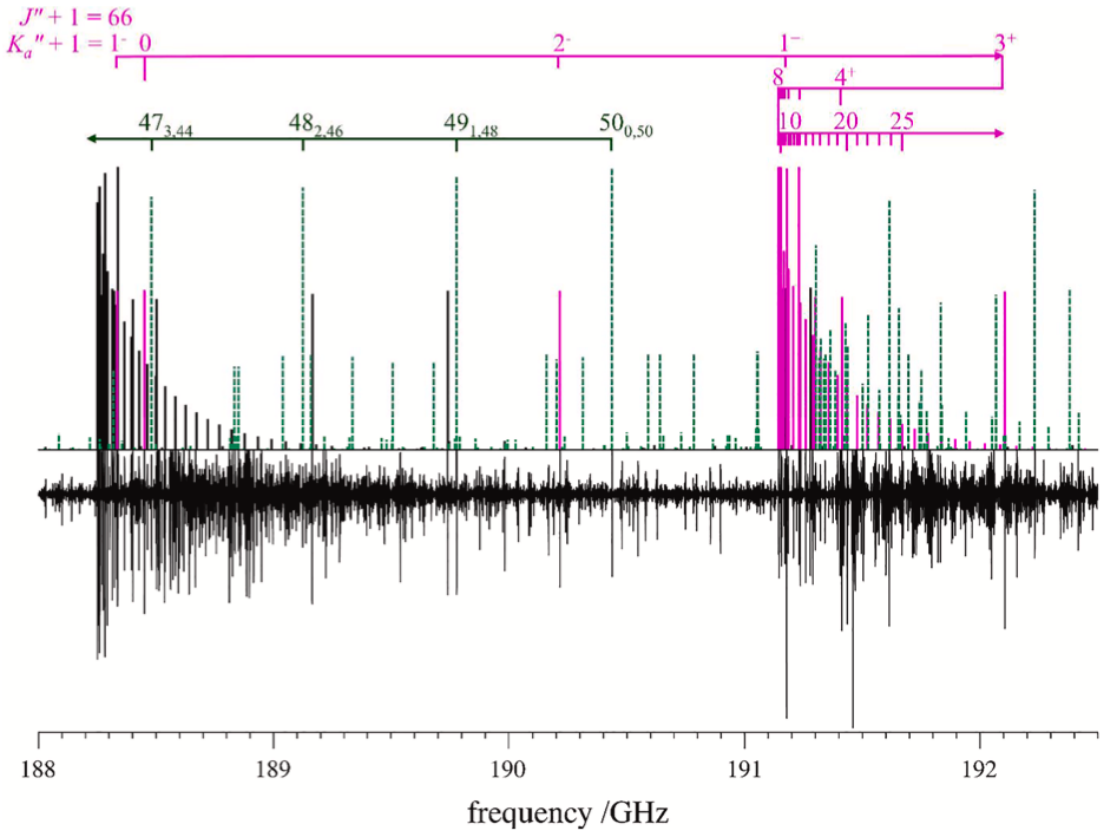


Fig. 4. Rotational spectrum of 4-cyano-1-butyne from 188.0 GHz to 192.5 GHz (bottom) and stick spectrum of the ground vibrational states (top). Dashed green lines mark transitions of *gauche*-4-cyano-1-butyne, and solid-colored lines mark transitions of *anti*-4-cyano-1-butyne. Solid lines highlighted in magenta belong to the $J'' + 1 = 66$ series of *anti*-4-cyano-1-butyne, and the corresponding $K_a'' + 1$ values are marked above. Many transitions belonging to other vibrational satellites are also visible in the experimental spectrum.

the S and A reductions, I^r representation in Table 1, and the output files for the least-squares fit are included in the Supplementary Material. In the microwave region, transitions are resolved into hyperfine multiplets that are well-predicted by the distorted-rotor model. In the millimeter-wave region, low-K_a series also demonstrate distorted-rotor behavior, but the experimental frequencies begin to subtlely deviate from those predicted at $K_a = 21$, even at the lowest J values. With increasing J, the transitions continue to further deviate from predicted frequencies until reaching a maximum deviation at $J'' + 1 = 104$. As the value of J continues to increase, transitions slowly migrate back toward their predicted distorted-rotor frequencies. A single-state, distorted-rotor model including transitions from $K_a = 0$–20 can be fit to low error ($\sigma_{fit} = 0.027$ MHz), while fits that incorporate observable transitions with $K_a > 20$ dramatically increase the error (σ_{fit}). This issue cannot be treated by inclusion of higher-order centrifugal distortion terms, making it evident that the ground state of *anti*-4-cyano-1-butyne is not amenable to a single-state, distorted-rotor Hamiltonian. It is apparent that the ground state is coupled to the lowest vibrationally excited state. Diminishing signal intensity and spectral congestion with higher-energy vibrational states make the extent to which transitions in the $K_a > 20$ series experience perturbation unclear. To obtain an effective fit for the *anti* conformer, all $K_a > 20$ transitions were excluded from the data set to allow the least-squares fit to produce minimally perturbed spectroscopic constants. Over 2,100 independent transitions were measured, including R-branch transitions with J'' values ranging from 0 to 126. The range of quantum number values for the newly measured ground-state transitions of *anti*-4-cyano-1-butyne is provided in the Fig. 5 data distribution plots.

The spectroscopic constants for the ground state of *anti*-4-cyano-1-butyne are provided in Table 1 in both the A and S reductions. The rotational constants show excellent agreement between the computed values (MP2/cc-pVTZ) and the effective experimental constants (within 0.7% for A_0, 0.3% for B_0, and 0.3% for C_0). The quartic centrifugal distortion constants are predicted by MP2 within 7.5% of the experimental values, and the sextic centrifugal distortion constants are all within 36.1%. Hyperfine-resolved transitions were not observed in the millimeter-wave region, but transitions observed in the microwave region were resolved into hyperfine multiplets arising from quadrupolar coupling to nitrogen. Experimental values of the nitrogen nuclear quadrupole coupling constants χ_{aa}, χ_{bb}, and χ_{cc} show reasonable agreement with predicted values (errors of 9.2%, 11.3%, and 7.5%, respectively). Although our analysis does not address the coupling evident in the millimeter-wave region, the agreement between the experimental and predicted constants, large number of transitions fit to low error ($\sigma_{fit} = 0.027$ MHz), and lack of obvious perturbation in the fitted series make us confident the current spectroscopic constants are physically meaningful.

Table 1
Effective experimental and predicted spectroscopic constants for the ground vibrational state of *anti*-4-cyano-1-butyne (I^r representation).

S reduction, I^r representation			A reduction, I^r representation		
	Calculated[a]	Experimental		Calculated[a]	Experimental
$A_0^{(S)}$ (MHz)	24,886	25064.23614 (34)	$A_0^{(A)}$ (MHz)	25,128	25064.23616 (34)
$B_0^{(S)}$ (MHz)	1473.0	1477.085286 (16)	$B_0^{(A)}$ (MHz)	1478.1	1477.087567 (21)
$C_0^{(S)}$ (MHz)	1415.0	1419.396089 (15)	$C_0^{(A)}$ (MHz)	1420.3	1419.393803 (20)
D_J (kHz)	0.1486	0.1501005 (14)	Δ_J (kHz)	0.1493	0.1507951 (33)
D_{JK} (kHz)	−8.209	−8.13277 (13)	Δ_{JK} (kHz)	−8.213	−8.13735 (13)
D_K (kHz)	301.8	307.79 (25)	Δ_K (kHz)	301.8	307.83 (25)
d_1 (kHz)	−0.01330	−0.0131037 (16)	δ_J (kHz)	0.01330	0.0131051 (17)
d_2 (kHz)	−0.0003219	−0.0003479 (15)	δ_K (kHz)	1.056	1.1421 (50)
H_J (Hz)	0.00007211	0.000070810 (63)	Φ_J (Hz)	0.00007357	0.00007258 (17)
H_{JK} (Hz)	−0.004470	−0.0046249 (41)	Φ_{JK} (Hz)	−0.003748	−0.0039381 (42)
H_{KJ} (Hz)	−0.06956	−0.07285 (32)	Φ_{KJ} (Hz)	−0.1034	−0.07600 (32)
H_K (Hz)	6.956	[6.956]	Φ_K (Hz)	6.958	[6.958]
h_1 (Hz)	0.00001399	0.000013003 (78)	ϕ_J (Hz)	0.00001404	0.000013048 (78)
h_2 (Hz)	0.0000007264	0.000000910 (83)	ϕ_{JK} (Hz)	0.001043	0.0061 (27)
h_3 (Hz)	0.00000005569	[0.00000005569]	ϕ_K (Hz)	0.3878	[0.3878]
χ_{aa} (MHz)[b]	−3.31	−3.6448 (36)	χ_{aa} (MHz)[b]	−3.31	−3.6448 (36)
χ_{bb} (MHz)[b]	1.43	1.6158 (17)	χ_{bb} (MHz)[b]	1.43	1.6158 (17)
χ_{cc} (MHz)[b]	1.88	2.0290 (19)	χ_{cc} (MHz)[b]	1.88	2.0290 (19)
Δ_i (uÅ^2)[c, d]	−6.24	−6.257342 (5)	Δ_i (uÅ^2)[c, d]	−6.24	−6.256241 (7)
N_{lines}[e]		128, 1994	N_{lines}[e]		128, 1994
$\sigma_{\mu\text{-wave fit}}$ (MHz)		0.0031	$\sigma_{\mu\text{-wave fit}}$ (MHz)		0.0031
$\sigma_{\text{mm-wave fit}}$ (MHz)		0.027	$\sigma_{\text{mm-wave fit}}$ (MHz)		0.027
$\sigma_{\text{total fit}}$ (MHz)		0.027	$\sigma_{\text{total fit}}$ (MHz)		0.027
$\sigma_{\text{total w.fit}}$[f]		0.587	$\sigma_{\text{total w.fit}}$[f]		0.588

[a] Evaluated at MP2/cc-pVTZ.
[b] Constants converted from the field gradient axis system to the inertial moment axis system.
[c] Inertial defect ($\Delta_i = I_c - I_a - I_b$).
[d] Calculated using PLANM from the B_0 constants.
[e] Number of independent transition frequencies for microwave and millimeter wave regions, respectively.
[f] Weighted deviation of global fits, where 2 kHz is assumed for microwave measurements and 50 kHz for millimeter-wave measurements.

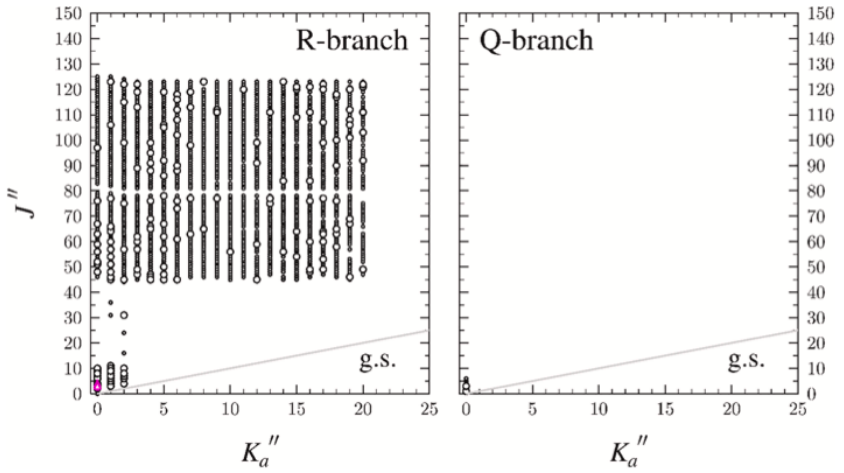


Fig. 5. Data distribution plots for the least-squares fit of spectroscopic data for the vibrational ground state of *anti*-4-cyano-1-butyne. R- and Q-branch transitions are represented by black circles, while P-branch transitions are represented as pink triangles. The size of the outlined shape is proportional to the value of $|(f_{obs.} - f_{calc.})/\delta f|$, where δf is the frequency measurement uncertainty and all values are<3.

4.4. *gauche*-4-cyano-1-butyne ground state

The *gauche* conformer was successfully identified in the millimeter-wave spectrum utilizing the MP2/cc-pVTZ predicted constants, and the assignments were confirmed by the microwave data. The microwave transitions are well-modeled by a distorted-rotor Hamiltonian, but transition frequencies begin to deviate due to coupling in the 130–360 GHz frequency region, even in the lowest K_a series. As done for the *anti* conformer, an effective fit for the *gauche* conformer was obtained by excluding transitions that deviated from distorted-rotor predicted frequencies. In the 130–360 GHz region, most quadruply degenerate transitions from $K_a = 0$–10 were fit to low error ($\sigma_{fit} < 50$ kHz) with distortion constants that compared reasonably (signs and orders of magnitude) with the predicted values. Including transitions with $K_a >$ 10 resulted in a substantial increase in the error of the least-squares fit. As with the *anti* conformer, this issue cannot be treated by inclusion of higher-order centrifugal distortion terms, making it evident that the ground state of *gauche*-4-cyano-1-butyne is not amenable to a single-state, distorted-rotor Hamiltonian. Over 250 distinct transitions including *a*- and *b*-type R-branch transitions with J'' values ranging from

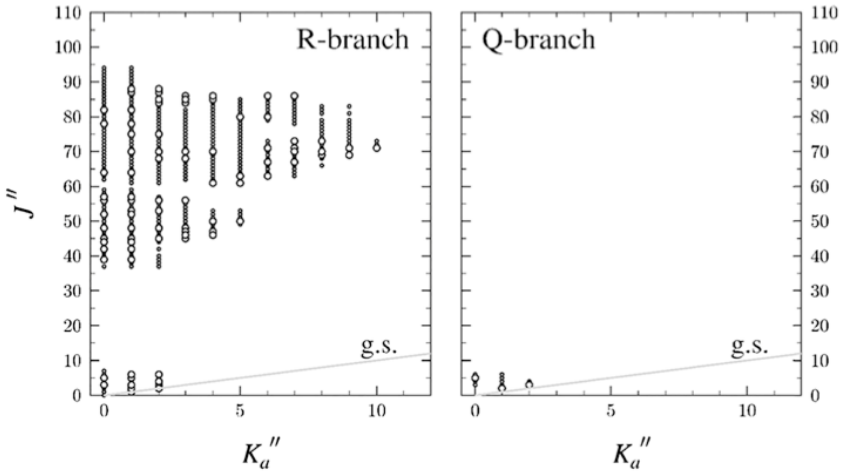


Fig. 6. Data distribution plots for the least-squares fit of spectroscopic data for the vibrational ground state of *gauche*-4-cyano-1-butyne. The size of the outlined circle is proportional to the value of $|(f_{obs.} - f_{calc.})/\delta f|$, where δf is the frequency measurement uncertainty and all values are<3.

0 to 95 and $K_a \leq 10$ were measured for the *gauche* conformer and are represented in the data distribution plot in Fig. 6.

The experimental spectroscopic constants for the ground state of the *gauche* conformer, along with the MP2-predicted constants, are reported in Table 2. In the A-reduced least-squares fit, the effective experimental rotational constants and the MP2/cc-pVTZ computed values show modest agreement (within 2.6% for A_0, 2.1% for B_0, and 0.8% for C_0), and the experimental quartic distortion constants are predicted within 12.3%. Because a limited number and type of K_a series were able to be included in the least-squares fit, some distortion terms were not well-determined. Terms Φ_{KJ} and Φ_K were held constant at their predicted values, which afforded a satisfactory fit with an error (σ_{fit}) commensurate with the experimental uncertainty. The remaining sextic centrifugal distortion constants differ substantially from their computed values. Constant Φ_{JK} has a different sign compared to the predicted value – a typical indication that a constant is absorbing coupling. There is considerable disagreement between the experimental and calculated values of the Φ_J, Φ_{JK}, and ϕ_J constants (196%, 128%, and 202%, respectively). (In the S-reduced least-squares fit, the corresponding Φ_J and ϕ_J terms are predicted within 105% and 89%, but the experimental value of Φ_{JK} differs from the prediction by almost 640%). Fixing any of these constants to their predicted value, however, massively increases

Table 2
Effective experimental and computed spectroscopic constants for the ground vibrational state of *gauche*-4-cyano-1-butyne (I^r representation).

S reduction, I^r representation			A reduction, I^r representation		
	Calculated[a]	Experimental		Calculated[a]	Experimental
$A_0^{(S)}$ (MHz)	6381	6548.45862 (12)	$A_0^{(A)}$ (MHz)	6381	6548.45742 (14)
$B_0^{(S)}$ (MHz)	2474	2422.661403 (29)	$B_0^{(A)}$ (MHz)	2474	2422.672036 (43)
$C_0^{(S)}$ (MHz)	1910	1894.290818 (15)	$C_0^{(A)}$ (MHz)	1910	1894.280311 (21)
D_J (kHz)	3.726	3.67941 (25)	Δ_J (kHz)	3.886	3.83687 (41)
D_{JK} (kHz)	−24.32	−25.7254 (43)	Δ_{JK} (kHz)	−25.28	−26.7203 (50)
D_K (kHz)	53.02	60.510 (11)	Δ_K (kHz)	53.82	61.331 (13)
d_1 (kHz)	−1.398	−1.37935 (16)	δ_J (kHz)	1.398	1.37548 (20)
d_2 (kHz)	−0.08003	−0.082600 (60)	δ_K (kHz)	4.869	5.4147 (51)
H_J (Hz)	0.02737	0.013356 (74)	Φ_J (Hz)	0.03059	0.010348 (97)
H_{JK} (Hz)	−0.1564	0.0290 (24)	Φ_{JK} (Hz)	−0.1001	0.3532 (55)
H_{KJ} (Hz)	−0.2009	[−0.2009]	Φ_{KJ} (Hz)	−0.4371	[−0.4371]
H_K (Hz)	1.231	[1.231]	Φ_K (Hz)	1.4074	[1.4074]
h_1 (Hz)	0.01409	0.007450 (34)	ϕ_J (Hz)	0.0144	0.004763 (49)
h_2 (Hz)	0.001609	0.001493 (12)	ϕ_{JK} (Hz)	0.0174	0.724 (18)
h_3 (Hz)	0.0003110	0.0003189 (18)	ϕ_K (Hz)	0.8080	1.742 (15)
χ_{aa} (MHz)[b]	0.0738	0.07500 (67)	χ_{aa} (MHz)[b]	0.0738	0.07493 (87)
χ_{bb} (MHz)[b]	−1.957	−1.84832 (19)	χ_{bb} (MHz)[b]	−1.957	−1.84807 (23)
χ_{cc} (MHz)[b]	1.884	1.77332 (85)	χ_{cc} (MHz)[b]	1.884	1.7731 (11)
Δ_i (uÅ^2)[c,d]	−18.95	−18.989536 (4)	Δ_i (uÅ^2)[c,d]	−18.95	−18.987155 (5)
N_{lines}[e]		200, 250	N_{lines}[e]		200, 250
$\sigma_{\mu\text{-wave fit}}$ (MHz)		0.0018	$\sigma_{\mu\text{-wave fit}}$ (MHz)		0.0018
$\sigma_{\text{mm-wave fit}}$ (MHz)		0.024	$\sigma_{\text{mm-wave fit}}$ (MHz)		0.024
$\sigma_{\text{total fit}}$ (MHz)		0.018	$\sigma_{\text{total fit}}$ (MHz)		0.026
$\sigma_{\text{total w.fit}}$[f]		0.557	$\sigma_{\text{total w.fit}}$[f]		0.691

[a] Evaluated at MP2/cc-pVTZ.
[b] Constants converted from the field gradient axis system to the inertial moment axis system.
[c] Inertial defect ($\Delta_i = I_c - I_a - I_b$).
[d] Calculated using PLANM from the B_0 constants.
[e] Number of independent transition frequencies for microwave and millimeter wave regions, respectively.
[f] Weighted deviation of global fits, where 2 kHz is assumed for microwave measurements and 50 kHz for millimeter-wave measurements.

the error of the least-squares fit and does not allow incorporation of many transitions into the data set. Under these circumstances, the constants represent a convolution of the effects of coupling and centrifugal distortion. As a result, the physical meaningfulness of these centrifugal distortion constants is dubious, as is the ability of the constants to predict transitions in the millimeter-wave region, where the effects of centrifugal distortion are important. With a substantial reduction in the size of the transition data set, it is not surprising that there is poorer agreement between the computed and observed spectroscopic constants. As in the *anti* conformer, hyperfine-resolved transitions were not observed in the millimeter-wave region for the *gauche* conformer, but several microwave transitions were resolved into hyperfine multiplets that were incorporated into the data set. The nitrogen nuclear quadrupole coupling constants χ_{aa}, χ_{bb}, and χ_{cc} show excellent agreement with predicted values (errors of 1.7%, 5.9%, and 6.2%, respectively). Despite the shortcomings of the current analysis – the fact that some of the spectroscopic constants differ from those predicted by MP2 and may not be physically meaningful – the analysis includes only transitions that appear to be devoid of perturbation and predicts, successfully, the highest-intensity transitions up to 360 GHz. A comparison of all predicted and experimental spectroscopic constants can be found in the Supplementary Material.

5. Conformational energy difference from relative intensity measurements

The energy difference between the *gauche* and *anti* conformers of 4-cyano-1-butyne was estimated by comparing differences in the intensities of their corresponding ground-state transitions (from 150 to 185 GHz) at 294 K [43]. The full analysis is presented in the Supplementary Material, from which we estimate an energy difference of $E_{gauche} - E_{anti} = 1.00\ (5)$ kcal/mol for 4-cyano-1-butyne. This energy difference is slightly larger than the predicted value (0.42 kcal/mol; MP2/cc-pVTZ) but is within range of the corresponding energy difference previously determined for the isomer, 4-isocyano-1-butyne (0.69 (14) kcal/mol) [34]. As expected, the structurally similar nitrile and isonitrile functional groups do not exhibit significantly different steric or electronic influences on the conformational equilibria.

6. Lowest excited vibrational states

The computed vibrational manifold of *anti*-4-cyano-1-butyne below 500 cm^{-1} is shown in Fig. 7(a). Given the large value of the A_0 rotational constant, the small value of the C_0 rotational constant, the predicted low energy of its vibrational states, and indications of coupling in the vibrational ground state, higher-energy vibrational states of the *anti* conformer were expected to exhibit intense coupling interactions. The C_s symmetry of the *anti* conformer and respective symmetries of the two lowest-energy excited vibrations, ν_{27} (torsion, A″, 73 cm^{-1}) and ν_{17} (in-plane bend, A', 118 cm^{-1}), allows for Coriolis coupling between the fundamental states along the *a*- and *b*- inertial axes (computed Coriolis coupling terms $G_a = 47803$ MHz, $G_b = 935$ MHz). Attempts to identify and assign ν_{27} and ν_{17} were made using the predicted vibration–rotation interaction constants (MP2/cc-pVTZ). The computed *a*-axis vibration–rotation interaction constants, however, have unusually large magnitudes and opposing signs from each other (1849.7 MHz for ν_{27} and –1784.9 MHz for ν_{17}) – a hallmark for strongly coupled states. The computed vibration–rotation interaction constants, applied to the experimental ground-state rotational constant values, did not lead to the identification of these fundamental states in the spectra. Nonetheless, the excited vibrational states of the *anti* conformer form smooth series that are visible in the Loomis-Wood plots of the ground vibrational state near $K_a = 21$. We were able to use the location of the intense bandhead transitions and the same band pattern of the ground state to assign the quantum numbers of the most intense transitions for states ν_{17} and ν_{27}. Unsurprisingly, we were unable to fit any of these states to low error using a distorted-rotor Hamiltonian, and we saw behavior indicative of intense coupling for each assignable state. A satisfactory distorted-rotor fit of even the lowest-K_a series of these vibrational states was not possible, even when using many higher-order centrifugal distortion constants. Given the observed behavior of the ground and excited vibrational states, a multistate analysis will be required to treat the perturbations in this system and obtain the spectroscopic constants of the excited vibrational states of *anti*-4-cyano-1-butyne. Such an analysis is beyond the scope of the current work. The situation for the *anti* conformer of the related isonitrile, 4-isocyano-1-butyne, is not dissimilar. Although the spectroscopic constants of the vibrational ground state appear to be free of perturbation in the measured frequency range (12–78 GHz), the vibrationally excited torsional modes show signs of

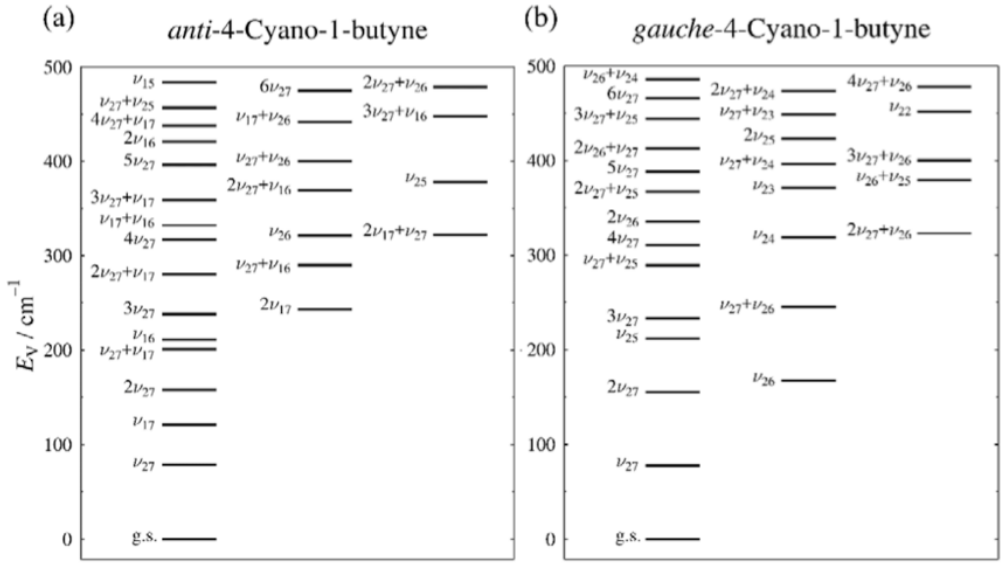


Fig. 7. Vibrational energy levels of (a) *anti*- and (b) *gauche*-4-cyano-1-butyne below 500 cm^{-1} from computed fundamental frequencies (MP2/cc-pVTZ).

unaddressed coupling [34]. The reported rotational constants do not display the expected linear relationship when plotted as a function of vibrational state [44,45].

The *gauche* conformer of 4-cyano-1-butyne exhibits a similarly complex vibrational manifold below 500 cm^{-1} (Fig. 7(b)). The predicted energies of its first two fundamental states, ν_{27} (torsion, A, 74 cm^{-1}) and ν_{26} (bend, A, 169 cm^{-1}), are low, and the vibrational manifold is comprised of many combination and overtone states. Due to the asymmetry of the *gauche* conformer (C_1), Coriolis coupling can appear between the states along all three primary axes (computed Coriolis coupling terms $G_a = 4841$ MHz, $G_b = 205$ MHz, $G_c = 94$ MHz). The predicted vibration–rotation interaction constants for ν_{27} and ν_{26}, along both *a*- and *b*-axes, are large in magnitude, similar in size, and opposite in sign – features indicative of coupling. Instead of using the vibration–rotation interaction constants to identify the vibrationally excited states, it was straightforward to identify transitions for the vibrationally excited states of the *gauche* conformer due to their appearance as straight series in the $K_a = 0$, Loomis-Wood plot of the vibrational ground state. Once again, we were unable to fit any of these states to low error using a distorted-rotor Hamiltonian, and we observed behavior indicative of intense coupling for each assignable state.

7. Conclusion

The ground vibrational states of both *anti*- and *gauche*-4-cyano-1-butyne show coupling to their excited states. Utilizing a Hamiltonian that models these couplings may allow the fitting of additional transitions, but would likely require assignment of many vibrational states for each conformer to completely address the spectroscopic deviations. With highly perturbed rotational spectra of astrochemically important molecules such as open-chain organic nitriles, we are often faced with choosing between a perturbation analysis involving numerous states or an effective distorted-rotor analysis to present to the spectroscopic community. Measuring substantial portions of a molecule's rotational spectrum, while avoiding inclusion of transitions that show obvious perturbation, appears to effectively model the most intense rotational transitions. While not ideal, this method may be useful in characterizing molecules likely to be sought by radioastronomers. In the current study, we generated effective fits for *anti*- and *gauche*-4-cyano-1-butyne and expect the constants presented above to enable those seeking either of these C_5H_5N conformers in harsh interstellar environments to identify them using the most intense transitions at frequencies up to 360 GHz.

Declaration of Competing Interest

The authors declare that they have no known competing financial interests or personal relationships that could have appeared to influence the work reported in this paper.

Acknowledgements

We gratefully acknowledge the National Science Foundation for support of this project (CHE-1954270, Wisconsin; AST-1908576, Center for Astrophysics). P.M.D thanks the Graduate School, University of Wisconsin-Madison, for support as an Advanced Opportunity Fellow.

Appendix A. Supplementary material

Supplementary data to this article can be found online at https://doi.org/10.1016/j.jms.2022.111604.

References

[1] H.S.P. Müller, F. Schlöder, J. Stutzki, G. Winnewisser, The cologne database for molecular spectroscopy, CDMS: a useful tool for astronomers and spectroscopists, J. Mol. Struct. 742 (2005) 215–227.
[2] H.S.P. Müller, S. Thorwirth, D.A. Roth, G. Winnewisser, The cologne database for molecular spectroscopy, CDMS, Astron. Astrophys. 370 (3) (2001) L49–L52.
[3] B.A. McGuire, A.M. Burkhardt, S. Kalenskii, C.N. Shingledecker, A.J. Remijan, E. Herbst, M.C. McCarthy, Detection of the aromatic molecule benzonitrile (*c*-C_6H_5CN) in the interstellar medium, Science 359 (6372) (2018) 202–205.
[4] B.A. McGuire, R.A. Loomis, A.M. Burkhardt, K.L.K. Lee, C.N. Shingledecker, S. B. Charnley, I.R. Cooke, M.A. Cordiner, E. Herbst, S. Kalenskii, M.A. Siebert, E. R. Willis, C.i. Xue, A.J. Remijan, M.C. McCarthy, Detection of two interstellar polycyclic aromatic hydrocarbons via spectral matched filtering, Science 371 (6535) (2021) 1265–1269.
[5] M.C. McCarthy, K.L.K. Lee, R.A. Loomis, A.M. Burkhardt, C.N. Shingledecker, S. B. Charnley, M.A. Cordiner, E. Herbst, S. Kalenskii, E.R. Willis, C.i. Xue, A. J. Remijan, B.A. McGuire, Interstellar detection of the highly polar five-membered ring cyanocyclopentadiene, Nat. Astron 5 (2) (2021) 176–180.
[6] K.L.K. Lee, P.B. Changala, R.A. Loomis, A.M. Burkhardt, C.i. Xue, M.A. Cordiner, S. B. Charnley, M.C. McCarthy, B.A. McGuire, Interstellar detection of 2-cyanocyclopentadiene, C_5H_5CN, a second five-membered ring toward TMC-1, Astrophys J. 910 (1) (2021) L2.
[7] M.C. McCarthy, B.A. McGuire, Aromatics and cyclic molecules in molecular clouds: a new dimension of interstellar organic chemistry, J. Phys. Chem. A 125 (2021) 3231–3243.
[8] K.L.K. Lee, B.A. McGuire, M.C. McCarthy, Gas-phase synthetic pathways to benzene and benzonitrile: a combined microwave and thermochemical investigation, PCCP 21 (2019) 2946–2956.
[9] J. Cernicharo, M. Agúndez, C. Cabezas, B. Tercero, N. Marcelino, J.R. Pardo, P. de Vicente, Pure hydrocarbon cycles in TMC-1: Discovery of ethynyl cyclopropenylidene, cyclopentadiene, and indene, Astron. Astrophys. 649 (2021) L15.
[10] L.W. Avery, N.W. Broten, J.M. MacLeod, T. Oka, H.W. Kroto, Detection of the heavy interstellar molecule cyanodiacetylene, Astrophys. J. 205 (1976) L173–L175.
[11] N.W. Broten, T. Oka, L.W. Avery, J.M. MacLeod, H.W. Kroto, The detection of cyanooctatetrayne (HC_9N) in interstellar space, Astrophys. J. 223 (1978) L105–L107.
[12] H.W. Kroto, C. Kirby, D.R.M. Walton, L.W. Avery, N.W. Broten, J.M. MacLeod, T. Oka, The detection of cyanohexatriyne, $H(C{\equiv}C)_3CN$, in Heiles's cloud 2, Astrophys. J. 219 (1978) L133–L137.
[13] C.M. Walmsley, G. Winnewisser, F. Toelle, Cyanoacetylene and cyanodiacetylene in interstellar clouds, Astron. Astrophys. 81 (1980) 245–250.
[14] N.W. Broten, J.M. MacLeod, L.W. Avery, W.M. Irvine, B. Hoeglund, P. Friberg, A. Hjalmarson, The detection of interstellar methylcyanoacetylene, Astrophys. J. 276 (1984) L25–L29.
[15] F.F. Gardner, G. Winnewisser, Detection of interstellar vinyl cyanide (acrylonitrile), Astrophys. J. 195 (1975) L127–L130.
[16] L.E. Snyder, J.M. Hollis, P.R. Jewell, F.J. Lovas, A. Remijan, Confirmation of interstellar methylcyanodiacetylene (CH_3C_5N), Astrophys J. 647 (1) (2006) 412–417.
[17] F.J. Lovas, A.J. Remijan, J.M. Hollis, P.R. Jewell, L.E. Snyder, Hyperfine structure identification of interstellar cyanoallene toward TMC-1, Astrophys J. 637 (1) (2006) L37–L40.
[18] P.M. Solomon, K.B. Jefferts, A.A. Penzias, R.W. Wilson, Detection of millimeter emission lines from interstellar methyl cyanide, Astrophys. J. 168 (1971) L107–L110.
[19] A. Belloche, R.T. Garrod, H.S.P. Müller, K.M. Menten, Detection of a branched alkyl molecule in the interstellar medium: *iso*-propyl cyanide, Science 345 (2014) 1584–1587.
[20] A. Belloche, R.T. Garrod, H.S.P. Müller, K.M. Menten, C. Comito, P. Schilke, Increased complexity in interstellar chemistry: detection and chemical modeling of ethyl formate and *n*-propyl cyanide in Sagittarius B2(N), Astron. Astrophys. 499 (2009) 215–232.
[21] R.A. Loomis, A.M. Burkhardt, C.N. Shingledecker, S.B. Charnley, M.A. Cordiner, E. Herbst, S. Kalenskii, K.L.K. Lee, E.R. Willis, C.i. Xue, A.J. Remijan, M. C. McCarthy, B.A. McGuire, An investigation of spectral line stacking techniques and application to the detection of $HC_{11}N$, Nat. Astron 5 (2) (2021) 188–196.
[22] M.C. McCarthy, K.L.K. Lee, P.B. Carroll, J.P. Porterfield, P.B. Changala, J. H. Thorpe, J.F. Stanton, Exhaustive product analysis of three benzene discharges by microwave spectroscopy, J. Phys. Chem. A 124 (25) (2020) 5170–5181.
[23] R.J. Halter, R.L. Fimmen, R.J. McMahon, S.A. Peebles, R.L. Kuczkowski, J. F. Stanton, Microwave spectra and molecular structures of (Z)-pent-2-en-4-ynenitrile and maleonitrile, J. Am. Chem. Soc. 123 (49) (2001) 12353–12363.
[24] M.A. Zdanovskaia, B.J. Esselman, R.C. Woods, R.J. McMahon, The 130–370 GHz rotational spectrum of phenyl isocyanide (C_6H_5NC), J. Chem. Phys. 151 (2019) 024301.
[25] M.A. Zdanovskaia, B.J. Esselman, H.S. Lau, D.M. Bates, R.C. Woods, R.J. McMahon, Z. Kisiel, The 103–360 GHz rotational spectrum of benzonitrile, the first interstellar benzene derivative detected by radioastronomy, J. Mol. Spectrosc. 351 (2018) 39–48.
[26] P.M. Dorman, B.J. Esselman, J.E. Park, R.C. Woods, R.J. McMahon, Millimeter-wave spectrum of 4-cyanopyridine in its ground state and lowest-energy vibrationally excited states, ν_{20} and ν_{30}, J. Mol. Spectrosc. 369 (2020) 111274.
[27] P.M. Dorman, B.J. Esselman, R.C. Woods, R.J. McMahon, An analysis of the rotational ground state and lowest-energy vibrationally excited dyad of 3-cyanopyridine: Low symmetry reveals rich complexity of perturbations, couplings, and interstate transitions, J. Mol. Spectrosc. 373 (2020) 111373.
[28] M.A. Zdanovskaia, P.M. Dorman, V.L. Orr, A.N. Owen, S.M. Kougias, B.J. Esselman, R.C. Woods, R.J. McMahon, Rotational spectra of three cyanobutadiene isomers

(C_5H_5N) of relevance to astrochemistry and other harsh reaction environments, J. Am. Chem. Soc. 143 (2021) 9551–9564.

[29] B.J. Esselman, S.M. Kougias, M.A. Zdanovskaia, R.C. Woods, R.J. McMahon, Synthesis, purification, and rotational spectroscopy of (cyanomethylene) cyclopropane—an isomer of pyridine, J. Phys. Chem. A 125 (25) (2021) 5601–5614.

[30] S.M. Kougias, S.N. Knezz, A.N. Owen, R.A. Sanchez, G.E. Hyland, D.J. Lee, A. R. Patel, B.J. Esselman, R.C. Woods, R.J. McMahon, Synthesis and Characterization of Cyanobutadiene Isomers – molecules of astrochemical significance, J. Org. Chem. 85 (9) (2020) 5787–5798.

[31] M.A. Zdanovskaia, B.J. Esselman, S.M. Kougias, A.R. Patel, R.C. Woods, R. J. McMahon, The 130–370 GHz rotational spectrum of *syn*-2-cyano-1,3-butadiene (C_5H_5N) – a molecule of astrochemical relevance, Mol. Phys. 119 (2021) 1964629.

[32] H.H. Smith, S.M. Kougias, B.J. Esselman, R.C. Woods, R.J. McMahon, Synthesis, purification, and rotational spectroscopy of 1-cyanocyclobutene (C_5H_5N), J. Phys. Chem. A (2022) (in press).

[33] R. Moreno, E. Silla, I. Tunon, A. Arnau, Ab initio rotational constants of the nitriles derived from cyanodiacetylene (HC_4CN), Astrophys. J. 437 (1994) 532–539.

[34] S. Samdal, H. Møllendal, J.-C. Guillemin, Microwave spectrum and conformational properties of 4-Isocyano-1-butyne ($HC{\equiv}CCH_2CH_2N{\equiv}C$), J. Phys. Chem. A 117 (40) (2013) 10304–10310.

[35] M.J. Frisch, G.W. Trucks, H.B. Schlegel, G.E. Scuseria, M.A. Robb, J.R. Cheeseman, G. Scalmani, V. Barone, G.A. Petersson, H. Nakatsuji, X. Li, M. Caricato, A.V. Marenich, J. Bloino, B.G. Janesko, R. Gomperts, B. Mennucci, H.P. Hratchian, J.V. Ortiz, A.F. Izmaylov, J.L. Sonnenberg, D. Williams-Young, F. Ding, F. Lipparini, F. Egidi, J. Goings, B. Peng, A. Petrone, T. Henderson, D. Ranasinghe, V.G. Zakrzewski, J. Gao, N. Rega, G. Zheng, W. Liang, M. Hada, M. Ehara, K. Toyota, R. Fukuda, J. Hasegawa, M. Ishida, T. Nakajima, Y. Honda, O. Kitao, H. Nakai, T. Vreven, K. Throssell, J.A. Montgomery, Jr. , J.E. Peralta, F. Ogliaro, M.J. Bearpark, J.J. Heyd, E.N. Brothers, K.N. Kudin, V.N. Staroverov, T.A. Keith, R. Kobayashi, J. Normand, K. Raghavachari, A.P. Rendell, J.C. Burant, S.S. Iyengar, J. Tomasi, M. Cossi, J.M. Millam, M. Klene, C. Adamo, R. Cammi, J.W. Ochterski, R.L. Martin, K. Morokuma, O. Farkas, J.B. Foresman, D.J. Fox, Gaussian 16 rev C.01. Gaussian, Inc., Wallingford, CT, USA, 2016.

[36] J.R. Schmidt, W.F. Polik, WebMO Enterprise, version 19.0; WebMO LLC: Madison, WI, USA, 2019. http://www.webmo.net (accessed August, 2019).

[37] B.J. Esselman, B.K. Amberger, J.D. Shutter, M.A. Daane, J.F. Stanton, R.C. Woods, R.J. McMahon, Rotational spectroscopy of pyridazine and its isotopologs from 235–360 GHz: equilibrium structure and vibrational satellites, J. Chem. Phys. 139 (2013) 224304.

[38] J.-U. Grabow, E.S. Palmer, M.C. McCarthy, P. Thaddeus, Supersonic-jet cryogenic-resonator coaxially oriented beam-resonator arrangement Fourier transform microwave spectrometer, Rev. Sci. Instrum. 76 (2005) 093106.

[39] Z. Kisiel, L. Pszczółkowski, B.J. Drouin, C.S. Brauer, S. Yu, J.C. Pearson, I. R. Medvedev, S. Fortman, C. Neese, Broadband rotational spectroscopy of acrylonitrile: vibrational energies from perturbations, J. Mol. Spectrosc. 280 (2012) 134–144.

[40] Z. Kisiel, L. Pszczółkowski, I.R. Medvedev, M. Winnewisser, F.C. De Lucia, E. Herbst, Rotational spectrum of *trans–trans* diethyl ether in the ground and three excited vibrational states, J. Mol. Spectrosc. 233 (2) (2005) 231–243.

[41] H.M. Pickett, The fitting and prediction of vibration-rotation spectra with spin interactions, J. Mol. Spectrosc. 148 (2) (1991) 371–377.

[42] P. Klaeboe, M. Moneeb, E. Törneng, H. Hopf, I. Böhm, B.N. Cyvin, S.J. Cyvin, The conformation and vibrational spectra of 1-cyano-3-butyne, Z. Naturforsch. A 35 (1980) 537–548.

[43] N. Wehres, M. Hermanns, O.H. Wilkins, K. Borisov, F. Lewen, J.-U. Grabow, S. Schlemmer, H.S.P. Müller, Rotational spectroscopy of the two conformers of 3-methylbutyronitrile (C_4H_9CN) between 2 and 400 GHz, Astron. Astrophys. 615 (2018) A140.

[44] Z. Chen, J. van Wijngaarden, The ν_{21} ring puckering mode of 3-oxetanone: a far infrared spectroscopic investigation using synchrotron radiation, J. Mol. Spectrosc. 279 (2012) 31–36.

[45] V.L. Orr, B.J. Esselman, P.M. Dorman, B.K. Amberger, I.A. Guzei, R.C. Woods, R. J. McMahon, Millimeter-wave spectroscopy, X-ray crystal structure, and quantum chemical studies of diketene: resolving ambiguities concerning the structure of the ketene dimer, J. Phys. Chem. A 120 (2016) 7753–7763.

Appendix H

The 130–360 GHz Rotational Spectrum of Isocyanocyclobutane (C_4H_7NC) and Cyanocyclobutane (C_4H_7CN)

Brian J. Esselman
Samuel M. Kougias
Madison D. Fellows
R. Claude Woods
Robert J. McMahon

Journal of Molecular Spectroscopy, 2022, *388*, 111684

Journal of Molecular Spectroscopy 388 (2022) 111684

Contents lists available at ScienceDirect

Journal of Molecular Spectroscopy

journal homepage: www.elsevier.com/locate/yjmsp

The 130–360 GHz rotational spectrum of isocyanocyclobutane (C_4H_7NC) and cyanocyclobutane (C_4H_7CN)

Brian J. Esselman, Samuel M. Kougias, Madison D. Fellows, R. Claude Woods *, Robert J. McMahon *

Department of Chemistry, University of Wisconsin–Madison, Madison, WI 53706, USA

A B S T R A C T

The 130–360 GHz rotational spectrum of isocyanocyclobutane is reported herein for the first time. Over 2200 transitions were measured, assigned, and least-squares fit to a partial-octic distorted-rotor Hamiltonian with small deviation ($\sigma_{fit} < 50$ kHz) for the *equatorial* conformer. The *axial* conformer has so far remained elusive. For cyanocyclobutane, we measured the rotational spectra of both *equatorial* and *axial* conformers in the same frequency region to allow a direct comparison between the isomers. Transition frequencies for each conformational isomer of cyanocyclobutane were similarly fit to partial octic distorted-rotor Hamiltonians with small deviation. The experimental spectroscopic constants are in very good agreement with the predicted values (B3LYP) for all three species and with those reported in an earlier microwave study of cyanocyclobutane. Measurement of the relative transition intensities provides an updated energy difference of 0.69 (7) kcal/mol between the two conformers, with the equatorial conformation being the more stable one. Analysis of the *axial* conformation of cyanocyclobutane reveals coupling of its ground state to the vibrationally excited states of the *equatorial* conformation. Our observations of the vibrationally excited states of the *equatorial* conformer suggest that there are many Coriolis interactions between these states that were not described previously. Combined with literature values of nuclear quadrupole coupling constants, these spectroscopic constants and reported transition frequencies provide the basis for future astronomical searches for isocyanocyclobutane and cyanocyclobutane.

1. Introduction

Nitriles (R–CN) are prominently represented in the list of more than 260 molecules detected in extraterrestrial environments [1,2] due to their stability, relative abundance, and intrinsically large dipole moments. In many instances, the corresponding isonitriles (R–NC) have also been detected, *e.g.*, R = H [3,4], R = CH_3 [5,6], and R = HCC [7]. These molecules reflect the full range of unsaturation (hydrogenation) available to organic species – from maximally unsaturated carbon chains [7–14] to intermediate levels of unsaturation (aromatic nitriles [15,16] and cyanocyclopentadienes [17,18]) to fully saturated frameworks (propyl [19] and isopropyl cyanide [20]). All of these molecular detections provide evidence for a rich chemistry involving organic nitriles in extraterrestrial environments. While none of the previously detected species includes a four-membered organic ring, the detections of propyl and isopropyl cyanide raise the possibility of detecting species such as cyanocyclobutene [21], cyanocyclobutane, and isocyanocyclobutane. Astronomical detection of these species is dependent on accurate experimental and predicted transition frequencies across the spectral range of available radiotelescopes.

Cyanocyclobutane and isocyanocyclobutane (Fig. 1) exist as equilibrium mixtures of two C_s conformational isomers, each with *a*- and *c*-type rotational transitions. The lower energy isomer, cyanocyclobutane (*c*-C_4H_7-CN) has been well-studied spectroscopically. Its vibrational spectra (infrared and Raman) have been reported and assigned in the solid, liquid, gas, and matrix phases [22–24] for both the *equatorial* and *axial* conformational isomers. In contemporaneous microwave spectroscopy works from 1973, two groups reported the rotational spectra of *equatorial* cyanocyclobutane [25,26]. Fong *et al.* reported the spectrum from 13 to 32 GHz and determined the ^{14}N nuclear quadrupole coupling constants, dipole moment components, and spectroscopic constants for the ground vibrational state and four vibrationally excited states of the ring-puckering (ν_{20}, A′) and out-of-plane vibrational modes (ν_{33}, A″) [25]. Durig *et al.* measured the spectrum from 26 to 40 GHz and reported dipole moment components and spectroscopic constants for the ground vibrational state and five vibrationally excited states of the ring-puckering (ν_{20}) and out-of-plane nitrile bending (ν_{33}) vibrational modes [26]. Caminati *et al.* reinvestigated the spectrum of cyanocyclobutane and improved the set of spectroscopic constants by determining the quartic centrifugal distortion constants [27]. They also observed the *axial* conformer for the first time [27], after a combined *ab initio* study and electron diffraction study of 1,1-dicyanocyclobutane suggested the

* Corresponding authors.
E-mail addresses: rcwoods@wisc.edu (R.C. Woods), robert.mcmahon@wisc.edu (R.J. McMahon).

https://doi.org/10.1016/j.jms.2022.111684
Received 20 May 2022; Received in revised form 20 June 2022; Accepted 25 July 2022
Available online 29 July 2022
0022-2852/© 2022 Elsevier Inc. All rights reserved.

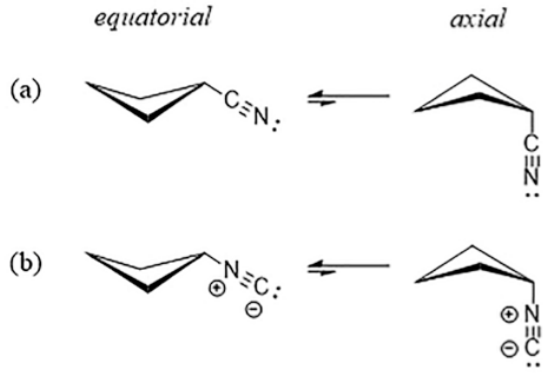


Fig. 1. (a) *Equatorial* and *axial* conformers of cyanocyclobutane. (b) *Equatorial* and *axial* conformers of isocyanocyclobutane.

existence of distinct *axial* and *equatorial* substituent positions [28]. In a related work, Caminati *et al.* analyzed the ring-puckering potential and reported spectroscopic constants for an additional five vibrationally excited states of *equatorial* cyanocyclobutane and five vibrationally excited states of *axial* cyanocyclobutane, including the out-of-plane nitrile-bending vibrational mode (ν_{19}, A′) [29]. Importantly, the latter work corrected the previous assignments of the vibrationally excited state spectra of the *equatorial* conformers. The data sets in these studies contained limited numbers of low-*J* transitions (<60 transitions) with frequencies less than 40 GHz. Thus, it is not surprising that no Coriolis coupling was reported between the vibrationally excited states despite several small energy spacings between states.

Like other cycloalkanes, the non-planarity of the cyclobutane ring gives rise to two non-equivalent conformational isomers of mono-substituted cyclobutane derivatives in which the substituent can occupy an *equatorial* or an *axial* position [22,29–32], (Fig. 1). Experimentally, the enthalpy difference between the *axial* and *equatorial* conformations of cyanocyclobutane has been reported to be 0.73 (14) kcal/mol, favoring the *equatorial* conformation with a barrier to conformational interconversion of less than 2.3 kcal/mol [22,27,29]. The potential energy surfaces of cyano- and isocyano cyclobutane are similar to those of chloro- or bromocyclobutane, whose rings are likewise substituted with σ electron-withdrawing substituents with a low steric profile [33]. Isomerization of isocyanocyclobutane (R–NC) to the lower energy nitrile isomer (R–CN occurs thermally at 200 °C. Although the enthalpies of formation and isomerization have not been measured directly for R = cyclobutyl, such isomerizations have been well studied and are remarkably similar, regardless of the R group [34]. As a result, the isocyano isomer is expected to be ~ 21 kcal/mol higher in energy than the cyano isomer, with an isomerization energy barrier of ~ 38 kcal/mol [35,36]. Thus, the rate of gas-phase isomerization at room temperature is negligible, and each of these cyclobutane derivatives can be studied independently.

Compared to cyanocyclobutane, relatively little is known about isocyanocyclobutane [37,38]. Isocyanocyclobutane has been synthesized previously [37,39,40], though its characterization is limited. It was recently used to generate a substituted tetrazole *via* an Ugi-azide, three-component reaction [41]. The present work describes the synthesis, purification, and characterization of isocyanocyclobutane and the rotational spectroscopy of both isocyano- and cyanocyclobutane.

2. Computational methods

Electronic structure calculations were carried out with Gaussian 16 [42] using the WebMO interface [43] to obtain theoretical spectroscopic constants. Optimized geometries at the B3LYP/6-311+(2d,p) level were obtained using "verytight" convergence criteria and an "ultrafine" integration grid, and subsequent anharmonic vibrational frequency calculations were carried out. All computational output files can be found in the supplemental material.

3. Experimental methods

3.1. Synthesis

We are not aware of commercial sources of isocyanocyclobutane. Like many other isonitriles, it can be readily prepared by dehydration of the corresponding formamide [37,44]. The requisite formamide, *N*-cyclobutylformamide, is generated *via* nucleophilic acyl substitution with excess ethyl formate in a 97 % yield (Scheme 1). Subsequently, *N*-cyclobutylformamide is dehydrated using a slight excess of *p*-toluenesulfonyl chloride (TsCl) in quinoline. Isocyanocyclobutane is then distilled into a liquid nitrogen-cooled receiving flask and purified *via* trap-to-trap vapor distillation twice, to remove any residual quinoline. Isocyanocyclobutane was obtained in a 40 % yield, characterized, and its rotational spectrum obtained. Characteristically of isonitriles, the odor of this compound is both intense and foul, and all contaminated glassware should be soaked in a bleach solution. A detailed experimental procedure and characterization is provided in Section 6 (*vide infra*).

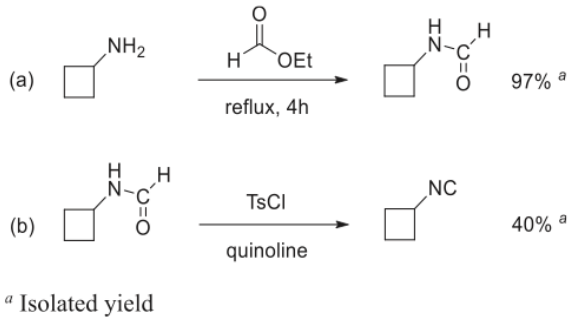
3.2. Spectroscopy

Using a millimeter-wave spectrometer that has been previously described [45,46], the rotational spectra of both cyclobutane derivatives were collected from 130 to 230 and from 235 to 360 GHz, in a continuous flow at room temperature, with a sample pressure of 3 mTorr. A commercial sample of cyanocyclobutane was used without further purification, while isocyanocyclobutane was synthesized as described. The separate spectral segments were combined into a single broadband spectrum using Kisiel's Assignment and Analysis of Broadband Spectra (AABS) software [47,48]. The complete spectrum from 130 to 360 GHz was obtained automatically over approximately six days using the following experimental parameters: 0.6 MHz/*sec* sweep rate, 10 ms time constant, and 50 kHz AM and 500 kHz FM modulation in a tone burst design. Pickett's SPFIT/SPCAT [49] were used for least-squares fits and spectral predictions [47,48], along with Kisiel's PIFORM, PLANM, and AC programs for analysis [47,48]. A uniform frequency measurement uncertainty of 0.050 MHz was assumed for all measurements.

4. Results

4.1. Cyanocyclobutane

Equatorial cyanocyclobutane (Fig. 2a) is a highly prolate ($\kappa = -0.927$), asymmetric top with dipole moment components along its *a*- and *c*-principal axes ($\mu_a = 4.04 \pm 0.09$ D, $\mu_c = 0.92 \pm 0.03$ D [26]) resulting in strong *a*- and much weaker *c*-type rotational transitions. The *axial*



Scheme 1. Syntheses of *N*-cyclobutylformamide and isocyanocyclobutane.

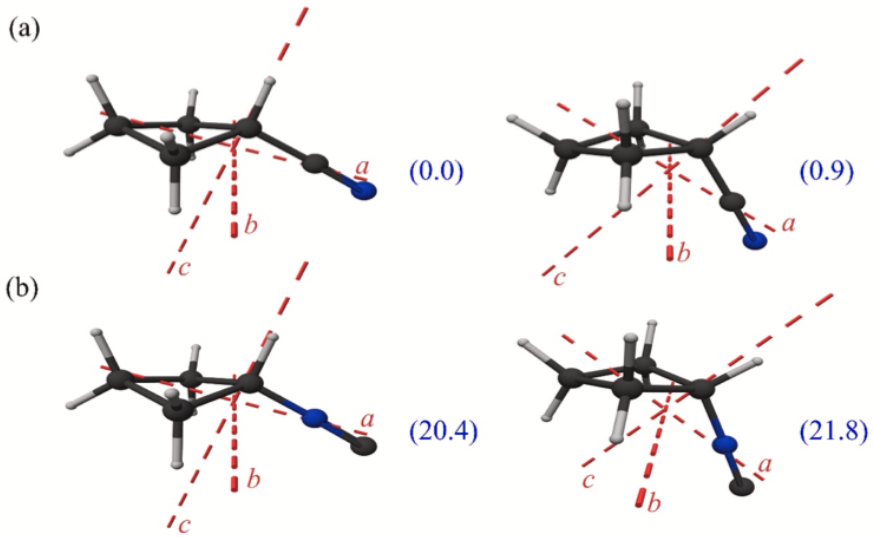


Fig. 2. (a) *Equatorial* ($\mu_a = 4.04 \pm 0.09$ D, $\mu_c = 0.92 \pm 0.03$ D [26]) and *axial* ($\mu_a = 3.81 \pm 0.03$ D, $\mu_c = 1.34 \pm 0.03$ D [27]) conformers of cyanocyclobutane. (b) *Equatorial* ($\mu_a = 4.01$ D, $\mu_c = 0.92$ D, B3LYP) and *axial* ($\mu_a = 3.90$ D, $\mu_c = 1.26$ D, B3LYP) conformers of isocyanocyclobutane. The computed relative energies in kcal/mol are presented in parenthesis, including zero-point vibrational energy correction.

conformer (Fig. 2a) is also a highly prolate ($\kappa = -0.931$) asymmetric top with a dipole along its *a*- and *c*-principal axes (($\mu_a = 3.81 \pm 0.03$ D, $\mu_c = 1.34 \pm 0.03$ D [27]). Caminati *et al.* determined an energy difference of 0.73 ± 0.14 kcal/mol [27], favoring the *equatorial* conformation [27]. The resulting spectrum from 130 to 360 GHz of cyanocyclobutane is dominated by $^{a}R_{0,1}$ transitions from the *equatorial* conformation, with weaker Q-branch transitions. Additionally, there are many R- and Q-branch transitions from its vibrationally excited states and its *axial* conformational isomer. Previously reported spectroscopic constants were combined with computed sextic centrifugal distortion constants to guide our initial search and assignment. Fig. 3 shows the rotational spectrum from 191.5 to 199.2 GHz, with the typical prolate-band structure of a highly prolate asymmetric top created by transitions of the same J'. The $J' = 43$ and $J' = 44$ bands of *equatorial* cyanocyclobutane (Fig. 3) are created by degenerate K_a^+ and K_a^- transitions (those where $K_a + K_c = J$ and $K_a + K_c = J + 1$, respectively) that progress to lower frequency and, at moderate K_a, turnaround and then progress toward higher frequency. Similar, but less intense bands ($J' = 37$ and $J' = 38$) are visible for *axial* cyanocyclobutane. The prominence of these features, combined with the excellent initial spectroscopic predictions for both conformational isomers, made the preliminary assignments and least-squares fitting relatively straightforward.

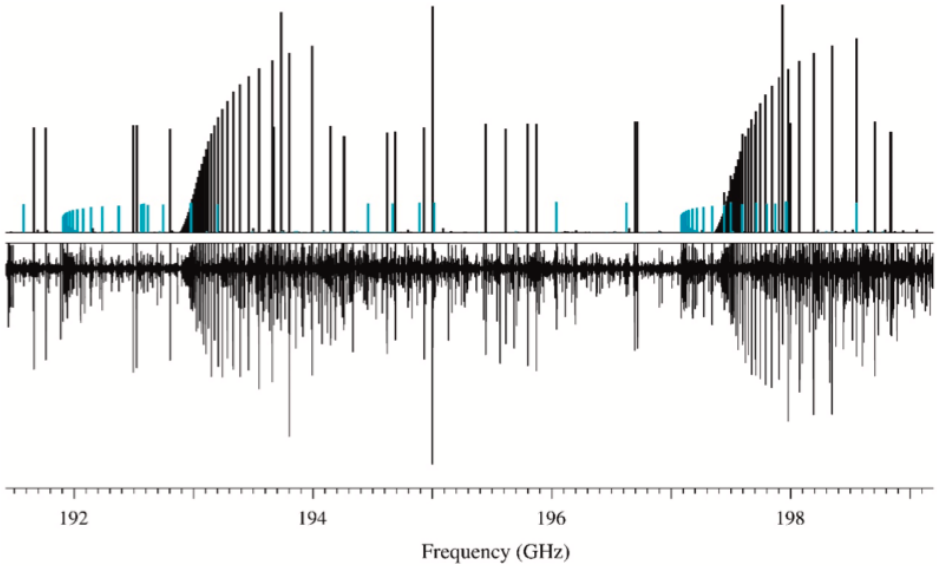


Fig. 3. Predicted (top) and experimental (bottom) rotational spectra of cyanocyclobutane from 191.5 to 199.2 GHz. Ground-state *equatorial* cyanocyclobutane transitions for the $J' = 43$ and $J' = 44$ bands appear in black. Ground-state *axial* cyanocyclobutane transitions for the $J' = 37$ and $J' = 38$ bands appear in cyan. Unassigned transitions are predominantly attributable to vibrationally excited states of *equatorial* cyanocyclobutane.

4.2. Equatorial cyanocyclobutane

Over 3100 R- and Q-branch transitions have been measured, assigned, and least-squares fit for *equatorial* cyanocyclobutane to both an A- and S-reduced, partial-octic centrifugally distorted Hamiltonian models in the I^r representation. Across the frequency range of this study, nuclear quadrupole splitting from the nitrogen nucleus was not resolved. Thus, these terms were not included in the Hamiltonian. The broad range of J' (2 to 86) and K_a' (0 to 54) values shown in the data set distribution plot in Fig. 4, necessitated the inclusion of a complete set of sextic centrifugal distortion constants and two octic centrifugal distortion terms (L_{JK} and L_{KKJ}) in both the S- and A-reductions ($\sigma_{fit} = 0.032$ MHz). While the data set is dominated by $^aR_{0,1}$ transitions, approximately 10 % of the R-branch transitions included in the data set, and all of the Q-branch transitions, are *c*-type transitions. Previously reported microwave transitions from Caminati *et al.* [27] were included in the data set and are represented in Fig. 4 by blue symbols. The resulting spectroscopic constants are presented in Table 1, and the least-squares fitting output files can be found in the supplemental material. Computed spectroscopic constants, where available, are presented alongside the experimental values in Table 1 for comparison. As expected, the computed A_0, B_0, and C_0 terms are within 1.6, 0.4, and 0.5 %, respectively, of their experimental values in both reductions. The computed quartic centrifugal distortion terms are in generally good agreement – within 7 % of their experimental values, except for D_{JK} and Δ_{JK}. These computed values D_{JK} and Δ_{JK} deviate by 25 and 28 % from their experimental values, respectively. The experimental Δ_{JK} value (0.776529 (84) MHz) determined in this work is in closer agreement with the value from the partial-quartic least-squares fit presented by Caminati *et al.* (0.96 (1) MHz) [29]. Given the extensive data sets, low σ_{fit} value, and the underestimate of the corresponding constant in each reduction, we attribute the discrepancy almost entirely to the computational model and not to the experimental least-squares fit. All of the computed sextic centrifugal distortion constants are in reasonable agreement (within 10 %) of the experimental values, except h_1, h_2, Φ_{JK}, and ϕ_{JK}. Without a data set that supports determination of a complete set of octic distortion constants, it is more challenging to ascertain the source of the deviation in these constants. The discrepancy may be an extension of the issue with the computed values of D_{JK} and Δ_{JK} or could be due to a truncation of the model and the incorporation of missing effects of the octic terms into the sextic terms during the least-squares fitting. With all experimental constants well-determined and of the expected sign and magnitude, we are confident in their physical meaning and that the ground state of the *equatorial* conformation is generally free of Coriolis coupling with its vibrationally excited states across the frequency range of our measurements.

Even though it was not noted in previous studies, our preliminary analysis of the vibrationally excited states of *equatorial* cyclobutane in the 130 to 360 GHz range revealed that there are clearly Coriolis interactions between ν_{20} (142 cm^{-1} [24]) and ν_{33} (192 cm^{-1} [24]) preventing either state from being adequately treated by a single-state Hamiltonian model. Given the close proximity of the next fundamental ν_{19} (262 cm^{-1} [24]) and the first set of overtones and combination $2\nu_{20}$ (~284 cm^{-1}), $\nu_{20} + \nu_{33}$ (334 cm^{-1}), and $2\nu_{33}$ (384 cm^{-1}), it is not yet clear whether ν_{20} and ν_{33} could be treated as an isolated dyad or must be analyzed as part of a larger polyad. Analysis of this complex system of vibrationally excited states is beyond the scope of the current work.

4.3. Axial cyanocyclobutane

As shown in Fig. 3 (cyan), the rotational spectrum of *axial* cyanocyclobutane ($\mu_a = 3.81 \pm 0.03$ D, $\mu_c = 1.34 \pm 0.03$ D, $\kappa = -0.931$ [27]) is readily identifiable by the distinct prolate-type bands of lesser intensity than the *equatorial* conformer. With a larger value of C_0, these bands appear to migrate across the spectrum with respect to the ground state and vibrationally excited states of the *equatorial* conformer. The initial prediction was based upon the previous reported spectroscopic constants [29] combined with computed centrifugal distortion constants. This prediction was sufficient to assign the transitions of the *axial* conformation in a straightforward manner. The least-squares fitting of *axial* cyanocyclobutane, however, is not as straightforward, as its transitions are *not* well-modeled by a single-state Hamiltonian. This is not surprising given the close energy spacing of the *axial* ground state (~240 cm^{-1}) and $2\nu_{20}$ (~284 cm^{-1}) of the *equatorial* conformer. The close energy spacing, ring-puckering potential function, and wave function for the lowest several ring-puckering vibrational states of both conformers were first described by Caminati *et al.* and are well-illustrated in Fig. 2 of that work [29] where $2\nu_{20}$ is vibrational state 2 (also labeled v(0, 2) by Durig *et al.* [26]). The spectroscopic constants presented in Table 2 are from an effective least-squares fit that is

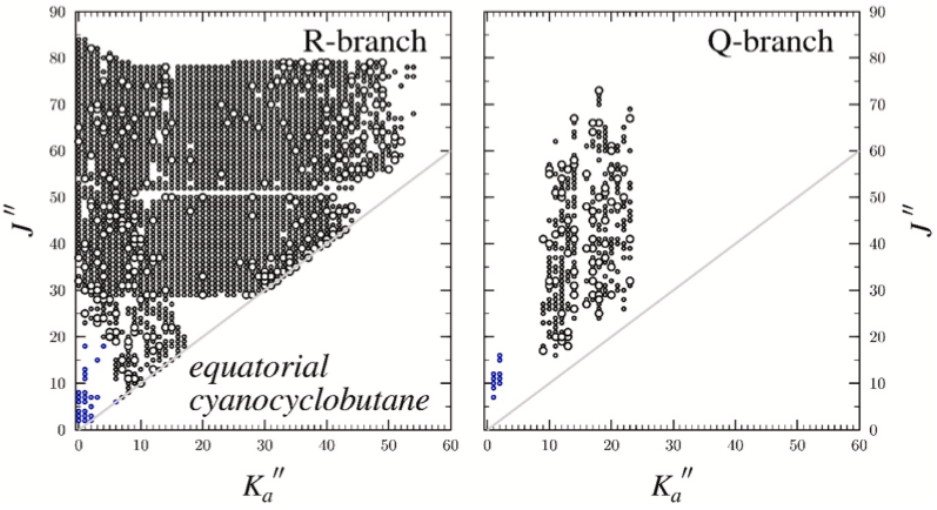


Fig. 4. Data distribution plots for the least-squares fit of spectroscopic data for the vibrational ground state of *equatorial* cyanocyclobutane. The size of the symbol is proportional to the value of $|(f_{obs.} - f_{calc.})/\delta f|$, where δf is the frequency measurement uncertainty, and all values are smaller than 3. Transitions from Caminati *et al.* [27] are in blue.

Table 1
Spectroscopic constants for the ground vibrational state of *equatorial* cyanocyclobutane (S- and A-reduced Hamiltonian, I^r representation).

	S Reduction, I^r representation			A Reduction, I^r representation	
	Experimental	B3LYP [a]		Experimental	B3LYP [a]
A_0 (MHz)	9761.90298 (22)	9604.	A_0 (MHz)	9761.90288 (22)	9604.
B_0 (MHz)	2383.395088 (44)	2375.	B_0 (MHz)	2383.398238 (44)	2375.
C_0 (MHz)	2105.124237 (47)	2094.	C_0 (MHz)	2105.121126 (48)	2094.
D_J (kHz)	0.3575750 (96)	0.349	Δ_J (kHz)	0.372006 (12)	0.362
D_{JK} (kHz)	0.863158 (66)	0.643	Δ_{JK} (kHz)	0.776529 (84)	0.562
D_K (kHz)	14.41358 (79)	15.4	Δ_K (kHz)	14.48570 (79)	15.5
d_1 (kHz)	−0.0152819 (70)	−0.0152	δ_J (kHz)	0.0152839 (70)	0.0152
d_2 (kHz)	−0.0072134 (39)	−0.00680	δ_K (kHz)	1.56035 (87)	1.45
H_J (Hz)	0.00045004 (82)	0.000437	Φ_J (Hz)	0.0004624 (13)	0.000451
H_{JK} (Hz)	−0.0045818 (83)	−0.00492	Φ_{JK} (Hz)	−0.00193 (18)	−0.00259
H_{KJ} (Hz)	0.063659 (53)	0.0628	Φ_{KJ} (Hz)	0.05457 (62)	0.0549
H_K (Hz)	−0.19705 (83)	−0.207	Φ_K (Hz)	−0.19079 (94)	−0.202
h_1 (Hz)	−0.00001113 (74)	−0.0000134	ϕ_J (Hz)	−0.00000792 (78)	−0.0000106
h_2 (Hz)	0.00000580 (54)	0.00000678	ϕ_{JK} (Hz)	0.00116 (11)	0.00122
h_3 (Hz)	0.00000301 (22)	0.00000282	ϕ_K (Hz)	0.0871 (66)	0.0767
L_J (mHz)	[0.]		L_J (μHz)	[0.]	
L_{JJK} (mHz)	[0.]		L_{JJK} (μHz)	[0.]	
L_{JK} (mHz)	−0.0005260 (42)		L_{JK} (μHz)	−0.0005922 (57)	
L_{KKJ} (mHz)	0.002274 (16)		L_{KKJ} (μHz)	0.002479 (21)	
L_K (mHz)	[0.]		L_K (μHz)	[0.]	
Δ_i (uÅ^2) [b,c]	−23.741314 (7)		Δ_i (uÅ^2) [b,c]	−23.740679 (7)	
P_{bb} (uÅ^2) [c,d]	39.899885 (3)		P_{bb} (uÅ^2) [c,d]	39.900203 (3)	
N_{lines} [e]	3158		N_{lines} [e]	3158	
σ_{fit} (MHz)	0.032		σ_{fit} (MHz)	0.032	

[a] Evaluated with the 6–311+G(2d,p) basis set. The computational output files label the representation as II^l, though we are confident that those constants are I^l which have been converted to I^r.
[b] Inertial defect, $\Delta_i = I_c - I_a - I_b$.
[c] Calculated using PLANM from the B_0 constants.
[d] Second moment, $P_{bb} = (I_c + I_a - I_b)/2$.
[e] Number of fitted transition frequencies.

Table 2
Effective spectroscopic constants for the ground vibrational state of *axial* cyanocyclobutane (S- and A-reduced Hamiltonian, I^r representation).

	S Reduction, I^r representation			A Reduction, I^r representation	
	Experimental	B3LYP [a]		Experimental	B3LYP [a]
A_0 (MHz)	7591.981 (25)	7834.2	A_0 (MHz)	7592.078 (22)	7834.2
B_0 (MHz)	2681.97940 (47)	2590.3	B_0 (MHz)	2681.98130 (48)	2590.3
C_0 (MHz)	2505.93868 (48)	2381.0	C_0 (MHz)	2505.93695 (50)	2381.0
D_J (kHz)	1.332174 (35)	1.37	Δ_J (kHz)	1.339432 (38)	1.39
D_{JK} (kHz)	−3.21013 (12)	−4.72	Δ_{JK} (kHz)	−3.25344 (15)	−4.80
D_K (kHz)	12.34 (16)	18.1	Δ_K (kHz)	12.29 (16)	18.2
d_1 (kHz)	0.128959 (74)	0.150	δ_J (kHz)	−0.129066 (75)	−0.150
d_2 (kHz)	−0.003906 (39)	−0.00635	δ_K (kHz)	0.8223 (20)	1.34
H_J (Hz)	−0.0000667 (37)	−0.00191	Φ_J (Hz)	−0.0002301 (38)	−0.00209
H_{JK} (Hz)	0.011221 (13)	0.0304	Φ_{JK} (Hz)	0.011729 (13)	0.0310
H_{KJ} (Hz)	−0.042825 (40)	−0.149	Φ_{KJ} (Hz)	−0.041946 (41)	−0.148
H_K (Hz)	[0.463]	0.463	Φ_K (Hz)	[0.462]	0.462
h_1 (Hz)	0.0002759 (80)	0.000767	ϕ_J (Hz)	0.0002650 (81)	0.000767
h_2 (Hz)	−0.0000405 (54)	−0.0000909	ϕ_{JK} (Hz)	[−0.0163]	−0.0163
h_3 (Hz)	[−0.000000544]	−0.000000544	ϕ_K (Hz)	[−0.0246]	−0.0246
Δ_i (uÅ^2) [b,c]	−53.33002 (23)		Δ_i (uÅ^2) [b,c]	−53.32890 (20)	
P_{bb} (uÅ^2) [c,d]	39.902465 (3)		P_{bb} (uÅ^2) [c,d]	39.902176 (3)	
N_{lines} [e]	987		N_{lines} [e]	987	
σ_{fit} (MHz)	0.040		σ_{fit} (MHz)	0.040	

[a] Evaluated with the 6–311+G(2d,p) basis set. The computational output files label the representation as II^l, though we are confident that those constants are I^l which have been converted to I^r.
[b] Inertial defect, $\Delta_i = I_c - I_a - I_b$.
[c] Calculated using PLANM from the B_0 constants.
[d] Second moment, $P_{bb} = (I_c + I_a - I_b)/2$.
[e] Number of fitted transition frequencies.

predictive for many of the most intense spectroscopic features of the spectrum of the *axial* conformer, but for which noticeably perturbed transition frequencies were removed from the data set. As with the *equatorial* conformation, previously reported microwave transitions from Caminati *et al.* [27] were included in the data set and are represented in Fig. 5 by blue symbols. The data set distribution plot (Fig. 5) shows curving gaps created by perturbed transitions that could not be included in the least-squares fit. Despite the removal of many hundreds of transitions, it is not possible to obtain a single-state fit of *axial* cyanocyclobutane with centrifugal distortion constants that match the sign and magnitude of the computed constants. In order to model these transitions adequately, a multi-state Hamiltonian model would be

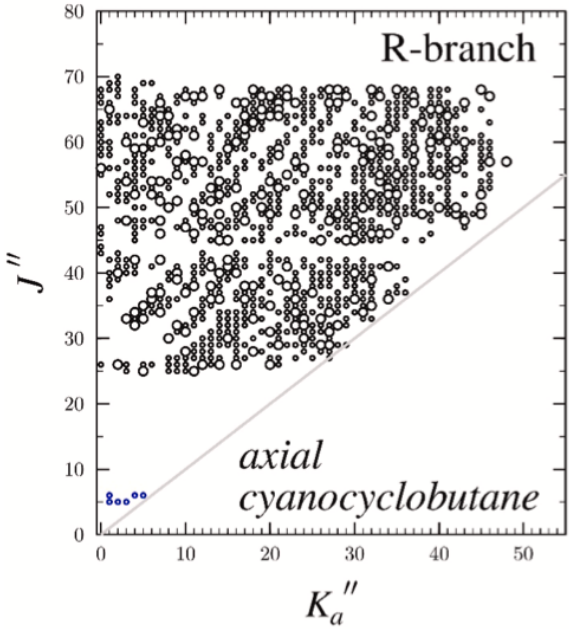


Fig. 5. Data distribution plot for the least-squares fit of spectroscopic data for the vibrational ground state of *axial* cyanocyclobutane. The size of the symbol is proportional to the value of $|(f_{obs.} - f_{calc.})/\delta f|$, where δf is the frequency measurement uncertainty. The curving gaps in the data distribution plot are suggestive of strongly perturbed transitions and untreated Coriolis coupling. Transitions from Caminati *et al.* [27] are in blue.

necessary, including the *c*-axis Coriolis interactions of the *axial* ground state (A′), $2\nu_{20}$ (A′) of the *equatorial* conformer, and ν_{19} (A′) of the *equatorial* conformer. Analysis of these interactions is beyond the scope of the current work.

4.4. Equatorial isocyanocyclobutane

Like the cyano isomer, *equatorial* isocyanocyclobutane (Fig. 2b) is a highly prolate ($\kappa = -0.916$), asymmetric top with dipole moment components along its *a*- and *c*-principal axes ($\mu_a = 4.12$ D, $\mu_c = 0.92$ D, B3LYP). No previous rotational constants have been reported for this molecule, so the initial predictions of its rotational spectrum were based upon computed rotational and centrifugal distortion constants. Using this method, over 2200 transitions of the *equatorial* conformer of isocyanocyclobutane were readily measured, assigned, and least-squares fit to a sextic A- and S-reduced, partial-octic centrifugally distorted Hamiltonian models in the I^r representation. These transitions span a comparable J and K_a range (Fig. 6) to those of *equatorial* cyanocyclobutane (Fig. 4). The rotational spectrum of isocyanocyclobutane (Fig. 7) displays a very similar structure and appearance to that of cyanocyclobutane (Fig. 3). This result is to be expected because the structural differences between the isomers (isocyano vs cyano group) lead to relatively small differences in the rotational and centrifugal distortion constants. Relative to *equatorial* cyanocyclobutane (Table 1), the spectroscopic constants of *equatorial* isocyanocyclobutane (Table 3) change by only a moderate amount. With the CN-moiety lying quite close to the *a*-principal axis, the change in A_0 is quite small (0.63 %). The changes in B_0 and C_0 are larger, reflecting the exchange of the carbon and nitrogen masses on their respective moments of inertia, but they still change by only 6.7 and 5.7 %, respectively. The changes in the centrifugal distortion constants are larger, but nevertheless the constants are generally consistent between the two isomers. Due to the decreased number of transitions available in the spectrum of isocyanocyclobutane – possibly due a lower partial pressure of isocyanocyclobutane in the gas sample, overlapping signals with impurities in the synthesized sample, or vibrationally excited states across the experimental spectrum – two of the off-diagonal sextic constants could not be satisfactorily determined. These values were held constant at their computed values. Based upon the satisfactory agreement between the computed and experimental spectroscopic constants, we believe that the spectroscopic constants provided in each least-squares fit are physically meaningful.

4.5. Search for the elusive axial isocyanocyclobutane

Unlike the cyano isomer, transitions for *axial* isocyanocyclobutane were not able to be assigned in the spectrum. They were not readily apparent as small bands moving across the equatorial spectrum like those seen for *axial* cyanocyclobutane (compare Figs. 3 and 7). The inability to assign *axial* isocyanocyclobutane may be due to several factors: lower abundance, as a consequence of the larger *axial / equatorial* energy difference for the isonitrile (1.4 kcal/mol) vs the nitrile

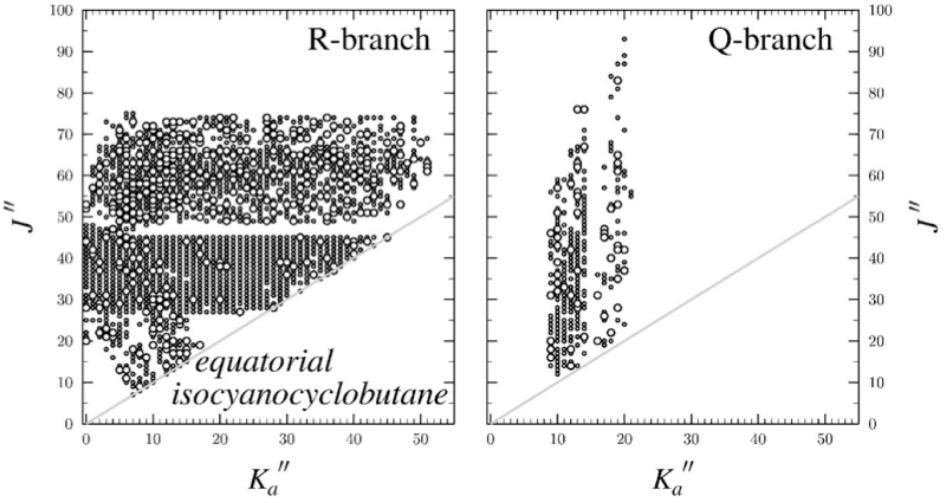


Fig. 6. Data distribution plots for the least-squares fit of spectroscopic data for the vibrational ground state of *equatorial* isocyanocyclobutane. The size of the symbol is proportional to the value of $|(f_{obs.} - f_{calc.})/\delta f|$, where δf is the frequency measurement uncertainty.

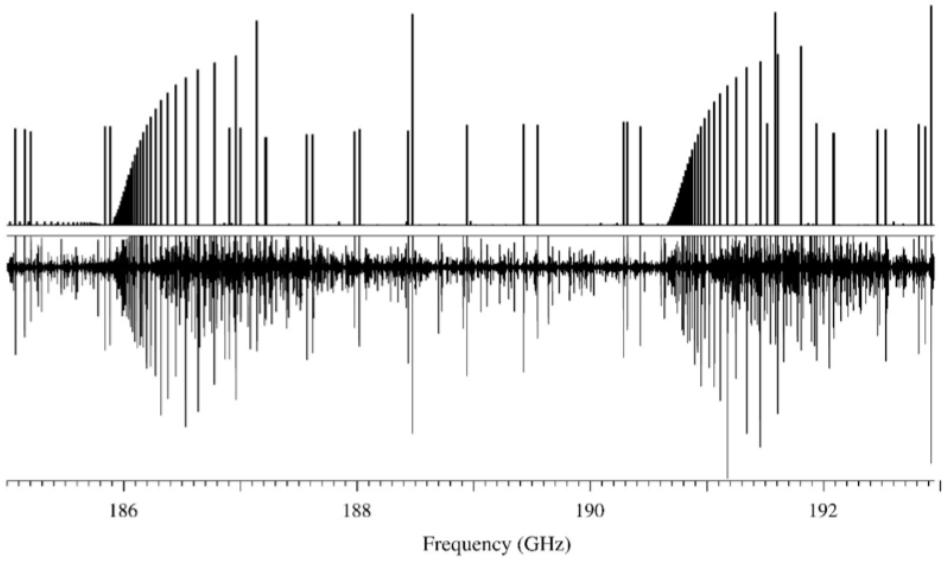


Fig. 7. Predicted (top) and experimental (bottom) rotational spectra of isocyanocyclobutane from 185 to 193 GHz. Ground-state *equatorial* isocyanocyclobutane transitions are shown for the $J' = 39$ and $J' = 40$ bands. Unassigned transitions are predominantly attributable to vibrationally excited states of *equatorial* isocyanocyclobutane.

Table 3
Spectroscopic constants for the ground vibrational state of *equatorial* isocyanocyclobutane (S- and A-reduced Hamiltonian, I^r representation).

	S Reduction, I^r representation			A Reduction, I^r representation	
	Experimental	B3LYP [a]		Experimental	B3LYP [a]
A_0 (MHz)	9823.21409 (36)	9686.7	A_0 (MHz)	9823.21373 (35)	9686.7
B_0 (MHz)	2542.019190 (63)	2525.6	B_0 (MHz)	2542.022183 (65)	2525.6
C_0 (MHz)	2226.550990 (71)	2208.5	C_0 (MHz)	2226.547590 (78)	2208.5
D_J (kHz)	0.366903 (17)	0.361	Δ_J (kHz)	0.383450 (21)	0.377
D_{JK} (kHz)	1.10893 (11)	0.965	Δ_{JK} (kHz)	1.00867 (12)	0.869
D_K (kHz)	13.3823 (16)	14.4	Δ_K (kHz)	13.4655 (16)	14.4
d_1 (kHz)	−0.016038 (14)	−0.0158	δ_J (kHz)	0.016059 (14)	0.0158
d_2 (kHz)	−0.0083226 (31)	−0.00796	δ_K (kHz)	1.57059 (57)	1.49
H_J (Hz)	0.0004756 (17)	0.000464	Φ_J (Hz)	0.0004816 (21)	0.000481
H_{JK} (Hz)	−0.004378 (16)	−0.00380	Φ_{JK} (Hz)	−0.001738 (30)	−0.000977
H_{KJ} (Hz)	0.055259 (91)	0.0492	Φ_{KJ} (Hz)	0.045768 (97)	0.0395
H_K (Hz)	−0.1540 (21)	−0.166	Φ_K (Hz)	−0.1483 (21)	−0.159
h_1 (Hz)	−0.0000342 (20)	−0.0000252	ϕ_J (Hz)	−0.0000272 (20)	−0.0000213
h_2 (Hz)	[0.00000833]	0.00000833	ϕ_{JK} (Hz)	[0.00141]	0.00141
h_3 (Hz)	[0.00000389]	0.00000389	ϕ_K (Hz)	[0.0831]	0.0831
L_J (mHz)	[0.]		L_J (μHz)	[0.]	
L_{JJK} (mHz)	[0.]		L_{JJK} (μHz)	0.0000246 (30)	
L_{JK} (mHz)	−0.0004526 (92)		L_{JK} (μHz)	−0.000554 (10)	
L_{KKJ} (mHz)	0.001076 (30)		L_{KKJ} (μHz)	0.001283 (30)	
L_K (mHz)	[0.]		L_K (μHz)	[0.]	
Δ_i (uÅ^2) [b,c]	−23.279075 (9)		Δ_i (uÅ^2) [b,c]	−23.278496 (10)	
P_{bb} (uÅ^2) [c,d]	39.807881 (3)		P_{bb} (uÅ^2) [c,d]	39.808173 (3)	
N_{lines} [e]	2296		N_{lines} [e]	2296	
σ_{fit} (MHz)	0.039		σ_{fit} (MHz)	0.039	

[a] Evaluated with the 6–311+G(2d,p) basis set. The computational output files label the representation as II^l, though we are confident that those constants are I^l which have been converted to I^r.
[b] Inertial defect, $\Delta_i = I_c - I_a - I_b$.
[c] Calculated using PLANM from the B_0 constants.
[d] Second moment, $P_{bb} = (I_c + I_a - I_b)/2$.
[e] Number of fitted transition frequencies.

(0.73 kcal/mol); additional spectral congestion arising from impurities in the synthesized sample, making the patterns less recognizable; or increased perturbation of transition frequencies due to coupling with the vibrationally excited states of the equatorial conformation, relative to the nitrile isomer. Attempts to predict the spectrum using the computed constants (B3LYP) or from empirical shifts derived from the experimental and computed constants of *axial* cyanocyclobutane were insufficient to identify this conformer by Loomis-Wood plots of its predicted series. While we are confident that the *axial* conformational isomer should have transitions with observable intensities in our frequency range, a successful detection appears to require higher sample purity of isocyanocyclobutane, better initial predictions, and/or addressing the

Coriolis coupling of this conformer to other vibrational states.

4.6. Ratio of axial and equatorial cyanocyclobutane

Utilizing transitions for the *equatorial* and *axial* conformers of cyanocyclobutane that have been confidently assigned and measured, it is possible to estimate the *equatorial* to *axial* ratio using the same methodology recently employed for determining the ratio of *anti*- to *gauche*-4-cyano-1-butyne [50]. This method, which relies on predicted intensities from SPCAT using the previously reported dipole moments for each conformer [26,27], yields an energy difference of 0.69 (7) kcal/mol for the *equatorial* and *axial* conformers of cyanocyclobutane. This value is consistent with the value reported by Caminati *et al.* of 0.73 (14) kcal/mol [27]. The newly determined value of 0.69 (7) kcal/mol is in good agreement with the computed value of 0.9 kcal/mol (B3LYP; Fig. 2). This close agreement for cyanocyclobutane gives us confidence that the conformational equilibrium of *axial* and *equatorial* isocyanocyclobutane is also being reasonably modeled *via* B3LYP. Using the computed energy difference of 1.4 kcal/mol, the *axial* to *equatorial* ratio for isocyanocyclobutane should be approximately 0.09 at 298 K. Details of the analysis are provided in the supplementary material.

4.7. Structural interpretation of the rotational constants

For the set of non-planar, C_s symmetry molecules presented in this work, a few conclusions are possible concerning these structures by analyzing the Δ_i and P_{bb} constants provided in Tables 1, 2, and 3 [51]. The inertial defect values (Δ_i) provide structural information regarding the extent to which all of the atoms are not located on the *ab* plane. The similarity between the inertial defects of *equatorial* cyano- and isocyanocyclobutane (differing by less than 2 %) is not surprising given their structural similarity. As is shown in Fig. 2., the *ab* plane lies just below the carbon atom bonded to the CN group and nearly bisects the CN substituent. In contrast, when the CN group is *axial*, the principal axes rotate to place the ring atoms and CN group further from the *ab* plane, nearly causing a doubling of the inertial defect. The second moment P_{bb} is arguably a more meaningful structural parameter. Due to the C_s nature of these species, where the plane of symmetry coincides with the *ac* plane, P_{bb} provides direct information about the distance of the CH_2 groups relative to the *ac* plane. For *axial* and *equatorial* cyanocyclobutane the S-reduction value of P_{bb} is remarkably consistent (39.902 and 39.900, respectively), indicating that the ring-puckering is not substantially impacted by the orientation of the cyano group. There are only slight differences in the P_{bb} values of mono-substituted cyclobutanes shown in Table 4, which indicates that the structure of the cyclobutane rings are reasonably consistent regardless of substitution of σ electron-withdrawing substituents with low steric profile. This is expected given the aforementioned consistency of the potential energy surfaces of these species.

5. Conclusion

The transition frequencies and spectroscopic constants for cyanocyclobutane and isocyanocyclobutane, presented in this work, provide the foundation for future astronomical searches for these molecules. Combined with nuclear hyperfine coupling constants, these constants should be useful for predicting lower or slightly higher energy transition frequencies reliably. Nuclear hyperfine coupling constants for isocyanocyclobutane need to be measured or estimated from high level *ab initio* calculations to enable this analysis. Our study also revealed previously unrecognized Coriolis-coupling interactions between the *axial* conformation of cyanocyclobutane and the vibrationally excited states of the *equatorial* conformation. In order to implement the challenging analysis of these couplings, additional spectroscopy including high resolution infrared spectroscopy would be very beneficial, due to the potentially large number of involved vibrational states and their close energy spacing.

Table 4
Second Moments (P_{bb}) for Mono-substituted Cyclobutanes.

Species	P_{bb} (uÅ^2)	Reference
fluorocyclobutane (*ax*)	39.967	[52]
fluorocyclobutane (*eq*)	39.805	[52]
chlorocyclobutane (*ax*)[a]	39.830	[53]
chlorocyclobutane (*eq*)[a]	39.842	[53]
bromocyclobutane (*eq*)[a]	39.943	[54]
cyanocyclobutane (*ax*)	39.902	this work
cyanocyclobutane (*eq*)	39.900	this work
isocyanocyclobutane (eq)	39.808	this work

[a] Data provided for the most abundant isotopologue.

6. Synthetic procedures and characterization

***N*-Cyclobutylformamide** [37,44]. In a single-neck 100 mL round-bottom flask, 6.12 g (86 mmol) cyclobutylamine and 60 mL (742 mmol) ethyl formate were combined. The reaction flask was connected to a water-cooled reflux condenser, and the stirred reaction was heated to reflux for 4 hr. After cooling to room temperature, excess ethyl formate was removed *in vacuo* to yield the crude product as a yellow oil. The crude oil was purified *via* short-path vacuum distillation (bp = 72 °C, 1 Torr) to yield *N*-cyclobutylformamide as a viscous, colorless oil (8.29 g, 97 %). ^{1}H NMR ($CDCl_3$, 400 MHz): The product was observed as two separate conformational isomers in a 4:1 ratio. δ (ppm) ***equatorial*:** 8.03 (s, 1H), 7.30 (brs, 1H), 4.43 (m, 1H), 2.31 (m, 2H) 1.97 (m, 2H), 1.72 (m, 2H). ***axial*:** 8.06 (s, 1H), 7.20 (brs, 1H), 4.00 (m, 1H), 2.31 (m, 2H) 1.97 (m, 2H), 1.72 (m, 2H). ^{13}C NMR ($CDCl_3$, 100 MHz): δ (ppm) ***equatorial*:** 160.6, 43.3, 30.7, 15.1. ***axial*:** 163.5, 47.3, 31.6, 14.4. IR (neat): (cm^{-1}) 3269 (m), 3047 (w), 2978 (m), 2862 (m), 1652 (s), 1528 (m), 1384 (m), 1344 (m), 1303 (m), 1253 (m), 730 (m), 600 (w), 455 (m). HRMS: $[M + H]^+$ Calculated for $C_5H_{10}NO$: 100.0757. Found: 100.0755; $[M + Na]^+$ Calculated for C_5H_9NONa: 122.0576. Found: 122.0574.

Isocyanocyclobutane [37]. In a flame-dried, single-neck 100 mL round-bottom flask (cooled under a stream of N_2), 24.23 g (127 mmol) *p*-toluenesulfonyl chloride and 49 g (380 mmol) dry quinoline were combined. The flask was then connected to a one-piece Claisen-type distillation apparatus with a 50 mL receiving vessel. The Claisen head was sealed with a rubber septum and the system was purged (2 ×) *via* vacuum/N_2 backfill cycles. The receiving vessel was cooled with liquid nitrogen and the boiling flask was heated to 50 °C in an oil bath. *N*-Cyclobutylformamide (8.29 g, 83.7 mmol) was then added dropwise to the heated solution of *p*-toluenesulfonyl chloride/quinoline over a course of 10 min *via* syringe needle. A vacuum (100 Torr) was applied to the system, and the crude distillate was collected over the next 40 min. The resulting distillate was further purified (to remove traces of quinoline) *via* trap-to-trap distillation (2 ×) to yield isocyanocyclobutane (2.71 g, 40 %) as a volatile, colorless oil with an intense, foul odor. ^{1}H NMR ($CDCl_3$, 500 MHz): δ (ppm) 3.95 (*p*, 1H, *J* = 8 Hz), 2.42 (*m*, 2H), 2.32 (*m*, 2H), 1.90 (*m*, 1H) 1.79 (*m*, 1H). ^{13}C NMR ($CDCl_3$, 125 MHz): δ (ppm) 155.3, 45.0, 31.1, 15.9. IR (neat): (cm^{-1}) 2994 (m), 2955 (m), 2874 (w), 2137 (s), 1444 (w), 1347 (m), 1248 (w), 1123 (w), 1052 (m), 937 (m), 896 (m), 746 (w), 467 (m). HRMS: $[M + H]^+$ Calculated for C_5H_8N: 82.0651. Found: 82.0648.

Declaration of Competing Interest

The authors declare that they have no known competing financial interests or personal relationships that could have appeared to influence the work reported in this paper.

Data availability

Data will be made available on request.

Acknowledgments

We gratefully acknowledge the National Science Foundation for support of this project (CHE-1954270). We thank Michael McCarthy for the loan of an amplification-multiplication chain. We thank the following organizations and individuals for support of shared departmental facilities: Bruker AVANCE 400 NMR spectrometer (NSF CHE-1048642), Bruker AVANCE 500 NMR spectrometer (gift from Paul J. and Margaret M. Bender), and Thermo Scientific Q Exactive Plus mass spectrometer (NIH 1S10 OD020022-1). We thank Maria Zdanovskaia for her assistance with generating figures.

Appendix A. Supplementary material

Computational chemistry output files, least-squares fitting output files from SPFIT, and experimental IR, ^{1}H NMR, ^{13}C NMR, and mass spectra of all synthesized compounds.

Supplementary data to this article can be found online at https://doi.org/10.1016/j.jms.2022.111684.

References

[1] H.S.P. Müller, F. Schlöder, J. Stutzki, G. Winnewisser, The Cologne Database for Molecular Spectroscopy, CDMS: a Useful Tool for Astronomers and Spectroscopists, J. Mol. Struct. 742 (1–3) (2005) 215–227.
[2] H.S.P. Müller, S. Thorwirth, D.A. Roth, G. Winnewisser, The Cologne Database for Molecular Spectroscopy, CDMS, Astron. Astrophys. 370 (3) (2001) L49–L52.
[3] L.E. Snyder, D. Buhl, Detection of Several New Interstellar Molecules, Ann. New York Acad. Sci. 194 (1 Interstellar) (1972) 17–24.
[4] B. Zuckerman, M. Morris, P. Palmer, B.E. Turner, Observations of CS, HCN, U89.2, and U90.7 in NGC 2264, Astrophys. J. 173 (1972) L125–L129.
[5] J. Cernicharo, C. Kahane, M. Guelin, J. Gomez-Gonzalez, Tentative Detection of CH_3NC towards SGR B2, Astron. Astrophys. 189 (1988) L1–L2.
[6] P.M. Solomon, K.B. Jefferts, A.A. Penzias, R.W. Wilson, Detection of Millimeter Emission Lines from Interstellar Methyl Cyanide, Astrophys. J. 168 (1971) L107–L110.
[7] K. Kawaguchi, M. Ohishi, S.-I. Ishikawa, N. Kaifu, Detection of Isocyanoacetylene HCCNC in TMC-1, Astrophys. J. 386 (1992) L51–L53.
[8] N.W. Broten, J.M. MacLeod, L.W. Avery, W.M. Irvine, B. Hoglund, P. Friberg, A. Hjalmarson, The detection of interstellar methylcyanoacetylene, Astrophys. J. 276 (1984) L25–L29.
[9] N.W. Broten, T. Oka, L.W. Avery, J.M. MacLeod, H.W. Kroto, The detection of HC_9N in interstellar space, Astrophys. J. 223 (1978) L105–L107.
[10] F.F. Gardner, G. Winnewisser, The detection of interstellar vinyl cyanide (acrylonitrile), Astrophys. J. 195 (1975) L127–L130.
[11] F.J. Lovas, A.J. Remijan, J.M. Hollis, P.R. Jewell, L.E. Snyder, Hyperfine Structure Identification of Interstellar Cyanoallene toward TMC-1, Astrophys. J. 637 (1) (2006) L37–L40.
[12] C.N. Shingledecker, K.L.K. Lee, J.T. Wandishin, N. Balucani, A.M. Burkhardt, S. B. Charnley, R. Loomis, M. Schreffler, M. Siebert, M.C. McCarthy, B.A. McGuire, Detection of interstellar H_2CCCHC_3N, Astron. Astrophys. 652 (2021) L12.
[13] M.A. Siebert, K.L.K. Lee, A.J. Remijan, A.M. Burkhardt, R.A. Loomis, M. C. McCarthy, B.A. McGuire, CH_3-Terminated Carbon Chains in the GOTHAM Survey of TMC-1: Evidence of Interstellar CH_3C_7N, Astrophys. J. 924 (1) (2022) 21.
[14] L.E. Snyder, T.L. Wilson, C. Henkel, P.R. Jewell, C.M. Walmsley, Detection of Interstellar Methylcyanodiacetylene in the Dark Dust Cloud TMC 1, Bull. Am. Astron. Soc. 16 (1984) 959.
[15] B.A. McGuire, R.A. Loomis, A.M. Burkhardt, K.L.K. Lee, C.N. Shingledecker, S. B. Charnley, I.R. Cooke, M.A. Cordiner, E. Herbst, S. Kalenskii, M.A. Siebert, E. R. Willis, C.i. Xue, A.J. Remijan, M.C. McCarthy, Detection of two interstellar polycyclic aromatic hydrocarbons via spectral matched filtering, Science 371 (6535) (2021) 1265–1269.
[16] B.A. McGuire, A.M. Burkhardt, S. Kalenskii, C.N. Shingledecker, A.J. Remijan, E. Herbst, M.C. McCarthy, Detection of the aromatic molecule benzonitrile (c-C_6H_5CN) in the interstellar medium, Science 359 (6372) (2018) 202–205.
[17] K.L. Kelvin Lee, P.B. Changala, R.A. Loomis, A.M. Burkhardt, C.i. Xue, M. A. Cordiner, S.B. Charnley, M.C. McCarthy, B.A. McGuire, Interstellar Detection of 2-cyanocyclopentadiene, C_5H_5CN, a Second Five-membered Ring toward TMC-1, Astrophys. J. 910 (1) (2021) L2.
[18] M.C. McCarthy, K.L.K. Lee, R.A. Loomis, A.M. Burkhardt, C.N. Shingledecker, S. B. Charnley, M.A. Cordiner, E. Herbst, S. Kalenskii, E.R. Willis, C.i. Xue, A. J. Remijan, B.A. McGuire, Interstellar detection of the highly polar five-membered ring cyanocyclopentadiene, Nat. Astron. 5 (2) (2021) 176–180.
[19] A. Belloche, R.T. Garrod, H.S.P. Müller, K.M. Menten, C. Comito, P. Schilke, Increased complexity in interstellar chemistry: detection and chemical modeling of ethyl formate and *n*-propyl cyanide in Sagittarius B2(N), Astron. Astrophys. 499 (1) (2009) 215–232.
[20] A. Belloche, T. Garrod Robin, S.P. Müller Holger, M. Menten Karl, Detection of a branched alkyl molecule in the interstellar medium: *iso*-propyl cyanide, Science 345 (6204) (2014) 1584–1587.
[21] H.H. Smith, S.M. Kougias, B.J. Esselman, R.C. Woods, R.J. McMahon, Synthesis, Purification, and Rotational Spectroscopy of 1-Cyanocyclobutene (C_5H_5N), J. Phys. Chem. A 126 (12) (2022) 1980–1993.
[22] D.L. Powell, A. Gatial, P. Klaeboe, C.J. Nielsen, A.J. Kondow, W.A. Boettner, A. M. Mulichak, Vibrational spectra and conformations of cyanocyclobutane, Acta Chem. Scand. 43 (5) (1989) 441–449.
[23] F. Vazart, C. Latouche, P. Cimino, V. Barone, Accurate Infrared (IR) Spectra for Molecules Containing the C≡N Moiety by Anharmonic Computations with the Double Hybrid B2PLYP Density Functional, J. Chem. Theor. Comput. 11 (9) (2015) 4364–4369.
[24] J.R. Durig, A. Ganguly, J.J. Klaassen, G.A. Guirgis, The r_0 structural parameters, conformational stability, and vibrational assignment of *equatorial* and *axial* cyanocyclobutane, J. Mol. Struct. 923 (1) (2009) 28–38.
[25] M.Y. Fong, M.D. Harmony, Microwave spectrum, dipole moment, quadrupole coupling constants, and conformation of cyanocyclobutane, J. Chem. Phys. 58 (10) (1973) 4260–4264.
[26] J.R. Durig, L.A. Carreira, W.J. Lafferty, Spectra and structure of small ring compounds. Microwave spectrum of cyanocyclobutane, J. Mol. Spectrosc. 46 (2) (1973) 187–193.
[27] W. Caminati, B. Velino, M. Dakkouri, L. Schäfer, K. Siam, J.D. Ewbank, Reinvestigation of the microwave spectrum of cyanocyclobutane: Assignment of the *axial* conformer, J. Mol. Spectrosc. 123 (2) (1987) 469–475.
[28] M. Dakkouri, H. Ephardt, K. Siam, L. Schäfer, C. Van Alsenoy, A combined ab initio and gas electron diffraction study of the molecular structure of 1,1-dicyanocyclobutane, J. Mol. Struct. 159 (1) (1987) 123–135.
[29] W. Caminati, B. Velino, R.G. Della Valle, Rotational spectra of several vibrational excited states of *axial* and *equatorial* cyanocyclobutane and potential energy function of the ring puckering, J. Mol. Spectrosc. 129 (2) (1988) 284–292.
[30] T. Egawa, T. Fukuyama, S. Yamamoto, F. Takabayashi, H. Kambara, T. Ueda, K. Kuchitsu, Molecular structure and puckering potential function of cyclobutane studied by gas electron diffraction and infrared spectroscopy, J. Chem. Phys. 86 (11) (1987) 6018–6026.
[31] D.L. Powell, A. Gatial, P. Klaeboe, C.J. Nielsen, A.J. Kondow, Conformational behaviour of five cyclobutane derivatives, J. Mol. Struct. 173 (1988) 389–396.
[32] R. Pasternak, A.Y. Meyer, Cyclobutane: a unified theoretical approach, J. Mol. Struct. 13 (2) (1972) 201–210.
[33] A. Gatial, P. Klaeboe, C.J. Nielsen, D.L. Powell, D. Sülzle, A.J. Kondow, Vibrational spectra and conformations of chloro- and bromo-cyclobutane, J. Raman Spectrosc. 20 (4) (1989) 239–250.
[34] M. Meier, B. Dogan, D. Beckhaus, C. Ruechardt, Heats of formation and heats of isomerization of isocyanides, New J. Chem. 11 (1) (1987) 1–6.
[35] M. Meier, B. Mueller, C. Ruechardt, The isonitrile-nitrile rearrangement. A reaction without a structure-reactivity relationship, J. Org. Chem. 52 (4) (1987) 648–652.
[36] W. Dianxun, Q. Ximei, Z. Qiyuan, The isonitrile-nitrile isomerization: kinetic parameters, reaction mechanism and relative photoionization cross-section of the HOMO. A HeI photoelectron spectroscopy study, Chem. Phys. Lett. 266 (5) (1997) 560–567.
[37] J. Casanova Jr., R.E. Schuster, N.D. Werner, Synthesis of aliphatic isocyanides, J. Chem. Soc. (Aug.) (1963) 4280–4281.
[38] J. Casanova, N.D. Werner, R.E. Schuster, The Isonitrile—Nitrile Isomerization, J. Org. Chem. 31 (11) (1966) 3473–3482.
[39] Z. Li, X. Xu, Y. Chen, J. Liu, W. Li, Preparation of 6-substituted benzodiazepine-2,4-dione compounds for treating cancer, East China University of Science and Technology, Peop. Rep. China; Chinese patent, CN 103435562 (Dec 11, 2013).
[40] M.J. Orwat, D.J.P. Pinto, L.M. Smith, II, S. Srivastava, Preparation of substituted tetrahydroisoquinoline compounds as factor Xia inhibitors, Bristol-Myers Squibb Company, USA; WO patent, WO 2013056034 (Apr 18, 2013).
[41] P. Capurro, L. Moni, A. Galatini, C. Mang, A. Basso, Multi-Gram Synthesis of Enantiopure 1,5-Disubstituted Tetrazoles Via Ugi-Azide 3-Component Reaction, Molecules 23 (11) (2018) 2758.
[42] M.J. Frisch, G.W. Trucks, H.B. Schlegel, G.E. Scuseria, M.A. Robb, J.R. Cheeseman, G. Scalmani, V. Barone, G.A. Petersson, H. Nakatsuji, X. Li, M. Caricato, A.V. Marenich, J. Bloino, B.G. Janesko, R. Gomperts, B. Mennucci, H.P. Hratchian, J.V. Ortiz, A.F. Izmaylov, J.L. Sonnenberg, D. Williams-Young, F. Ding, F. Lipparini, F. Egidi, J. Goings, B. Peng, A. Petrone, T. Henderson, D. Ranasinghe, V.G. Zakrzewski, J. Gao, N. Rega, G. Zheng, W. Liang, M. Hada, M. Ehara, K. Toyota, R. Fukuda, J. Hasegawa, M. Ishida, T. Nakajima, Y. Honda, O. Kitao, H. Nakai, T. Vreven, K. Throssell, J.A. Montgomery, Jr. , J.E. Peralta, F. Ogliaro, M.J. Bearpark, J.J. Heyd, E.N. Brothers, K.N. Kudin, V.N. Staroverov, T.A. Keith, R. Kobayashi, J. Normand, K. Raghavachari, A.P. Rendell, J.C. Burant, S.S. Iyengar, J. Tomasi, M. Cossi, J.M. Millam, M. Klene, C. Adamo, R. Cammi, J.W. Ochterski, R.L. Martin, K. Morokuma, O. Farkas, J.B. Foresman, D.J. Fox, Gaussian 16 rev C.01, Gaussian, Inc., Wallingford, CT, USA, 2016.
[43] J.R. Schmidt, W.F. Polik, WebMO Enterprise, version 19.0; WebMO LLC: Madison, WI, USA, 2019; http://www.webmo.net (accessed August, 2019).
[44] G. Giardina, G.D. Clarke, G. Dondio, G. Petrone, M. Sbacchi, V. Vecchietti, Selective.kappa.-Opioid Agonists: Synthesis and Structure-Activity Relationships of Piperidines Incorporating an Oxo-Containing Acyl Group, J. Med. Chem. 37 (21) (1994) 3482–3491.

[45] B.K. Amberger, B.J. Esselman, J.F. Stanton, R.C. Woods, R.J. McMahon, Precise Equilibrium Structure Determination of Hydrazoic Acid (HN_3) by Millimeter-wave Spectroscopy, J. Chem. Phys. 143 (10) (2015), 104310.
[46] B.J. Esselman, B.K. Amberger, J.D. Shutter, M.A. Daane, J.F. Stanton, R.C. Woods, R.J. McMahon, Rotational spectroscopy of pyridazine and its isotopologs from 235–360 GHz: Equilibrium structure and vibrational satellites, J. Chem. Phys. 139 (22) (2013), 224304.
[47] Z. Kisiel, L. Pszczółkowski, B.J. Drouin, C.S. Brauer, S. Yu, J.C. Pearson, I. R. Medvedev, S. Fortman, C. Neese, Broadband rotational spectroscopy of acrylonitrile: Vibrational energies from perturbations, J. Mol. Spectrosc. 280 (2012) 134–144.
[48] Z. Kisiel, L. Pszczółkowski, I.R. Medvedev, M. Winnewisser, F.C. De Lucia, E. Herbst, Rotational spectrum of *trans–trans* diethyl ether in the ground and three excited vibrational states, J. Mol. Spectrosc. 233 (2) (2005) 231–243.
[49] H.M. Pickett, The fitting and prediction of vibration-rotation spectra with spin interactions, J. Mol. Spectrosc. 148 (2) (1991) 371–377.
[50] P.M. Dorman, B.J. Esselman, P.B. Changala, S.M. Kougias, M.C. McCarthy, R. C. Woods, R.J. McMahon, Rotational spectrum of *anti*- and *gauche*-4-cyano-1-butyne (C_5H_5N) – An open-chain isomer of pyridine, J. Mol. Spectrosc. 385 (2022), 111604.
[51] R.K. Bohn, J.A. Montgomery, H.H. Michels, J.A. Fournier, Second moments and rotational spectroscopy, J. Mol. Spectrosc. 325 (2016) 42–49.
[52] W. Caminati, L.B. Favero, A. Maris, P.G. Favero, Microwave spectrum of the *axial* conformer and potential energy function of the ring puckering motion in fluorocyclobutane, J. Mol. Struct. 376 (1) (1996) 25–32.
[53] B. Velino, L.B. Favero, W. Caminati, Rotational Spectrum of the *Axial* Form and Conformational Equilibrium in Chlorocyclobutane, J. Mol. Spectrosc. 179 (1) (1996) 168–174.
[54] W.G. Rothschild, B.P. Dailey, Microwave Spectrum of Bromocyclobutane, J. Chem. Phys. 36 (11) (1962) 2931–2940.

Appendix I

Precise Equilibrium Structures of 1*H*- and 2*H*-1,2,3-Triazoles ($C_2H_3N_3$) by Millimeter-wave Spectroscopy

Maria A. Zdanovskaia
Brian J. Esselman
Samuel M. Kougias
Brent K. Amberger
John F. Stanton
R. Claude Woods
Robert J. McMahon

The Journal of Chemical Physics, 2022, *157*, 084305

The Journal of Chemical Physics ARTICLE scitation.org/journal/jcp

Precise equilibrium structures of 1*H*- and 2*H*-1,2,3-triazoles ($C_2H_3N_3$) by millimeter-wave spectroscopy

Cite as: J. Chem. Phys. **157**, 084305 (2022); doi: 10.1063/5.0097750
Submitted: 1 May 2022 • Accepted: 15 July 2022 •
Published Online: 23 August 2022

View Online Export Citation CrossMark

Maria A. Zdanovskaia,[1] Brian J. Esselman,[1] Samuel M. Kougias,[1] Brent K. Amberger,[1] John F. Stanton,[2,a)] R. Claude Woods,[1,a)] and Robert J. McMahon[1,a)]

AFFILIATIONS

[1] Department of Chemistry, University of Wisconsin–Madison, Madison, Wisconsin 53706, USA
[2] Quantum Theory Project, Departments of Physics and Chemistry, University of Florida, Gainesville, Florida 32611, USA

[a)] **Authors to whom correspondence should be addressed:** johnstanton@chem.ufl.edu, rcwoods@wisc.edu, and robert.mcmahon@wisc.edu

ABSTRACT

The 1*H*- and 2*H*-1,2,3-triazoles are isomeric five-membered ring, aromatic heterocycles that may undergo chemical equilibration by virtue of intramolecular hydrogen migration (tautomerization). Using millimeter-wave spectroscopy in the 130–375 GHz frequency range, we measured the spectroscopic constants for thirteen 1*H*-1,2,3-triazole and sixteen 2*H*-1,2,3-triazole isotopologues. Herein, we provide highly accurate and highly precise semi-experimental equilibrium (r_e^{SE}) structures for the two tautomers based on the spectroscopic constants of each set of isotopologues, together with vibration–rotation interaction and electron-mass distribution corrections calculated using coupled-cluster singles, doubles, and perturbative triples calculations [CCSD(T)/cc-pCVTZ]. The resultant structures are compared with a "best theoretical estimate" (BTE), which has recently been shown to be in exceptional agreement with the semi-experimental equilibrium structures of other aromatic molecules. Bond distances of the 1*H* tautomer are determined to <0.0008 Å and bond angles to <0.2°. For the 2*H* tautomer, bond angles are also determined to <0.2°, but bond distances are less precise ($2\sigma \leq 0.0015$). Agreement between BTE and r_e^{SE} values is discussed.

Published under an exclusive license by AIP Publishing. https://doi.org/10.1063/5.0097750

INTRODUCTION

1*H*- and 2*H*-1,2,3-Triazole ($C_2H_3N_3$, Fig. 1) are near-oblate, asymmetric rotors ($\kappa = 0.94$, C_s and 0.82, C_{2v}, respectively). The tautomers, as well as a few of their isotopologues, have been studied using ultraviolet,[1] infrared (IR),[1–4] Raman,[3] and microwave[5–8] spectroscopy. The 1*H*/2*H* tautomerism and equilibrium have received a fair amount of interest.[5,8–15] Both of the tautomers are present in the solid,[11] liquid,[4,10,12,13] and gas[5,9,10,13–15] phases. Although 1*H*-1,2,3-triazole is preferentially stabilized in polar solvents,[12] the 2*H*-1,2,3-triazole tautomer is estimated to be more stable by ~3.5–4.5 kcal/mol in the gas phase.[5,9,10,13] Despite the greater abundance of the 2*H* tautomer in the gas phase, its smaller dipole moment (μ_b = 0.10 D) relative to that of the 1*H* tautomer (μ_a = 4.2 D, μ_b = 0.77 D) results in both molecules being observable in the gas phase by millimeter-wave spectroscopy at room temperature.

While the structures of the triazoles have been computed at a variety of levels of theory,[3,16,17] and there has been a crystal-structure determination,[11] there has been only a single attempt to determine a gas-phase, equilibrium structure of 1,2,3-triazole. Begtrup *et al.*[5] used electron diffraction and microwave spectroscopy data to approximate an equilibrium structure for 2*H*-1,2,3-triazole. That structure determination, however, used microwave data from only three isotopologues. To date, there have been no attempts to determine the gas-phase structure of 1*H*-1,2,3-triazole. Following the pioneering work of Pulay, Meyer, and Boggs,[18] semi-experimental structure (r_e^{SE}) determination has evolved into a powerful method for establishing gas-phase molecular structure.[19,20] Semi-experimental structures for a variety of small heterocyclic compounds have been reported using a density functional theory version of the method.[21] Recently, we used coupled-cluster computations to achieve high-accuracy and high-precision semi-experimental equilibrium structure (r_e^{SE}) determinations of

Published under an exclusive license by AIP Publishing

The Journal of Chemical Physics ARTICLE scitation.org/journal/jcp

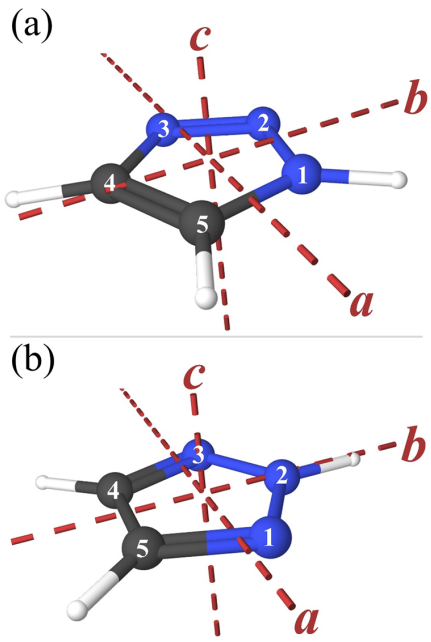


FIG. 1. (a) 1*H*-1,2,3-triazole and (b) 2*H*-1,2,3-triazole structures with principal inertial axes and atom numbering.

pyrimidine,[20] pyridazine,[22] thiophene,[23] thiazole,[24] and benzene.[25] We, therefore, sought to determine semi-experimental equilibrium structures for the 1,2,3-triazoles.

In our recent studies of structures of the six-membered ring molecules (which include only first- and second-row elements), the r_e^{SE} structures displayed exceptional agreement with the purely computational, "best theoretical estimate" (BTE) structures. Structures of two sulfur-containing, five-membered ring molecules, however, had BTE parameters that did not uniformly fall within the r_e^{SE} parameter uncertainties. Those discrepancies were plausibly ascribed to the proximity of certain atoms to principal axes,[23,24,26] combined with the inability to shift those atoms from the principal axes upon isotopic substitution (because the heavy sulfur atom essentially set the axes' orientation). 2*H*-1,2,3-Triazole offers the possibility to examine the above assertion—one nitrogen atom and one hydrogen atom lie directly on the *b*-axis, but the principal axes are easily rotated upon isotopic substitution. The ability to obtain well-determined parameters involving the on-axis atoms would support the idea that the near-axis sulfur atom was the culprit behind difficulties in previously examined five-membered ring structure determinations.

The precise determination of spectroscopic constants of the 1,2,3-triazoles achieved in the current study—particularly the determination of the centrifugal distortion constants—enables accurate prediction of the high-intensity transitions across a large range of frequencies for possible search in the interstellar medium (ISM) or in other harsh environments, such as Saturn's moon, Titan. There is considerable current interest in identifying aromatic molecules[27] and nitrogen heterocycles[28,29] in these environments, and such studies may be particularly relevant to the nitrogen-rich atmosphere of Titan, where the structurally related molecule, 1*H*-1,2,4-triazole, has been suggested as a likely tholin component.[30,31] Although these molecules are not believed to be naturally occurring on Earth, they have been found to act as effective mimics in a variety of biological applications[32,33] with beneficial properties, such that 1,2,3-triazole-containing species are now widely targeted pharmaceuticals.[34] In terms of organic chemistry, 1*H*-1,2,3-triazole is the stable product of the Huisgen cycloaddition (a 1,3-dipolar cycloaddition) between hydrazoic acid and acetylene.[35] This is a quintessential example of "Click chemistry" where two small molecules generate an aromatic product in a highly exothermic reaction.[36,37] Acetylene has been detected in the ISM[38,39] and on Titan.[40] Amberger *et al.* assigned the rotational spectrum of hydrazoic acid,[41] allowing for its search and potential identification. The detection (or not) of these molecules could be informative regarding the chemistry in various environments.

In this study, we observed transitions between 130 and 375 GHz for 1*H*- and 2*H*-1,2,3-triazoles, as well as several of their heavy-atom and deuterium-substituted isotopologues. Spectroscopic constants for many of the non-standard isotopologues are reported for the first time, and the spectroscopic constants for the standard isotopologues determined here include a full set of quartic, along with several sextic, centrifugal distortion constants. Presently, these and the spectroscopic constants of the isotopologues are used to obtain semi-experimental equilibrium structures for 1*H*- and 2*H*-1,2,3-triazoles, using a total of 13 isotopologues for the former and 16 for the latter.

EXPERIMENTAL METHODS

1*H*-1,2,3-triazole and 2*H*-1,2,3-triazole were obtained from Sigma-Aldrich (97% purity) and Oakwood Chemical (98% purity). The initial sample obtained (from Sigma-Aldrich) was pink and that from Oakwood was colorless. Initial rotational spectra were collected using the Sigma-Aldrich sample without further purification. In order to observe low-abundance isotopologues, a sample was later purified by Kugelrohr distillation. The sample from Sigma-Aldrich contained pyridazine and pyrazole as major impurities, identified by the previously collected rotational spectrum,[42] and measured rotational constants.[43–45] Deuteriated samples were prepared as described later.

Continuous broadband spectra in the 130–230 and 250–375 GHz ranges were collected using 5–30 mTorr sample pressures at room temperature. The instrument has been described previously.[41,42,46] The low- and high-frequency spectra were combined into a single spectral file using Assignment and Analysis of Broadband Spectra (AABS) software.[47,48] Additional short-frequency-range scans were collected with increased numbers of scans for low-abundance isotopologues. Data were analyzed using ASFIT and ASROT,[49] along with the AC program.[50,51] In our least-squares fits, we assume a uniform 50 kHz frequency measurement uncertainty for all transitions, including those from Stiefvater *et al.*[8] All least-squares output files are provided in the supplementary material.

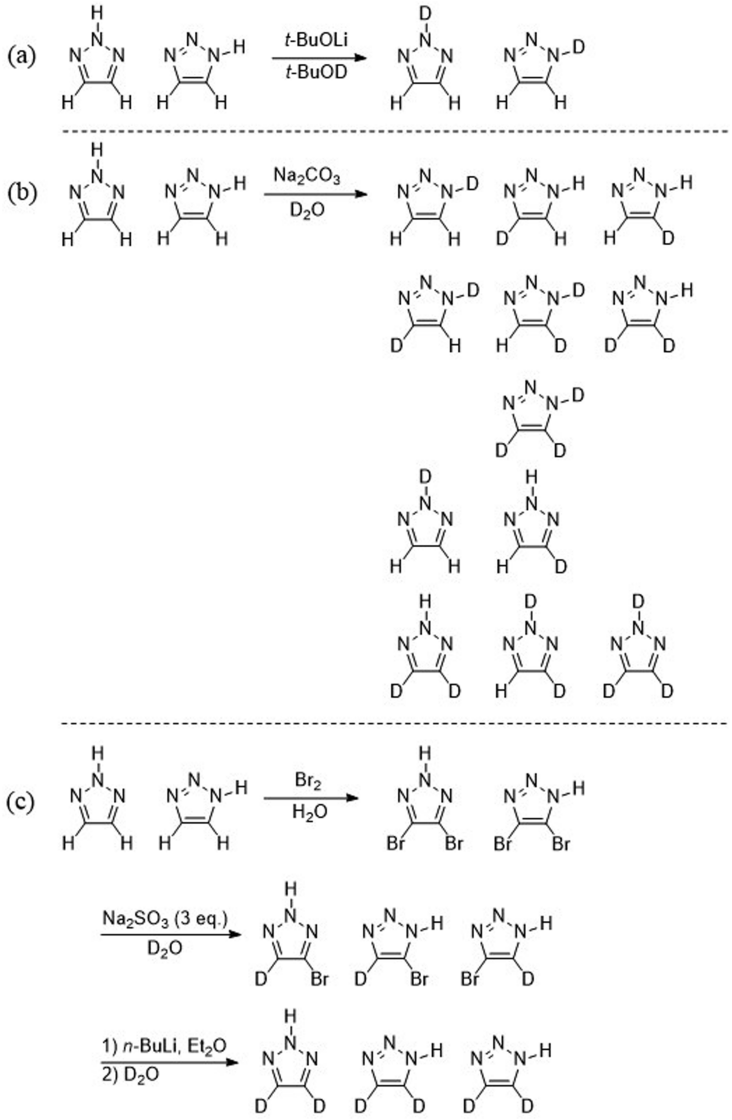
Published under an exclusive license by AIP Publishing

The Journal of Chemical Physics ARTICLE scitation.org/journal/jcp

COMPUTATIONAL METHODS

Calculations were carried out using a development version of CFOUR.[52] The 1*H*- and 2*H*-1,2,3-triazole structures were first optimized at the CCSD(T)/cc-pCVTZ level of theory. The optimized geometries and the same level of theory were subsequently used for anharmonic, second-order vibrational perturbation theory (VPT2) calculations, wherein cubic force constants are evaluated using analytical second derivatives at displaced points,[53–55] for each 1,2,3-triazole tautomer and magnetic properties calculations for each isotopologue. The "best theoretical estimate" (BTE) for each tautomer was evaluated as described previously,[20,22–24] and details are provided in the supplementary material.

Using the experimental, averaged determinable rotational constants and computational electron-mass distribution and vibration–rotation interaction corrections as input, the *xrefit* module of CFOUR calculates the moments of inertia and semi-experimental equilibrium structure. Since (1) the *Z*-matrix whose parameters are determined in this routine must comprise the minimal parameters necessary to geometrically define the entire



SCHEME 1. Deuterium incorporation in 1*H*- and 2*H*-1,2,3-triazoles: (a) *N*-deuteriation by strong base, (b) *C*-deuteriation by weak base, and (c) three-step sequence to achieve a high level of deuterium content at C-4 and C-5.

Published under an exclusive license by AIP Publishing

The Journal of Chemical Physics ARTICLE scitation.org/journal/jcp

molecular structure and (2) standard error propagation assumes independent uncertainties, multiple *Z*-matrices had to be employed for each 1,2,3-triazole tautomer in order to obtain all parameters of interest and their proper uncertainty values. The *xrefiteration* routine,[22] which begins by determining a structure using a single isotopic substitution at each position and then sequentially adds the most uncertainty-minimizing isotopologue to the structural least-squares fit until all available isotopologues are incorporated, was used to determine the suitability of the triazole isotopologues for the structure determination.

Computational output files are provided in the supplementary material.

SYNTHESIS OF DEUTERIO TRIAZOLES

The preparation of deuterium-containing isotopologues of 1,2,3-triazole was not as straightforward as for pyridazine[42] and pyrimidine.[20] H/D exchange using a strong base (*t*-BuOLi/*t*-BuOD), adapted from Esselman *et al.*[42] and depicted in Scheme 1(a), was attempted, but produced a detectable quantity of only the *N*-deuteriated species. Alternate synthetic routes involving Grignard or organolithium reagents were considered, and the route depicted in Scheme 1(c) resulted in the successful generation of 1,2,3-triazole isotopologues with deuterium at the carbon positions. During the course of attempting to generate singly carbon-deuteriated 1,2,3-triazole using a set of steps similar to those in Scheme 1(c), however, it was recognized that weak bases, such as carbonate, result in the exchange of both bromine and hydrogen/deuterium at the carbon atoms. This observation led us to develop the reaction in Scheme 1(b). Detailed synthetic procedures for the reactions depicted in Scheme 1 are provided in the supplementary material.

ANALYSIS OF ROTATIONAL SPECTRA

Transitions of 2*H*-1,2,3-triazole are more intense than those of the 1*H* tautomer, despite the larger dipole moment of the latter, confirming the greater population of the 2*H* than 1*H* tautomer in the gas phase. The spectrum of 2*H*-1,2,3-triazole (normal isotopologue) features *b*-type, R-branch transitions ($^{b}R_{1,1}$, and $^{b}R_{-1,1}$). The spectrum of 1*H*-1,2,3-triazole (normal isotopologue) exhibits both *a*- and *b*-type, R-branch transitions ($^{a}R_{0,1}$, $^{b}R_{1,1}$, and $^{b}R_{-1,1}$), of which the *a*-type transitions are more intense. Certain isotopic substitutions in both triazole tautomers result in substantial rotation of the principal axes. For the 1*H* tautomer, such rotations can alter which of the dipole components (and corresponding transitions) are larger, and for the 2*H* tautomer, some isotopologues have *a*-type or both *a*- and *b*-type transitions. Figure 2 shows a small portion of an experimental spectrum in the 291.0–296.5 GHz range, which includes four isotopologues of each tautomer. Despite the presence of multiple triazole species, the spectrum is quite sparse as a result of each tautomer's bands being separated by ~10 GHz (~2*C*). Such a separation fortuitously made it possible to analyze multiple isotopologues in a single spectrum without substantial loss of useable transition data. Even so, several of the lowest-intensity species could not be identified in the experimental spectra using their purely computationally predicted spectroscopic constants. These species were identified only after an r_e^{SE} structure of each tautomer (obtained using most, but not all, of the isotopologues in the final isotopologue set) was used to reverse-predict the rotational constants. These constants, combined with the computational centrifugal distortion constants, enabled the identification and fitting of transitions for the very low-intensity isotopologues.

Transitions of the ground vibrational states of observed isotopologues have typical oblate-type band structures; transitions progress to higher frequency away from the $K_a = 0$ transition with increasing K_a and concurrently decreasing J in our frequency region. Bandheads of 1*H*-1,2,3-triazole appear as four degenerate transitions: two $^{a}R_{0,1}$ ($J = K_a + K_c$ and $J + 1 = K_a + K_c$) transitions and two *b*-type ($^{b}R_{1,1}$ and $^{b}R_{-1,1}$), while those of the 2*H* tautomer are made up of the two degenerate *b*-type transitions. For both tautomers, these transitions lose degeneracy near $K_a = 12$ in our frequency

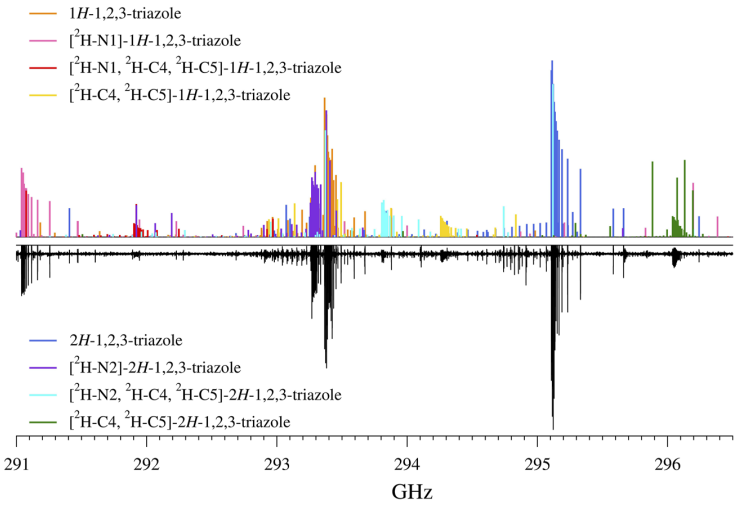


FIG. 2. Predicted stick spectra from 291.0 to 296.5 GHz (top) and experimental spectrum (bottom) of the normal and several deuteriated isotopologues of 1,2,3-triazoles. Transitions belonging to vibrationally excited states are also discernible.

Published under an exclusive license by AIP Publishing

The Journal of Chemical Physics ARTICLE scitation.org/journal/jcp

region. Q-branch transitions were also observed for both tautomers. Data distribution plots for the all isotopologues, showing the breadth of quantum numbers observed, are provided in the supplementary material.

Table I provides the 1*H* and 2*H*-1,2,3-triazole spectroscopic constants determined in this work alongside those determined by Begtrup *et al.*[5] and those predicted computationally in the S reduction, III^r representation. The predicted rotational constants for both triazoles are within 0.1% of the experimental values. All of the predicted centrifugal distortion constants are within 10% of the experimental values for the 1*H* tautomer, with the exceptions of d_2 and H_J (whose predicted values are in error by 50% and 80%, respectively). All of the predicted centrifugal distortion constants of the 2*H* tautomer are within 22% of their experimental values. Despite the previous determination of the spectroscopic constants by Begtrup *et al.*[5] using only partial quartic Hamiltonians (using τ terms), the rotational constants are in reasonable agreement with those determined in the current work. The spectroscopic constants of the triazoles determined in the A reduction (provided in the supplementary material) are also in reasonable agreement with the computed values, validating the use of the computed values when centrifugal distortion constants could not be determined experimentally. (Due to the similar values of A_0 and B_0 for each of the triazoles, the A reduction, III^r representation does not effectively determine the spectroscopic constants, so only the A reduction, I^r representation constants were determined.) Using both reductions enabled us to calculate the determinable constants from each reduction, compare the values, and use their average in the structure determination to eliminate the effects of reduction on the structure. A comparison of the determinable constants calculated from each reduction is provided in the supplementary material and gives confidence that the parameters used for the r_e^{SE} were determined accurately.

The heavy-atom isotopologues for both triazoles were observed at natural abundance in the same spectrum as the normal isotopologues. Using the previously described deuteriation methods, isotopologues substituting each H atom, and even some of their heavy-atom variants, were also analyzed. In total, 13 isotopologues were used for the 1*H*-1,2,3-triazole structure determination, and 16 isotopologues contributed to that of 2*H*-1,2,3-triazole. Although the 1*H* tautomer benefitted from the presence of both *a*- and *b*-type transitions, its smaller transition intensity and its lower symmetry (C_s) relative to that of the 2*H* tautomer (C_{2v}) made analyzing heavy-atom isotopologues more challenging. Where isotopologues substituting two of the nitrogen atoms and both of the carbon atoms of the 2*H* tautomer had their transition intensities doubled due to symmetry in any species that retained C_{2v} symmetry prior to heavy-atom substitution, none of the 1*H* isotopologues had such intensity enhancement. Most of the isotopologues were identified in the spectra based on their predicted spectroscopic constants, although some of the very low-intensity species required a more accurate prediction of their rotational constants using *xrefit* after the other isotopologues had been analyzed and included in the structural least-squares fit. For species where some spectroscopic constants could not be

TABLE I. Experimental and computational spectroscopic constants for 1*H*- and 2*H*-1,2,3-triazole, normal isotopologue, ground vibrational state (S-reduced Hamiltonian, III^r representation).

	1*H*-1,2,3-triazole			2*H*-1,2,3-triazole		
	CCSD(T)[a]	Current work	Begtrup *et al.* (Ref. 5)[b]	CCSD(T)[a]	Current work	Begtrup *et al.* (Ref. 5)[b]
A_0 (MHz)	10 036	10 030.800 90(26)	10 030.785(8)	10 257	10 252.030 69(14)	10 255.006(13)
B_0 (MHz)	9 877	9 870.690 16(27)	9 870.675(8)	9 783	9 776.988 76(14)	9 776.969(13)
C_0 (MHz)	4 976	4 972.941 28(21)	4 972.933(8)	5 005	5 002.457 56(15)	5 002.448(10)
D_J (kHz)	3.61	3.683 91(31)		3.58	3.653 40(22)	
D_{JK} (kHz)	−5.65	−5.772 36(19)		−5.59	−5.716 73(11)	
D_K (kHz)	2.43	2.490 22(25)		2.41	2.465 545(99)	
d_1 (MHz)	0.036 3	0.039 02(35)		0.093 5	0.113 422(57)	
d_2 (kHz)	0.008 04	0.016 033(77)		0.018 5	0.015 176(85)	
H_J (Hz)	0.001 38	0.000 77(15)		0.001 43	0.001 18(11)	
H_{JK} (Hz)	−0.006 00	−0.006 040(54)		−0.006 05	−0.006 138(35)	
H_{KJ} (Hz)	0.007 85	0.007 94(13)		0.007 80	0.007 836(58)	
H_K (Hz)	−0.003 23	−0.002 95(15)		−0.003 18	[−0.003 18]	
h_1 (Hz)	0.000 154	[0.000 154]		0.000 013 8	[0.000 013 8]	
h_2 (Hz)	−0.000 248	[−0.000 248]		−0.000 145	[−0.000 145]	
h_3 (Hz)	0.000 125	[0.000 125]		0.000 015 7	[0.000 015 7]	
N_{lines}[c]		838[d]			915	
σ (MHz)		0.033			0.023	

[a] B_e values evaluated using the cc-pCV5Z basis set and corrected for vibration–rotation interaction and electron-mass distribution evaluated using the cc-pCVTZ basis.
[b] Constants as reported in Ref. 5.
[c] Number of independent transitions.
[d] Transitions reported by Stiefvater *et al.*[8] are included in the least-squares fit.

Published under an exclusive license by AIP Publishing

The Journal of Chemical Physics ARTICLE scitation.org/journal/jcp

determined, these parameters were held constant at their predicted values. Tables of spectroscopic parameters for all measured isotopologues of 1*H*-1,2,3-triazole and 2*H*-1,2,3-triazole (S reduction, III^r representation; A reduction, I^r representation; comparison of determinable constants), along with data distribution plots, are provided in the supplementary material.

SEMI-EXPERIMENTAL EQUILIBRIUM STRUCTURE (r_e^{SE})

Spectroscopic constants determined in both A and S reductions (B_0) were converted to determinable constants (B'') using Eqs. S(1)–S(6) in the supplementary material. The agreement between these two sets of parameters (within 0.04 MHz) confirmed that the rotational and quartic centrifugal distortion constants were determined with sufficient accuracy for use in the structure determination. The two sets of determinable constants were averaged and input into *xrefit*, along with vibration–rotation interaction and electron-mass distribution corrections predicted at the CCSD(T)/cc-pCVTZ level of theory. The *xrefit* module uses the values to calculate the equilibrium rotational constants (B_e) using Eq. (1), where the second term is the vibration–rotation interaction correction, $\frac{m_e}{M_p}$ is the electron-to-proton mass ratio, B'' is the determinable constant, and $g^{\beta\beta}$ is the corresponding magnetic g-tensor component.

$$B_e^{\beta} = B''^{\beta} + \frac{1}{2}\sum_i \alpha_i^{\beta} - \frac{m_e}{M_P} g^{\beta\beta} B^{\beta}. \quad (1)$$

These rotational constants are then used to calculate the inertial defect (Δ_i), which is precisely zero for a rigid, planar molecule. Absent either of the computational corrections, it is evident from Table II that the observable inertial defect (Δ_{i0}) is ~0.04 uÅ^2 for both triazole tautomers. As observed for other heterocyclic molecules,[20–24] inclusion of the vibration–rotation interaction correction decreases the inertial defect (Δ_{ie}) to a small negative value, and subsequent application of the electron-mass correction brings the magnitude of the inertial defect (Δ_{ie}) quite close to zero. In close similarity to several other heterocyclic aromatic molecules, all of the fully corrected inertial defect values for 1*H*-1,2,3-triazole are positive, with an average value of 0.0013 ± 0.0001 uÅ^2. Strikingly, the fully corrected inertial defect values for the 2*H* tautomer are both positive and negative. Their average value is 0.000 09 ± 0.0003 uÅ^2, a value that is approximately two orders of magnitude smaller than that observed in previous structure determinations. For the nitrogen-substituted benzene analog, pyrimidine,[20] and pyridazine,[22] the fully CCSD(T)-corrected inertial defect values were consistently negative with an average value of −0.0011 uÅ^2. For thiophene[23] and thiazole,[24] these inertial defect values were consistently positive with average values also close to 0.001 uÅ^2. It is, therefore, interesting, but not obvious as to why, the 2*H*-1,2,3-triazole isotopologues exhibit corrected inertial defect values over an order of magnitude smaller than those observed previously. The numbers of transitions observable for the 2*H*-1,2,3-triazole species are smaller than those observable for other previously examined molecules, many of whose transitions numbered in the thousands. It is, therefore, unlikely that the spectroscopic constants for 2*H*-triazole are somehow better determined than those for other molecules. It is alternately conceivable that the spectroscopic constants used for the structure determination were heavily affected by having too

TABLE II. Inertial defects (Δ_i) of triazole isotopologues from various determinations of the moments of inertia.

1*H*-1,2,3-triazole				2*H*-1,2,3-triazole			
Isotopologue	Δ_{i0} (uÅ^2)	Δ_{ie} (uÅ^2)[a]	Δ_{ie} (uÅ^2)[b]	Isotopologue	Δ_{i0} (uÅ^2)	Δ_{ie} (uÅ^2)[a]	Δ_{ie} (uÅ^2)[b]
$C_2H_3N_3$	0.043 0	−0.008 86	0.001 35	$C_2H_3N_3$	0.0399	−0.009 60	0.000 239
[4-^{13}C]-	0.043 6	−0.008 94	0.001 27	[4-^{13}C]-	0.0404	−0.009 68	0.000 162
[5-^{13}C]-	0.043 6	−0.008 85	0.001 35	[2-^{15}N]-	0.0401	−0.009 76	0.000 087
[1-^{15}N]-	0.043 3	−0.008 98	0.001 23	[1-^{15}N]-	0.0405	−0.009 58	0.000 258
[2-^{15}N]-	0.043 4	−0.009 02	0.001 18	[4-^{2}H]-	0.0401	−0.009 47	0.000 380
[4-^{2}H]-	0.043 1	−0.008 97	0.001 23	[2-^{2}H]-	0.0343	−0.009 97	−0.000 123
[5-^{2}H]-	0.042 7	−0.008 86	0.001 34	[2-^{2}H, 4-^{13}C]-	0.0349	−0.009 82	0.000 030
[1-^{2}H]-	0.038 5	−0.008 93	0.001 27	[2-^{2}H, 1-^{15}N]-	0.0347	−0.009 88	−0.000 028
[1,4-^{2}H]-	0.038 5	−0.009 04	0.001 17	[2,4-^{2}H]-	0.0343	−0.009 86	−0.000 010
[1,5-^{2}H]-	0.038 2	−0.008 95	0.001 26	[2,4,5-^{2}H]-	0.0346	−0.010 05	−0.000 201
[1,4,5-^{2}H]-	0.038 3	−0.009 01	0.001 20	[1,2,3–^{15}N]-	0.0413	−0.009 55	0.000 288
[1,2,3-^{15}N]-	0.044 6	−0.008 78	0.001 43	[2-^{2}H, 1,2,3-^{15}N]-	0.0356	−0.009 83	0.000 015
[4,5-^{2}H]-	0.042 93	−0.008 88	0.001 33	[4,5-^{2}H]-	0.0405	−0.009 69	0.000 153
Average (x̄)	**0.041 8**	**−0.008 9**	**0.001 3**	[4,5-^{2}H, 4-^{13}C]-	0.0411	−0.009 32	0.000 528
Std. Dev. (s)	**0.002 4**	**0.000 1**	**0.000 1**	[4-^{2}H, 4-^{13}C]-	0.0404	−0.009 65	0.000 199
				[4-^{2}H, 5–^{13}C]-	0.0398	−0.010 35	−0.000 503
				Average (x̄)	**0.0383**	**−0.009 75**	**0.000 092**
				Std. Dev. (s)	**0.0029**	**0.000 25**	**0.000 245**

[a]Vibration–rotation interaction corrections only.
[b]Vibration–rotation interaction and electron-mass corrections.

Published under an exclusive license by AIP Publishing

The Journal of Chemical Physics ARTICLE scitation.org/journal/jcp

few transitions measured to determine many parameters, resulting in many parameters held constant at their predicted values, generating an artificially close agreement between the experimentally determined and computed constants. If the experimental constants were to agree perfectly with computed values, then the corrections at the same level of theory would result in ideal inertial defect values. This, however, is not the case, as some isotopologues with a small number of transitions (21 for [4-^{2}H, 5-^{13}C] and 41 for [4,5-^{2}H, 4-^{13}C]) and with the fewest spectroscopic parameters able to be determined have the largest magnitude of fully corrected inertial defect values. Meanwhile, those species with inertial defect values particularly close to zero vary from 60 to 632 transitions analyzed and have between three and all five quartic centrifugal distortion constants determined. Importantly, this discrepancy between 2*H*-1,2,3-triazole and other molecules does not appear to indicate a problem. The small values of the fully corrected inertial defects for both 1*H* and 2*H* tautomers indicate again that the spectroscopic constants are sufficiently well determined to be used in the structure determination.

The semi-experimental equilibrium structure parameters of 1*H* and 2*H*-1,2,3-triazole resulting from 13 to 16 isotopologues, respectively, are depicted in Fig. 3 and enumerated in Tables III and IV. The 2σ statistical uncertainties of the 1*H*-1,2,3-triazole bond distances are all <0.0008 Å. Corresponding uncertainties in the internal bond angles are <0.06°, while those of external angles are <0.2°. Overall, the parameters are determined to a similar degree of precision as those of thiazole.[24] Surprisingly, despite the larger number of isotopologues used to determine fewer structural parameters, the 2σ bond distance uncertainties for 2*H*-1,2,3-triazole are approximately a factor of two greater than for 1*H*-1,2,3-triazole. The only bond distance in the symmetrical isomer determined to better than 0.001 Å is that of the two equivalent C–H bond distances. All three angles of 2*H*-1,2,3-triazole have uncertainties just under 0.1°. The observation that the 2*H*-1,2,3-triazole structure is less well-determined than the 1*H* tautomer would seem to suggest that perhaps some of the isotopologues in the structure determination were providing conflicting information, resulting in larger parameter uncertainties. While the effect of isotopologue inclusion on structure indeed supports this idea, it is unclear whether the inclusion of the isotopologues in question is detrimental to the accuracy of the resultant parameters (*vide infra*).

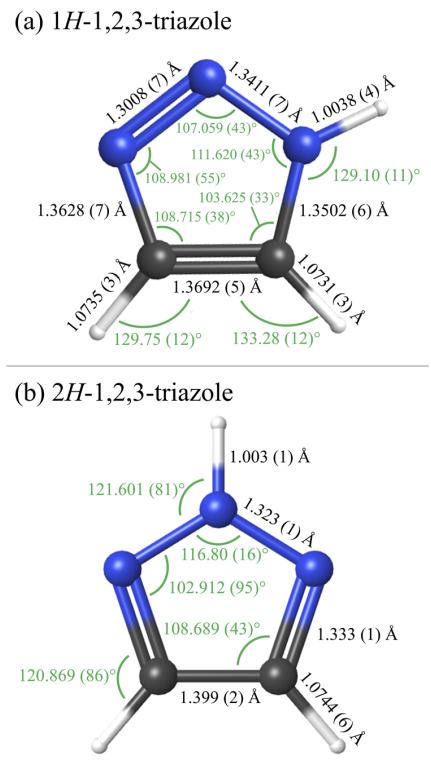


FIG. 3. Semi-experimental equilibrium structures (r_e^{SE}): (a) 1*H*-1,2,3-triazole and (b) 2*H*-1,2,3,-triazole with 2σ statistical uncertainties from least-squares fitting the isotopologue moments of inertia.

TABLE III. Structural parameters of 1*H*-1,2,3-triazole.

	r_e^{SE} CCSD(T)/ cc-pCVTZ	CCSD(T) BTE	CCSD(T)/ cc-pCV5Z
R_{C4-H} (Å)	1.073 5(3)	1.073 69	1.073 58
R_{C4-C5} (Å)	1.369 2(5)	1.369 49	1.369 39
R_{C5-H} (Å)	1.073 1(3)	1.073 30	1.073 2
R_{N3-C4} (Å)	1.362 8(7)	1.362 72	1.362 22
R_{N1-C5} (Å)	1.350 2(6)	1.350 35	1.349 90
R_{N2-N3} (Å)	1.300 8(7)	1.301 14	1.300 07
R_{N1-H} (Å)	1.003 8(4)	1.003 90	1.003 70
R_{N1-N2} (Å)	1.341 1(7)[a]	1.342 21[b]	1.340 26[b]
$\theta_{C5-C4-H}$ (°)	129.75(12)	129.662	129.636
$\theta_{C4-C5-H}$ (°)	133.28(12)	133.421	133.360
$\theta_{N3-C4-C5}$ (°)	108.715(38)	108.714	108.693
$\theta_{N1-C5-C4}$ (°)	103.625(33)	103.654	103.603
$\theta_{N2-N3-C4}$ (°)	108.981(55)	109.003	109.000
$\theta_{C5-N1-H}$ (°)	129.10(11)	128.900	129.152
$\theta_{N2-N1-C5}$ (°)	111.620(43)[a]	111.59[b]	111.63[b]
$\theta_{N1-N2-N3}$ (°)	107.059(43)[a]	107.04[b]	107.07[b]
$N_{isotopologues}$	13		

[a]Redundant parameters and uncertainties determined by using alternate *Z*-matrices.
[b]Redundant parameters not determined directly; calculated using geometry.

BEST THEORETICAL ESTIMATE

As described previously,[20,22–25] the best theoretical estimate (BTE) is based on a CCSD(T)/cc-pCV5Z optimized structure with four additional corrections that address:

1. residual basis set effects beyond cc-pCV5Z,
2. residual electron correlation effects beyond the CCSD(T) treatment,
3. effects of scalar (mass-velocity and Darwin) relativistic effects,
4. the fixed-nucleus approximation *via* the diagonal Born–Oppenheimer correction.

Published under an exclusive license by AIP Publishing

The Journal of Chemical Physics ARTICLE scitation.org/journal/jcp

TABLE IV. Structural parameters of 2*H*-1,2,3-triazole.

	Begtrup *et al.* (Ref. 5)	r_e^{SE} CCSD(T)/cc-pCVTZ	CCSD(T) BTE	CCSD(T)/cc-pCV5Z
R_{N2-H} (Å)	0.997	1.003(1)	1.003 48	1.003 3
R_{N1-N2} (Å)	1.317	1.323(1)	1.322 37	1.321 0
R_{N1-C5} (Å)	1.339	1.333(1)	1.333 54	1.332 9
R_{C4-H} (Å)	1.069	1.0744(6)	1.074 16	1.074 06
R_{C4-C5} (Å)	1.398	1.399(2)[a]	1.399 35[b]	1.399 41[b]
$\theta_{N1-N2-H}$ (°)	121.5[c]	121.601(81)	121.569	121.560
$\theta_{N2-N3-C4}$ (°)	103.0[c]	102.912(95)	102.894	102.92
$\theta_{N1-C5-H}$ (°)	138.5[c]	120.869(86)	120.887	120.928
$\theta_{N1-N2-N3}$ (°)	117.1[d]	116.80(16)[a]	116.862[b]	116.881[b]
$\theta_{N1-C5-C4}$ (°)	108.5[c]	108.689(43)[a]	108.675[b]	108.636[b]
$N_{isotopologues}$	3[e]	16		

[a]Parameters and uncertainties determined by using alternate *Z*-matrices.
[b]Parameters not determined directly; calculated using geometry.
[c]Parameters not determined directly in original work; calculated here for comparison.
[d]Angle held constant at *ab initio* value.
[e]Microwave work examined standard isotopologue, as well as [1,2,3-^{15}N]- and [2-^{2}H, 1,2,3-^{15}N]-2*H*-1,2,3-triazoles.

Equations used to calculate these corrections and the values of each of these corrections for both 1,2,3-triazole tautomers are provided in the supplementary material (Tables S-VIII and S-IX). One of the most important factors of the algorithm used to determine the BTE is the estimation of residual basis set effects, specifically estimated as the difference between the (directly computed) cc-pCV5Z geometry at the CCSD(T) level of theory and the estimate of the CCSD(T) geometry at the basis set limit. Following others,[19] the latter is obtained by assuming an exponential convergence pattern with respect to the highest angular momentum basis functions present in the basis. For 1*H*-1,2,3-triazole, there are decidedly non-exponential patterns exhibited by a few of the geometrical parameters, as revealed by careful consideration of the computational data that is provided in the supplementary material. For example, the N–H bond distance computed with the cc-pCVQZ basis is actually shorter (but minimally so) than that with cc-pCV5Z, a direct violation of the standard pattern of decreasing bond lengths with respect to basis expansion. In this case—where the cc-pCV5Z distance is shorter than cc-pCVTZ and longer than cc-pCVQZ—the behavior is not even qualitatively exponential, and extrapolation is meaningless. Similarly, while the angles $\theta_{C4-C5-H}$ and $\theta_{C5-N1-H}$ exhibit a monotonic pattern of change between cc-pCVTZ and cc-pCV5Z, the cc-pCVTZ/QZ difference is smaller than the cc-pCVQZ/5Z difference. The triple- to quintuple-zeta N-H bond distance and $\theta_{N1-C5-H}$ of the 2*H* tautomer also exhibit non-exponential behavior. This leads to quite unreliable extrapolated values for all of these parameters.

It is notable that two of the three problematic parameters of 1*H*-1,2,3-triazole correspond to those which are conspicuous in the comparison of BTE and semi-experimental parameters. For the $\theta_{C4-C5-H}$ angle, the BTE (133.42°) falls just above the range of the semi-experimental determination (133.28 (12)°), while the respective values for $\theta_{C5-N1-H}$ are 128.90° and 129.10 (11)° (Table III). If the cc-pCV5Z angles are used instead of the dubious extrapolated values, the so-modified BTE angles become 133.36° and 129.16°, respectively, both of which lie within the corresponding semi-experimental uncertainty ranges. The source of the non-exponential behavior is unclear, although challenges posed by the electronic structure effects associated with the corresponding geometric displacements might be at work here. To further investigate this issue, calculations were carried out with the core-weighted (cc-pwCV*X*Z) basis sets (Table S-VIII), but the three problematic parameters still exhibit the same qualitative behavior. The dubious nature of the corresponding extrapolations is further evidenced by the fact that all extrapolated distances and angles with the cc-pwCV*X*Z extrapolation are within 0.0002 Å and 0.02°, respectively, of the corresponding cc-pCV*X*Z results for the non-problematic results, but differences in the problematic parameters are at least an order of magnitude larger (Table S-VIII). This results from the fact that the underlying data are not well-described by the approximation of exponential convergence, and it might well be better here to substitute the cc-pCV5Z results for those obtained by the extrapolation procedure.

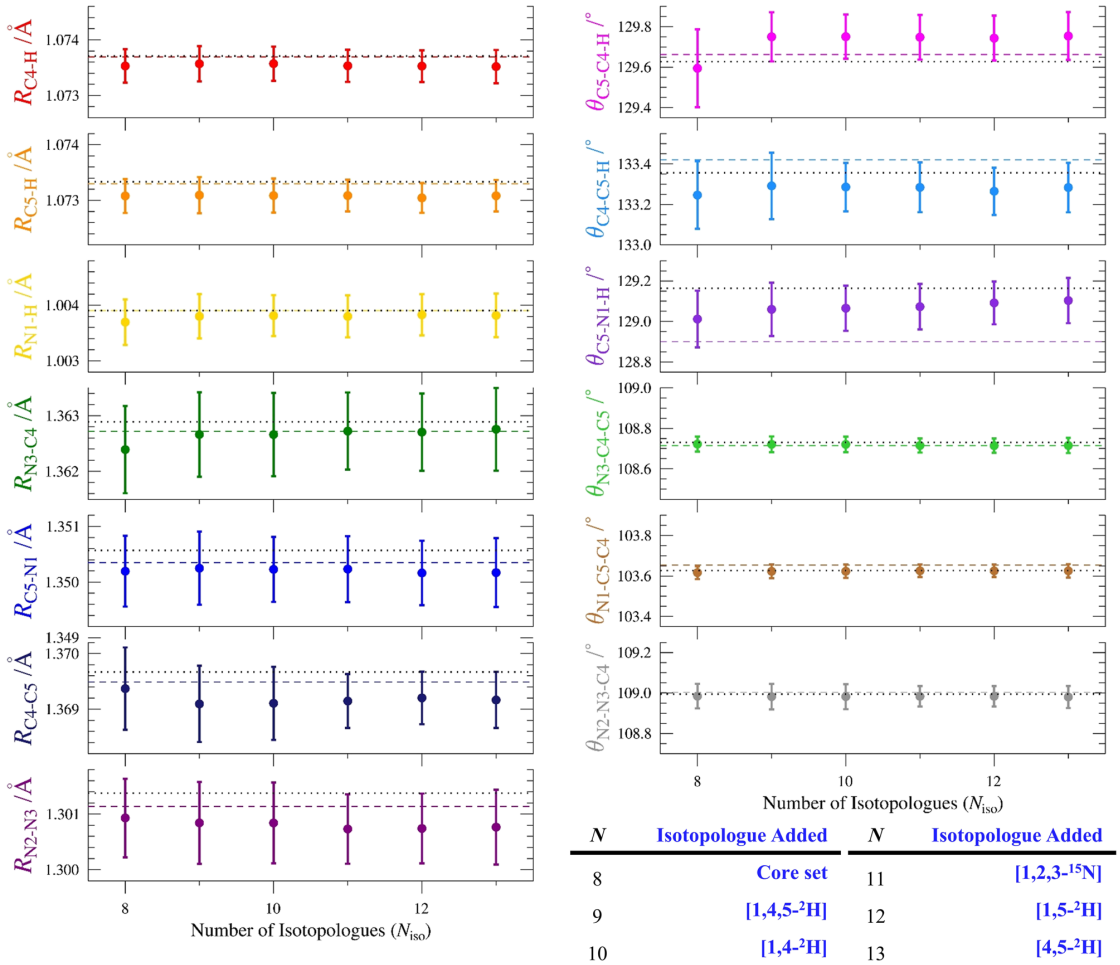
DISCUSSION

As has become standard in our recent structure determinations, the effect of including the available isotopologues in the r_e^{SE} structure is examined using *xrefiteration*. This script has been described in detail previously.[22] Briefly, the analysis provides the r_e^{SE} parameters based on a set of isotopologues substituting each unique atom once. The program then iteratively adds one isotopologue at a time to sequential r_e^{SE} determinations until all isotopologues are incorporated. The order in which the isotopologues are incorporated is based on the extent to which they decrease the uncertainty in the parameters; those that most decrease the uncertainty are added first. Figures showing a composite structural uncertainty as a function of a number of incorporated isotopologues are provided in the supplementary material. Figure 4 shows the structural parameter values and their uncertainties as a function of number of

Published under an exclusive license by AIP Publishing

The Journal of Chemical Physics ARTICLE scitation.org/journal/jcp

isotopologues for 1*H*-1,2-3-triazole. As depicted in the left-side plots, bond distances appeared to be fairly well converged even using single isotopic substitutions at each atom, though the incorporation of even a single additional isotopologue results in a noticeable change that brings the value into closer agreement with the BTE value (dashed, colored line) for several parameters (*e.g.*, R_{N1-H}, R_{N2-C4}). The inclusion of further isotopologues has only a minor effect on the uncertainties in the bond distances, but it is not possible to know *a priori* how many isotopologues are necessary to converge a parameter. Examination of the angles in the right-hand column, similarly, reveals that $\theta_{C5-C4-H}$ does not converge until the ninth isotopologue is incorporated, and the additional isotopologues appear important for the determination of the external, H-involving angles of 1*H*-1,2,3-triazole (the top three plots in the right-hand column of Fig. 4). As mentioned previously, the BTE values for two angles ($\theta_{C4-C5-H}$ and $\theta_{C5-N1-H}$) fall outside the 2σ uncertainties of the semi-experimental values. If, however, the correction for residual basis set effects beyond cc-pCV5Z (which are manifestly unreliable for these parameters) is omitted (black, dotted lines), these two parameters fall into agreement with the computed values. In fact, the value of $\theta_{C5-N1-H}$ moves farther from the BTE value and closer to that excluding the basis set correction with the incorporation of more isotopologues. One parameter whose basis set extrapolation is reasonable (*vide supra*), $\theta_{C5-C4-H}$, falls into disagreement, though

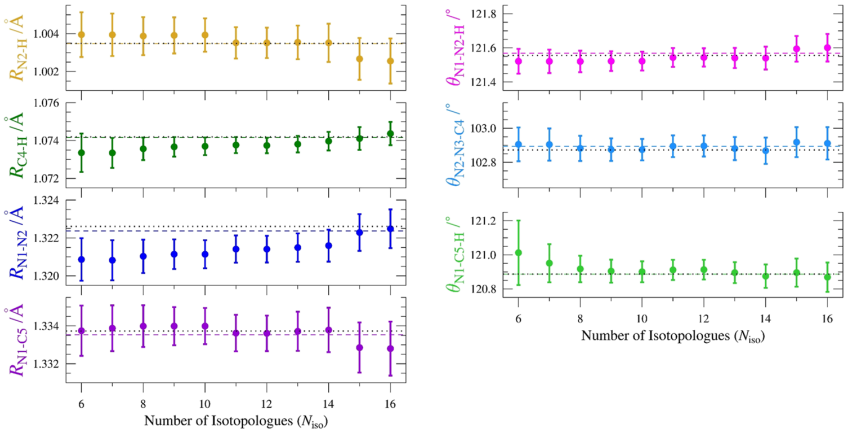


N	Isotopologue Added	*N*	Isotopologue Added
8	Core set	11	[1,2,3-^{15}N]
9	[1,4,5-^{2}H]	12	[1,5-^{2}H]
10	[1,4-^{2}H]	13	[4,5-^{2}H]

FIG. 4. Plots of the structural parameters of 1*H*-1,2,3-triazole as a function of the number of isotopologues (N_{iso}) and their 2σ uncertainties with consistent scales for each distance and for each angle. The table at the bottom indicates the *x*th isotopologue added to the r_e^{SE}. Colored dashed lines indicate the BTE value; black dotted lines indicate the value obtained by adding all corrections *except* the basis set extrapolation to the CCSD(T)/cc-pCV5Z value.

Published under an exclusive license by AIP Publishing

The Journal of Chemical Physics ARTICLE scitation.org/journal/jcp



N	Isotopologue Added
6	Core set
7	[4,5-^{2}H]
8	[1,2,3-^{15}N]
9	[2-^{2}H, 1,2,3-^{15}N]
10	[2,4,5-^{2}H]
11	[2-^{2}H, 4-^{13}C]
12	[2,4-^{2}H]
13	[4-^{2}H, 4-^{13}C]
14	[4,5-^{2}H, 4-^{13}C]
15	[2-^{2}H, 1-^{15}N]
16	[4-^{2}H, 5-^{13}C]

FIG. 5. Plots of the structural parameters of 2*H*-1,2,3-triazole as a function of the number of isotopologues (N_{iso}) and their 2σ uncertainties with consistent scales for each distance and for each angle. The table at the right indicates the *x*th isotopologue added to the r_e^{SE}. Colored dashed lines indicate the BTE value; black dotted lines indicate the value obtained by adding all corrections except the basis set extrapolation to the CCSD(T)/cc-pCV5Z value.

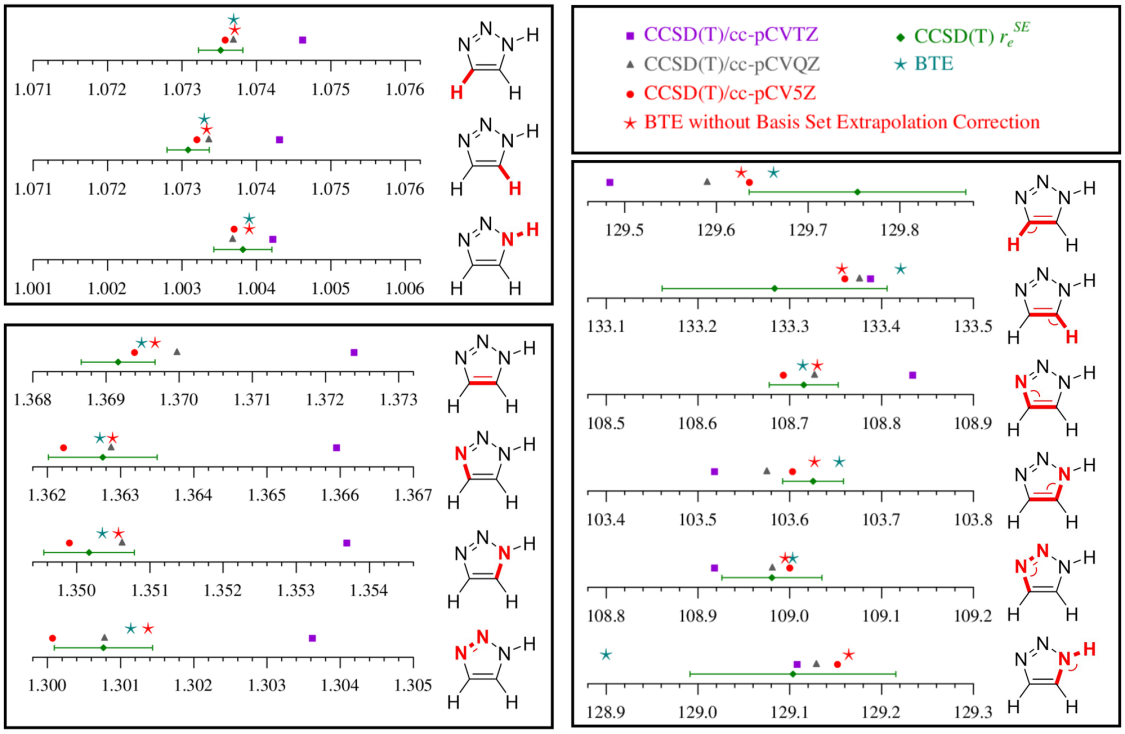


FIG. 6. Graphical comparison of the 1*H*-1,2,3-triazole structural parameters with bond distances in angstroms (Å) and angles in degrees (°). Bond distances are set to the same scale, and bond angles are set to the same scale. Uncertainties shown for current, CCSD(T) r_e^{SE} are 2σ. Cyan star indicates the BTE value; red star indicates the value obtained by adding all corrections except the basis set extrapolation to the CCSD(T)/cc-pCV5Z value.

Published under an exclusive license by AIP Publishing

The Journal of Chemical Physics ARTICLE scitation.org/journal/jcp

this may be an indication that all corrections are important for some parameters, as observed previously.[20,22]

Figure 5 shows the analogous structural parameter plots for the 2*H*-1,2,3-tautomer. In this case, the $\theta_{N1-N2-H}$ and $\theta_{N2-N3-C4}$ values are reasonably stable through the 14th isotopologue. The value of $\theta_{N1-C5-H}$, however, changes with the incorporation of even a few isotopologues beyond the minimal set, and its uncertainty decreases noticeably. The bond distance values and some of their uncertainties are refined by the inclusion of numerous isotopologues. It is visually striking that, with the last two isotopologues, [2-^{2}H, 1-^{15}N] and [4-^{2}H, 5-^{13}C], several of the parameters change in a discontinuous way. Furthermore, inclusion of the last four . . . increases the uncertainty of several parameters (see also Fig. S27). The inclusion of these four species is responsible for the aforementioned surprisingly lower precision of multiple parameters in the 2*H* tautomer relative to the 1*H* tautomer. Such effects may be due to errors in the data (rotational constants or corrections) used for the corresponding isotopologues or due to the fact that these isotopologues provide new or different information than the prior isotopologues. The last four isotopologues are indeed those whose spectroscopic constants are determined using the fewest transitions: 11 transitions for [4-^{2}H, 4-^{13}C], 41 transitions for [4,5-^{2}H, 4-^{13}C], 60 transitions for [2-^{2}H, 1-^{15}N], and 21 transitions for [4-^{2}H, 5-^{13}C]. Potential support for the hypothesis that the relatively small

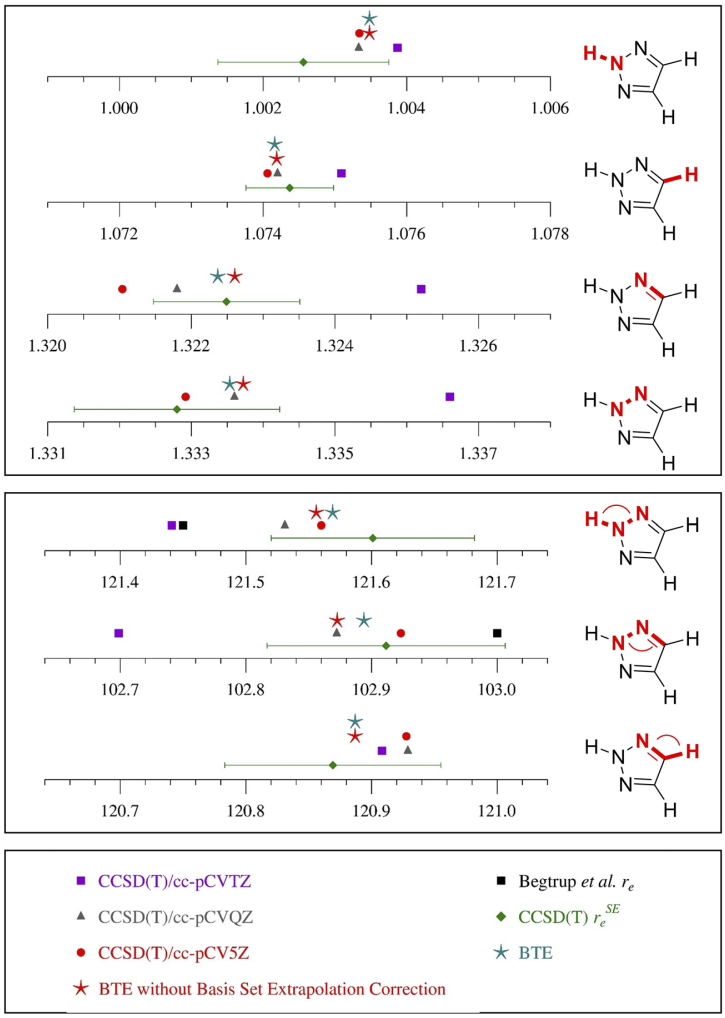


FIG. 7. Graphical comparison of the 2*H*-1,2,3-triazole structural parameters with bond distances in angstroms (Å) and angles in degrees (°). Bond distances are set to the same scale, and bond angles are set to the same scale. Uncertainties shown for current, CCSD(T) r_e^{SE} are 2σ. Where symbols of predicted values do not appear, they are sufficiently far from the CCSD(T) r_e^{SE} as to not fit within the respective displayed ranges. Cyan star indicates the BTE value; red star indicates the value obtained by adding all corrections except the basis set extrapolation to the CCSD(T)/cc-pCV5Z value.

Published under an exclusive license by AIP Publishing

The Journal of Chemical Physics ARTICLE scitation.org/journal/jcp

number of transitions identified for these species results in inaccurate rotational constants could be that the fully corrected inertial defects (Table II) of two of the carbon-deuteriated species ([4,5-^{2}H, 4-^{13}C] and [4-^{2}H, 5-^{13}C]) have the largest magnitudes of the 2*H* isotopologues, ranging from 0.000 50 to 0.000 53 uÅ^{2}. The *N*-deuterio isotopologue, [2-^{2}H, 1-^{15}N], however, has a quite small inertial defect magnitude (0.000 03 uÅ^{2}), and the other carbon-deuteriated species, [4-^{2}H, 4-^{13}C], also has among the lowest magnitudes (0.000 20 uÅ^{2}).

Moreover, all of these inertial defect values would have been considered not only acceptable but also among the smallest values of previous r_e^{SE} structures examined in this way. If these four isotopologues are excluded (x = 12 in Fig. 5) from the r_e^{SE} of 2*H*-1,2,3-triazole, the 2σ uncertainties of all bond distances fall to <0.001 Å, but two of the bond distances (R_{N1-N2} and R_{C4-H}) fall out of agreement with the corresponding BTE values. If only the last two isotopologues are excluded, the BTE and r_e^{SE} remain in complete agreement, but the desired precision is still not achieved. Parameters for four additional sets of r_e^{SE} structures for 2*H*-1,2,3-triazole, excluding the isotopologues in question here, are provided in the supplementary material. It is typical to consider the agreement of computational results in comparison to experimental (or semi-experimental) results, the latter being generally accepted to be more accurate in reality. Based on the exceptional agreement of several other BTEs and their respective r_e^{SE} structures (especially those containing only C, N, and H atoms),[20,22,25] however, it would appear surprising for the BTE presented here—calculated using the same levels of theory in all components as those of the cited works—to suddenly fail to predict the structural parameters of the triazoles to the same degree of accuracy. Since two bond distances that fall out of agreement upon removal of the last four isotopologues are expected to be properly estimated by the BTE (*i.e.*, their basis set extrapolation correction is appropriate), we consider the r_e^{SE} parameters of 2*H*-1,2,3-triazole presented here to be the most accurate. The inclusion of all 16 isotopologues in the determination of the parameters is necessary, albeit at the cost of the parameters' precision.

Figures 6 and 7 provide, respectively, for 1*H*- and 2*H*-1,2,3-triazole, a means to visualize the effects of the sum corrections on the respective CCSD(T)/cc-pCVXZ parameters and the agreement between r_e^{SE} and computational structures. The patterns that emerge upon examination of these plots are similar for both tautomers. In many cases, the triple–zeta parameter value is substantially outside of the r_e^{SE} 2σ uncertainty. The quadruple-zeta values fall within the 2σ uncertainty for approximately half of the 1*H* parameters and nearly all of the 2*H* parameters. The quintuple-zeta values are within the 2σ uncertainty of the r_e^{SE} value for all of the 2*H* parameters and all but a single 1*H* parameter. The 1*H* parameter whose quintuple-zeta value falls outside the r_e^{SE} value ($\theta_{C5-C4-H}$) shows a relatively large spread in the triple-, quadruple-, and quintuple-zeta values (Fig. 6, right-hand panel, top graph). The corresponding BTE value is in agreement with the r_e^{SE}. Conversely, the three direct computational values are closely clustered and all within the r_e^{SE} uncertainty for the $\theta_{C4-C5-H}$ and $\theta_{C5-N1-H}$ parameters of 1*H*-1,2,3-triazole (Table S-VIII)—it is the corrections applied to obtain the BTE (in particular, the aforementioned problematic extrapolated basis set correction) that put the BTE values out of agreement with the semi-experimental structure.

CONCLUSION

This work represents a continuation of our recent research efforts to determine highly accurate equilibrium structures and, in particular, extends the number of heterocyclic organic molecules that have been studied.[20,22–24] Unlike pyrimidine[20] and pyridazine,[22] however, the 1,2,3-triazole structures presented in this work are exceptional in the sense that 1*H*-1,2,3-triazole is the first molecule containing only carbon, nitrogen, and hydrogen for which the BTE and r_e^{SE} structures are not in complete agreement. These differences—two of the BTE parameters fall outside the 2σ uncertainties of the parameters of the r_e^{SE} structure—have been traced to issues associated with the extrapolation of structural parameters computed with large core-correlating basis sets (cc-pCV*X*Z, with *X* = T, Q, and 5) to the complete basis set limit. The atypical behavior observed in this study might be ameliorated by using alternative extrapolation strategies, but it is by no means obvious how this might be accomplished. It is only certain from our analysis that the use of the raw, uncorrected cc-pCV5Z result is a superior strategy to a nonsensical extrapolation correction.

In other respects, however, the results obtained for the 1,2,3-triazole isomers are among the best that we have been able to obtain in studies of this sort. For example, in recent studies on thiophene[23] and thiazole,[24] the process of determining accurate semi-experimental structures has been compromised by the presence of atoms that lie near, but not along, inertial axes. Although the N3 and C4 atoms of 1*H*-1,2,3-triazole are also fairly close to inertial axes, they are easily rotated away from principal axes by isotopic substitution and geometric parameters involving these atoms are readily determined with high accuracy. The positions of N2 and the bonded H atom of the 2*H* tautomer, which lie along an inertial axis in the main isotopologue, appear no less poorly determined than other positions in the molecule. The inertial defects defects obtained from the semi-experimental equilibrium rotational constants in this work are the smallest (by more than an order of magnitude) yet found in our recent semi-experimental structural determinations. Furthermore, the high quality of data in this work facilitated the detection of several low-abundance isotopologues in the experimental spectrum. The latter underscores the virtue of using such highly accurate r_e^{SE} structures to predict rotational constants that can subsequently be used to seek isotopologues of interest in complex spectra, including observational astronomical spectra. Finally, this work supplies the scientific community with spectroscopic constants including quartic and sextic centrifugal distortion constants necessary to identify these species in the ISM or other harsh environments. The detection (or lack thereof) of these triazoles in various locations would be interesting and potentially shed light on the types of chemistry in these environments.

SUPPLEMENTARY MATERIAL

Computational output files, least-squares fitting for all isotopologues, data distribution plots for all isotopologues, mass spectra, *xrefiteration* outputs, equations used for calculating determinable constants and BTE corrections, and tables of S reduction, A reduction, and determinable constants, as well as 2*H*-1,2,3-triazole r_e^{SE} parameters determined using 12–15 isotopologues, are provided in the supplementary material.

Published under an exclusive license by AIP Publishing

The Journal of Chemical Physics ARTICLE scitation.org/journal/jcp

ACKNOWLEDGMENTS

We gratefully acknowledge funding from the National Science Foundation (Grant No. CHE-1954270 to R. J. M.) and the U.S. Department of Energy, Office of Basic Energy Sciences (Grant No. DE-SC0018164 to J. F. S.) for support of this project, as well as the National Institutes of Health for support of shared Departmental mass spectrometry resources (Thermo Scientific Q Exactive Plus mass spectrometer, Grant No. 1S10 OD020022-1). We thank Michael McCarthy for the loan of an amplification-multiplication chain and the Harvey Spangler Award (to B.J.E.) for funding that supported the purchase of the corresponding detector.

AUTHOR DECLARATIONS

Conflict of Interest

The authors have no conflicts to disclose.

Author Contributions

Maria A. Zdanovskaia: Formal analysis (equal); Writing – original draft (lead). **Brian J. Esselman**: Formal analysis (equal); Writing – review and editing (equal). **Samuel M. Kougias**: Methodology (equal). **Brent K. Amberger**: Investigation (supporting). **John F. Stanton**: Conceptualization (equal); Formal analysis (equal); Writing – review and editing (equal). **R. Claude Woods**: Conceptualization (equal); Formal analysis (equal); Supervision (equal); Writing – review and editing (equal). **Robert J. McMahon**: Funding acquisition (lead); Project administration (lead); Supervision (equal); Writing – review and editing (equal).

DATA AVAILABILITY

The data that support the findings of this study are available within the article and its supplementary material.

REFERENCES

[1]L. W. Hartzel and F. R. Benson, "Synthesis of 4-Alkyl-v-triazoles from acetylenic compounds and hydrogen azide," J. Am. Chem. Soc. **76**, 667–670 (1954).

[2]E. Borello, A. Zecchina, and E. Guglielminotti, "A vibrational assignment for 1,2,3-triazole," J. Chem. Soc. B **1969**, 307–311.

[3]F. Billes, H. Endrédi, and G. Keresztury, "Vibrational spectroscopy of triazoles and tetrazole," J. Mol. Struct.: THEOCHEM **530**, 183–200 (2000).

[4]S. G. Aziz, S. A. Elroby, A. Alyoubi, O. I. Osman, and R. Hilal, "Experimental and theoretical assignment of the vibrational spectra of triazoles and benzotriazoles. Identification of IR marker bands and electric response properties," J. Mol. Model. **20**, 2078 (2014).

[5]M. Begtrup, C. J. Nielsen, L. Nygaard, S. Samdal, C. E. Sjøgren, and G. O. Sørensen, "The molecular structure and tautomer equilibrium of gaseous 1,2,3-triazole studied by microwave spectroscopy, electron diffraction and *ab initio* calculations," Acta Chem. Scand. A **42a**, 500–514 (1988).

[6]G. L. Blackman, R. D. Brown, F. R. Burden, and W. Garland, "Nuclear quadrupole coupling in the microwave spectrum of 1,2,3-triazole," J. Mol. Spectrosc. **65**, 313–318 (1977).

[7]G. O. Sorensen, L. Nygaard, and M. Begtrup, "Microwave spectrum of 1-deuterio-1,2,3-triazole," J. Chem. Soc., Chem. Commun. **1974**, 605–606.

[8]O. L. Stiefvater, H. Jones, and J. Sheridan, "Double-resonance-double-search assignment of the microwave spectrum of 1,2,3-triazole," Spectrochim. Acta, Part A **26**, 825–833 (1970).

[9]Z. Zhou, R. Liu, J. Wang, S. Li, M. Liu, and J.-L. Brédas, "Intra- and intermolecular proton transfer in 1*H*(2*H*)-1,2,3-triazole based systems," J. Phys. Chem. A **110**, 2322–2324 (2006).

[10]J.-L. M. Abboud, C. Foces-Foces, R. Notario, R. E. Trifonov, A. P. Volovodenko, V. A. Ostrovskii, I. Alkorta, and J. Elguero, "Basicity of *N*-H- and *N*-methyl-1,2,3-triazoles in the gas phase, in solution, and in the solid state—An experimental and theoretical study," Eur. J. Org. Chem. **2001**, 3013–3024.

[11]R. Goddard, O. Heinemann, and C. Krüger, "Pyrrole and a Co-crystal of 1*H*- and 2*H*-1,2,3-triazole," Acta Crystallogr., Sect. C: Cryst. Struct. Commun. **53**, 1846–1850 (1997).

[12]J. R. Cox, S. Woodcock, I. H. Hillier, and M. A. Vincent, "Tautomerism of 1,2,3- and 1,2,4-triazole in the gas phase and in aqueous solution: A combined ab initio quantum mechanics and free energy perturbation study," J. Phys. Chem. **94**, 5499–5501 (1990).

[13]F. Tomas, J. L. M. Abboud, J. Laynez, R. Notario, L. Santos, S. O. Nilsson, J. Catalan, R. M. Claramunt, and J. Elguero, "Tautomerism and aromaticity in 1,2,3-triazoles: The case of benzotriazole," J. Am. Chem. Soc. **111**, 7348–7353 (1989).

[14]J. Catalán, M. Sánchez-Cabezudo, J. L. G. De Paz, J. Elguero, R. W. Taft, and F. Anvia, "The tautomerism of 1,2,3-triazole, 3(5)-methylpyrazole and their cations," J. Comput. Chem. **10**, 426–433 (1989).

[15]M. H. Palmer, I. Simpson, and R. H. Findlay, "^{14}N nuclear quadrupole coupling in heterocyclic compounds, Part 2. A comparison of *ab initio* calculations and experimental results for the azoles and azines," Z. Naturforsch., A **36 A**, 34–50 (1980).

[16]C. Törnkvist, J. Bergman, and B. Liedberg, "Correlated *ab initio* geometries and vibrations of 1H- and 2H-1,2,3-triazole," J. Phys. Chem. **95**, 3123–3128 (1991).

[17]Y.-L. Lu, X.-D. Gong, X.-H. Ju, G.-F. Ji, and H.-M. Xiao, "Structures and properties of 1,2,3-triazoles and 1,2,4-triazoles," Chin. J. Struct. Chem. **25**, 582–588 (2006).

[18]P. Pulay, W. Meyer, and J. E. Boggs, "Cubic force constants and equilibrium geometry of methane from Hartree–Fock and correlated wavefunctions," J. Chem. Phys. **68**, 5077–5085 (1978).

[19]C. Puzzarini, J. Bloino, N. Tasinato, and V. Barone, "Accuracy and interpretability: The devil and the holy grail. New routes across old boundaries in computational spectroscopy," Chem. Rev. **119**, 8131–8191 (2019).

[20]Z. N. Heim, B. K. Amberger, B. J. Esselman, J. F. Stanton, R. C. Woods, and R. J. McMahon, "Molecular structure determination: Equilibrium structure of pyrimidine (*m*-$C_4H_4N_2$) from rotational spectroscopy (r_e^{SE}) and high-level *ab initio* calculation (r_e) agree within the uncertainty of experimental measurement," J. Chem. Phys. **152**, 104303 (2020).

[21]A. G. Császár, J. Demaison, and H. D. Rudolph, "Equilibrium structures of three-, four-, five-, six-, and seven-membered unsaturated N-containing heterocycles," J. Phys. Chem. A **119**, 1731–1746 (2015).

[22]A. N. Owen, M. A. Zdanovskaia, B. J. Esselman, J. F. Stanton, R. C. Woods, and R. J. McMahon, "Semi-experimental equilibrium (r_e^{SE}) and theoretical structures of pyridazine (*o*-$C_4H_4N_2$)," J. Phys. Chem. A **125**, 7976–7987 (2021).

[23]V. L. Orr, Y. Ichikawa, A. R. Patel, S. M. Kougias, K. Kobayashi, J. F. Stanton, B. J. Esselman, R. C. Woods, and R. J. McMahon, "Precise equilibrium structure determination of thiophene (*c*-C_4H_4S) by rotational spectroscopy—structure of a five-membered heterocycle containing a third-row atom," J. Chem. Phys. **154**, 244310 (2021).

[24]B. J. Esselman, M. A. Zdanovskaia, A. N. Owen, J. F. Stanton, R. C. Woods, and R. J. McMahon, "Precise equilibrium structure of thiazole (*c*-C_3H_3NS) from twenty-four isotopologues," J. Chem. Phys. **155**, 054302 (2021).

[25]B. J. Esselman; M. A. Zdanovskaia; A. N. Owen; J. F. Stanton; R. C. Woods; R. J. McMahon, "Precise equilibrium structure of benzene from eleven isotopologues," (unpublished work) (2021).

[26]L. Nygaard, E. Asmussen, J. H. Høg, R. C. Maheshwari, C. H. Nielsen, I. B. Petersen, J. Rastrup-Andersen, and G. O. Sørensen, "Microwave spectra of isotopic thiazoles. Molecular structure ^{14}N quadrupole coupling constants of thiazole," J. Mol. Struct. **8**, 225–233 (1971).

Published under an exclusive license by AIP Publishing

The Journal of Chemical Physics ARTICLE scitation.org/journal/jcp

[27]J. Cernicharo, A. M. Heras, A. G. G. M. Tielens, J. R. Pardo, F. Herpin, M. Guélin, and L. B. F. M. Waters, "Infrared space observatory's discovery of C_4H_2, C_6H_2, and benzene in CRL 618," Astrophys. J. **546**, L123–L126 (2001).
[28]S. B. Charnley, Y.-J. Kuan, H.-C. Huang, O. Botta, H. M. Butner, N. Cox, D. Despois, P. Ehrenfreund, Z. Kisiel, Y.-Y. Lee, A. J. Markwick, Z. Peeters, and S. D. Rodgers, "Astronomical searches for nitrogen heterocycles," Adv. Space Res. **36**, 137–145 (2005).
[29]Y.-J. Kuan, C.-H. Yan, S. B. Charnley, Z. Kisiel, P. Ehrenfreund, and H.-C. Huang, "A search for interstellar pyrimidine," Mon. Not. R. Astron. Soc. **345**, 650–656 (2003).
[30]B. Cunha de Miranda, G. A. Garcia, F. Gaie-Levrel, A. Mahjoub, T. Gautier, B. Fleury, L. Nahon, P. Pernot, and N. Carrasco, "Molecular isomer identification of Titan's tholins organic aerosols by photoelectron/photoion coincidence spectroscopy coupled to VUV synchrotron radiation," J. Phys. Chem. A **120**, 6529–6540 (2016).
[31]C. He and M. A. Smith, "Identification of nitrogenous organic species in Titan aerosols analogs: Nitrogen fixation routes in early atmospheres," Icarus **226**, 33–40 (2013).
[32]E. Bonandi, M. S. Christodoulou, G. Fumagalli, D. Perdicchia, G. Rastelli, and D. Passarella, "The 1,2,3-triazole ring as a bioisostere in medicinal chemistry," Drug Discovery Today **22**, 1572–1581 (2017).
[33]I. E. Valverde, A. Bauman, C. A. Kluba, S. Vomstein, M. A. Walter, and T. L. Mindt, "1,2,3-Triazoles as amide bond mimics: Triazole scan yields protease-resistant peptidomimetics for tumor targeting," Angew. Chem., Int. Ed. **52**, 8957–8960 (2013).
[34]K. Bozorov, J. Zhao, and H. A. Aisa, "1,2,3-Triazole-containing hybrids as leads in medicinal chemistry: A recent overview," Biorg. Med. Chem. **27**, 3511–3531 (2019).
[35]R. Huisgen, "Kinetics and mechanism of 1,3-dipolar cycloadditions," Angew. Chem., Int. Ed. **2**, 633–645 (1963).
[36]H. C. Kolb, M. G. Finn, and K. B. Sharpless, "Click chemistry: Diverse chemical function from a few good reactions," Angew. Chem., Int. Ed. **40**, 2004–2021 (2001).
[37]N. K. Devaraj and M. G. Finn, "Introduction: Click chemistry," Chem. Rev. **121**, 6697–6698 (2021).
[38]F. Lahuis and E. F. V. Dishoeck, "ISO–SWS spectroscopy of gas–phase C_2H_2 and HCN toward massive young stellar objects," Astron. Astrophys. **355**, 699–712 (2000).
[39]P. Sonnentrucker, E. González-Alfonso, and D. A. Neufeld, "Detection of acetylene toward Cepheus A East with *Spitzer*," Astrophys. J. **671**, L37–L40 (2007).
[40]S. Singh, T. B. McCord, J.-P. Combe, S. Rodriguez, T. Cornet, S. L. Mouélic, R. N. Clark, L. Maltagliati, and V. F. Chevrier, "Acetylene on Titan's surface," Astrophys. J. **828**, 55 (2016).
[41]B. K. Amberger, B. J. Esselman, J. F. Stanton, R. C. Woods, and R. J. McMahon, "Precise equilibrium structure determination of hydrazoic acid (HN_3) by millimeter-wave spectroscopy," J. Chem. Phys. **143**, 104310 (2015).
[42]B. J. Esselman, B. K. Amberger, J. D. Shutter, M. A. Daane, J. F. Stanton, R. C. Woods, and R. J. McMahon, "Rotational spectroscopy of pyridazine and its isotopologs from 235–360 GHz: Equilibrium structure and vibrational satellites," J. Chem. Phys. **139**, 224304–224313 (2013).
[43]G. Wlodarczak, J. Demaison, B. P. van Eijck, M. Zhao, and J. E. Boggs, "*Ab initio* and experimental quartic centrifugal distortion constants of acetone, pyrazole, and γ-pyrone," J. Chem. Phys. **94**, 6698–6707 (1991).
[44]L. Nygaard, D. Christen, J. T. Nielsen, E. J. Pedersen, O. Snerling, E. Vestergaard, and G. O. Sørensen, "Microwave spectra of isotopic pyrazoles and molecular structure of pyrazole," J. Mol. Struct. **22**, 401–413 (1974).
[45]W. H. Kirchhoff, "The microwave spectrum and dipole moment of pyrazole," J. Am. Chem. Soc. **89**, 1312–1316 (1967).
[46]M. A. Zdanovskaia, B. J. Esselman, R. C. Woods, and R. J. McMahon, "The 130–370 GHz rotational spectrum of phenyl isocyanide (C_6H_5NC)," J. Chem. Phys. **151**, 024301 (2019).
[47]Z. Kisiel, L. Pszczółkowski, B. J. Drouin, C. S. Brauer, S. Yu, J. C. Pearson, I. R. Medvedev, S. Fortman, and C. Neese, "Broadband rotational spectroscopy of acrylonitrile: Vibrational energies from perturbations," J. Mol. Spectrosc. **280**, 134–144 (2012).
[48]Z. Kisiel, L. Pszczółkowski, I. R. Medvedev, M. Winnewisser, F. C. De Lucia, and E. Herbst, "Rotational spectrum of *trans–trans* diethyl ether in the ground and three excited vibrational states," J. Mol. Spectrosc. **233**, 231–243 (2005).
[49]Z. Kisiel and E. Białkowska-Jaworska, "Sextic centrifugal distortion in fluorobenzene and phenylacetylene from cm-wave rotational spectroscopy," J. Mol. Spectrosc. **359**, 16–21 (2019).
[50]Z. Kisiel, "Assignment and analysis of complex rotational spectra," in *Spectroscopy from Space*, edited by J. Demaison, K. Sarka and E. A. Cohen (Kluwer Academic Publishers: Dordrecht, 2001), pp. 91–106.
[51]See http://info.ifpan.edu.pl/~kisiel/prospe.htm for "PROSPE–programs for ROtational SPEctroscopy".
[52]CFOUR, Coupled-Cluster techniques for Computational Chemistry, a quantum-chemical program package by J. F. Stanton, J. Gauss, L. Cheng, M. E. Harding, D. A. Matthews, P. G. Szalay with contributions from A. A. Auer, R. J. Bartlett, U. Benedikt, C. Berger, D. E. Bernholdt, Y. J. Bomble, O. Christiansen, F. Engel, R. Faber, M. Heckert, O. Heun, C. Huber, T.-C. Jagau, D. Jonsson, J. Jusélius, K. Klein, W. J. Lauderdale, F. Lipparini, T. Metzroth, L. A. Mück, D. P. O'Neill, D. R. Price, E. Prochnow, C. Puzzarini, K. Ruud, F. Schiffmann, W. Schwalbach, C. Simmons, S. Stopkowicz, A. Tajti, J. Vázquez, F. Wang, J. D.Watts and the integral packages MOLECULE (J. Almlöf and P. R. Taylor), PROPS (P. R. Taylor), ABACUS (T. Helgaker, H. J. Aa. Jensen, P. Jørgensen, and J. Olsen), and ECP routines by A. V. Mitin and C. van Wüllen. For the current version, see http://www.cfour.de.
[53]J. F. Stanton, C. L. Lopreore, and J. Gauss, "The equilibrium structure and fundamental vibrational frequencies of dioxirane," J. Chem. Phys. **108**, 7190–7196 (1998).
[54]W. Schneider and W. Thiel, "Anharmonic force fields from analytic second derivatives: Method and application to methyl bromide," Chem. Phys. Lett. **157**, 367–373 (1989).
[55]I. M. Mills, "Vibration-rotation structure in asymmetric- and symmetric-top molecules," in *Molecular Spectroscopy: Modern Research*, edited by K. N. Rao and C. W. Mathews (Academic Press, New York, 1972), Vol. 1, pp. 115–140.

Published under an exclusive license by AIP Publishing